

1985-16937

Space Shuttle Technical Conference

(NASA-CP-2342-Pt-2) SPACE SHUTTLE TECHNICAL
CONFERENCE, PART 2 (NASA) 530 p
HC A23/MF A01

CSCL 22A

N85-16937

THRU

N85-16980

Unclas

G3/12

13561



NASA Conference Publication 2342^{N85-16937}
Part 2

Space Shuttle Technical Conference

Norman Chaffee, *Compiler*
Lyndon B. Johnson Space Center
Houston, Texas

Papers prepared for a conference
sponsored by the National Aeronautics
and Space Administration and held at
Lyndon B. Johnson Space Center
Houston, Texas
June 28-30, 1983

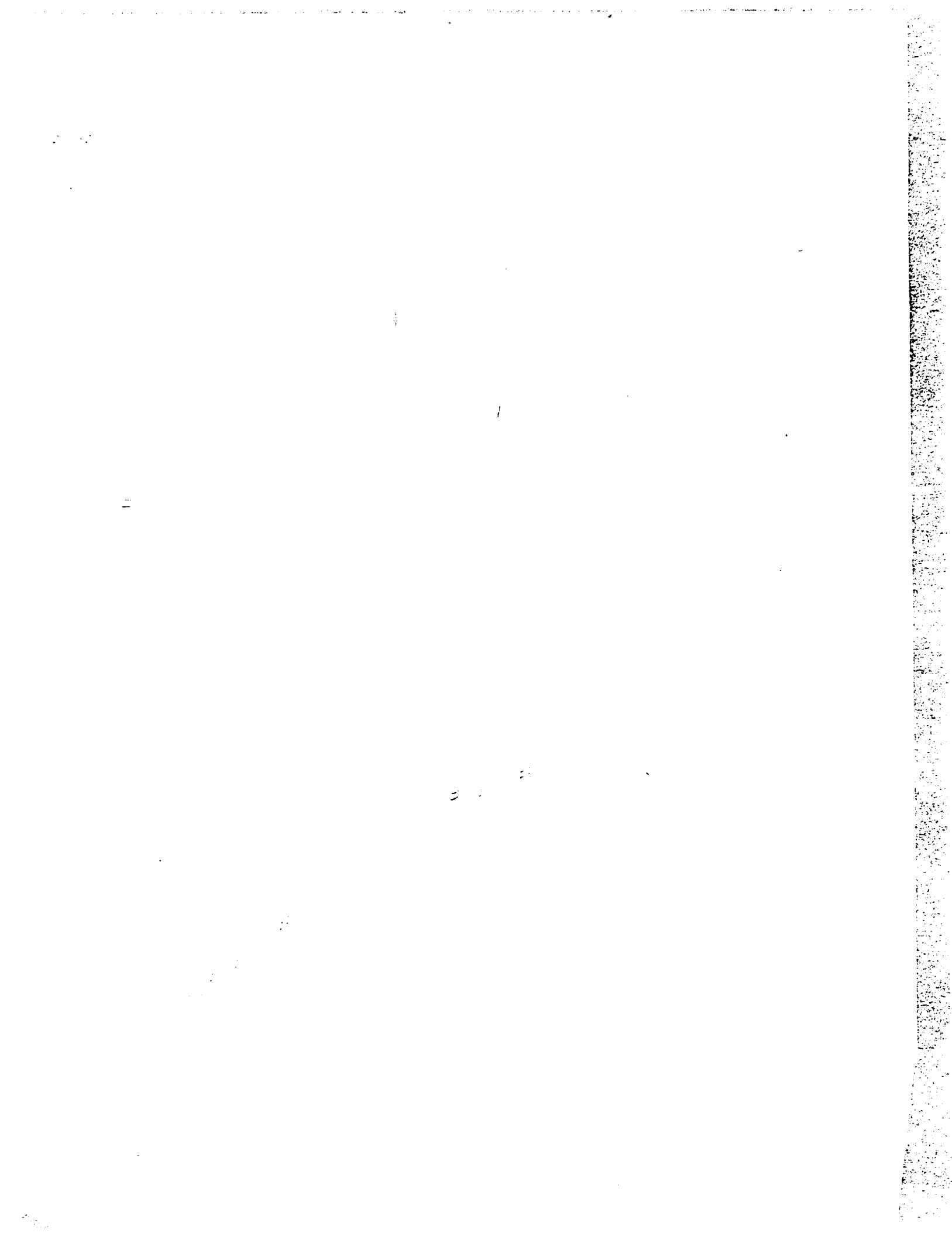
NASA

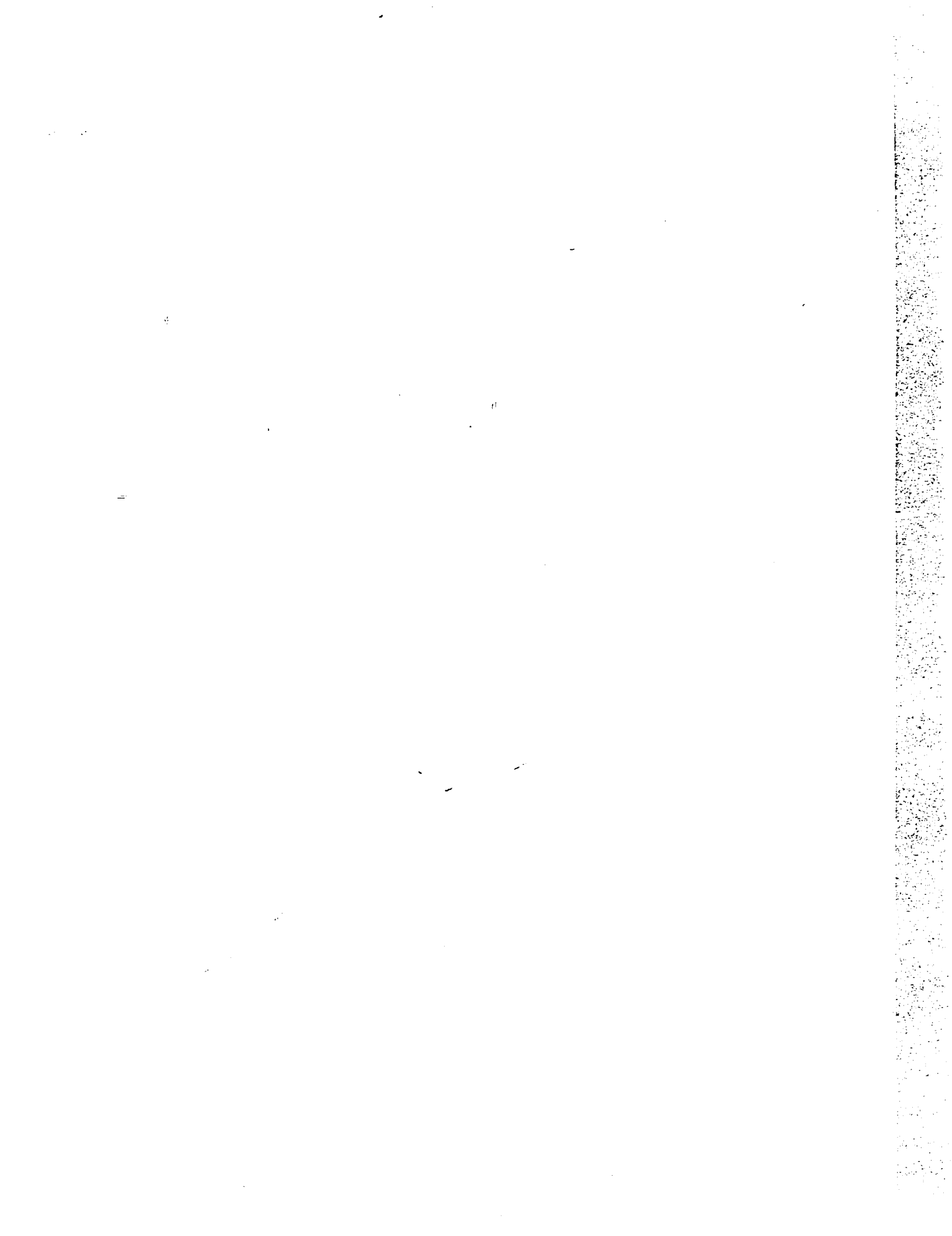
National Aeronautics
and Space Administration

Scientific and Technical
Information Branch

1985

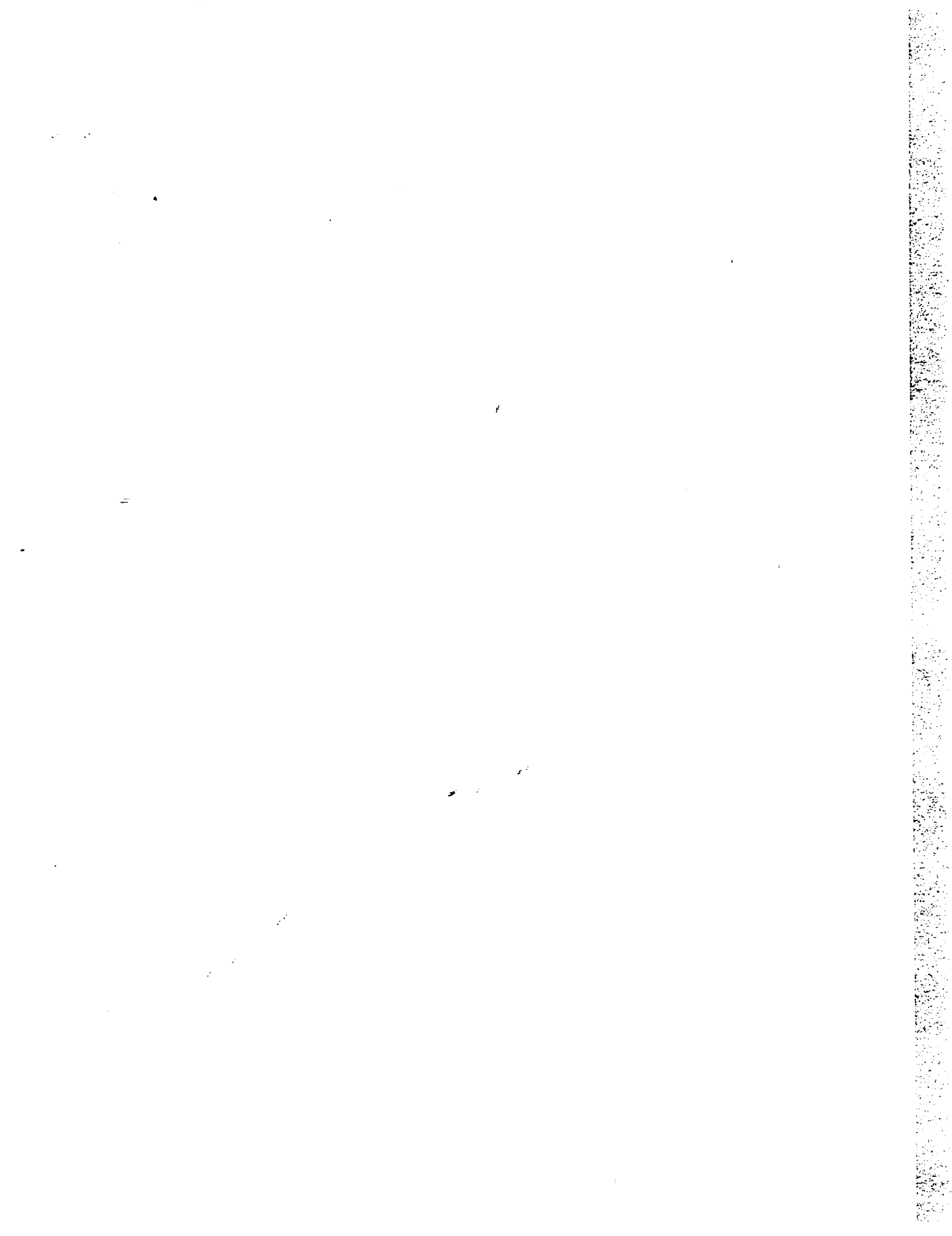
530





NOTICE

THIS DOCUMENT HAS BEEN REPRODUCED FROM THE BEST COPY FURNISHED US BY THE SPONSORING AGENCY. ALTHOUGH IT IS RECOGNIZED THAT CERTAIN PORTIONS ARE ILLEGIBLE, IT IS BEING RELEASED IN THE INTEREST OF MAKING AVAILABLE AS MUCH INFORMATION AS POSSIBLE.



PREFACE

This publication is a compilation of the papers prepared for the Space Shuttle Technical Conference held at the NASA Lyndon B. Johnson Space Center, Houston, Texas, June 28-30, 1983. The purpose of this conference was to provide an archival publication for the retrospective presentation and documentation of the key scientific and engineering achievements of the Space Shuttle Program following the attainment of full operational status by the National Space Transportation System.

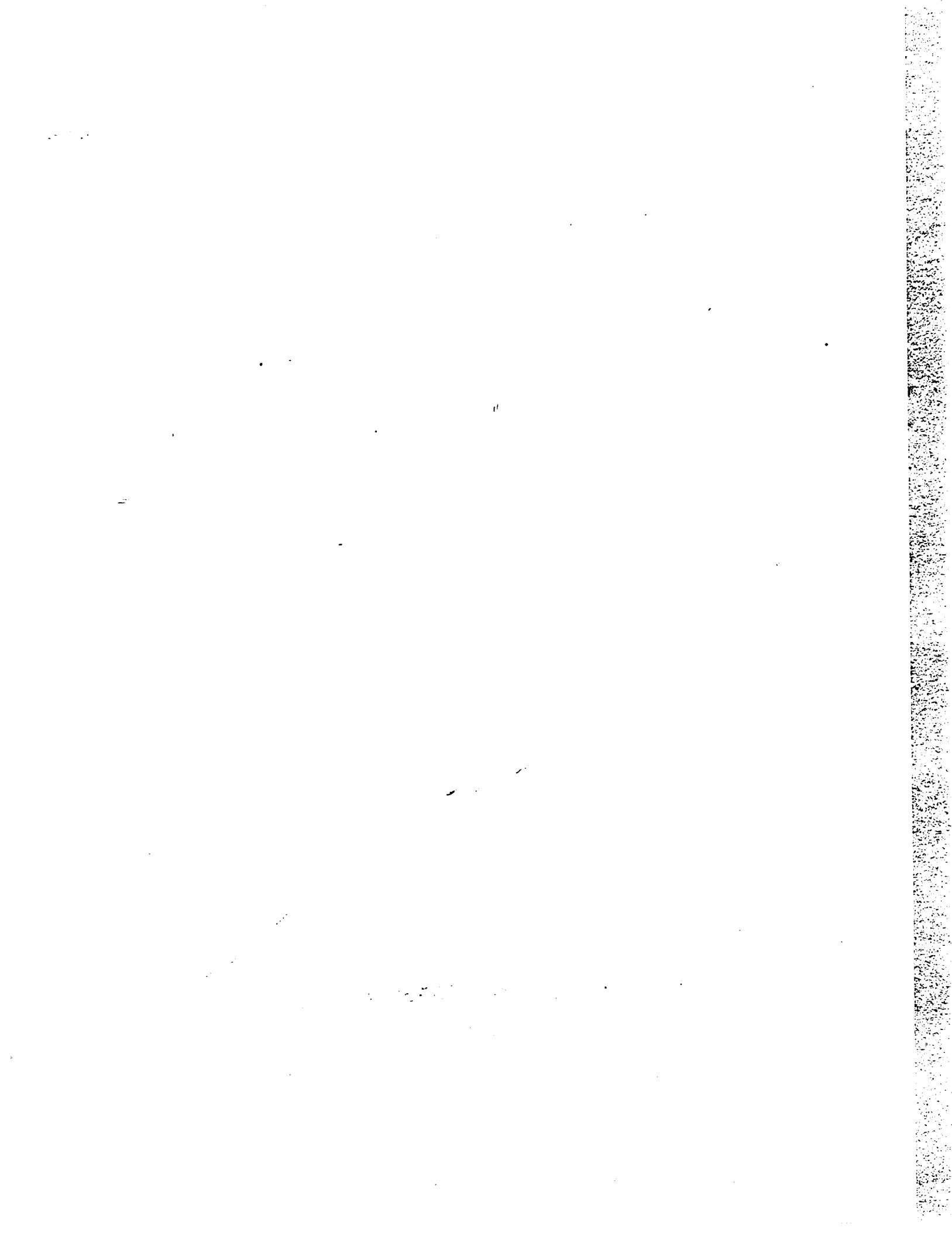
To provide technical disciplinary focus, the conference was organized around 10 technical topic areas: (1) Integrated Avionics, (2) Guidance, Navigation, and Control, (3) Aerodynamics, (4) Structures, (5) Life Support, Environmental Control, and Crew Station, (6) Ground Operations, (7) Propulsion and Power, (8) Communications and Tracking, (9) Mechanisms and Mechanical Systems, and (10) Thermal and Contamination Environments and Protection Systems.

The papers in each technical topic which were presented over the 3-day conference period provide a historical overview of the key technical problems and challenges which were met and overcome during the development phase of the Space Shuttle Program. Taken as a whole, these papers provide a valuable archival reference to the magnitude and scope of this major national achievement.

Because of the large volume of material prepared for the conference, this publication is divided into two parts.

This publication was prepared through the efforts of the staff of the Technical Information Branch, Management Services Division, Johnson Space Center.

PRECEDING PAGE BLANK NOT FILMED



FOREWORD

The achievement of operational status of the National Space Transportation System represented a historic accomplishment for the National Aeronautics and Space Administration (NASA), its contractors, and for the United States. To recognize this accomplishment, NASA organized a technical conference focusing on the design and development phase of the Space Shuttle Program. The purpose of the conference was to permit a presentation by key members of the NASA-Industry-Department of Defense team of the outstanding achievements of the program. Toward this end, the conference theme "The Space Shuttle Program: From Challenge to Achievement" was selected.

To provide a comprehensive and balanced program for the conference, the Conference Organizing Committee selected 10 broad, technical topic areas for which papers were invited from individuals who played key technical roles in the success of the design and development program. An extraordinarily fine selection of 91 papers was submitted for the conference representing the contributions of 6 NASA field centers, the Department of Defense, 2 universities, and 27 industrial organizations. Over the 3-day period of June 28-30, 1983, these papers were presented at the Lyndon B. Johnson Space Center in a format of multiple, parallel technical sessions, fully satisfying the "Achievement" portion of the conference theme.

The "Challenge" aspect of the conference theme was provided by Lieutenant General James A. Abrahamson, NASA Associate Administrator for Space Flight, who presented the conference keynote address; and by Dr. Maxime A. Faget, President of Space Industries Incorporated and former Director of Engineering and Development at the Johnson Space Center, who organized and moderated the discussions of a panel of distinguished government and industry executives who presided over the early days of the program. Excellent retrospective presentations were also made by Dr. Glynn S. Lunney, Manager of the National Space Transportation System Program, and by Donald K. (Deke) Slayton, President and Vice Chairman of Space Services Incorporated of America and former NASA astronaut and management official. The complementary combination of technical papers, addresses, and panel discussions provided a satisfying, synergistic package for the more than 1200 conference attendees.

As former Manager of the Orbiter Project, it was my privilege to serve as General Chairman of the Space Shuttle Technical Conference and to recognize and honor the team of men and women responsible for this historic accomplishment.

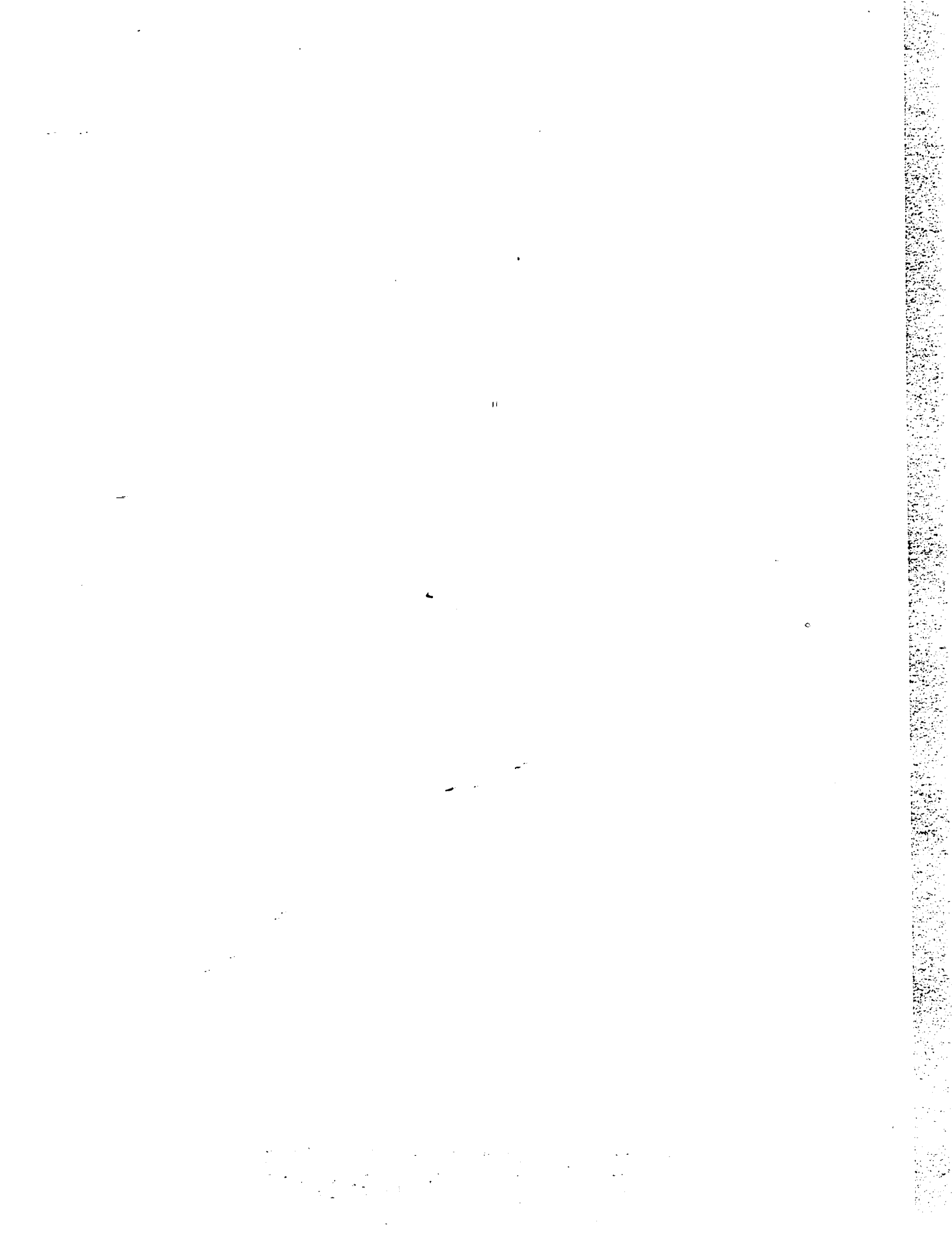
I am grateful for the help and support of the other members of the Conference Organizing Committee: Elwood W. Land, Jr. (NASA Headquarters); James E. Kingsbury (Marshall Space Flight Center); and Peter A. Minderman (Kennedy Space Center); and to Norman H. Chaffee (Johnson Space Center) who served as Conference Arrangements Chairman.

Aaron Cohen
General Chairman

Preceding page blank

v

PRECEDING PAGE BLANK NOT FILMED



CONTENTS

Page

PART 1

SESSION 1: INTEGRATED AVIONICS

Cochairmen: H. E. Smith, Johnson Space Center
W. C. Bradford, Marshall Space
Flight Center
J. A. Anderson, Kennedy Space Center

EVOLUTION OF SHUTTLE AVIONICS REDUNDANCY MANAGEMENT/FAULT TOLERANCE	1
Jack C. Boykin, Joseph R. Thibodeau, and Henry E. Schneider	
SHUTTLE AVIONICS SOFTWARE -- TRIALS, TRIBULATIONS AND SUCCESSES . . .	19
O. L. Henderson	
SHUTTLE AVIONICS SOFTWARE DEVELOPMENT -- TRIALS, TRIBULATIONS, AND SUCCESSES: THE BACKUP FLIGHT SYSTEM	30
Edward S. Chevers	
FLIGHT SOFTWARE FAULT TOLERANCE VIA THE BACKUP FLIGHT SYSTEM	35
Terry D. Humphrey and Charles R. Price	
SSME DIGITAL CONTROL DESIGN CHARACTERISTICS	38
Walter T. Mitchell and Richard F. Searle	
MAN-MACHINE INTERFACE AND CONTROL OF THE SHUTTLE DIGITAL FLIGHT SYSTEM	47 -
Richard D. Burghdoff and James L. Lewis, Jr.	
SPACE SHUTTLE MAIN ENGINE HARDWARE SIMULATION	54
H. G. Vick and P. W. Hampton	
DEVELOPMENT AND IMPLEMENTATION OF THE VERIFICATION PROCESS FOR THE SHUTTLE AVIONICS SYSTEM	64
H. E. Smith, W. B. Fouts, and J. Mesmer	
GROUND/MAN-MACHINE INTERFACES FOR ORBITER CHECKOUT	76
F. Herb Blackmon	
INTEGRATION OF GROUND AND ON-BOARD SYSTEM FOR TERMINAL COUNT	81
Charles A. Abner and Don H. Townsend	
INTEGRATED DESIGN CHECKOUT OF SHUTTLE PAYLOAD AVIONICS INTERFACES	87
John F. Muratore and Kathy K. Whitcomb	

Preceding page blank

vii

PRECEDING PAGE BLANK NOT FILMED

	Page
AUTOMATION OF CHECKOUT FOR THE SHUTTLE OPERATIONS ERA	97
Judith A. Anderson and Kenneth O. Hendrickson	

SESSION 2: GUIDANCE, NAVIGATION, AND CONTROL

Cochairmen: Dr. K. J. Cox, Johnson Space Center
K. J. Szalai, Ames Research Center/
Dryden Flight Research Facility

SHUTTLE NAVIGATION STATUS	102
Emil R. Schiesser	
DESCENT GUIDANCE AND MISSION PLANNING FOR SPACE SHUTTLE	113
B. Kent Joosten	
SOME EFFECTS OF DIGITAL SAMPLING ON ORBITER FLIGHT CONTROL SYSTEM OPERATION	125
S. V. Murray	
SPACE SHUTTLE HANDLING QUALITIES	137
David W. Gilbert	
LOW-SPEED LONGITUDINAL ORBITER FLYING QUALITIES	143
Bruce G. Powers	

SESSION 3: AERODYNAMICS

Cochairmen: B. G. Jackson, Johnson Space Center
C. D. Andrews, Marshall Space
Flight Center
W. I. Scallion, Langley Research
Center

THE SPACE SHUTTLE ASCENT VEHICLE AERODYNAMIC CHALLENGES -- CONFIGURATION DESIGN AND DATA BASE DEVELOPMENT	151
Charlie C. Dill, J. C. Young, B. B. Roberts, M. K. Craig, J. T. Hamilton, and W. W. Boyle	
THE SPACE SHUTTLE LAUNCH VEHICLE AERODYNAMIC VERIFICATION CHALLENGES	177
R. O. Wallace, L. D. Austin, J. G. Hondros, T. E. Surber, L. M. Gaines, and J. T. Hamilton	
THE AERODYNAMIC CHALLENGES OF SRB RECOVERY	189
D. L. Bacchus, D. A. Kross, and R. D. Moog	

	Page
THE AERODYNAMIC CHALLENGES OF THE DESIGN AND DEVELOPMENT OF THE SPACE SHUTTLE ORBITER	209
James C. Young, Jimmy M. Underwood, Ernest R. Hillje, Arthur M. Whitnah, Paul O. Romere, Joe D. Gamble, Barney B. Roberts, George M. Ware, William I. Scallion, Bernard Spencer, Jr., James P. Arrington, and Deloy C. Olsen	
THE DEVELOPMENT AND APPLICATION OF AERODYNAMIC UNCERTAINTIES; AND FLIGHT TEST VERIFICATION FOR THE SPACE SHUTTLE ORBITER	264
Joe D. Gamble, Douglas R. Cooke, Jimmy M. Underwood, Howard W. Stone, Jr., and Donald C. Schlosser	
AERODYNAMIC CHALLENGES OF ALT	295
Ivy Hooks, David Homan, and Paul Romere	
THE ORBITER AIR DATA SYSTEM	313
Ernest R. Hillje	

SESSION 4: STRUCTURES

Cochairmen: D. C. Wade, Johnson Space Center
R. S. Ryan, Marshall Space
Flight Center

SHUTTLE STRUCTURAL DYNAMICS CHARACTERISTICS -- THE ANALYSIS VERIFICATION	325
C. Thomas Modlin, Jr., and George A. Zupp, Jr.	
STRUCTURAL LOAD CHALLENGES DURING SPACE SHUTTLE DEVELOPMENT	335
Alden C. Mackey and Ralph E. Gatto	
ORBITER STRUCTURAL DESIGN AND VERIFICATION	345
Philip C. Glynn and Thomas L. Moser	
SPACE SHUTTLE EXTERNAL TANK PERFORMANCE IMPROVEMENTS -- THE CHALLENGE	357
Harold R. Coldwater, Richard R. Foll, Gayle J. Howell, and Jon A. Dutton	
STRUCTURAL AND MECHANICAL DESIGN CHALLENGES OF SPACE SHUTTLE SOLID ROCKET BOOSTERS SEPARATION AND RECOVERY SUBSYSTEMS	365
William R. Woodis and Roy E. Runkle	
SSME LIFETIME PREDICTION AND VERIFICATION, INTEGRATING ENVIRONMENTS, STRUCTURES, MATERIALS; THE CHALLENGE	386
Robert S. Ryan, Larry D. Salter, George M. Young III, and Paul M. Munaf0	

	Page
THE CHALLENGING "SCALES OF THE BIRD" (SHUTTLE TILE STRUCTURAL INTEGRITY)	403
William C. Schneider and Glenn J. Miller	
SESSION 5: LIFE SUPPORT, ENVIRONMENTAL CONTROL, AND CREW STATION	
Cochairmen: W. W. Guy, Johnson Space Center P. D. Quattrone, Ames Research Center	
CHALLENGES IN THE DEVELOPMENT OF THE ORBITER ATMOSPHERIC REVITALIZATION SUBSYSTEM	414
R. Norman Prince, Joe Swider, John Wojnarowski, Angelo Decrisantis, George R. Ord, James J. Walleshauser, and John W. Gibb	
CHALLENGES OF DEVELOPING AN ELECTRO-OPTICAL SYSTEM FOR MEASURING MAN'S OPERATIONAL ENVELOPE	426
Barbara Woolford	
CHALLENGES IN THE DEVELOPMENT OF THE SHUTTLE EXTRAVEHICULAR MOBILITY UNIT	435
Harold J. McMann and James W. McBarron II	
CHALLENGES IN THE DEVELOPMENT OF THE ORBITER ACTIVE THERMAL CONTROL SUBSYSTEM	450
John R. Nason, Frederic A. Wierum, and James L. Yanosy	
OTHER CHALLENGES IN THE DEVELOPMENT OF THE ORBITER ENVIRONMENTAL CONTROL HARDWARE	465
John W. Gibb, M. E. McIntosh, Steven R. Heinrich, Franz Schubert, E. P. Koszenski, R. A. Wynveen, Emory Thomas, Mike Steele, R. W. Murray, J. D. Schelkopf, and J. K. Mangialardi	
CHALLENGES IN THE DEVELOPMENT OF THE ORBITER RADIATOR SYSTEM	480
J. L. Williams, J. A. Oren, H. R. Howell, and M. F. Modest	

SESSION 6: GROUND OPERATIONS

Cochairmen: D. E. Phillips, Kennedy Space Center
W. C. Fischer, Johnson Space Center

OVERVIEW OF STS GROUND OPERATIONS/ORBITER TURNAROUND: STS-1 THROUGH STS-7	490
Richard Schwartz	
EXTERNAL TANK PROCESSING FROM BARGE TO PAD	498
J. E. Carpenter	
SOLID ROCKET BOOSTER RETRIEVAL OPERATIONS	505
Anker M. Rasmussen	
SPACE SHUTTLE FLIGHT READINESS FIRING -- DRESS REHEARSAL FOR STS-1	510
Lt. Col. Warren L. Riles	
TRANSITION TO THE SPACE SHUTTLE OPERATIONS ERA	525
William F. Edson, Jr.	
LAUNCH PROCESSING SYSTEM -- CONCEPT TO REALITY	532
William W. Bailey	
AUTOMATIC SOFTWARE FOR CONTROLLING CRYOGENIC SYSTEMS	539
James W. Rudolph	
MATHEMATICAL MODELS FOR SPACE SHUTTLE GROUND SYSTEMS	550
Edward G. Tory	
MANAGING COMPUTER-CONTROLLED OPERATIONS	558
John B. Plowden	
SUPPORT SYSTEMS DESIGN AND ANALYSIS	565
Robert M. Ferguson	
HISTORY, DESIGN, AND PERFORMANCE OF THE SPACE SHUTTLE HAZARDOUS GAS DETECTION SYSTEM	573
William R. Helms	

PART 2

SESSION 7: PROPULSION AND POWER

Page

Cochairmen: H. O. Pohl, Johnson Space Center
J. A. Lombardo, Marshall Space
Flight Center

PROPULSION AND POWER SYSTEMS PERSPECTIVE	581
Joseph G. Thibodaux, Jr.	
CRYOGENIC PROPELLANT MANAGEMENT -- INTEGRATION OF DESIGN, PERFORMANCE, AND OPERATIONAL REQUIREMENTS	585
Armis L. Worlund, John R. Jamieson, Jr., Timothy W. Cole, and Tibor I. Lak	
SPACE SHUTTLE MAIN ENGINE -- INTERACTIVE DESIGN CHALLENGES	600
John P. McCarty and Byron K. Wood	
SOLID ROCKET MOTOR CERTIFICATION TO MEET SPACE SHUTTLE REQUIREMENTS: FROM CHALLENGE TO ACHIEVEMENT	618
John Q. Miller and Joe C. Kilminster	
DEBRIS CONTROL DESIGN ACHIEVEMENTS OF THE BOOSTER SEPARATION MOTORS	628
Gerald W. Smith and Charles A. Chase	
ORBITAL MANEUVERING SYSTEM DESIGN EVOLUTION	639
Cecil Gibson and Clarence Humphries	
DESIGN EVOLUTION OF THE ORBITER REACTION CONTROL SUBSYSTEM	656
Ralph J. Taeuber, W. Karakulko, Don Blevins, Carl Hohmann, and John Henderson	
SPACE SHUTTLE ORBITER AUXILIARY POWER UNIT DEVELOPMENT CHALLENGES	673
Renee Lance and Dwayne Weary	
THE SOLID ROCKET BOOSTER AUXILIARY POWER UNIT -- MEETING THE CHALLENGE	690
Robert W. Hughes	
SPACE SHUTTLE ELECTRICAL POWER GENERATION AND REACTANT SUPPLY SYSTEM	702
William E. Simon	

SESSION 8: COMMUNICATIONS AND TRACKING

Cochairmen: R. S. Sawyer, Johnson Space Center
R. L. Owen, Goddard Space
Flight Center

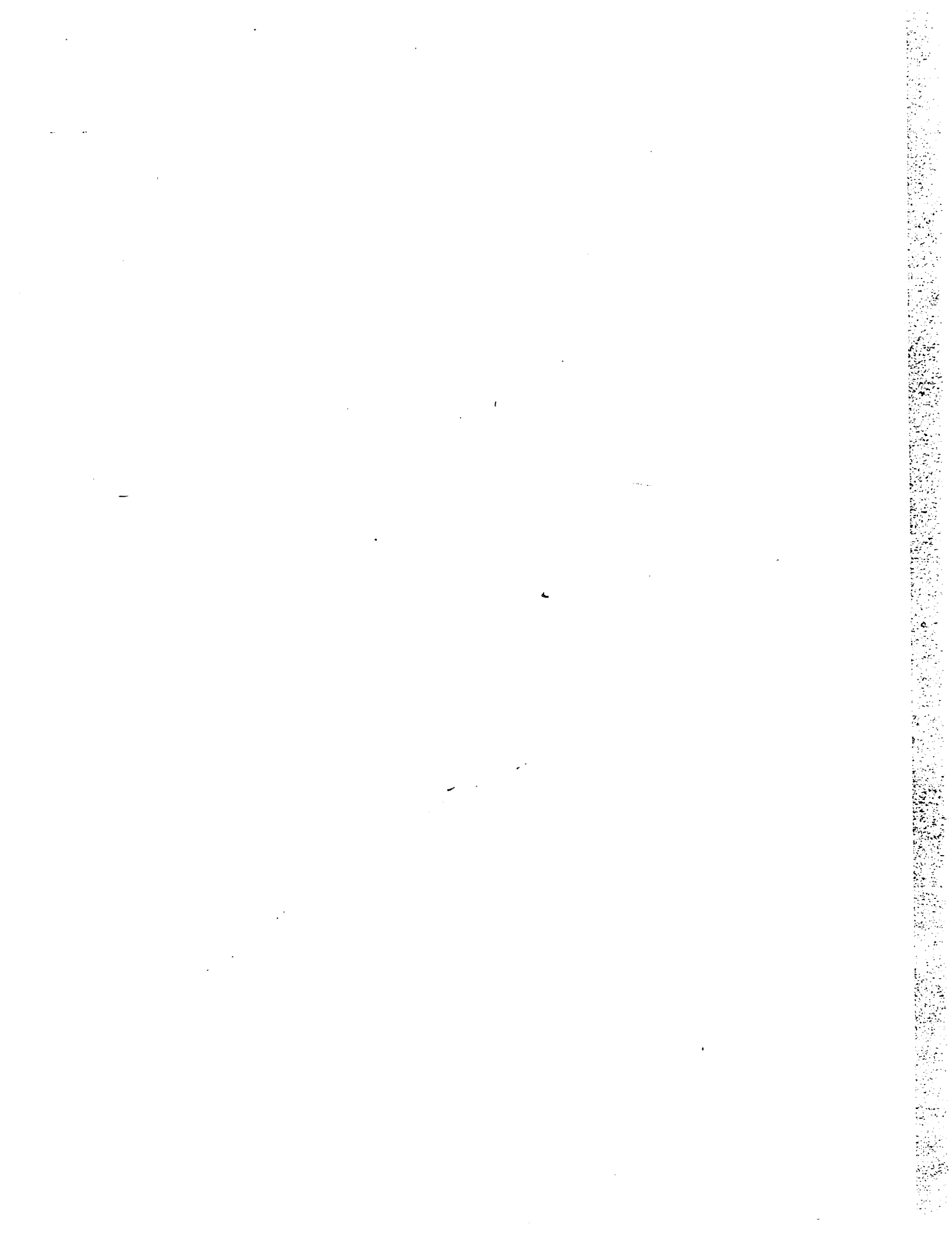
SHUTTLE S-BAND COMMUNICATIONS TECHNICAL CONCEPTS	720
J. W. Seyl, W. W. Seibert, J. A. Porter, D. S. Eggers, S. W. Novosad, H. A. Vang, S. D. Lenett, W. A. Lewton, and J. F. Pawlowski	
SHUTTLE Ku-BAND COMMUNICATIONS/RADAR TECHNICAL CONCEPTS	757
J. W. Griffin, J. S. Kelley, A. W. Steiner, H. A. Vang, W. E. Zrubek, and G. K. Huth	
SHUTTLE PAYLOAD S-BAND COMMUNICATIONS SYSTEM	767
Bartus H. Batson, William E. Teasdale, James F. Pawlowski, and Oron L. Schmidt	
TDRSS S-SHUTTLE UNIQUE RECEIVER EQUIPMENT	777
John J. Schwartz, Robert Spearing, and Aaron Weinberg	
THE COMMUNICATIONS LINK ANALYSIS AND SIMULATION SYSTEM (CLASS)	787
Robert D. Godfrey	
MODELING TECHNIQUES USED IN THE COMMUNICATIONS LINK ANALYSIS AND SIMULATION SYSTEM (CLASS)	798
Walter R. Braun and Teresa M. McKenzie	
VALIDATION OF THE COMMUNICATIONS LINK ANALYSIS AND SIMULATION SYSTEM (CLASS)	804
Walter R. Braun and Teresa M. McKenzie	
THE STATISTICAL LOOP ANALYZER (SLA)	810
William C. Lindsey	
DIGITAL SCRAMBLING FOR SHUTTLE COMMUNICATION LINKS: DO DRAWBACKS OUTWEIGH ADVANTAGES?	815
Khaled Dessouky	
NOVEL APPLICATIONS OF THE NASA/GSFC VITERBI DECODER HARDWARE SIMULATOR	821
Denver W. Herr, John J. Schwartz, Dirk J. M. Walvis, and Aaron Weinberg	
ELECTRONICS SYSTEMS TEST LABORATORY TESTING OF SHUTTLE COMMUNICATIONS SYSTEMS	831
C. Jack Stoker and Linda K. Bromley	

SESSION 9: MECHANISMS AND MECHANICAL SYSTEMS

Cochairmen: W. K. Creasy, Johnson Space Center
J. D. Phillips, Kennedy Space
Center

ORBITER WHEEL AND TIRE CERTIFICATION	850
Carlisle C. Campbell, Jr.	
SPACE EXPLORATION ROLLING ON TIRES	857
G. L. Felder	
SPACE SHUTTLE ELEVON SEAL PANEL MECHANISM	861
John G. Ripley	
SPACE SHUTTLE WHEELS AND BRAKES	872
Renton B. Carsley	
THE SPACE SHUTTLE ORBITER REMOTE MANIPULATOR POSITIONING MECHANISM	883
J. H. Hardee	
AN OVERVIEW OF THE SHUTTLE REMOTE MANIPULATOR SYSTEM	892
T. H. Ussher and K. H. Doetsch	
SPACE SHUTTLE RUDDER/SPEEDBRAKE ACTUATION SUBSYSTEM	905
Ruth A. Naber	
DEVELOPMENT OF THE SPACE SHUTTLE BODY FLAP ACTUATION SUBSYSTEM . . .	910
Clifton R. Boggs	
MECHANICAL FEATURES OF THE SHUTTLE ROTATING SERVICE STRUCTURE . . .	920
John M. Crump	
ORBITER PROCESSING FACILITY: ACCESS PLATORMS	935
Michael Haratunian	
EXTERNAL TANK GH ₂ VENT ARM.	942
Garland E. Reichle and Charles W. Glassburn	
PAYLOAD TRANSPORTATION AT KSC	952
Michael E. Donahue	
STS PAYLOAD GROUND HANDLING MECHANISM AT JOHN F. KENNEDY SPACE CENTER	961
Vincent Cassisi and Bemis C. Tatem, Jr.	
THE ORBITER MATE/DEMATE DEVICE	972
Arthur J. Miller and William H. Binkley	

	Page
COMPUTER AIDED PROCESSING USING LASER MEASUREMENTS	986
Richard M. Davis and John C. Koch	
SESSION 10: THERMAL AND CONTAMINATION ENVIRONMENTS AND PROTECTION SYSTEMS	
Cochairmen: D. H. Greenshields, Johnson Space Center Dr. J. W. Littles, Marshall Space Flight Center	
IN-FLIGHT TESTING OF THE SPACE SHUTTLE ORBITER THERMAL CONTROL SYSTEM	995
J. Thomas Taylor	
SHUTTLE SYSTEM ASCENT AERODYNAMIC AND PLUME HEATING	1022
Lee D. Foster, Terry F. Greenwood, and Dorothy B. Lee	
THERMAL DESIGN OF THE SPACE SHUTTLE SOLID ROCKET BOOSTER	1030
Robert R. Fisher, Jerold L. Vaniman, and William J. Patterson	
THERMAL DESIGN OF THE SPACE SHUTTLE EXTERNAL TANK	1041
Frederick D. Bachtel, Jerold L. Vaniman, James M. Stuckey, Carroll Gray, and Bernard Widofsky	
ORBITER ENTRY AEROTHERMODYNAMICS	1051
Robert C. Ried	
ORBITER THERMAL PROTECTION SYSTEM	1062
Robert L. Dotts, Donald M. Curry, and Donald J. Tillian	
SHUTTLE ON-ORBIT CONTAMINATION AND ENVIRONMENTAL EFFECTS	1082
L. J. Leger, S. Jacobs, H. K. F. Ehlers, and E. Miller	



PROPULSION AND POWER SYSTEMS PERSPECTIVE

Joseph G. Thibodaux, Jr.*
NASA Lyndon B. Johnson Space Center
Houston, Texas 77058

The Space Shuttle has its roots in a number of studies and programs dating back to the early 1940's. The first of these was the A-10, a V-2 derivative proposed as a winged hypersonic glide bomber capable of reaching the east coast of the United States when launched from Germany. After World War II, similar studies were conducted in the United States as secret Air Force programs named ROBO and Brass Bell. These studies evolved into the Dynasoar program of the mid 1950's. Dynasoar went through various phases and missions. By 1957, Dynasoar was proposed as a manned orbiting vehicle capable of reuse after landing. A conference of National Advisory Committee for Aeronautics (NACA) experts in all of the aeronautical research disciplines was convened at the NACA Ames Research Laboratory in October 1957 to review the feasibility of such a program. This group concluded that although there were many difficult engineering research and development problems to be solved, there were no fundamental reasons why such a vehicle could not be successfully developed. Dynasoar, for various reasons, was not immediately funded. It was later revived on a smaller scale and then canceled.

The NASA manned and unmanned space program had its beginnings at that conference even though NASA was not formed until a year later. There were serious discussions between various factions at the conference on the desirability of basing a manned orbital vehicle on the supersonic and hypersonic research airplane technology being developed at Edwards Air Force Base or on ballistic missile launch vehicle and reentry technology. There were also serious discussions about starting an all-solid-propellant launch vehicle to compete with the Vanguard Program.

The ballistic missile launch vehicle and reentry technology approach was studied in detail by a small group of engineers at the Pilotless Aircraft Research Division of the NACA Langley Research Center for the year following the conference. The same group did detailed studies and planning on a four-stage solid-propellant vehicle capable of placing small satellites in orbit. These studies were thorough enough to become the basis for Project Mercury and the Scout missile with the creation of NASA in October 1958. Project Mercury was successful, cost effective, and completed on a relatively short schedule because it bypassed all of the different engineering research and development problems associated with Dynasoar and utilized existing ballistic missile launch vehicle and reentry technology. The Scout program was successful because it was based on 15 years of small solid-propellant launch vehicle technology developed at Wallops Island.

Unmanned space operations used liquid-propellant launch vehicles such as Redstone, Thor, Atlas, and Titan, and their uprated derivatives. These launch vehicles had been rendered surplus by the introduction of smaller solid-propellant systems such as Pershing, Polaris, and Minuteman. The smaller solid-propellant systems were not capable of launching large satellites or manned vehicles into orbit. The number of surplus large liquid-propellant launch vehicles was limited, and there were no active production lines or programs to replace them. The Saturn V production line was shut down before completion of the Apollo Program. In the early 1970's, the future of manned and unmanned space programs looked bleak.

While the Apollo Program was winding down, some of the same engineers who started Project Mercury along with veterans of Mercury, Gemini, and Apollo missions began an in-house study of a reusable manned operational vehicle which could handle all the foreseen manned and unmanned space launch requirements. The vehicle was, in essence, a large upgraded version of Dynasoar with a different mission. Many things had happened since the Dynasoar proposal of 1957. Mercury, Gemini, Saturn, Apollo, X-15, manned reentry body research programs, and new ballistic missile systems had spawned advances in structures, materials, fabrication, processing, propulsion, aerodynamics, avionics, communications, guidance and navigation, and other technologies not available to Dynasoar in 1957. A reusable spacecraft did not seem so difficult any more. The initial reaction was to recover everything possible and to design both the booster and the orbiter around existing Saturn-Apollo technology. The vehicle was sized to accommodate the largest existing known payloads of the time.

Evolution from the original vehicle size and configuration to the present Shuttle was not easy. The number of different concepts, configurations, designs, payload weights and volumes, and operational requirements was unlimited, and everyone in the government and industry aerospace business had a legitimate reason for wanting a specific vehicle size and configuration to be selected. There were serious differences in philosophy regarding the cost effectiveness of using existing technology as opposed to tying the success of the program to promising, new, sophisticated but unproven technology.

*Retired.

Propulsion and power subsystems usually constitute 85 to 90 percent of the weight and volume of the entire system and have a profound effect on the overall launch vehicle size and configuration. Programmatic requirements and factors also have a significant effect on the overall propulsion system design and configuration. Some of these factors and requirements are shown in figure 1. The program requirements will generally be responsible for sizing the propulsion and power systems and establishing minimum system requirements. The program factors affect the selection of the configuration and have a strong influence on component design. The interaction between these factors is so complex that it defies any logical explanation or comment, and the success of the Shuttle is the result of hundreds of wise technical and management decisions that would have challenged Solomon.

When the Shuttle requirements were better defined and management decisions were made concerning the relative importance of some of the factors, the process of selecting one of the various configurations, design concepts, and system components from the many available options was started. Some of the more serious configuration options are presented in figure 2. Each of these was the subject of extensive contractor and government studies. The configuration option selected is enclosed by a rectangle.

Single stage to orbit is the goal or ideal of every space vehicle designer. Unfortunately, extremely low structural and subsystem weight fractions are required to keep the vehicle size manageable, and predictable high propulsion system performance is required. Very small percentage of weight growth or reduction in propulsion system performance in the course of vehicle development could result in negative payload margins. Commitment to a single-stage-to-orbit concept did not appear worth the risk. The integral propellant tank would result in a very large orbiter, and there was no experience in recovery of eggshell tanks reentering from orbital activities over a dispersed area. A recoverable drop-tank option is a possibility for future operations.

When boosting an aerodynamic vehicle with a large lifting surface in one plane, tandem booster arrangements produce extremely high structural bending loads and high control-moment requirements. Experience in launching many airplane configurations at Wallops Island in the 1950's showed that piggyback arrangements with parallel staging could alleviate this problem. Parallel staging of small solid-propellant launch vehicles was also developed at Wallops Island in the 1950's and successfully applied to the Delta and Titan programs on a much larger scale. An asymmetric piggyback configuration with large lifting surfaces in one plane and dual propulsion systems located above and below the center of gravity having different and varying thrust levels with large shifts in the vertical center of gravity is a control system nightmare.

A serious proposal was made to locate the Space Shuttle main engines (SSME's) aft on the external tank and to transport the engines into an empty payload bay using permanently attached mechanical arms. Such an arrangement could, it was reasoned, more easily track the center of gravity shifts as propellant was expended, reduce the overall required control authority, and possibly use a fixed-nozzle solid rocket booster (SRB).

PROGRAM REQUIREMENTS

- PAYLOAD WEIGHT
- PAYLOAD VOLUME
- ORBIT ALTITUDE AND INCLINATION
- ON ORBIT OPERATIONS

PROGRAM FACTORS

- TRAFFIC MODELS
- REUSABILITY AND REFURBISHMENT
- MAINTAINABILITY
- GROUND OPERATIONS
- TURNAROUND
- PRODUCTION COSTS
- OPERATIONS COST
- MANUFACTURING, TEST AND LAUNCH SITES
- SCHEDULE

FIGURE 1.- PROGRAM REQUIREMENTS AND PROGRAM FACTORS.

- NUMBER OF STAGES
 - SINGLE STAGE TO ORBIT
 - TWO STAGES
- PROPELLANT TANK
 - INTEGRAL WITH ORBITER
 - EXTERNAL - NON-RECOVERABLE
 - EXTERNAL - RECOVERABLE
- BOOSTER ORBITER ARRANGEMENT
 - TANDEM STAGING
 - PARALLEL STAGING (PIGGYBACK)
- ORBITER MAIN ENGINE LOCATION
 - AFT ON ORBITER
 - AFT ON EXTERNAL TANK (SWING ENGINE)

FIGURE 2.- CONFIGURATION OPTIONS.

Many of the reasonable propulsion and power system options considered are presented in figures 3 to 8 without comment. The selected options generally used existing military or Saturn-Apollo technology except where these systems would not permit reuse or where the system or component performance could not be easily upgraded to Shuttle requirements. Some of the reasons which led to selection of a specific design or concept and factors which contributed to successful development and operation of the system in a cost-effective manner are discussed in other papers in this session. Each reader can determine whether he thinks the selected approaches were cost effective and were indeed the best choice. No justification for the choices is necessary as the success of the program to date provides confirmation that options selected are adequate.

Some of the work is still unfinished. The Shuttle must yet demonstrate the originally advertised payload capability and turnaround time. Costs per launch must be reduced. There is little or no growth available in the existing propulsion and power systems without major redesign. There are, however, many system design features to take care of problems with low probability of occurrence and areas of excessive redundancy and design margins which have been incorporated into the program at the expense of payloads.

For the first time, there will be a small fleet of operational vehicles which will fly many missions and provide the necessary operational experience and a data base to eliminate the difference between real and imagined performance and design requirements. The existence of this data base alone should result in substantial increases in payload capability. This data base will also provide information to eliminate unnecessary design complexity, design margins, redundancy, and excessive estimate of propellant requirements for enhanced versions of the Shuttle and future space transportation systems.

- LIQUID PROPELLANT
 - LOX-H₂
 - LOX-HYDROCARBON
 - EARTH STORABLE
 - FLYBACK - REUSABLE
 - BIG DUMB BOOSTER
- SOLID PROPELLANT
 - NONRECOVERABLE
 - RECOVERABLE
 - CASE
 - MONOLITHIC
 - SEGMENTED
 - METAL
 - FILAMENT WOUND
- TVC
 - NONE
 - LIQUID INJECTION
 - GIMBALLED NOZZLE
- THRUST TERMINATION
 - NO
 - YES
- PROPELLANT
 - PBAA
 - HTPB
 - OTHER

FIGURE 3.- CONCLUDED.

FIGURE 3.- BOOSTER OPTIONS.

- ORBITER MAIN ENGINE (SSME)
 - J-2, J2-S
 - NEW HIGH PRESSURE GAS GENERATOR
 - HIGH PRESSURE STAGED COMBUSTION
 - AEROSPIKE
- ORBITAL MANEUVERING ENGINE
 - RL-10
 - LOX-HYDROCARBON
 - EARTH STORABLE
 - COOLING
 - ABLATION
 - REGENERATIVE
 - FEED SYSTEM
 - PRESSURE FED
 - PUMP FED
- MOUNTING
 - INTEGRAL WITH VEHICLE
 - EXTERNAL POD MOUNT
- PROPELLANT ACQUISITION
 - GRAVITY-THRUST SETTLING
 - CAPILLARY SCREENS

FIGURE 5.- ORBITER MANEUVERING SYSTEM OPTIONS.

FIGURE 4.- ORBITER PROPULSION OPTIONS.

- PROPELLANT
 - GASEOUS O₂-H₂
 - LOX-LH₂
 - LOX-HYDROCARBON
 - **EARTH STORABLE**
 - MONOPROPELLANT
- INSTALLATION
 - FIXED
 - **REMOVABLE POD OR MODULE**
- TANKS
 - BLADDERS
 - OTHER POSITIVE DISPLACEMENT
 - **CAPILLARY SCREENS**
- VALVES
 - SOLENOID
 - **LINE PRESSURE ACTUATED**

FIGURE 6.- REACTION CONTROL SYSTEM OPTIONS.

- (1) HYDROGEN-OXYGEN
- (2) EARTH STORABLE BI-PROPELLANT
- (3) LOX-HYDROCARBON
- (4) **MONOPROPELLANT**
 - POWER (SPEED) CONTROL
 - (1) PRESSURE MODULATION
 - (2) **PULSE MODULATION**
- PYROTECHNIC SYSTEMS
 - NO
 - **YES**

FIGURE 7.- AUXILIARY POWER UNIT OPTIONS.

- (1) TURBINE - ALTERNATOR
- (2) BATTERIES
- (3) **FUEL CELLS**
 - **BASIC**
 - ACIDIC
- (4) SOLAR CELLS
- REACTANT STORAGE SYSTEM
 - **SUPERCRITICAL STORAGE**
 - SUBCRITICAL STORAGE

FIGURE 8.- ELECTRICAL POWER OPTIONS.

Another reason for presenting the various propulsion and power system options without comment is that the issues are not yet settled. In the past years, numerous studies of enhanced or next generation space transportation systems were based on many of the options originally rejected, as well as on such new propulsion concepts as the dual fueled engine. Remembering that it was 15 years between the Dynasoar of 1957 and the Shuttle, and that 10 years have already elapsed since the Shuttle design concepts converged, it is not unreasonable to assume that new information or technology is or will be available which would result in selection of an entirely new concept or design, or one originally rejected, when future Space Transportation System (STS) programs are undertaken. The propulsion and power systems used technology from Department of Defense (DOD) programs, Saturn, Apollo, and some developed concurrently with the Shuttle. The success of the Shuttle program to date speaks for itself. Unfortunately, with the introduction of solid-propellant rockets into the ballistic missile program, recent emphasis on cruise missiles, and assignment of responsibility for all space transportation to NASA, DOD is no longer funding the large liquid-propellant technology programs which have benefited NASA in the past.

Lack of funding of new technology, cancellation of old launch vehicle programs, and no new production in sight threatens the existence of old line companies capable of developing and manufacturing the propulsion systems required for future space transportation systems. If new technology programs with substantial funding are not forthcoming soon, there may not be a single surviving company capable of conducting new technology and development and production programs required to support the Space Transportation System. The responsibility is now NASA's and the future of propulsion and power technology rests solely in the hands of NASA management.

CRYOGENIC PROPELLANT MANAGEMENT -
INTEGRATION OF DESIGN, PERFORMANCE AND OPERATIONAL REQUIREMENTS

Arnis L. Worlund
George C. Marshall Space Flight Center
National Aeronautics and Space Administration
Marshall Space Flight Center, Alabama

John R. Jamieson, Jr.
John F. Kennedy Space Center
National Aeronautics and Space Administration
Kennedy Space Center, Florida

Timothy W. Cole
Martin Marietta Corporation - Michoud Operations
New Orleans, Louisiana

Tibor I. Lak
Rockwell International Corporation
Space Transportation and Systems Group
Downey, California

ABSTRACT

The integration of some of the unique design features of the Shuttle elements into a cryogenic propellant management system is described. The implementation and verification of the design/operational changes resulting from design deficiencies and/or element incompatibilities encountered subsequent to the critical design reviews are emphasized. Major topics include subsystem designs to provide liquid oxygen (LO₂) tank pressure stabilization, LO₂ facility vent for ice prevention, liquid hydrogen (LH₂) feedline high point bleed, pogo suppression on the Space Shuttle Main Engine (SSME), LO₂ low level cutoff, Orbiter/engine propellant dump, and LO₂ main feedline helium injection for geyser prevention.

INTRODUCTION

America's Space Shuttle program challenged the cryogenic propulsion disciplines to extend the single launch Saturn-Apollo technology into a multilaunch space vehicle. Some of the parametric studies that were conducted to define the features of a reusable cryogenic propulsion system are summarized in reference 1. The design of each Space Shuttle element (SSME, Orbiter, External Tank (ET), and ground support facilities) was influenced by the reusability requirements and by the program goal of low cost per flight. The design and development of the ET cryogenic components and subsystems are presented in references 2, 3, and 4. The challenge to the engineers/designers of the Cryogenic Propellant Management System was to assure functional and operational compatibility of the interfacing elements. A primary emphasis was to resolve design deficiencies or to implement requirement changes encountered in the development process. The implementation of many of the changes encountered was accomplished by (1) utilizing software and control functions in lieu of hardware redesign and (2) extending the function of existing components. These approaches were selected in order to minimize impact to the program schedule and the cost objectives.

CRYOGENIC PROPELLANT MANAGEMENT OVERVIEW

The design and operation of the Cryogenic Propellant Management System are to provide LO₂ and LH₂ propellants at conditions that are compatible with the requirements/capabilities of the interfacing subsystem. The facility and vehicle propellant conditions are controlled during the prelaunch operations to preclude undefined loads from being imposed on the elements and to assure that the engine prestart requirements are achieved. Ascent performance requires that (1) the nominal usable propellant mass be 1,345,000 pounds \pm 0.5% of LO₂ and 225,000 pounds \pm 0.65% of LH₂ and (2) the residual propellants in the Orbiter and engine be dumped after SSME cutoff.

The LH₂ propellant delivery system shown in Figure 1 consists of main tankage with level control sensors and dual-function vent/relief valve, an internal "siphon" feedline, ET/Orbiter disconnect, Orbiter manifold and feedlines to the three SSME's, fill and drain line, LH₂ recirculation and high point bleed subsystem, and the SSME's. Propellant is loaded at high flow rates through the fill and drain line which connects the LH₂ ground servicing facility to the manifold. The low flow rates for

topping and replenish are routed from the fill and drain line through the recirculation return line to the LH₂ tank, bypassing the Orbiter/ET feedline. The SSME LH₂ preconditioning is accomplished by recirculation pumps mounted on the Orbiter manifold. Each pump forces LH₂ around the pre valve, through the feedline and engine. Downstream of the engine, the recirculation flow joins the replenish flow in the recirculation return line. The recirculation pumps are powered by electric motors operated with ground power, since their function is completed prior to lift-off.

LH₂ liquid level control during replenish utilizes the duty cycle (percent-wet) of the ET point (warm wire) sensors as the input to the facility Launch Processor System (LPS). The LPS adjusts the position of a ground control valve to provide makeup fluid to compensate for boiloff losses. This system maintains the propellant level within ± 2 inches ($\pm 0.1\%$) of the desired level. The balance of the loading accuracy error budget is allocated to propellant density and ET dimensional uncertainties.

The LO₂ propellant delivery system shown in Figure 2 consists of main tankage with level control sensors and dual-function vent/relief valve, ET feedline (with accompanying antigeysers line on vehicles 1-4), ET/Orbiter disconnect, Orbiter manifold and feedlines to each of the three SSME's, and the SSME's which contain the LO₂ bleed system and pogo suppressor system. LO₂ is loaded through the fill and drain line which connects the manifold to the LO₂ ground servicing facility. During periods of low flow rate into the ET (slow fill, to 2%, topping from 98 to 100%, and replenish at 100%), subcooled liquid is maintained in the LO₂ main feedline by using the thermal pumping of the 4-inch diameter antigeysers line to circulate liquid from the tank down the main feedline and back up the antigeysers line. Subcooled liquid in the ET's main feedline is essential to preclude LO₂ geysers (the formation of gaseous oxygen (GO₂) vapor pockets in the feedline which expand rapidly, expelling liquid from the feedline into the tank, leading to a sudden and damaging refill "water-hammer"). Helium is injected into the aft elbow of the antigeysers line to assure flow circulation. Throughout the loading and replenish operations, LO₂ is bled through the SSME turbopumps and then overboard through the engine/Orbiter bleed system.

LO₂ liquid level control during replenish is similar to LH₂ level control. The LO₂ replenish system must make up the boiloff losses and provide the bleed flow required for SSME thermal conditioning. The LO₂ level is maintained within ± 3 inches ($\pm 0.15\%$) of the desired level. The balance of the loading accuracy error budget is allocated to propellant density and ET dimensional uncertainties.

DEVELOPMENT AND INTEGRATION OF DESIGN

An integrated system approach to the development and operation of the Cryogenic Propellant Management System is illustrated by Figure 3, which contains subsystem requirements that were changed subsequent to element critical design reviews (CDR's). These requirement changes were the most cost effective/timely solutions to problems or element incompatibilities encountered during the development process. The subsystem designs to provide LO₂ tank pressure stabilization, LO₂ facility vent for ice prevention, LH₂ feedline high point bleed, pogo suppression on the SSME, LO₂ low level cutoff, Orbiter/engine propellant dump, and LO₂ main feedline helium injection for geysers prevention will be discussed.

LO₂ TANK PRESSURE STABILIZATION

A design goal of the ET program was a free-standing unpressurized structure. However, the forward ogive of the LO₂ tank of the ground vibration test article buckled while being filled with liquid. Subsequent analyses and testing of the structural test article defined a pressure requirement of 1.7 psig to preclude buckling of the forward ogive for liquid levels above 2%. The methods to satisfy the pressure requirement without major impact on other subsystems were developed on the Main Propulsion Test Article (MPTA), a flight hardware test facility used to verify the performance of the integrated cryogenic propulsion system. The initial approach to meet the pressure requirement was based on increasing the vent flow resistance with a corresponding increase in ullage pressure and liquid saturation temperature. A 2.75-inch diameter orifice in each of the two 5.5-inch diameter vent ducts (downstream of the vent/relief valve) maintained the ullage pressure above 1.7 psig when the tank was loaded at approximately 5000 gallons-per-minute. The orifices would not maintain adequate tank pressure during replenish or fill at KSC flow rates of 1400 gpm. Therefore, the ET vent valve capability to control ullage pressure during loading and replenish was evaluated.

The use of the vent/relief valve for pressure control was complicated by the design that placed the valve control functions on the facility. However, tank pressure control by vent valve cycling was accomplished by experimentally determining acceptable control limits and modifying the LPS software to provide the valve control functions. Narrow range pressure transducers were added to the tank and used by LPS to determine when to close the valve. During loading, LPS closes the valve at 2.2 psig and opens the valve at 8 psig. The 2.2 psig limit accounts for system reaction time and instrumentation

errors such that the minimum ullage pressure is ≥ 1.7 psig. The 8 psig upper limit allows time for the LPS to identify a valve failed closed and then perform alternate procedures which will maintain the ullage pressure below 17 psig, the maximum pressure that would not put a pressure cycle on the tank. During replenish, the valve is closed at 2.2 psig and opened 3 minutes later. The time limit ensures consistency of cycles for any replenish flow rate. The lightweight tank (LWT) design (ET-7 and subs) includes additional structure (250 pounds) to eliminate the pressure stabilization requirements for levels above 98%.

The vent valve cycling to provide tank pressure stabilization makes the ground control function critical for structural integrity. The LPS monitoring, control logic, and corrective actions must be able to compensate for component failures and off-nominal operating conditions. In addition to increasing the quantity and criticality of the software, two design changes were required. Specifically, the helium vent valve closure actuation flow was separated from the helium injection flow to the anti-geyser line (originally the design had helium inject off whenever the vent valve was actuated closed), and the gaseous nitrogen (GN_2) auxiliary pressurization flow rate was increased so that the auxiliary system could maintain the ullage pressure during an emergency drain with the vent valve failed open.

LO₂ FACILITY VENT FOR ICE PREVENTION

The ET LO₂ tank and protuberances were uninsulated in the initial design concept. During the development of the Orbiter reentry thermal protection system, it became apparent that ice/frost falling off the ET due to lift-off vibrations could damage the tiles and endanger the Orbiter during reentry. The requirement to eliminate ice/frost formation on the ET was imposed just prior to the CDR. The design changes incorporated to satisfy this requirement included: (1) ground controlled, heated purges for the intertank compartment, nose cone cavity, and pressurization lines; (2) insulation on the ET acreage and small protuberances; and (3) electrical heaters under insulation on large protuberances. The addition of insulation to the LO₂ tank reduced the heat input to the cryogen such that one of the two vent valves was eliminated from each tank.

A test program to assess the effectiveness of ET design changes for ice/frost prevention determined that the GO₂ vent louvers would accumulate ice. The resulting requirement to preclude ice/frost on vent louvers was unique, i.e., prior launch vehicles exhausted GO₂ directly into the atmosphere. Modifications to provide a hard disconnect umbilical for the GO₂ vent similar to that used for gaseous hydrogen (GH_2) would have been extensive. Therefore, a facility GO₂ vent hood was selected to remove the vent gases from the tank with an inflatable dock seal (Figure 4) to provide a soft "footprint" on the ET insulation surface.

The vent hood has a dock seal for each of the vent louvers. These seals are attached in a retractable vent hood tip assembly mounted on a service arm off the launch pad fixed service structure. The dock seals are inflatable Herculite cloth with an LO₂ compatible beta cloth liner. The dock seals are inflated to 0.5 psig and are used to duct the vent gases from the louvers to a pair of exhaust ducts that remove the gases from the immediate vicinity of the LO₂ tank. A GN_2 purge in the vent hood volume, external to the dock seals, eliminates the accumulation of hazardous gases. A separate GN_2 flow purge (25 lb/min) through the dock seals provides thermal conditioning of the flexible material, thus ensuring no leakage under the dock seal "footprint" on the tank surface.

The design verification testing of this system, presented in reference 5, utilized a complete LO₂ tank vent system and nose cone assembly to assure realistic system performance. The test conditions for tank pressures, vent temperatures, and flow rates were derived from the MPTA. The LO₂ tank pressure range during operation varied from 22 to 2.2 psig with vent temperatures ranging from ambient to -220°F. Subsequent to a dock seal failure during the initial test series, testing revealed velocity pressures resulting from the nonsymmetrical flow downstream of the 2.75-inch orifices in the vent manifold. Experimental evaluation of the tank vent system showed that the 2.75-inch orifices in the two ET vent ducts should be removed and the vent valve stroke changed from 2.6 to 1.1 inches. These changes substantially reduced velocity pressures at the louvers as shown in Figure 5. Testing with two pairs of service arm ducts (12-in OD X 62-ft long and 24-in OD X 27-ft long) showed that duct size was a significant factor in reducing the pressure spike in the dock seal plenum when the vent valve was opened, i.e., the forces required for acceleration of the residual gases in the facility ducts produced substantial pressures in the dock seal plenums. The 24-inch diameter by 27-foot long ducts were selected for the Pad 39A launch facility.

The changes to the tank vent system and facility ducting, in conjunction with component optimizations, i.e., bungee sizes, dock seal sizes, and internal pressure, resulted in a functional LO₂ vent hood system that prevents ice accumulation on the LO₂ tank due to GO₂ venting. The design also provides reconnect capability to the tank if required by a countdown recycle and minimizes possible damage to the tank insulation. The dock seals are deflated prior to service arm retraction and the bungee cords retract the seals from the tank surface approximately 2 1/2 minutes prior to launch. If

reconnect of the vent hood to the tank is required, the service arm is moved back over the tank, the vent hood is lowered, and the dock seals are inflated.

LH₂ FEEDLINE HIGH POINT BLEED SYSTEM

The LH₂ propellant feed system of the Shuttle elements (Figure 1) resulted in an inverted U-tube design that traps the warmer propellant flowing upwards from the tank bottom and collects it at the high point of the Orbiter 17-inch feedline. Integrated system analysis showed that the stratified fuel would vaporize, forming a large pocket of hydrogen vapor in the feedline during tank replenish. This vapor volume would grow, cavitating the recirculation pumps and resulting in cessation of engine thermal conditioning and violation of the SSME start requirement. Analysis indicated that the hydrogen bubble in the feedline would not recondense during tank prepressurization, resulting in bubble ingestion by the SSME's during start or mainstage operation with potentially catastrophic results. Therefore, a high point bleed system was added to prevent vapor accumulation in the hydrogen feed manifold.

The system consists of a 3/4-inch insulated line connected to the Orbiter disconnect with a high point bleed valve approximately 2 feet downstream of the inlet and a disconnect valve at the Orbiter/facility interface. An orifice in the facility line limited the bleed flow rate. Extensive high point bleed system testing on MPTA resulted in removal of the flow-limiting orifice in the facility. Bleedline performance was sensitive to the facility vent line back-pressure due to the low pressure head available (2.8 psi) to expel the hydrogen vapor. Therefore, a separate facility vent line was provided for the high point bleed system. The MPTA data showed that the high point bleed system should be chilled and operational prior to the start of the recirculation pump in order to ensure normal pump performance. The prelaunch operation of the bleed system is continued until the recirculation pumps are turned off to assure bubble free operation at engine start. System performance is monitored by the LH₂ feed manifold disconnect temperature and the high point bleed temperatures in the Orbiter and facility line. A manifold disconnect temperature less than 45°R indicates a vapor free feedline when the tank is unpressurized.

The high point bleed system also helps to reprime the recirculation pumps after a recirculation flow interrupt resulting from power failure to the pumps or test sequence recycling. A further use of the high point bleed system being considered is the removal of trapped LH₂ feedline residuals (70 pounds) following an aborted mission with a return to launch site (RTLS). This function could be accomplished by connecting a facility line to the bleedline disconnect, pressurizing the feedline through the on-board feedline repressurization system, and allowing the liquid residual to be expelled through the high point bleed system.

POGO SUPPRESSION ON SSME

Longitudinal vehicle instability due to closed-loop coupling of the structural, propellant delivery, and engine subsystems (commonly called pogo) was encountered on Thor, Titan II, and Saturn vehicles during development flights. The remedial solutions that provided vehicle stability were feedline accumulators. Spring/piston and contained gas accumulators were used on the Titan II program and overflow gas (helium) accumulators were utilized on the Saturn S-IC and S-II stages. The emphasis from early in the design phase of the Space Shuttle program was to ensure vehicle stability by the inclusion of an engine mounted accumulator in the liquid oxygen system. The primary concern with an engine accumulator mounted upstream of the high pressure oxidizer turbopump (HPOTP) was the overflow of a non-condensable gas (helium) from the accumulator, resulting in pump cavitation and overspeed. The design goal was an accumulator that could be pressurized with oxygen, a condensable gas. To make this goal a reality required (1) a solution to the problem of accumulator ullage collapse caused by heat and mass transfer at the liquid/gas interface and (2) the integration of the pogo system with the engine helium and oxygen pressurization subsystems and the Orbiter propellant feed subsystem.

The initial engine mounted pogo accumulator used a blanket of floating Teflon balls to separate the liquid/gas interface, and a pleated Dutch twill screen in the neck of the accumulator prevented the Teflon balls from entering the HPOTP. The structural integrity and reliability of a pleated Dutch twill screen and the problems with batch testing Teflon material for LO₂ compatibility necessitated a design improvement. Tests with turning vanes to inhibit the turbulent flow in place of the pleated Dutch twill screen and the Teflon balls were marginally successful, i.e., some accumulators collapsed during engine tests due to spraying of LO₂ into the GO₂ ullage. The addition of parallel perforated splash plates above the turning vane, shown in Figure 6, resulted in a semiquiescent liquid/gas surface and successful accumulator performance at all SSME power levels. Accumulator ullage collapse during the SSME start transient was precluded by helium charges prior to engine start and at 2.4 seconds after start command. Ullage collapse subsequent to SSME shutdown command was prevented by a helium

post-charge initiated at cutoff command. The post-charge was subsequently extended and used in the in-flight shutdown sequence as described in the LO₂ low level cutoff section of this paper.

The pogo suppression system is shown schematically in Figure 7. The LO₂ normally closed bleed valve and the normally open recirculation isolation valve (RIV) are powered from a common pneumatic source to assure that the RIV is closed during the prestart period when the SSME is being thermally conditioned with LO₂ flow through the bleed system. This also assures that the valves are in the proper positions for the SSME start, i.e., bleed valve closed and RIV open. The Orbiter pogo recirculation valves change the flow path from overboard LO₂ bleed to GO₂ recirculation at SSME start. The Orbiter pogo recirculation valves and SSME bleed valves are launch commit criteria monitored by the LPS. The accumulator precharge pressure is an SSME parameter verified by the SSME controller during start. During engine operation, the accumulator GO₂/LO₂ overflow is routed to the Orbiter through the engine bleedline. This dual use of the bleedline minimized engine weight and interface connections. In the Orbiter, the overflow is routed to the feed manifold near the ET/Orbiter disconnect to maximize the time available for the GO₂ to collapse before entering the low pressure oxidizer turbopump (LPOTP).

The SSME mounted pogo suppressor has been tested extensively to verify functional and dynamic characteristics (reference 6). Pump subsystem tests defined the accumulator diffuser and thermal barrier configuration. Single engine tests defined: (1) the helium precharge and post-cutoff charging times; (2) pressurant flow rate/engine power level relationship; and (3) the baffle configuration to assure an adequate thermal barrier for all operating conditions. The integrated system tests refined the precharge and post-charge times and verified the overall vehicle performance.

LO₂ LOW LEVEL CUTOFF

A low level cutoff (LLCO) system is needed to satisfy the minimum SSME LO₂ net positive suction pressure (NPSP) requirement and to preclude the catastrophic consequences of an LO₂ depletion shutdown. The uniqueness of the LO₂ feedline design, which is over 100 feet long containing 15,000 pounds of LO₂, resulted in the engine cutoff (ECO) sensors being mounted in the Orbiter feedline to reduce the LO₂ residual dispersion at LLCO, and to make the ECO sensors reusable along with the signal conditioner electronics. ECO sensors mounted in the Orbiter feedline had to be reliable and able to quickly respond to the fast-moving liquid interface. A warm wire ECO sensor design was selected because of fast response, simple electronic design, light weight, and similarity to the ET liquid level control sensors.

The generation and propagation of cavitation bubbles within the feed system and their effect on ECO sensor performance had to be determined experimentally because of the complex routing of the LO₂ feedline. A series of full scale LO₂ flow tests were performed. Although the ECO sensors performed normally in the tests, a pressure dropout recorded prior to ECO dry indication showed NPSP requirements would not be satisfied. The presence of a large concentration of bubbles was also photographed at the simulated SSME inlet. The concern relative to the pressure dropout and the vapor volume in conjunction with Orbiter location inability to support the MPTA tests due to 1-G limitations resulted in the ECO sensors being moved to the vertical portion of the ET feedline. The pressure dropout phenomenon was later identified as a facility data problem, and the bubble concentration was determined by single SSME tests to be acceptable. However, the ET location for ECO sensors was retained for the development flights because of increased LO₂ NPSP requirements and to obtain flight performance data.

The ECO system currently incorporates three timers that are entered into the Orbiter General Purpose Computer in order to minimize the LO₂ residual. The timer values correspond to a normal mission shutdown of three engines from minimum power level (MPL), two engines from MPL for an RTLS abort, and two engines from full power level for an abort once-around. The timer values were determined from terminal drain tests with correction for flight acceleration rate and predicted thrust angle. For STS-12 and subsequent flights, the ECO sensors will be mounted in the original Orbiter design location.

The original SSME NPSP requirement was only defined for mainstage operation with the engines accepting the self-generated shutdown NPSP transient. During engine development, tests and analyses indicated a potentially catastrophic overspeeding of the oxidizer turbopumps due to inadequate NPSP during an in-flight shutdown. This condition is a result of the vehicle acceleration transient and the SSME fuel flow transient. The SSME staged combustion cycle (Figure 8) routes the LH₂ propellant flows through the preburners and turbines prior to entering the main combustion chamber. The fuel-rich engine shutdown (to prevent turbine and main injector damage due to high combustion temperatures) is accomplished by a main fuel valve closure profile that allows fuel flow to continue to the preburners for approximately 5.5 seconds. A helium purge initiated 1.8 seconds into the cutoff transient to purge the oxygen trapped downstream of the preburner oxidizer valves results in power being reapplied to the high pressure pumps as this oxygen combusts with the incoming fuel. The rapid decay in available NPSP due to loss of vehicle acceleration could result in pump cavitation as power is reapplied to the HPOTP.

Three potential solutions to this problem were: (1) a preburner fuel valve added to the engine to stop fuel flow to the preburners, precluding combustion when the oxygen is purged out; (2) a purge pressure increase from 750 psi to 2000 psi to allow the oxygen to be purged earlier in the cutoff sequence when NPSP is higher; or (3) the NPSP level could be increased during shutdown by pressurizing the engine inlet. The third option was selected as the most cost effective and timely solution. The SSME LO₂ inlet pressurization would be accomplished by closing the existing prevalues located in the Orbiter feedline earlier during engine shutdown, and pressurizing the engine and feedline with the pogo accumulator helium supply.

The Orbiter pneumatically operated prevalues were not designed to close rapidly. For this concept to work, the prevalues had to be closed prior to the start of the preburner purge. If the prevalues closed too soon, the prevalues would starve the engine of LO₂ flow, resulting in a more severe pump cavitation and overspeed problem. If the prevalues closed too late, feedline pressurization would be delayed, resulting in possible damage to the HPOTP.

A ground test program was utilized to demonstrate the use of the prevalues and the pogo suppressor pressurization system to prevent turbopump overspeed during cutoff. The tests were devised to simulate worst case flight NPSP and prevalue closing response ranges. A single engine stand was modified by installing a long vertical feedline from the LO₂ tank to the horizontal plane of the engine inlet. The LPOTP was rotated 90 degrees on its discharge flange and a flight Orbiter feedline and prevalue were installed horizontally between facility feedline and the LPOTP inlet. This configuration allowed the LO₂ liquid level to be drained very low in the vertical feedline, simulating the engine NPSP decay in-flight, without starving the engine. The ability of the engine to cut off safely for all prevalue closure tolerances was demonstrated. The first test series qualified the engine cutoff sequence for STS-1 by demonstrating the engine's ability to shut down safely with a transient NPSP of 10 psi at ECO to 2.0 psi at prevalue closure. After the STS-1 flight, a second test series was conducted to qualify the shutdown sequence for low level shutdown and shutdown from rated power level. The engine test stand was reconfigured for this series of tests by adding a separate feedline vent system. This allowed the vertical feedline to be drained much lower before engine cutoff while maintaining the required main-stage NPSP with the tank pressurization system. The valve at the tank bottom and the feedline vent valve were sequenced during the shutdown transient to simulate the in-flight NPSP decay because the feedline volume was much smaller than the tank. The incorporation of prevalue sequencing and an extended pogo accumulator post-charge into the SSME shutdown were effective in preventing HPOTP overspeed for worst case flight conditions. The test also demonstrated that the engine could shut down safely in-flight with a minimum of 80 pounds of LO₂ upstream of the LPOTP inlet.

ORBITER/ENGINE PROPELLANT DUMP

The cryogenic subsystems of the reusable Space Shuttle Orbiter are a fixed part of the orbital and reentry vehicle. The liquid propellants trapped in the SSME's and feedlines at main engine cutoff (MECO) must be dumped to (1) reduce system weight for on-orbit and reentry operations and (2) minimize the hazards associated with venting combustible propellants during post-landing operations. The original concept was to dump both propellants through the SSME's with helium pressurization provided to accelerate the dump. The propellants were to be dumped in series. The LO₂ residual (4600 pounds) was to be dumped first because of its higher temperature and greater mass, followed by the LH₂ residual (300 pounds) dump. The 300-second dump was to be accomplished during OMS-1 burn to provide impulse to the Orbiter, reducing the Orbital Maneuvering System propellant requirement by approximately 130 pounds.

The concept was changed because of a potential HPOTP overspeed problem during LH₂ dump. The potential overspeed results from the SSME staged combustion design where all the LH₂ propellant flows through both preburners and turbines before going into the main combustion chamber. With the engine LO₂ system empty, the hydrogen dump flow would accelerate the unloaded oxygen pump to catastrophic speeds. Since an alternate LH₂ dump path requirement was identified late in the program (May 1980), the solution was to use existing Orbiter components to preclude impacting initial Shuttle launch date. Both the LH₂ fill and drain system and the recirculation/replenish system, shown in Figure 9, were used with only software changes to perform the on-orbit dump function. This modified dump concept allowed a shorter dump sequence by simultaneously dumping the LO₂ and LH₂. The LH₂ dump time is minimized by a short (6-second) dump through the 8-inch inboard and outboard fill and drain valve. This is followed by a 114-second dump that allows the LH₂ residual to be expelled from the 12-inch Orbiter feedlines, and the SSME's through the LH₂ replenish valve and the outboard fill and drain valve. The LH₂ component of impulse was no longer usable for vehicle delta V since the LH₂ dump flow is routed out the side of the Orbiter.

Extensive analytical modeling of LH₂ two-phase flow to vacuum was required to define the dump period and to determine if solid hydrogen formation could inhibit the dump system capability. The performance analysis of the LO₂ and LH₂ dump systems was important because the flight characteristics could not be determined by sea level tests due to 1-G and ambient pressure limitations. Sea level

tests of the LO₂ and LH₂ dump systems were performed on a single SSME test stand and on the MPTA to verify the software sequences and component responses.

The LO₂ and LH₂ dump systems performance analysis, using the Lockhart-Martinelli correlation for two-phase flow, agrees with flight data. The correlation between the reconstructed LO₂ dump thrust and flow rate histories and analytical predictions is presented in Figure 10. The LO₂ dump thrust was determined from accelerometer data by converting the measured acceleration rates to total vehicle thrust and subtracting the effects of the Orbital Maneuvering Engine. The LO₂ dump flow rate was verified two ways: (1) the reconstructed dump thrust was divided by the calculated Isp and (2) dump flow was calculated from the helium pressurization flow rate. The LO₂ dump flow rate reconstruction from flight data indicated approximately 1100 pounds remained at the end of dump. The high LO₂ residual, due to loss of helium pressurant which tunnels through the liquid core under the low-G environment, is vented to space as a result of normal leakage through the engine HPOTP seals and during feedline vacuum inerting. Table 1 summarizes the predicted and reconstructed LO₂ dump performances for the development flights.

The LH₂ dump prediction also agrees well with the flight data. Flight data analysis was based on using temperature data to indicate when the liquid interface passed the transducer locations. The predicted and measured dump times for the first SSME to complete dump (engine number 3) are shown below:

	<u>Predicted</u>	<u>Measured</u>
STS-1	71 seconds	60 seconds
STS-2	52 seconds	47 seconds
STS-3	52 seconds	56 seconds
STS-4	52 seconds	52 seconds

Following the STS-1 flight, a 30-second vent of the LH₂ feedline was added to the ET separation sequence (MECO + 10 seconds) in order to protect the system if a relief valve failed. This vent resulted in a reduced post-shutdown pressure rise in the Orbiter feedlines due to heat soakback. The 30-second vent reduced the predicted LH₂ dump time by 19 seconds. The only change to the LO₂ and LH₂ dump sequences, subsequent to the development flights, was to reduce the feedline pressurization period by 18 seconds to save 5 pounds of helium.

The current on-orbit dump sequence presented in Figure 11 cannot be used during an RTLS abort because aerodynamic drag on the Orbiter settles the liquid away from the SSME's and from the LH₂ fill and drain line. A separate LH₂ dump system, from the Orbiter feedline disconnect to the vehicle exterior, dumps the residuals during an RTLS abort. The LH₂ dump, initiated 15 seconds after ET separation with the opening of the RTLS dump valves and manifold repressurization valve, removes approximately 230 pounds of hydrogen. Seventy pounds of the LH₂ in the Orbiter feedlines cannot be dumped due to vehicle attitude. An Orbiter LO₂ RTLS dump system is not required since the LO₂ residual is not hazardous and its effect on the vehicle center of gravity is acceptable. For an RTLS abort, the SSME main oxidizer valves are opened to remove 1280 pounds of the LO₂ residuals from the SSME.

LO₂ MAIN FEEDLINE HELIUM INJECTION

Concurrent with the development program for the Shuttle elements, there was continuous emphasis on performance improvement. One objective was a weight and cost reduction of the ET. The changes implemented on the LWT included deletion of the LO₂ antigeysers line, which resulted in weight and cost reductions of 700 pounds and \$113,000 per flight, respectively. The major problems with antigeysers line deletion were geyser prevention, increased SSME LO₂ prestart temperature, and tank liquid level control.

The development activities for the main feedline helium injection system, summarized in Figure 12, were necessary to resolve design incompatibilities with the Shuttle elements. Geyser prevention was accomplished by using main feedline helium injection and facility flow control. Successful geyser prevention depends on the LPS to monitor the feedline conditions and to take corrective action. Feedline temperature redlines are established to assure subcooled propellant for each phase of loading. For a redline exceedance, the LPS initiates a stop flow and changes the facility flow direction to remove the warm propellant from the vehicle. Extensive testing on the MPTA: (1) defined the LPS control requirements and redlines; (2) evaluated procedural and design changes; and (3) demonstrated adequacy of corrective actions. Experience has shown that the characteristics of all components must be well defined for proper operation of this configuration. For example, STS-5 loading was satisfactorily accomplished with Mobile Launch Platform No. 1 (MLP-1). STS-6 loading with the identical LPS sequence using MLP-2 encountered two stop flows and a nondamaging geyser during the slow fill to 2% operation. This condition resulted from a difference in the flow characteristics of two facility

replenish control valves for the same position setting. Subsequent to STS-6, additional parameters are being controlled at the facility/Orbiter interface to preclude a reoccurrence of this situation.

Deletion of the antigeysers line resulted in increased LO₂ feed system temperatures that were incompatible with the SSME prestart requirement. An SSME test facility was modified to experimentally evaluate the impact of the higher temperature. The test results allowed the SSME preburner pump discharge temperature requirement to be changed from 178°R to 183.5°R, eliminating the temperature incompatibility.

The use of main feedline helium injection changed the flow profiles in the tank, resulting in the inability of the level control sensors to define the liquid level. A special test series on MPTA defined the reorientation and baffling of the sensors necessary to regain the level control function.

CONCLUSION

The government/contractor team has met the challenge to develop a cryogenic propellant management system that integrated the design features of the Shuttle elements. The flights of the Space Shuttle Columbia and Challenger portray the success of these efforts. Future emphasis will be on the automation of the prelaunch operations, integration/activation of the Western Test Range, and performance improvements that increase vehicle payload. These performance improvements include: (1) removing the LO₂ tank pressure stabilization requirement for liquid levels above 98% (for increased propellant density); (2) reducing the ullage volume (for higher loading levels and shorter drain-back time); and (3) reducing the liquid residuals at engine cutoff. These improvements can result in an additional increase in the Shuttle capability by about 1500 pounds.

REFERENCES

1. Paul, Hans G.: Development Trends of Space Vehicle Propulsion in the 1970's. 10th International Technical and Scientific Conference on Space (Rome, Italy), March 1970.
2. Norquist, Lawrence: External Tank for the Space Shuttle Main Propulsion System. AIAA/SAE 12th Propulsion Conference (Palo Alto, California), Paper No. 76-595, July 1976.
3. Norquist, Lawrence: Development Progress, External Tank for the Space Shuttle Main Propulsion System. AIAA/SAE 14th Propulsion Conference, Paper No. 78M0-1044, July 1978.
4. Norquist, Lawrence: Preflight Status of the External Tank Portion of the Space Shuttle Main Propulsion System. AIAA/SAE/ASME 15th Joint Propulsion Conference (Las Vegas, Nevada), Paper No. 79-1143, June 1979.
5. Franklin, William G.: Space Shuttle External Tank Gaseous Oxygen Vent System. 16th Aerospace Mechanisms Symposium (Kennedy Space Center, Florida), NASA CP-2221, May 1982.
6. Fenwick, J. R.; Jones, J. H.; and Jewell, R. E.: Space Shuttle Main Engine (SSME) Pogo Testing and Results. 52nd Shock and Vibration Symposium (New Orleans, Louisiana), October 1981.

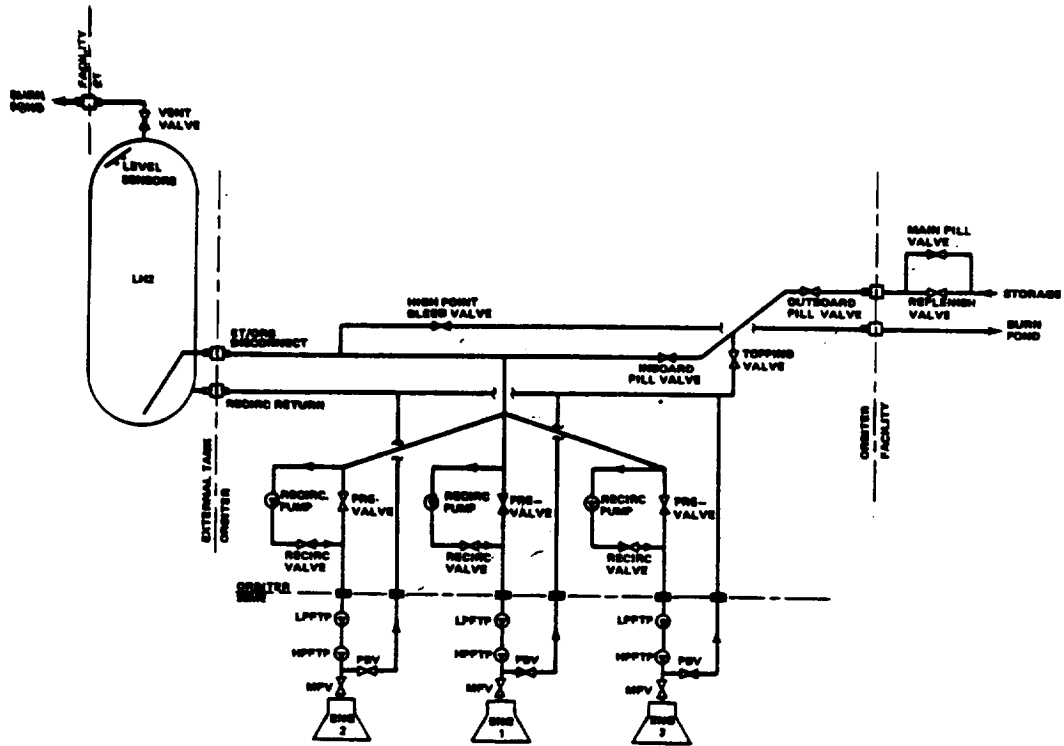


FIGURE 1. LH₂ PROPELLANT DELIVERY SYSTEM

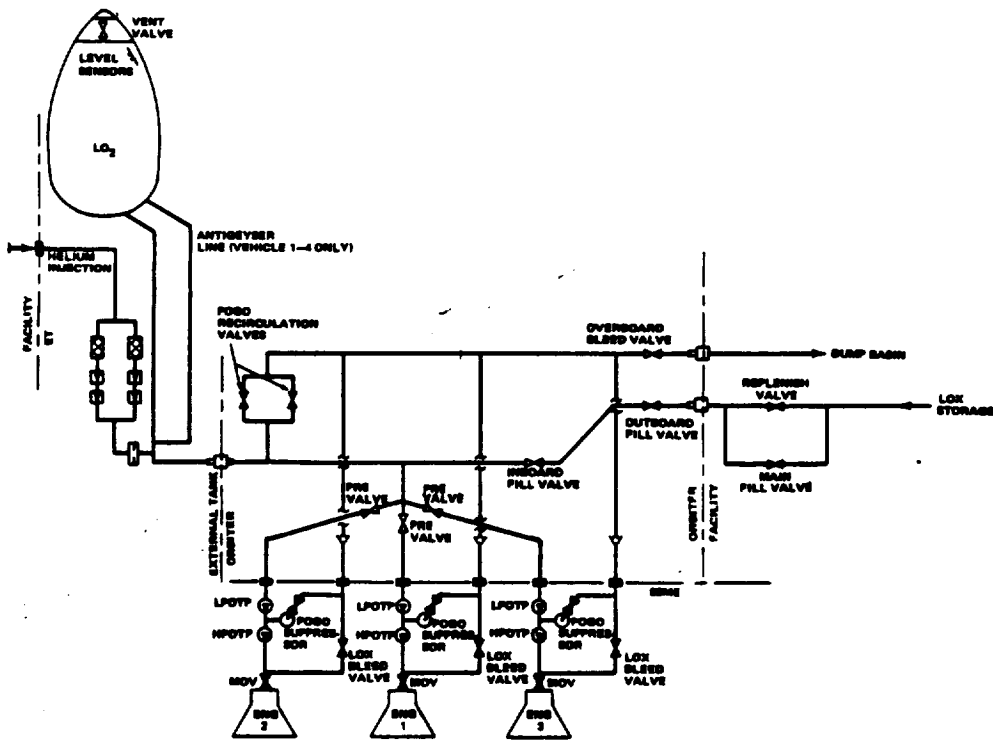


FIGURE 2. LO₂ PROPELLANT DELIVERY SYSTEM

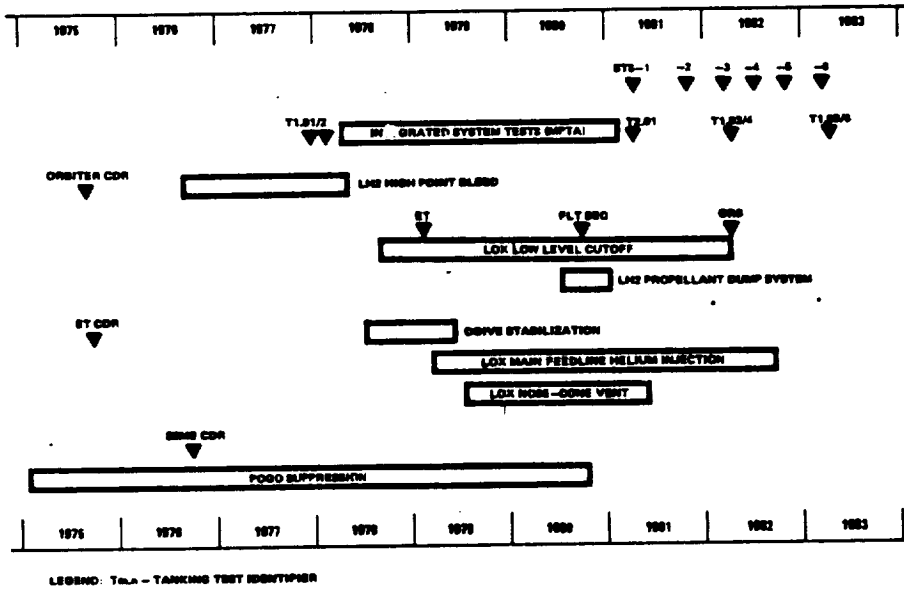


FIGURE 3. CRYOGENIC PROPPELLANT MANAGEMENT SYSTEM CHRONOLOGY

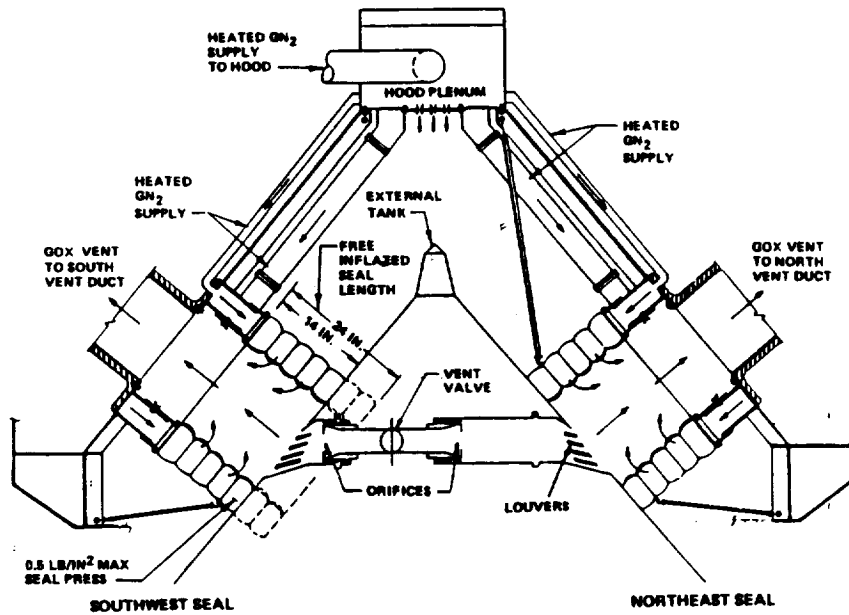
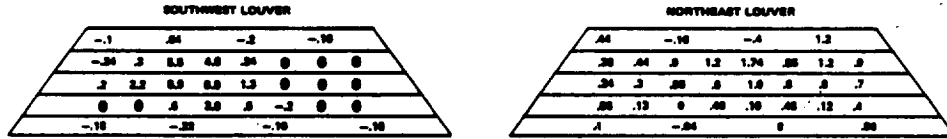


FIGURE 4. VENT HOOD CUTAWAY WITH DOCK SEALS AND EXTERNAL TANK COMPONENTS

ORIGINAL PAGE IS
OF POOR QUALITY

26 INCH VALVE STROKE
2.75 INCH DRIFICES
T = -80°F, P = 8.1 PSIG



⊙ OFF SCALE NEG

1.1 INCH VALVE STROKE
NO DRIFICES
T = -80°F, P = 8.1 PSIG



FIGURE 5. GO₂ VENT SYSTEM PRESSURE DISTRIBUTION 3/4" INSIDE LOUVERS

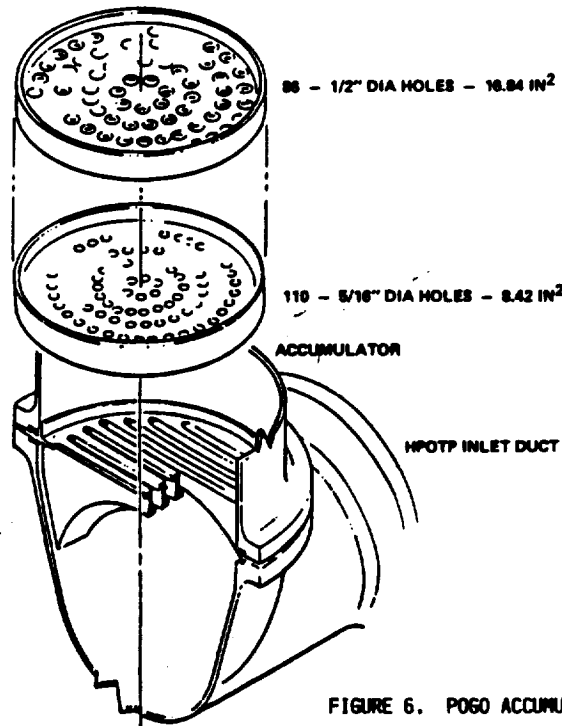


FIGURE 6. POGO ACCUMULATOR SPLASH PLATE

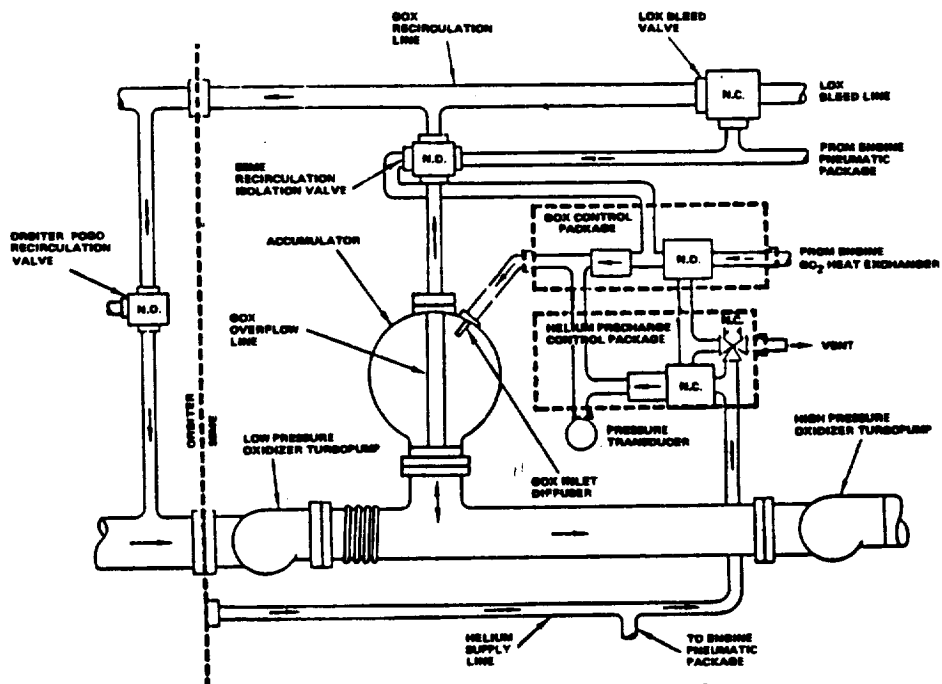


FIGURE 7. POGO SUPPRESSION SYSTEM SCHEMATIC

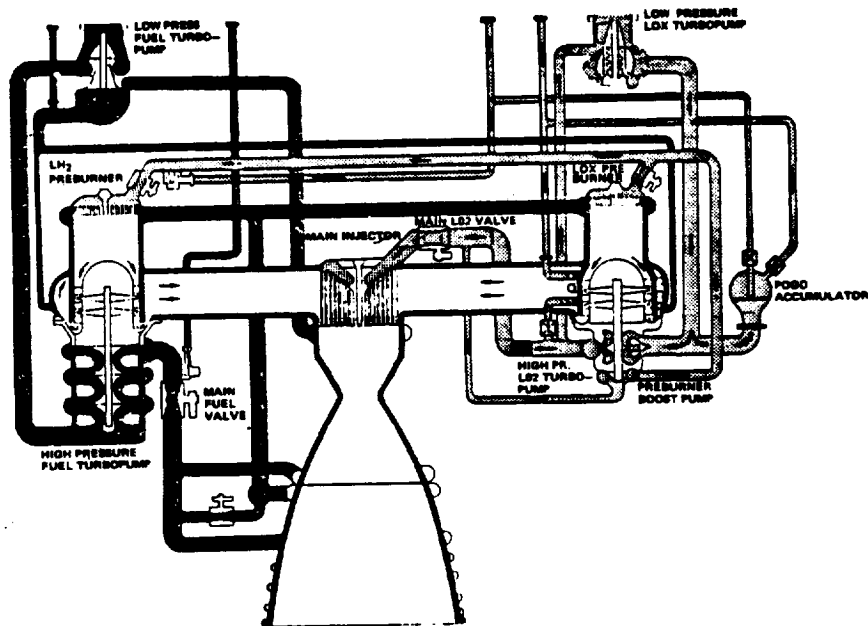


FIGURE 8. SSME PROPELLANT FLOW SCHEMATIC

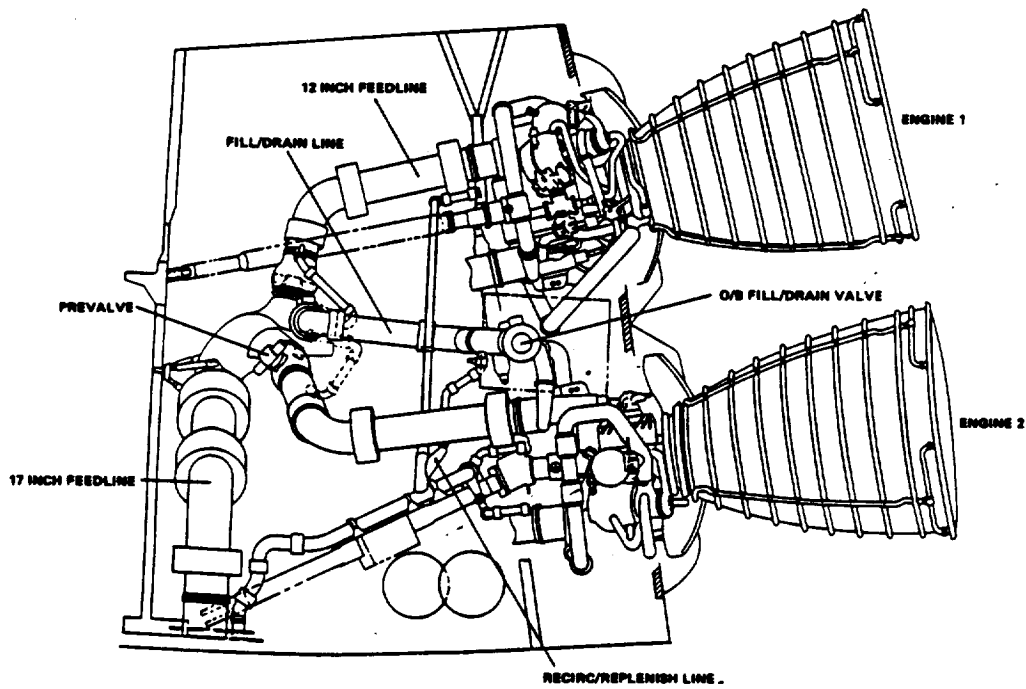


FIGURE 9. LH₂ MPS PROPELLANT DUMP

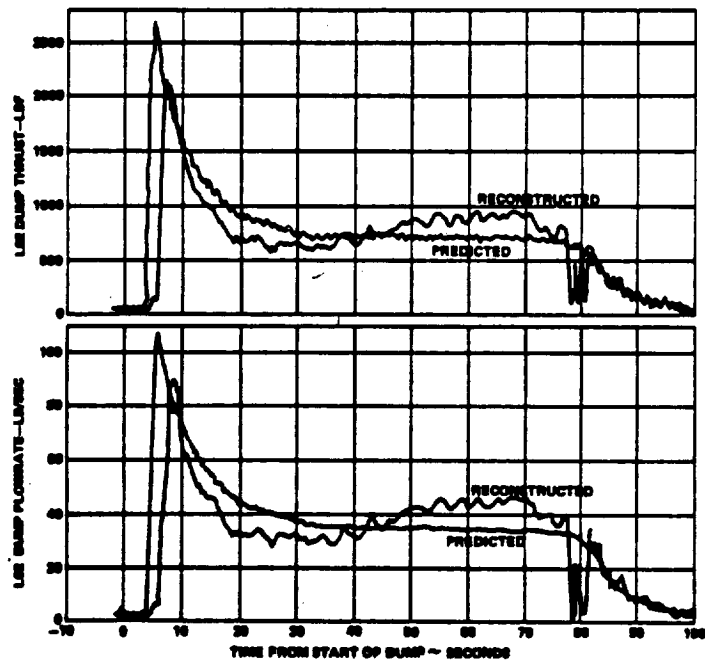


FIGURE 10. LO₂ PROPELLANT DUMP MODEL CORRELATION (STS-2)

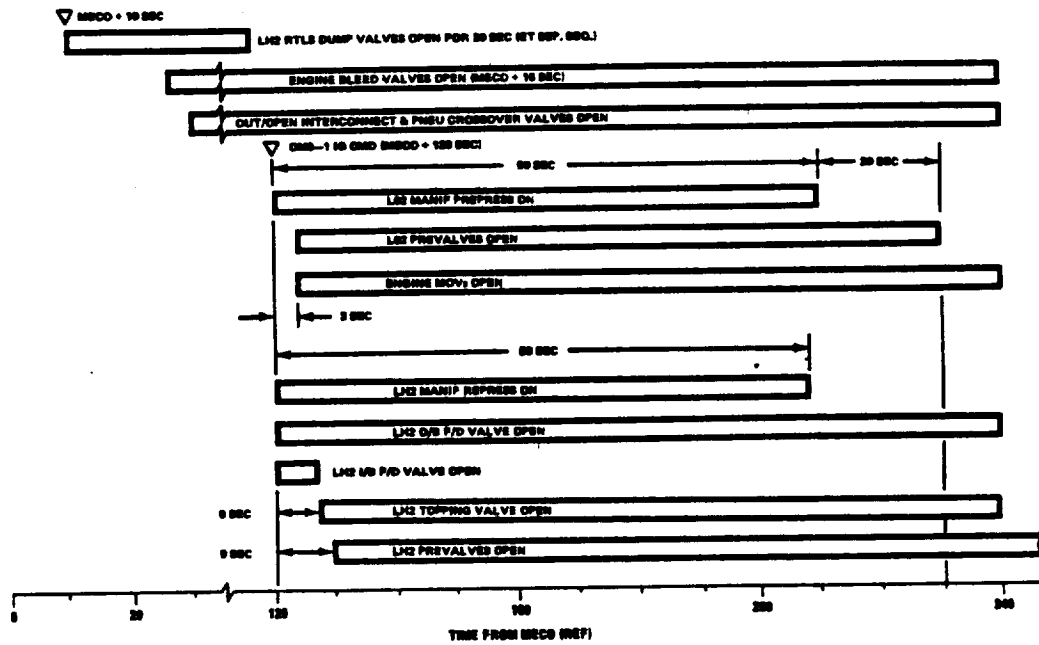


FIGURE 11. MPS DUMP SEQUENCE - NOMINAL (STS-5 AND SUBS)

TEST	RESULT	1976	1977	1978	1979	1980	1981	1982
FULL SCALE FEEDLINE HELIUM INJECTION	DEVELOPMENT OF MATH MODEL FAILURE MODES EVALUATION SOME START TEMP RESET				■			
SINGLE SUMP	SOME START AT INCREASED TEMP SOME START WITH 4% HELIUM GAS					■	■	
SUBSCALE FEEDLINE	INSIGNIFICANT HELIUM IN ORBITER FEED SYSTEM DURING START					■		
MPTA STATIC FIRING 12	IDENTIFIED FILL TO 2% ISSUES VERIFIED INLET TEMP, JUNE START IDENTIFIED VENT UNDERSHOOT ISSUE IDENTIFIED LEVEL CONTROL WADSWORTH						■	
MPTA TANKING-02	FILL TO 2% PROCEDURE INADEQUATE HELIUM INJECT FAILURE MODE/LIMITS						■	
MPTA TANKING-03	VERIFIED MATH MODEL VERIFIED LEVEL SENSOR DESIGN CHANGE							■
MPTA TANKING-04	DEVELOPED FILL TO 2% PROCEDURE DEMONSTRATED KSC REVERT AT 2% AND 70%							■
STS 1, 2, 3 LOADING/LAUNCH	VERIFIED FACILITY CHARACTERISTICS/ OPERATIONS						■	■
STS 4 TANKING	VERIFIED FACILITY OPERATIONS FOR FILL TO 2% AND STOP FLOW							■
STS 5 TANKING	DEMONSTRATED LOADING SEQUENCE W/O ANTIVEYER LINE							■

FIGURE 12. DEVELOPMENT/IMPLEMENTATION OF LO₂ MAIN FEEDLINE HELIUM INJECTION

TABLE 1. MPS LD2 PROPELLANT DUMP PERFORMANCE SUMMARY FOR STS-1 THRU STS-4

STS	ANALYSIS BASED ON ACCEL. DATA				ANALYSIS BASED ON FEED PRESS DATA				AVERAGE	
	IMPULSE (LBF-SEC)	DELTA V (2) (FT/SEC)	LEZ DUMPED (4) (LBM)	RESIDUAL (LBM)	IMPULSE (LBF-SEC)	DELTA V (2) (FT/SEC)	LEZ DUMPED (4) (LBM)	RESIDUAL (LBM)	IMPULSE (LBF-SEC)	LEZ DUMPED (4) (LBM)
1	ACCELEROMETER DATA NOT AVAILABLE				7207	10.7	2000	797	7207	2000
2	86201	0.4	3213	1000	79144	10.8	2412	801	87718	3213
3 (1)	48812 (2)	0.3 (2)	2100 (2)	2104 (2)	88338	7.8	2048	1654	48825	2370
4	88700	0.4	2400	800	87825	8.2	2340	900	88318	2370

- (1) DUMP THROUGH SINE NO. 1 & 2 ONLY (EARLY APV NO. 3 & 5).
 (2) BASED ON BUICK-LOGG ACCELEROMETER DATA.
 (3) DELTA V GENERATED IS A FUNCTION OF ORBITER MASS AT ONE-1 POSITION.
 (4) 270 LB LEZ LEAKED THROUGH NPOTP SEALS PRIOR TO DUMP INITIATION.

D3
N85-16940

SPACE SHUTTLE MAIN ENGINE - INTERACTIVE DESIGN CHALLENGES

John P. McCarty
National Aeronautics and Space Administration
George C. Marshall Space Flight Center, Alabama

and

Byron K. Wood
Rocketdyne Division
Rockwell International Corporation

ABSTRACT

The operating requirements established by NASA for the SSME were considerably more demanding than those for earlier rocket engines used in the military launch vehicles or Apollo program. The SSME, in order to achieve the high performance, low weight, long life, reusable objectives, embodied technical demands far in excess of its predecessor rocket engines.

The requirements dictated the use of high combustion pressure and the staged combustion cycle which maximizes performance through total use of all propellants in the main combustion process. This approach presented a myriad of technical challenges for maximization of performance within attainable state-of-the-art capabilities for operating pressures, operating temperatures and rotating machinery efficiencies. Controlling uniformity of the high pressure turbomachinery turbine temperature environment was a key challenge for thrust level and life capability demanding innovative engineering. New approaches in the design of the components were necessary to accommodate the multiple use, minimum maintenance objectives. Included were the use of line replaceable units to facilitate field maintenance, automatic checkout and internal inspection capabilities.

INTRODUCTION

The National Program to develop a Space Shuttle and replace the "one-shot" expendable rocket vehicles with a reusable Space Transportation System promises to be a turning point in liquid propellant rocket engine history.

The requirements for reuse with a minimum refurbishment and turnaround cycle introduced stage requirements such as reusable reentry thermal protection, wing surfaces and landing gears. These features, and others, contributed to a relatively high hardware weight when compared to non-reusable systems. In addition, reentry and landing flight characteristics put a premium on high engine thrust-to-weight and small engine envelopes. As a result the search for performance for the Shuttle Systems, i.e., more payload delivered to orbit at reduced cost, focused main engine performance requirements on increases in specific impulse, thrust-to-weight and thrust-to-engine exit area. Engine operational requirements consistent with reusable, low-cost transportation, included long life and low maintenance to reduce recurring cost and minimum development program to reduce non-recurring cost.

THE CHALLENGE

It can readily be seen that the search for performance can be pursued along two directions, more specific impulse and lower rocket engine weight.

The early history of the application of liquid propellant rockets has seen the succession of more energetic propellant combinations. The use of hydrogen/oxygen for the propellants of the Space Shuttle Main Engine (SSME) represents a propellant choice near the peak of readily available chemical propellant combinations. This succession of more energetic propellants has been accompanied by a drive to reduce rocket engine weight necessary to achieve a given installed performance level. Figure 1 shows that increased thrust-to-weight is accomplished by increasing the ratio of engine thrust to nozzle exit area. Increasing the engine thrust per unit exit area also has the effect of reducing the nozzle exit area at a given thrust, thereby reducing vehicle drag associated with the attendant base area.

Using this relationship and the theoretical performance characteristics shown in Figure 2 which are representative of LH_2/LO_2 , one can construct Figure 3 which displays the path necessary to achieve improvements in installed performance.

Figure 3 shows that to increase specific impulse at a given thrust-to-weight, or to increase thrust-to-weight at a given specific impulse, or to increase both requires an increase in the combustion pressure. This combustion pressure increase can be traced in the LO_2/LH_2 family of engines where

capability has progressed from the RL-10 at 400 psia, through the J-2 at 632 psia and the J-2S at 1200 psia to the current development of the SSME at 3000 psia. The J-2 and J-2S combustion pressures noted above result from these engines using the gas generator power cycle. In this cycle a small portion of the incoming propellant is used to power the turbopumps which feed propellant to the main thrust chamber, instead of producing thrust. If these engines had used the staged combustion or preburner cycle, in which all of the fuel powers the turbopumps before being used in the main thrust chamber, like the RL-10 and SSME, the combustion pressure would be close to that shown in the Figure.

These increases in combustion pressure have been accomplished through improvements in component technology, improved materials, higher speed and head rise pumps, higher turbine inlet temperatures, and improved cooling techniques for higher heat fluxes to name but a few. To place the SSME challenges in perspective it is appropriate to compare a few key operating characteristics to those of prior systems.

Increased combustion pressures require increased power to feed the propellants to the combustion chamber. The generation of these high power levels must employ a highly efficient working cycle to minimize, or preferably avoid any performance loss. The well developed gas generator cycle, which served adequately for most prior engines, is shown in a simplified schematic in Figure 4 along with the more efficient preburner cycle. Also shown is a comparison of the specific impulse and the lower value which results from the inefficient utilization of the turbine exhaust gases in producing thrust. On the other hand, the preburner cycle requires considerably higher pump discharge pressures, as shown in Figure 5, to accommodate the pressure drop which occurs in the turbines.

The need for very high pump discharge pressures must be met by increased head rises from the individual pump stages to minimize the number of stages and pump weight. Impeller tip speeds, as shown on Figure 6, increased substantially. In parallel, the focus on minimum weight pushed the design sophistication and speed, as shown in Figure 7, beyond levels then in use.

High chamber pressure has a significant impact on combustion chamber cooling. Gas side heat transfer coefficients increase with chamber pressure to approximately the 0.8 power. These high film coefficients increase the heat flux, as shown in Figure 8, which must be accommodated by the cooling system to meet the long life requirements.

One of the prime characteristics of the Space Shuttle, and consequently the SSME, is design for reusability and long life with minimum maintenance. These requirements must be achieved despite the extreme physical environments imposed upon the engine components and the demand that the hardware be fully utilized to just short of the point where safety and performance are impaired.

Basic to this concept of reusability is the extension of design life typically required for expendable engines - 10 starts and 3600 sec which is sufficient for acceptance tests and the single flight - to that required for the SSME - 55 starts and 27000 sec which should be sufficient for 50 to 55 missions after acceptance tests. Field maintenance with minimum between flight activity required advances relative to prior rocket engine experience and practices. Examples include the identification and design of line replaceable units that are interchangeable without system recalibration, establishing and verifying effective inspection and automatic checkout procedures to facilitate the short turnaround goals of the Shuttle system, and integration of development experience, field maintenance records and flight data analysis to extend the time between component replacements and engine overhaul.

Equally ambitious to the technical challenges outlined above was the programmatic challenge to accomplish the design, development and certification with the utilization of resources substantially less than required in previous, comparable development programs. A measure of the resources is represented by the engine test programs shown in Figure 9. As can be seen the projected number of tests and development engines were reduced by some 40%.

THE ENGINE

The SSME primary flow schematic is shown in Figure 10 and briefly described as follows:

The fuel flow enters the engine at the low-pressure turbopump inlet and pressure is increased to meet high-pressure pump inlet requirements. After the fuel leaves the high-pressure pump, the flow is divided and distributed to provide: preburner fuel, nozzle coolant, main combustion chamber coolant, low-pressure turbine drive gas and hot gas manifold coolant.

The oxidizer flow enters the engine at the low-pressure turbopump inlet. The low-pressure oxidizer pump increases the pressure to meet high pressure pump inlet requirements. From the high pressure pump discharge, the majority of the oxidizer is fed to the main injector. The remaining oxidizer is increased to preburner inlet pressure by the high-pressure boost stage of the oxidizer pump. Liquid oxygen from the high pressure pump discharge is used to drive the low pressure oxidizer turbine.

Individual preburners are used to supply power for the high pressure fuel and oxidizer turbines. Preburners provide the flexibility to adjust the power split between the two high pressure turbines by the control of valves which govern the oxidizer flow to the preburners.

The majority of the high pressure fuel is used in the turbine drive system. The remainder is used to cool components and power the low pressure fuel turbopump. A portion of the oxidizer flow also is used in the preburners; the remainder is routed directly to the main combustion chamber. The propellants combusted in the preburners power the high pressure turbopumps and are then routed to the main combustion chamber.

In the main combustion chamber, the gases from the preburners are burned with the propellants.

The major engine physical arrangement, Figure 11, provides for a central structural member called the powerhead wherein are located the main injector and respective fuel and oxidizer preburners. The main combustion chamber and the two high pressure turbopumps "plug in" and are bolted to the powerhead.

CONSTRAINING DESIGN CONSIDERATIONS

The significant system development challenges can be grouped around the central issue of how to develop sufficient turbomachinery horsepower to meet the high pressure performance demands and maintain turbine operating temperature both transient and steady state within life limit practicality.

In the preburner cycle hydrogen flow availability and pressure schedule are the prime design considerations. Unlike most prior operational systems which use a small percentage (10%) of the engine fuel flow to drive high pressure ratio turbines the SSME preburner cycle seeks to use 100% of the engine fuel flow to drive low pressure ratio turbines. In Figure 5 this directly dictates the pumping system required head, and therefore, the system pressure schedule.

The available power to produce these conditions is in turn limited by turbomachinery efficiency, turbine flowrate and turbine temperature. In very simplified terms the relationship can be represented by the following:

$$\eta (1 + MR) T C_p \left[1 - \left(\frac{P_c}{P_D} \right)^{\frac{\gamma-1}{\gamma}} \right] = P_D \left(\frac{1}{\rho_F} + \frac{MR}{\rho_O} \right)$$

η = Turbopump Efficiency

T = Turbine Gas Temperature

P_c = Chamber Pressure

P_D = Pump Discharge Pressure

ρ = Density

MR = Mixture Ratio

γ = Specific Heat Ratio.

Figure 12 illustrates the premium paid to maximize turbomachinery efficiency and design for high temperature operation. Taken all together the relationship between pressure (weight) and turbomachinery efficiency at a fixed structural temperature limit are depicted in Figure 13 by parametric solution of the above equation.

DEVELOPMENT

To drive the three stage centrifugal high pressure fuel turbopump with a demonstrated pump efficiency between 74 and 78 percent a maximum first stage turbine blade metal temperature of 1960 degrees R was selected or a gas temperature of approximately 2000 R. The material properties for the Mar-M-246-DS blades are shown in Figure 14 which for steady state stresses would provide essentially infinite life at 1960 degrees R.

SSME development testing at full thrust exhibited erosion of the first stage turbine blade platform leading edges with accelerating damage test-to-test and high maintenance. This precipitated the

removal of the turbopumps for replacement of the first stage blades. In addition, a number of blades exhibited transverse leading edge high cycle fatigue cracks above the blade root giving rise to concern for blade failure.

As a consequence a specially instrumented turbopump, Figure 15, was fabricated with circumferential inlet blade O.D. and I.D. temperature thermocouples. Testing with the special instruments revealed the problem to be both start transient and steady state mainstage oriented. Hot gas temperature spikes approaching 4000 degrees R were recorded as the preburner ignited. In addition, a radial temperature distribution was confirmed in which the inner core gases approach 3000 degrees R with the outer diameter gases near 1900 degrees R, Figure 16. The inner core gases by stream tube analysis would be the ones aggravating the blade root erosion problem as illustrated in Figure 17.

DESIGN INNOVATION

The Fuel Preburner is a fuel cooled, double walled chamber producing energy to drive the High Pressure Fuel Turbopump. The injector is a concentric element with 264 elements and three baffles to aid stability. The preburner is ignited by an augmented spark igniter (ASI) which is a small central combustion chamber with two spark igniters. The injector has a single pair of impinging oxidizer orifices surrounded tangentially by eight hydrogen orifices. The injection flow pattern creates an oxidizer-rich condition at the spark igniters for ignition. An oxidizer-rich core surrounded by fuel provides a high mixture ratio torch to ignite the preburner.

The resolution of the blade erosion challenge was approached in two ways. First the preburner face hot gas temperature distribution was modified to reduce the inner core temperature by raising the outer diameter temperature in a region where a higher allowable blade temperature can be tolerated, Figure 17. This assumes the blade stress to be a linear function of height. This was accomplished by enlarging the preburner baffle center coolant holes, providing a 20% increase in center core cooling, Figure 18. In addition, the preburner injector face coolant holes were modified by enlarging 132 existing holes and adding 36 holes in the inner zones of the injector face, Figure 19.

These modifications resulted in the reprogrammed temperature distribution shown in Figure 20 and a verified blade temperature distribution shown in Figure 21.

The second innovation addressed the ignition temperature spike. The ignition of the preburner is accomplished by regulation of the oxidizer flow to the preburner by the inlet valve. The resulting temperature at ignition directly correlates to the oxidizer accumulated up to the point of ignition. The SSME onboard control system provides the flexibility to adjust the scheduling of the engine control valves.

As a result a notch was added to the preburner oxidizer control opening, Figure 22. The notch was programmed to limit oxidizer flow at the time of ignition but subsequently increase flow at a time of higher fuel flow availability in order to not affect the total start time integrated oxidizer flow.

The effect of the modification on the resulting temperature transient is shown in Figure 22. This and the above modification were successful in adjusting the design on a simple but innovative basis to produce the desired environment. Since the modification, test and flight hardware have shown a marked improvement in observed erosion and cracking, thereby, significantly reducing required and projected maintenance.

REUSABILITY, LIFE AND MAINTENANCE

The preceding was just one example of many innovative concepts essential in the SSME design to meet the reusable Shuttle life challenge. Each component that experiences cyclic loading during operation was designed to have a minimum high cycle fatigue life of at least 10 times the number of cycles it will experience during service life. All components were designed to have a minimum low-cycle fatigue life of at least four times service life. A factor of 4 was also maintained on the time to rupture to account for creep effects. For those components experiencing both high and low cycle fatigue a generalized life equation is used to assess the accumulative damage capability versus time and thrust level.

The SSME has matured to a current 10-flight capability with a safety factor of 2. Testing will seek to keep pace with operational use and extend the operational life goal to 55 starts and 27,000 sec with a factor of 2, Figure 23. The testing will define components not capable of full life and spares requirements will be adjusted accordingly. The redesign of short-life components will be undertaken only if clearly economical to the program.

Test results will also become part of the mechanized information system developed to track critical hardware for operational exposure and life-limiting conditions. The system provides fingertip information with respect to component remaining available life by a system of interactive computer terminals located at key user sites.

As a consequence nearly all SSME components were designed as Line Replaceable Units (LRU's) to accommodate field maintenance for the operational phase of the program. Turbopumps, valves, ducts, instrumentation, igniters, nozzle and controller are considered normal LRU's. After manufacture or refurbishment, the performance characteristics of selected LRU's is determined by special "green run" tests. With the operating characteristics known, any LRU component can be replaced in the field and the pertinent controller software can be updated to reflect the new LRU component characteristics; assuring proper operation of the engine. Removed components are recycled through a depot maintenance program and made available as spares for future changeouts.

The high pressure turbopumps have the most demanding field maintenance requirements. The fuel pump turbine end sections must be inspected every other flight, and blade replacement is mandatory after eight flights. The oxidizer pump turbine end sections must be inspected and turbine blades replaced every eight flights. Current development testing is being focused on these areas to extend life and reduce operational maintenance.

Internal visual inspection of critical parts replaces the engine disassembly method used in past programs for routine inspection of parts. Routine maintenance tasks include automatic checkout, external inspection of engine hardware, turbomachinery torque checks and "life" inspections with internal inspection of key components using borescopes. Borescope ports, Figure 24, have been included in the design to permit internal visual inspection, by simply removing a plug and inserting the borescope. Routine use of the fibrous optic devices developed by the medical field is now common practice for SSME, Figure 25. These borescopes can be connected to still or TV cameras to record life data, Figure 26.

Maintenance data and flight data together are analyzed to determine if corrective maintenance or component replacement is required. Since corrective maintenance represents the largest single expenditure of time and resources during the turnaround cycle, full utilization of the service life available in each component is a necessary goal.

CONCLUSION

The quest for high performance, low weight and small envelopes through the use of more energetic propellants and increased combustion pressure has recorded a high level of refinement with the successful certification and flight of the SSME on Columbia and Challenger.

The next objective is to increase the operating life and reusability of these engines through repeated engine testing to extend the demonstrated basic ten flight usage. During this testing, life limits for specific LRU's will be determined and maintenance procedures will be developed to assure satisfactory flight performance. Should any new problems relating to life occur in the ground tests, they can then be defined and solutions developed to avoid similar problems in flight. Minor design improvements will be made to life-limiting parts.

As a companion effort, a product improvement study will address the complete engine in terms of design margins and ultimate life potential. NASA's supporting research and technology (SRT) program will continue to seek means to improve the life and reliability of launch vehicle engines such as the SSME. It includes for example work to increase the life of the turbine blades in the high-pressure pump and of heavily loaded bearings.

The Space Shuttle will be the backbone of this nation's space transportation for the remainder of this century and beyond. Use of the SSME should extend well into the next century. Other potential new vehicles will undoubtedly draw on the existing SSME capabilities. Through the planned improvements, and possibly uprated thrust, the SSME should meet the national requirements for launch-vehicle propulsion to space for decades.

REFERENCES

F. P. Klatt and V. J. Wheelock, "The Reusable Space Shuttle Main Engine Prepares for Long Life," presented at ASME Winter Annual Meeting, 14-19 November 1982.

J. P. McCarty and J. A. Lombardo, "Chemical Propulsion - The Old and the New Challenges," AIAA Student Journal, December 1973.

J. P. McCarty, "Space Shuttle Main Engine Concepts Technical Assessment", Unpublished Marshall Space Flight Centre Presentation, July 1969.

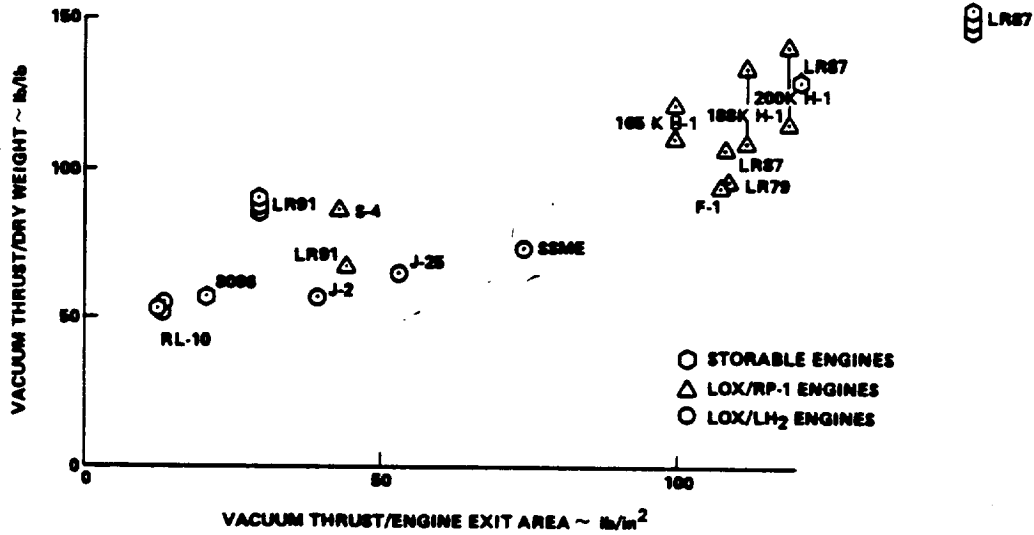


Figure 1. Engine System Weight.

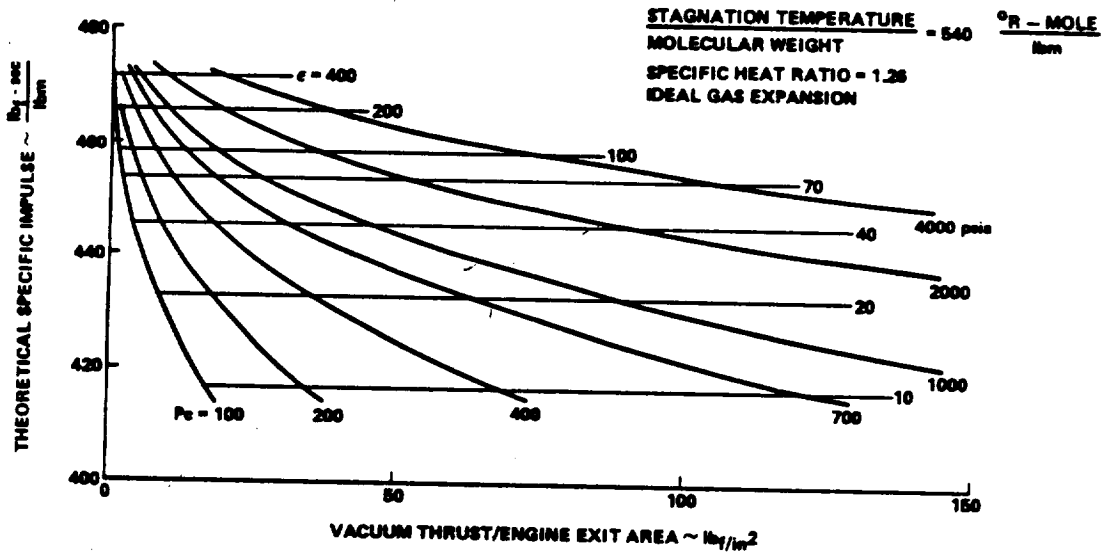


Figure 2. Theoretical LH₂/LO₂ Propellant Performance.

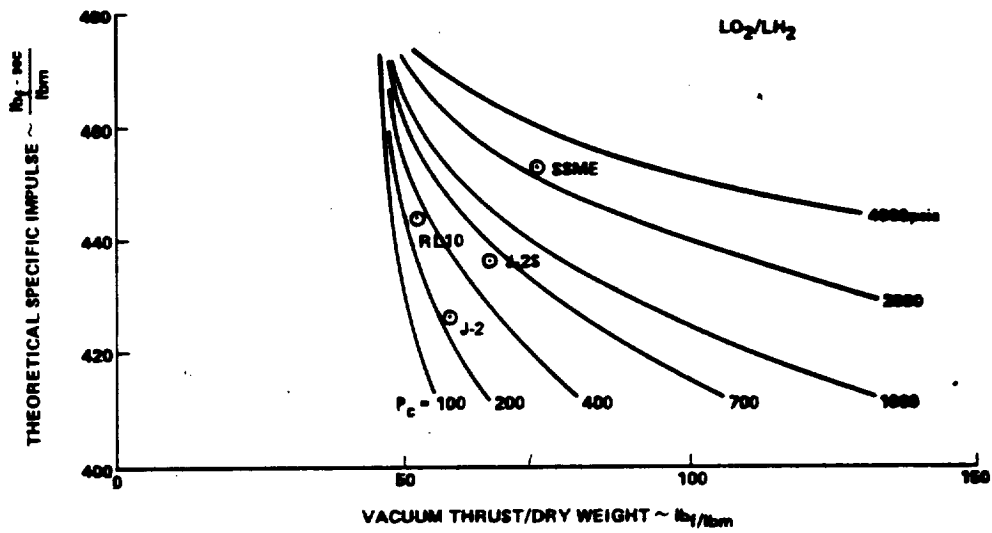


Figure 3. LH_2/LO_2 Rocket Engine Performance Characteristics.

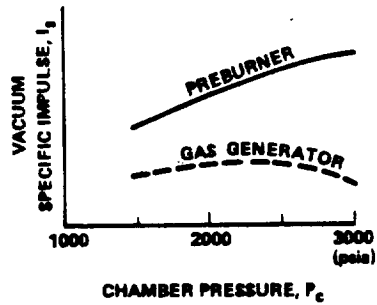
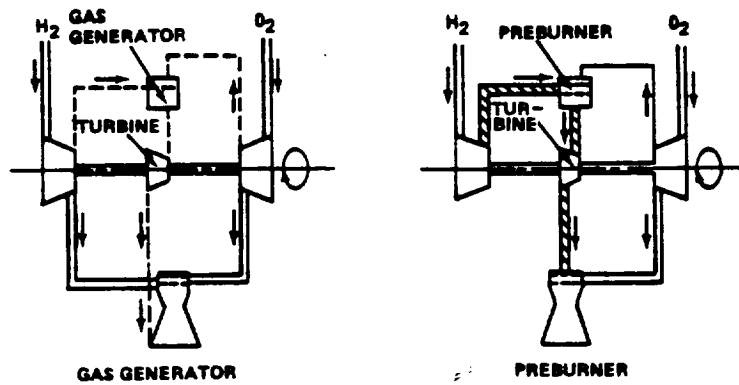


Figure 4. Gas Generator and Preburner Systems (Simplified).

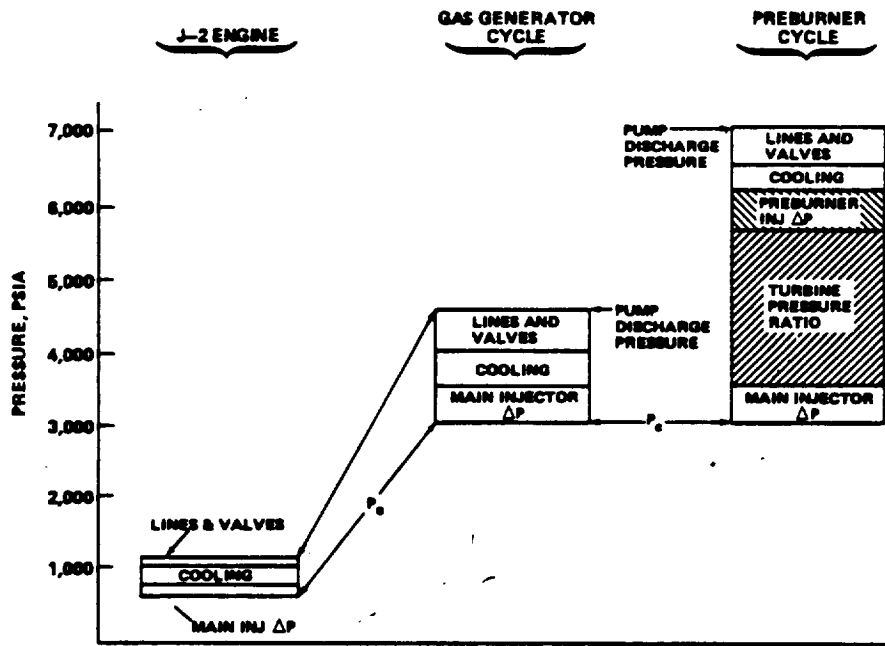


Figure 5. Rocket Engine Pressure Schedule.

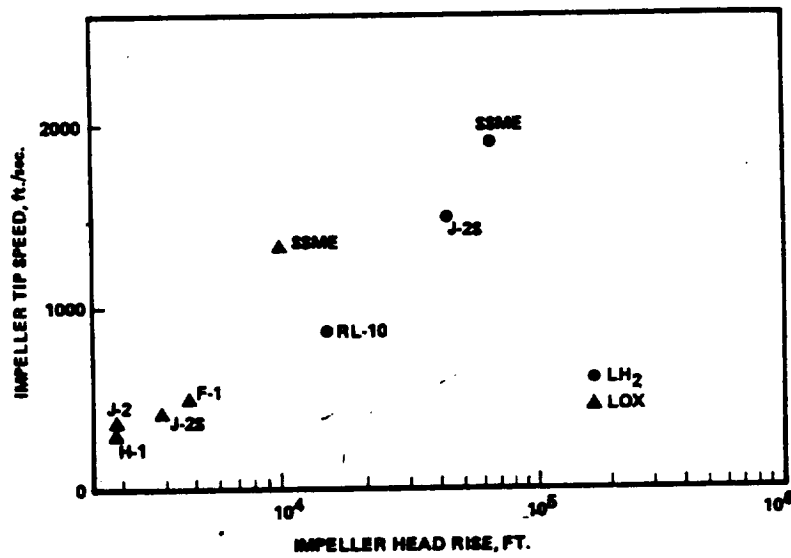


Figure 6. Impeller Design Experience.

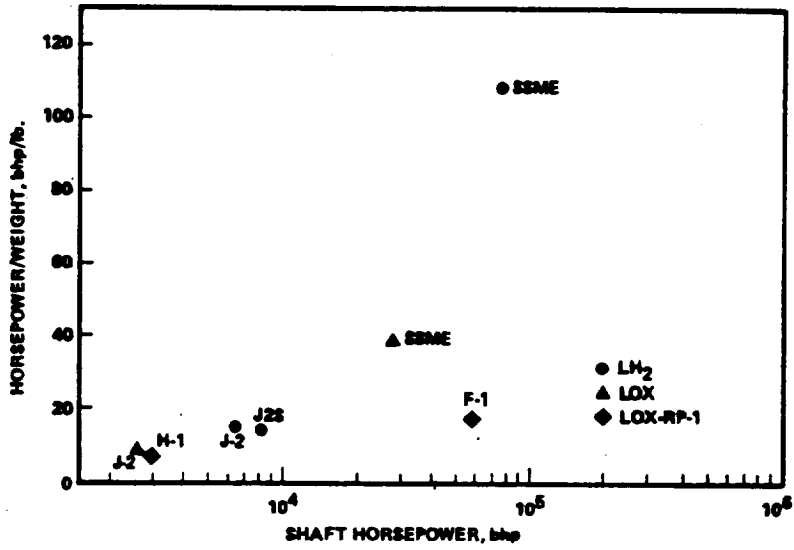


Figure 7. Turbopump Power/Weight Experience.

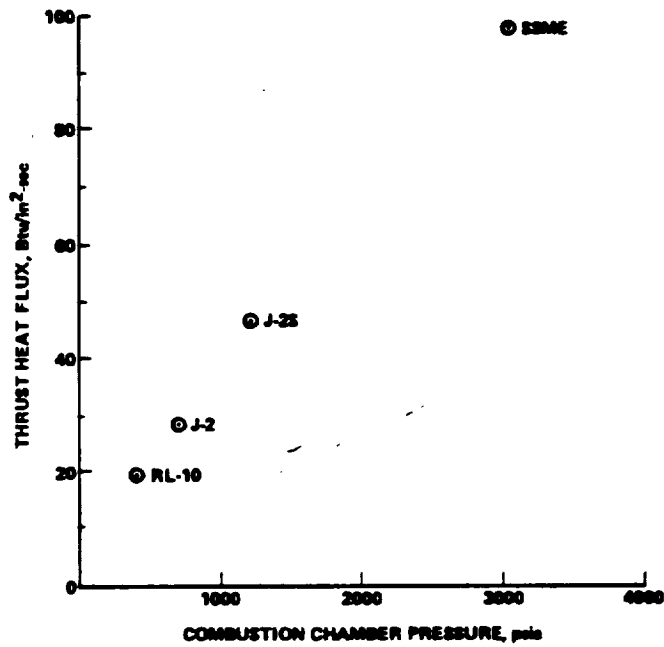


Figure 8. Combustion Chamber Heat Flux.

OPTIMIZATION OF FLOOR QUALITY

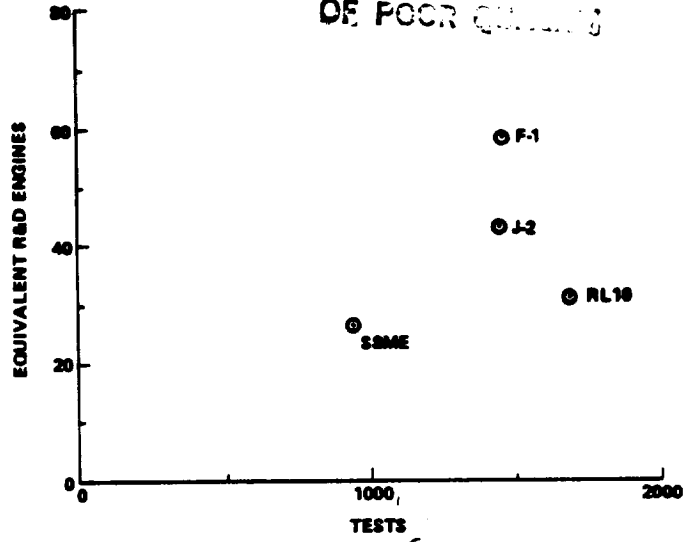


Figure 9. Development Resources.

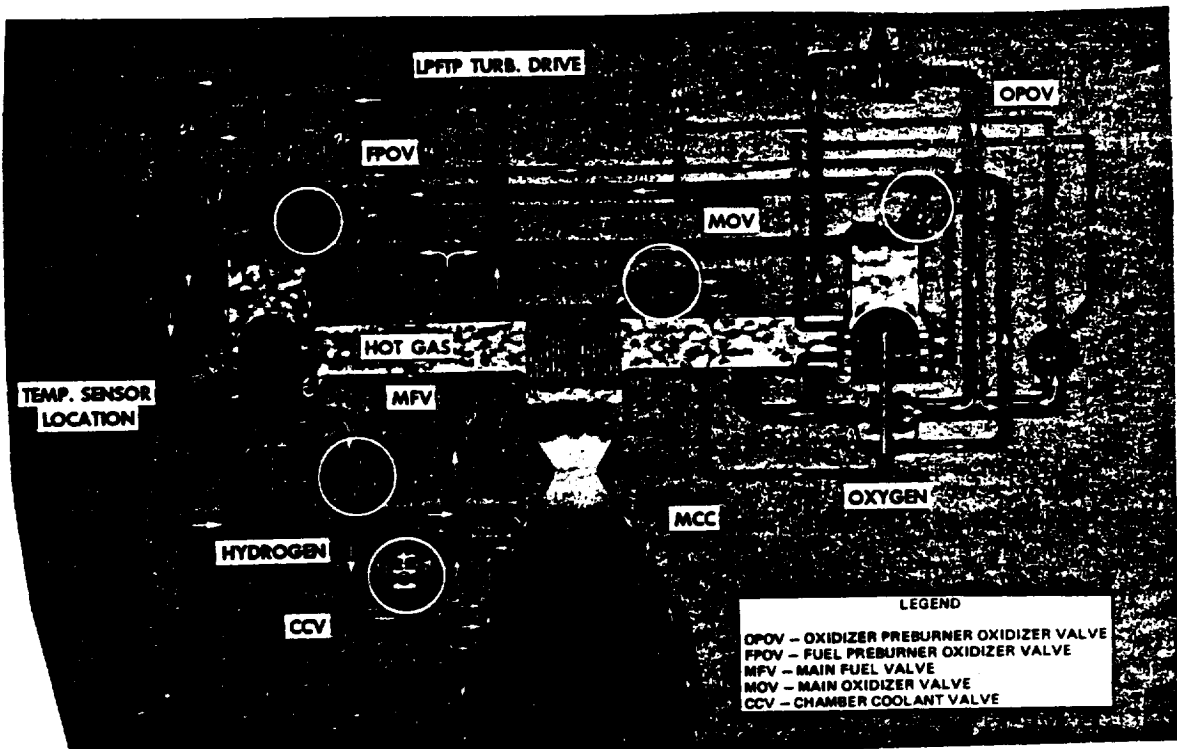


Figure 10. SSME Propellant Flow Schematic.

Reproduced from best available copy.

ORIGINAL PAGE IS
OF POOR QUALITY.

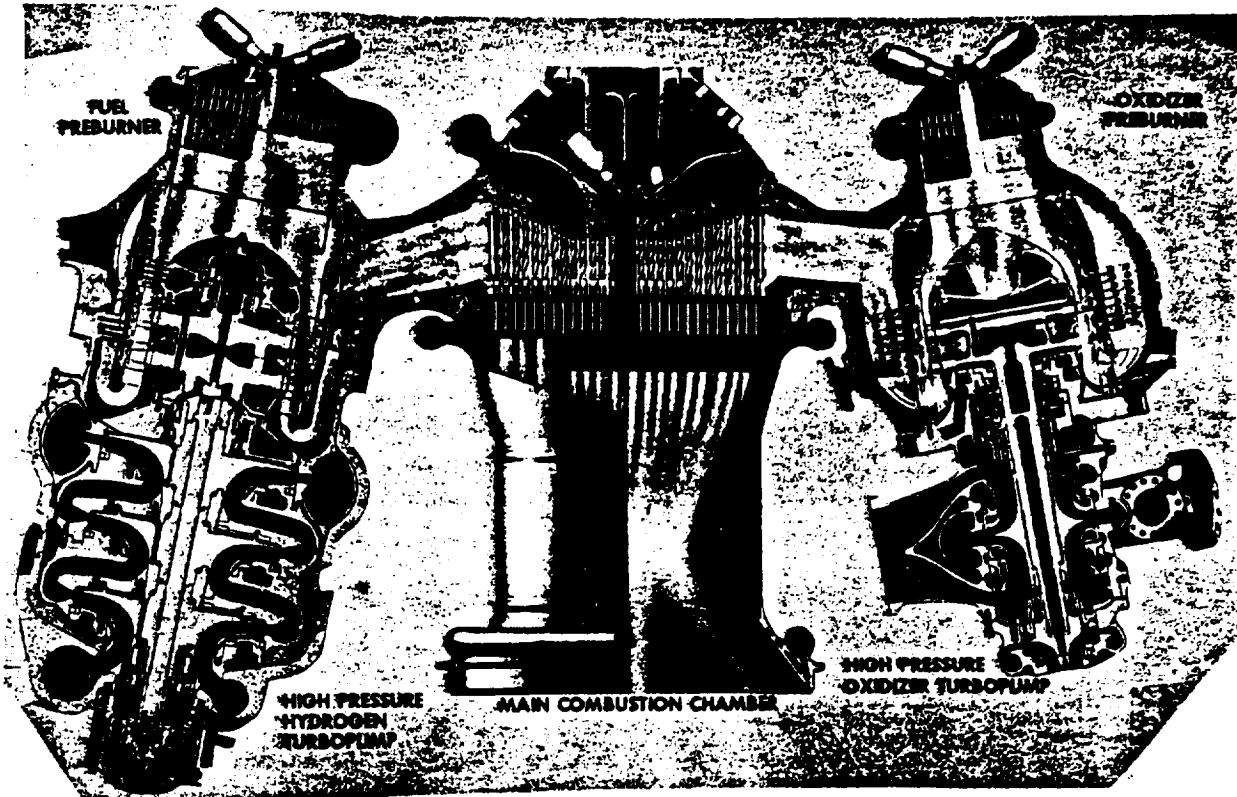


Figure 11. SSME Powerhead Component Arrangement.

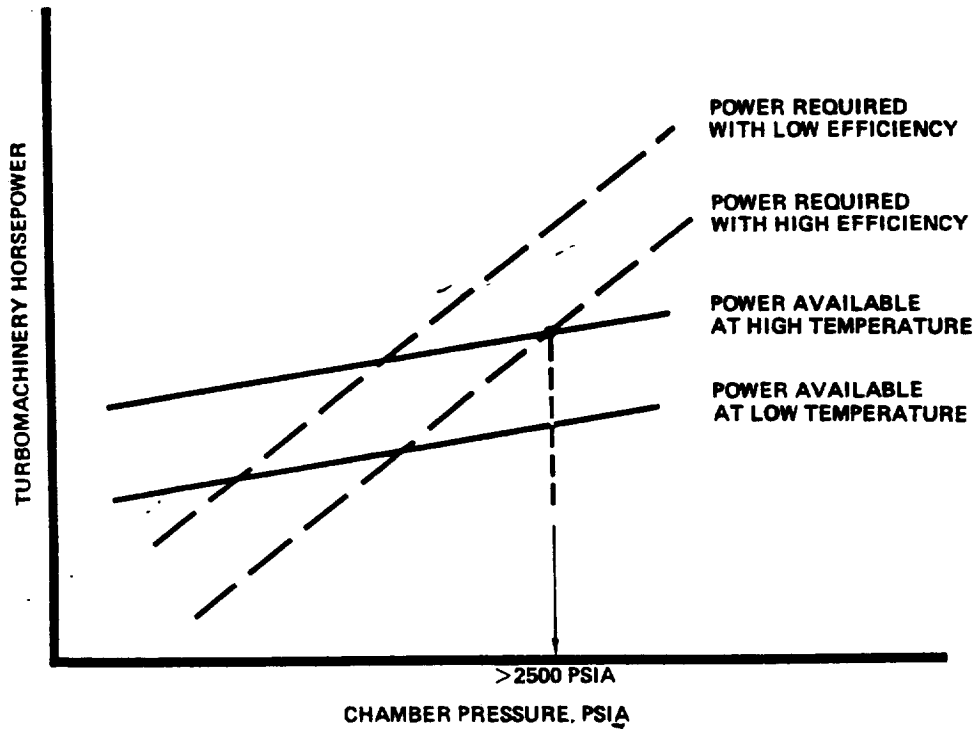


Figure 12. Staged Combustion Cycle.

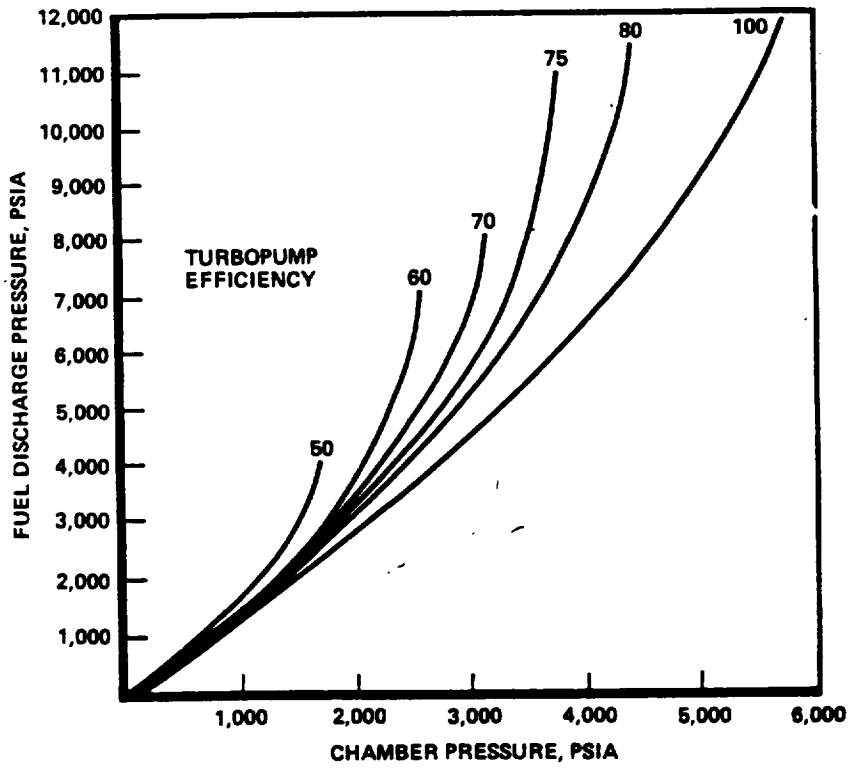


Figure 13. Staged Combustion Cycle.

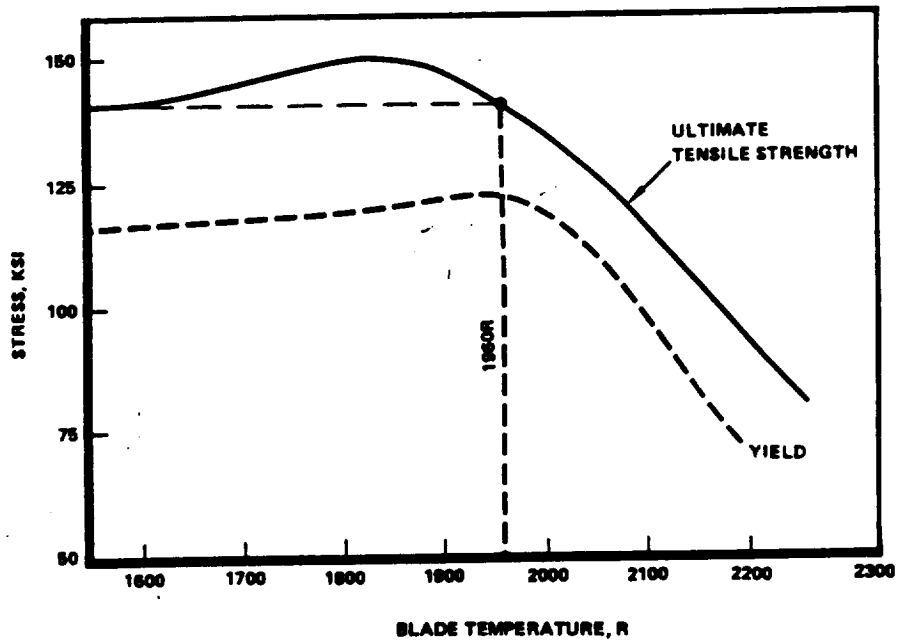


Figure 14. HPFTP Turbine Blade Metal Temperature (MM-246-DS).

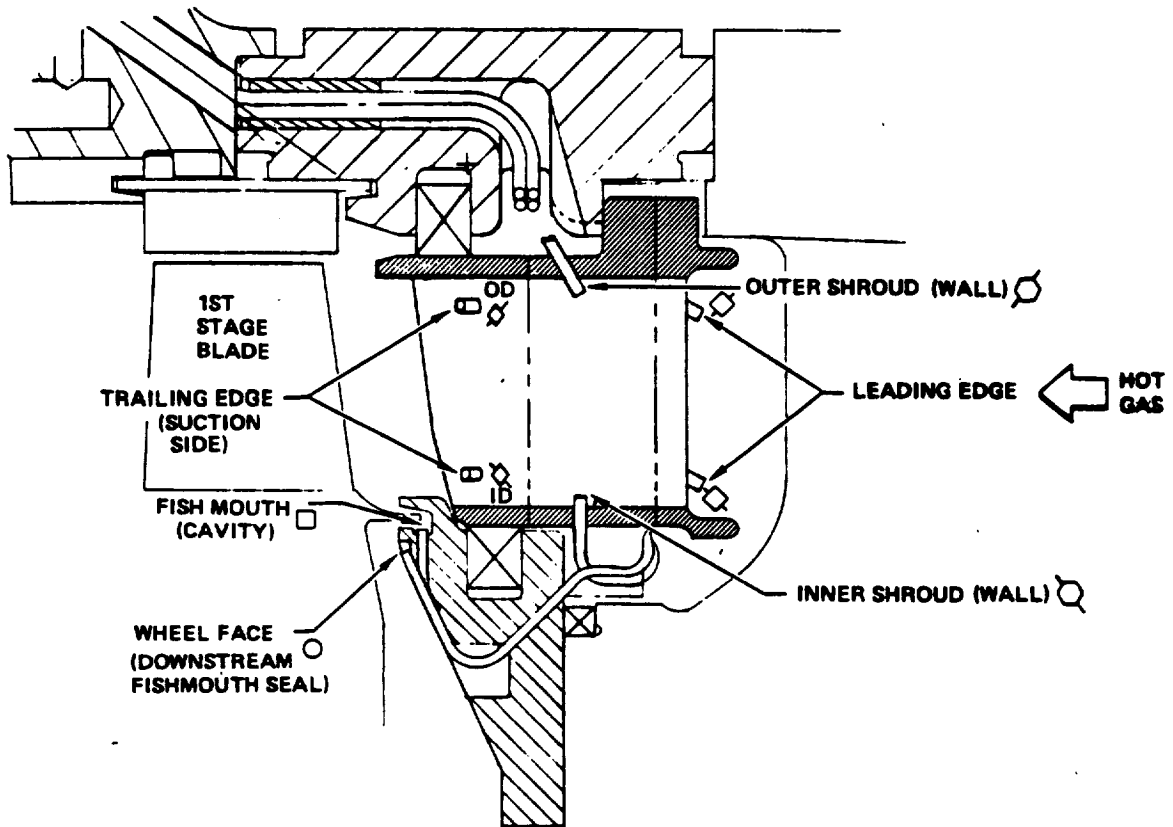


Figure 15. HPFTP Instrumented Nozzle.

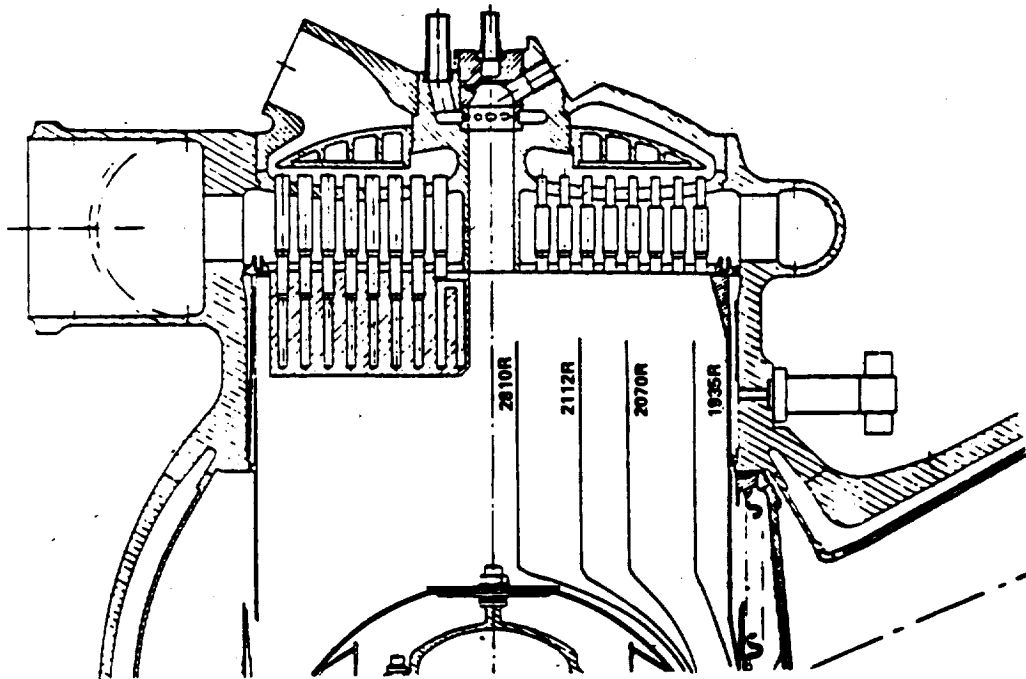


Figure 16. Fuel Preburner Temperature Distribution.

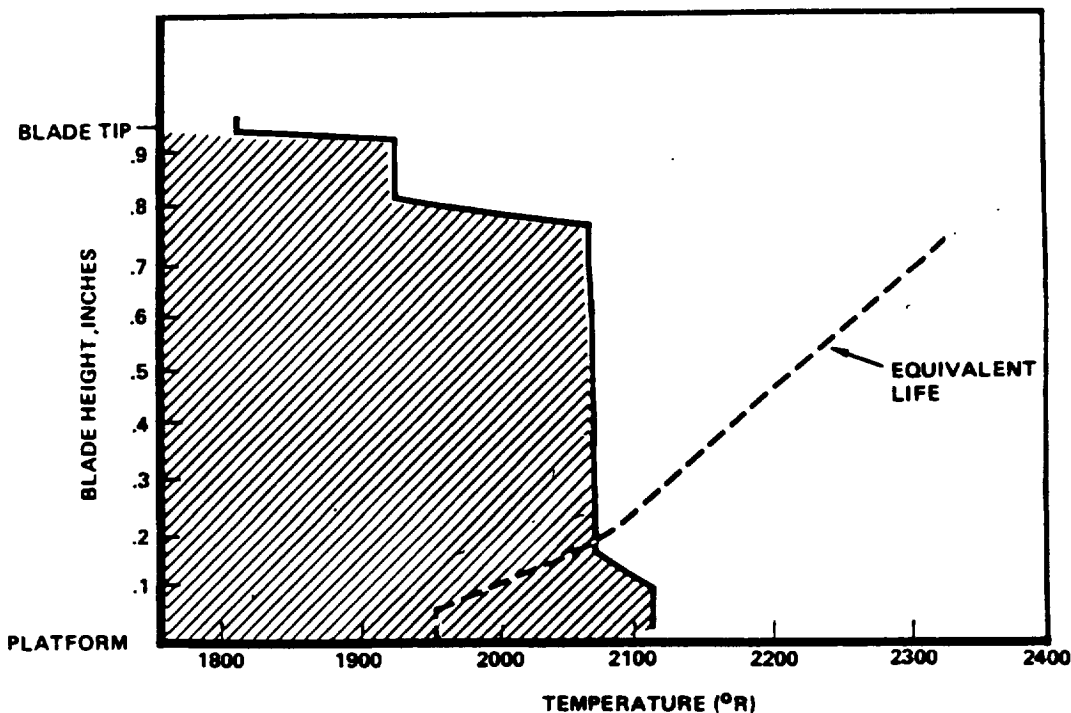


Figure 17. HPFTP First Stage Blade Temperature Profile.

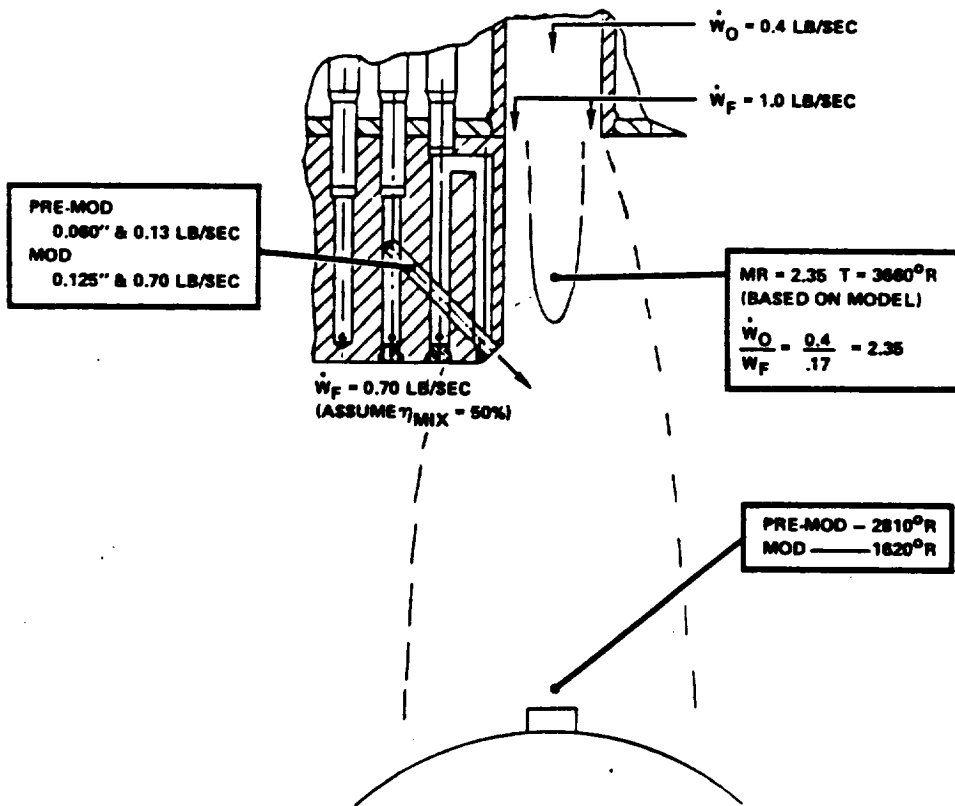


Figure 18. Fuel Preburner Baffle Modification (ASI Core Temp.).

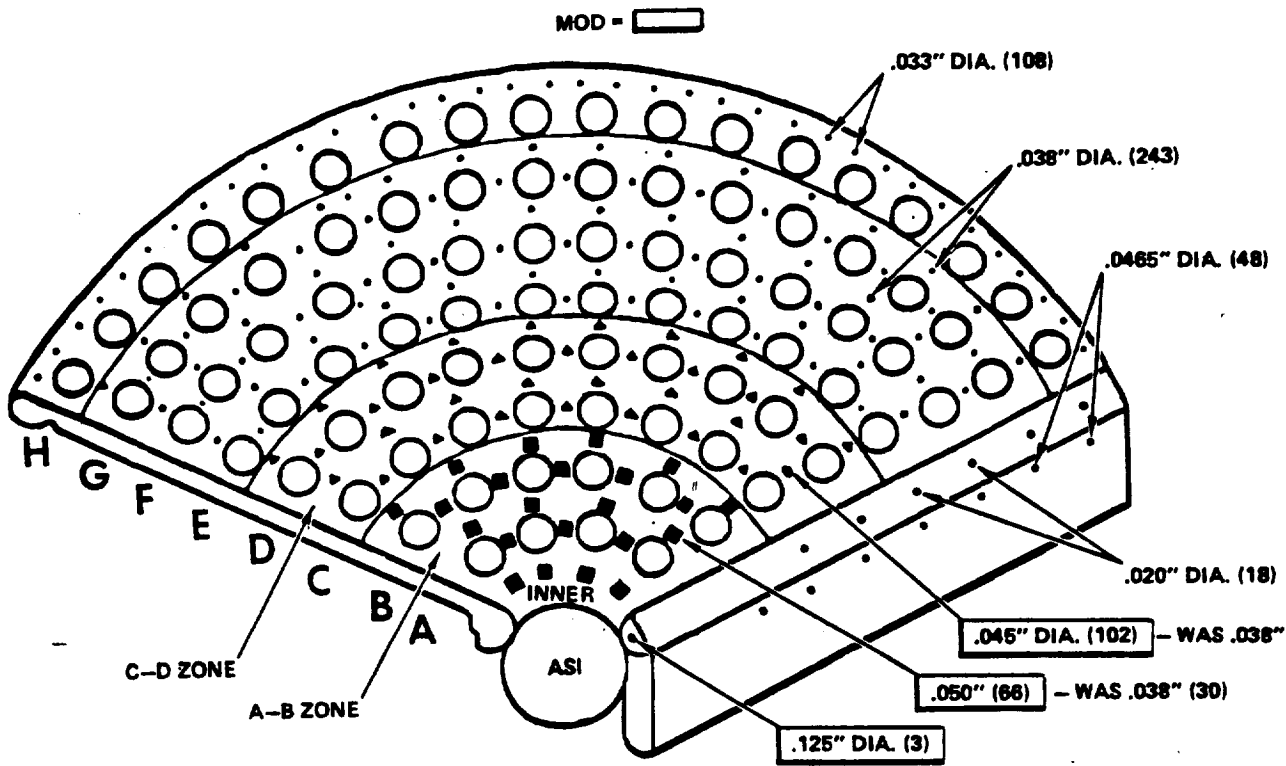


Figure 19. Fuel Preburner Injector Modification.

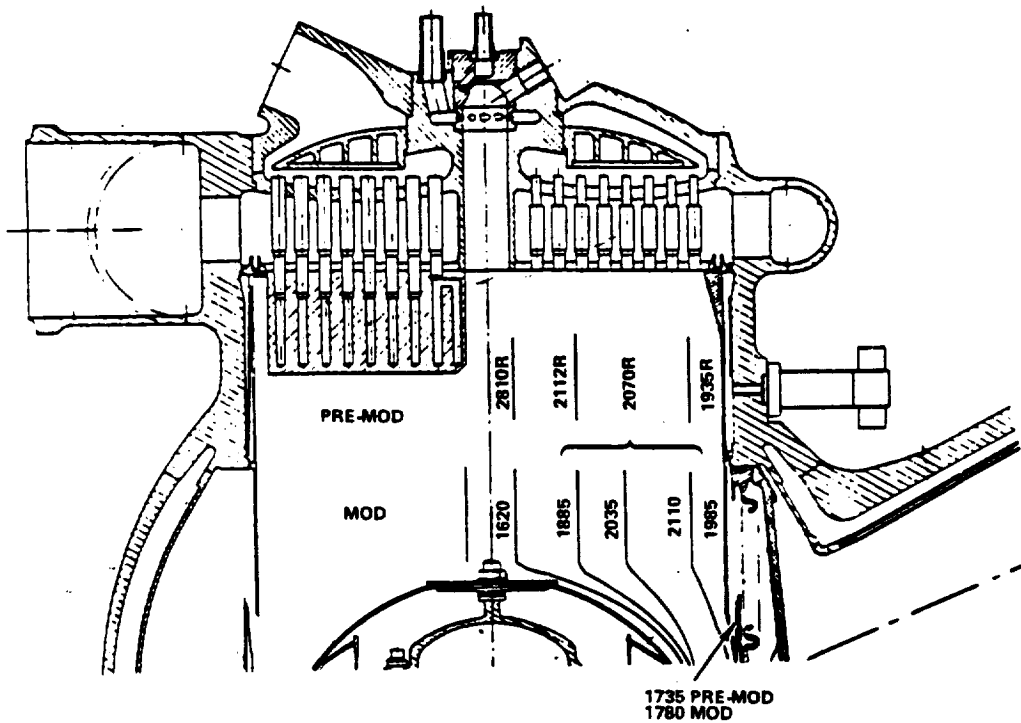


Figure 20. Fuel Preburner Temperature Comparisons Radial Distribution.

ORIGINAL
OF POCING

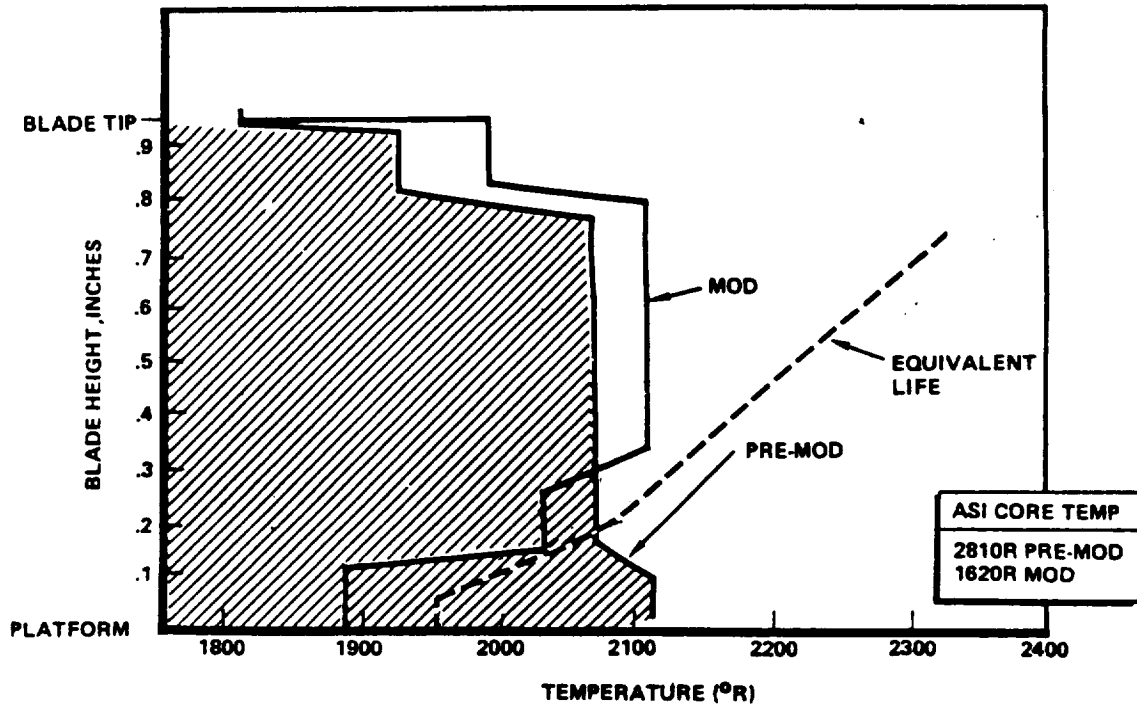


Figure 21. HPFTP First Stage Blade Temperature Profile.

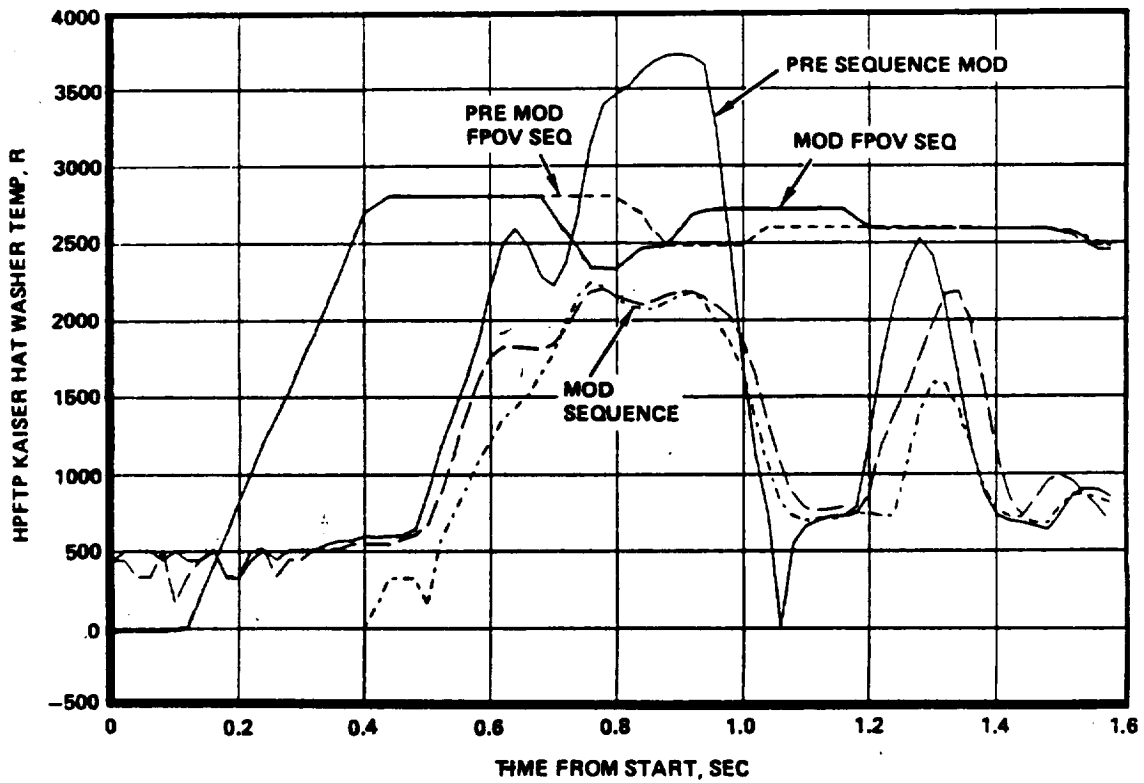


Figure 22. Ignition Temperature Spike Sequence Modification.

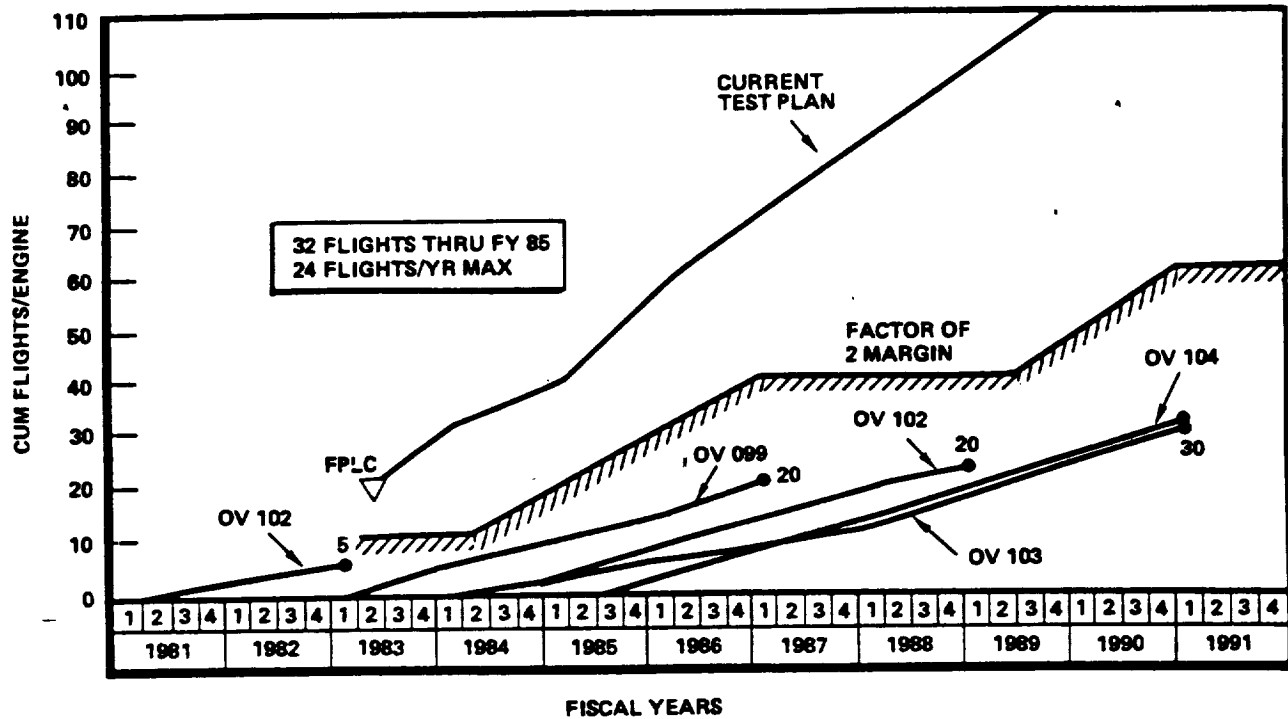


Figure 23. Flight Certification Extension Testing Plan Exceeds Factor of 2 Margin Requirements.

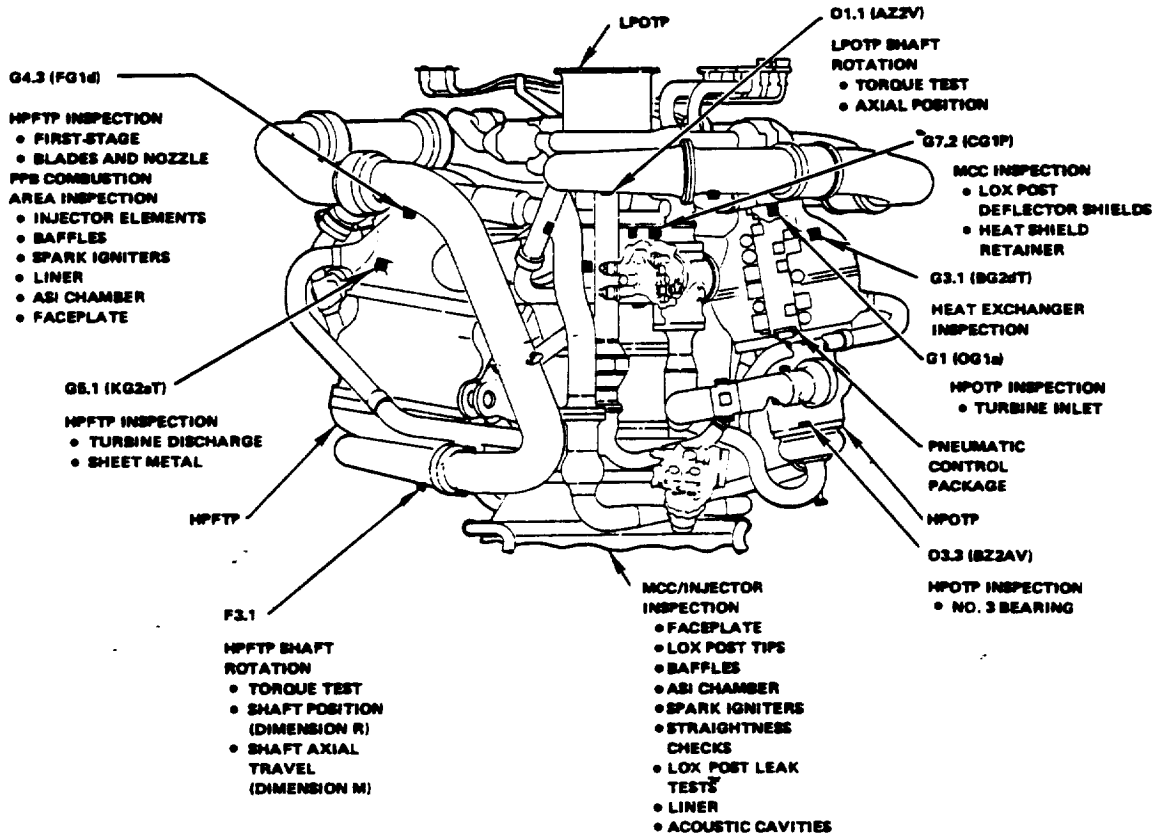


Figure 24. Internal Inspection and Shaft Rotation Access LPOTP Side of Engine.

ORIGINAL PAGE IS
OF POOR QUALITY

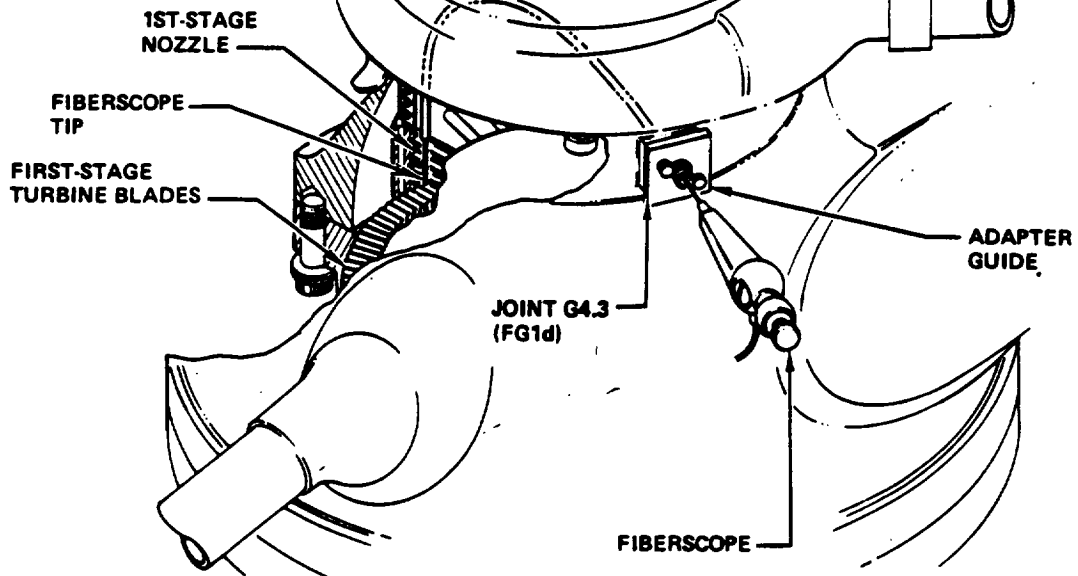


Figure 25. HPFTP First Stage Turbine Blades and Nozzle.

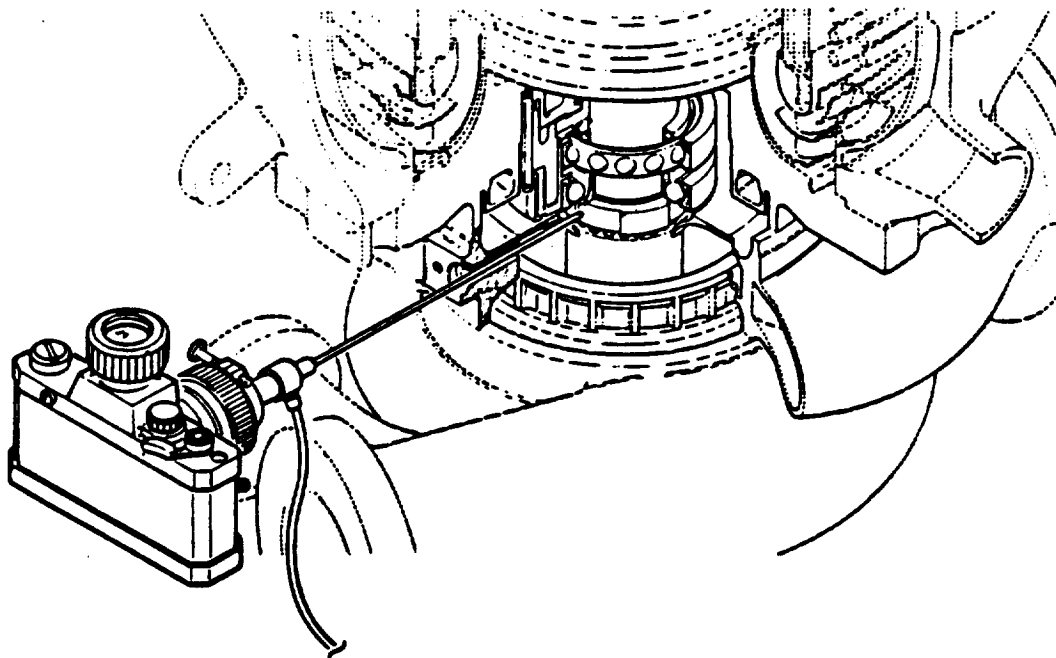


Figure 26. HPOTP No. 3 Bearing Photographic Condition Recording.

SOLID ROCKET MOTOR CERTIFICATION TO MEET SPACE SHUTTLE REQUIREMENTS:
FROM CHALLENGE TO ACHIEVEMENT

John Q. Miller, National Aeronautics and Space Administration
George C. Marshall Space Flight Center, AL and
Joe C. Kilminster, Morton Thiokol, Inc., Brigham City, UT

ABSTRACT

The Solid Rocket Motor (SRM) for the Space Shuttle was by contract requirement, a state-of-the art motor design to the maximum extent possible.

There were three design requirements for which there was no existing solid rocket motor experience. These were: the requirement for a unique thrust-time trace to meet unique Space Shuttle requirements, the requirement for 20 uses of the principal hardware, and the requirement for a moveable nozzle with an 8° omniaxial vectoring capability.

These three unique requirements are discussed and the solutions presented.

DESCRIPTION

THRUST-TIME TRACE

The development of the solid rocket motor thrust-time trace requirements and certification will be discussed.

Requirement

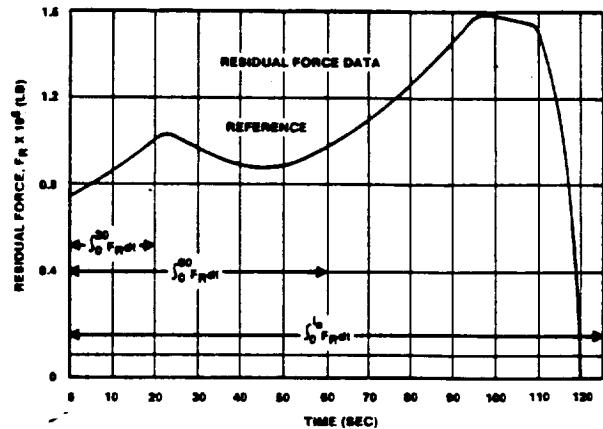
Establishment of the SRM thrust-time characteristic was based upon a residual force requirement derived from Shuttle system flight synthesis (Figure 1). Residual force is the force required to accelerate the Shuttle vehicle along a flight path after subtracting the thrust of the SSME's. Associated with this requirement was a vehicle liftoff thrust to weight ratio of 1.5, a maximum vehicle dynamic pressure of 650 psf, and a vehicle maximum acceleration limit of 3g. The specification of SRM residual force requirements enabled the SRM contractor to conduct design trade studies which culminated in the definition of a thrust-time history meeting system requirements. The results of these studies led to a more conventional definition of SRM thrust-time history requirements (Figure 2) which are currently included in the SRM Contract End Item specification.

Analytical Design Approach

The large size of the SRM, combined with a limited number of development tests (4), precluded a "cut-and-try" approach to curve shape tailoring. Rather, analytical assessments of the various mechanisms that can affect curve shape had to be made. Results of these assessments were then used as guidelines in establishing reasonable Contract End Item (CEI) specification limits on the nominal thrust trace shape. They also were used for contingency planning in the mandrel procurement, wherein enough flexibility was built into the initial mandrel configuration to counteract the most probable extremes in curve shape. The first two static tests (DM-1 and DM-2) showed that the actual curve shape, while containing some variations, was sufficiently close to the original prediction to preclude major mandrel modification.

It was determined that the payload performance of the system was quite sensitive to the SRM thrust trace shape. In order to achieve sufficient control of the trace shape, Rockwell International (RI) and NASA decided to delineate requirements on the nominal thrust-time shape and also impose impulse gate requirements at 20 seconds and 60 seconds through which the impulse-time performance must pass.

The basic predictability limits that apply to the thrust-time curve shape of a solid rocket motor were analyzed based on previous large motor history. Results of this analysis were used to generate the envelope requirements within which the nominal thrust must fit and the impulse gate requirements on nominal performance (Figure 2).



NOMENCLATURE:
 F_R - INSTANTANEOUS RESIDUAL FORCE, LBF
 L_0 - MAXIMUM ALLOWABLE ACTION TIME, SEC

FIGURE 1. SRM PERFORMANCE REQUIREMENTS

Historic data were examined to determine the nature of the significant factors which contribute to predictability of solid motor ballistic performance. Examination was limited to those factors that contribute to predictability of thrust-time curve shape and thus affect the mandrel design. Easily countered factors such as the propellant burn rate were not considered, since a minor tailoring of the propellant formulation can easily modify the burning rate in accordance with a change in target rate. These changes can be implemented at any time in the program.

One of the most widely recognized factors that is not entirely predictable and which affects curve shape is erosive burning. Examination of large motor data, particularly Titan seven-segment data, indicated that large motor erosive burning did not significantly affect ballistic performance. It was concluded that limiting the Shuttle port mass velocities to levels at or below those experienced by the Titan seven-segment motors would preclude or minimize erosive burning.

Early in this literature search, a peculiar factor affecting curve shape was recognized. In many motors, both large and small, the actual trace shapes were more "humped" than the theoretical traces. Generally, actual traces are initially lower than the theoretical, higher in the middle of burn, and lower again near the end of web time. This phenomenon was given the acronym BARF--Burning Anomaly Rate Factor.

BARF was found in almost all of the 156 in. motors. It was also found in all the Aerojet 260 in. motors and apparently in the Titan seven-segment motor to a small degree. However, BARF did not occur in the Titan III C/D (five-segment motor). It is also found in many smaller motors, a notable example being the 5 in. circular perforation motor (5 in. CP) used by Thiokol for burn rate evaluation. A similar phenomenon is found in the Super BATES motor.

Based upon the frequency of occurrence of BARF in large motors, it was decided that the BARF phenomenon was a distinct possibility in the Shuttle SRM and that planning for the mandrel fabrication should include the flexibility to counter it, should it occur.

The other parameters which were considered potentially significant to a degree that could affect mandrel design were predictability of I_{sp} and nozzle throat erosion. It should be pointed out that the I_{sp} loss prediction technique was, at the time, in a relatively early stage of development. Since then, the model has been improved such that the prediction of delivered I_{sp} is well within 1%.

From the standpoint of mandrel design, a low I_{sp} is far more of a problem than a high I_{sp} because the constraint imposed by the maximum design pressure, used in the hardware design, precluded any increase in mass flow rate during the first 20 seconds without an increase in throat area. Any increase in throat area was precluded by hardware/schedule constraints. Thus the ability to recover from the effects of low I_{sp} impacts was considered in this analysis.

It should be noted that a 1% predictability degradation was being imposed upon a baseline nominal vacuum I_{sp} prediction of 262.2 seconds, which was itself felt to be slightly conservative since, at that time, the I_{sp} loss prediction technique indicated the I_{sp} would be slightly higher. The philosophy of introducing a small degree of conservatism into the prediction of I_{sp} was suggested by MSFC.

The nominal baseline vacuum specific impulse was conservatively predicted to be 262.2 seconds. The throat erosion rate was assumed to be 0.008 ips; and accuracy of throat erosion predictability was assumed to be $\pm 15\%$, based upon judgment of experienced nozzle designers.

It was assumed that I_{sp} , BARF and throat erosion rate were independent variables. This led to a statistical approach in the analysis wherein each effect was treated as an independent variable, and its effect was assessed independently. Impact of BARF on thrust performance is presented in Figure 3. The one percent low I_{sp} would result in a uniform one percent thrust reduction throughout operation.

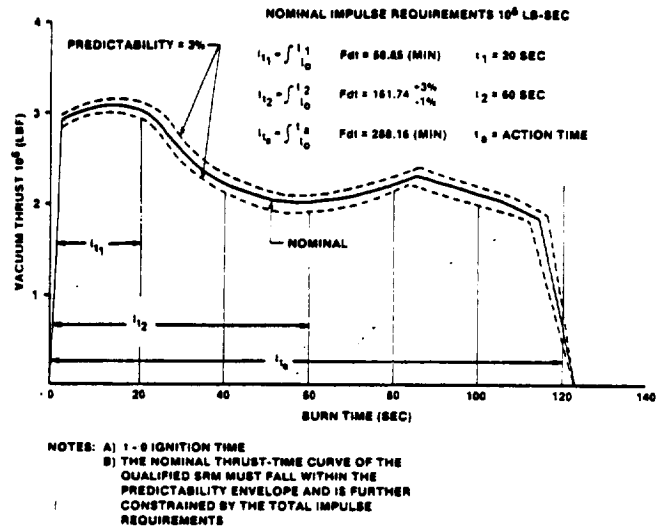


FIGURE 2. SRM NOMINAL PERFORMANCE REQUIREMENTS (VACUUM, 60°F)

Effect of throat erosion rate variation (+ 15%) proved to be minimal; at no time did the thrust deviation exceed 0.26% of nominal.

Since a mandrel modification after the first static test was allowed for in the planning, analytical grain design modifications were undertaken to counteract the effects of the assumed BARF and low I_{sp} .

Care was taken in the analytical redesign phase to limit the mandrel changes, since any mandrel modification is a relatively expensive, long lead time effort. Given this constraint, it was impossible to completely counteract these effects and small residual impulse deviations remained at the various gates as well as small residual deviations in the thrust-time curve shapes. The total residual thrust and impulse deviations at the various times were then determined by a root sum squaring of the three components. These residual deviations then formed the base for establishing specification limits, although more information was needed to completely quantify the limits.

Figure 4 presents the basic grain design. No design modifications were necessary to counteract low I_{sp} or to counteract BARF.

At this point, information was not available to completely quantify CEI specification limits on impulse gates and the thrust envelope. This was because the grain design modifications were to be made only after one motor firing and there was a distinct possibility that it would not be a nominal motor, due to normal ballistic performance reproducibility. Further, the accuracy of the data acquisition system (+ 0.5%) impact on these uncertainties needed to be assessed and added into the specified tolerances.

The potential dispersion that a particular motor could have from the nominal performance of a population was estimated by reviewing Stage I Minuteman data. A population of 23 motors was examined to determine the coefficient of variation in impulse yielded at 38% of web burn. This variation, when multiplied by an appropriate K factor, was assumed to represent the maximum limit that the DM-1 impulse could be dispersed from the true population nominal at 20 seconds (17.8% of web burn) and 60 seconds (53.3% of burn) with a 90% confidence and 99% probability. The resulting dispersion was 1.55%. This also is a reasonable estimate for the instantaneous thrust dispersion at any time.

The assessment of impulse reproducibility at a fixed percent web burn was made to factor out the effect of burn rate, since predictability of nominal burn rate was not a pertinent variable in this study.

The total potential dispersion in impulse values at 20 and 60 seconds and in the thrust time curve were then estimated by root-sum-squaring the residual components due to BARF, I_{sp} predictability, throat erosion rate predictability, normal motor reproducibility, and instrumentation accuracy. Tables I and II present the value of each component and the total (RSS) value, respectively, for impulse gates and thrust-time curve, and compare these estimates to those finally selected for the CEI specification.

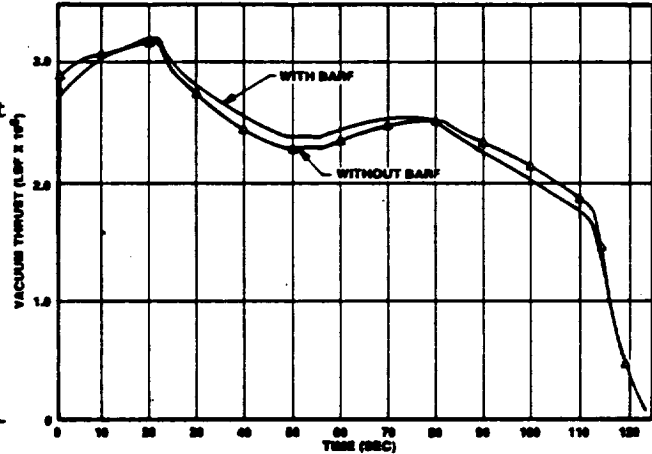


FIGURE 3. EFFECT OF BARF ON TC-227A-75 THRUST PERFORMANCE

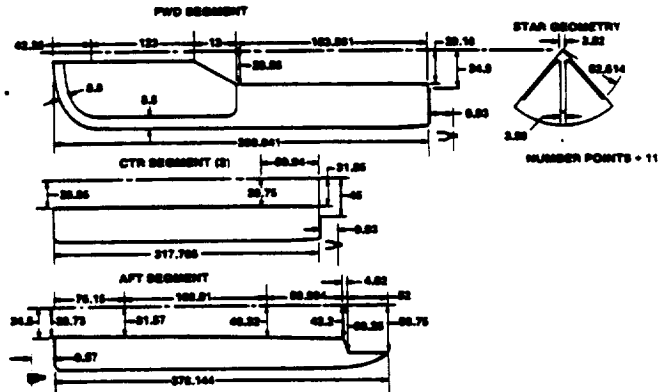


FIGURE 4. BASIC GRAIN DESIGN

TABLE I
POTENTIAL DEVIATION FROM PREDICTED IMPULSE AT 20 SEC, 60 SEC, AND ACTION TIME

Time (sec)	Nominal Predicted Vacuum Impulse (Mlb-sec)	Potential Deviation From Predicted Normal (%)					Total (RSS)	Selected CEI Specification Limit About Population Nominal (%)
		Due to BARF	Due to I _{sp}	Due to Throat Erosion	Due to Instrumentation	Due to Motor Reproducibility		
20	60.03	0.611	1.017	0.05	0.90	1.525	+ 2.0	-2.0 (minimum)
60	161.74	0.178	0.479	0.125	0.90	1.525	+ 1.7	+3.0, -1.0
Action Time	291.07	0.070	0.872	0.130	0.90	0.0	+ 1.0	-1.0 (minimum)

TABLE II
POTENTIAL DEVIATION FROM PREDICTED THRUST AT VARIOUS TIME

Time (sec)	Nominal Predicted Vacuum Thrust (lb)	Potential Deviation From Predicted Nominal Thrust, Percent Nominal					Total (RSS)	Selected CEI Specification Limit About Population Nominal, % Nominal
		Due to BARF	Due to Low I _{sp}	Due to Throat Erosion	Due to Instrumentation	Due to Motor Reproducibility		
1	2,849,000	+0.663	-0.718	0.0	± 0.5	± 1.5	1.9	3.0
10	3,065,000	+1.095	-0.852	0.05	± 0.5	± 1.5	2.1	3.0
20	3,157,000	-0.394	-1.017	0.10	± 0.5	± 1.5	1.9	3.0
30	2,729,000	+0.465	+4.504	0.13	± 0.5	± 1.5	4.8	3.0
40	2,453,000	-0.487	+5.992	0.17	± 0.5	± 1.5	6.2	3.0
50	2,259,000	-0.436	+1.195	0.21	± 0.5	± 1.5	2.0	3.0
60	2,325,000	-0.233	-1.831	0.25	± 0.5	± 1.5	2.4	3.0
70	2,465,000	-0.321	-1.982	0.25	± 0.5	± 1.5	2.7	3.0
80	2,523,000	-0.542	-2.324	0.25	± 0.5	± 1.5	2.9	3.0
90	2,330,000	-1.428	-2.588	0.26	± 0.5	± 1.5	3.4	3.0
100	2,131,000	+1.243	-2.862	0.26	± 0.5	± 1.5	3.5	3.0
110	1,881,000	+1.228	-2.355	0.26	± 0.5	± 1.5	3.1	-3.6 +3.0
120	416,000	-3.299	-6.331	0.26	± 0.5	± 1.5	7.3	-87.6 +54.6

Test Results

Data from the first two static test firings were analyzed and, based upon these data, the following observations were drawn.

1. No erosive burning was observed.
2. The BARF phenomenon did not occur.
3. Vacuum delivered specific impulse was about 265 seconds, based upon expended propellant weight.

4. During the first 6 seconds, flow conditions in the star region produced head-to-aft end stagnation pressure drops in excess of theoretical one-dimensional predictions. The flow field in the star region appears to offer the most reasonable explanation for this phenomenon. The flow in the valleys at the aft end of the star, where the valleys end (Figure 4), must be directed radially inward towards a central core of axial flow. At the star/CP transition, this core must be constrained to the diameter of the CP. If throughout the star the flow is contained within approximately this diameter, the effective port area for axial flow is considerably less than the star cross-sectional port area. The resulting pressure drops, due to axial velocity, would be of the magnitude observed. This effective port area then gradually increases until around 6 seconds, when the full port area of the star is utilized for axial flow and measured pressure drops are in good agreement with theoretical predictions.

Since there was such excellent agreement between the predicted curve shape made with the analytical model and test data, no major mandrel modification from the DM-1 configuration was required to satisfy nominal curve shape and impulse gate requirements. Figure 5 compares the projected final flight motor configuration thrust-time performance with the CEI thrust requirements, and Table III compares the projected 20 and 60 second impulse values with specification requirements. As can be seen, the nominal thrust performance will essentially satisfy the requirements in all areas.

SOLID ROCKET MOTOR CASE

The overall design philosophy for the Solid Rocket Motor case was to develop a simple, rugged and effective design based upon the use of proven techniques and concepts. Major emphasis was placed on reusability and performance reproducibility.

Each motor case consists of 11 individual case segments that are assembled into casting segments prior to propellant loading. The casting segments consist of two interchangeable center segments and forward and aft segments. There are four deliverable casting segments per SRM.

The intent here is to discuss those criteria, testing and certification requirements affecting the reusability of the SRM case.

Design Requirements

The design requirements for the Space Shuttle SRM case were evolved from three major sources: those specified by the contracting organization (NASA), those self-imposed by the motor manufacturer (Thiokol) and those which inherently exist due to fabrication, processing and transportation limits. It is not within the scope of this paper to list all requirements, but rather to list only the requirements which were considered to be the major drivers in the evolution of the current case design.

Basic Strength/Toughness/Elongation

Minimum ultimate tensile strength = 195 ksi
 Minimum tensile yield strength = 180 ksi
 Typical fracture toughness = 90 ksi $\sqrt{\text{in.}}$
 Minimum elongation = 8%
 Minimum reduction in area = 25%

General Safety Factors

Before SRM separation
 Yield factor of safety = 1.10
 Ultimate factor of safety = 1.40

After SRM separation
 Yield factor of safety = 1.10*
 Ultimate factor of safety = 1.25*

Safety Factors for Pressures

Before SRB separation
 Yield pressure = 1.2 x limit pressure
 Ultimate pressure = 1.40 x limit pressure
 After SRB separation (water recovery, etc.)
 Yield pressure = 1.10* limit pressure
 Ultimate pressure = 1.25* x limit pressure

* This is a design goal only for water impact loads.

The SRM case and its components must be capable of reuse following recovery and retrieval after submersion in sea water for up to seven days (168 hrs.) The SRM case and its components must meet the refurbishment and reuse cycle that supports the Space Shuttle System turnaround time from lift-off to lift-off.

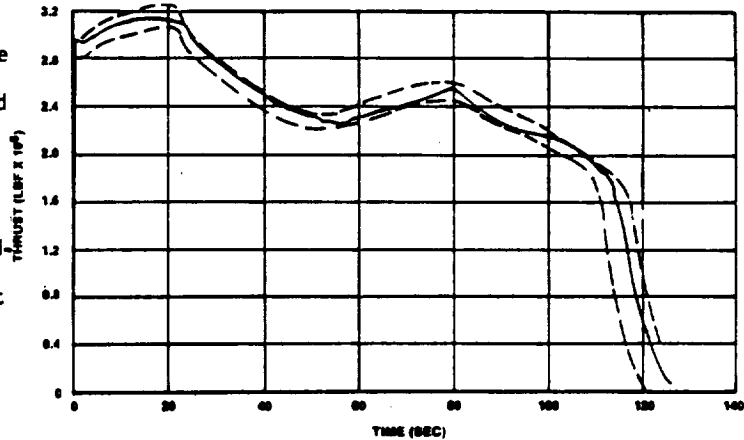


FIGURE 5. SRM-3 PRELIMINARY PREDICTION

TABLE III

FLIGHT MOTOR SRM IMPULSE COMPARED WITH
 CEI REQUIREMENTS NOMINAL, 60°F

Time (sec)	CEI Required Impulse (Mlb-sec)		Predicted Impulse (Mlb-sec)
	Min	Max	
20	58.83	----	61.20
60	160.12	166.69	164.89
Action Time	288.16	----	293.63

Design Description

The baseline SRM case design utilizes D6AC material with minimum yield and ultimate strengths of 180,000 psi and 195,000 psi, respectively.

D6AC was selected as the baseline material primarily for strength, high fracture toughness, cost, and schedule credibility. The material has been used broadly in SRM applications, and its use has resulted in a successful case program.

The baseline design has a cylindrical wall minimum thickness of 0.477 in. and a maximum expected operating pressure (MEOP) of 936 psig. The minimum burst pressure is predicted to be 1,310 psig, providing a 1.4 safety factor. The proof test pressure for each segment is 1,123 psig.

Figure 6 shows the case design schematically, with the basic dimensional data.

The segmented concept consists of nine cylindrical segments, plus a forward and an aft segment. Clevis type mechanical joints allow for a completely weld-free case assembly.

Segment Joint Testing

The segment joint, which is utilized to connect each segment to the adjacent segment(s), is in the form of a tang and clevis (Figure 7). This general type of joint has been used successfully on both 120 and 156 in. diameter test cases and on the Titan III SRM. However, the man-rating and reusability requirements of the Space Shuttle SRM case created a need for additional design features and further testing.

Initially, the general structural behavior of the joint was assessed in a bench test program. In this program, strength, fatigue, corrosive effects, and selected manufacturing anomalies were assessed through the use of full scale tension sections of the segment joint. A total of 10 tests were conducted which included combinations of: nominal, oversized holes, flawed, missing pins, abnormally low toughness and highly corroded specimens. A summary of the results obtained is presented in Table IV. All testing was highly successful and resulted in predicted factors of safety well above the required 1.4 value.

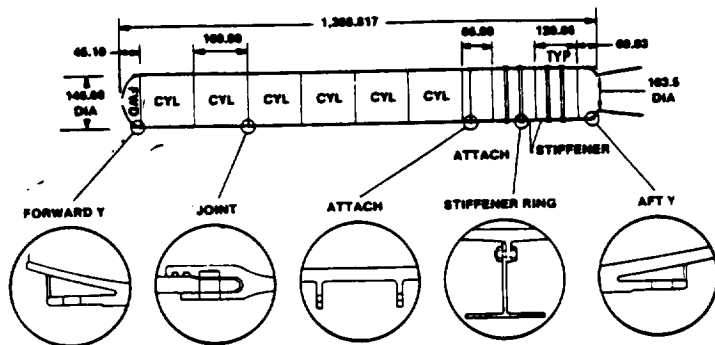


FIGURE 6. SRM CASE

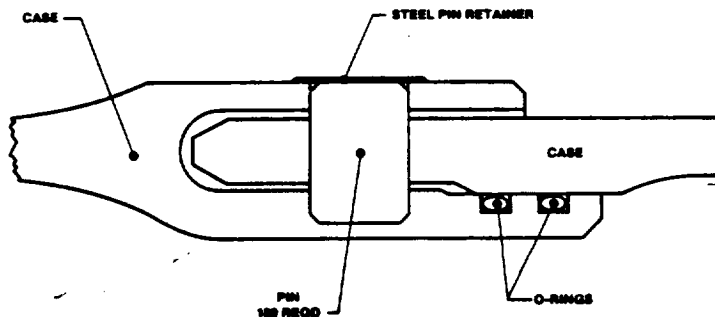


FIGURE 7. SEGMENT JOINT DETAIL

Reusability

Technological excellence is required to develop a highly reliable SRM booster on the basis of the multiple reuse concept. Fracture control is an important area of technology that demands close attention.

The need for a comprehensive, well controlled fracture control program is the underlying theme in all case design, fabrication, inspection and refurbishment efforts that relate to case reuse. Accordingly, a program was developed that integrates checks and controls into the case design fabrication procedure to insure that the case will completely fulfill the cyclic (reuse) mission requirements.

There are basically two methods of insuring that a critical flaw does not exist in design hardware. It must be precluded by nondestructive inspection NDI techniques, or the hardware must be demonstrated by proof testing prior to use. The requirements of the Space Shuttle program are such that both techniques are employed.

TABLE IV
SUMMARY OF JOINT TESTS

Specimen	Test No.	Type	Test	Failure Load (10 ⁶ lb)	Factor of Safety	Cycles	Remarks
1	1	5 Pin - Nominal	Burst	1.04	2.23	---	Pin and clevis arm failure.
2	2	5 Pin - Nominal	Burst	1.00	2.27	---	Pin and clevis arm failure.
3	3	5 Pin - Nominal	Cyclic and Burst	1.01	2.17	240	After cycling, no pin marked and minor hole elongation. Clevis arm failure.
4	6	5 Pin - Oversize Hole (0.010 in. large dia)	Burst	1.00	2.15	---	Clevis holes bearing failure. Clevis arms spread.
5	5	4 Pin - Nominal	Burst	0.80	2.15	---	Specimen did not separate. Pin bending and clevis hole bearing failure.
6	7	5 Pin - Bushing (0.050 in. wall thickness - DGAC)	Cyclic and Burst	1.025	2.20	160	No bushing deformation after cycling. Clevis arm failure.
7	4	5 Pin - 1st Flaw (0.050 deep - Jewelers File)	Cyclic and Burst	0.80	1.72	160	No crack growth. Notch failure between tang holes at 800 K.
8	8	5 Pin - 2nd Flaw (0.050 deep - EPDM)	Cyclic and Burst	0.855	1.83	160	Crack between tang holes at 685 K on burst cycle. Burst 855 K.
9	9	5 Pin - Low KJC - Flaw (0.050 deep - EPDM)	Cyclic and Burst	0.825	1.77	1	Crack between holes at 453 K during 1st cycle at tang flaw.
10	10	5 Pin - Corrosion	Cyclic and Burst	1.025	2.20	240	Clevis Failure.

4 Pin Joint
Limit Load = 373,000 lb (Maximum Flight Load)
Ultimate = 1.4 Limit = 523,000 lb

5 Pin Joint
Limit Load = 466,000 lb (Maximum Flight Load)
18: Proof = 515,000 lb
Ultimate = 1.40 Limit = 653,000 lb

The first requirement stipulates that the largest flaw which can escape detection with specified NDI will not grow to critical size through 20 uses of the case. One use of the case encompasses all events associated with its use as it proceeds through the fabrication, loading, launch, recovery, refurbishment and proof test sequence. Compliance to this requirement is demonstrated through the application of principles of linear fracture mechanics.

The second requirement for the SRM case associated with fracture mechanics/flaw growth principles requires that the case be proof tested prior to flight to a load level which will screen out (by case failure) all existing flaws which are critical for flight, or would become critical if the flaw were allowed to grow (theoretically) through four missions. One mission is defined as one motor operating (pressure) cycle plus one water impact sequence.

MOVABLE NOZZLE WITH 8° OMNIAxIAL VECTOR CAPABILITY

The Solid Rocket Motor nozzle is a convergent-divergent moveable design containing an aft pivot point flexible bearing as the gimbal mechanism (Figures 8 and 9). The nozzle is partially submerged to minimize erosive conditions in the aft end of the motor and to fit within envelope length limitations. The nozzle provides attach points for the thrust vector control (TVC) actuators, an attachment structure to mate with the motor aft closure, a capability for jettisoning a part of the aft exit cone after burnout to reduce water impact damage to the nozzle flexible bearing.

TVC for the Space Shuttle SRM is obtained by omniaxial vectoring of the nozzle. The vector requirements of the system, the impact of multiple reuse on the components, and the unique problems associated with a large flexible bearing are discussed. The subscale bearing development program is also presented.

Requirements

Omniaxial requirements for the SRM nozzles are shown in Figure 10. The 7.1 deg of nozzle vectoring required in the vehicle's pitch and yaw axes decreases to 5 deg in the 45 deg plane between the pitch and yaw axes. By locating the actuators in this 45 deg plane, they could be designed with a stroke equivalent to 5 deg, yet, when operated in unison, provide the total 7.1 deg required in the

pitch and yaw planes. The flexible bearing which permits the movement of the nozzle was designed for a maximum omniaxial nozzle vectoring of ± 8 deg; thus, allowance of 0.9 deg was incorporated in the design to allow for geometric misalignment and actuator overtravel. Requirements for the nozzle bearing are tabulated on Table V.

The requirement was placed upon the nozzle flexible bearing elastomer that it be reused nine times. The reuse requirement was a significant driver in the design of the nozzle flexible bearing. Components were designed so that they would withstand the high loads encountered at the time of water impact.

Flexible Bearing Design

The flexible bearing consists of alternate lamina of natural rubber elastomer and steel shims between a forward and aft end ring (Figure 11). Ten metal shims and 11 layers of elastomer are vulcanized to each other and the end rings. The elastomer provides the flexibility that permits the nozzle to vector. The flexible bearing is designed to be used 10 times without replacing the elastomer pads. After each flight the flexible bearing is disassembled from the nozzle and placed in a test fixture, where extensive tests are conducted to insure its integrity prior to reuse in another nozzle. Calculations and subscale test data show that the elastomer will be suitable for a minimum of 10 uses. Should the testing between flights indicate that the bearing elastomer has been damaged during a flight or recovery operation, the bearing can be disassembled by cutting it apart and the metal parts can be refurbished and reused. The parts can then be cleaned and the bearing remolded with new elastomer pads. Experience in the flight program has shown that bearing reuse is feasible and a bearing in STS-7 has been used three times in static tests as well as on STS-2 flight.

Testing

The flexible bearing is the largest ever built for a flight program. While the design concepts were state-of-the-art, it was deemed advisable to conduct a development program to assure that the bearing could

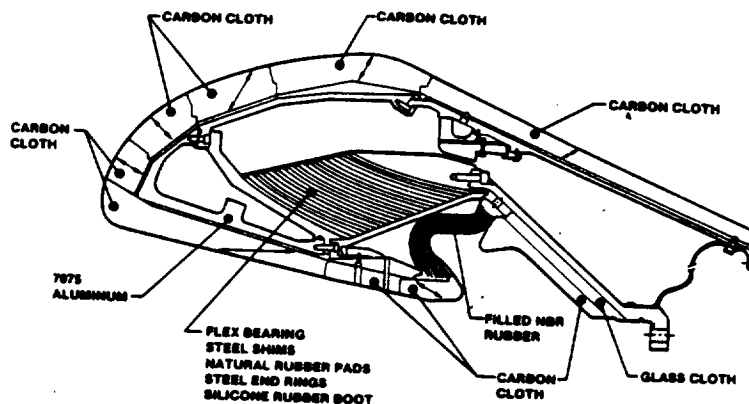


FIGURE 8. NOZZLE FORWARD ASSEMBLY

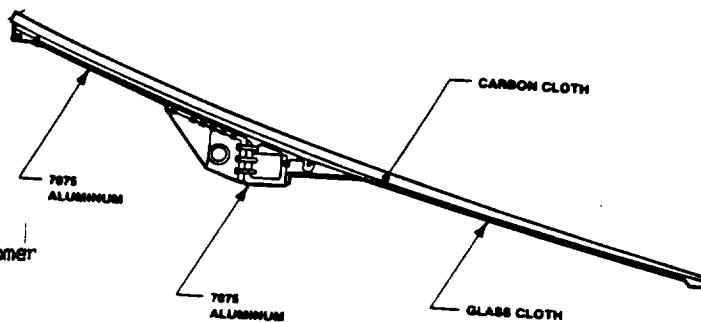


FIGURE 9. NOZZLE EXIT CONE ASSEMBLY

OMNIAXIAL DEFLECTION REQUIREMENT

- 7.1 DEG CONTROL REQUIREMENT
- 0.9 DEG GEOMETRICAL MISALIGNMENT
- 0.4 OVERTRAVEL
- 8.9 TOTAL OMNIAXIAL REQUIREMENT

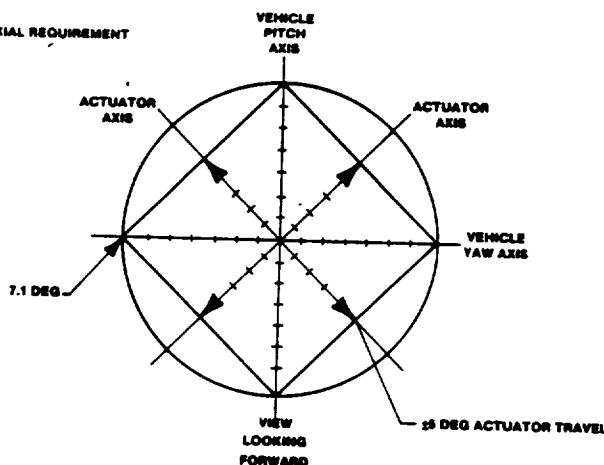


FIGURE 10. SOLID ROCKET MOTOR TVC REQUIREMENTS

be reused as required and to obtain performance characteristics such as torque, various spring constants, and the center of rotation when vectored. The development program consisted of fabricating three subscale bearings approximately one-quarter size (Figure 12) and three full size prototype bearings. Two of the three subscale bearings were, in fact, true geometric subscales designed by scaling all of the dimensions to approximately one-quarter the size of the full size bearing. The other subscale was of the same general size as the first two, but had only two metal shims and three elastomer pads, whose thicknesses were not scaled down but were the same as on the full scale bearing. The true subscale 10-shim bearings were fabricated and tested and provided data which, when scaled up to full size, indicated that the performance of the bearing would be acceptable. The bearings have also been vectored through duty cycles equivalent to the actual flight service (plus acceptance testing) that would be experienced in 10 flights. These data indicated that the fatigue characteristics of elastomer are adequate for the 10 uses required.

The major problems in the development of the full size flex bearing were the complexity of the mold (Figure 13) necessary to fabricate the bearing and the requirement to uniformly heat the rubber to the 300°F temperature without overheating the rubber next to the heating elements. Several of the early bearings experienced uneven heating and the subsequent lack of vulcanization between the rubber pads and metal shims. A very severe test has been developed where the flex bearing is longitudinally stretched two inches and inspected for unbonds. This test has shown that while several of the early bearings lacked areas of vulcanization and had to be disassembled and rebuilt, the more recent bearings have all been properly vulcanized.

The two-shim subscale bearing was primarily designed to provide processing data to confirm that thick pads of elastomer could be manufactured that would have the desired fatigue characteristics. Some performance data were also obtained with this bearing.

As mentioned, three prototype flexible bearings were also included in the development program. These bearings were fabricated and extensively tested to confirm that performance was within specifications and that the fatigue life of the elastomer in the flexible bearing environment meets the minimum 10-use criteria. These three bearings also provided repeatability data and confirmed that the abbreviated acceptance tests to be conducted on each bearing prior to use are adequate to insure that it is suitable for reuse.

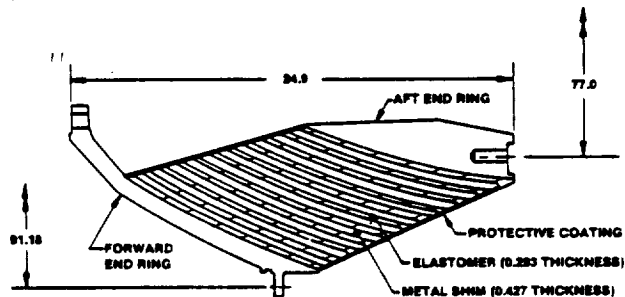
CONCLUSIONS

There have been four development motor tests and three qualification motor tests in the basic SRM development program. There have been six DDT&E (twelve instrumented SRM's) flights.

All pressure-time traces for the development, qualification and flight test motors in the DDT&E program, (less STS-6, data not yet available) when corrected to standard burn rate, pressure and propellant mean bulk temperature have fallen well within the predictability limits established in the CEI specification (Figure 14).

TABLE V
NOZZLE BEARING DESIGN REQUIREMENTS

Omniaxial Vector Capability	±8 deg	
Actuator Stall Load	103.424 lb	
Plane of Actuator		
Total Use Requirements		
Metal Parts	20 times	
Bearing Elastomer	10 times	
Safety Factors	Prior to Separation	After Separation
Structure	1.4 Ultimate	1.25 Ultimate
Nonpressure Vessel	1.1 Yield	1.1 Yield
Pressure Vessel	1.2 Yield	1.2 Yield



WEIGHT SUMMARY (LB)	
FORWARD END RING	1.357
SHIMS	3.757
ELASTOMER	29.1
AFT END RING	1.332
MISCELLANEOUS	0.3
TOTAL	6.880

FIGURE 11. FLEXIBLE BEARING CROSS SECTION

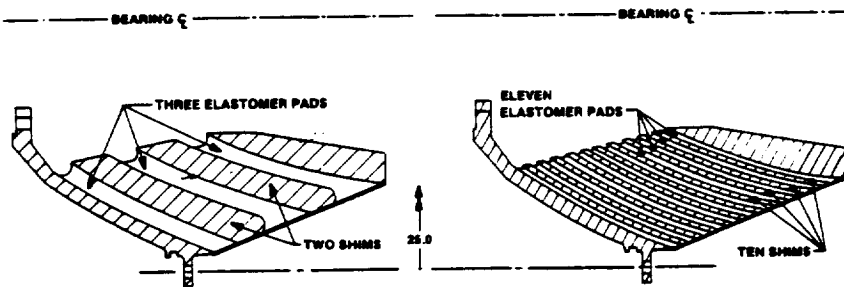


FIGURE 12. SUBSCALE FLEXIBLE BEARING DETAILS

42 motor case components used in static firings during the development program have been reused in flight. DDT&E flight six had 4 motor case components reused from DDT&E flight one.

A nozzle flexible bearing has been reused three times during the DDT&E program. Four nozzle flexible bearings have been reused in the DDT&E flight program, and one of the nozzle flexible bearings in STS-6 was reused from DDT&E flight one. It was nearly 5 years old. In all cases the demonstrated torque has been less than the limits established in the CEI specification.

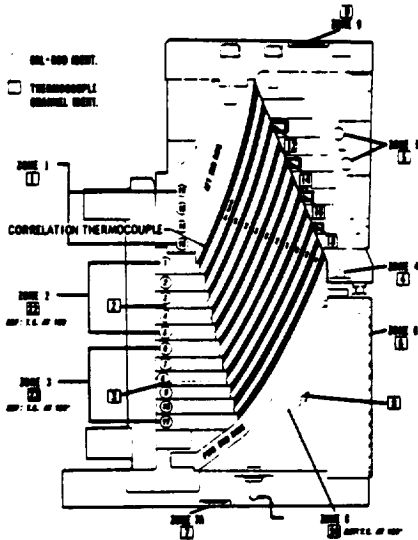


FIGURE 13. NOZZLE FLEXIBLE BEARING MOLD

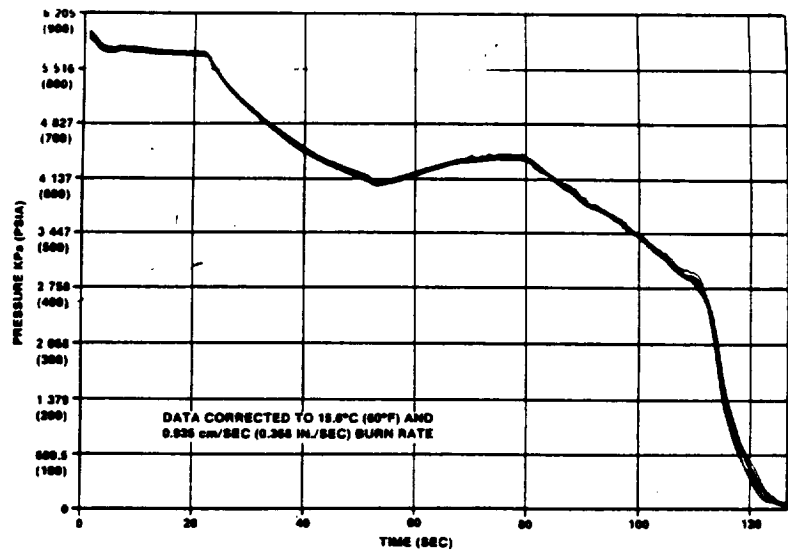


FIGURE 14. COMPOSITE OF 13 BASELINE 5M PRESSURE TRACES

ORIGINAL PAGE IS
OF POOR QUALITY.

D5
N85-16942

DEBRIS CONTROL DESIGN ACHIEVEMENTS OF THE BOOSTER SEPARATION MOTORS

Gerald W. Smith
Marshall Space Flight Center
Huntsville, Alabama

Charles A. Chase
United Technologies Corporation, Chemical Systems Division
Sunnyvale, California

ABSTRACT

The stringent debris control requirements imposed on the design of the Space Shuttle booster separation motor are described along with the verification program implemented to ensure compliance with debris control objectives. The principal areas emphasized in the design and development of the Booster Separation Motor (BSM) relative to debris control were the propellant formulation and nozzle closures which protect the motors from aerodynamic heating and moisture. A description of the motor design requirements, the propellant formulation and verification program, and the nozzle closures design and verification are presented.

INTRODUCTION

The Space Shuttle solid rocket booster separation system is designed to ensure safe separation of each of the Solid Rocket Boosters (SRBs) from the External Tank (ET) without damaging or recontacting the Shuttle Orbiter/ET during or after separation. Eight solid BSMs, four mounted in the SRB nose frustum and four mounted externally on the aft skirt (Fig. 1), provide the impulse and momentum required to move each SRB radially outward from the ET. As the SRBs move outward from the ET, the slightly downward thrust vector of the SSME (Fig. 2) causes the orbiter to be exposed to the exhaust plume of the forward BSMs.

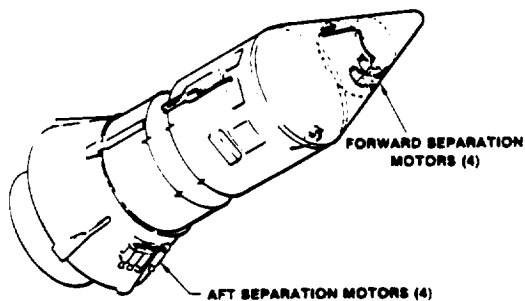


Figure 1. BSM Locations.

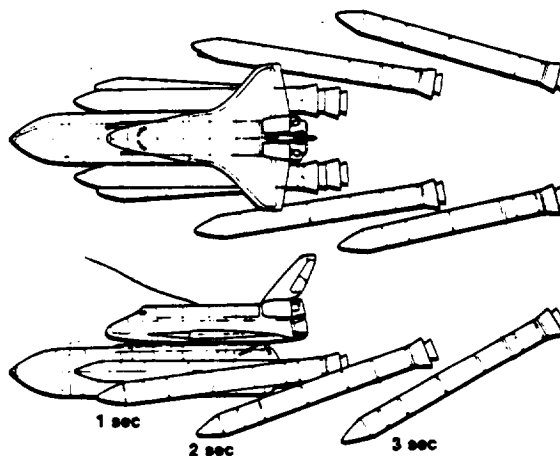


Figure 2. Computer Simulation of SRB Separation Sequence.

SRB separation nominally occurs at a flight time of 124 sec, an altitude of approximately 140,000 ft, and a mach number of 4.5. The initial conditions for separation (dynamic pressure, angle of attack, sideslip angle, and body angular rates) will be different for each flight depending on ascent winds, atmospheric conditions, SRB thrust talloff mismatch, flight control system status, and SSME operating status. A set of design initial conditions was defined which reflected a composite of nominal and malfunction flight conditions and provided the basis for sizing the system. The BSM thrust and total impulse requirements were derived from these design initial conditions (Table 1).

DESIGN DRIVERS FOR DEBRIS CONTROL

Plume exposure tests of Orbiter and ET Thermal Protection System (TPS) materials conducted at the Air Force Arnold Engineering Development Center indicated that even short-term exposure of these

TABLE 1. BSM PERFORMANCE AND DESIGN REQUIREMENTS

o PERFORMANCE

Thrust level (max), lbf	29,000
Web action time average thrust (min), lbf	18,500
Web action time impulse (min), lb-sec	14,000
Action time impulse (min), lb-sec	15,000
Web action time (max), sec	0.8
Ignition interval to 75% max thrust, msec	30 to 100
Time to thrust equal to or greater than web action average thrust (max), msec	200
Time from end of web action time (EWAT) to 50% of pressure at EWAT, msec	100
Maximum pressure at EWAT, psi	2,000
Propellant bulk temperature, °F	30 to 120

o DESIGN

Weight (max), lb	154
Length (max), in.	34.6
Diameter (max) in.	12.88
Nozzle cant angle, degrees	20
Propellant stability additives (max) %	2
Propellant burning rate additives (max) %	1

materials to the solid rocket motor exhaust plume resulted in extensive material damage. TPS materials exposed to exhaust plumes in a manner that simulated the anticipated flight conditions relative to separation distance and exposure time experienced rather significant erosion and particle debris damage. The Orbiter insulation, consisting of rigidized silica fiber felt with a thin borosilicate glass coating, is designed for multiple reuses, and replacement of the TPS tiles is a costly process. Aluminum oxide particles and debris from sources such as igniter tape, igniter propellant, and nozzle materials eroded and fractured the TPS coating to the extent that similar erosion during flight would require replacement of the TPS.

The sensitivity of the Orbiter/ET TPS to exhaust plume debris resulted in relocation of the BSMs on the SRB and a reduced motor burning time requirement. The forward BSMs were moved from the SRB forward skirts to the nose frustum and oriented as shown in Figure 3. This location and orientation, combined with a maximum burning time requirement of 0.8 sec, minimizes exposure of the TPS to the plume during normal separation conditions. In a similar manner, the aft BSMs were moved to the SRB aft skirt and the nozzle canted 20 deg to eliminate plume impingement on lower surfaces of the Orbiter. Since the TPS can be exposed to the motor exhaust plumes for short periods in off-nominal or abort separations, additional design constraints were imposed on the BSM to minimize the amount of damage.

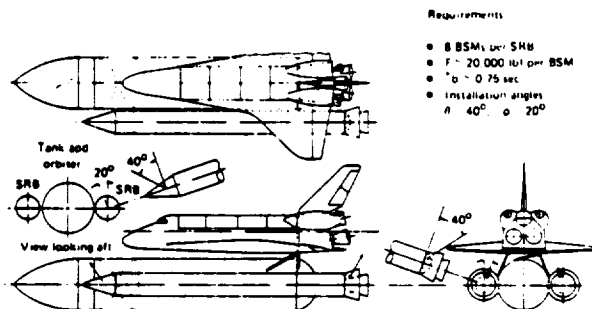


Figure 3. Shuttle Separation System.

PERFORMANCE AND DESIGN CONSTRAINTS

The BSM performance requirements reflect an emphasis on control of exhaust debris. The requirements that motor burning time shall not exceed 0.8 sec and that tailoff pressure shall decay to 50% within 100 msec were established to terminate the motor burning time and collapse the exhaust plume before the Orbiter could intersect the motor plume boundary. In addition, the contoured nozzle is designed to minimize the expansion of the gaseous and particulate plume at EWAT and during tailoff.

Control of exhaust debris is reflected in the design requirements for the igniter, nozzle, nozzle closures, and propellant. The nozzle and igniter were designed to preclude the generation of debris thus limiting the types of materials and coatings that could be used. Propellant particulate debris is controlled by limiting the amount of burning rate and stability additives to 1 and 2%, respectively. A similar constraint is imposed on the igniter propellant. Additionally, the igniter design was modified to eliminate the ejection of unburned igniter and boost charge particulates. The igniter design features a booster charge retainer with mylar sheet to contain the charge during handling and shipping and a radially perforated igniter case to ensure complete burning of the booster charge and igniter propellants before exiting the nozzle.

PROPELLANT FORMULATION

The selection of 1% and 2% limitations on the burn rate and stability additives represented a compromise between minimizing particulate debris and ensuring adequate combustion stability margin. Rigorous combustion stability requirements were imposed on the motor design and the development program to ensure stable operation of the motor. Two propellant formulations were selected for initial development testing, the baseline propellant containing 2% aluminum powder and an alternate containing a mix of aluminum and alumina. The baseline propellant selected for the BSM is an 86% solids/2% aluminum HTPB propellant with formulation and key properties as shown in Table 2.

TABLE 2. UTP - 19,048 BSM PROPELLANT

o FORMULATION	
Hydroxy-terminated polybutadiene binder, %	14.0
Iron oxide catalyst, %	0.25
Aluminum powder, %	2.00
Ammonium perchlorate, %	83.75
o PROPERTIES	
Theoretical specific impulse, sec	250
Theoretical density, lb/in. ³	0.0614
Burning rate at 1500 psia/70°F, in./sec	0.8
Pressure exponent	0.45
Tensile strength at 70°F, psi	200
Elongation at 70°F, %	40
End of mix viscosity (140°F), kps	5
Pot-life, hr	20
Autoignition temperature, °F	
10 sec	685
30 sec	570
60 min	420

Combustion stability was a major consideration in the design of the BSM since propellants with low solid particles in the exhaust tend to produce chamber pressure oscillations. The evaluation of combustion stability included (1) a preliminary stability evaluation based on an analysis of interactions between combustion and flowfield and (2) pulse tests in prototype and development motors to determine experimentally the stability of the motor. The stability of pressure disturbances of small amplitude is balanced between the combustion processes that supply energy to the disturbance and other processes that remove energy (i.e., nozzle, flow turning, and particulate damping). The evaluation of the mechanisms contributing to motor stability were evaluated using a combination of analytical techniques for particle and nozzle losses and flow turning and experimental data for pressure coupled response using T-burner results. The T-burner characterization program was conducted using the baseline propellant formulation. The tests were run at 1350 psia using the pulse-variable area method which had been used extensively for testing highly aluminized propellants. Cylindrical grains were used with area ratio variations from 2.67 to 6.67 and frequency variations from 480 to 900 hz. One series of tests was conducted with the grains preheated to approximately 130°F. The test results revealed a low response function for combustion driving indicating a reduced susceptibility towards instability in the motor.

The uncertainties involved in completely defining and characterizing the mechanisms effecting motor stability necessitated full-scale motor pulse tests. Four prototype and several development motors were pulsed at a 5% overpressure at 200 and 400 msec after ignition to demonstrate stability throughout web burn time. The results of these tests, which revealed a highly damped response to the overpressure, verified the stability of the propellant-motor combination over a wide frequency range in both the axial and transverse modes.

NOZZLE ENVIRONMENTAL COVER

The BSMs have their nozzle exit cones exposed to the atmospheric elements that exist at the Kennedy Space facility as well as the environments of launch. In order to preclude the ability of these environments from affecting the condition of components within the motor (such as, the propellant grain and igniter) it was necessary to provide a nozzle closure. This closure had to satisfy the following basic requirements:

1. Provide a humidity seal for the motor for a time period of 6 months on the launch pad.
2. Be hermetic (no leaks) when the closure is subjected to a differential pressure of 4 psi.
3. Protect the BSMs from all launch and ascent thermal and acoustic environments.
4. Open completely during the ignition transient time.
5. Do not produce any debris during ascent, separation, or booster re-entry that could possibly impact the Shuttle Orbiter.

The latter requirement is particularly challenging for the nozzle closure of the BSMs mounted within the nose cone of the Solid Rocket Boosters (SRBs). The location of the forward and aft mounted BSMs is shown in Figure 1. From Figure 2 it can be seen that the SRB nose cones are mounted forward of the Orbiter. Also, in order to obtain the outward and downward movement of the SRBs relative to Orbiter, it is necessary for these forward BSMs to have their nozzles pointed upward and inward toward the Orbiter. This creates a significant problem in that any portion of the nozzle closure that might be ejected during booster separation could severely damage the Orbiter and potentially cause loss of the mission. Thus, a major requirement imposed on the forward BSMs is that the nozzle environmental closure not only seal the motor from outside elements, open almost instantaneously during motor ignition, but that upon opening the nozzle closure must remain attached to the BSM and not allow any solid ejecta. Figures 1 and 2 show that the aft mounted BSMs are located aft of the Orbiter with their nozzles directed aft of the Orbiter. Therefore, nozzle closure debris from these motors is acceptable since it poses no threat to the Orbiter.

FORWARD BSM NOZZLE CLOSURE

A debris-free nozzle closure posed a unique design problem. Many propulsion systems have nozzle closures but they are simply ejected upon motor ignition. Therefore, no data/experience base existed upon which the BSM program could draw information. Numerous concepts were evaluated including various kevlar reinforced rubber closures that were configured to petal open and then slide forward to avoid ablation of the petals by the BSM exhaust plume. This system had promising features but introduced potential hermetic sealing problems, aeroheating concerns, and possible flight dynamics interactions that would be difficult to simulate in ground testing.

After further evaluation of potential approaches it was decided to design and test a rigid metal cover that could be made to hinge open during motor ignition as shown in Figure 4. Motor ignition was required to open the closure because this nozzle cover concept was retrofitted to the existing booster separation system and no additional ordnance devices were to be considered. The resulting primary design requirements for the forward mounted BSMs nozzle closure were:

1. Protect the BSM from ascent aeroheating (1600°R).
2. Induce no modifications or additions to the existing electrical or ordnance systems.
3. No solid ejecta can emanate from the closure during all phases of booster flight from launch through water impact.
4. Nozzle closure must survive the aerodynamic heating, acoustic, vibration, and shock environments of the booster from launch through water impact.
5. Nozzle closure must open solely from the impetus provided by motor ignition.
6. Nozzle closures cannot interfere with either the closures or exhaust plumes of adjacent BSMs (Fig. 5).

7. The hinged cover must open a minimum of 145° in order to avoid interference with the BSM exhaust plume (Fig. 6).
8. The hinged cover must open a maximum of 180° in order to avoid impacting the skin of the SRB nose fairing.

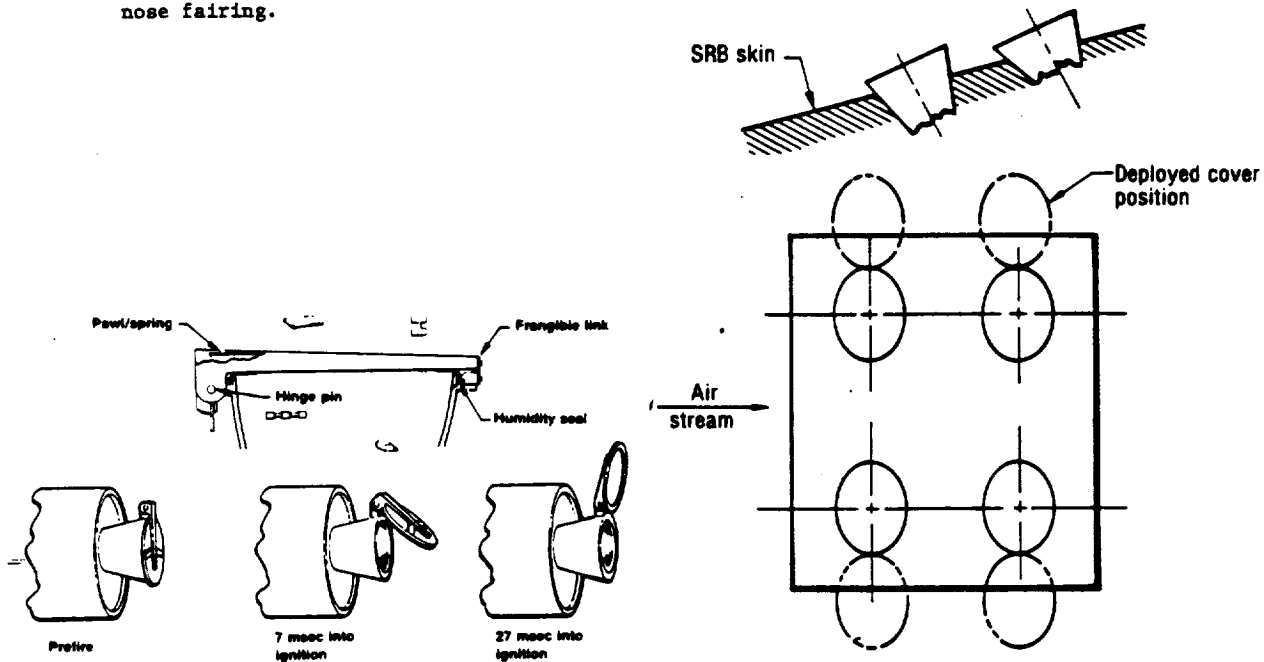


Figure 4. Basic Concept for Hinged Cover.

Figure 5. Forward BSM Nozzle Closure Relative Orientation.

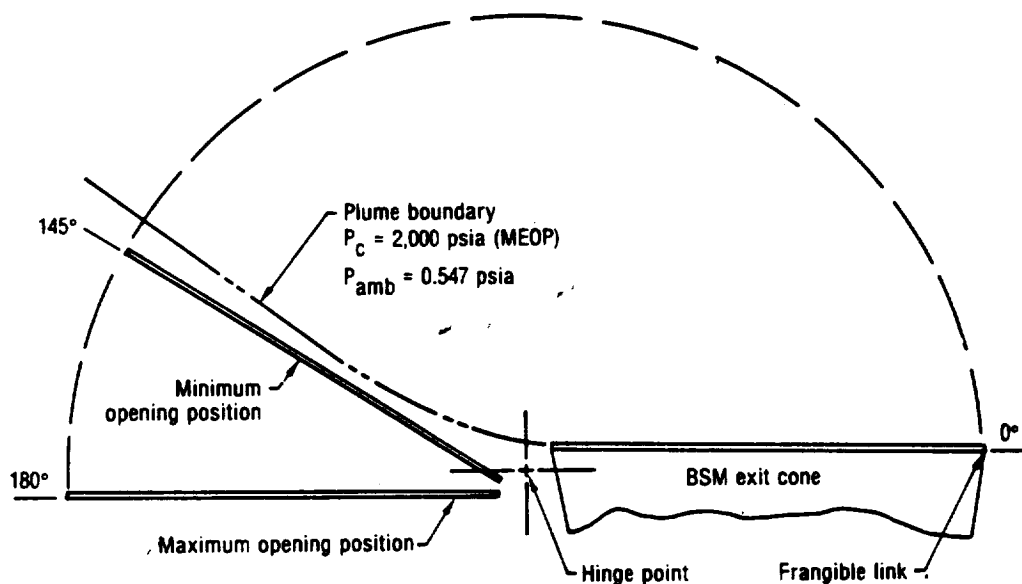


Figure 6. Forward BSM Nozzle Closure Allowable Opening Angles.

The primary design challenge for the hinged cover was to determine how the large amount of rotational energy could be absorbed in time to stop the cover between the angular position of 145 and 180 deg. Extensive study of the problem resulted in the use of a hinge-pin (axis of rotation) that would twist during cover rotation. This twisting action allowed absorption of a significant portion of the rotational energy. To absorb the remaining energy, a cantilevered secondary stop was incorporated which could accurately limit rotational travel to a maximum of 180 deg. To prevent springback to an angle less than 145 deg, a ratchet engagement device was used.

The metal hinged cover, shown in Figure 7, consists of a structurally reinforced disc supported at two points 180 deg apart. At one point, a hinge pin undergoes torsional plastic strain during operation. At the second point, 180 deg from the hinge pin, the disc is held closed by a stainless steel frangible link. At a given ignition pressure, the frangible link will break and the cover will swing open. During the opening process, the hinge pin will deform torsionally and absorb the accumulated rotational energy of the cover. At 151 deg the cover engages a locking ratchet, then finally comes to rest and locks at about 166 deg. At 155 deg the cover engages a deformable secondary stop (Fig. 8). Between 155 deg and 180 deg the cover energy is, therefore, being absorbed by both the torsion pin and the secondary stop.

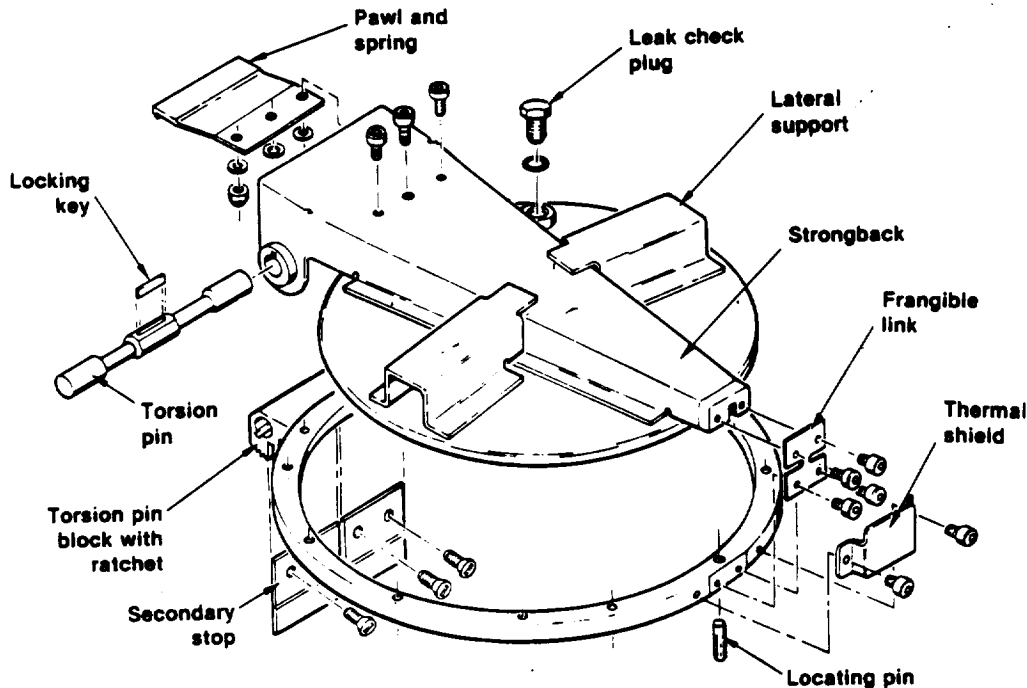


Figure 7. Exploded View of Forward BSM Nozzle Closure.

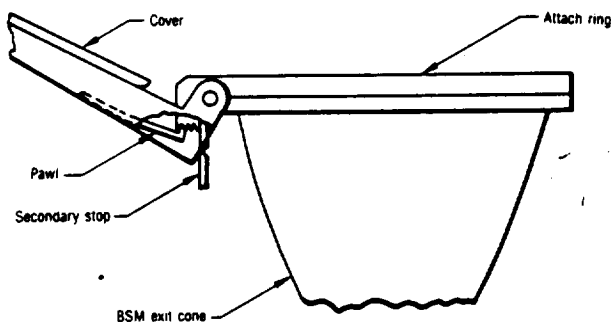


Figure 8. Open Cover Immediately Before Secondary Stop Engagement.

The cover plate is spin-formed from a flat sheet of 321 stainless steel. The strongback and lateral support structure, also 321 stainless steel, are spot welded to the cover plate. The subassembly is mated to the attachment ring by aligning the holes and the keyway in the strongback tabs to those in the torsion pin block, then inserting the torsion pin. After the cover is properly positioned, the torsion pin (304L stainless steel) is welded to the bosses on the strongback tabs. The frangible link is attached to the cover and the entire assembly is bolted to a flange on the exit cone. Figure 9 shows the cover assembled to the exit cone.

Major tasks for the hinged cover aeroheating shield were to demonstrate that the rotational energy given to the cover could be absorbed by the hinge pin via plastic torsional deformation without

resultant fracture of the pin. Additional objectives were to demonstrate repeatable performance, large margins of safety, and zero debris during operation.

The frangible link was designed to fail during ignition. The torsion pin was sized to allow the cover to swing open to an angle greater than 145 deg (to clear the expanded plume) but less than 180 deg (to avoid impacting the SRB skin).

A series of component bench tests were performed to characterize the torsion pin and secondary stop energy absorption at the predicted high strain rates. A laboratory fixture was designed and built which could be preset to impart the required amount of torsional work to a flywheel simulating one-half

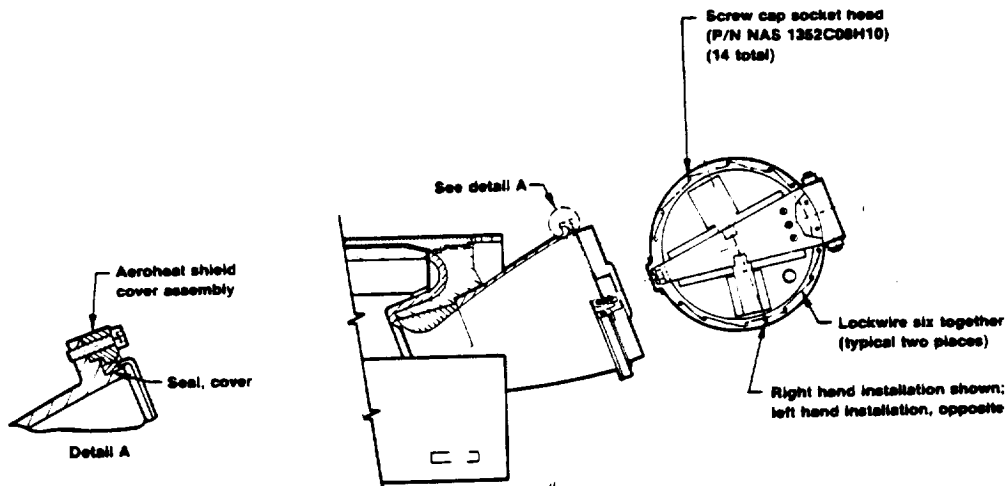


Figure 9. Hinged Cover Assembled to BSM Exit Cone.

of the mass properties of the hinged cover. The flywheel was restrained by a single torsion pin specimen simulating one-half of the hinged cover torsion pin and was set to contact a secondary stop specimen after approximately 145 deg rotation.

Twenty-five torsion pins and four secondary stop specimens were tested. The results demonstrated repeatable performance in that all the input energy was absorbed and the flywheel came to rest within the position range of 145 deg to 180 deg required for hinged cover operation. Twist angles of approximately 1,000 deg were required to fracture the torsion pin.

From the above results, component sizing data were generated to support a prototype hinged cover design. Three tests were conducted in which the hinged cover was assembled to an empty BSM motor case powered with only an igniter. The cover was tested also during two BSM motor firing tests. All tests were successful in that the cover opened to the predicted angles, no debris was ejected, and no physical degradation of hardware was observed.

Fifty-seven empty case tests and three motor firings were conducted on the hinged cover to evolve critical component dimensions, demonstrate repeatability, and verify large margins of safety. Vibration, structural, and leakage tests also were performed. The development tests and their objectives are given in Table 3.

TABLE 3. TEST OBJECTIVES SUMMARY

Test Category	Objective
Component sizing	Verify soundness of current design
	Establish dimensions for critical components
Repeatability	Demonstrate repeatable dynamic operation
Margin Test	Demonstrate survivability under all single point failure modes
Vibration	Verify cover remains intact under full ascent vibration spectrum
	Verify cover remains closed with frangible link omitted
	Verify cover remains intact and open during reentry
Structural	Verify integrity of ratchet pawl under simulated reentry loads
	Verify large margins in critical design areas
Leakage	Verify integrity of environment seal

Empty case tests consisted of a BSM, motor assembly with an igniter, and an epoxy filler to simulate propellant volume. It was determined that the same initiator system as would be used in flight was required to yield representative test results. Both Tabor and Kistler pressure transducers were used to provide the required frequency response. Pressure data were taken in the motor case and in the exit cone.

ORIGINAL PAGE IS
OF POOR QUALITY

The frangible link, torsion pin, and secondary stops were critical components requiring final design definition. Since these components were all functionally interrelated, many iterations were required for final sizing. To assist in this effort, NASA/MSFC-developed dynamics computer programs were used.

Initial hardware was sized from static test results, then incorporated into a cover assembly and tested. High speed photographic records were analyzed to determine the cover position versus time. These results were combined with the pressure data and the initial test conditions and input to a computer curve-fit program to determine the ratio of motor pressure to pressure against the cover (P/P_c) and the cover dynamics. The values of P/P_c , cover mass properties, and initial design/performance conditions were input to a dynamics program. The output of this program was compared to the observed dynamics of the cover and the value of the opening pressure was adjusted until predicted and actual test results agreed.

Component resizing is simulated by changing the initial design conditions and inputting these new values to the dynamics program. The output will determine the hardware dimensions for subsequent tests. Figures 10 and 11 show a typical cover (test 2-15) in the pretest and posttest conditions. In the test, the final opening angle was 168 deg.



Figure 10. Pretest Condition of Typical Hinged Cover Test.

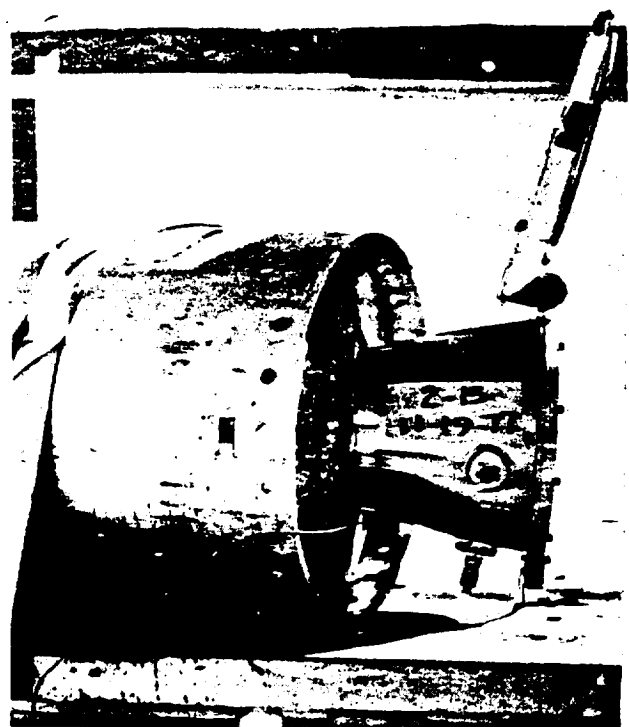


Figure 11. Post-Test Condition of Typical Hinged Cover Test.

A series of margin tests were conducted to verify that single point failure modes would not result in catastrophic failure. The results clearly demonstrated the cover's ability to survive under extreme test conditions. Vibration tests were conducted with the cover assembly attached to a BSM exit cone and successfully demonstrated large margins of safety. A series of structural tests were performed to verify large margins of safety during ascent and cover operation. Leakage tests with GN_2 verified the integrity of the environmental seal to 4 psi.

The design shown in Figure 7 has been incorporated into all flight BSM systems. To date, six Shuttle launches have been completed. All BSMs have performed as designed. Figure 12 shows the hinged cover properly intact after the recovery of one of these flights.

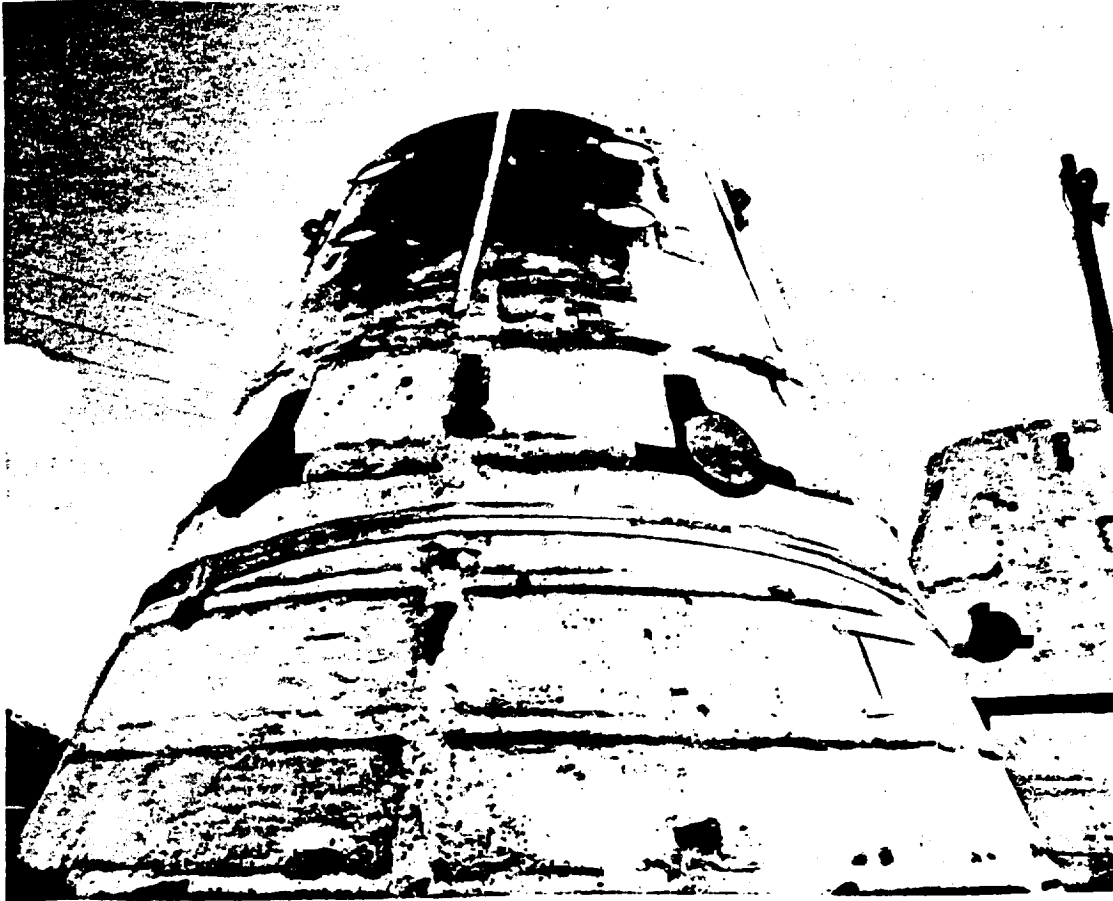


Figure 12. BSM Hinged Covers on Nose Cone of Recovered Shuttle Booster After Flight.

AFT BSMs NOZZLE CLOSURE

As previously mentioned, the aft mounted BSMs do not have a nozzle cover debris requirement since their nozzles are directed away from the direction of the Orbiter. The design of this cover simply involves clamping an 1100 series aluminum disc over the end of the nozzle. The disc has a circumferential notch to provide a clean rupture. The design is shown in Figure 13. Figures 14 and 15 show this closure pretest and posttest. All tests were successful and the design has been incorporated for flight. Figure 16 shows the aft mounted BSMs with their covers clearly ejected after ignition in flight on board the Shuttle SRBs.

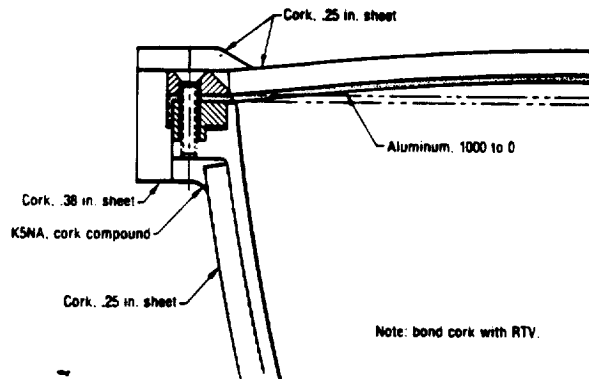


Figure 13. Aft Mounted BSM Nozzle Closure Configuration (After Proof Test).



Figure 14. Aft Mounted BSM Nozzle Closure - Pretest.

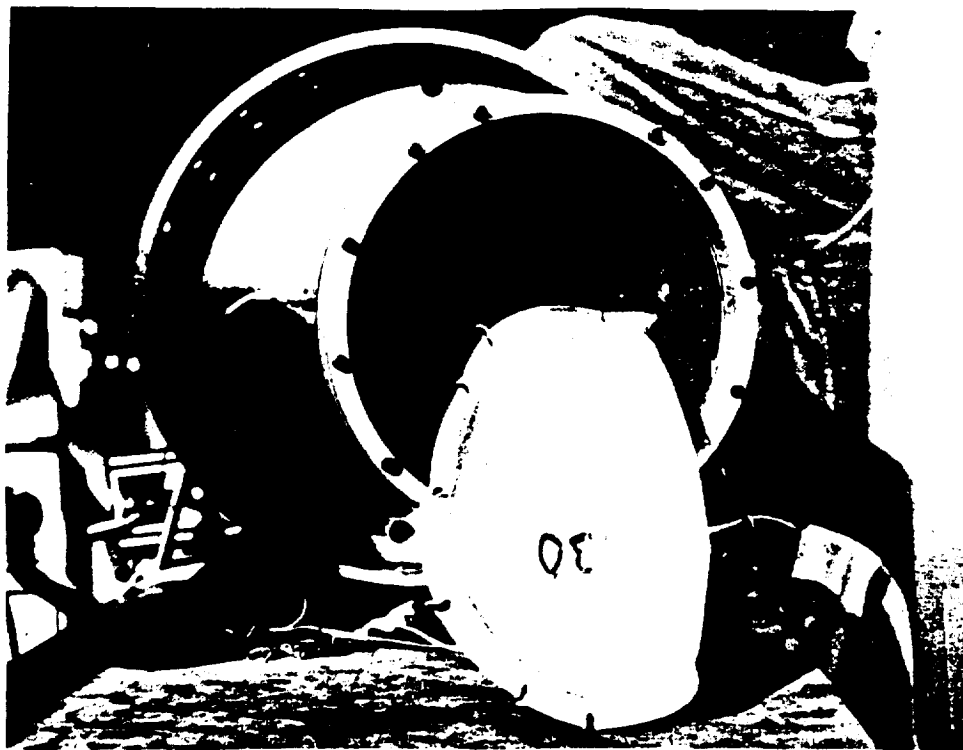


Figure 15. Aft Mounted BSM Nozzle Closure - Post-Test.

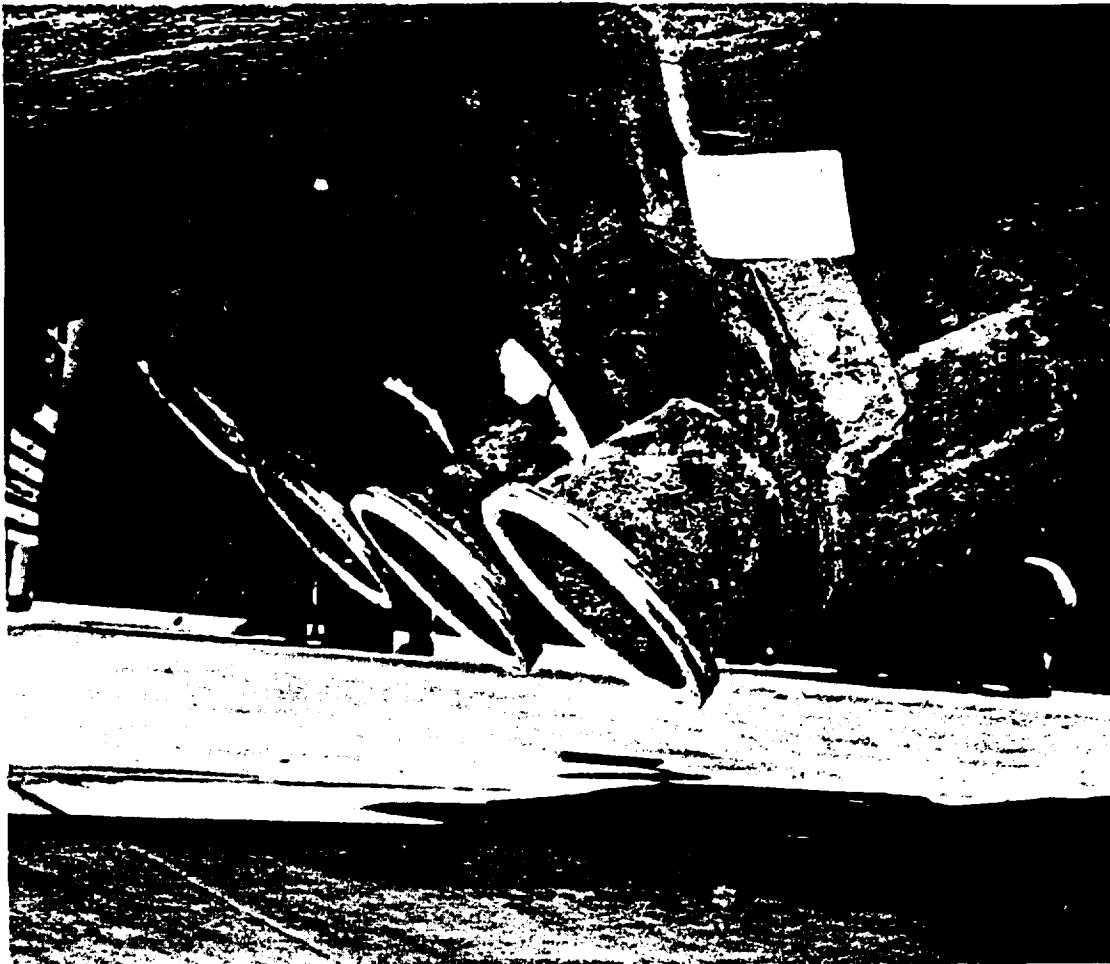


Figure 16. Aft Mounted BSMs After Recovery From Flight.

CONCLUSION

The seven successful flights of the Space Shuttle Transportation System (STS) have verified the design of the BSM relative to control of debris that would be damaging to the Orbiter. Post flight inspections have not revealed any Orbiter TPS damage resulting from BSM operation. The flight program has validated the BSM design approach and the extensive development and certification test program that was implemented to ensure debris free operation.

ORBITAL MANEUVERING SYSTEM DESIGN EVOLUTION

C. Gibson and C. Humphries
NASA Lyndon B. Johnson Space Center
Houston, Texas 77058

ABSTRACT

NASA and industry Shuttle configuration studies conducted in 1969 and 1970 baselined a liquid oxygen/liquid hydrogen (LO₂/LH₂) orbital maneuvering system (OMS), for a series of 15 000-pound to 25 000-pound payload class vehicles. Although the initial OMS guidelines were limited and general in nature, they established the basic architecture for future trade studies. Multiflight reuse, fail-operational/fail-safe redundancy, and a 10-year/100-mission life were required. The propellant tanks were sized for a 2000-ft/sec delta velocity, which included a 1500-ft/sec on-orbit requirement. In 1970, conceptual design studies were conducted for a 50 000-pound, 15- by 60-foot payload bay Orbiter. To minimize overall vehicle length and reduce subsystem development costs, the OMS baseline was changed to Earth-storable nitrogen tetroxide/Aerozine-50 propellants using a single Apollo lunar module (LM) descent engine. In 1971, several Shuttle configurations using external main propulsion system propellant tanks were studied. In a continuing effort to reduce Orbiter length and weight, trade-off studies were conducted using the Apollo LM ascent engine and new 5000- and 6000-pound hypergolic-propellant engines. Because of increased interest in an Earth-storable-propellant OMS system, engine technology contracts were initiated in 1972 to investigate chamber cooling, injector design, and combustion stability concepts. The results of these and system storable-propellant studies provided critical design data that later proved to significantly reduce the mainstream development effort.

In 1972, the Rockwell International Company was awarded the Orbiter Shuttle contract and they selected the McDonnell Douglas Astronautics Company (MDAC) to design and develop the OMS pods. The initial configuration contained a wedge in the OMS pod envelope for a separate reaction control system (RCS) pod. The forward end of the pod interfaced with a nose fairing that was part of the Orbiter payload bay doors. The OMS propellant tanks employed an acquisition system but did not have an RCS feed requirement; the pod skin was of conventional aluminum aircraft construction. Configuration trade studies and design evolution continued after the MDAC contract was awarded. The most significant change was integration of the RCS module into the OMS pod structure. This concept reduced cost and weight and allowed easier interconnection of the OMS and RCS systems. The integrated pod was also redesigned to allow elimination of the payload bay nose fairing, and the structural material was changed to graphite epoxy. In 1974, the Aerojet Liquid Rocket Company was selected as the OMS engine contractor. The baseline engine incorporated a platelet injector, acoustic cavities for stability, a fuel regeneratively cooled combustion chamber, a pneumatic-operated quad redundant ball valve, and an all-columbium nozzle.

The current OMS consists of two identical pods that use nitrogen tetroxide (NTO) and monomethylhydrazine (MMH) propellants to provide 1000 ft/sec of delta velocity for a payload of 65 000 pounds. Major systems are pressurant-gas storage and control, propellant storage supply and quantity measurement, and the rocket engine, which includes a bipropellant valve, an injector/thrust chamber, and a nozzle. The subsystem provides orbit insertion, circularization, and on-orbit and deorbit capability for the Shuttle Orbiter.

PRELIMINARY DESIGN CONSIDERATIONS

In-house Space Shuttle configuration studies conducted at the NASA Lyndon B. Johnson Space Center in early 1970 addressed the concerns of the lack of convergence of requirements, the high development and total program cost, the high technical risk, and the long development time associated with previous studies. A revised set of guidelines and constraints was developed and continually modified during the study. The payload weight was established as between 10 000 and 15 000 pounds; a resizing of the vehicle resulted in a 15-foot-diameter by 30-foot-long payload bay. Extensive examination was made of all current spacecraft and aircraft hardware to minimize cost of new developments and to reduce technical risks. Where no existing system could satisfy vehicle requirements, a new system development was considered assuming 1970-71 state of the art. The Orbiter was designed for a life of 100 missions, or 10 years combined storage and operations. To obtain reuse, limited refurbishment was permitted, where practical. This refurbishment was accepted at the expense of slightly higher flight operational costs. A general redundancy philosophy of fail operational/fail safe was established for the orbital maneuvering system (OMS). The liquid oxygen/liquid hydrogen (LO₂/LH₂) orbital maneuvering system had propellant tankage sized for 2000-ft/sec delta velocity, with payload quoted at a propellant loading giving 1500 ft/sec. Additional propellant for missions requiring in excess

of 1500-ft/sec delta velocity was provided by offloading payload. The on-orbit engines and the main engines were not required to operate simultaneously.

Late in 1970, studies were continued to refine the OMS for Orbiter vehicles of alternate configurations. The airframe, avionics, crew station, and propulsion subsystems were evaluated, and a preliminary design was developed for a series of 009-1 configurations. The OMS is shown in figures 1 and 2. The tanks were sized for 22 000 pounds of usable propellant. With a 5-percent allowance for residuals and ullage, the resulting volumes were 1206 cubic feet for the LH₂ tanks and 261 cubic feet for the LO₂ tank. The LO₂ tanks were located on each side of the LH₂ tank. The propellant tanks included interior baffling and structure, propellant retention devices, and gaging systems. Two gimbaled RL10A3-3 engines mounted to a thrust bulkhead integral with the fuselage structure were installed at the forward end of the Orbiter and were forward firing. The feedline to the reaction control system (RCS) used LO₂/LH₂ drawn from the OMS tanks; the RCS gas generator was connected to the OMS engine feedline downstream of the shutoff valve. The OMS tanks were pressurized by the OMS engines, by the main propellant tanks, or by the gas-generating device for the RCS system. A forward umbilical plate contained the OMS LH₂ and LO₂ fill valves; the umbilical panel was located on the left side of the Orbiter. Each OMS tank was vented through 1-inch-outside-diameter lines overboard through a redundant vent valve located on the aft fuselage structure.

Configurations ranging from long slender fuselages to short stubby fuselages, and various fuselage taper ratios, tank arrangements, and payload access schemes were investigated in the 012 series of vehicles. The payload weighed 50 000 pounds and the payload bay was 15 feet diameter by 60 feet long. All of the configurations were generated by varying the type and location of the main propellant tanks as well as the OMS. Internal volume constraints and concerns regarding the complexity of the O₂/H₂ OMS and RCS led to consideration of storable hypergolic propellants (nitrogen tetroxide (NTO)/Aerozine-50) as used in the Apollo lunar module (LM) and command and service modules. The tankage was sized for a delta velocity of 2000 ft/sec with a specific impulse (I_{sp}) of 310 seconds with a 1:6 mixture ratio and contained 31 300 pounds of usable propellant. Single LM engines were also investigated. The 013 series of Orbiter configurations (fig. 3) was generated to investigate the possibilities of forcing the vehicle center of pressure aft by means of an arrowhead type of fuse-

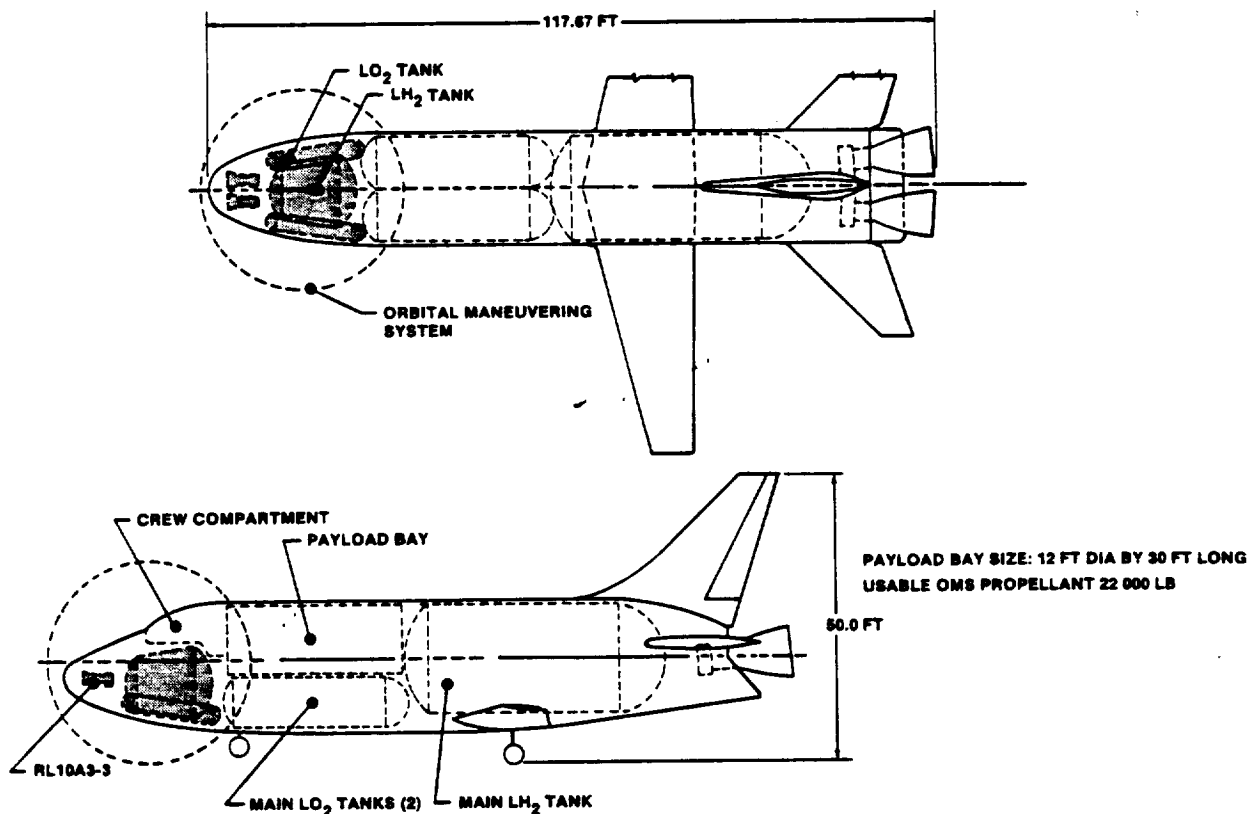


FIGURE 1.- ORBITER CONFIGURATION 009.

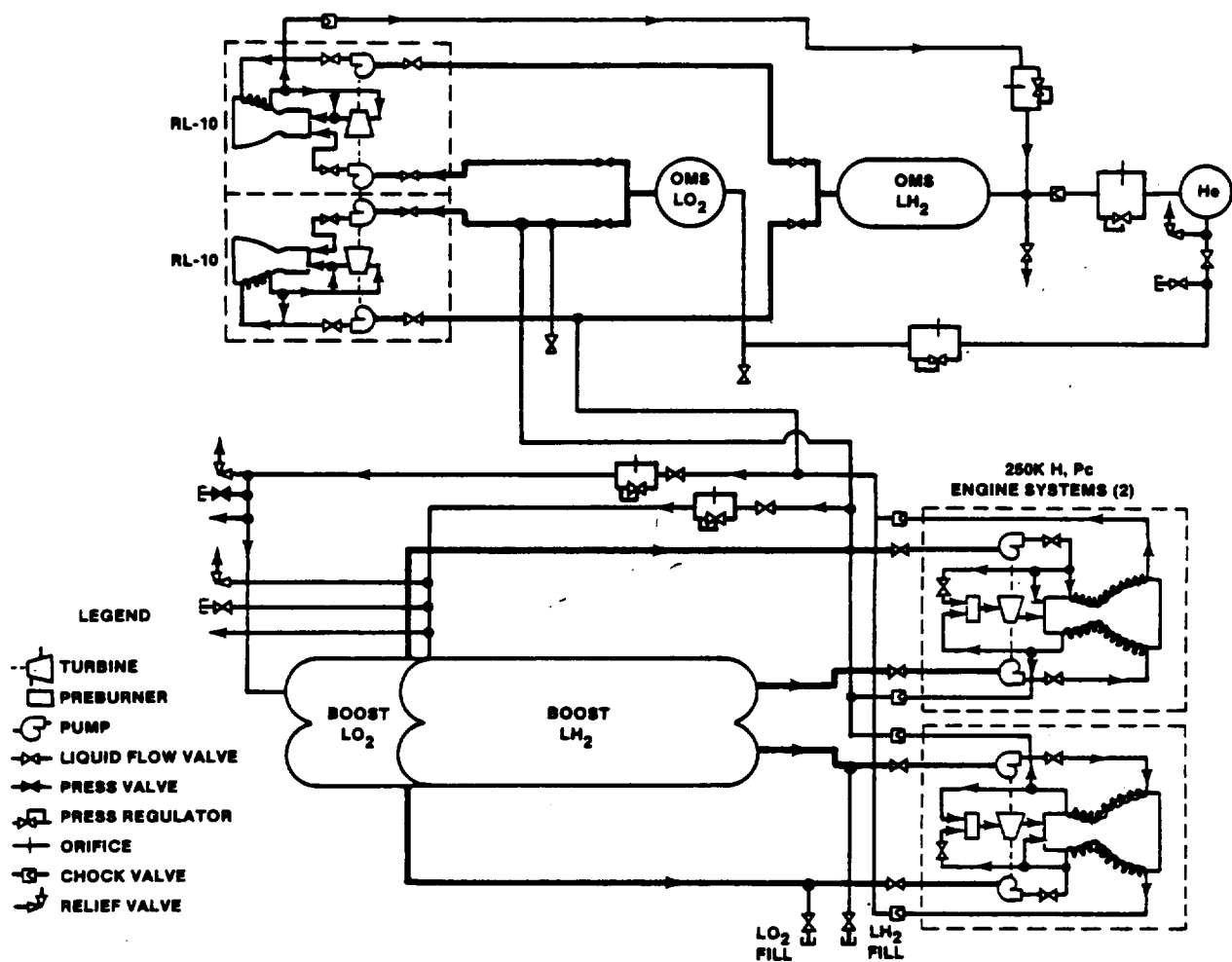


FIGURE 2.- ORBITER FEED AND PRESSURIZATION SCHEMATIC.

lage. Four configurations were generated by varying length, diameters, and fineness ratios of the injection tanks, as well as, in the case of Orbiter configuration O13-1, the location of the crew compartment. The OMS propellants were storable, hypergolic (NTO/Aerozine-50), and sized for a delta velocity of 2000 ft/sec at an I_{sp} of 310 seconds. The OMS tankage was loaded to provide a delta velocity of 1395 ft/sec.

In 1971, a series of Orbiter configurations using external main propulsion system propellant tanks was evaluated. Results of these vehicle studies showed that smaller Shuttle Orbiters with external, expendable main engine tankage would provide a more cost-effective approach compared to the large vehicles used to generate previous baseline requirements. The Orbiter weight reduction resulting from this change enabled a significant reduction of OMS impulse requirements. This effect, together with a decision to allow scheduled OMS refurbishment, stimulated further consideration of Earth-storable propellant systems. For the smaller, lighter Orbiter with external main tanks, sufficient internal volume for an oxygen/hydrogen OMS was a significant penalty; higher density storable propellants were also attractive from this standpoint. To be consistent with Orbiter Shuttle philosophy at that time, only existing engines were considered. Earlier trade studies indicated an OMS using the LM ascent engine would provide the lightest system weight of the Earth-storable-propellant configurations. However, because of engine burn-time considerations, the Agena and the LM descent engine were also considered. The maximum engine mission-duty-cycle firing duration of the LM ascent engine (500 seconds) combined with its relatively low thrust (3500 pounds) dictated the need for the three engines to meet the 1550-second burn-time requirement associated with the 1500-ft/sec delta-velocity maneuvering capability. The LM ascent engine had demonstrated mission-duty-cycle firing durations as high as 900 seconds, but a detailed thrust chamber thermal analysis substantiated with hot

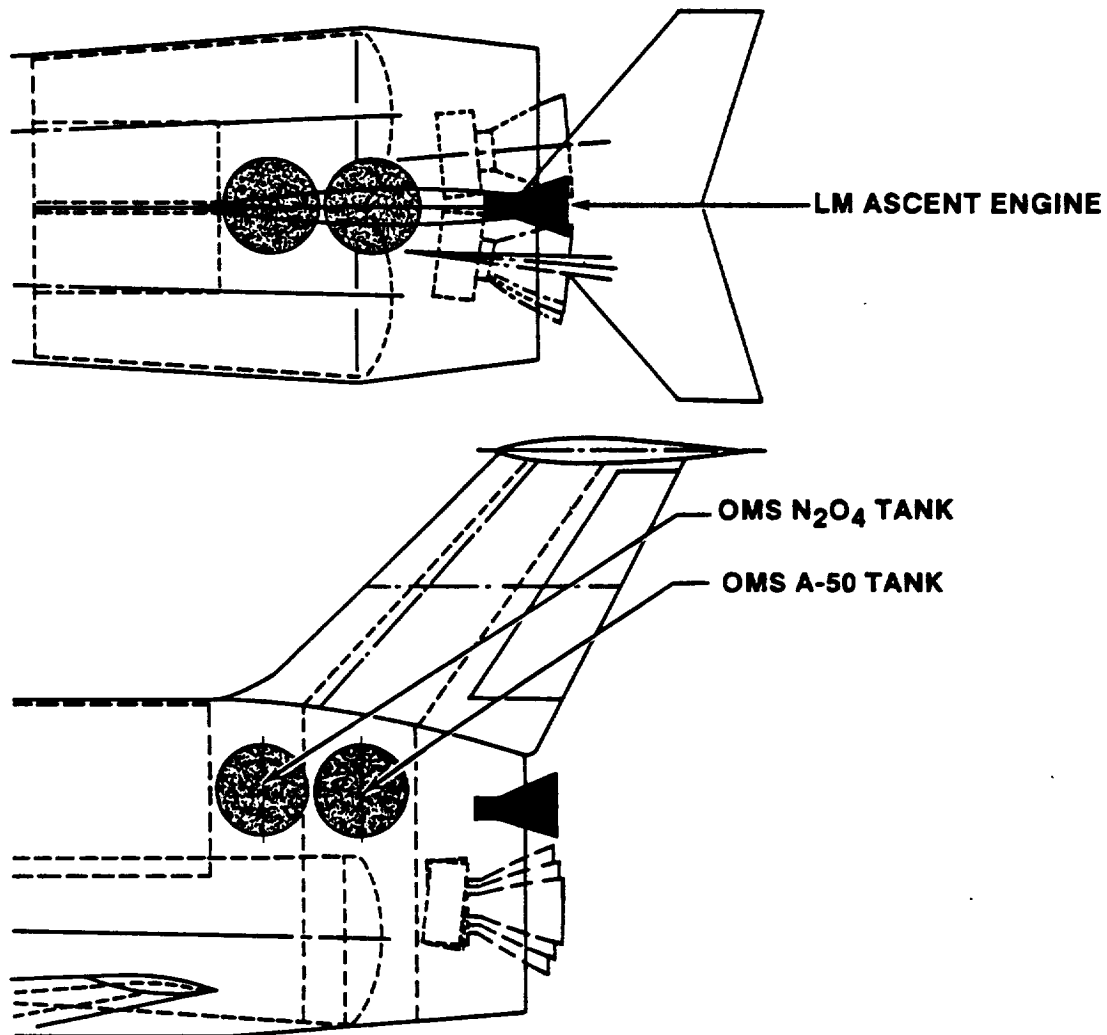


FIGURE 3.- ORBITER CONFIGURATION 013.

firings would be required to justify using only three engines for a 2000-ft/sec delta-velocity capability.

Major perceived disadvantages of the storable-propellant system were the higher maintenance requirements resulting from the corrosive nature of the propellants and personnel exposure concerns resulting from propellant toxicity. These considerations were addressed by incorporating the OMS (and the RCS) into modular pods that could be readily removed from the Orbiter. Thus, OMS maintenance or refurbishment could be decoupled from Orbiter turnaround activities.

The O40C orbital maneuvering system (fig. 4) had two propulsion pods, each self-contained and capable of producing 500 ft/sec delta velocity for an on-orbit vehicle weight of 250 000 pounds, which included 65 000 pounds payload. The engine for each pod had the capability of using propellant from a storage system located in the payload bay and/or propellants from the other pod. Using auxiliary propellant tankage in the payload bay, the OMS would produce a total of 2500 ft/sec delta velocity. The baseline engine was a new 5000-pound-thrust, reusable, Earth-storable-propellant engine. This change was based on the following reasons.

1. The thrust-to-weight ratio (T/W) was marginal using the LM ascent engine (LMAE) and left no tolerance for vehicle weight growth.

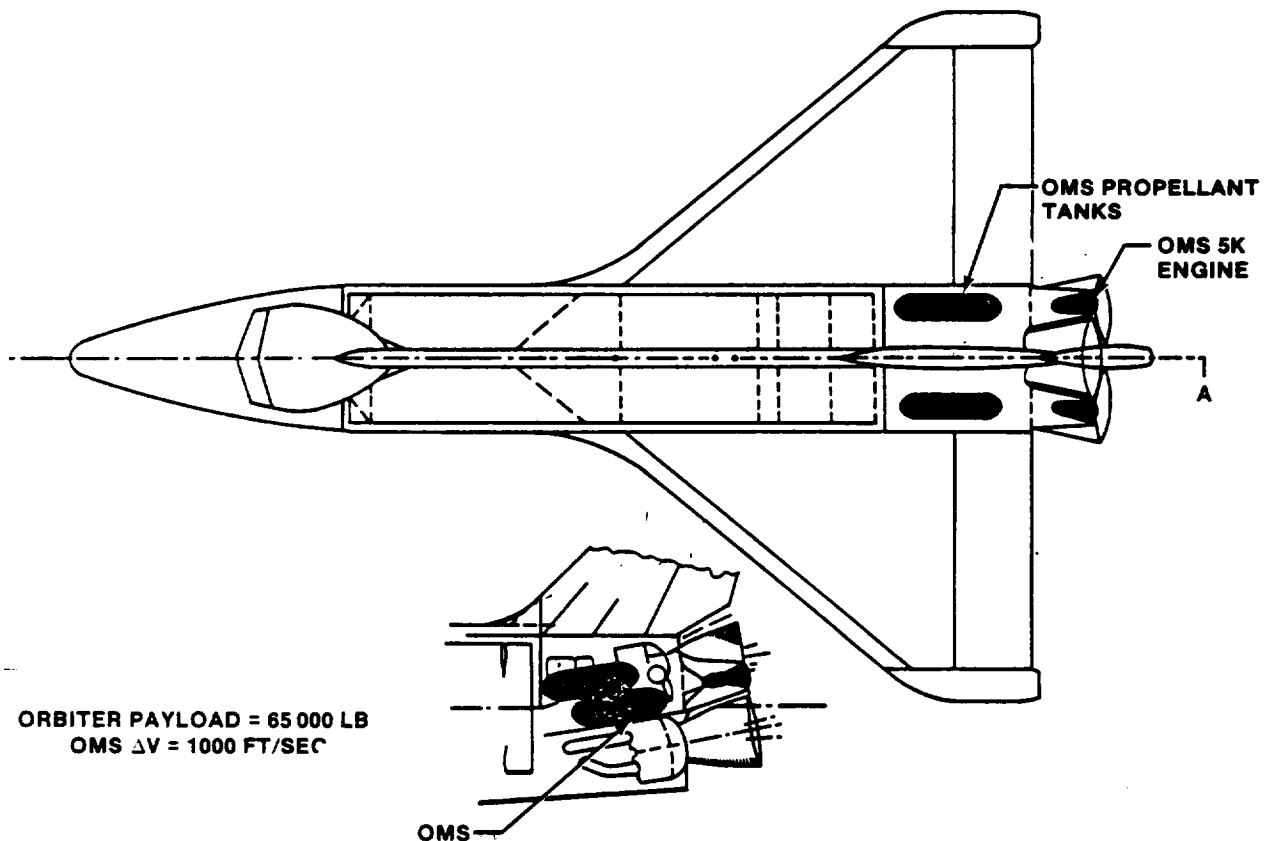


FIGURE 4.- ORBITER O40C CONFIGURATION.

2. The burn time for the LMAE to perform the total delta-velocity requirement was 2800 seconds for each engine; this duration dictated a new ablative chamber.
3. The burn time for the LM descent engine (LMDE) to perform the total delta-velocity requirement was 995 seconds for each engine, an indication of marginal engine capability to perform an engine-out deorbit burn without chamber modifications.
4. The refurbishment cost of the LMAE and LMDE made building a new reusable engine cost effective.
5. The new OMS engine allowed for vehicle and requirement growths.

Figure 5 is a schematic of one of the two OMS pods. Each pod consisted of a pressurization system, a propellant storage and feed system, a liquid-propellant rocket engine, and the structure. The system used hypergolic propellants of NTO/Aerozine-50 and was pressure fed. The propellants were pressurized by gaseous ambient-temperature helium supplied by one tank per pod. The module was assembled, tested, checked out, installed, and removed independent of other vehicle systems. The design goal for the OMS was 15 hours life (100 missions) with maintenance-free operation for 1 year.

ENGINE CRITICAL ISSUE INVESTIGATIONS

During the post-Apollo period, several NASA technology contracts were conducted to resolve key technical issues associated with development of the orbital maneuvering engine (OME). The first of these contracts had a program objective of improving the Apollo service propulsion system (SPS) bipropellant valve. The SPS valve had two major problems: marginal life cycle characteristics (i.e., excessive leakage after cycling) and complicated assembly and repair procedures. The original scope of work consisted of design, fabrication, and test of one preprototype valve assembly. Primary

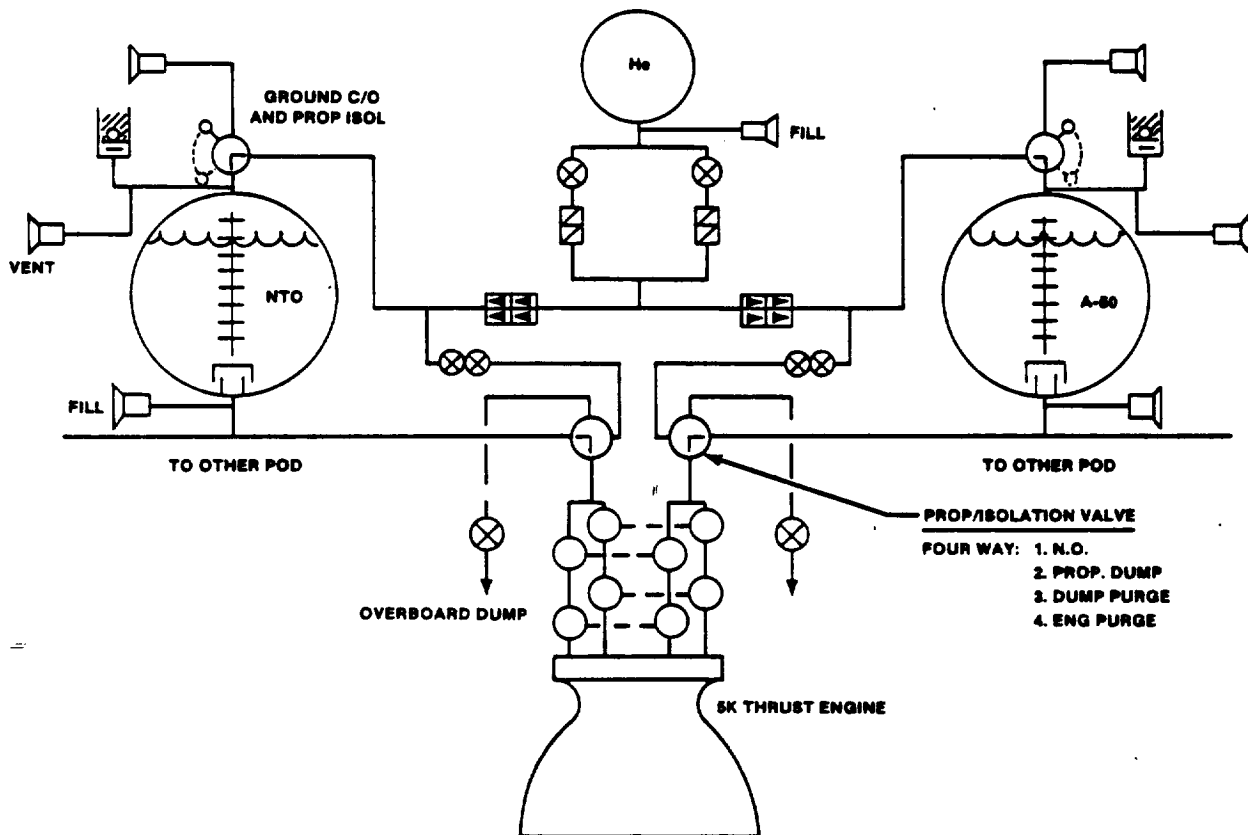


FIGURE 5.- ORBITER O40C OMS SCHEMATIC.

emphasis was placed on improved leak rates and assembly procedures. The results were ultimately used to design the OMS valve.

Two contracts were awarded to investigate reusable thrust chamber concepts for determining the optimum configuration for OMS application. The primary objective of these programs was to evaluate and determine the feasibility of reusable thrust chambers with storable propellants. The programs provided basic engine data to potential vehicle contractors to assist them in evaluating and selecting various OME configurations. One contract was directed toward investigation of a fuel regeneratively cooled thrust chamber. The analyses and tests conducted during the program led to the general conclusion that a regeneratively cooled NTO/monomethylhydrazine (MMH) engine could provide a lightweight, stable, reusable propulsion system with high performance. The propellant and cooling method analyses led to the conclusion that a regeneratively cooled NTO/MMH engine was the preferred concept of various candidates studied based on considerations of performance, weight, development risk, cost, safety, maintainability, life, and reliability. It was concluded from results of sub-scale injector tests that the like-doublet injector would produce higher and more stable performance than injectors using either unlike-doublet or triplet elements. Full-scale injector test programs demonstrated that a like-doublet injector provided safe, stable operation with moderately high performance. The injector could be stabilized with an acoustic cavity having a gradual contoured entrance. Results of the thrust chamber cooling tests using electrically heated tubes and channels led to the conclusion that regenerative cooling at design and off-design conditions could be accomplished with reasonable design parameters and factors of safety. Data obtained with simple round-tube tests were used to define steady-state safety factors for chambers having channel wall construction. The engine could be started safely when the chamber was hot from a previous firing or from exhaust plume impingement from other engines. The chamber could also tolerate large continuous helium bubbles in the fuel, but the safety factor was degraded by the presence of frothlike propellant. A flight-weight thrust chamber was fabricated and safe operation was demonstrated at nominal and anticipated off-design conditions. It was shown that the thrust chamber and the injector could survive a fuel deple-

tion condition and that the engine was stable in the blowdown mode to approximately 70 psia chamber pressure. Propellant saturation did not significantly affect either the performance or the heat-transfer characteristics of the engine. Performance tests demonstrated an I_{sp} of 317 seconds with an OME-sized nozzle.

The second thrust chamber design study emphasized an insulated columbium chamber. The insulated columbium thrust chamber was tested to prove the capability both of fabrication and of the fuel film cooling to limit the chamber wall temperature to 2400° F. Several lengths of chamber were tested and a final performance of slightly more than 310 seconds I_{sp} was accomplished. Subsequent interest in the columbium chamber concept was reduced as further studies of the regeneratively cooled chamber indicated that cyclic requirements and high performance using the regeneratively cooled chamber could be achieved.

Injector designs combined with acoustic cavity concepts were investigated by several companies. Acoustic cavities, used either independently or in conjunction with baffles, had been demonstrated as an effective method of suppressing acoustic modes of combustion instability in rocket engines. In propulsion applications with requirements for both long-duration firings and reusability, cavities had an advantage over baffles because they were easier to cool and, therefore, less subject to failure from either burnout or thermal cycling. Acoustic cavities, therefore, were particularly attractive for use in the orbital maneuvering engine. Extensive tests had been made with LM ascent-engine-type hardware, an unbaffled injector, and the MTO/Aerazine-50 propellant combination. Dynamic stability was demonstrated with a relatively wide range of cavity configurations. Moreover, analytical design techniques had been developed for the design of cavities. Nevertheless, the stability of an engine with or without acoustic cavities could not be predicted analytically with confidence. As the regeneratively cooled engine concept advanced, data from extensive testing with LMAE-type hardware were available to aid in the design of cavities for the OME case, but all of these tests had been made with ambient-temperature propellants and with operating conditions near those of the LMAE. A principal concern was the effect of the high fuel temperature associated with regenerative cooling. Therefore, technology programs were begun to evaluate the effectiveness of acoustic cavities under conditions closer to those of the OME. The results from these programs clearly indicated that dynamic stability could be ensured in regeneratively cooled OMS engines through the use of acoustic cavities. Stable operation was demonstrated with a range of cavity configurations, an indication that a moderate stability margin could be obtained. Further, adequate suppression was demonstrated with doubly tuned cavity configurations that prevented occurrence of the first and third tangential modes and the first radial mode. All three of these modes were encountered when insufficient suppression was provided.

The OME platelet injector program was undertaken to evaluate a platelet face injector as a means of obtaining additional design margin and lower cost. The program was conducted in three phases. The first phase consisted of evaluating single injector elements; it involved visual flow studies, mixing experiments using propellant simulants, and hot firings to assess combustion efficiency, chamber wall compatibility, and injector face temperatures. In the second phase, subscale units producing 600 pounds thrust were used to further evaluate orifice patterns chosen on the basis of unelement testing. Full-scale testing of selected patterns at 600 pounds thrust was performed in the third phase. Performance, heat transfer, and combustion stability were evaluated over the anticipated range of OMS operating conditions. Among these conditions were the effects of combustion stability on acoustic cavity configuration, including cavity depth, open area, and inlet contour.

INITIAL SUBSYSTEM REQUIREMENTS DEFINITION

As the Shuttle configuration became more defined in 1972, so did the OMS requirements and challenges that had to be met. An accurate evaluation and comparison of candidate OMS configurations required a consistent and well-defined set of requirements. The requirements that evolved were that the Shuttle system should, as a design objective, have a service life of 10 years and be capable of low-cost refurbishment and maintenance for 100 missions. The OMS turnaround time from landing and return to launch readiness was less than 160 working hours, covering a span of 14 calendar days for any mission. The OMS had to be capable of launch readiness from a standby condition within 2 hours and hold in a standby status for 24 hours.

The Space Shuttle was planned to accomplish a wide variety of missions. The reference mission (satellite delivery/retrieval to a 100-nautical-mile circular orbit) for the Shuttle was used in conjunction with other requirements to size the OMS. The spacecraft was launched from the NASA John F. Kennedy Space Center due east and required a payload capability of 65 000 pounds with the Orbiter vehicle. The Orbiter was inserted into a 50- by 100-nautical-mile orbit; circularization at apogee required an OMS delta velocity of 90 ft/sec. The Orbiter remained on station for approximately 6 days and, in this timespan, 12 orbit maintenance burns were required to retain the 100-nautical-mile parking orbit; each burn required a 4.5-ft/sec velocity increment. Before satellite retrieval, a 32-ft/sec OMS burn was required for terminal phase initiation. The crossrange capability of the

delta wing Orbiter eliminated the need for preorbit phasing, and, at the appropriate time, the Orbiter deorbited and returned to the launch site. The OMS also provided the 250-ft/sec deorbit burn. The anticipated on-orbit and descent OMS requirement was 372 ft/sec (neglecting the orbit maintenance burns), but a total delta-velocity capability of 1000 ft/sec was provided.

The required thrust of the OMS was principally determined by vehicle orbital maneuver and abort requirements. The orbital maneuvers performed by the OMS ranged from small velocity corrections to relatively large maneuvers such as plane changes and retrograde firings. From the standpoint of defining thrust requirements, the smaller maneuvers were more efficiently performed at a low thrust level, but low thrust increased the burn time and, consequently, the impulse required for large velocity corrections. Since the latter consideration was more significant for the Shuttle vehicle, a thrust level of approximately 6000 pounds was determined to be a reasonable nominal value with 4000 pounds as the lower limit.

The propulsion functions that the OMS had to perform set the design requirements, e.g., total impulse, thrust level, burn time, etc. However, the system designed to meet these requirements was strongly influenced by interpretation of the Shuttle reliability criterion. Two factors were of predominant importance: the number of engines and the propellant available for maneuvering and deorbit. Based on Apollo experience, the use of two OMS engines in conjunction with other component redundancy represented an acceptable level of safety and was a ground rule for system design. This rule meant that the system was designed for full mission capability, after an engine failure, and, thus, definition of the thrust level and the total impulse was based on operation of a single engine for all mission functions. Systems using a common propellant supply inherently have the capability to use all the system impulse through either of the two OMS engines. However, modular-type (pod) systems, using separate propellant and pressurant supplies for each engine, would effectively be reduced to half the system impulse capability in the event of an engine failure unless each module was designed for full system capacity. Design of the separate modules with full capacity resulted in an excessive weight penalty. Since engine failures were entirely possible at times when the propellant remaining in one module was insufficient for retrograde firing, the capability to transfer propellant to the operational engine was necessary for crew survival. Hence, for the modular system, a requirement was that the OMS be designed for the capability to expend all propellant through either engine. The effect of this requirement was to dictate dry, isolated propellant interconnects between modules to achieve minimum weight. The interconnects allowed propellant supply components to be only doubly redundant and still provide the Shuttle with fail-operational/fail-safe OMS capability.

TRADE STUDIES AND DESIGN APPROACHES

After selection of the Rockwell International Company as the Space Shuttle prime contractor, the OMS was changed from an internal installation to a separate module mounted on the aft sides of the Orbiter and projecting into the fuselage, as shown in figure 6. After selection of the McDonnell Douglas Astronautics Company (MDAC) to build the pod, the configuration became shoulder mounted because of aerodynamic considerations. This configuration had the pod extending to the payload bay, and required a fairing on the payload bay doors.

Figures 7 and 8 identify major component parts for the MDAC configuration. Helium pressurant for propellant tank pressurization and for flight purge of the rocket engine assembly was contained in a single composite aluminum bottle. From the bottle, the pressurant flow divided into two branches; each branch supplied helium to a pressurization panel containing series-parallel regulators, regulator isolation solenoid valves, quad redundant check valves, and a solenoid valve. The components were arranged so that redundant components were isolated from each other and were not subjected to identical dynamic environments. Primary and secondary relief mechanisms at the outlet of each pressurization panel protected the propellant tanks against an overpressure condition. Manual selector valves allowed independent checkout of the regulators without pressure cycling the propellant tanks. The propellant tanks were made of annealed titanium. Each contained point sensors for measuring propellant quantity (when the propellant was settled) and a refillable trap propellant acquisition assembly to assure gas-free propellant delivery to the rocket engine. A propellant line and quad redundant valve assembly on each tank provided the capability for rapid propellant dump during a launch abort. The engine was regeneratively cooled. Pneumatic two-position valves in the engine feedlines provided engine isolation and purge. Complete servicing or safing of the engine, propellant, and pressurant assemblies was accomplished from a ground servicing panel in the pod base heat shield. The pods were constructed of conventional aluminum, with emphasis on low cost and ease of field inspection and maintenance. The pod was attached to the Orbiter at four points with shear pins and threaded fasteners to provide quick mate and demate capability.

The cargo bay kit employed the same components and pressurization panels as the pods. It contained as many as six propellant tanks mounted on an all-aluminum structure for a maximum additional delta-velocity capability of 1500 ft/sec. Propellant was transferred to the pod by vehicle-mounted transfer lines, which joined the engine feedlines upstream of the engine isolation purge

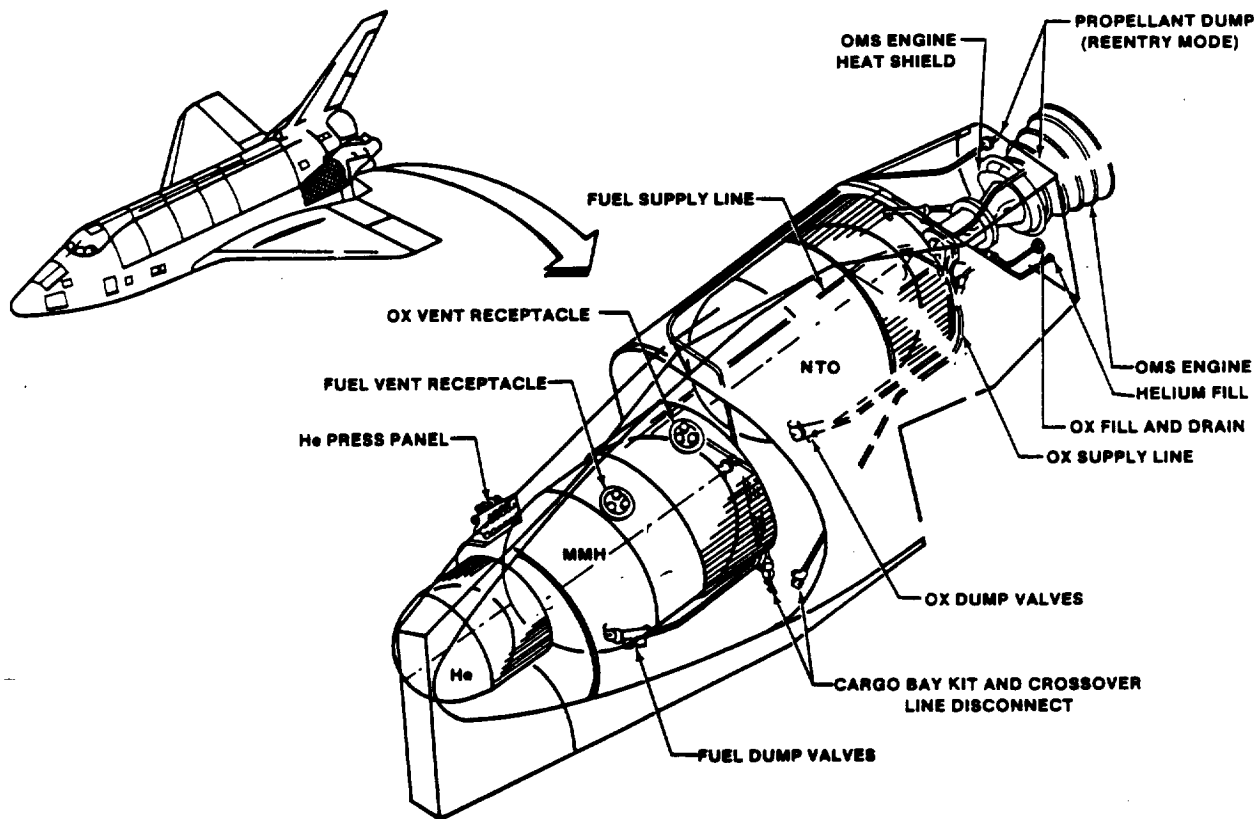


FIGURE 6.- OMS CONTRACTOR PROPOSAL BASELINE.

valves. Normally closed valves in the pod kept the vehicle-mounted transfer lines dry, unless the lines were needed for feed from cargo bay tankage or for crossfeed between pods.

Several trade studies performed and different design approaches investigated early in the program resulted in significant changes. Through design studies, it was found that both cost and weight would be saved with a common integrated structure for the OMS and the reaction control system. This change, combined with selection of RCS NTO/MMH propellants, resulted in initiation of trade studies - to investigate several degrees of integration between the two propulsion systems. The design study included common propellant tanks, clustered RCS engines for the OMS, and an interconnect system by which the RCS used OMS propellants. The interconnect system was baselined because of cost, weight, and low development risk considerations.

With the decision to interconnect the RCS and OMS propellant tanks, design requirements for the OMS acquisition and gaging system changed. A refillable trap was no longer adequate to supply propellant to the RCS. The basic requirement imposed on the OMS acquisition system was a capability to supply 1000 pounds of propellant to the RCS while maintaining a capability to restart the OMS 10 times. The design that evolved was a compartmentalized refillable trap as shown in figure 9. As a result of this change in the acquisition system, it was desirable to monitor propellant quantity in the lower compartment. Therefore, the gaging system was redesigned from point sensors to a capacitance probe. The OMS pod and later OMS/RCS pods were fabricated using aluminum and conventional aircraft construction. When it was recognized that a large weight savings could be accomplished by using a graphite epoxy skin similar to that being used for the payload bay doors, a design change was made to reduce each pod weight by 250 pounds.

Initially, the OMS and the RCS were considered as separate systems with redundancy requirements for fail operational/fail safe. After the OMS/RCS interconnect lines were incorporated, the criteria for the OMS were reduced to a fail-safe condition. This change resulted in removal of the third regulation leg of the pressurization system. It was later found to be cost and weight effective to have a common regulation source for both oxidizer and fuel. This configuration further reduced the regulated flow path from separate to coupled propellant tanks and allowed closer control of mixture

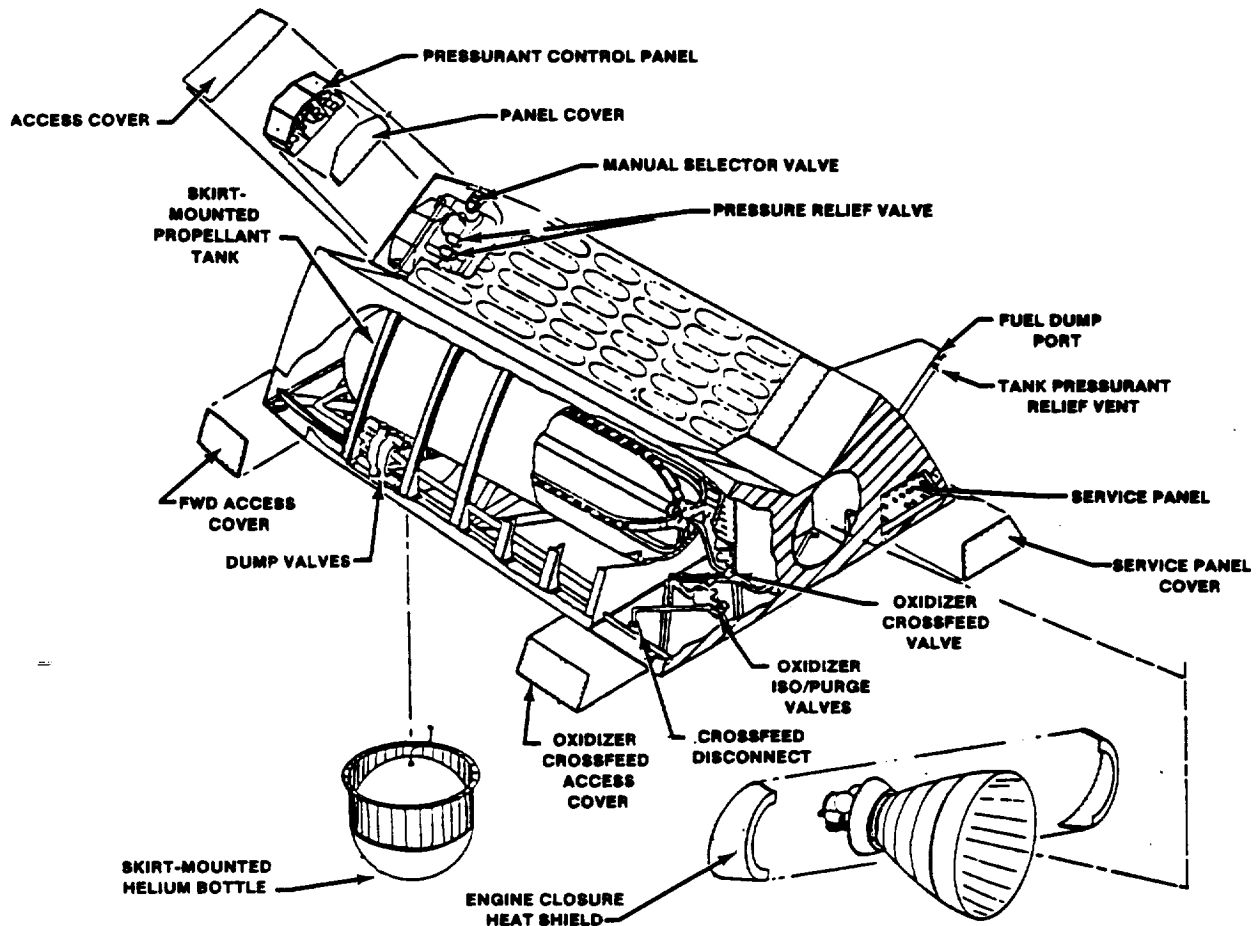


FIGURE 7.- OMS POD DESIGN.

ratio with a common pressure source. To assist in preventing the migration of vapor from the oxidizer tank to the fuel tank, parallel solenoid valves were installed upstream of the check valves on the oxidizer side. The initial design had a valve to purge the engines before reentry following the deorbit burn. The valve was later determined to not be required and was removed. During return to launch site (RTLS) abort, it is required to dump propellant in the OMS tanks to an acceptable level for landing. The configuration at the beginning of the program used quad redundant valves for propellant dump. This configuration was later changed to series valves with the ground rule modification that RTLS operation would not consider additional failures. Subsequent analysis indicated that the dump could be accomplished through the OMS and RCS engines by use of the interconnect, and the separate dump system was deleted. The final OMS design is shown pictorially in figure 10 and schematically in figure 11.

The OMS engine is illustrated schematically in figure 12. The design drivers were life, envelope, applied environment, specific impulse, combustion stability, reusability, and propellant inlet feed pressure. A single overriding consideration was that no single-point failure would result in a safety hazard to ground or flight personnel. The basic design concepts were direct applications of predevelopment technology activities. The key requirement was long life and this influenced design of the acoustically stabilized, flat-face, photo-etched injector; the regeneratively cooled, slotted combustion chamber; and the redundant ball valve. The engine nozzle area ratio was 55:1, which efficiently used the allocated envelope length but only 44 inches of the 50-inch envelope diameter. The resulting configuration reduced weight because the nozzle skirt was smaller. The engine used a fuel inlet torus-mounted gimbal ring which was selected on the basis of cost, weight, stiffness, and maintainability considerations. The side-mounted, series redundant propellant valve reduced feedline length, and engine length, and allowed for shock mounting to modulate engine input. Filters were contained at the inlets of the feedlines for ease of access. Static leakage was controlled by

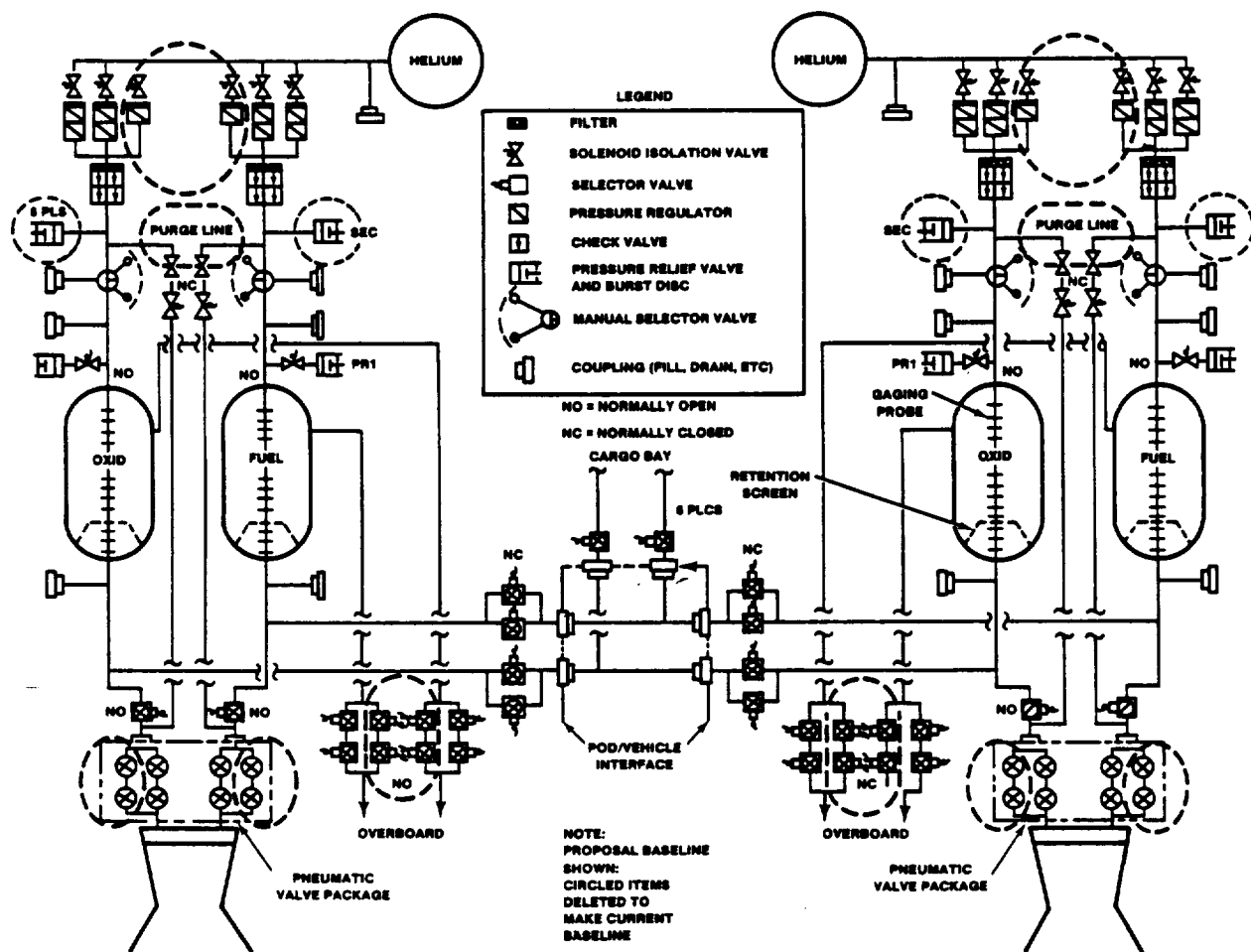


FIGURE 8.- OMS CONFIGURATION CHANGES.

redundant seals at all flanges and interconnecting fluid joints. Inlet line routing to the engine was through propellant lines located in the same plane as the gimbal ring and chamber throat. Maintenance, installation, and servicing were simplified by designing the engine as a line replaceable unit (LRU) and mounting it on the inlet manifold-mounted gimbal ring. Large tolerance stackups were also eliminated and thrust alignment was simplified.

The development injectors were designed to be mechanically joined to a fuel manifold acoustic cavity assembly, which simulated the forward end of the regeneratively cooled thrust chamber. This design allowed stability assessment of the flight configuration to be accomplished with uncooled workhorse thrust chambers. Removal of the injector flange enabled welding of the same injectors directly to the regeneratively cooled chamber. The X-doublet injector developed under a technology contract was later replaced by a like-on-like pattern composed of eight photo-etched platelets but in all other respects identical. The basic reason for the change was the inability to reproduce the X-doublet injector. This discrepancy became obvious when the first like-on-like injector was tested and found to have impaired stability characteristics. An exhaustive inspection of both injectors disclosed a slight variation in platelet flatness in the technology injector that resulted in minor stream variations. Because of the subtle nature of differences between the two injectors, it was almost impossible to define all of the effects. As a consequence, the like-on-like pattern (fig. 13) was selected for the baseline engine.

The combustion chamber, shown in figure 14, was regeneratively cooled by fuel flowing in a single pass through nontubular coolant channels. Its design was based on regeneratively cooled thrust chambers fabricated on technology contracts. The design configuration was similar to that of the Space Shuttle main engine chamber. The chamber was constructed from a stainless steel liner with

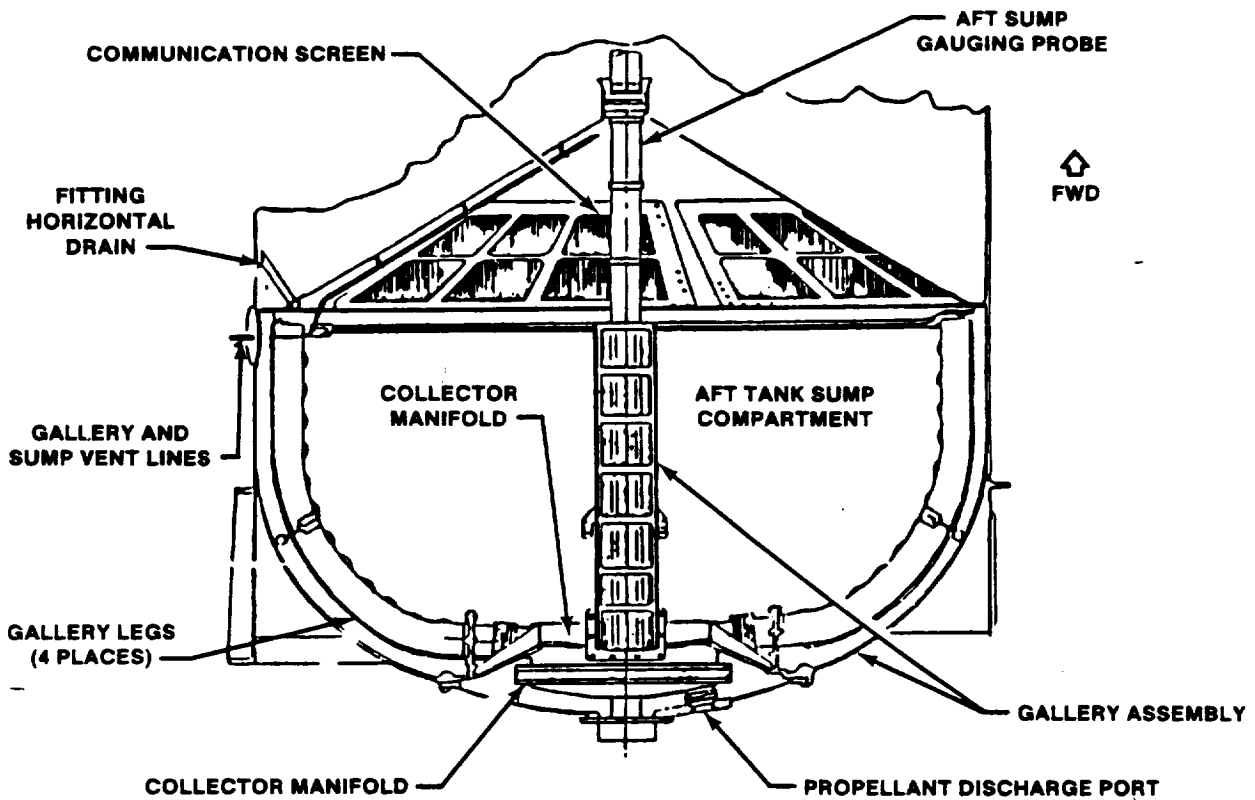


FIGURE 9.- PROPELLANT ACQUISITION SYSTEM.

rectangular coolant channels enclosed with an electroformed nickel shell. Because the electroformed shell and the liner were independently capable of withstanding the structural loads, the criticality of the interface bond was removed. The upper chamber was cylindrical with a contraction ratio of 1:9. The distance from the injection plane to the throat is 15.9 inches. The thrust chamber assembly extends to a 6:1 area ratio, where the nozzle extension was attached by means of a bolted joint. The chamber contained 120 longitudinal, milled, rectangular-shaped passages. The cooling channels had constant widths but varied in depth to provide an optimum configuration for cooling effectiveness, chamber life, and engine performance. The combustion chamber was composed of three main parts: a stainless steel liner, an electroformed nickel shell, and an aft flange and fuel inlet manifold assembly. The liner was fabricated from 304L stainless steel, selected because of its adequate strength properties at operating temperature, chemical compatibility with the combustion environment, and superior machining and electron beam (EB) welding characteristics. The chamber structural design was based on life cycle requirements; mechanical loads such as pressure, thrust, and aerodynamic loading on the nozzle; fabricability; and weight. The main structural consideration for the stainless steel liner was thermal fatigue due to temperature gradient and channel pressure. The nickel outer shell thickness was governed principally by the moment along the length of the chamber resulting from aerodynamic loading on the nozzle.

The nozzle extension (fig. 15) was radiation cooled and was constructed entirely of columbium commensurate with experience gained in the Apollo Program. The nozzle extended from the regeneratively cooled interface to an area ratio of 55:1. The aft section was reinforced by three external stiffeners to provide for the large external pressure loads encountered by the nozzle during ascent. The entire surface of the nozzle was constructed of three parts: a flange, a forward section, and an aft section. The mounting flange consisted of a bolt ring made from a forging and a tapered section which could either be made from a forging or spun. This tapered region provided a transition from the 0.100-inch-thick flange to the 0.050-inch-thick forward nozzle section. The forward and aft sections were made from two panels each; the aft section was 0.030 inch thick. The panels were butt-welded to form two cones; the cones were welded circumferentially to each other at the flange region. This assembly was bulge-formed to the final configuration, and the stiffening

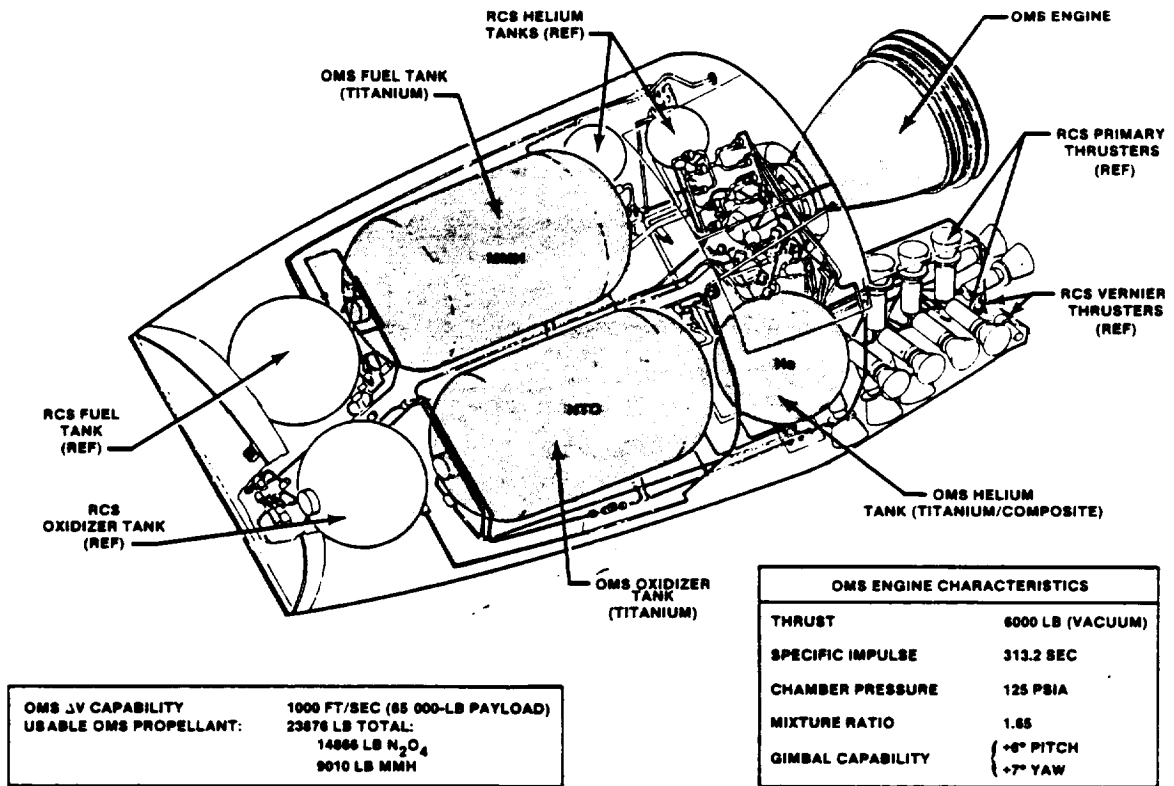


FIGURE 10.- BASELINE ORBITAL MANEUVERING SYSTEM.

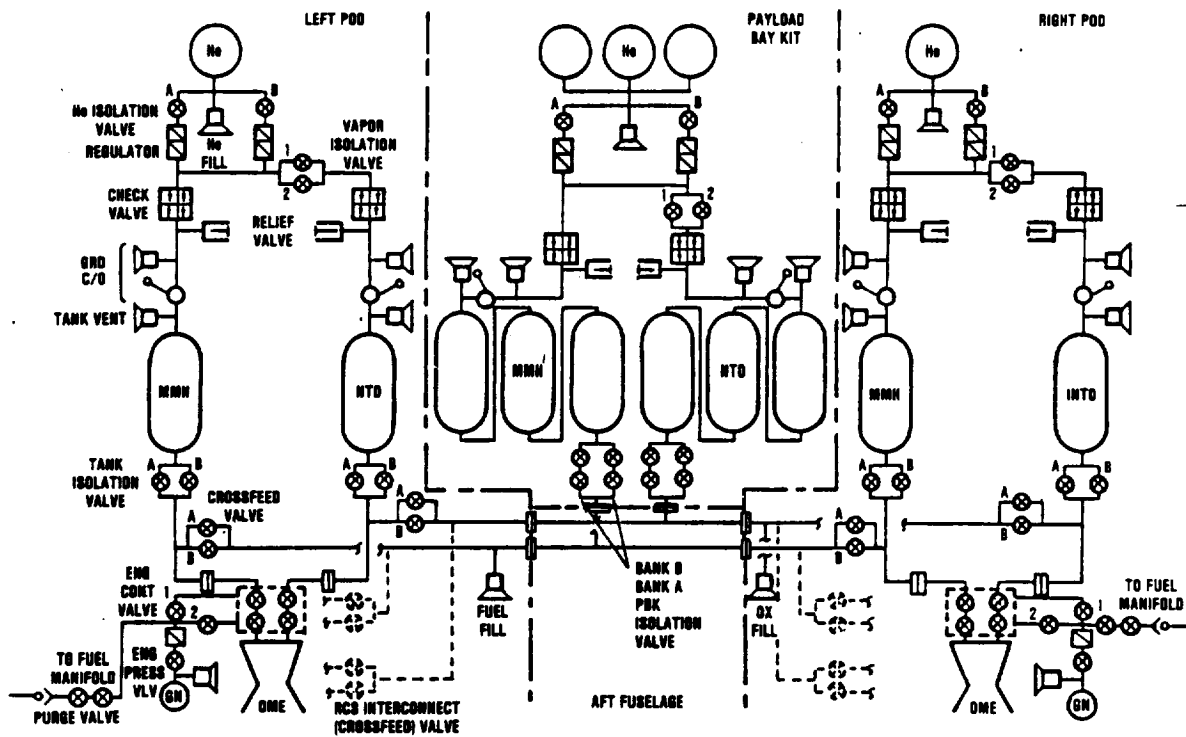


FIGURE 11.- BASELINE OMS SCHEMATIC.

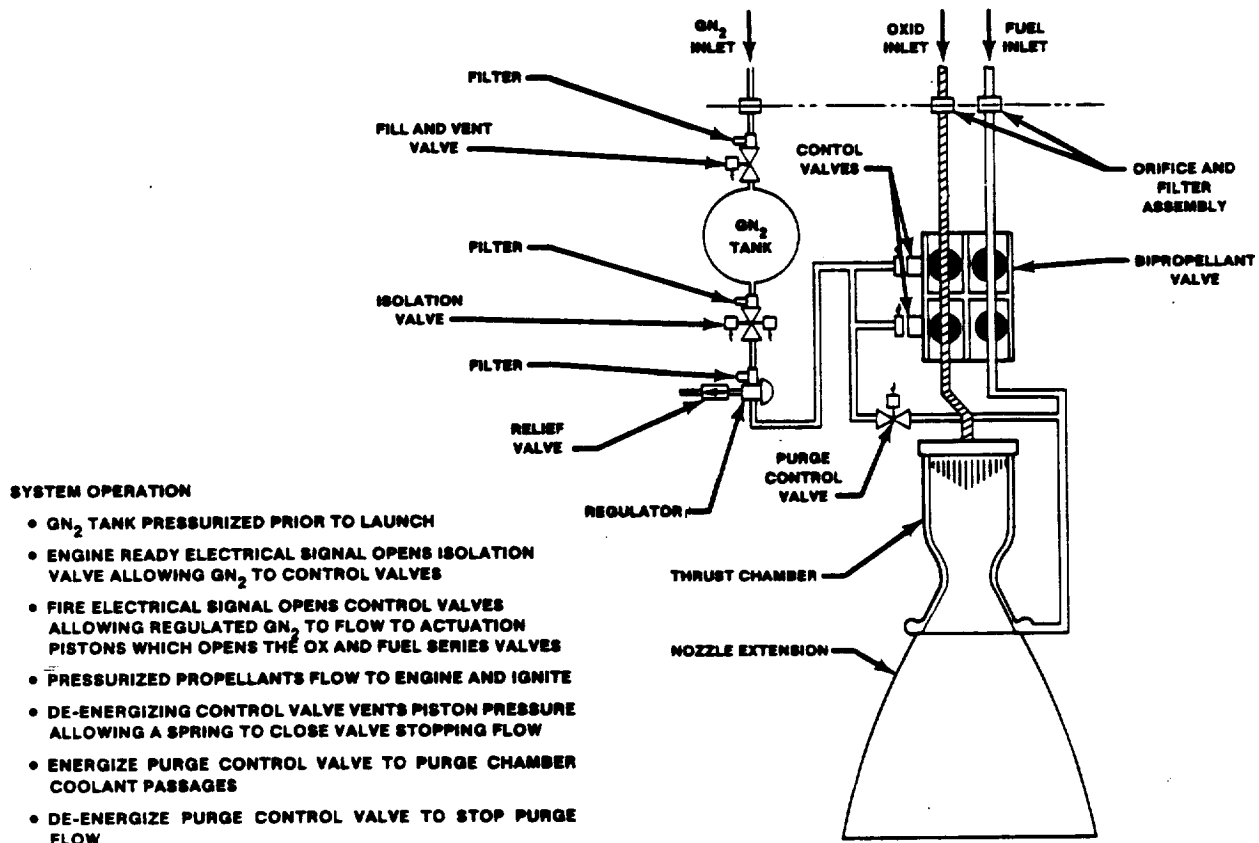
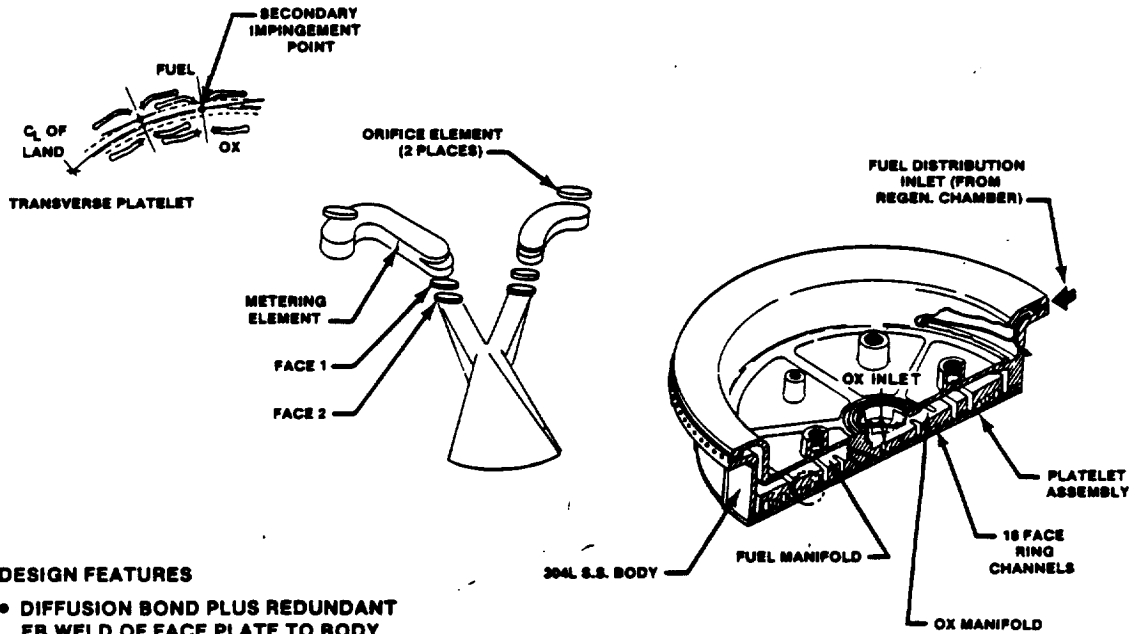


FIGURE 12.- OMS ENGINE SCHEMATIC.

rings were attached by welding. The oxidation barrier diffusion operation was done after all machining was completed. The nozzle extension also underwent some minor design changes as a result of the development program. As previously mentioned, the original design included three stiffening rings located approximately at the midpoint of the nozzle. Changes in both the magnitude and the location of aerodynamic loading combined with changes to the expected aerodynamic noise level dictated the current design with a single flange at the nozzle exit. With the exception of minor changes in shell thickness and in number of circumferential welds, the nozzle and the manufacturing process are identical to those proposed.

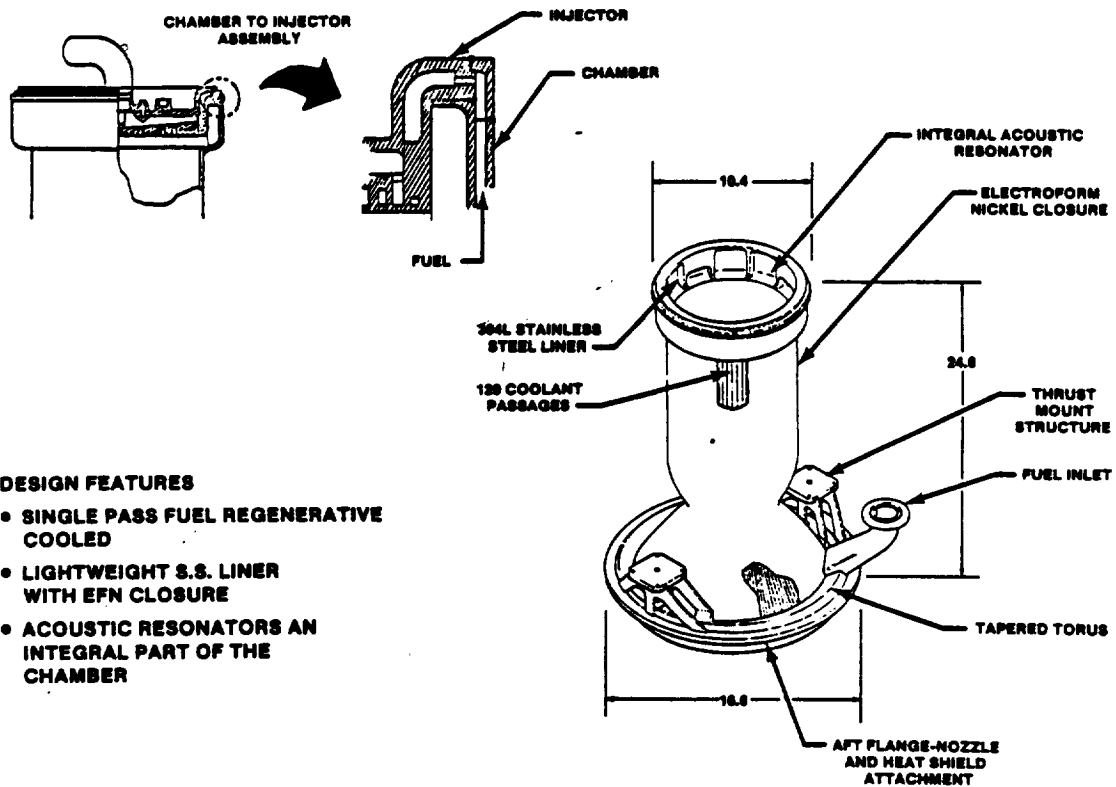
A basic design consideration for the bipropellant valve (figs. 16 and 17) was the elimination or the reduction of problems that occurred with the Apollo quad redundant valves. The selection was accomplished first by subjective trade-offs, to narrow the number of candidates, and then by quantitative comparisons to evaluate major candidates. A basic design premise was requirement of a modular-type valve as a cost-effective approach, not only for maintenance and servicing but also for fabrication and test. Primary reasons for this selection were the potential for low-risk attainment of operating requirements and credible, substantiated costs. One fuel and one oxidizer valve were mechanically linked, with each of four linked pairs driven through a rack and pinion assembly by a piston actuator. Opening force was produced by pneumatic pressure, which was controlled by a close-coupled, three-way solenoid valve located at each actuator. Closing force was provided by nested, counterwound, helical compression springs. The three-way solenoid valves were included in the actuator module of the valve assembly to reduce fluid volumes and actuation delay times. Actuation gas control was achieved by a pneumatic pack. The pneumatic pack included a gas storage tank, a two-way solenoid valve, a pressure regulator, a pressure relief valve, related filters, and access ports for servicing and instrumentation. In addition to selection of the basic subcomponent parts of the valve assembly, there were options regarding the physical arrangement of these subcomponents relative to the engine. The primary aspect of the assembly design was modularization. The capability to preassemble subassemblies and install and remove them without disturbing other parts of the valve was the key to a cost-effective program. This capability would reduce fabrication problems, reduce development time, and allow servicing and maintenance goals to be met with lower inventory. The quad



DESIGN FEATURES

- DIFFUSION BOND PLUS REDUNDANT EB WELD OF FACE PLATE TO BODY
- PHOTO-ETCHED INJECTOR PATTERN
- STABILITY ACHIEVED WITH ACOUSTIC RESONATORS

FIGURE 13.- OMS ENGINE INJECTOR.



DESIGN FEATURES

- SINGLE PASS FUEL REGENERATIVE COOLED
- LIGHTWEIGHT S.S. LINER WITH EFN CLOSURE
- ACOUSTIC RESONATORS AN INTEGRAL PART OF THE CHAMBER

FIGURE 14.- OMS ENGINE COMBUSTION CHAMBER.

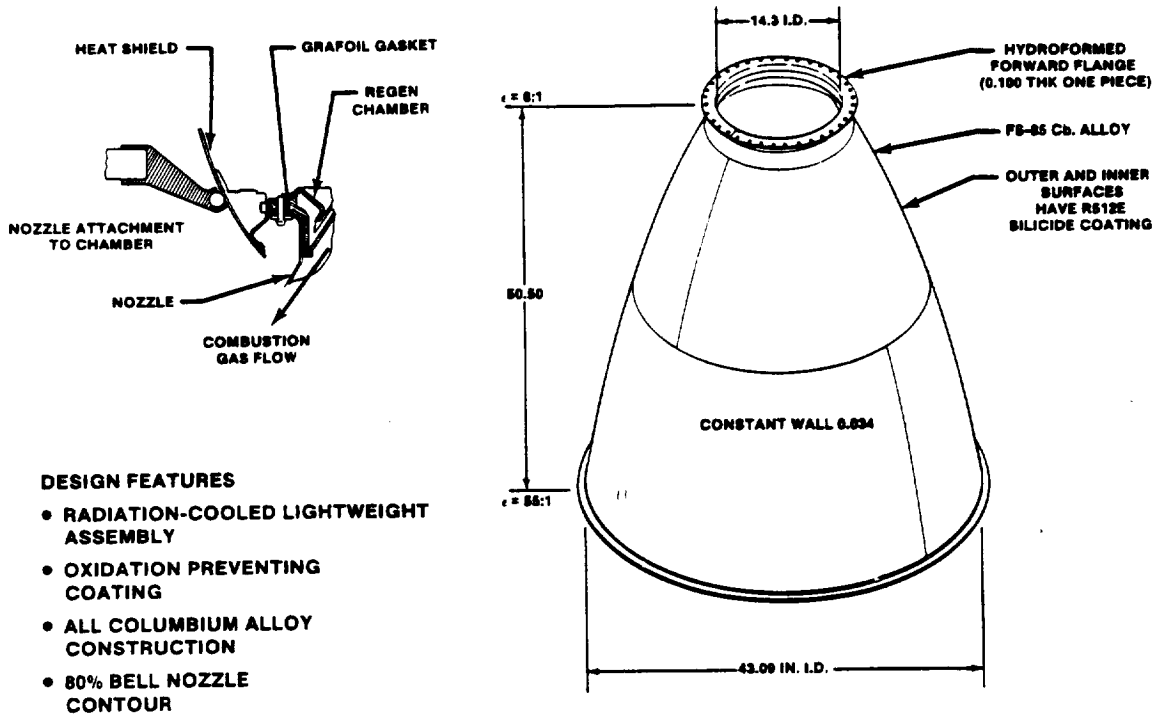


FIGURE 15.- OMS ENGINE NOZZLE EXTENSION.

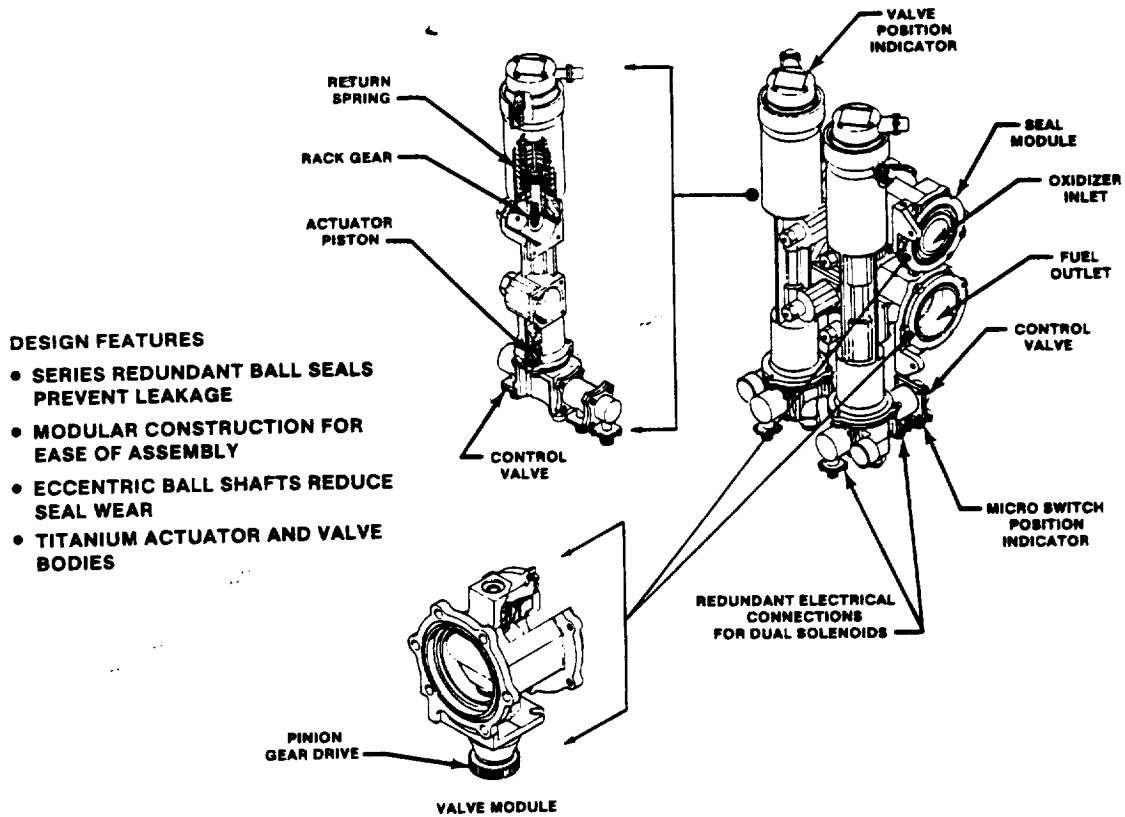


FIGURE 16.- OMS ENGINE BI-PROPELLANT VALVE.

DESIGN FEATURES

- INTEGRAL TITANIUM TANK AND MANIFOLD ASSEMBLY
- "PLUG-IN" COMPONENTS MOUNTED ON MANIFOLD
- REDUNDANT COIL SOLENOID ON ISOLATION VALVE
- PRESSURE RELIEF VALVE INTEGRAL WITH REGULATOR
- PROVIDES REGULATED PNEUMATIC PRESSURE FOR 10 ENGINE PURGES AND 40 VALVE ACTUATIONS

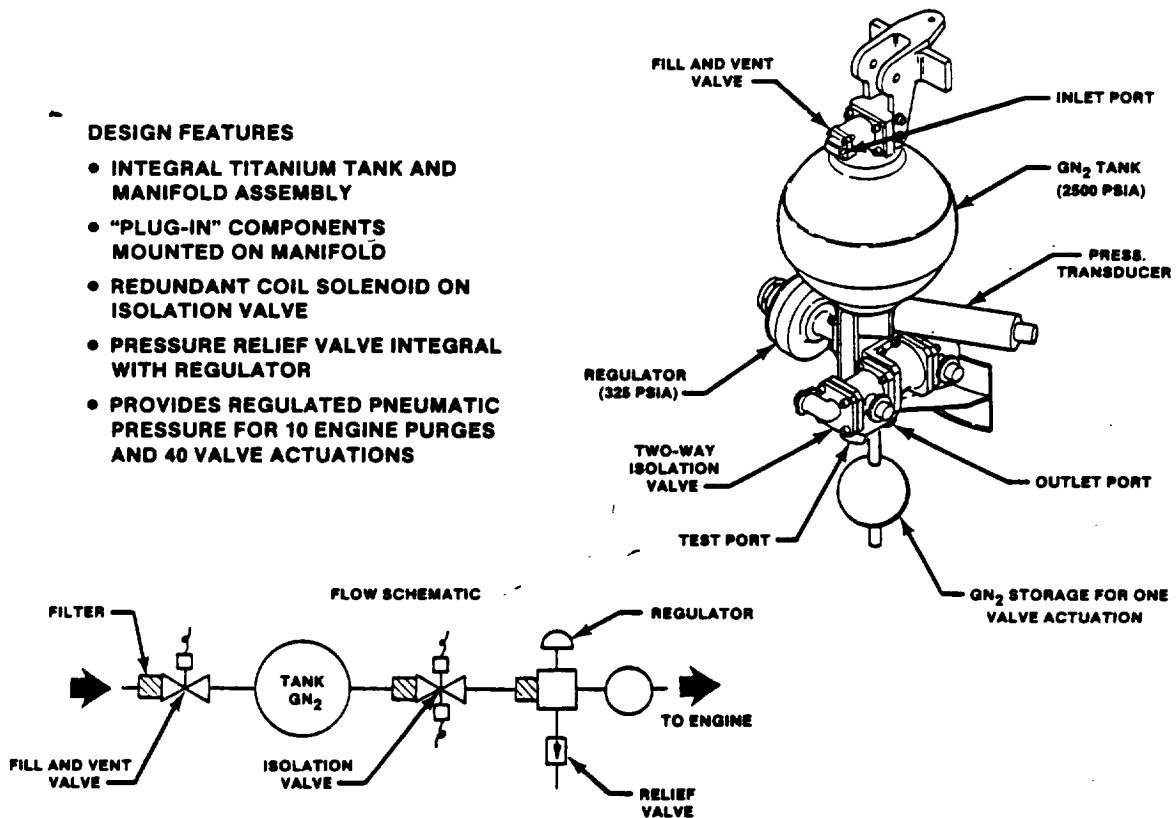


FIGURE 17.- OMS ENGINE VALVE ACTUATION SYSTEM.

redundant bipropellant valve was subsequently changed to a series redundant valve in the interest of weight and complexity. The quad redundant concept is advantageous from the standpoint of a failure to open because parallel flow paths are provided; however, the added complexity is not desirable from the standpoint of the added leak paths. Upon reevaluation of the quad redundant concept, it was decided that series redundancy was appropriate to the OMS system because, unlike the Apollo SPS engine, the OMS engines were redundant to each other and the tankage and propellant supply lines could be configured to provide complete functional redundancy in the event of a failed-closed condition. In addition, it was determined that the most probable cause of failure of the bipropellant valve to open was a failure of one of the solenoid control valves which control the flow of gaseous nitrogen (GN₂) (the actuation gas) to the valve actuators. Consequently, all solenoid valves include dual coils to provide redundancy. Finally, a second GN₂ storage tank was added immediately downstream of the pressure isolation valve. This tank provides sufficient GN₂ to open the bipropellant valve once even if the pressure isolation valve fails to open.

CONCLUSIONS

The most significant lesson learned from the OMS program was the advantage of developing critical technology before initiating full-scale hardware designs. The successful completion of pre-development studies undoubtedly reduced total contracted costs and minimized schedule delays that had been experienced in previous propulsion programs.

ACKNOWLEDGMENT

The many talented and dedicated technicians, engineers, and managers who made the Shuttle Program a success through their contributions to development of the Orbital Maneuvering System are gratefully acknowledged. In particular, the Manager, Orbital Maneuvering System, Rockwell, Mr. Don Jones; the Manager, OMS Engineering, Aerojet, Mr. Clyde Teague; and the Chief Program Engineer, Aft Propulsion System, McDonnell Douglas, Dail Stone are recognized.

DESIGN EVOLUTION OF THE ORBITER
REACTION CONTROL SUBSYSTEM

Ralph J. Taeuber, W. Karakuiko, D. Blevins, C. Hohmann, and J. Henderson
NASA Lyndon B. Johnson Space Center
Houston, Texas 77058

ABSTRACT

The challenges of Space Shuttle Orbiter reaction control subsystem development began with selection of the propellant for the subsystem. Various concepts were evaluated before the current Earth-storable, bipropellant combination was selected. Once that task was accomplished, additional challenges of designing the system to satisfy the wide range of requirements dictated by operating environments, reusability, and long life were met. Verification of system adequacy was achieved by means of a combination of analysis and test. The studies, the design efforts, and the test and analysis techniques employed in meeting the challenges are described in this paper.

INTRODUCTION

The requirements for the Space Shuttle Orbiter reaction control subsystem (RCS) were replete with challenges; however, four requirements had the greatest impact on system development: (1) a fail-operational/fail-safe design, (2) 10 years of life, (3) a 100-mission reuse capability, and (4) the capability for operation both in orbit and during reentry. The requirement of a fail-operational/fail-safe design not only introduced the complexity of additional hardware but, perhaps more importantly, introduced a complex, critical redundancy management (RM) system. The calendar life and reuse requirements posed problems in material selection and material compatibility and in ground handling and turnaround procedures, as well as classical wearout problems. The requirement for both on-orbit and entry operation complicated propellant-tank acquisition system design.

Because requirements did not identify the need for a specific propellant or propellant combination, an early issue that had to be resolved was that of selecting propellants. The ultimate propellant selection had a significant impact on the four requirements identified previously.

In subsequent sections of this paper, the most significant challenges incurred in development of the Orbiter RCS are identified and the manner in which those challenges were met in the ultimate certification of the system for operational flight is described.

PROPELLANT SELECTION

One of the first major issues to be resolved concerning the Space Shuttle Orbiter RCS was that of selecting the propellant(s) to be used. Early in the program definition phase, oxygen (O_2) and hydrogen (H_2) were baselined as the reactants for all propulsion and power systems. This choice was made for a number of reasons. As a propellant combination, O_2 - H_2 provides high specific impulse. Logistics are simplified and less costly with a single propellant combination for all vehicle propulsion systems. The exhaust products are noncorrosive, and the propellants are relatively clean and nontoxic - all attributes desired in a reusable system. As a result of the oxygen/hydrogen baselining, all early technology work addressed improving the technology posture of O_2 - H_2 systems. This improvement was necessary because O_2 - H_2 systems were far from state of the art when used for reaction control purposes. As the component technology and systems study programs progressed, the weight advantage thought to exist with O_2 - H_2 propellant systems gradually diminished. The heavy accumulators (two per system) in combination with redundant turbopumps (six per system) and heat exchangers (six per system) offset the weight advantage afforded by the better performance in the total impulse range being considered. Because system dry weight was high, the O_2 - H_2 systems also added to the vehicle landing weight penalty.

A further factor that became more and more apparent as technology work progressed was that the oxygen-hydrogen systems would be very expensive to develop and build as well as extremely complex systems to operate. The complexity generated real concerns with respect to the reliability of the overall system. When it became clear that the weight of the O_2 - H_2 system would be no better than that of a monopropellant system (fig. 1), the baseline was changed to a monopropellant hydrazine system to reduce cost and complexity. The monopropellant system baseline was retained through the award of the Orbiter prime contract. As the Orbiter design evolved and the total impulse requirement approached 2 million pound-seconds, performance again became a more important factor and the trade swung in favor of the bipropellant (monomethyl hydrazine (MMH) and nitrogen tetroxide (NTO)) systems, which were still lighter and much cheaper and simpler than O_2 - H_2 systems. Another factor being con-

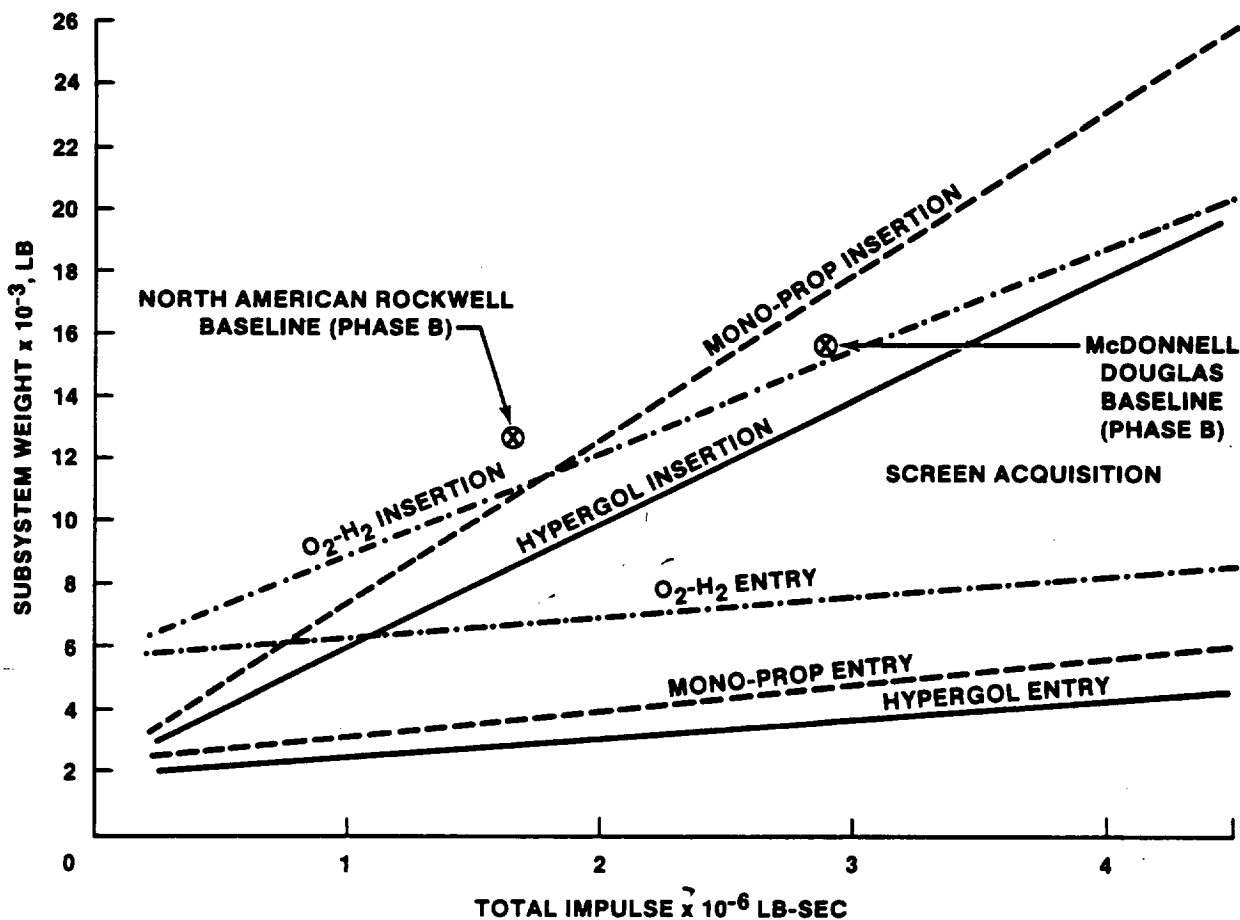


FIGURE 1.- WEIGHT AS A FUNCTION OF TOTAL IMPULSE FOR CANDIDATE PROPELLANTS.

sidered at the time was the potential for integration of the RCS with the orbital maneuvering system (OMS), which also used the MMH/N₂O propellant combination. This propellant combination ultimately was selected because of the favorable weight trade-off, the reasonable development cost, and the minimal development risk.

COMPONENT DEVELOPMENT CHALLENGES

During the course of readying each component for flight, a distinct set of development and certification problems arose. Some were the result of well-defined, but rigid requirements. Others were the result of ill-defined or changing requirements; still others were the result of being unable to readily demonstrate satisfaction of requirements. Some of the more significant challenges encountered during the development of the Orbiter RCS components are described next.

SHUTTLE ORBITER RCS PROPELLANT TANKS

For a number of reasons, Orbiter Program management selected a tank concept employing a screen propellant acquisition device (PAD), which is used to acquire and deliver gas-free liquid to the thrusters. In previous spacecraft, a Teflon membrane was used to separate the propellant from the pressurant. However, Teflon membranes rupture after relatively few expulsive cycles and, therefore, would be unsuitable for 100-mission life. No elastomeric membranes that are sufficiently compatible with the RCS propellants to assure a 10-year life have been developed. For these reasons, and because of its weight advantage over the bellows-type tanks, a screen tank was chosen to provide gas-free liquid outflow. See figures 2 and 3 for the forward and aft configuration tanks, respectively. This device works by using the surface tension of the liquid to form a barrier to the pressurant gas. The PAD is made up of channels which are covered with a very finely woven stainless steel mesh, or

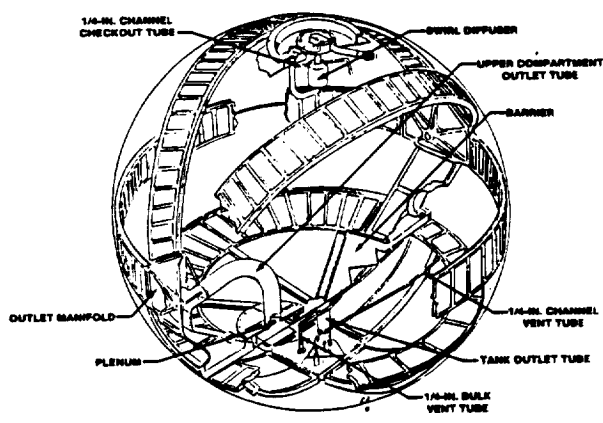


FIGURE 2.- FORWARD TANK.

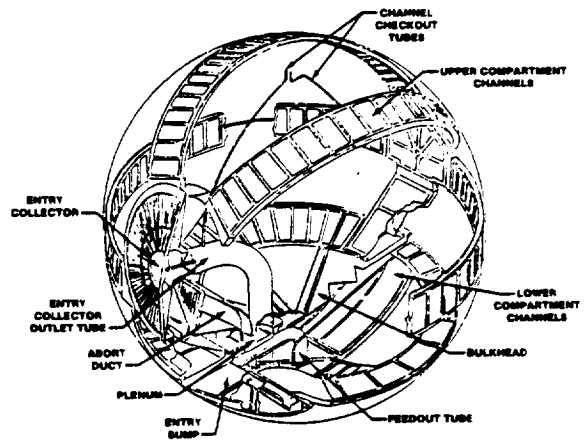


FIGURE 3.- AFT TANK.

screen. Contact with liquid wets the screen, and the surface tension of the liquid prevents the passage of gas. The strength of the liquid barrier is finite, and the pressure differential at which gas will be forced through the wetted screen is called the bubble point. When the bubble point is exceeded, the screen is said to "break down," or to transfer gas. However, if the pressure difference is less than the bubble point, gas cannot penetrate the liquid barrier and only liquid will be pulled through into the channels. Therefore, the goal in designing the tank is to minimize the pressure loss while maximizing the amount of propellant expelled, or expulsion efficiency. The pressure loss is made up of two major components: the flow loss, due to viscous loss, turning loss, entrance loss, etc., and the hydrostatic head loss (fig. 4). The latter is a function of the acceleration to which the tank is subjected. The flow losses depend on the puddle size. As the volume of propellant decreases, the screen surface area in contact with the puddle decreases; thus, to supply the same volume flow rate, the velocity must be greater and, therefore, the pressure differential must be greater.

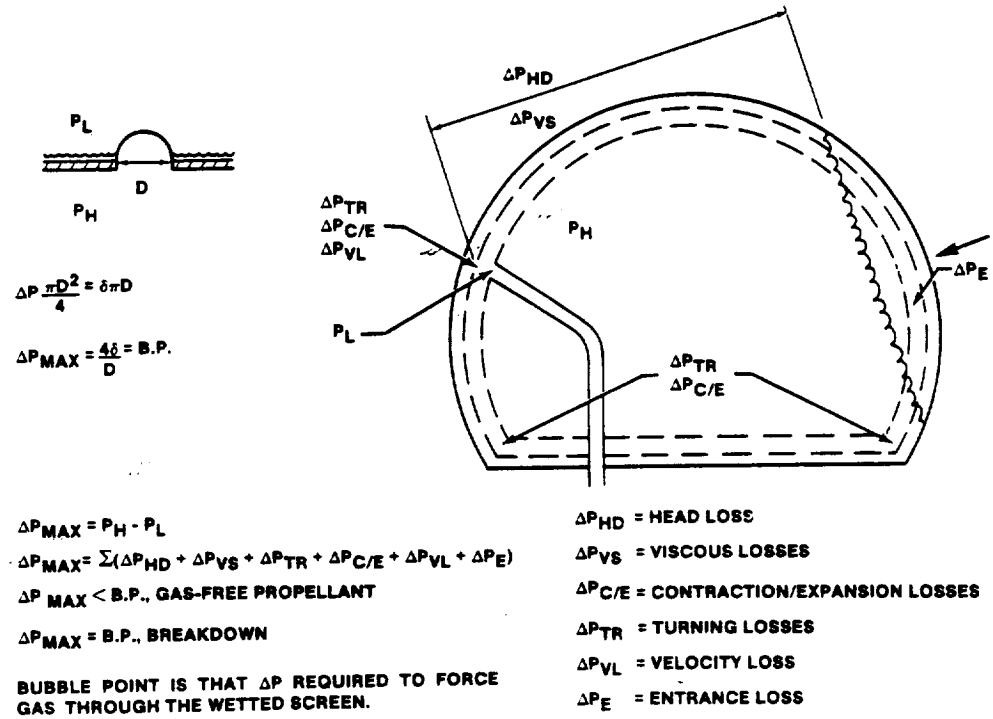


FIGURE 4.- TANK PRESSURE LOSSES.

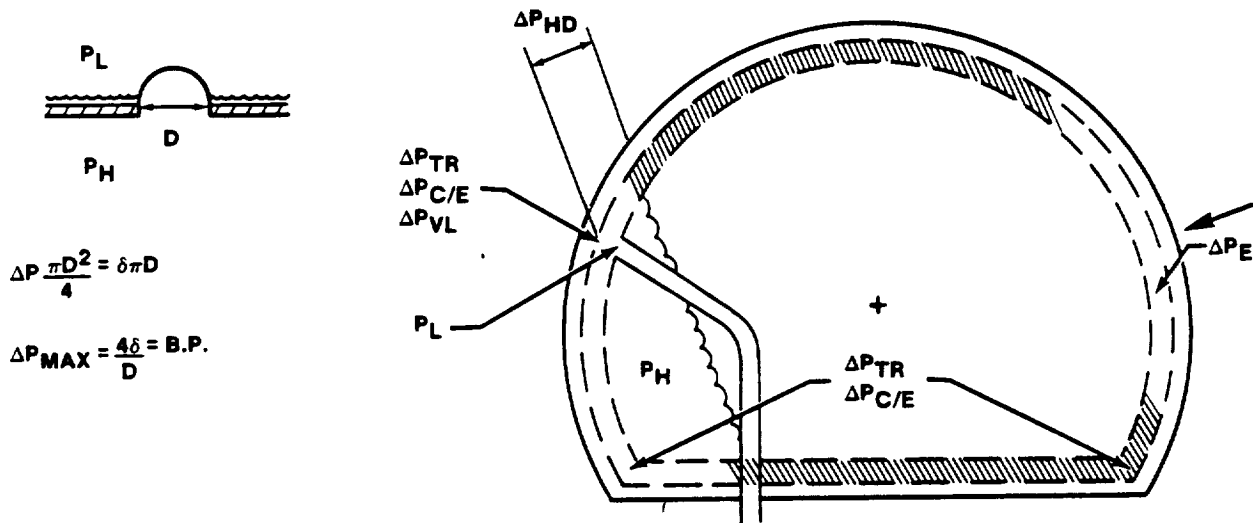
The greatest flow losses occur with the smallest puddle. The expulsion efficiency of a tank is defined as the smallest residual at which the flow and hydrostatic head-pressure losses, combined, are equal to the bubble point of the screen. Because the tank is designed to work primarily in a low-g environment, the hydrostatic head-pressure term is small. However, any ground testing has to be performed in a one-g environment, and the hydrostatic head-pressure loss very quickly becomes the dominant term and, therefore, the tank performance cannot be directly determined or demonstrated in ground tests. This problem was the greatest engineering challenge encountered in the tank development program.

To get around this problem, sophisticated math models were developed to characterize the on-orbit performance of the tank. The math models were developed using ground test of subassemblies in which flow losses of each device in the PAD were measured.

In early 1980, testing at the system level revealed a serious deficiency in the math models. In addition to the steady-state pressure drops, a transient-pressure drop, due to thruster pulsing, was discovered. This loss had not been considered in previous analyses and was unexpected. An additional analysis indicated that when combinations of thrusters were commanded simultaneously, the pressure drop associated with the opening of the thruster valves was being transmitted through the supply lines to the tank. There, the analysis showed, the pressure drops were high enough, with more than three thrusters pulsing, to cause gas ingestion and momentary screen breakdown. Because of the transient problem, gas could be fed out to the thruster and perhaps cause a thruster to misfire and be deselected during a critical mission phase. To avoid this possibility, the number of thrusters which could be simultaneously commanded per system was constrained to three thrusters for all mission phases except entry and return to landing site (RTLS) abort. For entry, the acceleration vector causes the propellant to cover the outlet; therefore, no transient problem is encountered. The RTLS case, however, still required seven thrusters. To satisfy this requirement, it was necessary to "overfill" the aft RCS tanks. Overfill means that the tanks are loaded completely full leaving no ullage volume; therefore, the upper compartment screens are entirely wet and the risk of gas ingestion is almost eliminated. However, overfill entailed a lengthy list of operational problems and procedures and it was viewed as a temporary solution to the transient problem.

Shortly after the problem was discovered, an intensive effort was initiated to quantify the transient problem. Again, because the tank performance could not be defined by direct test in a one-g environment, an advanced transient-pressure math model was developed. It was then correlated with preliminary test data obtained by the contractor from tests on a tank in one g using a test fluid and simulated thruster valves. A more detailed model-validation test plan was then developed using a tank that was specially instrumented with highly sensitive pressure transducers, and a test entitled "OV-102 Aft RCS Tank On-Orbit Performance Test" was run. This test provided pressure transient data from an actual system. The tests were run in the worst case attitude and, because of the large hydrostatic head-pressure loss, with a large residual puddle. The math model predictions for one-g operation agreed fairly closely with the test results, and the model was then used to predict the expulsion efficiency of the tanks for on-orbit conditions. A conservative safety factor was included in the predicted on-orbit performance to account for test uncertainties.

The "on-orbit" tests, along with the math model, indicated that the abort duct in the aft RCS tank was the device most affected by start transients in the upper compartment and also was the device that determined the entry expulsion efficiency. Because the abort duct for which it was designed had been eliminated, it was decided to remove this abort duct from the OV-099 tank. With this change, the updated math model indicated that the upper compartment would not be sensitive to on-orbit pressure transients after the screens are initially wetted. To test this prediction, and also to test the OV-099 modification tank, a new test concept was proposed. (See fig. 5.) A way had been found to minimize the test uncertainty due to hydrostatic head-pressure loss and to simulate the worst case "terminal" puddle in a one-g environment. By wrapping the screen channels with Teflon tape, leaving a small area uncovered at the bottom of the tank and the aft entry collector uncovered, a simulated low-g expulsion test could be run. With the collector as a high point, and with liquid filled until the level is just below it, thrusters are fired. Because only a small screen area is exposed to propellant flow, the steady-state and transient losses are maximized. Because the height below the collector is small, the hydrostatic head-pressure loss is minimized and thus on-orbit conditions are simulated. The initial results indicated that the tank was performing better than the math model predictions. The math model developed for the forward tanks indicated that the start transients were not as severe as in the aft system. Therefore, no redesign of the forward RCS (FRCS) tank was required. As mentioned earlier, during the first flight, as well as on all subsequent flights, the digital autopilot (DAP) was constrained to firing a maximum of three thrusters simultaneously. A study by the tank contractor, employing the latest model, indicates that a four-thruster capability can be attained on normally filled aft tanks. A five-thruster capability could be achieved on an overfilled aft OV-099 tank; however, because of the problems associated with overfill, this capability will not be pursued. The only major roadblock to deleting overfill is the RTLS, in which the DAP can command as many as seven thrusters simultaneously. Additional analysis performed for RTLS



$$\Delta P_{MAX} = P_H - P_L$$

$$\Delta P_{MAX} = \sum(\Delta P_{HD} + \Delta P_{VS} + \Delta P_{TR} + \Delta P_{C/E} + \Delta P_{VL} + \Delta P_E)$$

$$\Delta P_{MAX} < \text{B.P.}, \text{ GAS-FREE PROPELLANT}$$

$$\Delta P_{MAX} = \text{B.P.}, \text{ BREAKDOWN}$$

BUBBLE POINT IS THAT ΔP REQUIRED TO FORCE GAS THROUGH THE WETTED SCREEN.

ΔP_{HD} = HEAD LOSS

ΔP_{VS} = VISCOUS LOSSES

$\Delta P_{C/E}$ = CONTRACTION/EXPANSION LOSSES

ΔP_{TR} = TURNING LOSSES

ΔP_{VL} = VELOCITY LOSS

ΔP_E = ENTRANCE LOSS

FIGURE 5.- PRESSURE DROPS WITH MASKED SCREEN.

using avionic simulations has shown that no significant quantities of gas are ingested. Therefore, overfill will be eliminated by STS-8.

With the conclusion of this study, and the OV-099 performance testing, the RCS tank performance certification will be complete.

THRUSTERS

One of the major challenges in the Orbiter RCS development was design of the primary thruster. The thrust size was almost an order of magnitude larger than that used on previous manned spacecraft reaction control systems. The large thrust size coupled with a need for 38 primary thrusters made weight a prime consideration in component design. Because early technology work had shown that a hydraulically operated valve was considerably lighter than a conventional solenoid valve for a Shuttle Orbiter-size engine, that concept was chosen for use on the primary thruster (fig. 6). The new concept introduced new problems. The valve relied on pressure imbalances established by a pilot poppet to provide the necessary opening force. These valve-actuating pressure imbalances could also be created by transient-pressure waves generated by other thruster or isolation valve operation within the system. These inadvertent, momentary valve openings were demonstrated to be safe in flight but unacceptable for ground operation. Furthermore, it was discovered that gas entrapped in recesses of the valve could slow down both opening and closing valve response and also increase the tendency for the valve to "bounce" with pressure transients. To minimize the possibility of valve "bounce" during ground operations, isolation valve operation was procedurally limited to cases in which the pressure differential across the valve was below 25 psid. To accommodate the slowed valve response with the presence of gas in the valve, the minimum thruster firing time was increased from 40 to 80 milliseconds, which was still satisfactory for control purposes.

An ongoing problem that has a potential for considerable downstream program impact is the tendency of some primary thruster valves to leak when subjected to low temperature. The problem was first discovered when liquid was observed to be dripping from the system-level test article engines during a cold environment test. Additional testing at the NASA Lyndon B. Johnson Space Center (JSC)

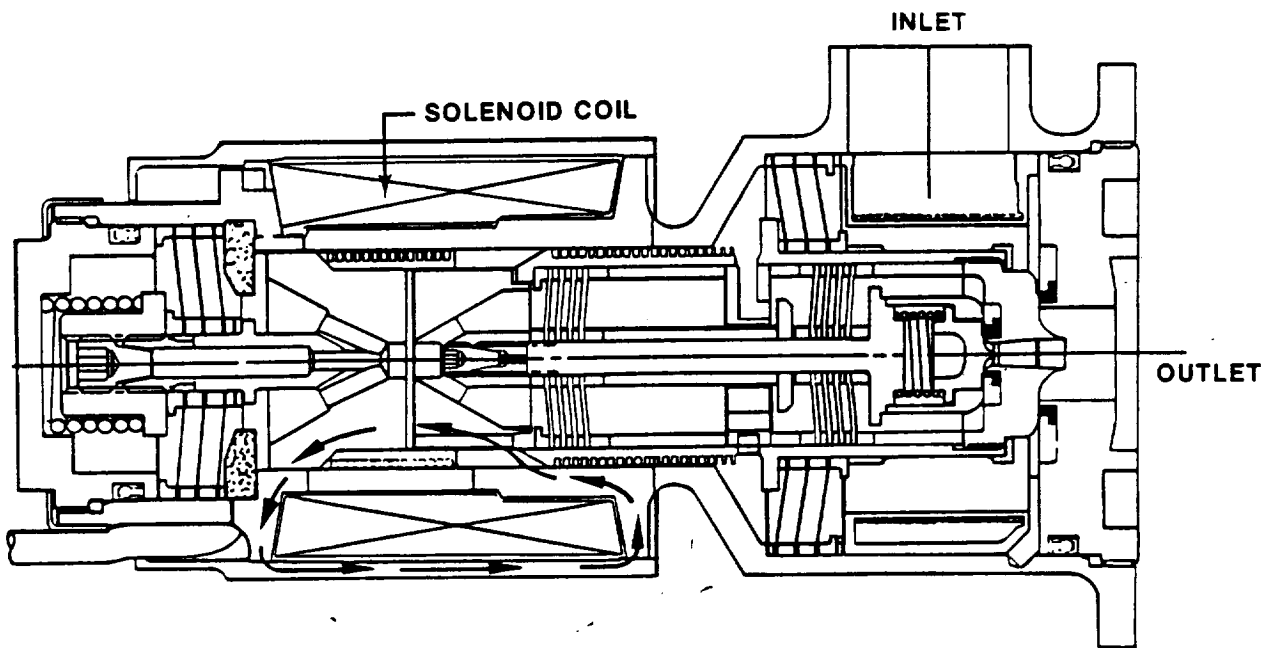


FIGURE 6.- CROSS SECTION OF PRIMARY THRUSTER VALVE.

revealed that one out of three valves leaked when chilled from ambient temperature to 300° F. Furthermore, the leakage became progressively worse with increased cycling. Preliminary corrective action in the form of a 400°-F screening test was introduced to eliminate "cold leakers." Continued investigation of the problem indicated that the TFE Teflon underwent a marked change in thermal expansion rate in the 65°- to 77°-F temperature range. Because machining, done as a part of seat fabrication, was accomplished in this temperature range, some parts had insufficient seat material exposed at reduced temperature. The flat-seat, non-temperature-compensating design made the unit very sensitive to temperature changes. Therefore, to further reduce susceptibility to cold leakage, two actions, in addition to the screening, were implemented. First, the Teflon is machined at 320° F to ensure uniform dimensions with adequate seat material exposed at reduced temperatures. Second, the thruster heater set points have been raised to maintain valve temperature above 600° F. Even with these actions implemented, there have been instances of cold leakage when heater power had to be turned off during ferry flight operations. Whether the incidence of cold leakage increases as valve seat wear occurs with use still remains to be seen and will determine whether additional work is required.

Another environment-induced development problem involved the requirement for the valve to be capable of withstanding salt fog exposure. Care was exhibited in selecting materials for the valve, and all those selected (Inconel 718, Custom 455, and A-286) were individually compatible with salt fog. However, when all the factors and materials were assembled, a galvanic crevice corrosion on the Custom 455 occurred. The completed series of ingredients that resulted in the corrosion was the stacking of the three valve materials against either of the thruster materials, titanium or columbium, plus the addition of a propellant-soaked crevice around the valve seat, and lastly, the electrolyte, sodium chloride. Severe and rapid pitting occurred on the valve poppet (Custom 455), and leakage ensued. Results of material testing confirmed the four-material problem and suggested a material change as a corrective action. Because the failure occurred late in the production process, the first flight units had already been manufactured and shipped. This situation dictated considering an immediate corrective action for existing hardware and implementing the material change for future replacements. The immediate corrective action was to keep the thrusters sealed against moisture and salt air intrusion by keeping plugs and desiccant protection in place at all times when on the ground. To date, this approach has been satisfactory, and the long-term solution has not been pursued.

Another subtle material problem occurred in the fabrication of the injectors. During waterflow tests of the injectors for the OV-102 thrusters, water was observed to be externally leaking from the injector adjacent to the acoustic cavities (fig. 7). No confirmed cause for the cracking was determined; however, an ultrasonic screening test was invented to isolate the cracked injectors. The

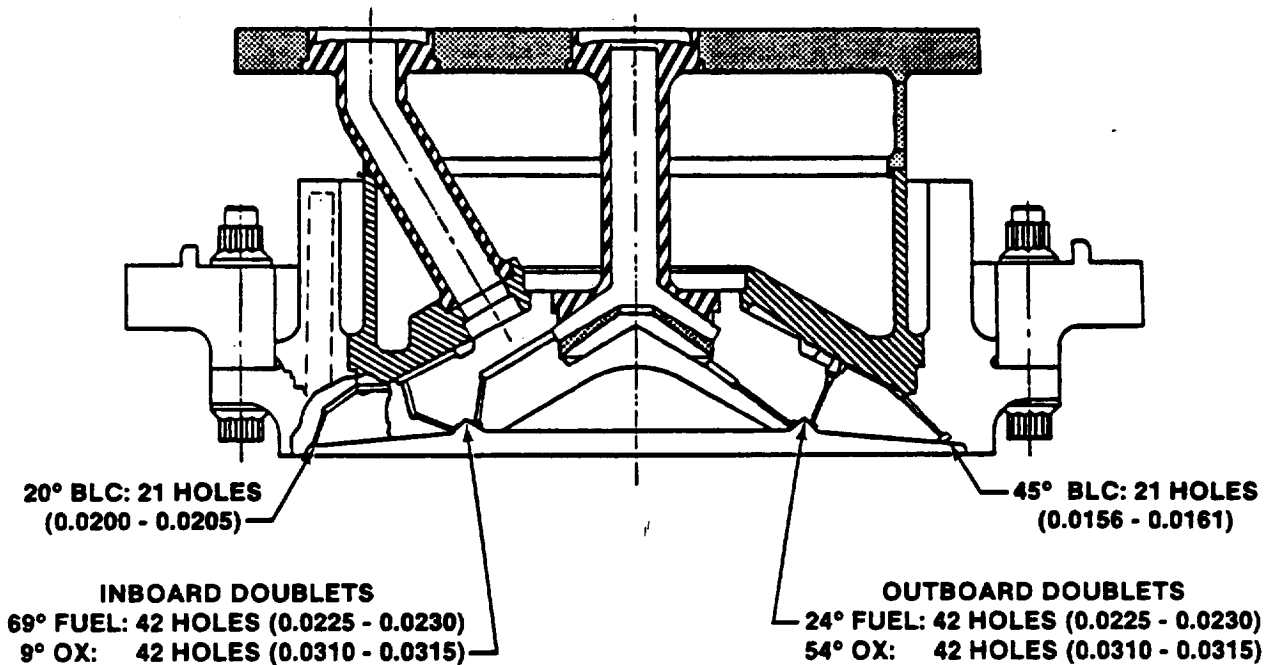


FIGURE 7.- INJECTOR CROSS SECTION.

screening test was imposed at several stages in the manufacturing process in hopes of determining the cause. During the manufacture of the OV-103 hardware, the problem reoccurred and the screening test paid off. With some good metallurgical investigative efforts, it was determined that the columbium was cracking because of hot salt stress corrosion and that fluoride salt exposure, temperature, and stress all had to be present for cracking to occur. The fluoride salt was a residue from an inadequate rinse of a chemical etch used in preparation for welding. The problem was solved by eliminating the use of the etchant after reaching a certain stage of the injector fabrication process.

One of the latest challenges encountered in the development of the Space Shuttle RCS thrusters was a premature failure of the disilicide coating on the vernier engines (fig. 8). Coating failures were first experienced in the component qualification program and later on the flight hardware. Failures occurred over quite a range of burn times. At first, it was thought to be a single generic problem with the coating itself, but as testing and investigation progressed, it was shown to be a multifaceted problem. The qualification engine coating spalled after 80 000 seconds of burn time, whereas two of the OV-102 engines developed coating defects at about 10 000 seconds of burn time. Thus, it was theorized that not only burn time but thermal cycling as well was critical. The qualification and flight hardware both had approximately equal thermal cycles. This theory was negated when one engine spalled at 10 thermal cycles and others were spall-free after more than 800 thermal cycles. Evidence pointing to one potential cause was revealed during an inspection of the OV-099 engines performed to document their condition before their first flight. Two of the engines were found to have defects, with nothing more than acceptance-test burn time. Examination of the ground-support throat plugs revealed that metallic fingers on the plug had broken and dislodged pieces from the new engine coating. These throat plugs were abandoned and new ones designed to preclude high loads being put into the coating. It was now obvious that the coating could have been and probably was mechanically damaged in some of the failures, but this mechanism did not explain all of them. Samples tested at the JSC White Sands Test Facility (WSTF) in a special coating test that had never been exposed to any throat plugs developed coating defects. Further investigation determined that poor quality control in manufacture of the combustion chamber was probably contributing to the early wearout. Ridges, undercuts, and smeared material were found in the chamber before coating. Coating over these imperfections was producing weak areas, which, when cycled, were causing coating pinholes or spalling to occur. Combustion chamber machining was subsequently revised to control intersecting cuts, and the finishing cut now is made in one direction in a single pass. Use of this new technique minimizes smearing and ridging. Chemical milling was implemented before coating to further remove any smears and ridges remaining from machining and to remove any contaminants buried in the surface. Testing to verify the improved manufacturing process is underway.

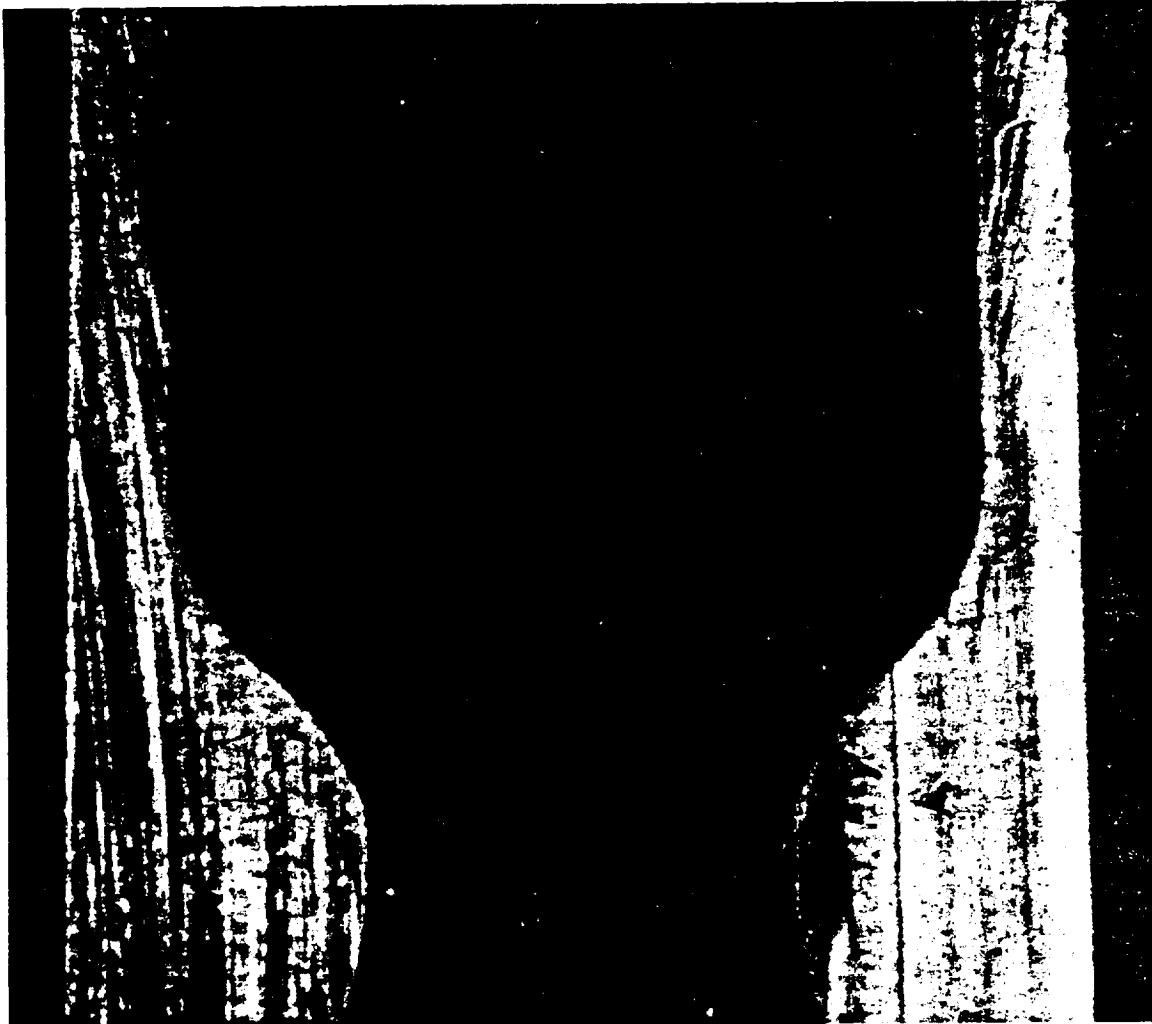


FIGURE 8.- VERNIER THRUSTER COATING FLAW.

A/C MOTOR ISOLATION VALVES

An interesting subsystem interface issue that arose on the flight vehicle involves the RCS A/C motor isolation valves and their control circuitry. The RCS isolation valves are ball valves that are driven by high-speed alternating-current motors (fig. 9). The response of the ball is slow, approximately 1 second for full travel in either direction, but the motor is rotating at 8000 rpm. The gear reduction is large, and large inertia force in the gear train is partly removed by a friction brake upon stopping. The valve was built with microswitches for terminating power at the end of valve travel. The original design accommodated the large inertia by removing power from the motor before the mechanism came to rest. By this means, the ball and gear train could "coast down" before impacting the friction energy absorber. The absorber was designed to marginally handle the anticipated inertia load. The valves cycled without problems when operated individually and had in fact completed development testing and part of qualification life testing without mishap. However, when used in the vehicle, the oxidizer and fuel isolation valves were actuated as pairs. Power was left on until the slowest of the two valves completed its cycle. This mode of operation drove the gear train of the fastest valve hard into the energy absorber and left stall torque on the motor until the slower valve completed travel and power was shut off. The added momentum of the gear train as a result of powered impact with the energy absorber caused the absorber to recoil and produce a sudden inelastic reaction load into the gear train. Repeated cycling of the paired valves could cause the nylon teeth of the third-stage planetary gear to strip and, thus, disable the valve. The first in-

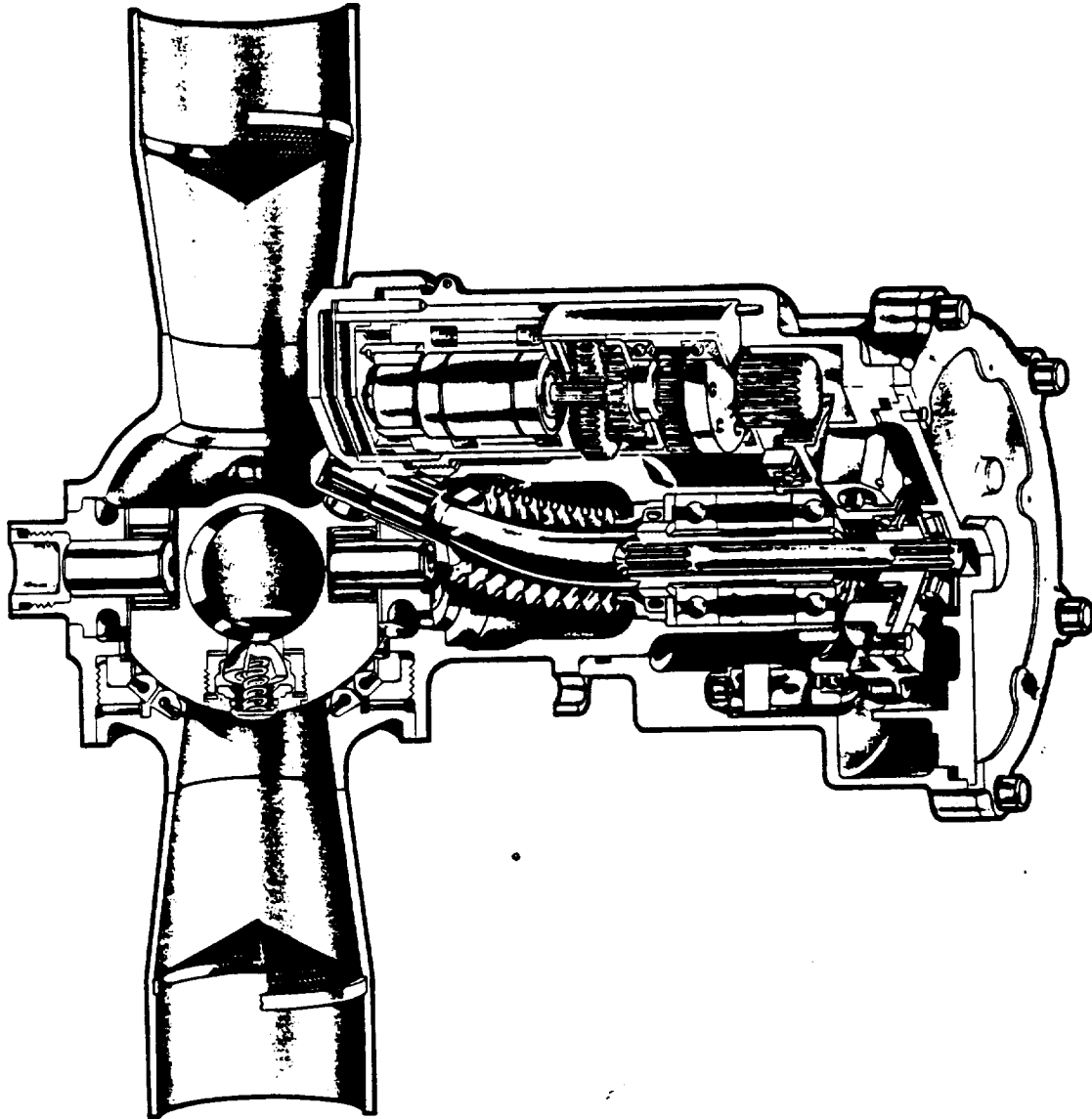


FIGURE 9.- A/C MOTOR VALVE CROSS SECTION.

dication of this problem occurred when the OV-102 forward module RCS was checked out at the NASA John F. Kennedy Space Center (KSC). The valves were being cycled with a 2-second timing circuit, and it was noticed that the microswitch feedbacks were intermittent. On closer investigation, it was discovered that power in excess of 1.15 seconds could cause intermittent open/close indications because the gear train would backlash enough to cause an open circuit to occur on the microswitch. Further investigation indicated that the vehicle wiring would leave power on for greater than 1.15 seconds and, therefore, could cause intermittent indications. Driving a valve beyond the microswitch turnoff signal was known as a "hard cycle." Testing on the A/C motor valve was begun to pursue the effects of "hard cycling" on "paired" valves. It was discovered that the reliable life of the valve was no more than several cycles. Work was initiated on redesigning the gear train to accommodate the larger loads. The resultant product was a new, all-metal gear train incorporating a magnetic brake in the motor and a different, and significantly better, energy absorber for the inertia load, designed to sustain the full inertia load plus motor stall torque driving into the stop. Certification testing of the new valve verified that the new configuration could achieve the required full 100-mission life in the hard-cycle mode.

RCS SYSTEM-LEVEL DEVELOPMENT AND CERTIFICATION

A major challenge with any liquid propulsion system such as the Space Shuttle RCS is to verify that all the components combined as a system operate as a unit during all expected operating modes and that the interaction between components will not cause problems. A second significant activity required on a system-level test article is the development and verification of all ground checkout and servicing procedures necessary for a multiuse vehicle. To ensure that these goals were met and also to verify system structural integrity, a major ground test program was performed on the RCS (fig. 10). This ground test program included the following major elements.

1. FRCS and ARCS Breadboard Development Test
2. FRCS and ARCS Development Tests
3. FRCS and ARCS Qualification Tests
4. FRCS Thruster Installation Tests
5. ARCS Pressure Panel Tests
6. FRCS and ARCS Vibroacoustic Tests

The major objectives of these test programs were as follows.

1. FRCS and ARCS Breadboard Development-Test - Provide early system data to support the analysis and design efforts and to evaluate servicing and checkout procedures. Simulated propellants were used in this test.

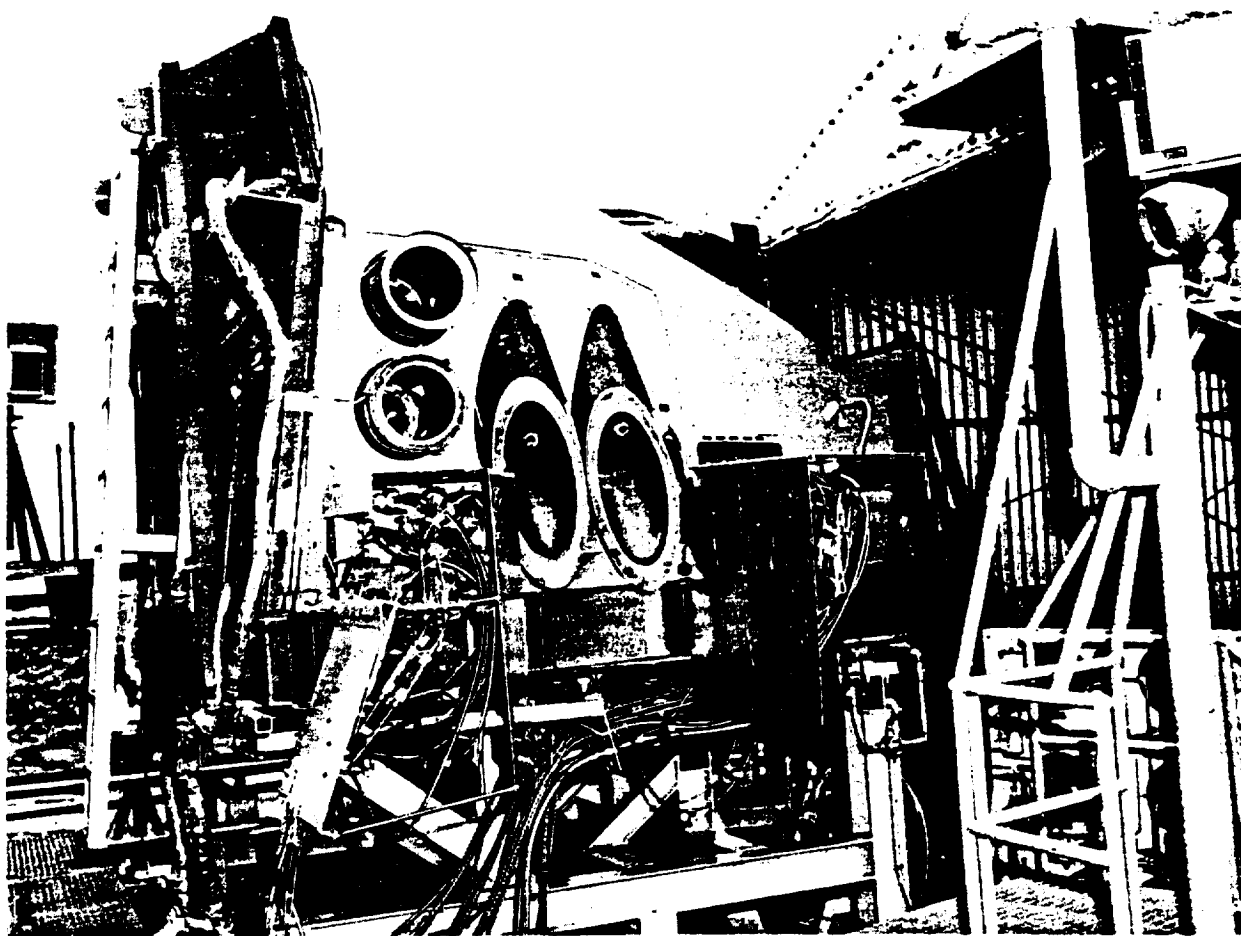


FIGURE 10.- TYPICAL SYSTEM TEST ARTICLE (FRCS).

2. FRCS and ARCS Development Tests - Conduct 12 test series on the FRCS and 11 test series on the ARCS at WSTF to verify RCS design, including evaluation of steady-state and transient performance under all operating conditions, and develop and evaluate servicing and checkout procedures. This was the first actual system hot-fire testing on complete FRCS and ARCS test articles.

3. FRCS and ARCS Qualification Tests - Conduct sufficient test series on the FRCS and ARCS to certify the system for development and operational flights. These tests were divided into Qual I (STS-1), Qual II (operational flights), and Qual III (OV-099 and subsequent modifications). Thirteen test series were performed on the FRCS and 15 on the ARCS with each series approximately equivalent to one mission.

4. FRCS Thruster Installation Tests - Provide data for thermal and structural certification of the complex RCS thruster installation. The firing tests were performed at simulated altitude at WSTF, and the vibroacoustic tests were performed at Rockwell International (RI).

5. ARCS Pressure Panel Tests - Certify the RCS helium pressurization system for simulated series regulator failures including relief system limit testing.

6. FRCS and ARCS Vibroacoustic Tests - Provide data to certify FRCS and ARCS primary and secondary structure, components, and tubing for the acoustic environments experienced during ascent. The FRCS test was conducted at RI and the ARCS at JSC.

Numerous challenges resulted from the problems discovered during the ground test programs listed. Some of the major challenges and the eventual technical solutions are discussed next.

The breadboard test program revealed two major problems requiring resolution.

1. Servicing procedures resulted in propellant residual entrapment in the helium pressurization lines. Subsequent activation of the system by opening the fast-response helium isolation valves produced pressure surges that would sometimes rupture the burst disk in the helium relief system. This problem was solved procedurally for the OV-102 vehicle by implementing a series of pressure cycles called "breathing cycles" which cleared the liquid from the helium lines. For OV-099 and subsequent vehicles, the problem was solved by a change in the helium system plumbing to add a separate, dedicated propellant vent line.

2. The ARCS breadboard test revealed that certain combinations of engine firings produced pressure transients in the propellant feed system in excess of the design limits. The pulse characteristics were also erratic under these conditions. As a result of this finding and parallel findings from the development testing at WSTF, the minimum pulse on/off duration and frequency were changed from an initial value of 0.040 second on/0.040 second off with a maximum frequency of 12.5 hertz to 0.080 second on/0.080 second off with a maximum frequency of 6.25 hertz. This change resulted in more propellant usage in some cases but eliminated the pressure transient concern and resulted in much more repeatable pulse performance with the corresponding reduced risk of engine pressure spikes and erroneous deselections by the Shuttle RM system. This change was a major step in improving the reliability of the RCS.

Challenges resulting from RCS system-level development and qualification testing were numerous. Some of the major challenges involved engine valve problems, servicing and activation problems, propellant-tank checkout, propellant-tank surge-flow evaluation, and subsystem life certification. The first major challenge occurred very early in development testing and involved engine/system incompatibilities. The initial plan was to fill the RCS tanks with propellant and the manifolds with low-pressure gas. During system activation, the propellant isolation valves were opened and the gas was compressed; these actions left large gas bubbles in the RCS feed system and engine valves. As discussed in another section of this report, the primary engine valve operation is adversely affected by gas entrapment. During initial FRCS system-level testing, major problems occurred including missed pulses, failure of valves to close between pulses, long ignition delays, cold flows of one propellant due to oxidizer and fuel valve mismatch, and valve bounce due to system pressure transients. This inefficient operation also caused concern for potential hard-start (spike) problems resulting from residue accumulation in the combustion chambers. The following plan was implemented to solve these problems.

1. Change the loading procedure to a vacuum-fill process to eliminate gas bubbles.

2. Perform bench tests on the thruster valves to map performance characteristics as a function of gas entrapment/flow, static and dynamic pressure, propellant saturation, etc.

3. Install linear variable differential transformers on some thruster valves on the FRCS and ARCS test articles to determine effects of gas bubbles, saturated propellants, and system pressure transients.

4. Change minimum pulse on and off times from 0.040 second to 0.080 second.
5. Run system-level tests with vacuum-filled manifolds and saturated propellants to verify adequacy of modification.
6. Perform single engine pulse tests at altitude simulating conditions seen in step 5 to determine whether oxidizer and fuel residuals cause problems at altitude.

This program was successful in characterizing the valve and valve/system interactions. The test program also revealed that the corrective actions of vacuum filling and changing the minimum pulse time were adequate to allow the thruster valve to be used for flight without major valve or system design changes.

Problems of engine valve leakage at cold temperatures and low pressure and engine valve bounce caused by upstream isolation valve or quick-disconnect cycles were also discovered in system-level testing. These problems were solved by procedural controls and are discussed more fully in the section entitled "Thrusters."

Checkout of the RCS propellant-tank surface-tension acquisition screens proved to be another major challenge. For the screens to perform properly in flight, there must not be any holes in the screen that will cause a reduction of the bubble-point pressure. It is desirable to have a technique that allows contingency and periodic checkout of the screens during operations without removing the propellant tanks or using fluids other than the propellants. The basic process proposed for this checkout involves filling the tanks with propellants, draining them without drying the propellant from the screens, and then determining the bubble point (pressure at which gas penetrates the wet screen surface) through the special checkout ports provided for this purpose. This process proved to be fairly easy to implement for the fuel tank because of the low vapor pressure of MMH. Implementing the process for the oxidizer tank, however, proved to be a very difficult task because of the high vapor pressure of NTO. All initial attempts to check out screens on the system level with oxidizer proved to be unsuccessful because the screens dried out. This challenge was met by implementing a special test program on the tank alone with simulated system-level checkout access plumbing and valves. This approach allowed for experimentation with thermal control, tank orientation, and propellant saturation level of the nitrogen gas introduced into the tank. This approach finally revealed the key controls that must be used to allow checkout with oxidizer. The most important parameter requiring control is the saturation level of the gas. The incoming pressurant gas (nitrogen) must be saturated with propellant. Second, the incoming gas must be at the same temperature as, or warmer than, the tank, and third, the tank pressure should be in the 60- to 70-psi range. The concept was then proven on system-level tests, and current plans are to implement it for the operational phase of the program at KSC.

Test effort on the system level caused the development of some very effective techniques for evaluating the complex surface-tension acquisition devices. The use of X-rays was found to be very effective in determining the locations of propellants in the tank for evaluating performance, loading and drain procedures, and potential acquisition device gross damage. Elaborate instrumentation concepts were also developed to evaluate surge-flow pressure differentials in the tank. These were used to evaluate pressure differentials for high flow rates into and out of the tank associated with crossfeed/interconnect operations and propellant manifold repressurization. High-response piezoelectric instrumentation was also used to determine differential pressures across the screens to evaluate engine start transient effects in the tank.

Another challenge associated with system-level testing involved life certification for 10 years and 100 missions. Obviously, a 10-year/100-mission life test would be very expensive. Therefore, the concept used was to certify the individual components in bench-type environments for 100 missions of cycle life and vibration exposure and to run short, 90-day screening tests for propellant compatibility. The components and the system were then tested in a development program representing 11 to 13 missions over an approximately 9-month period. This test was followed by a qualification test program representing 13 to 15 missions spread over a 3-year period. Including other special tests, the qualification hardware was exposed to 4 to 5 years of operation. All operations on the systems were designed to be representative of actual Space Shuttle servicing, flight, and repair procedures. The acoustic test articles were exposed to a full 100-mission or more equivalent exposure in a short time period except for the FRCS module, which was exposed for only 10 missions and analyzed for the remaining 90 missions. All failures or problems were analyzed for any life-limiting indications, and, if a life limit was indicated, it was so noted and identified as limited-life hardware. The described approach was then used for 10-year/100-mission certification with any exceptions being noted.

The ARCS vibroacoustic test revealed a problem very late in the certification program that required extensive effort to solve. Initial testing on an ARCS pod structure revealed that vibration levels on individual components and zones in the pod were higher than had been previously predicted

and were higher than the levels used for component certification. This pod was originally equipped with "mass simulated," nonfunctional components with the idea that the levels would be equal to or less than the levels used in component tests. Therefore, component tests could be used for certification. Since the levels were higher, a decision was made to use the vibroacoustic pod for component certification. This decision required a last minute change to install functional components in the pod and complete the component and system certification in this manner. Since the levels were higher in the ARCS, test results could also be used to certify the FRCS components for 100 missions. The FRCS had only been tested for 10 missions as a system.

RCS INTERFACES

The Orbiter RCS is the most complex RCS ever designed. To use it effectively requires major RCS interfaces with avionics/software, wiring, instrumentation, thermal control, and structures subsystems. A major challenge in the RCS design was to ensure that compatible interfaces exist within these areas. Although difficult interface challenges existed in each of the areas, perhaps the most difficult was the RCS/avionics/software interface. Only this interface will be discussed here. Principal functions performed in the Shuttle avionics/software for the RCS are redundancy management, quantity monitoring, RCS crossfeed sequencing, OMS-to-RCS interconnect sequencing and gaging, FRCS propellant dump, trickle-current testing, and system monitoring and annunciation functions. All these functions required extensive exchange of information between subsystems to ensure that the software and the avionics hardware were compatible with the RCS hardware in terms of timing, sequencing, limit sensing, redundancy requirements, etc. The most complex avionics/software interface is the area of redundancy management. The purpose of the RM system is to monitor the 44 RCS engines, announce and isolate failures, and reconfigure the system to maintain vehicle control during all mission phases. This function is necessary to effectively maintain the RCS fail-operational/fail-safe redundancy. The major elements of the final system design are as follows.

1. Fail-off detection - compares computer fire command with engine chamber pressure feedback to determine whether engine has fired. If no response occurs in an appropriate time, the engine is declared failed-off, annunciated to the crew, and taken out of the available jet table in the computers.
2. Fail-on detection - compares jet driver output with computer fire command to determine whether an engine is firing with no command. If a failed-on engine is detected, it is annunciated to the crew so that the appropriate manifold may be isolated to prevent excessive propellant loss.
3. Valve leak detection - monitors engine fuel and oxidizer injector temperatures to determine whether engine valve leakage is occurring. If the temperature of the oxidizer injector tube is below 300° F or of the fuel is below 200° F because of rapid propellant evaporation, a leak is indicated. For a leak indication, the problem is annunciated to the crew and the engine is taken out of the available jet table. The crew may then manually close the appropriate isolation valves if propellant loss is excessive.
4. Manifold status monitor - monitors RCS manifold isolation valve positions to determine whether valves are open or closed. If the valves are closed, the engines on that manifold are removed from the available jet table.
5. Jet fault limit monitor - limits number of jets which may be automatically removed from the available jet table in response to failure indications. This function is designed to ensure that the RM system will not automatically remove engines to levels at which insufficient control authority exists.

All RM functions may be overridden by the crew in all phases except for ascent, for which only limited override capability is available. To date, this system has been very effective in detecting RCS engine problems and managing RCS redundancy in flight.

The other major avionics/software interfaces are now briefly described. Quantity monitoring uses RCS helium and propellant-tank pressure and temperature measurements to calculate and display the RCS propellant status at all times using the pressure/volume/temperature relationship to determine the quantity of helium gas that has been transferred from the helium tank to the propellant tank. The RCS crossfeed sequence provides automatic sequencing of 28 RCS/OMS valves to feed RCS engines in both aft pods from the RCS propellant tanks in a single pod. The sequence will also reconfigure to normal feed and is operational only in ascent and entry phases. The OMS-to-RCS interconnect sequencing and gaging performs the OMS/RCS valve sequencing required to feed OMS propellants to RCS engines during abort dumps and to reconfigure to normal feed after the dump is completed. During on-orbit operations of normal missions, the OMS-to-RCS interconnect sequence initiates OMS-to-RCS gaging and automatically pressurizes the OMS tanks as required. The on-orbit valve sequencing is a manual operation. The FRCS propellant dump sequence provides capability for the crew to dump the FRCS propellant through opposing Y-axis engines for center-of-gravity control. The trickle-current

test is used to check the electrical circuits that provide voltage to fire the RCS engines. Various RCS pressures and temperatures are limit sensed, displayed, and annunciated by the avionic/software interface to alert the crew of potential RCS problems.

OPERATIONS

Operations challenges for the RCS can be divided into two major categories: ground operations and flight operations. More emphasis is placed on ground operations because most major operations challenges have occurred in that area. As an introduction to ground operations, the basic operational concept for the RCS and the OMS is described.

The basic design concept for the hypergolic systems with their toxic, flammable propellants is to include the systems in modules or pods that can be removed from the Shuttle Orbiter and taken to a dedicated maintenance facility for hazardous repair or checkout operations. This facility is called the Hypergolic Maintenance Facility (HMF). By performing hazardous operations in the HMF, the work can be done in parallel with other Orbiter work and, thus, valuable turnaround time between flights can be saved. The HMF is also used to perform lengthy checkout operations, whether hazardous or not, to save serial turnaround time. The modules or pods are also provided with access panels and numerous plumbing access connections to enable performance of most checkout functions in the Orbiter Processing Facility (OPF) without removal from the vehicle. The decision on whether to perform repair or checkout in the OPF or the HMF is usually based on access and turnaround time considerations.

Development of ground checkout philosophy has been a major challenge for a reusable system that contains highly corrosive propellants, is used on a continuous basis in flight, and has considerable redundancy. The general philosophy that has been developed is as follows. A complete electrical and mechanical checkout on the FRCS module and the ARCS pods is performed by the manufacturer before the units are delivered to be installed on the Orbiter. The interfacing Orbiter electrical and instrumentation wiring is also checked out using module and pod simulators before the actual hardware is installed. The most critical components and the system plumbing integrity are checked again in the HMF before final installation on the Orbiter. After the module and pods are installed for the first Orbiter flight, the electrical components are checked for proper end-to-end channelization where possible by actual physical response, e.g., flow, pressure, or temperature response. The system is then loaded with propellants and helium on the launch pad. During the actual flight, the system pressures, temperatures, quantities, and valve positions are monitored closely for any indication of malfunction. Special procedures are also used to get as much component functional data as is reasonably possible by changing from one operational component to a redundant component during each mission; this is done with regulator paths, heaters, and engines. Special hot-fire tests are also performed to check out engines that might not normally be used. Use of this technique verifies the functional capability of as many components as possible to reduce ground checkout requirements. After the Orbiter lands, component checkout is performed on a very limited number of components every flight based on their criticality and whether they can be checked out in flight. Most components are only checked out on a 5- or 10-mission basis to screen for unexpected deterioration. The system plumbing is leak checked by monitoring for pressure decay at normal turnaround pressures after every flight. The engine chamber and nozzle coating is also inspected for defects after every flight. By using the described approach, the turnaround time is minimized without excessive sacrifice in reliability.

One of the first major challenges encountered in actual operations was the need to provide rain protection for some of the Orbiter engines after the protective structure was moved away and the protective ground covers were removed from the RCS engines. The requirement was to protect the three upward-facing engines and eight of the left side engines from rainwater accumulation on the launch pad. The upfiring engine covers had to prevent water accumulation that could freeze in the injector passages during ascent. The side-firing engine covers had to prevent water from accumulating in the bottom of the chamber and to protect the chamber pressure-sensing ports. Freezing of accumulated water during ascent could block the sensing port and cause the engine to be declared "failed off" when it was first used. The original design concept was to install Teflon plugs in the engine throats (side-firing) and a combination Teflon plug tied to a Teflon plate that covered the nozzle exit (upfiring). This concept added vehicle weight, required special procedures to eject the plugs in flight, and had the risk of accidental ejection in ascent that could damage tiles. The second concept evaluated involved Teflon sheets that were glued to the nozzle exits and pulled off by lanyards when the crew access structure was retracted. This concept was considered to be unnecessarily complex and did not provide protection all the way to launch or for all the engines. The final solution was a novel approach of using ordinary plastic-coated freezer paper cut to fit the exit plane of the nozzle and glued in place (fig. 11). Tests proved this concept would provide a reliable seal under all expected rain and wind conditions. Wind-tunnel tests revealed that the covers could blow off in ascent before Mach 1. The covers were, therefore, very low cost, simple, and added no significant weight.

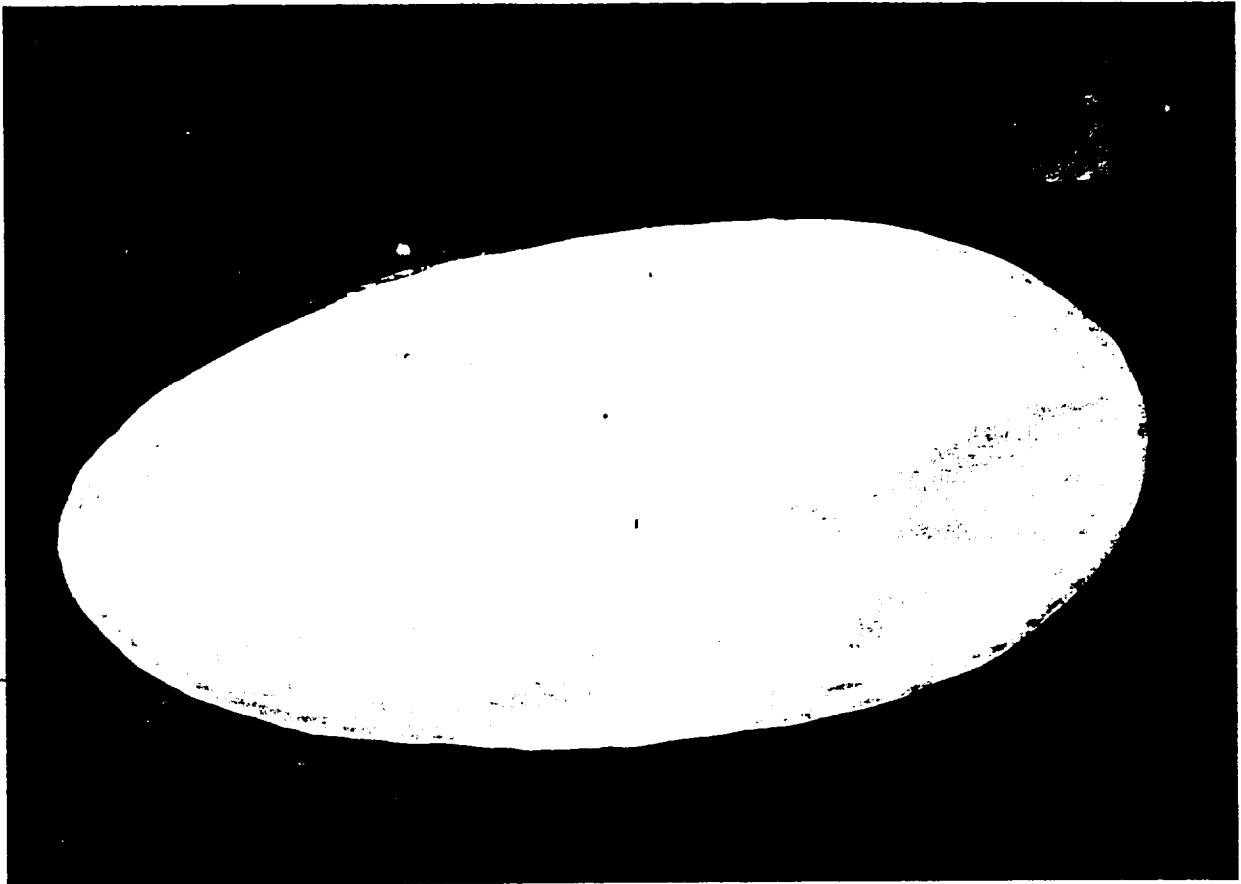


FIGURE 11.- PAPER ENGINE COVER.

The next major operational challenge involved RCS engine valve leakage problems during ground turnaround. Following the first orbital flight of the Shuttle, the FRCS module and the ARCS pods were removed for inspection and checkout. A test was performed to evaluate the capability to evacuate the manifolds after they had been drained of propellant but not completely dried. Following this test, four RCS engine oxidizer valves developed high gas-leak rates. This leakage caused great concern because the leak rate was high enough to indicate that the valves might leak liquid. To understand the problem, one of the engines was removed for failure analysis. This failure analysis, in combination with the analysis performed on another engine removed for a different reason, revealed the causes for the leakages. The valves had low Teflon seal height and some nitrate deposits in the seal area. The drying of the oxidizer system by evacuation caused Teflon shrinkage, which, in combination with the nitrates, caused leakage. It was expected that rewetting the seal with liquid oxidizer would swell the seal and dissolve the nitrates and, therefore, prevent liquid leakage. Experience has shown that this does happen. The KSC turnaround procedures were changed to preclude drying the RCS manifolds by evacuation unless they are to be refilled immediately with liquid. The problem of oxidizer valve gas leakage during turnaround has not recurred.

Prevention of iron nitrate contamination in the RCS oxidizer proved to be another operational challenge. Storage of oxidizer in tanks and plumbing that contain iron has been found to cause iron contamination in the propellant. This contamination can form a nitrate that can precipitate and cause valve leakage, filter blockage, interference in sliding fits, etc. Several RCS component failures were related to this problem; the most prominent one was the failure of a ground-half quick disconnect to close resulting in an oxidizer spill on the launch pad just before STS-2. A program was implemented at WSTF to determine the parameters that cause iron nitrate formation and then to implement procedures to prevent their formation in Shuttle propellants. This program resulted in understanding the relationship between iron, water, and nitric oxide content and nitrate formation. Also, production and storage controls and filtration techniques to remove the iron were developed. With the implementation of these controls, the iron nitrate problem appears to have been solved.

Another major operational challenge was development of the best procedures for ferry flight of the Orbiter RCS after a mission. Because of the initial concern for engine valve leakage at cold temperatures and propellant slosh effects on tank screens, the RCS propellants were drained at the landing site before ferry flight. Following STS-2, the drain operation had two valve sequencing errors that subjected the RCS propellant tanks to potentially damaging surge flows. These errors were attributed to the remote location of the drain site and the difficulty of communications between the drain site and KSC, where the systems data were available. Consequently, the operations site (KSC) recommended that the propellant not be drained before ferry flight. This recommendation was accomplished after STS-3 by turning the RCS thruster heaters and FRCS area heaters on through a special hookup to the carrier airplane. The carrier airplane was also instrumented with a special accelerometer to monitor for excessive slosh loads on the RCS tanks. A recognized risk was taken that 15 to 25 percent of the RCS thruster valves might leak as much as 10 cm³/hr of liquid propellant during ferry flight even with the heaters on. This approach has been successful on all ferry flights from STS-3 to the present with only minor leakage occurring in a few engines. Damaging slosh loads have never been encountered.

The incidents that occurred during draining at the landing site created another major operations challenge. There was concern that the RCS tank screens and/or internal bulkhead structure might have been damaged by the surge flow into the tanks. Since the RCS tank checkout procedures by bubble-point technique had not been fully developed at that time and no ground-support equipment (GSE) was available to perform in-place tank checkout, the only way to check the tanks was to remove them and send them to the manufacturer for checkout. This action would have been a major impact to the program schedule and to hardware deliveries for subsequent vehicles. To avoid this impact, a decision was made to attempt to duplicate the surge incidents on the ARCS test system at WSTF and then to check out the test tanks to determine whether damage occurred. This resulting test program required a meticulous duplication of all the procedures that had been performed on the systems at the landing site. This duplication was particularly challenging since data were not available during some periods at the landing site and the crossfeed plumbing and the GSE were different at WSTF than on the Orbiter. The test program was successfully completed, and results indicated that the tanks on the vehicle were not damaged. This testing resulted in saving about 2 months on the Shuttle schedule, since the tests at WSTF were run in parallel with the other Orbiter operations and no checkout times were required for the tanks.

The next major operations challenge occurred after STS-3, when the Shuttle Orbiter landed at White Sands, New Mexico. Just after landing, high winds blew gypsum sand into the RCS engines before they could be covered. This event caused concern that the injector orifices could be blocked and thus cause unstable combustion and/or improper cooling of the combustion chamber walls. Results of bench tests revealed that the gypsum would migrate into the passages of the injector, particularly on the upfiring engines, where the gypsum accumulated on the injector face. Results of bench tests also revealed that the gypsum would harden and cake when exposed to propellants or water such as seen in ferry flight (cold leakage and moisture from the air). To solve this problem, a plan was implemented to remove and replace all nine of the upfiring engines and to remove three horizontal-firing engines. The three horizontal-firing engines were inspected and test fired to ensure that no detrimental effects were seen. Data from these three engines were then used to clear the other horizontal engines for flight.

A general program goal during the operational phase has been to improve/reduce turnaround time and operations. The RCS program has been very successful in this area to date, and additional reductions are expected in the near future. Major turnaround improvements to date include the following.

1. Deleted screen drying requirement - 16 hours.
2. Developed computer program to track nitric oxide content in oxidizer and thus deleted requirement for postflight oxidizer samples - 8 hours.
3. Deleted requirement to drain and refill tanks and manifolds between flights - 2 to 3 days.

Turnaround improvements in work include the following.

1. Delete overflow requirement on the ARCS propellant tanks - 1 to 2 days.
2. Improve loading procedures - 8 hours.

These improvements have been achieved primarily by implementing special programs on the test articles at WSTF to ensure that the changes are acceptable. The testing has also been supplemented by analysis efforts in some cases.

Numerous problems or challenges and their solutions have been identified in this paper. The solutions to the problems have produced satisfactory operational hardware. The real achievement in completing the development program, however, was not in the final hardware itself but in what was learned to make that hardware possible. Those real achievements on this program must become the routine working tools for the next major effort so that the creative engineers of tomorrow may spend their time constructively in dealing with tomorrow's challenges.

SPACE SHUTTLE ORBITER AUXILIARY POWER UNIT
DEVELOPMENT CHALLENGESRenee Lance and Dwayne Weary
NASA Lyndon B. Johnson Space Center
Houston, Texas 77058ABSTRACT

When the flying spacecraft was approved for development, a power unit for the hydraulic system had to be developed. Unlike other systems on the Orbiter, there was no precedent in earlier spacecraft for a hydraulic system nor for the power unit to drive the hydraulic pumps. The only prototypes available were airplane auxiliary power units, which were not required to operate in the severe environments of a spacecraft nor to have the longevity of an Orbiter hydraulic power unit. The challenge was to build a hydraulic power unit which could operate in 0g or 3g, in a vacuum or at sea-level pressure, and at -65° F or 225° F, which would be capable of restarting while hot, and which would be capable of sustaining the hydraulic loads for the life of the Orbiter. This paper describes the challenges of building such a machine and the manner in which they were met.

INTRODUCTION

This paper deals with the problems associated with providing power to aerodynamic control surfaces and other functions, such as steering and braking, for a vehicle intended to function as both a spacecraft and an aircraft. The approach selected to accomplish these tasks for the Space Shuttle Orbiter Program was to use a conventional hydraulic system and thereby to establish conventional aircraft hydraulic system technology as the foundation of the Orbiter system. This approach minimized the technology development requirements except for the power supply unit. Developing a power supply unit to drive the hydraulic pumps thus became one of the major challenges for the Space Shuttle Orbiter Program.

The basic approach to providing hydraulic power for the Orbiter was to use a small, high-speed, monopropellant-fueled turbine power unit to drive a conventional aircraft-type hydraulic pump. Although a misnomer, the power unit was labeled an auxiliary power unit (APU) because of its similarity to conventional aircraft emergency power units, traditionally called APU's. Here, in the name, much of the similarity ends. The stringent requirements imposed on the Orbiter APU quickly made this machine different from existing aircraft APU's.

REQUIREMENTS

Basically, the Orbiter APU's were required to operate in temperature environments of -54° C (-65° F) to 107° C (225° F), in acceleration environments of 0g (on orbit), 3.3g (boost), and 1.5g (landing shock), and in pressure environments of sea level to space vacuum. The units were required to operate for 92 minutes each mission at power levels from 8 to 148 horsepower. A minimum of two restarts was required during each mission. In addition, the APU's were to be used for the 100-mission life of the Orbiter. A breakdown of APU design requirements is shown in table 1. During the ascent, descent, and landing portions of a mission, reliance is placed on the Orbiter hydraulic system (fig. 1) for critical flight control functions. These functions include providing power for the Orbiter control surfaces (rudder/speedbrake, body flap, and elevon actuation systems), main engine gimbaling and propellant control during ascent, landing gear deployment, and steering and braking during landing. Operations occur during launch/ascent, on-orbit checkout, reentry/descent, and landing/rollout.

Operational effectiveness of the APU is predicated on reliable, failure-free operation during each flight, on mission life (reusability), and on serviceability between flights (turnaround). Achieving these elements was the challenge presented to the APU development team consisting of the NASA Lyndon B. Johnson Space Center (JSC), Rockwell International, Sundstrand Corporation, and the Sundstrand subcontractors.

SYSTEM DESCRIPTION

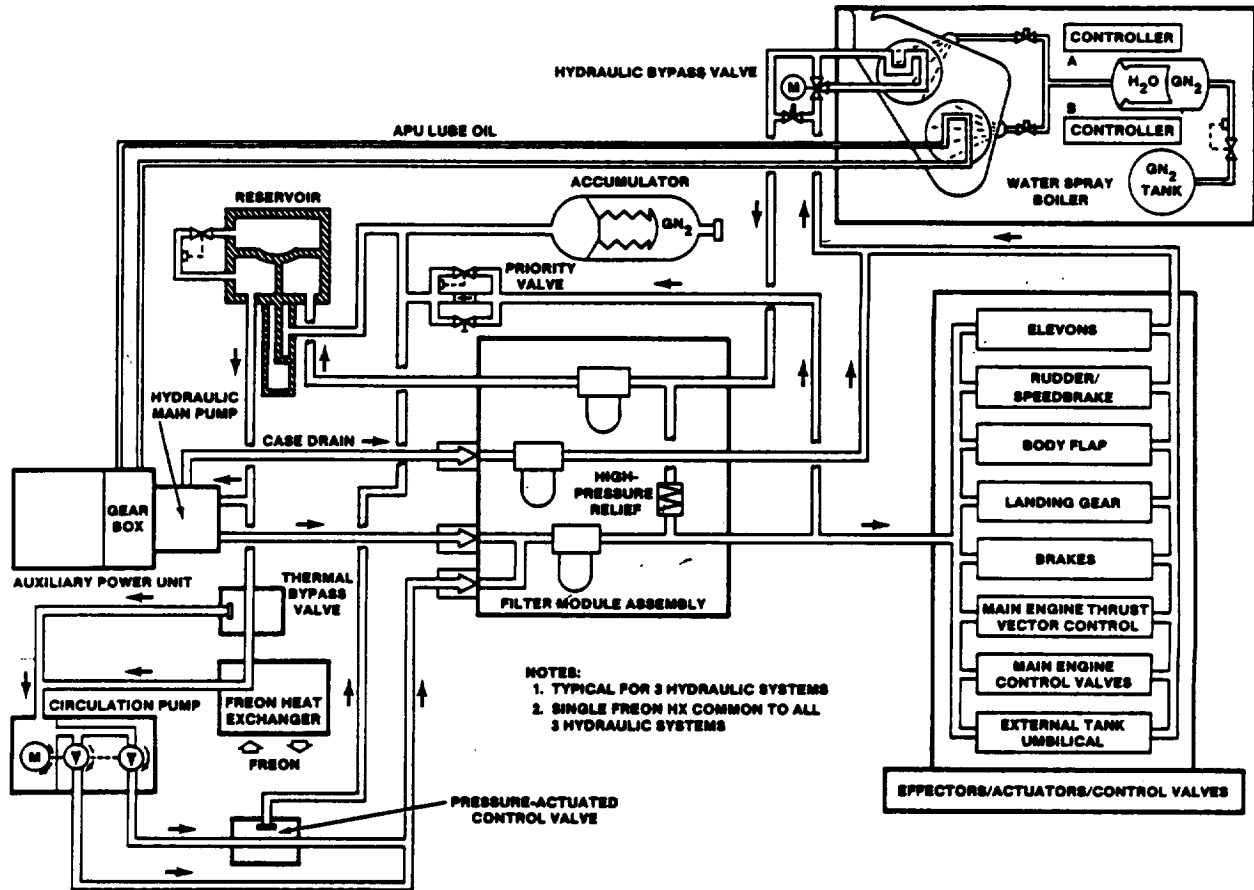
The Orbiter vehicle uses three complete APU subsystems and three hydraulic systems. The APU's, including their fuel systems, are isolated from each other. Pressure-actuated cross-links are provided between the hydraulic systems so that in case of a failure in a single APU or hydraulic system, the remaining two systems can accommodate the total hydraulic load.

TABLE 1.- ORBITER APU DESIGN REQUIREMENTS

Parameter	Requirement
Basic	Provide shaft power for 3 hydraulic pumps to operate aerodynamic control surfaces, main engine thrust vector control, main engine valves, landing gear, brakes, and steering
Design	3 independent APU subsystems; liquid hydrazine fuel supply, filter, valve, APU, controller, lubrication system, thermal management, cooling provisions
Operation	
Power, hp	
Nominal (normal speed)	134
Maximum (high speed)	148
Life between scheduled maintenance, hr	20
Starts	Prelaunch, hold, checkout, contingency checkout, and reentry
Thermal control	Maintain fuel, lubrication oil, and water temperature at 45° to 150° F (7° to 65° C); control fuel system soakback to <200° F (<93° C)
Tank capacity, nominal, lb (kg)	350 (158.8)
Duty cycle, min	
Nominal	92
Abort once around	120
Environmental	
Temperature, °F (°C)	
Min. prelaunch	0 (-18)
Min. on-orbit	-65 (-54)
Min. atmospheric flight	-40 (-40)
Max. reentry soakback	225 (107)
Acceleration, g	
Boost	3.3
Orbit	0
Landing shock	1.5
Vibration, g _{rms}	
Level A	
X-axis	8.2
Y-axis	4.1
Z-axis	4.1
Level B	
X-axis	5.3
Y-axis	2.6
Z-axis	2.6
Pressure	Sea-level to space vacuum

The APU's are hydrazine fueled, turbine driven, and restartable a multiple of times. Power is delivered to the hydraulic pump through a lubricated zero-g, all-attitude gearbox. The units have a thermal control system to prevent both freezing of the fuel during periods of low-temperature environmental exposure and overheating during heat soakback following operation and shutdown. An electronic controller provides all of the functions to check out key APU status parameters before launch, control during operation (startup, speed control, shutdown, redundancy management), and thermal management before and after operation.

A functional schematic of the APU subsystem is presented in figure 2. Figure 3 shows the APU configuration. The Orbiter installation is shown in figure 4, in which the locations of the fuel feed system, the fuel tankage, the water cooling system, and the water tankage are indicated.



NOTES:
 1. TYPICAL FOR 3 HYDRAULIC SYSTEMS
 2. SINGLE FREON MIX COMMON TO ALL 3 HYDRAULIC SYSTEMS

FIGURE 1.- ORBITER HYDRAULIC SYSTEM SCHEMATIC.

Monopropellant-grade hydrazine fuel is supplied to the inlet of the fuel pump at pressures ranging from 80 psia (5.5 bars) to 370 psia (24.5 bars). The fuel pump increases the pressure to approximately 1500 psia (103 bars). The high-pressure fuel is directed through the gas generator valve module (GGVM) to the gas generator (GG). The GG catalytically decomposes the fuel into gas at a temperature of 1700° F (927° C) and at a nominal pressure of 1260 psia (86.5 bars); the gas is then directed through a two-stage, supersonic reentry turbine. After work is extracted by the turbine, the gas is used to cool the gas generator by flowing over it before exiting the APU.

Once turbine operating speed is achieved, it is controlled within +8 percent by the GGVM, the electronic controller, and speed sensors. Three redundant speed sensors mounted at the turbine shaft provide the electronic controller with pulsed speed signals. The primary nominal turbine operating speed is 75 000 rpm. If the primary speed control mode fails, a secondary speed control mode of 81 000 rpm is activated automatically. This secondary mode may also be selected manually in the event the APU is required to have greater load-carrying capacity. Should the secondary speed control mode fail, a backup (part of the primary circuit) control mode of 83 000 rpm is activated automatically. If both primary and secondary control modes are inoperative, automatic shutdown occurs at 93 000 rpm.

The power from the turbine shaft is transmitted to the hydraulic pump, the fuel pump, and the lubrication pump through the gearbox. The gearbox design features piston accumulators that function as variable-capacity oil reservoirs and gearcase walls that closely conform to the gears. These features enable the lubrication system to function in any attitude and in zero g (ref. 1). Component description and performance may be obtained through references 2 and 3.

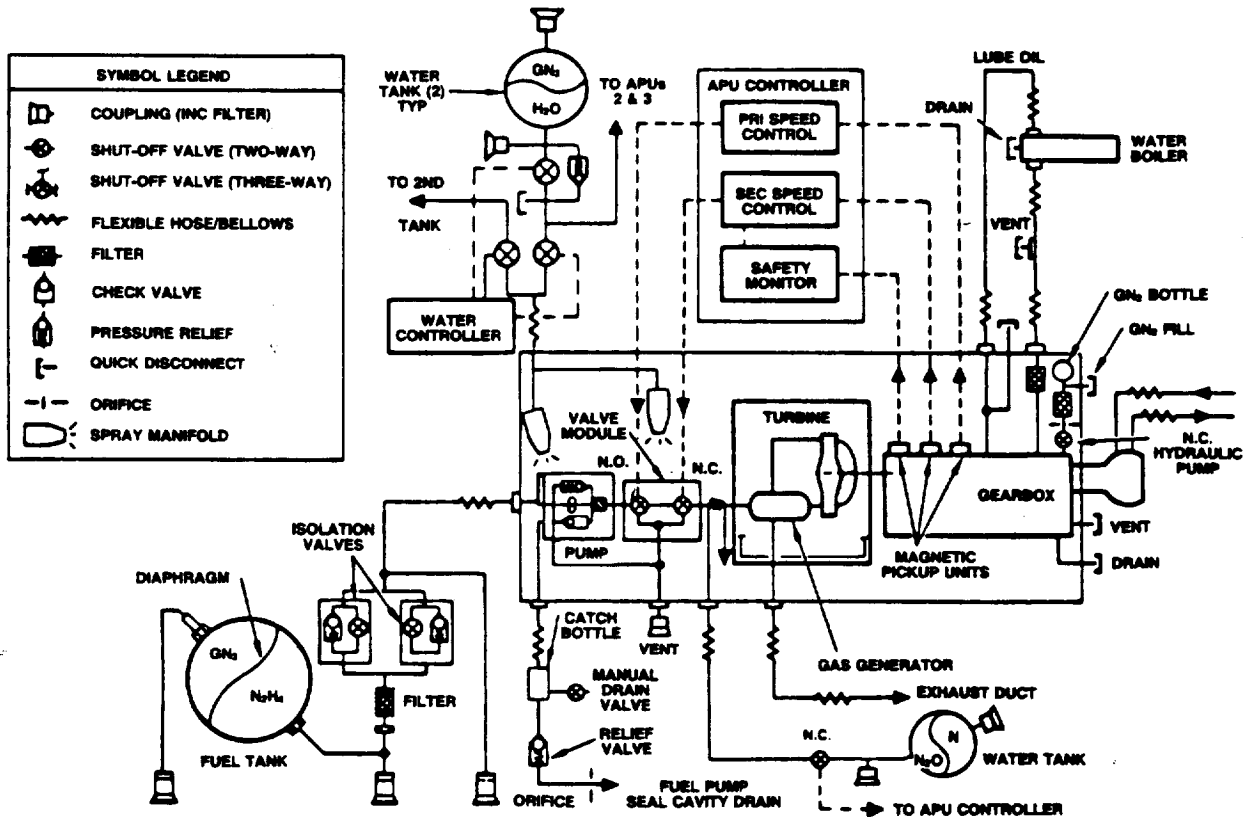


FIGURE 2.- AUXILIARY POWER UNIT SUBSYSTEM SCHEMATIC.

EARLY DESIGN PROBLEMS AND SOLUTIONS

Early in the APU development program, several significant technology issues arose. Key among these were problems with fuel pump life and performance, turbine wheel blade and shroud cracking, gas generator life and hot-restart capability, control valve seat/poppet life and valve performance, gearbox accumulator performance, turbine shaft seal leakage, lubrication oil silting, gearbox performance at low ullage pressures, exhaust turbine containment housing life (cracking), turbine overspeed containment, and controller manufacturing. In the paragraphs to follow, these problem areas are described and the solutions or actions taken discussed.

FUEL PUMP

Because of the very poor lubricity properties of hydrazine, galling of the fuel pump gears was an early problem that significantly limited pump life. The approach taken to resolve this problem was to reduce the pitch velocity, to design the gear teeth to minimize sliding contact between the gears, and to use a gear material less sensitive to galling. This change was accomplished by using a very hard material and many small teeth rather than a few large ones. The resultant design was a 16-pitch, 17-tooth gear made from M2 tool steel. This design is in use today and effectively provides unlimited fuel pump life (fig. 5).

Poor performance (volumetric efficiency) was another problem characteristic of the early fuel pump. This problem was found to be associated with dimensional instability of the graphite sleeve bearings, which permitted internal leakage. The solution was found in the area of clever manufacturing processes rather than in the primary material selection. By partly machining the bearings, then soaking them in hydrazine before final machining, reasonable dimensional stability was achieved. This process was augmented by the use of O-ring seals between the bearing-face ends and the cover plate (body). These changes improved the basic pump performance to such an extent that a controlled

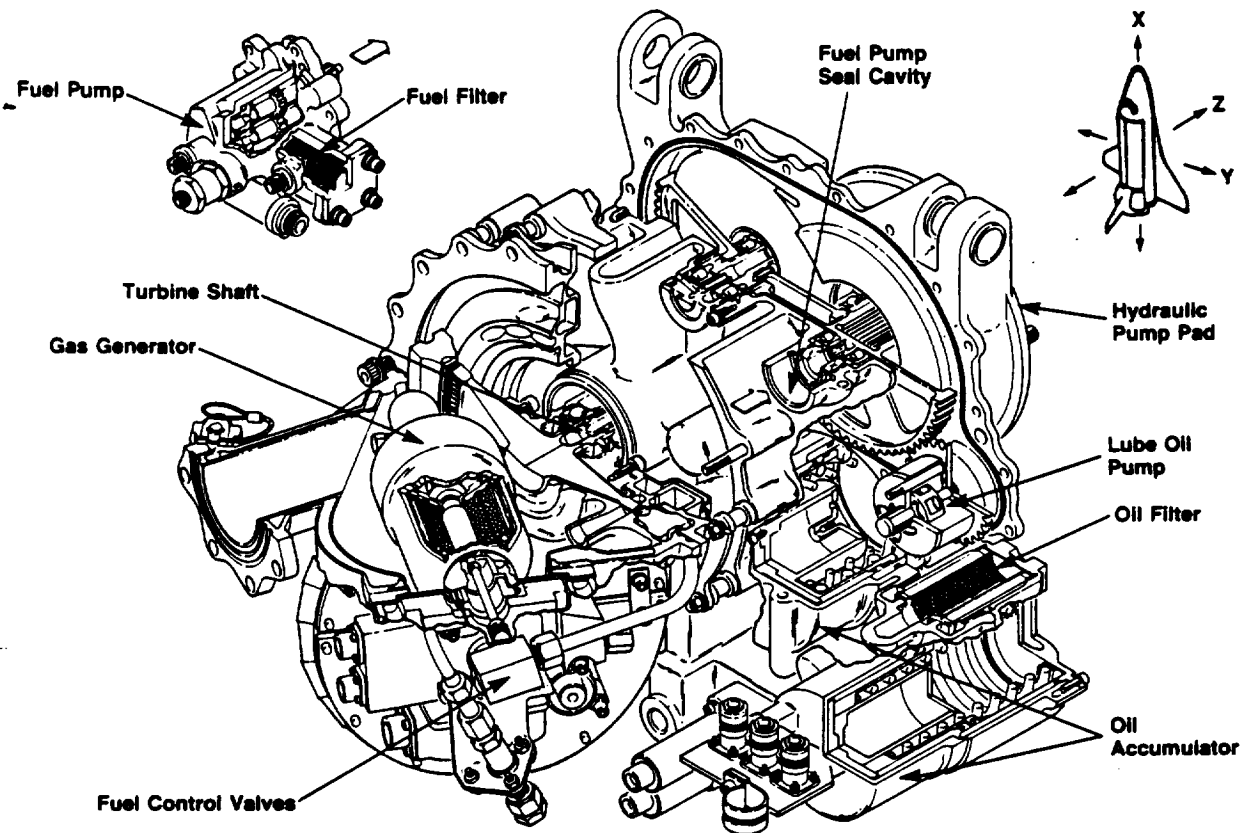


FIGURE 3.- AUXILIARY POWER UNIT ASSEMBLY.

leak (drilled passage from the high-pressure side of the pump to the low-pressure side) is now used to match (lower) the output pressure to levels required by the gas generator design.

During development testing, fuel pump drive-shaft seal leakage problems resulted in several design iterations of the bellows in the seal. These changes were not successful, and after a bellows failure during an Approach and Landing Test (ALT) flight, the bellows-type shaft seal was replaced with a seal that uses an O-ring in place of the bellows to seal between the carbon-face seal holder and the seal case. No further problems with massive fuel leakage due to seal failures have been experienced. A disassembled fuel pump is shown in figure 6.

TURBINE WHEEL

The APU turbine wheel is a 5-1/4-inch-diameter, impulse-type turbine using a blade tip shroud (fig. 7). Early problems with the wheel included blade root cracks (fig. 8), shroud cracks, inadequate welds between the blade tips and the shroud (fig. 9), and blade trailing-edge cracks at the blade tips. The trailing-edge cracks propagated to the point at which pieces of the blades would break off. The combination of blade root cracks and shroud cracks led to at least one instance of loss of a blade and a portion of the shroud during APU operation (fig. 10). The trailing-edge cracking was found to be caused by aerodynamically induced fatigue acting on the very thin (0.005 inch) trailing edge near the tip of the blade. Analysis results indicated that this part of the blade could be removed with a small 45° chamfer at the blade tip without significant effect on performance. Testing later verified this as an acceptable solution for the problem.

The blade root cracking was resolved by carefully controlling the blade root corner radiuses. Stress caused by sharp radiuses was found to cause the cracking. Careful design and dimensional control of the electrochemical-machining (ECM) tooling successfully resolved this problem. The shroud cracking situation was found to be related to both material selection and the welding process.

ORIGINAL DRAWING
OF POOR QUALITY

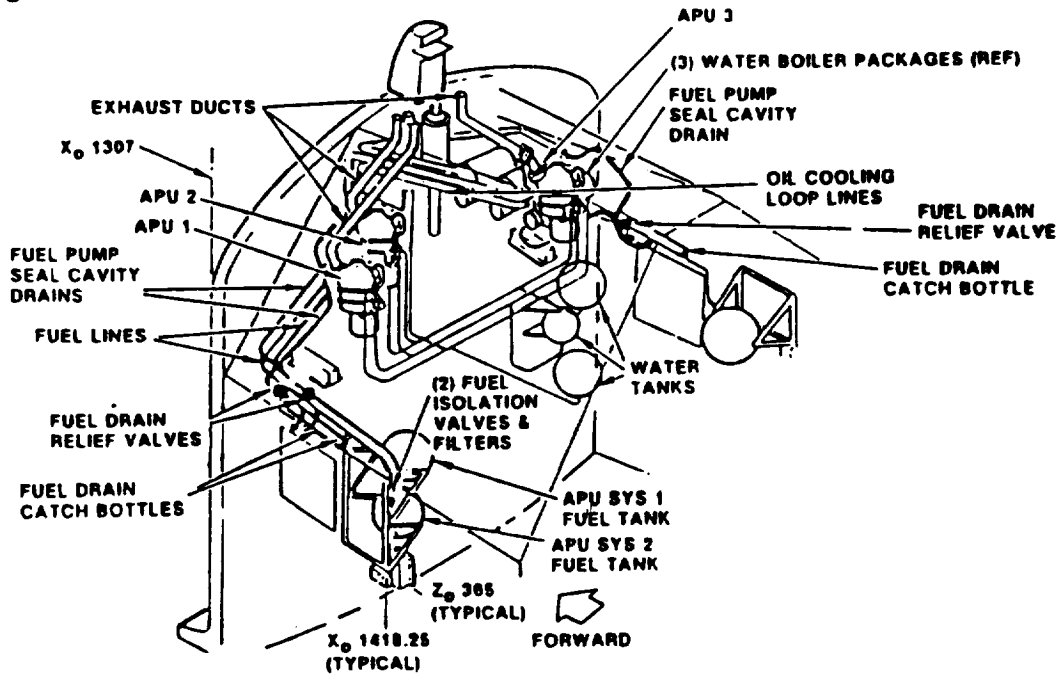


FIGURE 4.- AUXILIARY POWER UNIT SUBSYSTEM INSTALLATION DESCRIPTION.

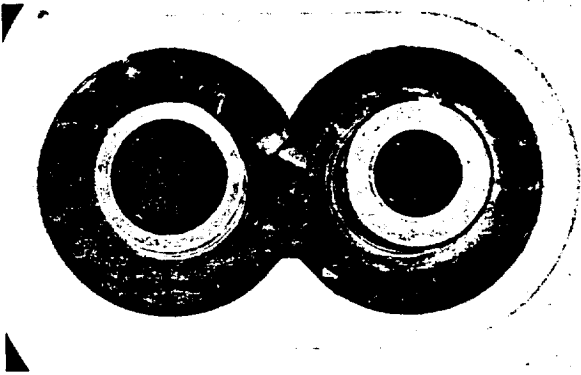


FIGURE 5.- APU FUEL PUMP GEARS, 17 TOOTH/16 PITCH.

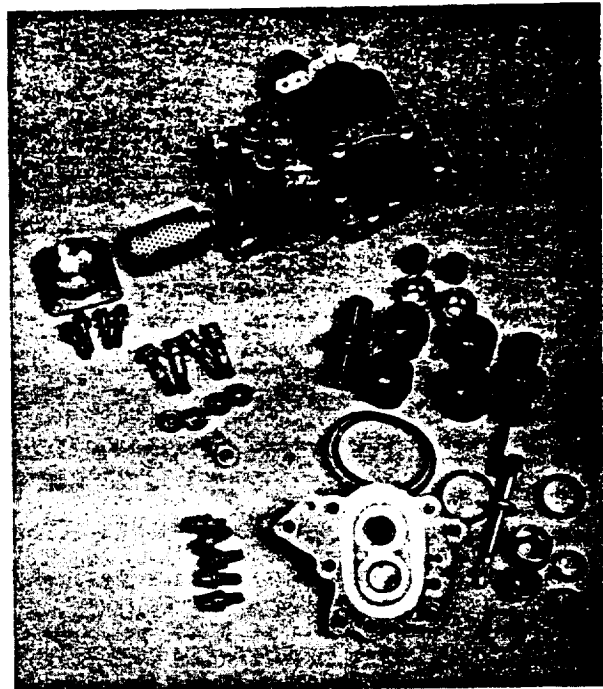


FIGURE 6.- APU FUEL PUMP.

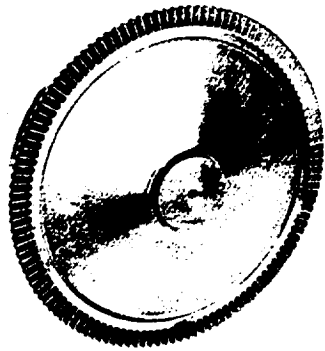


FIGURE 7.- TURBINE WHEEL.

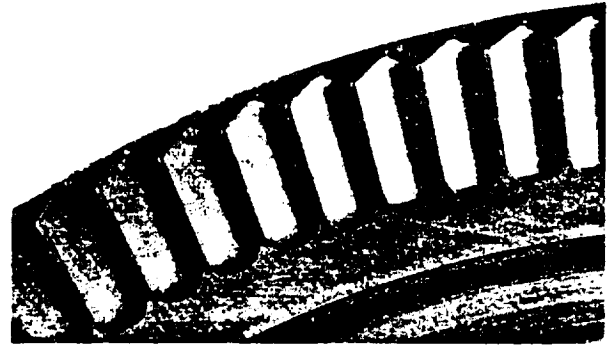
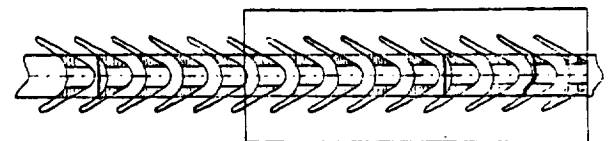


FIGURE 8.- AIRFOIL ROOT CRACKS AFTER 28 HOURS IN APU 102.



FIGURE 9.- METALLOGRAPHIC SAMPLE OF EB-WELDED JOINT RANDOMLY SELECTED. ARROWS DENOTE UNWELDED AREA IN CENTER OF JOINT (14X).



SHROUD CRACK SCHEMATIC BEFORE FAILURE

VIEW OF INSET AREA (ABOVE)
SHOWN AFTER FAILURE

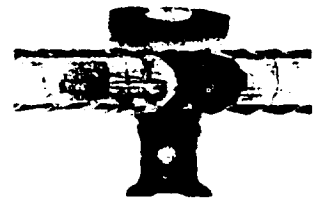


FIGURE 10.- SHROUD CRACK. TOP: SCHEMATIC BEFORE FAILURE. BOTTOM: VIEW OF INSET AREA (ABOVE) SHOWN AFTER FAILURE.

Increased strength and weldability characteristics were achieved by changing the shroud material from Hasteloy X to Inconel 625. Then, a very precisely controlled electron-beam (EB) weld procedure was developed to ensure full penetration weld across the chord of the blades without overheating the shroud. These actions eliminated the shroud crack problem.

GAS GENERATOR VALVE MODULE

Development of a reliable valve (fig. 11) to control the fuel flow into the APU gas generator proved to be one of the most challenging tasks of the APU program. The valve is required to "pulse" fuel into the GG at frequencies of 1 to 3 hertz. Leakage requirements were stringent for both safety and efficiency reasons. In addition, the valve is exposed to significant pressure fluctuations (80 to 1500 psia per cycle) and must provide high response, yet have high reverse-cracking capability to seal against the GG pressure at valve closing.

The primary problems with the valve centered around leakage and limited life due to wear and failure (breakage) of the tungsten carbide valve seat. Considerable effort was invested in redesign

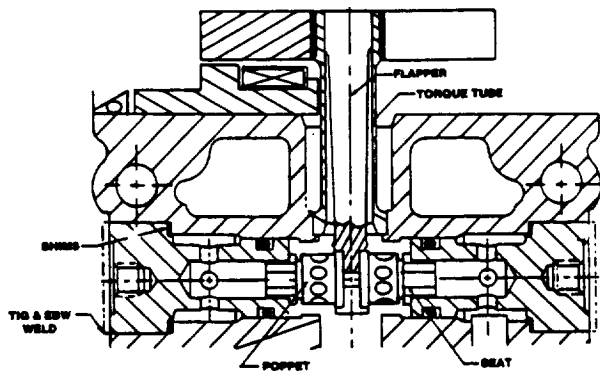


FIGURE 11.- CURRENT VALVE CONFIGURATION.

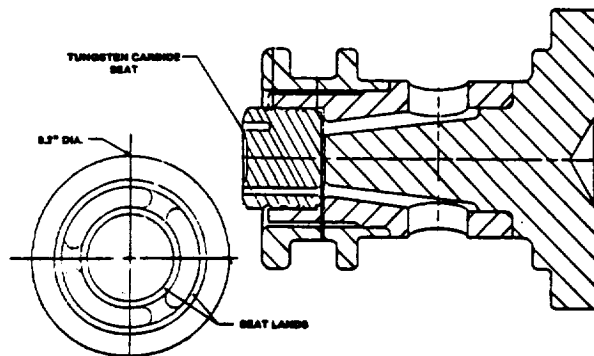


FIGURE 12.- APU SUBSYSTEM GGVM REDESIGNED SEAT AND MANIFOLD.

of the seat, in stress analysis, and in developing manufacturing processes. This effort resulted in an intricate seat design with concentric, dual-sealing surfaces and redesigned internal flow passages (fig. 12). The seat was diamond slurry honed as part of the manufacturing process to remove the recast layer left by the electrodischarge machining (EDM). This recast layer is a source of stress risers (cracks) and was considered one of the primary factors causing seat failure. The machining and manufacturing process turned out to be almost an art, and all seats and poppet assemblies were manufactured in a small, one-man shop.

Key lessons learned during the development of the GGVM include the following.

1. The tungsten carbide seat material is sensitive to many solvents and other fluids. Leaching of the binder material can significantly reduce strength and initiate intergranular cracking.
2. The seat configuration (internal corners, interfaces, etc.) caused residual internal stress that greatly affected the cracking characteristics.
3. The condition of the seat material surface significantly affected the cracking characteristics. The irregular, porous, cracked recast layer left after the EDM process was directly related to seat cracking.
4. Seat wear characteristics (life) were directly related to concentricity between the seat and the poppet, to seat-land width, to seat-poppet impact velocity, to closing spring force (reverse-cracking pressure), to poppet self-alignment design features, and to overall seat-poppet alignment established during the valve assembly process.
5. The use of damping oil in the valve armature area reduced rebound and was effective in reducing seat wear and seat-land edge chipping problems.

GAS GENERATOR

A key component of the APU is the gas generator. The GG receives hydrazine from the GGVM in short controlled pulses. The fuel is injected (flows) radially into a Shell 405 catalyst bed, where it is decomposed into hydrogen, nitrogen, and ammonia. The resultant gas mixture leaves the bed at approximately 1200 psia and 1700° F. The performance and the useful life of the GG are measured by the stability of the decomposition process. Pressure fluctuations (roughness) of greater than ± 10 percent of the steady-state level, pressure spikes (pulse spiking) of 2000 psia, or three consecutive pulses greater than 1900 psia indicate that the GG is no longer serviceable.

Key design features developed to extend useful GG life centered around the fuel injector and the catalyst bed. The size, the shape, the distribution, and the retention scheme for the catalyst granules were factors receiving significant development effort. The final design used had concentric, cylindrical beds separated by a cylindrical divider (figs. 13 and 14). The inner bed was packed with 14- to 18-mesh catalyst retained within a unique metal foam. The outer bed did not contain the metal foam. The technique used to pack the bed was found to be critical to good performance. This is an art-life operation consisting of pouring, shaking, tapping, and, in general, handworking the proper amount of catalyst into the bed. Because of the subjective nature of the operation, it has been, and still is, a basic concern in the manufacturing process.

ORIGINAL DESIGN
OF POOR QUALITY

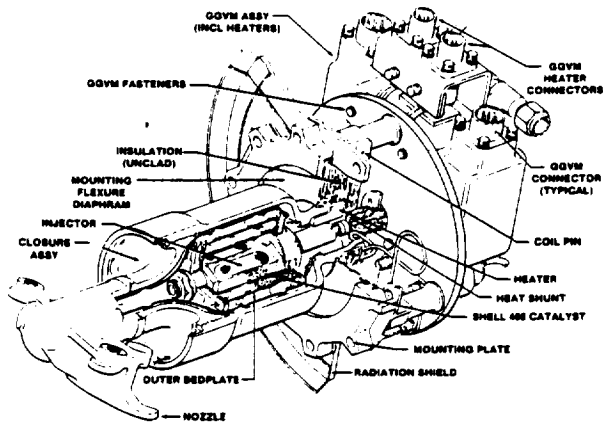


FIGURE 13.- MIN-MOD GAS GENERATOR - BASELINE.

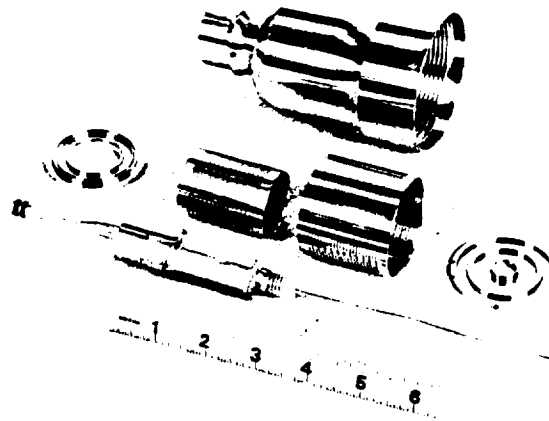


FIGURE 14.- APU GAS GENERATOR.

Injector design was also a critical element of GG performance. The current design consists of a core body with shaped fuel distribution channels feeding four injector panels. The injector panels are made from a sintered metal mesh material called Rigimesh (fig. 14). These panels produce uniform radial and axial distribution of fuel being fed radially into the catalyst bed. Design of the injector to produce uniform fuel distribution was a key element in extending GG life.

Another primary driver relative to GG bed life was vibration. Each piece of the GG was carefully analyzed and designed to minimize vibration within the GG. Specifically, the unit and its components were designed such that their natural frequencies did not tune with the APU or the hydraulic pump characteristic frequency. In some early configurations, resonances discerned at the 600-hertz pump frequency and at the 1250-hertz turbine frequency resulted in very early GG performance deterioration (roughness) due to mechanical breakup of the catalyst. The catalyst breakup caused bed voids, which allowed small accumulations of fuel to decompose violently and cause pressure roughness.

Thermal control within the GG was another area of significant concern. Overheating of the injector assembly during soakback after APU shutdown caused damage to the GG, damage to GGVM seals, decomposition of residual fuel in the injector upstream of the injector Rigimesh panels, and damage to the panels themselves (fig. 15). Early corrective actions included using a copper heat shunt between the injector and the GGVM mounting plate to dissipate some of the heat in the injector, and decreasing the thermal mass of the injector such that the incoming fuel could better cool the injector.

Even though these changes resolved the thermal concerns about the operating APU, it was found that if the APU restarted before the injector cooled to less than 400° to 450° F, the fuel would thermally decompose behind the injector panels and cause damage to the injector and would even feed back upstream to damage the GGVM. Limited hot-restart capability was finally achieved by adding an active water cooling system to the GG to be used only for hot restarts. This system injects water into a cavity within the injector. The steam thus generated is vented overboard (fig. 16). Use of this system enables restarts at any time after the cooling process, which requires a 210-second delay, is completed.

HYDRAZINE

In addition to the hot-restart problems discussed previously, the thermal instability of hydrazine also caused major problems with the APU fuel feed system (GGVM and fuel pump). After APU shutdown, soakback temperatures of 275° F and higher were causing excessive fuel decomposition within the GGVM and the fuel pump. Although the process was low order and did not damage the hardware, it did produce gas bubbles in the fuel system. After an "explosion" severely damaged a GGVM during an APU test (fig. 17), subsequent testing and analysis revealed the potential for adiabatically compressing hot gas bubbles within the GGVM and thereby increasing the temperature of the fuel vapor in the bubble to the point at which detonations occurred. This situation was controlled by limiting the maximum soakback temperatures in the fuel feed system (200° F) to minimize bubble formation and, by the same action, eliminating any APU starts when fuel feed system temperatures were higher than 200° F.



FIGURE 15.- APU GG INJECTOR FAILURE.

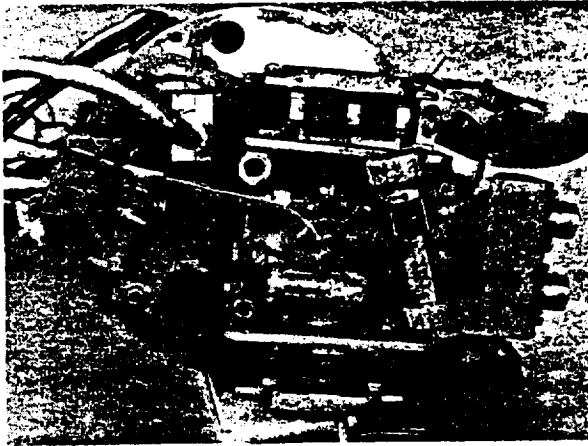


FIGURE 17.- GGVM DETONATION DAMAGE.

ORIGINAL PAGE IS
OF POOR QUALITY

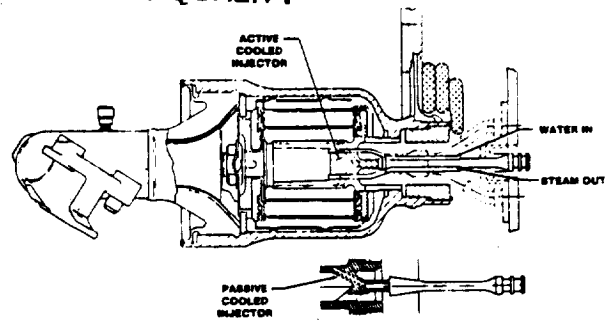


FIGURE 16.- GAS GENERATOR.

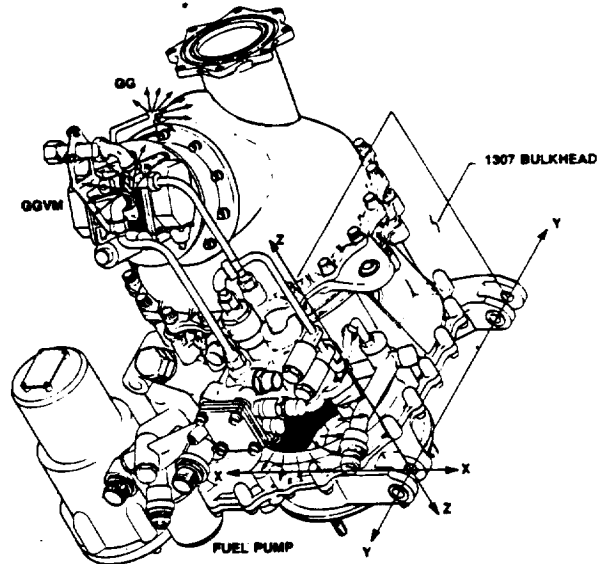


FIGURE 18.- ORBITER APU COOLING REGIONS.

The fuel pump and GGVM temperatures were controlled by use of an active water cooling system that sprays water externally onto the components (fig. 18).

During the course of the APU development, the sensitivity of hydrazine to decomposition has been a continual concern. Critical elements involved are temperature, materials in contact with the fuel, and purity of the fuel. High-purity hydrazine in contact with certain materials decomposes at significant rates at fairly low temperatures. Contamination within the feed system is always a concern and has the potential of causing detonations. Rust in any form is a catalyst and causes great concern.

A series of tests at the JSC White Sands Test Facility (WSTF) is being performed to define the compatibility of hydrazine with various materials and to define the sensitivity of hydrazine to the adiabatic-compression phenomenon. In addition, the effects of shock-wave propagation through the fuel and its vapor are being investigated. This work is being done to gain a better understanding of hydrazine in its application as a fuel and to ensure that, for use in the APU's, there are adequate safety margins relative to temperature limitations, to material compatibility, to shock and compression phenomena, and to the composition and chemical control of the fuel.

GEARBOX

The APU gearbox is required to reduce the 75 000-rpm turbine shaft speed to the hydraulic pump speed of 3700 rpm. It also drives the fuel pump and the lubrication oil pump. Development challenges were associated with the oil accumulators (required to control the oil-gas ratio in the gearbox), operation at low gearbox pressure, shaft sealing, and lubrication oil contamination. The oil accumulators in the gearbox control the quantity of oil in the lubrication circuit. To maintain proper lubrication oil flow and pressure, the ratio between oil and gas (void volume) must be controlled. Excessive oil causes churning and oil overheating, whereas insufficient oil causes inadequate oil flow. The original accumulators were pistons, sealed with an elastomeric diaphragm (Belloram, fig. 19). Failures of the diaphragm were common because of wear, scuffing, and folding as the pistons moved. The end results were contamination of the lubrication oil, leaks between the oil and gas side of the accumulators, and occasionally oil flow restrictions when a damaged diaphragm blocked the accumulator oil outlet passage. This problem was resolved by replacing the diaphragm with piston-ring-type seals made of Teflon.

During the development test program, it was determined that if the pressure within the gearbox was less than approximately 1 psia, the oil pump was incapable of functioning in a satisfactory manner (i.e., low pressure could develop on orbit because of seal leakage). The problem was primarily due to low net positive suction head (NPSH) pressure at the pump, but because the system is a closed loop which is not completely filled, voids could also form at the pump inlet. It, therefore, became necessary to provide a fluid (gas or oil) for the pump to displace to assure presence of oil at the inlet. This problem was resolved by adding a gaseous nitrogen pressurization system which guarantees a minimum of 4 to 7 psia in the gearbox at startup and during operation (fig. 20).

Shaft seal design was also one of the significant technical development challenges, especially the turbine shaft seal. When operating at high speeds and high temperatures, leakage was a continuing problem. Acceptable performance was finally achieved by using a hand-lapped, carbon-face seal with special provisions to ensure high face loading and stable rotational dynamics. Special lubrication oil cooling was also required for satisfactory performance.

Leakage of the turbine exhaust products through the turbine shaft seal caused another unusual secondary problem. The ammonia in the exhaust gases reacted with a particular additive in the lubrication oil to produce a silt that was plugging the oil filter and adversely affecting lubrication system performance. Once the additive was identified, a new oil was selected and the silting problem resolved.

The gearbox shaft seal at the fuel pump interface (bellows-type carbon-face seal) coupled with the shaft seal on the fuel pump posed problems that have not been solved (fig. 21). Slight leaks through these seals result in contamination of the lubrication oil with hydrazine. The reaction of the hydrazine with the lubrication oil produces contamination in the gearbox composed of a waxy, long-chain polymer (hydrazide) and a salt (pentaerythritol). The search for a hydrazine-tolerant oil is still in progress. Because free hydrazine in 270° F oil is dangerous because of the poten-

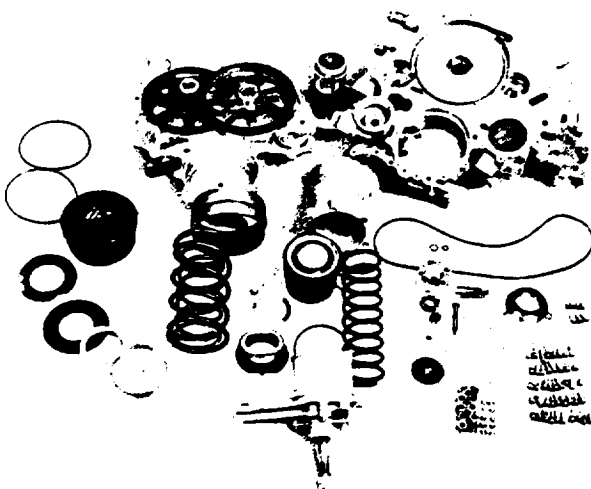


FIGURE 19.- GEARBOX.

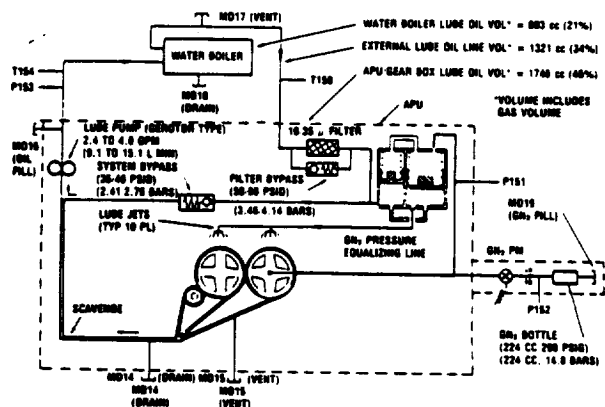


FIGURE 20.- APU LUBRICATION SYSTEM.

tial for detonation of the hydrazine, the most promising approach has been to add scavenging agents to the oil. However, this method has tended to cause some incompatibility problems between the oils and certain metals within the APU. Efforts in this area continue.

TURBINE HOUSINGS

Early in the development test program, it was discovered that the Stellite turbine containment housings and exhaust housings were cracking because of thermal cycling stresses (figs. 22 to 24).

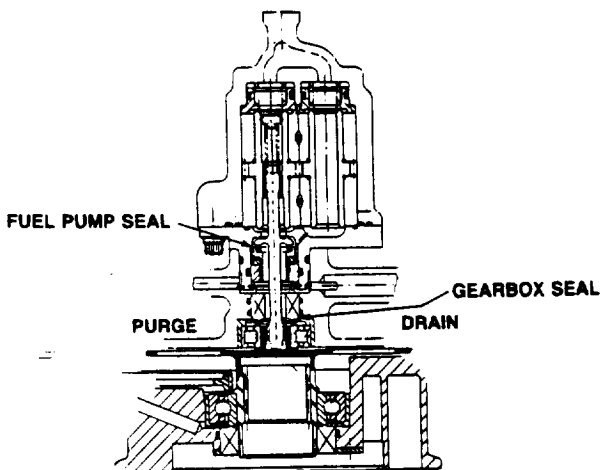


FIGURE 21.- APU FUEL PUMP.

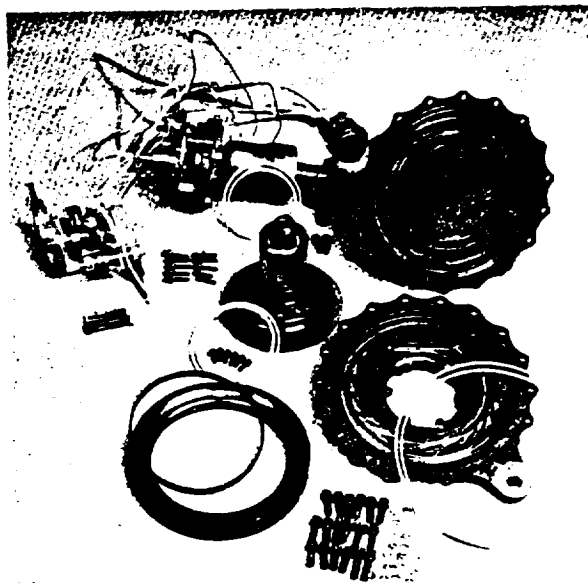


FIGURE 22.- GAS TURBINE MODULE.

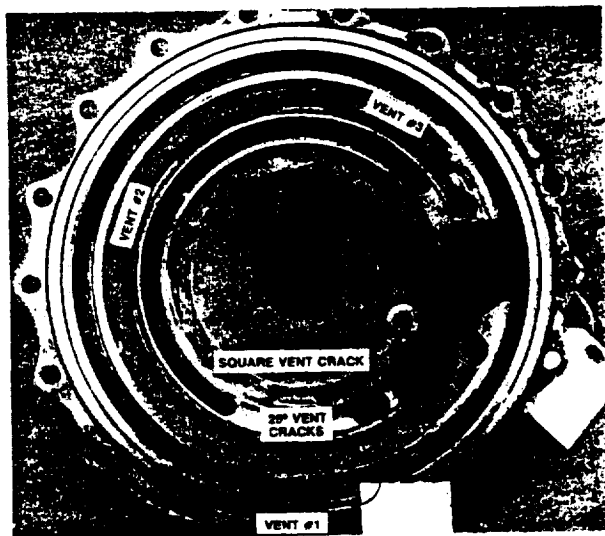


FIGURE 23.- TYPICAL EXHAUST HOUSING CRACKS.



FIGURE 24.- CRACK AT 25° VENT, APU EXHAUST HOUSING.

ORIGINAL DESIGN OF POOR QUALITY

Analysis results showed that the normal thermal cycles associated with starting and stopping the APU were causing stresses that exceeded the elastic limits of the Stellite. These cracks would develop within as little as 5 hours of APU operation. However, they were in noncritical areas and never adversely affected APU operation. The housings were qualified for 20 hours of operation with cracks. Part of the rationale used to support qualification with the cracks was that several cracked housings were used for more than 40 hours and two for more than 70 hours without any problems. The cracks were a concern, however; if the cracks were to continue to grow, housing failure would be theoretically possible. For this reason, a housing material change has always been high on the list of potential APU product improvement items. Sundstrand has fabricated housings using Udimet LX. Early development testing indicates that this material change could eliminate the cracking problem.

TURBINE FAILURE CONTAINMENT

The basic APU was designed with a turbine wheel radial containment ring and a blade tip seal and rub ring to safely control failures of the high-speed assembly (fig. 25). The honeycomb seal and rub ring was designed to dissipate rotational energy of a failing turbine wheel. The containment ring was intended to then keep any fragments of a wheel that was breaking up from leaving the APU envelope. Overspeed failure tests showed that speeds of greater than 155 percent (of 72 000 rpm) were required to destroy the turbine wheel. At these speeds, the containment features of the APU were incapable of totally containing wheel fragments. Typical overspeed tests resulted in damaged APU fuel lines, damaged housings, broken containment rings, and the escape of several wheel fragments with sufficient energy to dent test cell facility lines and equipment (figs. 26 and 27).

Attempts to improve the APU containment capability were made by redesigning the rub-ring features and strengthening the containment ring. Both size and material changes were considered in attempts to redesign the containment ring. Within reasonable design practices, these attempts were not successful. Containment rings capable of containing 155-percent speed ruptures were not practical because of size, weight, and configuration considerations. In the end, no physical changes were made to the APU relative to containment.

The approach finally taken to address this issue was to provide safety features that would allow operation within the existing degree of containment. An overspeed safety circuit is used to automatically shut down an APU at 93 000 rpm (129 + 1 percent). Additionally, this overspeed signal is used to close the fuel tank isolation valve to minimize any potential loss of fuel because of line damage on the APU. To provide further insurance against wheel failure, stringent flaw-detection inspections were imposed. With these controls, results of fracture-mechanics analysis showed the theoretical life to be many (approximately 10) times the 100-mission requirement.

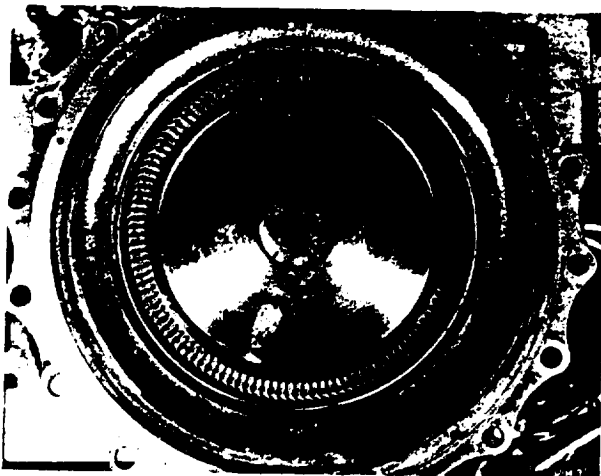


FIGURE 25.- CONTAINMENT RING.



FIGURE 26.- TURBINE OVERSPEED TEST.

CONTROLLER

The critical problem areas associated with the development of the APU electronic controller (fig. 28) were basically not in design. There were some design iterations associated with reducing the complexity of the unit, primarily in the built-in test equipment (BITE) circuits, and some changes were made to provide redundancy for the higher stressed components. However, the significant challenges were associated with manufacturing. Basic deficiencies in manufacturing procedures, equipment, specifications, and technician skill caused problems in being able to repeatedly build high-quality hardware. Development of proper wave soldering techniques and procedures was also required. Once adequate specifications, manufacturing procedures, and quality control procedures were written, and the technicians were properly trained, the controller became a very reliable and trouble-free component.

The only problem encountered in qualification was stress corrosion on the rivets in the controller frame. This problem was resolved by installing the rivets with a wet coat of Super Korpon paint.

Although not an integral part of the controller, there was a manufacturing problem with the magnetic pickup units (MPU's) that feed the APU-speed signal to the controller. During assembly, it was necessary to braze a 0.002-inch lead wire from the MPU coil to a 20-gage output wire. This operation went through several iterations. At one point, a special holding fixture was used to position the wires during brazing. In the end, however, the most reliable joints were those done by hand by a skilled technician.

TEST FACILITIES

Specialized facilities were required to test the APU in all attitudes and environments that the APU would encounter during flight. The Integrated Test Article (ITA) built to simulate the entire APU subsystem included proper line lengths and routing and all the components in the APU subsystem. Capabilities of the ITA included turning the subsystem from launch to landing attitudes, temperature variations from -18°C (0°F) to 52°C (125°F), and exhaust pressures from sea level to 100 mmHg (50 000 feet). The ITA did not include a vacuum environment around the APU. This test facility was used to prove the APU subsystem could operate in various attitudes and prelaunch temperatures, to size the heaters for prelaunch environments, and to exercise the vehicle-servicing ground-support equipment.



FIGURE 27.- TURBINE WHEEL FRAGMENTS.

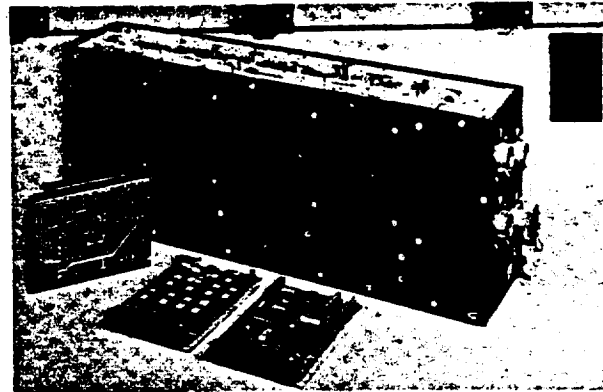


FIGURE 28.- ORBITER APU CONTROLLER.

ORIGINAL PAGE IS
OF POOR QUALITY

To test the APU in a vacuum environment, a vacuum chamber at the JSC Thermochemical Test Area (TTA) (fig. 29) was used. The TTA vacuum chamber was capable of pressure conditioning from ambient pressure to 0.365 mmHg (180 000 feet) with a nonoperating APU or 2.49 mmHg (130 000 feet) with an operating APU and of temperature conditioning from -54°C (-65°F) to 107°C (225°F). This facility was used to prove that the APU could operate in a vacuum environment at the temperatures expected in space and, also, that the design of the heaters was adequate for on-orbit conditions. Testing in this chamber defined the cooldown rate of the APU and showed that the APU could not be shut down and restarted for an abort once around without performing an actively cooled hot restart. Testing in this chamber also revealed the problem of adiabatic compression of bubbles at high temperature by which an APU was destroyed after an attempted hot start.

To test the capability of the gearbox to function in zero g, a KC-135 aircraft was used to fly Keplerian parabolas while the onboard gearbox was operating.

None of the testing facilities used was a perfect simulation of the operating environments of the APU, but the facilities were sufficient to isolate and correct problems in the design of the APU. The full test of the APU with the vehicle hydraulic system and correct environments was performed during the Approach and Landing Test and the Orbital Flight Test (OFT) Programs.

FLIGHT EXPERIENCE

The APU was tested in flight for the first time during ALT for three captive/active flights and five free flights. In all flights, the APU was proved capable of handling flight loads (ref. 4).

Several problems were encountered during ALT. First, during a ground test, an APU gearbox was improperly serviced with an excessive quantity of oil causing an overtemperature of the gearbox. That problem was solved by a more accurate tool for measuring ullage volume in the gearcase. During



FIGURE 29.- JSC THERMAL VACUUM TEST.

captive/active flight 1, APU 1 developed a fuel leak which was large enough to be observed by a chase plane. Subsequent investigation showed that the bellows of the fuel pump seal was highly stressed in that it was exposed to dynamic pressures from tank pressure to 68 atmospheres (1000 psi). Because of the high stresses, the bellows design was abandoned and replaced with an elastomeric seal. No failures have occurred with the elastomeric seal design.

The exhaust-gas temperature (EGT) transducer was troublesome throughout the ALT flights and did not perform well in the extreme temperatures of the exhaust-gas environment. The crew was trained to shut down the APU upon indication of an exhaust-gas overtemperature. During captive/active flight 3, APU 1 was shut down because of the EGT transducer failure and erroneous indication of an overtemperature. After that incident, the crews were instructed to confirm the exhaust-gas overtemperature on a backup EGT instrument before taking action to shut down the APU. The EGT transducer was tackwelded to the exhaust duct, where the delicate leads were not adequately protected from vibration, and breakage of the leads caused the overtemperature indication. Following ALT, the EGT was changed to a probe which screwed into the exhaust duct and the leads were better protected.

The first Space Transportation System orbital flights (STS-1 to STS-4) proved the design concept of the APU for performance in zero g, vacuum, and extreme temperatures. These flights proved that the APU was well capable of handling the hydraulic loads in the extreme environments of space (ref. 4).

During STS-1, both APU 2 gas generator heaters failed. The heaters shared a common case, in which argon gas acted as a heat-transfer medium. A crack in a weld allowed the argon gas to escape. Long-term operation of the heaters caused overheating of the wire and subsequent failure of both heaters. During the qualification tests, the heaters passed an evacuated test. It was not a long-term, steady-state test, but consisted of many heater actuations, which was believed to be the worst case. After the flight, an inspection procedure was developed for all heater cases in which the heater was placed in a vacuum chamber and the resistance measured during the heatup cycle. If there was a leak in the case, the heater wire would get hotter and consequently have a higher resistance. For long-term redesign, as part of the improved APU program, the heater will be redesigned to have separate cases for each of the redundant heaters and the watt density will be lowered.

Also during STS-1, there was an indication of bubbles trapped in the fuel feedline as revealed by the gas generator pressures. This condition introduces the potential for the adiabatic compression of hydrazine discussed earlier. As a result of ground testing, a water system had been added to cool the GGVM and the pump after shutdown to prevent the decomposition of hydrazine. Also, care had been taken to service the flight system so as to prevent the trapping of bubbles in the feedline. Therefore, the appearance of bubbles on STS-1 was surprising. Tests run on the ITA indicated that bubbles could still be in the feedline from servicing; therefore, for STS-2, even more care was taken with servicing. During STS-2, bubbles were again evident in the APU 1 gas generator trace, and, after that mission, the APU was removed for investigation. The results of that investigation showed that significant decomposition of the fuel could take place at lower temperatures during a long exposure period. Servicing on the vehicle occurred several months before the actual flight. Also, it was determined that the fuel pump filter could act as a surface-tension device in trapping bubbles for some time before being flushed through the gas generator. These two results were convincing that the APU would have to operate with bubbles. A requirement was instituted that the APU should not be started unless the fuel feed system temperature was less than 200° F. This limit was backed up with APU and adiabatic-compression testing. Work is continuing on a filter that will not trap a bubble but allow it to be purged through the gas generator during startup before the first high compression occurs.

During the STS-2 prelaunch period, APU's 1 and 3 had high lubrication oil outlet pressure, an indication that the lubrication oil filter was plugged and that the gearbox was operating on the relief valve around the filter. The filter was determined to be contaminated with pentaerythritol, a compound formed when hydrazine fuel penetrates the gearbox. The gearboxes were flushed, and elaborate turnaround procedures were developed for keeping hydrazine out of the gearbox. Between every mission, the gearbox is flushed with lubrication oil and the filter replaced. The seal cavity drain (the common drain between the fuel pump and the gearbox) is flushed with alcohol to prevent a buildup of the waxy contaminant. The seal cavity drain pressure is maintained below the gearbox pressure to keep the driving force away from the gearbox. All of these procedures are time consuming, and none is totally successful. The APU 3 filter plugged again on STS-4. Work is continuing on redesigning the seal cavity drain and developing a compatible lubrication oil. Other minor problems on the APU during OFT included drain relief-valve leaks, "fuzz" leaks of the servicing quick-disconnect fittings, and a misthreaded fitting in the APU 1 GGVM/fuel pump water cooling line.

IMPROVED APU

The APU was developed under schedule constraints; consequently, as problems arose, modifications were made that were not necessarily optimum. The goal of the improved APU program is to optimally de-

ORBITER
OF POOR QUALITY

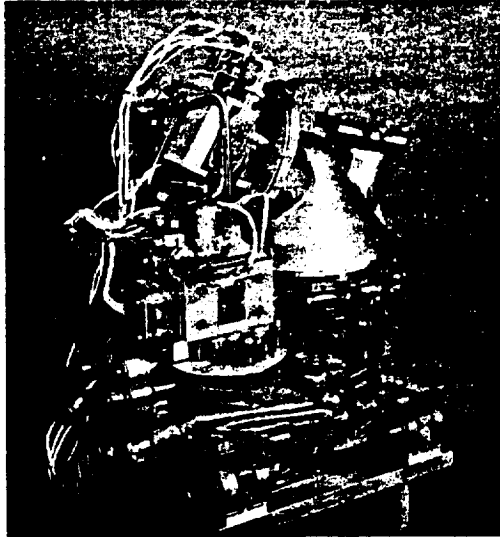


FIGURE 30.- IMPROVED APU.

sign the APU for durability and for performance, and to solve the flight and development problems. The design goal is for a 75-hour life, a passively cooled valve and pump, exhaust and containment housings that do not crack, a fuel pump filter that does not trap bubbles, and a redesigned seal cavity that prevents hydrazine from penetrating the gearbox (fig. 30). Development tests are already underway, and if implementation is approved by Orbiter management, the redesigned APU could be on the Orbiter by early 1987.

SUMMARY

The APU suitability for orbital flight, durability, and reusability have been demonstrated during OFT flights. More than 862 hours of APU operation (29.3 hours in OFT vehicle) and 1574 starts (72 starts in vehicle) have been accumulated with 100 percent success.

Enhancements have been identified to extend life to 75 hours (50 missions), to reduce weight (150 pounds (68 kilograms) per vehicle), to improve the lubrication system, and to reduce turnaround time. These enhancements are directed toward significantly reduced life-cycle cost, turnaround, and weight, and increased reliability, maintainability, and operational effectiveness.

The performance of the APU system has both proved the effectiveness of the APU development program and revealed the areas in which additional efforts could be effective. The necessity for a thorough development program with adequate test hardware, test programs, and design support and analysis has been emphatically shown. Where shortcuts have been taken, problems have often developed late in the program with significant adverse impacts. Timely and thorough development effort has been invaluable in guaranteeing safe, reliable, operationally effective systems.

REFERENCES

1. Reck, M. W.; and Baughman, J. R.: Space Shuttle Orbiter Auxiliary Power Unit Configuration and Performance. AIAA paper 78-1007, 1978.
2. Tuthill, W. C.: APU Gearbox Test. Rep. JSC-14693, NASA Lyndon B. Johnson Space Center (Houston, Tex.), Apr. 1979.
3. McKenna, R.; Wicklund, L.; Baughman, J.; and Weary, D.: Space Shuttle Orbiter APU. SAE paper 820838, 1982.
4. McKenna, R.; Wicklund, L.; Baughman, J.; and Weary, D.: Space Shuttle Orbiter APU Flight Performance. SAE paper 821513, 1982.

09
N85-16946

THE SOLID ROCKET BOOSTER AUXILIARY POWER UNIT -- MEETING THE CHALLENGE

Robert W. Hughes
Structures and Propulsion Laboratory
Marshall Space Flight Center, Alabama

ABSTRACT

The thrust vector control systems of the solid rocket boosters are turbine-powered, electrically controlled hydraulic systems which function through hydraulic actuators to gimbal the nozzles of the solid rocket boosters and provide vehicle steering for the Space Shuttle. Turbine power for the thrust vector control systems is provided through hydrazine fueled auxiliary power units which drive the hydraulic pumps.

The solid rocket booster auxiliary power unit resulted from trade studies which indicated significant advantages would result if an existing engine could be found to meet the program goal of 20 missions reusability and adapted to meet the seawater environments associated with ocean landings. During its maturation, the auxiliary power unit underwent many design iterations and provided its flight worthiness through full qualification programs both as a component and as part of the thrust vector control system. More significant, the auxiliary power unit has successfully completed six Shuttle missions.

THE SOLID ROCKET BOOSTER CHALLENGE

The challenge associated with the development of the Solid Rocket Booster (SRB) Auxiliary Power Unit (APU) was to develop a low cost reusable APU, compatible with an "operational" SRB. This challenge, as conceived, was to be one of adaptation more than innovation. As it turned out, the SRB APU development had elements of both.

During the technical trade studies to select a SRB thrust vector control (TVC) system, several alternatives for providing hydraulic power were evaluated. A key factor in the choice of the final TVC system was the Orbiter APU development program, then in progress at Sundstrand Aviation. This program was implemented under contract with Rockwell International Corporation and Johnson Space Center. The Orbiter APU design requirements very closely approximated or exceeded the ascent phase performance needed by the SRB and was physically compatible with the SRB concept¹ (Table I). Because of this comparability in requirements and physical compatibility, the Orbiter APU was selected as the basic power element for the SRB. With this selection came the expectation of reduced development costs and early hardware availability.

This paper deals with the challenge in adaptation of the Orbiter APU to meet the SRB need.

TABLE I. APU OPERATIONAL REQUIREMENTS

<u>PARAMETER</u>	<u>ORBITER</u>	<u>SRB</u>
Horsepower Shaft (HP)	135/151	135/148
Operation/Mission (Min)	82	2.4
Missions (Min)	40	20
Total Operating Time (Hr)	50	2
Useful Life (Hr)	250	10
Cold Gas Checkout	No	Yes
All Attitude Operation	Yes	No
Zero G Operation	Yes	No
Redundant Control	Yes	Yes

SRB AND ORBITER

Although the Orbiter APU is used as the basic power element for the SRB APU and both fly on the same Shuttle vehicle, the APUs are, in fact, quite different. These differences range from the obvious to the barely detectable and are the factors which make the SRB APU of interest.

In order to understand the development challenge of the SRB APU it helps to have a basic understanding of the differences between the Orbiter and the SRB missions and the environments these missions induce (Fig. 1).

The Orbiter mission requires the APUs to be functional during all phases of operation (Table II). Orbiter APUs start about 5 min prior to lift-off and operate continuously throughout ascent into Orbital insertion before they are shutdown. In preparation for de-orbit and reentry the APUs are restarted and operate throughout atmospheric maneuvering to a runway landing. Total APU operating time for each Orbiter APU is about 82 min.

In comparison, the SRB APUs are started approximately 25 sec before lift-off and function only during the ascent phase of the mission terminating at SRB separation 161 sec later (Table II). From separation at approximately 200,000 ft altitude, the remaining 6 min of the SRB flight mission consisting of atmospheric reentry, parachute slowed descent, and ocean splashdown are performed with nonfunctional APUs. Once in the water, the SRB mission becomes one of survival. From SRB splashdown at 91 ft/sec to SRB removal from the ocean at dockside, the APUs are subjected to various combinations of seawater immersions and water pressures for 7 days during SRB recovery and retrieval.

Complicating the SRB APU situation is its installation. Where the Orbiter APU is installed in an aircraft type compartment offering protection from aerodynamic, vibration, and thermal extremes, during all phases of operation, the SRB APU is located in the aft skirt section of the SRB next to the engine where protection is available only during ascent (Fig. 2).



Figure 1. SRB Mission Sequence.

Reproduced from
best available copy.

TABLE II. APU MISSION COMPARISON - SRB VERSUS ORBITER

<u>APU OPERATION</u>	<u>ORBITER</u>	<u>SRB</u>
PRELAUNCH	YES	YES
BOOST	YES	YES
ORBITAL	YES	NO
REENTRY	YES	NO
LANDING	YES	NO
POSTLANDING	YES	NO
TOTAL TIME	4200 Seconds	161 Seconds

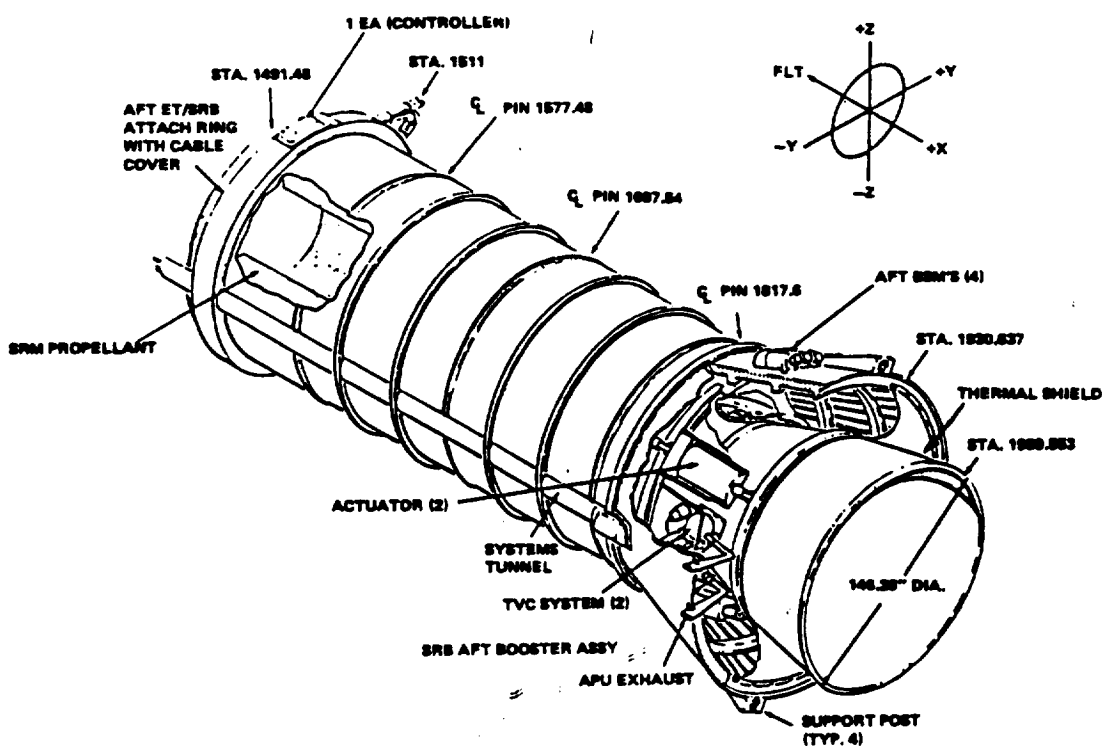


Figure 2. SRB TVC Subsystem and Actuators.

Table III shows the major environmental differences between the SRB and the Orbiter APUs. The main differences were in the vibration and landing loads, and in the seawater pressures and immersions. It was obvious the Orbiter APU was not designed for the SRB severe conditions, and modifications would be necessary. The majority of the SRB APU developmental effort was expended in these areas.

In this developmental phase of the SRB program, the decision to use the Orbiter APU proved most valuable since test hardware for modification became available without long lead times.

Modifications made to create the SRB APU may be categorized in four basic ways:

- a. Elimination of unneeded features
- b. Hardening of existing components
- c. Reduction of production/replacement costs
- d. Implementation of servicing and checkout aids.

TABLE III. ENVIRONMENTAL COMPARISON

<u>ENVIRONMENT</u>	<u>ORBITER</u>	<u>SRB</u>
VIBRATION		
LIFT-OFF	18.1 grms	21.7 grms
BOOST	18.1 grms	32.0 grms
REENTRY	5.7 grms	47.0 grms
LANDING LOADS	1.5 g (93M/S)	40 g (140M/S) Axial lateral
ACCELERATION (ASCENT)	3.3 g	3.3 g
WATER IMPACT PRESSURE	None	120 psi
WATER IMMERSION PRESSURE	None	57 psi
SALT WATER IMMERSION	None	4 to 7 days
ZERO G	Yes	No
VACUUM	Yes	No

An example of a modification for each of the categories is presented. To facilitate understanding these examples, a basic description of the APU is necessary.

DESCRIPTION OF THE APU

The SRB APU is a monopropellant hydrazine-fueled gas turbine engine used to drive a variable displacement hydraulic pump (Fig. 3). The APU features a gear type fuel pump, driven through the APU speed reduction gearbox, in a bootstrapping mode, to provide high pressure hydrazine fuel to a catalytic type hydrazine gas generator. Flow of fuel to the gas generator is controlled by the gas generator valve module (GGVM), which contains two control valves in a series configuration. In the gas generator, the hydrazine is decomposed to create hot gas for driving the reentry type turbine, turning the gearbox, and driving the hydraulic pump. Speed control of the turbine is accomplished through a pulse counting, logic circuit called the controller. The controller issues open or close signals to the GGVM to control fuel flow in response to electrical pulses generated by the turbine. The controller can control APU speed at 100 percent speed (72,000 rpm) for normal control; at 110 percent speed (79,200 rpm) for redundant TVC operation; or at 112 percent speed (80,640 rpm) for redundant internal APU control. The 100 percent and 110 percent control modes operate the primary control valve of the GGVM and the 112 percent control mode operates the secondary control valve of the GGVM.

ELIMINATION OF UNNEEDED FEATURES

The best example of how "elimination of unneeded equipment" was used in the development of the SRB APU is found in the gearbox.

The Orbiter gearbox, as it was developed, had an intricate externally attached lubrication oil cooling loop; externally attached oil accumulator; and an externally attached gearbox pressurization system to support long duration and on-orbit operations in zero G and vacuum environments (Fig. 4). If necessary for the SRB, these features would have meant additional complication of the TVC system and additional weight and volume in the aft skirt. In addition, the projected effort to design the externally mounted components to meet the vibration and water entry loads; to select materials which would survive in the corrosive seawater environment; and to flight qualify these components would also have been expensive.

The solution to the problem was obvious. Eliminate as many components as possible. Through analysis of APU operational times and the heating loads induced, it appeared to be feasible to tailor the SRB APU operational profile to stay within the 300°F thermal limit of the gearbox without the external components. The results of this analysis were confirmed by a series of tests duplicating expected worst case APU operations. With this verification, the coolant loop, the accumulator, and the pressurization

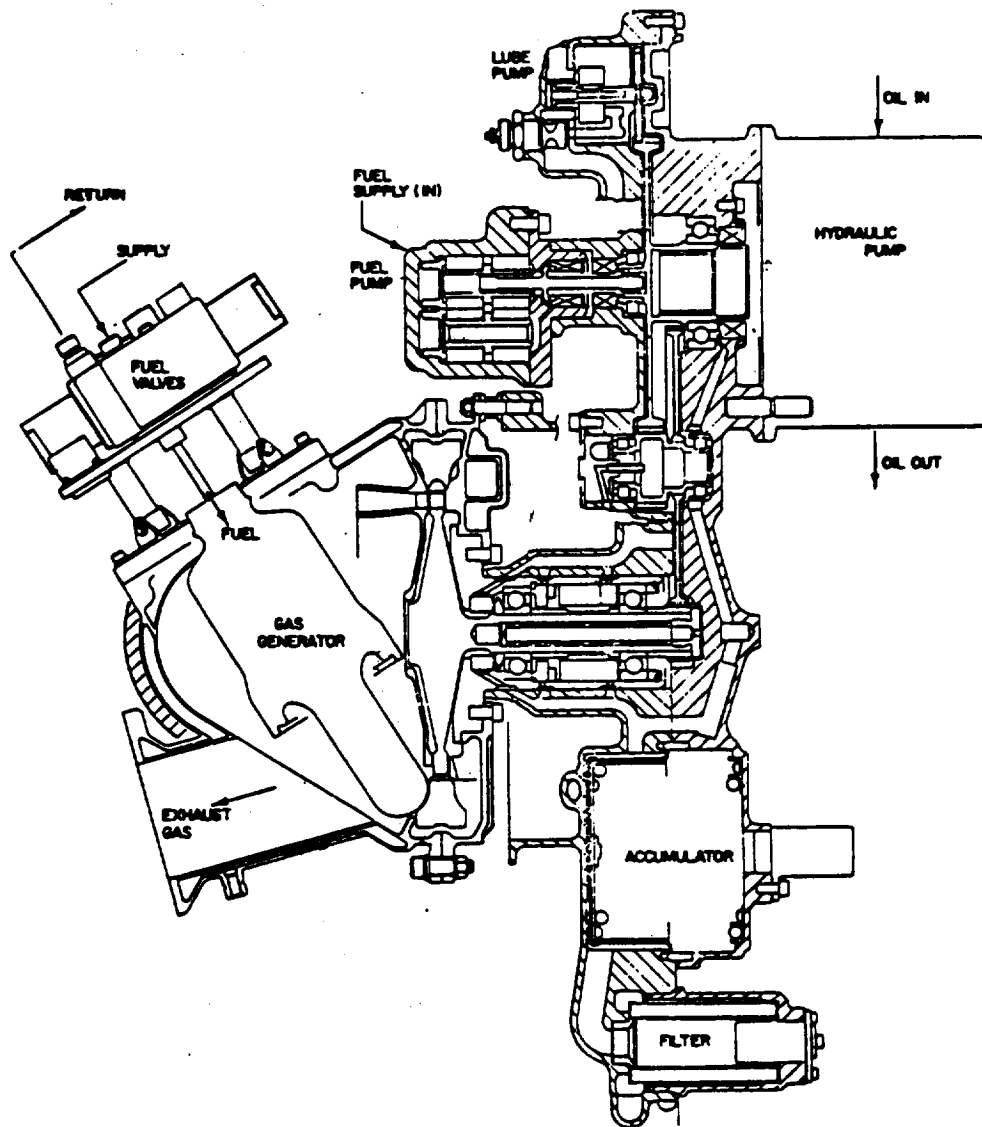


Figure 3. SRB APU.

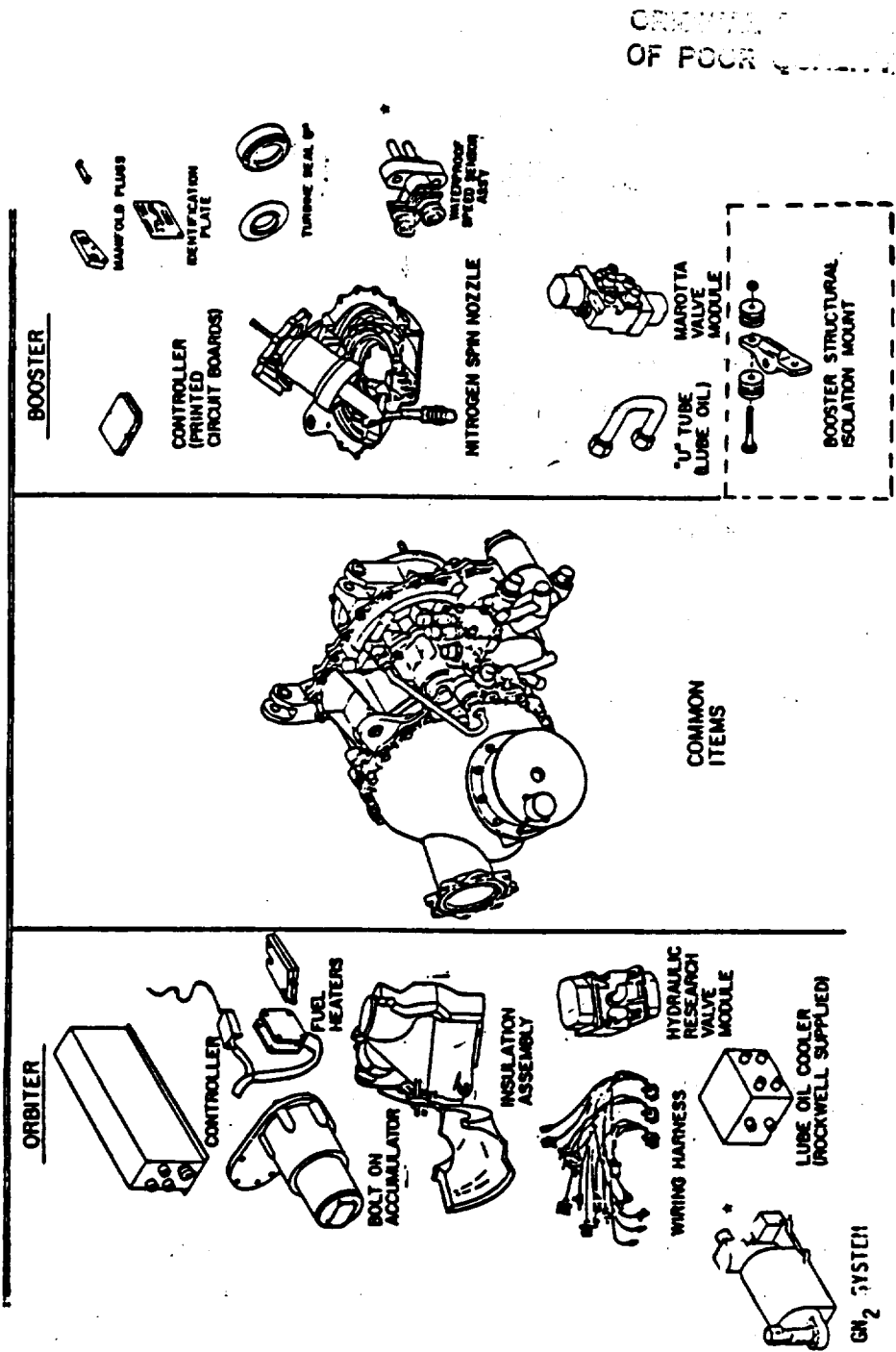
system were eliminated. An advantage in this elimination was the fact that the components in question were all bolted on externally so that their removal did not significantly alter the design of the basic gearbox.

HARDENING OF COMPONENTS

Hardening, as used in this paper, is meant to describe efforts to improve the resistance of the Orbiter APU components to damage and make them suitable for SRB.

The largest example of hardening is the SRB APU vibration isolation system.

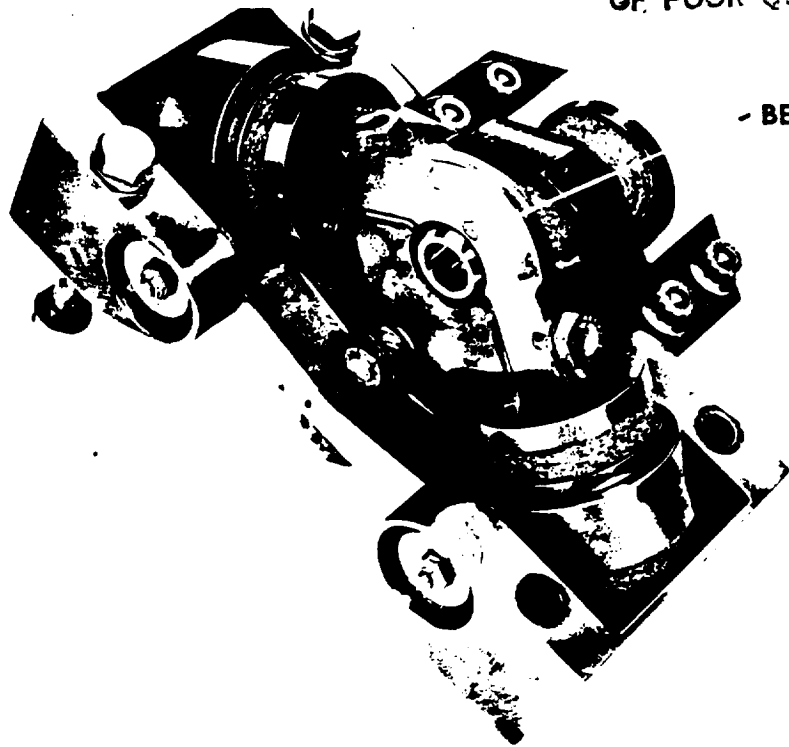
In all cases, the vibration loads expected for SRB APU exceeded those expected for Orbiter. This exceedence caused concern for the operability and life of several APU components such as the gas generator and the fuel pump. To preclude having to redesign these components, a vibration isolation system was developed for the APU (Figs. 5, 6, and 7). The system consisted of three individually tuned vibration damping mounts attached between the APU at its mounting lugs and the primary mounting structure. The result was attenuation of the vibration loads input to the SRB APU to levels well below those for a hard mounted APU and, in some cases, below those experienced by the Orbiter (Table IV).



ORBITER
OF FOUR

Figure 4. Pictorial Hardware Comparison - Booster Versus Orbiter.

ORIGINAL DRAWING
OF POOR QUALITY



- BEARING CAP



Figure 5. Isolation Mount M-3.

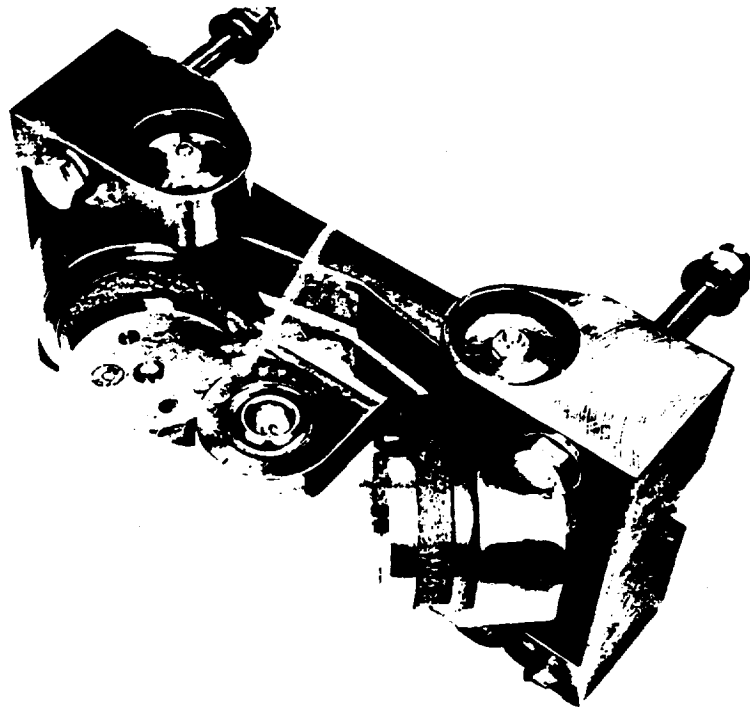


Figure 6. Isolation Mount M-2.

CRITICAL TO
OF POOR QUALITY

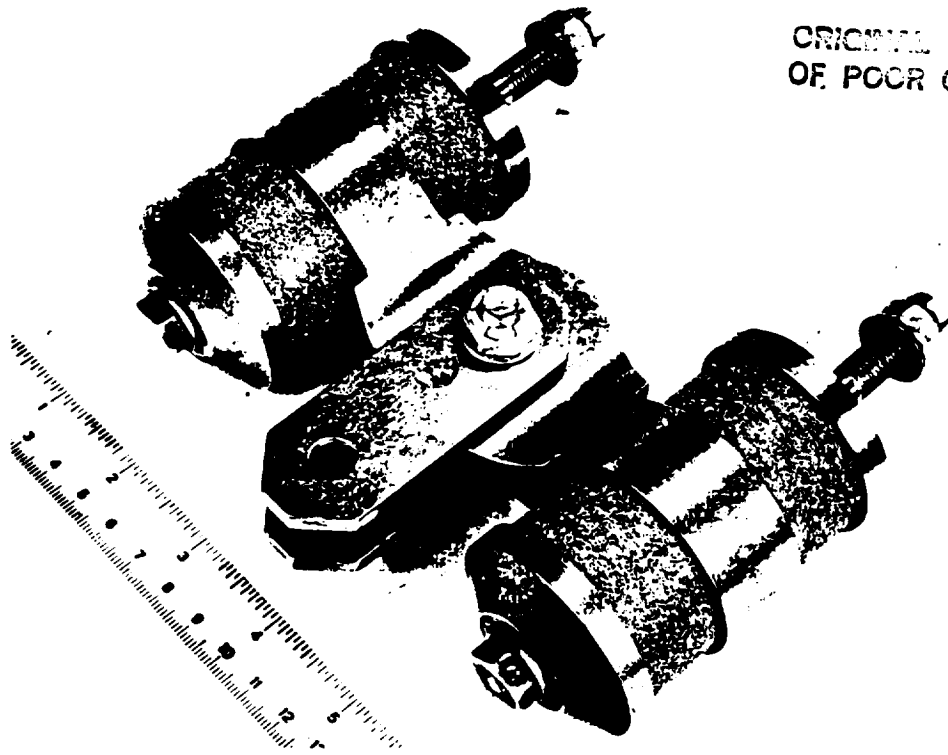


Figure 7. Isolation Mount M-1.

TABLE IV. APU VIBRATION ISOLATION SYSTEM

	INPUTS TO SRB APU ²		ORBITER HARD MOUNTED (G RMS)
	HARD MOUNTED (G RMS)	ISOLATED (G RMS)	
X (AXIS)			
LIFT-OFF	21.7	5.3	
BOOST	32.0	7.8	18.1
REENTRY	41.5	10.0	
Y (AXIS)			
LIFT-OFF	21.0	11.0	
BOOST	31.1	16.0	5.7
REENTRY	47.0	18.5	
Z (AXIS)			
LIFT-OFF	16.9	5.8	
BOOST	24.0	5.7	5.7
REENTRY	28.1	8.8	

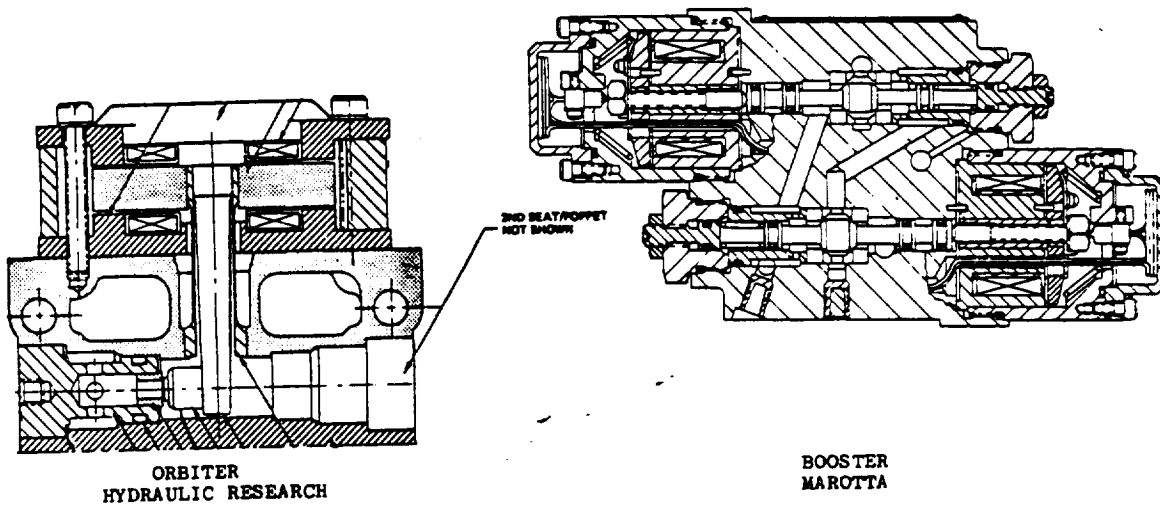
REDUCED COMPLEXITY

This category of modification is mentioned separately, because it covers circumstances where SRB made changes to the Orbiter APU primarily to achieve significant cost advantages. The gas generator valve module is presented as a good example.

The Orbiter gas generator valve module (GGVM) is a complex component utilizing many sophisticated production and operational techniques (Fig. 8). The design incorporated features like welded actuator torque tubes, torque motors, and metal to metal seats. These features were necessary in the Orbiter to meet the demands of reduced fuel consumption; prolonged cycle life; and elevated operating temperatures. Associated with these features were high development and unit costs.

In evaluating GGVM requirements, the SRB realized that its needs were far exceeded by the Orbiter GGVM. Coupled with high Orbiter development and unit costs, this realization lead the SRB to investigate the availability of a less sophisticated GGVM to meet the SRB needs. The resulting SRB GGVM was a direct actuating, poppet type, solenoid valve module with elastomeric type seats (Fig. 8). This unit was produced at approximately one quarter of the unit cost of the Orbiter GGVM. This savings was considerable when multiplied by the projected 400 SRB APU unit buys, and an attrition rate as high as 12 percent.

ORIGINAL DESIGN
OF POOR QUALITY



	<u>HYDRAULIC RESEARCH</u>	<u>MAROTTA</u>
WEIGHT		
ORBITER BOOSTER	3.2 POUNDS MAXIMUM	2.5 POUNDS MAXIMUM WITH SWITCHES
CONSTRUCTION	FLEXURE TUBE, HARD SEATS	SLIDING SPOOL, SOFT SEATS
LIFE	1.5×10^6 CYCLES	ESTIMATED 130,000 CYCLES
REFURBISHABILITY	LOW	HIGH

Figure 8. Comparison of Gas Generator Valve Modules.

PROCESS STREAMLINING

The Shuttle program had a very ambitious operational schedule projected to be as high as one flight per month. This high rate of activity made it mandatory for the SRB to incorporate all practical conveniences which would decrease the numbers of in-flow operations and reduce the total operational turnaround times. Several streamlining features were developed for the SRB APUs to accomplish this. One of these will be discussed.

The most successful streamlining modification undertaken for the SRB APU was the cold gas turbine spin (Fig. 9). This feature was added in the reentry nozzle block of the SRB turbine to provide an easy method to rotate the APU turbine without a full hot-fire operation or disassembly of the TVC system. Some of the advantages of this are: easy checkout of the APU at speeds up to 76 percent of full operational speed; easy checkout of the SRB TVC system at demands up to 26 horsepower; easy servicing of the hydraulic system; and easy fuel system servicing. The total TVC system time savings realized through the incorporation of cold gas spin is measured in days (approximately 6 days/mission). This is significant when compared to an operational turnaround time measured in weeks.

The examples presented were intended to explain the challenge presented in developing the SRB APU from the Orbiter APU and to demonstrate how the SRB APU became a unique entity in the answering of this challenge. Other examples of how the challenge has been met are found in the following:

- a. SRB controller
- b. SRB fuel pump
- c. SRB fuel system
- d. SRB gearbox
- e. SRB turbine
- f. SRB gas generator
- g. SRB electrical system.

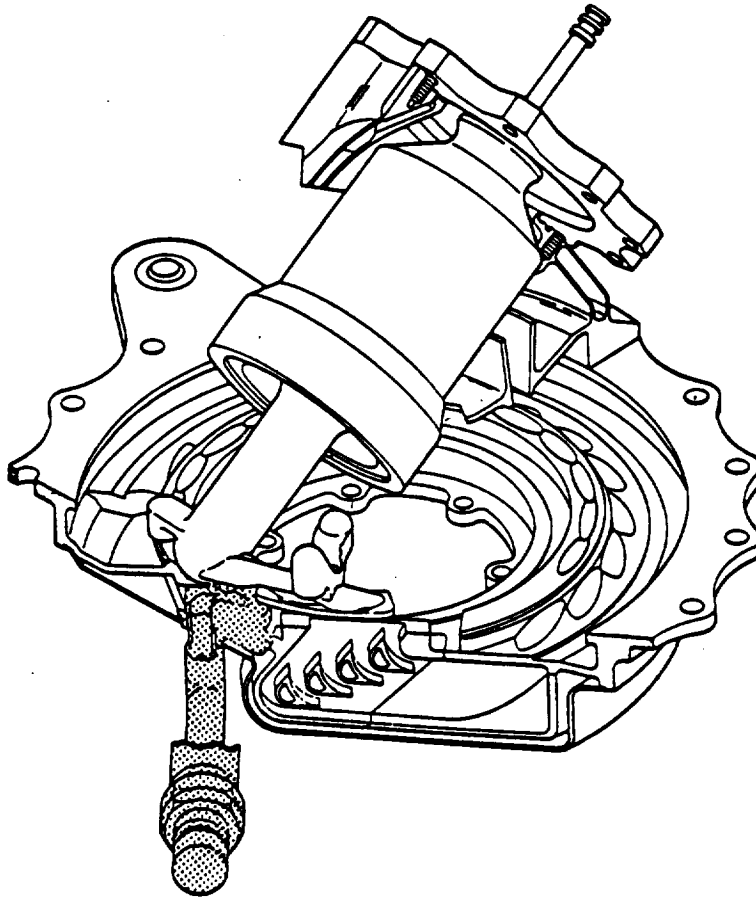


Figure 9. SRB GN₂ Spin Nozzle.

THE SCORE CARD/RESULTS

To evaluate how well a challenge has been met, a score in some form must be kept. Table V gives an indication of the score.

TABLE V. SRB APU OPERATIONAL SCORE CARD

<u>STS</u>	<u>SUCCESSFUL APU ASCENT/OPERATION</u>	<u>RECOVERED APU'S</u>	<u>APU DAMAGE</u>
1	4	4	20%
2	4	4	15%
3	4	4	10%
4	4	SRB'S LOST	100%
5	4	4	3%
6	4	4	1%

To date, all APUs recovered have been slated for return to service. It should be noted that all APUs from STS-5 and STS-6 could have been reused without off-line repair.

A second challenge was to reduce development cost. In this, the program can again be declared successful. The cost for development of the SRB APU resulted in a program savings of approximately 50 percent over the costs anticipated for a totally new development. This savings can be attributed almost totally to the decision to use the Orbiter APU as a basis for development.

WHAT NOW

The challenge of the SRB continues and will until the damage column on the score card reads 0 and hardware turnaround becomes routine.

Efforts to improve the APU continue with the objectives of:

- a. Reducing preparation, servicing, and turnaround times.
- b. Reducing costs.
- c. Improving reliability.

Toward this end, the SRB is presently pursuing major product improvement programs with a primary focus on the development of a low cost SRB gas generator, the most expensive component of the APU. A 40 percent reduction in APU unit costs is a goal for this effort.

Also in work is the development of an unpumped fuel system for the SRB APU. This effort will have significant impacts on APU reliability, servicing, preparation, turnaround, and cost.

CONCLUSIONS

An overall assessment of the SRB APU program leads to several important conclusions.

- a. The challenge to use the basic Orbiter APU as the design basis for the SRB APU has been met and has produced positive dividends in cost and schedule.
- b. The present SRB APU has been highly successful and has met the challenge of SRB APU reusability.
- c. The APU problems encountered during Shuttle operations pose a new challenge wanting real solutions which are cost effective and timely.
- d. The challenge to bring an SRB APU into operational status has been met and future challenges are in the category of product improvements.

REFERENCES

1. McCool, A. A.; Verble, A. J.; and Potter, J. H.: Space Transportation System Solid Rocket Booster Thrust Vector Control System; Journal of Spacecraft and Rockets, Volume 17, Number 5, September - October 1980, pp. 407-412.
2. Koenings, D. A. and Johnson, B.: Qualification Report for Solid Rocket Booster Thrust Vector Control System Auxiliary Power Unit Model APU-02; Sundstrand Aviation AER-1539-6, Rev. A., 1979.
3. SRB Systems Data Book, Marshall Space Flight Center, SE-019-083-2H, Rev. A, Vol. 1, June 1977.

SPACE SHUTTLE ELECTRICAL POWER GENERATION
AND REACTANT SUPPLY SYSTEM

William E. Simon
Lyndon B. Johnson Space Center
Houston, Texas 77058

ABSTRACT

A review of the design philosophy and development experience of fuel cell power generation and cryogenic reactant supply systems is presented, beginning with the state of technology at the conclusion of the Apollo Program. Technology advancements span a period of 10 years from initial definition phase to the most recent Space Transportation System (STS) flights. The development program encompassed prototype, verification, and qualification hardware, as well as post-STS-1 design improvements. The review is concentrated on the problems encountered, the scientific and engineering approaches employed to meet the technological challenges, and the results obtained. Major technology barriers are discussed, and the evolving technology development paths are traced from their conceptual beginnings to the fully man-rated systems which are now an integral part of the Shuttle vehicle.

INTRODUCTION

Minimal energy requirements of the earliest spacecraft permitted the use of batteries for electrical power. However, for longer, higher power missions with energy requirements in the hundreds of kilowatthours, the fuel cell has obvious performance and weight advantages which enhance payload carrying capability. During the past 20 years, this potential for better performance and reduced weight has spurred electrochemical technology toward substantial increases in current density (amperes per square foot) and life, with concurrent decreases in specific weight (pounds per kilowatt) (ref. 1) as shown in figure 1. At the same time, increasing fuel cell reactant storage requirements for longer missions and higher energy production rates created a corresponding need for improved performance in reactant cryogenic storage. This need provided the driving force for the development of more sophisticated cryogenic storage techniques (ref. 2). Additionally, the practical application of these systems in advanced spacecraft was contingent upon the availability of necessary component technology for controlling fluid pressures and temperatures, for regulating heat- and mass-transfer processes, and for measuring fluid quantities. These growing requirements motivated significant advances in component technology in both the fuel cell and the cryogenics areas.

One of the most interesting combinations of these technologies is the Space Shuttle fuel cell and reactant supply system, which is the power workhorse and sole primary electrical power source for the Orbiter vehicle (refs. 3 to 5). This system is a highly efficient power generating system that produces electrical power by the electrochemical conversion of hydrogen (H₂) and oxygen (O₂) to potable water. Additionally, the reactant supply system provides breathing oxygen for the crew. This fuel cell and cryogenic system represents a major technological advance over that used for the Apollo missions. The fuel cells used in the Orbiter Columbia's original flights are 50 pounds lighter than and deliver as much as eight times as much power as the Apollo powerplants. A weight comparison to a battery system would indicate that today's advanced batteries would weigh about 10 times as much for the same amount of energy, and weight of the most readily available, or "off-the-shelf," batteries would be as much as 25 times greater than that of this fuel cell/cryogenic system combination. The subsequent addition (effective for the ninth Space Transportation System flight (STS-9)) of a third substack of cells to each Orbiter powerplant further improves the specific weight picture and assures a lifetime 10 times greater than that of the Apollo powerplant. The Shuttle reactant storage tanks are essentially scaled-up Apollo-type tanks, but they are far superior to the Apollo tanks in that they contain significantly improved insulation and support schemes. Moreover, the reusability of the tanks and the technical challenges thereby presented are particularly important for this paper (ref. 6).

Accordingly, in this report, the status of the fuel cell and cryogenic technologies at the conclusion of the Apollo Program is summarized, and the predevelopment technology activity which contributed substantially toward the formation of a firm technology basis for the Space Shuttle Program is discussed. Relevant technology issues are investigated, and the most significant innovations are noted. The manner in which the lessons learned from Apollo and pre-Shuttle technology programs were directly applied to the Shuttle development program is shown. Finally, major achievements in the test and evaluation programs supporting Orbiter development are discussed, and flight experiences are described.

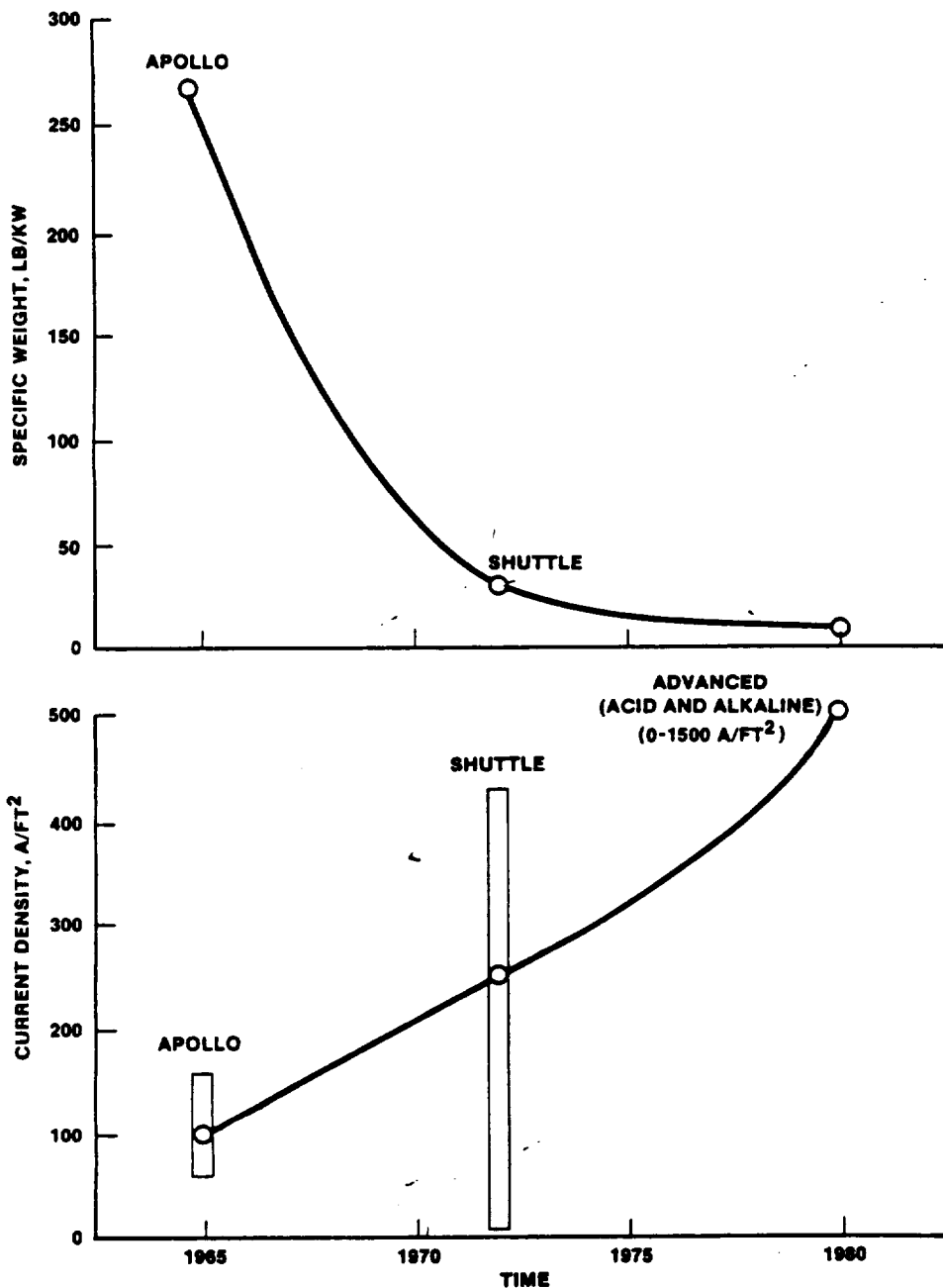


FIGURE 1.- NASA FUEL CELL TECHNOLOGY ADVANCES.

BACKGROUND

STATE OF TECHNOLOGY AT APOLLO PROGRAM CONCLUSION

The end of the Apollo Program marked the achievement of significant milestones in the development history of fuel cell power and cryogenic reactant supply systems. The flight-proven Apollo system could generate electrical energy at the rate of approximately 2 kilowatts for 14 days, with an available peak power of more than 4 kilowatts for limited periods of time, while supplying potable water and metabolic oxygen for a crew of three. This system consisted of three fuel cell powerplants of the Bacon cell technology, with accompanying supercritically stored hydrogen and oxygen reactants.

In the early 1960's when it was chosen for Apollo, the technology state of this fuel cell concept was extremely low, and many developmental difficulties were encountered from the beginning of the program (ref. 7). Although many of these problems were solved, some were merely "fixed" using work-around techniques because of the pressing schedule. This approach resulted in many inherent system design difficulties and features which made the fuel cell sensitive to operator error and necessitated the use of more complicated operational procedures than desired.

Initially, problems were encountered with pressure sealing in the 500°-F potassium hydroxide (KOH) environment. Also, a lightweight, long-life pump and water removal system which would operate satisfactorily in a 60-psi, 200°-F wet-hydrogen environment was needed. A highly reliable low-power coolant pump which could function well in a thermal vacuum environment at temperatures from -40° F to 140° F also had to be developed.

Contamination and corrosion in fluid flow loops with critical hardware tolerances were serious problems for many spacecraft systems and the fuel cell was no exception, as evidenced by sluggish valves and pumps failing to start. These difficulties were overcome mainly by improved servicing and operational procedures; material or design changes (or both) were made when there was no other means of dealing with the problem. Other problems with valves, accumulators, cell separation, and internal cell shorting were met and dealt with during the component development, production, and ground test phases of the program. As the production phase of the program was begun, a new set of problems evolved. Careful attention was needed in areas of process control, servicing, spares production, and traceability to ensure reliable flight-qualified hardware.

Although the actual Apollo space flights were relatively free of fuel cell failures, two classic fuel cell problems discovered in flight are worthy of note. The first involved air and particulate contamination trapped in the coolant system in the normal-gravity servicing environment. In low- or null-gravity conditions, the gas and particles freely migrated through the fluid loop and resulted in coolant pump cavitation and reduced thermal control capability. Improved servicing procedures precluded recurrence of the problem in later flights. The second problem involved condenser exit temperature oscillations occurring first in lunar orbit and found to be caused by a low-gravity, two-phase flow instability manifested only under certain powerplant operating conditions. Complex mathematical models and extensive in-house testing were required to characterize the instability and to quantify the operating conditions at which it occurred, so that valve schedule changes could be devised to accommodate this idiosyncrasy of the system (ref. 8).

At the end of the Apollo Program, a much improved cryogenic reactant storage system over the one originally conceived was seen, partly because of the Apollo 13 oxygen tank failure (ref. 9). Although low-gravity, two-phase fluid handling problems were avoided through the use of supercritical storage, development problems occurred early in the Apollo Program with insulation, heaters, pressure vessels, fans, and other components (ref. 10). These difficulties were resolved largely through design modifications and changes in hardware suppliers, and through tighter control of manufacturing processes, techniques, and quality. Other problems that developed during the flight phase required some redesign and requalification of flight hardware, but, overall, the state of technology in supercritical cryogenic storage supply dewars was advanced significantly during the Apollo years.

In the area of dewar insulation, significant design innovations involving multilayer insulation schemes with an embedded vapor-cooled shield were introduced during Apollo. Early insulation schemes were completely load-bearing, but excessive heat leak led to the use of semi-load-bearing insulation straps encircling the hydrogen pressure vessel and contacting the pressure vessel at specific points where the load is transmitted to a girth ring.

Apollo heater design schemes started with an original static heater concept and settled on a fan and heater combination which reduced system weight and minimized fluid stratification. After the Apollo 13 incident, the fans were deleted from the oxygen tanks, and the performance of the resulting static fluid heaters depended to a large extent on the effective gravity level.

Early pressure-vessel problems with the hydrogen tanks involved vessel failures due to room-temperature creep in the titanium alloy (5 Al-2.5 Sn), titanium hydride formation, and resultant spalling which caused vent-disconnect weld failures, and to problems encountered in the electron-beam welding process. Resolution of these problems was accomplished by changes in materials and fabrication processes, and by improved weld specifications and quality control, including the use of a borescope for weld inspection.

Major advances in the technology of other cryogenic components were seen by the end of Apollo. Included were significant improvements in fan motor design and the development of better vacuum potting techniques for the vac-ion pump package to prevent electromagnetic interference (EMI) and corona effects.

Three significant failures associated with the cryogenic storage system during Apollo had an impact on the technology base. These were failure of the automatic pressure control system in a hydrogen tank (Apollo 9); loss of vacuum in a hydrogen tank annulus, detected during loading (Apollo 12); and, of course, the Apollo 13 incident in which an oxygen tank failed in translunar flight. Through a diligent effort on the part of the Apollo team, a successful recovery from each of these failures was effected. Thus, at the end of the Apollo Program, significant technological improvements were seen in cryogenic system design, particularly in pressure-vessel fabrication and welding, bimetallic joints, vapor-cooled shields in high-performance insulation, vacuum acquisition and retention, EMI control, and metallurgical techniques.

In addition to the numerous system hardware technology advances, much progress was made in the development of analytical modeling techniques for electrical power and cryogenic storage systems (refs. 11 to 14). Also, certain advances in electronics technology were ready for application in future power systems. Collectively, these achievements constituted a firm technology base from which the Space Shuttle development program could begin.

RELEVANT TECHNOLOGY PROGRAMS PRECEDING SHUTTLE

Although the Apollo system was satisfactory for its intended use, it nonetheless left much to be desired as a means of power generation for future spacecraft. Even as far back as the days of Apollo, the NASA Lyndon B. Johnson Space Center (JSC), with awareness of the limitations of the Apollo fuel cell design, initiated technology development programs using NASA Office of Aeronautics and Space Technology (OAST) funding with both the Allis-Chalmers Manufacturing Company and the General Electric Company (GE). At that time, Allis-Chalmers was advancing the alkaline capillary matrix concept, which held the promise not only of longer life but also of alleviating the severe operational constraints experienced with the Apollo design. General Electric, on the other hand, was continuing development on an early version of the acid solid polymer electrolyte (SPE) fuel cell. The Allis-Chalmers concept was ultimately selected to be developed for the Orbital Workshop in the NASA Apollo Applications Program (AAP) and for the U.S. Air Force Manned Orbiting Laboratory (MOL). Later, the MOL program was canceled, and the Orbital Workshop concept was restructured and renamed Skylab. At this point, for economic reasons, a programmatic decision was made to use existing Apollo fuel cells for Skylab. These two events led to the curtailment of all Allis-Chalmers fuel cell activities. The Power Systems Division (PSD) of United Technologies Corporation, in recognition of the Apollo design limitations, had also been developing the alkaline capillary matrix technology, which has become its mainstay for the Shuttle fuel cell. Meanwhile, a technological breakthrough involving reactant prehumidification in the GE fuel cell made it a viable option for the projected Shuttle Orbiter power system.

During this same time period, the Bendix Company had been chosen to build cryogenic storage tanks for the Orbital Workshop and the Garrett AiResearch Corporation was selected to provide tankage for the MOL. However, cancellation of both these programs halted this effort before any significant technology advancements were realized.

By the close of the decade, although technological progress had been achieved in both fuel cells and cryogenic storage, much of it was fragmented and affected heavily by programmatic decisions outside the realm of these technologies. It was thus recognized in early 1970 that for the Space Shuttle, additional technology improvements would be required. For this reason, JSC initiated a competitive procurement activity with United Technologies Corporation and GE aimed at upgrading the state of hydrogen-oxygen fuel cells for Shuttle needs (ref. 15). Additionally, two technology programs for advancing the state of the art in cryogenic oxygen and hydrogen storage vessels were begun by JSC with the Beech Aircraft Corporation, Boulder Division: the Oxygen Thermal Test Article (OTTA) and the Hydrogen Thermal Test Article (HTTA) programs (refs. 16 and 17). At this time in the early Shuttle conceptual definition, a cryogenic orbital maneuvering system (OMS) was being considered; therefore, the vessels were sized for both OMS propellants and power reactants, as well as for metabolic oxygen. These programs brought about such improvements as silver-plated H-film insulation, S-glass support straps, and a refined vapor-cooled shield. Concurrently with these fuel cell and cryogenic technology programs, JSC also initiated a cryogenic supply system optimization study, one of the principal objectives of which was to investigate the feasibility of a totally integrated cryogenic fluid storage and supply system for the Orbiter that would provide fluids for propulsion, power generation, and life support (ref. 18). After selection of the present solid rocket booster/external tank combination in lieu of the all-cryogenic Shuttle, this activity was reoriented to a cryogenic cooling study. Perhaps the most useful result of this work was the establishment of a comprehensive data base for cryogenic system component design. This information was used extensively in the design and development phase of the Shuttle reactant supply system.

TRANSITION TO THE SHUTTLE ERA

GREATER DEMANDS THAN APOLLO

With the refocusing of the space program to near-Earth orbit following the lunar exploration phase, plans emerged for larger crews and increased activities with experiments and other flight hardware. Thus, electrical power requirements increased by more than an order of magnitude over the modest levels of previous programs and produced greater demands for high-performance power generation systems. With the emphasis on economy, this objective could only be attained through extended life and reusability. The concept of reusability required high operational tolerance and flexibility to achieve acceptable turnaround rates at launch and landing sites. Furthermore, to optimize total vehicle design, plans were laid for an increase in system integration for the Shuttle compared to previous spacecraft. Taken all together, these increased demands pointed up the requirement for a quantum jump in technology over that of the Apollo Program. Fortunately, these needs had been recognized earlier by fuel cell and cryogenic storage technologists and by the NASA OAST, and technology development in both areas had been evolutionary, building up from modest levels beginning just after the Apollo design was frozen in the early sixties to the competitive technology programs of the seventies resulting in the selection of the present Shuttle system. Through these programs, major technological barriers were overcome and the fuel cell and cryogenic storage system was placed in the enviable position of being one of the few systems truly ready, from a technology standpoint, for the development program. The development effort was reduced to solving engineering problems, though not at all insignificant, for which no major scientific breakthroughs were required. This state of technological preparedness earned for the power generation and reactant storage system the distinction of being the only subsystem which reached the end of the originally defined Shuttle development program on schedule and within the allocated budget (ref. 19).

LESSONS LEARNED FROM PREVIOUS PROGRAMS

The completion of JSC's competitive fuel cell technology programs in 1973 marked the end of a decade of significant accomplishments in fuel cells and cryogenic storage, and it was a time for reflection by the technical community on the successes and failures of these programs during that brief period before the Shuttle development program began. In retrospect, two things were clear to the fuel cell and cryogenics experts who were to be involved in the Orbiter project: (1) the features of a power generation and reactant storage system that were to be avoided in the Orbiter design were known from the Apollo Program and (2) technical risks in the development program could be minimized by using certain techniques and ideas which had evolved from the technology programs. Most unworkable methods had by this time been eliminated, and feasible techniques had been found, for the most part, to achieve the Orbiter goals of increased life, higher power, improved operational flexibility, and lower specific weight and volume.

Two fuel cell approaches were successful: the PSD fuel cell, with its improved alkaline electrolyte matrix, and the GE fuel cell, with its acid solid polymer electrolyte and hydrogen prehumidifier. Both of these concepts had undergone significant improvements during the competitive technology program, and engineering models of each had been subjected to a 5000-hour test program, with small stacks (four to six cells) and other components accumulating more than 10 000 operating hours.

Cryogenics specialists had reached a similar plateau in the development of reactant storage and supply systems, and although it was generally felt that the basic technology (supercritical cryogenic storage) would be adequate for the Shuttle, it was also agreed that certain improvements over the Apollo technology would be required to satisfy higher power levels, a different vibration environment, and requirements for increased operational flexibility and safety. High on the list of needed improvements was a better method of loading the reactant tanks because of significant loading problems with the Apollo tanks and the larger fluid quantities to be handled on the Shuttle. Consequently, a clear need was established for greatly improved ground-support equipment (GSE) and operations.

The Apollo 13 incident had led to improved static heater pressurization systems, and much had been learned about low-gravity thermal stratification and its effects in the oxygen tanks on later Apollo flights. Insulation and pressure-vessel mounting improvements had been made as a result of the OTTA and HTTA technology programs, and techniques were available to avoid the compressive, load-bearing insulation scheme of Apollo. A simplified vapor-cooled shield which further increased the thermal efficiency of the hydrogen vessel had been developed. Progress in electronics virtually assured electrical control and protective circuitry for the reactant storage and supply system that was greatly improved compared to the previous electromechanical pressure-switch system.

When the technology and flight programs for the development of fuel cell and cryogenic reactant storage systems in the years preceding the Shuttle are reviewed, it is clear that the availability of

the technology is attributable to the failures as well as the successes encountered in these programs, and to the penetrating insight and attention to detail on the part of the technical specialists involved. Although funding was modest in these areas compared to other systems in the Shuttle program, the combination of talented manpower, in-house test capability, and well-planned technology programs was responsible for the "ready" technology state of these systems at the start of the Shuttle development program. A composite summary of these technology and development programs is shown in figure 2.

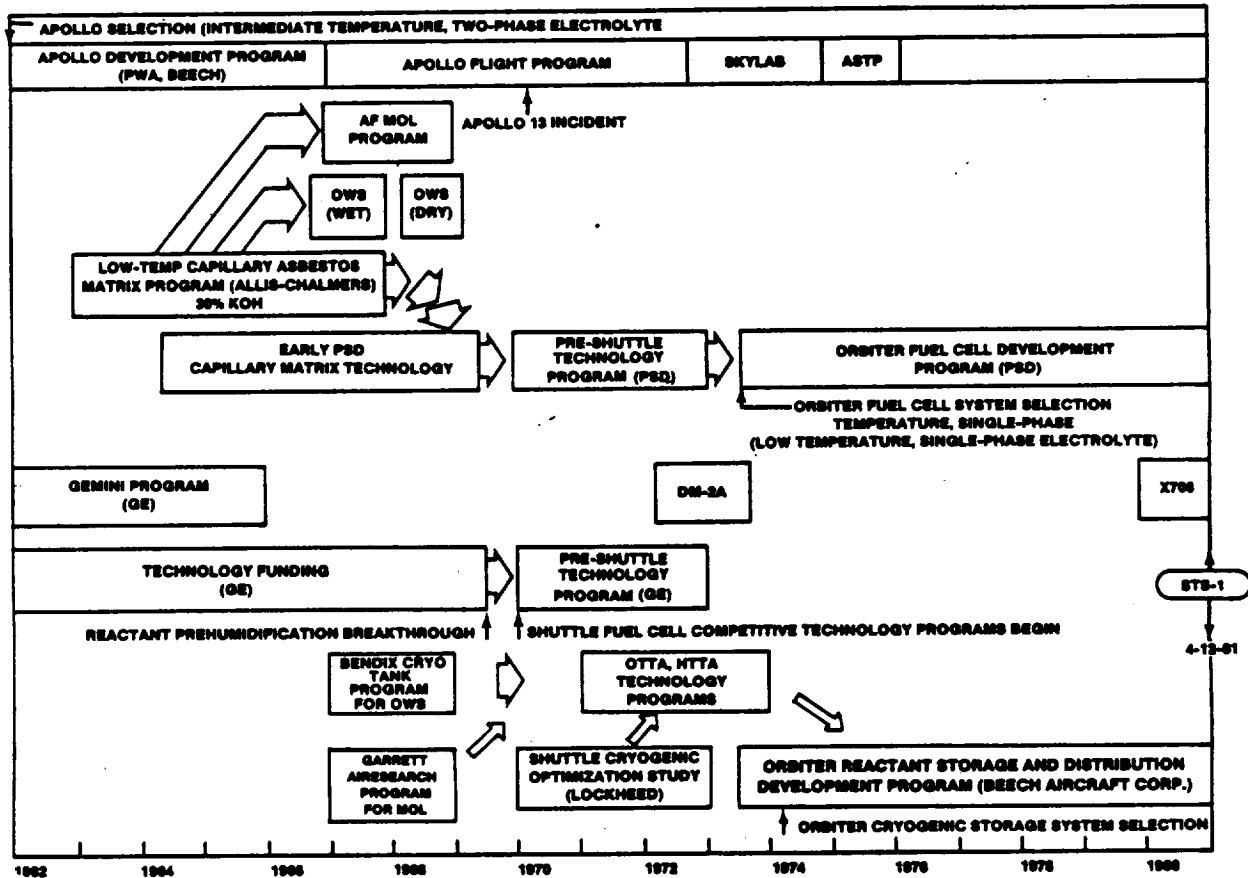


FIGURE 2.- FUEL CELL AND CRYOGENIC REACTANT STORAGE DEVELOPMENT AND TECHNOLOGY PROGRAMS.

THE DEVELOPMENT PROGRAM

TEST AND EVALUATION PROGRAMS

Unlike electrical power system development in the Apollo Program, which was richly endowed with supporting analytical activity, the principal development channel in Shuttle fuel cell and cryogenic system development was its test program. However, because of the increased emphasis on economy in the Shuttle program, the approach taken in the development phase for both the fuel cell and the cryogenic storage system included a minimum test program which would satisfy program requirements. This test program consisted of element and component supplier tests, thermal vacuum tests, vibroacoustics tests, and checkout tests in the Orbiter, with final integrated system checkouts in the horizontal flight test, the flight readiness firings, and the operational flight test program (STS-1 to STS-4).

Very early in the development program, cell test work at the NASA Lewis Research Center resulted in a change from the original platinum-palladium catalyst to the gold catalyst now used in all cells. This change provided increased efficiency and thereby a significant system weight decrease, since two powerplant substacks could then be used instead of the three originally required for each fuel cell powerplant.

Early development fuel cell units of the compact capillary matrix type were the PC8B-1 and the PC8B-4. Tests of the PC8B-1 led to many changes in the proposed Shuttle design, including the innovative dual-feed oxygen system and Moryl end plates. The PC8B-1 test program emphasized the need for aligned nubbins and other flow field changes.

Other tests performed at JSC also provided direction for the development program. One example is the investigation of the cold cathode activation procedure, found to be beneficial through early PSD testing, whereby the cells were starved of oxygen after shutdown by supplying an inert gas to the cathode, with hydrogen on the anode, while applying a load to the system. This procedure prevented the 0.5-millivolt per cell unrecoverable voltage losses associated with conventional shutdown procedures and enabled accurate performance predictions, thus reducing the rate of performance degradation of the powerplant. This is one of the reasons the flight powerplants have performed better than originally predicted from the qualification test results.

In addition to the designated qualification powerplants and development units, two developmental powerplants and some component hardware were purchased by JSC for special tests and evaluations to complement the mainstream development program. The DM2A fuel cell was a Shuttle prototype unit consisting of one flight-configured, 32-cell electrical generating stack and a nonflight accessory section. This powerplant was tested at the JSC Thermochemical Test Facility, primarily to provide insight into long-term thermal vacuum environment performance and degradation characteristics early in the Shuttle development program (ref. 20). It successfully ran for 5000 hours at a simulated Shuttle average load of 4.5 kilowatts, with an average loss of less than 1 volt over this time period. In addition to determining degradation characteristics, test engineers mapped the operating characteristics of the powerplant for the full range of Shuttle conditions and evaluated power-up capabilities, transient load responses, purge requirements, and diagnostic techniques. Procedures for starting and stopping the powerplant were also developed and verified in this program.

Another development powerplant, X708, was tested at JSC in 1978 (ref. 21) to evaluate a fully flight-configured Orbiter powerplant over various operating regimes at sea-level pressure and in a thermal vacuum environment. Although there were minor differences, the stack was essentially identical to the present Shuttle fuel cell stack and consisted of two 32-cell, power-producing stacks electrically connected in parallel. The powerplant arrived at JSC having approximately 2000 equivalent hours of operation, and approximately 1000 equivalent hours were added in the course of the tests. Such things as the effects of long periods of open circuit, postlanding cooldown, and short-term high power levels were evaluated. These tests confirmed operation within specification limits for the sea-level and vacuum tests and were extremely useful in thermal mapping of the coolant loop during the cooldown, high power, and open-circuit tests.

Other fuel cell tests were performed at JSC on its FC-40 fluid breadboard test loop. An example is the investigation performed to develop techniques and procedures for removing dissolved gas from the fuel cell coolant fluid before vacuum filling the coolant system.

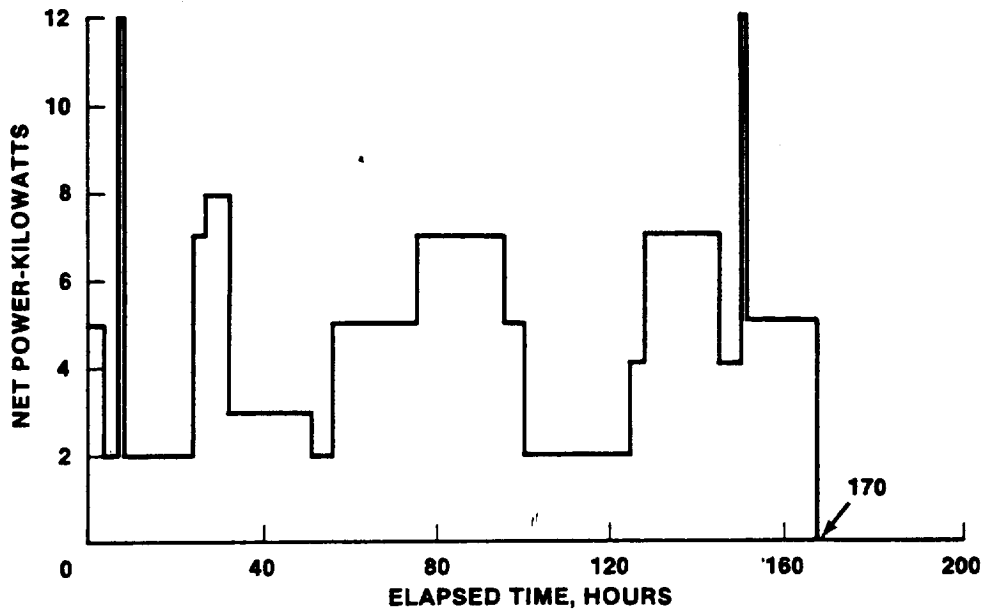
Although development problems in the fuel cell program could well be classified as "system level" and "component level," it is perhaps more meaningful in this paper to discuss in some detail the three most important problem areas from the standpoint of meeting and solving the challenges of system development. The first important area was a water removal problem first evidenced in 1975 by hydrogen pump seize-up during vibration testing of a powerplant simulator. A failure investigation revealed impeller interference within the housing, as well as contamination inside the pump. Consequently, the hydrogen pump was redesigned to include a circulating filter, increased clearances, and a larger diameter impeller to maintain existing pumping capacity despite the larger clearances. The redesigned pump-separator unit successfully completed vibration and other tests, and it was not until the next year, when attitude position testing on development powerplant X707 began, that further problems arose. Surge and stall problems occurred in the right-hand launch attitude tests. Investigation revealed that impeller rim purging during startup would eliminate surge and stall during right-hand position starts and operation. This revelation led to the third-generation production pump, which incorporated two purge ports in the impeller rim. Tests on this design revealed that purging did not solve the surge and stall problem in the right-hand position during startup, and out of this series of additional problems arose a fourth-generation, self-aspirated pump. Unfortunately, this design did not eliminate the surge and stall problems. It was also determined during pump testing that condenser backflow was sometimes experienced during certain expected launch acceleration loads (-Z). The fuel cell specification was then changed to incorporate expected launch and landing accelerations, and a condenser backflow investigation was initiated. This investigation resulted, in 1978, in further pump development activity in which 10 design changes were made and, subsequently, in a fifth-generation pump. The condenser backflow investigation also precipitated other changes in the condenser inlet header and the condenser aspirator pickup points. The result of these changes was the designation of "left-hand" and "right-hand" powerplants, according to their position, and resultant orientation, in the vehicle. Aspirator suction tube kits were fabricated for field conversion from the "right-hand" to the "left-hand" configuration. The redesigned condenser and fifth-

generation hydrogen pump successfully completed all attitude tests as well as a 2000-hour qualification test. In fabricating the redesigned condenser, it was observed that inadequate deburring before the welding process left metal "burrs" inside the condenser which could have led to serious contamination problems in the flow system had this problem not been corrected by tightening quality control procedures. This quality problem is considered minor in comparison to the other problems associated with the water removal system.

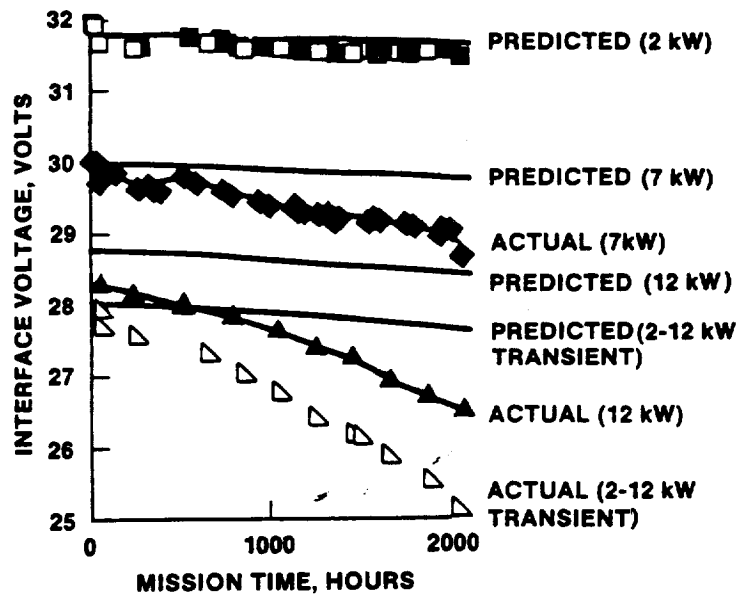
The second important fuel cell development problem occurred in the process of plating the magnesium separator plates which provide the flow channels for the reactant gases and the coolant. Magnesium was chosen for the plates because of its lighter weight, and it was used in the fabrication of the hydrogen and oxygen plates as well as the coolant plates. To isolate the magnesium from water in the stack to prevent corrosion, it was necessary to cover these plates with a thin (1.5 mil) layer of nickel. Then, to preserve electrical conductivity and to provide oxidation protection for the nickel, a layer of gold 0.2 mil in thickness was electroplated onto the nickel coating. The magnesium plates were first dipped in a zincate solution to promote adhesion of an intervening layer of copper, which was required by the industry-standard process to facilitate adhesion of the nickel coating. The problem involved plating defects in the nickel layer, and was ultimately found to be caused by insufficient process control and quality checks. Flow distribution requirements necessitated the use of a complex waffle-pattern plate geometry, which contributed to the formation of tiny blisters on the plate surface. These blisters were the result of a coating system breakdown which exposed the magnesium. The industry-standard process, although well established for other applications, was found to be inadequate for this specific application. To complicate matters, two vendor changes occurred in the manufacture of the finished plates during this time period. An investigation was then conducted which resulted in a better understanding of quality issues and requirements in plate production and in improvement of visual and X-ray standards. After process control was tightened, the improved inspection techniques helped in reducing scrap rates.

The third fuel cell problem of major import involved an abnormally high performance degradation in the qualification unit. The specification requirement for a fuel cell powerplant dictates a voltage regulation between 27.5 volts and 32.5 volts at the fuel cell terminals for loads between 2 kilowatts and 12 kilowatts. This specification applies in either a power-up or a power-down direction, as well as in steady state, over a period of 2000 hours when the average load on the powerplant is 4.5 kilowatts. The qualification power profile is shown in figure 3(a), and these loads were to be repeated for the qualification test until the powerplant had been operated for the required 2000 hours. At approximately 600 hours into the test, the powerplant fell below the 27.5-volt minimum requirement during a 2-kilowatt to 12-kilowatt power-up transient as shown in figure 3(b). This figure also shows performance losses at various steady-state power levels. It was decided at that point to continue the test for the purpose of certifying the powerplant accessory section for the required 2000 hours, and this was accomplished. The powerplant accumulated 2061 hours, with 53 starts, before teardown and analysis began. Meanwhile, because of this problem, production powerplants could only be considered qualified for 600 hours, or the equivalent of about four Shuttle flights. An exhaustive investigation was launched into the manufacturing history and build characteristics of the cell and into multicell rig and powerplant operational differences to find the cause of the premature performance degradation. The historical data search revealed that the performance decay was a function of numerous extensive powerplant load variations, start/stop cycles, and extended operation between cycles. Additionally, the anode (H_2 electrode) was suspected, since its voltage decay was worse than that of the cathode at high power levels. The post-test teardown confirmed this suspicion, since white calcium silicate deposits were found on the anode surface and were judged to be a primary contributor to anode performance degradation. Examination of used, new, and virgin electrolyte matrix material (asbestos) showed significant quantities of calcium (as much as several percent) in the asbestos material. Tests indicated that the calcium deposit transferred to the anode, where it inhibited the hydrophobicity of the anode. Without hydrophobicity, the catalyst reactant sites become excessively wetted by electrolyte, which masks reactant from the catalyst area and causes a decrease in performance. Cathode (O_2 electrode) performance was essentially unchanged from initial conditions, although the occurrence of small (10 mV/cell) positive and negative shifts caused performance changes from one start to the next (cathode activation losses). After the matrix material was found to be the source of the calcium deposits, it was theorized that electrolyte volume changes (i.e., a washing effect of electrolyte back and forth in the electrolyte reservoir plate (ERP) as a result of load changes and start cycles) provided the mechanism for calcium deposition. At this point, a plan of action was initiated to develop methods for calcium removal. Adding cells to the stack and even changing fuel cell vendors were options discussed. Tests on a two-cell stack using new cells to investigate the high initial performance degradation and the effects of startup and shutdown were initiated by JSC.

Approximately 1 year of intensive effort on the part of JSC, its prime contractor, Rockwell International, and the fuel cell manufacturer, the United Technologies Corporation PSD, was required to solve this problem, and the solution came in the form of two processes. The first, an electrode floccing process, consisted of adding a floccing agent to the colloidal dispersion of catalyst agent



(a) QUALIFICATION POWER PROFILE.



(b) QUALIFICATION TEST RESULTS (P760105).

FIGURE 3.- ORBITER FUEL CELL QUALIFICATION PARAMETERS.

used to coat the surface of the electrodes. Use of the floccing agent produced an electrode of more uniform consistency, thereby minimizing cell-to-cell performance variations. The floccing process was already in use in the PSD fuel cell developed for the U.S. Navy and in the NASA Lewis Research Center fuel cells, and it was incorporated as a no-cost improvement in the Orbiter program. The other process, that of leaching the asbestos matrix material to remove calcium impurities, involved reacting the calcium in the matrix with an organic acid and rinsing away the soluble reaction product. Figure 4 is a comparison of original qualification powerplant performance with later performance obtained after incorporation of the floccing and leaching processes. Here, individual cell

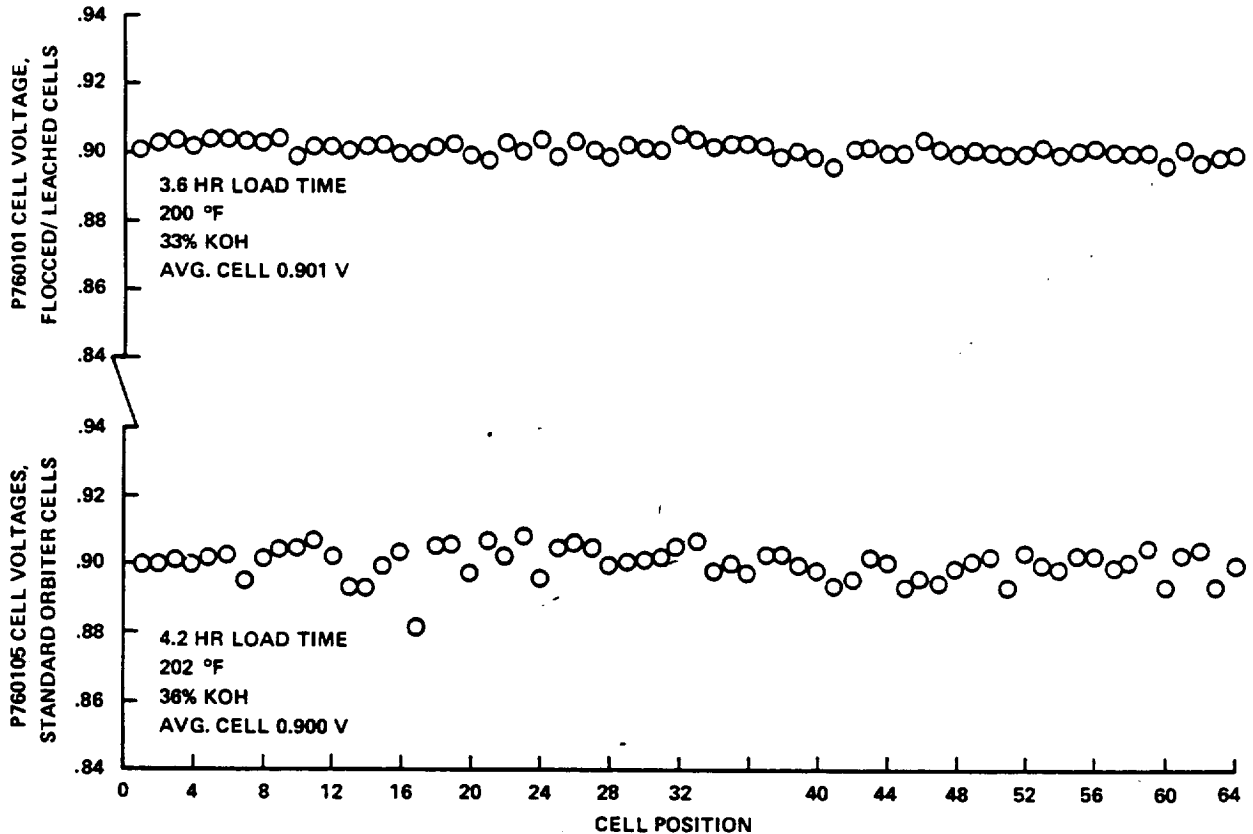


FIGURE 4.- COMPARISON OF STANDARD AND FLOCCED/LEACHED VOLTAGE PROFILES AT 12 kW.

performance is plotted at various loads for both powerplants. Although operating time is insufficient to accurately evaluate these cell process changes, NASA expects powerplant life to reach the 2000-hour goal with the present two-stack configuration. This powerplant is literally being qualified in flight, and all units currently are at or above predicted voltage levels. One powerplant has accumulated approximately 800 hours of flight operation with no noticeable degradation.

A further change later in the development program to a three-stack powerplant configuration was implemented in response to increased power requirements for the Orbiter. This change provides two avenues for additional operational flexibility, namely, longer life (NASA predicts more than 4000 hours) at a design average power level of 4.5 kilowatts or higher load capability (15-kilowatt peak per powerplant) for Shuttle missions. Figure 5 is a comparison of the two- and three-substack configurations for various steady-state powerplant loads.

Other fuel cell development problems, although significant, are considered relatively minor in comparison to the three just described in terms of impact to the program. These less important problems are listed below the major ones in table 1. The problems, the time of occurrence, the causes, and the corrective actions taken are shown.

Cryogenic storage development testing was accomplished for the most part at the Beech Aircraft Corporation, Boulder Division, where two test units, a dynamic model and a thermal test article, were extensively utilized. The dynamic unit was used in the development of the girth ring, the support straps, and the pressure vessel and to solve fill and vent line problems. The thermal test article was important in understanding the thermal-acoustic oscillation phenomenon and in the development of calibration procedures for the capacitance quantity gage inside the tanks. These test units are still in use today and have been used at JSC for relief valve and fill and vent line testing.

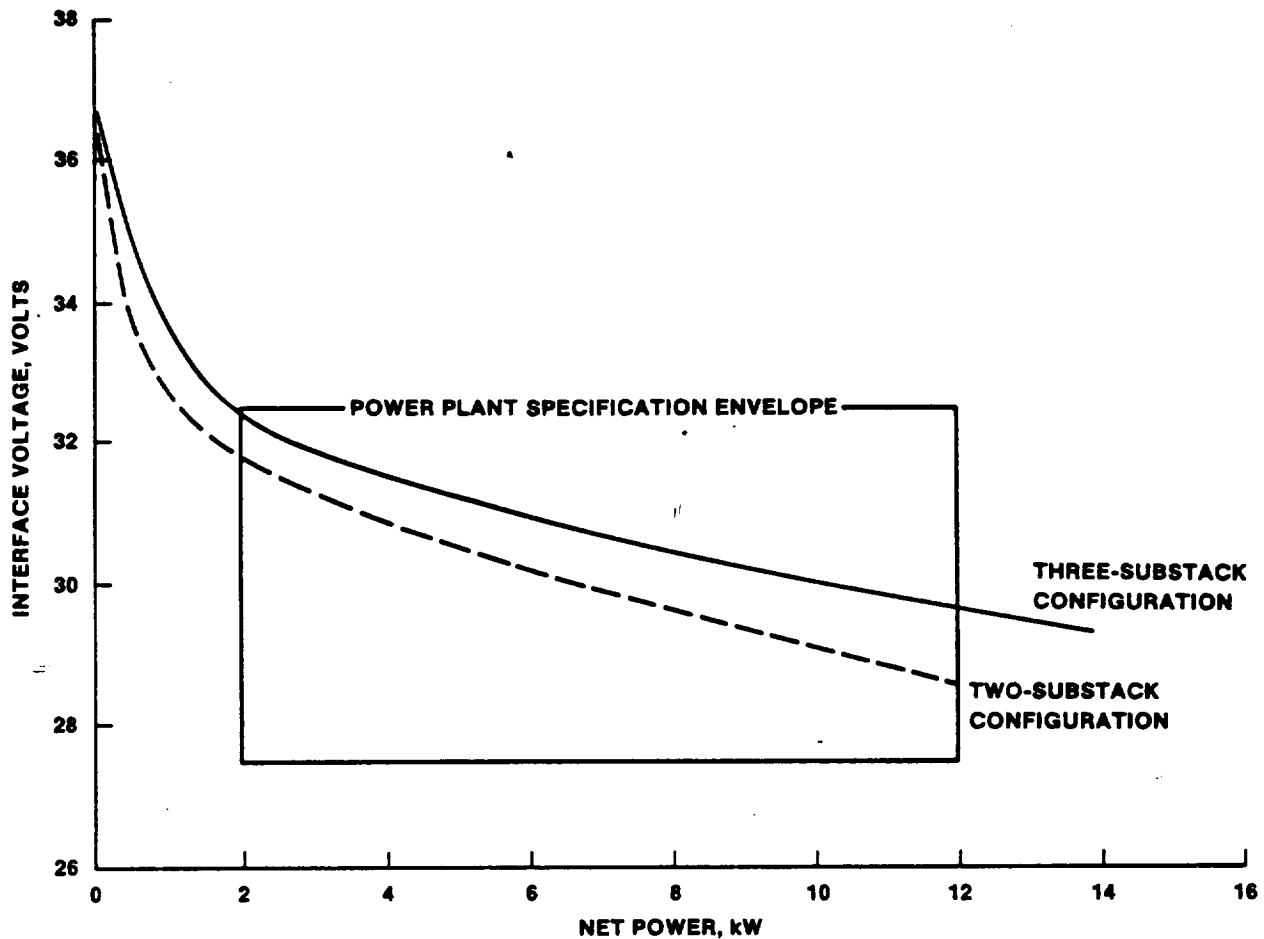


FIGURE 5.- COMPARISON OF PERFORMANCE DATA FOR TWO-SUBSTACK AND THREE-SUBSTACK POWERPLANTS.

Engineering improvements in cryogenics were needed in four areas: tank pressurization, inner vessel suspension, protective electrical circuitry, and GSE. The Apollo 13 incident had led to improved static heater pressurization systems, and although internal and external pressurization methods were being considered for the Shuttle, the general consensus was to maintain the internal scheme used on Apollo but to use no fans in either the Shuttle hydrogen or the Shuttle oxygen tank. Although the static internal pressurization technique had been flight-proven in the redesigned oxygen tanks used on later Apollo and subsequent flights, the reactant flow demands of the Shuttle system were approximately seven times greater than those of Apollo, and the increase caused a sharply higher localized heat influx at the heater probes. For example, the maximum heat input to the single heater probe in the redesigned Apollo oxygen tank was 150 watts. In the Shuttle oxygen tank, maximum heat input is 1000 watts. For this reason, the heater element configuration was changed and two heater probes are used in each tank as opposed to the single Apollo probe. The major unknown factors in the pressurization area at the beginning of the tank development program were the degree of thermal stratification expected in these larger tanks and the effects of stratification on system performance. These unknowns were later quantified and understood in the course of the development and flight test programs.

In remembrance of the problems encountered in the Apollo pressure-vessel suspension system, Shuttle designers used the increased knowledge gained in the OTTA and HTTA technology programs by choosing filament-wound S-glass support straps and using them in a tensile-loaded configuration, as opposed to the Apollo compressive load-bearing insulation scheme. This choice eliminated not only mechanical problems caused by internal vessel rotation but also localized high-heat-leak areas through the compressed insulation. Here again, the technology programs were rewarding in providing an increased level of intelligence for Shuttle development.

TABLE 1.- PROBLEMS ENCOUNTERED IN ORBITER FUEL CELL DEVELOPMENT PROGRAM

Problem	Time frame	Cause	Corrective action
Major			
Water removal system			
H ₂ pump stall	1975	Low impeller clearance, contamination in pump	Pump redesign (filter, increased clearance, larger diameter impeller)
Right-hand launch attitude stall	1976-78	Water buildup in pump rim	Impeller rim purge port and aspirator installation, pump current measurements, pump/separator redesign, left-hand/right-hand powerplants (aspirator suction tube kits)
STS-2 fuel cell failure	1981	Pump rim aspirator blocked by small foreign object; caused progressive fuel cell flooding with resultant high pH and voltage loss	Improved contamination control; pump redesign (eliminated pump rim aspirator); material change (parts changed to stainless; stainless steel filters)
Nickelplating (Mg plates)	1974-75	Insufficient process control and quality checks	Improved process control in plate production and improved nondestructive evaluation techniques
Performance degradation, qualification powerplant	1979-80	Calcium deposits on anode	Floccing and leaching
Other			
Dynamics (vibration)	1975	Allowable component stress levels exceeded	Support lines added, other fixes implemented to reduce stress levels
Condenser fabrication (burrs)	1982	Lack of quality control in condenser retrofit aspirator	Manufacturing procedures revised to include deburring; condensers reworked
Thermal control valves	1977	Contamination in piston relief slot	Improved cleaning methods
	1982	Thermal expansion, entrapped fluid	Improved manufacturing requirements, groove redesign for 3-substack fuel cell
Water trap	1979	Corrosion in housing - material incompatibility	Material change - Al to Inconel 600
Coolant pump seizure	1980	Coolant fluid expanded with increased temperature forcing can into stator	Stator can perforated to accept coolant volume change
Dual pressure regulator (venting)	1979	Contamination	Quality control improved

The optimization techniques developed in the OTTA and HTTA technology programs led to the selection of double silverized Kapton multilayer insulation with nylon net spacers, although heat leak minimization requirements were not as demanding because of planned higher reactant usage rates. Collectively, these improvements resulted in significantly lower cost, complexity, and weight for the Shuttle reactant storage system.

A third major improvement in the Shuttle tanks compared to the Apollo tanks is in the electrical protective circuitry. Each Shuttle hydrogen/oxygen tank set contains an electrical control box (mounted on avionics cold plates), which contains differential current level detectors, control pressure conditioners (CPC's), remote power controllers (RPC's), control drivers, and the logic required to control the tank heaters and to provide overload protection in case of heater fault.

The fourth item requiring considerable attention in the development program was GSE. In an effort to avoid the difficulties of loading the Apollo tanks, much consideration was given to the GSE early in the program. As a result, larger lines, better insulation, and the absence of tank loading problems were characteristics of the Shuttle program. At JSC and Beech Aircraft, hydraulic pressurization techniques were developed to pressurize the tanks after loading, and procedures were developed at JSC to assure adequate reactant purity at filling. These techniques and procedures resulted in decreased tank loading times.

Although the reactant storage system development program was relatively smooth compared to the fuel cell program, several problems were encountered. These problems can be loosely separated into three categories: dynamics, thermal-acoustic phenomena, and fabrication techniques.

Dynamics (i.e., vibration) problems were of two types. The first - definition of the vibration environment for the system - involved no hardware failures but has been an annoyance from the beginning of the program to the present time. Because of the complex configuration of the

interreacting support struts and straps with their multiple degrees of freedom, it has been virtually impossible to perform an adequate dynamic analysis of the system to determine correct vibration levels for dynamic testing. This difficulty has caused many changes in the test requirements, and this issue is still not fully resolved, although the latest tank configuration has been certified for the required 100 missions. The second dynamics problem was related to the first in that it was partly due to a lack of understanding of the vibration environment, but was strictly a components problem. Many components (e.g., tank heaters, capacitance probe, and vac-ion pump) were failing when vibrated to a level believed to be much more severe than that expected in flight. The support straps failed because of fatigue, and the electrical signal-conditioning box almost completely disintegrated during an early development test. The signal-conditioning box was found to be reaching a resonant frequency on the girth ring on which it was mounted, and vibration isolators were required to solve this problem. The fill and vent lines cracked in the hydrogen tank, and this failure led to a complete redesign of these lines in both the hydrogen and oxygen tanks. (The oxygen tank redesign is in work.) Only the pressure vessel, the outer shell, and the tank's girth ring needed no modification after vibration tests. Electrical problems occurred with transistors and diodes failing in the CPC. An embrittlement problem arose in connecting the lead wires to the heater elements; this problem required a manufacturing process change. Thermal-acoustic oscillations discovered early in the program in the hydrogen tank caused pressure change amplitudes of 20 ± 10 psi, which not only produced problems for the pressure control system but also increased tank heat leak by 200 percent. To damp these oscillations, an orifice was put in the fill line and the line was insulated. Extensive JSC in-house testing resulted in both the discovery of this problem and the evaluation of the design fix.

Although extensive spark ignition tests had been performed in the Apollo Program to determine minimum energy levels required for ignition of combustible materials in a high-pressure oxygen environment, later discoveries in the 10 years following the Apollo 13 incident modified these results somewhat. The most significant of these discoveries was that Teflon will ignite in this environment at energy levels lower than originally expected. Extensive testing was performed on the Shuttle signal conditioner to determine whether it was capable of delivering localized energies in the vicinity of the capacitance probe (the only tank component containing Teflon) sufficient to produce ignition. The results were negative and no changes had to be made to the system.

Another Shuttle development problem which constituted a significant challenge concerned the manufacturing process for the pressure vessel. To complete a pressure vessel, its two preformed hemispherical shells are clamped together carefully at many points and, after precision alignment and measurement checks, the hemispheres are welded together. Because no problem was suspected, the measurements originally were not rechecked after the welding process was completed. Later, discovery of pressure-vessel mismatches caused concern for the integrity of the vessel. An additional qualification test was run on a pressure vessel with a known severe mismatch, and, following this test, the vessel was subjected to a burst test which proved that excessive mismatch did not cause burst pressure problems. Tanks currently are being flown with a lower degree of mismatch than that of the burst-test specimen, but two significant corrective actions have been initiated. The first was a procedural modification requiring recheck of the vessels for mismatch after welding is complete. The second corrective action involved the development of an ingenious nondestructive evaluation (NDE) procedure to X-ray for pressure vessel mismatch on existing tanks, viz, completely fabricated tanks with an outer vessel. Considerable cost savings were realized using this procedure, since not all tanks have the mismatch problem.

Table 2 is a summary of major reactant supply system development problems, the time frame in which they occurred, the determined cause, and the corrective actions taken. This table, as with the comparable fuel cell table presented earlier, is not intended as a complete problem list but only to highlight some of the most challenging problems encountered in the program.

Although testing and evaluation is continuing on such issues as certification of empty reactant storage vessels for launch, fuel cell startup heater design issues, and higher-than-anticipated vibration levels in flight, a technological plateau was reached in 1981 when both the fuel cell and cryogenic systems were declared ready for the first orbital flight test. From this plateau, one could look back down the steep slope representing the challenges which had been overcome in bringing these two systems to a state of flight readiness. Many improvements had been made in these systems since the Apollo Program. A comparison of the most significant characteristics of these Shuttle systems with those of Apollo is shown in tables 3 and 4. The pause at this plateau was brief, however, because on April 12, 1981, the launch of STS-1 signaled the beginning of a new era of developmental flight testing in the early Shuttle flights which held still more surprises.

FLIGHT EXPERIENCES

In the first four development flight tests, several problems were encountered in the fuel cell and reactant storage systems. Only one of these problems could be considered major, that being the STS-2 fuel cell failure. This problem was traced to contamination in the water removal system. It

TABLE 2.- PROBLEMS ENCOUNTERED IN SHUTTLE REACTANT SUPPLY SYSTEM DEVELOPMENT PROGRAM

Problem	Time frame	Cause	Corrective action
Environmental			
Inadequate tank/component vibration environment definition	1974-present	Complex configuration; multiple degrees of freedom	Vibration requirements modified by flight test data
Component vibration failures	1974-80	Inadequate component vibration environment definition led to overly severe test conditions	Redesign of some components (e.g., fill/vent lines); retest of others at reduced vibration levels; vibration isolators
Thermal-acoustic oscillations (H ₂)	1977-78	Thermal instability	Installed orifice in the fill line and improved insulation on H ₂ and O ₂ fill and vent lines
Electrical			
Control pressure conditioner	1980-present	Cold solder joints, unpotted filters	Component redesign and improved manufacturing techniques
Reactant valve switch	1977	Excessive voltage drop across contacts	Revised manufacturing procedures
H ₂ shutoff valve lead wire short	1977	Wire contact with valve cover during welding	Improved inspection techniques
O ₂ shutoff valve short	1976	Sharp bends in wires, insulation failed, causing shorting	Wiring and insulation redesign
Signal conditioner combustion hazard	1979	Potential shorting in capacitance probe	Performed hazard analysis and additional off-limits testing to prove adequacy of design and to define design margins
Manufacturing			
Heater wire embrittlement (H ₂ tank)	1982 (STS-4)	High stresses developed during high-temperature annealing and gold braze operations, causing embrittlement	Design changes to eliminate heater stress concentration bends; improved inspection techniques
Pressure vessel mismatch	1980-81	Welding process for hemispheres introduced errors; not rechecked after welding	Improved clamping procedures; began using improved radiographic technique to detect mismatch on existing vessels (those produced before the problem was discovered)
Instrumentation			
H ₂ quantity transducer shift	1982 (STS-4)	Unresolved to date	Tank depletion can be tracked by quantity comparison with other tanks and known fuel cell usage
O ₂ quantity transducer shift	1982	Suspected shift in calibration; cause unresolved to date	Same as H ₂ transducer
H ₂ quantity gage off-scale high	1982 (STS-3)	Two simultaneous open-circuit conditions in EMI filter sections of signal conditioner	Revised repair/inspection techniques
O ₂ pressure transducer	1976	Transducer instability	Revised acceptance test procedure
Control logic failure in H ₂ T-O valve	1981	H ₂ T-O valve control logic defective	Valve replaced, control logic revised

was found that the hydrogen pump was not operating properly because of contaminant blockage of the pump impeller rim aspirator. The blockage caused water backflow through the pump rim into the hydrogen discharge port and eventually all the way to the power section and flooded several cells. This problem resulted in yet another redesign of the hydrogen pump and the water removal system. Included were material changes, the incorporation of filters in the water removal section of the pump, and the elimination of the hydrogen pump rim aspirator in favor of a passive recirculation system. Also, ground checkout monitoring of pump current was emphasized. No further problems have been experienced with this system. A three-substack fuel cell powerplant has also been produced; this unit has recently completed qualification testing and will be flown for the first time on STS-9. The redesigned hydrogen pump was installed on the three-substack powerplant and qualified along with the powerplant after successful completion of powerplant qualification testing. Other fuel-cell-related flight problems include reactant flowmeter malfunctions and a shift in thermal control set points. Both of these are minor by comparison to the hydrogen pump problem, and design or process changes have remedied both problems.

The reactant storage system has performed well on all flights through STS-7 with few problems, none of which caused a mission compromise. The heater wire embrittlement problem, thought to have been solved earlier, did recur on STS-4, resulting in a powered-down heater mode for entry, but per-

TABLE 3.- COMPARISON OF SALIENT APOLLO AND SHUTTLE
FUEL CELL CHARACTERISTICS

Characteristic	Apollo	Shuttle ^a
Net powerplant output, steady state		
Min-max, kW	0.6-1.4	2-12
Average, kW	0.9	7
Voltage, V	27 to 31	27.5 to 32.5
Thermal control	Dedicated radiators	Integrated with vehicle ATCS ^b
In-flight restart capability	No	Yes
Restarts allowed	N/A	50 starts with no maintenance 125 starts with maintenance
Reactant purity required (by volume)	0.99995 O ₂ 0.99995 H ₂	0.99989 O ₂ 0.99990 H ₂
Powerplant life, hr	400	2000 with no maintenance 5000 with maintenance
Powerplant weight, lb	245	202
Powerplant specific weight, lb/kW	270	29
Current density at average load, A/ft ²	90	230
Cost		
Development program, million dollars ^c	61.1	22.6 (through OV102)
Production powerplant, million dollars ^c	1.2	2.2

^aTwo-substack powerplant.

^bActive thermal control system (Freon loops).

^cApollo costs in 1971 dollars; Shuttle costs in 1982 dollars.

formance remained nominal with no mission impact. This problem is under investigation, but because of extensive ground checkout, an extremely low failure rate, and an adequate amount of redundancy to cover uncertainties, no flight impact has occurred. Only two other component failures have occurred in the flight program (excluding random instrumentation failures): a remote power controller and a hydrogen quantity gage. The RPC problem was traced to an electrical problem and resolved, and the quantity gage signal conditioner was replaced (twice) to preclude recurrence. The tank pressure control system works consistently, with no control band drift from flight to flight. Compared to the Apollo pressure control system, the Shuttle system is very sophisticated. It allows predelivery setting of the pressure control band higher for selected tanks, with all tanks in the "auto" position, to avoid callup requirements to the crew for manual tank management. Occasionally, pressure drops of as much as 100 psi in the oxygen tanks, caused by destratification, have been observed during vehicle maneuvers, but these cause no concern since the tank operates at a pressure near 900 psia and the fuel cell minimum pressure requirement is 100 psia. Other minor problems that have occurred, primarily instrumentation problems, are not mentioned here. Review of flight data for the STS-1 to STS-4 missions revealed tank vibration levels which were higher than expected during ascent. This revelation necessitated certain modifications to the oxygen tank fill line and resulted in a redesign and certification of the tank for the more stringent dynamic environment.

TABLE 4.- COMPARISON OF SALIENT APOLLO AND SHUTTLE
REACTANT STORAGE SYSTEM CHARACTERISTICS

Characteristic	Apollo	Shuttle
Tank capacity (100% quantity), lb	29 H ₂ ^a 330 O ₂	92 H ₂ ^b 781 O ₂
Tank heat leak at dQ/dm min, Btu/hr	7 H ₂ 26 O ₂	6.7 H ₂ 20 O ₂
Flow rate at dQ/dm min, lb/hr . . .	0.07 H ₂ 0.73 O ₂	0.07 H ₂ 0.62 O ₂
Insulation	Aluminized Mylar	Silverized Kapton with nylon net
Vapor-cooled shield	O ₂ (limited) H ₂ (forerunner to Shuttle)	O ₂ - not required H ₂ - simplified
Structural support	Compressive O ₂ : load bearing H ₂ : partly load bearing	Tensile Epoxy-impregnated S-glass support straps
Reusability	None	100 missions
Tank operation control	Pressure switches	Cryogenic control box (electronic)
Heater protection	Fuses Stainless steel sheath (O ₂ : static)	Differential current level detector Double stainless steel sheath (O ₂) High-emissivity coating
Tank weight, lb		
H ₂	91	227
O ₂	80	215
Cost		
Development program, million dollars ^c	15.1	14.4
Production tank set (two tanks), million dollars ^c	0.8	1.6

^aApollo baseline: before Apollo 14 - two tank sets (H₂ and O₂); after Apollo 14 - three tank sets.

^bShuttle baseline: two tank sets, but as many as five complete tank sets can be installed below payload bay liner.

^cApollo costs in 1971 dollars; Shuttle costs in 1982 dollars.

CONCLUSION

Looking back on the vast amount of activity occurring from the early days of the technology programs to the present time, peaks of accomplishment stand out in meeting the challenges faced in developing the present fuel cell and reactant storage systems. These accomplishments include major advances in electrochemical technology, significant mechanical and electrical improvements, much progress in dynamics and thermal engineering, and major breakthroughs in nondestructive testing and manufacturing techniques. Many of these achievements can be traced directly to the NASA predevelopment technology programs.

Collectively, the decisions and efforts of a large number of design and development experts, test engineers, project personnel, and subsystem managers, under the direction of the Orbiter Project Manager, have successfully guided the development of these two Shuttle systems through many problems.

This success was the result of a dedicated team effort by all involved, both NASA and contractor personnel. All should be proud that the challenge has been met and major difficulties overcome to produce the systems which are flying in the Shuttle Orbiter today.

In summary, no failures have occurred in flight which have compromised either crew safety or mission success, although the STS-2 fuel cell failure did cause this mission to be shortened to preplanned minimum mission guidelines; however, more than 90 percent of all high-priority flight tests were accomplished (ref. 22). The STS-2 mission incident also demonstrated important "designed-in" operational capabilities in the presence of a significant subsystem failure. From this standpoint, it can be concluded that these systems have performed well. Development problems still exist, however, which are being diligently worked on at the present time (examples are cryogenic tank heater wire embrittlement and fuel cell startup heater failures in ground test). Because of this continuing effort, future flights should be even safer and better from an operational standpoint. As in any high technology area, further improvements may be required and problems as yet unforeseen may arise in the future, and we must remain prepared to face these new challenges.

VITA

William E. Simon is Deputy Chief of the Power Generation Branch of the JSC Propulsion and Power Division. After joining JSC in 1963, he was involved in the development of the Apollo fuel cell and performed a computerized transient thermodynamic analysis of this system. He served as the Division's senior thermal control coordinator for Propulsion and Power Division Shuttle subsystems from 1972 to 1975. He performed the thermal dynamic power system technology trade-off studies in 1976 for the JSC in-house Solar Power Satellite Study. From 1977 to 1980, he was involved in the development and verification of the Shuttle Integrated Main Propulsion System (MPS). Dr. Simon assumed his present duties in November 1980 which involved responsibility for the Shuttle's onboard fuel cell and cryogenic subsystems, as well as the JSC Government furnished equipment battery program, and advanced electrical power system development for Space Station application.

ACKNOWLEDGMENT

The author gratefully acknowledges the suggestions, insights, and data provided by former JSC subsystem managers Robert R. Rice, Shelby L. Owens, James R. Briley, Fulton M. Plauché, and present subsystem manager Thomas L. Davies. Appreciation is also extended to Rockwell International Project Manager James F. Williams as well as to William E. Romanoski and Henry J. DeRonck, system engineers with United Technologies Corporation, Power Systems Division. Gratitude is expressed to Richard B. Ferguson, former Deputy Chief of the JSC Propulsion and Power Division for valuable insight into the JSC early technology programs. Thanks also go to Mrs. Lynn S. Murgia for her review and comments on the mechanisms theorized for performance degradation within the fuel cell. Recognition is given to the JSC Thermochemical Test Branch, specifically to power systems test engineers David R. Saucier and Norman C. Luksa and to Branch Chief Chester A. Vaughan, for review of the paper and for vital information on the JSC in-house test programs. The author also acknowledges the informative discussions and information on system and component problem histories provided by Marvin F. LeBlanc, quality engineer with the Boeing Company. Finally, thanks go to Mr. William A. Chandler, Chief of the JSC Power Generation Branch, for his review and comments.

REFERENCES

1. Simon, William E.: Energy Conversion Technology. AIAA Fortune 500 Conference Briefing, NASA Johnson Space Center, Houston, Tex., Jan. 22, 1981.
2. Davis, Michael L.; Allgeier, Robert K., Jr.; Rogers, Thomas G.; and Rysavy, Gordon: The Development of Cryogenic Storage Systems for Space Flight. NASA SP-247, 1970.
3. Shuttle Operational Data Book, vol. 1, Shuttle Systems Performance and Constraints Data. JSC-08934, Oct. 1976.
4. Fraser, Wilson M., Jr.: Orbiter Electrical Power Generation Subsystem Handbook. NASA Johnson Space Center, Houston, Tex., in writing at publication of this paper.
5. Fraser, Wilson M., Jr.: Orbiter Power Reactant Storage and Distribution Subsystem Handbook. NASA Johnson Space Center, Houston, Tex., Second Edition, January 1983.
6. Colaprete, Stephen J.: Cryogenic Technology - Contribution to Space Shuttle Achievement. Electronic Progress (The Raytheon Company), vol. XXIII, No. 4, Winter 1981, pp. 3-9.

7. Bell, David, III; and Plauché, Fulton M.: Apollo Experience Report - Power Generation System. NASA TN D-7142, 1973.
8. Low, George M.: What Made Apollo A Success? *Astronautics and Aeronautics*, vol. 8, No. 3, March 1970, p. 41.
9. Report of Apollo 13 Review Board. National Aeronautics and Space Administration, June 15, 1970.
10. Chandler, William A.; Rice, Robert R.; and Allgeier, Robert K., Jr.: Apollo Experience Report - The Cryogenic Storage System. NASA TN D-7288, 1973.
11. Simon, William E.: Transient Thermodynamic Analysis of a Fuel Cell System. NASA TN D-4601, 1968.
12. Davies, Thomas L.: Heat Transfer Analysis of a Vapor-Cooled Shield. The University of Houston, unpublished Master's Thesis, 1970.
13. Patterson, H. W.; and Forester, C. K.: Shuttle Orbiter Cryogenic Tank Stratification Analysis. The Boeing Aerospace Company, Seattle, Wash., Feb. 1975.
14. Chen, I. M.; and Anderson, R. E.: Prediction of the Effects of Thermal Stratification on Pressure and Temperature Response of the Apollo Supercritical Oxygen Tank. MSC Cryogenics Symposium, MSC-04312, 1971, pp. 274-300.
15. Blaski, Marvin F.; and Owens, Shelby L.: Electrical Power Generation Subsystem for Space Shuttle Orbiter. AIAA Symposium, Aug. 1974, p. HP-32.
16. Chronic, William L.; Baese, C. L.; and Conder, R. L.: Oxygen Thermal Test Article (OTTA) Final Report/Design Manual. The Beech Aircraft Corporation, contract NAS 9-10348, 1973.
17. Chronic, William L.: Hydrogen Thermal Test Article (HTTA) Final Report. The Beech Aircraft Corporation, contract NAS 9-12105, 1975.
18. Shuttle Cryogenic Supply System Optimization Study - Final Report. vol. 1, Management Summary, sec. 1 through 3, Lockheed Missiles and Space Company, LMSC-A-991396, 1973.
19. Apollo CSM Cost/Schedule/Technical Characteristics Study, Final Report, vol. I. North American Rockwell Corporation, Space Division, SD71-35-1, Apr. 30, 1971.
20. Saucier, David R.: Performance and Degradation Evaluation of the Shuttle Prototype DM2A Fuel Cell, JSC-12543, 1977.
21. Luksa, Norman C.: Performance Evaluation of the Orbiter Fuel Cell. JSC-13904, 1978.
22. STS-2 Orbiter Mission Report. NASA Johnson Space Center, Houston, Tex., JSC-17959, Feb. 1982.

SHUTTLE S-BAND COMMUNICATIONS TECHNICAL CONCEPTS

J. W. Seyl, W. W. Seibert, J. A. Porter, D. S. Eggers,
S. W. Novosad, H. A. Vang, S. D. Lenett, W. A. Lewton,
and J. F. Pawlowski
NASA Lyndon B. Johnson Space Center
Houston, Texas 77058

ABSTRACT

The Shuttle S-band communications system provides the Shuttle Orbiter with the capability to communicate directly with the Earth by way of the Ground Spaceflight Tracking and Data Network (GSTDN) or by way of the Tracking and Data Relay Satellite System (TDRSS), which relays Orbiter information signals through a geosynchronous satellite to/from the Earth. S-band frequencies provide the primary links for direct Earth and TDRSS communications during all launch and entry/landing phases of Shuttle missions. While on orbit, the Orbiter uses its S-band links when TDRSS K_u -band is not available, when conditions require Orbiter attitudes unfavorable to K_u -band communications, or when the payload bay doors are closed. The Shuttle S-band communications functional requirements, the Orbiter hardware configuration, and the NASA S-band communications network are described. The requirements and implementation concepts which resulted in new or unique techniques for Shuttle S-band hardware development are discussed. These areas include (1) digital voice delta modulation, (2) convolutional coding/Viterbi decoding, (3) critical modulation index for phase modulation using a Costas loop (phase-shift keying) receiver, (4) optimum digital data modulation parameters for continuous-wave frequency modulation, (5) intermodulation effects of subcarrier ranging and time-division multiplexing data channels, (6) radiofrequency coverage, and (7) despreading techniques under poor signal-to-noise conditions. The performance of these new and unique communication channels is reviewed, with analytical and experimental results of performance provided.

INTRODUCTION

The Shuttle functional communication requirements are met through the use of three basic communication network modes. The NASA Ground Spaceflight Tracking and Data Network (GSTDN) mode provides for communication links from the Shuttle to the NASA network ground stations. The U.S. Air Force (USAF) Space Ground Link System (SGLS) mode provides for communication to the Air Force Satellite Control Facility (AF/SCF) by way of a remote tracking site (RTS). The NASA Tracking and Data Relay Satellite (TDRS) mode provides for communication links from the Shuttle to a geosynchronous orbiting satellite for relay to the NASA White Sands Ground Terminal. These S-band links represent the primary communication capability of the Shuttle for all mission phases when the TDRS K_u -band communication link is not available. All Shuttle missions through STS-6 depended solely on the NASA GSTDN and/or the AF/SCF SGLS S-band communication modes.

Figure 1 illustrates the communication links associated with the Shuttle S-band modes. Each mode uses a common Orbiter network subsystem, which is also shown functionally in figure 1. Table 1 defines the link capabilities, the modulation techniques employed, and unique design features. The frequencies for each of the S-band communication modes are given in table 2. The SGLS mode uplink is actually in the L-band frequency range for compatibility with the AF/SCF RTS transmitters.

To provide the multiple functions such as two duplex voice channels and command data on the uplinks, a time-division multiplexing (TDM) technique is incorporated. Similarly, TDM is used on the downlinks to allow simultaneous transmission of two duplex voice channels and telemetry data on a single carrier signal.

To achieve optimum performance on these digital channels, a phase modulation (PM) system was developed. In addition, a frequency-modulated (FM) channel is provided for transmission of television or other analog/digital data which cannot be handled by the PM links. The PM link used for communications through the Tracking and Data Relay Satellite can operate at two digital data rates. The low-data-rate mode is provided to ensure adequate link margins if communication channel parameters operate near their worst case tolerances. When operating through the TDRS, the phase modulation index is optimized at $\pm 90^\circ$, which is referred to as phase-shift keying (PSK).

An important characteristic of the S-band links is the coverage provided by the S-band PM switched-beam antennas, which are flush mounted at four locations on the Shuttle vehicle. These antennas allow nearly continuous communication when a network element is visible, without requiring Shuttle attitude constraints.

The Shuttle S-band GSTDN network (fig. 2) consists of 13 NASA ground stations and 2 USAF AF/SCF

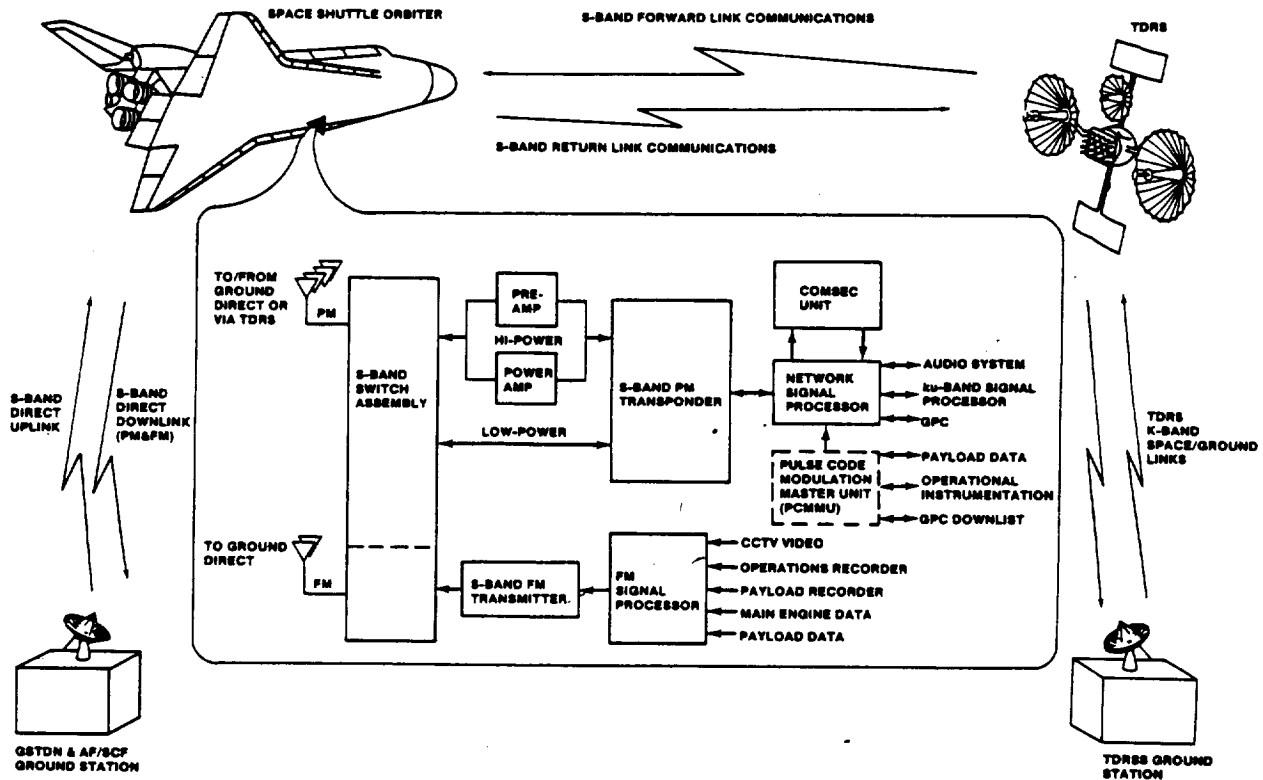


FIGURE 1.- ORBITER OPERATIONAL S-BAND SYSTEM.

remote sites. The TDRS system (TDRSS) is scheduled to be available after STS-6. The TDRSS network (fig. 2) consists of two satellites and a spare satellite. The TDRSS network will provide significantly more coverage than previously available. When the TDRSS is operational, the number of NASA ground stations will be reduced and only those necessary to cover launch and landing phases will be retained for Shuttle support.

In the following sections, the S-band communication modes are discussed in detail. The unique techniques and designs incorporated in the Orbiter S-band network hardware to provide these links are highlighted. Performance characteristics, including the effects of nonideal hardware parameters for links that incorporate new or advanced communication concepts, are reviewed.

TRACKING AND DATA RELAY SATELLITE SYSTEM MODE TECHNIQUES

To communicate with the Earth by way of the TDRS, the Shuttle S-band network subsystem design incorporated several new and sophisticated techniques. Many of these techniques are necessary to enhance the channel performance for adequate circuit margins, whereas some resulted from operational requirements and constraints.

To optimize performance and to provide a secure communications capability, an all-digital link design emerged. Thus, a method for digitizing voice and multiplexing the voice and data channels was required. To maintain the data rate as low as possible for link margin purposes, a delta modulation process was selected for voice digitizing. This technique allows the minimum number of bits (one) to be used for each voice sample. In addition, the voice sampling rate was reduced to as low a value as practical consistent with good quality. Two modes are provided for the TDRSS links. In mode 2, two duplex voice channels are available, each operating at a 32-kbps sample rate on the forward and return links. In mode 1, a single duplex voice channel is available. The forward link sample rate is reduced to 24 kbps, whereas the return link sample rate is maintained at 32 kbps.

Even with the efforts to minimize the required data rates for the forward and return links, other factors eventually forced incorporation of convolutional coding to achieve the needed performance. For example, communications through the TDRS must be maintained independent of Shuttle attitude. This requirement dictates use of relatively broad beam, low-gain antennas to maximize the

TABLE 1.- SHUTTLE S-BAND COMMUNICATIONS LINK CAPABILITIES, MODULATION TECHNIQUES, AND UNIQUE FEATURES

Frequency	Communications link	Capability	Modulation technique	Unique features
S-band (Hi-Lo)	Orbiter-GSTDN downlink	Telemetry (Hi-Lo data rates) Voice (1 or 2 channels) Ranging Doppler (2-way)	Phase modulation (PM)	Linear PM baseband data with ranging on 1.7-MHz sub-carrier
S-band	Orbiter-GSTDN downlink	Payload data Recorded data Operational Payload Television	Frequency modulation (FM)	FM deviation optimized for maximum digital data rates
S-band (Hi-Lo)	GSTDN-Orbiter uplink	Command Voice (1 or 2 channels) Ranging	PM or phase-shift keyed (PSK)	Linear PM baseband data with ranging on 1.7-MHz sub-carrier
S-band (Hi-Lo)	Orbiter-TDRSS return link	Telemetry (Hi-Lo data rates) Voice (1 or 2 channels) Doppler (2-way)	PSK	Convolutional encoding rate 1/3, Viterbi decoding
S-band (Hi-Lo)	TDRSS-Orbiter forward link	Command Voice (1 or 2 channels)	PSK/spread spectrum	Spread spectrum to meet CCIR reqmts, TDM convolutional encoded rate 1/3, Viterbi decoding
S-band (Hi-Lo)	Orbiter-AF/SCF downlink	Telemetry (Hi-Lo data rates) Voice (1 or 2 channels) Doppler (2-way)	PM	Secure links, telemetry and voice
S-band	Orbiter-AF/SCF downlink	P/L data (real-time) Recorded data Operational Payload	FM	Secure data links
S-band (Hi-Lo)	AF/SCF-Orbiter uplink	Command Voice (1 or 2 channels)	PM	Secure command and voice links

radiofrequency (rf) coverage. A network of four (quad) antennas flush mounted on the Shuttle fuselage with computer-driven switching logic is used to accomplish the needed coverage. As a result of these antenna characteristics, the transmitter power and receiver sensitivity had to be pushed to state-of-the-art values. A 140-watt power amplifier (traveling-wave tube (TWT)) was developed by Watkins-Johnson, and a receiver with less than a 3.0-decibel noise figure was developed by TRW. Even with these state-of-the-art rf components, convolutional encoding was necessary to achieve adequate link performance margins. A nontransparent rate one-third code with constraint length of 7 was selected. The decoding algorithm used was that developed by A. J. Viterbi (ref. 1); it has been shown to be optimum in the maximum likelihood sense.

The modulation process was also selected on the basis of optimizing the channel performance; hence, PSK was chosen. A Costas loop provides for carrier reconstruction and data recovery of both forward and return link signals.

TABLE 2.- SHUTTLE S-BAND MODE FREQUENCIES

Communications mode	S-band frequencies, MHz	
	Uplink/forward link	Downlink/return link
GSTDN - high frequency	2106.4063	2287.5
GSTDN - low frequency	2041.9479	2217.5
AF/SCF - SGLS - high frequency	1831.7870	2287.5
AF/SCF - SGLS - low frequency	1776.7330	2217.5
TDRSS - high frequency	2106.4063	2287.5
TDRSS - low frequency	2041.9479	2217.5

Because the TDRS satellites continuously radiate the Earth with S-band energy, the forward link S-band signal power flux density in a 4-kilohertz bandwidth must be maintained below the level consistent with international agreements. To meet this requirement, a pseudorandom code is used to spread the TDRS-transmitted energy over a significantly larger bandwidth than would normally be required for the information rates involved. This technique of "spread spectrum" modulation greatly increases the complexity of the Shuttle S-band TDRS receiver, since a despread version of the information signal must be developed before the data can be recovered with conventional phase-lock loop techniques. The following paragraphs describe these new and unique techniques resulting from the TDRSS communications mode requirements.

DIGITAL VOICE/TIME-DIVISION MULTIPLEXING

There are two reasons for including a digital (TDM) link in the Shuttle Program. The first is that the use of the TDRSS for NASA missions provides a high rf coverage capability but results in relatively weak S-band links. Analog signal designs could not provide adequate margins, but digital links with channel coding can. The second reason for use of a digital TDM link is to satisfy the requirement for message privacy.

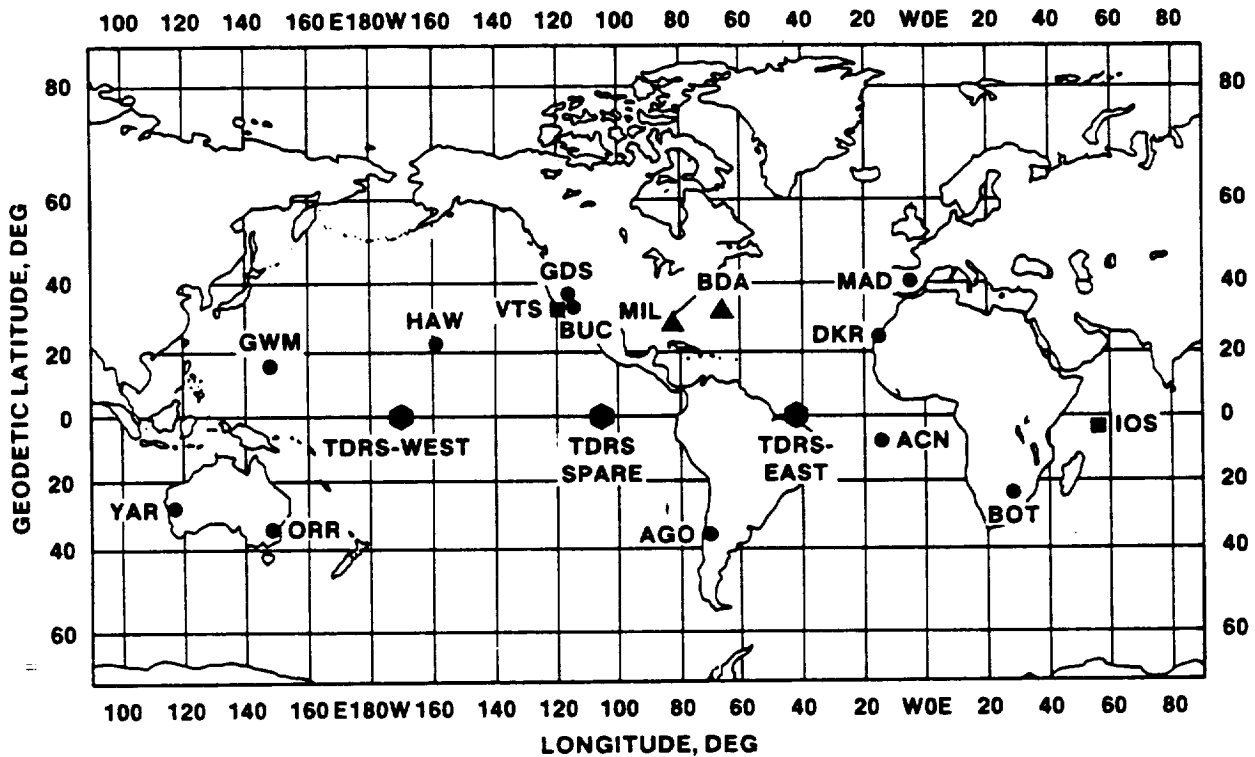
The Shuttle system incorporated a signal design in which one or two digitized speech channels are time-division multiplexed with commands or telemetry. The composite data stream is convolutionally encoded prior to rf transmission. This approach is more efficient than analog since no power is wasted in unrecoverable intermodulation products and a substantial reduction in rf power is achieved using error correction coding.

Digitizing of Shuttle voice is accomplished by delta modulation techniques. Figure 3 is a simplified functional diagram of the delta modulation process. Also illustrated are the analog input and resulting digital output signals. In the modulation process, the input analog signal's instantaneous value is digitized according to a particular algorithm. Based on the generated data (bit) stream, the step size processor and feedback device reproduces the analog input $m(t)$ for comparison with the actual input signal $m(t)$. If $m(t) < m(t)$, then a binary one output results. If $m(t) > m(t)$, then a binary zero output results. In the demodulation process, the data (bit) stream is the input to the step size processor and the feedback portion of the demodulator, which then reproduces a replica of the original input analog signal. The output is filtered to smooth the samples and remove unwanted noise components which may result from the delta modulation processing.

Delta modulation is employed on the Shuttle because it provides approximately the same voice intelligibility as pulse code modulation (PCM), but at one-half the bandwidth. Delta modulation is intelligible, with speaker recognition and bit error rates as low as 10^{-1} for some adaptive delta modulation (ADM) techniques. Several ADM algorithms were tested by NASA to select one that would maintain high word intelligibility with reasonable voice quality at sampling rates of 32 or 24 kbps in the presence of very high channel errors (i.e., bit error rates approximately 10^{-1}). The delta modulation algorithm selected by NASA to satisfy these requirements is a modified version of the "ABATE" algorithm (ref. 2).

The TDRSS link margins are small, and convolutional encoding is used for efficient operation. The errors for such a coded channel will exhibit a burst characteristic. The need to maintain voice communications as long as possible in a burst-error environment was a key factor in the selection of the "Modified ABATE" algorithm. The Modified ABATE algorithm equation is illustrated in figure 4.

The unique feature of the Modified ABATE algorithm is that it was designed to adaptively follow the received signal with an extremely high channel error rate (approximately 10^{-1}). When an error



■ AF/SCF STATION	} OFT & FIRST FEW OPS	▲ GROUND STATION	} OPERATIONAL TDRSS ERA
● GSTDN STATIONS		● GEOSYNCHRONOUS SATELLITE	

ACN - ASCENSION ISLAND	GDS - GOLDSTONE, CA
AGO - SANTIAGO, CHILE	GWM - GUAM
BDA - BREMUDA	HAW - HAWAII
BOT - BOTSWANA	IOS - INDIAN OCEAN
BUC - BUCKHORN, CA	MAD - MADRID, SPAIN
DKR - DAKAR, SENEGAL	MIL - MILA AND PONCE DELEON, FL

ORR - ORRORAL VALLEY, AUSTRALIA
 VTS - VANDENBERG AFB
 YAR - YARGADEE, AUSTRALIA

(PERCENTAGE COVERAGE FOR A TYPICAL SHUTTLE MISSION:
 GSTDN ~ 15%, TDRSS ~ 80%)

FIGURE 2.- SHUTTLE S-BAND NETWORK (GSTDN, AF/SCF, AND TDRSS).

occurs in the received data stream, the step size processor will produce erroneous step sizes until a correctly received data transition is detected. The average number of erroneous step sizes following a received error in the Modified ABATE algorithm is less than in other popular ADM algorithms (ref. 3). It is this feature that gives the Modified ABATE algorithm its good performance in the presence of channel errors. The Modified ABATE algorithm sounds significantly better at an error rate of 10^{-1} than do other ADM algorithms. This improved error performance is obtained at the expense of frequency response and dynamic range.

The ADM is relatively immune to channel errors whether they occur randomly or in bursts. Some of the results obtained by NASA from word-intelligibility tests of the Modified ABATE algorithm are summarized in table 3. The burst errors scored in table 3 were limited to burst lengths of 10 bits. These bursts occurred randomly, but, during a burst, the probability of error was 0.5. The bit error rate (BER) presented in table 3 is the average error rate. Note that the ADM is more immune to burst errors than to random errors. Figure 5 shows word intelligibility as a function of BER for random

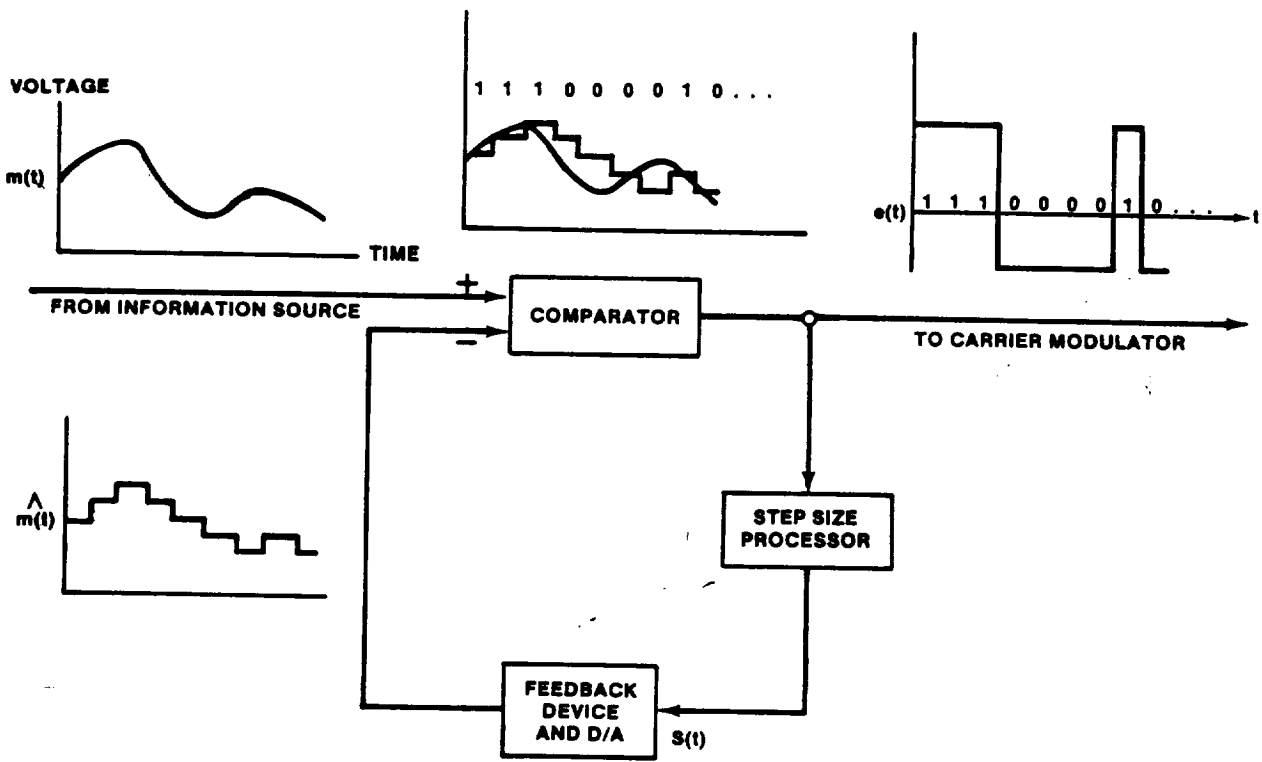


FIGURE 3.- DELTA MODULATION PROCESS.

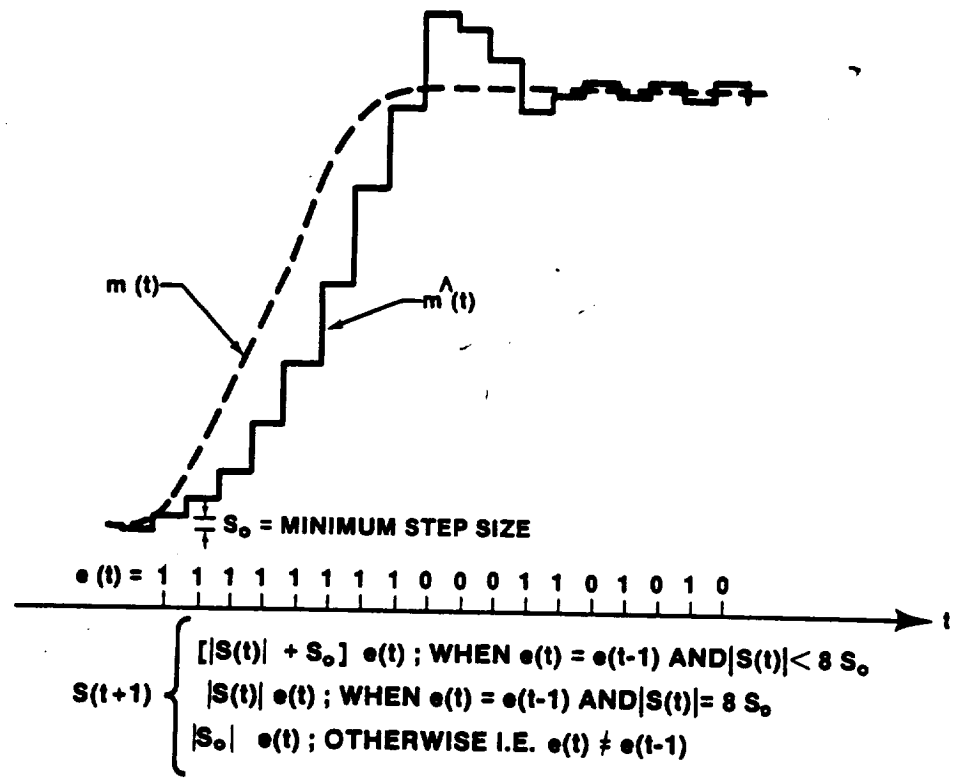


FIGURE 4.- MODIFIED ABATE ADAPTIVE DELTA MODULATION ALGORITHM.

TABLE 3.- PERFORMANCE OF THE MODIFIED ABATE ALGORITHM

Sampling rate, kbps	Bit error type	Bit error rate	Word-intelligibility score
32	Random	3.5×10^{-5}	96.5
		2.7×10^{-2}	95.2
		1.3×10^{-1}	76.1
16	Random	4.6×10^{-5}	95.1
		1.7×10^{-2}	93.6
		8.8×10^{-2}	88.8
32	Burst	9.2×10^{-5}	94.7
		2.3×10^{-2}	94.7
		1.5×10^{-1}	87.5

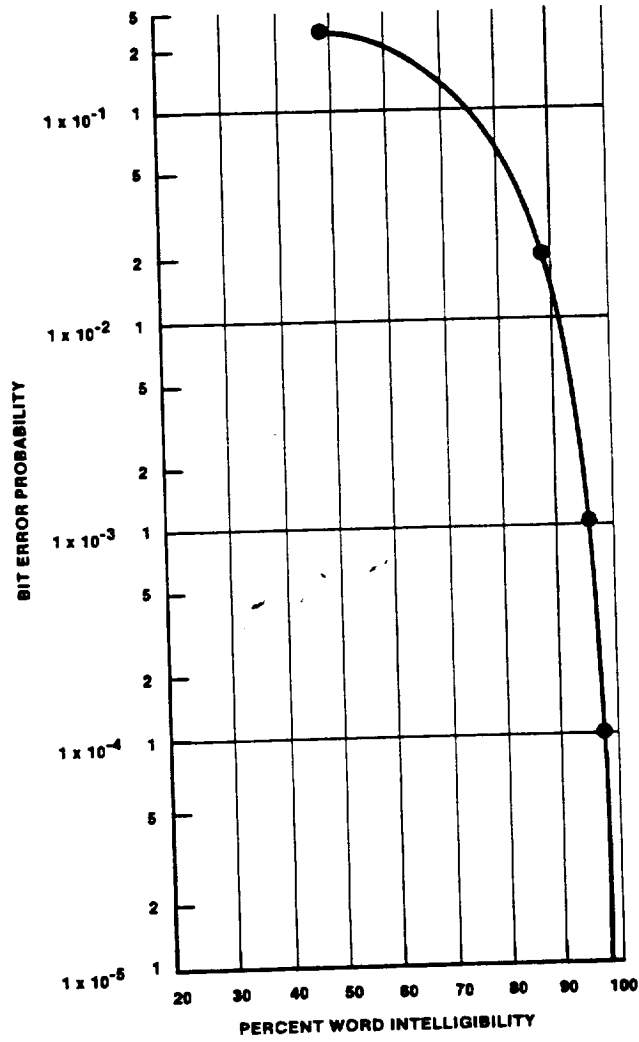


FIGURE 5.- MEASURED WORD INTELLIGIBILITY FOR RANDOM BIT ERRORS - MODIFIED ABATE DELTA MODULATION ALGORITHM.

errors (i.e., not burst errors) resulting from Shuttle voice channel verification tests performed in the NASA Lyndon B. Johnson Space Center (JSC) Electronic Systems Test Laboratory (ESTL) (ref. 4).

Word intelligibility of 87.5 percent with an average BER of 1.5×10^{-1} can be achieved with burst errors. The word-intelligibility results in table 3 and figure 5 were achieved using postdemodulation band-pass filtering (300 to 2300 hertz). The delta demodulator is essentially an integrator; thus, its output noise power spectrum is approximately kf^{-2} , where k is a constant the value of which depends on the BER. The 300-hertz high-pass filter was used to eliminate a large portion of this low-frequency noise due to channel errors. The 2300-hertz low-pass filter was chosen to eliminate the higher frequency components due to sampling.

CONVOLUTIONAL CODING/VITERBI DECODING

Because of the long range to the TDRS (geosynchronous orbit) and the Shuttle's antenna characteristics, the required performance for the Shuttle/TDRSS links could not be achieved by brute force methods, i.e., by increased transmitter power and reduced receiver noise temperatures. In fact, even with the 140-watt Shuttle transmitter power, and a low-noise parametric amplifier receiver, the forward and return TDRSS links required error correction channel encoding to achieve the design goal BER performance.

A simplified functional diagram for a digital communication channel is shown in figure 6. Because the received data bit is corrupted with noise, a finite probability of error exists in the bit decision process. For a PSK-modulated channel assuming optimum matched-filter detection, the probability of error at the receiver has been shown to be

$$P_e = \frac{1}{2} \operatorname{erfc} \sqrt{\frac{E_c}{N_0}} \quad (1)$$

where E_c is the signal energy of a channel bit at the input to the decision device, N_0 is the noise spectral density of the receiver system, and erfc is the complementary error function.

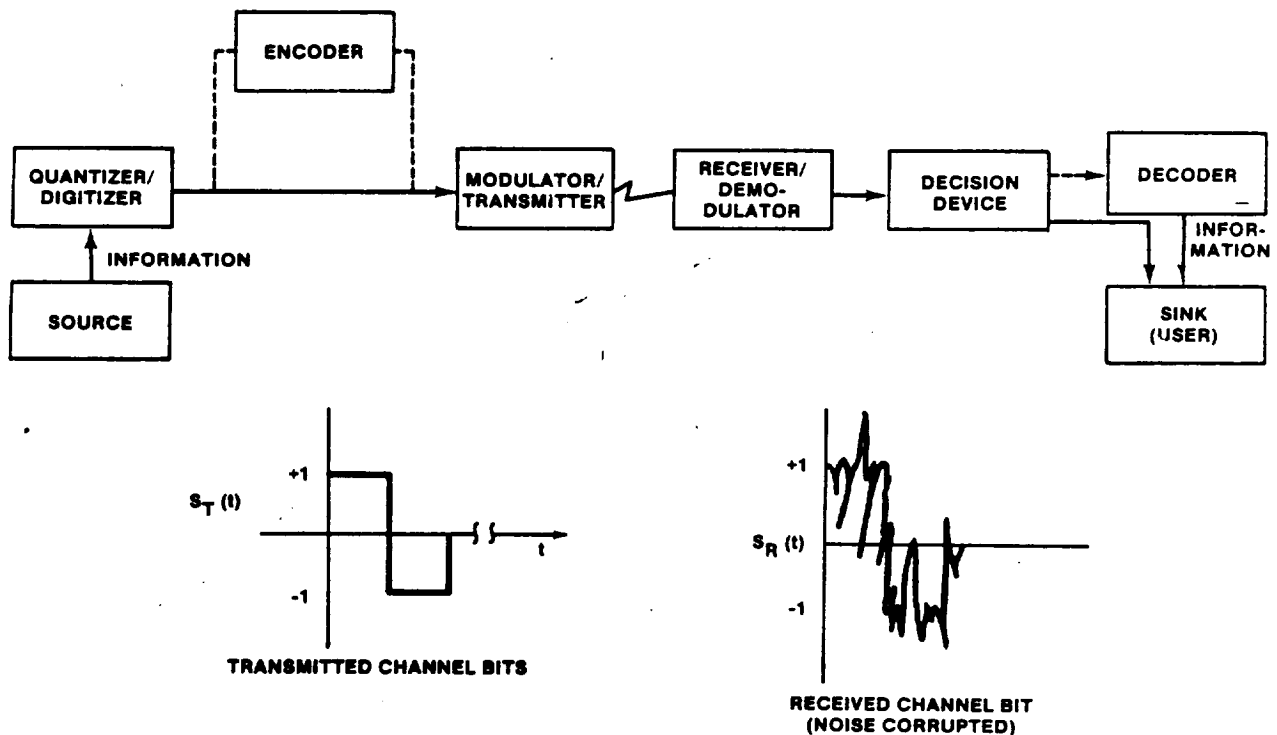


FIGURE 6.- FUNCTIONAL BLOCK DIAGRAM OF A DIGITAL COMMUNICATION CHANNEL.

If coding is not employed, the received bit is directly equivalent to the transmitted bit. The receiver bit decision is thus made on information bits directly. If transmitted and received power is held constant for coded and uncoded channels, then more energy is available for decisions on information bits than for decisions on channel bits (symbols), since each information bit is represented by two or more symbols. This redundancy results in lower energy-to-noise density ratios for the coded symbols and hence a higher error rate. The decoder's task is to correct as many of these bit errors as possible resulting in a net coding gain. For coding gain to be achieved, the information BER must be less after decoding than it would have been for an uncoded channel.

The choice of coding parameters selected for the Orbiter/TDRSS link was the culmination of a series of trade studies, hardware constraints, link margins, and empirical tests. It is well documented that convolutional codes can outperform block codes with comparable decoding hardware. The decision then centered upon selecting either a sequential decoder or a Viterbi decoder and their associated rates and constraint lengths.

Use of coding was dictated by link margin considerations, and the design goal was to improve channel performance by 4 to 5 decibels. Since voice quality could be maintained with error rates on the order of 10^{-1} , the overall communication link had to be designed to ensure a graceful degradation of the system to prevent premature loss of voice communications.

The decoding of convolutional codes is by far a more complex operation than encoding. Since size, weight, and power are at a premium on the Orbiter, a study of the complexity of both sequential and Viterbi decoders was conducted for the maximum uplink data rate of 72 kbps. The complexity of the decoder is a function of the rate of the code, the constraint length, the quantization of the demodulated data bits, and the required output BER. It was found that as the code rate is decreased and the quantization is increased, the Viterbi decoder performance for a given complexity improves in relation to the sequential decoder. In addition, at the BER crossover point, the Viterbi decoder degrades gracefully but the sequential decoder does not. For the link robustness, ease of resynchronization, and relative insensitivity to data bit quantization, the Viterbi decoder was chosen.

The coding gain of the Viterbi decoder at a BER of 1×10^{-5} can roughly be summarized as follows, for constraint lengths on the order of 3 to 8. The coding gain improves roughly 0.5 decibel for every increase in the constraint length. An increase of 2 decibels in coding gain can be obtained by increasing the symbol bit decision quantization from 2 to 8 levels (i.e., soft decision compared to hard decision performance improvement). Another 0.5 decibel gain can be achieved by decreasing the code rate from one-half to one-third. The Viterbi decoder complexity at these data rates roughly doubles with each increase in constraint length. The design goal of 5 decibels coding gain could have been achieved with a rate one-half, constraint length 7 code. However, an additional 0.4 decibel coding gain was achieved by changing the code rate from one-half to one-third. This change in code rate did not significantly affect decoder complexity.

The symbol synchronization performance is critical in a coded communication system in which large coding gains are expected. This coding gain corresponds to a reduction in the energy per symbol to noise spectral density available for symbol synchronization and detection. To achieve the expected coding gains, the symbol synchronizer must introduce negligible degradation. The Shuttle channel coding that was selected is the rate one-third, constraint length 7 code. Since there is still intelligible voice at BER's of 10^{-1} , the symbol synchronizer must still operate properly at this error rate. This requirement forces the symbol synchronizer to acquire and lock at approximately -5 decibels E_c/N_0 , which was met with a digital implementation of the symbol synchronizer to ensure repeatable and reliable operation.

The Viterbi decoder implements a maximum likelihood algorithm to estimate the transmitted data bit. To save hardware, the algorithm performs 2^{K-1} decisions every bit time, where K is the constraint length of the system. With timing overhead, the decoder must perform an operation every 190 nanoseconds for a constraint length equal to 7. This is the limit at which the hardware can process data with the logic family selected (low-power Schottky). The Orbiter Viterbi decoder implementation provides a coding gain of 5.4 decibels at a BER of 1×10^{-5} . Figure 7 illustrates the theoretical performance improvement of the Shuttle convolutional encoded, Viterbi decoded channel over the optimum PSK uncoded channel (ref. 5).

SPREAD SPECTRUM MODULATION

The application of spread spectrum techniques to communications systems provides several capabilities which cannot be obtained with conventional techniques. Some of the capabilities for which spread spectrum techniques are commonly adapted include antijamming, multiple-access communication, message privacy, and navigation. In most of these applications, the ratio of the spreading chip rate to the information data rate is large ($>10^3$) and the signal-to-noise ratio (SNR) in the information rate bandwidth is high (>10 decibels). For the Shuttle Orbiter application, the spreading process is

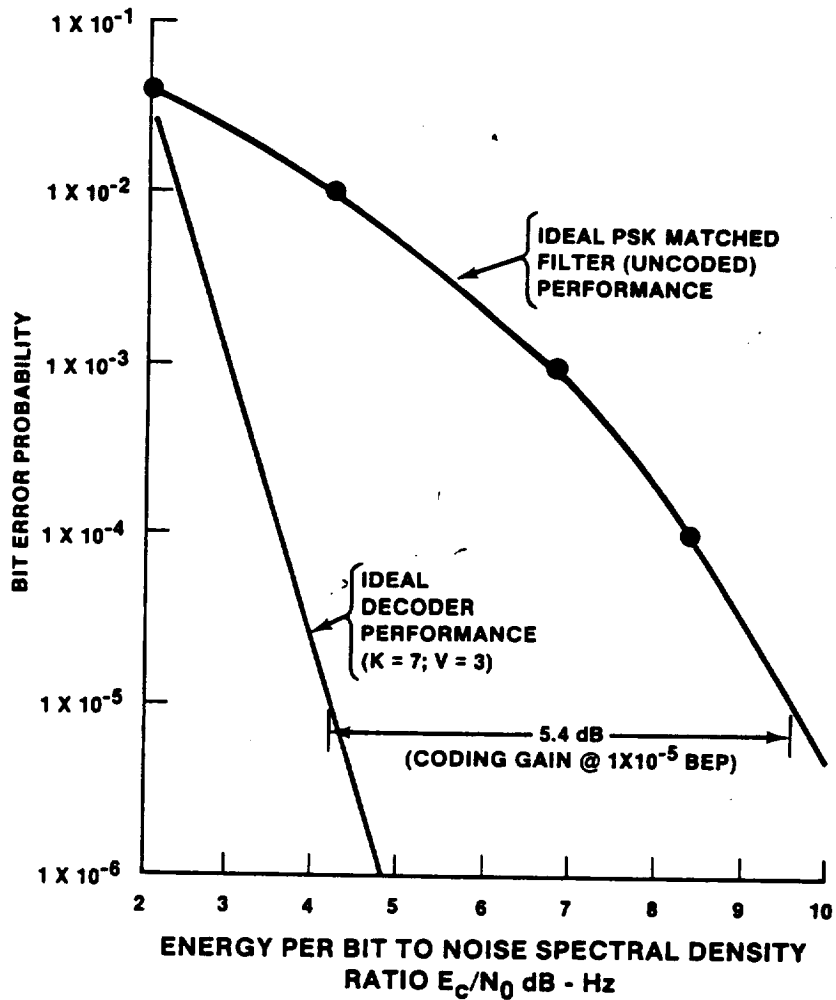


FIGURE 7.- BIT ERROR PROBABILITY PERFORMANCE IMPROVEMENT FOR IDEAL CODED CHANNEL.

used to reduce the rf power spectral density. For this case, the spreading chip rate is purposely selected as low as possible to just meet the required power spectral density levels. Hence, the ratio of spreading chip rate to information rate is considerably less than that normally encountered. In addition, the information is Manchester encoded, and an information bandwidth of approximately twice the data rate is required for the despreading process. These factors, together with operations required at SNR's close to 0 decibel in the information bandwidth, make the Shuttle Orbiter despreading system design unique.

The International Radio Consultative Committee (CCIR) of the International Telecommunication Union (ITU) recommends various criteria concerning rf signals and their spectra. The rf frequency bands currently used by commercial communications satellites are the same as those used by the common carriers for microwave relay systems on Earth. To allow frequency sharing, various criteria are established by CCIR to prevent mutual interference. Many studies were made by international experts on the subject, and several recommendations have resulted. One particular item specifies the maximum allowable power flux density received at the Earth's surface from an Earth-orbiting satellite (space station). The power flux density is defined by

$$F = EIRP/4\pi d^2 \quad (2)$$

where

- \bar{F} = flux density
- EIRP = effective isotropic radiated power
- d = distance between spacecraft and Earth in meters

Table 4 presents the maximum allowable power flux density at the Earth's surface from an Earth-orbiting satellite for the Shuttle Orbiter S-band frequency. The values tabulated show that the most stringent requirements occur for signals having an angle of incidence above the horizontal plane of 0° to 5° and indicate how the flux-density requirements vary as a function of the angle of arrival of the rf signal.

The TDRS to Shuttle Orbiter S-band forward communication link would exceed the CCIR requirements without additional modulation to spread the flux density over a much larger bandwidth. Thus, a spread spectrum signal design was developed for Shuttle to maintain compliance with the CCIR requirements on flux density. In the spread spectrum concept, the signal spectrum is expanded at the transmitter before transmission. This expansion distributes the signal energy over a bandwidth much greater than the information bandwidth normally required. The spreading technique chosen for Shuttle involves direct-sequence, pseudorandom code biphasic modulation of the information carrier signal. Figure 8 is a simplified block diagram of a spread spectrum system using pseudonoise (PN) code modulation.

TABLE 4.- CCIR FLUX-DENSITY GUIDELINES

Frequency band	Maximum flux density in 4-kHz bandwidth, dBW/m ² , for angle of arrival (δ) above the horizontal plane of -		
	0° to 5°	5° to 25°	25° to 90°
S-band	-154.0	$-154 + \frac{\delta - 5^\circ}{2}$	-144

The rf carrier which is modulated with the data signal of rate R_d is passed to a balanced PSK modulator. The PN code generator supplies a binary sequence of ones and zeros to the PSK modulator. Typically, a binary "1" is sent as unperturbed carrier phase, whereas a binary "0" is sent by a change in phase of the carrier of 180°. This process has the effect of "spreading" the signal over a bandwidth roughly equal to twice the rate of the PN code (R_c). The resulting spread signal is then transmitted over the communication channel. At the receiver, after downconverting to a suitable intermediate frequency (i.f.), an identical PN code is correlated with the received code. After de-spreading, only the original data modulation remains and is passed to a conventional PSK demodulator. Other (interfering) signals received will not be correlated and are effectively spread by the receiver PN code, thus appearing as noise to the data demodulator. Figure 9 is a sketch of typical spectra for the transmitted and received signals at various points in the system as indicated by the circled numbers in figures 8 and 9.

If a uniformly distributed, transmitted spread spectrum is assumed, it can be shown that the spreading code rate must satisfy equation (3) (ref. 6).

$$10 \log R \geq \text{EIRP} |_{\text{dBW}} + \log B/2 - 22 \text{ dB} - 20 \log d - \text{CCIR} |_{\text{dBW/m}^2/\text{Hz}} \quad (3)$$

where

- R = the spreading code rate
- $\text{EIRP} |_{\text{dBW}}$ = the satellite transmitted EIRP in decibels referenced to 1 watt
- B = measurement bandwidth (4 kilohertz for CCIR requirement)
- d = range from the satellite to the Earth surface in meters
- $\text{CCIR} |_{\text{dBW/m}^2/\text{Hz}}$ = CCIR power flux-density requirement

For the case of the TDRS in geosynchronous orbit and assuming the worst case CCIR requirement for less than 5° elevation angles, the Shuttle minimum spreading code rate is 10.7 Mbps for the S-band forward link. The actual S-band spreading code rate is 11.232 Mbps, and the code length is 2047 chips.

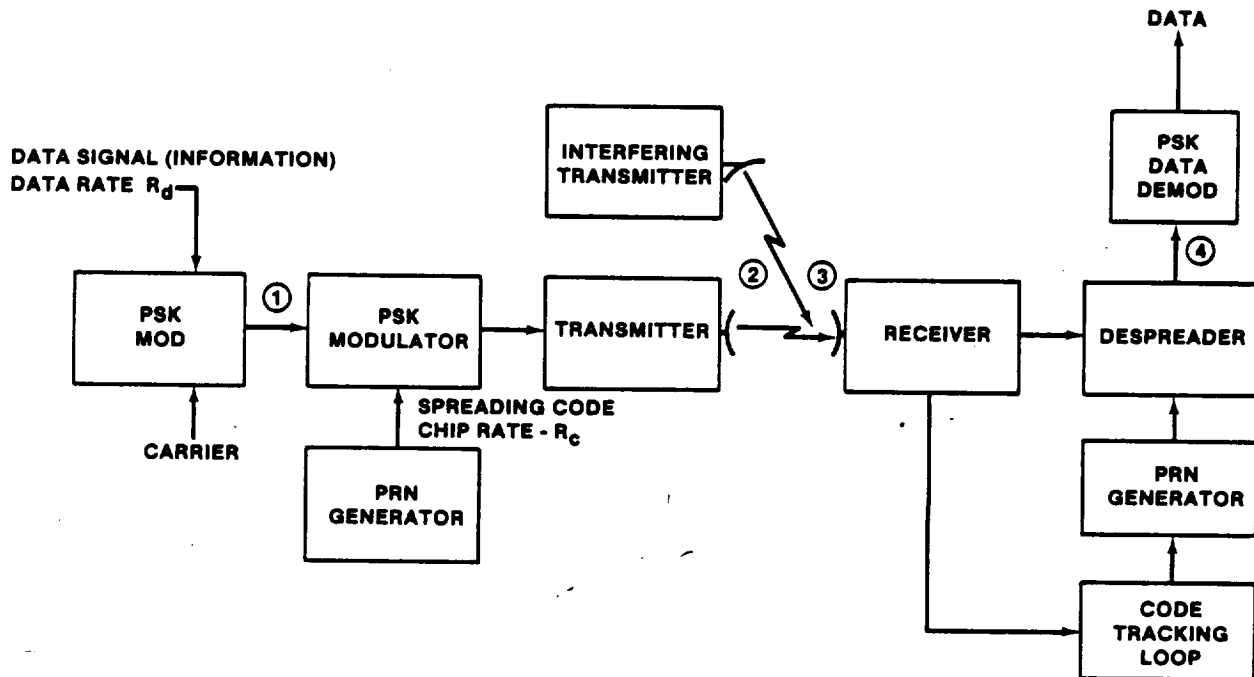


FIGURE 8.- SPREAD SPECTRUM SYSTEM CONFIGURATION.

As noted earlier, the Orbiter despreader design is unique because of several factors associated with the TDRSS forward communication channel. To meet the CCIR flux-density requirements, the forward link rf signal is spread using a PN sequence with chip rate $R = 11.232$ Mbps and the sequence length $N = 2047$ bits. The information transmitted over the TDRSS forward link to the Orbiter can be either 32 kbps or 72 kbps of data, rate one-third, convolutionally encoded. Since the despreader must operate for either rate, the worst case condition is encountered for the 72-kbps mode. For this case, the effective despreader information rate is the channel encoded symbol rate of 216 kbps. Thus, the ratio of chip rate to information rate is

$$\frac{R_c}{R_d} = \frac{11.232 \times 10^6}{216 \times 10^3} = 52 \quad (4)$$

This ratio is considerably lower than normally encountered in spread spectrum systems; as a result, several potential system design problems exist. The TDRSS forward link transmitted power is 46.5 decibels (referenced to 1 watt), which results in a nominal carrier-to-noise spectral density (C/N_0) at the Orbiter despreader of 54 decibel-hertz. Since the system must operate with a Manchester data format and allow for Doppler frequency offsets and hardware frequency uncertainties, the despreader bandwidth must be on the order of 500 kilohertz. Thus, the nominal despread signal-to-noise ratio P_s/N , assuming 3 decibels correlation and filter losses, is approximately -7.0 decibels under nominal conditions during acquisition. With the condition just described, a critical signal detection problem exists for reliably acquiring and tracking the spreading code.

Figure 10 is a simplified block diagram of the Orbiter despreading system. The spread signal is filtered in a band-pass filter (BPF) with 3-decibel bandwidth of approximately 20 megahertz. The filtered spread signal is then coupled to three product detectors (multipliers), where it is multiplied by a local replica of the PN spreading code. The process involved in acquiring code synchronization is now discussed. The local PN code is periodically stepped in phase by one-half of a chip width at a rate sufficiently slow to allow integration of the signal plus noise for detection purposes, but sufficiently rapid to ensure that maximum Doppler offset does not reduce the effective search rate by an unreasonable amount. When a phase is found at which the integrated signal plus noise reaches a value greater than the predetermined threshold setting, then phase synchronization is assumed, and the code stepping signal is removed. If the phase is truly correct, then the code tracking loop automatically pulls in, and code tracking is established.

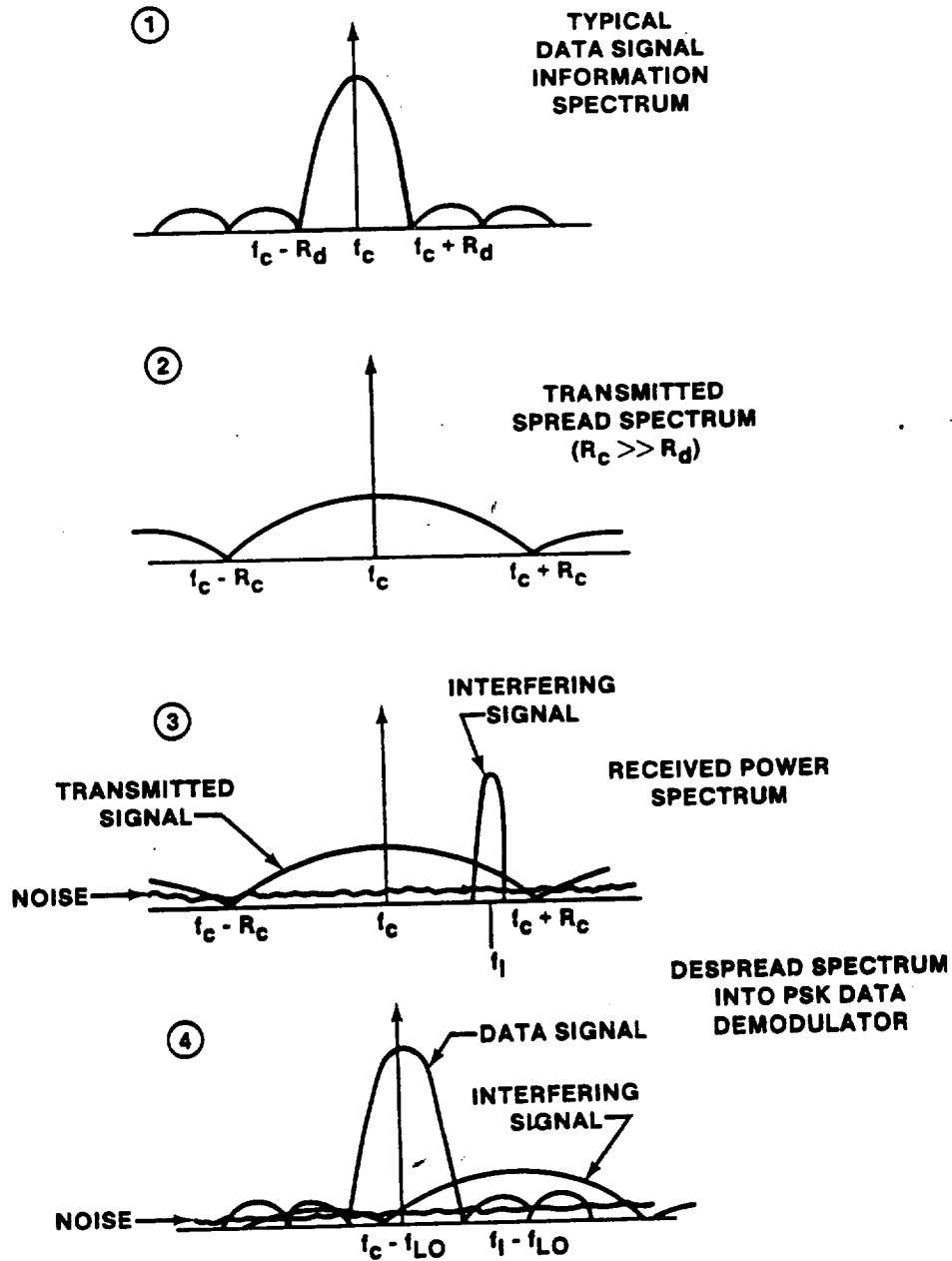


FIGURE 9.- SPREAD SPECTRUM TRANSMISSION.

Although the basic operation seems simple enough, several problems were encountered. A unique mechanization approach was necessary for updating the threshold setting in the lock decision process to ensure that drifts in channel gain and/or noise characteristics did not significantly affect the detection statistic. It is important to note that the same decision channel is used for signal detection and threshold updating. The threshold level is updated periodically, even when the system is untracking, by offsetting the PN code to the acquisition channel multiplier and thereby creating an uncorrelated condition and allowing the detector to sample system noise for threshold adjustment. This process is required to remove variations in system noise level due to channel gain variations and is referred to as an adaptive threshold.

Because of the low SNR's and the Doppler frequency offsets, the design of the code tracking loop required two loop bandwidths: a wideband acquisition loop and a narrow tracking loop. To ensure that

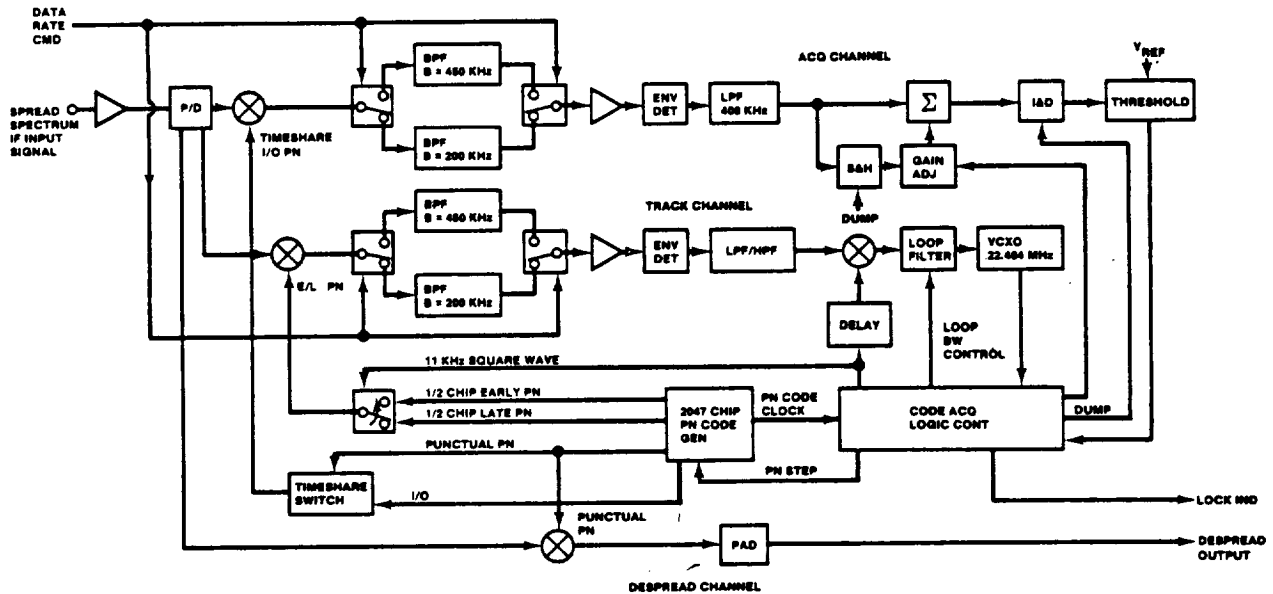


FIGURE 10.- S-BAND SPREAD SPECTRUM PROCESSOR (SSP) FUNCTIONAL DIAGRAM.

the loop will remain in lock sufficiently long after acquisition occurs, it is required that the loop bandwidth be reduced after tracking has been achieved. Care must be exercised in the bandwidth reduction to ensure that the switching transient does not cause the loop to unlock. A time delay before the loop bandwidth was switched and a stepped reduction in bandwidth was necessary to accomplish the desired results.

Of primary importance is the strategy employed in the process of acquiring code synchronization. Because of the low signal-to-noise condition and the desire for rapid acquisition, a strategy is needed by which synchronization can be achieved as quickly as possible, but with a high degree of confidence that the lock state is reached only when a valid synchronization condition is detected, and by which lock will be maintained for a significant length of time (90 minutes). To accomplish this, a serial search lock strategy is employed. The acquisition algorithm is illustrated by the flow diagram in figure 11 (ref. 7). The process followed is outlined in the following paragraphs.

Search is initiated and each phase position (cell) of the code is tested for some period of time T , which is selected to provide sufficient integration for a high probability of detection but small enough to allow rapid dismissal and to ensure that Doppler offset does not significantly increase the search time. Once a cell in which the integrated signal-plus-noise level exceeds the preset threshold is reached, a hit is declared. The system advances to the lock state, and the code tracking loop parameters discussed previously are switched. Once the system is in lock, five consecutive misses are required to cause loss of lock and reinitiation of the search process. Some of the significant features and critical parameters which are required in such a search/lock strategy are as follows.

1. The search mode threshold setting should be such that the probability of false alarm is in the vicinity of 10^{-2} . Lower probabilities of false alarm (10^{-6}) will result in extremely rapid degradation (increase) in acquisition time as the SNR decreases.

2. In lock, the probability of false alarm can be low since the desire here is to ensure that the system remains locked and, thus, a high probability of detection is necessary. The lock mode employs reset counters to reduce the probability of false dismissal to a sufficiently low value. A mean time to unlock on the order of 5400 seconds at a C/N_0 of 54 decibel-hertz is required for the Shuttle.

The theoretical mean acquisition time as a function of carrier-to-noise density and code Doppler offset in chips per second, for the Shuttle acquisition algorithm, is shown in figure 12.

For the Shuttle TDRS link, the forward link channel performance degradation in bit error probability (BEP) was specified to be less than 1.0 decibel. Test results obtained at the JSC ESTL verified that this specification was met. Tests also indicated that at strong C/N_0 values (65 decibel-hertz), the code tracking loop would false lock. Prior to the C/N_0 at which a solid false

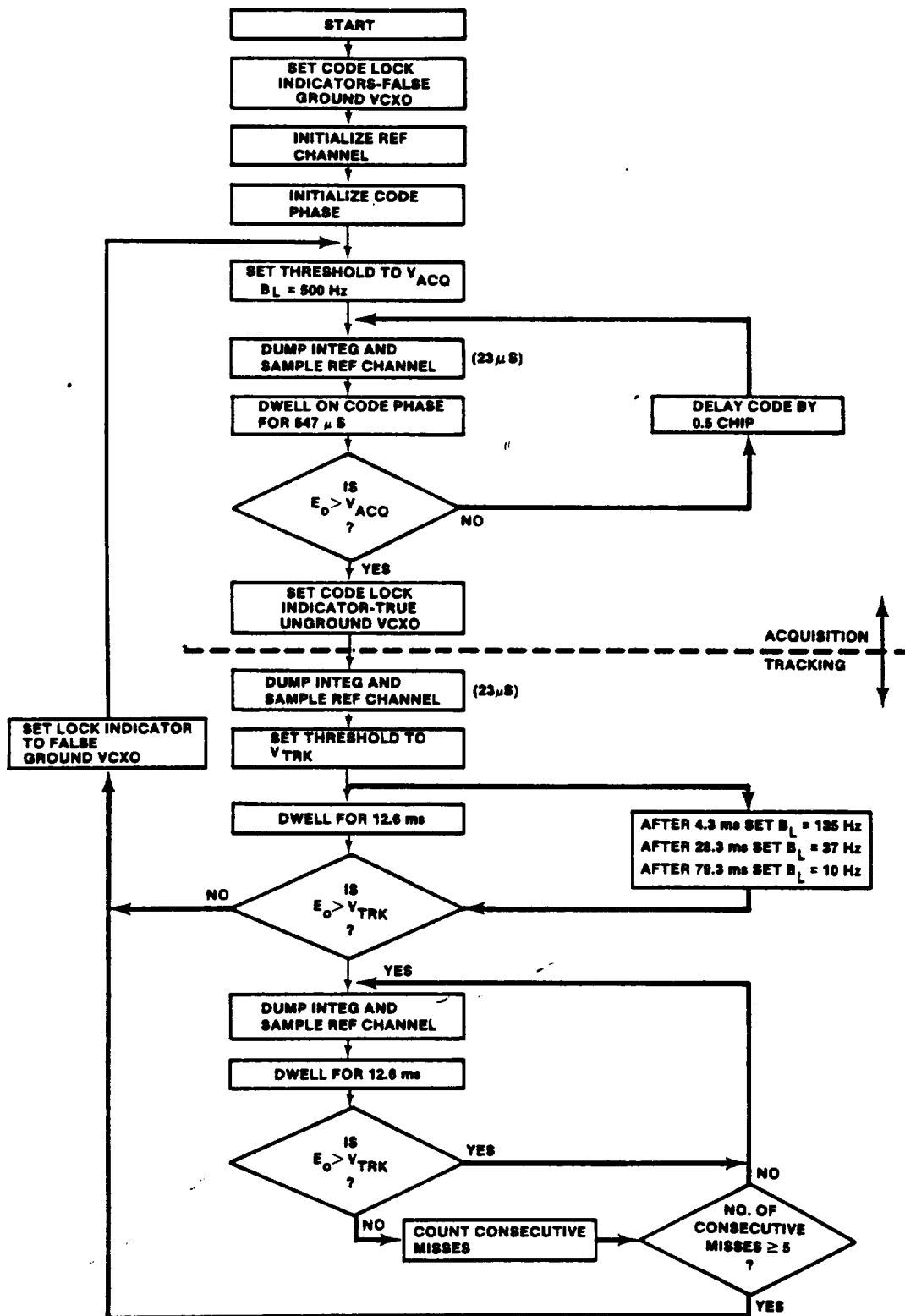


FIGURE 11.- SSP ACQUISITION-TRACKING ALGORITHM (S-BAND).

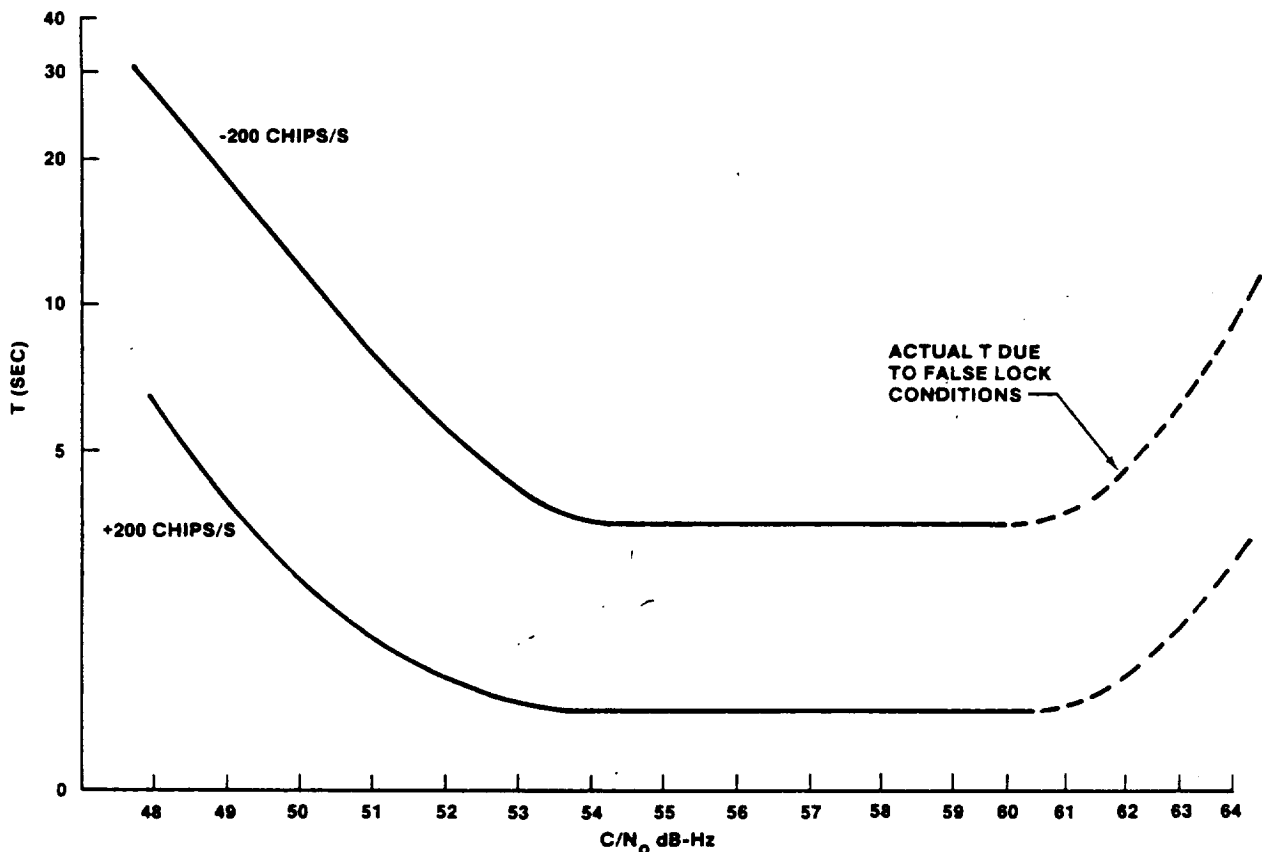


FIGURE 12.- S-BAND MEAN ACQUISITION TIME THEORY (WITH CODE DOPPLER OFFSET), LOW DATA RATE.

lock occurs, an increase in acquisition time is seen. This effect is illustrated by the dashed portion of the curves in figure 12, and is attributed to filtering effects giving rise to partial correlation outside the desired lock region. Figure 13 illustrates the unwanted correlation effects of a Tchebycheff band-pass filter on a typical Tau dither loop error signal (ref. 8).

ANTENNA GAIN/COVERAGE

Four quad antennas are used for the TDRS S-band communications. These antennas are located approximately 90° apart in the Orbiter roll plane and conform to the Shuttle inner moldline (fig. 14), which is the contour of its aluminum skin. The multiple-layer thermal protection system (TPS) is installed over the antennas.

Each of the four quad antennas has two beam positions, providing eight total beams around the Shuttle. These two beam positions are required to cover an angular sector of 140° in the pitch plane by 100° in the roll plane. This sector coverage is required to produce the specified gain coverage of 4 decibels over 85 percent of the sphere.

The quad antenna is a two-element array, which is oriented in the Shuttle nose-to-tail direction. The two elements are fed in quadrature, and their excitations are interchanged by an electro-mechanical transfer switch. The element itself is a crossed dipole in a square cavity, which provides circular polarization.

A typical measured composite coverage is shown in figure 15 for the 2041.9-megahertz frequency. This coverage is 63 percent at the 4-decibel gain level and is substantially less than the specified 85 percent. The coverage difference between theoretical and measured corresponds to a gain difference of approximately 0.5 to 1.0 decibel depending on the S-band operational frequency. This difference may be a result of the TPS effects and loss variations in stripline, switch, and cable components (ref. 9). The initial specified coverage of 85 percent at the 4-decibel level has been relaxed to an average value of 50 percent for the four operational S-band frequencies.

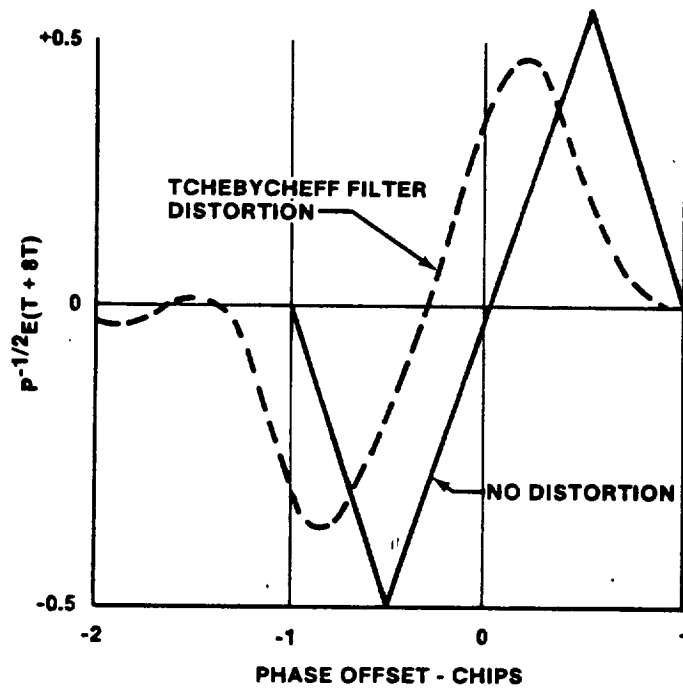


FIGURE 13.- EFFECT OF TCHEBYCHEFF BAND-PASS FILTER ON A TYPICAL TAU DITHER LOOP ERROR SIGNAL.

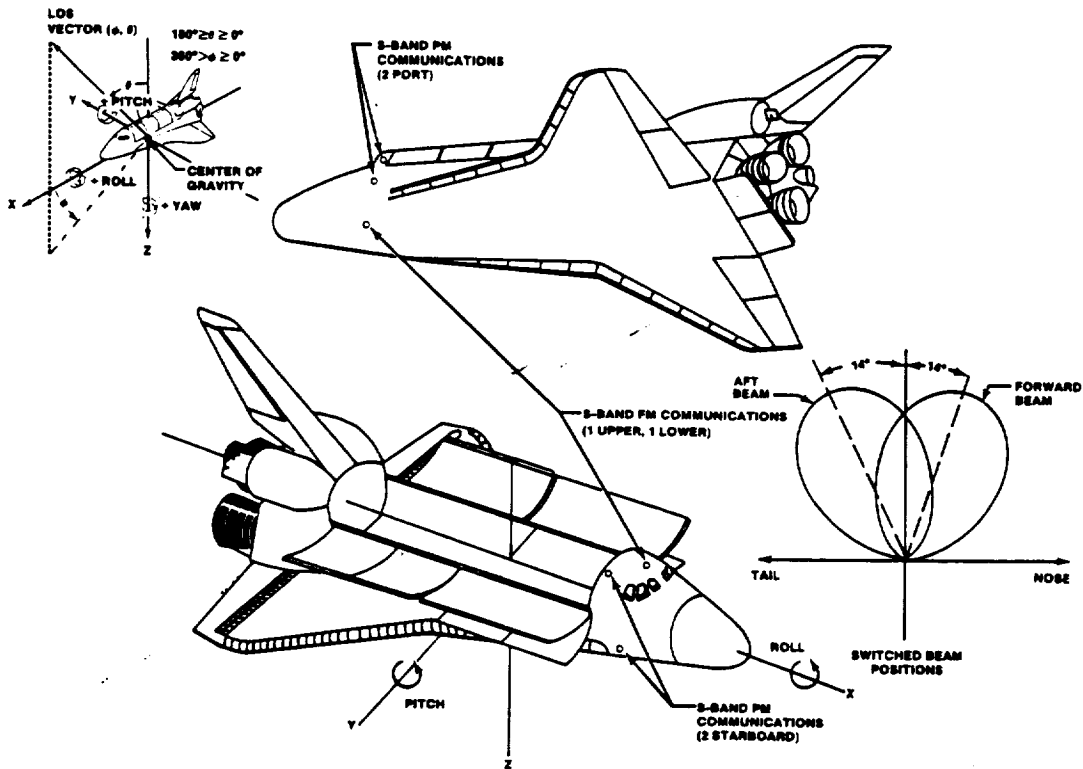


FIGURE 14.- SHUTTLE S-BAND ANTENNA LOCATIONS.

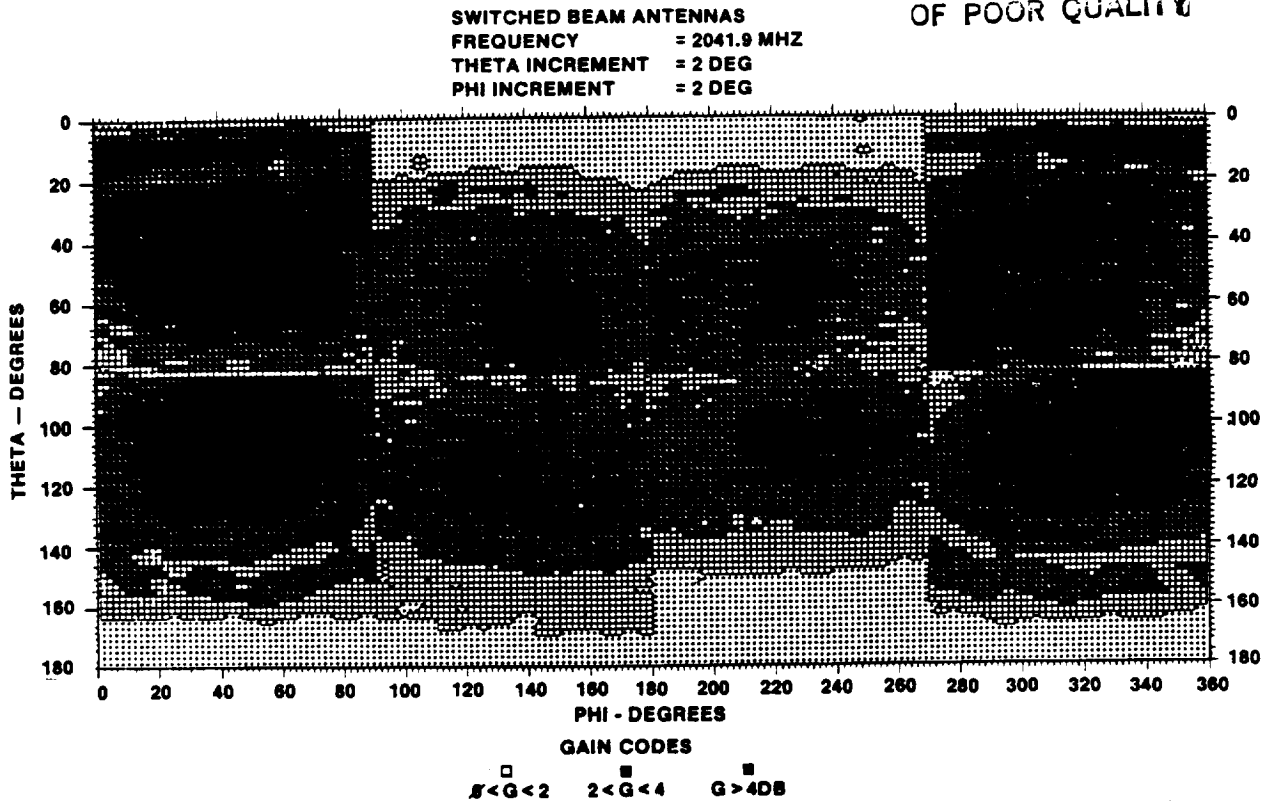


FIGURE 15.- MEASURED S-BAND QUAD ANTENNA SYSTEM COMPOSITE COVERAGE.

Since the desired gain/coverage capability has not been achieved with the existing TDRS switched-beam quad antenna system, some limited phased-array antenna development is continuing. A software simulation has been developed to analyze potential spherical coverage capability as a function of the number of beams formed by the switching array. Figure 16 illustrates the simulation results of gain over 85 percent of the sphere compared to the number of beams. Breadboard arrays are being evaluated at JSC for potential future applications on the Shuttle.

GSTDN AND AF/SCF COMMUNICATION MODE TECHNIQUES

One of the key areas of concern for the direct Shuttle to Earth communications system was the desire for rapid and automatic signal acquisition of the PM frequency links. Since an all-digital link design was dictated by TDRS and other operational considerations, a PSK modulation technique should allow acquisition with data modulation present on the carrier signal. However, navigational requirements established the need for a ranging function on the S-band communications channel. This requirement resulted in addition of a subcarrier to the uplinks and downlinks which carried the ranging signals of the GSTDN tone ranging system. The subcarrier was phase modulated by the ranging tones, and both the data and the subcarrier phase modulated the uplink and downlink S-band carriers. The net result of this ranging function addition was that PSK modulation could no longer be used for the GSTDN links. The ground station receiver was not capable of receiving a PSK signal; therefore, the downlink design was residual carrier PM from conception.

The television and recorded data are transmitted over a wideband FM link to provide sufficient bandwidth for the video signal or to allow dump of recorded data simultaneously with transmission of operational data on the PM links. The GSTDN and AF/SCF downlink frequencies are identical; however, the uplinks differ in frequency. Thus, the network transponder design had to be capable of operating with two coherent turnaround ratios (one for NASA GSTDN and the other for the USAF AF/SCF). Also, since the range from the Shuttle to the Earth is much closer than the range from the Shuttle to TDRS, a low-power transmit mode and less sensitive receive mode was provided for the direct Earth PM links. Broad antenna patterns for nearly continuous coverage with a minimum of vehicle attitude constraints were required for the PM and FM antenna systems.

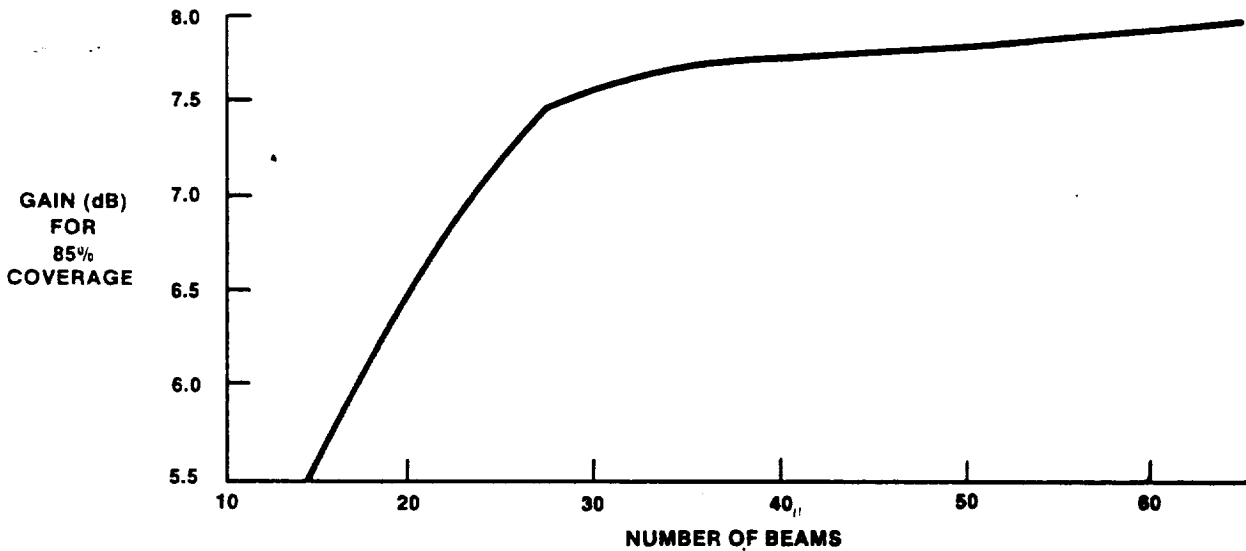


FIGURE 16.- SOFTWARE SIMULATION RESULTS OF GAIN FOR 85 PERCENT SPHERICAL COVERAGE WITH NUMBER OF BEAMS AS A VARIABLE.

RADIOFREQUENCY ACQUISITION AND CRITICAL PM MODULATION INDEX

As initially designed, the Shuttle S-band network receiver was to operate with a PSK uplink signal modulation format. Traditionally, a Costas loop is used in such receivers to reconstruct the totally suppressed carrier. However, for the Shuttle S-band uplink when ranging and data are both present, the Costas loop must acquire and track a residual (PM) carrier. As a result, several questions arise relative to the Costas loop performance under these conditions. It was also found that automatic acquisition could not be achieved even when PSK modulation was present because of the distortion effects of the Costas loop arm filters (ref. 10). These effects created stable false-lock points at frequencies related to the data rate and submultiples of the data rate as a result of data format repetitions, such as synchronization words and multiplexed voice words which contain alternate ones and zeros a vast majority of the time (when no speech is present). False locks become prevalent for some modes at carrier-to-noise density ratios as low as 58 decibel-hertz, which is only 4 decibels greater than expected levels for TDRS operations.

The rf acquisition problem is illustrated in figure 17, which shows the primary false-lock components associated with the uplink GSTDN mode using the high-rate data format. The TDM data rate in this case is 72 kbps; hence, a strong false-lock component results at the carrier frequency ± 72 kilohertz. As seen in figure 17, false locks can also occur for carrier offsets of ± 18 and ± 54 kilohertz as a result of the multiplexed voice channel idle patterns (alternate ones and zeros), and at ± 36 kilohertz as a result of the basic TDM format.

If voice is present, the ± 18 - and ± 54 -kilohertz lock points disappear because of the randomizing of the voice multiplexed word patterns. This fact, together with the introduction of rate one-third coding to increase the basic channel symbol rate to 216 kbps, was effectively employed to alleviate false-lock susceptibility for most of the launch trajectory (i.e., until Doppler shifts cause the one-half data-rate term to be within the receiver acquisition sweep range (ref. 11)). Figure 18 illustrates the uplink false-lock components of this special launch communication mode. To ensure that false-lock points do not exist within the carrier acquisition sweep range for a significant portion of launch communications coverage, two basic changes were made to the launch communication mode. First, a continuous low-level-noise modulation is introduced into the voice delta modulators. This continuous modulation in effect randomizes the voice word patterns and removes the associated false-lock components. Second, the data-rate multiplication due to encoding increases the channel symbol rate to 216 kbps; therefore, the one-half data-rate term now occurs at 108 kilohertz, which is beyond the acquisition sweep range of the Shuttle receiver with zero Doppler offset. As Doppler effects shift the received carrier frequency, a point is reached at which the 108-kilohertz term will fall within the acquisition sweep region. The time into launch at which this occurs is maximized by offsetting the launch-site transmitter frequency to compensate for Doppler effects as much as possible without causing the opposite 108-kilohertz component to appear within the sweep range.

The on-orbit acquisition process is normally accomplished without modulation applied to the up-

(ZERO DOPPLER, ± 85 KHz ABOUT CARRIER)

72 Kbps TDM, 1-0 VOICE IDLE PATTERN, RANGING-ON

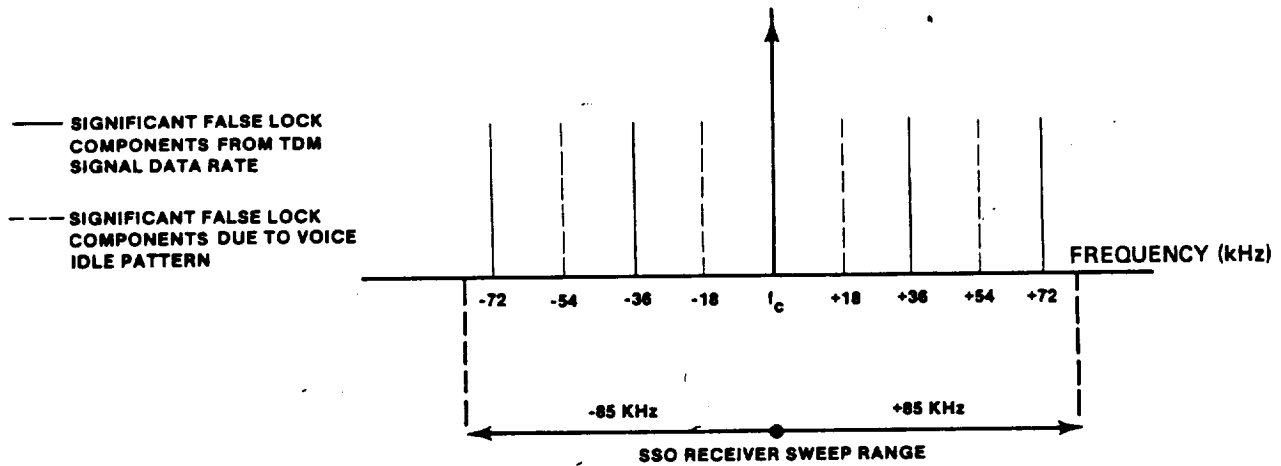


FIGURE 17.- GSTDN UPLINK SIGNAL FALSE-LOCK COMPONENTS.

(ZERO DOPPLER, ± 108 KHz ABOUT CARRIER)

216 Kbps CONVOL. ENCODED TDM, 1-0 VOICE IDLE PATTERN RANGING-ON

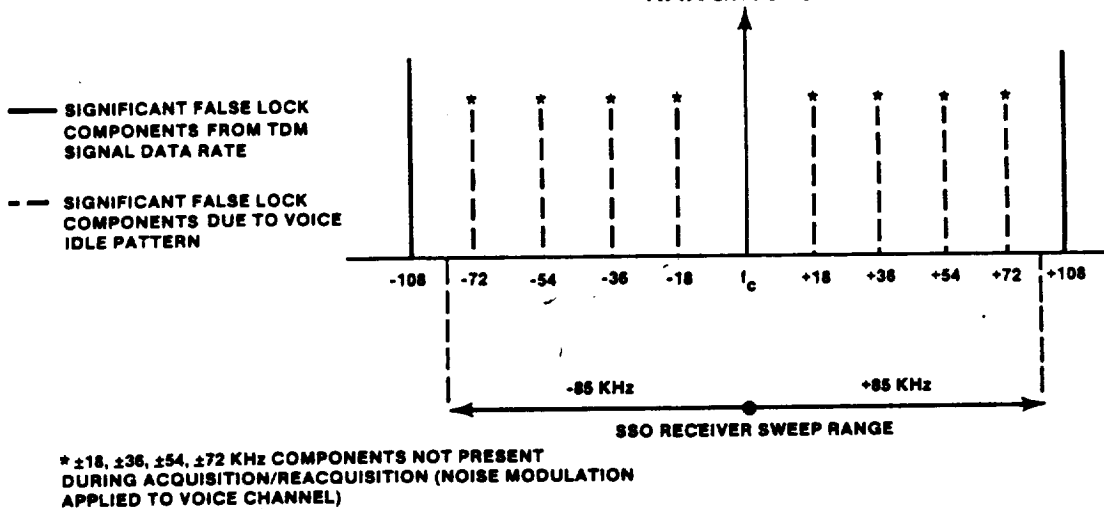


FIGURE 18.- UPLINK SIGNAL FALSE-LOCK COMPONENTS OF THE SPECIAL LAUNCH COMMUNICATION MODE.

link carrier for both direct (GSTDN) links and TDRS links. Since the ground receiver designs incorporate anti-sideband lock features, no significant false-lock problems were encountered by the GSTDN or TDRS ground station receivers.

In addition to the basic false-lock problems encountered with the Shuttle transponder, a phenomenon referred to as "critical modulation index" effect was encountered. Traditionally, a Costas loop is intended for use in receivers that must reconstruct a carrier reference from an input signal hav-

ing a completely suppressed carrier component (i.e., PSK modulation). However, for the Shuttle direct (GSTDN) uplink mode with ranging, the Orbiter transponder Costas loop is required to acquire and track a PM signal (i.e., when a residual carrier component is present in the signal spectrum), as is illustrated in figure 19. The means by which the ranging subcarrier is extracted using the in-phase modulation reference signal generated by the Costas loop is shown in the figure.

For the case of a Costas loop operating on a linear modulated signal with digital TDM data and a sine-wave ranging subcarrier, the error signal in the loop can be defined as follows.

If the input signal is given by equation (5)

$$s(t, \theta) = \sqrt{2A} \sin \left[\omega_0 t + \underbrace{\theta_1 d(t)}_{\text{TDM data}} + \underbrace{\theta_2 \sin(\omega_{SC} t + BR(t))}_{\text{Ranging subcarrier}} \right] \quad (5)$$

then the error signal in the loop $Z_0(t)$ can be shown to have the form of equation (6).

$$Z_0(t) = AJ_0^2(\theta_2) \left[D \sin^2 \theta_1 - \cos^2 \theta_1 \right] \sin \psi \quad (6)$$

where

- ω_{SC} = ranging subcarrier radian frequency and $\omega_{SC} \gg$ than the low-pass arm filter 3-decibel bandwidth
- D = filter distortion factor; $D = 1$ for infinite-bandwidth arm filters
- θ_1 = TDM data PM modulation index (radians)

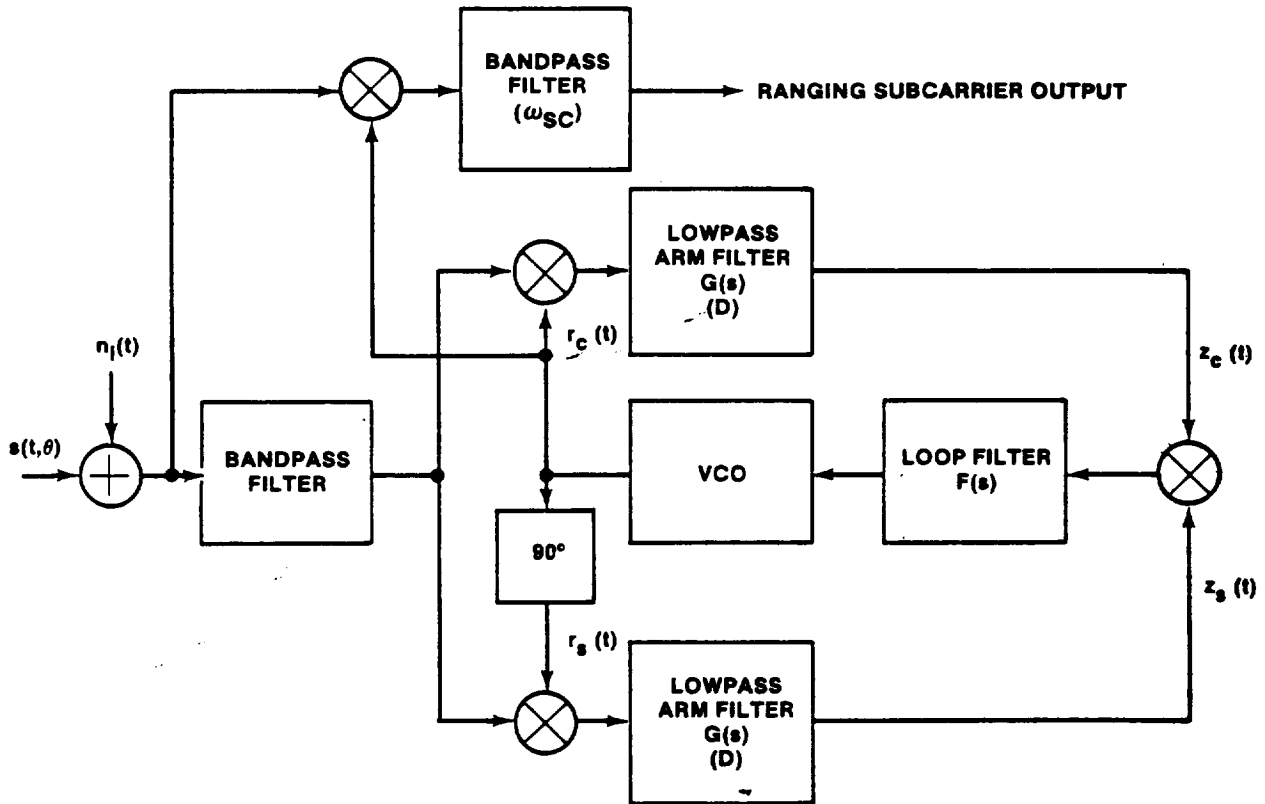


FIGURE 19.- COSTAS LOOP AND RANGING DEMODULATOR.

θ_2 = ranging subcarrier modulation index (radians)
 β = ranging tone PM modulation index (radians)
 $R(t)$ = ranging tone signals
 J_0 = Bessel function of first kind and order zero
 $A \sin \omega_0 t$ = carrier signal (unmodulated)

Note that the error signal $Z_0(t)$ disappears (i.e., goes to zero) for the following conditions.

1. $J_0^2(\theta_2) = 0$; when $\theta_2 = 2.4$ radians
2. $\theta_1 = \cot^{-1} \sqrt{D}$; when $\theta_1 = \pi/4$ radians or 45° and infinite bandwidth (i.e., $D = 1$) is assumed

For the Shuttle network transponder, the Costas loop filter distortion factors have been rigorously defined (ref. 12). The critical modulation index $(\theta_1)_{cr}$ for which the Shuttle Costas loop cannot acquire or track the GSTDM ranging modes for the various TDM data rates of interest is given in table 5.

It is obvious from equation (6) that as the filter distortion factor approaches unity, the signal power available for tracking (i.e., error signal) approaches that for the PSK channel. For PSK, the error signal would become

$$Z_0(t) = AD \sin 2\psi \quad (\text{since } \theta_2 = 0 \text{ and } \theta_1 = \pi/2 \text{ radians}) \quad (7)$$

The acquisition performance of the loop in the PM mode of operation will always be degraded over that for a PSK modulation mode. Table 6 illustrates the calculated and measured acquisition threshold for a representative Shuttle network transponder Costas loop in the PSK and PM (residual carrier) modes of operation.

TABLE 5.- CRITICAL MODULATION INDEX $(\theta_1)_{cr}$

TDM data rate	Costas loop arm filter, 3-dB bandwidth, kHz	Filter distortion factor (D)	$(\theta_1)_{cr}$, rad
32 kbps (Low data rate, uncoded)	147.5	0.886	0.8157
96 kbps (Low data rate, coded)	147.5	.6636	.8872
72 kbps (High data rate, uncoded)	147.5	.8884	.851
216 kbps (High data rate, coded)	147.5	.670	1.003

The performance of the ranging channel is also dependent on the selection of the TDM data modulation index. The ranging subcarrier is extracted by demodulating the input signal with an in-phase reference generated by the Costas loop. The signal power available to the ranging channel is given by

$$P_r = 2P \cos^2(\theta_1) J_1^2(\theta_2) \cos^2\psi \quad (8)$$

where

P_r = the power available in the ranging channel
 θ_1 = the data PM mode index
 θ_2 = the ranging subcarrier modulation index
 P = the total received power level
 ψ = the Costas loop dynamic phase error
 J_1 = the first-order Bessel function of the first kind

TABLE 6.- ACQUISITION THRESHOLDS

Parameters			Threshold P_r/N_0 , dB-Hz	
Data PM index, rad	Subcarrier PM index, rad	Arm filter bandwidth, kHz (a)	Calculated	Test (a)
PSK (216-kbps data)				
$\pi/2$	0	147.5	47.68	45.6
216-kbps data plus ranging				
1.25	1.0	147.5	55.84	56.1
1.1	1.0	147.5	61.15	61.6
1.125	1.0	147.5	59.66	60.6
1.375	1.0	147.5	54.26	53.8

^aSeptember 1980 ESTL test results.

As the data modulation index is increased above its critical value, the Costas loop tracks better. However, the factor $\cos \theta_1$ decreases and hence the ranging power is reduced. Obviously, a trade-off exists with respect to selection of θ_1 . If the data modulation index falls below the critical value or if data are removed completely, the in-phase and quadrature demodulation reference signals switch roles and the ranging channel power P_r tends toward zero depending on the exact value of the loop phase error ψ . Thus, to extract ranging modulation, the data modulation must be present and at a modulation index above its critical value.

FREQUENCY MODULATION OPTIMUM FREQUENCY DEVIATIONS

For the Shuttle digital FM links, it was necessary to optimize the modulation parameters because of the relatively low transmitter power (10 watts) and the low antenna gains of the FM hemispherical coverage antennas. For a digital frequency-shift keying (FSK) system with coherent matched-filter detection and assuming "zero" correlation between transmitted symbols, the performance has been shown to be 3 decibels worse than for coherent PSK systems. For such a system, the probability of error is given by equation (9).

$$P_e = \frac{1}{2} \operatorname{erfc} \sqrt{\frac{(1 - \rho) E_b}{2N_0}} \quad (9)$$

where

- E_b = the energy per bit time
- N_0 = the receiver noise spectral density
- erfc = the complementary error function

and ρ is the normalized symbol correlation coefficient given by equation (10).

$$\rho = \frac{1}{E_b} \int_0^T S_1(t) S_2(t) dt \quad (10)$$

where $S_1(t)$ and $S_2(t)$ are the transmitted symbols. However, it is not necessary that there be zero correlation between transmitted symbols $S_1(t)$ and $S_2(t)$. For the case of continuous-phase (i.e., nonswitched) digital FM links, it can be shown that ρ can take on negative values. Equation (11) represents the value of ρ for a continuous-phase FM transmitter modulated with binary non-

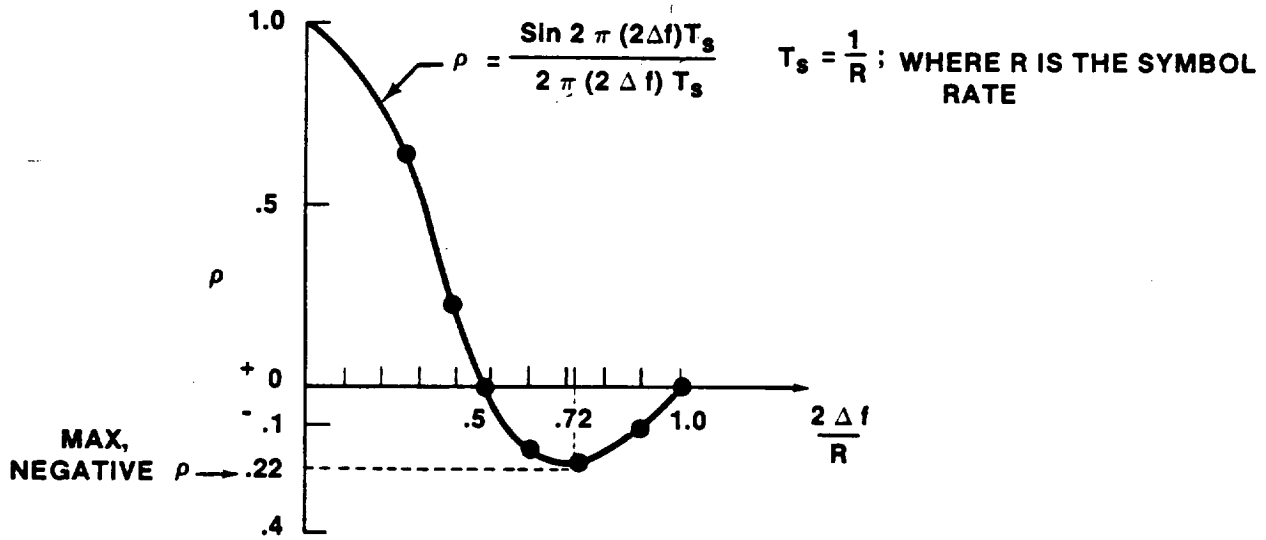
return to zero (NRZ) symbols.

$$\rho = \frac{\sin[2\pi(2\Delta f) T_s]}{2\pi(2\Delta f) T_s} \quad (11)$$

where

- Δf = the peak frequency deviation of the FM transmitter (hertz)
- R = symbol data rate
- T_s = NRZ symbol bit time

As seen from figure 20 for orthogonal performance (i.e., $\rho = 0$), the frequency deviation is $\Delta f = 0.25R$. However, for optimum "best" performance, $\rho = -0.22$ and the frequency deviation is $\Delta f = 0.36R$. Thus, performance of an optimum continuous-phase digital FM channel should be only 2.2 decibels worse than performance of an optimum PSK channel. This surprising result constitutes a performance bound on FSK systems using suboptimum detection schemes.



$$P_{E_o} = \frac{1}{2} \operatorname{erfc} \sqrt{\frac{.5 E_b}{N_o}} \rightarrow \text{ORTHOGONAL PERFORMANCE} \left[\rho=0, \frac{2\Delta f}{R} = .5 \right]$$

$$P_{E_B} = \frac{1}{2} \operatorname{erfc} \sqrt{\frac{.61 E_b}{N_o}} \rightarrow \text{BEST PERFORMANCE} \left[\rho = -.22, \frac{2\Delta f}{R} = .72 \right]$$

P_{E_B} \rightarrow REPRESENTS PERFORMANCE BOUND ON COHERENT FSK 2.2 dB WORSE THAN COHERENT PSK

FIGURE 20.- ρ VERSUS FREQUENCY DEVIATION FOR CONTINUOUS-PHASE FM DIGITAL MODULATION.

In the Shuttle case, the FM link was designed for the optimum Δf at the highest channel digital data rate of 1024 kbps. Another parameter which affects the optimum performance of the linear FM digital channel is the ratio of i.f. filter bandwidth to the data rate. Table 7 shows the values of normalized optimum Δf and ratios of i.f. filter bandwidth to data rate B/R for NRZ and biphase data formats (ref. 13).

Experimental results of Shuttle link performance using a linear FM discriminator followed by an integrate-and-dump bit synchronizer (fig. 21) agreed quite well with the theoretical performance for NRZ data. Figures 22 and 23 illustrate the experimental results obtained during tests at the JSC

TABLE 7.- OPTIMUM PARAMETERS FOR FM DIGITAL LINK

Data format	$\Delta f/R$	B/R
NRZ	0.360	1.4
Biphase ^a	.62	2.7

^aBiphase optimum Δf was determined experimentally.



FIGURE 21.- SHUTTLE DIGITAL FM LINK DETECTION PROCESS.

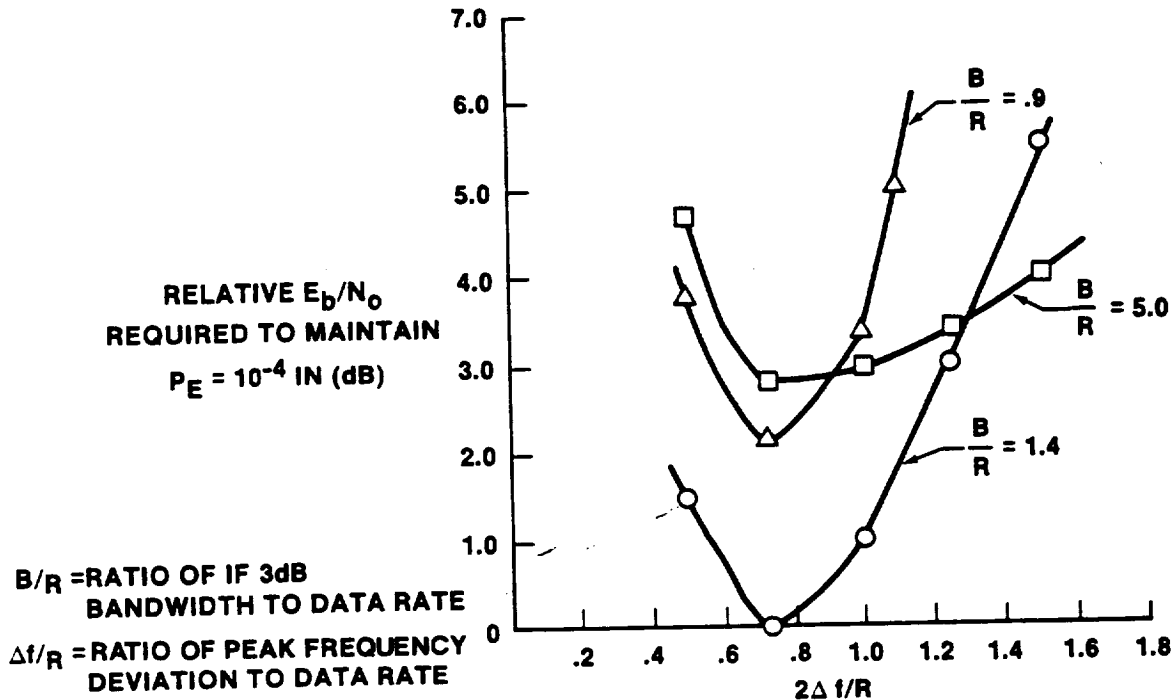


FIGURE 22.- RELATIVE BIT ERROR PERFORMANCE (NRZ DATA): DISCRIMINATOR DETECTION OF CONTINUOUS-PHASE FM MODULATION.

ESTL (ref. 13). Performance in terms of the relative E_b/N_0 required to maintain a 1×10^{-4} BER is shown as a function of frequency deviation Δf and receiver 3-decibel bandwidth B to digital data rate R ratio B/R . The optimum case tested is for $B/R = 1.4$ and a Δf of $0.36R$ as seen from figure 22 for NRZ digital data, and $B/R = 2.7$ and $\Delta f = 0.65$ for biphase digital data as seen from figure 23.

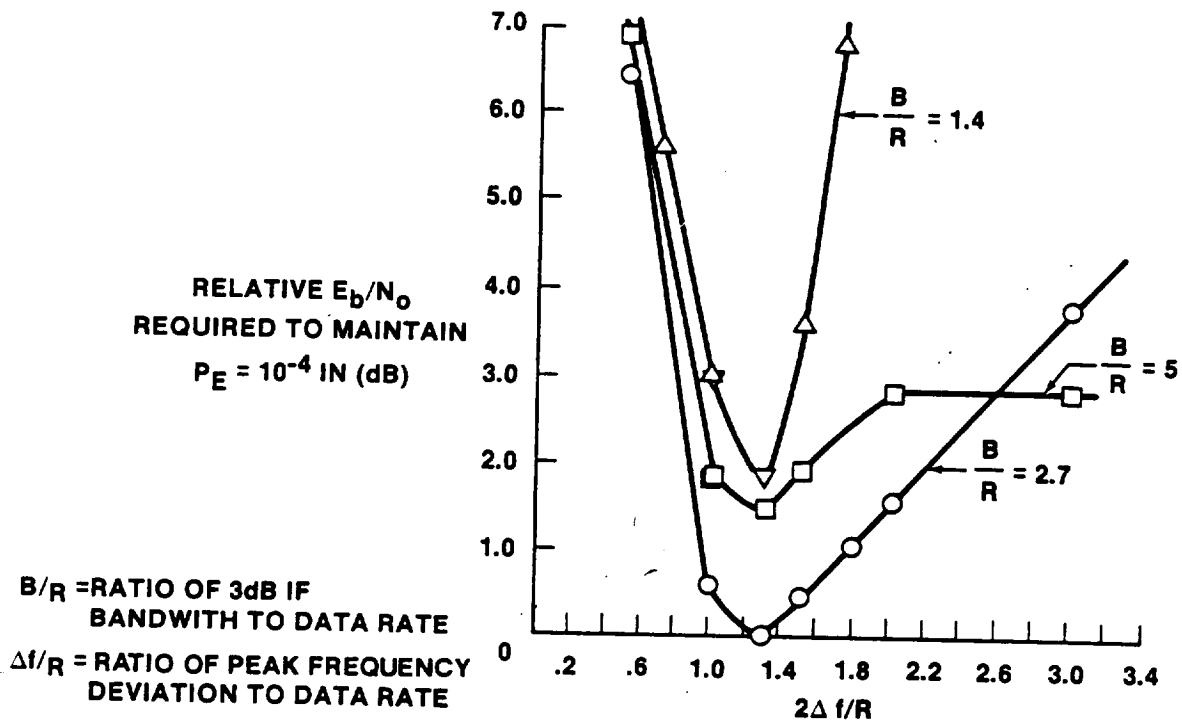


FIGURE 23.- RELATIVE BIT ERROR PERFORMANCE (BIPHASE DATA): DISCRIMINATOR DETECTION OF CONTINUOUS-PHASE FM MODULATION.

RANGING CHANNEL (SUBCARRIER MODULATION)

General Description

The ranging channel is used primarily during ascent and entry to provide a precision analog measurement of slant range between a GSTDN ground station and the Orbiter. The ranging signal consists of a combination of tones which are generated by the GSTDN ground station. This analog signal phase modulates a 1.7-megahertz subcarrier, which is then frequency-division multiplexed (FDM) with a baseband digital signal (32, 72, 96, or 216 kbps biphas-level format operational data). The resulting FDM signal then phase modulates the uplink carrier frequency. In the Orbiter receiver, a phase demodulator recovers the FDM signal; the 1.7-megahertz tone-modulated subcarrier is separated from the FDM signal by a BPF and amplified by an automatic gain control (AGC) circuit. This filtered, amplified ranging subcarrier is then FDM with a downlink baseband digital signal (96, 192, 288, or 576 kbps biphas-level format operational data). The resulting FDM signal phase modulates the downlink carrier frequency (which is coherent with the uplink carrier frequency). At the GSTDN station, a phase demodulator recovers the 1.7-megahertz tone-modulated subcarrier, which is then demodulated by a subcarrier phase demodulator. The recovered range tones are routed to a processor, in which slant range is determined.

Range Measurement

The range measurement data are instantaneous values of the total phase delay of a major tone from the time of transmission of the tone from the GSTDN station to the Shuttle to the time of reception of the tone back at the GSTDN station. The round-trip phase delay is provided in nanoseconds with a 1-nanosecond resolution. Each phase-delay measurement has a time tag; the measurement corresponds to the phase delay at a time within ± 50 nanoseconds of the associated time tag. Each measurement is independent of previous measurements and is unambiguous to a range of 15 000 kilometers, with maximum 3σ range measurement errors of 10 meters noise and 20 meters bias.

The major tone currently used is 500 kilohertz. To resolve the total phase delay through the rf communications system, a series of lower frequency tones must be simultaneously transmitted through the system during initial acquisition. After an initial measurement of the total phase delay has been made, the transmission of low-frequency tones is discontinued until a loss of lock occurs and a

reacquisition is required. The modulation steps in obtaining the initial total phase-delay measurement are listed in table 8. The 500-kilohertz tone is modulated on the 1.7-megahertz subcarrier and transmitted to the Orbiter in step 1. When the return 500-kilohertz tone has been received on the

TABLE 8.- RANGING MODULATION SEQUENCE

Sequence step	Tones phase modulated on 1.7-MHz subcarrier	Remarks
1	500-kHz major tone	
2	500-kHz major tone 100-kHz minor tone	
3	500-kHz major tone 20-kHz minor tone	
4	500-kHz major tone 4-kHz minor tone	The 4-kHz minor tone is modulated by an 800-Hz tone using upper single sideband suppressed carrier (USSBSC) modulation with the lower sideband filtered so that it is 20 dB down.
6	500-kHz major tone 4-kHz minor tone	The 4-kHz minor tone is modulated by a 160-Hz tone using double sideband suppressed carrier (DSBSC) modulation.
7	500-kHz major tone 4-kHz minor tone	The 4-kHz minor tone is modulated by a 40-Hz tone using DSBSC modulation.
8	500-kHz major tone 4-kHz minor tone	The 4-kHz minor tone is modulated by a 10-Hz tone using DSBSC modulation.
9	500-kHz major tone	

ground and phase lock to the 500-kilohertz tone has occurred, the ranging equipment automatically changes to step 2 by adding a 100-kilohertz tone to the uplink. The equipment automatically proceeds through the remaining steps until only the 500-kilohertz tone remains. At this point, the first total phase-delay measurement is completed. Subsequent measurements can be provided at selected rates as high as 10 per second.

S-BAND NETWORK COMMUNICATION SUBSYSTEM

The S-band network equipment consists of 10 line replaceable units (LRU's) and associated antennas as shown in figure 24. The subsystem is redundant with the exception of the rf contacts in the antenna switch, the diplexers in the preamplifier, and the antennas with their associated rf cables. The general redundancy approach is to use the equipment in strings and avoid cross-strapped operations. A minimal amount of status information such as temperatures, AGC values, and rf power outputs is provided by the LRU's for relay in either real-time or delayed (recorded) telemetry.

The hardware is environmentally sealed and cold-plate cooled. The environmental design requirements were based on the controlled areas of the Shuttle equipment bays, and the equipment cannot withstand exposure to space environments. All S-band LRU's operate from 28-volt dc buses, and each LRU has the capability to operate from either of two redundant buses. The power distribution is carefully designed to maintain the string-redundancy approach. Internal LRU redundancy is maintained by physical separation and by including structural elements to provide isolation and prevent propagation of failures. See table 9 for LRU physical information.

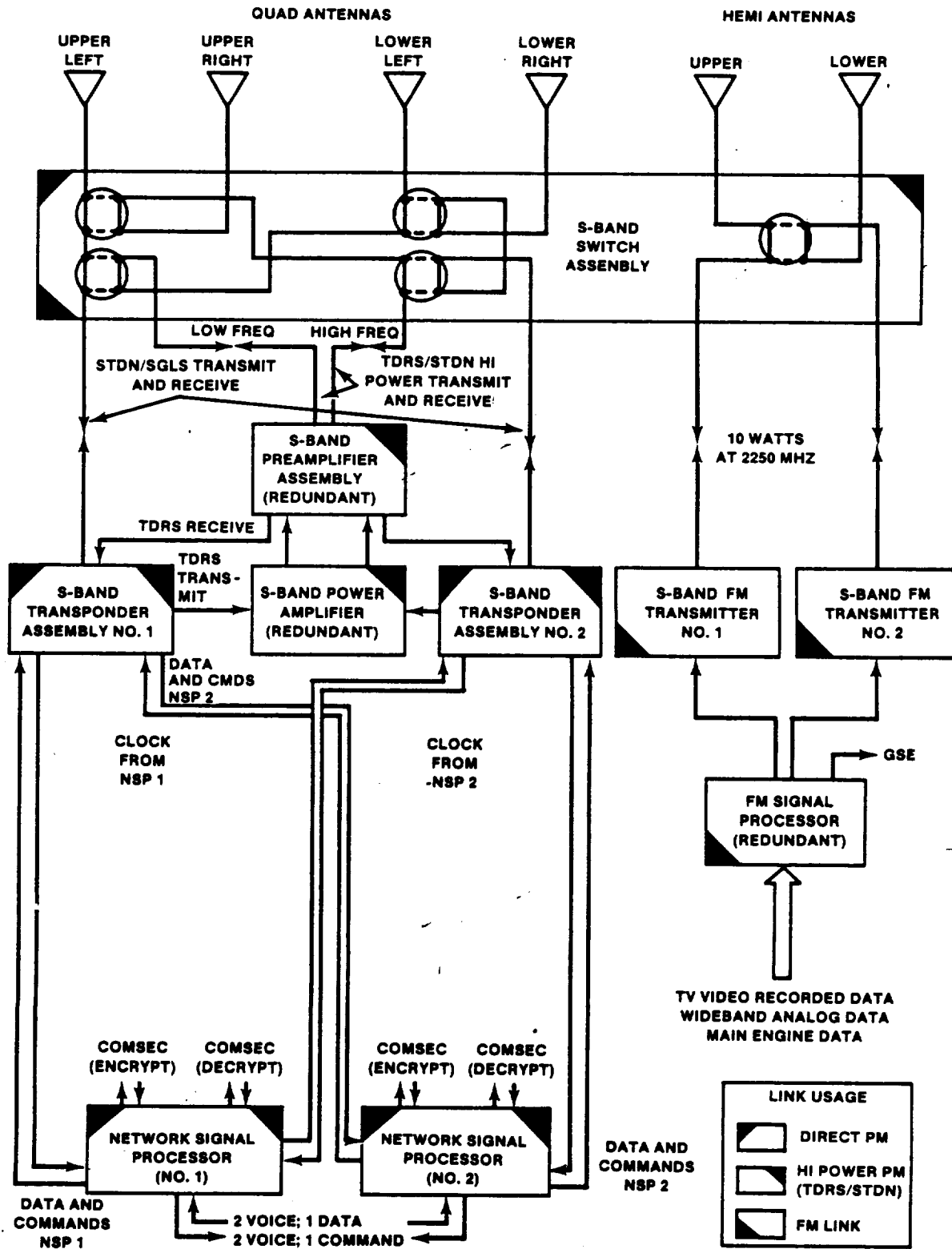


FIGURE 24.- S-BAND NETWORK COMMUNICATION EQUIPMENT.

TABLE 9.- S-BAND LRU PHYSICAL CHARACTERISTICS

LRU	Weight, lb	Approximate volume, in ³	Power, W
Network transponder (2 required)	35.8	1120	65 STDN/SGLS 48 STDN-HI/TDRS
Preamplifier	25.6	790	35 Turn-on 25 After 10 min
Power amplifier	32.5	850	415 Operate 20 Standby
Switch assembly	7.7	335	2 Steady state 150 Switching
FM transmitter (2 required)	6.8	115	120
FM signal processor	12	395	9
Network signal processor (2 required)	18	720	30

As indicated in figure 24, the S-band network equipment is functionally divided into the PM and FM systems. The only common LRU is the antenna switch assembly, which provides similar but separate rf signal routing services for both systems. In the Shuttle operational era, the FM system will be a "kittable" (optional) flight item since it provides services on direct links only. The PM equipment provides four basic modes of operation, two of which are "low power" (SGLS and GSTDN) direct links and two, "high power." One high-power mode is a direct link (GSTDN-Hi Pwr) and the other is the satellite relay link (TDRS). In all cases, system control signals for operational modes are routed through the Ground Communications Interface Logic (GCIL) and configuration control is exercised by forward link commands. In contingencies, these controls can be exercised by onboard panel switches or keyboard entries to the onboard general-purpose computers (GPC's).

The heart of the S-band PM system is the network transponder (fig. 25). In all primary modes, it supports full duplex operation and is also capable of receive-only service. The LRU operates in a phase-coherent mode with a specified turnaround ratio and has the capability to turn around ranging data. The double conversion receiver employs a Costas detector. A spread spectrum processor is activated in the TDRS mode. The baseband and control module chooses various parameters in accordance with mode selection and controls the acquisition scenarios. In the low-power modes, all the transmitter power amplifier stages are active and the rf output is 5 watts. When a high-power mode is selected, the final stages are inactive to provide a lower (1 watt) level to drive the S-band power amplifier.

The S-band preamplifier supplies the duplex function in the high-power modes and also provides low-noise preamplification for the network transponder receiver. The preamplification is provided by uncooled parametric amplifiers followed by transistor amplifiers. The duplex function is not redundant. There are two duplexers; one is used for the high STDN frequency pair and the other, for the low STDN frequency pair. Internal switching allows the use of either preamplifier with either transponder and either power amplifier.

The S-band power amplifier is used in the high-power modes to amplify the output of the transponder. The LRU consists of two TWT's with their associated power converters and control circuits. The input portion of the LRU incorporates an rf switch to route either transponder output to either of the internal amplifiers. The LRU incorporates several protective devices for the TWT's. Each output is protected from mismatch damage by a circulator and load. The tubes are further protected from po-

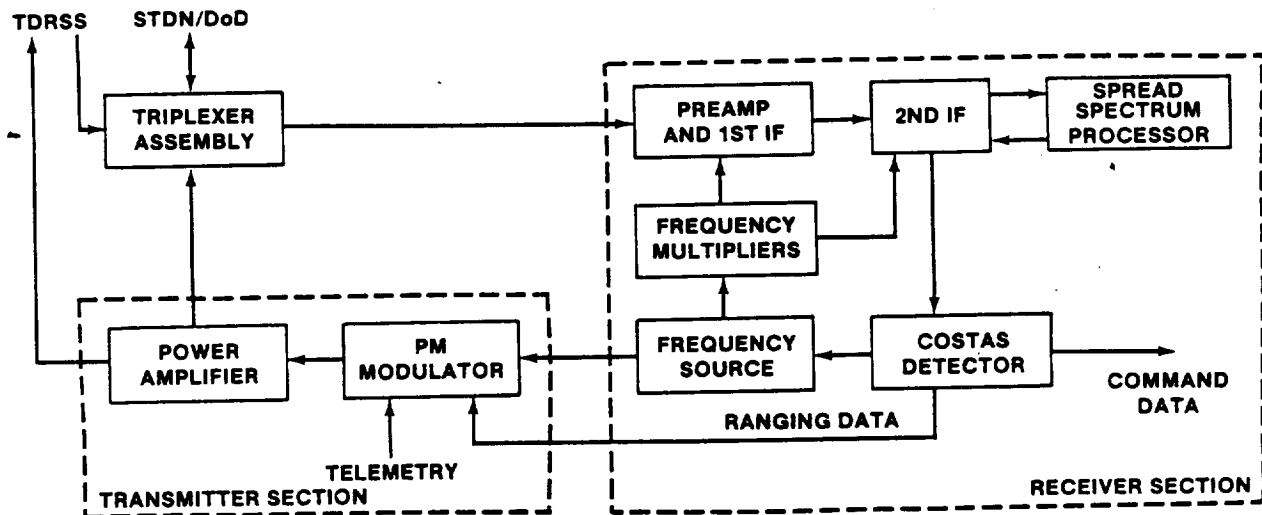


FIGURE 25.- NETWORK TRANSPONDER FUNCTIONAL BLOCK DIAGRAM.

tential collector thermal shock damage by a circuit which senses the absence of rf drive and shuts down the power supply or the high voltage to the tube. The power amplifiers typically produce 120 to 140 watts of rf output power.

The S-band antenna switch is internally redundant except for the rf head assembly. The LRU provides four transfer switches for the PM signal routing and one switch for the FM system. The input logic and switch drives are fully redundant. Control signals originate with the GPC system in the automatic mode and with the Orbiter control panel in the manual mode. The LRU logic receives inputs that indicate the equipment in use and the mode of operation. The internal logic then recognizes commands to select a given antenna and configures the rf switches accordingly. There are 16 potential rf paths in the PM and 4 in the FM section. In all cases, the rf assembly consists of movable and fixed reeds and fixed contacts. The contact areas are hard anodized and sealed to prevent buildup of oxides. By careful design and process control, these contact areas provide capacitive, low-loss coupling across the frequency range of interest. It should be noted that there is no interruption of the rf during switching and the antenna switch is a "hot switch" design with the capability to switch a 175-watt rf signal. The rf head also includes mechanical contacts which are slaved to the rf contacts and provide status information on switch positions for telemetry and antenna management use.

The network signal processor (NSP) (fig. 26) essentially provides the interface between the S-band PM equipment and the other onboard systems. As shown, the forward link information is routed from the transponder receiver into a symbol synchronizer. When coding is in use, the NSP then routes the signal to the Viterbi decoder, and, in the case of secure data, the data are routed through the outboard COMSEC device. The information is then demultiplexed and demodulated or decoded as required. The signals are then routed to the users at the proper level and impedance. In the return link, the inverse functions are provided; onboard voice signals are received from the audio system and digitized in a delta modulation process using a Modified ABATE algorithm. The telemetry signals are then multiplexed with the voice. Then, depending on the operational mode, the signal is routed through the convolutional encoder or the COMSEC unit or both. The final processing is to convert from NRZ-L to biphasic L and route the information at the proper level to the transponder modulator for rf transmission or to the ground-support equipment (GSE) data bus. The LRU has self-contained logic that recognizes the desired system configuration and internally controls the routing and processing.

The FM transmitter is frequency modulated by the output of the FM signal processor. The input modulates a 98.5-megahertz oscillator. This signal is then mixed with the eighth harmonic of a stabilized oscillator. The resulting 750-megahertz signal is filtered, amplified, and multiplied by 3 to drive the output power amplifier. The solid-state output amplifier produces a minimum of 10 watts rf. The companion FM signal processor (fig. 27) provides the interface function between the FM system and the various Orbiter data sources. Such signals as main engine data, television, and payload data are selected, level and impedance controlled, modulated on internally generated subcarriers, and provided as the modulating signal to the FM transmitter. An important function is the processing of high-speed telemetry playback data from the Orbiter recorders.

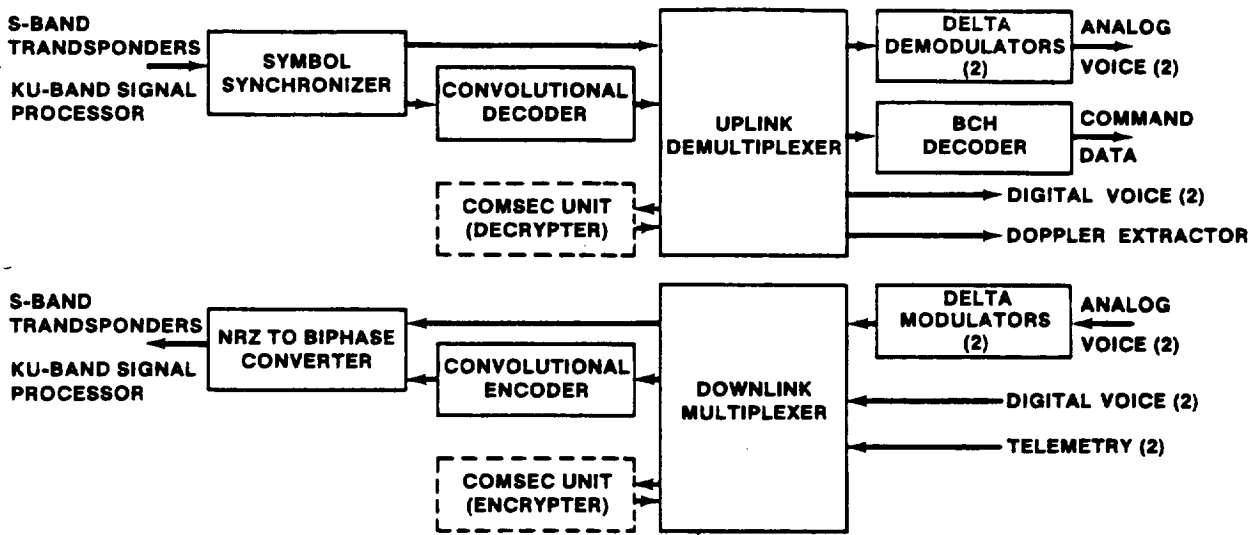


FIGURE 26.- NETWORK SIGNAL PROCESSOR FUNCTIONAL BLOCK DIAGRAM.

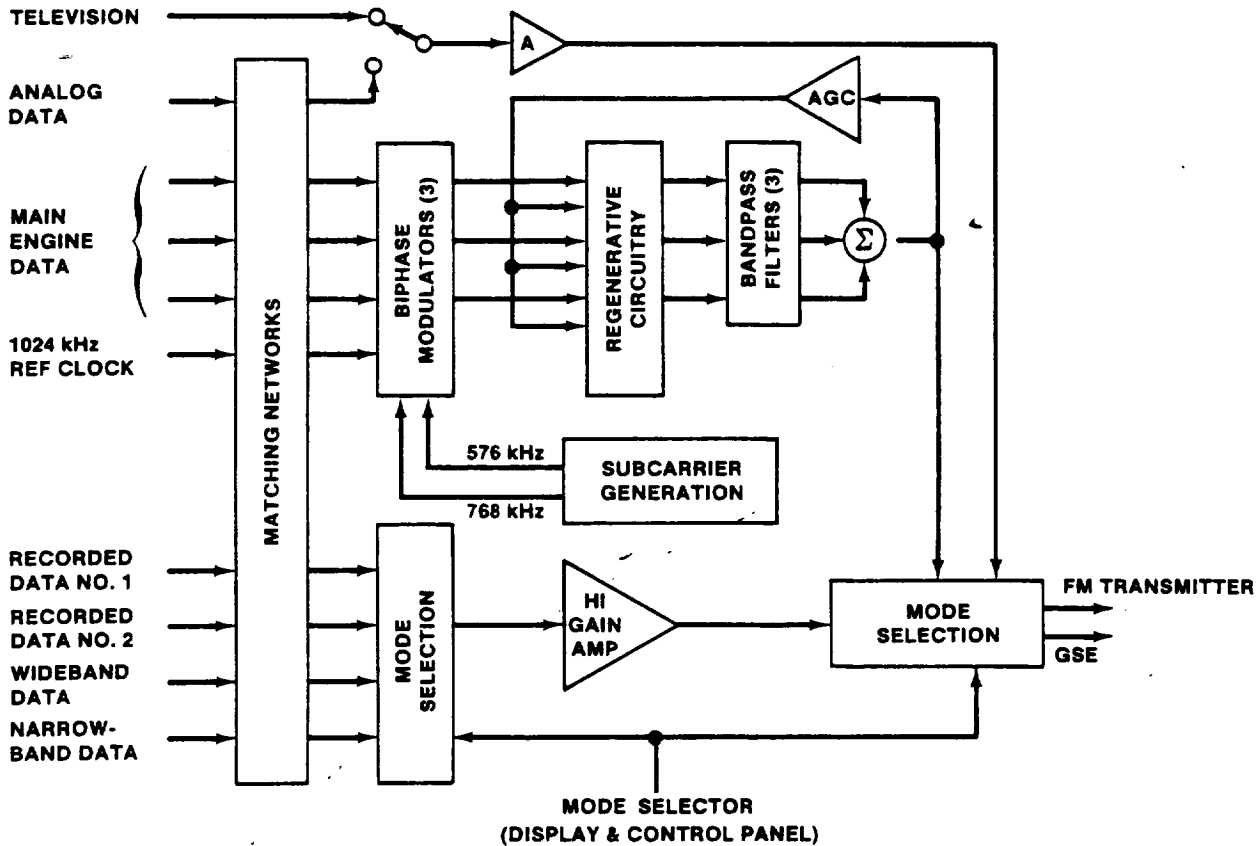


FIGURE 27.- FM SIGNAL PROCESSOR FUNCTIONAL BLOCK DIAGRAM.

GSTDN/TDRSS PERFORMANCE MARGINS

End-to-end data performance for communications or tracking links can be expressed in terms of a required SNR in an appropriate bandwidth at some point in the receiving system. For an analog chan-

nel, this may be the final demodulator output SNR or it may be the first demodulator input SNR which is necessary to provide the required final output SNR. For a digital channel, the SNR in the data-rate bandwidth at the bit detector input that is required for a given BEP is frequently used. For either analog or digital channels, the performance margin (or circuit margin) is the amount, in decibels, by which the calculated (or measured) SNR exceeds the required SNR at the chosen reference point in the receiving system. The required SNR (and thus the performance margin) can also be expressed in terms of the received signal-to-noise power spectral density ratio P_r/N_0 .

Table 10 summarizes Shuttle S-band network performance margins for a representative selection of Orbiter and ground station/TDRSS modes. These margins reflect conservative, end-of-life parameter values but are not considered to be worst case in the sense of using worst case tolerances. The TDRSS margins reflect Orbiter antenna performance for an average 50-percent spherical coverage. The return link margins do not include any degradation due to ground-based rf interference.

TABLE 10.- SHUTTLE S-BAND PERFORMANCE MARGIN SUMMARY

Configuration	Channel	Performance margin
GSTDN-to-Orbiter uplink		
1. GSTDN: 9.1 m ant; 2 kW xmtr ORB: Preamp bypass Both: On-orbit modulation, ranging off, high-data-rate mode, 270 n. mi. orbit	72 kbps data	45.7 dB (10^{-4} BEP)
2. Same as 1, except ranging on	72 kbps data Ranging	42.9 dB (10^{-4} BEP) 54.8 dB ($P_r/N_0 = 49.4$ dB-Hz)
3. GSTDN: 9.1 m ant; 2 kW xmtr ORB: Preamp in Both: Launch modulation, ranging on, high-data-rate mode, range = 460 n. mi.	72 kbps data Ranging	62.2 dB (10^{-4} BEP) 65.6 dB ($P_r/N_0 = 49.4$ dB-Hz)
AF/SCF-to-Orbiter uplink		
AF/SCF: 14 m ant; 1 kW xmtr ORB: Preamp bypass Both: High-data-rate mode, 225 n. mi. orbit	72 kbps data	40.4 dB (10^{-5} BEP)
Orbiter-to-GSTDN PM downlink		
GSTDN: 9.1 m ant; 140 K syst temp ORB: Power amp bypass, coherent mode Both: Ranging on, high-data-rate mode	192 kbps data Ranging	14.2 dB (10^{-4} BEP) 31.4 dB ($P_r/N_0 = 53.5$ dB-Hz)
Orbiter-to-AF/SCF PM downlink		
AF/SCF: 14 m ant; 220 K syst temp ORB: Power amp bypass, coherent mode Both: High-data-rate mode, 225 n. mi. orbit	192 kbps data	14.1 dB (10^{-5} BEP)

TABLE 10.- Concluded

Configuration	Channel	Performance margin
Orbiter-to-GSTDN FM downlink		
GSTDN: 9.1 m ant; 140 K syst temp		
Both: 270 n. mi. orbit		
(1) Recorder playback	1024 kbps data	7.9 dB (10^{-4} BEP)
(2) Main engine subcarriers	60 kbps data	8.1 dB (10^{-4} BEP)
(3) Digital payload data	5 Mbps data	.1 dB (10^{-4} BEP)
(4) Analog payload data	4 MHz data	1.1 dB (SNR = 13.5 dB)
(5) Television	3 MHz video	1.4 dB (SNR = 33.0 dB)
Orbiter-to-AF/SCF FM downlink		
AF/SCF: 14 m ant; 220 K syst temp, SGLS receiver		
Both: 225 n. mi. orbit		
(1) Recorder playback	960 kbps data	9.0 dB (10^{-5} BEP)
(2) Digital payload data	256 kbps data	14.1 dB (10^{-5} BEP)
TDRSS-to-Orbiter forward link		
(1) Low-data-rate data	32 kbps	2.1 dB (10^{-4} BEP)
(2) High-data-rate data	72 kbps	-1.4 dB (10^{-4} BEP)
Orbiter-to-TDRSS return link		
(1) Low-data-rate data	96 kbps	3.5 dB (10^{-4} BEP)
(2) High-data-rate data	192 kbps	.5 dB (10^{-4} BEP)

DATA/RANGING INTERFERENCE EFFECTS

Interchannel compatibility of the GSTDN/Orbiter data and ranging channels has been well demonstrated during the first Shuttle flights. However, earlier versions of the design had significant interference problems which were exposed in ESTL system performance verification testing at JSC. These initial-design problems and the resulting interference effects on link performance are described in the following paragraph.

The initial data/ranging design used a major ranging tone of 100 kilohertz instead of 500 kilohertz. Tests using nominal modulation indexes and the 100-kilohertz major tone resulted in unusable ranging data. Tests using nominal modulation indexes and the 500-kilohertz major tone indicated degraded but acceptable ranging performance (25 meters compared to 10 meters specified range accuracy, 20 seconds average acquisition time, and 2 percent probability of incorrect acquisitions). Ranging test results using the 500-kilohertz major tone and worst case modulation indexes, however, were unacceptable (100 meters accuracy, 30 to 95 seconds acquisition time, and 30 to 40 percent probability of incorrect acquisition). Based on subsequent tests and analyses, the downlink data modulation index was reduced from 1.1 ± 10 percent radians to 0.55 ± 10 percent radians, providing good ranging performance (5 meters accuracy, 17 seconds acquisition time, and no incorrect acquisitions). Downlink data performance was degraded by 4.6 decibels as a result of the modulation index reduction, but performance margins for 10^{-4} BEP were still very high (+18 decibels for the low-power mode).

RADIOFREQUENCY COVERAGE ANALYSIS

Radiofrequency coverage analysis is to be distinguished from the closely related activity known as circuit margin analysis. Both deal with link performance assessment and prediction, but the latter is a generalized and limited assessment. It excludes the mission time-variable factors: spacecraft orientation and trajectory. Circuit margins are calculated for a fixed range or distance and, in the case of omnidirectional antennas, a nominal reference value of antenna gain and polarization. The rf coverage analysis, on the other hand, is keyed to mission time and spacecraft position and at-

titude and thus provides a dynamic analysis of the rf links as the spacecraft moves along its trajectory with ever-changing attitude and range to ground stations or the TDRSS. It is the only end-to-end rf link performance assessment that analyzes rf links in their real form, combining the mission-fixed and mission time-varying link characteristics.

Radiofrequency coverage analysis is also reiterative. It is repeated during early planning stages as mission changes or new inputs occur and, in fact, is itself sometimes the catalyst for trajectory and attitude changes. When a mission's final operational trajectory is released, a formal rf coverage report is published, giving performance predictions for that particular mission. After the mission, rf coverage postmission analysis addresses anomalies, assesses actual compared to expected rf link performance, and considers whether changes are needed to subsequent mission plans.

Figure 28 characterizes the rf coverage and performance analysis process (ref. 14). The basic characterization of the rf links is given by the familiar range equation

$$P_r = P_t \frac{G_t G_r c^2}{16\pi^2 R^2 f^2 L_c L_m} \quad (12)$$

where

- P_r, P_t = received and transmitted signal power, respectively
- G_r, G_t = receive and transmit antenna gain, respectively
- f = frequency
- R = range
- c = speed of light
- L_c = circuit losses (transmit and receive)
- L_m = miscellaneous losses (pointing, polarization, etc.)

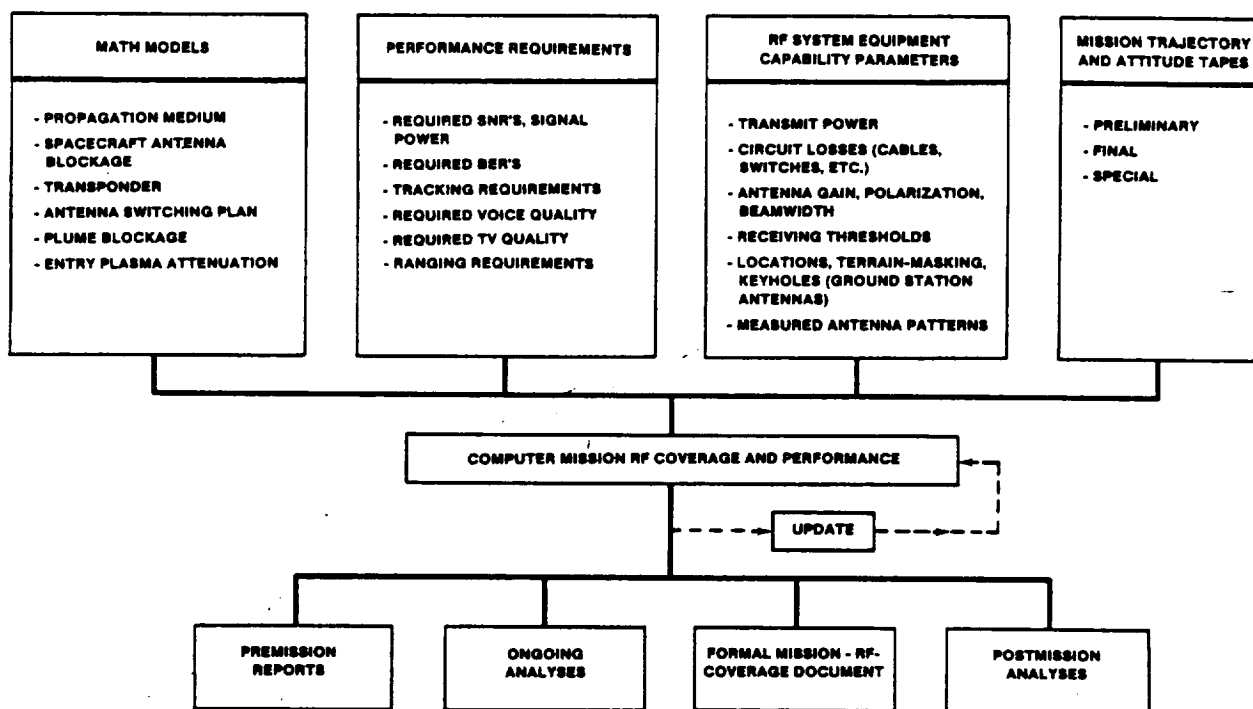


FIGURE 28.- RF COVERAGE AND PERFORMANCE ANALYSIS PROCESS.

With the Shuttle moving along its trajectory with changing attitude, its range and antenna gain (for omnidirectional antennas) are time variables and must be continuously computed as a function of time. The position and attitude at each instant is given by the state vector (position and velocity compo-

nents, $X, Y, Z, \dot{X}, \dot{Y}, \dot{Z}$) and directional cosines, respectively. The Shuttle omnidirectional antennas generally receive a final reference set of measurements at the JSC antenna test range facility, whereas vehicle antenna blockage is usually modeled from physical structural measurements.

MISSION PHASE CONSIDERATIONS

Ascent and descent mission phases have strict navigation requirements, and the Shuttle trajectory and attitude cannot be tailored to communication needs. With certain exceptions, on-orbit navigation requirements are more flexible and vehicle attitude (but not trajectory) can be planned to at least partly favor communications.

During ascent, Shuttle attitude relative to the Merritt Island (MIL) ground station changes rapidly; therefore, antenna gain of the S-band PM and FM antennas and hence the link signal strength varies considerably. There are four PM link antennas, one for each quadrant about the spacecraft. Switching can be manual but is normally automatic, initiated by onboard computer identification of which quadrant contains the line of sight.

As the Shuttle ascends and heads downrange, the radio links to MIL operate in the low-gain aft region and also in the solid rocket booster (SRB) exhaust plume. Figure 29 shows a typical plot of the S-band PM signal strength at MIL from the Shuttle, from lift-off until MIL loss of sight. The period when the line of sight with MIL passes through the plume is indicated on the graph. The signal strength during this period is much lower than shown because of plume attenuation (as much as 60 decibels has been observed) and also erratic because of phase distortion. Figure 30 is typical of the variation of the Shuttle-to-MIL line of sight during the ascent phase. Continuous communications with MIL cannot be assured when the line of sight is close to or within the dashed-box plume-blockage region. A decision was made in 1977 to locate a ground station at Ponce De Leon (PDL), somewhat north of the MIL site, so that its line of sight would be outside this blockage region. Shuttle missions have confirmed that MIL does lose communications during this period and that PDL is largely unaffected.

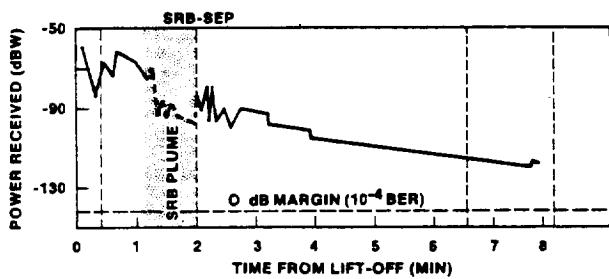


FIGURE 29.- ASCENT-PHASE PM SIGNAL STRENGTH, SHUTTLE TO MIL (TYPICAL).

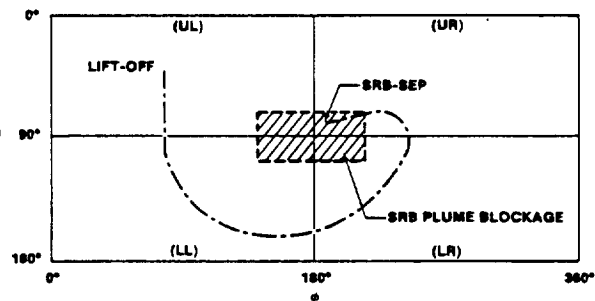


FIGURE 30.- ASCENT-PHASE LOOK ANGLES, SHUTTLE TO MIL (TYPICAL).

Circuit margin analysis for the S-band PM links between the Shuttle and the TDRS show 2 to 4 decibels margin when the line of sight lies in the main coverage region of the Shuttle S-band PM link antennas. During ascent, however, the line of sight from the Shuttle to the TDRS is in and out of the main coverage region (or the external tank/SRB blockage region) during the first few minutes and continuous communication by way of TDRS is highly unlikely until after the first 4 to 6 minutes as illustrated in figure 31. The MIL/PDL stations, on the other hand, are expected to have a strong signal from lift-off through about the first 7 to 8 minutes. Figure 32 illustrates the coverage using MIL/PDL for the first 8 minutes and TDRSS thereafter. The MIL/PDL/TDRS combination is the baseline projected when TDRS becomes operational.

During the descent phase, communications will again be through the S-band quads. Figure 33 illustrates the signal strength of the S-band Shuttle link to both TDRSS satellites, as predicted, using a typical descent trajectory for a landing at Edwards Air Force Base in California. Figure 33 encompasses the period from an altitude of 170 000 feet to an altitude of about 10 000 feet. The look angles are in and out of the fore and aft regions of the Shuttle, where the PM quad antennas have their lowest gain, as a result of large attitude excursions by the Orbiter as it dissipates excess energy. Reliable communications for descent, like ascent, probably will require a ground station assist to the TDRSS. Ground station links for descent are very strong, as has been demonstrated in missions to date, because of ground station proximity (compared to the TDRSS satellites being some 23 000 nautical miles farther away).

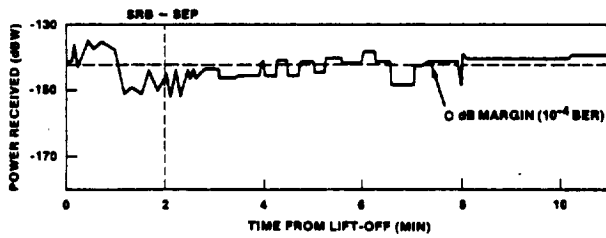


FIGURE 31.- ASCENT-PHASE PM SIGNAL STRENGTH, SHUTTLE TO TDRS EAST (TYPICAL).

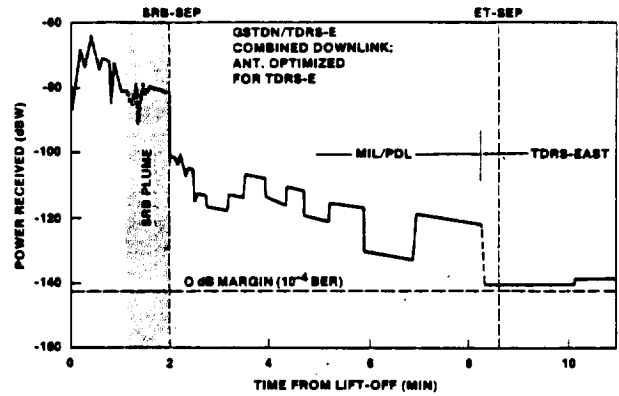


FIGURE 32.- ASCENT-PHASE GROUND STATION/SATELLITE COMPOSITE COVERAGE. PM SIGNAL STRENGTH, SHUTTLE TO MIL/PDL/TDRS EAST (TYPICAL).

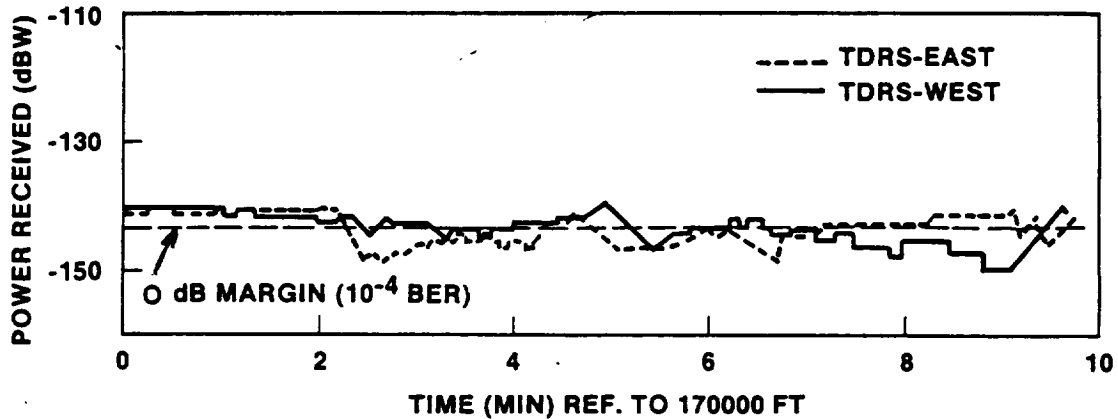


FIGURE 33.- DESCENT-PHASE PM SIGNAL STRENGTH, SHUTTLE TO TDRS EAST AND TDRS WEST (TYPICAL).

A communications "blackout" occurs during descent because of a plasma/shock sheath created by the Shuttle's high-speed entry into the Earth's atmosphere. The blackout has been extensively analyzed, but, because the sheath and its effects are not fully amenable to analytical methods, explicit analytical predictions should be treated only as preliminary estimates. Furthermore, results may be different for different missions since trajectory, velocity, and attitude all have an effect on sheath thickness, flow, and intensity. Also, since the thickness, flow, and intensity vary at different points around the vehicle, the amount of blackout likewise depends on which antenna is being used and the line-of-sight direction to the ground station (or TDRS).

Blackout for the Shuttle has been predicted to be only a "grayout." For example, the peak S-band signal attenuation is predicted to be on the order of 20 to 25 decibels compared to 100 decibels in the Apollo Program. The maximum effect is predicted to occur around 250 000 feet altitude or higher, decreasing to little or none by about 200 000 feet, which is before the Shuttle normally comes into view of descent-phase ground stations (typically approximately 180 000 feet). Hence, no blackout has been observed at these ground stations for missions to date. Because of the alternate landing at Northrup strip of STS-3, the Hawaii ground station had the Shuttle within line of sight and received signals briefly from about 290 000 feet to 250 000 feet, as did an advanced range instrumentation aircraft during STS-2 at about 210 000 feet. Although the data were not conclusive, there were indications that plasma attenuation on the order of 5 to 15 decibels was present during the STS-3 Hawaii pass.

REFERENCES

1. Viterbi, Andrews: Error Bounds for Convolutional Codes and Asymptotically Optimum Decoding Algorithms. IEEE Transactions On Information Theory, vol. IT-13, no. 2, Apr. 1967, pp. 260-269.
2. Abate, J. E.: Linear and Adaptive Delta Modulation. Proc. IEEE, vol. 55, Mar. 1967, pp. 298-308.
3. Shelling, Donald L.; et al.: Voice Encoding for Space Shuttle Using Adaptive Modulation. IEEE Transactions, vol. COM-26, Nov. 1978, pp. 1652-1659.
4. ESTL NASA Task 501 Orbiter/TDRSS S-Band Forward Link TDM System Verification Test Report. JSC-16689, Oct. 1980.
5. Batson, Bartus H.; Moorehead, Robert W.; et. al.: Simulation Results for the Viterbi Decoding Algorithm. NASA Technical Report, MSC-07027, July 1972.
6. Seyl, J. W.; and Kapell, M. H.: Applications of Spread Spectrum to the Shuttle Orbiter Communication System. Proceedings National Telecomm Conference, Dec. 1976.
7. Alem, Waddah K.: Spread Spectrum Acquisition and Tracking Performance for Shuttle Communication Links. IEEE Transactions, vol. COM-26, Nov. 1978, pp. 1689-1703.
8. Lindsey, W. C.: False Lock Phenomenon in the Shuttle S-Band PN Code Tracking Loop. LINCOM Corp. Report - TR-0382-1080 (NASA Contract NAS 9-16097), Mar. 1982.
9. Cubley, Dean H.: Antenna Development for the Space Shuttle Orbiter Vehicle. IEEE Transactions, vol. COM-26, Nov. 1978, pp. 1713-1722.
10. Wso, Kai T.; et al.: False Lock Performance of Shuttle Costas Loop Receivers. IEEE Transactions, vol. COM-26, Nov. 1978, pp. 1703-1712.
11. Novosad, Sidney; and Schmalz, Mark: An Automatic (Hands-off) Acquisition Technique for STS-1 S-Band PM Links. JSC-16981, Nov. 26, 1980.
12. Simon, Marvin K.: The Effects of Residual Carrier on Costas Loop Performance as Applied to the Space Shuttle Orbiter S-Band Link. IEEE Transactions on Communications, vol. COM-26, no. 11, Nov. 1978, pp. 1542-1548.
13. Seyl, J. W.; Smith, B. G.; and Batson, Bartus H.: Experimental Results for FSK Data Transmission System Using Discriminator Detection. Proceedings, National Telecomm Conference, Dec. 1976.
14. Loh, Yin-chung; and Porter, James A.: RF Coverage Analysis and Performance for Shuttle Communication Links. IEEE Transactions on Communications, vol. COM-26, no. 11, Nov. 1978, pp. 1745-1757.

SHUTTLE K_U-BAND COMMUNICATIONS/RADAR TECHNICAL CONCEPTS

J. W. Griffin, J. S. Kelley, A. W. Steiner, H. A. Vang,
and W. E. Zrubek
NASA Lyndon B. Johnson Space Center
Houston, Texas 77058

G. K. Huth
Axiomatix Corporation
Los Angeles, California 90045

CRITICAL ASPECTS
OF POOR QUALITY

ABSTRACT

Technical data on the Shuttle Orbiter K_U-band communications/radar system are presented. The emphasis is on the more challenging aspects of the system design and development. The technical problems encountered and the advancements made in solving them are discussed. The radar functions are presented first. Requirements and design/implementation approaches are discussed. Advanced features are explained, including Doppler measurement, frequency diversity, multiple pulse repetition frequencies and pulse widths, and multiple modes. The communications functions that are presented include advances made because of the requirements for multiple communications modes. Spread spectrum, quadrature phase shift keying (QPSK), variable bit rates, and other advanced techniques are discussed. Performance results and conclusions reached are outlined.

INTRODUCTION

Two important functions that the Orbiter must perform while orbiting the Earth are to detect and track other objects (targets) and to communicate with Earth via the Tracking and Data Relay Satellite (TDRS). Target tracking is required to support rendezvous operations; communications are needed to provide data, voice, and television transfer. By the time these program requirements were finalized, the Orbiter configuration had been set and the K_U-band system design had to be made compatible with it. As a result, the deployed assembly (DA) was mounted in the payload bay between the payload envelope and the payload bay doors (fig. 1). Since rendezvous target tracking is a short-term operation, it made possible the combining of the radar and communications functions in one system and thereby saved weight and cost and minimized impact to the Orbiter. The challenges and innovations in the K_U-band system are due in large part to the fact that the system had to meet two sets of complex and sometimes conflicting requirements.

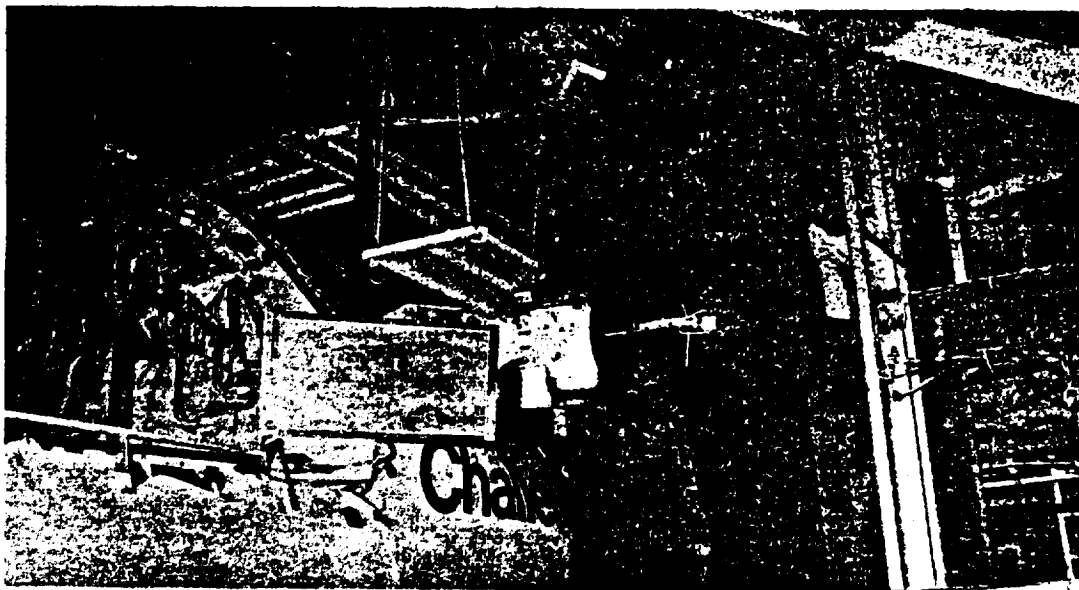


FIGURE 1.- DEPLOYED ASSEMBLY MOUNTED IN THE ORBITER PAYLOAD BAY.

Reproduced from
best available copy.



An overall diagram of the Ku-band system is shown in figure 2. Note that the system tracks targets and communicates, but not simultaneously. The block diagram shows that the system consists of the DA, electronic assembly 1 (EA-1), electronic assembly 2 (EA-2), and the signal processor assembly (SPA). Display, control, and electrical power interfaces are not shown.

The radar challenges/design approaches are presented first, followed by the communications discussion. Emphasis is given to technical advancements, and only limited details about the Ku-band system are presented. Further information can be found in the references given at the end of this paper.

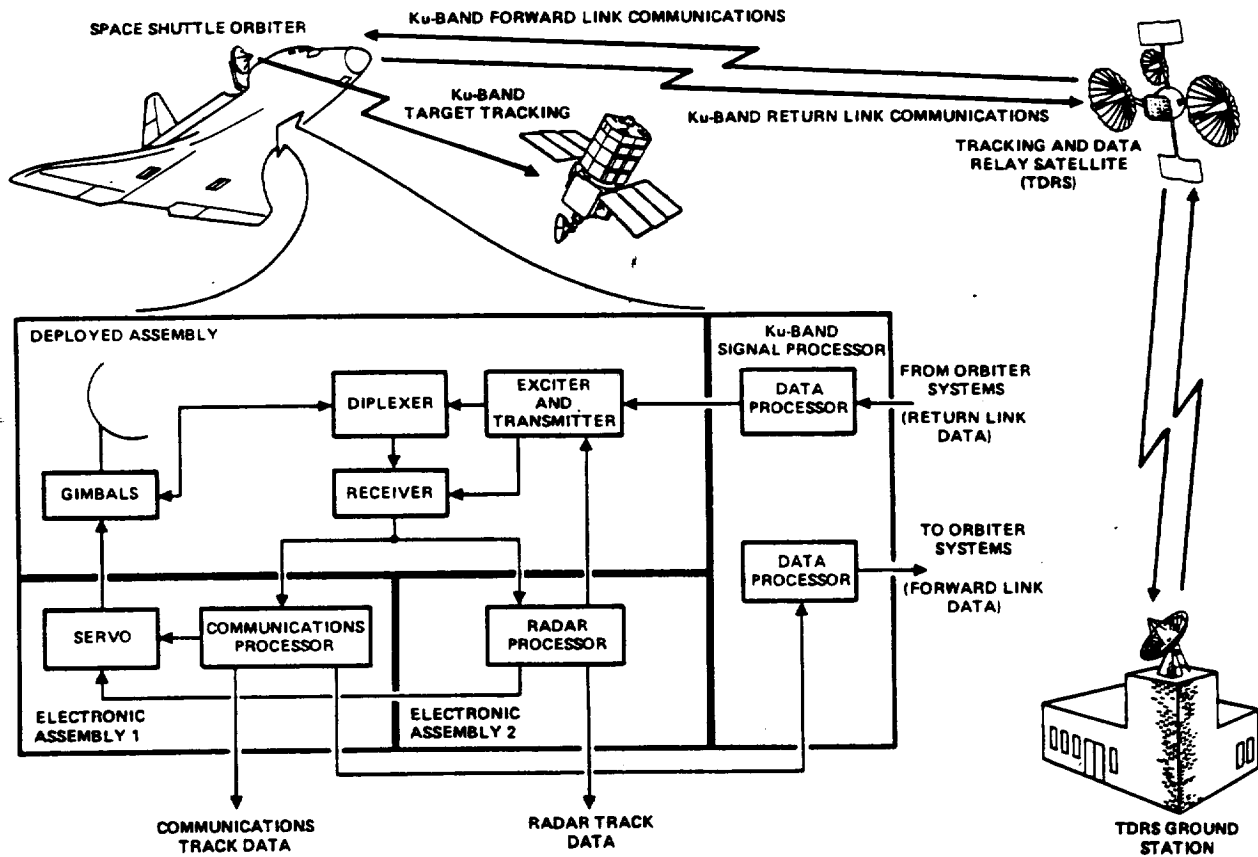


FIGURE 2.- ORBITER Ku-BAND RADAR/COMMUNICATIONS SYSTEM.

Ku-BAND SYSTEM DESIGN

GENERAL

Early in the Ku-band system design phase, it was determined that the functions common to radar and communications that could use common hardware were transmission, reception, and antenna control. The system, therefore, has in common a traveling-wave tube (TWT) transmitter, a receiver, an antenna, an antenna controller, and microwave components (refs. 1 and 2). The TWT transmitter provides both continuous-wave (CW) and pulsed operation. The TDRS dictates a forward link (Ku-band receive) frequency of 13.775 gigahertz and a return link (Ku-band transmit) frequency of 15.0034 gigahertz. The radar center frequency is 13.883 gigahertz, which allows common use of receiving circuits and the TWT.

The common components (receiver, transmitter, antenna and servo, and microwave components) must satisfy diverse requirements. Specific technical challenges resulting from these requirements were in the development of an efficient TWT; a narrow beam antenna with a lightweight, high-gain, paraboloidal reflector and monopulse feed; and a multifunction servo system to accomplish search, acquisition, and track during either radar or communications operation.

The requirements for high TWT efficiency at 15.0034 gigahertz CW and variable duty cycle pulse operation at 13.883 gigahertz resulted in the development of a permanent periodic magnet focused helix TWT with three stages of depressed collectors. The TWT provides 55 to 60 watts of radio-frequency (rf) power over the frequency band from 13.75 to 15.1 gigahertz with a gain of greater than 40 decibels. The electron gun is designed to provide a 65-milliampere beam at 7 kilovolts. A modulating anode is incorporated to switch the beam current on and off. A dual-pitch helix is used to provide optimum rf characteristics in both the radar and the communications bands with low distortion. A beam scraper is introduced between the electron gun and the input end of the helix to provide thermal protection for the helix in the case of power supply malfunction or electron gun arcing. The TWT is 14 inches long, 3.5 inches wide, and 2.7 inches high and weighs approximately 5.5 pounds.

The main technical challenges encountered in the development of the K_u -band antenna system were (1) minimum weight and restricted stowage volume, (2) space environment, (3) right-hand circular polarization for communications and linear polarization for radar, (4) angle search, acquisition, and tracking, and (5) minimum losses. These challenges were met in the design of the DA (refs. 2 and 3).

The DA consists of the antenna, a gimbal mechanism, and all electronics that are required to be near the antenna. Transmission line losses at this frequency made it necessary to locate all rf (K_u -band) functions near the antenna. Therefore, the DA contains all electronics to convert from intermediate frequency (i.f.) to rf and to amplify and transmit at the K_u -band frequency, along with the front end of the receiver, the low noise amplifier, and the down converter. The location selected for the DA led to two constraints on the antenna. First, the antenna depth was restricted to approximately 14 inches. Second, a boom and a deployment mechanism were required to obtain a maximum field of view. The stowage space constraint led to an edge gimbal attachment for the antenna dish. Therefore, the resonant frequency of the boom/gimbal/dish varies with pointing angle, as does the dish inertia. A switchable-bandwidth servo was implemented to achieve stability while meeting the radar search requirements.

The antenna is a prime-fed paraboloidal reflector and uses a five-element monopulse feed with a monopod feed support. The 36-inch parabola has a focal length to diameter (f/D) ratio of 0.28 and is constructed of epoxy-impregnated graphite tape formed over four main supporting ribs. The graphite construction provides excellent thermal characteristics and results in a very stable and lightweight antenna. The unique monopulse feed uses a crossed-probe-fed, dielectrically loaded waveguide horn as a sum channel element and four resonant slots as difference channel elements. The sum port transmits and receives either linear or right-hand circular polarization (selected by system mode of operation) and is independent of the monopulse tracking function. This five-feed approach provides minimum communications system signal loss since the monopulse comparator is only associated with the difference channel elements and is not in the transmit or sum channel signal paths. The monopulse comparator combines the difference channel signals to produce azimuth (ΔAZ) and elevation (ΔEL) error signals. These error signals are phase coded and time division multiplexed before they are added to the sum channel.

Another engineering challenge resulting from the location constraint was antenna sidelobe levels. Design of a short-focal-length antenna, with a focal-point feed to minimize weight on the gimbal, was required. The initial design consisted of a 4- by 4-inch feed, which included the monopulse bridge. The sidelobe levels were much too high, on the order of -17 decibels for circular polarization and -15 decibels for linear polarization. The monopulse bridge was moved and the feed was redesigned into a 2- by 2-inch package. This change resulted in sidelobe levels of about -21 decibels for circular polarization. Even these reduced sidelobe levels may not eliminate all acquisition difficulties.

The combination of boom length and deployment mechanism (one-axis turntable) had a significant impact on the angle servo system design. Resonant frequencies in the 8- and 12-hertz region severely limited the stable bandwidth of the servo. The first design was found to be unsatisfactory. The radar search requirements required a wide bandwidth, whereas stability indicated a narrow bandwidth. Other challenges surmounted in the development of the K_u -band servo system were (1) wide angular coverage, (2) adaptive response dependent on search, acquisition, or track function, (3) antenna scanning to provide coverage and sufficient time on target for detection, (4) multimode capability providing for designation by the general-purpose computer (GPC), manual slewing, scanning variable sectors at variable rates, operation as an autotrack system, inertial or body stabilization, and control by an internal system microprocessor, and (5) providing coordinate transformations between the antenna and the Orbiter coordinate axes.

To obtain the nearly 4π steradians of spatial coverage using a two-axis elevation over azimuth gimbal system, the servo provides rapid whiparound in azimuth whenever the elevation or azimuth mechanical limits are approached. These whiparounds must be accomplished in minimum time because spatial coverage for moving targets is lost whenever whiparound occurs.

A passive thermal design was implemented that is adequate for "beginning of life" surface conditions. The design includes silvered Teflon on parts of the DA. This surface is rather delicate and requires careful handling of the antenna assembly. A replacement schedule for the thermal surface will be developed as the system is used.

RADAR DESIGN

To perform the radar function, the K_U-band system is required to do the following.

1. Search for, detect, and track passive (nonaugmented) and active (transponder-augmented) targets
2. Measure and provide target data (range rate, range, angle rates, angles) to the Orbiter for use in rendezvous operations
3. Provide for signal flow to and from the Orbiter for displays and command/control

Table 1 summarizes the radar performance requirements. The main challenges arise from the angle rate and range rate accuracy requirements for the passive target case.

TABLE 1.- K_U-BAND RADAR REQUIREMENTS

Parameter	Passive target (1 m ² cross section)	Augmented target
Search, acquisition, track volume:		
Angle search, acquisition	±30°	±30°
Track	Orbiter obscuration	
Range	100 ft to 12 n. mi.	100 ft to 300 n. mi.
Probability of detection (FAR = 1/hr) ^a	0.99	0.99
Range accuracy, 3σ		80 ft or 1%
Velocity accuracy, 3σ		1 ft/sec
Angle accuracy, 3σ		8 mrad
Angle rate accuracy, 3σ		0.14 mrad/sec

^aFalse alarm rate.

The angle tracking servo is shown in figure 3. The servomechanism includes rate integrating gyros, gimbal torque motors, shaft encoders, a microprocessor, and other elements. The antenna position and motion is controlled by the Orbiter GPC, by the astronaut, or (when the servo loop is closed) by the target's relative motion. A spiral scan is used to find the target. When the loop is first closed, a type 2 transfer function with a short time constant is used to rapidly reduce the angle error. A switch to a longer time constant type 2 servo then provides the required angle rate and position accuracies. The servo time constants are switched as the range changes to meet the dynamics and accuracy requirements.

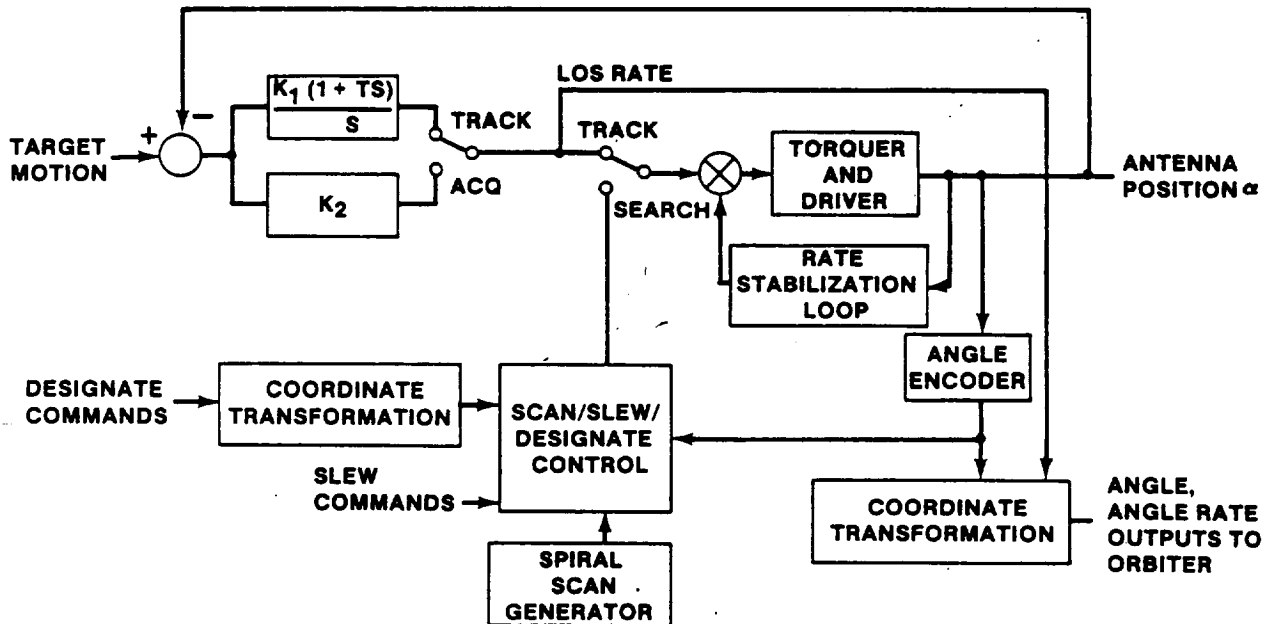


FIGURE 3.- ANGLE TRACKING SERVO BLOCK DIAGRAM.

The K_u -band radar uses a number of advanced techniques to obtain optimum performance (refs. 4 and 5). Frequency diversity (five frequencies) is used to obtain increased detection range. Pulse Doppler techniques provide range measurement and the required range rate accuracy. The transmitted pulse repetition frequency (PRF) and pulse width are changed with range to maximize detection probability and range rate accuracy. To allow for tracking at short ranges and reduce the probability of sidelobe acquisition, a TWT bypass mode is provided. Fourier transform filtering and logarithmic discriminant techniques are used to determine the Doppler frequency (range rate), the angle rate, the angle position, and the range.

RADAR TESTING

Various tests of the K_u -band radar have been conducted. Successful testing during STS-7 was performed using the SPAS-01 payload as a target. Detailed tests, using dynamic targets, are to be conducted at the NASA Lyndon B. Johnson Space Center (JSC) White Sands Test Facility (WSTF) later this year to obtain performance and error model data. Some early system data obtained by Hughes and Rockwell (K_u -band and Orbiter contractors) while tracking a helicopter are shown in figure 4. A reference system was not used; hence, the accuracy of such data remains to be determined by the WSTF tests.

COMMUNICATIONS DESIGN

To meet the communications requirements, the K_u -band system in the communications mode receives/transmits signals from/to the TDRS (table 2) (refs. 6 and 7). This capability provides a significant increase (relative to earlier missions) in the percent of time during which the Orbiter is in communications contact with the ground. This capability also meant that the K_u -band system design (ref. 2) had to meet a number of advanced requirements including those arising from (1) mutual acquisition of the narrow-beam K_u -band and TDRS antennas, (2) reception and processing of a spread-spectrum signal,

(3) processing, modulating, and transmitting several data sources, and (4) synchronizing with high-rate payload data routed over Orbiter cables.

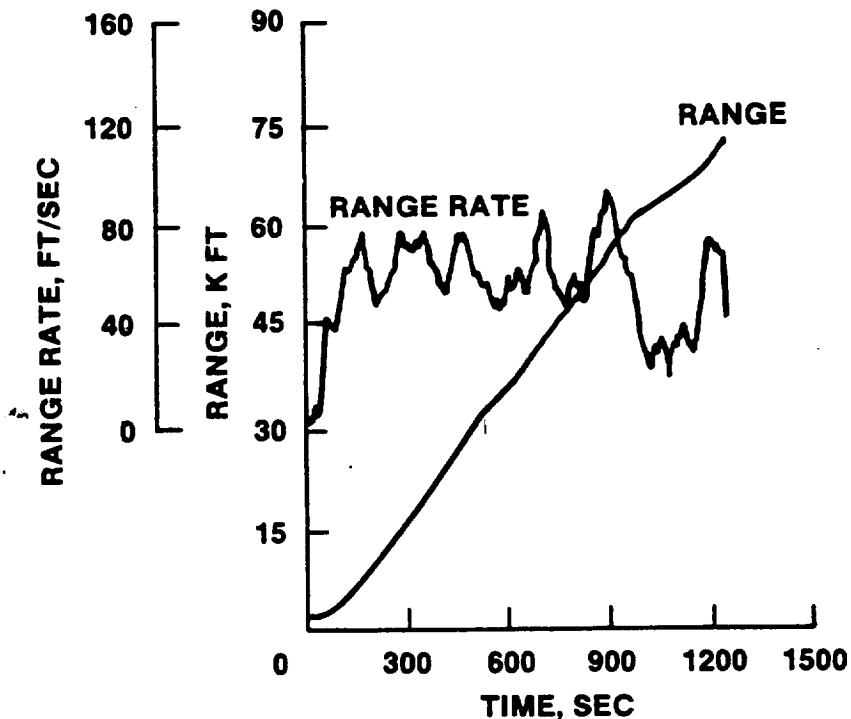


FIGURE 4.- RADAR TEST DATA, HELICOPTER TARGET.

The K_u -band forward link design was influenced by the need to be compatible with the S-band link (ref. 8) resulting in the bit rates shown in table 2. High antenna gains and the relatively low maximum bit rate of 216 kbps eased the design difficulties.

TDRS signal acquisition involves the following: (1) TDRS open-loop pointing at the Orbiter, (2) Orbiter acquiring the forward link by doing a spiral scan, (3) Orbiter transmitting the return link, and (4) TDRS acquiring the Orbiter return link and pointing with a maximum of 0.5 decibel pointing loss. Several aspects of this acquisition procedure proved challenging. First, because the TDRS first points its antenna at the Orbiter, there is a large dynamic signal amplitude range at the K_u -band system. Second, because of the uncertainty of K_u -band pointing at the TDRS, a spiral scan is required to find the TDRS. Finally, the dynamic range of the TDRS signal level, the Orbiter antenna sidelobe levels, and Orbiter monopulse tracking loop pull-in characteristics are such that the Orbiter antenna could stop in the scan before pointing its main beam at the TDRS. This problem has been solved by transmitted power control by the TDRS.

Another major design challenge involved bit synchronization of the high-rate payload data (refs. 9 and 10). The payload data rate can vary from 2 to 50 Mbps and can have significant data asymmetry (ref. 11). In addition, the Orbiter cables from the payload to the K_u -band system introduce risetime degradation and amplitude modulation (ref. 12). The first K_u -band interface circuit was found to have a range of clock/data phase offsets and to make unstable bit detections at high data rates. A redesign was also found to have inadequate margins for bit detection. Finally, an adaptive threshold bit synchronizer was designed and extensively analyzed to provide adequate performance margins with respect to clock/data phase offset, amplitude, transition time, and data jitter.

Table 2(b) shows that the return link communications design is more complex than the forward link. To transmit TV signals (Mode 2), frequency modulation (FM) was selected because of its maturity relative to digital techniques. To allow simultaneous transmission of TV and two channels of lower rate digital data, the TV signal frequency modulates at baseband, and the digital data modulate a subcarrier using unbalanced quadrature phase shift keying (UQPSK). Alternatives considered but not used include time division multiplexing (TDM) and use of two subcarriers. The alternatives involved complexity (TDM of variable bit rates) and large bandwidths/intermodulation products with two subcarriers. The selected UQPSK technique uses a subcarrier frequency of 8.5 megahertz.

TABLE 2.- K_U-BAND COMMUNICATIONS MODES AND CHANNELS

(a) Forward link (ground to Orbiter, 13.775 GHz)

Mode	Modulation	Data		
1	Bi-phase-L	Ch. 1	Voice 1	32 kbps
			Voice 2	32 kbps
			Command	6.4 kbps
			Sync	1.6 kbps
				<u>72 kbps</u>
		Ch. 2	Text/graphics	128 kbps
			Sync	16 kbps
				<u>144 kbps</u>
2	Bi-phase-L		Voice 1	32 kbps
			Voice 2	32 kbps
			Command	6.4 kbps
			Sync	1.6 kbps
				<u>72 kbps</u>

(b) Return link (Orbiter to TDRS, 15.0034 GHz)

Mode	Modulation	Data		
1	Unbalanced QPSK	Ch. 1	Voice 1	32 kbps
			Voice 2	32 kbps
			TLM	128 kbps
				<u>192 kbps</u>
		Ch. 2 One of the following:		
		A. P/L digital data, 16 kbps to 2 Mbps		
		B. P/L recorder playback, 25.5 kbps to 1024 kbps		
		C. OPS recorder playback, 60 kbps to 1024 kbps		
		D. Detached payload bent-pipe data, 16 kbps to 2 Mbps		
		Ch. 3 Attached P/L digital data (realtime or playback, 2 Mbps to 50 Mbps)		
2	High modulation index FM	Ch. 1 - Same as mode 1		
		Ch. 2 - Same as mode 1		
		Ch. 3 - One of the following:		
		A. Television composite video, dc to 4.5 MHz		
		B. Attached P/L analog data, dc to 4.5 MHz		
		C. Detached P/L bent-pipe analog data, dc to 4.5 MHz		

Mode 1 includes the high bit rate payload data. For this mode, it was desirable to use the same UQPSK-modulated subcarrier for the operational data and the low-rate payload data or digital recorder data. An innovative signal design was developed (ref. 13) to combine the high-rate payload data with the UQPSK-modulated subcarrier. The phase-multiplexing technique used is applicable to five channels or less and is a hybrid approach which has some of the features of both quadrature modulation and the interplex approach (ref. 14) used for deep-space communication.

An additional signal design consideration for the high-rate data in Mode 1 was signal power required to transmit 50 Mbps from the Orbiter through the TDRS. Error-correction coding was investigated, but convolutional coding was chosen because the decoding algorithms (sequential and Viterbi) provide significant coding gains at the required bit-error probability of 10^{-5} and could be implemented at 50 Mbps with moderate hardware (ref. 15). As a result of evaluating the convolutional decoding approaches, five multiplexed 10-Mbps Viterbi decoders were chosen. This approach provided the best possible performance (5.1 decibels coding gain at probability of bit error of 10^{-5}) without

severe penalties in cost, complexity, and reliability. In addition, the system degrades gracefully (a coding gain of 2.7 decibels is available at a probability of error of 10^{-2}), the Orbiter encoder was simple to implement, and ground-based decoders were available and could be combined in a straightforward manner. It appears reasonable to extend the parallel 10-Mbps Viterbi decoder concept to systems requiring operation at data rates well in excess of 100 Mbps, although reliability becomes a concern as the number of parallel decoders becomes large. In fact, this parallel approach was expanded and adopted as the TDRS System (TDRSS) standard.

COMMUNICATIONS PERFORMANCE

Various tests of the K_U -band communications function have been conducted by the contractors at JSC and at the NASA John F. Kennedy Space Center. A sample test result, obtained at the JSC Electronic Systems Test Laboratory (refs. 16 and 17), is shown in figure 5.

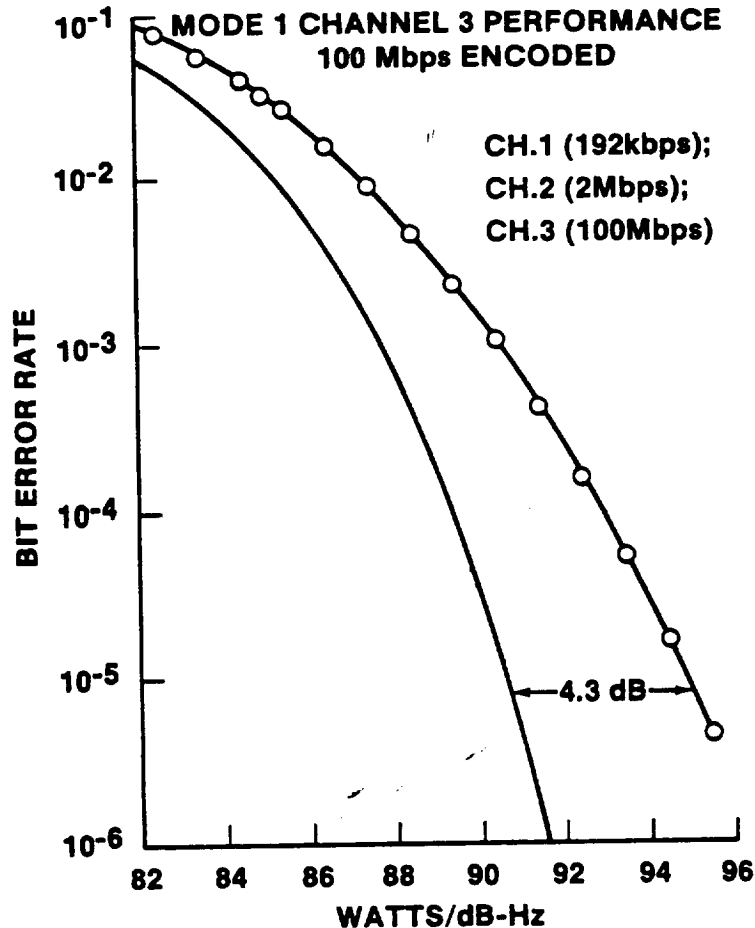


FIGURE 5.- SAMPLE K_U -BAND COMMUNICATIONS TEST RESULTS.

The first flight use of the K_U -band system was on STS-7 in June 1983. Communications performance was not tested because the TDRS was not in position. It is expected that the communications functions will be checked out on STS-8.

CONCLUSIONS

Even though complete and detailed flight performance of the K_U -band system remains to be demonstrated, some concluding remarks can be made. Development of a combined radar and communications system is feasible under the proper conditions. Weight, volume, and antenna locations can be

reduced when the functions are combined. In such a case, however, both functions cannot be performed at the same time. One disadvantage of combining is that development and test activities for the two functions are interdependent. Thus, a design change or a problem in one of the functions may affect the other function and slow its progress. The more complex the system, the more likely it is that difficulties will be encountered. Also, testing of a more complex system is more challenging and requires more time because the functions cannot be tested in parallel unless more test units are built. Factors like these should all be considered and weighed in implementing future radar and communications requirements.

The development of the K_u -band system involved advances in both radar and communications. It is expected that the system will operate as specified. However, the system is complex, and performance anomalies may occur. Nevertheless, it is expected that the K_u -band system will, for many years, fulfill its role in the Shuttle Orbiter mission.

REFERENCES

1. Carrier, Louis M.; and Pope, Warren S.: An Overview of the Space Shuttle Orbiter Communication and Tracking System. IEEE Transactions on Communications, vol. COM-26, no. 11, Nov. 1978, pp. 1494-1506.
2. Cager, Ralph H.; LaFlame, David T.; and Parode, Lowell C.: Orbiter Ku-Band Integrated Radar and Communications Subsystem. IEEE Transactions on Communications, vol. COM-26, no. 11, Nov. 1978, pp. 1604-1619.
3. Cubley, H. Dean; and Ellis, Haynes: Antenna Development for the Space Shuttle Orbiter Vehicle. IEEE Transactions on Communications, vol. COM-26, no. 11, Nov. 1978, pp. 1713-1722.
4. Iglehart, S. C.: The Space Shuttle Ku-Band Rendezvous Radar. Proceedings 1980 National Telecommunications Conference, Houston, Tex., Nov. 30 to Dec. 4, 1980, pp. 66.1.1-66.1.5.
5. Alem, Waddah K.; and Weber, Charles L.: Performance Analysis of Pulse Doppler Digital Radars with Application to the Shuttle Ku-Band System. IEEE Transactions on Communications, vol. COM-26, no. 11, Nov. 1978, pp. 1620-1635.
6. Schwartz, John J.; and Feinberg, Eugene J.: STON in the TDRSS and Shuttle Era. IEEE Transactions on Communications, vol. COM-26, no. 11, Nov. 1978, pp. 1506-1513.
7. Spearing, R. E.; Schwartz, J. J.; and Herr, D. W.: Shuttle Unique TDRS Communications. Paper presented at Space Shuttle Program Technical Conference, Houston, Tex., June 28-30, 1983.
8. Seyl, J. W.; Seibert, W. W.; Porter, J. A.; et al.: Shuttle S-Band Communications Technical Concepts. Paper presented at Space Shuttle Program Technical Conference, Houston, Tex., June 28-30, 1983.
9. Teasdale, W. E.: Payloads and Data Handling Accommodations. IEEE Transactions on Communications, vol. COM-26, no. 11, Nov. 1978, pp. 1557-1567.
10. Batson, Bartus H.; Teasdale, William E.; Pawlowski, James F.; and Schmidt, Oron L.: Shuttle Payload S-Band Communications System. Paper presented at Space Shuttle Program Technical Conference, Houston, Tex., June 28-30, 1983.
11. Simon, Marvin K.; Tu, Kwei; and Batson, Bartus H.: Effects of Data Asymmetry on Shuttle Ku-Band Communications Link Performance. IEEE Transactions on Communications, vol. COM-26, no. 11, Nov. 1978, pp. 1639-1651.
12. Vang, H. A.; and Schadelbauer, S.: Risettime Distortion of Shuttle Ku-Band Payload 50 Mbps Data Due to Coaxial Cable Skin Effects. Proceedings 1980 National Telecommunications Conference, Houston, Tex., Nov. 30 to Dec. 4, 1980, pp. 66.3.1-66.3.5.
13. Batson, B. H.; Huth, G. K.; and Udalov, S.: Phase Multiplexing for Three-Channel Data Transmission. Proceedings 1976 National Telecommunications Conference, Dallas, Tex., Nov. 29 to Dec. 1, 1976, pp. 21.6-1-21.6-7.
14. Butman, S.; and Timov, U.: Interplex - An Efficient PSK/PM Telemetry System. IEEE Transactions on Communications, vol. COM-20, no. 3, June 1972, pp. 415-419.

15. Batson, B. H.; and Huth, G. K.: Convolutional Coding at 50 Mbps for the Shuttle Ku-Band Return Link. Proceedings 1976 International Telemetry Conference, Los Angeles, Calif., Sept. 28-30, 1976, pp. 175-183.
16. Stoker, C. Jack; and Bromley, Linda K.: Electronic Systems Test Laboratory Testing of Shuttle Communications Systems. Paper presented at Space Shuttle Program Technical Conference, Houston, Tex., June 28-30, 1983.
17. Seyl, Jack W.; and Travis, Arthur D.: Shuttle Communication Systems Compatibility and Performance Testing. IEEE Transactions on Communications, vol. COM-26, no. 11, Nov. 1978, pp. 1732-1744.

SHUTTLE PAYLOAD S-BAND COMMUNICATIONS SYSTEM

Dr. Bartus H. Batson, William E. Teasdale, Dr. James F. Pawlowski, and Oron L. Schmidt
NASA Lyndon B. Johnson Space Center
Houston, Texas

ABSTRACT

The Shuttle payload S-band communications system design, operational capabilities, and performance are described in detail in this paper. System design requirements, overall system configuration and operation, and laboratory/flight test results are presented.

Payload communications requirements development is discussed in terms of evolution of requirements as well as the resulting technical challenges encountered in meeting the initial requirements. Initial design approaches are described along with cost-saving initiatives that subsequently had to be made. The resulting system implementation that was finally adopted is presented along with a functional description of the system operation. A description of system test results, problems encountered, how the problems were solved, and the system flight experience to date is presented. Finally, a summary of the advancements made and the lessons learned is discussed.

INTRODUCTION

In the Shuttle payload S-band communications system, one Earth-orbiting satellite monitors and controls various functions of another Earth-orbiting satellite. Previously, this capability resided only in large Earth stations specifically implemented to monitor and control various manned and unmanned satellites.

Since a wide variety of satellites will be deployed and/or retrieved by the Shuttle, a major challenge was to engineer a communications system that could (1) generate commands having payload-compatible formats, data rates, and carrier frequencies and (2) monitor telemetry signals having various standard formats, data rates, subcarrier frequencies, and carrier frequencies. In addition, it was determined that to keep the implementation complexity within the realm of possibility, the system should provide the capability to relay nonstandard telemetry (via the Orbiter K_u -band communications system) to the ground without onboard subcarrier demodulation and bit synchronization. Similarly, it was decided that the system should be capable of accommodating nonstandard commands generated onboard the Orbiter by payload-unique processors.

This paper describes the early activities that resulted in an initial definition of the detailed functional and performance requirements of the Shuttle payload S-band communications system. It also describes the design concept developed to satisfy the initial requirements and discusses a reduced set of requirements which was later developed to simplify the implementation. The simplified implementation approach is also described in some detail.

The results of system-level testing in the Electronic Systems Test Laboratory (ESTL) are summarized, with emphasis on the problem areas encountered and on the solutions. The flight experience on the S-band payload communications system (PCM) is also discussed. Finally, the advancements made in the S-band payload communications system and some of the lessons learned by the NASA and contractor engineers directly involved in its development are briefly addressed.

INITIAL PAYLOAD COMMUNICATIONS REQUIREMENTS

The Shuttle payload S-band communications system requirements evolved over a period of several years during the mid 1970's through a series of meetings with various government and commercial organizations engaged in developing free-flying satellites for the 1980's. A set of general requirements directed by Level I program operational requirements concerning payload accommodations in the areas of safety, on-orbit payload deployment, checkout and retrieval mandated implementation of a short range payload radiofrequency (RF) communications system on the Orbiter. In the summer of 1974, an extensive meeting was held at the NASA Johnson Space Center (JSC) with representatives from many prospective Shuttle payload organizations. They were invited to make suggestions on how the Shuttle could best service their specific payloads (satellites). Their main points of interest were in terms of data and command rates, formats, modulation schemes, and carrier and subcarrier frequencies. The inputs received were quite varied. It soon became apparent that the Shuttle payload communications system would have to be designed as an orbital S-band ground station (indeed, three ground stations) that would be able to support Ground Space Flight Tracking and Data Network (GSTDN), Deep Space Network (DSN), and Tracking and Data Relay Satellite System (TDRSS) compatible payloads (satellites). In

TABLE 1.- SHUTTLE PAYLOAD S-BAND COMMUNICATIONS SYSTEM
(INITIAL REQUIREMENTS)

Requirement	Return link (telemetry)	Forward link (commands)
Carrier modulation	PM	PM
Modulation index	1.0 rad	1.0 rad
Data rates	16, 8, 4, 2, 1 kbps 256, 128, 64, 32, 16, 8, 4, 2, 1 bps	2000, 1000, 500, 250, 125, $\frac{125}{2}$, $\frac{125}{4}$, $\frac{125}{8}$, $\frac{125}{16}$, $\frac{125}{32}$, $\frac{125}{64}$, $\frac{125}{128}$ bps
Subcarriers	1.7 and 1.024 MHz 512, 256, 128, 64, 32, " 16, 8, 4, 2, 1 kHz	16 kHz
Subcarrier modulation	All subcarriers PSK except 1.7 MHz - IRIG FM/FM	PSK
PCM formats	Biphase L, M, S NRZ L, M, S	Biphase L, M, S NRZ L, M, S
Special processing	Spread spectrum demodulation ^a	Spread spectrum demodulation ^a

^aRequired for TDRS-compatible payloads.

TABLE 2.- SHUTTLE PAYLOAD S-BAND COMMUNICATION SYSTEM RF CHANNELIZATION
INITIAL REQUIREMENTS

Requirement	Frequency range, MHz	No. of channels	Channel spacing, kHz
<u>GSTDN/TDRS compatible payloads</u>			
Orbiter transmit	2025.833 to 2118.7	808	115
Orbiter receive	2200 to 2300.875	808	125
<u>DSN compatible payloads</u>			
Orbiter transmit	2110.243 to 2119.792	29	241.049
Orbiter receive	2290.185 to 2299.814	27	370.37

addition, because the Shuttle would act like a ground station as far as its payloads were concerned and would simultaneously communicate with some of the same ground station elements that employed the same signal characteristics as the Shuttle, a technique was needed to minimize the expected interference between S-band links.

The initial system requirements and modulation characteristics from this meeting and from subsequent interaction between JSC and the payload community resulted in adoption of the characteristics shown in table 1 and the RF channelization shown in table 2 to support GSTDN, TDRSS, and DSN compatible satellites. These initial requirements approved by the Shuttle Program were intended to accommo-

date virtually every conceivable payload RF system implementation that might be fabricated to fly against any one of the three existing ground networks (TDRSS, GSTDN, and DSN).

The RF communication accommodation for deployable payloads was again driven by the top-level operational requirement to provide onboard, real-time, command control, and monitoring of payloads to support deployment, checkout, and retrieval activities.

INITIAL DESIGN APPROACH

The design concept initially conceived to provide the system capabilities outlined above centered around fabrication of two line replaceable units (LRU's) and one flush-mounted S-band antenna located on top of the Orbiter just forward of the payload bay opening. The two LRU's consisted of a highly flexible multichannel S-band transponder called the payload interrogator (PI) and a many-faceted, multifunction, extremely complex payload signal processor (PSP). Figure 1 illustrates the functional configuration of the payload S-band communications system as it interfaces with a typical deployed payload.

The initial system requirements resulted in a number of stringent system design drivers for the two LRU's. Specifically, the payload interrogator would be required to (1) generate more than 800 pairs of transmit and receive frequencies, (2) provide multiple modulation/demodulation schemes, and (3) perform spectrum spreading and despreading for TDRSS compatible payloads. The payload signal processor would have to (1) generate and modulate many command subcarrier frequencies, (2) detect and demodulate many telemetry subcarrier frequencies, (3) generate and process six pulse-code modulated (PCM) formats, (4) bit synchronize on over 100 possible bit rates, and (5) perform frame synchronization for many formats.

To perform all these functions on the ground would require enormous complexity (the equivalent of three ground stations in one); to try to perform all of these functions in space was quickly recognized as too costly and impractical. Technically, the challenges could have been met, given an unlimited source of funding and sufficient time to develop and package the flight hardware. However, with the funding problems the Shuttle program was beginning to encounter at that time across the board, the need to greatly simplify the payload S-band communications system was recognized.

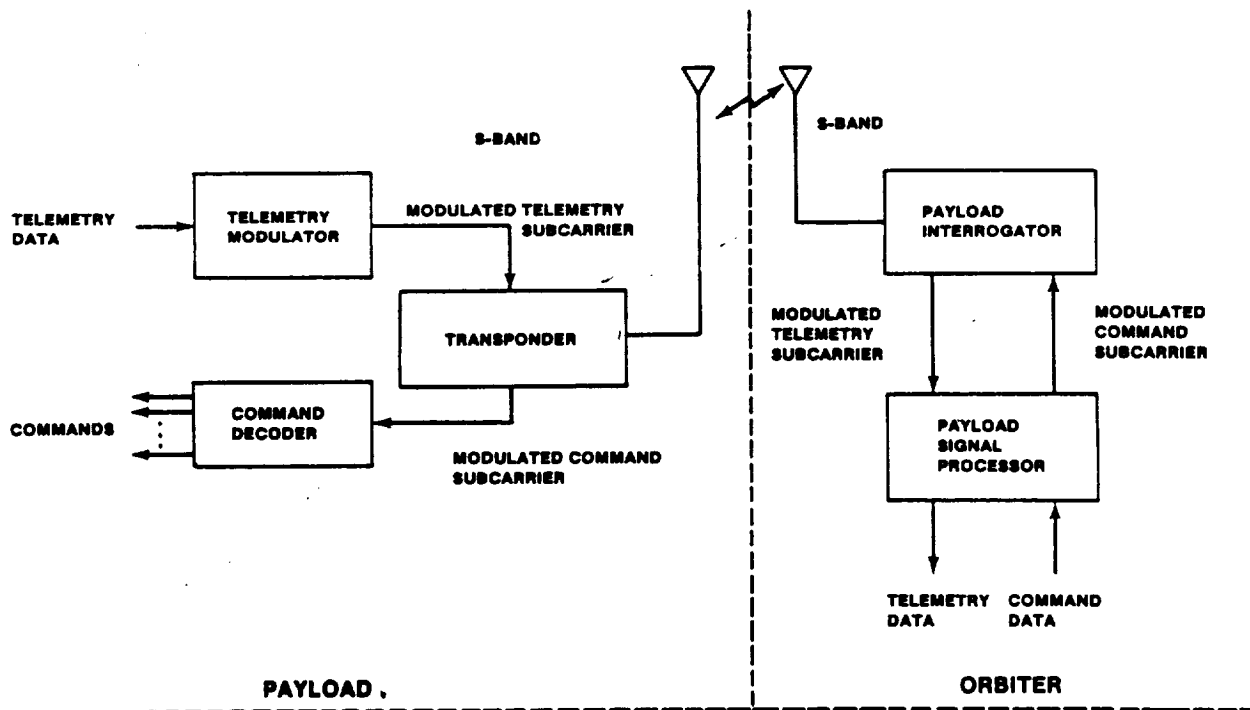


FIGURE 1.- ORBITER PAYLOAD S-BAND COMMUNICATIONS SYSTEM FUNCTIONAL CONFIGURATION (INITIAL).

The Shuttle program management then initiated a review of payload RF communications requirements along with technical factfinding of various system simplification options. This series of reviews and technical assessments resulted in the program management decision to make the following changes.

1. Delete the forward and return link spread spectrum capability.
2. Provide normal baseband signal processing functions for only a limited number of modulation schemes, subcarriers, bit rates, PCM formats, etc. (i.e., a set of "standard" signals).
3. Implement a transparent throughput "bent-pipe" capability to relay "nonstandard" payload signals to the ground via the Orbiter K_u-band link for ground monitoring.

It was decided that these changes would result in greatly simplified Orbiter hardware and significant reductions in cost, weight, and development risk to the Orbiter. The total savings to the program as a result of these changes was estimated at the time to be approximately \$20 million.

Tables 3 and 4 show the revised set of payload S-band communications system characteristics based on the updated system requirements and adopted standard versus nonstandard payload concept. The RF channelization reflected in table 3 was unchanged from the initial concept. The decision was made to pursue implementation of the total GSTDN/TDRSS/DSN complement of operating frequencies using a frequency synthesizer approach. Table 4 shows the revised command and telemetry signal processing characteristics for the standard payload.

TABLE 3.- SHUTTLE PAYLOAD S-BAND COMMUNICATION SYSTEM RF CHANNELIZATION

Requirement	Frequency, MHz	No. of channels	Channel spacing, kHz
GSTDN/TDRS			
Transmit	2025.833 to 2117.916	801	115
Receive	2200 to 2300	801	125
DSN			
Transmit	2110.243 to 2119.792	29	241.049
Receive	2290.185 to 2299.814	27	370.37

TABLE 4.- SHUTTLE PAYLOAD S-BAND COMMUNICATIONS SYSTEM STANDARD COMMAND AND TELEMETRY REQUIREMENTS

Requirement	Return link (telemetry)	Forward link (commands)
Carrier modulation	PM	PM
Modulation index	1.0 rad	1.0 rad
Subcarrier frequency	1.024 MHz	16 kHz
Subcarrier modulation	PSK	PSK
Data rates	16, 8, 4, 2, 1 kbps	2000, 1000, 500, 250, 125, $\frac{125}{2}$, $\frac{125}{4}$, $\frac{125}{8}$, $\frac{125}{16}$ bps
PCM formats	NRZ L, M, S Biphase L, M, S	NRZ L, M, S

IMPLEMENTATION APPROACH SELECTED

The simplified Shuttle payload RF communications concept on which the final implementation approach was based called for a standard interface capability to provide normal baseband processing functions for a defined set of standard signals and nonstandard interface capability to provide a telemetry throughput to the ground via a transparent channel (bent pipe) or to the Orbiter aft flight deck payload station. Functionally, the nonstandard mode would be accomplished by having the payload interrogator strip out a baseband (or intermediate frequency (IF)) unprocessed version of the nonstandard signal and route it to the ground via the K_u -band TDRSS link, time shared with television (FM mode 2), or by routing the signal to a payload-supplied unique signal processor located in the aft flight deck payload station.

Simplification of the initial requirements and implementation concept did not change the basic LRU concept shown in figure 1; however, it did allow a great reduction of internal LRU complexity. The payload interrogator complexity was reduced by eliminating the spread spectrum capability. The PSP complexity was reduced by eliminating several modulation scheme, subcarrier, data rate, command rate, and PCM format options and the attached payload (hardline) telemetry capability. This capability already existed in the payload data interleaver (PDI) design.

Figure 2 shows the functional configuration of the final payload S-band communications system implementation, including the added interfaces with the K_u -band signal processor and the aft flight deck payload station. Figure 2 also shows LRU redundancy. Figure 3 illustrates how the final system configuration interfaces with the overall Orbiter avionics system. In figure 2, either nonstandard or standard telemetry formats can be sent directly to ground (unprocessed) via the K_u -band system in the bent-pipe mode. Nonstandard payload telemetry, which must be processed onboard for display, recording, or monitoring, is routed from the PI to the payload station distribution panel where it is sent to a payload-supplied unique signal processor. This same processor may also be used to generate nonstandard command formats and output them to the PI for transmission to the detached payload. Standard telemetry and command formats listed in table 4 are processed onboard by the PSP as a standard Shuttle service.

PAYLOAD INTERROGATOR

The PI provides the RF communication link between the Orbiter and detached payloads. For communications with the standard payloads, the PI operates in conjunction with the PSP.

During most nonstandard missions, the PI is interfaced with a Payload Station Distribution Panel (PSDP) unique signal processor. Nonstandard data received by the PI can also be routed to the K_u -

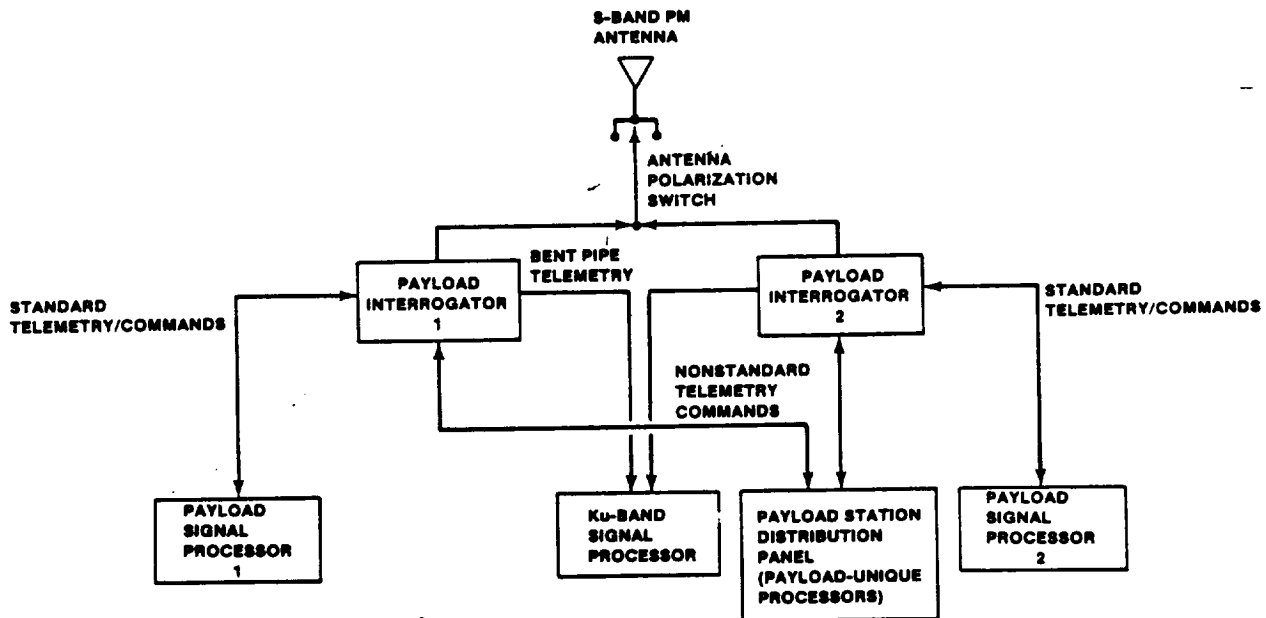


FIGURE 2.- ORBITER PAYLOAD S-BAND COMMUNICATIONS SYSTEM FUNCTIONAL CONFIGURATION (FINAL).

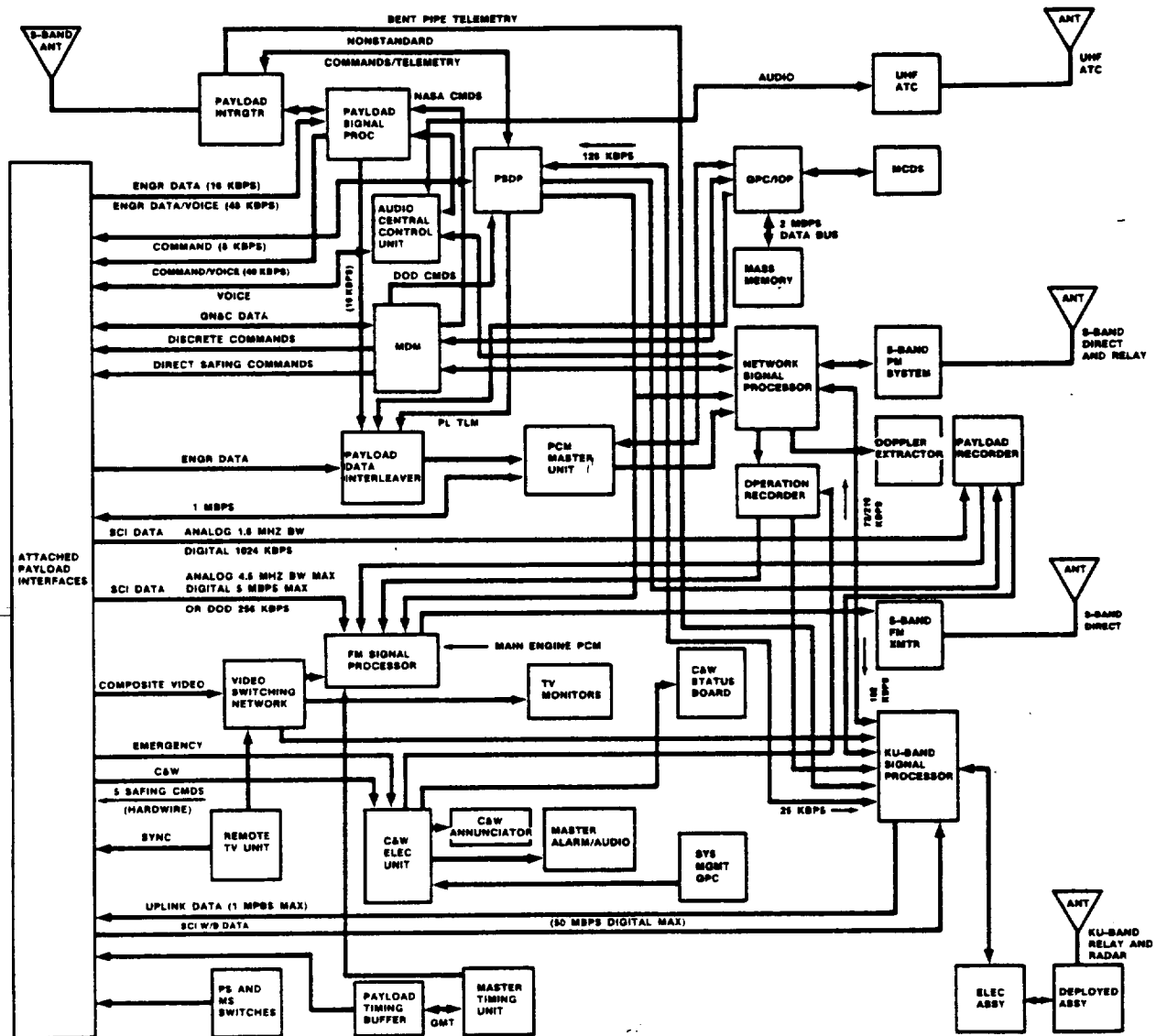


FIGURE 3.- SHUTTLE ORBITER AVIONICS SYSTEM.

band signal processor, where it is processed for transmission to the ground via the Shuttle K_U -band/TDRSS link (bent pipe).

Simultaneous RF transmission and reception is the primary mode of PI operation with both standard and nonstandard payloads. The Orbiter-to-payload link carries the commands, while the payload-to-Orbiter link communicates the telemetry data. In addition to this duplex operation, the PI provides for "transmit only" and "receive only" modes of communication with some payloads.

Figure 4 shows the functional block diagram for the PI. The antenna connects to an input/output RF port which is common to the receiver and the transmitter of the PI unit. A dual triplexer is used because of a requirement to operate the PI simultaneously with the Shuttle/ground S-band network transponder, which radiates and receives on the same frequency bands. The Shuttle S-band network transponder emits a signal at either 2217.5 or 2287.5 megahertz. Both frequencies fall directly into the PI receive band of 2200 to 2300 megahertz. Conversely, the payload transmitter, operating in the 2025- to 2120-megahertz band, can interfere with uplink signal reception by the S-band network transponder receiver. Therefore, by use of the triplexer and by simultaneously operating the PI and network transponder in the mutually exclusive subbands, the interference problem is effectively eliminated.

In addition to the problem of potential interference due to the mutual, simultaneous operation of the S-band payload and S-band network communications system, there is also the problem of an extremely large range of power levels that must be accommodated. When detached payloads are in the immediate vicinity of the Orbiter, excessive RF power levels may impinge on the interrogator antenna. Thus, the RF preamplifier of the receiver is protected by a combination of sensitivity control attenuators and a diode breakdown limiter. The output of the preamplifier is applied to the first mixer where it is converted to the first IF for amplification and level control. The first local oscillator frequency, f_{L01} , is tunable and its frequency corresponds with the desired PI receive channel frequency. Except for channel selection, however, f_{L01} is fixed. Consequently, any unspecified frequency difference between the received payload signal and f_{L01} will appear within the first IF amplifier and at the input to the second mixer.

The receiver frequency and phase tracking loop begins at the second mixer. As shown in figure 4, the output of the first IF amplifier is down-converted to the second IF as a result of mixing with a variable second LO frequency, f_{L02} . The portion of the second IF which involves only the carrier tracking function is narrowband, passing the received signal residual carrier component and excluding the bulk of the sideband frequencies. Demodulation to baseband of the second IF signal is accomplished by mixing with a reference frequency, f_R . The output of the tracking phase detector, after proper filtering, is applied to the control terminals of a voltage controlled oscillator (VCO) which provides the second local oscillator signal, thereby closing the tracking loop. Thus, when phase track is established, f_{L02} follows frequency changes of the received payload signal.

For the purpose of frequency acquisition, the f_{L02} may be swept over a ± 50 -kilohertz uncertainty region. Sweep is terminated when the output of the coherent amplitude detector (CAD) exceeds a present threshold, indicating that the carrier tracking loop has attained lock. The output of the CAD also provides the automatic gain control (AGC) to the first IF amplifier. To accommodate payload-to-Orbiter received signal level changes caused by range variation from a few feet to 10 nautical miles, 110 decibels of AGC is provided in the first intermediate frequency amplifier (IFA).

A wideband phase detector is used to demodulate the telemetry signals from the carrier. The output of this detector is filtered, envelope level controlled, and buffered for delivery to the PSP, PSDP, and K_u -band signal processor units.

The PI receiver frequency synthesizer provides the tunable first LO frequency and the corresponding exciter frequency to the transmitter synthesizer. It also delivers a reference signal to the transmitter phase modulator. Baseband standard or nonstandard command signals modulate the phase of this reference signal, which is in turn supplied to the transmitter synthesizer where it is upconverted to the transmit frequency and applied to the power amplifiers.

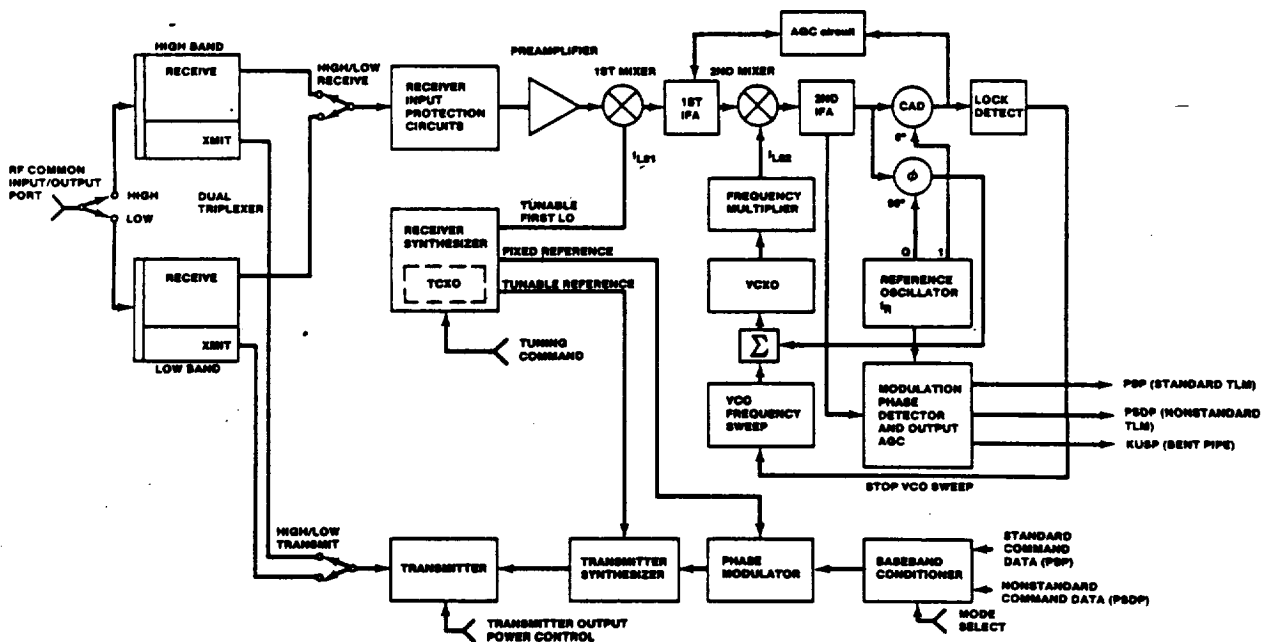


FIGURE 4.- PAYLOAD INTERROGATOR FUNCTIONAL BLOCK DIAGRAM.

Depending on the operating band selected, transmitter output is applied to either the high- or low-band triplexer. To compensate for varying distances to payloads, each transmitter has three selectable output power levels (5 to 10 dBm, 28 to 33 dBm, and 38 to 42 dBm).

PAYLOAD SIGNAL PROCESSOR

The payload signal processor (PSP) (1) modulates standard payload commands onto a 16-kilohertz sinusoidal subcarrier and delivers the resultant signal to the PI and to the attached payload umbilical, (2) demodulates the payload telemetry data from the 1.024-megahertz subcarrier signal provided by the PI, and (3) performs bit and frame synchronization of demodulated data and delivers these data and its clock to the payload data interleaver.

The PSP also transmits status messages to the Orbiter's general-purpose computers (GPC's). The status messages allow the GPC's to control and configure the PSP and validate command messages before transmission.

The functional block diagram for the PSP is shown in figure 5. The PSP configuration and payload command data are input to the PSP via a bidirectional serial interface. Transfer of data in either direction is initiated by discrete control signals. Data words 20 bits in length (16 information, 1 parity, 3 synchronization) are transferred across the bidirectional interface at a burst rate of 1 Mbps, and the serial words received by the PSP are applied to word validation logic which examines their structure. Failure of the incoming message to pass a validation test results in a request for a repeat of the message from the GPC.

Command data are further processed and validated as to content and the number of command words. The function of the command buffers is to perform data rate conversion from the Mbps bursts to one of the selected standard command rates. Command rate and format are specified through the configuration message control subunit.

From the message buffers, the command bits are fed via the idle pattern selector and generator to the subcarrier biphase modulator. The idle pattern, which often consists of alternating "ones" and "zeros," precedes the actual command word and is usually also transmitted in lieu of command messages. Subcarrier modulation is biphase non-return-to-zero (NRZ) only.

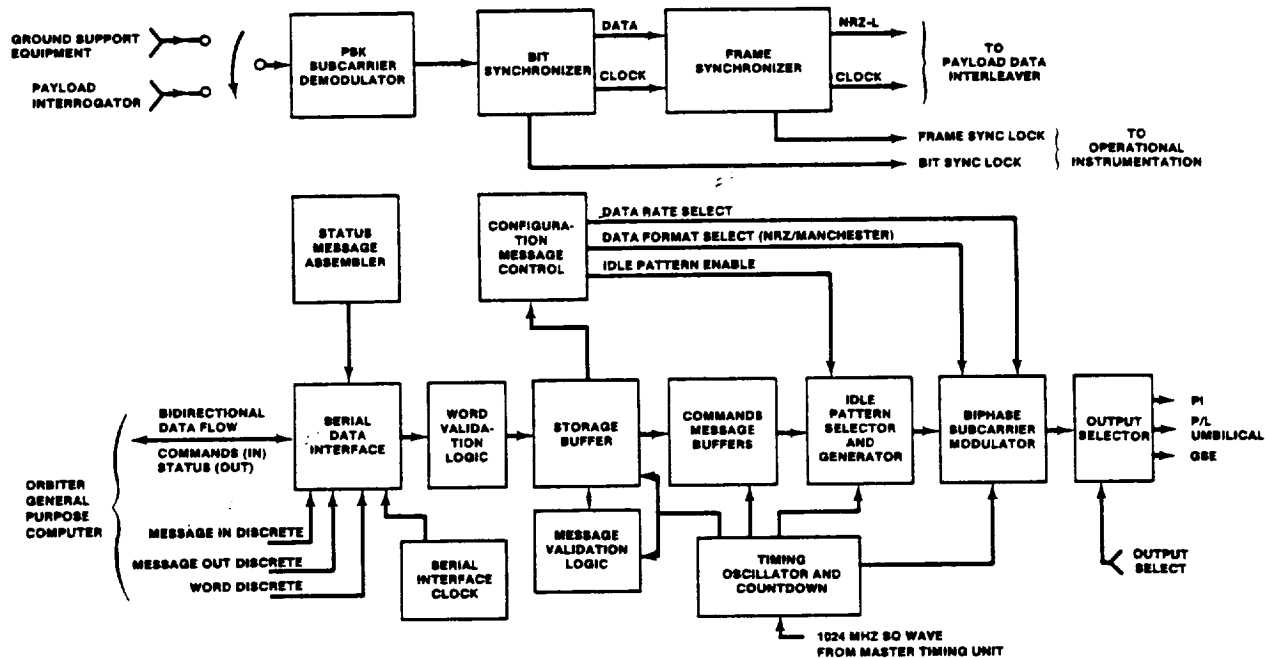


FIGURE 5.- NASA PAYLOAD SIGNAL PROCESSOR FUNCTIONAL BLOCK DIAGRAM.

The 1.024-megahertz telemetry subcarrier from the PI is applied to the PSK subcarrier demodulator. Since the subcarrier is biphase modulated, a Costas-type loop is used to lock onto and track the subcarrier. The resulting demodulated bit stream is input to the bit synchronizer subunit, where a DTTL bit synchronization loop provides timing to an integrate-and-dump matched filter which optimally detects and relocks the telemetry data.

Detected telemetry bits, together with clock data, are input to the frame synchronizer where frame synchronization is obtained for any one of the four NASA standard synchronization words. The frame synchronizer also detects and corrects the data polarity ambiguity caused by the PSK demodulator Costas loop.

From the frame synchronizer, the telemetry data with corrected frame synchronization words and clock data are fed to the PDI. The telemetry detection units also supply appropriate lock signals to the Orbiter's operational instrumentation equipment, thus acting to indicate the presence of valid telemetry.

TEST RESULTS AND FLIGHT PERFORMANCE

RF compatibility tests were performed in the Electronic Systems Test Laboratory (ESTL) using the Orbiter's PI and PSP to communicate with several classes of payload communications systems. The payload communications systems tested were the Inertial Upper Stage (IUS); the Shuttle Pallet Satellite-01 (SPAS-01); the Tracking and Data Relay Satellite (TDRS) Telemetry, Tracking, and Command (TT&C) system; and the NASA near-Earth and TDRS user's transponders. Additionally, the PI and PSP were used during the fifth Shuttle flight (STS-5) to receive telemetry from the Satellite Business System (SBS) payload. During the sixth flight (STS-6), the PI was used to send commands to and receive telemetry from the IUS spacecraft. The PI and PSP were used for TDRS predeployment communication checkout.

PAYLOAD SIGNAL PROCESSOR PERFORMANCE

A major PSP problem, uncovered during the SPAS-01 transponder testing in the ESTL, was false locking of the bit synchronizer on NRZ-L telemetry. PSP false lock could occur by thresholding the PI receiver (similar to going through an antenna pattern null) and then increasing the total received power (TRP) to a value above data threshold.

The PSP bit synchronizer is implemented in a microprocessor. The modification to remedy the false lock problem consisted of changing the microprocessor software and making cuts and installing jumpers in the microprocessor printed circuit board.

The PSP was used for the first time during flight to process the telemetry from the SBS payload during STS-5. The aforementioned modifications had not been made to the STS-5 PSP to remedy the false lock problem for this mission; however, the conditions for false locking did not occur during SBS deployment and the PSP performance was excellent. The modifications to prevent false locking were made in the PSP used to support the predeployment checkout of TDRS-A during STS-6. Again, the PSP performance was excellent for both telemetry and command processing.

PAYLOAD INTERROGATOR PERFORMANCE

The ESTL RF compatibility tests using the PI with each major class of payload communication system showed that the PI was compatible with each and that all performance requirements were met. The most significant finding during the IUS and SPAS-01 tests was that simultaneous transmission of television via the FM transmitter on 2250.0 megahertz could interfere with the PI return link telemetry reception. This interference is most certain to occur (1) when the payload transmit frequency is within 15 megahertz of the FM transmitter frequency, (2) when the payload is greater than 1 kilometer from the Orbiter, and (3) when television video is being transmitted via the upper FM hemispherical antenna. The simultaneous occurrence of these conditions can be avoided operationally.

Excessive phase noise was detected on the ESTL prototype unit. After the unit was returned to the vendor for repair, a faulty capacitor was found and replaced. No further design deficiencies were uncovered during ESTL testing.

The PI was used for the first time during a mission to receive the return link telemetry signal from the SBS payload during STS-5. The PI performance was excellent. The PI was also used on STS-6 for transmitting commands and receiving telemetry in conjunction with the predeployment checkout and deployment of the IUS and TDRS-A spacecraft. Again, the PI performance was excellent.

CONCLUSIONS

Development of a spaceborne system to provide the capability for monitoring and controlling nearby satellites is a significant milestone. Expansion of this capability will most assuredly be required if a space station is to be developed. Such expansion will undoubtedly include a multi-access capability to allow simultaneous monitoring and control of multiple satellites as well as an extended range capability.

The merits of designing a multipurpose system such that a standard onboard processing capability is provided for most users while a "bent-pipe" relay capability is provided for the relatively few nonstandard users were found to be more than theoretical. Significant savings in cost, weight, and complexity were realized. These savings clearly demonstrate the necessity to "scrub" requirements and to explore alternate design approaches before implementing a complex system.

The necessity of performing end-to-end system performance testing for complex communications systems was (once again) demonstrated. Although the S-band payload system LRU's underwent extensive vendor-level testing (prototype, qualification, and acceptance testing) and a certain level of prime contractor integrated system testing, the major problems that occurred were not manifested until the system was thoroughly tested in ESTL. Uncovering these problems through ESTL testing (detailed end-to-end system compatibility testing) rather than during real-time mission operations allowed the opportunity to adequately analyze and resolve the system performance deficiencies early on instead of risking compromised mission success.

REFERENCES

1. Space Shuttle Payload Data Handling and Communication Description and Performance Document. JSC-14241, Rev. B, May 1981.
2. Shuttle Orbiter/Cargo Standard Interfaces. JSC-07700, Vol. XIV, Attachment 1 (ICD 2-19001), Rev. G, Sept. 1980.
3. Springett, James C.; and Udalov, Sergei: Communications with Shuttle Payloads. In IEEE Transactions on Communications, Special Issue, Nov. 1978.
4. Teasdale, W. E.: Space Shuttle Payloads and Data Handling Accommodations. In IEEE Transactions on Communications, Special Issue, Nov. 1978.
5. Carrier, L. M.; and Pope, W. S.: An Overview of the Space Shuttle Orbiter Communications and Tracking System. In IEEE Transactions on Communications, Special Issue, Nov. 1978.
6. Houston, S. W.; Martin, D. R.; and Stine, L. R.: Microprocessor Bit Synchronizer for Shuttle Payload Communications. In IEEE Transactions on Communications, Special Issue, Nov. 1978.
7. Orbiter/Shuttle Pallet Satellite-01 (SPAS-01) Transponder Verification Test Report. JSC-18647, Oct. 1982.
8. TDRS User's NASA Standard Transponder Test Report. JSC-18676, Nov. 1982.
9. Orbiter/Inertial Upper Stage (IUS) System Verification Test Report. JSC-18700, Nov. 1982.

TDRSS S-SHUTTLE UNIQUE RECEIVER EQUIPMENT

Aaron Weinberg
Stanford Telecommunications, Inc.
McLean, VA 22101

John J. Schwartz
Robert Spearing
NASA/GSFC
Greenbelt, MD 20771

ABSTRACT

Beginning with STS-9, the Tracking and Data Relay Satellite System (TDRSS) will start providing S- and Ku-band communications and tracking support to the Space Shuttle and its payloads. The most significant element of this support takes place at the TDRSS White Sands Ground Terminal, which processes the Shuttle return link S- and Ku-band signals. While Ku-band hardware available to other TDRSS users is also applied to Ku-Shuttle, stringent S-Shuttle link margins have precluded the application of the standard TDRSS S-band processing equipment to S-Shuttle. It was therefore found necessary to develop a unique S-Shuttle Receiver that embodies state-of-the-art digital technology and processing techniques. This receiver, developed by Motorola, Inc., enhances link margins by 1.5 dB relative to the standard S-band equipment and its bit error rate performance is within a few tenths of a dB of theory. The goal of this paper is to provide an overview description of the SSRE, which includes the presentation of block diagrams and salient design features. Selected, measured performance results are also presented.

1. INTRODUCTION

Beginning with STS-9 the Tracking and Data Relay Satellite System (TDRSS) will start providing communications and tracking support to the Space Shuttle and its payloads under a broad range of operating conditions and data throughput requirements. Such support will take place at both S- and Ku-band frequencies, under forward (JSC-to-Shuttle) and return (Shuttle-to-JSC) link conditions, during launch (S-band only) and, of course, during in-orbit operation.

To support forward link operation the TDRSS ground terminal at White Sands, New Mexico (WSGT) will act as a ground relay between JSC and the TDRS-Shuttle link. At WSGT, necessary processing such as PN spreading, data format conversion, doppler compensation, and baseband-to-RF conversion is performed. No other data-related processing is performed at WSGT and the TDRS satellite further acts as a bent pipe repeater between WSGT and Shuttle. Figure 1 highlights salient interfaces between JSC, Shuttle and the TDRSS, while Figure 2 amplifies on TDRSS Ground Network support to Shuttle operations.

The most significant communications and tracking support provided by the TDRSS to Shuttle takes place at WSGT in the processing of return link S- and Ku-band signals. Here, WSGT receiver hardware performs demodulation, symbol synchronization and data detection (coded and uncoded), and relays the detected data via NASCOM to JSC. Additional return link processing at WSGT involves doppler tracking, phase ambiguity resolution and closed-loop autotracking of the TDRS Ku-band antenna in the direction of Shuttle.

To support Ku-Shuttle return link operation, WSGT receiver hardware that is available to other TDRSS Ku-band Single Access (KSA) users is uniquely configured to handle the Shuttle 3-channel modulation schemes. This involves appropriate application of the KSA High and Medium Rate Demodulators and Symbol Synchronizers, and a multiplexed set of Viterbi decoders to handle coded data rates up to 50 Mbps.

For S-Shuttle return link operation the originally planned TDRSS support also called for the application of WSGT receiver hardware available to other TDRSS S-band Single Access (SSA) users. Due to stringent Shuttle link budget considerations, however, the link margins available via the standard SSA equipment were found to be insufficient, and it was found necessary to develop a unique S-Shuttle receiver that embodies state-of-the-art digital technology and processing techniques. The uniqueness of this S-Shuttle Receiver Equipment (SSRE), developed by Motorola, Inc., may be highlighted by several significant features:

- all-digital processing after IF-to-baseband conversion
- integrated carrier loop/symbol sync design
- link margin enhanced by 1.5 dB relative to existing SSA equipment
- bit error rate performance within a few tenths of a dB of theory

The SSRE represents an important achievement in the development of state-of-the-art digital hardware that implements near-optimal communication signal processors. It also serves as a benchmark for future hardware research and development to be undertaken by NASA in support of TDRSS operations over the next decade, and for on-going support during the post-TDRSS era.

The goal of this paper is to provide an overview description of the SSRE, involving the presentation of block diagrams and salient design features. Selected, measured performance results are also presented. Toward this end Section 2 begins with a summary of S-Shuttle signal characteristics that must be supported by the SSRE and is followed in Section 3 by an overview of the SSRE and associated interfaces. Section 4 proceeds to focus on several of the SSRE components, highlighting their specific functions and significant features. Selected results are presented in Section 5 and conclusions are contained in

2. TDRSS/S-SHUTTLE RETURN LINK SIGNAL CHARACTERISTICS AND OPERATIONS CONSIDERATIONS

Salient S-Shuttle return link signal characteristics are as follows:

- BPSK modulation
- Data Rate
 - Mode 1: 96 KBPS
 - Mode 2: 192 KBPS
 - Mode 3: Unmodulated Carrier
- Coding
 - Convolutional
 - Rate 1/3, constraint length 7
 - Non-transparent
- Signal Format
 - Bi- ϕ (Manchester)

From an operational viewpoint three additional aspects that warrant mentioning in this context are:

- signal dynamics
- antenna switching transients
- degraded signal level

Under normal conditions, S-Shuttle will operate in a coherent turnaround mode, which implies that the uncompensated doppler at the SSRE input can exceed 130 KHz; typically, however, doppler compensation will reduce residual doppler to well below this value. This doppler value may be significant during signal acquisition, since under certain conditions a large doppler offset may lead to false carrier lock.

Antenna switching transients must also be contended with. In particular, S-Shuttle employs one of four quad antennas at a time, and when switching from one antenna to the next takes place, a brief signal dropout occurs (e.g., ≤ 50 ms). While data bits will, of course, be lost during the antenna switch, it is imperative that the SSRE demodulator stay in lock or recover quickly after the antenna switching process is complete.

A third operational aspect of importance involves S-Shuttle operation under degraded EIRP conditions. To compensate for this contingency both of the TDRS SSA antennas may be used simultaneously to relay Shuttle signals to WSGT, where they may be appropriately combined to provide up to 2.5 dB SNR enhancement.

It is clear from the above discussion that the SSRE must handle three distinct data modulation modes and simultaneously contend with a variety of other signal and channel conditions. SSRE design features and selected performance results, and how they relate to the above discussion, are treated in the sections that follow.

3. SSRE OVERVIEW

The WSGT contains two SSRE components. Under normal operating conditions only one will be necessary, but a second is available to support the SSA antenna combining operation briefly discussed in Section 2.

A simplified block diagram overview of the SSRE, and associated interfaces, is presented in Figure 3. A preliminary discussion of the SSRE components shown is presented here with more detailed discussion to follow in Section 4. The information here is primarily based on [1, 2].

ANALOG/DIGITAL INTERFACE

The incoming 35 MHz IF signal is first processed by a wideband (~ 10 MHz) noncoherent AGC to control the dynamic range of the composite signal + noise into the coherent AGC and the remainder of the receiver. As seen in Figure 3, the coherent AGC output is then processed by an analog voltage controlled amplifier (VCA), in-phase and quadrature mixed to baseband, and each low pass filtered in an analog fashion. It is at this point that digitation takes place, via 8 bit A/D conversion, and all remaining processing through NCO carrier reconstruction is then performed digitally.

The analog/digital interface is clearly identified in Figure 3. The treatments of the coherent AGC and the NCO are to be noted. Specifically, both are treated as lying directly on the interface since they both accept digital inputs while producing analog outputs.

Also noteworthy are the analog in-phase and quadrature low pass filters. The one-sided 3 dB bandwidth of each filter may take on one of three values, depending on the Shuttle mode of operation. The bandwidths are as follows:

- Mode 1 (288 KSPS): 1.75 MHz
- Mode 2 (576 KSPS): 3.5 MHz
- Mode 3 (unmodulated): 54 KHz

The significance of Mode 1 and 2 low pass filter bandwidths, as they relate to subsequent processing, is discussed in Section 4.

CARRIER LOOP/SYMBOL SYNCHRONIZER

Probably the heart of the SSRE is the "integrated" carrier tracking loop/symbol synchronizer. The term "integrated" is employed here since, contrary to conventional receivers which first perform carrier tracking and demodulation followed by symbol synchronization, the SSRE performs both operations simultaneously. Implementation of this design feature involves the use of digital, integrate-and-dump (I-D) arm filters in both the carrier loop and symbol synchronizer. Application of I-D arm filtering leads to a design which is near-optimum in nature and is therefore a very significant aspect of the SSRE in maximizing the efficient use of available carrier-to-noise ratio. A more detailed discussion of this portion of the SSRE will be presented in Section 4.

AMBIGUITY RESOLVER

Because the signal format of S-Shuttle data is Bi- ϕ in nature, timing ambiguity associated with the mid-symbol and end-symbol instants, may exist. Resolution of this potential ambiguity is straightforwardly accomplished by this component of the SSRE.

LOCK DETECTOR

The lock detector implements the post-detection accumulated $\{|I|-|Q|\}$ characteristic which is used to ascertain when the carrier loop is in lock; the algorithm employed also prevents false carrier lock from occurring. Noteworthy here, once again, is an interesting departure from conventional receivers. While the typical receiver employs two separate lock detection circuits to monitor lock-up of the carrier loop and symbol sync, the present "integrated" design requires only once such circuit. The Lock Detector component is also expanded upon in Section 4.

SSRE OUTPUT INTERFACES

As seen in Figure 2 the SSRE provides several distinct outputs:

- recovered carrier
- recovered symbol clock
- 8 bit soft decision data
- lock status

The recovered carrier is externally used for doppler extraction and is further available as an output to be used in conducting laboratory measurements (e.g., for cycle slipping measurements). The recovered clock drives the external Viterbi decoder and also serves as an output for laboratory measurements (e.g., for data bit jitter measurements). The 8 bit soft decision data outputted by each SSRE may be combined as shown to enhance the effective output signal-to-noise ratio by approximately 2.5 dB. Whether or not combining is employed, the 3 most significant bits per detected information are then used as inputs to the Viterbi decoder. Finally, lock status output data is used both by WSGT and JSC for real-time performance monitoring.

The next section proceeds to provide some more detailed design information on selected portions of the SSRE.

4. SSRE DESIGN DETAILS

4.1 INTRODUCTION

Of the SSRE components identified in Figure 3, the following are treated in more detail in this section:

- Integrated Carrier Loop/Symbol Synchronizer
- NCO
- Lock Detector
- Coherent AGC

Each is individually considered in the subsections that follow, with the major consideration being the first item.

4.2 INTEGRATED CARRIER LOOP/SYMBOL SYNC

4.2.1 Overview

Figure 4 provides a simplified description of the carrier loop/symbol sync integrated structure, which motivates the subsequent more detailed discussion. The I and Q A/D converter outputs of Figure 3 are fed into the carrier loop portion of the SSRE, with the I component simultaneously employed by the symbol sync. The carrier loop accumulates I and Q samples, with each accumulator dumped once per symbol time, under the control of the clock shown. Of special significance here is the fact that each of the I and Q accumulators implements a digital, integrate and dump (I-D) filter and therefore each also requires an appropriate Bi- ϕ inversion operation to be performed on each of the samples accumulated during the second half of the accumulating period. The I-accumulator output represents desired soft decision data for external combining and Viterbi decoding. This output is also sign detected to yield a hard decision estimate of the data, denoted by \hat{d}_i , which is used to implement a decision directed carrier tracking loop. The I/Q multiplier output is then digitally filtered to yield the error signal for carrier reconstruction via the NCO.

The I input samples are simultaneously applied to symbol synchronization. As seen, mid-symbol and end-symbol accumulations are performed, dumped by the clock at appropriate intervals and processed by a Data Transition Tracking Loop (DTTL)-type of algorithm that is optimized for the Bi- ϕ signal format. Specifically, a mid-symbol polarity transition always occurs in each and every Bi- ϕ symbol, while end symbol transitions occur at an average rate equal to one minus the symbol transition density. The manner in which the symbol sync algorithm takes advantage of this will be clarified shortly. Note also from Figure 4 that the hard decision estimate, \hat{d}_i , is simultaneously employed by the carrier loop and symbol sync portions.

The integrated nature of the carrier loop/symbol sync structure is apparent from Figure 4 and the above discussion. Clearly, satisfactory operation of one portion is intimately dependent on satisfactory operation of its counterpart. This complicates the signal acquisition procedure, but once acquisition is complete and tracking takes over, the benefit of enhanced SNR operation, via the carrier loop I and Q I-D matched filters, readily presents itself. This benefit is, of course, coupled with the important advantage all digital processing provides in minimizing implementation losses.

4.2.2 Carrier Loop Details

A more detailed block diagram characterization of the carrier loop component is shown in Figure 5.

As seen, 16 samples per symbol are accumulated in each of the I and Q arms, independent of mode of operation; this independence makes the SSRE digital processing essentially transparent to the underlying nature of the analog input to WSGT. What is necessary, however, is that the sample clock rate be adapted appropriately. This is accomplished as follows.

The SSRE employs an underlying clock reference of 27.648 MHz, which is used to generate a sample clock rate matched to the mode of operation. In addition, the 3 dB bandwidth of each of the I and Q analog arm filters in Figure 3 is chosen for compatibility with sampling rate. Specifically, from Section 2, the one-sided 3 dB bandwidth for Mode 1 is 1.75 MHz, which implies a somewhat greater effective noise bandwidth. From a system theoretic viewpoint, noise samples taken at the Nyquist rate (based on the noise bandwidth) are statistically independent. Accordingly, the 1.75 MHz 3-dB bandwidth implies that more than 12 independent samples may be accumulated over the Mode 1 symbol duration.* This is

* I.e., $2 \times (\text{one-sided noise bandwidth})/\text{symbol rate} = 2 \times 1.75 \times 10^6 / 2.88 \times 10^5 > 12$.

the basis for the 16 sample accumulation per symbol employed by the SSRE. Note that the associated nominal sampling rate is 4.608 MHz, which represents 6 cycles of the 27.648 MHz clock reference. Similarly, for Mode 2 the nominal sampling rate is 9.216 MHz and the associated low pass arm filter 3dB bandwidth is 3.5 MHz. As discussed below, these nominal sampling rates may be adjusted by the symbol sync component.

The number of quantized bits available at the input to each subcomponent is also indicated in Figure 4. The quantization scaling inherent in the 8 bit input to the I and Q accumulators is derived from the coherent AGC; the scaling reflects a dynamic range of $\pm 8|m|$ and a quantization stepsize of $|m|/16$, where $|m|$ is the estimated signal mean absolute amplitude. It is apparent that negligible amplitude information is lost via the SSRE quantization scheme.

The I/Q multiplier output is further accumulated over 16 symbol intervals to enhance SNR and is fed into the phase and frequency components of the digital loop filter; this implementation leads to a second order carrier loop with a nominal damping factor of 0.707. Several additional aspects of the loop filtering should also be noted:

- the symbol accumulator is an integral part of the overall loop filter and, it, coupled with the other filter components shown, specifies the carrier loop bandwidth.
- frequency and phase scaling are also necessary for loop bandwidth specification and must reflect the symbol accumulation rate.
- phase and frequency clipping are employed to prevent overflow, but the probability of an overflow occurrence is very low.
- for carrier acquisition frequency sweeping is implemented by adding an appropriate digital word as shown in Figure 5; the frequency sweep limits are ± 70 kHz.

Also of importance with regard to frequency sweeping is the issue of false lock, under Mode 1 and 2 conditions. Because of the decision-directed nature of the loop, and the fact that it employs digital I-D arm filters, the potential for false lock presents itself at frequency offsets which are rational multiples of half the symbol rate [3]. The greatest possibility occurs at a frequency offset equal to half the symbol rate which is 144 kHz for Mode 1 and 288 kHz for Mode 2. For anticipated doppler offsets, however, these components do not occur, and other potential false lock states are automatically bypassed via the SSRE lock detector circuitry.

To complete the discussion on the carrier loop we include Figure 6 which describes the NCO. As seen, a 10 bit word is provided to the Sine Generator ROM which, in turn, generates an 8 bit word for D/A conversion to yield the desired updated carrier reference. The associated reference frequency varies over the range $500 \text{ kHz} \pm 50 \text{ kHz}$. Note that this reference is mixed with a fixed 34.5 MHz IF, the output of which yields the recovered carrier — nominally equal to 35 MHz — and is also an externally available output of the SSRE.

A summary of salient carrier loop parameters is presented in Table 1.

4.2.3 Symbol Sync Details

A more detailed block diagram characterization of the symbol sync component is shown in Figure 7. The symbol sync error signal is generated by using a DTL-type of algorithm that is matched to the Bi- ϕ symbol format employed by Shuttle. Specifically, as seen, both "end-symbol" and "mid-symbol" accumulations are performed, with each involving 8 samples - i.e., a time interval equal to half a symbol duration. The mid-symbol accumulator sums up to the 5th thru 12th samples of the 16 samples encompassing the assumed symbol period. Under tracking conditions, the timing error will be a small fraction of a symbol and, by virtue of the Bi- ϕ format, a polarity transition will always occur during the mid-symbol accumulation interval; accordingly, a measure of the timing error is always available from the mid-symbol accumulator. The output of this accumulator is multiplied by the estimate of the given symbol's polarity, which is derived from the I accumulator output as shown; this multiplication is necessary for appropriate error signal generation, since it provides the direction of the timing error.

Under tracking conditions, when the timing error is sufficiently small (less than a quarter of a symbol period) the end-symbol accumulator straddles two adjacent symbols. For the end symbol, a polarity transition will only occur when the adjacent symbols are equal in polarity — this occurs at an average rate equal to one minus the symbol transition density. Note that the multiplication

by $(\hat{d} + \hat{d}_{n-1})/2$ generates the proper sense, or direction, of the timing error when a symbol transition does not occur and equals zero, otherwise. The fact that both end-symbol and mid-symbol transitions can be taken advantage of is a benefit of using the Bi- ϕ format, relative to NRZ.

The end-symbol and mid-symbol error signals are differenced to yield the composite error signal for processing by a second order loop filter. This loop filter consists of an N symbol accumulator followed by appropriate phase and frequency scaling and processing. The accumulation interval N is given by:

- N = 16 for wideband loop (acquisition)
- N = 128 for narrowband loop (tracking)

The composite effect of the N symbol accumulation and phase and frequency scaling specifies the loop bandwidth. Also of interest is the manner in which the sample clock rate is updated. The phase scale output is clipped to 4 bits for both Modes 1 and 2. This provides a capability for changing the clock phase as follows:

- Mode 1: up to 2 sample intervals in 1/6 sample ($\sim 0.04\mu s$) increments
- Mode 2: up to 4 sample intervals in 1/3 sample ($\sim 0.04\mu s$) increments

The frequency scale output is also clipped and the output is used to either stuff or delete clock pulses so that the effective clock rate may be effectively increased or decreased, respectively. The stuffing or deletion is uniformly spread over the N symbol accumulation interval prior to scaling. This frequency correction capability of the SSRE is useful in compensating for data bit jitter that may be present in the incoming signal.

Salient parameters of the symbol sync are summarized in Table 2.

4.3 LOCK DETECTOR

The Lock Detector circuit is shown in Figure 8. It provides lock status information to the SSRE output, to reflect lock of the integrated carrier loop/bit sync, and further initiates loop bandwidth adjustments to reflect switchover from acquisition-to-tracking and vice versa, if loss of lock occurs. The algorithm displayed by the figure is self-explanatory and need not be expanded upon. As a companion to Figure 8, Figure 9 displays the SSRE state diagram which describes the flow of the acquisition/tracking/reacquisition procedures performed by the SSRE.

4.4 COHERENT AGC

Figure 10 describes the coherent AGC circuit. The I accumulator output, under lock conditions, will typically exceed the noise level substantially. Thus, the 256 symbol accumulator output represents a close estimate of the signal amplitude under lock conditions. This then serves as a reference for gain control in a typical fashion. Note that the Coherent AGC represents one of the digital/analog interfaces of the SSRE.

5. SSRE PERFORMANCE

Selected SSRE performance results are presented in this section to reflect both demodulator and symbol error rate (SER) performances. These results reflect tests performed both by Motorola, Inc. and by the Electronic Systems Test Laboratory (ESTL) at JSC.

Figures 11 and 12 display results generated on SER performance and reflect SER results for both Modes 1 and 2, respectively. As seen, both modes behave in essentially identical fashions, with measured results extremely close to theoretical predictions — i.e., discrepancies < 0.5 dB for SER values from 10^{-1} to 10^{-5} . Note that the Mode 1 $E_s/N_0 \sim 2.8$ dB is the worst case Shuttle operating value. For Mode 2 the worst case E_s/N_0 is approximately -0.2 dB.

Figure 13 illustrates carrier tracking loop performance, wherein rms phase jitter is plotted vs E_s/N_0 . As seen, both Mode 1 and Mode 2 performances are substantially better than spec requirements. Furthermore, Mode 3 results (not shown here) display phase jitter performance very similar to that of Fig. 13.

Numerous additional tests were run at ESTL [4] to assess in-depth SSRE performance under both acquisition and tracking conditions. A brief summary of several of these results, together with pertinent observations now follow.

- For anticipated doppler uncertainties during acquisition Mode 2 never experienced false lock.
- For Mode 1 and under sufficiently strong signal conditions, temporary false lock occurrences were observed at frequency offsets of ± 36 kHz, ± 48 kHz, and ± 72 kHz, but the SSRE prevented a false lock from taking hold; these temporary false locks are consistent with the alias lock predictions of [3] and reflect the active arm filters employed by the SSRE. Furthermore, at an offset of ± 144 kHz a solid false lock did occur, but offsets of this magnitude are not anticipated during normal operation. Again, theory predicts the dominance of this 144 kHz component and its potential for yielding a false lock; specifically the dominance of this component is based on the decision-directed implementation of the carrier tracking loop.

Acquisition Time

- At expected C/N_0 levels (~ 62.8 dB-Hz), the SSRE mean acquisition time never exceeded 0.5 seconds for both Modes 1 and 2.
- In the absence of doppler compensation mean acquisition time never exceeded 1 second.

Acquisition Threshold

- Thresholds and margins are summarized in Table 3. Note the much lower Mode 3 threshold which is based on the use of a much narrower acquisition loop bandwidth (See Table 1).

Cycle Slipping

- Under typical operating conditions, wherein the return link C/N_0 exceeds its forward link counterpart by 7.9 dB, and coherent turnaround tracking operation is in progress, the cycle slip thresholds are:

Mode 1: 55.9 dB-Hz

Mode 2: 57.4 dB-Hz

This compares to a nominally expected C/N_0 level of 62.8 dB-Hz.

Antenna Switching

- The switching from one Shuttle quad antenna to another requires a break-before-make operation which, in turn leads to a signal dropout interval. At nominal C/N_0 values (~ 62.8 dB-Hz) and break intervals less than 25 ms, carrier loop lock was found to be lost with a 45% probability and < 1600 symbol errors were made. Note that recovery from an antenna switch requires relocking of both the carrier and symbol sync loops. The rapid recovery of the SSRE once again displays its excellent performance.

6. CONCLUSIONS

The Tracking and Data Relay Satellite Systems, once operational, will significantly enhance the communication capabilities of Shuttle at both S- and Ku-band frequencies. Because of the unique nature of the Shuttle mission and its associated communication requirements, specialized supporting hardware and ground station configurations had to be developed. This paper focussed on the Shuttle S-band component and described in detail the unique S-Shuttle Receiving Equipment (SSRE) developed for incorporation into the TDRSS White Sands Ground Terminal.

To support S-Shuttle stringent link budget requirements, a state-of-the-art all digital SSRE design was pursued by its developer, Motorola, Inc. This paper described several of its significant features, including its integrated carrier-loop/sync component and its use of near-optimum digital-integrate-and-dump arm filters in the carrier loop. Selected performance results were also presented and the closeness ($< .5$ dB) of its error rate performance to theory was highlighted.

The SSRE represents an achievement that should serve as a basis for future state-of-the-art developments to be supported by NASA. One such TDRSS project is already under way. It involves the development, by Harris Corporation, of an all digital demodulator that performs A/D conversion at IF and implements third order carrier tracking loops to significantly enhance tracking performance under high dynamics conditions — such as occur during spacecraft unstable orbit conditions. An integrated carrier loop/symbol sync feature is also included. This new demodulator should be incorporated into the White Sands receiver, and become operational by 1985, at which time it will begin supporting S-band TDRSS users with data rates up to 300 kbps.

REFERENCES

1. Motorola, Inc., SSRE CRITICAL DESIGN REVIEW PACKAGE.
2. Motorola, Inc., Government Electronics Division, Operation & Maintenance Instructions: S-Band Shuttle Return Equipment for TDRSS Tracking, Return and Modulation Equipment (TRAM), Document No. 68-P09801M.
3. Marvin K. Simon and Kai T. Woo, "Alias Lock Behavior of Sampled-Data Costas Loops," IEEE Trans. Comms., Vol. COM-28, No. 8, August 1980, pp. 1315-1325.
4. Electronic Systems Test Laboratory, TDRS/Orbiter SSA Return and Two-Way RF Acquisition Test Report, JSC 18723, January 1983.

TABLE 1

CARRIER LOOP PARAMETERS

- INPUT IF: 35 MHz
- DECISION-DIRECTED LOOP
 - DIGITAL INTEGRATE-AND-DUMP ARM FILTERS
 - 16 SAMPLES/SYMBOL
- SECOND ORDER LOOP
- 0.707 DAMPING FACTOR
- ACQUISITION SWEEP RANGE: = 70 KHZ

CARRIER LOOP BANDWIDTHS (ONE-SIDED)

	ACQUISITION	TRACKING
MODE 1	1500 HZ	290 HZ
MODE 2	2400 HZ	510 HZ
MODE 3	250 HZ	24 HZ

- NCO FREQUENCY RANGE: 500 KHZ ± 50 KHZ

TABLE 2

SYMBOL SYNC PARAMETERS

- DATA TRANSITION-TRACKING-LOOP TAILORED TO BI-PHASE SYMBOL FORMAT
 - MID-SYMBOL AND END-SYMBOL ACCUMULATORS
 - HALF-SYMBOL ACCUMULATION WINDOWS
- SECOND ORDER LOOP

SYMBOL SYNC LOOP BANDWIDTHS (ONE-SIDED)

	ACQUISITION	TRACKING
MODE 1	2.88 KHZ	360 HZ
MODE 2	5.76 KHZ	720 HZ
MODE 3	N/A	N/A

- TIMING (PHASE) ADJUSTMENT CAPABILITIES
 - MODE 1: UP TO 2 SAMPLE INTERVALS IN 4 SAMPLE INCREMENTS
 - MODE 2: UP TO 4 SAMPLE INTERVALS IN 4 SAMPLE INCREMENTS
- FREQUENCY ADJUSTMENT CAPABILITIES
 - MODE 1: UP TO 1.0% CHANGE IN ~ .008 INCREMENTS
 - MODE 2: UP TO 2.0% CHANGE IN ~ .016 INCREMENTS

TABLE 3

SSRE ACQUISITION THRESHOLDS AND MARGINS

MODE	THRESHOLD C/N ₀ (DBHZ)	REQUIRED C/N ₀	MARGIN (DB)
1	51.2	60.2	9.0
2	48.9	57.2	8.3
3	29.3	N/A	N/A

ORIGINAL PAGE IS
OF POOR QUALITY

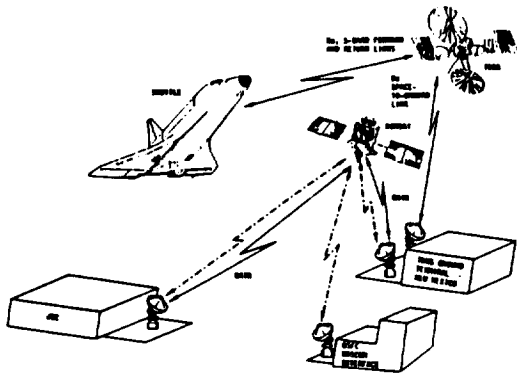


FIGURE 1: JSC, SHUTTLE AND TDRSS INTERFACES

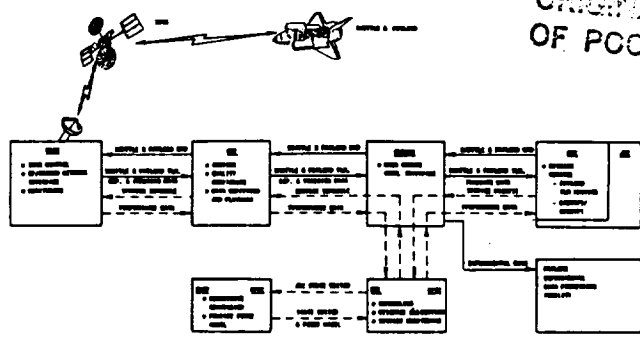


FIGURE 2: TDRSS NETWORK SUPPORT TO STS MISSION - AN OVERVIEW

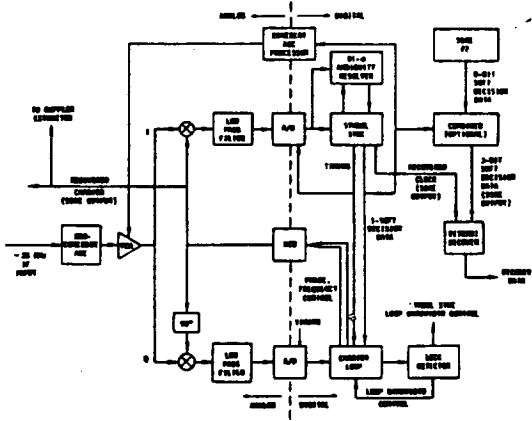


FIGURE 3: SDRS OVERVIEW AND ITS INTERFACES

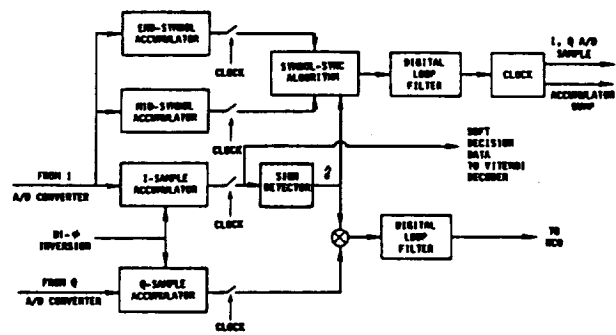


FIGURE 4: OVERVIEW OF SDRS, INTEGRATED CARRIER LOOP/SYMBOL SYNC

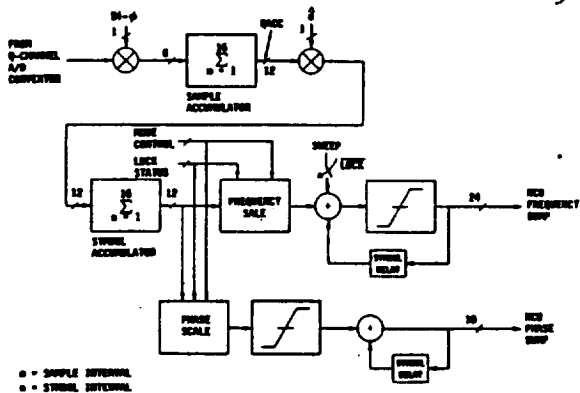


FIGURE 5: CARRIER TRACKING LOOP

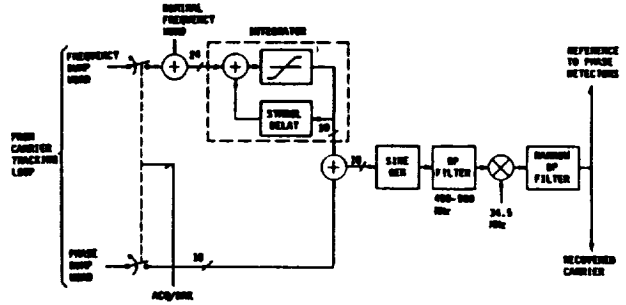


FIGURE 6: INVERSELY CONTROLLED OSCILLATOR (ICO)

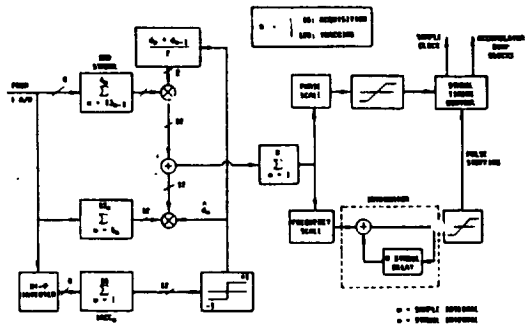


FIGURE 7: SYMBOL SYNCHRONIZER

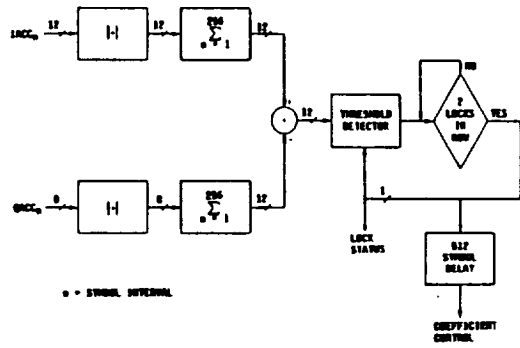


FIGURE 8: LOCK DETECTOR

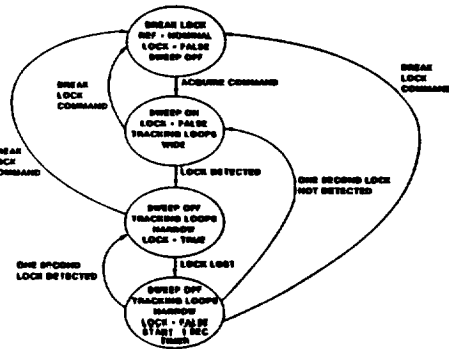


FIGURE 9: SRE STATE DIAGRAM

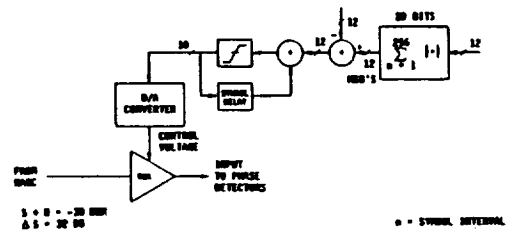


FIGURE 10: COHERENT AIC

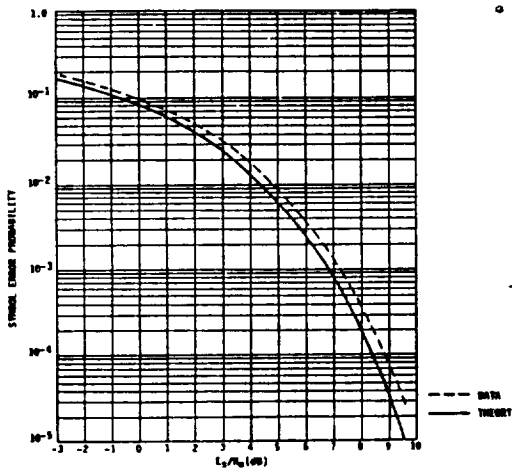


FIGURE 11: PROBABILITY OF ERROR FOR PSK DATA - MODE 1

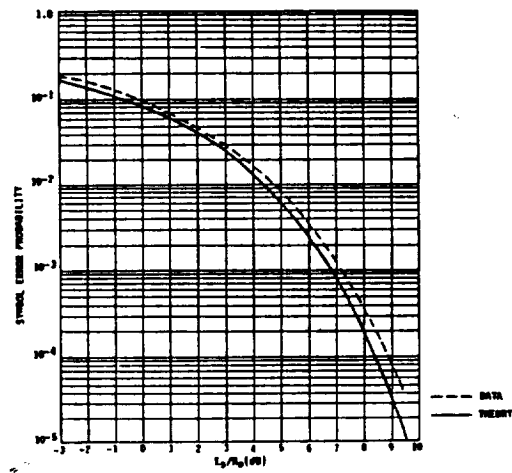


FIGURE 12: PROBABILITY OF ERROR FOR PSK DATA - MODE 2

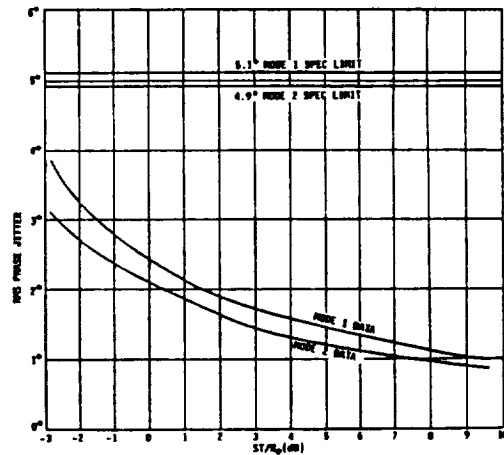


FIGURE 13: MODES 1 AND 2: DEGREES OF PHASE JITTER

... OF POOR QUALITY.

THE
COMMUNICATIONS LINK ANALYSIS
AND
SIMULATION SYSTEM
(CLASS)

Robert D. Godfrey
CLASS Development Manager
NASA/GSFC Code 831

ABSTRACT

The Communications Link Analysis and Simulation System (CLASS) is a comprehensive, computerized communications and tracking system analysis tool under development by the Networks Directorate of the NASA/GSFC. The primary use of this system is to provide the capability to predict the performance of the Tracking and Data Relay Satellite System (TDRSS) User Communications and Tracking links through the TDRSS. This paper describes, in brief form, the general capabilities and operational philosophy of the current and final versions of the CLASS along with some examples of analyses which have been performed utilizing the capabilities of this system.

1. INTRODUCTION

The CLASS is a computerized analysis system for evaluating the performance of communications and tracking links with respect to all performance parameters. The system has been developed specifically to permit the performance evaluations of the forward (command) and return (telemetry) link communications through the TDRSS. The system modeling is, however, designed to permit other systems to be analyzed as will be done when the CLASS is used as a design tool to support future NASA Networks development programs such as TDAS. The initial versions of the system are currently in operational use providing performance analysis of the TDRSS User/TDRSS interface to insure compatibility between the TDRSS Users communications system and TDRSS requirements. The system is also currently in use providing TDRSS user design analysis in an effort to help these users optimize their communications link performance when transmitting through the TDRSS.

The CLASS models all elements of the communications link from the point at which the data is generated to the point at which the data is utilized. A diagram of the modeled TDRSS and TDRSS User systems is shown in Figure 1. The communications channel environment models and data bases are also shown in this figure. A diagram of the TDRSS system as modeled is shown in Figure 2. The performance of the system modeled can be evaluated by analytical or simulation techniques or by a combination of the techniques as appropriate. A pictorial representation of the capabilities of the CLASS system is shown in Figure 3.

The CLASS system has been under development since 1976 and is scheduled for completion in mid 1985. The final system, which is coded in Fortran, is expected to exceed 500,000 lines of code. The initial versions of the system are operational on a dedicated Perkin Elmer 3244 computer and accessed by remote terminals. This computer facility is also utilized in the development of the system. The system is being developed through the efforts of contractors (primarily the LinCom Corporation and Stanford Telecommunications Incorporated) and inhouse NASA/GSFC elements. The development and operation of the system is controlled by NASA/GSFC.

A brief description of the modeling techniques used within the CLASS and the techniques that have, and will, be used to validate the CLASS is contained in the papers by Walter R. Braun and Teresa McKenzie of the LinCom Corporation which are contained in these proceedings. The first paper is titled "Modeling Techniques Used in the Communications Link Analysis and Simulation System (CLASS)" and the second is titled "Validation of the Communications Link Analysis and Simulation System (CLASS)".

2. SYSTEM PHILOSOPHY

The CLASS system is designed to permit reliable and accurate operation by a diverse group of CLASS system users. This operation is attained through the use of authority levels where, at the lowest level (General User Level), it is configured to provide a basic end-to-end system bit error rate analysis capability where only TDRSS User communications system parameters can be varied. The inputs and outputs at this level are heavily protected to insure accurate properly documented analysis. All communications with the system at this level are conversational and self prompting since the user is not required or expected to have a detailed knowledge of the CLASS or of the TDRSS.

The next higher level is the Network Systems Engineer Level and is designed for use by personnel with a good knowledge of the TDRSS and TDRSS User systems but with little or no knowledge of the CLASS. This level provides the capability to analyze all communications link parameters on an end-to-end basis. Here again, only TDRSS User parameters can be modified for the analysis.

The highest level provides the capability to analyze the system on an end-to-end, system by system or subsystem basis. At this level any communications system parameter, TDRSS User, TDRSS or environment, can be varied or modified for the analysis. The user at this level is required to have a detailed knowledge of the CLASS, the TDRSS and the TDRSS User systems.

At all levels, the CLASS system is configured to provide conversational, self prompting inputs and outputs in an effort to simplify the operation of a very complex analysis system and to insure that the results derived at each level are correct and reliable. The system itself is currently being validated and will be fully validated when complete to insure the accuracy of the analysis techniques and models. The system is operated under a central control system which links the appropriate analysis/simulation modules to provide the required analysis. At the General User and Network Systems Engineer levels, the control system selects all analysis and system modules (except for user system data) and fully controls all execution. At the highest level, the CLASS user can override the control system as desired to perform other non-standard types of analysis.

The currently operational analysis capabilities of the CLASS system (the initial system is called Interim CLASS) are shown in Figure 4 by authority level for the General User and NSE levels. These lists represent a subset of the capabilities that will be available when the system is completed.

3. CLASS ANALYSIS CAPABILITIES

The TDRSS, which will be the primary spaceflight communications and tracking support element of the NASA Networks, is a threshold communications system where normal operating margins are expected, and in some cases encouraged, to be small. This results in a communications or tracking link where maximum efficiency must be used, where signal distortions must be minimized, where all channel environment parameters must be considered, and where accurate, thorough and rapid analysis of all appropriate performance parameters must be conducted. The classical communications system analysis techniques in use cannot provide the analysis capabilities and accuracies required, they cannot consider simultaneously all of the significant parameters and cannot consider the non-gaussian communications channel environment of the TDRSS. These classic techniques also can not provide the rapid analysis capability needed by the Networks to ensure performance and compatibility of the TDRSS User/TDRSS interface in a dynamic analysis environment.

The solution to this problem is the development of the CLASS system which can provide all necessary analyses in the required time frame and to the required accuracy. The CLASS also permits many of the analyses to be performed by personnel who are not experts in the area of communications system analysis thereby reducing the demand on this limited resource. This user can for example, by inputting a description of the TDRSS user data system, transmitter and antenna systems, perform an analysis to determine the bit error rate of the data at the output of the TDRSS this analysis can consider simultaneously the users specific link parameters, all signal distortion parameters, antenna characteristics, user vehicle dynamics, the impact of RFI, multipath, atmospheric and TDRSS hardware and software characteristics. This analysis can be performed for all TDRSS compatible signal configurations, both forward (command) and return (telemetry), as well as certain classes of signal structures which are not totally compatible with TDRSS interface requirements.

The primary performance parameters which can be analyzed by the CLASS are data/symbol bit error rate, data/symbol slippage statistics, cycle slippage statistics, signal/data acquisition statistics, loss of lock probabilities, tracking data accuracies, false lock statistics, system interference, and autotrack system performance. These parameters can be analyzed on an end-to-end system basis or on a system-by-system basis. They can be performed as a single point analysis for a single value of each variable, on a sensitivity basis where the performance parameter is computed against the variation of one or more variables or the evaluation can be on a time line basis where the performance parameters are evaluated against a mission time line. Any or all elements of the communications channel can be included in the performance analysis. In general the current operating CLASS system evaluates these performance parameters on an individual basis whereas the final system will provide for the simultaneous evaluation of all applicable performance parameters. These parameters can be used to evaluate the performance capabilities of the TDRSS User link or to evaluate the performance of the TDRSS system or any component of the system.

The CLASS also provides a group of ancillary, or secondary, capabilities which complement or supplement those previously described. These provide the capability to plot or compute statistics relative to TDRSS communications coverage of user spacecraft, prediction of forward and return link flux density restrictions as they affect support capabilities for the user, subprograms to provide formatted data for Interface Control Documents, and other TDRSS/user interface efforts, as well as the ability to evaluate total signal compatibility when any end-to-end evaluation is performed. Also, since the CLASS inherently contains a current description of the interface capabilities of the TDRSS system, this information is provided to the system user, at his request, on a subject by subject basis.

4. CURRENTLY OPERATIONAL ANALYSIS TYPES

The current CLASS system (the Interim CLASS) is capable of performing a variety of analyses based upon the capabilities discussed in Section 3. Some of the more frequently used types are discussed below to provide examples of the CLASS capabilities.

Evaluation of the effect of signal distortions on bit error rate: This evaluation is performed to determine the User Constraint Loss parameter for use in link performance predictions as shown in Figure 5. It can also be utilized to evaluate the sensitivity of the TDRSS in response to variations in one or more link or channel parameters as shown in Figure 6.

Evaluation of TDRSS User bit error rate performance margins: This type of analysis is utilized to evaluate the BER performance of a given set of user parameters on a single point or time line basis. The result is usually expressed as a user EIRP margin relative to achieving a 1 in 10^5 BER. The primary purpose of the CLASS is to provide the User Constraint Loss, RFI Loss, Dynamics Loss, Atmospheric Loss, Antenna Switching Loss, and Multipath Loss data as shown in the example in Figure 7. When operated in this mode, the system also provides a full compatibility evaluation and a link diagram showing all models included in the analysis along with the values of the TDRSS variables involved. An example of this link diagram is shown in Figure 8.

Link acquisition time analysis: This analysis determines the acquisition time statistics for the user link including all elements (total link) or for just one element (e.g., PN acquisition). A total link acquisition time analysis is shown in Figure 9 for a forward link.

The effect of antenna switching of system performance: This type of analysis is conducted to evaluate the effect of antenna switching on user communications channel BER performance, loss of lock statistics and acquisition times. An example is shown in Figure 10. This capability provides both a performance evaluation and an aid in user design activities.

Self interference analysis: A system capability which is executed to monitor the interference caused by the other users of the TDRSS system when support is being provided to a specific user. The results of this continuing analysis are utilized in NASA network planning and user mission design and planning. An example of this type of analysis is shown in Figure 11.

TDRSS user time line performance: A capability to provide a mission time line analysis of any performance parameter while considering all channel and TDRSS elements. An example of a Centaur return link BER performance margin analysis for a planetary insertion trajectory time line is shown in Figure 12. This example analysis includes the effect of Centaur dynamics, antenna switching, plume attenuation and signal characteristics.

TDRSS system performance evaluations: These analyses are conducted to evaluate the performance of the TDRSS system, in total or on a subsystem-by-subsystem basis, relative to specification requirements or to characterize the system performance for the purpose of providing the TDRSS users with current accurate performance predictions. Examples of these analyses are shown in Figure 13 and 14.

5. SYSTEM AVAILABILITY AND USE

Access to the CLASS analysis is currently available through the Network Systems Engineers who are a part of the Networks Mission Support Team. The Network System Engineer will either perform the analysis or refer the request to a CLASS analyst. CLASS system analyses are automatically performed by the NSE as a part of the ICD development efforts. The use of the CLASS for mission design or mission optimization type efforts will normally be executed through the CLASS development contractors. More information on this subject can be provided by contacting the CLASS Development Manager.

For certain TDRSS users, direct access to the CLASS system will be available at the General User authority level. The capabilities available at this level are designed to permit TDRSS user communications system sizing and planning types of analysis. Access at this level may be limited due to computer loading considerations.

ACKNOWLEDGEMENT

I would like to acknowledge the contributions of the LinCom Corporation, especially Dr. William Lindsey, Dr. Walter Braun and Terese McKenzie, for their invaluable aid in the development of the CLASS concept and the development of many of the components of the CLASS system.

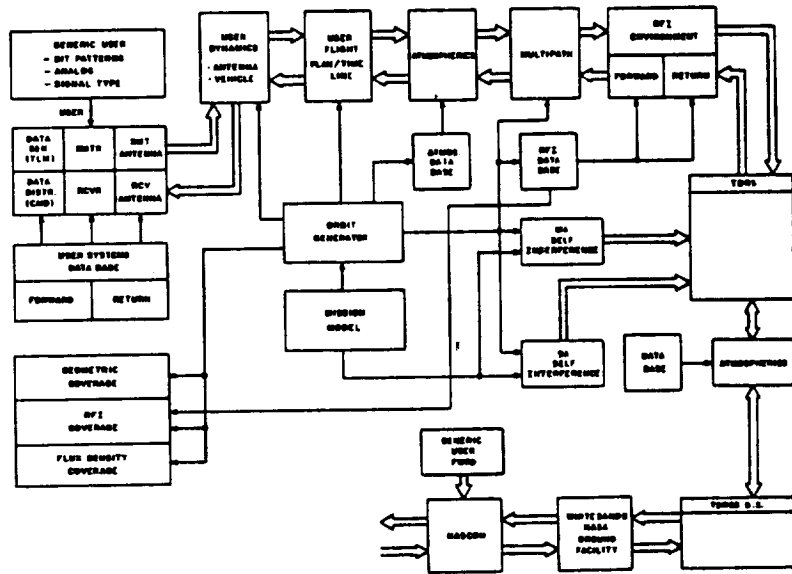


FIGURE 1: CLASS MODEL DIAGRAM

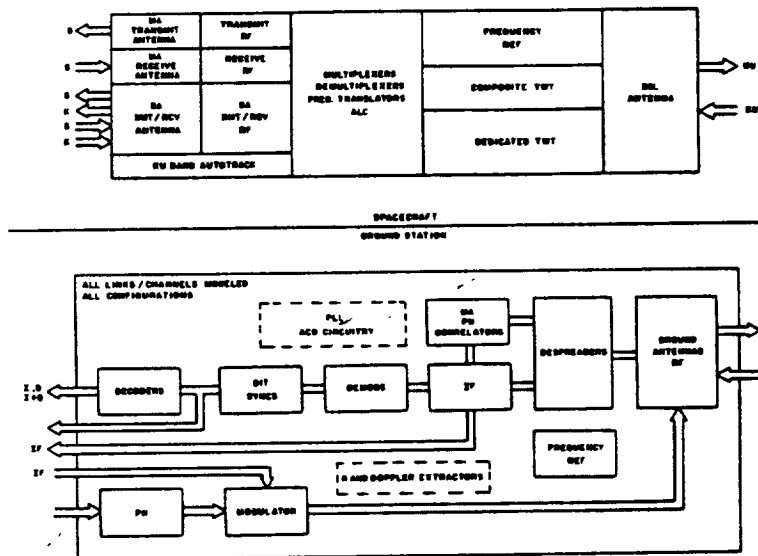


FIGURE 2: CLASS TDRSS COMPONENT COMPONENT MODEL

INTERIM CLASS CAPABILITIES

BY AUTHORITY LEVEL

General User Level

1. TDRSS Capabilities Description - Return Link
2. TDRSS Capabilities Description - Forward Link
3. User/TDRSS Link Signal Margin Calculation - Forward Link
and Return Link
(Reduced)

Network Support Engineer Level

1. TDRSS Capabilities Description - Return Link
2. TDRSS Capabilities Description - Forward Link
3. User/TDRSS Link Signal Margin Calculation - Forward and
Return Link
(Full)
4. User/TDRSS Link BER Evaluation - Forward and Return Link
5. User/TDRSS Link Signal Performance Time Line - Forward and
Return Link
EIRP Margin
or BER
6. User Constraint Analysis - Sensitivity
7. Total Link Acquisition Time
8. TDRSS Coverage
9. TDRSS/User Coverage Statistics
10. User Data Base
11. Forward Link Flux Density Analysis
12. Return Link Flux Density Analysis

FIGURE 4

COMMUNICATIONS LINK ANALYSIS AND SIMULATION SYSTEM

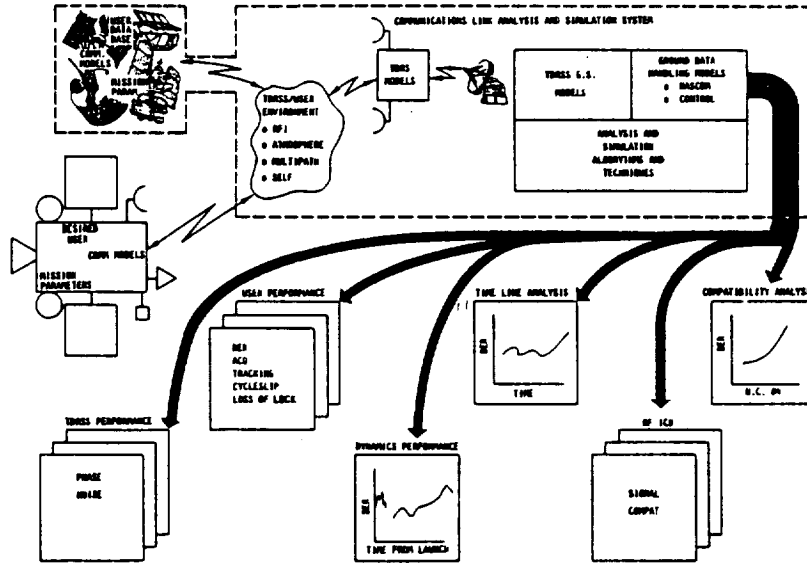


FIGURE 3: CLASS SYSTEM CAPABILITIES

LINK PERFORMANCE DEGRADATION DUE TO EXCEEDING USER CONSTRAINT LIMITS

SHUTTLE S-BAND LINK

S-BAND SIGNAL DESCRIPTION

- DATA RATE 192 kbps
- DG 2, MODE 1, NRZ, CODED, BPSK, TWT TRANSMITTER REPRESENTATION

CONSTRAINT PARAMETER	STDN 101.2 LIMIT	SHUTTLE ^a VALUE	INDIVIDUAL DEGRADATION (dB)
PHASE NOISE/COHERENT	<1° rms	<10° rms	.3
PHASE NOISE/NOH-COHERENT	<1° rms	<10° rms	.3
MODULATOR PHASE IMBALANCE(BPSK)	± 3° peak	± 11° peak	.1
DATA ASYMMETRY (PEAK)	± 3%	± 3.8%	.1
AM/PM	≤ 12 deg/dB	≤ 14 deg/dB	.2
GAIN FLATNESS (PEAK)	± .3 dB	± .4 dB	0
COMBINED TOTAL			≤ 0.8

^aAS PER REFERENCED LETTER

^bROUNDED TO NEAREST .1 dB

FIGURE 5: SHUTTLE USER CONSTRAINT DEGRADATION ANALYSIS

```

-PRINT OUT THE RESULTS:
-CASE 1 FOR DCF PERFORMANCE, 2 FOR SENSITIVITY
) FOR BOTH, 3 FOR PRINT-OUT
*)
.
.
.
VALUE OF PARAMETER 12 : 0.00 DESIGN VALUE: 0.00
.
UP-CM BIT ERROR RATE RMS PK. ERR. (DEG) IDEAL DEG
-CASE VAR. 1 CHAN. 0 CHAN. 1 CHAN. 0 CHAN. 1 CHAN. 0 CHAN.
.
1 -0.00 1.95E-04 1.95E-04 3.72E+00 3.72E+00 2.48E-06 2.48E-06
2 -0.00 3.80E-06 3.80E-06 3.67E+00 3.67E+00 3.11E-09 3.11E-09
3 -2.00 3.50E-08 3.50E-08 3.64E+00 3.64E+00 9.13E-10 9.13E-10
4 0.00 1.26E-10 1.26E-10 3.61E+00 3.61E+00 7.28E-21 7.28E-21
5 2.00 3.27E-11 3.27E-11 3.60E+00 3.60E+00 5.56E-32 5.56E-32
.
.
.
VALUE OF PARAMETER 12 : 5.00 DESIGN VALUE: 0.00
.
UP-CM BIT ERROR RATE RMS PK. ERR. (DEG) IDEAL DEG
-CASE VAR. 1 CHAN. 0 CHAN. 1 CHAN. 0 CHAN. 1 CHAN. 0 CHAN.
.
1 -0.00 1.76E-04 1.76E-04 3.72E+00 3.72E+00 2.48E-06 2.48E-06
2 -0.00 5.38E-06 5.38E-06 3.67E+00 3.67E+00 3.11E-09 3.11E-09
3 -2.00 6.16E-08 6.16E-08 3.64E+00 3.64E+00 9.13E-10 9.13E-10
4 0.00 3.16E-10 3.16E-10 3.61E+00 3.61E+00 7.28E-21 7.28E-21
5 2.00 1.22E-12 1.22E-12 3.60E+00 3.60E+00 5.56E-32 5.56E-32
.
.
.
VALUE OF PARAMETER 12 : 6.00 DESIGN VALUE: 0.00
.
UP-CM BIT ERROR RATE RMS PK. ERR. (DEG) IDEAL DEG
-CASE VAR. 1 CHAN. 0 CHAN. 1 CHAN. 0 CHAN. 1 CHAN. 0 CHAN.
.
1 -0.00 3.37E-04 3.37E-04 3.72E+00 3.72E+00 2.48E-06 2.48E-06
2 -0.00 8.94E-06 8.94E-06 3.67E+00 3.67E+00 3.11E-09 3.11E-09
3 -2.00 1.49E-07 1.49E-07 3.64E+00 3.64E+00 9.13E-10 9.13E-10
4 0.00 1.22E-09 1.22E-09 3.61E+00 3.61E+00 7.28E-21 7.28E-21
5 2.00 8.51E-12 8.51E-12 3.60E+00 3.60E+00 5.56E-32 5.56E-32

```

FIGURE 6: TYPICAL TABULATED PERFORMANCE RESULTS

CRITICAL
OF POOR QUALITY

SPACE TELESCOPE
RETURN LINK PERFORMANCE MODEL
LINK NO. 1

NO. SERVICE, DATA GROUP = 1, MODE = 2, 200.0 MHz, LCP
NAME = 04294.0 00

1-CHANNEL

DATA RATE = 4.0 MBPS
MOD 2 ADDED TO 00
DATA TYPE = 000-4
RATE 1/2 CODED

0-CHANNEL

DATA RATE = 32.0 MBPS
MOD 2 ADDED TO 00
DATA TYPE = 000-4
RATE 1/2 CODED

PARAMETER	LINK DATA		TELESCOPE		REMARKS
	1-CHANNEL	0-CHANNEL	1-CHANNEL	0-CHANNEL	
1. USER TRANSMITTED POWER - dBm	6.2	6.2	.0	.0	NOTE A
2. USER POSITIVE LOSS - dB	6.2	6.2	0	0	NOTE A
3. USER ATTEN. LOSS - dB	26.4	26.4	0	0	NOTE A
4. USER POSITIVE LOSS - dB	.2	.2	0	0	NOTE A
5. POLARIZATION LOSS - dB	.2	.2	0	0	NOTE A
6. USER DATA/TOTAL POWER RATIO - dB	-2.0	-2.0			NOTE A
7. PREAMP SPACE LOSS - dB	126.4	126.4			NOTE A
8. PREAMP RECEIVED POWER - WATT @ 0.01m	-100.5	-100.5			SEE 1 THRU 7
9. USER CARRIER LOSS - dB	.0	.0	0	0	NOTE B
10. OTHER LOSSES - dB	0	0	0	0	NOTE C
11. RFL LOSS - dB	.0	.0	0	0	NOTE D
12. REMAINDER EFFECTIVE POWER - WATT @ 0.01m	-176.5	-176.5			SEE 0 THRU 11
13. REMAINDER EFFECTIVE POWER - WATT @ 0.01m	-100.0	-171.2			SEE 100.2
14. EFFECTIVE USER CHANNEL NUMBER - dB	16.2	1.2	-1.0 000 -1.0 000	-1.0 000 -1.0 000	12 REMARK 13
15. EFFECTIVE CHANNEL NUMBER - dB					NOTE E

NOTE A - PREAMP REFERENCE SUBJECT TO CHANGE BY USER
NOTE B - PREAMP CLASS ANALYSIS
NOTE C - PREAMP CLASS ANALYSIS IF COMPUTED
NOTE D - ANTENNA SWITCHING LOSS - dB -
ATMOSPHERIC LOSS - dB - .00 dB
MULTIPLEX LOSS - dB - .00 dB
NOTE E - PREAMP CLASS ANALYSIS
REQUIREMENTS AND ANALYSIS GROUP
000 - CLASS
1/2/3/4/5
NOT APPLICABLE IF NOT COMPUTED

LINK CARRIER/QUALITY EVALUATION
LINK IS ESSENTIALLY CARRIER/QUALITY -
1. REMARK 13 EXCESSIVE FOR SERVICE
ALL OTHER CHECKED ITEMS ARE CARRIER/QUALITY -

FIGURE 7: SAMPLE RETURN LINK PERFORMANCE EVALUATION

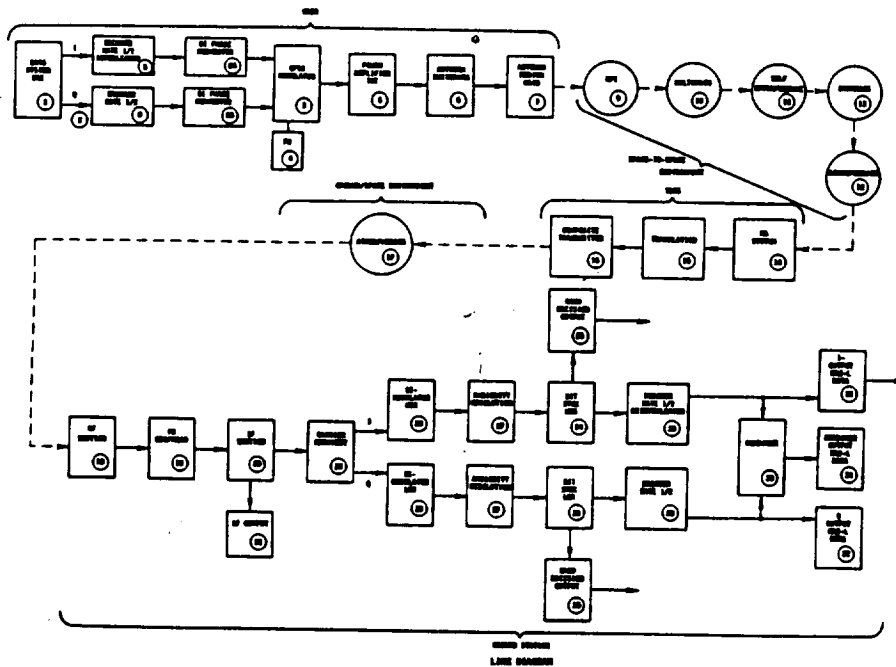


FIGURE 8: RETURN LINK - EXAMPLE

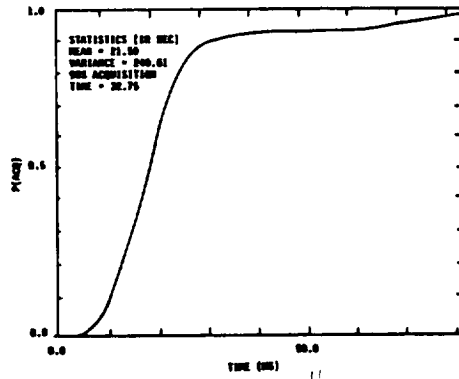


FIGURE 9: EXAMPLE OF CUMULATIVE PDF PLOT FOR FORWARD LINK USER

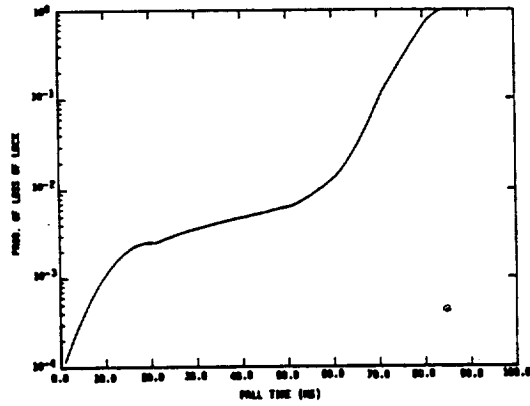


FIGURE 10: PROBABILITY OF LOSS OF LOCK AS A FUNCTION OF TIME RELATIVE TO THE BEGINNING OF FRAME. ANTENNA SWITCHING ANALYSIS

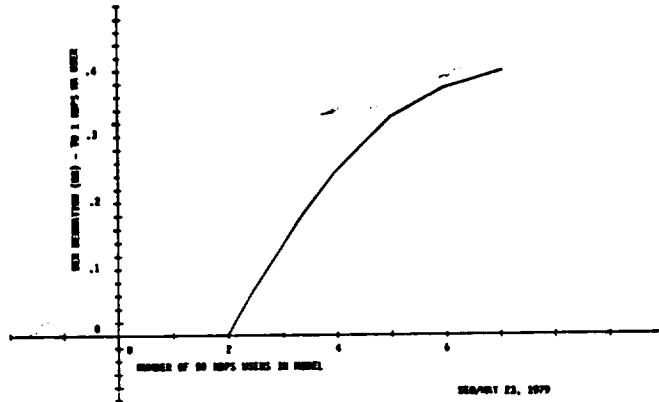


FIGURE 11: IA SELF INTERFERENCE ANALYSIS TOTAL NUMBER OF USERS-20

GR. P. 1111

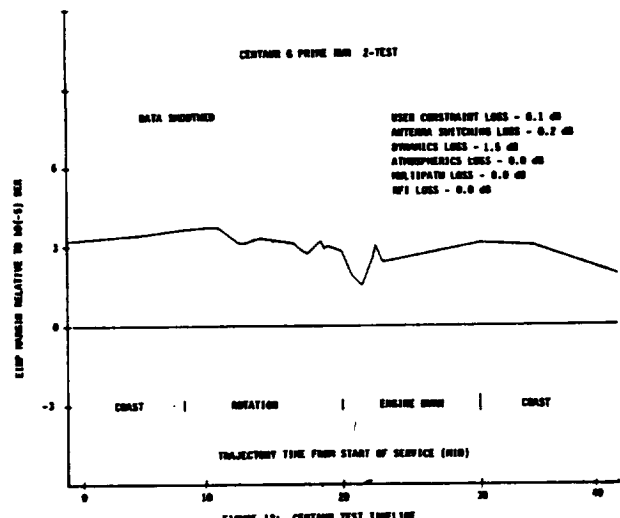


FIGURE 12: CENTAUR TEST TIMELINE

USER SEARCH SCHEME \ EIRP (DBW)	4	5	6	7	8	9	10
Expanding Window Search	116.5	70.3	47.0	37.6	30.5	26.0	20.0
Abbreviated Expanding Window Search	121.4	73.7	46.5	38.6	21.1	18.9	18.4
Extended Search	122.2	74.5	46.7	31.6	22.4	18.0	12.6
Alternate Expanding Window Search	118.1	68.8	46.4	34.2	28.5	21.7	16.5

*Applies to symbol rates < 3 bps and 8 kHz protection filter.

FIGURE 13: MODE 1 ACQUISITION TIME (SEC) VS USER EIRP FOR 90% ACQUISITION PROBABILITY*

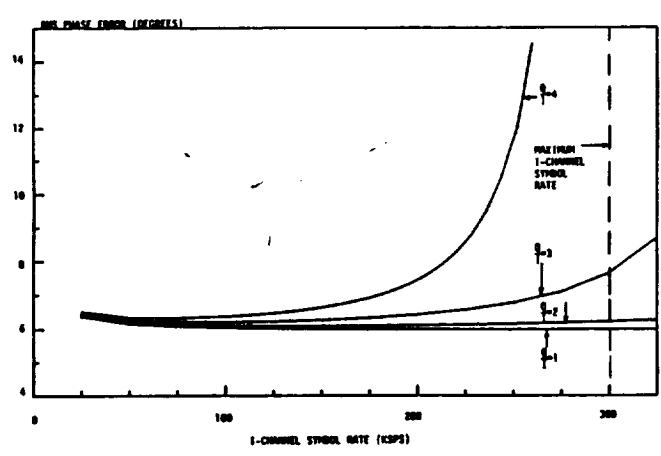


FIGURE 14: MODE 2 TRACKING RMS PHASE ERROR PERFORMANCE - CORDED MODE, 90% IN LOOP DENSITY

D116
N85-16953

MODELING TECHNIQUES USED IN THE COMMUNICATIONS LINK ANALYSIS AND SIMULATION SYSTEM (CLASS)[†]

Walter R. Braun*
Teresa M. McKenzie

LinCom Corporation
P.O. Box 15897
Los Angeles, CA 90015-0897
(213) 381-3701

ABSTRACT

CLASS (Communications Link Analysis and Simulation System) is a software package developed for NASA to predict the communication and tracking performance of the Tracking and Data Relay Satellite System (TDRSS) services. This paper describes some of the modeling techniques used in CLASS.

1. INTRODUCTION

The Communications Link Analysis and Simulation System (CLASS) presently under development for NASA/Goddard Space Flight Center (GSFC) is an integrated set of FORTRAN programs capable of predicting the compatibility and performance of the communication and tracking links for all services and signal formats supported by the Tracking and Data Relay Satellite System (TDRSS). CLASS contains detailed models for the TDRSS spacecraft and ground terminal hardware, including Shuttle-unique equipment, and models for the effects of the transmission medium (rain attenuation, multipath, radio frequency interference (RFI)). CLASS allows the modeling of the transponder of a TDRSS user such as Shuttle either based on a specific hardware implementation or based on a set of parameters describing the signal characteristics at the RF interface between TDRSS and the user transponder. These parameters are used by NASA/GSFC to specify the quality of the user's signal at this interface and are, therefore, referred to as user constraints [1].

CLASS is capable of verifying the compatibility of a particular transponder design with the TDRSS signal formats and predicting the system performance in terms of all the performance parameters of interest to the user. These include data integrity (bit error probability, bit slippage probability, probability of carrier phase slips in MPSK systems), synchronization (tracking jitter, slip rates, loss of lock probability), tracking (range and range rate), and acquisition (acquisition time, probability of false lock) performance.

The capabilities and structure of CLASS are presented in more detail in another paper in these Proceedings, "Communications Link Analysis and Simulation System" by Robert Godfrey. The effort made to validate CLASS is described in another paper in the Proceedings, "Validation of the Communications Link Analysis and Simulation System (CLASS)" by the same authors as the current paper.

The purpose of this paper is to describe some of the modeling techniques used in CLASS. The components of TDRSS and the performance parameters to be computed by CLASS are too diverse to permit the use of a single technique to evaluate all performance measures. Hence, each CLASS module applies the modeling approach best suited for a particular subsystem and/or performance parameter in terms of model accuracy and computational speed. It was one of the challenges of the CLASS development to design a software structure which allows these diverse modules to share one system database.

The following sections provide a brief description of the modeling techniques used for four major parts of CLASS: the bit error rate performance computation (Section 2), the synchronization/tracking subsystem (Section 3), the acquisition subsystem (Section 4), and the evaluation of RFI effects (Section 5).

2. COMPUTATION OF BIT ERROR RATE

The channel model for the bit error rate analysis must account for the signal distortion occurring in the transmitter, the relay satellite, as well as the receiver. A typical return link channel model is shown in Figure 1. The complexity of this channel model, particularly the mixing of linear and nonlinear elements, prevents the use of strictly analytical performance evaluation techniques. Similarly, the low bit error probabilities of interest (the design BER is 10^{-5}) make Monte Carlo type simulations prohibitively slow. The approach used in CLASS combines elements of both techniques. The signal is represented as a sampled waveform which allows the modeling of all user constraints. Linear

[†]This work was supported by NASA Goddard Space Flight Center under contracts NAS 5-27240, NAS4-25681, NAS5-23591.

* W. Braun is currently with Brown, Boveri & Co., Limited, Baden, Switzerland.

signal distortions are easily incorporated through a fast Fourier transformation (FFT) of the waveform and appropriate processing in the frequency domain. The interaction between the signal, adjacent channel waveforms, and thermal noise in nonlinear elements (power amplifiers, limiters) is modeled through a modified Barrett-Lampard expansion developed for this program and described elsewhere [2].

The receiver model operates on the sampled signal and a statistical representation of the thermal noise and interference. First, the effect of the signal characteristics on the synchronization systems (PN code, carrier, clock recovery) is computed. The effect of these subsystems on the recovered symbols is then included in the bit error performance evaluation by computing first the BER conditioned on the various synchronization errors and then averaging over the appropriate probability densities. The BER in the case of coding and 8-level quantization at decoder input is computed via the R_0 approximation [3]. The channel cut-off rate R_0 , computed from the channel output probabilities conditioned on channel input, is assumed to fully characterize the channel. The BER is assumed to be a function of code rate and R_0 only, those functions being given in [4].

The above approach is not intended as a universal modeling tool for nonlinear channels. The modified Barrett-Lampard expansion describes the spectral characteristics of the output of the nonlinearity and it requires an excessive number of terms when highly nonlinear elements, such as hard limiters, are included in the channel model. Similarly, the approximations made in the statistical representation of the noise and interference become inaccurate when highly nonlinear elements are modeled. However, for the characteristics of the TDRSS channels the accuracy of the models was verified by analysis and comparison to Monte Carlo simulations.

To point out the importance of a comprehensive link model, the single parameter sensitivities with a perfect signal and a linear, wideband channel are compared in Figure 2 with sensitivity results obtained with a typical TDRSS link model. The plots show that single parameter sensitivity results with a perfect signal and a linear, wideband channel can be quite misleading. Similarly, Table 1 shows that for another typical link the sum of the degradations that result from increasing each of several parameter values separately can be different from the degradation that results from increasing all the values at once.

3. MODELING OF THE SYNCHRONIZATION/TRACKING OPERATION

The synchronization subsystems modeled are the PN code, carrier, and clock recovery loops in their various implementations in the TDRSS ground station. Several performance parameters are of interest:

- (1) the tracking jitter due to thermal noise and signal amplitude and phase variations,
- (2) the tracking offset due to loop stress and vehicle dynamics (Doppler, acceleration),
- (3) the rate of cycle slips due to all the above sources and to untracked clock jitter,
- (4) the probability of dropping lock due to vehicle and antenna dynamics and signal dropouts.

These subsystems are modeled by a combination of analysis and simulation. The analysis accounts for the effect of thermal noise, phase noise (clock jitter), and vehicle and antenna dynamics on the synchronization performance (based on nonlinear tracking models [5]), while the signal waveform generated for the BER performance evaluation is used to characterize the effect of waveform distortions. The phase-tracking jitter generated by these signal distortions is generally referred to as pattern jitter. By linearly combining it with the thermal noise effect the overall subsystem performance is obtained.

The characterization of the tracking performance requires, in addition to the above aspects, an accurate model of the low-frequency phase noise in the TDRSS and user transponder. All TDRSS links can operate in a coherent turnaround mode. This means that the phase noise processes on the ground, in the TDRS, and in the user equipment are correlated. However, due to the small phase error values of interest, linear models apply and the system can be characterized by a linear network. A thorough description is provided in [6].

4. MODELING OF SIGNAL ACQUISITION

The signal acquisition process includes the search for the PN code epoch (for spread spectrum signals), the carrier frequency and phase acquisition, and the clock synchronization. In addition, the Ku-band links require the spatial acquisition of the autotrack system.

Analytical models were developed for the different hardware implementations used in the TDRSS ground station and various user transponders. The signal model used reflects the user constraints as well as the linear and nonlinear distortion effects of the channel.

The PN acquisition model computes the characteristic function of the search time based on the a priori code epoch uncertainty and the search algorithm. Specific cases of interest include single dwell time, dual dwell time, and variable dwell time systems for a circular search over the whole code

or an expanding window search over a small part of the long code (e.g. during reacquisition). A detailed description of the analytical approach is given in [7,8].

The carrier acquisition algorithms modeled include frequency-locked loop (FLL) aiding, swept acquisition, and frequency pull-in (self acquisition). The modeling is based on analytical models [5,9,10] with appropriate modifications to account for signal distortions (user constraints and channel effects). The FLL may operate with a low SNR at the input to the frequency discriminator. The model includes, therefore, a spike noise component at the discriminator output. The FLL bandwidth is small, however, which permits the use of a linearized loop model.

A major component of these models is the acquisition/tracking monitor and the transition between the two modes. The response time of the monitor can contribute significantly to the overall acquisition time. Also, the implementation of this monitor determines the probability of false lock.

The clock recovery loops modeled are all self-synchronizing. With typical clock stabilities, these systems do not contribute significantly to the acquisition time.

5. MODELING OF RFI EFFECTS

It is expected that some of the TDRSS links will be subject to high-powered RFI. This interference may be a mixture of pulsed CW signals and noise pulses of a few microseconds duration with random arrival times.

CLASS is designed to account for the RFI effect on all aspects of TDRSS performance. First we discuss modeling of the effect on BER, then on synchronization and acquisition, and last on tracking.

Two approaches were taken in the case of BER. First an analytical model was developed based on assumptions that hold for the general TDRSS S-band user. The model breaks down for the Shuttle S-band return link in the prediction of decoder performance. For this reason, a second approach, a Monte Carlo type simulation, was also taken. A benefit of having both approaches is that they serve to verify each other.

The analytical approach in the case of BER is based on the sample-sum approximation to the matched-filter output [11]. The approach is implemented in different ways depending on whether the symbol rate is high or low relative to the inverse of the RFI pulse duration. In both cases the characteristic function of the matched-filter output is obtained. From it, in the case of a convolutionally encoded link, the cut-off rate R_0 is computed, from which in turn BER is computed. An early account of the modeling approach is given in [12]. However, extensive testing demonstrated the need for a host of refinements to insure good accuracy for all RFI environments and data rates. These updated models are described below.

In the high-rate analytical model for BER at most one RFI pulse is assumed to occur in a symbol duration. The Gaussian or non-Gaussian characteristic function of the matched-filter output is obtained, conditioned on no RFI or on the type and power of RFI occurring in the symbol. For CW RFI conditioning is also on the RFI frequency and initial phase. The conditional characteristic functions are weighted and summed to yield the unconditional function. Since interleavers are used by the general TDRSS S-band user (but not Shuttle) for high symbol rates, it can be assumed for the decoder model in that case that the channel is memoryless.

In the low-rate analytical model for BER, each RFI pulse is assumed to be wholly contained in one symbol. The characteristic function of the contribution to the matched-filter output of one RFI pulse is computed, conditioned as above. This characteristic function is normalized by the characteristic function of no RFI occurring for the pulse duration. The average of all such functions is obtained. Poisson pulse arrival statistics are employed to form the non-Gaussian characteristic function of the matched-filter output as the product of a term involving the function just described and the no-RFI characteristic function.

In the Monte Carlo type simulation to model the RFI effect on BER, no interleaver or deinterleaver is present, which reflects the case of the Shuttle return links.

The models of the RFI effect on all the synchronization subsystems and most of the acquisition subsystems are similar. In these subsystems there are a filter with bandwidth roughly equal to the symbol rate, a nonlinear element and possibly some other elements, and then a filter with a bandwidth less than the lowest symbol rate. As in the BER model, two analytical models are actually used. For low symbol rates the first filter is assumed to average the RFI conditions. For high symbol rates the first filter is assumed wide enough to pass the RFI undistorted and the second filter is assumed narrow enough to do the averaging. The results are insensitive to the exact symbol rate that is chosen for the cross-over point between the models. For swept carrier acquisition the time during which the loop

can pull in is assumed long enough to contain many pulses of each type of RFI.

The RFI affects Doppler tracking by increasing carrier phase jitter and cycle slips.

REFERENCES

- [1] "Tracking and Data Relay Satellite System (TDRSS) Users' Guide, Revision 4," STDN No. 101.2, NASA Goddard Space Flight Center, January 1980.
- [2] Chie, C. M., "A Modified Barrett-Lampard Expansion and Its Application to Bandpass Nonlinearities with Both AM-AM and AM-PM Conversion," IEEE Trans. on Comm., Vol. COM-28, November 1980.
- [3] Massey, J. L., "Coding and Modulation in Digital Communications," Proceedings, Int'l. Zurich Seminar on Digital Communications, Switzerland, March 12-15, 1974.
- [4] Weinberg, A., "The Impact of TDRSS User and Transponder Constraints on BER, Acquisition, and Tracking Performance," STI/E-TR-8013, Stanford Telecommunications, Inc., McLean, VA, March 1978.
- [5] Lindsey, W. C., Synchronization Systems in Communication and Control, Prentice-Hall, Englewood Cliffs, New Jersey, 1972.
- [6] Gagliardi, R. M., et al., "Phase Noise Analysis of the TDRSS," Proc. NTC'77, Los Angeles, CA, 1977.
- [7] Braun, W. R., "Comparison Between Variable and Fixed Dwell-Time PN Acquisition Algorithms," Proc. ICC 1981, Denver, CO, 1981.
- [8] Braun, W. R., "Performance Analysis for Variable Dwell Time Expanding Search PN Acquisition Algorithm," IEEE Trans. on Comm., Vol. COM-30, No. 3, March 1982.
- [9] Klappner, J., and Frankle, J. T., Phase-Locked and Frequency-Feedback Systems, Academic Press, New York, 1972.
- [10] Gardner, F. M., Phaselock Techniques, Second Edition, John Wiley and Sons, New York, 1979.
- [11] Davisson, L. D., and Milstein, L. B., "On the Performance of Digital Communications Systems with Bandpass Limiters--Part I," IEEE Trans. on Comm., Vol. COM-20, October 1972.
- [12] Huang, T. C., and Braun, W. R., "Evaluation of Pulsed RFI Effects on Digital Satellite Repeaters," Proc. NTC 1981, Houston, TX, 1980.

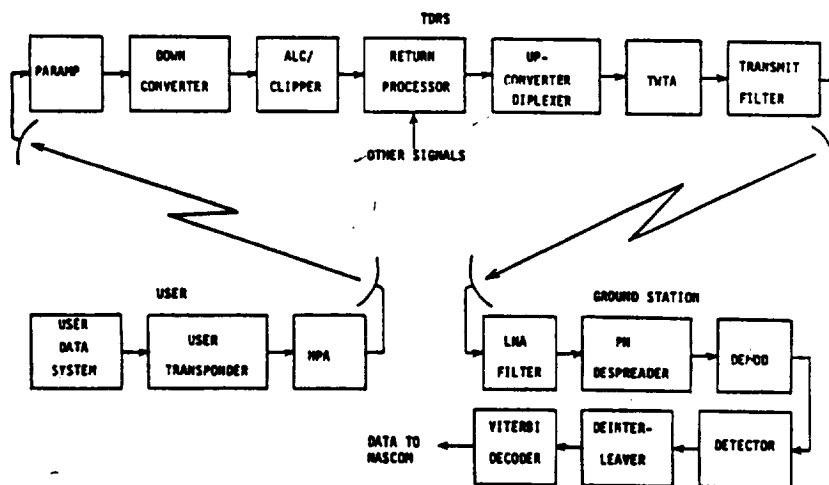


Figure 1. TYPICAL LINK MODEL.

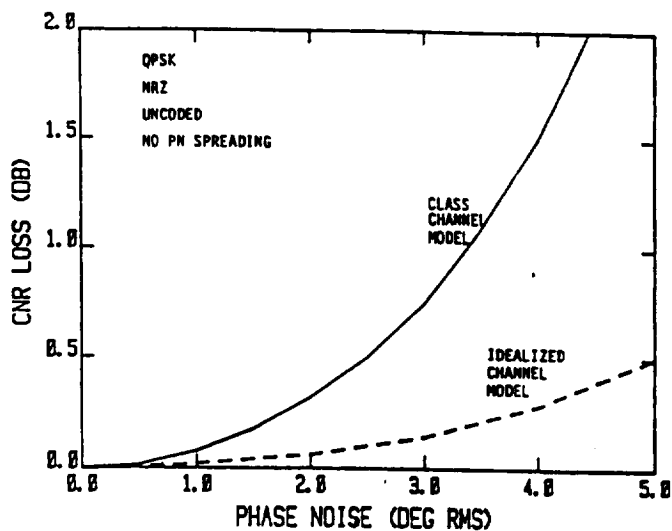


Figure 2a. COMPARISON OF PARAMETER SENSITIVITIES FOR CLASS CHANNEL MODEL AND IDEALIZED CHANNEL MODEL FOR UNTRACKED PHASE NOISE.

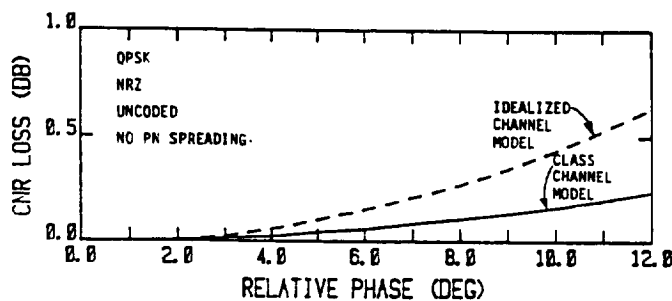


Figure 2b. COMPARISON OF PARAMETER SENSITIVITIES FOR CLASS CHANNEL MODEL AND IDEALIZED CHANNEL MODEL FOR MODULATOR PHASE ERROR.

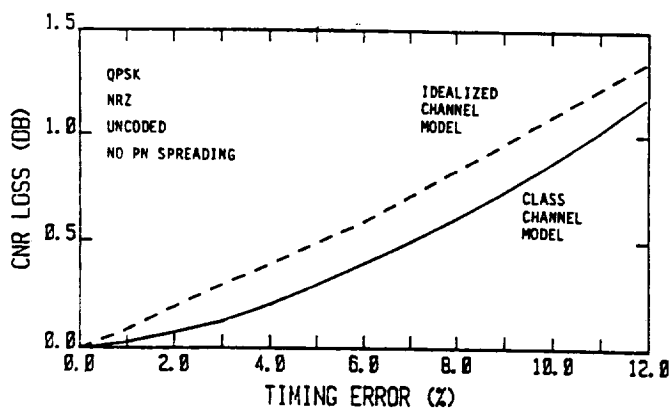


Figure 2c. COMPARISON OF PARAMETER SENSITIVITIES FOR CLASS CHANNEL MODEL AND IDEALIZED CHANNEL MODEL FOR RECOVERED CLOCK PHASE ERROR.

Table 1. CNR LOSS DUE TO SEVERAL PARAMETERS EXCEEDING NOMINAL VALUES (COURTESY OF ROBERT GODFREY OF NASA).

	Parameter	Nominal Value	Actual Value	CNR Loss
1.	Modulator Phase Imbalance	3°	7°	0.2 dB
2.	Modulator Gain Imbalance	+0.25 dB	+0.8 dB	0.87
3.	Phase Nonlinearity	+3°	+9°	0.5
4.	Gain Flatness	+0.3 dB	+3 dB	--
5.	Gain Slope	+0.1 dB/MHz	1	0.15
6.	AM/PM	12°/dB	20°/dB	0.58
7.	Phase Noise	1°	3°	0.1
	Composite Impact			3.18 dB

(BPSK, NRZ, Rate-1/2 Coding, No PN Spreading)

D17
N85-16954

VALIDATION OF THE COMMUNICATIONS LINK ANALYSIS AND SIMULATION SYSTEM (CLASS)[†]

Walter R. Braun*
Teresa M. McKenzie

LinCom Corporation
P.O. Box 15897
Los Angeles, CA 90015
(213) 381-3701

ABSTRACT

CLASS (Communications Link Analysis and Simulation System) is a software package developed for NASA to predict the communication and tracking performance of the Tracking and Data Relay Satellite System (TDRSS) services. This paper describes the methods used to verify CLASS.

1. INTRODUCTION

The Communications Link Analysis and Simulation System (CLASS) presently under development for NASA Goddard Space Flight Center is an integrated set of FORTRAN programs capable of predicting the compatibility and performance of the communication and tracking links for all services and signal formats supported by the Tracking and Data Relay Satellite System (TDRSS).

The capabilities and structure of CLASS are presented in another paper in these Proceedings, "Communications Link Analysis and Simulation System" by Robert Godfrey. Models of major components of CLASS are described in a second paper in the Proceedings, "Modeling Techniques in the Communications Link Analysis and Simulation System (CLASS)" by the same authors as the current paper.

The usefulness of a software tool such as CLASS depends strongly on the reliability and accuracy of the results it produces. For this reason, considerable attention was paid to validation throughout the CLASS development. The purpose of this paper is to describe those efforts. The models mentioned in this paper were discussed in the second paper cited in the above paragraph.

Verification has been and continues to be done by making four types of comparisons: comparisons with analysis (Section 2), with Monte Carlo-type simulations (Section 3), with measurements (Section 4), and with TDRSS test data (Section 5). The prediction of bit error rate (BER) on links both with and without radio-frequency interference (RFI) has been verified in the first three ways. The prediction of pseudo-noise (PN) code acquisition has been checked by comparison with analysis. Finally, in the next couple of years the entire CLASS will be validated on both subsystem and system levels by TDRSS test data.

2. COMPARISON WITH ANALYSIS

One approach taken to verify CLASS is to compare its predicted results with those obtained by analyses, both in-house and published. In this section we describe such efforts for single-parameter sensitivities of BER, the Viterbi decoder performance, BER for a link with RFI, and PN-code acquisition time.

The BER sensitivity to each user constraint (member of a set of distortion parameters that characterize the TDRSS user's transmitter [1]) was evaluated with CLASS using an otherwise perfect signal and a linear, wideband channel. The results were then compared to analytical single-parameter sensitivity results. Typical results are shown in Figure 1. The slight discrepancy in Figure 1c is due to the fact that the sampled signal model does not allow the modeling of instantaneous phase transitions. It can be seen that agreement is excellent.

Comparison of CLASS with purely analytical models of non-ideal channels is not practical because of the limitations the latter place on the channel that can be treated. Figure 2 shows that a typical channel model for analysis does not include filtering effects on the transmitted signal, in distinction from even a minimal model for simulation.

The R_0 approximation method for computing the BER for a convolutionally encoded Gaussian channel from E_b/N_0 (ratio of bit energy to noise one-sided power spectral density) was checked by comparing it

[†]This work was supported by NASA Goddard Space Flight Center, Greenbelt, MD, under contracts NAS5-27240, NAS5-25681, and NAS5-23591.

*W. Braun is currently with Brown, Boveri, & Co., Limited, Baden, Switzerland.

with two other models: a Linkabit Corporation software model probably based on the union bound and an in-house Monte Carlo-type simulation. Figure 3 shows that the R_0 approximation matches the simulation for BER's above about 10^{-5} and is upper-bounded by the Linkabit model for all BER's, as it should be. The validation of the R_0 approximation for non-Gaussian, RFI links is discussed in Section 3.

The analytical model for BER on an RFI link was partially validated by showing that the two sub-models, one for high bit rates and one for low, give similar results in the range of bit rates near the bit rate which is the cross-over point between the sub-models, even though the sub-models themselves are quite different. Figure 4 shows the good agreement for a typical link. The vertical scale on the plot is omitted for national security reasons.

Finally, the model for PN code acquisition performance, applicable to both variable and fixed dwell-time systems, was verified by showing excellent agreement between its predictions and exact results for the fixed dwell-time algorithm, as described in [2].

3. COMPARISON WITH MONTE CARLO-TYPE SIMULATIONS

A variety of BER predictions made by Monte Carlo-type simulations were compared to those made by CLASS. The CLASS link was configured as near as possible to the link used in the Monte Carlo simulations. Three simulation programs of no-RFI links and one of an RFI link were used.

The first comparison for a no-RFI link was with Champ, a simulation program of Comsat Corp. for the evaluation of BER and synchronization (tracking) (see, e.g., [3]). BER results for a TDMA link agreed within 0.5 dB.

The second such comparison was with Link, a program of TRW, Inc., which is usually run without uplink noise (see, e.g., [4]). Such published results were duplicated by CLASS.

The third comparison for a no-RFI link was with an in-house program that modeled the BPSK link shown in Figure 2a. Here, the pulse shaping filter is modeled as a half-Nyquist filter with a roll-off parameter $\alpha = .1$. The satellite input and output filters are of the Chebyshev type with a bandwidth equal to three times the data rate and a ripple of .1 dB. The receiver low-pass filter is matched to the pulse-shaping filter. The high-power amplifier is linear while the satellite TWT characteristic is given by Figure 5. For the Monte Carlo simulation the same 63-bit signal used in CLASS was combined with 32 different uplink noise waveforms to find the uplink waveform contribution to the detector input. The downlink noise effect was modeled analytically. No effort was made to smooth the resulting performance curves in order to demonstrate the slow convergence of the results. Typical results are shown in Figure 6 for two different operating points of the TWT. Note that the Monte Carlo curves follow the CLASS results quite well, but with some wild variations, despite the large number of bits simulated.

The predictions of the analytical program for BER on an RFI link have been compared with those from an in-house Monte Carlo-type program for coded links without interleaver. The two data rates used in the comparison were low enough that the analytical model also included no interleaver. The BPSK link had uplink noise, a non-linearity, and no downlink noise or receiver losses. The RFI was severe. The BER's were identical within 10%. This finding confirms not only the approach taken in the analytical program to model the matched filter output in RFI but also the applicability of the R_0 approach for coded BER computation on a channel which is not nearly Gaussian.

4. COMPARISON WITH MEASUREMENTS

Probably the most convincing validation of results obtained with software is close agreement with hardware results. Both no-RFI and RFI link predictions were checked this way.

One comparison of CLASS with hardware was with Harris, Corp., breadboard measurements made in 1978 for a TDMA satellite communication system. The link was nonlinear and included uplink and downlink thermal noise and adjacent channel interference. Agreement was within 1 dB.

The RFI BER model was verified with Harris Corp. breadboard measurements using TDRSS hardware and an RFI test generator. Four RFI scenarios were used. Two distributions of RFI power and pulse arrival rate were used, a benign environment and a severe environment. On each environment were based two scenarios, one with only noise-type pulses and one with the pulses divided between noise-type and continuous wave (CW)-type. The results in Table 1 demonstrate that the predictions were accurate in most cases and that they were in all cases pessimistic. The model was designed not to underestimate the RFI effect.

5. COMPARISON WITH TDRSS TEST DATA

Currently an effort is under way to develop a comprehensive CLASS validation plan using the first TDRS in orbit and the TDRSS ground station. Baseline hardware losses of TDRSS subsystems will be measured. Then the sensitivity of all the performance measures predicted by CLASS to all the sources of signal distortion and interference will be verified. A great effort has been made to reduce the number of tests to the minimum necessary for a complete validation.

REFERENCES

1. "Tracking and Data Relay Satellite System (TDRSS) Users' Guide, Revision 4," STDN No. 101.2, NASA Goddard Space Flight Center, January 1980.
2. Braun, W. R., "Performance Analysis for the Expanding Search PN Acquisition Algorithm," IEEE Trans. on Comm., Vol. COM-30, No. 3, March 1982.
3. Palmer, L. C., and Lebowitz, S., "Including Synchronization in Time-Domain Channel Simulations," Comsat Technical Review, Vol. 7, No. 2, Fall 1977.
4. Poza, H. B., and Berger, H. L., "Performance Characterization of Advanced Wideband Data Links," International Conference on Communications, 1975.

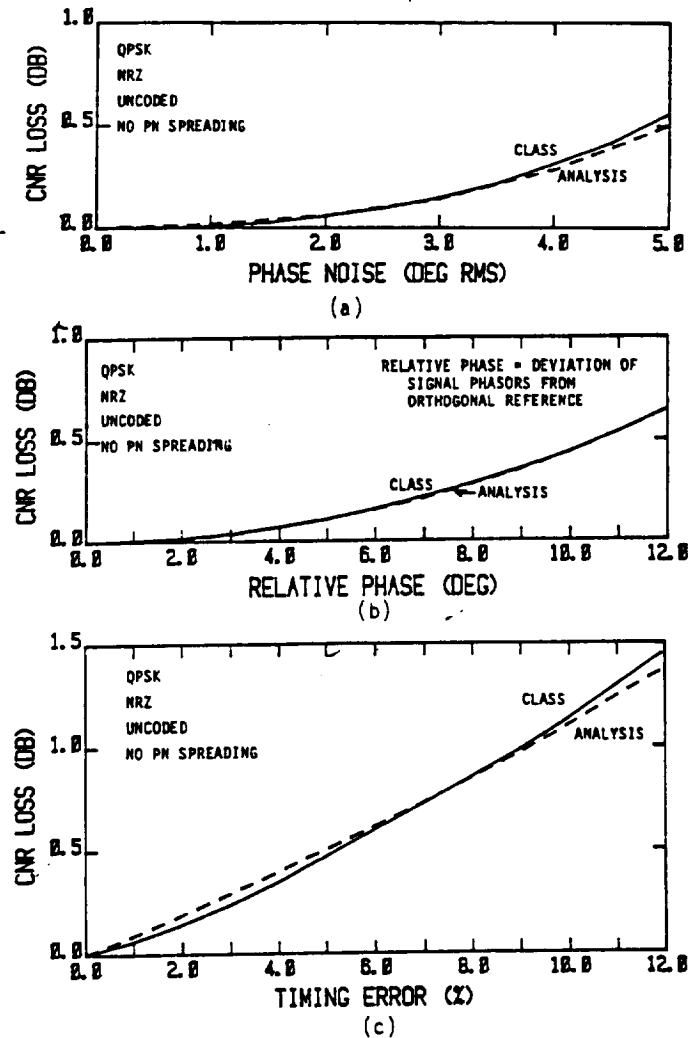


Figure 1. COMPARISON OF ANALYTICAL AND SIMULATED SINGLE PARAMETER SENSITIVITIES. (A) UNTRACKED PHASE NOISE, (B) MODULATOR PHASE ERROR, (C) RECOVERED CLOCK PHASE ERROR.

ORIGINAL QUALITY
OF POOR QUALITY

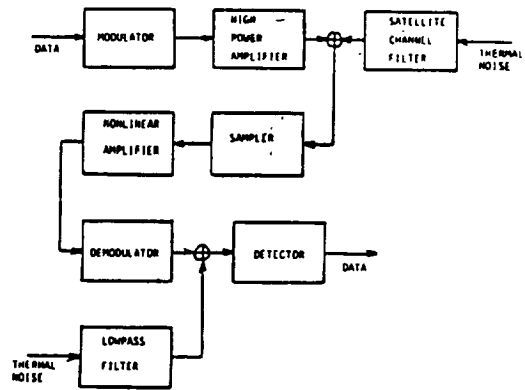
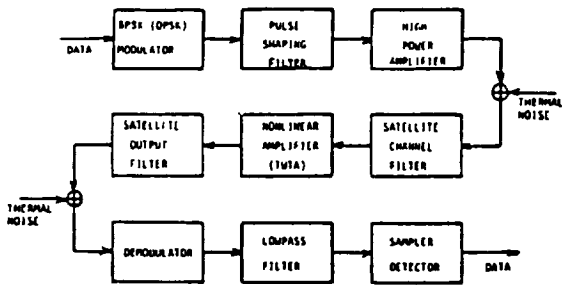


Figure 2a. MINIMAL CHANNEL MODEL FOR SIMULATION.

Figure 2b. TYPICAL CHANNEL MODEL FOR ANALYSIS.

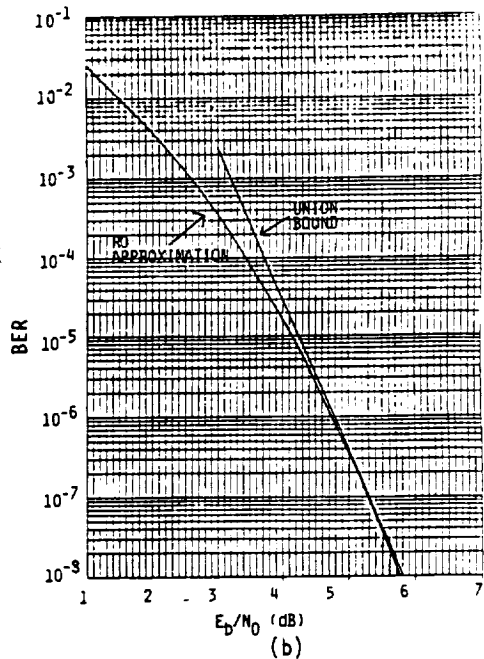
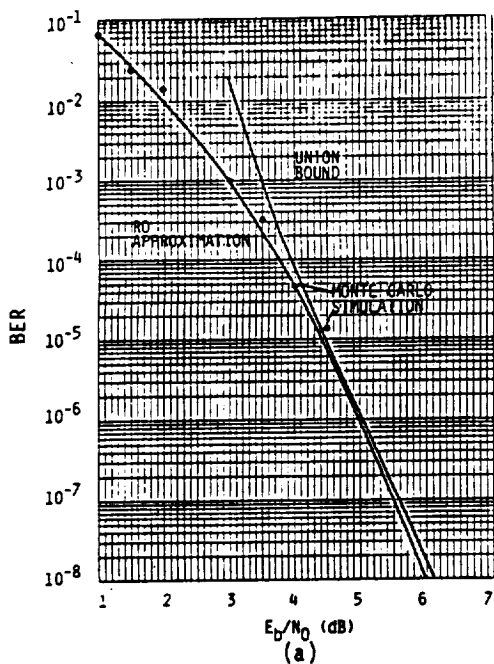


Figure 3. COMPARISON OF PERFORMANCE MODELS FOR (A) RATE-1/2 CODE, (B) RATE-1/3 CODE.

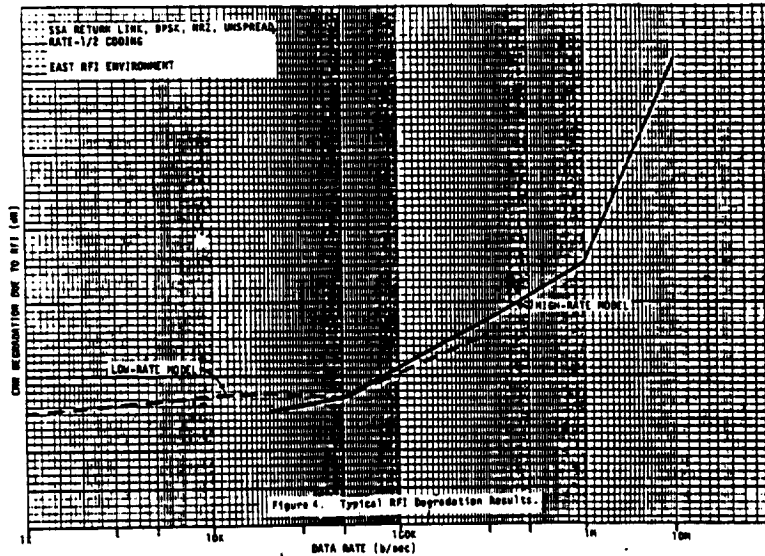


Figure 4. TYPICAL RFI DEGRADATION RESULTS.

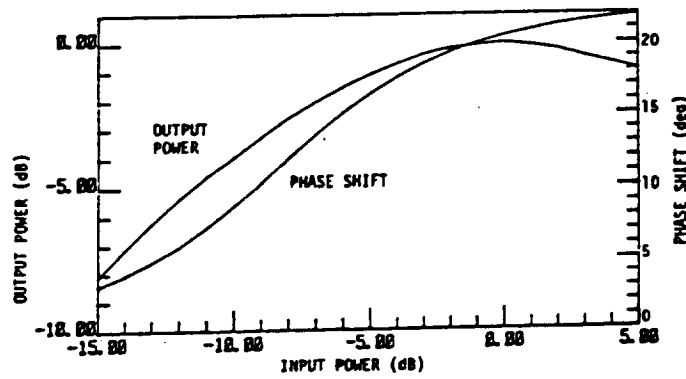


Figure 5. TYPICAL TWT CHARACTERISTIC.

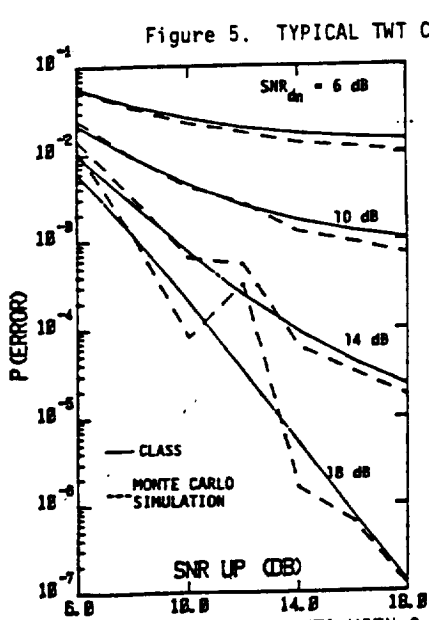


Figure 6a. BER PERFORMANCE FOR TWT WITH 3 dB INPUT BACKOFF.

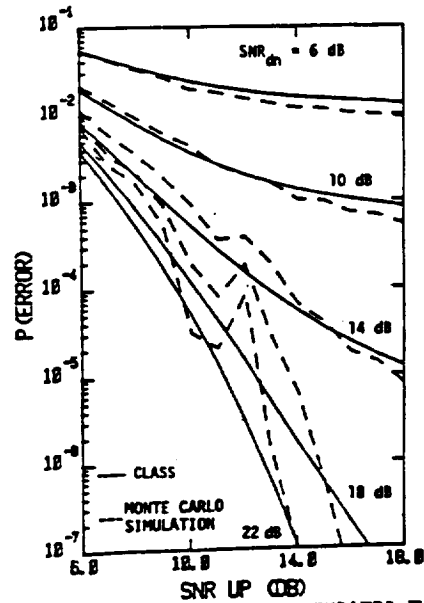


Figure 6b. BER PERFORMANCE FOR SATURATED TWT.

Table 1. VERIFICATION OF RFI MODEL: BER DEGRADATION.

RFI PULSES	NOISE-ONLY		NOISE+CW	
	BENIGN ENVIRONMENT		BENIGN ENVIRONMENT	
ENVIRONMENT	BENIGN ENVIRONMENT		BENIGN ENVIRONMENT	
DATA RATE	200 Kbps	6 Mbps	200 Kbps	6 Mbps
MEASUREMENT	.9 dB	1.5 dB	.6 dB	1.3 dB (1.9) ¹
CLASS PREDICTION	1.46	3.02	1.19	2.84

RFI PULSES	NOISE-ONLY		NOISE+CW	
	SEVERE ENVIRONMENT		SEVERE ENVIRONMENT	
ENVIRONMENT	SEVERE ENVIRONMENT		SEVERE ENVIRONMENT	
DATA RATE	200 Kbps	6 Mbps	200 Kbps	6 Mbps
MEASUREMENT	4.0 dB	8.0 dB	2.1 dB (3.6)	6.0 dB (9.8)
CLASS PREDICTION	5.32	11.51	5.22	11.67

¹Numbers in parentheses come from "RFI Test Study Second Interim Report" by Harris Corp., 26 February 1980. Others come from "RFI Test Study Final Report," by Harris Corp., 24 April 1980.

D/8

N85-16955

THE STATISTICAL LOOP ANALYZER (SLA)[†]

WILLIAM C. LINDSEY

LINCOM CORPORATION
P.O. BOX 15897
LOS ANGELES, CA 90015-0897

ABSTRACT

The Statistical Loop Analyzer is a new instrument for measuring acquisition, tracking and frequency stability performance characteristics of data acquisition and tracking systems.

1.0 INTRODUCTION

The Statistical Loop Analyzer (SLA) is designed to automatically measure the acquisition, tracking and frequency stability performance characteristics of symbol synchronizers, code synchronizers, carrier tracking loops, and coherent transponders. Automated phase-lock and system level tests can also be made using the SLA. Standard baseband, carrier and spread spectrum modulation techniques can be accommodated.

The SLA can be used to conduct tests during the initial design and checkout of breadboards, for conducting system level tests and acceptance testing. The tests can be performed on engineering breadboards thereby minimizing the risk of finding software (algorithm) and/or hardware problems during the manufacturing phase; thus the risk of schedule slips and associated increased costs are minimized. Utilizing the SLA in breadboards and system level test set ups eliminates the need for numerous monotonous and repetitive test procedures which require hand entry of test variables and hand recording of test results. The SLA approach to testing minimizes the changes for operator errors to enter into the experimental results as well as minimizing the time needed in the laboratory facility.

The test capability of the SLA is demonstrated in Table 1.1. The tests are automatically performed upon operator command so that manpower and laboratory test time requirements are minimized. The SLA can serve as a stand alone piece of test instrumentation (such as needed when testing breadboards) or it can be integrated into ground station test equipment and measurement laboratories via the SLA IEEE 488 and RS-232 interfaces.

The SLA is capable of collecting data and analyzing the statistics of discrete event indicators such as lock detectors, code sync detectors, frame sync detectors, etc. Through the SLA's phase-error jitter and cycle slip measurements the acquisition and tracking thresholds of the unit under test are determined; any false phase and frequency lock events are statistically analyzed and reported in the SLA output in probabilistic terms. Automated signal drop out tests can be performed in order to trouble shoot algorithms and evaluate the reacquisition statistics of the unit under test. Cycle slip rates and cycle slip probabilities can be measured using the SLA. These measurements, combined with bit error probability measurements, are all that are needed to fully characterize the acquisition and tracking performance of a digital communication system.

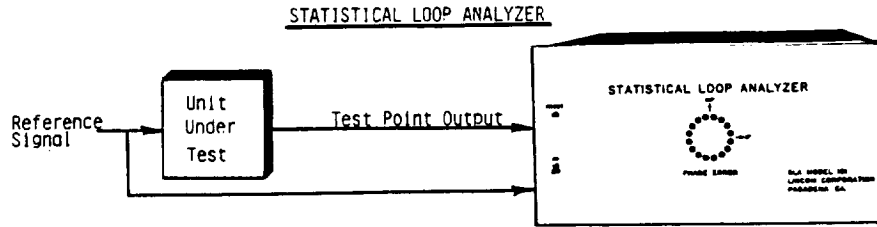
2.0 SLA TEST MENU AND SHUTTLE COMMUNICATIONS AND TRACKING TEST RESULTS

The test menu selectable by the test engineer is illustrated in Table 1.1. Four types of acquisition tests can be performed. Typical results obtained from performing the acquisition tests on the Space Shuttle's Payload Interrogator-Payload Signal Processor Unit is shown in Figure 2.1. Here the joint carrier, subcarrier, bit sync and frame sync probability distribution of acquisition is plotted for four different PSP-PI channels within the 100 MHz band. Similar SLA output data from RF signal drop out experiments is depicted in Fig. 2.2 for the Shuttle PSP-PI frame sync circuit. The RF signal drop-out time interval was one second.

Figures 2.3 through 2.6 illustrate typical test results obtained by performing the SLA's Tracking Test. Measured phase error jitter in the Shuttle PSP-PI bit sync and subcarrier sync loops is illustrated in Figures 2.3 and 2.4 for Channel 1 and Channel 210. Similar test data obtained by performing the SLA's tracking threshold test is depicted in Figure 2.5 to 2.6.

Figure 2.7 illustrates test data taken on the Frequency Stability of the Shuttle's Ku-Band high rate MUX clock. This data was taken using the SLA automated rms fractional frequency deviation test.

[†]This work was supported by NASA Lyndon Johnson Space Center under contract NAS 9-16691.



SLA FEATURES

- Automated Testing Under Microprocessor Control
- Automated Self Test and Calibration
- Automated Phase-Lock Tests
- Automated Phase and Frequency Stability Tests
- Automated Signal Drop-Out Tests
- Automated Testing of Acquisition and Tracking Algorithm Designs in Engineering Breadboards and at System Level
- Automated Data Reduction
- Compatible with Existing ATE via GPIB Interface
- Hard Copy Printing and Plotting via IEEE 488 Interface
- Visual Phase Error and Cycle Slip Transients
- Test Accuracy Selectable

Table 1.1. SLA Test Capability.

Acquisition Tests

- A - Probability Distribution of Acquisition Time
- B - Probability of Acquisition for a Fixed Time
- C - Probability Distribution of Reacquisition
- D - Signal Drop Out

Tracking Tests

- Phase Error Jitter-Slip Rate Tests
- A - Phase Noise Jitter
 - B - Phase Error Jitter and Slip Rate
 - C - Range Jitter

Threshold Tests

- D - Tracking Threshold
- E - Slip Rate

Phase and Frequency Stability Tests

- A - Doppler Accuracy
- B - RMS Phase Deviation
- C - RMS Fractional Frequency Deviation
- D - Allan Variance

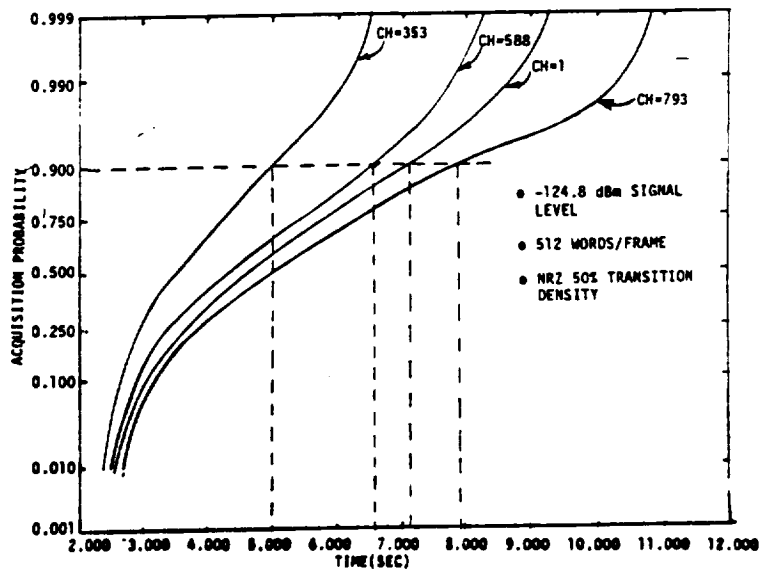
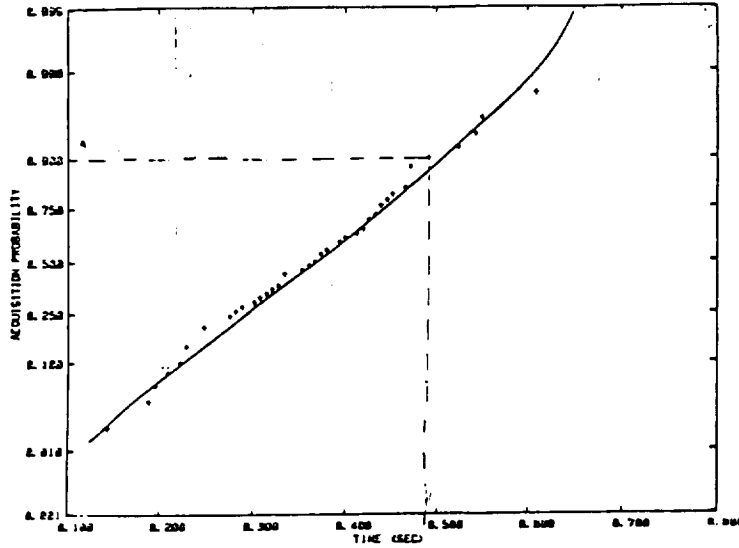


Figure 2.1. Shuttle PSP-PI Acquisition Test Result Comparison.



ORIGINAL PAGE IS
OF POOR QUALITY

Figure 2.2. Joint Probability of Carrier, Subcarrier, Clock and Frame Sync Acquisition vs Time for the Shuttle PSP-PI.

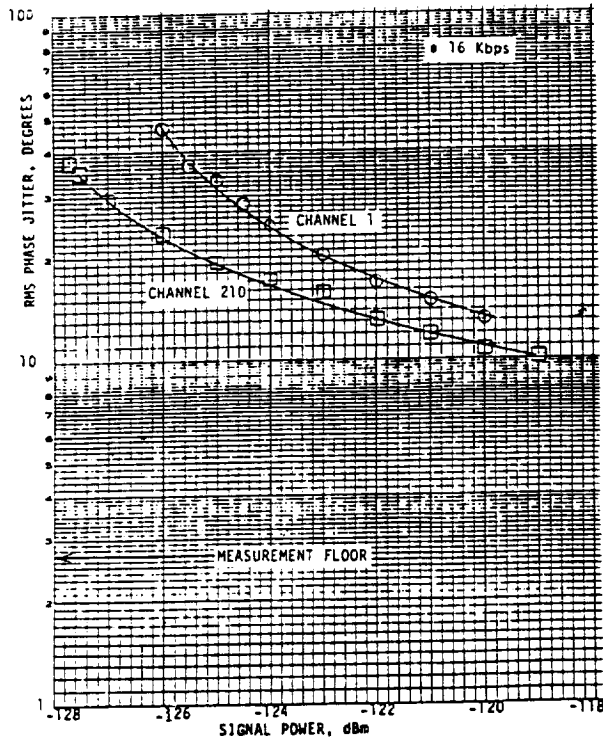


Figure 2.3. Shuttle PSP-PI Subcarrier Loop Phase Jitter Performance.

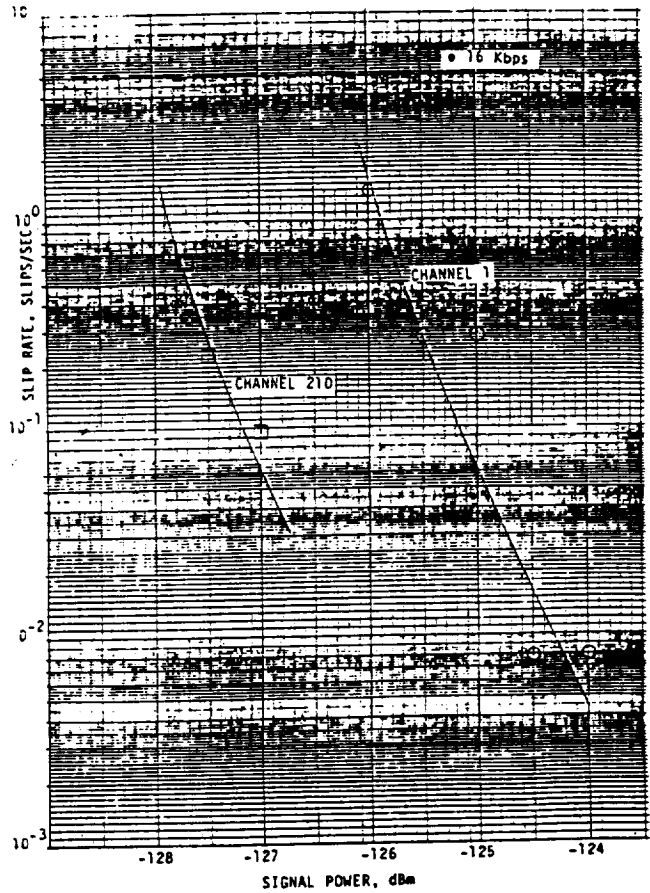


Figure 2.4. Shuttle PSP-PI Subcarrier Loop Slip Rate Performance.

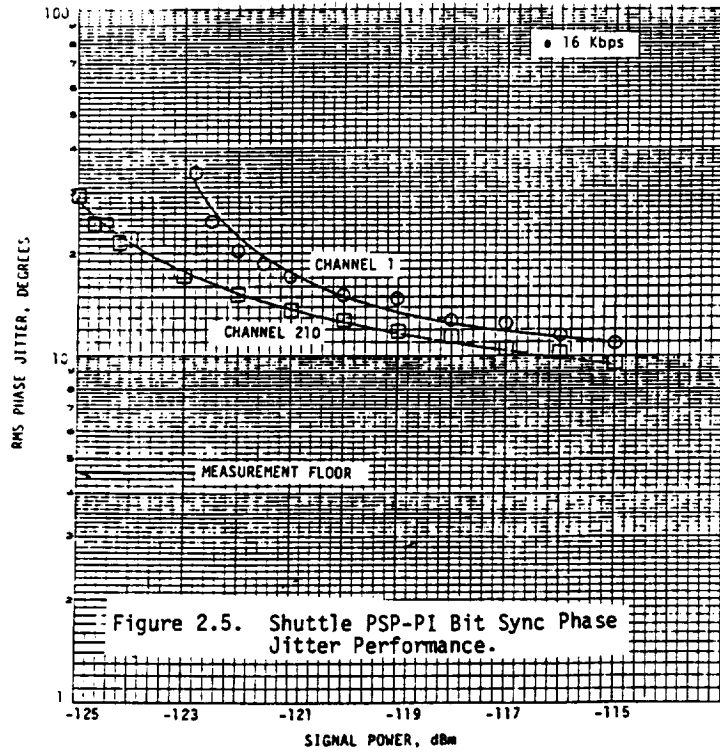


Figure 2.5. Shuttle PSP-PI Bit Sync Phase Jitter Performance.

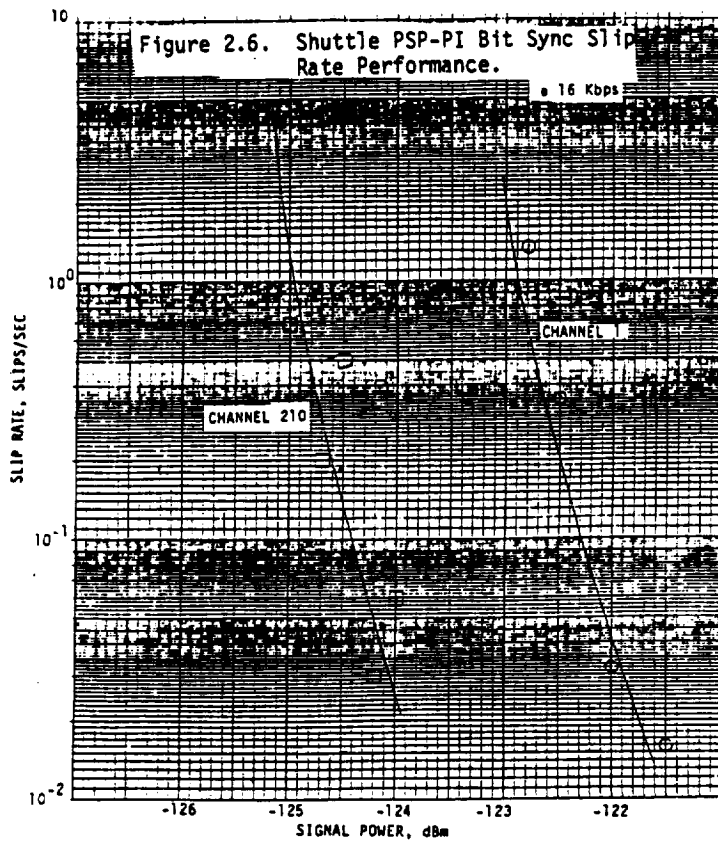


Figure 2.6. Shuttle PSP-PI Bit Sync Slip Rate Performance.

ORIGINAL PAGE IS
OF POOR QUALITY

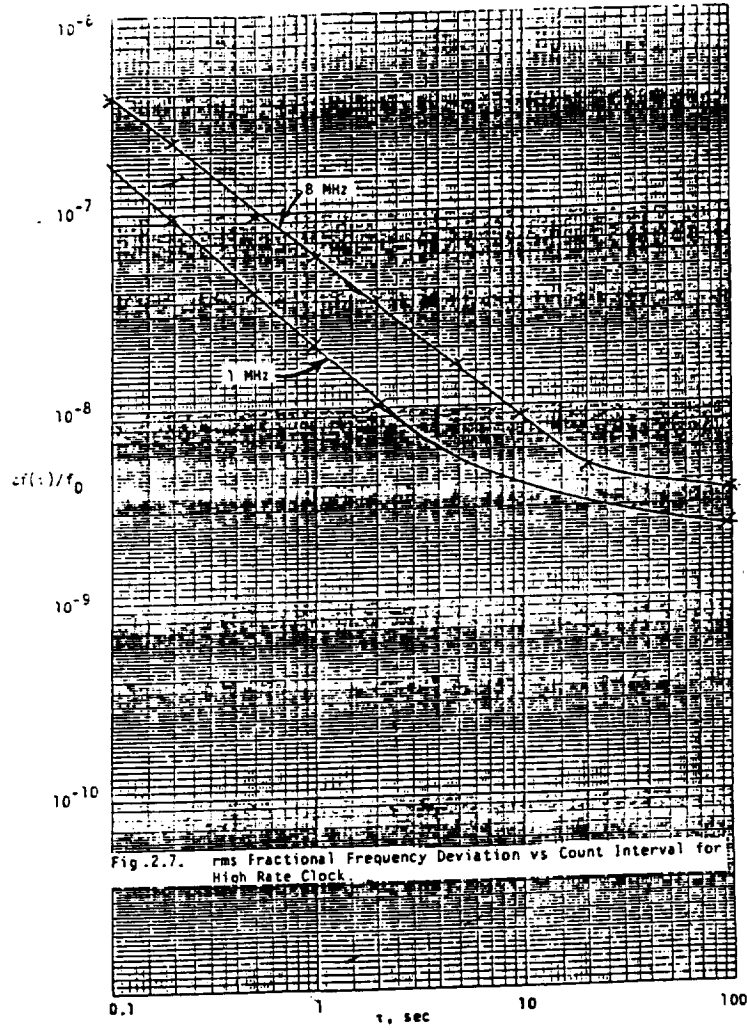


Figure 2.7. rms Fractional Frequency Deviation vs Count Interval for High Rate Clock.

DIGITAL SCRAMBLING FOR SHUTTLE COMMUNICATION LINKS:
DO DRAWBACKS OUTWEIGH ADVANTAGES?†

Khaled Dessouky

LinCom Corporation
P.O. Box 15897
Los Angeles, CA 90015
(213) 381-3701

ABSTRACT

Digital data scrambling has been considered for communication systems using NRZ symbol formats. The purpose is to increase the number of transitions in the data to improve the performance of the symbol synchronizer. This is accomplished without expanding the bandwidth but at the expense of increasing the data bit error rate (BER).

Models for the scramblers/descramblers of practical interest are presented together with the appropriate link model. The effects of scrambling on the performance of coded and uncoded links are studied. The results are illustrated by application to the Tracking and Data Relay Satellite System (TDRSS) links. Conclusions regarding the usefulness of scrambling are also given.

1. INTRODUCTION

In the communication links of the Space Shuttle, as in many other communication systems, data clock timing is extracted from the data transitions in the received signal. When NRZ baseband signaling format is used, long data streams of 0's or 1's may be encountered. This can result in the loss of data clock synchronization.

More than one approach may be considered for increasing the data transition density. One approach is using biphasic signaling format. This scheme provides frequent data transitions at the expense of increasing the bandwidth by roughly a factor of two over NRZ signaling. Biphasic signaling has the same BER performance as NRZ and is used in the Shuttle links when no bandwidth constraint is present.

An alternate approach which does not increase the bandwidth is digital data scrambling [1]. This provides a data transition density close to 50%. In the presence of channel noise, however, scrambling increases the data BER and may degrade the overall system performance.

For both of the above methods, coding may or may not be additionally used to improve the performance of the system. In the following sections we study the effects of scrambling on uncoded and coded communication links. We then attempt to weigh the benefits gained by scrambling against the price that has to be paid to obtain them (in terms of increased signal power to achieve the required BER performance).

In Sec. 2 we describe the model for a link that employs scrambling. In Sec. 3 we introduce the models for the scramblers and descramblers of interest. We then analyze the effects of scrambling on the link BER performance in Sec. 4. In Sec. 5 we illustrate the results of Sec. 4 by applying them to the TDRSS links. Conclusions are presented in Sec. 6.

2. LINK MODEL

Figure 1 depicts the model of a modern communication link employing digital scrambling/descrambling. In the transmitter the data may or may not be convolutionally encoded and interleaved. After scrambling PN-spreading may be introduced. In the channel, the transmitted waveform is corrupted by additive white Gaussian noise of power spectral density level N_0 (one-sided). The received waveform is despread (if applicable), demodulated, matched-filtered, hard-limited, descrambled, and deinterleaved and Viterbi decoded if appropriate.

Since the descrambler creates closely spaced multiple symbol errors from one channel symbol error, an interleaver is placed after the encoder to randomize the placement of symbol errors into the decoder. The hard-limiter after the matched filter is necessary for the operation of the descrambler. The Viterbi decoder therefore must operate on hard-limited symbols, on which its

†This work was supported by NASA Goddard Space Flight Center, Greenbelt, MD, under Contract No. NAS 5-27240.

performance is poorer than, for example, an 8-level-quantized symbols as frequently used in practice.

3. SCRAMBLER AND DESCRAMBLER MODELS

The scramblers and descramblers of interest here belong to the family of self-synchronizing scramblers/descramblers. They recover from the bit errors introduced by the noise in the channel [1].

Digital scramblers/descramblers achieve two goals both of which improve the performance of the bit synchronizer: (1) they introduce frequent transitions in the channel signal, (2) they increase the period of periodic source sequences (an all-0 or all-1 sequence is periodic with period 1). The scrambler consists of two elements: a "basic scrambler" and an associated "monitoring logic" [1].

The basic scrambler or descrambler is a shift register circuit. It consists of a linear sequential filter with feedback paths for the scrambler and feed-forward paths for the descrambler. The mathematical representation of a scrambler (or descrambler) takes the form of a polynomial. The polynomial $h_m(x) = x^m + c_1 x^{m-1} + \dots + c_{m-1} x + c_m$ is called the tap polynomial of an m-stage (m delay elements) scrambler. The tap constants for the scramblers considered here are either 1 (presence of a tap) or 0 (its absence). For the successful operation of the scrambler the tap polynomial has to be "primitive" over the binary field [1]. We shall see shortly that for practical purposes this will translate to the few simple but effective realizations shown in Figure 2.

The basic scrambler changes the period of the input, say period of length s, to the least common multiple (LCM) of s and $2^m - 1$ for all but one of the initial states of the scrambler where it remains s. At this point comes the role of the monitoring logic.

The monitoring logic consists of counters, storage elements and incidental logic. The monitoring logic detects the presence of the output data sequence that has period s and adds a '1' at intervals to break that periodicity [1]. The minimum output period then becomes $\text{LCM}(s, 2^m - 1)$.

There are two main considerations in the choice of the number of stages and taps in the basic scrambler. First, a suitable choice for m gives $2^m - 1$ which is prime. The minimum output period would then be $s(2^m - 1)$ for an output of period s. Second, since it is generally true that on the average the descrambler multiplies the channel errors at its input by $w(h)$, where $w(h)$ is the number of non-zero terms in the tap polynomial [1], it is important to use the minimum number of taps possible. Moreover, since this minimum number increases for larger values of m [2], it becomes necessary to use a scrambler with a smaller number of stages.

From the tables of primitive polynomials [2] we find that the scramblers that meet the above requirements correspond to the polynomials

$$h_3(x) = x^3 + x^2 + 1 \quad (1)$$

and

$$h_5(x) = x^5 + x^3 + 1 \quad (2)$$

or their reciprocals (over the binary field). The reciprocals are $h_3'(x) = x^3 + x + 1$ and $h_5'(x) = x^5 + x^2 + 1$ respectively. The basic scramblers and descramblers corresponding to (1) and (2) are shown in Figure 2. The alternate center taps which correspond to the realization of the reciprocal polynomials are shown dotted.

The 3- and 5-stage scramblers presented herein have values of $2^m - 1$ equal to 7 and 31, respectively, which are prime yielding good performance with periodic inputs. These scramblers are also the only 3- and 5-stage realizations with the minimum number of taps possible.

4. EFFECT OF SCRAMBLING ON LINK BER

In what follows we associate the term bit error rate (BER) with the output of the decoder, and use symbol error rate (SER) with the error rate at the input or output of the descramblers. For uncoded links BER and SER are equivalent.

4.1 Calculation of SER at Descrambler Output

Here we describe how an SER at descrambler input is mapped into an SER at descrambler

output. We first concentrate on the basic descrambler then discuss the impact of the monitoring logic.

For an m-stage basic descrambler the states at m+1 points in the descramblers are significant in evaluating the output SER. For the 3-stage descrambler these are indicated in Figure 2 by s_i, \dots, s_{i-3} . Only those states which have a connection to the output can actually cause an output symbol to be in error. The approach to obtain the output probability of symbol error is to examine all possible symbol patterns occupying s_i, \dots, s_{i-3} and determine if each pattern causes an output error. We then add the probabilities of occurrence of the patterns that lead to an output error. After examining $2^4 = 16$ patterns we have at the output of the 3-stage basic descrambler (for both of the possible realizations)

$$\text{SER} = 3(1-p)^3 p + 3(1-p)^2 p^2 + (1-p)p^3 + p^4 \quad (3)$$

where p is the input SER. Similarly we have at the output of the 5-stage descrambler (both realizations)

$$\text{SER} = 3(1-p)^5 + 9(1-p)^4 p^2 + 10(1-p)^3 p^3 + 6(1-p)^2 p^4 + 3(1-p)p^5 + p^6 \quad (4)$$

Equations (3) and (4) can be simplified by expanding the different terms. After simplification we find that the two equations yield the expression

$$\text{SER} = 3p - 6p^2 + 4p^3 \quad (5)$$

Equation (5) describes how the SER at the input of a 3- or 5-stage descrambler is translated into an SER at its output. It is interesting to note that at small value of input SER, the basic descrambler produces 3 output errors per input error, and 3 is the number of non-zero coefficients in the 3- and 5-stage descramblers used.

Now, how is the output SER of the basic descrambler affected by the monitoring logic? It has been shown [1] that for relatively infrequent channel errors, say for SER less than one over a few multiples of the number of stages, the monitoring logic has negligible effect on the SER at the output of the basic descrambler. For higher levels of input SER (closer to 0.5) the output of the basic descrambler tends to become completely garbled (output SER very close of 0.5). The effect of the monitoring logic in that case is of no significance.

In Figure 3 we illustrate the effects of scrambling and subsequent descrambling on $\text{BER} = \text{SER}$ for an uncoded link. Carrier and clock recovery are assumed perfect and for an unscrambled link the BER characteristics are given by $0.5 \operatorname{erfc}(\sqrt{E_b/N_0})$. The required increase in E_b/N_0 to offset the effect of scrambling depends on the desired BER performance. Typically, for $\text{BER} = 10^{-5}$ the required increase in E_b/N_0 is 0.5 dB. The degradation due to scrambling when other degradation sources are present in an actual system are discussed in Sec. 5.

4.2 Calculation of Coded BER

For the coded case the results are quite different. We first assume that the channel is Gaussian and that in the absence of scrambling the Viterbi decoder would work on an 8-level-quantized symbol at the output of the matched filter. The results of simulation reveal that the BER at the decoder output is strongly affected by the presence of scrambling/descrambling (and the necessary hard-limiting). This is seen in Figure 4 where a rate 1/2 constraint length 7 code has been used.

There are two components that contribute to the significant degradation of BER performance of the coded link. There is an effective loss of 2.2 dB in E_b/N_0 due to the necessary hard-limiting (as opposed to operation on 8-level-quantized signal) [3]. There is also the degradation due to the increase in the SER at the input of the decoder due to the descrambler. To understand the contribution of each of these factors, we have drawn in Figure 4 a hypothetical curve that depicts a situation where hard-limiting is used on an unscrambled link. This curve (curve c in Figure 4) is separated by 2 dB from curve a. The difference between curves c and b is due to the descrambler. This difference is largest (up to 2.5 dB) at smaller values of E_b/N_0 . In that region, the Viterbi decoder is very sensitive to any increase in SER at its input. As E_b/N_0 increases beyond 6 dB, the symbol errors at the decoder input become infrequent. As a result, the degradation in its output BER due to the increase in its input SER becomes less noticeable. At a typical 10^{-5} BER the degradation in E_b/N_0 due to scrambling is 3.7 dB. The degradation in the performance of the coded links of an actual system, where other sources of performance degradation are present, is discussed in the following section.

5. EXAMPLE: APPLICATION OF SCRAMBLING TO TDRSS LINKS

The model of a typical TDRSS return link follows closely the general link model presented in Figure 1. We shall discuss here the case where no radio frequency interference (RFI) disturbs the link.

Figures 5 and 6 show the results of simulation for the link using the simulation package LinCsim developed by LinCom Corporation for the NASA Goddard Space Flight Center. The results for a typical uncoded and coded return links of the single access S-band service (SSA) are shown in Figures 5 and 6 respectively. The results given reflect the presence of actual system disturbances such as imperfect carrier and clock recovery, and different signal distortions like gain and phase imbalance and data asymmetry etc. [4]. The figures give the BER performance as a function of delta uplink (user satellite to TDRS) CNR for BPSK at the maximum rate of 12 M symbols/sec. In each curve the nominal CNR is the CNR that yields the design BER of 10^{-5} . Each figure shows three curves: (a) unscrambled link and 50% data transition density, (b) unscrambled and 10% data transition density, (c) scrambled (hence 50% transition density) link. In obtaining these curves the effects of the other system disturbances have been appropriately averaged out [5]. For both figures the BER performance degrades as we go from curve a to b to c. In the uncoded case the degradation of 10^{-5} BER in the scrambled case exceeds the degradation in the unscrambled case with 10% transition density by 3.2 dB.

The above results are in close agreement with the general results of Sec. 4. It is worth noting, however, that in the TDRSS the rms timing error of the symbol synchronizer at 10% transition density is less than 1% of the symbol duration at the values of E_b/N_0 of interest [5]. This explains the relatively small degradation between curves a and b in Figures 5 and 6. It should be noted also that the curves of Figure 5 should not be compared to the curves of Figure 6. This is because of the differences in the nominal CNR's and averaging techniques used [5].

6. CONCLUSIONS

We have seen from Secs. 4 and 5 that the major drawback of digital data scrambling is the degradation in the overall BER performance of the communication link. This degradation is quite significant for coded links.

If the symbol synchronizer is capable of operating at most of the reduced data transition densities encountered (without a large degradation in the overall BER and bit slip rate) then scrambling should not be used. If we cannot make this assertion, perhaps because of the possibility of very low transition densities, then for uncoded links 0.5 dB is a very reasonable price to pay for stable symbol synchronization. For coded links, on the other hand, the large degradation in BER due to scrambling suggests that we rephrase the problem. Should we improve symbol synchronization by scrambling at a price of about 3.5 dB, or by simply raising the SNR by a comparable amount? The answer to this question depends on the required BER performance and the characteristics of the particular symbol synchronizer at hand. It is apparent, though, that scrambling is not well suited for coded links.

ACKNOWLEDGEMENT

The author wishes to thank Mrs. Teresa McKenzie for her valuable contributions, Mr. Song An for running the LinCsim simulations, and Dr. W. C. Lindsey for his constructive suggestions.

REFERENCES

- [1] J. E. Savage, "Some Simple Self-Synchronizing Digital Data Scramblers," Bell Sys. Tech. J., February 1967, pp. 449-487.
- [2] W. W. Peterson and E. J. Weldon, Jr., Error Correcting Codes, MIT Press, Cambridge, MA, 1972, Appendix C.
- [3] J. K. Omura and B. K. Levitt, "Coded Error Probability for Antijam Communication Systems," IEEE Trans. on Comm., Vol. COM-30, No. 5, May 1982, pp. 896-903.
- [4] "Tracking and Data Relay Satellite System (TDRSS) User's Guide," Revision 4, January 1980, NASA/GSFC, Greenbelt, MD.
- [5] "First Interim Report: Analytical Evaluation of Communications Features of TDRSS," LinCom Corp. Technical Report No. TR-0483-8214, April 1983.

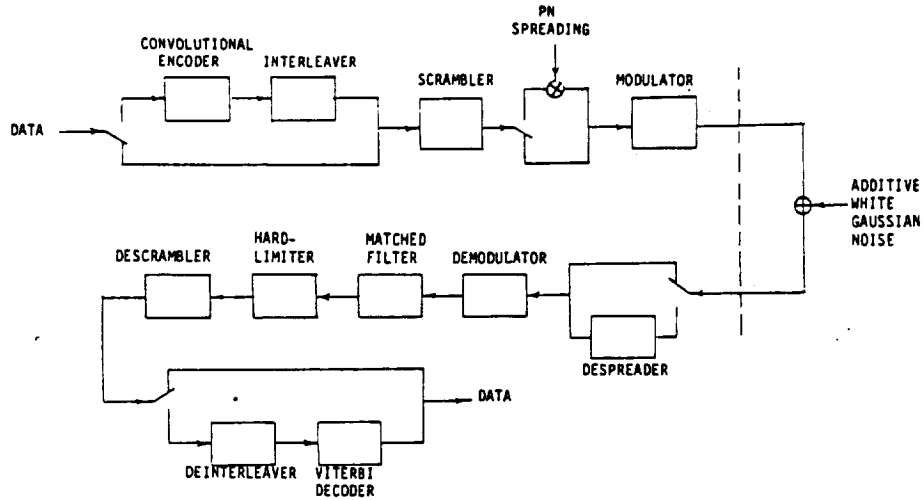


Figure 1. LINK MODEL.

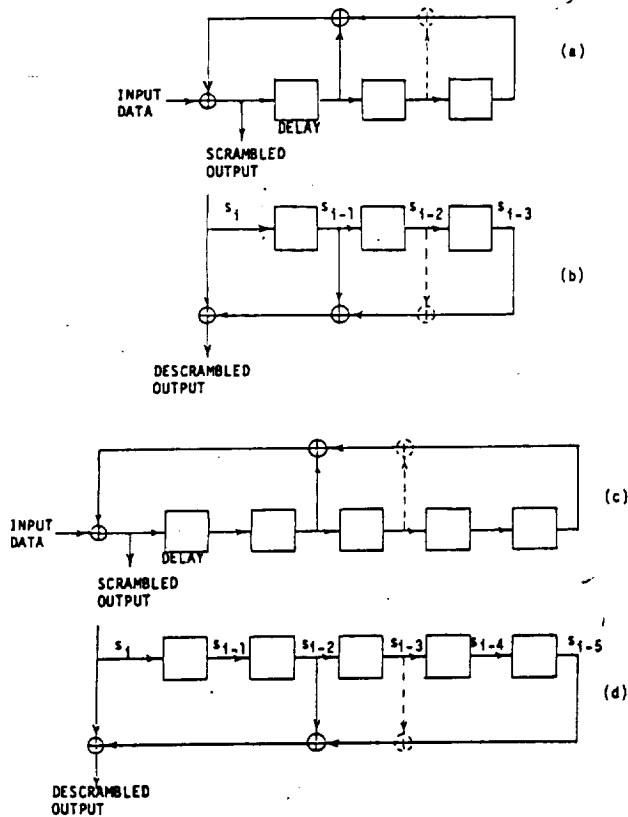


Figure 2. THREE AND FIVE STAGE SCRAMBLERS AND DESCRAMBLERS WITH MINIMUM NUMBER OF TAPS. (A) 3-STAGE SCRAMBLER; (B) CORRESPONDING DESCRAMBLER, (C) 5-STAGE SCRAMBLER; (D) CORRESPONDING DESCRAMBLER (SHOWN DOTTED ARE ALTERNATIVE CENTER TAPS FOR ALTERNATIVE REALIZATIONS.)

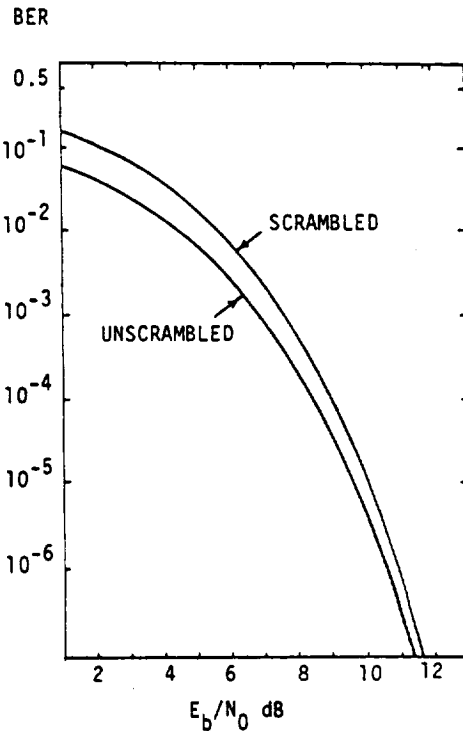


Figure 3. COMPARISON OF BER AS A FUNCTION OF E_b/N_0 IN SCRAMBLED AND UNSCRAMBLED CASES--UNCODED LINK; PERFECT CARRIER AND CLOCK RECOVERY.

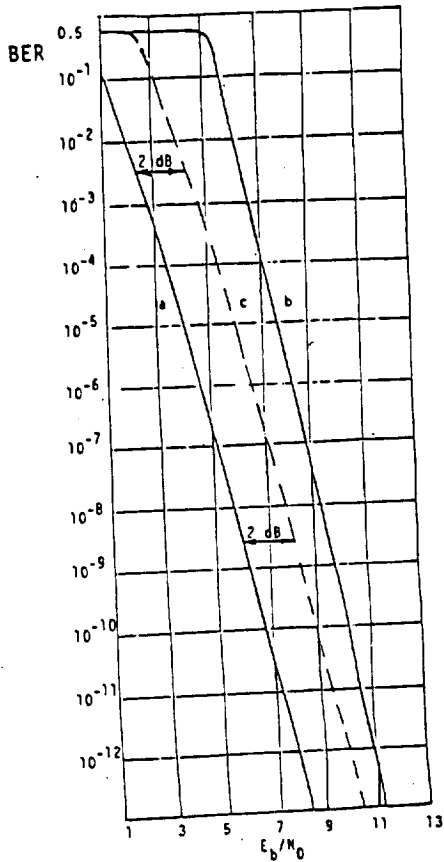


Figure 4. COMPARISON OF BER AS A FUNCTION OF E_b/N_0 FOR SCRAMBLED AND UNSCRAMBLED CASES— $R=1/2$, CONSTRAINT LENGTH 7 CODING; PERFECT CARRIER AND CLOCK RECOVERY.
 CURVE A: UNSCRAMBLED
 B: SCRAMBLED (AND HARD-LIMITED)
 C: UNSCRAMBLED BUT HARD-LIMITED

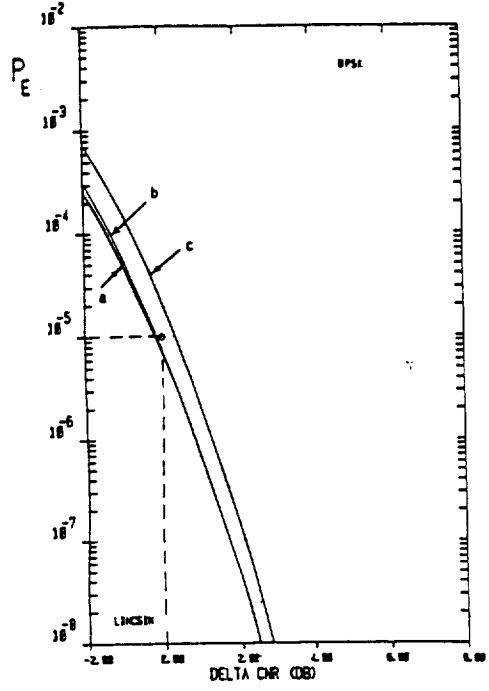


Figure 5. BER PERFORMANCE FOR A TYPICAL UNCODED TDRSS RETURN LINK. (A) UNSCRAMBLED, 50% TRANSITION DENSITY; (B) UNSCRAMBLED, 10% TRANSITION DENSITY; (C) SCRAMBLED.

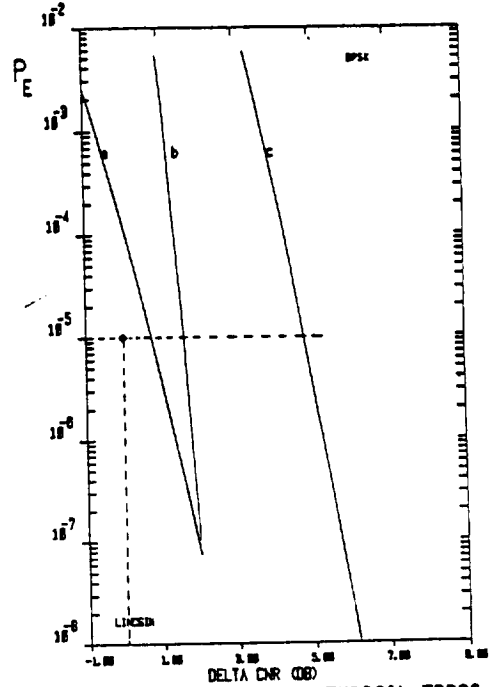


Figure 6. BER PERFORMANCE OF A TYPICAL TDRSS LINK CODED AT RATE 1/3 (CONSTRAINT LENGTH 7). (A) UNSCRAMBLED, 50% TRANSITION DENSITY; (B) UNSCRAMBLED, 10% TRANSITION DENSITY; (C) SCRAMBLED.

NOVEL APPLICATIONS OF THE NASA/GSFC VITERBI DECODER HARDWARE
SIMULATOR

Dirk J.M. Walvis
Aaron Weinberg
Stanford Telecommunication, Inc.
McLean, Va. 22101

Denver W. Herr
John J. Schwartz
NASA/GSFC
Greenbelt, Md. 20771

ABSTRACT

NASA/GSFC has had developed an all digital, real time, programmable Viterbi decoder simulator operating at rates up to 6 Msps. With this simulator, the BER performance of convolutionally encoded/Viterbi decoded Shuttle-TDRSS return link channels under pulsed RFI conditions has been predicted. The principles of the simulator are described with special emphasis on the channel simulator and the essential interaction between CLASS software and the simulator. The sensitivity of coded BER as function of several illustrative RFI parameters is discussed for two typical Shuttle-TDRSS return link configurations.

1. INTRODUCTION

The Shuttle - TDRSS return links, S-band and K-band mode 1, channel 3, employ convolutional encoding/Viterbi decoding. During certain periods the TDRSS ground receiver may have to contend with high level pulsed RFI. These pulses may affect many consecutive information symbols depending on the symbol rate and RFI pulse duration.

An analytical software package of CLASS (Communication Link Analysis and Simulation System), [1,6], has the capability to predict the performance of the decoders under RFI conditions when the channel can be modeled as a memoryless channel. To evaluate the performance when the decoder has to contend with a series of consecutive pulses affected by RFI (i.e. a non-memoryless channel), NASA GSFC engaged Linkabit Corporation to develop an all digital convolutional encoder/Viterbi decoder simulator. This simulator can be programmed to simulate a large variety of time-varying channels, including pulsed RFI, and operates at symbol rates up to 6 Msps. It has been used at NASA GSFC to predict the impact of RFI on the return link performance of TDRSS users such as Space Telescope and Shuttle.

This paper describes the major features of this simulator and its interfaces with CLASS. It presents the results of tests measuring the impact of illustrative RFI on some Shuttle - TDRSS return links.

2. OVERVIEW OF THE SIMULATOR

The present configuration of the simulator is shown in Figure 1 [2]. The simulator is configured and controlled via the desk top calculator, which provides the capability of automated testing. In addition, the configuration data generated with CLASS can be downloaded to the calculator. The error rate tester is controlled via the desk top calculator or via front panel controls. A PN sequence, which simulates the data source, is generated in the error rate tester and looped back to the tester for BER measurement after being processed by the encoder, transition probability generator and decoder. Interleaving and deinterleaving is optional. The error rate tester also generates the symbol rate clock, which allows symbol rates up to 6 Msps. The encoder and decoder are either rate 1/2 or rate 1/3, with constraint length 7. The deinterleaver is integrated with the decoder and the decoder metric growth is monitored to establish interleaver/deinterleaver synchronization.

The transition probability generator models the discrete channel formed by the modulator, channel characteristics and noise, and the quantized output of the demodulator/detector. The TPG maps each symbol into one of the possible 8 soft decision levels at the input of the deinterleaver/decoder, based on a probabilistic process for which the data is generated with CLASS.

CHANNEL MODELING

With the TPG the channel is modeled as follows: The time varying channel is divided into as many as 32 different channel conditions or states. Each of these channel conditions is time-invariant and is modeled as a discrete, binary input to 8-ary output, memoryless channel. The time variation is then achieved by selecting one of the available channel conditions for each transmitted symbol. The transitions between channel conditions are modeled as a zero or first order Markov process with up to 32 states. In addition, it is possible to specify the number of symbols the TPG is to stay (or hold) in a channel condition, once entered. This is particularly useful when modeling pulsed RFI as the hold time is equal to the number of channel symbols the RFI pulse overlaps. For the application described here the transitions between channel conditions are modeled as a zero order Markov process i.e. the probability of entering a channel condition is independent of the previous channel condition. For a pulsed RFI environment the channel condition transitions are then determined from the

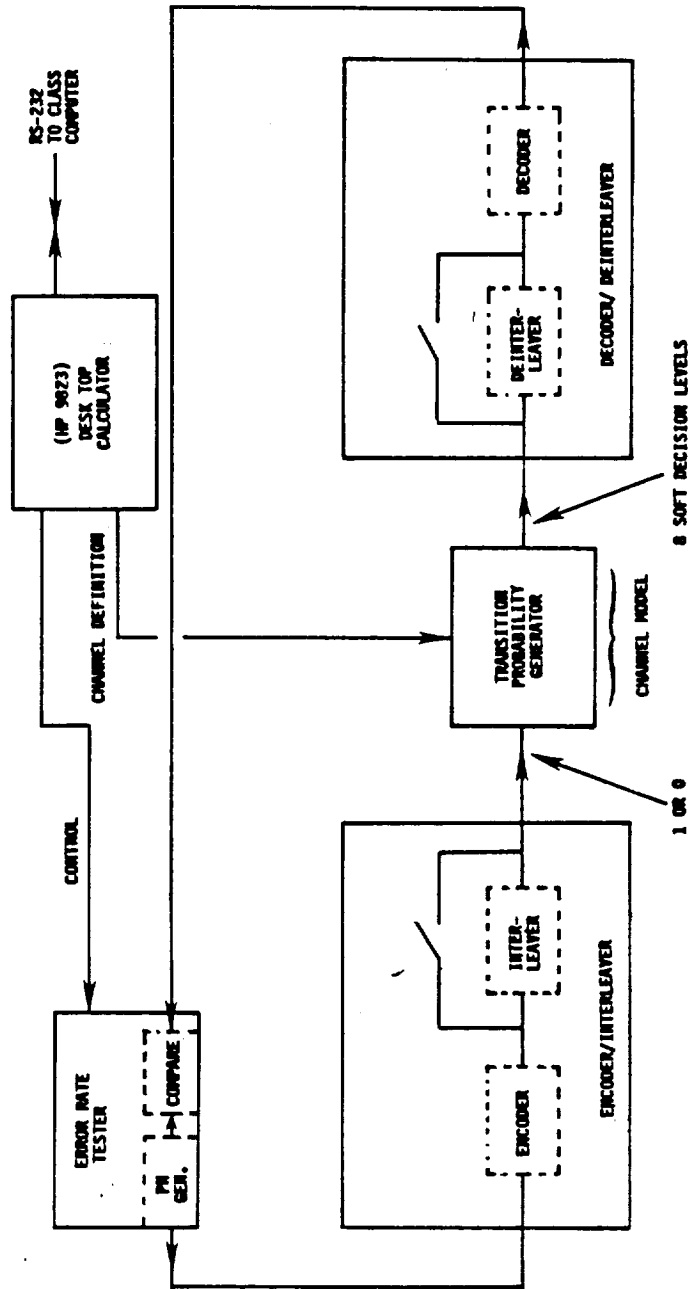


FIGURE 1: BLOCK DIAGRAM OF ALL DIGITAL, REAL-TIME SIMULATOR

duty cycle, T_j , and pulse duration, M_j , of each associated RFI condition. When the phenomenon of overlapping RFI pulses is neglected, which is a good approximation for low duty cycles, the probability of entering a channel condition is easily found to be:

$$Pr_j = \frac{T_j}{M_j} \left(\sum_{i=1}^{N_e} \frac{T_i}{M_i} \right)^{-1} \quad (1)$$

with:

- Pr_j - the probability of entering channel condition j.
- T_j - the duty cycle of the RFI associated with the j-th channel condition.
- M_j - the pulse duration of the RFI associated with the j-th channel condition.
- N_e - total number of different channel conditions.

Figure 2 shows a functional diagram of the TPG and a typical list of channel conditions. The two rightmost columns show the duty cycle and pulse duration from which CLASS software calculates the transition probabilities via (1). These probabilities are downloaded into the desk top calculator. Most channels are modeled with the pulse duration of the NO-RFI channel condition, approximately an AWGN channel condition, equal to 1 as shown in the table of Figure 1. This implies that the TPG is not forced to stay in the non-RFI condition and that the RFI channel conditions may be selected after any number of channel symbols which are not affected by RFI.

For each channel condition the discrete binary to 8-ary memoryless channel is fully characterized by calculating the 8-level soft decision statistics, assuming that a "1" is transmitted, as the TPG models each channel condition as a symmetric channel. These soft decision statistics are calculated by CLASS. For full details on the methods followed in these computations see [1]. In addition to the RFI parameters listed in Figure 2, the following parameters must be specified in order for CLASS to compute the soft decision statistics:

Shuttle: EIRP, Data rate

TDRSS : Return/down link noise, AM/AM, AM/PM, clipping level

The next section describes some results on decoder performance and shows typical soft-decision statistics.

3. SIMULATION RESULTS

The simulation results presented in this paper illustrate the capability of the simulator to assess the impact of several RFI parameters on the performance of the Viterbi algorithm decoder. As examples, the impact of illustrative RFI on the Shuttle - TDRSS K- and S-band has been simulated.

SHUTTLE-TDRSS K-BAND

For the simulation described here the configuration data for the TPG are computed with the following signal and channel parameters, [3]:

- Shuttle channel 3, up to 50 Mbps, characterized as BPSK with 47.3 dBW EIRP, rate 1/2 coding.
- Pulsed RFI
 - Duty cycle: < 1%
 - For each test a choice of:
 - In-band or out-of-band CW
 - Two illustrative RFI power levels
 - 1, 10 or 20 consecutive information symbols overlapped by a single RFI pulse
- TDRSS KSA return link transponder
 - 250 MHz noise bandwidth
 - 44 dBW thermal noise level
 - ALC with 10 dB clipper and 1.2 degrees per dB AM/PM

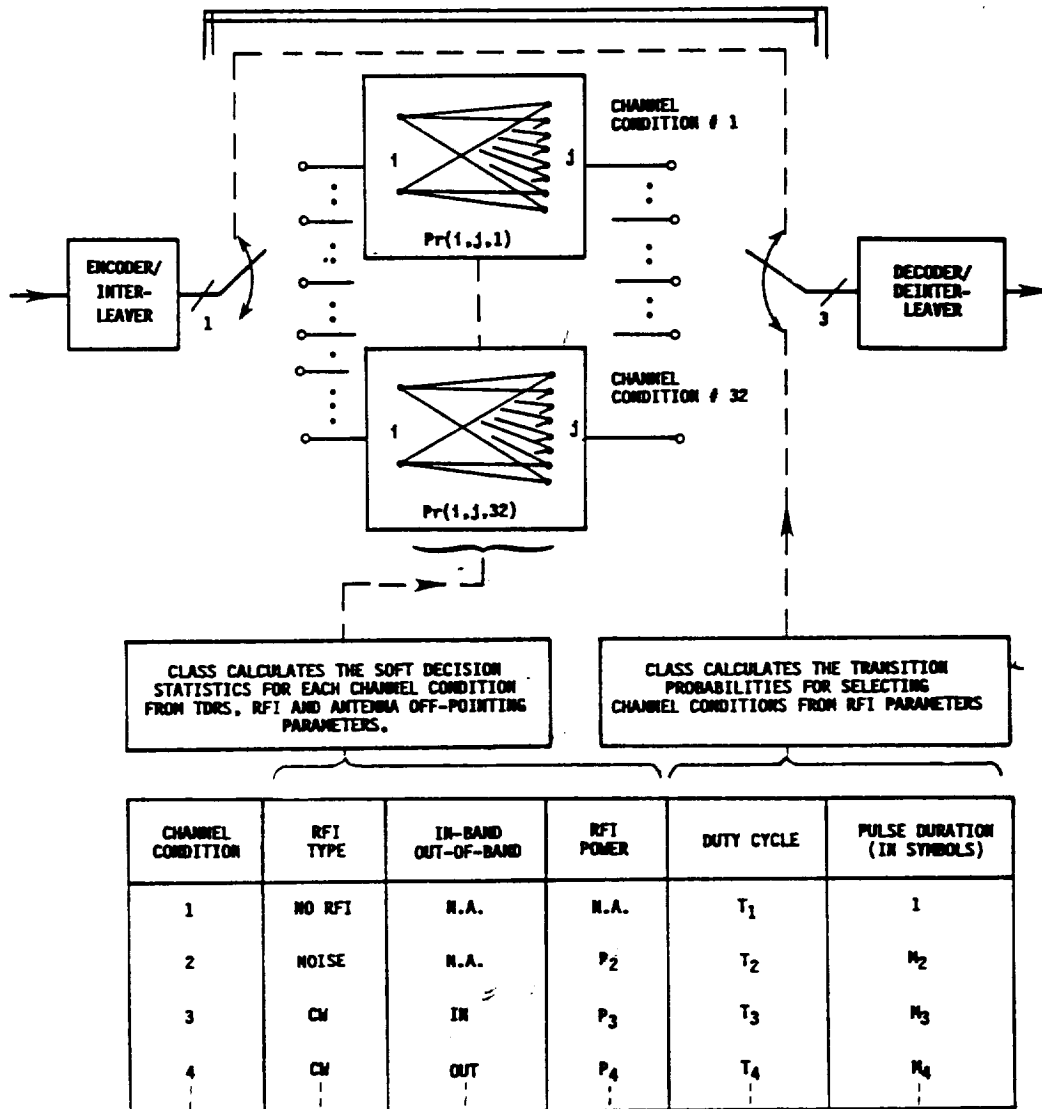


FIGURE 2: TRANSITION PROBABILITY GENERATOR

The BPSK signal characterization is an approximation to the actual QPSB signal structure and is reasonable due to the 6 dB dominance of the channel 3 signal relative to the composite of the channel 1 and 2 signals.

The TDRS transponder characteristics indicated reflect the actual KSA return link transponder. The thermal noise level of 44 dBW refers to the fact that the thermal noise power within the 250 MHz bandwidth may be equivalently obtained by having the TDRS point directly at a 44 dBW thermal noise source on the surface of the earth that is radiating via an omnidirectional antenna.

The duty cycle of less than 1% is purely illustrative, as is the number of consecutive symbols overlapped by RFI. The in-band RFI, modeled in CLASS with a RFI frequency which precisely coincides with the carrier, leads to worst case performance for a given RFI power level. Six combinations of the RFI parameters are evaluated. These are listed in Table 1. As a companion to Table 1, Table 2 summarizes the soft decision statistics that apply to each RFI presence. The NO RFI channel condition is the same for each scenario and is also listed in this table.

Table 3 shows the BER obtained through simulation, as well as the channel symbol error rate for each scenario. As seen, and expected, performance degradation is much more severe under in-band RFI conditions.

Also to be observed from Table 3 is the expected increasing degradation that occurs as the RFI EIRP and the number of symbols overlapped increases. Especially interesting is the approach of the decoded BER to the channel error rate for the particularly severe scenarios. This phenomenon reflects that for those scenarios virtual each RFI pulse is sufficiently severe and long to cause a burst of decoding errors. Note that the degradation of the channel during the out-of-band RFI pulses is not sufficiently severe to consistently cause a burst of decoding errors.

SHUTTLE-TDRSS S-BAND

For the simulation described here the configuration data for the TPG are computed with the following signal and channel parameters:

- Shuttle S-band return link, BPSK with typical EIRP and 96 or 192 Kbps, rate 1/3 coding.
- Illustrative pulsed RFI
 - Severe RFI with a duty cycle < 2%
 - 1, 2, 3 or 4 consecutive information symbols overlapped by RFI
- TDRSS SSA return link transponder
 - 20 MHz noise bandwidth
 - 29 dBW thermal noise level
 - ALC with 10 dB clipper and 1.2 degrees per dB AM/PM

The design of the rate 1/3 decoder of the Shuttle unique receiver of the TDRSS ground equipment is slightly different from the decoder used in the simulator. The major difference is the path memory length which is 64 decoded bits instead of the 32 decoded bits in the simulator. In addition, the metric assignment for the different decoder input quantization levels are probably different. The exact assignments are proprietary. As part of the evaluation of the impact of RFI on the Shuttle decoder, it was shown that degradation of performance for both decoders is very comparable. This was shown by configuring the software decoder simulator "CODES", which is part of CLASS, either as the Shuttle decoder or as the all digital, real time simulator and comparing the results.

Figure 3 shows the BER degradation due to RFI as function of the number of consecutive symbols affected by RFI, for a variety of margins of the Shuttle EIRP. We see that for the same margin the 192 kbps is degraded more severely than the 96 kbps. This is due to the higher duty cycle of the in-band RFI, which is a result of the wider receive filter. When we compare the A-margin curves with the B-margin curves, we see that the degradation due to consecutive symbols affected by RFI, is more severe when the margin is higher.

It is interesting, as well, to compare the simulation speed of the software package CODES, which allows detailed specification of different convolutional codes and hardware constraints, with the simulation speed of the hardware simulator. A ten million bit simulation takes 5 to 10 hours with CODES on the CLASS computer. With the hardware simulator such a simulation takes less than 20 minutes, which includes inputting the data into CLASS and operating the hardware simulator.

TABLE 1
RFI SCENARIOS CONSIDERED IN SECTION 3

Desired signal EIRP = 47.3 dBW

SCENARIO NO.	RFI DUTYCYCLE	RFI CLASS	RFI EIRP	NO. OF CONSECUTIVE SYMBOLS OVERLAPPED BY RFI PULSE
1	< 1%	IN-BAND	E_1^*	20
2	< 1%	IN-BAND	E_2^*	10
3	< 1%	IN-BAND	E_2	20
4	< 1%	OUT-OF-BAND	E_1	20
5	< 1%	OUT-OF-BAND	E_2	10
6	< 1%	OUT-OF-BAND	E_2	20

* $E_2 > E_1$

TABLE 2
CONDITIONAL SOFT DECISION PROBABILITY DISTRIBUTIONS FOR RFI SCENARIOS OF TABLE 1

QUANTIZATION LEVEL*	NO RFI	IN-BAND, E_1	IN-BAND, E_2	OUT-OF-BAND, E_1	OUT-OF-BAND, E_2
1	1.6×10^{-5}	.052	.270	.015	.066
2	10^{-4}	.044	.034	.013	.029
3	6.5×10^{-4}	.057	.031	.021	.035
4	3.1×10^{-3}	.064	.029	.033	.042
5	.011	.063	.027	.047	.048
6	.033	.058	.026	.063	.054
7	.074	.052	.026	.079	.059
8	.878	.610	.559	.729	.645

* Assumes transmission of a + symbol polarity. The channel is assumed to be symmetric.

TABLE 3

MEASURED ERROR RATES FOR RFI SCENARIOS OF TABLE 1

SCENARIO	DECODED BER	CHANNEL SYMBOL ERROR RATE
1	1.4×10^{-4}	4.7×10^{-3}
2	1.1×10^{-3}	5.3×10^{-3}
3	1.3×10^{-3}	5.3×10^{-3}
4	8.4×10^{-7}	4.2×10^{-3}
5	6.0×10^{-5}	4.6×10^{-3}
6	1.6×10^{-4}	4.6×10^{-3}

- HAD INTERLEAVING/DEINTERLEAVING BEEN EMPLOYED DECODED BER WOULD BE $\ll 10^{-6}$ IN ALL CASES.

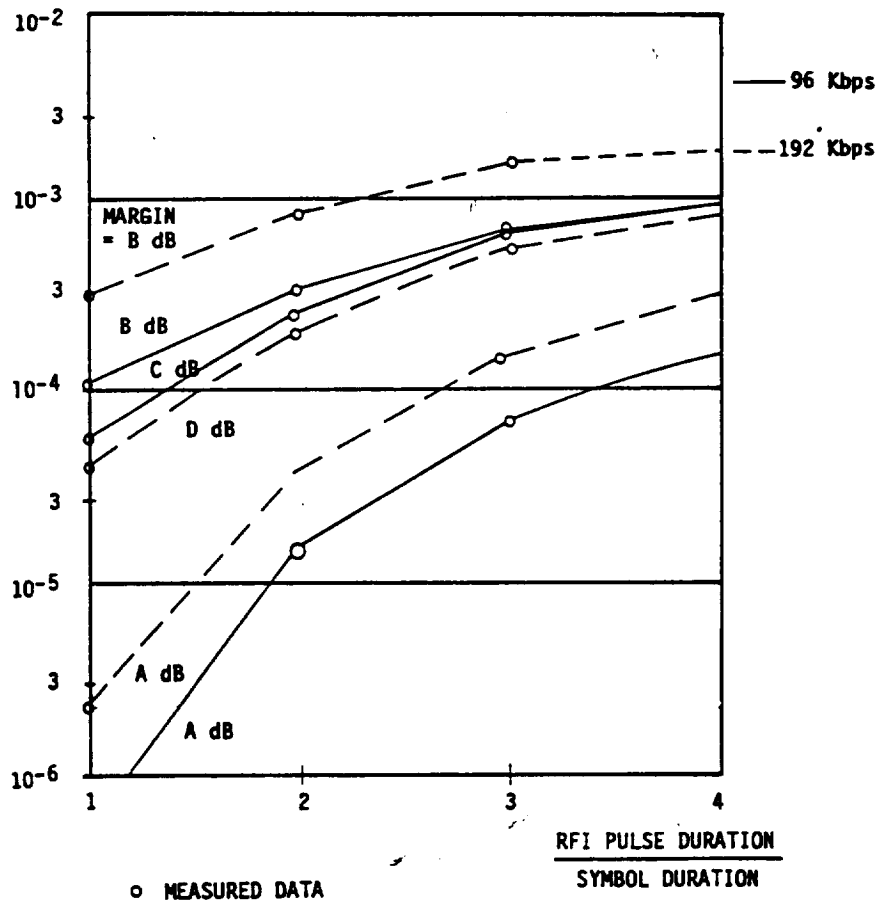


FIGURE 3: ILLUSTRATIVE IMPACT OF RFI PULSE DURATION ON SHUTTLE-TDRSS S-BAND RETURN LINK.
 (A ≥ D ≥ C ≥ B)

4. SUMMARY

The NASA/GSFC Viterbi decoder hardware simulator extends the capability of CLASS to include non-interleaved channels when the impact of pulsed RFI on the coded BER of the TDRSS return link is assessed. The discrete, bursty channel is simulated by computing a set of soft decision probability distributions with CLASS. The simulator chooses one soft decision probability distribution for each channel symbol.

The simulation results show the sensitivity of coded BER to a variety of illustrative RFI parameters. The sensitivity of coded BER to the RFI pulse duration can be easily assessed as is shown with the Shuttle-TDRSS S-band simulations. As an example of the impact of the RFI power levels, pulse duration and of the RFI being on-band/out-of-band, the coded BER of the Shuttle-TDRSS K-band is evaluated for some illustrative RFI parameters.

REFERENCES

1. Weinberg, A., "Coded BER Performance for the Nonlinear TDRSS Communication Channel Corrupted by RFI, STI/E-TR-8115, Stanford Telecommunications, Inc., McLean, VA (March 1980).
2. Final Report for a Simulation System for Validating the Analytical Prediction of Performance of the Convolutional Encoder and Symbol Interleaved TDRSS S-Band Return Link Service in a Pulsed RFI environment, Linkabit Corporation, San Diego, CA (1981).
3. Walvis, D.J.M., Zakrzewski, e., Wilkinson, W., Swerdlin, S., Weinberg, A.: Hardware and Software Simulation of Viterbi Decoder Performance in Pulsed RFI. STI/E-TR-25003A, Stanford Telecommunications, Inc., McLean, VA (1982).
4. COSAM User's Guide, Stanford Telecommunications, Inc., McLean, VA (1980).

ELECTRONICS SYSTEMS TEST LABORATORY TESTING
OF SHUTTLE COMMUNICATIONS SYSTEMSC. Jack Stoker and Linda K. Bromley
NASA Lyndon B. Johnson Space Center
Houston, TexasABSTRACT

Shuttle communications and tracking systems space-to-space and space-to-ground compatibility and performance evaluations are conducted in the NASA Johnson Space Center Electronics Systems Test Laboratory (ESTL). This evaluation is accomplished through systems verification/certification tests using Orbiter communications hardware in conjunction with other Shuttle communications and tracking external elements to evaluate end-to-end system compatibility and to verify/certify that overall system performance meets program requirements before manned flight usage. In this role, the ESTL serves as a multi-element major ground test facility. This paper provides a brief description of the ESTL capability and program concept. The system test philosophy for the complex communications channels is described in terms of the major phases. A summary of results of space-to-space and space-to-ground systems tests is presented. Several examples of the ESTL's unique capabilities to locate and help resolve potential problems are discussed in detail.

INTRODUCTION

The Electronic Systems Test Laboratory was established in 1964 as the only practical means of development, and subsequent certification by testing, of space/ground communications systems on an end-to-end basis. Space vehicle communications subsystems, unlike other subsystems, must interface not only with other subsystems on the space vehicle but also, by radiofrequency, with remotely located external equipment. These external interfaces include the Ground Space-Flight Tracking and Data Network (GSTDN), the Air Force Satellite Control Facility (AFSCF), the Tracking and Data Relay Satellite System (TDRSS), NASA and Department of Defense (DOD) detached payloads, and extravehicular communications systems. Descriptions of the Shuttle communications modes and systems configurations can be found in references 1 to 3.

Reliable communications between the Orbiter space vehicle and its external elements are mandatory for successful missions. The early manned-space-flight programs (Mercury and Gemini) used, primarily, off-the-shelf aircraft-type communications systems. These systems had been developed previously and a proven capability had been demonstrated, primarily by the military. These systems were accepted for space flight using ground support equipment to simulate the functions of the external communications equipment. The actual space vehicle and the external communications equipment were not interfaced until tests at the launch facility. As the communications systems became more complex, a new philosophy was needed. The advent of more complex high information rate communications systems, such as the Apollo unified S-band system and the Shuttle TDRSS space-to-space and space-to-ground multiple configurations, requires a more thorough and comprehensive program for compatibility and performance certification before the first use on manned missions. The ESTL was established as the most practical way to provide the unique capability to interface space vehicle communications equipment and its external counterparts in a laboratory environment. This capability is used to develop and verify that equipment is compatible and that the performance provided by these communication links meets program requirements.

The Space Shuttle communications system consists of major hardware elements that can be generally categorized as space elements and ground elements. Before release of hardware specifications, analytical models are developed to determine system feasibility and potential performance capabilities. As the analytical phase progresses, many problems/questions arise that are not analytically tractable but lend themselves to experimental evaluation. Thus, to supplement the analysis, early system-level tests are conducted using breadboard hardware. During hardware development (after contract award), the analysis and breadboard testing continue to be essential elements in resolving specification conflicts which arise as the hardware design matures. After design/development of the system hardware, system verification testing using prototype hardware is accomplished. These tests establish basic system compatibility and performance and provide a means to identify any modifications required if an incompatibility or performance deficiency exists. The final phase of hardware development includes system performance certification, which entails verification that the flight-configured systems are compatible and will meet mission performance requirements. If problems are encountered at this level of testing, either hardware modifications or mission constraints result. To avoid the serious consequences of performance certification problems, the Shuttle Program Office has established the Space Shuttle communications and tracking systems ground testing program at the NASA Johnson Space Center (JSC). This program provides three basic phases: (1) system design eval-

uation tests using breadboard hardware, (2) system verification/certification tests using prototype hardware (or flight-type hardware when differences exist between flight-type and prototype hardware), and (3) special tests involving operational configurations and/or concepts. The remainder of this paper describes, in more detail, the test philosophies, techniques, and results associated with each of these test phases.

ESTL TEST CONCEPT

The ESTL provides the unique capability to interface space vehicle communications equipment with its external counterparts in a laboratory environment under closely controlled conditions. Particular emphasis is placed on new, complex, and unproven system designs. Test conditions are closely controlled by any combination of such factors as the total received power levels and the presence or absence of static or dynamic Doppler, data encoding, spectrum spreading, bit jitter, and/or data asymmetry, etc. These factors can be varied individually to determine their effect on the system or set to their nominal mission values to determine overall expected end-to-end system performance. Use of the ESTL capabilities enables early verification of communications systems compatibility and performance.

The concept used in the implementation of testing in the ESTL is illustrated in figure 1 for certification test phases. Operational Shuttle Orbiter hardware electrically equivalent to flight hardware is obtained through the prime contractor and interconnected such that the resultant subsystem is equivalent to the Orbiter Communications and Tracking Subsystem. The hardware is then installed in one of four radiofrequency (RF) shielded enclosures in the ESTL. The ESTL Orbiter/spacecraft test area is shown in figure 2. The space vehicle communications subsystem is interconnected with the external elements (GSTDN, TDRSS, AFSCF, extravehicular systems, or payloads) through space loss simulators. The relay satellite, extravehicular systems, and payloads are also installed in shielded enclosures.

The space loss simulators provide precise control of the power levels for the K_u -band, S-band, and ultrahigh frequency (UHF) signals delivered to the receiving systems. The ESTL space loss simulator is shown in figure 3. For S- and K_u -band waveguide configurations, a dry air system is required to maintain constant waveguide characteristics and thus preserve the space loss simulator accuracy. The space loss simulator also provides the capability to induce dynamic or static Doppler onto the RF signal and its modulation. Patch panels enable routing of signals between any of the four shielded enclosures, the GSTDN ground station equipment, the AFSCF ground station equipment, and the TDRSS (space and ground segment) equipment.

The GSTDN equipment installed in the ESTL was obtained through the NASA Goddard Space Flight Center (GSFC) and is identical to the equipment located in NASA's worldwide network. Equipment from one of the AFSCF remote tracking sites was modified and provided by the Air Force to accommodate interface certification with the Shuttle Orbiter. The TDRSS ground station equipment (fig. 4) installed in the ESTL was procured from various vendors by part numbers and is identical to the S-band and K_u -band single access equipment in the ground station at White Sands, New Mexico. The TDRSS equipment located in the ESTL represents a functional simulation of the single access characteristics of the actual satellite. Specifications for the simulation system were developed in coordination with cognizant engineers at GSFC. A functional simulator of the TDRS (space and ground interface segments) is presently installed in the ESTL. TDRSS ground station hardware is updated as necessary to ensure that high-fidelity operational TDRSS configurations are maintained.

The test control center in the ESTL (fig. 5) serves as the central location for coordination of test activities. It also has the capability to generate test activities. Additionally, the generation and evaluation of audio and television video signals, measurement of bit error rates (to 150 Mbps), command evaluation, space loss simulator control, and remote control of GSTDN equipment are initiated from the test control center. The measurements and data comparisons performed in the test control center are recorded by keyboard entry into the real-time data analysis and prediction system.

To perform system-level tests, several types of measurement techniques must be employed. These techniques include the statistical measurement of bit error rate (BER) (probability), signal-to-noise ratios (SNR's), and voice quality (made in conjunction with the U.S. Army Test and Evaluation Command at Fort Huachuca, Arizona). Details of techniques to make these measurements can be found in reference 4. Several unique measurement techniques have been developed such as an automated system (Statistical Loop Analyzer, ref. 5) for measuring acquisition, tracking, and frequency stability performance characteristics. Evaluation of the performance of the Space Shuttle communications and tracking systems requires simulated Doppler frequency shifts applied to the RF carrier and to the modulation signal frequencies. A description of the ESTL computer-controlled range and Doppler simulation system can be found in reference 6. Additionally, a computerized Real-Time Data Analysis and Predictions System that makes data plots with performance predictions and tolerances and provides permanent data storage (ref. 7) is used to improve productivity by decreasing the time required to assess the performance of the link under evaluation. The ESTL Data Processing and Graphics System is used

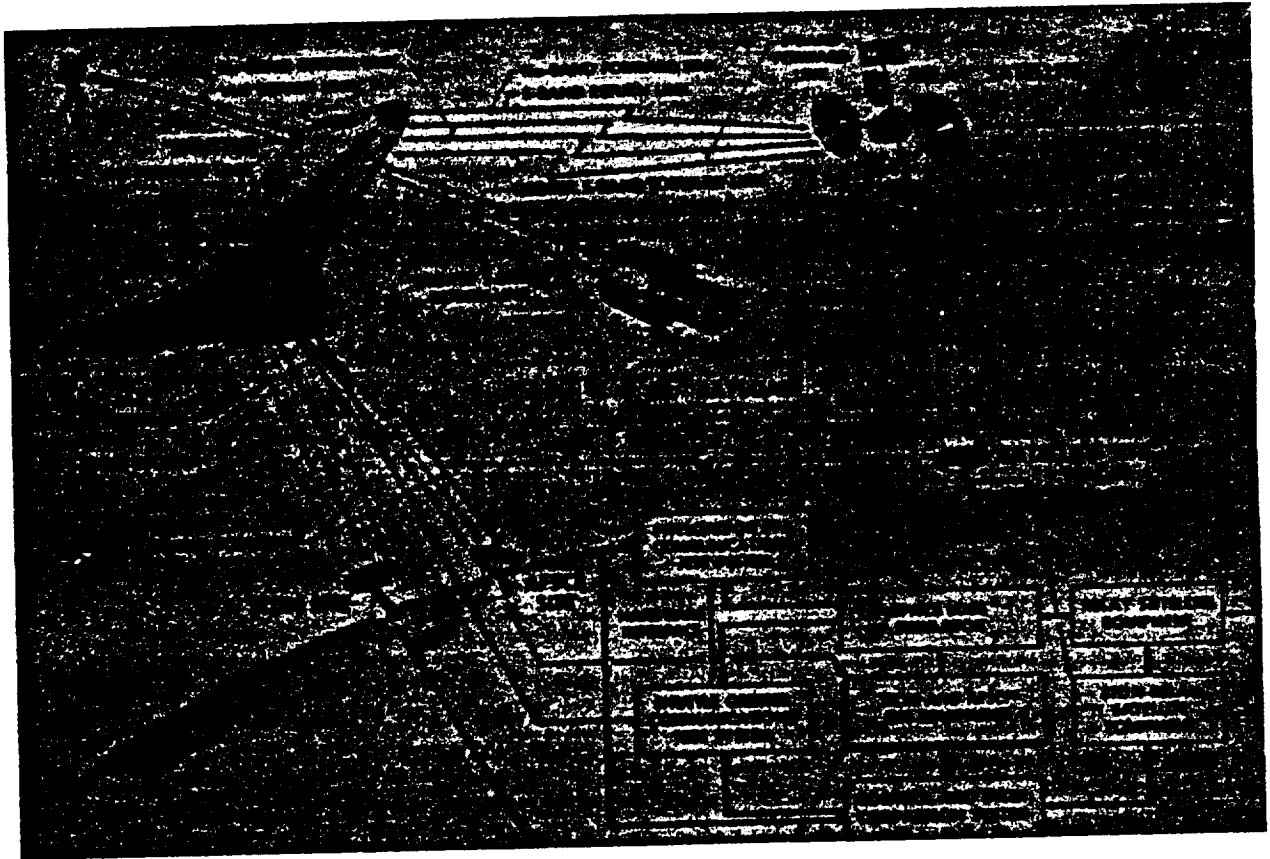


FIGURE 1.- ESTL TEST CONCEPT.

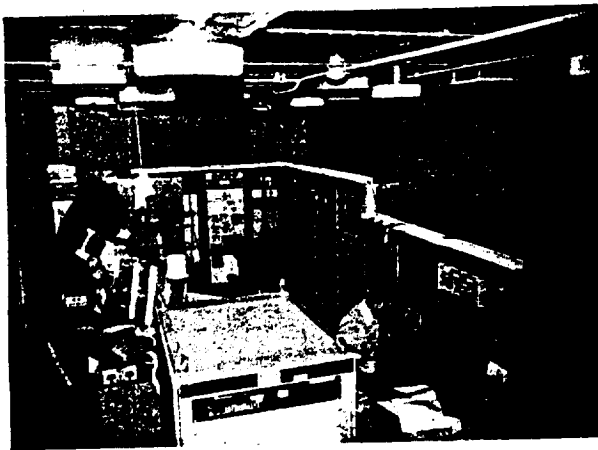


FIGURE 2.- ESTL ORBITER/SPACECRAFT TEST AREA.

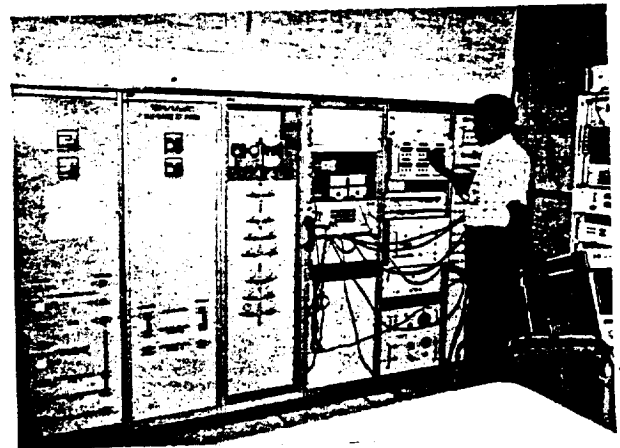


FIGURE 3.- ESTL SPACE LOSS SIMULATOR.

for data acquisition and statistical analysis and generation of digital data required to perform test operations. Techniques that can be used to evaluate early breadboards of telemetry channel performance (without RF receivers) are discussed in reference 8.



FIGURE 4.- ESTL TDRSS GROUND STATION EQUIPMENT.

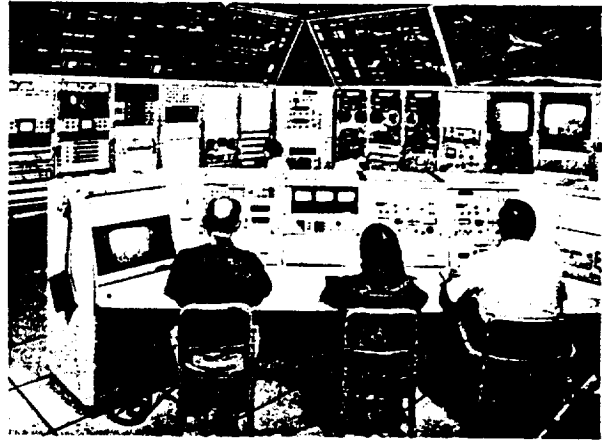


FIGURE 5.- ESTL TEST CONTROL CENTER.

SYSTEM COMPATIBILITY AND PERFORMANCE TESTS

Shuttle communications and tracking systems development testing in the ESTL was divided into two broad categories. The first category, system design evaluation tests, involved the use of Orbiter subsystem breadboards very early in the program. The purpose of these tests was to evaluate proposed communications techniques, hardware, and software implementations; to provide data for Orbiter and possibly network hardware specifications; to determine whether problems existed, evaluate cost-effective solutions to the problems as early as possible, and provide an early assessment of performance capability; and to establish test techniques and criteria for future tests. The second category, system certification tests, involves operational Orbiter and network hardware and results in the certification of the end-to-end systems compatibility and performance. Because of the complexity of the elements involved and the amount of time required to investigate and resolve problems when they occur, it is necessary that this category of testing begin as early as practical in the program. Using prototype Orbiter hardware, these tests are implemented initially to certify that the performance of the system is satisfactory and that the RF communications links between all elements meet program requirements and are ready for flight. The second category of testing is different from the design verification tests in that the space/ground hardware configurations used are flight equivalent. When differences exist between Orbiter prototype hardware and production (flight) hardware, either the prototype hardware is upgraded to be flight equivalent or the production/flight hardware is utilized.

SYSTEM DESIGN EVALUATION TESTS

System design evaluation tests are accomplished using breadboard system hardware configurations. Early tests were accomplished before the hardware procurement specification preparation and continued through the early vendor hardware development phase. Test results were effective in influencing specification parameter values and hardware mechanization/design. The type of tests conducted depended on the particular area of investigation but was generally conducted on an end-to-end basis to investigate system parameters whose interactions are not readily tractable through analytical means or in areas where new math models had been derived but not verified empirically. Particular emphasis was placed on the new, complex, and unproven aspects of end-to-end system compatibility and performance. Figure 6 illustrates the types of sources of breadboard hardware used. The Orbiter breadboard hardware obtained from in-house subsystem laboratories was integrated with a TDRSS (space segment) simulator in a laboratory environment. The integrated breadboard system was then evaluated on an end-to-end performance basis to determine whether any potential Orbiter hardware specification and/or design deficiencies exist. The results of these tests provide GSFC and DOD with performance criteria to establish system performance specifications for Shuttle-unique channels. Critical elements of both the TDRSS S-band and K_u -band single access channels were simulated and evaluated.

The Shuttle S-band and K_u -band system design evaluation tests included both preprocurement specification testing and hardware development support testing. ESTL capabilities include system concept and technique verification, hardware mechanization feasibility, system design requirements development for end-item specifications, and parameter definitions for interface control documents. The following specific examples are discussed to illustrate the nature of system design evaluation testing.

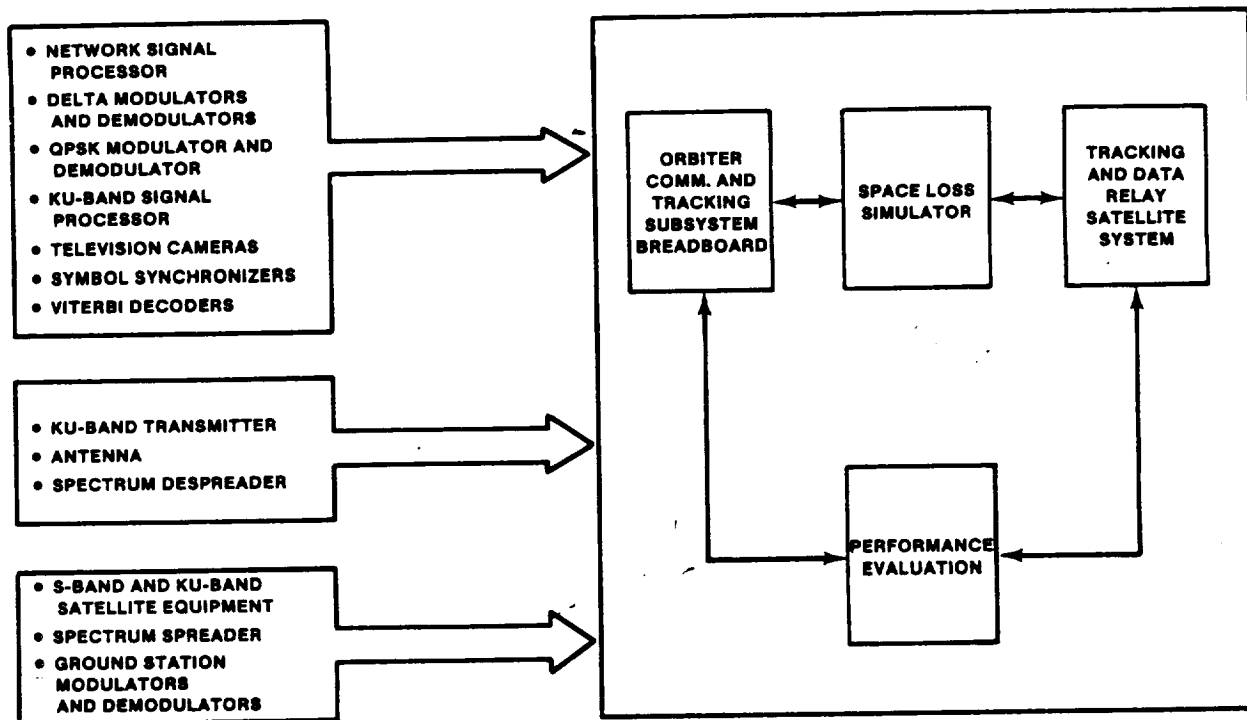


FIGURE 6.- ORBITER COMMUNICATIONS AND TRACKING SUBSYSTEM BREADBOARD SOURCES.

During early system design evaluation testing of the digital voice system, five separate algorithms were evaluated in combination with various audio processing techniques and requirements (automatic gain control, clipping, filtering, levels, etc.), including the effects of convolutional encoding/decoding (error statistics) on voice quality. Frequency modulation (FM) mode parameters were investigated before preparing the procurement specification for the K_u -band hardware. The major areas of investigation included carrier frequency deviations due to television video, receiver bandwidth requirements, subcarrier television interference effects including premodulation and postdetection filtering, quadriphase shift-keyed (QPSK) subcarrier demodulation techniques, and television channel performance criteria (i.e., SNR, response, etc.). Space system elements under evaluation included the wideband signal processor and the K_u -band wideband modulator. The ground system elements under evaluation included the K_u -band wideband demodulator (intermediate frequency (IF) bandwidth), the postdetection filter, and the QPSK demodulator. The system elements and parameters could be accomplished and optimum system specifications established. Results of these tests provided the data used in establishing the frequency deviation for television (± 11 megahertz), the premodulation filter specifications for the K_u -band signal processor, and the receiver IF and postdetection filter specifications for the ground station. In addition, it was verified that the television channel performance criteria used for circuit margin calculations provided high-quality video signals.

A second level of design evaluation testing occurs as the hardware design matures. During this phase, the ESTL end-to-end system compatibility was expanded and provided needed support to NASA prime contractors in evaluating vendor impacts resulting from specification deficiencies and/or hardware design deficiencies. Parameters such as frequency deviations, bandwidth requirements, subcarrier interference effects, digital voice quality, coding gain, bit jitter effects, and RF and spread spectrum acquisition probabilities were determined. For example, during S-band FM data performance testing, it was determined that the optimum frequency deviation (Δf) and IF for Manchester and nonreturn-to-zero (NRZ) data formats was $0.62R$ (Δf), $2.5R$ (IF) and $0.36R$ (Δf), $1.5R$ (IF) respectively, where R is the transmitted data rate.

Of particular interest (because of the high cost impacts associated with a "fix") was the investigation of the effects of data asymmetry on the high data rate (50 Mbps) channel performance during K_u -band tests. The ESTL system testing provided experimental results which, combined with performance simulations and analysis, led to the decision to relax data asymmetry requirements on Shuttle Orbiter data channels. This decision resulted in a significant cost avoidance. The results also indicated that initial analytical predictions of degradation due to asymmetry were highly pessimistic.

tic. Subsequently, it was found that analytical results varied significantly if bit synchronizer mechanizations were more exactly modeled. The data asymmetry analytical results (such as dc restoration) are discussed in references 9 and 10. The tests and analysis have shown that a general degradation model for all systems seems impractical. As a result of this activity, the K_u-band hardware vendor was directed to relax the asymmetry specification to 10 percent or less (from the 3 percent or less limitation that had previously been imposed). Relaxation of the specification resulted in a NASA cost savings of several million dollars. Summaries of S-band and K_u-band design evaluation testing are listed in tables 1 and 2 and discussed in reference 4.

During the design evaluation phase, the capability of the ESTL to perform end-to-end system tests proved highly effective in avoiding downstream costly hardware modifications and in allowing specification changes where reasonable. ESTL activities and hardware vendor test capabilities are complementary in nature and result in a high probability that the hardware will be compatible and will meet system performance requirements when integrated with the remaining communication system elements, while minimizing vendor system test equipment capital investment requirements. The net result of this type of system design evaluation testing is a significant program cost avoidance.

SYSTEM CERTIFICATION TEST

Shuttle communications certification tests were different from the system design evaluation tests in purpose, type of hardware used, and depth of testing. The purpose of the system certification tests is to certify that the Orbiter communications systems are ready for manned flight and will support the program requirements. For the most part, prototype Orbiter hardware that was electrically equivalent to space vehicle equipment was used to implement these tests. The use of flight-equivalent hardware ensures that differences between system design verification configurations and flight-type equipment which affect system performance are considered in the certification process and certifies that any problems encountered during the system design verification have been corrected. Shuttle system certification tests were initiated in the second quarter of 1979 and included all of the major space and ground element systems (i.e., GSTDN, AFSCF remote tracking station, TDRSS ground segment, extravehicular astronauts, Spacelab, and five detached payloads). The importance of performing system certification tests cannot be overemphasized. The effects of complex techniques and/or concepts such as unbalanced quadriphase modulation, convolutional encoding/Viterbi decoding, and spectrum spreading and despreading are ascertained. ESTL system test results together with theoretical predictions (analysis and simulation) have been used to characterize the system and to assess end-to-end RF system performance.

Where differences exist between theoretical and measured data, detailed system analysis is initiated. End-to-end system performance is characterized by making system test measurements as listed in table 3. A discussion of performance examples, such as coding gain, Doppler and intermodulation effects, link margins, etc., is beyond the scope of this paper (see refs. 14 to 21); however, some of the significant findings (and problems to be avoided) are summarized in the following paragraphs.

Launch Configuration RF Acquisition

The Shuttle S-band communications system design was intended to provide signal acquisition without interaction by the ground station operators. The Orbiter transponder and the multifunction receiver (MFR) at the ground station were both to begin sweeping about the nominal uplink and downlink

TABLE 1.- S-BAND DESIGN EVALUATION TEST SUMMARY

Issue under investigation	Type of tests	Results/outputs
Delta modulation techniques	Frequency response	Selected modified "ABATE" algorithm
	Output noise spectrum	Determined postdetection BPF response (300 Hz to 2.5 kHz)
	Voice quality	Determined 90-percent word intelligibility $\leq 10^{-2}$ BER
	COMSEC compatibility	Determined compatible with COMSEC

TABLE 1.- Concluded

Issue under investigation	Type of tests	Results/outputs
Convolutional encoding/decoding	Coding gain	Coding gains \leq 0.3 dB from theoretical were achievable
	Sensitivity to receiver parameters	Coding gain affected by receiver phase error and IF amplifier limiting
	Error statistics	Compatible with COMSEC - actually decreases sensitivity to channel errors
Television (FM link)	Signal-to-noise ratio and video-to-noise ratio	Determined 26-dB rms/rms SNR requirement consistent with good quality video
	RF spectrum	Determined Δf of 4.5-MHz optimum for direct S-band links
	Postdetection filter optimization	Determined RF spectrum with TV Δf of 4.5 MHz does not result in RFI problem for AF
	Frequency deviation optimization and IF amplifier (predetection)	Determined optimum IF bandwidth for TV approximately 2 Δf , for $\Delta f > 4.0$ MHz
Spread spectrum techniques	Adaptive threshold performance	Developed adaptive threshold technique
	Despreading algorithm evaluations	Determined acquisition algorithm sensitivities to system parameters (threshold levels, search, check, and lock stages, etc.)
	Acquisition time	Verified acquisition time predictions
	Tau dither loop evaluation	Developed tau dither loop bandwidth switching technique
	BER degradation due to spreading	Determined despreading degradation < 1.0 dB
FM data performance optimization (NRZ and Manchester formats)	BER sensitivity to Δf and to IF bandwidth	Determined optimum Δf and IF bandwidth for Manchester and NRZ data formats
	Main engine data channel premodulation filter optimization	Premodulation filter characteristics specified
Synchronization strategy evaluation	Data transfer versus bit error probability and voice quality (intelligibility versus data transfer)	Determined data transfer of 80 percent or more at a BER of 1×10^{-1} required to prevent additional voice intelligibility degradation

frequencies, respectively, with data modulating the carriers. The downlink frequency was to be provided by an auxiliary oscillator (AUX OSC) in the Orbiter transponder when the transponder was not locked to the uplink signal. When the transponder acquired the uplink signal, the downlink frequency

TABLE 2.- K_U-BAND COMMUNICATION SYSTEM DESIGN EVALUATION TEST SUMMARY

Issue under investigation	Type of tests	Results/outputs
Return link, FM mode (parameter evaluation)	Television signal-to-noise ratio, television quality, and TV/data interference	Determined TV frequency deviation $\Delta f = 11$ MHz Determined receiver IF BW = 45 MHz Determined postdetection filter BW = 4.5 MHz
	Baseband data BER	Specified premodulation filters to minimize subcarrier/TV interference
	Subcarrier channel BER	Determined sensitivity of subcarrier operational data channel to experimental data as a function of experimental data rates. (Worst case approximately 2 dB when experimental data are at same rate or twice the rate of the operational data.)
		Verified voice quality and data bit error probability performance Demonstrated feasibility of bent-pipe subcarrier mode
Return link, PM mode (parameter evaluation)	Dual QPSK technique	Verified dual QPSK modulation technique Determined signal suppression of low-level channel
	High rate channel BER (uncoded and coded)	Determined system performance at 100, 50, and 25 Mbps for uncoded and coded data
	High rate data asymmetry degradation (uncoded and coded)	Developed asymmetry degradation factor for high data rate channel
	Subcarrier channel BER and high rate/subcarrier channel interference	Verified subcarrier channel bit error probability performance and voice quality
	Bent-pipe channel evaluation	Demonstrated bent-pipe capability in PM mode (subcarrier channel)
Return link, PM mode (parameter evaluation) (cont)	PSK coding gain	Verified coding gain specifications achievable with real world hardware
	Three-channel interplex	Determined interference degradation Verified unbalanced QPSK performance

TABLE 3.- SYSTEM TEST MEASUREMENTS

System/function	Test measurement	System/function	Test measurement
Voice	Speech-to-noise ratio Word intelligibility Crosstalk Distortion	Data (command/ telemetry)	Bit error rates Percent information loss Message rejection rates Coding gain Recorder jitter effects
Ranging	Acquisition probability Range data accuracy	Doppler	Doppler accuracy Effects on BER
Acquisition	Costas loop acquisition probability Costas loop acquisition time Spread spectrum acquisition proba- bility Spread spectrum acquisition time Acquisition threshold Mean time to unlock	Television	Resolution Signal-to-noise ratios K-factor Differential phase Differential gain Picture quality

source was to be switched over from the AUX OSC to the voltage controlled oscillator (VCO) and the acquisition process would be completed automatically.

During the uplink acquisition tests, a problem was encountered in that Costas loop acquisition of a signal with modulation on the uplink carrier could be accomplished only at very low signal levels. At signal levels about 49 dB-Hz, the data components in the frequency spectrum became large enough for the transponder to false lock to them instead of the desired carrier. Figure 7 depicts the significant components in the uplink signal spectrum (amplitudes not to scale) for modulation by high and low data rates of 75 kbps and 32 kbps, respectively, and the transponder sweep range. As shown in figure 7, there are a large number of stationary spectral lines within the sweep range of the transponder.

Since a rework of the Shuttle transponder would have been costly and could impact flight schedules, a new acquisition procedure was developed to circumvent the false lock problems. Under the new procedure, the uplink would be transmitted carrier-only (i.e., no data modulation on the carrier) while the downlink would still be transmitted with data modulation present. After a good two-way lock has been achieved, the ground station exciter operator applies uplink modulation.

Tests of the new procedure proved that it circumvented the false lock problem during initial acquisitions. However, once the initial two-way lock has been achieved and modulation applied, if for any reason the uplink should lose lock, it is still likely to reacquire falsely since modulation would be on the carrier during a reacquisition process. In addition, this procedure adds significant ground operator involvement and results in greatly increased total two-way RF acquisition time (fig. 8). Long acquisition/reacquisition times are particularly undesirable during critical mission phases such as ascent and entry when communication dropouts will occur because of unavoidable phenomena such as solid rocket booster (SRB) plume effects, vehicle blockage from the external tank or other Orbiter structures, low-gain portions of the Orbiter antenna patterns, etc.

A new technique was developed and tested (ref. 11) to handle this problem. This technique allows modulation on the uplink during acquisition/reacquisition without ground operator involvement, thereby simplifying acquisition procedures and significantly reducing acquisition time. The technique involves convolutionally encoding the high data rate (72 kbps) time-division multiplexed (TDM) signal to provide a 216-kbps signal. As shown in figure 9, this alone will drive the stronger spectral components out farther. It was found that the strongest spectral components were caused by the voice idle pattern (alternating 1's and 0's) when no voice was being uplinked. Replacing this idle pattern with a random pattern (conventional noise source) effectively eliminates most spectral components except for those at one-half the data rate (i.e., 108 kilohertz, 216 kilohertz, etc.).

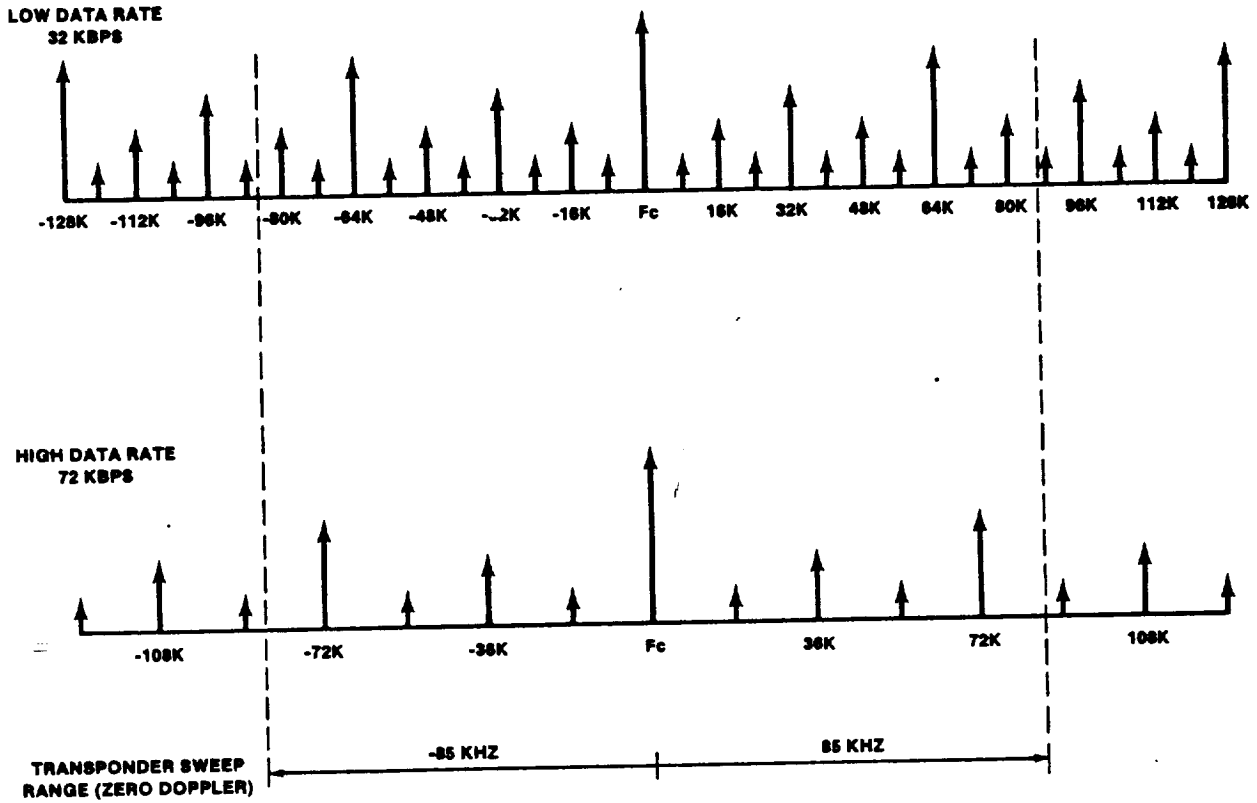


FIGURE 7.- S-BAND UPLINK SIGNAL SPECTRUM.

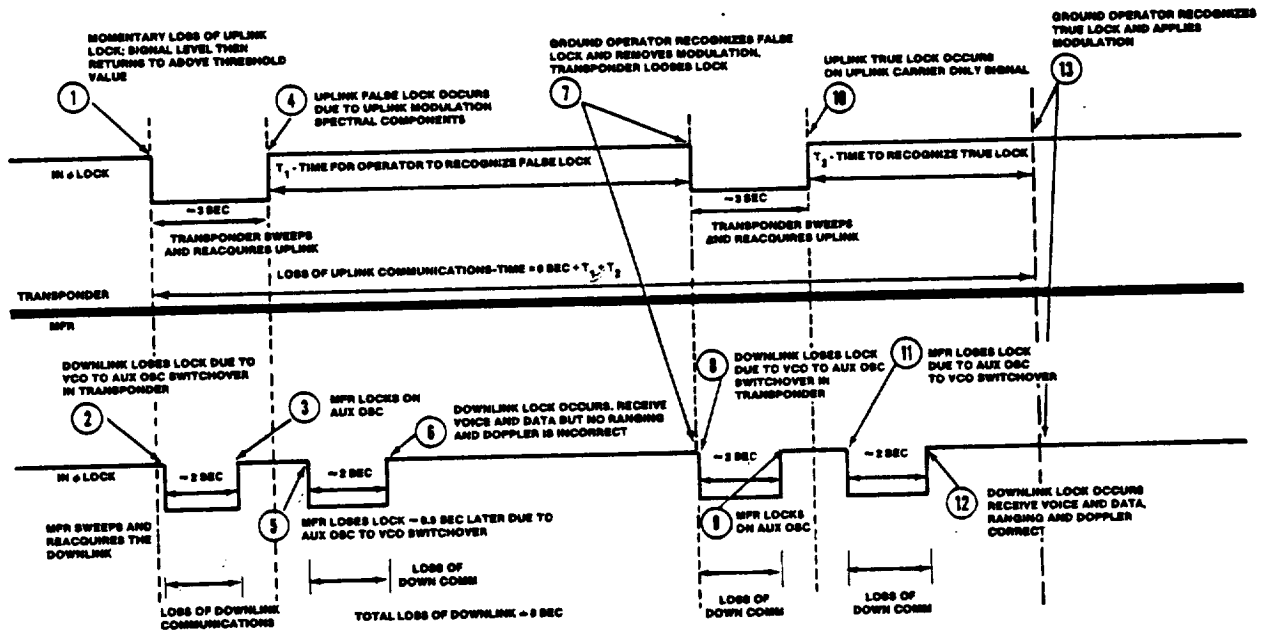


FIGURE 8.- ORBITER-GSTDN TWO-WAY RF REACQUISITION SEQUENCE (JSC/ESTL).

This technique was implemented at the ground stations covering the most critical phase of launch. As expected, the SRB plume effects do cause momentary dropouts. However, the implementation of this

HIGH DATA RATE ENCODED
72 KBPS X 3 = 216 KBPS

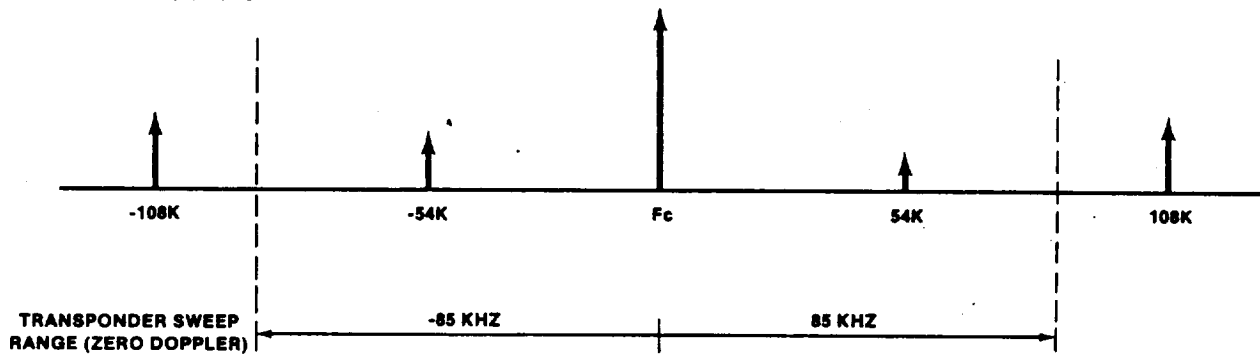


FIGURE 9.- UPLINK ENCODED 72-kbps SIGNAL SPECTRUM.

"noise mode" technique has very effectively prevented the occurrence of false locks during reacquisitions and has minimized the reacquisition time, thereby eliminating excessive loss of data.

Orbiter-GSTDN Ranging Channel Anomaly

A block diagram of the S-band direct link ranging channel is presented in figure 10. As shown in the figure, the range tones phase modulate a 1.7-megahertz subcarrier. This subcarrier is then frequency division multiplexed with the TDM and command data at the input to the transmitter phase modulator. In the Orbiter, the uplink signal is demodulated to a baseband composite in the wideband phase detector. The composite signal is passed through a bandpass filter which is centered at 1.7 megahertz and has a bandwidth of approximately 2 megahertz. The turned-around ranging subcarrier and noise are combined with the downlink TDM data in the transponder. The composite signal then phase modulates the downlink carrier. At the ground station, the 1.7-megahertz subcarrier is detected and then upconverted to 100 megahertz to be compatible with the GSTDN ranging equipment (SRE).

The SRE offers three combinations of tones which can be used to measure range. These combinations are shown in table 4. The high-frequency tone, called the major range tone, is used to obtain the fine (accurate) ranging data and is transmitted continuously after the start of the range acquisition process. The remaining lower frequency tones are used to resolve ambiguities. A more detailed discussion of the range tone transmission sequence is given in reference 13.

The Shuttle ranging system was designed to use the 100-kilohertz major range tone option. Tests showed that the three-sigma range errors were in excess of the specified value of 10 meters. While the three-sigma errors varied with test conditions, the measured errors were as large as 1042 meters when the ranging subcarrier was multiplexed with high rate (192 kbps) TDM data and 59 meters when the ranging subcarrier was multiplexed with low rate (96 kbps) TDM data.

Ranging acquisition probability and accuracy tests were repeated using the 500-kilohertz major range tone option. The three-sigma error was reduced to 20 to 25 meters. However, approximately 2 percent of the acquisition attempts resulted in incorrect correlation of the phase of the 100-kilohertz minor tone and a 300-meter error. Tests conducted with the expected worst-case TDM modulation index of 1.2 radians resulted in three-sigma errors of 1286 meters and a mean acquisition time of 95 seconds. Thus, the tests showed that the ranging system performance was not acceptable.

Further investigation of these problems revealed that the TDM signal itself contained a high-level 100-kilohertz component. The high-rate TDM format consists of 100 minor frames of data per second. Each minor frame contains forty 48-bit bytes. Thus, the bytes occur 4000 times a second. The combination of this 4-kilohertz component at one-half the bit rate (96 kilohertz) results in the high-level spectral component at 100 kilohertz.

The modulation process in which the algebraic sum of the ranging subcarrier and the TDM data phase-modulate the carrier also results in the TDM data phase-modulating the 1.7-megahertz subcarrier. Thus, the spectrum around the 1.7-megahertz subcarrier contains two 100-kilohertz components. One of these components is the desired 100-kilohertz major range tone. The other component is the desired 100-kilohertz component of the TDM data. Since they are derived from different reference oscillators, the phases of the two 100-kilohertz components vary slowly with respect to each other. The amplitude and phase of the resultant sum of these two 100-kilohertz components varied significantly as the relative phases of the two signals changed.

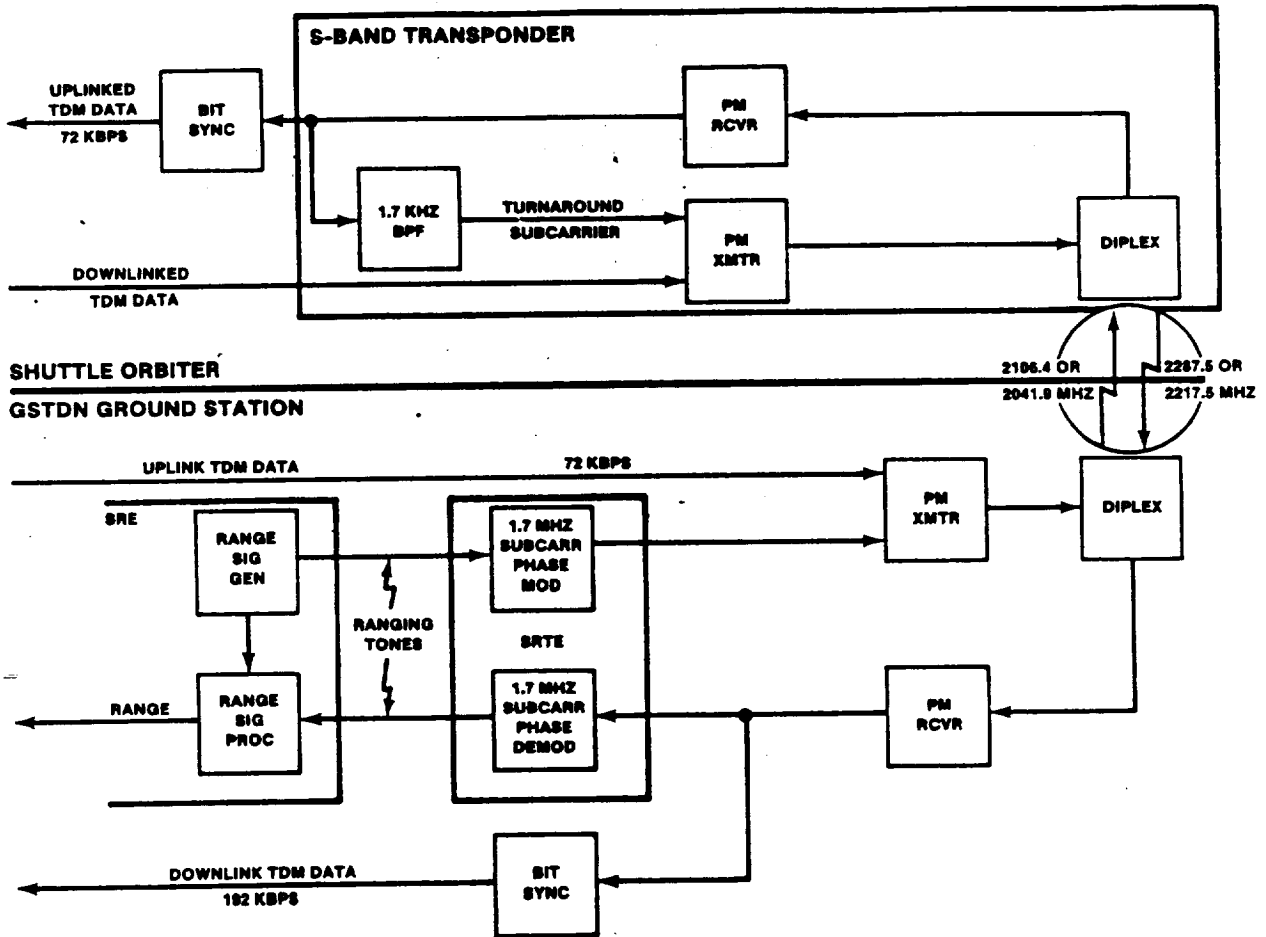


FIGURE 10.- S-BAND RANGING CHANNEL.

TABLE 4.- AVAILABLE RANGE TONE COMBINATIONS

Tone	Combination 1	Combination 2	Combination 3
Major tone	500 kHz	100 kHz	20 kHz
Minor tones	100 kHz 20 kHz 4 kHz 800 Hz 160 Hz 40 Hz 10 Hz	20 kHz 4 kHz 800 Hz 160 Hz 40 Hz 10 Hz	4 kHz 800 Hz 160 Hz 40 Hz 10 Hz

As a result of these investigations, a series of special tests was performed using the GSTDN transmitter and a frequency translator to simulate the downlink signal. Use of this combination allowed the peak deviation of the carrier due to the ranging subcarrier and TDM data to be varied. The reduction of the carrier deviation due to the TDM data to 0.55 radian significantly reduced the three-sigma errors and shortened the acquisition time.

An engineering model of the transponder was modified by reducing the modulation due to the TDM data to 0.55 radian. Tests of this unit showed that the three-sigma error was reduced to approximately 5 meters and the mean acquisition time was reduced to 17 seconds. Based on these results, the Shuttle Program Manager approved a change in the Orbiter S-band transponder design. The results of the tests accomplished with the modified transponder showed that the reduction of the TDM modulation index resolved the range accuracy and acquisition problems.

STS-1 AFSCF/ORBITER INTERFACE INCOMPATIBILITY

The Shuttle STS-1 mission included ground station coverage by the AFSCF remote tracking station located in the Indian Ocean (IOS). During DOD/AF premission readiness testing to functionally verify Orbiter communications system/ground station interfaces, it was observed that it was impossible to transmit Orbiter uplink data from facilities located at Sunnyvale, California, to the Orbiter equipment located at IOS. The problem existed to some extent at both uplink data rates. Bit jitter on the uplink data stream was considered to be the most likely cause of the problem. As a result of the ESTL capability, DOD representatives expedited delivery of affected positions of the IOS Defense Communications System Satellite Control Facility Interface System (DSIS) to supplement the existing ESTL Orbiter/Air Force ground station configuration, for detailed investigation and subsequent resolution of this anomaly. The anomaly was repeated in the ESTL with the DSIS equipment. Test results showed that the problem was caused by the lack of adequate dejitter capability of the dejitter hardware used at IOS. The dejitter hardware was subsequently modified in the laboratory by DOD representatives. Space/ground systems retests performed with the modified dejitter unit provided acceptable performance. ESTL tests confirmed that dejitter capability is mandatory for successful uplink with the Orbiter from IOS and that the DSIS and modified dejitter hardware are not overly sensitive to bit jitter. Return of the DOD hardware and final end-to-end (MCC-GSFC-STC-IOS) forward link integration verification testing were accomplished in time to enable IOS to successfully support the STS-1 mission.

VOICE DISTORTION DUE TO TIME DELAY

Another event that requires special treatment is the potential for voice distortion resulting from differential time delays when two paths are used for redundancy purposes. During Shuttle missions, audio signals are transmitted simultaneously to the Orbiter via UHF and S-band RF links. For example, voice signals routed from the Mission Control Center (MCC) to the Merritt Island Launch Area (MILA) utilize independent paths, resulting in differential delays before transmission. To alleviate the distortion, commonly referred to as the "barrel effect," tests were performed in the ESTL to determine the amount of reduction in the UHF onboard audio level required to substantially reduce the distortion effects but still allow for UHF communications in the event of an S-band failure. These settings were determined and have been successfully used in all Shuttle flights to date.

FORWARD LINK PERFORMANCE DEGRADATION DUE TO RETURN LINK

There have been several cases of the forward link performance being degraded in some manner when the return link transmitter is enabled. For example, during the GSTDN direct link tests, it was found that a degradation of 0.8 decibel in uplink performance occurred when the downlink power amplifier (PA) was enabled (fig. 11). While circuit margins for the direct link were such that an 0.8-decibel degradation would not be a problem, the degradation was critical in the TDRSS mode where the margins were small. Tests were conducted to determine the extent of the problem when the equipment was in the TDRSS mode and to search for its cause.

BER tests were performed for various uplink parameters (frequencies, data rates, spreading, etc.) with the PA in standby, on, and with magnets attached to the preamplifier assembly connectors. The tests with the magnets mounted on the preamplifier connectors were performed because an investigation by the preamplifier assembly vendor had shown that the use of magnets significantly reduced the noise figure degradation which occurs during the use of the PA. The vendor investigation and subsequent investigation by the ESTL were prompted by Alert No. Y1-A-75-01 (ref. 12), issued by the Naval Research Laboratory. The data presented in this alert showed that RF nonlinearities resulting from small quantities of ferromagnetic contaminants (in Kovar hermetically sealed connectors and stainless steel connector shells) caused generation of intermodulation products that can result in substantial performance degradation. This alert also pointed out that the presence of ferromagnetic nonlinearities could be detected by application of an external magnetic field positioned near the connector in question.

Tests were designed to determine what factors were contributing to the degradation and to determine the consequences of this degradation on forward link performance in the TDRSS mode. Three factors were found to be the major contributors to the degradation: ferromagnetic effects, thermal effects, and cable length variations. These contributions to the BER degradation anomaly are sum-

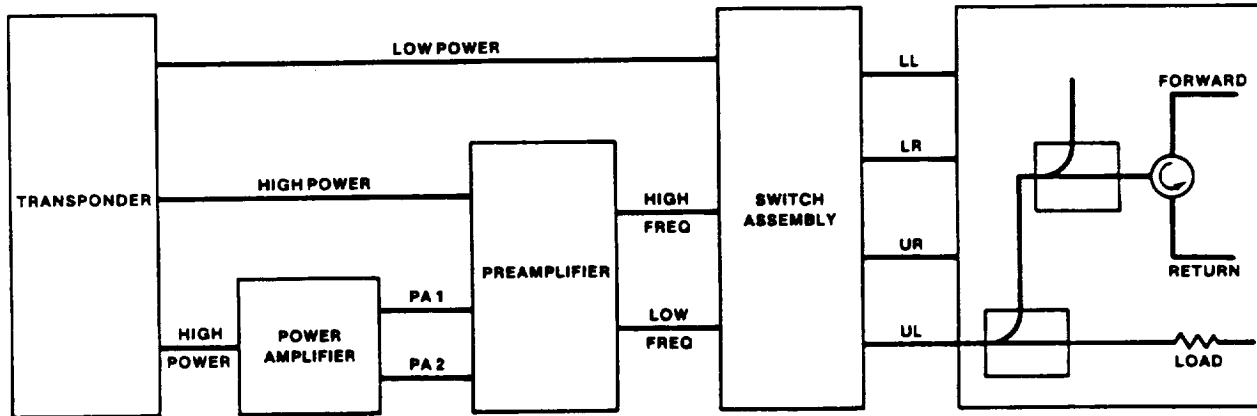


FIGURE 11.- ORBITER S-BAND SYSTEM.

TABLE 5.- BER DEGRADATION CONTRIBUTORS

Effect	Degradation, dB	
	Best case	Worst case
Ferromagnetic	0.4	0.5
Thermal	.1	.2
Cable length variation	0	.5
Unknown	0	.1
Total	0.5	1.3

marized in table 5. As a result of these investigations, the stainless steel connectors on the pre-amplifier assembly were replaced, resulting in an 0.4- to 0.5-decibel improvement.

A second example of forward link degradation due to the return link occurred during tests conducted on the Orbiter K_u-band system (fig. 12). During these tests, it was found that the forward link BER degraded 10 decibels when the return link transmitter was enabled with full modulation (48 Mbps). The initial assessment by the hardware vendor attributed the cause of this degradation to the failure to properly initialize a set of ferrite switches (fig. 13) when bringing up the system in the COMM mode. These switches are primarily used in the RADAR mode to provide a means of radar transmit/receive blanking to eliminate ambiguities. The "radar xmt safe" control line shown in figure 13 is used to first enable (i.e., place switches in clockwise path) the transmitted pulse, then disable the transmitter (i.e., counterclockwise path). While the transmitter is off, the system will "listen" for the return of the pulse just transmitted. The process is then repeated for the next pulse. The last switch in the set of four is used only in the RADAR mode to provide a path for cases when a very low power radar signal is desired to be transmitted. In this case, the traveling-wave tube (TWT) amplifier is bypassed and the unamplified signal will enter the diplexer through this last switch which will have been set to its counterclockwise position.

In the COMM mode, these switches are to be set in a counterclockwise position, effectively eliminating that path into the second diplexer. The initial assessment by the vendor considered that, if the ferrite switches are not properly set for COMM mode (fully counterclockwise), some wideband RADAR "noise" could be added with the desired COMM signal in the diplexer. This combined signal would then go through the FWD/RTN directional coupler. Although greatly attenuated, some of this combined return link signal could possibly leak through the coupler into the sum receive channel as depicted in figure 13. The bandpass filter is centered around 13.775 gigahertz and is 100 megahertz wide. This

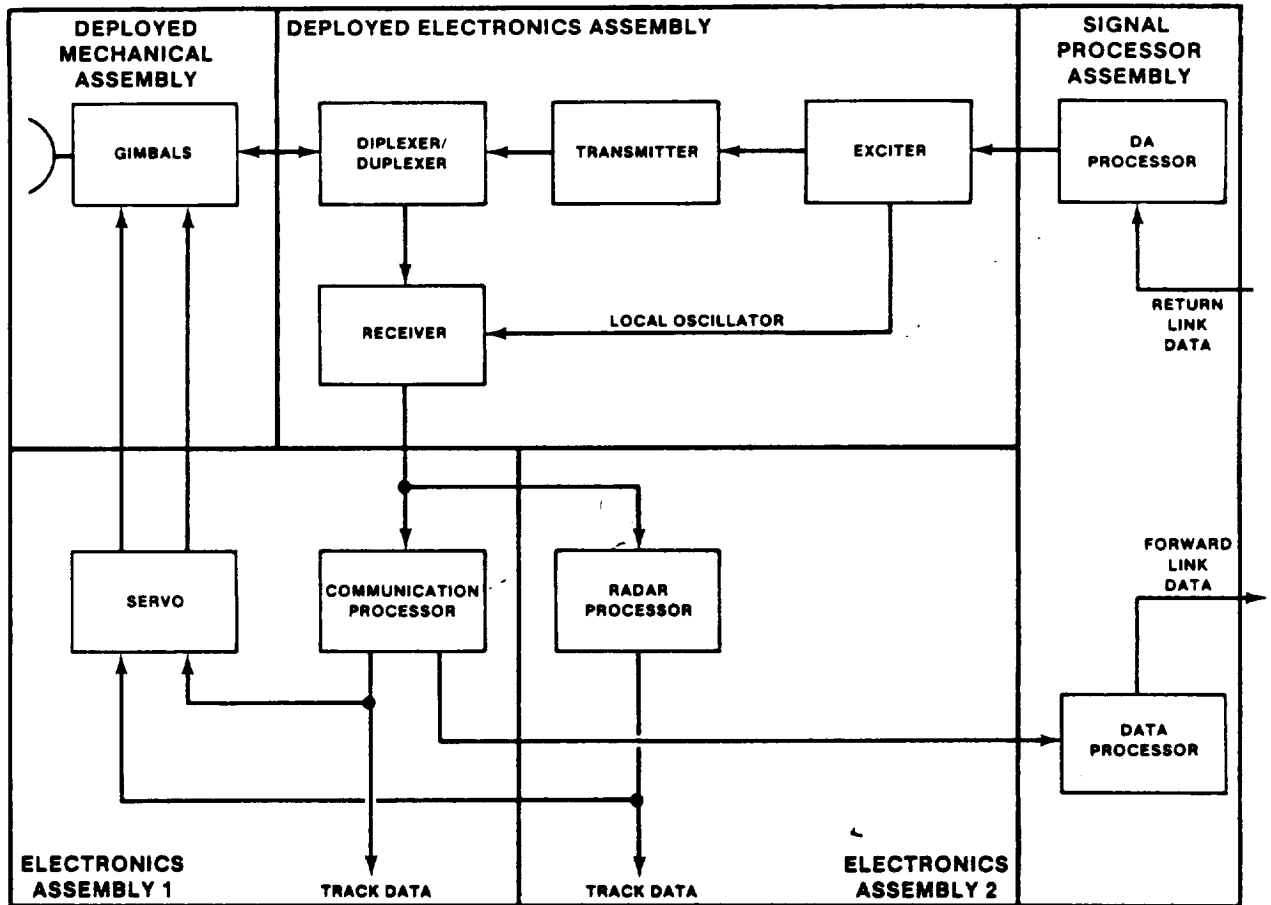


FIGURE 12.- K_u-BAND SYSTEM BLOCK DIAGRAM.

filter would remove virtually all of the narrowband 15.0034-gigahertz return link COMM signal but would pass a portion of the wideband RADAR "noise" and therefore degrade the forward link signal. It was considered that if the ferrite switches were removed or bypassed, the path for the "noise" would be eliminated and thereby the forward link degradation would be circumvented whenever the system is configured in the communications mode. (This modification was to provide a temporary quick-fix to enable the K_u-band system to meet communication system mission requirements; it disabled the high-power radar mode capability leaving the low-power capability which meets the initial radar mode mission requirements.)

Subsequently, the ESTL system was modified by the vendor (ferrite switches were removed). However, ESTL retest of the modified system revealed that only 1.6 decibels improvement was realized (i.e., degradation was reduced to 8.4 decibels at 48 Mbps). Further investigative testing identified the degradation to be caused by a diode signal sampler installed in the deployed assembly waveguide to provide indication of the transmit power level. Removal of this sampler and replacement with a "matched" load for testing purposes completely eliminated the degradation. Subsequent modification by the vendor to all flight units was made thus eliminating the problem.

PAYLOAD INTERFACE TESTING

Space Shuttle Orbiter missions will entail use of tandem communications links for mission operations. The payload links include the payload-to-Orbiter to GSTDN or AFSCF remote tracking station and payload/Orbiter/TDRS configurations. System certification testing is accomplished in the ESTL with particular emphasis placed on the Orbiter/payload RF interface. RF acquisition and data (command and telemetry) tests (table 3) are performed to provide an assessment of the Orbiter capability for a specific payload. The ESTL payload test capability is illustrated in figure 14. After completion of ESTL RF tests, and depending on new, unproven, or untested designs, joint Shuttle Avionics

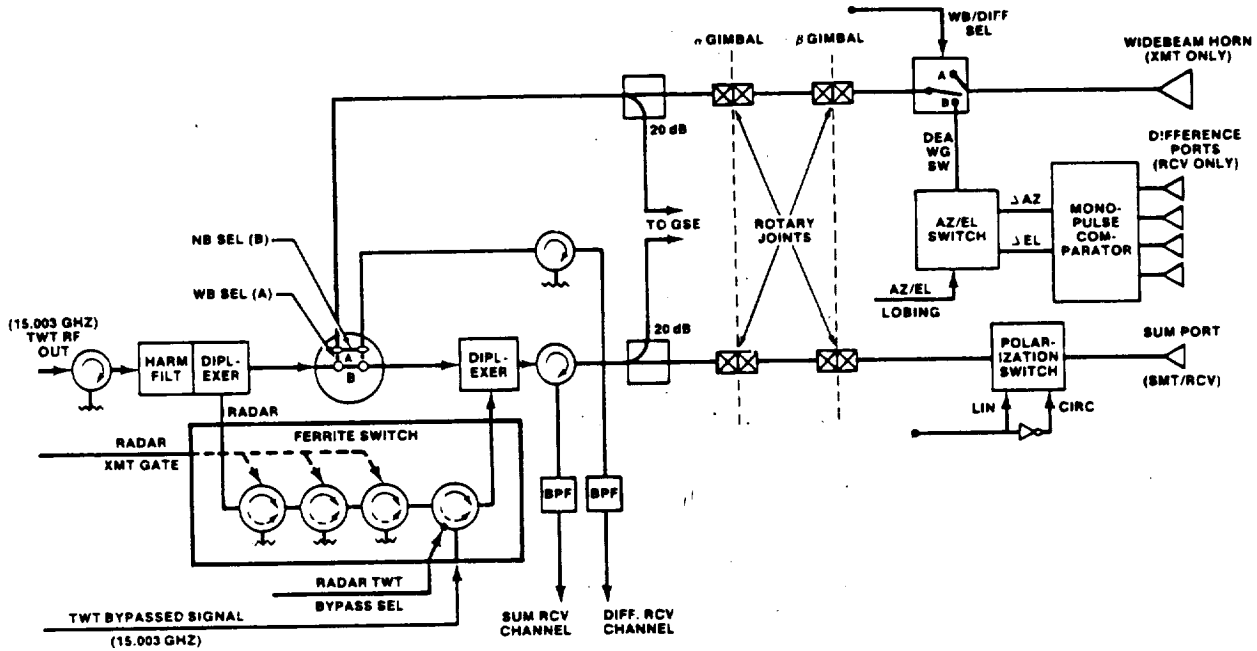


FIGURE 13.- K_U-BAND DEPLOYED ELECTRONICS ASSEMBLY FRONT-END DIAGRAM.

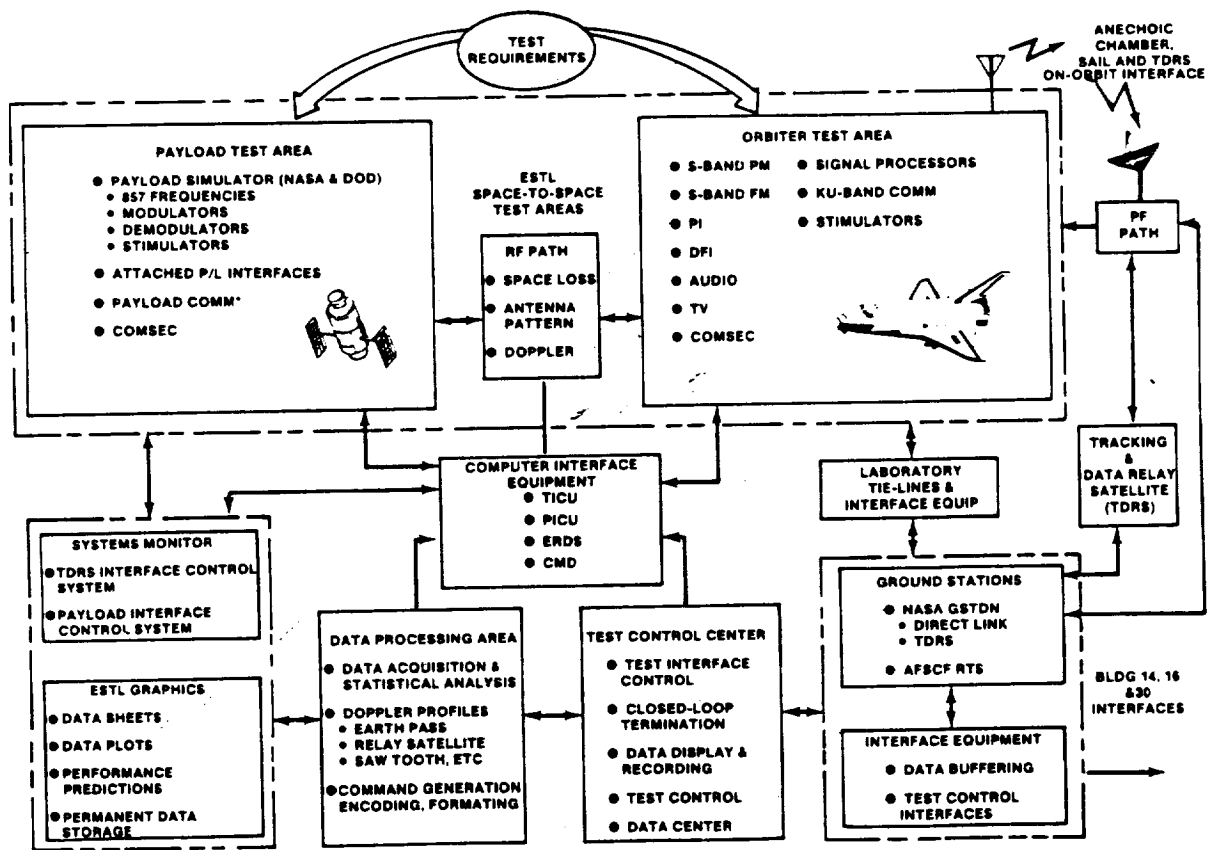


FIGURE 14.- ESTL PAYLOAD TEST CONFIGURATION.

Integration Laboratory (SAIL)/ ESTL tests are performed to provide an evaluation of the hardware/software and external RF interface capability. (Joint SAIL/ESTL tests are functional.)

To date, five payload RF communications configurations (including the Spacelab and DOD/Inertial Upper Stage) have completed the system certification test phase. Several problem areas and significant findings were identified as follows.

1. The Orbiter payload signal processor was susceptible to false-lock to telemetry data. Design changes were made and a retest verified the fix.
2. Payload transponders that did not incorporate anti-side-band lock features require the Orbiter to transmit an unmodulated carrier during RF acquisitions. This is an operational constraint that is particularly bothersome whenever a momentary loss of lock occurs such as during an antenna pattern null or blockage.
3. Test results show that some payload transponders when operating in the coherent mode (and no uplink) are susceptible to AUX OSC/VCO intermittent switching (causing Orbiter payload interrogator to lose lock) if the ranging channel is enabled.
4. There is a high probability of return link false lock on turned-around forward link data when ranging is enabled.
5. Sufficient Orbiter (onboard) crew displays of forward link status (AGC, static phase error, data good, etc.) are required to achieve and maintain good two-way acquisition. Additional information can be found in references 22 through 25.

ESTL OPERATIONAL SYSTEMS TEST

The third phase of ESTL testing involves operational configurations and/or concepts. Figure 15 depicts a series of end-to-end operations integration tests, performed in cooperation with GSFC, of the Integrated Space Shuttle Orbiter/Tracking and Data Relay Satellite (SSO/TDRSS) communication links utilizing SSO communications hardware, the operational TDRSS, with an on-orbit TDRS. These tests are to be accomplished after the Orbiter-TDRS basic certification testing has been completed in the ESTL and after Mission Control Center (MCC), Network Control Center (NCC), and MCC/NASA Ground Terminal (NGT) validation testing but before the first mission use of the TDRSS.

As depicted in figure 15, the SSO S-band and K_u -band communications subsystems will be located in the ESTL. The TDRSS Ground Terminal, located at White Sands, New Mexico, and the TDRS-A satellite, in geosynchronous orbit, constitute the first "satellite hop" configuration. The communications links are completed by the second "satellite hop" from White Sands to the JSC/MCC and GSFC/NCC by a Domestic Communications Satellite. This series of tests constitutes a final demonstration of the overall Shuttle/TDRSS operational readiness before first mission utilization. Primary test objectives include determination of RF acquisition tracking thresholds, demonstration of S-band two-way Doppler tracking capability for carrier-only and modulated-carrier conditions, determination of data, bit error rates for S-band and K_u -band as a function of total received power, and demonstration of the capability to accommodate the data channels (command, telemetry, and digital voice) of both the forward and return links. A description of tests can be found in reference 26.

SYSTEM TEST EFFECTIVENESS

During the Shuttle development phases, the ESTL results made significant impacts on hardware design parameters and specifications. As system hardware design progressed, system certification test results were utilized to avert serious program impacts. For example, as noted earlier, significant cost avoidance was accomplished by providing an understanding of the jitter characteristics affecting performance of the IOS DSIS link. Additionally, modification of the S-band transponder by reducing the TDM modulation index resolved unacceptable range accuracy and acquisition problems. The effectiveness of system performance and compatibility testing was well proven, both as a cost-effective system development tool and as a highly accurate system performance assessment method. The performance assessments achieved by these tests provide an engineering data base necessary to accomplish cost-effective mission anomaly resolutions, establish mission constraints, and/or evaluate proposed system updates/additions. At the conclusion of system certification tests for Shuttle, the performance capabilities of each communications link will be well documented, available link margins will have been measured, incompatibilities will have been identified, and alternate solutions developed to resolve the incompatibilities implemented.

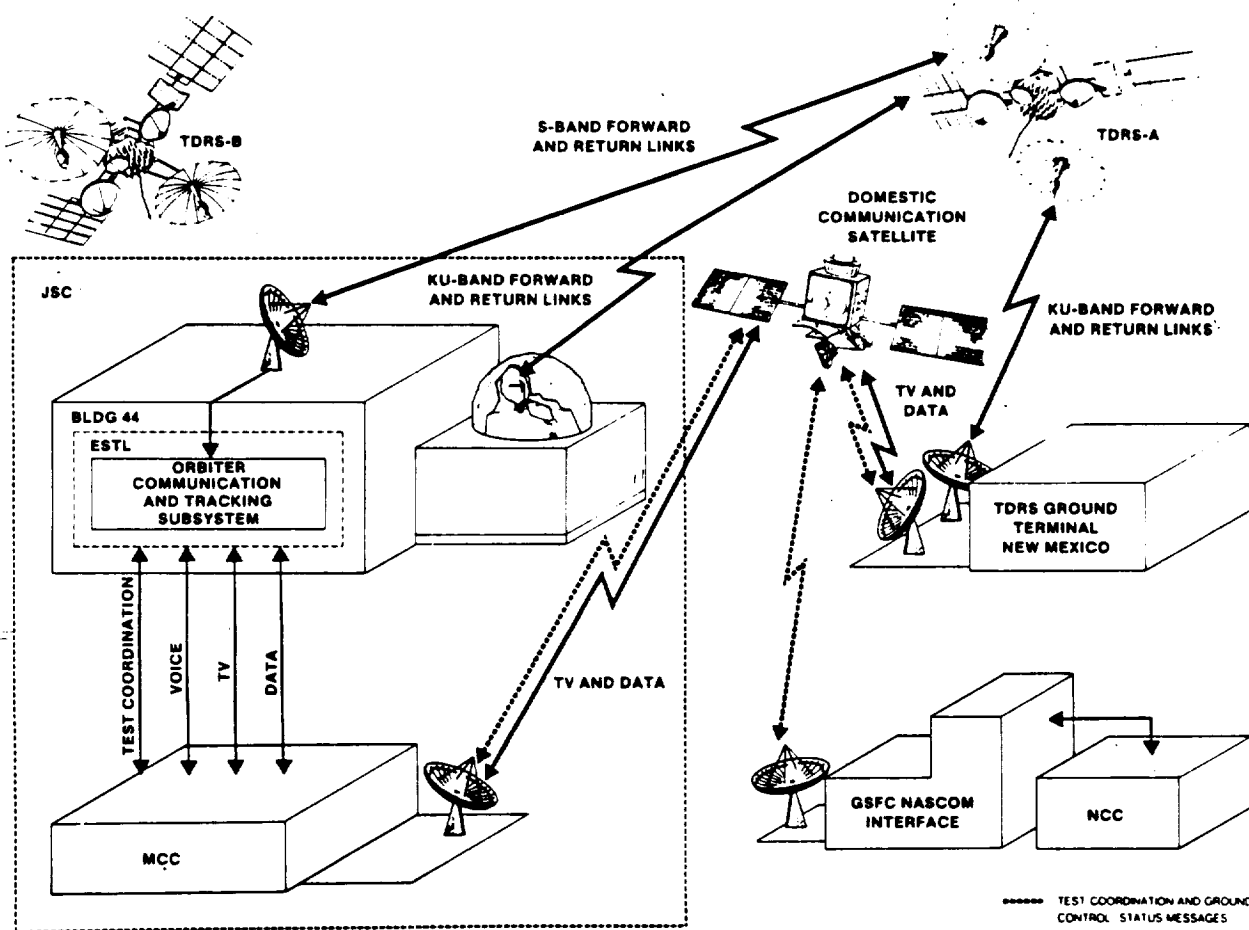


FIGURE 15.- TDRS INTERFACE TEST CONFIGURATION.

REFERENCES

1. Carrier, L. M.; and Pope, W. S.: An Overview of the Space Shuttle Communications and Tracking System. IEEE Transactions on Communications, Vol. COM-26, No. 11, Nov. 1978, pp. 1494-1506.
2. Bacinski, R.; and Helgeson, R.: Orbiter S-Band Communications Subsystem. IEEE Transactions on Communications, Vol. COM-26, No. 11, Nov. 1978, pp. 1521-1531.
3. Cager, R. H., Jr.; LaFlame, D. T.; and Parode, L. C.: Orbiter Ku-Band Integrated Radar and Communications Subsystems. IEEE Transactions on Communications, Vol. COM-26, No. 11, Nov. 1978, pp. 1604-1619.
4. Seyl, J. W.; and Travis, A. D.: Shuttle Communication Systems Compatibility and Performance Testing. IEEE Transactions on Communications, Vol. COM-26, No. 11, Nov. 1978, pp. 1732-1744.
5. Lindsey, W. C.; and Seyl, J. W.: Measurements of Phase Lock Loop Performance Using the Statistical Loop Analyzer. Globecom, Vol. C, Dec. 1982, pp. 670-675.
6. Wallingford, W. M.: ESTL Range and Doppler Simulation System. Rep. EE7-77-502A, LEC-10008A, Nov. 1978.
7. Bromley, L. K.: Realtime Data Analysis and Prediction System. Rep. EE7-79-803, Aug. 1979.
8. Hopkins, P. M.: Pseudorandom Noise for Telemetry Error Rate Measurement Applications, and Limitations. National Telecommunications Conference, Houston, Tex., Dec. 1972.

9. Simon, M. K.; Tu, K.; and Batson, B. H.: Effects of Data Asymmetry on Shuttle Ku-Band Communications Link Performance. IEEE Transaction on Communications, Vol. COM-26, No. 11, Nov. 1978, pp. 1639-1651.
10. Vanelli, J. C.: Effects of Bit Synchronizer DC Restoration on Performance Degradation Due to Data Asymmetry. Rep. EE7-77-311, LEC-10943, July 1977.
11. Novosad, S. W.; and Schmalz, M. D.: An Automatic (Hands-Off) RF Acquisition Technique for STS-1 S-Band PM Links. JSC-16981, 1980.
12. Young, C. E.: Intermodulation Generation Degradation Possibilities Resulting From the Use of RF Circuit Elements Containing Ferromagnetic Materials. Naval Research Laboratory, Alert No. Y1-A-75-01, Oct. 6, 1975.
13. Vermillion, B. K.: Orbiter/GSTDN PM Direct Link System Verification Test Report. JSC-16651, Aug. 1980.
14. Robinson, N. J.: ESTL System Verification Tests - Orbiter/GSTDN FM Channel Configuration. Rep. EE7-79-201, Feb. 1979.
15. Robinson, N. J.: System Verification Tests TDRSS/Orbiter/SSA Forward Link Configuration Test Report. Rep. EE7-80-201, May 1980.
16. Schmalz, M. D.: Orbiter/GSTDN Closed Circuit TV (CCTV) System Verification Test Report. JSC-16432, Apr. 1980.
17. Hamilton, M. W.: Orbiter - EVA/GSTDN UHF Link System Verification Test Report. JSC-16549, Apr. 1980.
18. Vermillion, B. K.: Orbiter/AFSCF S-Band Direct Link System Verification Test Report. JSC-16630, May 1980.
19. Bromley, L. K.: TDRS/Orbiter SSA (S-Band Single Access) Forward Link RF Acquisition Test Report. JSC-16963, Oct. 1980.
20. Robinson, N. J.: Orbiter/TDRSS S-Band Return Link TDM System Performance Test Report. JSC-18302, May 1982.
21. Bromley, L. K.: TDRS/Orbiter SSA (S-Band Single Access) Return and Two-Way RF Acquisition Test Report. JSC-18723, Dec. 1982.
22. Vermillion, B. K.: Orbiter/Shuttle Pallet Satellite-01 (SPAS-01) Transponder Verification Test Report. JSC-18647, Oct. 1982.
23. Robinson, N. J.: TDRS User's NASA Standard Transponder Test Report. JSC-18676, Nov. 1982.
24. Vermillion, B. K.: Orbiter/Inertial Upper Stage (IUS) System Verification Test Report. JSC-18700, Nov. 1982.
25. Batson, B. H.; Teasdale, W. E.; Pawlowski, J. F.; and Schmidt, O. L.: Shuttle Payload S-Band Communications System. Space Shuttle Program Technical Conference, NASA Johnson Space Center, Houston, Tex., June 28-30, 1983.
26. Orbiter/TDRS/MCC Communications Performance Verification Test Plan. JSC-17623, June 1982.

D22
N85-16959

ORBITER WHEEL AND TIRE CERTIFICATION

Carlisle C. Campbell, Jr.
NASA Lyndon B. Johnson Space Center
Houston, Texas

ABSTRACT

The Orbiter wheel and tire development has required a unique series of certification tests to demonstrate the ability of the hardware to meet severe performance requirements. Early tests of the main landing gear wheel using conventional slow-roll testing resulted in hardware failures. This resulted in a need to conduct high-velocity tests with crosswind effects for assurance that the hardware was safe for a limited number of flights. Currently, this approach and the conventional slow-roll and static tests are used to certify the wheel/tire assembly for operational use.

INTRODUCTION

The Space Shuttle Orbiter wheel and tire designs combined conventional aircraft materials into one of the most highly optimized assemblies yet developed. This is not obvious until the performance limits are compared to similarly sized equipment on commercial aircraft, which will reveal that the Orbiter's wheel/tire load capability is nearly twice as high.

To confirm that these wheels and tires were capable of meeting Space Shuttle requirements, an unusually stringent and highly realistic test and analysis program was developed to demonstrate the required capability as well as the performance margins available beyond the requirements. As more stringent requirements have arisen, the hardware has been proven acceptable in most cases without design changes.

GENERAL DESCRIPTION OF HARDWARE AND CERTIFICATION

The Orbiter main tire characteristics are as follows: 44.5-inch diameter, 16-inch width, 21-inch bead seat diameter, 34-ply rated, 200-pound weight, and 315-psi inflation pressure. The tire is of bias ply construction using conventional materials such as nylon, natural rubber, and steel bead wire (fig. 1). The tire's unique construction, developed by B. F. Goodrich, Akron, Ohio, has provided the desired very high load capability at a minimum weight. Consequently, reuses are limited when compared to military or commercial tires.

The main wheel is a split, forged aluminum alloy design with a steel hub pressed into the in-board half. The bearings have conventional tapered rollers but their uniquely high preload requirement provides a drastic increase in landing load capability at the sacrifice of reuse life.

The nose tire characteristics are 32-inch diameter, 8.8-inch width, 18-inch bead seat diameter, 20-ply rated, 50-pound weight, and 300-psi inflation pressure. The nose tire is also of bias ply construction and made of conventional materials.

The nose wheel is a split, forged aluminum alloy design but its bearings are located on a rotating or "live" axle rather than in the hub such as in the main wheel design. Both nose wheels are splined to the "live" nose axle providing a corotating feature which improves stability or reduces the tendency to shimmy.

Most of the vendor's qualification tests of the nose wheel and tire were similar to those of the main wheel and tire, the exception being that the main wheel and tire received additional off-limits tests because of a wider variety of performance requirements. In many cases, the main tire only was tested and its performance was extrapolated for nose tire use. Rather than repeat the many similar tests of the nose tire, the remaining material in this text will address the main tire only.

Nearly all wheel tests require the use of a flight-type tire to provide realistic wheel load paths and pressure seals. Tires are frequently tested on a high-strength (but heavy) laboratory wheel for safety and cost reasons. The most significant tests given the wheel/tire assembly are those that are most nearly representative of an abort landing load case. In such a test, the assembly is subjected to changing velocities, radial loads, and rollout yaw angles which duplicate those that can occur on an actual landing except that the tire rolls on a 10-foot diameter dynamometer "road wheel." This provides a cylindrical rolling surface, which is also smoother than a paved runway. The curved rolling surface is considered to provide an even more conservative or harsh test due to the increased stresses from the additional bending required as the tire tread conforms to the

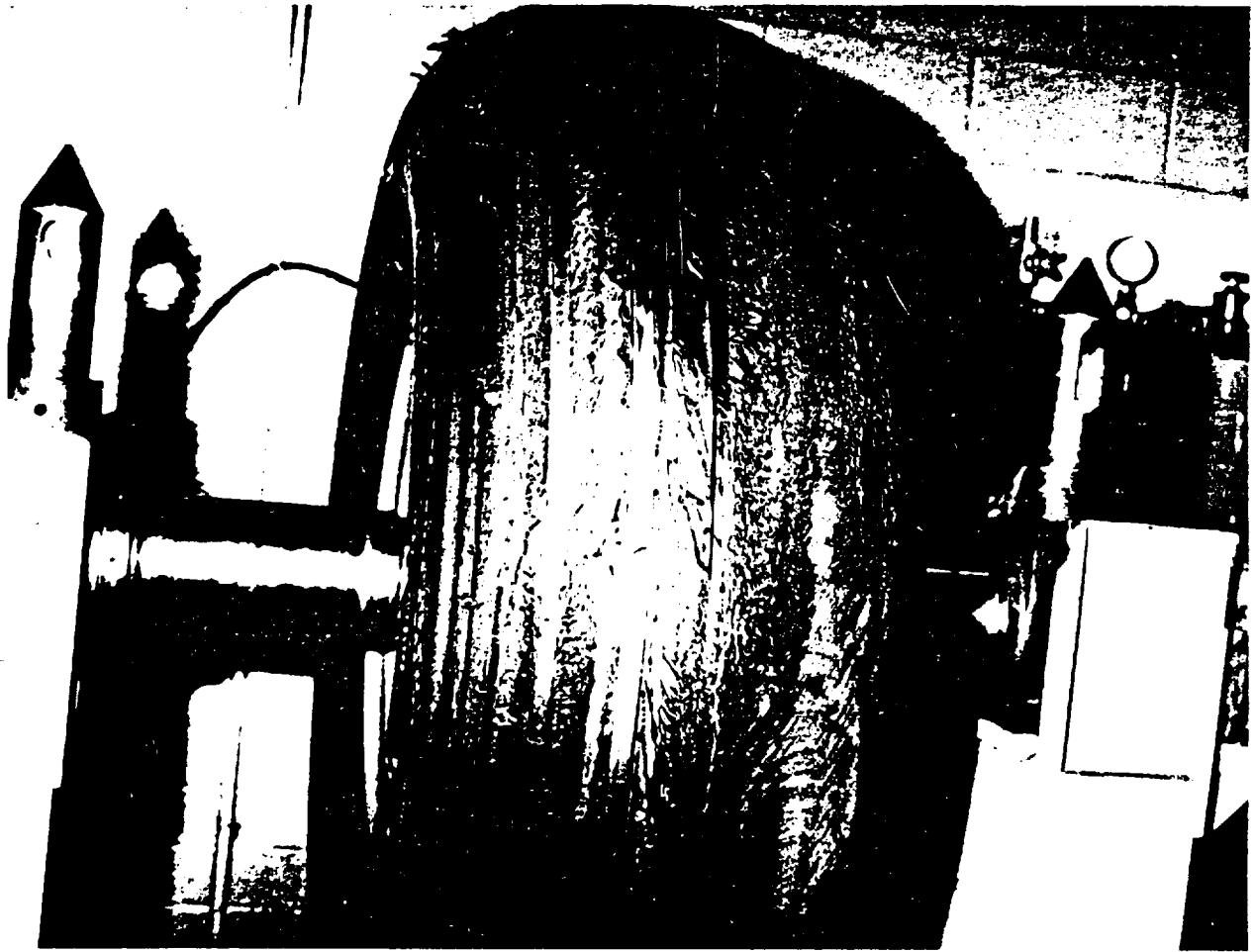


FIGURE 1.- MAIN WHEEL/TIRE ASSEMBLY AFTER CROSSWIND CERTIFICATION TESTS.

dynamometer surface. The tire inflation pressure must also be increased for a dynamometer test to maintain the same peak tire sidewall deflection at the center of the tire footprint when located against the dynamometer.

In addition to these dynamic landing load tests, the wheels and tires were also subjected to many other certification tests, such as burst pressure, slow-roll fatigue, leakage, thermal cycling, and static ultimate strength.

Other off-limits and engineering tests required are high velocity, extra heavy abort weight, lifetime fatigue, low pressure, thermal vacuum, sideload, and high crosswind.

It is interesting to note that commercial and military aircraft wheels are not subjected to dynamic landing load tests - only to slow-roll fatigue plus other static tests. The Orbiter could not be subjected to multiple high-speed taxi tests and numerous landings such as is practiced in conventional aircraft test programs. Therefore, the dynamic landing load tests plus the integrated system stability tests became necessary to demonstrate operational capability. In fact, the dynamic landing load tests have been used twice to certify the main wheel/tire assemblies for a limited number of orbital flights due to development problems uncovered in the wheel slow-roll fatigue life tests. Overall, wheel and tire certification requirements over the past several years have changed and increased into a more extensive program than the original concept.

HARDWARE DEVELOPMENT HISTORY RESULTING IN CERTIFICATION CHANGES

The wheel/tire design, as initially developed, was used during the five Approach and Landing Test (ALT) flights. It was lighter and had less load capability than the wheels and tires used for orbital flights. Even though the ALT vehicle weight was 66 percent of the original Orbiter abort weight, the requirements became more severe when the abort weight was then increased from 227 000 to 240 000 pounds. Testing attempts to pass these increased conditions resulted in hardware failure. Not only was the tire failing tests but the wheel was experiencing bearing problems. With this bearing problem realization, it was obvious that more realistic dynamic landing load conditions must be conducted which would include crosswind effects. This prompted the decision to conduct such tests at the Wright Patterson Air Force Base (WPAFB) Facility where the testing would include crosswinds and the testing was automated for a faster and more convenient test setup.

Subsequent test failures at WPAFB, which included crosswinds, graphically revealed the inability of the tires and wheel bearings to survive flight requirements. In addition, the wheel was subject to cracking during the slow-roll fatigue tests resulting in redesign of both pieces of hardware several times before arriving at the combination in use today.

The main tire has been modified from a 28-ply-rated, 260-psi inflation pressure model to a 34-ply-rated, 315-psi version. The wheel design has had its inboard bearings moved off the wheel centerline to a more inboard location and housed in a steel hub to achieve more evenly distributed bearing loads. A dual O-ring seal system between the two wheel halves was used during the first orbital flight because of its improved leakage characteristics, but this design feature caused additional cracks during fatigue tests so the design reverted back to the single O-ring approach. Finally, the forging thickness was increased in several areas to provide protection against fatigue cracks. This latest wheel design will start certification slow-roll fatigue tests this year.

TEST FACILITIES

The wheel and tire manufacturers both use conventional dynamic and static test equipment suitable for commercial and military requirements. However, the maximum load capacities cannot meet the Shuttle requirements, and their ability to set up and repeat dynamic tests is relatively slow. Changing a dynamometer test condition is tedious, since it requires construction of a new load profile template.

In contrast, the WPAFB test facility is automated and test conditions are easily varied. After a wheel/tire assembly is mounted on a test axle, it is not touched by hand as it is translated from a cooling cage to the dynamometer where it is clamped to a yoke. Then it can be hydraulically stroked into the motor-driven road wheel to provide the loads and velocities required. If loads, velocities, or yaw angles must be varied, these can be typed into the computer in a matter of minutes and the command system is ready before the tire can cool down for a subsequent test. All landing load data are recorded on stripcharts as well as on tape.

The WPAFB dynamometer used in Orbiter dynamic landing load tests has greater and more diversified capabilities than any other similar facility in the free world. It not only can provide high radial loads, it can also achieve high velocities, crosswind, and camber effects. Specific dynamic capabilities include radial load: 0 to 150 000 pounds in 0.1 second; velocity: 0 to 300 knots; acceleration: 0 to 24 ft/sec²; yaw angles: $\pm 20^\circ$; and camber angles: $\pm 20^\circ$.

The use of the WPAFB test facility has resulted in a better understanding of overall performance capability of the main wheels and tires than other types of aircraft that have flown. Since the effects of crosswind on wheels and tires during landing cannot presently be adequately analyzed, a realistic test is currently the safest approach.

Of the major achievements in the wheel and tire development programs, the most significant should include (1) development of the STS-2 34 ply-rated operational "K" model tire, (2) the main wheel bearing high preload concept, and (3) the use of the WPAFB test facility to test for crosswind effects.

DETAILED LISTING OF CERTIFICATION TESTS

B. F. Goodrich wheel certification tests	Table 1
JSC/Rockwell dynamic wheel/tire tests	Table 2
Typical load/time profile	Figure 2
B. F. Goodrich tire certification tests	Table 3
JSC/Rockwell off-limits tests	Table 4
High velocity	
Heavy weight	
Low pressure	
High crosswind	
Engineering tests	Table 5
Thermal vacuum	
Cornering force	
Flat tire (nose tire only)	
Tire leakage	
Integrated systems tests	Table 6
Bendix main gear dynamic stability	
Bendix nose gear dynamic stability	
Bendix main gear braking	
Langley Research Center (LaRC) nose gear stability tests	

TABLE 1.- B. F. GOODRICH MAIN WHEEL CERTIFICATION TESTS

Test	Wheel identification and test sequence								Test location
	A	B	C	D	E	F	G	H	
Acceptance	1	1	1	1	1	1	1	1	BFG
Combined static loads									
Inboard yield cond. I	2								BFG
Outboard yield cond. I	3								BFG
Inboard ultimate cond. I	4								BFG
Inboard yield cond. II		2							BFG
Outboard yield cond. II		3							BFG
Outboard ultimate cond. II		4							BFG
Burst pressure			2						BFG
Static pressure				2					BFG
Diffusion				3					BFG
Dynamic pressure				4					BFG
1000-mile roll test				5					WPAFB
Dynamic load profiles				6					WPAFB
STS-1 load profiles (INBD)					2				WPAFB
STS-1 load profiles (OUTBD)					3				WPAFB
Thermal relief plug					4				BFG
STS-2, STS-3, and STS-4 load profiles						2			WPAFB
Environmental tests							2		BFG
Structural torque							3		BFG
Dynamic brake test								2	BFG

TABLE 2.- JSC/ROCKWELL DYNAMIC WHEEL/TIRE TESTS
(APPLIED AFTER WHEEL COMPLETES 1000-MILE CERTIFICATION TESTS)

Landing weight, lb	Touchdown velocity, knots	Crosswind velocity, knots	Landing technique	No. of tests
207 000	212	0	Delay pitchover	2
207 000	212	10	Quick pitchover	3
240 000	225	20	Quick pitchover	1

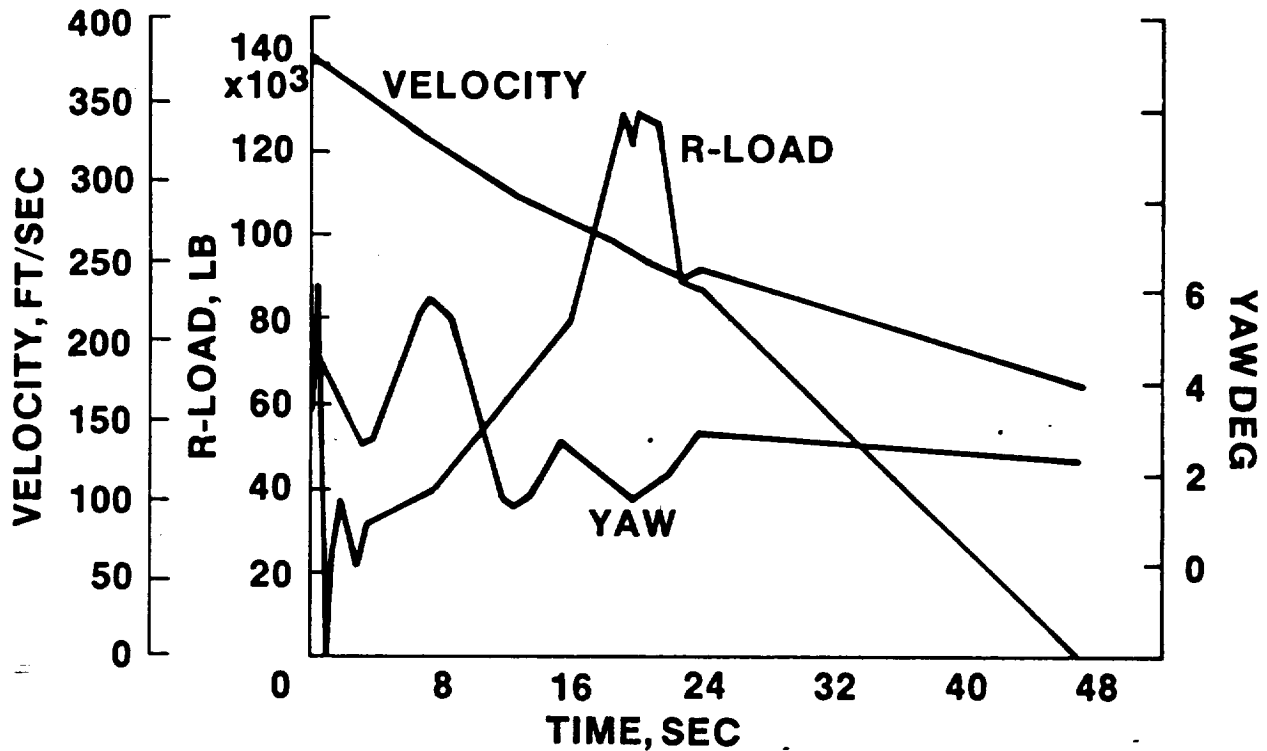


FIGURE 2.- TYPICAL LOAD/TIME PROFILE: 240 000-POUND VEHICLE WEIGHT, DELAYED PITCHOVER, 20-KNOT CROSSWIND.

TABLE 3.- B. F. GOODRICH MAIN TIRE CERTIFICATION TESTS

Test	Tire identification and test sequence				Test location
	A	B	C	D	
Acceptance	1	1	1	1	BFG
Deflection	2				BFG
Burst		2			BFG
Dynamic load profiles ^a					
Delayed nose pitchover			2		WPAFB
Quick nose pitchover				2	WPAFB

^aDynamic load profile tests include 6 landings and 6 taxi tests per tire of which: 1 landing is a tire chilled to -35° F, 1 landing is a tire preheated to $+135^{\circ}$ F, 5 landings represent a 207 000-pound landing weight, 1 landing represents a 240 000-pound landing weight and crosswinds, and range from 0 to 20 knots.

TABLE 4.- JSC/ROCKWELL OFF-LIMITS TESTS

	Landing weight, lb	Touchdown velocity, knots	Crosswind velocity, knots	Pressure, psi	No. of tests	Tire ID
High velocity	212 000	245	0 to 10	315	5	A
	212 000	255	0	315	2	B
	240 000	255	0 to 10	315	2	B
Heavy weight	245 000	240	15 to 0	315	4	C
	251 000	240	15 to 0	315	4	D
Low pressure	240 000	225	10	256	1	E
	212 000	215	10	256	2	E
Tire life	212 000	215	0 to 10	315	24	F
	212 000	215	10	315	9	G
	240 000	225	20	315	3	G
	212 000	215	10	315	6	H
	240 000	225	20	315	1-1/2	H
High crosswinds ^a						

^aTo be conducted.

TABLE 5.- ENGINEERING TESTS

Thermal vacuum

1. 7 days in vacuum at 1×10^{-5} and at +15° F.
2. Subsequently subjected to 4 dynamic landing load profiles representative of a 207 000-lb landing weight, in 0- to 20-knot crosswinds and using quick nose pitchover technique.

Cornering force

- Yaw angles: ±4°
- Velocity: 100 to 200 knots
- Radial load: 80 000 to 100 000 lb
- Tire pressure: 315 psi

Flat tire during rollout tests - nose tire only

Abrupt load increased at 12, 20, and 30 seconds into roll

Tire pressure leakage studies

- Temperature: ambient to -65° F
- Time: 7 to 197 days

TABLE 6.- INTEGRATED SYSTEMS TESTS

Bendix main gear dynamic stability tests

275 dynamometer runs including mass impact on tire
Velocity range: 4 to 217 knots
"Nose up" and "nose down" tests: -4° to $+19^{\circ}$
Tire pressures: 205 to 280 psi
Tire unbalance: 100 to 300 in-oz.
Strut vertical loads: 23 000 to 120 000 lb
Strut compression: 2 to 14 in.

Bendix nose gear dynamic stability tests

272 dynamometer runs including mass impact on tire
Velocity range: 29 to 204 knots
Tire pressures: 237 to 325 psi
"Nose up" and "nose down" tests: -4° to $+4^{\circ}$
Strut vertical load: 9000 to 60 000 lb
Strut compression: 3 to 20 in.
Nose wheel steering: on and off
Tire unbalance: 25 to 75 in-oz.

Bendix main gear braking/antiskid stability tests

18 braking tests include the following ranges
Energy: 3.2 to 34.7×10^6 ft-lb (36.5×10^6 ft-lb is reuse limit)
Velocity: 50 to 147 knots
Tires: one and two wet, one flat, all dry
Brake pressure: 0 to 1500 psi (maximum)
Antiskid: on and off
Strut vertical load: 40 000 to 114 000 lb

Langley Research Center nose gear dynamic stability tests on flat track test facility

65 runs including mass impact on tire
Velocity: 40 to 104 knots
Vertical load: 15 000 and 30 000 lb
Tire pressure: 0, 150, and 300 psi
Sink speed: 0.5 to 3 ft/sec
Runway conditions: dry, damp, wet, and sand covered
Nose wheel steering: on and off

SUMMARY

The Orbiter wheel and tire designs have been successfully subjected to an extensive and rigorous certification program to demonstrate all flight capability requirements. The approach of using a Government test agency (WPAFB) in conjunction with the manufacturer's test capability has proven to be cost and schedule effective. The unique dynamic landing loads testing imposed on Orbiter hardware has resulted in interest by other government agencies of the potential for application of similar testing on conventional aircraft.

The certification program appears to have demonstrated the full range of the hardware capability and has provided confidence that it is safe for flight under the conditions expected.

THE SPACE SHUTTLE PROGRAM
FROM CHALLENGE TO ACHIEVEMENT
SPACE EXPLORATION
ROLLING ON TIRES

G. L. Felder
Aircraft Tire R&D
BFGoodrich Co.
Akron, Ohio

ABSTRACT

The Space Shuttle Transportation System is the first space program to employ the pneumatic tire as a part of space exploration. For tires (Aircraft type), this program establishes new expectations as to what constitutes acceptable performance within a set of tough environmental and operational conditions. Tire design, stresses the usual low weight, high load, high speed, and excellent air retention features but at extremes well outside industry standards. Tires will continue to be an integral part of the Shuttle's landing phase in the immediate future since they afford a unique combination of directional control, braking traction, flotation and shock absorption not available by other systems.

INTRODUCTION

Unlike any preceding U.S. space venture, the decision to develop a reusable space exploration system; namely, the Shuttle system, carried with it needs and functions never before required by space travel. The particular need I'm referring to, is vehicle recovery by land rather than by sea; the particular function, and the focus of this talk, the use of landing gear tires. Recovery by land spelled out a set of requirements that could not be met more efficiently, within state-of-the-art technology, than by the use of a pneumatic tire system. These requirements include, in particular, braking traction, shock absorption, damping, directional control, and flotation characteristics.

The discussion to follow will include the tire design background, a description of key performance requirements which form the challenge, and the tire design which satisfied these punishing conditions. Both the nose landing gear tires and the main landing gear tires were developed and supplied by BFGoodrich. My comments will primarily focus on the main landing gear tire since it presented the greatest challenge and resulted in an unusual design.

TIRE DESIGN BACKGROUND

First some background information on the tire design's evolution.

Even before the Shuttle's first Orbital flight, BFGoodrich had developed three (3) successive generations of main landing gear tires, each in response to changing performance requirements and an ever growing vehicle weight. This total effort encompassed an eight (8) year time span starting in 1972. One basic objective of the tire development program was to avoid new exotic materials for which no track record existed. On this basis, nose and main gear tires were innovatively constructed from industry materials.

The first generation main landing gear tire, known as the baseline tire, was used exclusively on the Enterprise, the first Shuttle produced. At that time the vehicle's estimated maximum gross weight was at 88,906 Kgs. (196,000 lbs.); as it turns out, that would be the lightest weight vehicle compared to later models. The dynamic test requirement for qualification of the tire was based on only straight ahead landing rolls at the 88,906 Kg. (196,000 lbs.) vehicle weight. Within the spatial limits of the Orbiter wheel well and tire design optimization, a bias tire with a 28 PR designation was selected in a 1.13 M (44.5 in.) diameter, .41 M (16.0 in.) section width, fitted to a wheel with a .53 M (21.0 in.) diameter and a 15° bead seat taper.

During the preorbital approach and landing tests, Rockwell Engineers had instrumented the landing gear to measure forces upon landing. From these readings, a new set of test requirements evolved, and subsequently, a new tire meeting them. The new test parameters reflected a more accurate set of vehicle reaction loads, coupled with a higher vehicle weight, now 108,864 Kgs. (240,000 lbs.) maximum. The new dynamic test requirements included an oscillating yaw condition to simulate the effect of crosswind. To match these conditions, the 2nd generation tire was designed and stepped up to a 34 ply rating, while remaining the same size. (Ply rating, by the way, is an index of relative tire strength.)

There were difficulties in meeting the requirements for the heavier vehicle and the design work for the 2nd generation tire was pushed to the first flight, tire delivery cutoff date. At that point, the 2nd generation tire was reliably capable of test loads equal to the maximum weight of the first flight vehicle; namely, 93,895 Kgs. (207,000 lbs.). This design, the 2nd generation tire, was certified as a first flight tire only and performed superbly during the April, 1981, flight of the Columbia.

Before the Columbia had been launched, a 3rd generation tire was well on its way to final certification. This tire, as proven in development tests, would pass the test requirements for a 188,864 Kg. (240,000 lbs.) vehicle as well as the severe crosswind yaw condition. This tire is also 34 ply rated but of a slightly different internal design. It is this main landing gear tire that will be the focus of my comments; it is this tire that is currently in use on the Challenger and Columbia.

The nose landing gear tire complementing the main tire carries a smaller portion of the vehicle load and as such is smaller in size: .80M (31.5 in.) diameter, .24M (9.30 in.) section width, on a rim .41M (16.0 in.) diameter. This tire is designated 32x8.8/20 PR. Suspended on a castored gear, many of the changing side load and vertical load conditions experienced by the main landing gear, while the Shuttle's weight was growing, did not affect the nose gear, therefore only one generation of nose gear tire was developed.

THE CHALLENGE - KEY TIRE PERFORMANCE NEEDS

The Shuttle's landing configuration required a unique combination of shock absorption, damping, and flotation capability under a variety of environmental and load conditions; something only the pneumatic tire could provide. These performance requirements breakdown into a set of test requirements familiar to the aviation world.

TEMPERATURE & AIR RETENTION

First let's examine the temperature and air retention requirements. The Shuttle tire must be capable of withstanding soak temperatures in space that cycle as low as -51°C (-60°F) and as high as +93°C (+200°F). These extremes are controlled by exposure of the Shuttle's surfaces in and out of the Sun.

In the landing phase, the tire is required to perform dynamically to soak temperatures ranging from -37°C (-35°F) to +55°C (+131°F). Initial flight data has shown the lower half of this temperature range to be more significant.

Throughout these soaks, air retention must be kept at a maximum. After temperature, time is the toughest parameter in retaining pressure. As it turns out, from the time the Shuttle is mated to the main fuel tank in preparation for launch to the point of touchdown, the tire inflation pressure cannot be serviced, only monitored. This time span can vary from a few weeks to several months.

WEIGHT

As with any project of this type, the lowest possible tire weight is foremost, tempered by the design's ability to do the job. Each MLG tire for the Shuttle weighs in at approximately (89 Kgs.) 196 lbs. Some control over this weight was predetermined when the tire size selection was made. It would take a 1.32 meter (52.0 in.) diameter tire, such as is found on a Lockheed Tristar L-1011, of the same PR in a commercial aircraft tire size to carry approximately the same load as the Shuttle's 1.13 meter (44.5 in.) diameter tire. The consequence of selecting such an undersized tire for weight and size is overloading.

LOAD

In tests, the actual tire dynamic loading for a single tire reaches more than twice its rated load, or about 58,968 Kgs. (130,000 lbs.), to give a peak operating deflection of 66%, as compared to a conventional commercial aircraft tire at a maximum operating deflection of 35%. This loading comparison is made outside the instantaneous spike loading any aircraft tire could experience upon landing.

SPEED - YAW

Landing touchdown speeds range from 394 Km/h to 422 Km/h (245 to 262 MPH). A B-727, or Lockheed Tristar by comparison, would land at speed from 225 Km/h to 257 Km/h (140 - 160 MPH); about 161 Km/h (100 MPH) slower than the Shuttle.

The yaw test parameter attempts to simulate the Shuttle's crabbed final approach condition under crosswinds, a condition not fully corrected at touchdown. The Shuttle tire must be capable of withstanding the lateral forces generated at 3.0 - 5.4° yaw under high loads and high speeds. This test requirement, single-handedly, has doubled the difficulty of meeting the Shuttle's performance requirements.

In order to ensure that a tire will operate to a given performance level under a variety of temperature, load, speed, and yaw conditions, two separate conditions are tested on an indoor roadwheel dynamometer. The two landing test conditions are based on two possible landing configurations; the first designated "Quick Pitchover", the second designated "Delayed Pitchover". The term "Pitchover" refers to the lowering of the Shuttle's nose after touchdown.

In the delayed case, the nose is held up for a period of time (approximately 10 seconds) and then lowered. In the quick case, the nose is lowered immediately after touchdown. Each landing profile produces a different reaction loading at the main gear.

To create for you an appreciation of some of the dynamic test conditions (deflection, yawing, impact velocity), I have a brief film clip of a Shuttle main landing gear tire, testing under the conditions of a delayed pitchover landing. This film was taken at Wright-Patterson AFB, compliments of NASA. There are four test cycles in this clip each identified by maximum gross vehicle weight, crosswind velocity, and touchdown velocity. All four tests are conducted on the same tire.

THE TIRE DESIGN

To meet all of these requirements, the tire design had to be geared for high reliability under long term static conditions and short term punishing dynamic conditions. The key features of the design can be described in five categories.

MOLD SHAPE

The Shuttle main landing gear tire is molded to a shape which is described in the industry as semicantilevered. The term simply defines the shape of the mid and lower sidewall by specifying the relationship of the wheel flange spacing to the average inflated section width. For a semicantilevered tire, this ratio is in a range from 60% to 70%. This mold shape has been found to be favorable to high deflection capability since the tire can be molded closer to the inflated/deflected shape.

LINER

The Shuttle MLG tire has a heavy innerliner to maximize air retention. The key design variables to achieving a minimum pressure decay rate over an extended period of time are material gauge and compound. Balancing weight against air retention capacity, and compound against operating temperature, a 100 ga. liner compound was adopted for the Shuttle main with an effective air retention rate 1.6 times better than conventional military aircraft tire materials.

Still state-of-the-art technology could not provide a virtually non-diffusing liner material. To compensate for this, a leak rate history is established for the tire/wheel assembly. Overinflation is then based on the total anticipated pad checkout and flight time, and the assembly leak rate. The average long term static decay rate for main landing gear assemblies has been 1.38 Kilopascals/day (.20 PSI/day) on a base of 2172 Kilopascals (315 PSIG), for less than one-tenth of one percent per day. In a system that has no reinflate or service capability, the normal daily loss of 2-3% in the aviation industry would be totally unacceptable.

TREAD

At 2.54mm (.10 in.) skid depth, only a very thin skin of tread compound covers the outer carcass ply. High load and speed requirements limit the tire to a maximum of 6 landings. This results in a shallow skid design and a design that lacks groove definition across the tread (groove to rib ratio of 1:2.5). A very cool running compound is used in the tread, still, the phenomenon of surface blistering and reversion occur while testing on the dynamometer under extreme load and speed as demonstrated in the film.

CARCASS

The weight savings realized from the shallow tread allowed added strength to be designed back into the carcass design. The carcass design features a contoured cross section, very beefy in the lower sidewall and relatively thin in the upper sidewall. The exaggerated contouring controls the high flex point during radial loading but more importantly during lateral loading. The internal content of the tire was driven by the performance need (mindful of weight) and the ultimate manufacturing boundaries. A standard nylon carcass was selected but with a larger, stronger cord (12% stronger than conventionally used) to minimize the total number of plies. The insulating compound surrounding the cord, is non-uniformly distributed based on the needs of the critical stress points in the shoulder and lower sidewall. By minimizing insulation, the primary bias tire heat generator is reduced. But a tradeoff occurs, in that less rubber insulating material is available to distribute shear forces. The net result is a specialized bias tire matrix that performs in a satisfactory temperature range with good short term durability.

BEAD

The Shuttle tire bead base is of a more conventional design, however, it is large, to complement the contouring of the lower sidewall.

If you study the tire's total content in terms of three basic components--beadwire, fabric, and compound--and compare these to a conventional heavy duty commercial airline tire, the Shuttle tire contains 11% less insulating material but 6% more fabric.

CONCLUSION

The Shuttle tire program has been a story of innovative design within the boundaries of known materials. It has been an extensive and successful effort to balance material capability with performance requirements which fall well outside industry standards.

This tire design technology has been reapplied to other aircraft products but only to a very limited extent. More realistically, this technology has led to further investigation of materials and structures in an effort to minimize the less desirable tradeoffs of short operating intervals and short operating life; two tire characteristics not marketable in the aviation industry. Even with its life limitations, the pneumatic tire still provides that unique combination of directional control, shock absorption, flotation, and traction unlike any other system.

SPACE SHUTTLE ELEVON SEAL PANEL MECHANISM

John G. Ripley

Rockwell International

Downey, California

ABSTRACT

The orbiter elevon seal panel mechanism controls the position of fairing panels between the orbiter wing and elevon. Early mechanism designs used linkages which approximately matched the panel motion to elevon position, depending on panel deflections to maintain sealing. These linkages were refined during orbiter development to match panel motion to elevon motion more exactly, thus reducing panel deflections, loads, and weight. Changes to the adjacent cove seal resulted in the use of curved tension-compression links. Mechanism temperatures up to 750F (locally) posed difficulties in bearing lubrication. Despite the adverse effect of the many fabrication tolerances, the system has successfully prevented the entry of 1200F hot gases into the wing/elevon joint.

INTRODUCTION

Development of a space vehicle capable of both aerodynamic flight and entry into the atmosphere posed a number of challenges in sealing the moving control surfaces to prevent the entry of hot gases. The orbiter elevons, consisting of an inboard and an outboard elevon on each wing, posed a unique problem at the upper wing surface. The elevon hinge line was established near the lower wing surface, so elevon motion resulted in large changes in the position of the upper elevon forward edge. The structure and systems installations prevented use of a stationary seal riding on a large skin radius.

The gap between the elevons and wing required sealing sufficient to prevent interior heating by the hot entry gases, which reach up to 1200F in that area. These high temperatures would damage the aluminum structure (restricted to 350F maximum), and the hydraulic systems operating the surfaces could not be allowed to exceed 275F. In addition to thermal sealing, the upper wing/elevon junction required a fairing to provide aerodynamic smoothness in an area subject to high vibration, pressure differentials, and buffet/flutter loads.

INITIAL APPROACH

The approach to this challenge was initially developed by Grumman, the major subcontractor for the orbiter wings. A system of overlapping panels made of high-temperature alloys bridged the gap between the wing and the elevon. Each panel had rollers on its trailing edge, and the panels were preloaded to maintain roller contact. Seals between the rollers and at the panel hinges prevented hot gas ingestion.

The use of mechanisms came about in order to maintain contact of the rollers on the elevon surface. Predicted burst/crush loads, dynamic requirements, and magnitude of movement precluded spring loading the panels down. Therefore, at each panel, 2 four-bar linkages were used to cause the motion of the panel to approximately follow that of the elevon.

This initial design resulted in a set of interface points that became fixed for the remainder of the program. As shown in Figure 1, there were 15 panels per wing. A linkage (Figure 2) connected the elevon to a bellcrank (mounted on the rear wing spar) at 17 locations. The bellcrank, in turn, connected with either one or two panels, depending on the location, for a total of 29 connections to panels from the 17 bellcranks per wing. In general, the pivot axis of each bellcrank was skewed relative to the elevon and seal panel hinge lines in an attempt to compromise between the latter two, which were not parallel. Since the panel motion did not precisely follow the elevon motion, the clevis attaching the upper link to the panel was adjustable, and a high preload was put into each linkage by bowing the panel. This allowed the rollers to remain in contact without perfectly matched panel-to-elevon motion.

PROBLEMS WITH INITIAL DESIGN

The initial design was used on OV-101 (The Enterprise) for the Approach and Landing Tests (ALT). The seals and materials were not fully developed for high-temperature use at that time. The ALT program revealed that the high panel preload caused high wear on the interfaces. The rollers would sometimes fail to roll, giving high friction and a jolt at each new motion. The holes in the roller clevises elongated under the high loads, changing the adjustment and spoiling the pivot surfaces.

As a temporary measure to allow completion of the ALT program, the preload on the linkage was reduced. The bushings in the rollers were replaced by needle-type bearings to reduce friction. These measures provided acceptable performance in the low temperature ALT program, but the resulting gaps at the panel trailing edge were not acceptable for operational use. In addition, no anti-friction bearings were available that could meet the environmental requirements of the trailing edge rollers. At this point in the development, the mechanism (linkage) weight was approximately 221 pounds per vehicle.

CHANGES FOR ORBITAL FLIGHT TEST

Following the ALT program, Rockwell International undertook the further development of the subsystem to meet full orbital mission requirements. Primary goals were weight reduction, simplification, and a trailing edge configuration compatible with the high entry temperatures. The approach was to refine the kinematics so that an approximately constant gap would be maintained between the panel trailing edge and the elevon surface throughout the travel. This was envisioned as eliminating the rollers and reducing loads (a high preload would no longer be required to maintain panel trailing edge contact). A new metal seal configuration was developed by the thermal protection system designers to have greater initial deflection and thus tolerate greater variations in trailing edge gap. The lower loads, combined with use of lightweight swaged-end aluminum rod assemblies, gave an anticipated weight savings of 114 pounds per vehicle (52%).

TECHNIQUES USED

The challenge now faced by the designers was the sheer magnitude of the work required. Seventeen (17) lower stages and 29 upper stages had to be kinematically optimized to maintain the trailing edge gap within $\pm .060$ inch over the elevon travel. Since pivot axes, panel sizes, and wing contours were unique at each location, separate kinematic studies were required at each. At that time (1976), no Computer Aid Design (interactive graphics) facilities were available at Rockwell.

The kinematic optimization became a joint effort of the Mechanical Design Group, with Mr. I. Awtamonow as lead designer, and the Numerical Design Group, represented by R. Chu, Supervisor, A. Shapiro, and B. Rivera. The Numerical Design group's primary responsibility was the mathematical modeling of vehicle lines and the programming of large computer controlled plotters to generate lines drawings. Using this background, the analysts developed a geometry analysis program for the main frame digital computer. The program allowed the entry of data on the basic pivot points and lines at each location. The radii and angles of the bellcrank were the only parameters which could be varied without changing the interface points built into the structure. With the chosen values entered, the user could input the elevon angle, and the program would calculate the positions of all the joints and the size of the trailing edge gap.

This program was used at each location to develop the linkage geometry. The designers proceeded much as they would have "on the board," using the original ALT linkage as a start and converging on a satisfactory solution by observing the sensitivity of the gap to each variable at the elevon up, neutral, and down positions. By this process of "enlightened trial and error," the geometry of all the linkages was established in about one year.

DETAIL DESIGN

As a geometry was established at each location, spot layouts were made to assure adequate clearances. However, the resources were not available to allow a detailed check layout of each location. Design of link and bellcrank details followed the establishing of the geometry. Conventional aerospace light weight design practices were followed. The most significant obstacle to detail design was the high temperature anticipated at the rod end attaching to the seal panel. A rod end using carbon-graphite-MoS2 bearing inserts was specified in order to withstand the approximately 800F temperature predicted. Bearings of the same material, but in a different configuration, were used in other orbiter systems - e.g., the Payload Bay Door Hinges.

The final loads iteration for the subsystem was completed in 1977, when detail design was well underway. Analysis revealed that the light links had insufficient stiffness based on flutter/buffet criteria. As a result, most tube/link details were redesigned. The larger diameter and wall thickness resulted in a weight increase, but the subsystem weight remained close to the target weight of 107 pounds.

LATER CHANGES

The elevon cove seal on the lower wing/elevon surface was redesigned in 1977. The diameter of the seal increased to the point that the lower links would interfere with the seal as shown in Figure 3. This problem was discovered in spot layouts prior to completion of detail release. Changes in the critical seal were not feasible, so the lower links were redesigned to clear the seal. The resulting curved links added 21 pounds per vehicle to the subsystem.

The body of the curved links was hollow aluminum, the curved and straight portions being one continuous part (Figure 4). The initial fabrication sequence consisted of forming an oversized machined tube to the curvature, chemically milling and machining final dimensions, and heat treatment. Difficulties were encountered due to the higher rate of chemical material removal in the stretched (formed) areas as well as dimensional changes induced by heat treatment. Manufacturing technique development eventually produced trouble free fabrication. The sequence evolved into the following: machining the straight tube to final dimensions; forming the tube to a smaller radius of curvature than the final requirement; and heat treatment, during which the tube straightened out to final dimensions. The amount of overbending required to achieve the correct curvature after heat treatment was determined by experiment.

At some locations, an additional clearance problem precluded the use of the large diameter curved tubes. In these areas, the curved portion of the tube entered a channel fitting with the elevon up (Figure 5). An alternate design was developed as shown in Figure 6. The narrower section and anti-rotation lugs provided the additional clearance required. However, the greater weight of these links resulted in the total subsystem weight increasing to 196 pounds per vehicle. These heavier Inconel 718 links were used at seven of the nine inboard lower stages.

BEARING MATERIAL CHANGE

As described above, the high temperature end of the upper links used a carbon-graphite-MoS2 bearing insert material. This material will withstand temperatures up to 2500F. However, the manufacturer of the bearings found that the spherical ball rod end with carbon-graphite bore presented unanticipated fabrication problems. Cracking of the insert material during fabrication resulted in an extremely high rejection rate. Virtually no bearings were delivered 1-1/2 years after the first order.

In mid-1978, the decision was made to give up on the carbon-graphite inserts. A rod end using a ceramic MoS2 dry film lubricant was specified instead. The new lubricant was restricted to a maximum of 750F for short duration only, which corresponded to the expected environment with no margin. The dry film lubricant was therefore being pushed to perform at its maximum capability. However, experience had been gained by this time with this dry film lubricant in other orbiter mechanisms, resulting in confidence that the life would be adequate.

INITIAL INSTALLATION PROBLEMS

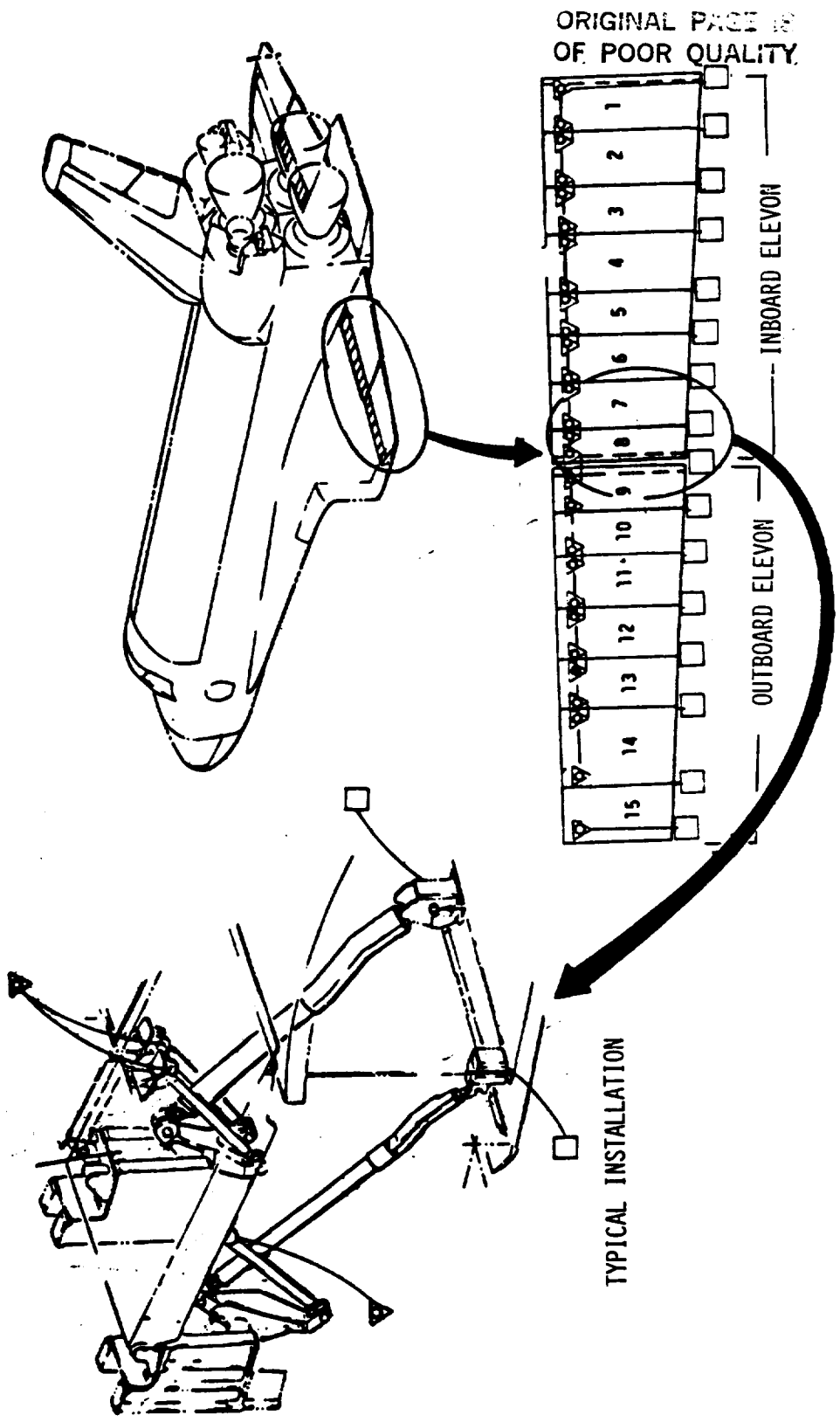
The installation and adjustment of the first operational system occurred on OV-102 (Columbia). Owing to the simplicity of the hardware and its similarity to other orbiter mechanisms, a full qualification program was not performed. Consequently, a number of problems were encountered on the first article. The primary problem was an inability to hold the trailing edge gap tolerances originally targeted. The buildup of fabrication tolerances was enough to force the gap tolerance to increase from + 0.060 (original) to + 0.130 (neutral position), + 0.160 (elevon down), and + .215 (elevon up). The tolerances involved included those on the elevon moldline (contour), panel details, bellcranks, wing spar fittings, elevon hingeline, and elevon clevis fittings. Adjustments of the link lengths (upper and lower) from nominal were made based on calculated sensitivity until the best results were achieved. Fortunately, the seal design had enough margin to absorb the increased gap variations.

Other first article problems included low clearances to hydraulic lines and fasteners, and rubbing of rod end locking devices against adjacent rod bodies. The problems were considered minor for the first installation of a system without complete check layouts or mockups. R. Holt of Rockwell International was the responsible engineer during the subsystem installation phase.

Installation of OV-099 (Challenger) encountered very few problems. However, many trailing edge gaps were at the low side of the tolerance band, and excessive seal wear was noted on many seals following elevon tests. The damage was found to be caused by rubbing of an area of the seal not intended to contact. A change in the seal mounting geometry solved this problem and avoided any change to the mechanism or the seal itself.

SUBSYSTEM PERFORMANCE SUMMARY

Figure 7 illustrates a typical linkage of the final configuration. The mechanism performance has been satisfactory on all orbital flights. No functional or leakage problems have been encountered. The final design, as developed from the ALT version, meets the original challenge in the intended way - simply and directly.



ORIGINAL PAGE IS
OF POOR QUALITY

FIGURE 1 PANEL AND LINKAGE LOCATION

- ELEVON ATTACH
- ▽ PANEL ATTACH

TYPICAL INSTALLATION

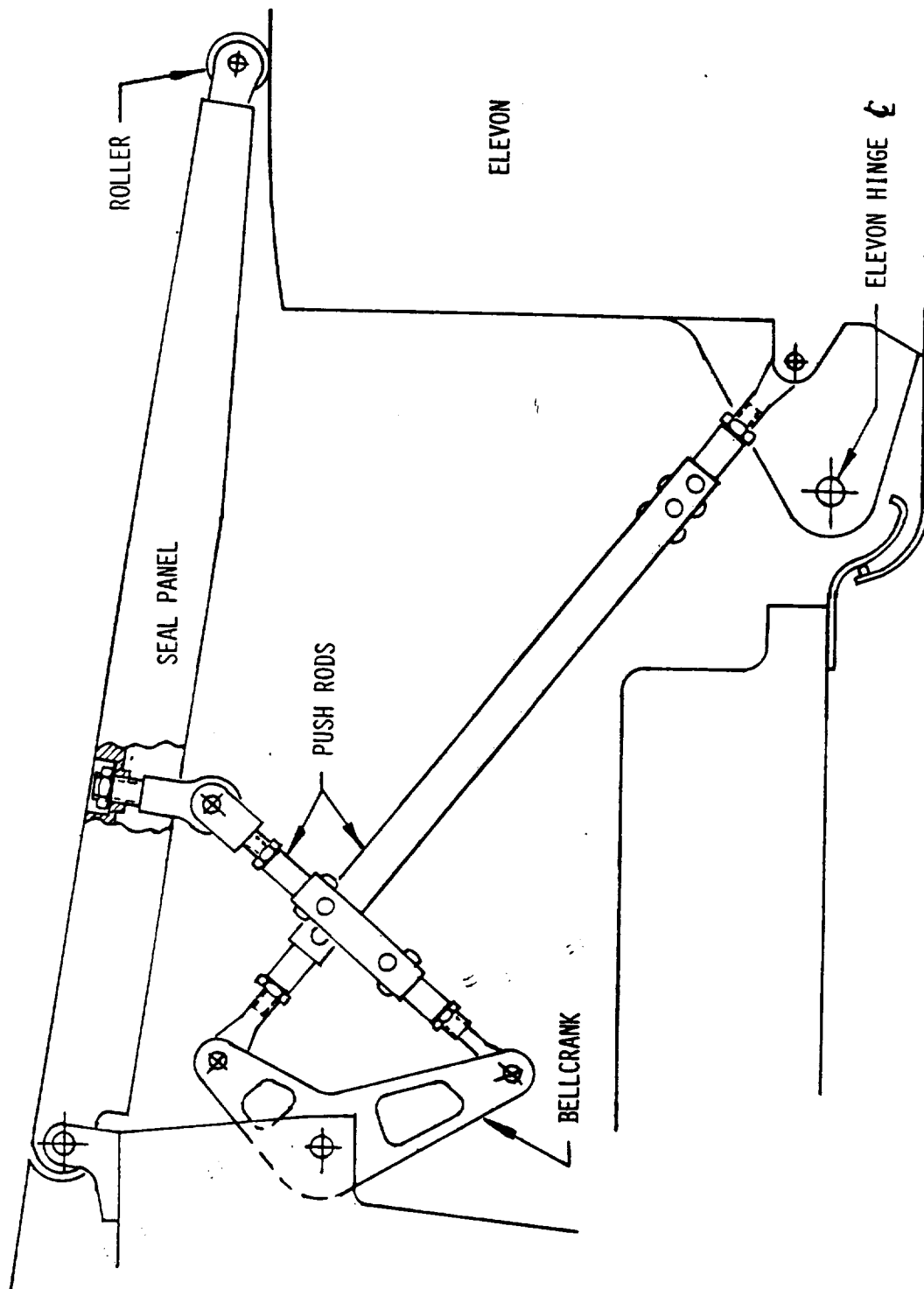


FIGURE 2. ORIGINAL LINKAGE CONFIGURATION (TYPICAL)

ORIGINAL PAGE IS
OF POOR QUALITY

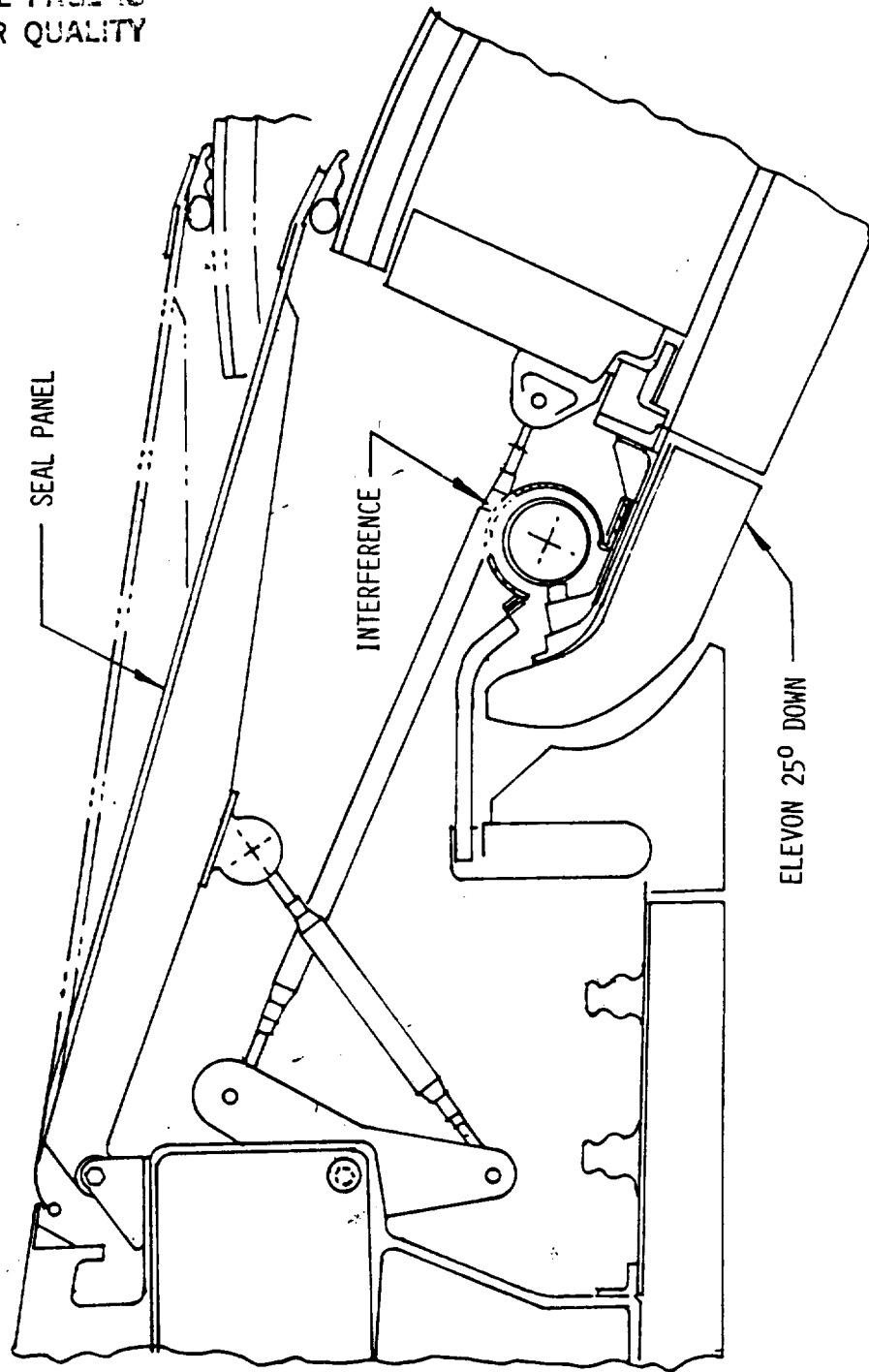


FIGURE 3. INTERFERENCE OF LOWER LINK WITH NEW COVE SEAL

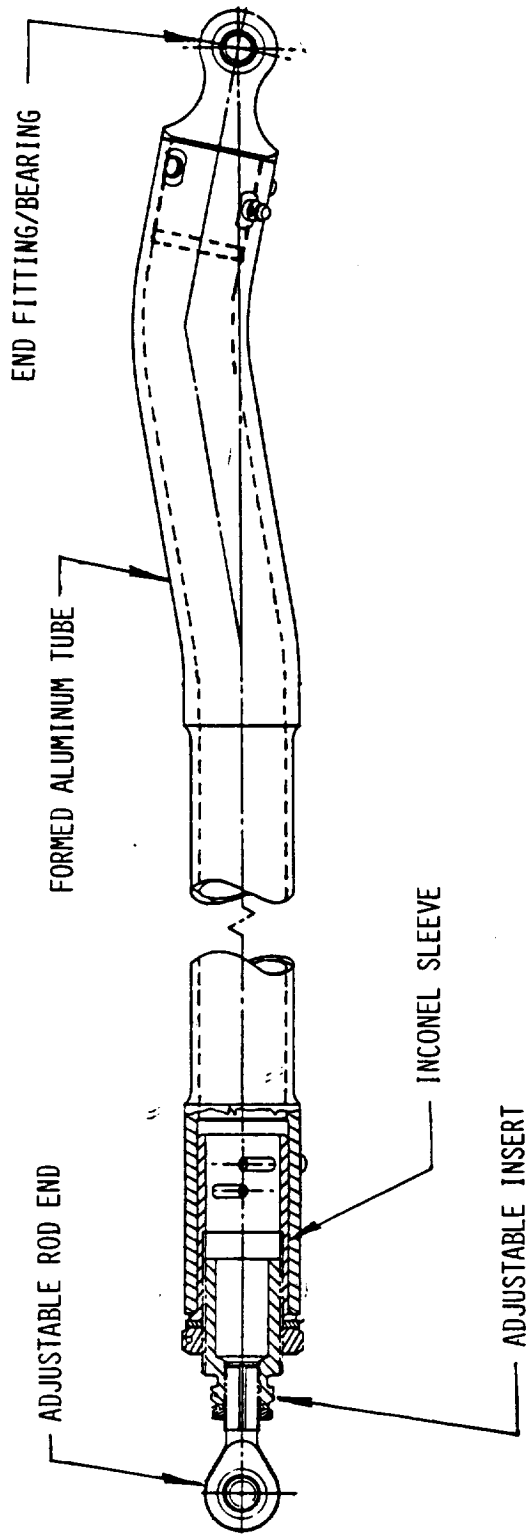


FIGURE 4. CURVED ALUMINUM LINK ASSEMBLY

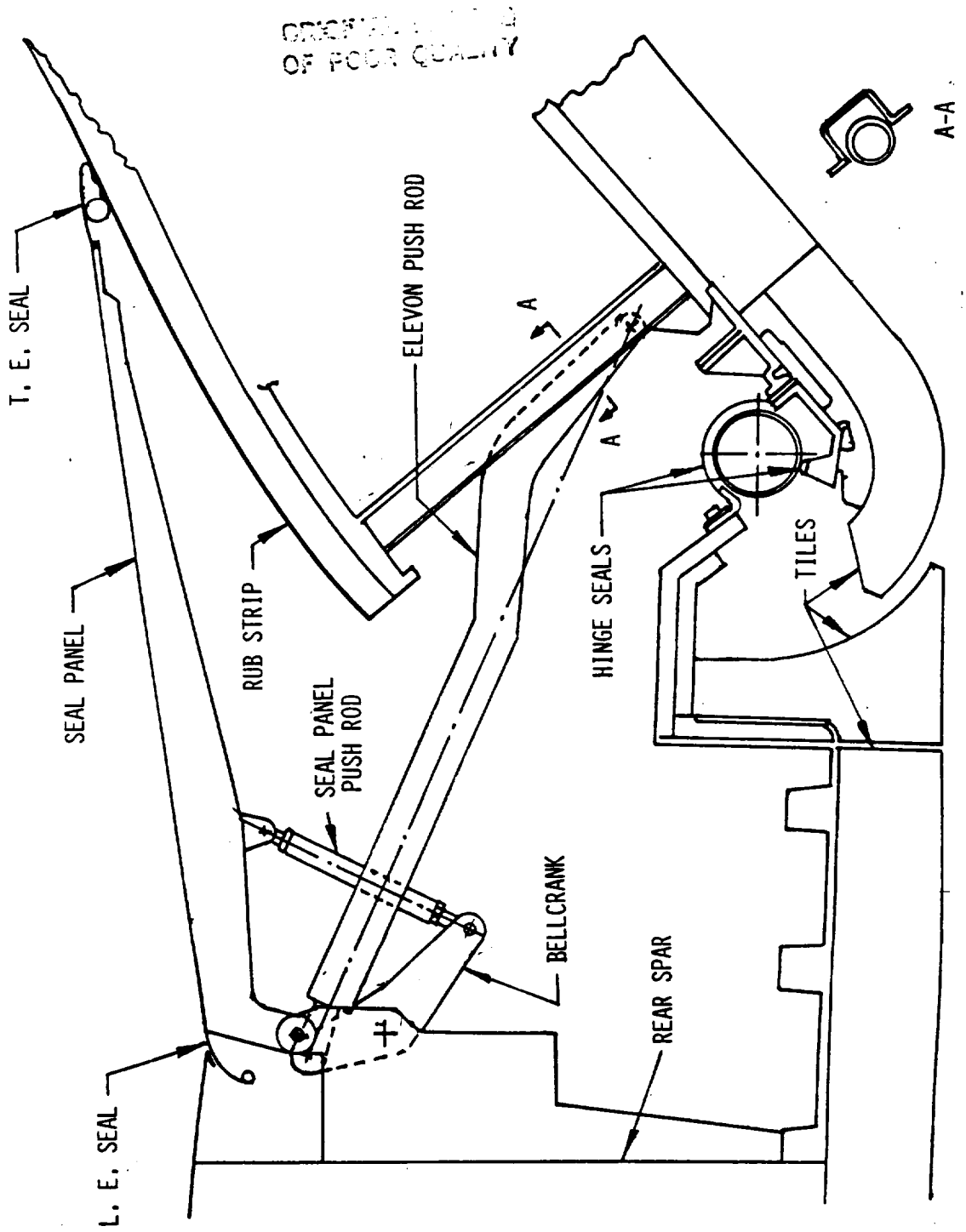


FIGURE 5. CURVED ALUMINUM LINK INTERFERENCE WITH ELEVON STRUCTURE (ELEVON UP)

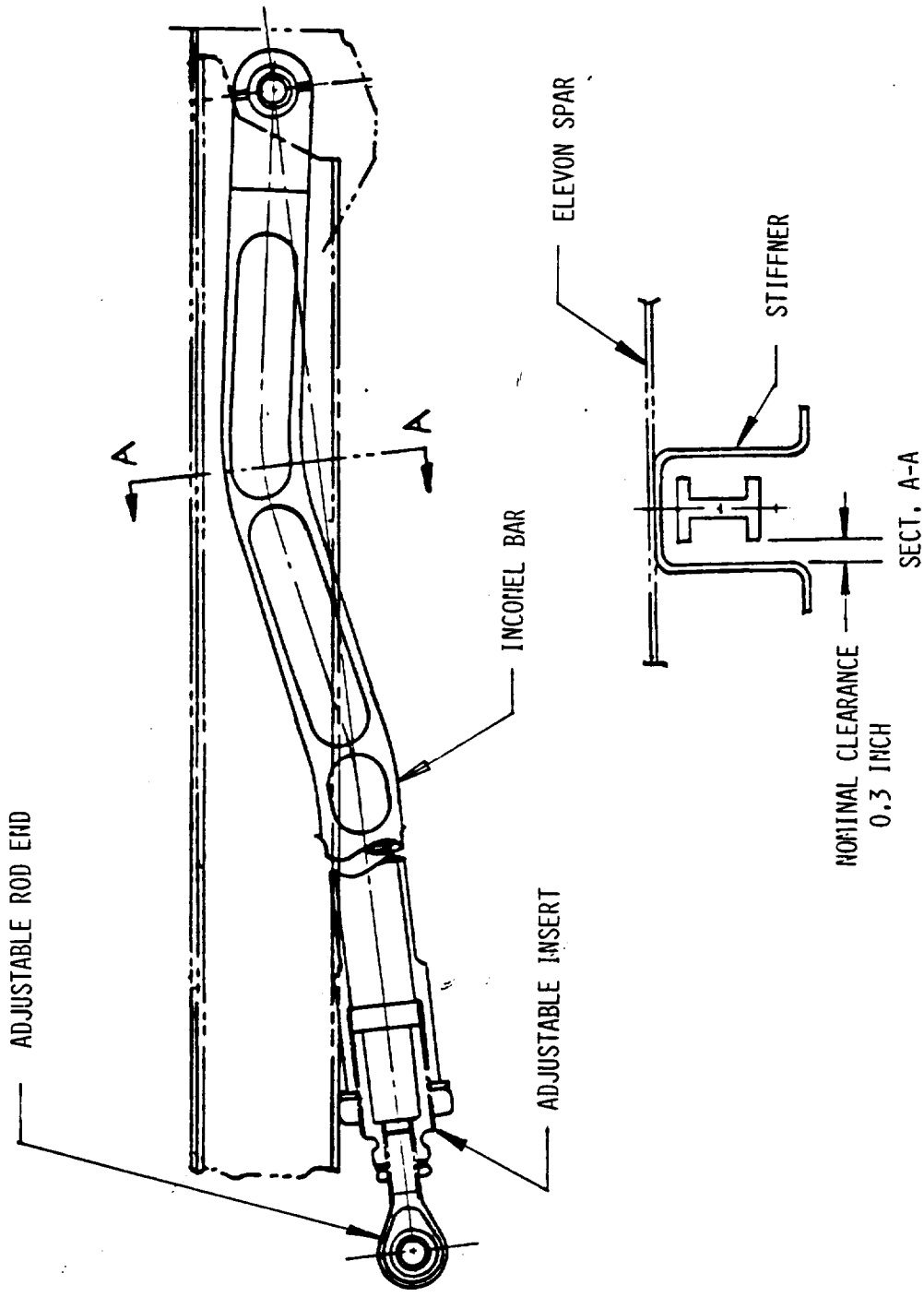


FIGURE 6. CURVED INCONEL LINK ASSEMBLY

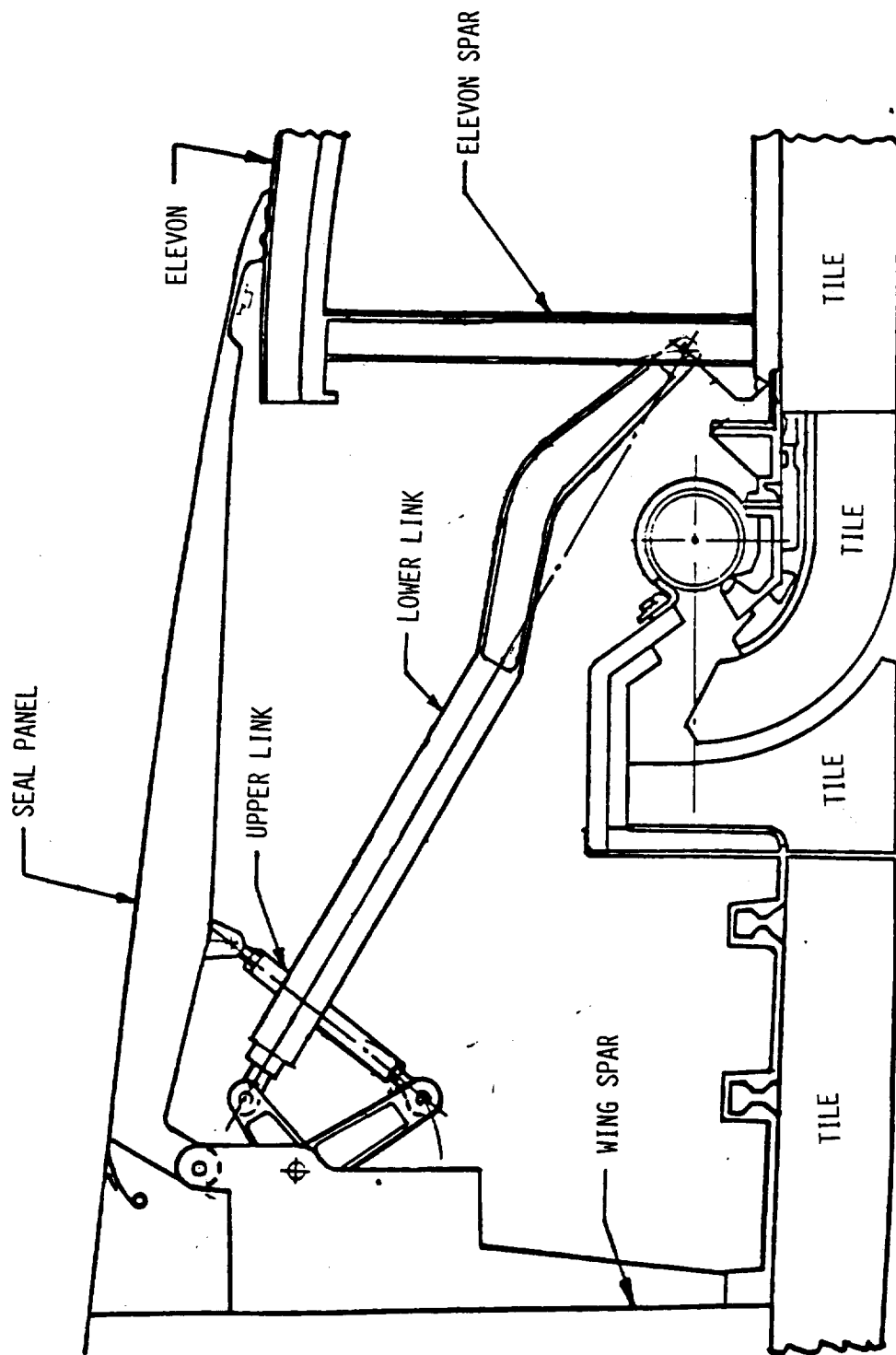


FIGURE 7. FINAL LINKAGE CONFIGURATION (TYPICAL)

25
N85-16962

SPACE SHUTTLE WHEELS AND BRAKES

Renton B. Carsley

Rockwell International Corporation

Downey, California

ABSTRACT

The Space Shuttle Orbiter wheels have been subjected to a combination of tests which are different than any previously conducted in the aerospace industry. The major testing difference is the computer generated dynamic landing profiles used during the certification process which subjected the wheels and tires to simulated landing loading conditions.

The orbiter brakes use a unique combination of carbon composite linings and beryllium heat sink to minimize weight. The development of a new lining retention method was necessary in order to withstand the high temperature generated during the braking roll. As with many programs, the volume into which this hardware had to fit was established early in the program, with no provisions made for growth to offset the continuously increasing predicted orbiter landing weight.

Both wheels and brakes were designed, manufactured, and certified for Orbiter operational use by B. F. Goodrich Company, Troy, Ohio.

I. INTRODUCTION

The Space Shuttle, as with all space vehicles, requires a minimum weight configuration in order to maximize the payload weight to orbit lift capability. Using this philosophy, and drawing from the years of experience and techniques utilized in commercial and military aircraft applications, the wheel/tire/brake/shock strut configuration was sized on a predicted Space Shuttle Orbiter landing weight established very early in the program.

The main wheel baseline design has many of the same features as a commercial aircraft wheel. An interface with the axle, brake and tire, an over-inflation plug, thermal fuse release plug, inflation valve, bearing housings, grease seals, and pressure seals.

A "live axle" configuration was chosen for the nose gear which differs in design for most current aircraft but has been used in experimental and operational aircraft. With the live axle design, the wheels are splined to the axle and rotate as a unit on bearings mounted in the shock strut. The resulting corotating wheels reduces the tendency for wheel shimmy and, therefore, increases the stability of the assembly.

Preliminary studies by B. F. Goodrich were conducted to evaluate various combinations of materials for both the brake heat sink and friction surfaces in order to minimize the brake weight for both reusable and non-reusable applications. The combinations studied included full carbon composite heat sinks, conventional beryllium heat sinks with mechanically attached sintered metallic friction materials and the combination of carbon composite linings and beryllium heat sink. The carbon composite lining/beryllium heat sink was finally selected for its relatively low peak temperatures (compared to steel and carbon composites) which allowed the minimum weight reusable heat sink. The

carbon composite heat sink was the lowest weight for a non-reusable application, requiring new wheels and tires to be installed after every stop. In comparing the levels of brake energies required for a normal landing when the brakes would be usable and a maximum brake energy stop where the brakes and wheels were expendable, the composite lining/beryllium heat sink was the most efficient for the very critical Space Shuttle weight requirements.

II. GENERAL DESCRIPTION OF THE ORBITER MAIN WHEEL

The Orbiter main wheel (See Figure 1) is similar to conventional aircraft wheels in most respects. It is made in two halves machined from 7049-T73 forgings and joined together by eighteen tie bolts and nuts of MP35 multi-phase 240 Ksi material.

The inboard wheel half has a 4340 steel sleeve pressed into the hub and supports the inboard bearing and grease seal. The wheel half, also contains the ports for the three thermal fuse plugs, over-inflation plug and inflation valve. Elevon brake drive lugs which interface with the brake rotors are also part of the inboard half and are protected from wear by 4130 steel hard chrome plated drive channels.

The outboard half contains the outboard bearing, grease seal and has mounting provisions for the hub cap.

The bearings are a standard Timken bearing size with special modifications and processing to help withstand the Orbiter landing speeds and loads.

Tire pressure sealing is accomplished by the compression of an O-ring in a seal cavity between the wheel halves. The O-ring material and seal geometry was established as the result of a separate NASA/B. F. Goodrich study contract. Extremely low leakage rate of the wheel/tire assembly was necessary because of the long "storage" time from gear retraction at vehicle mating to gear extension at landing. Access to the wheel wells for tire pressure check and reinflation during this time period was not possible.

III. GENERAL DESCRIPTION OF ORBITER NOSE WHEEL

The nose wheel (See Figure 2) differs from most conventional nose wheels in that it is mounted on a "live" axle with corotating wheels. That is, the axle rotates with the wheels using bearings mounted in the nose gear strut, thereby, eliminating the bearings from the wheel and replacing them with a spline/bushing configuration.

The nose wheel configuration is similar to the main wheel except for the lack of brake system interface. It is made in two halves of the same material, bolted together by attachments of the same material and has thermal fuse plugs, over-inflation plug and an inflation valve.

Thermal fuse plugs are used as blowout protection against nose wheel well overheat from plasma flow rather than brake heat as in the case of the main wheel. Pressure sealing is accomplished in the same manner as the main wheel.

IV. GENERAL DESCRIPTION OF THE ORBITER MAIN WHEEL BRAKE

The Orbiter brake (See Figure 3) is a four rotor, multiple disk brake using beryllium as the heat sink. The friction surfaces are carbon composite linings mechanically attached to the beryllium heat sink surfaces. The brake assembly consists of a pressure plate, back plate, rotors, stators, support torque tube and a hydraulic actuation piston housing. The piston housing has two separate hydraulic circuits for redundant actuation. The brake assembly is bolted to the landing gear shock strut with a bracket register to the axle for support of the outboard end of the brake assembly.

V. WHEEL DESIGN CHALLENGE TO OPERATIONAL CERTIFICATION

Modification to the wheel/tire testing philosophy, that is, the addition of the dynamic landing load profiles had little effect upon the original nose wheel design. The nose wheel loading is not impacted by crosswinds and only slight changes occur as the result of total vehicle weight change. This is because the nose gear is a semi-free castor design and can react a limited side load and the nose gear carries such a small percentage of the total vehicle static weight. In addition, the pitch over rate and resulting nose gear impact load or "slap down" has not changed. Therefore, the remaining portion of the text will address the challenges which had to be solved to certify the main wheel and brake.

As with many programs, requirements change over a period of time, and the Orbiter was certainly not different. Not only did the vehicle landing weight increase dramatically from the initial levels, but the methods of dynamic landing load profile simulation testing currently in use had never been performed on an aircraft wheel/tire assembly in the past. This advancement of the state-of-the-art caused several failures during the certification process.

The original or baseline wheel assembly design (See Figure 4) is similar to conventional aircraft wheels used throughout the aerospace industry. The baseline wheel was used during five Approach and Landing Tests (ALT) where the Orbiter was released at altitude from the 747 carrier aircraft to prove the flying and landing ability of the Orbiter. However, the Orbiter vehicle weight increased from approximately 150,000# for ALT to 227,000 pounds for an operational abort condition. The weight was subsequently increased again to the present 240,000 pound level. What are now called dynamic landing load profile tests were added to the baseline conventional MIL specification requirements at this time in the program. Because of the dramatic increase in loading conditions due to these changes, failures in the wheel bearings began to occur.

The dynamic load profiles (See Figure 5) are generated by computer programming that "lands" the Orbiter under given conditions of weight, velocity, aero surface configuration, c.g. location, tire sideload resistance capability, angle of attack, etc. Using these conditions, values for tire/wheel radial load, tire velocity, yaw angle and lateral load are obtained and used as inputs to the Wright Patterson Air Force Base (WPAFB) automated dynamometer.

In the baseline wheel configuration, the inboard bearing is located at approximately the tire centerline and is considerably larger than the outboard bearing. With the advent of the dynamic profiles the increased lateral load and corresponding increased moment on the wheel resulted in bearing failures.

At this point, a major redesign and development testing of the wheel was undertaken. The final wheel configuration (See Figure 1) which is still, as of this writing, being tested under straight roll, maintained the same interfaces between the wheel, brake and tire but the bearing configuration was drastically changed. By adding a steel sleeve pressed into the inboard wheel half, the distance between the bearings was increased and thereby equalized the load distribution on the bearings.

The use of the steel sleeve was required to carry the large cantilevered inboard bearings load and still fit within the inner diameter of the brake torque tube. Installation of the insert, however, proved to be a major design problem. During initial tests, it was discovered that the insert rotated in the inner wheel half when installed with approximately 0.007 inch interference. The interference was increased in steps until it reached the presently used whopping 0.022 inch interference.

During the testing to solve the sleeve rotation problem, a parallel program of bearing configuration, grease and bearing axial preload test series was being conducted. The tests showed that by "manicuring" and adding a phosphate process to a standard tapered roller bearings and installing them with a high axial preload, dramatically increased the load capability. The high preload is contrary to instructions in automobile maintenance manual for front wheel bearing installation.

The preload is applied as a measure of wheel rolling resistance and requires approximately 1500 foot pounds torque on the axle nut.

The initial redesigned or "heavy duty" wheel, flown on STS-1, had a second or redundant O-ring added at the split line to help reduce pressure loss during mated and orbit operations (See Figure 6). The O-ring groove placement and configuration proved to be a stress riser causing a complete circumferential crack in the outboard wheel half during the straight roll test.

The next configuration flown on STS-2, 3, 4, and 5 removed the second O-ring groove but failed in two areas at approximately 800 miles of straight roll. Cracks occurred in the inboard half originating from the fuse plug hole and in the outboard half in the tie bolt hole at the wheel split line.

In the third configuration, flown on STS-6, the fuse plug holes were repositioned to a reduced stress area and the outboard wheel half web thickness was increased and a larger radius added in the tie bolt hole at the split line. At the 500 mile point of straight roll for this configuration, non-destruction inspection revealed a crack in the steel sleeve at the outer surface of the bearing cup housing. The failure was traced to an inclusion in the 4340 steel material just below the outer diameter surface.

For the latest sleeve configuration, flown on STS-7, as of this writing is again in the straight roll test phase; the material specification was changed which limits the allowable size and number of inclusions. In addition, a shot peening process was added to the highly stressed bearing housing area.

VI. BRAKE DESIGN CHALLENGE TO OPERATIONAL USE

The main wheel brake design (See Figure 3) is an extension of the technology developed by B. F. Goodrich on other aircraft programs but with special emphasis on weight savings and performance. The beryllium heat sink is used on the military C-5A and F-14 aircraft. However, the combination of beryllium heat sink and mechanically attached carbon composite linings is used for the first time on the Orbiter.

As the program progressed, changes were made to the design requirements from a single stop and replacement to a multiple stop and refurbishment. Results of development tests on various combination of heat sink and friction lining materials as well as the design requirements changes led to the selection of beryllium as the heat sink and carbon composite for the linings. Beryllium was chosen for its light weight and efficient heat absorption capability and carbon composite was chosen because of its great wear resistant, light weight, high strength, and high temperature capability.

The major problems encountered in the development and certification testing were the method of mechanical attachment and physical configuration of the linings (See Figure 7). Several iterations of attachment, materials, and processing were tried before the final configuration was established. Included in the assembly are 1722 Rhodium plated steel for the "T" clips used to react the braking torque; Columbium rivets with molybdenum washers to attach the lining segment; and monel rivets to attach the "T" clips to the beryllium disks.

Design changes were also made in the attachment of the back plate to the torque tube and to the hydraulic piston seal configuration.

Certification testing included those normally associated with conventional aircraft brakes along with hydraulic burst and pressure cycle endurance tests. Because there was not a method to conduct the normal rejected takeoff test on the Orbiter, a simulated landing roll brake test was conducted using a dynamometer. The specification requirement stated that the brake assembly shall be capable of absorbing 36.5 million foot-pounds of energy in five separate "normal" stops and 55.5 million foot-pounds in one return to launch site (RTLS) stop, commonly referred to as an abort landing without failure. The certification test program verified these requirements could be met.

It must be pointed out at this time that the brake assembly certification document was dated August 1977. This was well over 3-1/2 years before the flight of STS-1. And because of the increased landing weights, changes in wheel and axle configuration, impact of crosswinds and other factors, certain brakes have been operated in the energy range which exceeds the reuse/refurbishment capability during the STS flights. For example, the brakes were designed for use on five landings with the maximum Orbiter landing weight of 188,000 pounds (32K pound payload) and refurbishable, followed by an emergency landing weight of 227,000 pounds (65K payload) with no reuse. Under these requirements all landings above 188,000 pounds were considered an emergency and, therefore, could result in the loss of the brakes. To date and for future planning all Orbiter landings have been above 188,000 pounds.

VIII. BRAKE PERFORMANCE DURING STS FLIGHTS

Brake pressure data obtained after the STS-1 landing indicated a considerably higher pressure was present at the right inboard brake than for the right outboard brake. This discrepancy was traced to a faulty connection in the brake skid control box. However, inspection of the right inboard brake showed that damage to the No. 3 rotor drive slot had occurred. The damage was determined to be lack of complete engagement between the wheel drive lug channels and the rotor drive slot face. Because of axle deflection relative to the brake assembly centerline, there is axial movement between the wheel lug and rotor slots as the wheel rotates. This axial in and out relative motion caused the end of the channel to displace the beryllium material at the rotor drive slot face outboard.

New longer channels were installed for STS-2 and post landing inspection revealed no further brake damage.

Initial inspection of brakes assemblies used on STS-3 and STS-4 and subsequent analysis revealed that the relative deflection between the wheel/brake/axle combination allow contact between rotating and stationary parts of the brakes and wheels. There was contact between the rotor I.D. and the torque tube lugs and between the stator O.D. and wheel lugs. Also, there was wear and displaced metal at some rotor drive slots. Subsequent inspection made by removing the carbon linings disclosed that beryllium carbide not previously visible, had formed in localized areas beneath the linings on both the rotors and stators (See Figure 8).

In this same time frame, the landing of STS-5 took place. During the last 60 feet of the landing roll, the left inboard tire skidded for 50 feet and then rolled the last 10 feet. When the brake assembly was disassembled, it was found that the No. 3 stator was broken into 5 segments.

An in-depth analysis of all the available data from STS-1 through -5 and the qualification test report established these conclusions.

1. Beryllium carbide formations are occurring in local "Hot spots" on rotors and stators of brake assemblies that are approaching or exceeding the reusability energy limit of 36.5 million foot-pounds. These formations occur when beryllium reaches its melting point of approximately 2400°F.
2. Heat generation is not distributed evenly across the lining surfaces in a radial direction, thereby causing local "hot spots" and results in carbide formations.
3. Carbide formation causes a bulge in the lining thus increasing the localized contact pressure and thereby self-perpetuates the temperature increase and carbide formation.

4. Heavy braking at high velocity and extended braking causes the "hot spots" to increase in size and spread to include the structural load path sections, resulting in stator failure.
5. Detection of beryllium carbide requires removal of linings. Beryllium carbide, upon cooling, is a porous material and leaves a pocket in the disk at the "hot spot." If the brake is reused, a new "hot spot" can form in a new location radially under the lining face.
6. Heat generation is not distributed evenly along the length of the brake assembly. Rotors and stators closer to the back plate show larger carbide formations than those close to the pressure plate. The formations are slightly larger at the bottom of the stator than at the top.
7. Brake on time during qual test reusability stops did not exceed 22 seconds. Brake on time for the flights has ranged from 26 seconds (STS-2) with no damage to 52 seconds (STS-5) with the failed stator.
8. Differential braking in a crosswind increases the potential for brake damage and reduces the total brake energy capability available for stopping.
9. Continued use of the brakes close to or exceeding the refurbishment limit will reduce the reusability capability of the assembly.
10. The stator failure on STS-5 was the result of loss of stator strength due to high heat build-up from "extended" medium to heavy braking.
11. Failure of a stator or rotor is not a safety issue. Loss of one or all stators reduces braking capability but does not cause complete loss. The brake would act as a single rotor brake in the case of an all stator failure.

Prior to STS-6, a support bracket was added to the brake assembly which fits between the torque tube I.D. and the axle O.D.. The purpose of the bracket is to reduce the relative deflection between the axle and brake assembly during landing rollout.

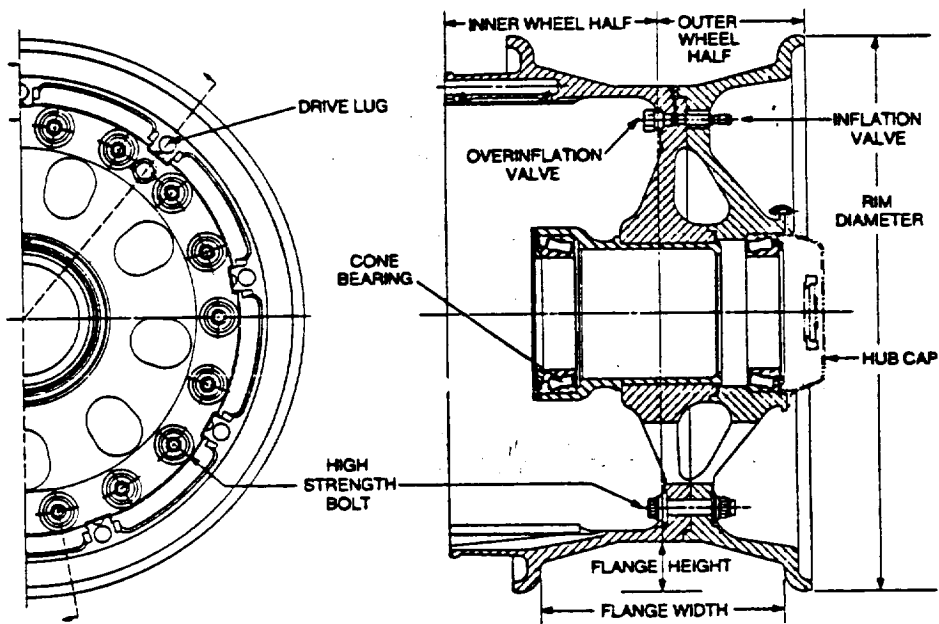
Inspection of the brakes after STS-6 landing did, indeed, show that the bracket eliminated the contact noted on previous flights. However, two brake assemblies approached the refurbishable energy level (34.7 and 32.6 million, respectively) resulting in carbide formations. In addition, three stators in one other brake had cracks in the beryllium. These cracks were traced to the forced interference fit of the "T" retainer spacer which caused scratches in the beryllium and subsequently caused crack propagation during brake use.

This condition has been corrected by rework on the brake assemblies installed on STS-7 as well as the addition of steel clips on the rotor and stator drive slot faces. The clips were added to eliminate the galling of the beryllium at slot faces caused by the relative motion of the drive keys and disks. An evaluation of the clip performance will be made after the STS-7 landing.

B. F. Goodrich is presently performing a study to determine the feasibility of increasing the brake energy capacity within the present limited space that is available, thereby increasing the refurbishment capability.

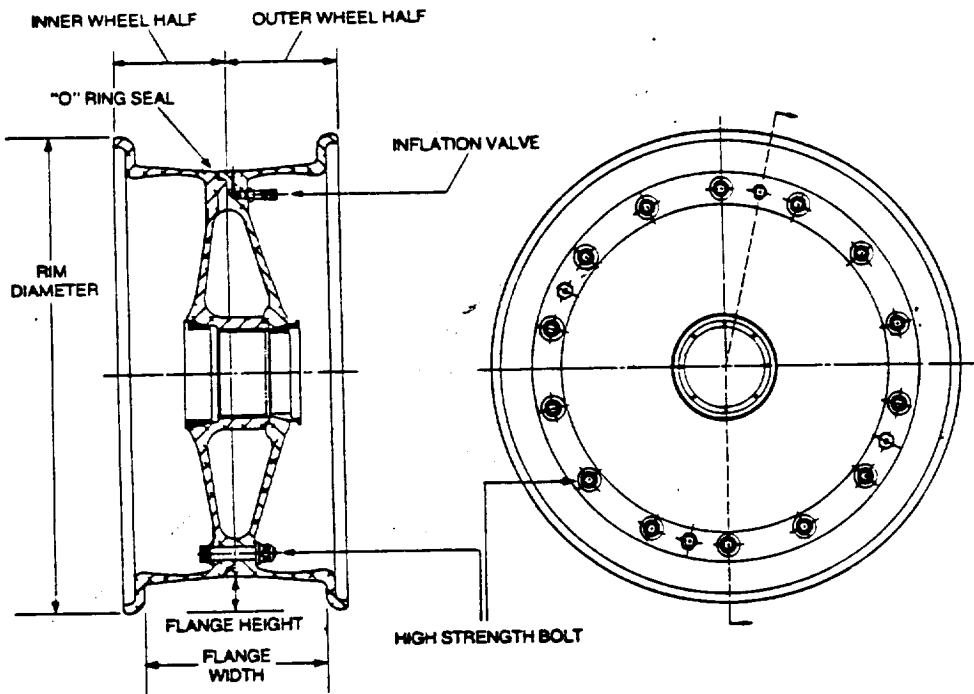
VIII. SUMMARY

The Orbiter wheels and brakes have been subjected to an extremely rigorous test program which far exceeds those used for any wheel and brake presently used in the aerospace industry. Changing requirements, increasing load conditions, and the use of landing load profiles has been the major contributor to the problems which occurred during the certification program and the Space Shuttle STS flights.



MAIN WHEEL OPERATIONAL CONFIGURATION

FIGURE 1

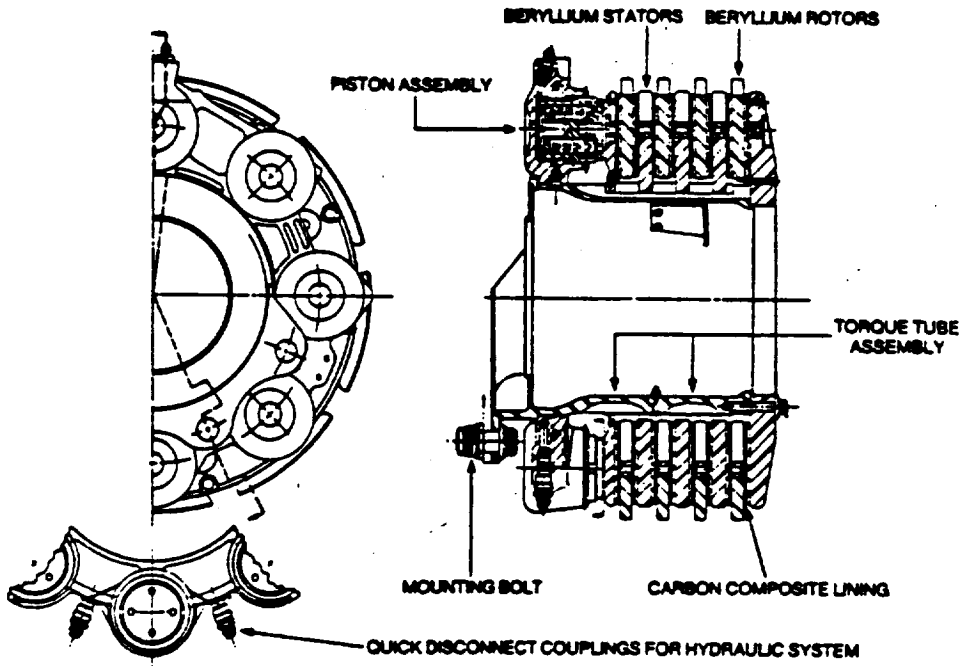


NOSE WHEEL OPERATIONAL CONFIGURATION

FIGURE 2

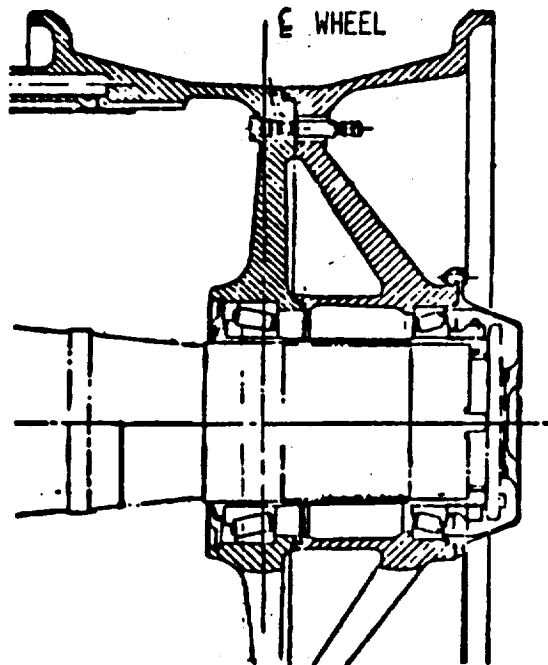
ORIGINAL PAGE IS
OF POOR QUALITY

ORIGINAL PAGE IS
OF POOR QUALITY



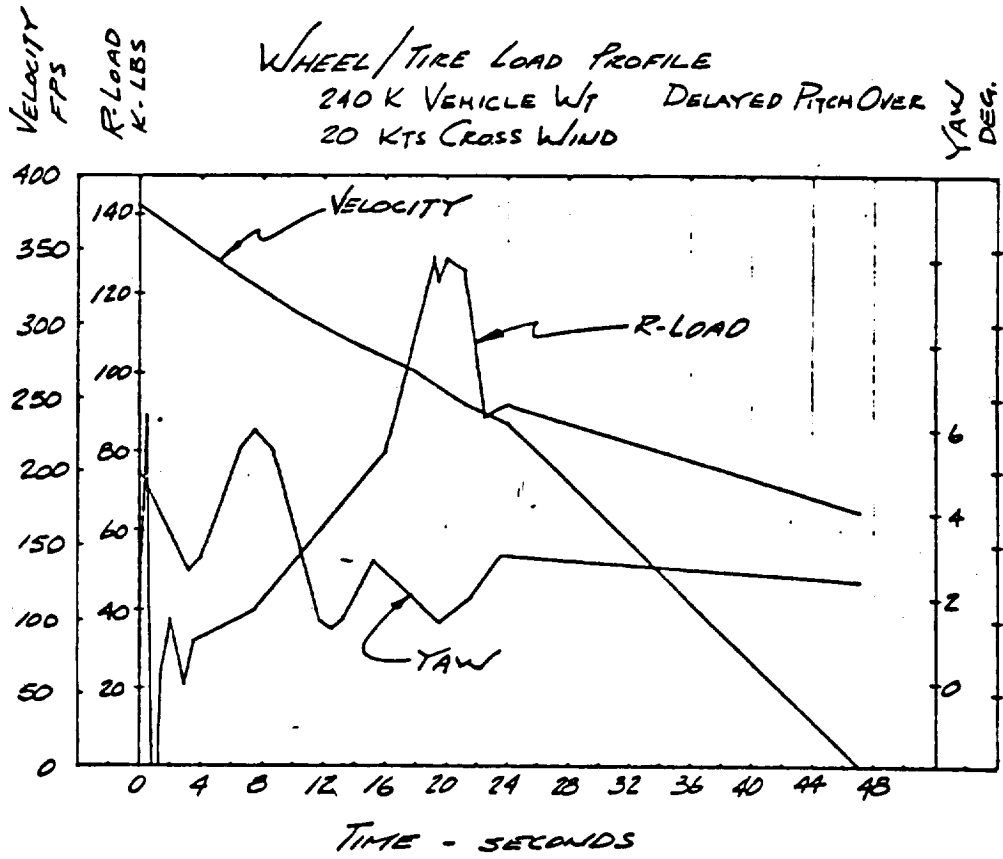
MAIN WHEEL BRAKE OPERATIONAL CONFIGURATION

FIGURE 3



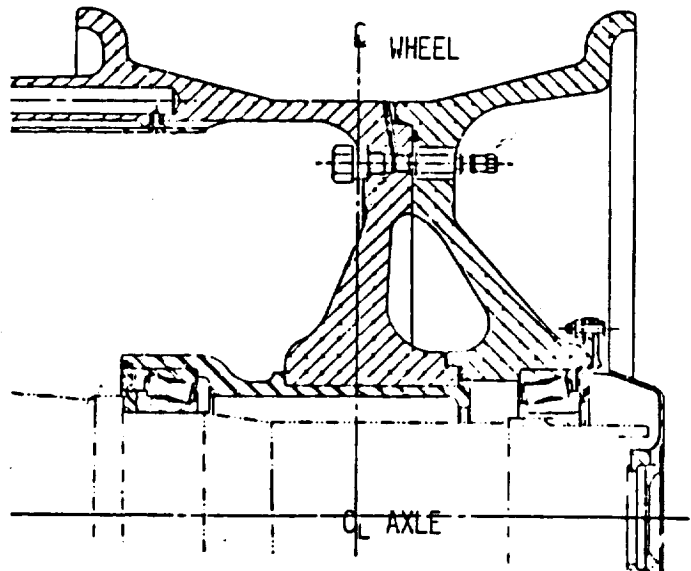
MAIN WHEEL BASELINE CONFIGURATION

FIGURE 4



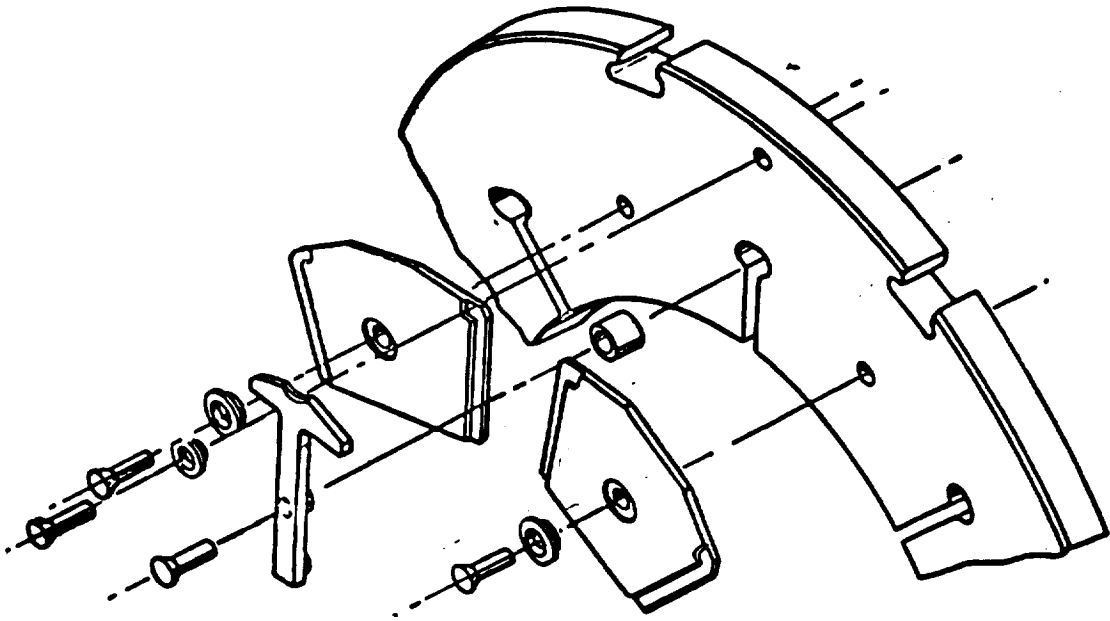
TYPICAL LANDING LOAD PROFILE

FIGURE 5

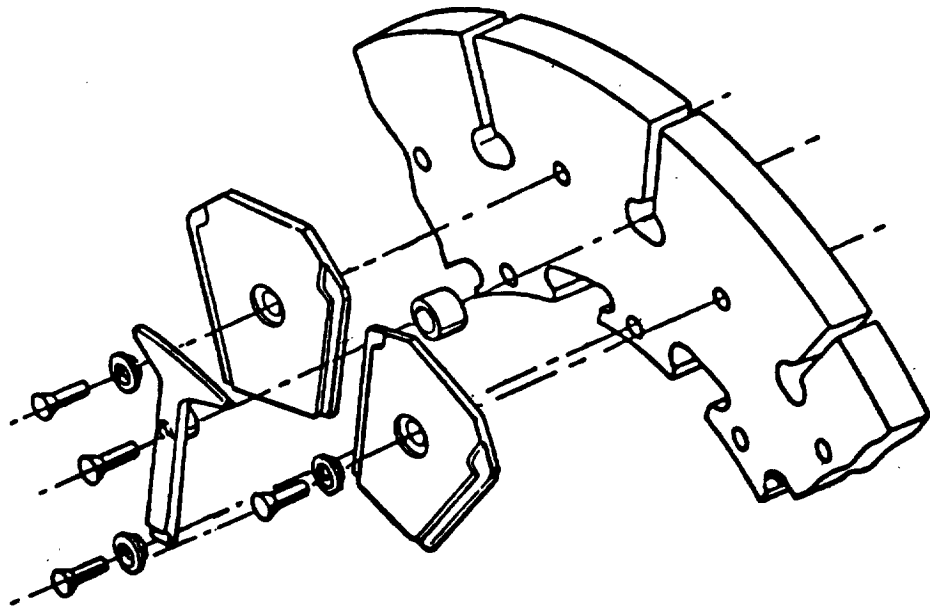


MAIN WHEEL DUAL O-RING CONFIGURATION

FIGURE 6



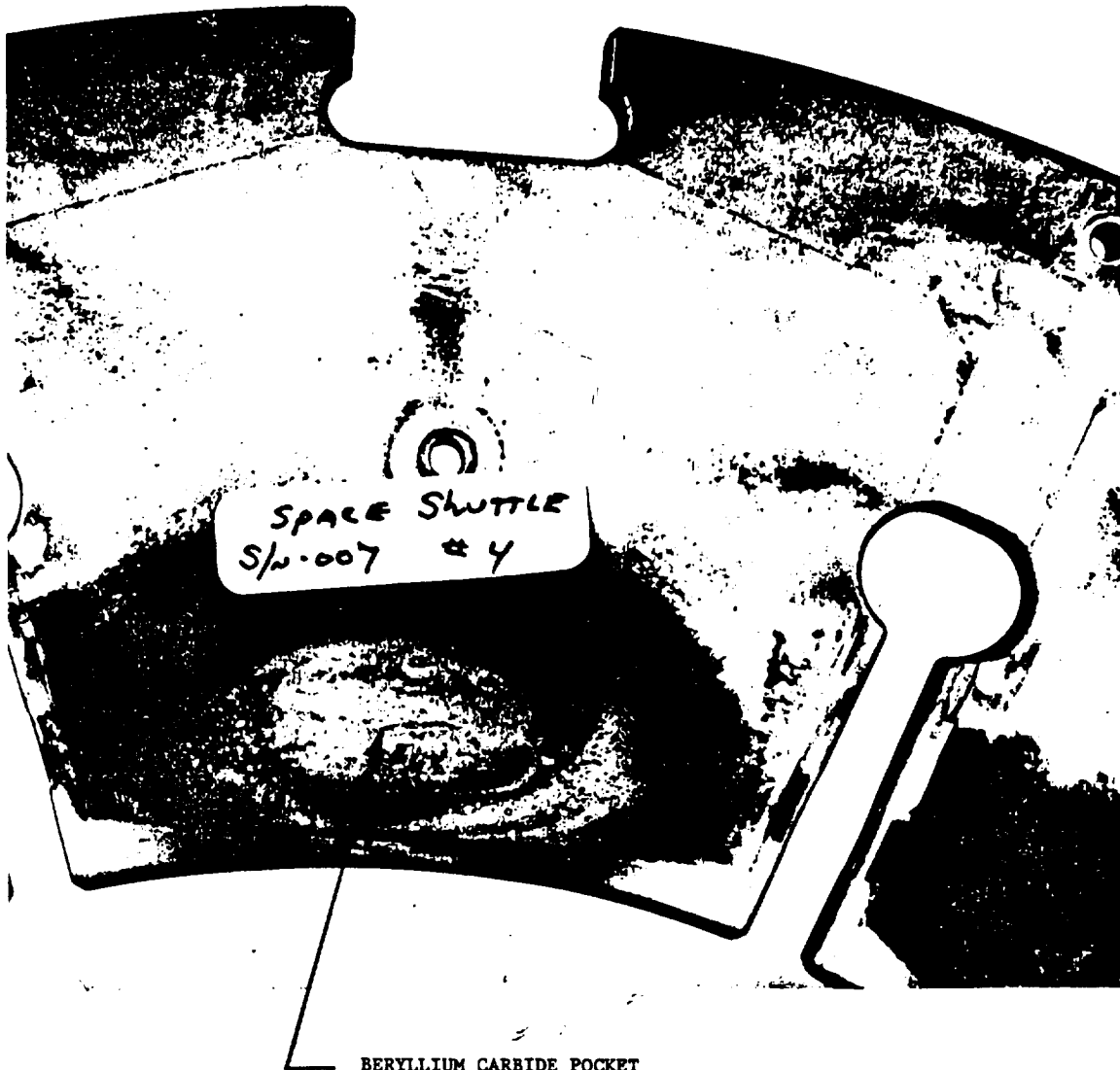
ROTOR



STATOR

ROTOR AND STATOR LINING ATTACHMENT METHODS

FIGURE 7



BERYLLIUM CARBIDE POCKET

ORIGINAL PAGE IS
OF POOR QUALITY

BERYLLIUM CARBIDE FORMATION ON ROTOR FACE

FIGURE 8

ORIGINAL PAGE IS
OF POOR QUALITY.

THE SPACE SHUTTLE ORBITER REMOTE MANIPULATOR POSITIONING MECHANISM

BY J. H. HARDEE

INTRODUCTION

The Space Shuttle Orbiter provides the Manipulator Positioning Mechanism (MPM). Manipulators may be mounted on either left or right sides of the Payload Bay or both sides if two are flown. This Manipulator Positioning Mechanism is provided on purpose of securing the remote arm in stowed position during lift-off, boost and landing, it also provides the deploy, latch and unlatch capabilities of the Remote Manipulator System Arm (RMS ARM). (See Figure 1 and 2).

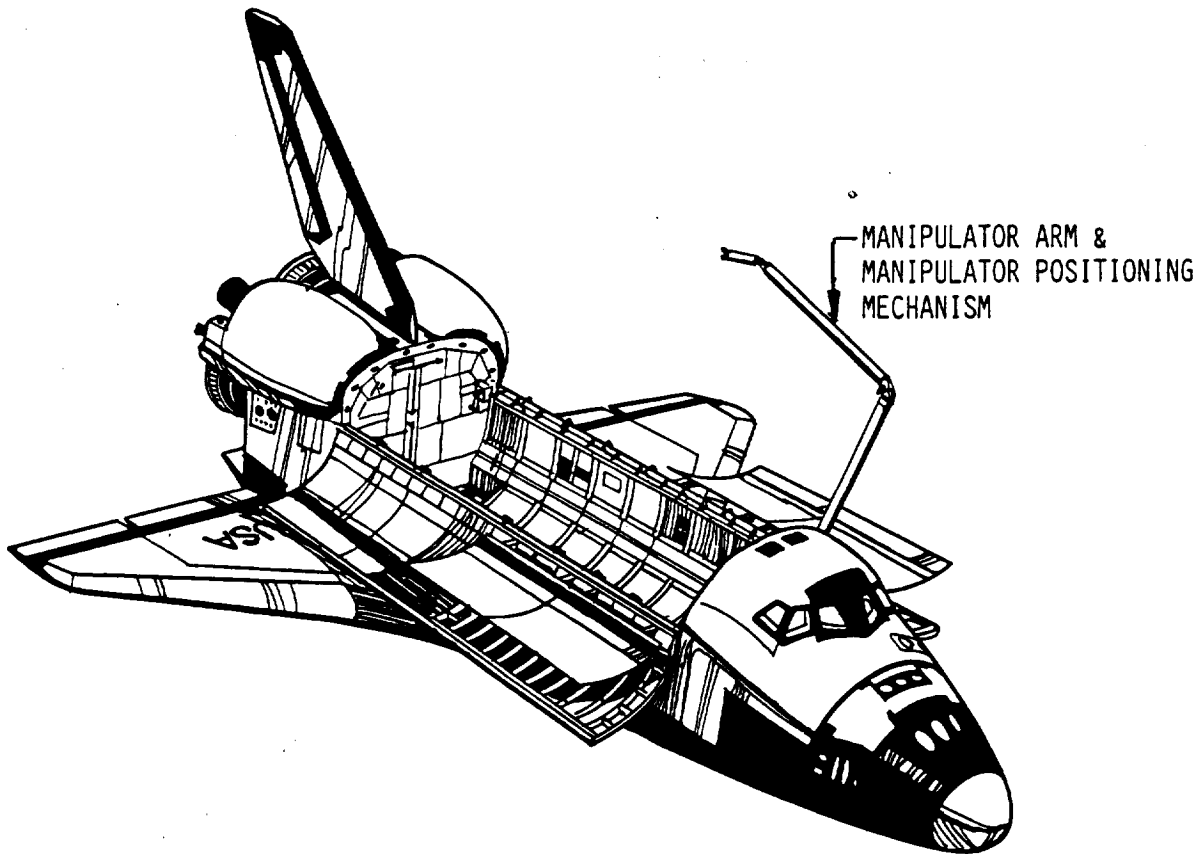


Figure 1. RMS ARM On Its On-Orbit Use Position

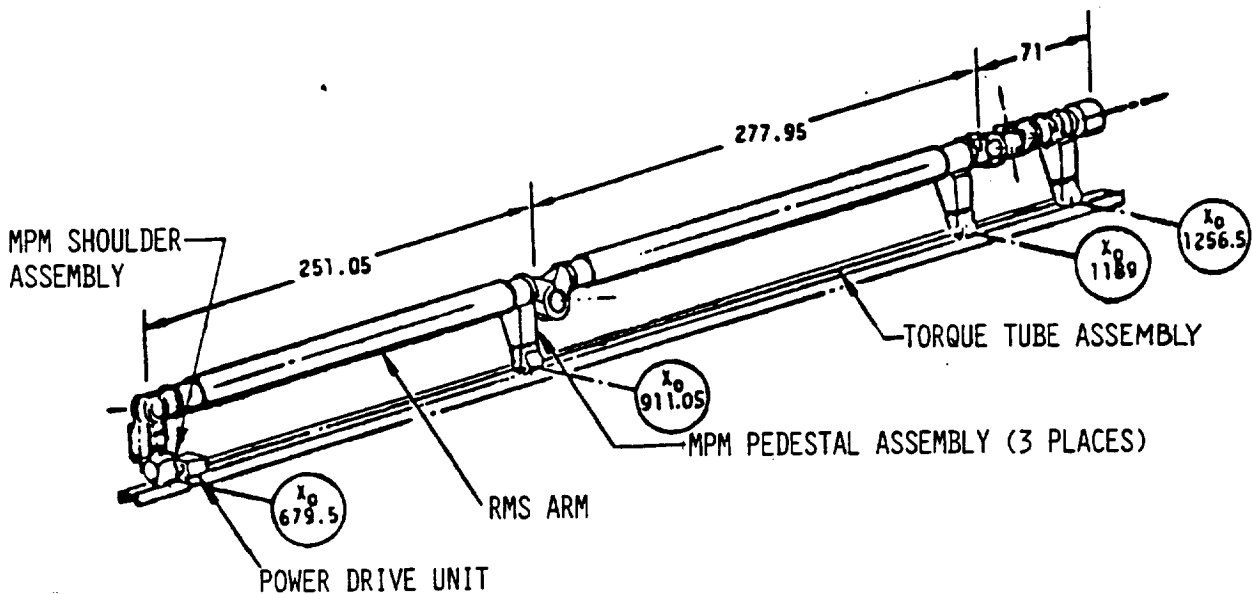


Figure 2. Manipulator Positioning Mechanism - General Arrangement
DESIGN MANIPULATOR POSITIONING MECHANISM (MPM)

The MPM is comprised of the following major assemblies:

- A. Shoulder Assembly - Support of all loads experienced as a result of in flight operation of the arm (See Figure 3).
 1. Electromechanical actuator - gear box, and redundant motor, power drive unit (PDU).
 2. Rotary actuator - planetary gear box.
 3. Base assembly - structural mount to bridge fitting.
 4. Fitting assembly - supporting fitting for RMS.
 5. Drive linkage - mechanical drive from gear box to fitting assembly.
 6. Hook assembly - securing device for deployed position.
 7. Switch Module - deploy and stow indicators.
 8. Retractor - device providing separation capability.
- B. Three Pedestal Assemblies - support of the arm in stowed position and provide latch and unlatch capabilities. (See Figure 4).
 1. Rotary actuator - planetary gear box.
 2. Base assembly - structural mount to bridge fitting.
 3. Fitting assembly - supporting fitting for RMS.
 4. Drive linkage - mechanical drive from gear box to fitting assembly.
 5. Switch modules - ready-to-latch and latch, deploy and stow indicators.
 6. Retractor - device providing separation capability.
 7. Retention latch hook - device providing latch and unlatch capabilities.
- C. Torque Tube Assembly - Drive shaft system providing capability of simultaneous drive on all four assemblies (Shoulder Assembly and Three Pedestal Assemblies).
- D. Thermal Blankets and Covers - Solar Shields.

OF FOUR QUALITY

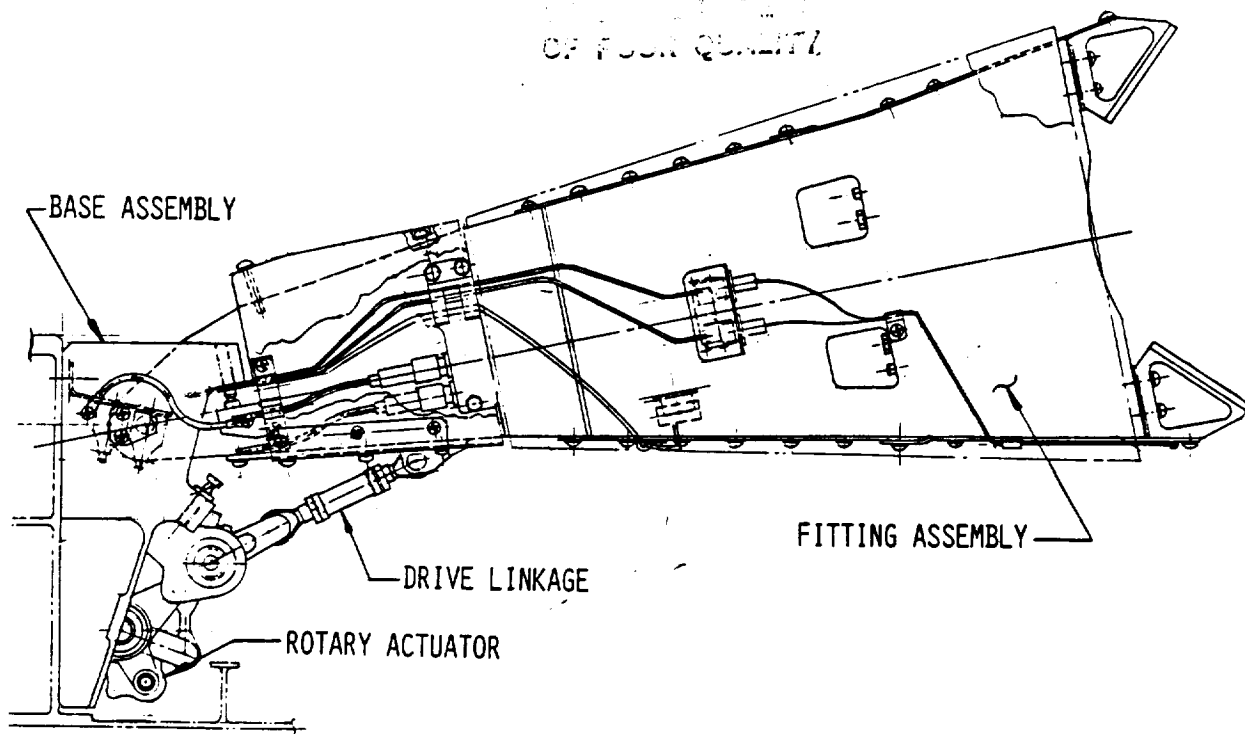


Figure 3. Manipulator Positioning Mechanism Pedestal Assembly
(3 Places)

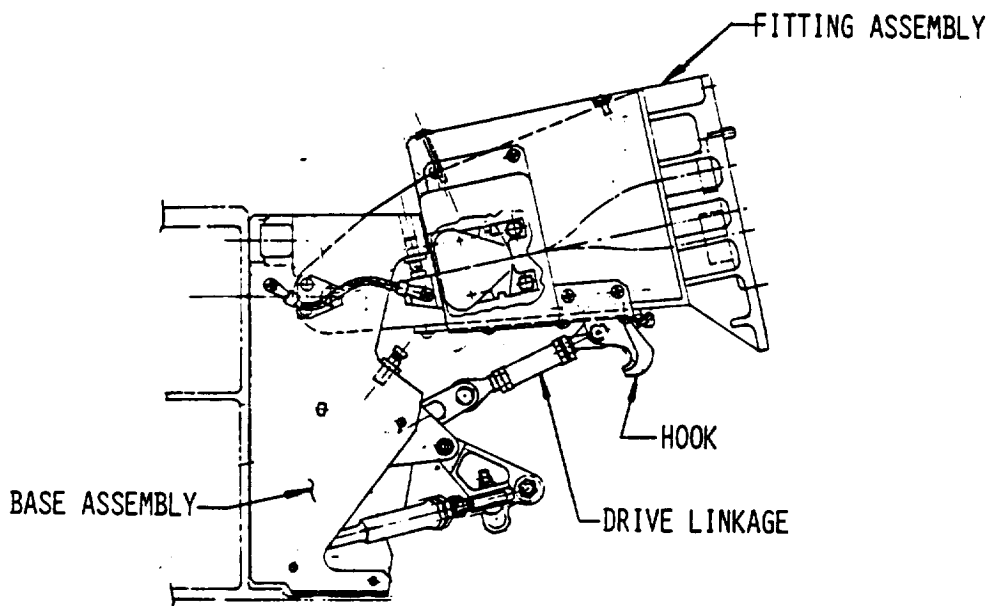


Figure 4. Manipulator Positioning Mechanism Shoulder Assembly

FUNCTIONAL DESCRIPTION

In stowed position, the drive linkage incorporates an overcenter lock to preclude backdrive of the actuation train (See Figures 5 and 6).

The MPM utilizes a single electromechanical actuator which drives through a torque tube to four gear boxes at the manipulator retention locations. Operation of these four gear boxes causes the arm to pivot outward to its on-orbit use position.

Once positioned outboard, the three pedestal assemblies release latches holding the manipulator arm, enabling the arm to articulate and perform its mission function (See Figure 7). On completion of its mission function, the arm articulates to its extended configuration and is rotated back to the locations of the three aft retention systems where they capture and latch the manipulator arm.

All four assemblies (Shoulder Assembly and Three Pedestal Assemblies) then rotate simultaneously to return the arm to its stowed position to allow closure of the Payload Bay Doors for entry.

In case of failures result in inability to stow or latch the arm for entry, a pyrotechnic separation system is provided at each manipulator retention location to allow jettison of the failed components and a safe orbiter configuration for entry (See Figure 8). One possibility to save the system is to stow it manually, this is called Extra Vehicular Activity (EVA).

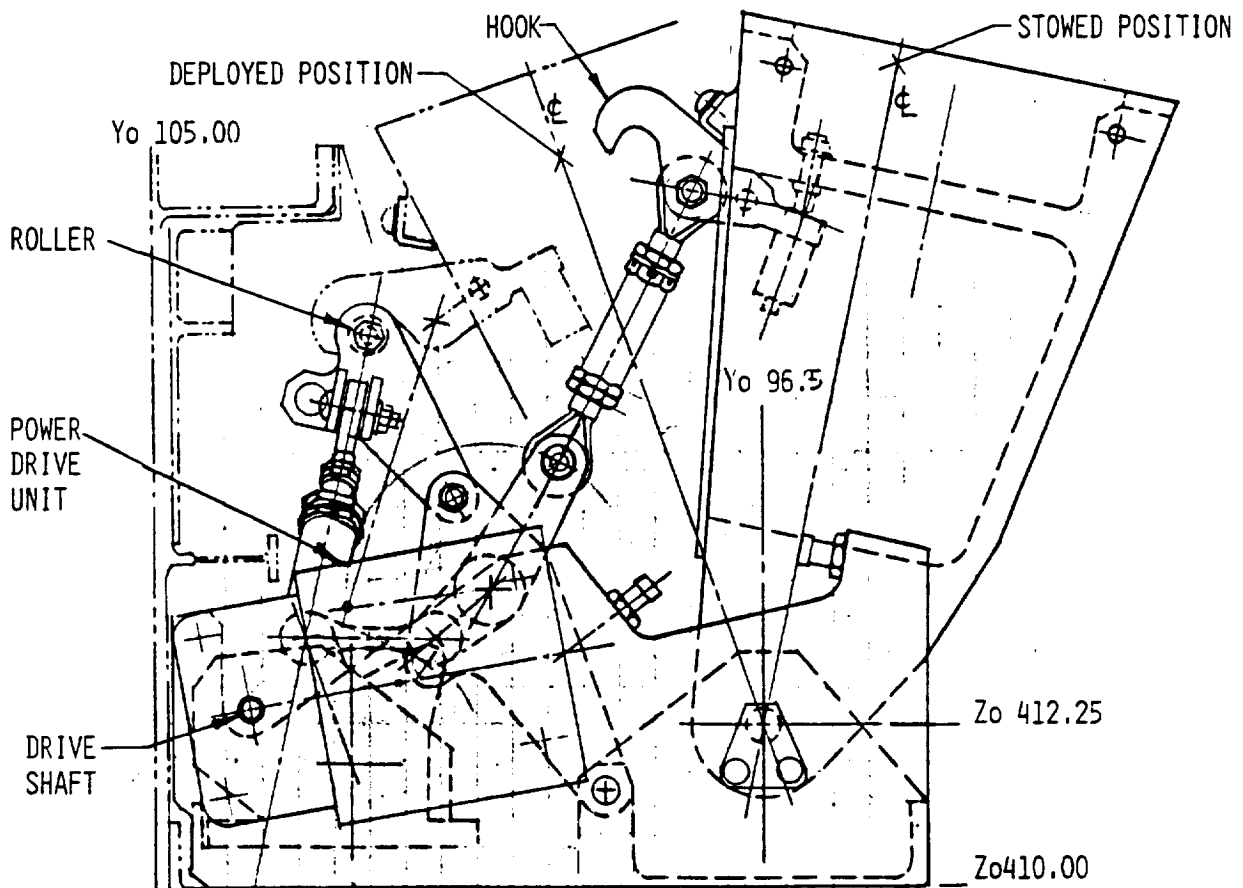


Figure 5. Shoulder Support - Stowed and Deployed Positions

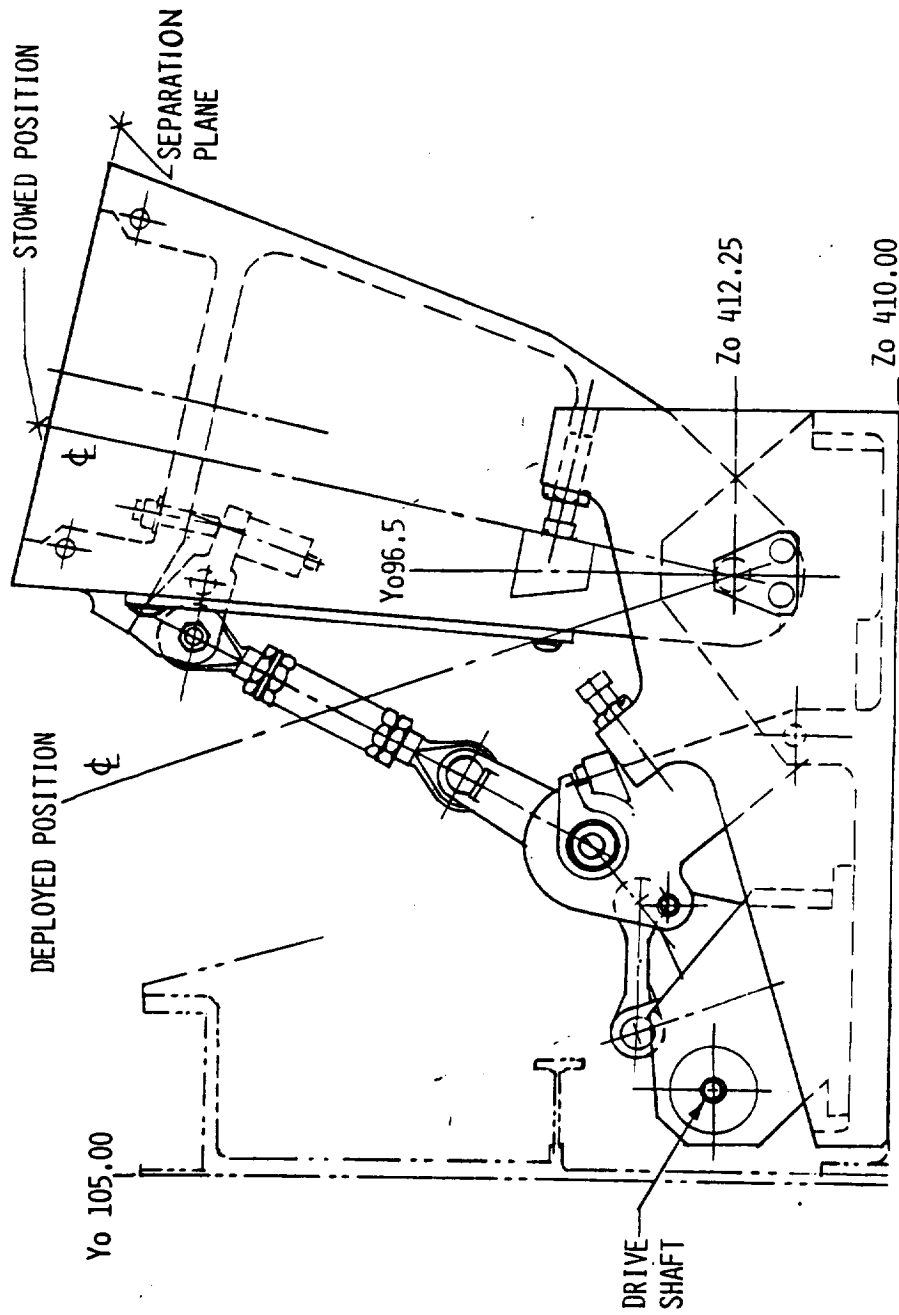


Figure 6. Retention Support - Stowed and Deployed Positions

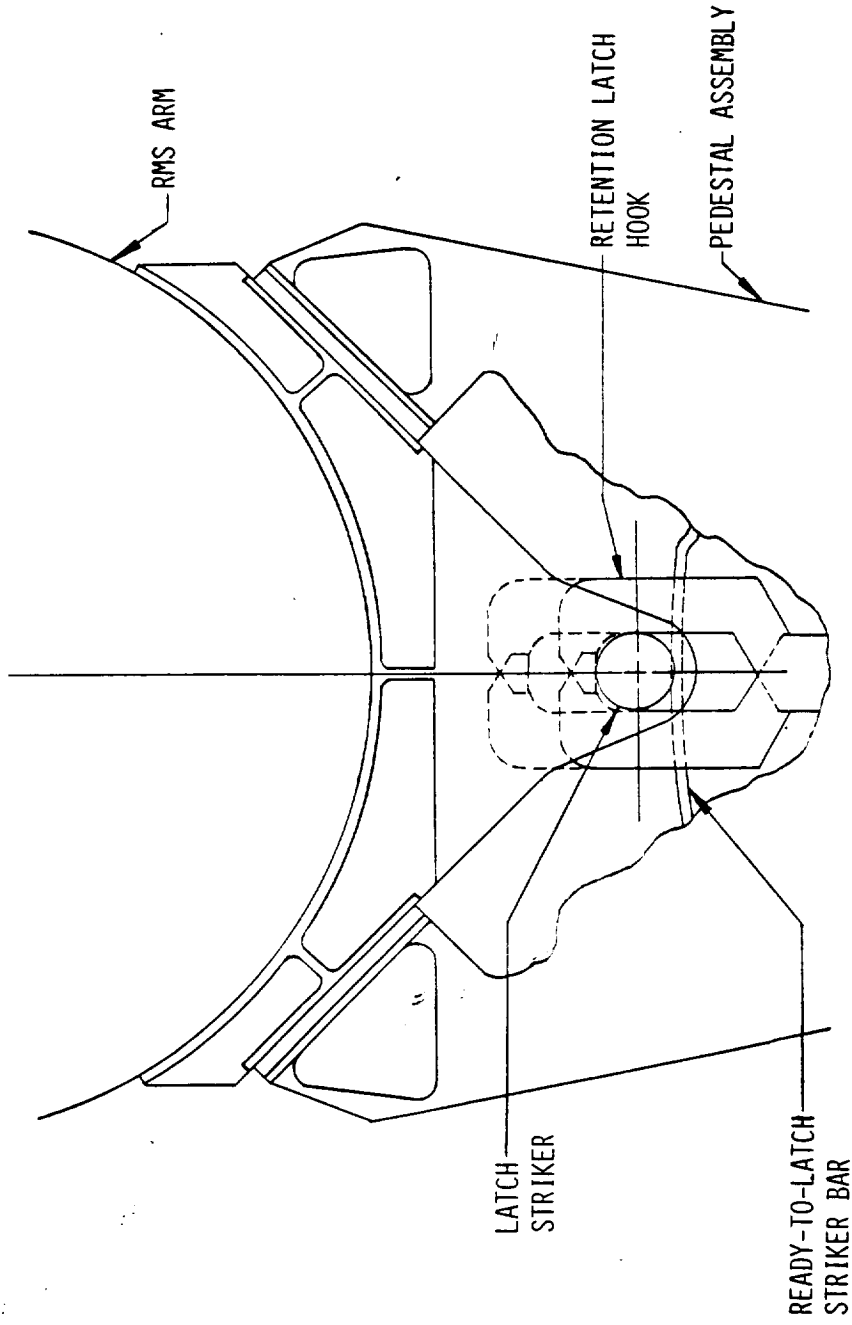


Figure 7. Manipulator Positioning Mechanism Latch and Unlatch Capabilities of RMS ARM

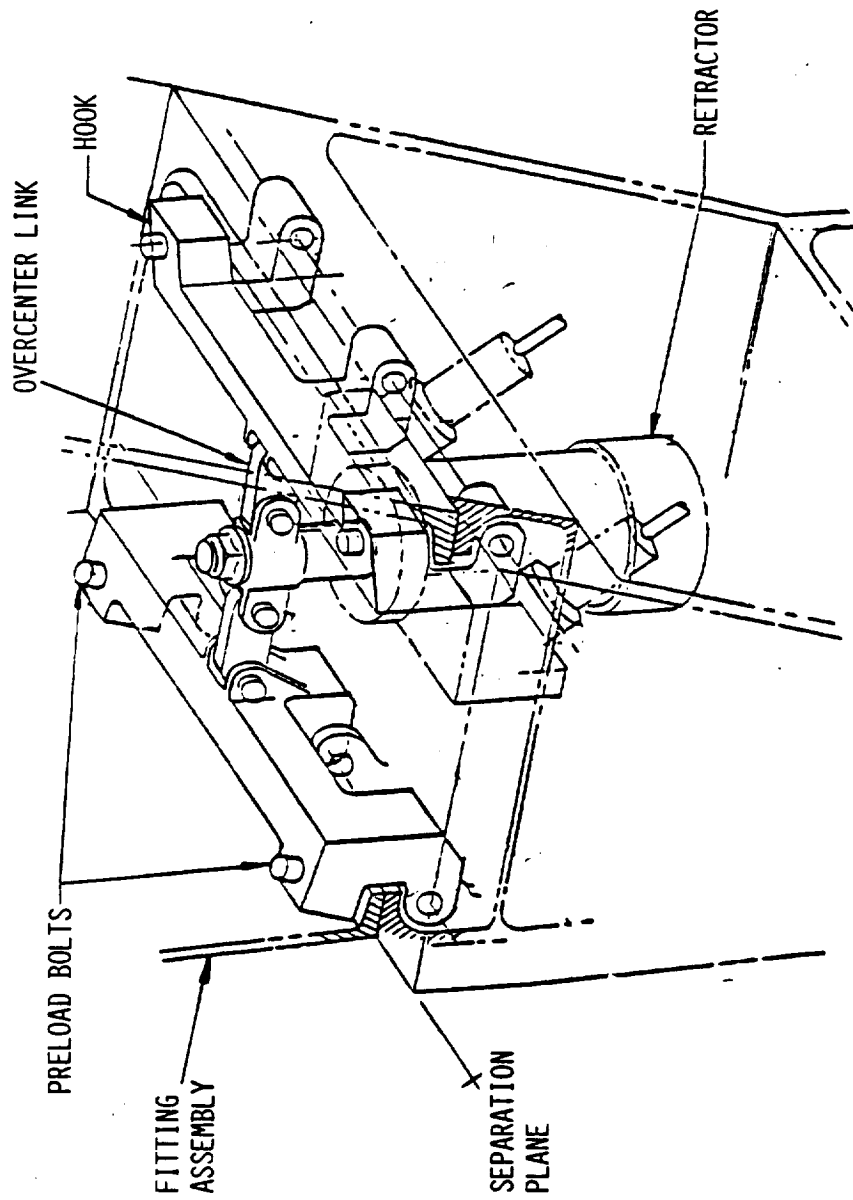


Figure 8. Manipulator Positioning Mechanism Separation System.

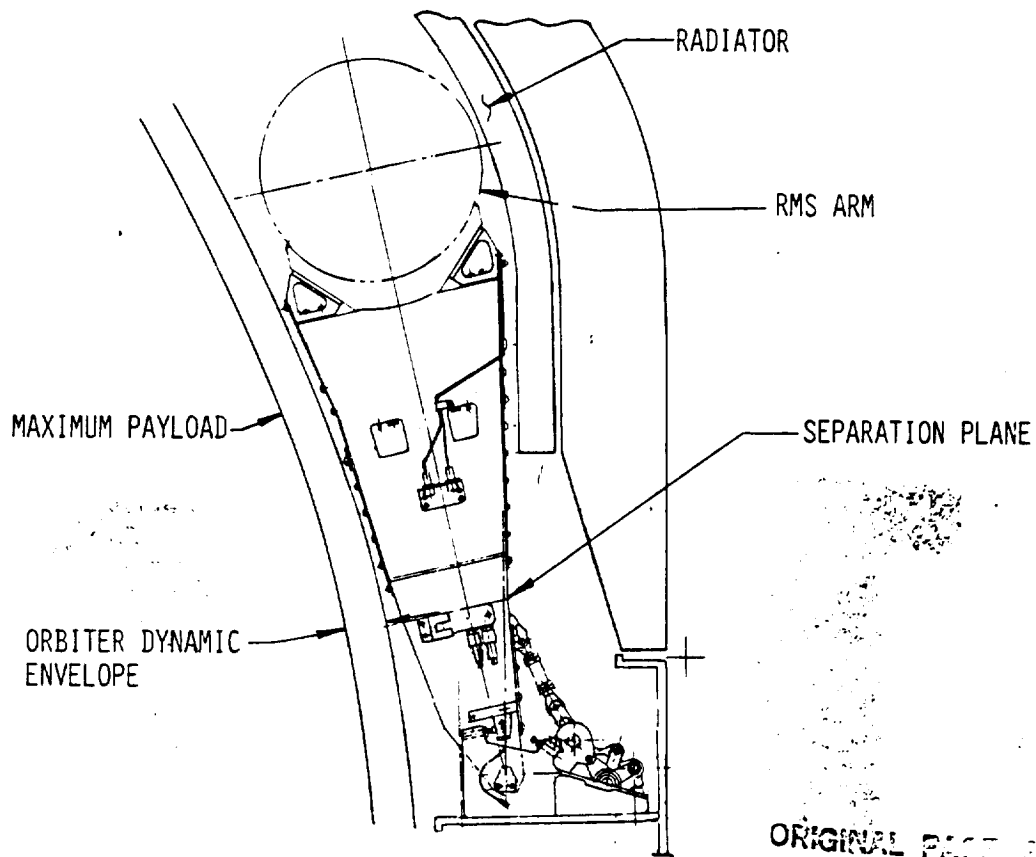


Figure 9. RMS/MPM Envelope

ORIGINAL PAGE IS
OF POOR QUALITY

DESIGN - RETENTION LATCH HOOK

Requirements

- o Secure Manipulator Arm in stowed position.
- o Lift-Off, boost and landing.
- o Latch & Stow capability of RMS Arm after usage.

Latch Design mechanically compatible with RMS Arm design & operation.

- o Latch Envelope - 0.875 - In. "Z" & \pm 1.50 - In. "Y" Axis.
- o Final travel of hook motion to be straight be straight line.
- o Z-Axis loading - approximately 2000 Lb.
- o Y-Axis Loading on hooks during latchup -150 Lb.
- o Operational time -7.5 sec, dual motors; 18 sec, single motor.

Reliability

- o Latch driven by redundant motors.
- o Dual rotating surfaces.

ORIGINAL PAGE IS
OF POOR QUALITY

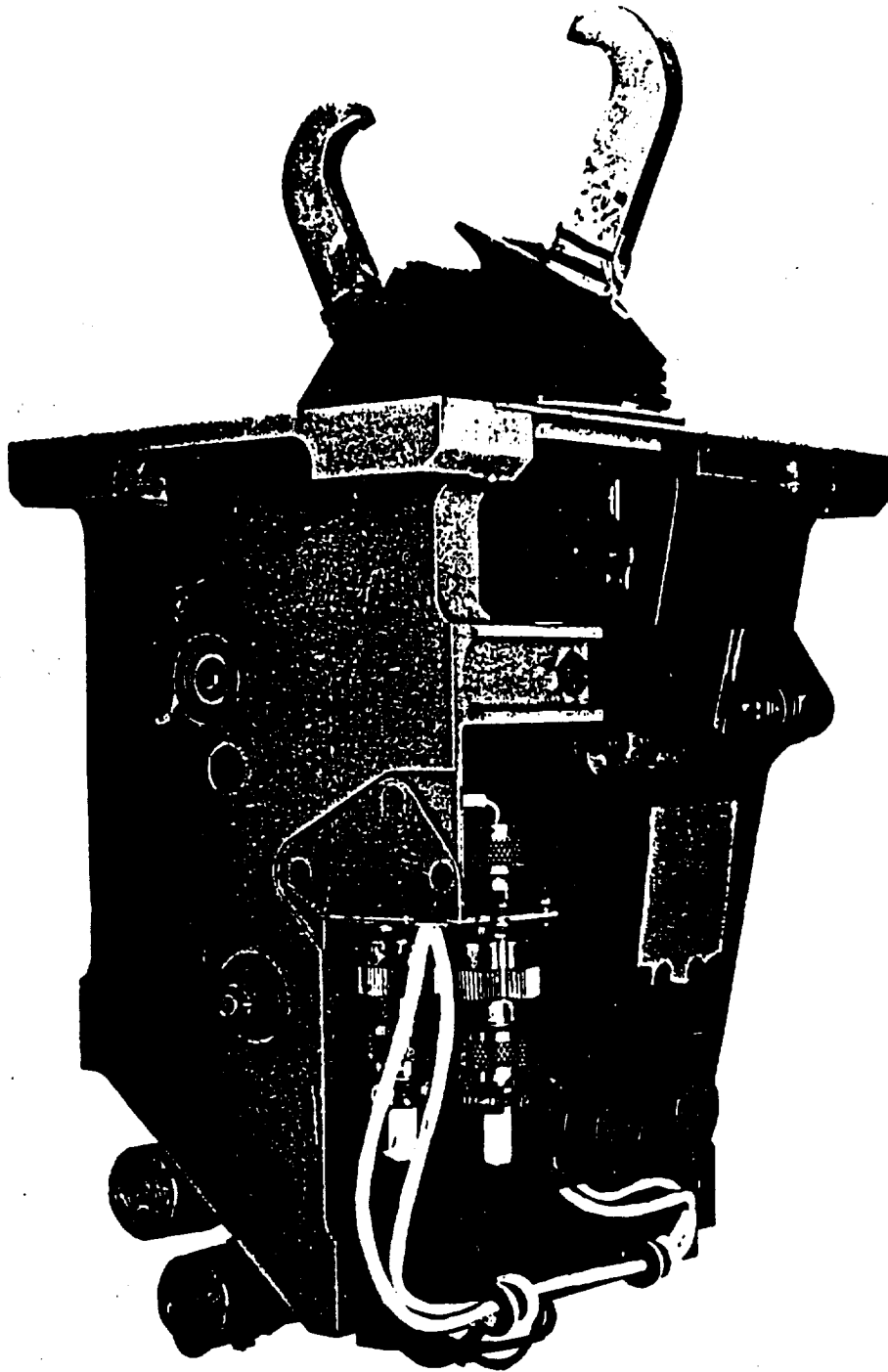


Figure 10. Manipulator Retention Latch

D27
N85-16964

AN OVERVIEW OF THE SHUTTLE REMOTE MANIPULATOR SYSTEM

T.H. Ussher
Director, Programs, Remote Manipulator Systems Division
Spar Aerospace Limited

K.H. Doetsch
Assistant Director, National Aeronautical Establishment
National Research Council of Canada

ABSTRACT

The development of the Shuttle Remote Manipulator System (SRMS) was the result of a cooperative program between the National Research Council of Canada, Spar Aerospace Limited (Prime Contractor) and NASA. The requirement to provide a six degree-of-freedom, remotely controlled manipulator for cargo deployment and retrieval during on-orbit operations of the Space Shuttle orbiter vehicle presented challenges in design, development, manufacture, test and program management, any one of which could be described in a paper in its own right.

This paper, however, presents an overview of the system requirements and performance of the SRMS, and provides data on some of the mechanical design considerations that were necessary during the development program.

The operational success of both the Orbiter and the SRMS during flights STS-2, -3 and -4 is ample evidence that the SRMS performed as expected and as desired.

While some minor improvements have been made in the follow-on production systems, one of which has been delivered and two are currently under construction, the system design has not changed significantly from that of the DDT&E hardware. Therefore, this paper is applicable to all four systems eventually to be operated by NASA.

PROGRAM DESCRIPTION

During the late 1960's, when the Apollo program was nearing completion, NASA approached the Government of Canada to determine if there was an interest by Canada in participating in the development of the Space Shuttle. Canada had an interest in remote manipulator systems, often referred to as tele-operators for operation in hostile environments such as underwater, nuclear power plant maintenance, arctic operations and mining. The National Research Council of Canada (NRCC) was selected as the government agency to interact with NASA. A memorandum of understanding was signed in July, 1975 between NASA and NRCC for the design, development, test and evaluation (DDT&E) of the SRMS. Spar and its industrial team members was chosen by NRCC as the prime contractor for the Canadian-funded DDT&E program. One of the more significant activities during the early design period (1975-1976) was to develop the system requirements, since there was no contract end item specification (CEI) in place. Spar and its subcontractors, DSMA ATCON (special ground handling and system test equipment), CAE Electronics Ltd., (display and control subsystem) and RCA Canada Ltd., (arm-based electronics) started work to define system requirements, subsystem specifications, statements of work and commence the control system design. Work proceeded towards a preliminary design review held in September, 1976, followed by a critical design review in April, 1978. Management of the program was controlled by Spar Aerospace Ltd. on behalf of NRCC, and a multi-agency Joint Review Board was set up to provide schedule review, program guidance, technical discussion and inter-agency coordination between NRCC, NASA (JSC, KSC, HQ), Rockwell International and Spar.

SYSTEM DESCRIPTION

System Requirements

The manipulator arm was to occupy a volume no larger than 50 ft. in length overall and having a 15 in. dynamic envelope. The overall system weight, including the display and control subsystem, closed-circuit television (CCTV), and manipulator controller interface unit (MCIU) was to be no more than 994 lb. The system was required to manoeuvre a "design case" payload of 32,000 lb. having dimensions 15 ft. in diameter and 60 ft. long. The maximum weight payload to be deployed (and

retrieved in a contingency operation) was 65,000 lb. A significant design problem immediately encountered was to develop a servo control system which would be stable under all loaded and unloaded arm conditions where the moment of inertia varies by a factor of approximately 10^6 . Further, a 32,000 lb. payload attached to the arm and translating at a velocity of 0.2 feet per second was required to be brought to rest within 2 feet. The unloaded arm had to achieve the same stopping distance criterion, but under a translational velocity of 2.0 f.p.s.

The initial design concept was a fail operational - fail safe system which required system redundancy, particularly in the joint motor drive. This resulted in a considerable weight penalty, and a decision was made in the early stages of the program to design a system that was fail safe only. This resulted in an overall system weight of approximately 950 lbs, or 44 lbs. under the specified control weight limit. Methods of redundancy, other than those requiring dual drive systems and dual electronics were incorporated.

The entire system has been designed to have a ten-year operational life, or the equivalent of 100 orbiter missions. Hence, considerable attention was paid to providing adequate margins in both the electrical-electronic and the mechanical systems. A mission, from an RMS standpoint, required the deployment and capture/berthing of up to 5 payloads.

System Configuration

Figure 1 shows the arm in diagrammatic form. It has a total of six degrees-of-freedom. A shoulder pitch and yaw joint, an elbow pitch joint and wrist pitch, yaw and roll joints. The shoulder and elbow joints are connected by a lightweight carbon composite boom approximately 13 in. in diameter and with a length of 16 ft. This is designated the upper arm boom. The lower arm boom, connecting the elbow joint output flange to the wrist forward electronics compartment, is 13 in. in diameter and approximately 19 ft. long. There are four major attachment points to the orbiter longeron; the main Manipulator Positioning Mechanism (MPM) for the arm is at the shoulder yaw pedestal, where a jettison system and cable cutter allows the arm to be separated from the orbiter in the event of a significant malfunction which would prevent stowage of the arm and closing of the payload bay doors. Three manipulator retention latch mechanisms (MRLs) support the arm at the elbow, wrist pitch and wrist roll electronics compartments. The MPM and MRLs roll inboard to allow payload bay doors to close. Further, the MRLs exert a force of about 2000 lb. on each latch roller on the arm, thus holding the arm firmly in position during launch.

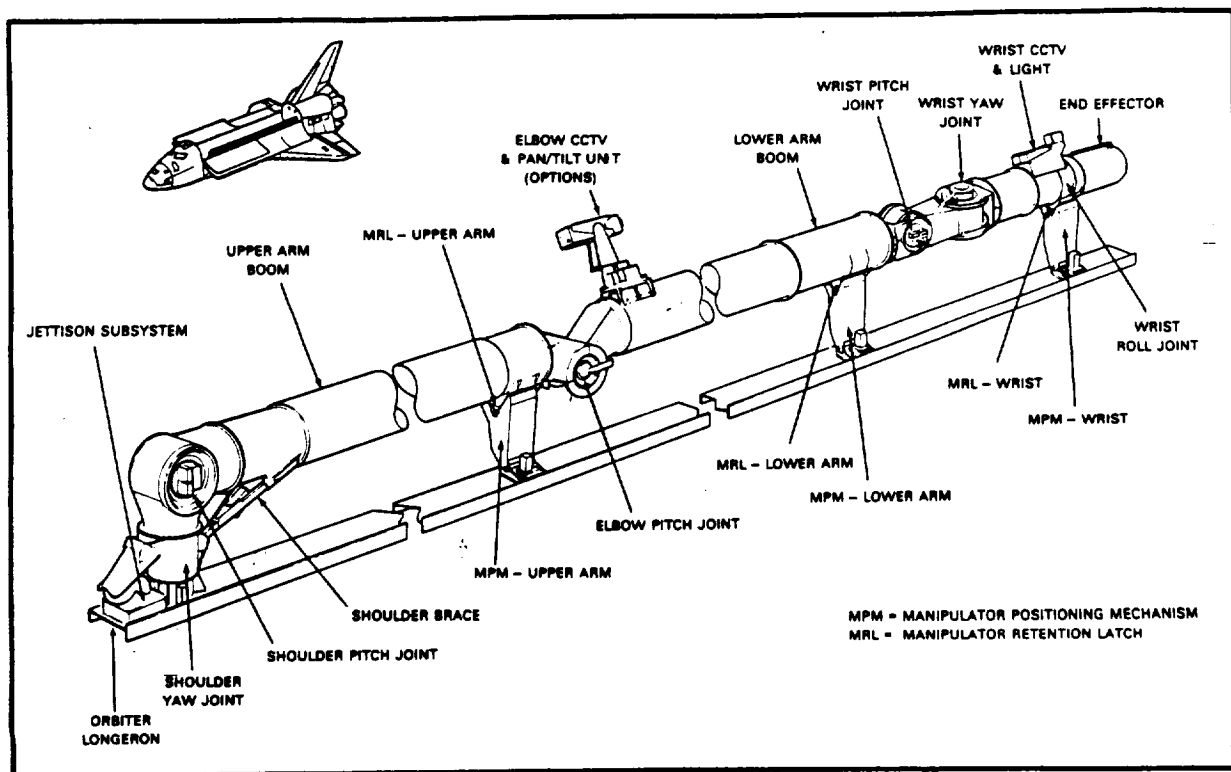


Figure 1 Manipulator Arm Configuration

Two CCTV cameras are located on the arm. The elbow camera has provision for pan, tilt and zoom and provides general payload bay, arm and payload viewing. The wrist camera is located on the wrist roll joint and rotates with that joint. Its purpose is to assist the mission specialist in manoeuvring the end of the arm (the end effector) over the payload-attached grapple fixture. The arm is covered over its entire length with a multi-layer insulation thermal blanket system which provides passive thermal control. This material consists of alternate layers of goldized Kapton, Dacron scrim cloth and a Beta cloth outer covering. The thermal blanket provides passive thermal control during most mission conditions, although during extreme cold case conditions, thermostatically controlled electric heaters (resistance elements) attached to critical mechanical and electronic hardware can be powered on.

The display and control subsystem provides the interface between the mission specialist and the RMS. Figure 2 shows the D&C panel and the translational and rotational hand controllers. The translational hand controller provides X, Y and Z translation at the tip of the arm, while the rotational hand controller provides pitch, yaw and roll commands, and is used primarily to manoeuvre the wrist joint. The D&C panel provides caution and warning information, mode of operation and arm health and status, commanded and actually achieved rates, digital readout information of individual joint angles or the end effector position in relation to a chosen coordinate system. Selection can also be made of various operating modes, automatic sequences and end effector operations.

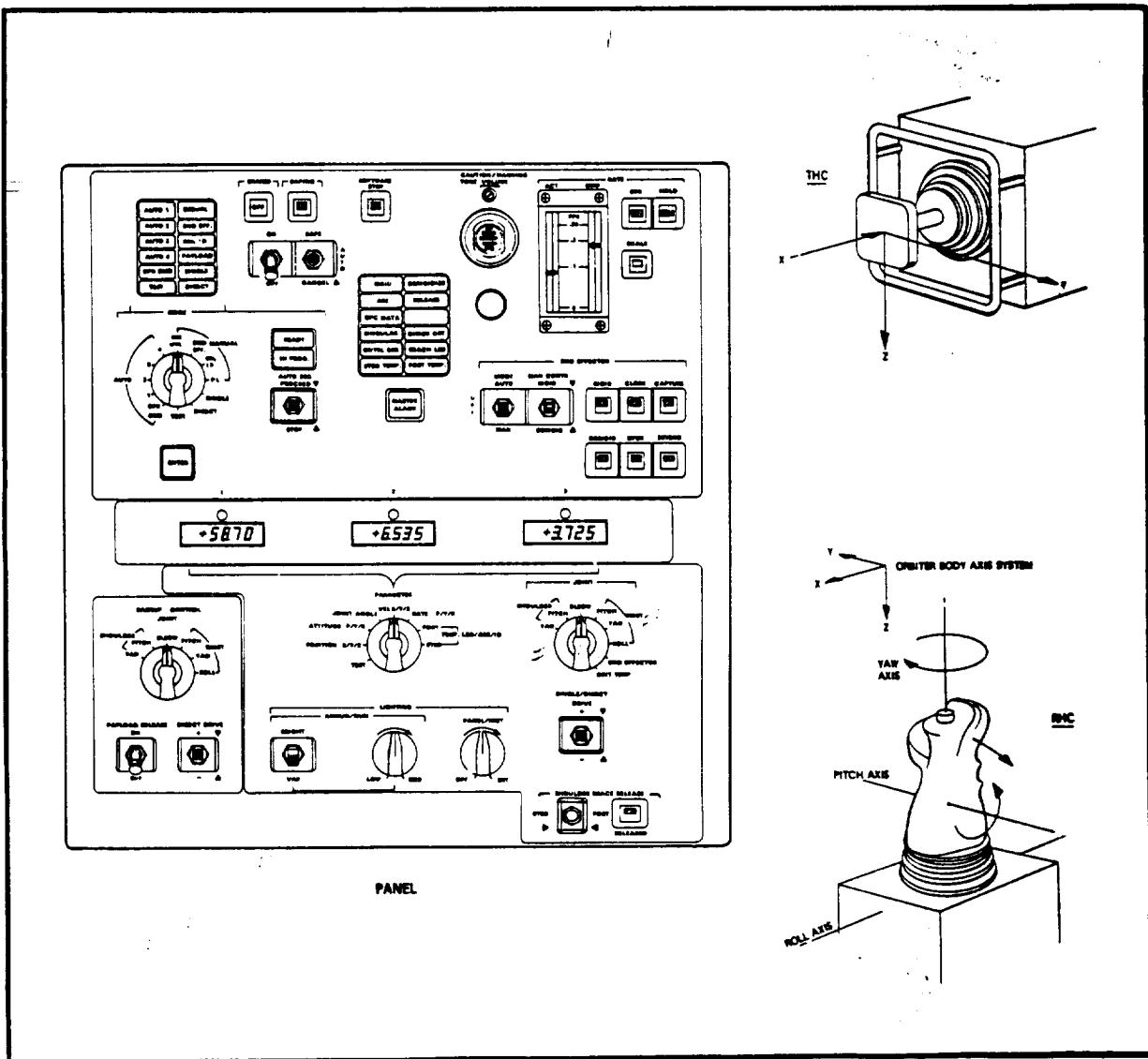


Figure 2 Display and Control Panel, and Hand Controllers

Electrical Subsystem

A block diagram of the electrical subsystem is shown in Figure 3. The interface between the orbiter general purpose computer (GPC) and the manipulator arm is via the Manipulator Controller Interface Unit (MCIU). Hand controller signals from the translational and rotational hand controllers are fed to the MCIU which then routes these commands to the GPC. The GPC provides reformatted commands back to the arm via the MCIU. A serial digital data bus routes commanded rates to the arm based electronics servo power amplifiers (SPA) which provide drive power to the joint motors. The GPC communicates with the MCIU every 80 ms, exchanging command and response data in this time frame. The MCIU also provides automatic safety features to protect the arm under certain operating conditions.

The software which controls the arm is resident in the GPC. There are ten software modules which perform command calculations, interface with the THC and RHC commands, provide drives for flags, meters and other annunciators, actuate the digital displays and provide caution and warning information. In the automatic mode of operation the GPC provides four preprogrammed automatic end-of-arm trajectories. Keyboard access also provides additional operator-derived automatic sequences which, when loaded in the computer, command the tip of the arm to move in a predefined trajectory.

There are six servo power amplifiers, one per joint servo motor. The shoulder electronics compartment contains two SPAs for the shoulder pitch and yaw joints plus a Joint Power Conditioner (JPC) essentially a DC-to-DC converter which supplies the various secondary bus voltages needed by the shoulder and elbow SPAs; a Backup Drive Amplifier (BDA) is also located in this compartment. The BDA is a replica (in part) of the servo power amplifier, but is used to command one joint at a time via a toggle switch on the D&C panel when the system is operated in the backup mode during contingency operations. The elbow electronics compartment contains a single SPA to drive its joint motor, while the wrist forward compartment houses the pitch and yaw SPAs and a single JPC; the wrist roll electronics compartment contains the SPA for that joint motor.

The arm is supplied with 28 volts nominal DC power and the D&C panel is provided with both DC power and 400 Hz, 115-volt, single phase AC power for lighting. During operation, the SRMS requires a maximum of 1 kilowatt of 28 volt DC for drive power, and a maximum of 1050 watts DC power for thermal control. In addition, 150 VA of 115-volt, 400 Hz, AC power at a power factor of 0.75 is provided for lighting control of the edge-lit D&C panel.

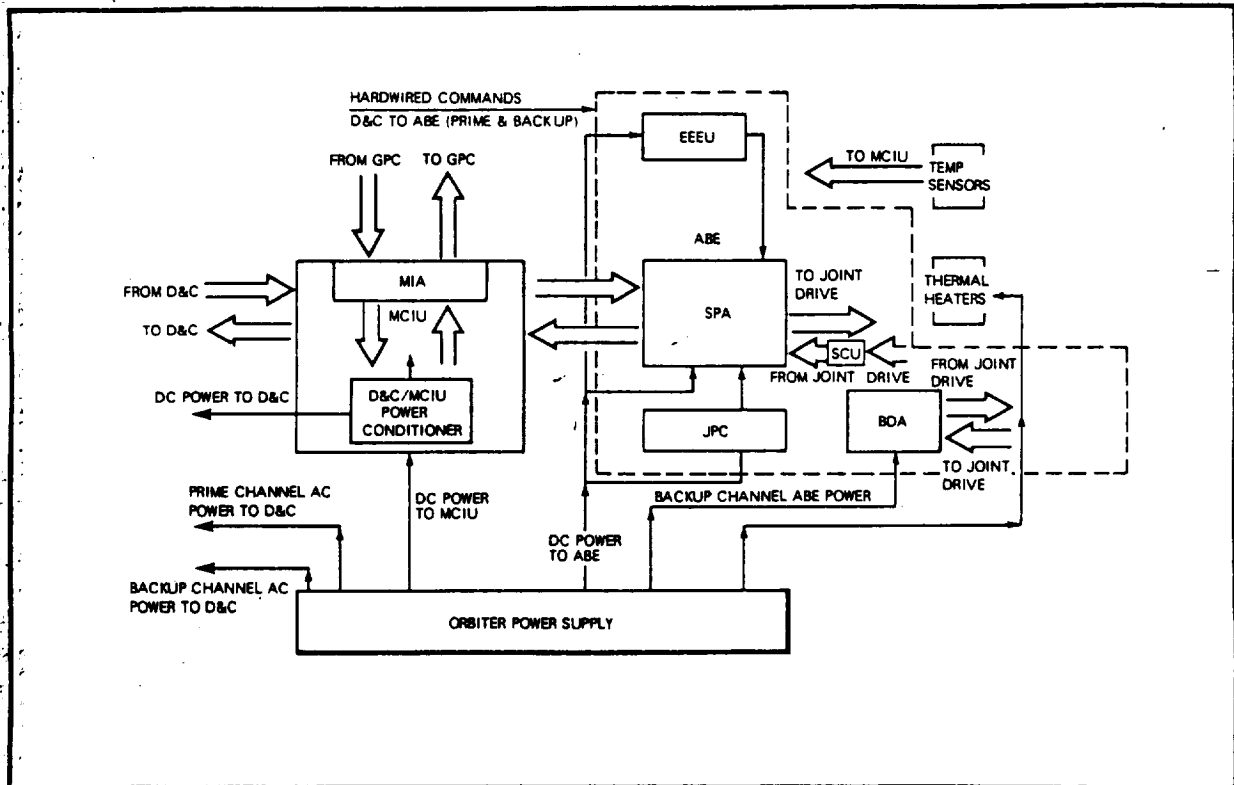


Figure 3 SRMS Electrical Subsystem Block Diagram

System Operating Modes

The SRMS can be switch-selected to operate in four standard modes. Three of these are supported by the GPC, that is, the commanded rate is fed to the joint SPAs via the serial data bus, and all joint operating commands to provide end point control of the RMS are carried out through calculations performed within the SRMS software resident in the orbiter GPC. The primary embodiment of this operating mode is in Manual Augmented. In this mode, the operator uses the two hand controllers to "fly" the end of the arm. Translational commands provided by the THC and rotational commands provided by the RHC are fed to the GPC via the MCIU whereupon the GPC performs a resolved rate algorithm calculation which provides serial control of each joint independently, although such joint-by-joint drive is not apparent to the operator. The servo system, shown in Figure 4, provides rate and position data at all times; two rate loops are used, an analog loop to maintain stability of the servo system itself, and a digital rate loops which is used to generate a rate error signal between the achieved and commanded rates.

Alternative modes of operation of the arm are available in (a) Single Joint control, wherein full GPC support is provided but the individual joints are controlled on a joint-by-joint basis, by applying a fixed drive signal to the control algorithms via a toggle switch on the D&C panel; this mode, rate commands are provided to drive the select joint while maintaining joint position control of unselected joints; (b) Direct Drive wherein the GPC is bypassed and a fixed rate command is supplied to the SPA motor drive amplifier summing junction via a toggle switch on the D&C panel and individual joints are driven on a joint-by-joint basis as selected on the D&C panel; (c) Automatic mode of operation, where the hand controllers are not used, all commands being generated by the GPC itself based on prestored or operator commanded (keyboard entry) auto sequence programs. Up to four preprogrammed auto trajectories may be selected using a selector switch on the D&C panel. GPC stored control algorithms output joint rate demands to obtain the required end effector position.

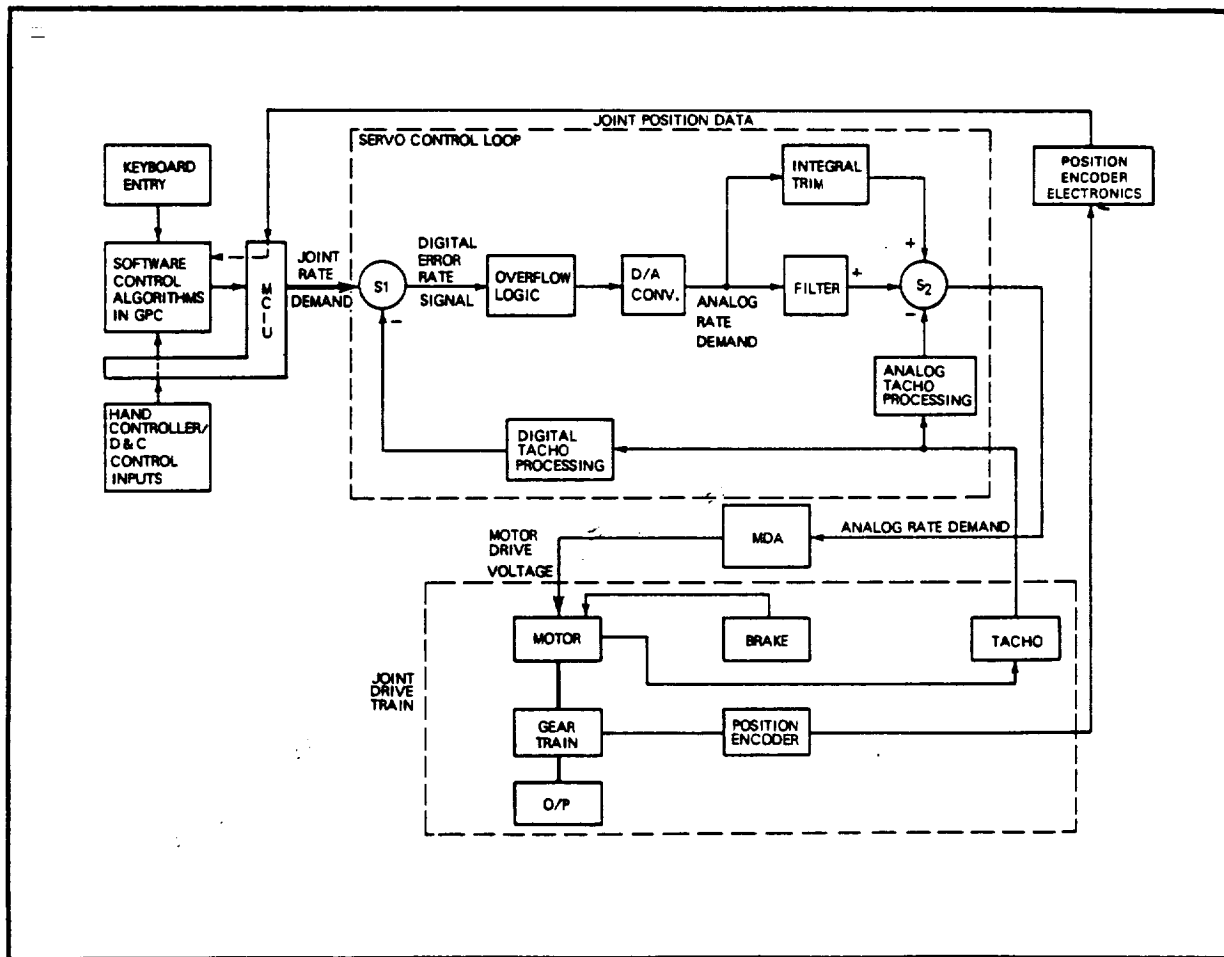


Figure 4 System Block Diagram - Typical Joint

MECHANICAL CONSIDERATIONS

Joint Design

Each SRMS joint is powered by an optically commutated, brushless DC motor providing a stall torque capability of 100 oz/in and a no-load speed of approximately 90 radians per second. Dual commutator electronics are used to provide redundancy in the sensitive area of the motor. Each motor is driven by an SPA which provides a pulse width modulated signal to the three motor windings. The command to the SPA via the serial data bus is a rate error signal, being the difference between the operator commanded rate and that rate fed back from the digital or low speed rate loop. The rate signals for feedback are obtained from an inductosyn tachometer mounted on the motor shaft. To obtain the high joint output torque needed from the relatively low motor torque available, an extremely high precision, high reduction gearbox with an epicyclic/planet system is used. Figures 5 and 6 show the joint motor and a cutaway of the shoulder pitch and yaw joints. The motor has its own internal gear train called the G1 which, through an output pinion, interfaces with the G2 of the main joint drive gear train system. All joints must be backdrivable; virtually zero backlash is demanded to maintain positioning accuracy and servo stability. Figures 7 and 8 show the general arrangement of the elbow and wrist joints. Dry type lubrication as opposed to the more traditional wet lubrication is used to maintain low friction and long lubricant life under the relatively low speed, high loading conditions experienced in the gearbox. Although these were mechanical design challenges presented early during the development phase, the gearbox has proven to be an extremely precise and trouble-free element of the overall design. A mechanical disc-type joint brake is provided as an integral part of the motor, and is used for maintaining the position of a joint during direct drive joint operation, and when the software-derived position hold mode is non-operative. Position information is obtained from an optical encoder with 16 bit resolution which provides precise joint angular position data. This is used as part of the overall joint control system, primarily when the arm is in the position hold mode as well as providing joint angular positions which are displayed by digital read-outs on the D&C panel.

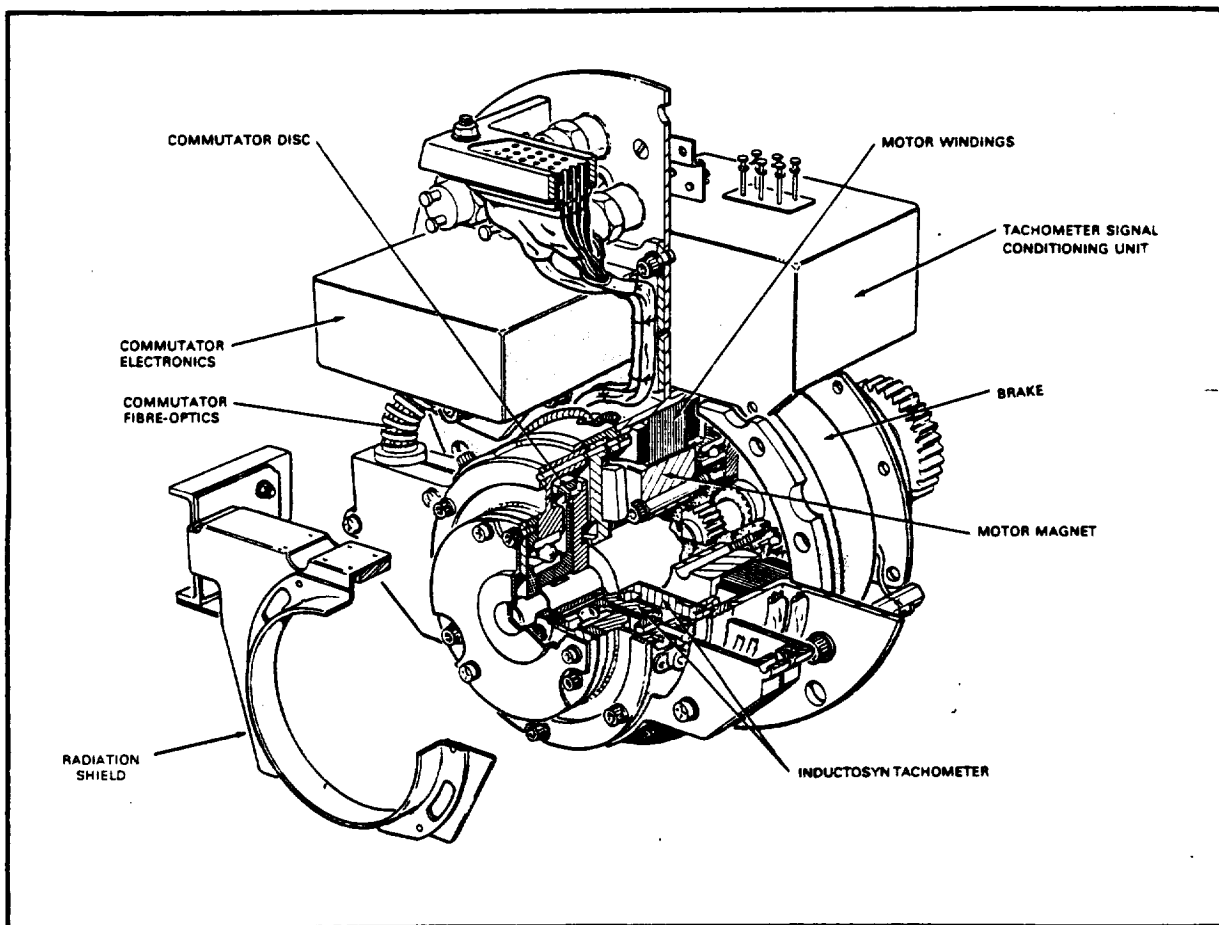


Figure 5 Motor Module Configuration

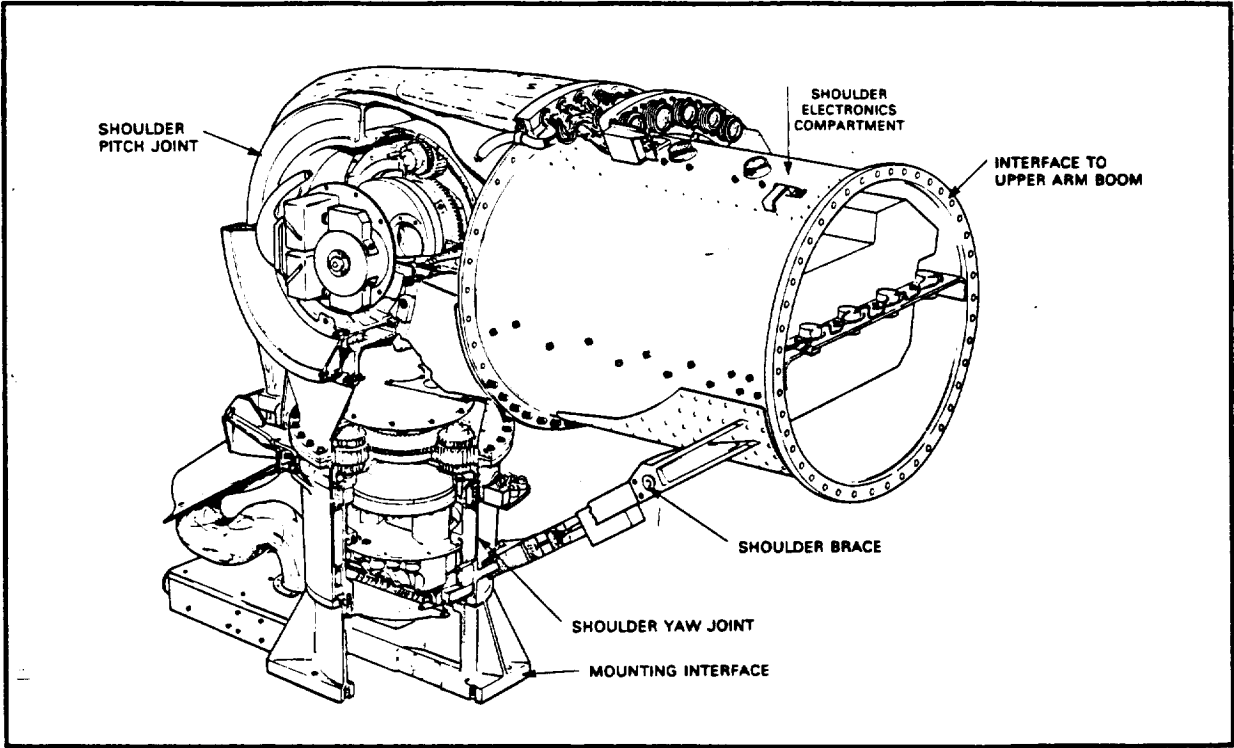


Figure 6 Overall Configuration of the Shoulder Joint

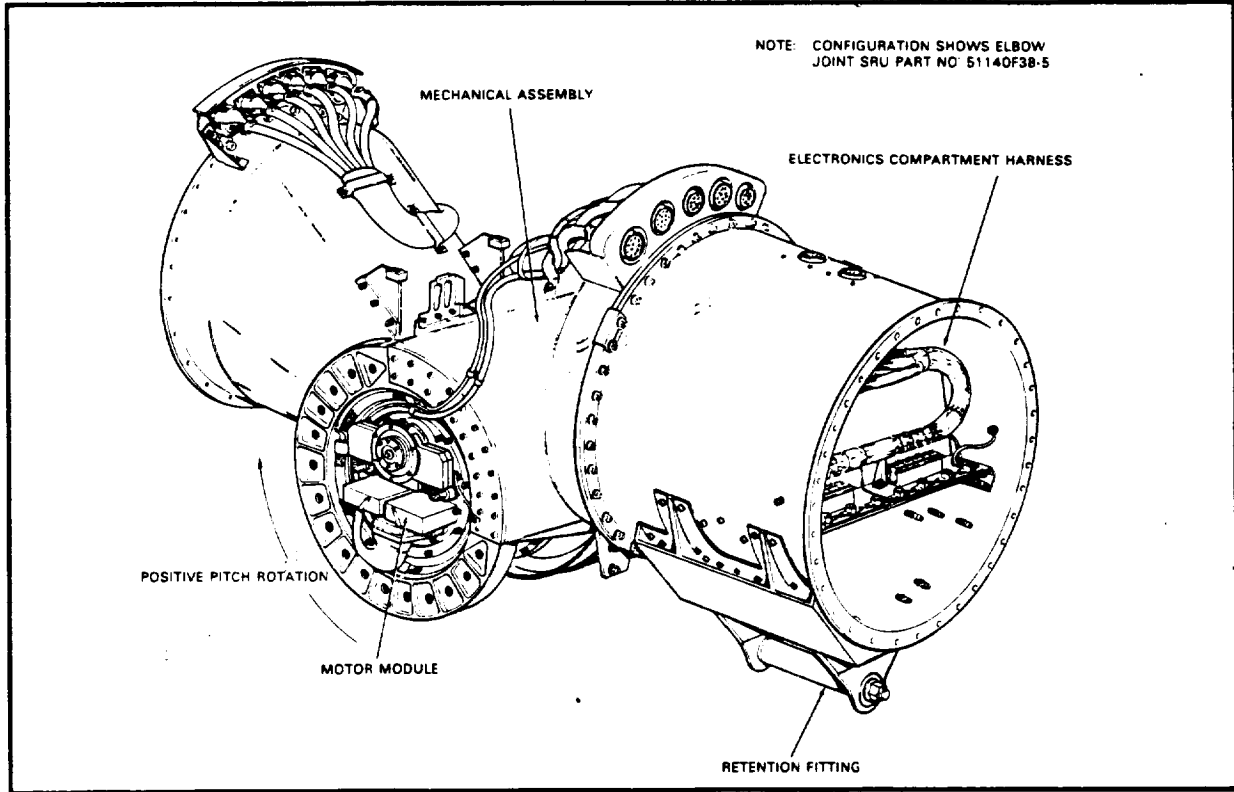


Figure 7 Overall Configuration of the Elbow Joint

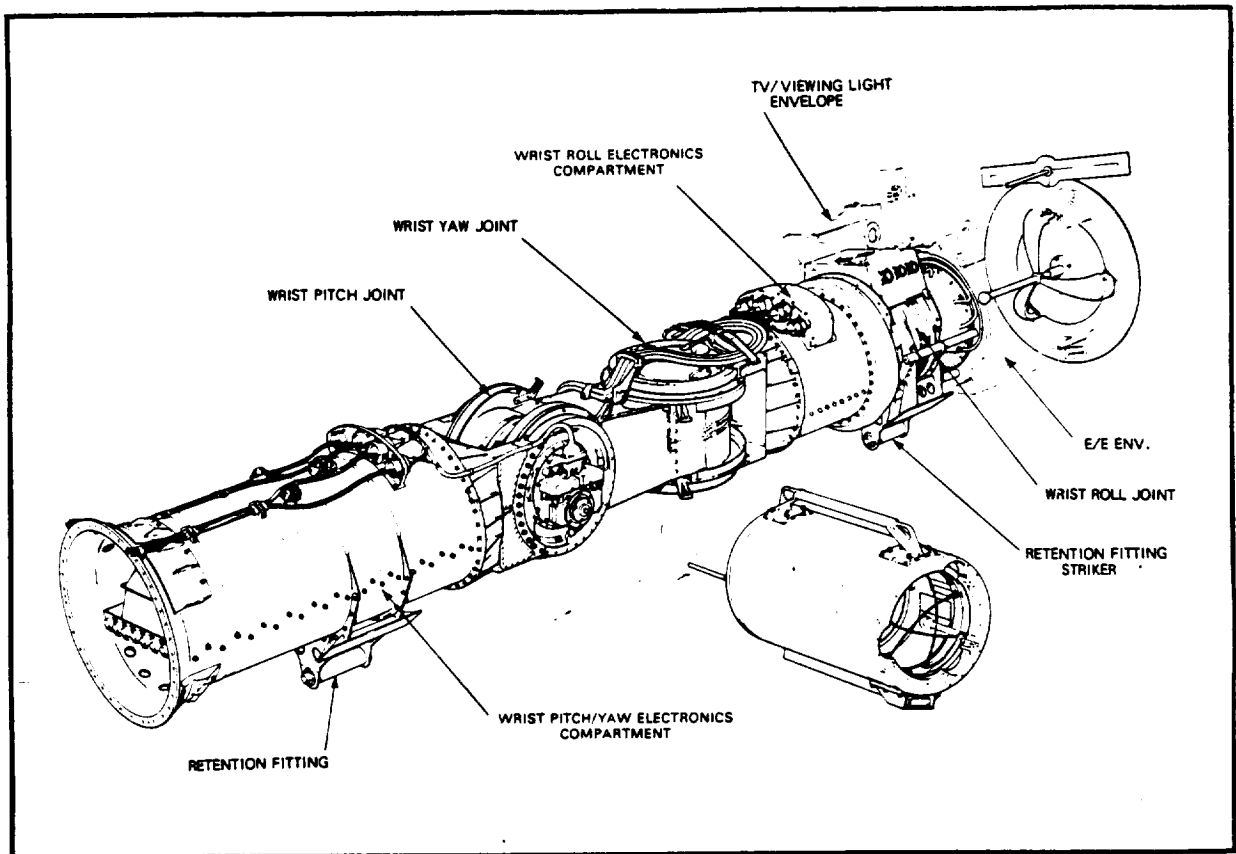


Figure 8 Overall Configuration of the Wrist Joint

Structural Considerations

Structural considerations during the design addressed the need to maintain adequate strength along the arm while minimizing arm weight. As a result, the output torques from each of the joints are graduated in descending order from the shoulder out to the wrist joint. Joint output torques and angular rotation limits are shown in Table 1 below.

TABLE 1		
Joint	Output Torque, ft-lbs	Maximum Angular Rotation, degrees
(a) Shoulder Pitch	1,158	-2, +145
(b) Shoulder Yaw	1,158	+180
(c) Elbow Pitch	792	+2.4, -161
(d) Wrist Pitch	347	+121.4
(e) Wrist Yaw	347	+121.3
(f) Wrist Roll	347	+447

Gear ratios for the various joints vary from 1,842 at the shoulder pitch and yaw to 739 at the wrist joints. The joints had to be backdrivable without damaging the gear train or overstressing the structure of any joint under conditions of a failed current limit circuit in the SPA. During dynamic braking conditions, the motor of each joint acts as a generator, and the electrical energy generated is dumped onto the DC bus. Normally the current so generated is limited, but should the current limit fail at maximum, the joints have to be able to withstand what essentially is a locked rotor condition.

The stiffness and weight distribution along the length of the arm has been optimized within the constraint of maintaining as great a commonality of parts as is possible, hence minimizing manufacturing costs and schedules. As a result, the stiffness in the wrist joint sections is somewhat less than the stiffness (and strength) in the shoulder joint area. The overall effect is to maintain an effectively tapered boom much like that seen in antenna tower supports. The joint structures, housings and gearboxes are designed with conventional materials such as 17-4PH and Custom 455 stainless steels, aluminum alloys of the A356, 7075-T7351 and 7050-T6 materials, and titanium alloys of the TI-6Al-4V category.

A balance of strength versus stiffness was needed in each of the joints. The shoulder joint, for example, is designed primarily for strength, generally to allow it to accommodate the failed current limit backdrive situation mentioned. The elbow and wrist are both a mixture of strength and stiffness designs. For example, the stiffness at the shoulder joint is 7.34×10^5 ft/lb per radian, while at the wrist joint it is 1.7×10^5 ft/lb per radian. The joint weights are 258, 117 and 186 lbs. for the shoulder, elbow and wrist, respectively. In some of the joints, fracture critical items require special non-destructive testing techniques to inspect for cracks. Hence, crack/flaw sizes are extremely small so that the 100 mission life can be achieved without significant crack propagation.

End Effector

The design of the end effector for the RMS was dictated by its main functional requirements:

- initial soft dock followed by rigidizing of the interface
- large capture envelope
 - o 4 inch deep, 8 inch diameter cylinder
 - o $\pm 15^\circ$ error in pitch, yaw and roll.

The configuration selected is shown in Figure 9 and its function is illustrated in Figure 10. It was selected in a trade-off with other types including internal and external claw-type, mainly because of its advantages in the two important areas mentioned as well as for its ability to provide a stiff load-path for handling heavy payloads. It is designed to be used in conjunction with special purpose end effectors (SPEEs) for the more intricate operations.

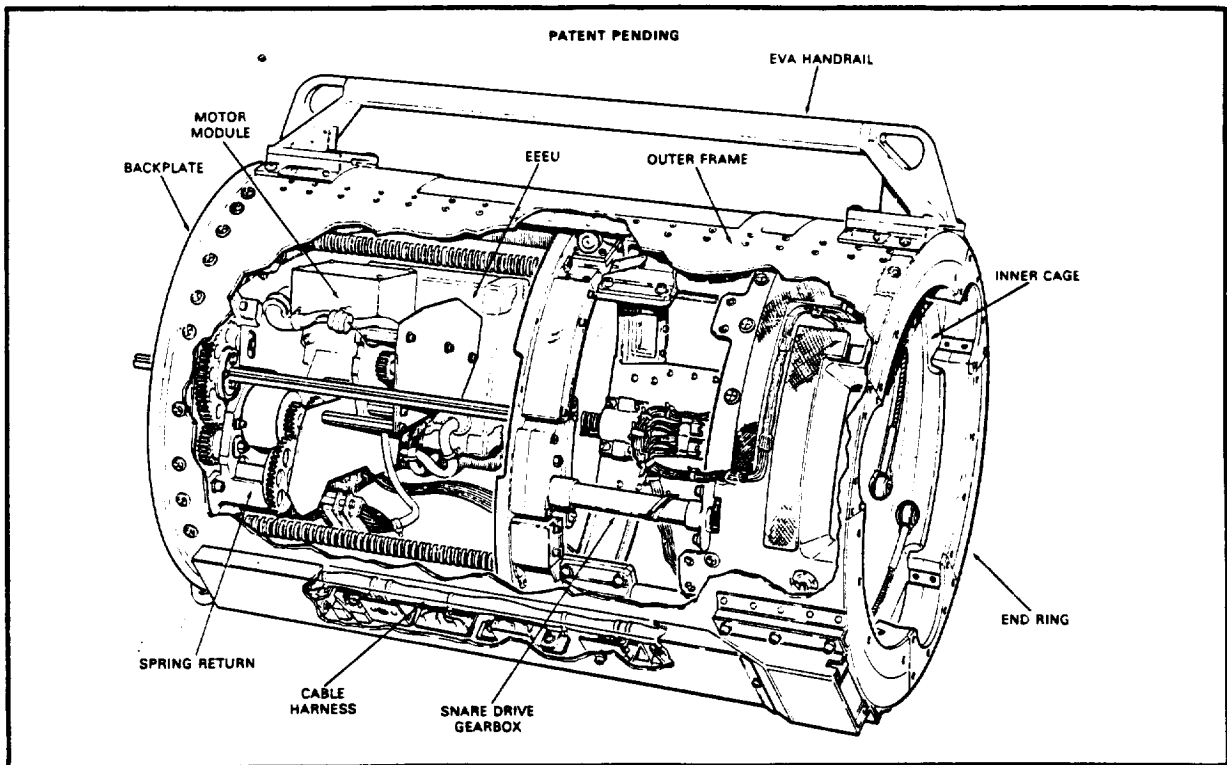


Figure 9 End Effector Arrangement

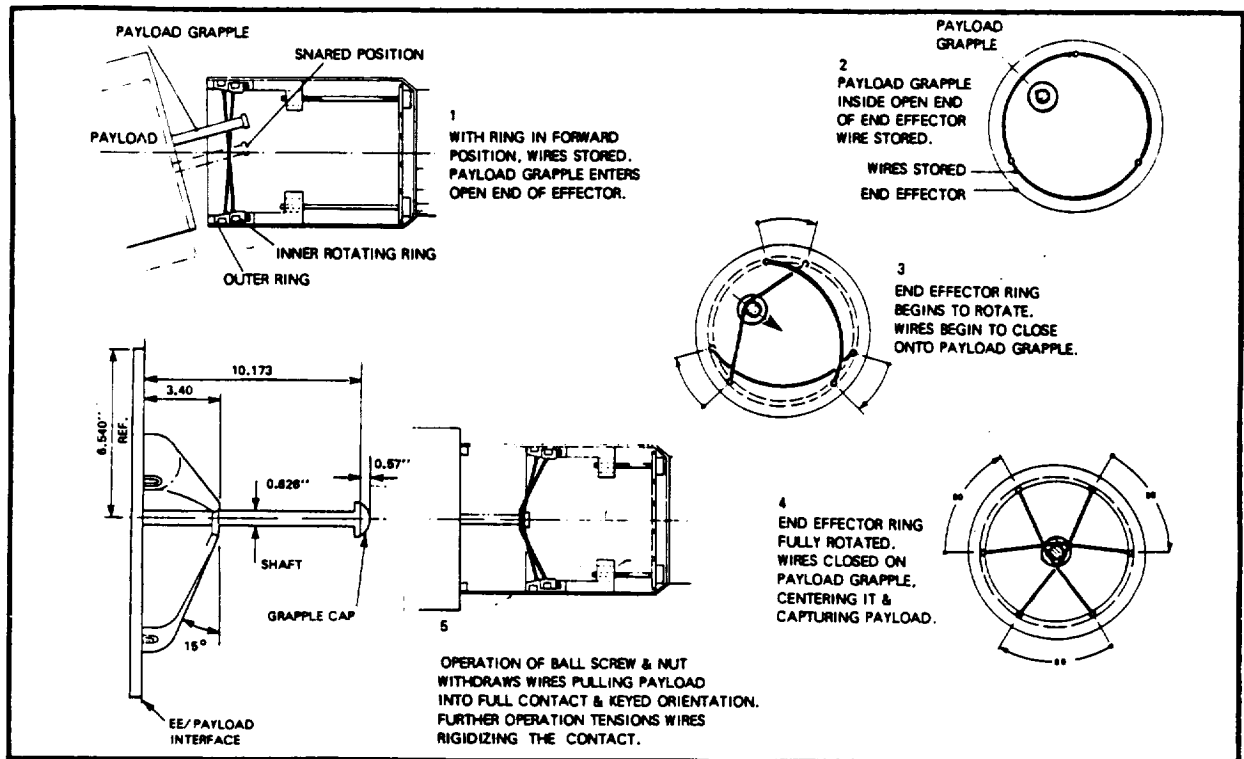


Figure 10 End Effector Capture and Rigidize Sequence

It functions by closing three snare wires around a pin attached to a payload so that the pin is centralized within the end effector. At this point the rigidization process starts when a ball-screw mechanism pulls the pin into the body of the end effector by means of the snares, thus bringing the alignment cams at the base of the pin into engagement with slots in the end effector. After these cams are mated, a preload force of 700 lbf is applied at the interface which provides the required stiffness for payload handling.

The device is thus a two-stage mechanism consisting of a large diameter snare drive ring and a mechanism for pulling this ring, and the snare cables, into the body of the end effector.

In the initial design, the end effector was to be an electrically redundant device whereby two electronic units drove a single motor coupled by clutches to the two drives. This was changed to simplify electrical interfaces and to save weight, so that the electronics drove both mechanisms as the primary drive but the redundant portion became a backup release system activated by a positive clutch release and driven by a negator spring motor.

End effector output forces and torques must be quite high while the inputs are current-limited and are therefore low torque systems amplified by gear boxes. This has meant that friction in the low torque systems has been a problem and a great deal of development effort has been devoted to solving this. Another problem has resulted from overestimating the capability of dry lubrication (LUBEKO) in an axially-loaded bearing configuration. This led to the introduction of Braycote grease which has since been utilized in several applications in the end effector where high speed, moderately loaded bearings are used.

Arm Booms

The arm booms, constructed of graphite-epoxy, were designed and manufactured by General Dynamics of San Diego, to requirements specified by Spar. Figure 11 shows schematic details of the boom construction. Ultra high modulus GY/70/934 graphite epoxy was selected to meet the requirements of stiffness and strength within the boom weight limits. The upper boom uses 16 plies of 0.005" each oriented at 0, +38 and -38 degrees. The lower boom has 11 plies oriented in the same fashion. To maintain the stability of the thin-walled booms, intermediate stiffening rings are located internally at regular intervals along the length of each boom. The rings prevent the Brazier affect which can cause

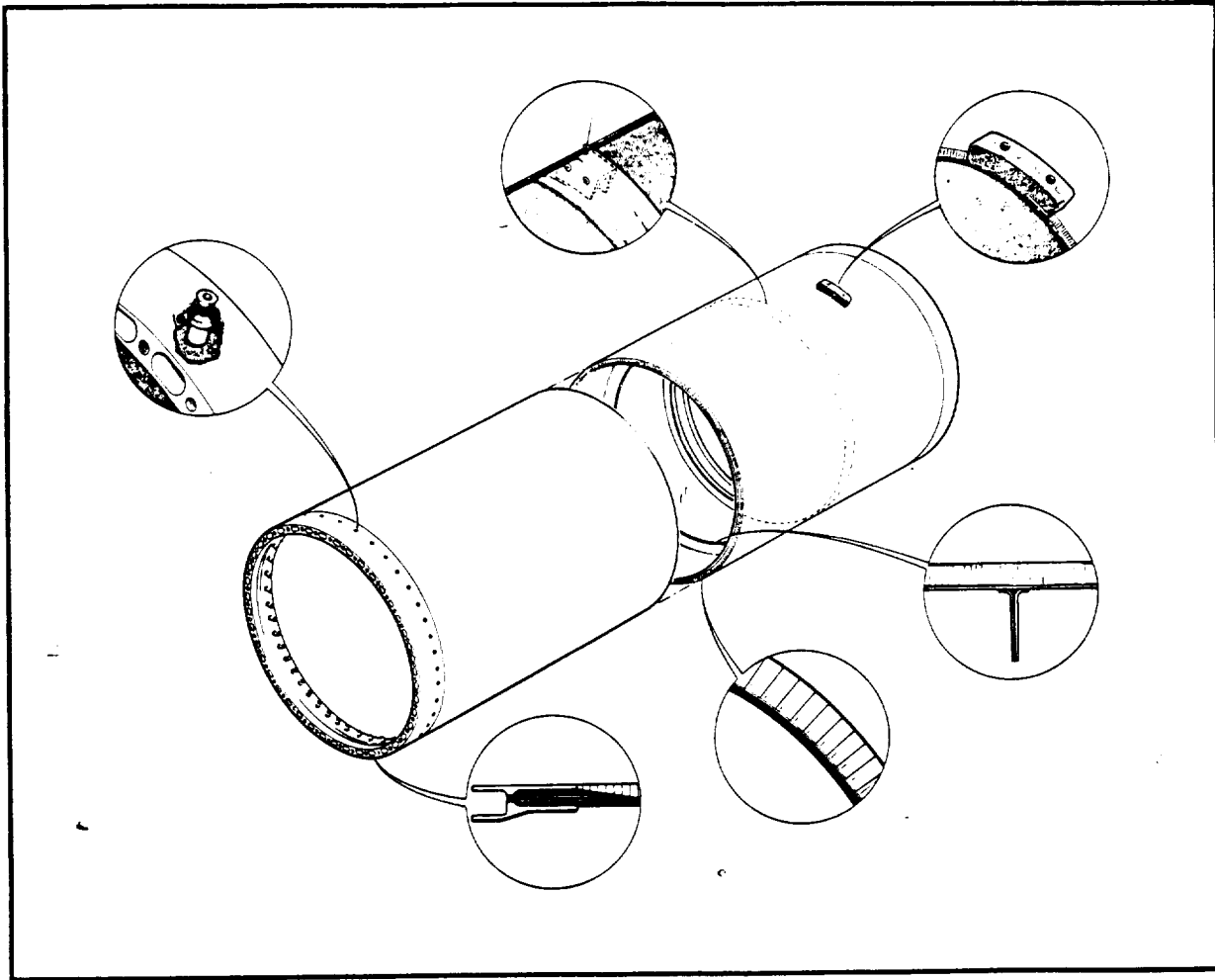


Figure 11 Arm Boom Construction

flattening of a thin-walled tube under bending, leading to premature collapse of the tube wall, and to increase the vibration frequency of the sidewall to well above the high energy acoustic range experienced during orbiter liftoff. Aluminum alloy (2124-T851) end rings are attached to the boom tubes at each end through a specially designed bolted joint. In this area, high strength T300/934 graphite/epoxy is used to increase the tube wall thickness locally for additional strength.

Because the booms are subject to damage from impact, a special bumper system is provided. The bumper system comprises precrushed HR-10 Nomex honeycomb bonded to a one-ply 102 Kevlar fabric skin bonded to the graphite/epoxy tube. The bumper system absorbs energy of up to 5 ft-lbs without indenting the bumper material. An impact of higher energy leaves a visible indentation on the bumper as an indication of possible local boom damage, requiring a local cutaway of the bumper material and visual or acoustic inspection of the graphite/epoxy subsurface. As a result of the combined stiffnesses of the individual joints and the arm booms, the unloaded arm provides the highest natural frequency of approximately 0.35 Hz in a straight arm configuration, and 0.027 Hz with a 32K payload attached.

SYSTEM PERFORMANCE SUMMARY

The on-orbit performance of the SRMS has met or exceeded expectations. The data taken from the unloaded and loaded arm during flights 2, 3 and 4 when handling the PDP and the IECM show excellent agreement with the predictions of control system performance derived from both non-real-time and real-time computer simulations. Thermal performance was well controlled, and both hot and cold case on-orbit testing showed that arm based electronics and mechanical drive temperatures were held between 28 and 96 degrees F, worst case.

Because of the problems of testing a system on the ground which is intended to operate in zero-g, certain joint-related tests were run which showed that the major system requirements (forces, torques, joint stiffness), were met. An exception to this was the overall arm stiffness, originally specified at 10 lb/in in the straight arm configuration, and which actually was measured at 8.4 lb/in. The stiffness of the individual joints was within specification, hence the reduction in stiffness is attributed to the boom-to-joint interface stiffness not being as high as was thought necessary in the early phases of the design. This has been reflected in both real and non-real-time computer simulations and has not been identified as a problem, nor has it affected on-orbit operations.

Overall force at the end of a 50 feet straight arm was to be not less than 15 lbs and was achieved. Indeed, in some arm geometry configurations, considerable force can be exerted where mechanical advantages are greater.

Stopping distance, position hold accuracy of ± 2 inch and ± 1 degree, rate hold accuracy, overall operating envelope and all operating modes, including automatic safeing, (a feature that commands zero rates to all joints) and auto-braking under conditions of uncommanded motion have all been successfully demonstrated. Qualification testing of the system has been conducted for life and environments equivalent to 100 missions.

Because of low signal levels existing in the inductosyn tachometer rate loop, there were concerns that radiated RF fields of 2 volts per metre over the frequency range 14 kHz to 10 GHz would cause joint instability. These were unfounded. Indeed, test frequencies at field strengths up to 20 V/m were shown to not degrade joint performance or stability. Conducted interference and susceptibility were also within specification.

The true test of a system such as this is the ease with which it performs its tasks on-orbit. While only lightweight payloads have been handled through STS-4 to date, (deployed, berthed and manoeuvred) the crew comments about arm behaviour, stability, predictability and ease of operation have all been highly complimentary.

The successful conclusion of this major Canada-NASA program was the completion of the Operational Readiness Review held in November, 1982, and, as the Space Transportation System continues regular operational service, the SRMS will form an important element of the new era of manned spaceflight.

ACKNOWLEDGEMENTS

Grateful acknowledgement is made to the National Research Council of Canada for permission to submit this paper.

Thanks are due to my colleague, Geoffrey Marks, for many helpful suggestions and for proof-reading the manuscript. Thanks are also due to many of my associates at Spar Aerospace Limited, RMS Division, for their assistance.

BIBLIOGRAPHY

1. Kumar P., Truss P., Wagner-Bartak C.G., "System Design Features of the Space Shuttle Remote Manipulator", Proceedings, Fifth World Congress on Machines and Mechanisms, July, 1979, Montreal, Canada.
2. Doetsch K., "The Remote Manipulator System for the Space Shuttle Orbiter", September, 1977, Jahrestagung, 1977 of the Deutsche Gesellschaft für Luft- und Raumfahrt eV, Berlin W. Germany.
3. Dunbar D., Robertson A., and Kerrison R., "Graphite/Epoxy Booms for the Space Shuttle Remote Manipulator", Aerospace Applications of Advanced Composite Materials, ICCM/2, April 16-20, 1978, Toronto, Canada.
4. Sharpe A., "The Shuttle Remote Manipulator Control System", presented at SAE Aerospace Control and Guidance System Committee Meeting No. 48, October 29, 1981.
5. Ravindran R., Trudel C.P.R., Nguyen P.K., "Shuttle Remote Manipulator Control System", presented at the 18th IEEE Controls and Dynamics Conference, Fort Lauderdale, Florida, December 12, 1979.
6. Gossain D.M., Quittner E., Sachdev S.S., "Analysis and Design of the Shuttle Remote Manipulator System Mechanical Arm for Launch Dynamic Environment", Shock and Vibration Bulletin No. 50, Naval Research Labs., Washington, D.C., September, 1980.
7. Gossain D.M., "Effect of a High Gear-Ratio Joint on Dynamics of an Articulated Structure", Canadian Aeronautics and Space Journal, Volume 25, No. 3, 1979.
8. McCullough J.R., Sharpe A., and Doetsch K.H., "The Role of the Real-Time Simulation Facility (SIMFAC) in the Design, Development and Performance Verification of the Shuttle Remote Manipulator System (SRMS) with Man-in-the-Loop", presented at the 11th Space Simulation Conference, Johnson Space Center, Houston, Texas, September 23-25, 1980.
9. Hunter J.A., Ussher T.H., Gossain D.M., "Structural Dynamic Design Considerations of the Shuttle Remote Manipulator System", presented at AIAA/ASME/ASCE 23rd Conference of Structures, Structural Dynamics & Materials, May 10-12, 1982.

SPACE SHUTTLE RUDDER/SPEEDBRAKE ACTUATION SUBSYSTEM

Ruth A. Naber
Sundstrand Advanced Technology Group
Rockford, Illinois

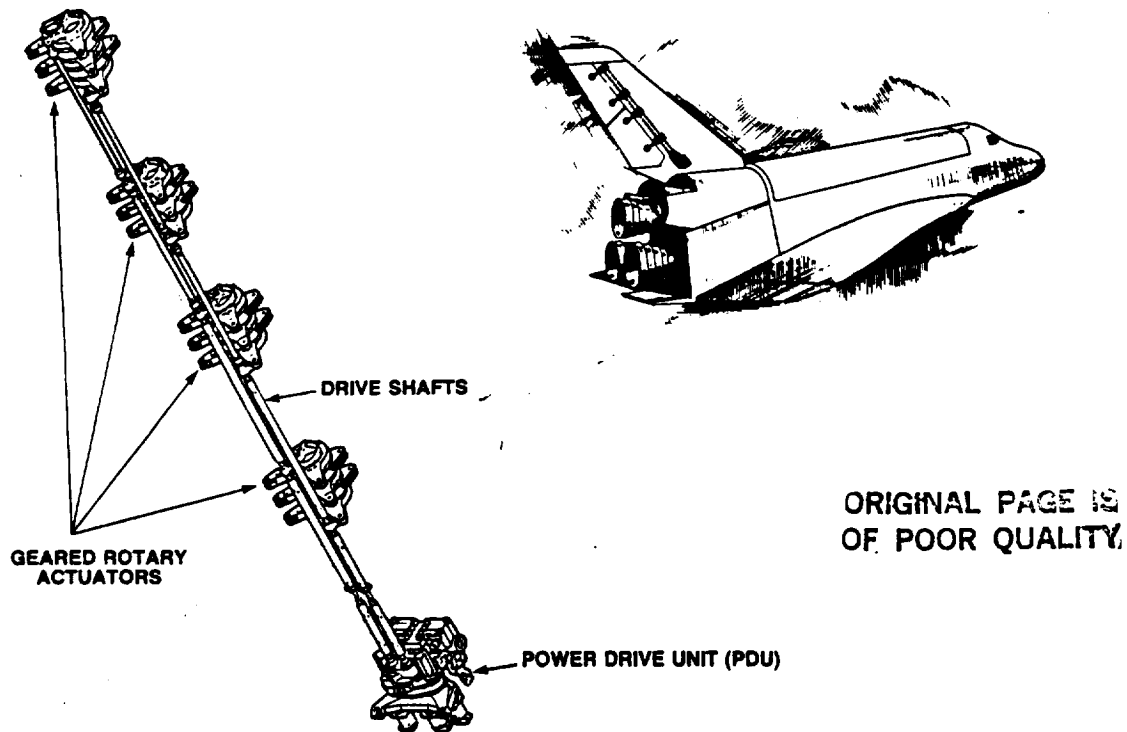
ABSTRACT

An electro-hydro-mechanical actuation system for control of the rudder and speedbrake aerosurfaces of the Space Shuttle orbiter was developed to meet the strict operational requirements imposed on this mission critical function. (Reference 1) The re-entry and landing portions of the Space Shuttle mission included a set of environmental and operational requirements which presented a significant engineering challenge. The design solutions derived during this effort served to provide a reliable, safe-life actuation system and to provide technology that will be useful in future engineering challenges.

INTRODUCTION

The Rudder/Speedbrake (R/SB) Actuation Subsystem supplied by the Sundstrand Corporation for use on the NASA Space Shuttle Orbiter is an electro-hydro-mechanical system which provides the control and positionary capability of the orbiter aero-dynamic primary flight control surface. The system is located in the vehicle's vertical stabilizer. The Geared Rotary Actuators provide a power hinge feature of the split panel rudder. Actuation of both panels in the same direction provides conventional rudder control; actuating the panels differentially provides a speedbrake function intended to control both speed and pitch. The commands may be superimposed on one another.

The system consists of one Power Drive Unit (PDU) which responds to quadredundant avionic signals to generate a rotary output, four Geared Rotary Actuators, which develop rotary position and torque as outputs, and ten torque transmitting Drive-shafts. (See Figure 1)



ORIGINAL PAGE IS
OF POOR QUALITY.

Figure 1
Rudder/Speed Brake Actuation System

The Power Drive Unit (PDU) responds to electrical command signals that operate electrohydraulic servovalves. The servovalve operation ports hydraulic pressure to hydraulic motors which in turn provide rotary power to PDU gearbox. The PDU is presented schematically in Figure 2.

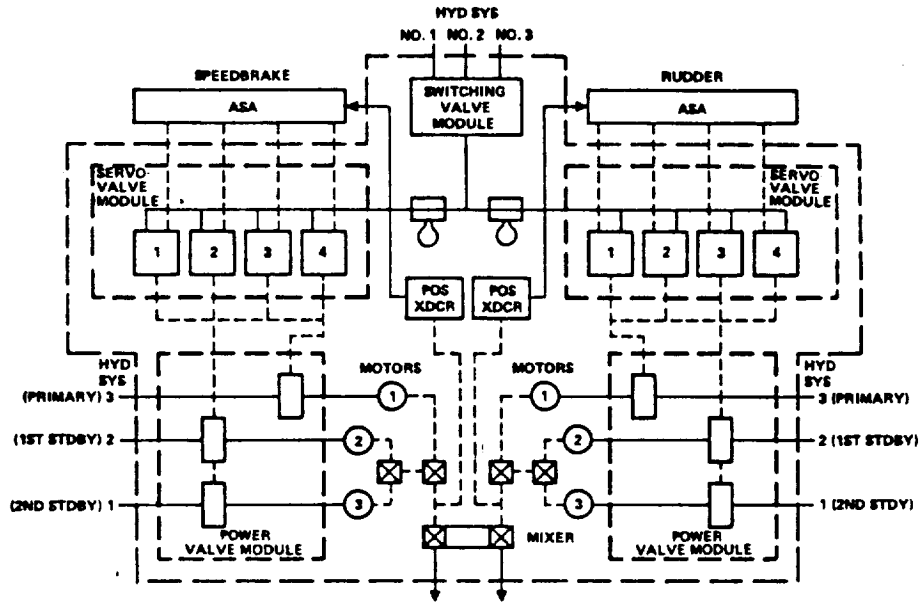


Figure 2
Power Drive Unit Schematic

Within the PDU design, the areas of engineering challenge to be discussed in this paper include the following:

1. Electrical/Hydraulic Fault Detection and Isolation,
2. Gearbox design to mechanically mix the rudder commanded movement with speedbrake commanded movement.

The Geared Rotary Actuator shown in Figure 3 presented a significant challenge on its own. As in all flight control systems, weight and volume are critical factors in determining the actuating mechanism package. This results in the use of highly stressed gears to accomplish the task. This gear design required refinement of the analytical technique and extensive testing.

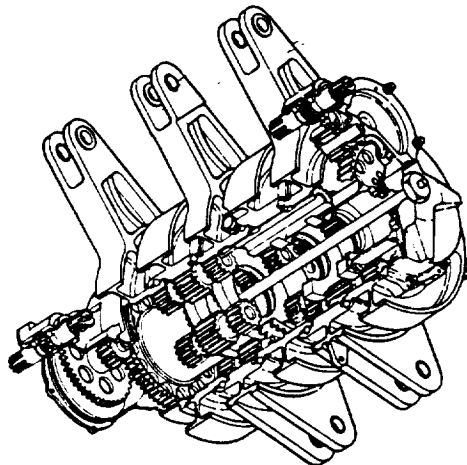


Figure 3
Rotary Actuator

ORIGINAL PAGE IS
OF POOR QUALITY

FAILURE DETECTION AND ISOLATION

The operational capability of the R/SB system is critical to the successful completion of the orbiter mission. Therefore considerable design emphasis was placed on electrical and hydraulic system redundancy and further fault detection and isolation. Referring to Figures 2 and 4, the electronic input commands are quadredundant, coming to the PDU from four independent avionic sources. These four commands act on four separate electro-hydraulic servovalves within the PDU. Pressures from the servovalve second stages act on areas of a single structural power spool valve, causing it to move from its null position. This movement opens ports that supply hydraulic pressure to the three hydraulic motors providing rotary power to the PDU gearbox.

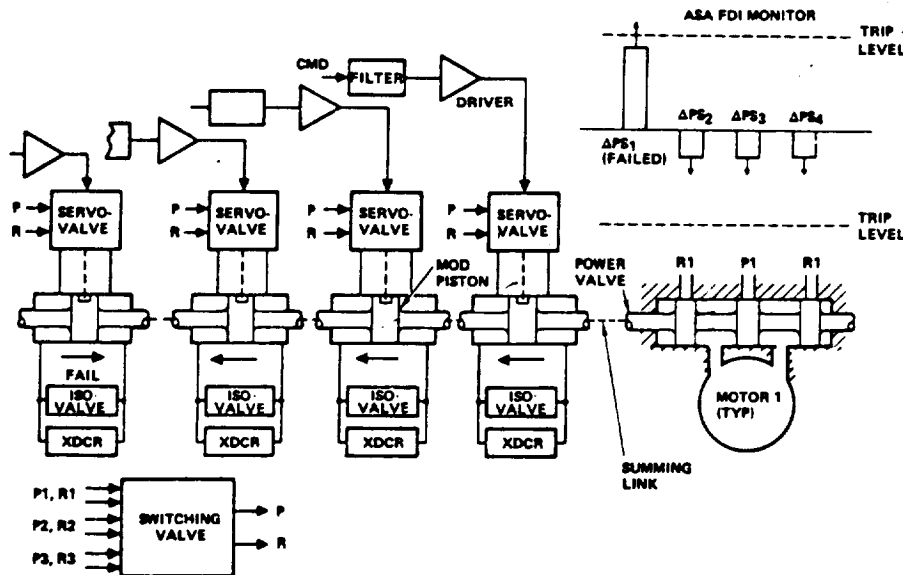


Figure 4
Channel Fault Detection

Should a servovalve output to the power valve be significantly different from the other three (due to failure of the valve, or its associated avionics, for instance), the second-stage differential pressure of that servovalve will rise as it force-fights the three opposing good servovalves. This rise in pressure (Figure 4) is monitored by second-stage pressure transducers, and, when a trip level is attained indicative of a failed channel, a solenoid valve is commanded to open, bypassing the failed channel. The PDU, meanwhile, continues operating normally in response to the commands of the three good channels. Should a second servovalve failure occur, a similar two-versus-one vote would result in its bypass. In this way, the PDU is tolerant of two avionic failures while maintaining full performance.

During early development testing of the PDU, it was found that channel failure and isolation, while the PDU was operating at a high output rate, could result in very high internal pressure pulses as a result of transfer of kinetic energy to potential energy by compressing the oil as a spring between the motor and the valve. This problem was resolved by making several system modifications, including avionic command filtering, elimination of a power valve positioning linkage, and strengthening of pressure passages within the PDU.

A hydraulic system failure is monitored by and managed by the switching valve. This pressure actuated valve is arranged to accept the three on-board independent hydraulic systems. The valve automatically switches from an out-of-tolerance hydraulic source to a standby source. Isolation of motor pressures is maintained.

MECHANICAL MIXER

The Space Shuttle Orbiter combines in the rudder flight control system two functions: conventional rudder operation and a speedbrake function. In order to produce the desired output of the functions the PDU gearbox design was required to accept the power inputs of either or both the rudder and speedbrake controls and integrate and deliver those inputs to the geared rotary actuators.

A combination of gears and differentials was selected to perform this PDU function (See Figure 5). In the first series of gears/differentials the three motor outputs of each flight control system (rudder or speedbrake) are speed summed into a single shaft entering the mixer. In the final series of gears/differentials, the mechanical mixer algebraically sums the rudder and speedbrake motor outputs and delivers the resultant to the aerosurface via the system drive shafts and actuators. Successful design and development of this mechanical mixer concept has greatly reduced the system complexity and weight while permitting simultaneous rudder and speedbrake motion.

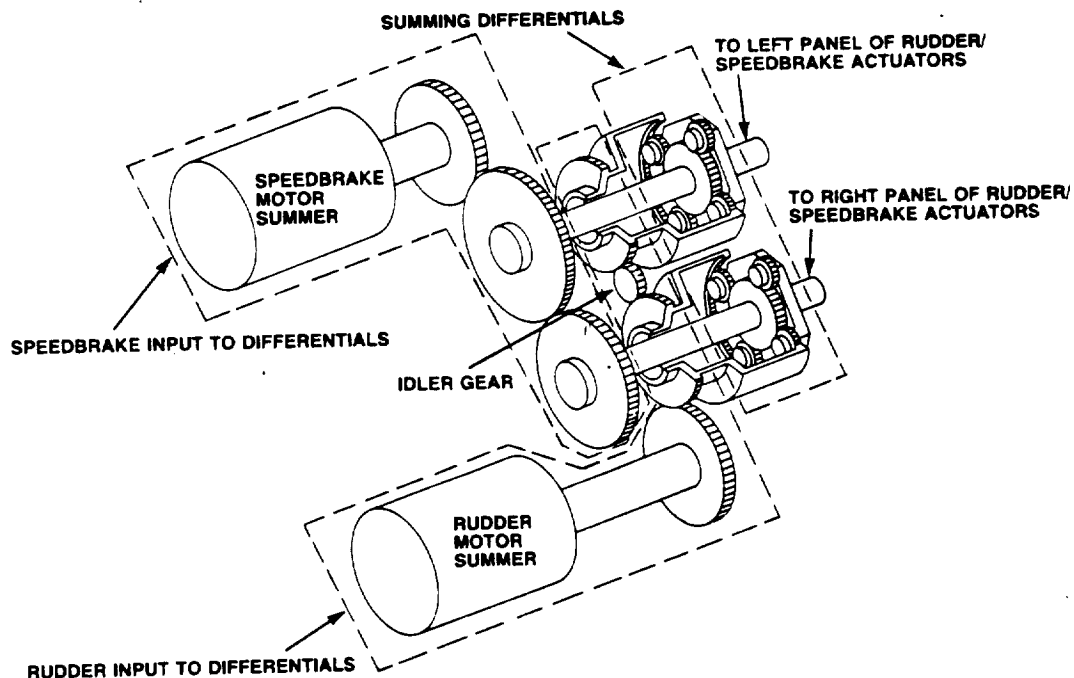


Figure 5
Mechanical Mixer

PLANET GEAR DESIGN

The Geared Rotary Actuator is a planetary-type gearbox with a 474-to-1 gear reduction system. The unit acts as a power hinge for the aerosurfaces. Within the system there are two basic sizes, with barrel diameters of 8.8 in. and 11.4 in. The two sizes are designed for maximum load capacity of 338,000 in lb. and 732,000 in lb.

The planet gears in the actuator assembly are the critical, life limiting component. These gears are designed to withstand high stresses in order to minimize weight and envelope. During early program testing a problem was encountered with root cracking in these highly stressed gears. This test result led to extensive evaluation of material and manufacturing processes as well as load distribution analysis and cumulative damage analysis.

The material and manufacturing processes' evaluation led to requirements for additional shot peening of the gear roots to increase precompression and for a new process: grit-blasting of gear roots to remove the presence of intergranular oxidation. The absence of these two items was not considered the cause of initial failure but provided added reliability to final design configuration.

Considerable test work and analysis was conducted to study the effect of load distribution on the planet gears. Testing revealed that under maximum load conditions the relatively long planet gears deflected several thousandths of an inch, resulting in a considerable load concentration on the inside corners of the gear teeth. Using the test information the analytical model was reviewed and after several iterations a solution was recommended. That solution required optimizing the gear tooth thickness and providing a crown on the mating ring gear so that under loaded conditions the planet would deflect into a more uniform gear contact. These changes were thoroughly tested and verified before implementation into production.

The ability to predict the fatigue life of a gear critical actuation system became the subject of concern. It was determined that a more detailed model of the mission load spectrum was required. In studying this design, Dr. Philip S. Oyoung developed a method to synthesize the load spectrum for the Rudder/Speedbrake mission profile so that actuator life capability could be calculated. The method, applicable to general fatigue analysis, provides a much improved accuracy to gear life prediction.

Conclusion

All of the design challenges of the Rudder/Speedbrake Actuation Subsystem, and specifically those addressed in this paper, have been met and solutions derived that yield a highly reliable actuation system. The channel self test features of the PDU and its ability to isolate bad control channels and to switch hydraulic power supplies combine to give a depth of redundancy that is unique to a flight control system. The mechanical mixer provided a light weight, simple gear system that permits simultaneous rudder and speedbrake operation. Safe-life design concepts for primary load carrying components were utilized to maximize output potential for given weight and envelope.

Successful test programs and, now, successful operational status of the orbiter vehicle are the evidence of meeting the challenge this aircraft has presented the technical community.

References

1. Technical Report Woolhouse, Dwight: Space Shuttle Orbiter Rudder/Speedbrake Actuation System. STS 81-0231
2. Technical Report Oyoung, Shio-ping Philip: Fatigue Life Optimization for Gear Critical Actuation Systems by Load Spectrum Synthesis and an Algorithm for S-N-R Curve Generation

DEVELOPMENT OF THE SPACE SHUTTLE BODY FLAP ACTUATION SUBSYSTEM

Clifton R. Boggs
Sundstrand Advanced Technology Group
Rockford, Illinois

ABSTRACT

Development of the Body Flap Actuation Subsystem included alterations from the original design to mechanical stops, planet gears, control valves, and solenoid valves. The mechanical stops were redesigned to absorb stall load and rotating inertia of the hydraulic motors instead of only stall load. The institution of a quill shaft (torsion spring) was a successful solution. The planet gears in the geared rotary actuators developed cracks during testing. This failure was alleviated via modification to the gears. A motor pressurization - brake release timing technique was developed thru analysis and testing. This resulted in a control valve configuration which would not permit "freewheeling" of the body flap surface. Finally, several solenoid valve configurations were tested to obtain the desired performance.

Conceptual redesigns and modifications were weighed against each other to optimize a solution. Tradeoffs were usually made between life, performance, failure tolerance, and reliability versus weight, envelope, and maintainability.

INTRODUCTION

The Body Flap of the Space Shuttle Orbiter is an aerosurface which protects the rocket engines from the heat of re-entry and also acts as a flight control surface to augment pitch control. The actuation system is an on-off system which consists of a hydraulic valve module/gearbox, (Power Drive Unit) and geared rotary actuators (Figure 1). The valve module contains three redundant valve packs, one for each hydraulic system. Each valve pack has a power control valve, which controls flow to a hydraulic motor. Two solenoid valves shift the control valve to the "up" or "down" position and are respectively marked. The three motor outputs are speed summed in the gearbox to obtain a single output. This output is further speed reduced in the gearbox before being transmitted to the geared rotary actuators. The actuators attach the body flap surface to the orbiter and also function as a hinge. The actuator transmits torque reduced loads to or from the gearbox via torque shafts.

The rate of movement for the body flap surface is controlled in the valve pack. A command in the "up" direction energizes the UP solenoid valve, thus hydraulically shifting the control valve. Flow is circulated thru orifices #2 and #3, which limit the flap rate of movement. A command in the "down" direction energizes the DOWN solenoid valve, thus shifting the control valve in the opposite direction. In this case, the flow rate is limited by orifice #1, which limits the flap rate of movement.

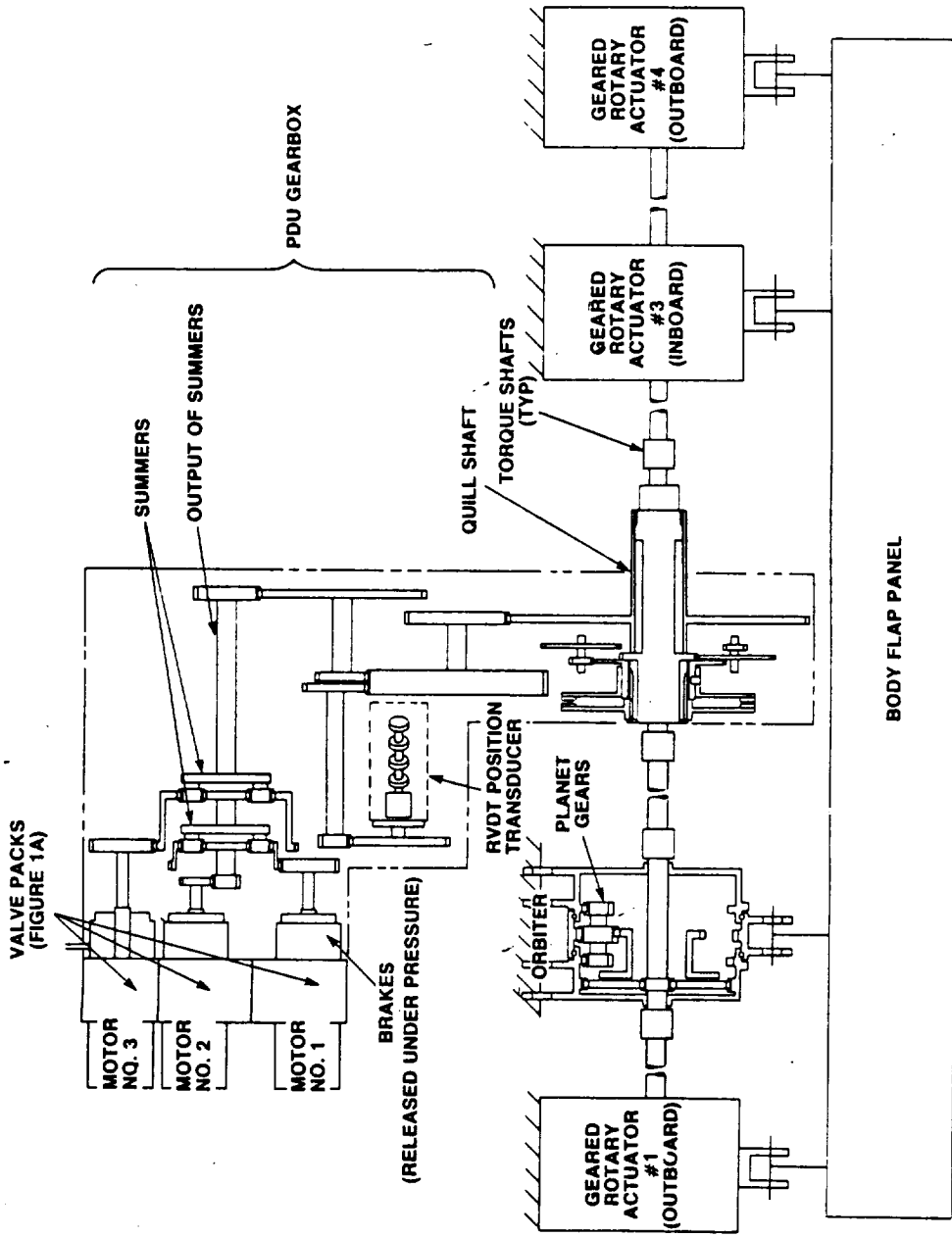


Figure 1
Body Flap Actuation Subsystem

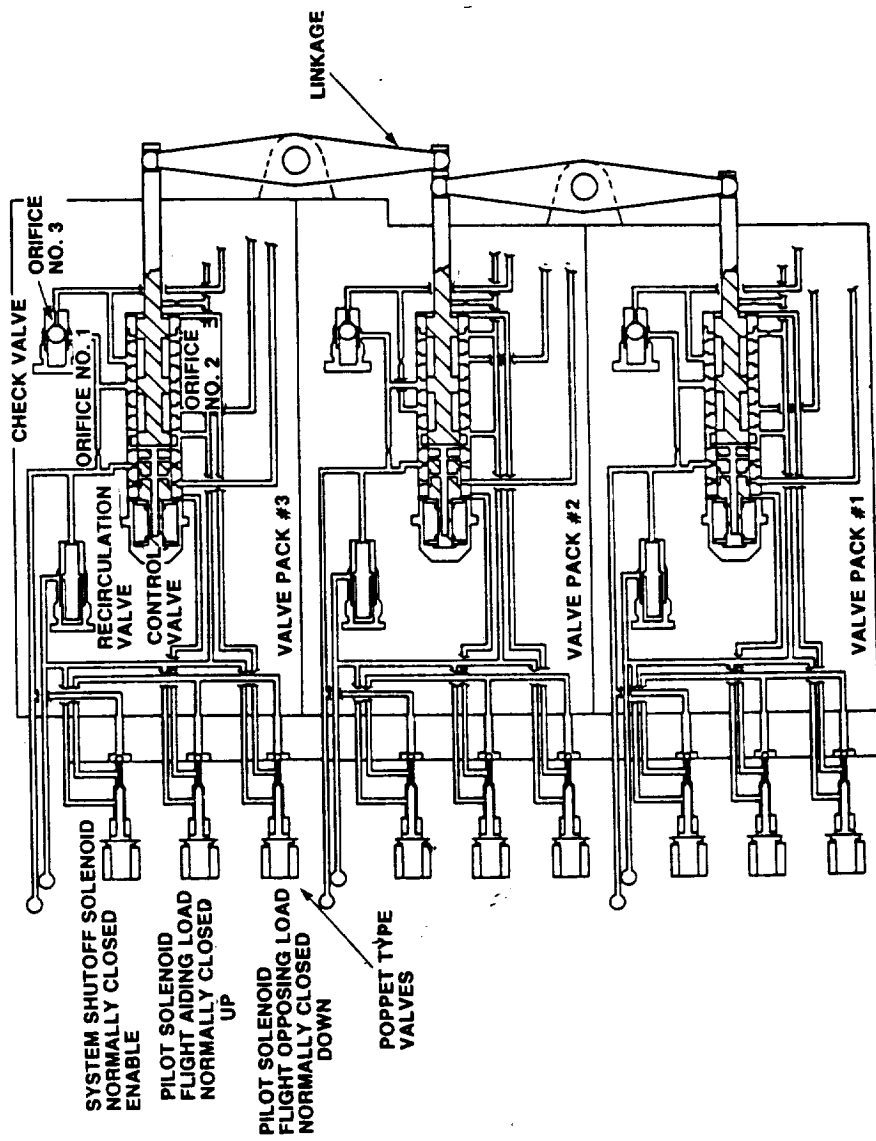


Figure 1A
Body Flap Actuation Valve Pack

Other features are included in the actuation subsystem. An enable valve isolates hydraulic supply to each valve pack. A pressure released brake at the output of each motor prevents backdriving of the motor when it is not pressurized. Mechanical stops limit travel of the body flap surface. A quill shaft (torsion spring) absorbs rotating inertia when the mechanical stops are engaged. A recirculation valve maintains a flow thru the valve pack to stabilize the valve pack temperature.

Development of the Body Flap Actuation Subsystem required the selection of various design concepts and optimization of the selected concepts thru analysis and testing. Areas requiring development effort were the mechanical stops, planet gears in the rotary actuators, brake release timing, and solenoid valves. The mechanical stops need to withstand the rotating inertia of the subsystem moving at full rate. The planet gears need to withstand extremely high loads. The brake needs to be engaged and released only when the motor is carrying the load - to prevent "freewheeling" of the body flap surface. Finally, the solenoid valves need to facilitate the specified subsystem response time (under 0.20 seconds) and withstand a burst pressure of 7500 psi. The following sections give a synopsis of the development effort given in the areas listed above.

MECHANICAL STOPS

Mechanical dog stops limit the amount of travel of the body flap surface. The initial design required the stops to react only the stall load expected by the hydraulic motors. This requirement was determined to be unacceptable. The requirement was upgraded to also require the stops to absorb the full load of the hydraulic motors going at full speed. The inertial loads of the motors would fail the dog stops of the original design. Several new design approaches were investigated and are detailed below.

- A. Mechanically driven limit switches could be used which would be tripped at the end of travel. The solenoid valves would be de-energized thereby stopping the motors and engaging the brakes. Note that the control valve automatically engages the brake when flow is restricted from the motors.
- B. Stops could be instituted on each of the four actuators as shown in Figure 2. The inertia of the hydraulic motors would be absorbed by the torque shafts (acting as torsion springs) between the actuators and gearbox.
- C. Stops which are located at the input to the two inboard actuators could be utilized as shown in Figure 3. The inertia of the motors would be absorbed by the two torque shafts between the gearbox and inboard actuators.
- D. Dog stops internal to the gearbox with a quill shaft (torsion spring) designed to absorb the motor inertia could be used. See Figure 4.

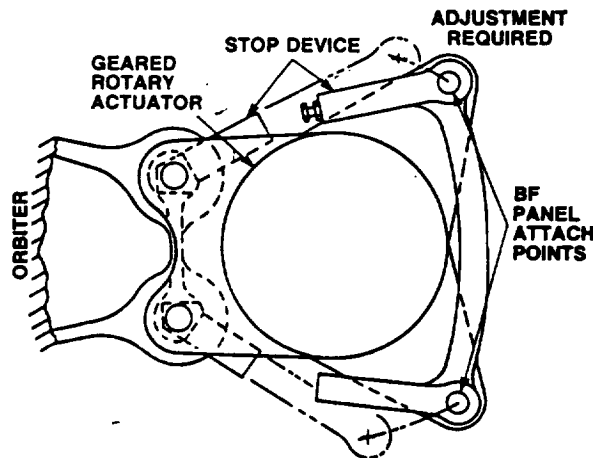


Figure 2
Stops Located on Actuator Output

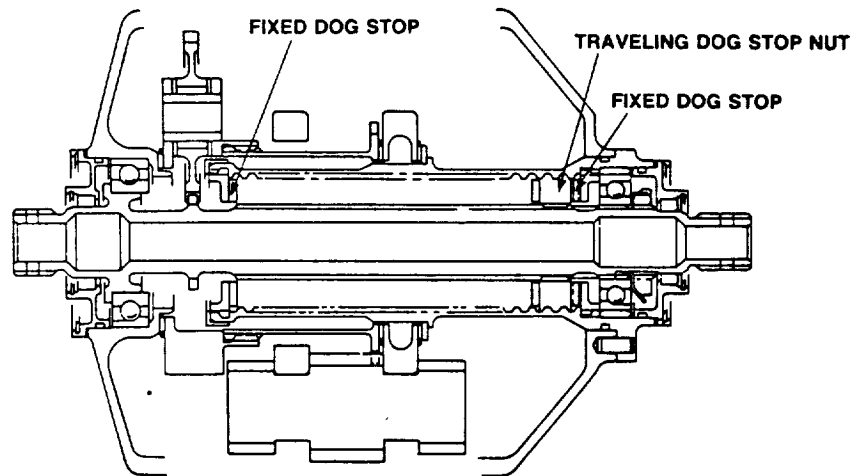


Figure 3
Stops Located on Inboard Actuator

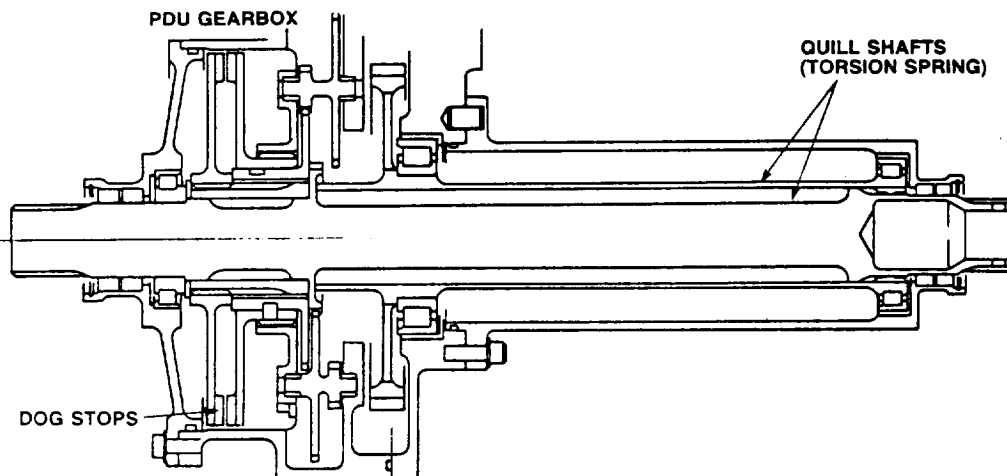


Figure 4
Quill Shaft and Dog Stops in PDU Gearbox

Investigation into each of these design techniques determined that option D was best. Design D required an increase in envelope dimensions along with a weight increase of 5 lbs. to the Power Drive Unit (PDU) (valve packs and gearbox) from 55 to 60 lbs. The other approaches were discarded for the following reasons:

- A. Electrical limit switches were considered to have a marginally acceptable reliability level. A mechanical solution was also philosophically preferred to an electrical solution.
- B. Actuator stops entailed a significant weight increase along with a major redesign of the rotary actuators.
- C. Inboard actuator stops would require a redesign of the inboard actuators along with the PDU. A weight increase of 11 lbs. would have occurred. In addition, testing and rigging of the subsystem would be more complicated.

The design utilizing the dog stops and quill shaft was incorporated into the subsystem. Development and qualification testing of the subsystem has proven the design with no further changes required.

PLANET GEARS

The planet gears in the Geared Rotary Actuators are highly stressed to minimize the weight and envelope of the Body Flap Subsystem. Inspection of planet gears after early development testing revealed cracks in the gear teeth roots (Figure 5). Analyses prior to development testing had shown that the planet gears would survive fatigue testing of 400 mission duty cycles without developing any cracks. Investigation into the failure showed that at maximum load the planet gears deflect several thousandths of an inch. This deflection caused the gear teeth to carry a higher percentage of the load on the inside of the gear teeth than was previously calculated. Refer to Figure 6. Several solutions to increasing the fatigue life were investigated.

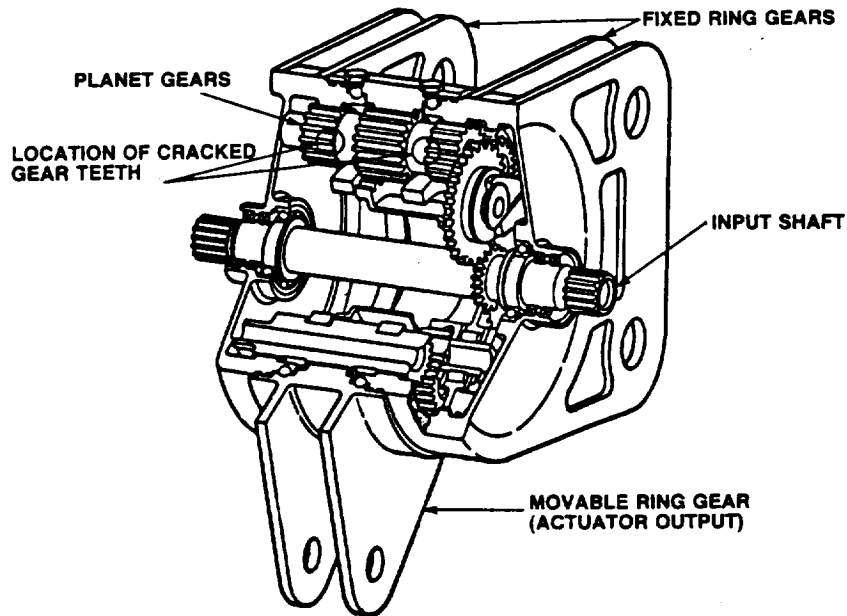


Figure 5
Geared Rotary Actuator

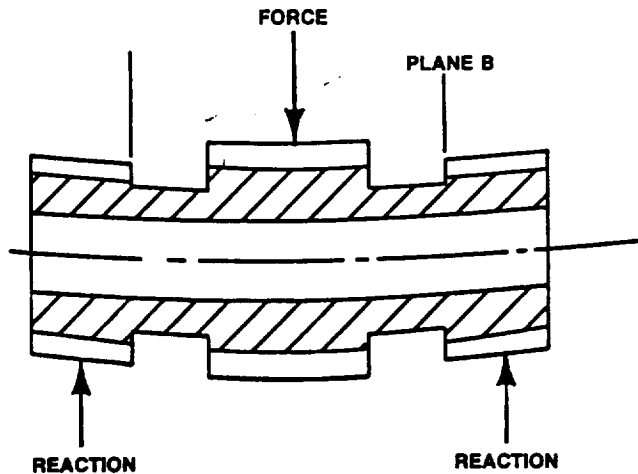


Figure 6
Deflection of Actuator Planet Gears Under Load

- A. The actuator could be increased in size.
- B. The tooth thickness of the planet teeth could be increased and the tooth thickness of the ring gear decreased.
- C. The planet gear teeth could be crowned.
- D. The ring gear teeth could be crowned. (See Figure 7)

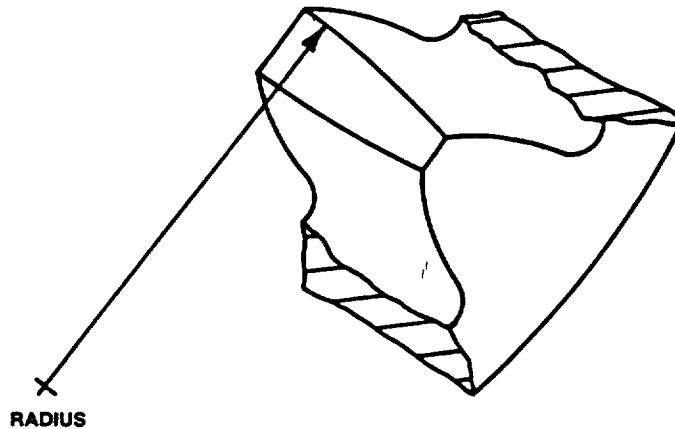


Figure 7
Crowned Ring Gear Tooth

A solution to rectify the failure was extensively investigated. Increasing the size of the actuator was least preferable since this type of change would have a significant weight impact. Crowning of the planet gear teeth would give a minimal increase in life. With this change the stress distribution across the gear tooth root would be improved but more material would be removed from a highly stressed tooth. The solution instituted was a combination optimizing gear tooth thicknesses as in B and crowning the ring gear teeth as in Figure 7. These changes alleviated the stress concentration at the ends of the planet gear teeth. The changes instituted resulted in a significant improvement in fatigue life analytically and was confirmed thru fatigue testing.

MOTOR PRESSURIZATION - BRAKE RELEASE TIMING

The motor pressurization and brake release sequence is considered critical to obtaining the desired operation characteristics of the Body Flap Actuation Subsystem. If a brake is released prior to pressurization of its respective motor, the body flap surface could "freewheel". The desired sequence is for the motor to become fully pressurized (stalled) against the brake. Then the brake can be released. When the system is de-energized the desired sequence is reversed. The motor pressurization - brake release timing was considered a development problem.

The initial design concept of the valve pack entailed a 4 land power valve with the brakes released off of pilot passages from the "up" and "down" solenoid valves. Refer to Figure 8. The pilot flow fed from a commanded solenoid valve and thru an orificed relief valve to release the brake. A remote type of relief valve failure could restrict the brake from engaging upon loss of pilot pressure and de-pressurization of the motor. This failure could permit the body flap surface to "freewheel". A single failure mode of this kind is not permitted. In addition, this concept could produce a timing sequence for the motor and brake which is not desirable or easily modified.

A design concept which showed the most indication of success entailed adding the brake release valve onto the spool and sleeve of the power valve as in Figure 10. Two slight hydraulic short circuits were designed into the valve, one in the brake section, and one in the motor section. This feature would soften brake and motor pressurization. As the spool travels from the null position to the up position (or down position) the short circuits occur just after the supply is opened and just prior to closing the return. See Figure 10. The short circuits occur in the brake and motor simultaneously. Tests on this design confirmed the intended results. As the brake reduced its load holding capability, the motor increased load holding capability, thus preventing a "freewheel" condition.

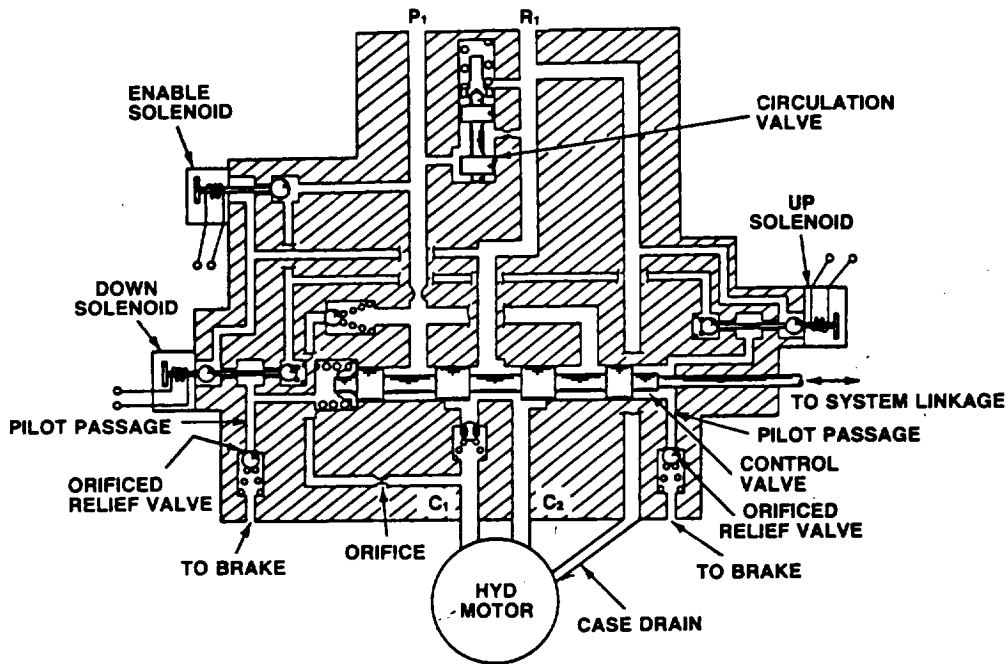


Figure 8
Initial Valve Pack Design Concept

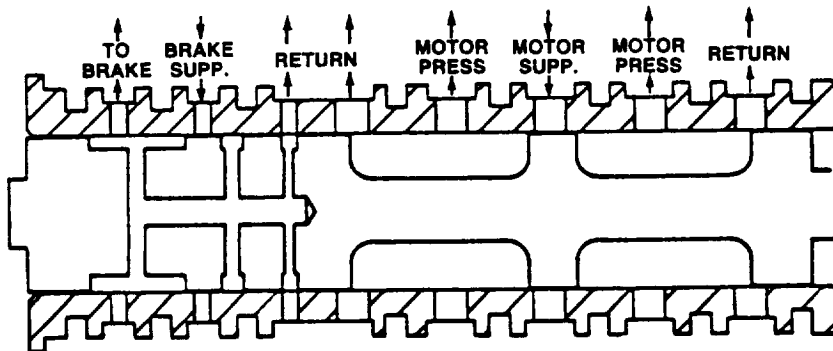


Figure 9
Control Valve in the Null Position

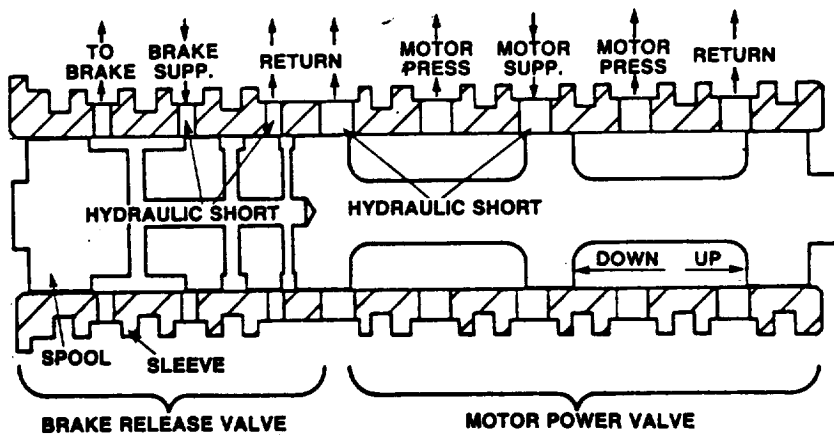


Figure 10
Control Valve Moving From Null to Up Position

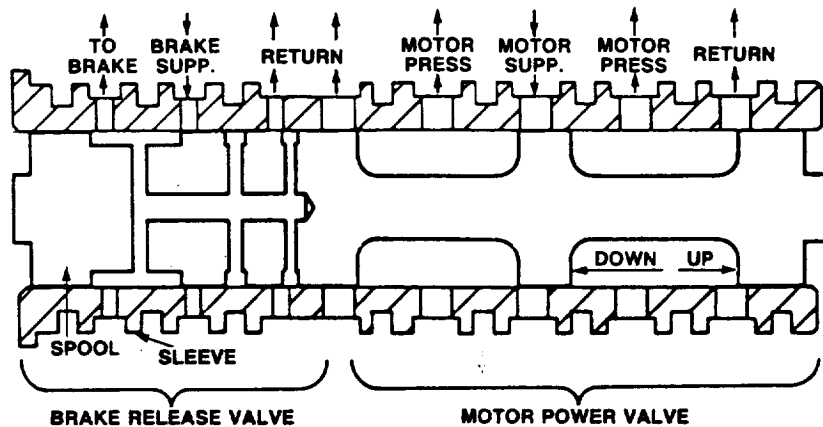


Figure 11
Modified Control Valve Moving From Null to Up Position

Several undesirable effects occurred with the "short-circuit" style design. The first effect was a pressure spike on the supply line as the spool moved into the up or down position. During transition a high flow occurred when the short circuits were open. This high flow quickly slowed, thus causing a pressure spike. The second effect occurred in failure mode testing. With hydraulic system #1 force driving electrically inhibited systems #2 and #3 an excessive amount of lost motion in the linkage would cause incomplete travel of spool #3. The #3 spool would travel to the short circuit position and stop, thus rendering the #3 system stalled.

The final design of the valve pack entailed minor modifications to the "short-circuit" design. The short-circuits were eliminated by increasing several land width dimensions. In addition, the lands were shifted slightly to permit complete motor pressurization prior to pressurizing the brake (i.e. releasing it). See Figure 11. The valve spool linkage was modified to minimize lost motion due to freewheel and bending. Development and qualification testing has shown this design to be very successful.

SOLENOID VALVES

Two types of solenoid valves considered for use in the valve pack were (a) spool and sleeve and (b) poppet. The initial valve pack design used the spool and sleeve type as shown in Figure 12. This type of solenoid has several advantages over the poppet type shown in Figure 13. The spool and sleeve solenoid valve requires a smaller coil for actuation, the valve portion of the solenoid can be made smaller and it is less expensive to manufacture than the poppet solenoid valve.

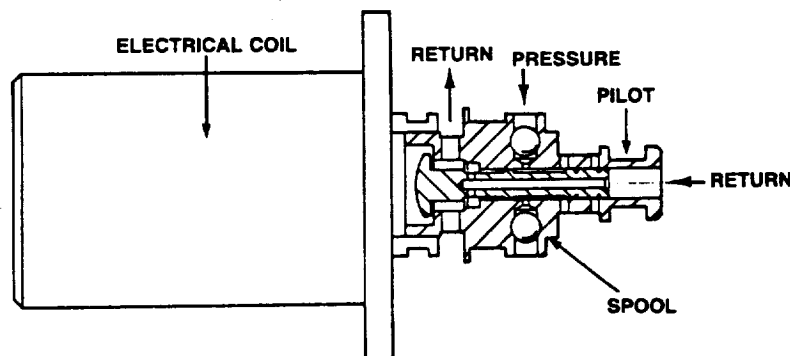


Figure 12
Spool and Sleeve Solenoid Valve 3-Way, 2-Position

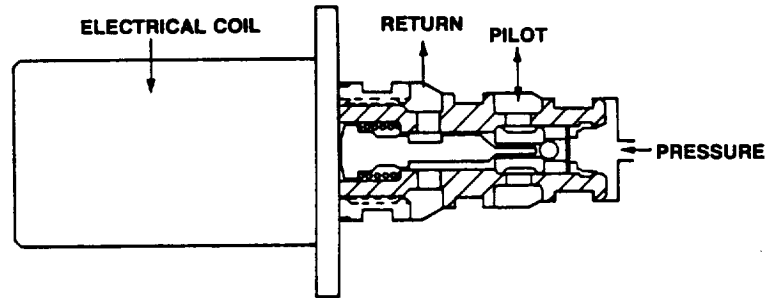


Figure 13
Poppet Solenoid Valve, 3-Way, 2-Position

Development tests performed with the initial valve pack gave an adequate response time for activating the subsystem (.15 seconds) but an inadequate response time for deactivating the subsystem (.20 seconds). An investigation determined that the ports from cylinder to return on the solenoid valve were too restrictive to permit the control valve to shuttle to the null position (from an UP or DOWN position) in the required time. The ports were enlarged and the valves successfully retested. Subsequent testing failures revealed that the edge of the spool land was catching on the edge of the enlarged port holes. These failures triggered a re-evaluation of the selection of a spool and sleeve type solenoid valve.

Re-evaluation of the solenoid valve led to the selection of a poppet style valve. The poppet solenoid valve is less prone to contamination type failures and has a lower leakage rate. In addition, the aerospace industry is somewhat biased towards poppet style solenoid valves. Development of this valve resolved problems with excessive time response and weak flanges. The flanges are designed to contain a burst pressure of 7500 psi. Qualification testing has shown the valve to have excellent performance and reliability.

CONCLUSION

Development of the Body Flap Actuation Subsystem entailed testing, small redesigns, and various modifications. Development testing assisted in identifying areas requiring improvements. The test results triggered redesigns and modifications in items such as stops, planet gears, control valves, and solenoid valves.

Conceptual redesigns and modifications were weighed against each other to optimize the solution to a problem. Tradeoffs were usually made between life, performance, failure tolerance, and reliability versus weight, envelope, and maintainability to obtain the optimum package.

Qualification testing has demonstrated the final configuration's ability to meet endurance, operation, and performance requirements for 4 times life. (Lifetime = 100 mission duty cycles). This configuration has high reliability and failure tolerance while meeting the performance and life requirements to minimize weight.

D30. N85-16967

MECHANICAL FEATURES OF THE
SHUTTLE ROTATING SERVICE STRUCTURE

John M. Crump
Reynolds, Smith and Hills
Jacksonville, Florida

ABSTRACT

With the development of the Space Shuttle launching facilities, it became mandatory to develop a Shuttle Rotating Service Structure to provide for the insertion and/or removal of payloads at the launch pads. The Rotating Service Structure is a welded tubular steel space frame 189 feet high, 65 feet wide, weighing 2,100 tons, bridge which rotates about a pivot column at one end and travels on two 8 wheel trucks at the opposite end. This structure, as shown in Figure 1, has three basic support points. At the pivot column the structure is supported on a 30 inch diameter hemispherical bearing. At the opposite terminus the structure is supported on two truck assemblies each having eight 36 inch diameter double flanged wheels.

INTRODUCTION

There was no known "first" Shuttle Rotating Service Structure upon which to adapt, develop, and base various fundamental decisions. Thus because of its first of a kind requirement, a number of interrelated functional features had to be determined simultaneously. The fundamental purpose of this structure is to position a 50 foot wide, 45 foot deep by 130 foot high environmentally controlled payload changeout room in a mated position with the Orbiter Cargo Bay such that payloads can be inserted and/or removed without exposure to the outside environment, following which the structure can be moved away from the launch pad during launch of the Shuttle from the Mobile Launchers. Certain features of the existing Saturn vehicle launch pad together with the existing flame trench and existing Mobile Launcher Mount Mechanism also influenced and placed restraints on the configuration of the Rotating Service Structure. Other related factors which influence the mechanical features of this structure are: location of Fixed Service Structure, Cabin Access Arm, routing of fuel piping systems and electrical services from the pad to the Orbiter, locations of Orbiter access requirements, hinged access stairs to tail service masts and Orbiter contingency access locations, Cargo Bay door torque arm hoists and access platforms, motor operated bi-fold 65 foot high doors, pneumatic environmental seals, payload canister hoisting and guide rails, HVAC and hypergol spill emergency purge system, telescopic platform for access to interior of Orbiter Cargo Bay, and related configuration of Launch Pad. All previous launch facilities utilized movable structures that moved to remote locations for vehicle launches. The approach used for the Space Shuttle is a relatively fast moving structure that remained in the immediate vicinity of the launch environment. The challenge clearly was to design a Rotating Service Structure that achieved all of the related functional requirements. The Rotating Service Structure was designed to satisfy these interrelated functions, and the significant mechanical features are described in this paper.

FROM CHALLENGE TO ACHIEVEMENT

Thus at the program's inception an intensive effort was made to investigate all feasible alternatives, innovative approaches and techniques in order to meet the challenge. Fundamental to the challenge was the question of how to provide for insertion and/or removal of payloads 15 feet in diameter by 65 feet long weighing up to 65,000 pounds within a controlled environment and without "hard physical contact" with the Space Shuttle Cargo Bay. The synergistic features demanded that this activity be accomplished using a rotating structure that could be moved into a mated position with the Orbiter and subsequently moved to a retracted position for Space Shuttle launch without interfering with the normal movement of the Space Shuttle to the launch pad from the Vehicle Assembly Building. The rotating service structure achieved this objective. Handling of the payload canister was explored using a variety of different innovative approaches, including movement through the rear, top and bottom of the rotating service structure. The technique selected was the most innovative and offered the highest degree of operational simplicity which would result in the maximum reliability. Basically the technique included a payload canister having an exterior mold line matching that of the Orbiter around the Cargo Bay. This provided for a synergistic effect whereby the side of the rotating service structure which mated with the Orbiter could be configured to mate with the payload canister and the Orbiter using the same environmental seal features. The payload hoisting machinery was located on top of the rotating service structure and provided the means for hoisting the payload canister to and from the pad surface, mating the canister with the payload changeout room environmental seals, opening the 65 foot tall payload changeout room doors, and opening the payload canister doors, all without exposing the payload to the

ambient environment. In this position, the payload can be removed from the canister into the payload changeout room, payload changeout room doors closed, canister doors closed, canister lowered to pad surface, and subsequently the rotating service structure rotated into mated position with the Orbiter. See Figure 2.

Once mated with the Orbiter, the same pneumatic seals that mated with the payload canister are used to provide an environmental seal with the Orbiter. Thus the 65 foot tall payload changeout room doors can be opened, the Orbiter cargo bay doors open and the payload inserted into, or removed from, the Orbiter Cargo Bay without exposure to the ambient environment. See Figure 3.

Since the rotating service structure performs a variety of other Shuttle related support functions, it remains mated with the Orbiter until the appropriate time in the launch countdown at which time it is rotated to its retracted position for launch. The entire front side of the rotating service structure is configured to allow for mating with the Orbiter with approximately 6 inches clearance between "hard points," thereby allowing for personnel access to numerous Orbiter access locations. See Figure 8.

Other secondary functions which illustrate innovative solutions to challenging requirements include flip down access platforms and pneumatic hoists, located on the payload changeout room 65 foot high bi-fold motor operated doors, for handling and installation of "torque arm" that must be installed on the Orbiter Cargo Bay doors prior to opening these doors while the Orbiter is in the vertical position at the launch pad. Flip down access stairs are provided on both sides of the rotating service structure providing access to the tail service masts and the Orbiter. Additional features of major rotating service structure elements are included in the following discussions and illustrated in the appended Figures 1 through 10.

BASIC STRUCTURE

The basic structure, as shown in Figure 1, is a tubular steel space frame bridge spanning 160 feet from the pivot column at one end to the two 8 wheel drive trucks at the other end. Central to the structure is the Payload Changeout Room which, in its mated position with the Orbiter Cargo Bay, determined its relative location to the Launch Pad and Flame Trench. The pivot column is located just outboard of the Mobile Launcher clearance envelope and in line with the front truss of the structure. At the outer end of the structure the two truck assemblies travel on a double 175 pound rail system having a 3 foot gauge. Mechanical wedge type tiedowns are provided at each terminus of the rail system. The 160 foot radius of the rail system being determined by the Mobile Launcher Mount Mechanism clearance on the opposite side of the flame trench from the pivot column. Thus the Rotating Service Structure rotates about a pivot column with two electric motor driven drive trucks traveling on a 160 foot radius curved track system.

PIVOT COLUMN AND BEARINGS

The pivot column is 42 inches outside diameter by 33 inches inside diameter. At the top of this pivot column, as shown in Figure 2, is a bearing assembly comprised of a 30 inch diameter ASTM B 148-955-HT aluminum bronze hemispherical thrust bearing race rotary on a 41 inch diameter ASTM A182-304 S.S. Alloy steel thrust bearing, the hemispherical ball. Just below this main support bearing is a 61 inch diameter side thrust bearing race and ball. This pivot bearing assembly has a 6 foot 2 inch diameter, A441 housing with a removable cover retained in the housing by means of a tapered shear key ring, thereby allowing for bearing changeout in the unlikely event the need should ever arise. The vertical resultant load support at this bearing assembly during rotation of the structure is in the order of 2,000,000 pounds (1,000 tons).

A lower side thrust bearing is provided on the pivot column to accommodate resulting side loads and is configured similarly to the side thrust bearing at the top of the column.

Figure 4 shows the 3 point support system comprised of the pivot column top hemispherical bearing assembly and two eight wheel drive truck assemblies. The relative size of the top hemispherical bearing assembly is illustrated in Figure 5 as it was being assembled on the ground prior to erection onto the pivot column during initial construction. Figure 5D shows the bearing assembly erected onto the pivot column.

BEARING CHANGE OUT

The bearing at the top of the pivot column incorporates provisions for installing six hydraulic jacks which in conjunction with three bearing changeout bolts will allow for complete bearing changeout should the need for repair ever occur. The jacks and locking belts allow the load to be removed from

the bearings after which the housing cover can be removed and the bearings subsequently removed from the housing, repaired and/or replaced.

The lower side thrust bearing assembly incorporates similar means for bearing changeout. An interesting feature of the hemispherical side thrust bearings is that the ball can be rotated 180 degrees to allow insertion or removal from the race. Thus the top side thrust bearing is made in one piece. The lower side thrust bearing is made in three segments to allow installation and/or removal from around the pivot column.

The uniqueness of the pivot column and bearing assemblies resides in their not so obvious relative simplicity together with the means to allow for the unlikely need for bearing repairs and/or changeout.

DRIVE TRUCK ASSEMBLIES

The configuration and functional requirements of the Rotating Service Structure made it necessary for the structure to travel on a 160 foot radius curved track utilizing two drive truck assemblies, thereby providing a stable three point support system for the structure. Each truck assembly has a resultant vertical load during rotation on the order of 1,400,000 pounds during rotation. The question of single rail versus double rail resolves itself down into a question of space requirements for the truck assemblies. Utilizing 36 inch diameter wheels a total of 8 wheels are required on each truck assembly. On a single rail, the length of the truck assembly when incorporated into a load equalization system would be extremely long. The length of single rail truck assemblies could not be utilized due to Space constraints when the structure is mated with the Orbiter and also when rotated to the retracted position. Thus a double rail truck assembly was selected as most feasible for this application.

Each truck assembly is comprised of four two wheel bogies connected to a structural wellment frame by means of load equalization pins. At one end of the truck assembly the load equalization system incorporates two load equalization pins perpendicular to one another, thereby providing load equalization not only along the axis of the rails but also between the two rails. This system functions much like a tricycle. Each truck assembly is 8 feet wide by 20 feet long, weighing in the order of 70,000 pounds. See Figures 6A and 6B.

The truck assembly is driven by four 15 HP D.C. drive motors which are capable of moving at any continuous speed between 1/8 inch per second and 4 inches per second when delivering maximum rated torque. Each individual 2 wheel bogie has a drive motor connected to the two wheels through a gear reducer and gear train. The control system is a four quadrant regenerative D.C. drive system with solid state components capable of maintaining a preset speed during varying wind conditions that would try to accelerate or decelerate the structure during rotation. The control system is split into two sections, each section driving 1/2 of the number of drive motors. The two drive units are interconnected with a load sharing logic system that will allow any combination of drive motors to provide the necessary driving force.

THERMAL EXPANSION/CONTRACTION OF STRUCTURE

Mounted on top of each drive truck assembly is a hemispherical ball joint which is connected to the main 36 inch diameter, tubular structural members supporting the Rotary Bridge Structure. This assembly will accommodate the normal thermal expansion and contraction of the 160 foot long structure while maintaining load equalization onto the "tricycle" type load equalization system of the main truck frame. See Figure 7.

HURRICANE TIE DOWNS

Incorporated into each main truck frame weldment is a provision whereby the two side skirts move between two related tie down plates located on the pad surface. Once the structure is positioned at either of its two extreme operating positions, four steel wedges can be inserted thereby locking the structure into position. Unique with the tiedown system is the capability of jacking the trucks up approximately 1/2 inch and moving the wedges in further, thereby placing the load onto the wedges during hurricane load conditions. This allows the wheels and bogies to be designed for a lesser load condition of 40 knot winds during rotation as opposed to 120 knot hurricane wind loads. This feature also allows for removal and/or replacement of truck components, should the need arise. See Figure 6C. Details of the drive trucks and hurricane tie downs are best seen in Figure 7.

PAYLOAD CHANGEOUT ROOM (PCR) MAIN DOORS AND PCR-TO-ORBITER SEALS

To provide for payload changeout without exposing the payloads to the outside environment, two sets of two-panel bi-fold doors 29 feet wide by 62 feet high are provided. These doors together with the PCR-to-Orbiter seals provide the means whereby this can be accomplished. After the Rotating Service Structure is moved into its mated position with the Orbiter, the pneumatic seals are inflated into contact around the periphery of the cargo bay doors of the Orbiter. Following this operation, the cavity space between the exterior of the main doors and Orbiter Cargo Bay is cleaned with an air wash which is part of the PCR environmental control system. After the cleaning operation the main doors are opened, following which the Cargo bay doors may be opened and payload changeout operations conducted. The main doors also provide hinged platform and hoist features whereby a special torque arm can be installed onto the Orbiter Cargo bay doors to allow their operation when in the vertical position. See Figure 8.

PAYLOAD GROUND HANDLING MECHANISM (PGHM)

This system located inside the PCR can be described as a bridge crane supporting a 217 ton manipulator for insertion or withdrawal of the 15 foot diameter by 60 foot long by 65,000 pound shuttle payloads into the Orbiter cargo bay. This system was designed by NASA and FMC.

PAYLOAD ACCESS PLATFORMS

Five adjustable platform access levels are provided on each side of the PCR to provide access to any size payload configuration. Each platform is composed of an 8 plank adjustable module whereby the planks are pneumatically adjusted in and out to interface and provide access to any payload configuration. See Figure 10A.

ORBITER CARGO BAY ACCESS

An adjustable cantilevered access platform is provided to allow for access to the cargo bay interior payload attachment features. This platform in its retracted position is stored below the PGHM. When utilized, it is rolled out into position in front of the Cargo bay connected to hoisting cables and stabilizers. The platform can then be hoisted to any level of the vertical Cargo bay. Incorporated into the platform are two telescoping platform segments which can extend out into the Cargo bay, thus allow operating personnel access to any location inside the Cargo bay. See Figure 10B.

PCR CONTROLLED ENVIRONMENT

The Payload Changeout Room (PCR) is a controlled environment room 50 feet wide by 45 feet deep by 130 feet high. The temperature, humidity, cleanliness and pressurization are controlled by circulating 52,000 cfm of air through HEPA filters mounted on the ceiling with the return air passing through a pre-filter bank and chilled water cooling coils located above the fan room. The room is maintained at 0.5 inch W.G. positive pressure to prevent outside air from entering the room. Provisions are also provided for shutdown of the normal HVAC cooling pressurization system in the event of toxic hypergolic propellant spillage within the PCR. Should a propellant spill occur, the normal HVAC system is changed to a fresh air purging system by the coordinated interlocks between control dampers outside air supply fan, and purge air exhaust fans. See Figure 9.

90 TON CANISTER HOIST

A 90 ton, 2 speed 176 feet left, payload canister hoist is located in the hoist room on the PCR roof. This hoist system provides the means for lifting from the launch pad, or lowering to the launch pad, a payload canister. The canister is raised into position in front of the PCR main doors and mated with the pneumatic seals similar to that which is done with the Orbiter. Thus a payload can be inserted into or removed from a canister without being exposed to the outside environment.

ORBITER ACCESS PLATFORMS

A system of hinged flip down access platforms are provided for access to all required Orbiter access locations including a rolling window access ladder for Orbiter windows.

ORIGINAL PAGE IS
OF POOR QUALITY

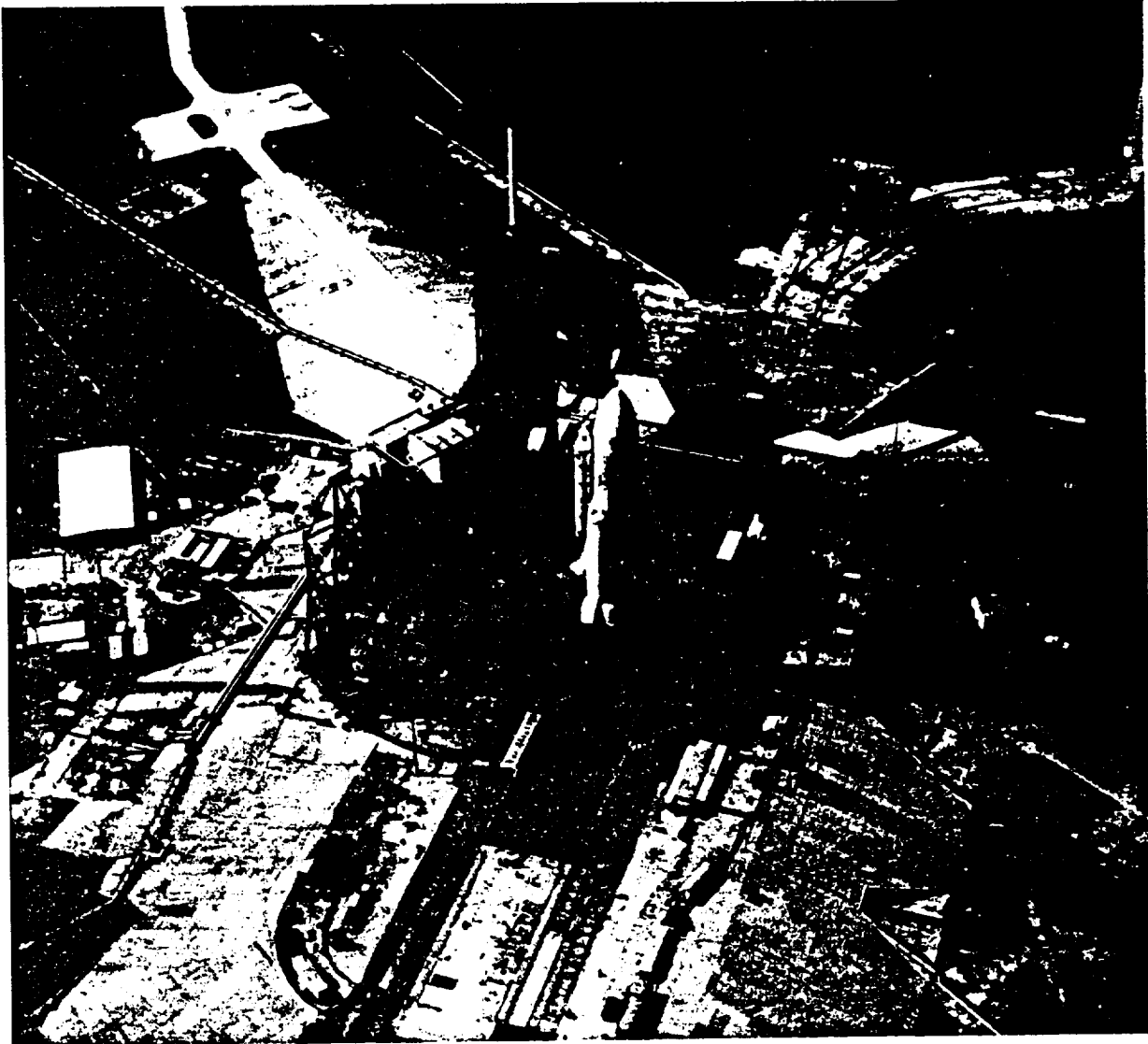


FIGURE 1. ROTATING SERVICE STRUCTURE SHOWN IN RETRACTED POSITION -
SHUTTLE READY FOR LAUNCH

LOADING OF FOUR QUARTERS

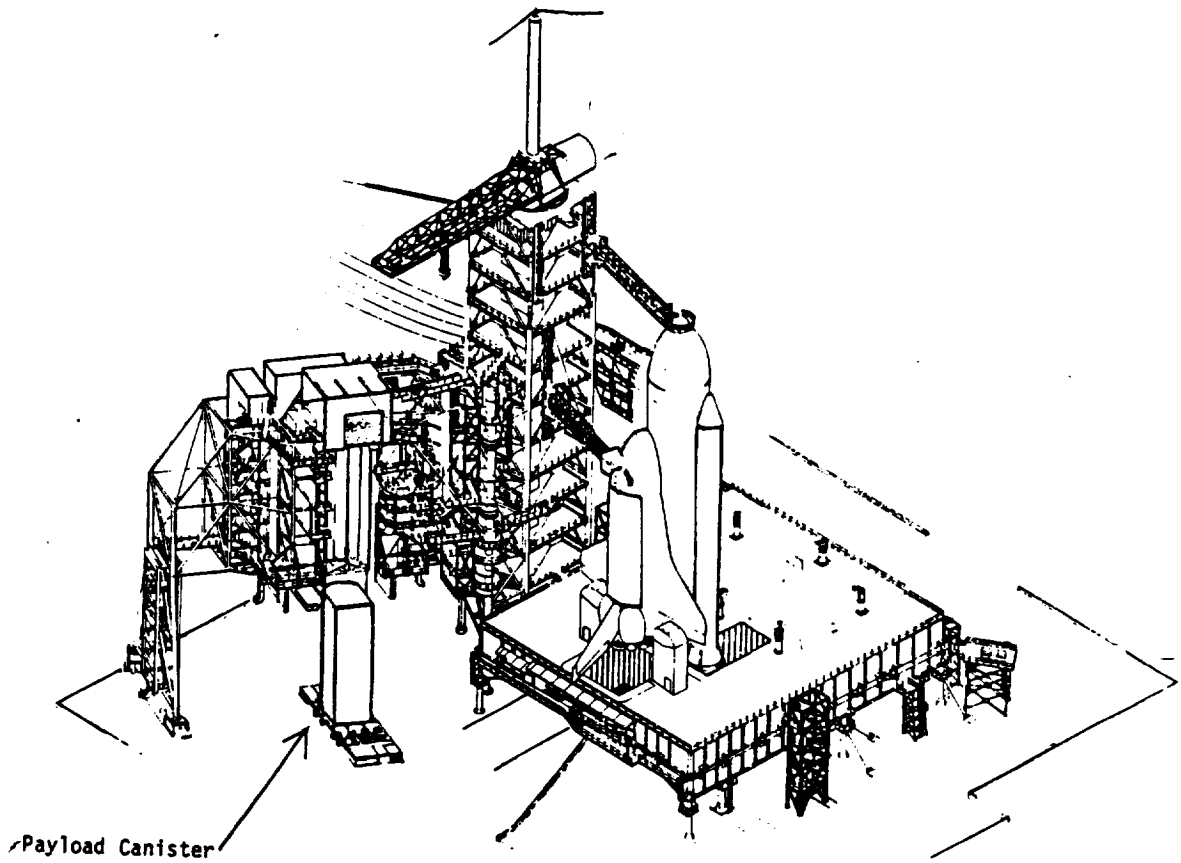


FIGURE 2. PAYLOAD CANISTER BEING HOISTED INTO PCR

ORIGINAL PAGE IS
OF POOR QUALITY

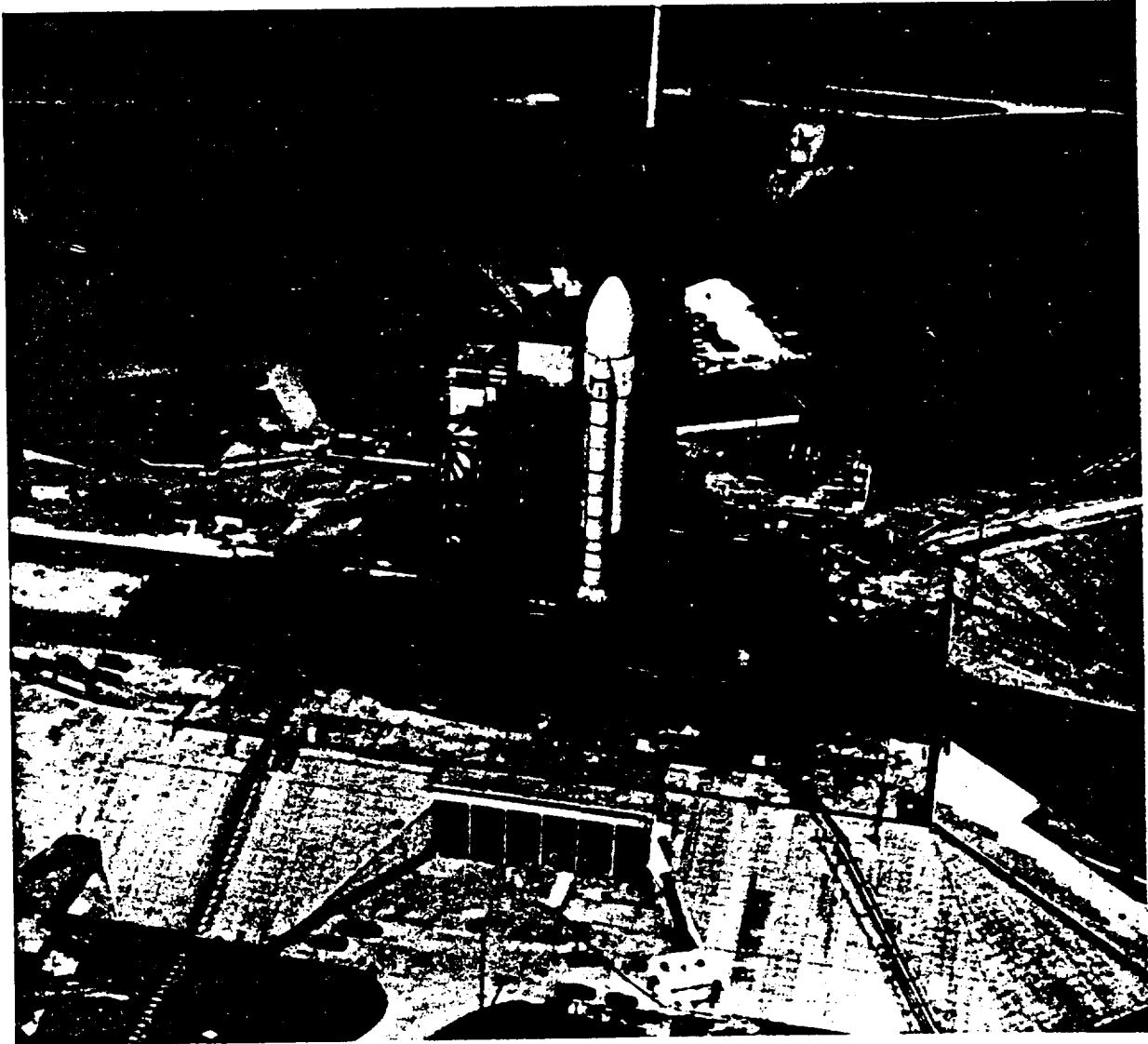
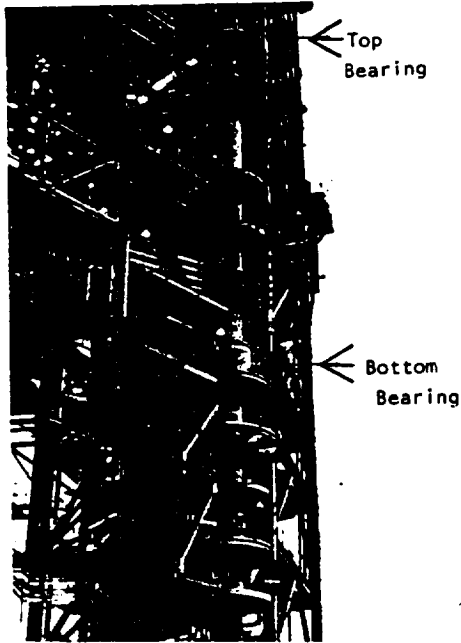


FIGURE 3. ROTATING SERVICE STRUCTURE SHOWN MATED WITH ORBITER FOR
PAYLOAD INSERTION OR REMOVAL

OF FOUR QUALITY



Pivot column bearings and utility crossover system designed for 120° of rotation with access and utility around the pivot column.

Figure 4A

The RSS is rotated on a 3 point support system comprised of a pivot column top bearing and 2 eight wheel drive trucks.

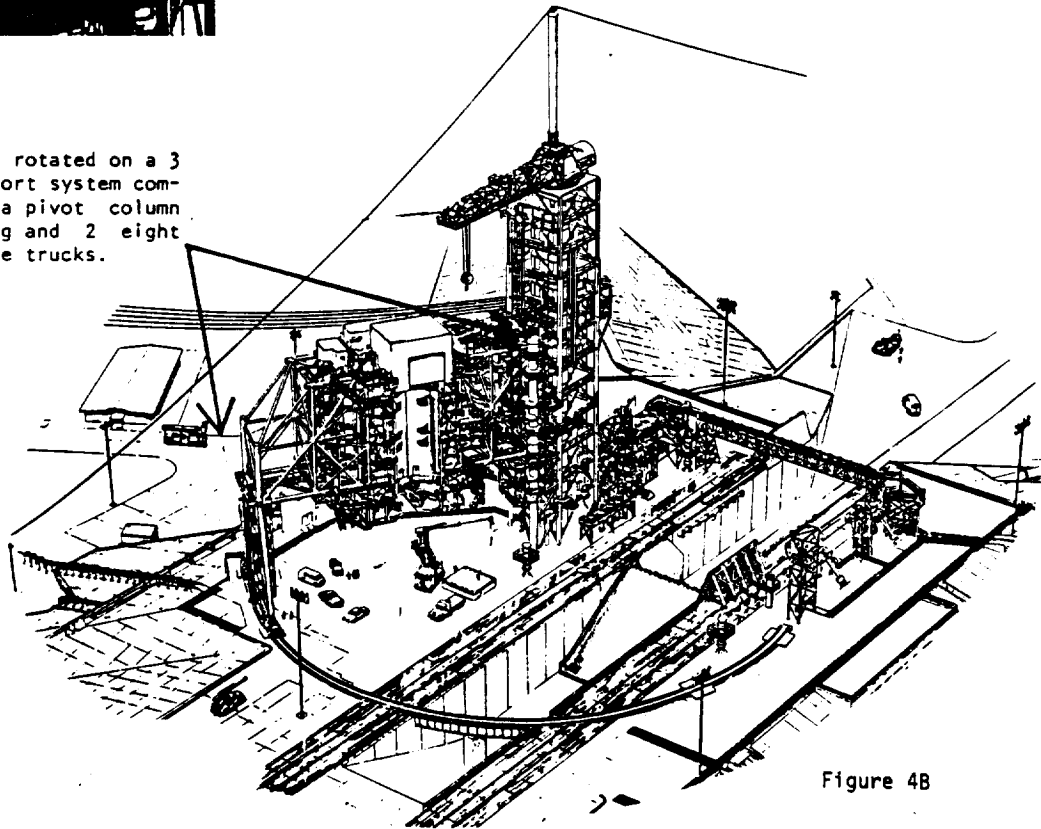


Figure 4B

FIGURE 4. 3 POINT SUPPORT SYSTEM

ORIGINAL FACE IS
OF POOR QUALITY



Figure 5A
Top Bearing Housing & Pivot
Column Being Assembled

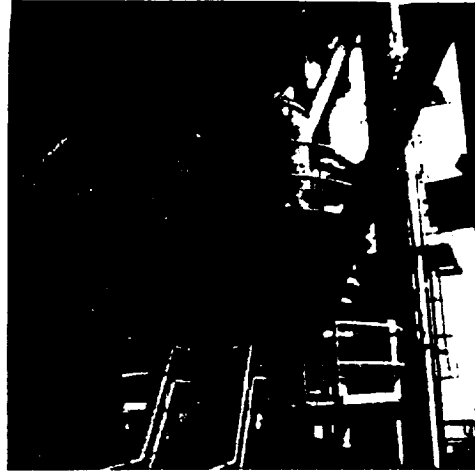


Figure 5D
Top Bearing Assembly Erected
on Top of Pivot Column

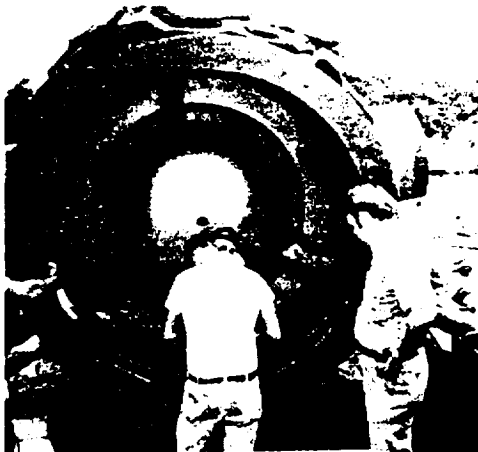


Figure 5B
Top Hemispherical Bearing
Assembled Inside Housing



Figure 5C

FIGURE 5. PIVOT COLUMN BEARING ASSEMBLY

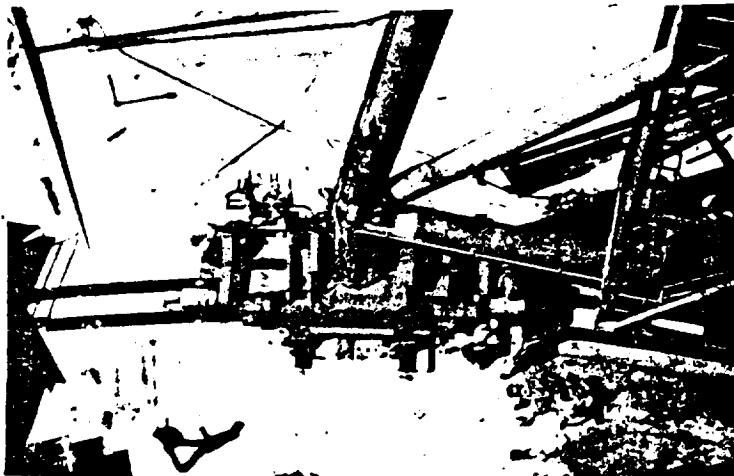


Figure 6A. Top View

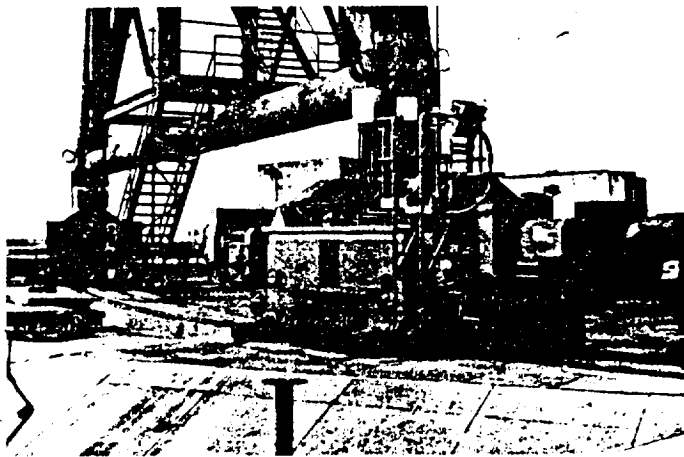


Figure 6B. Side View

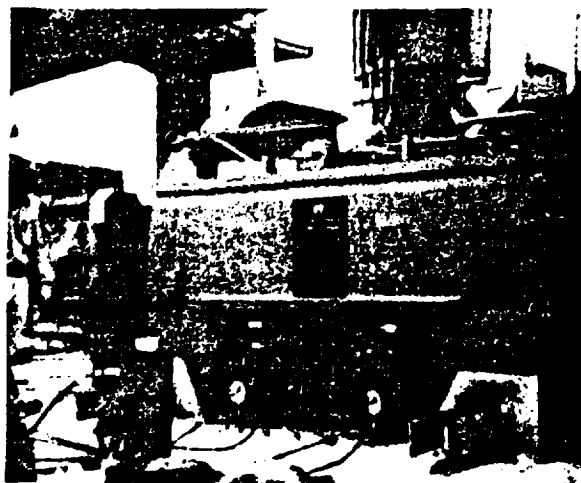


Figure 6C. Hydraulic Jacks and
Locking Wedges

FIGURE 6. DRIVE TRUCK ASSEMBLIES

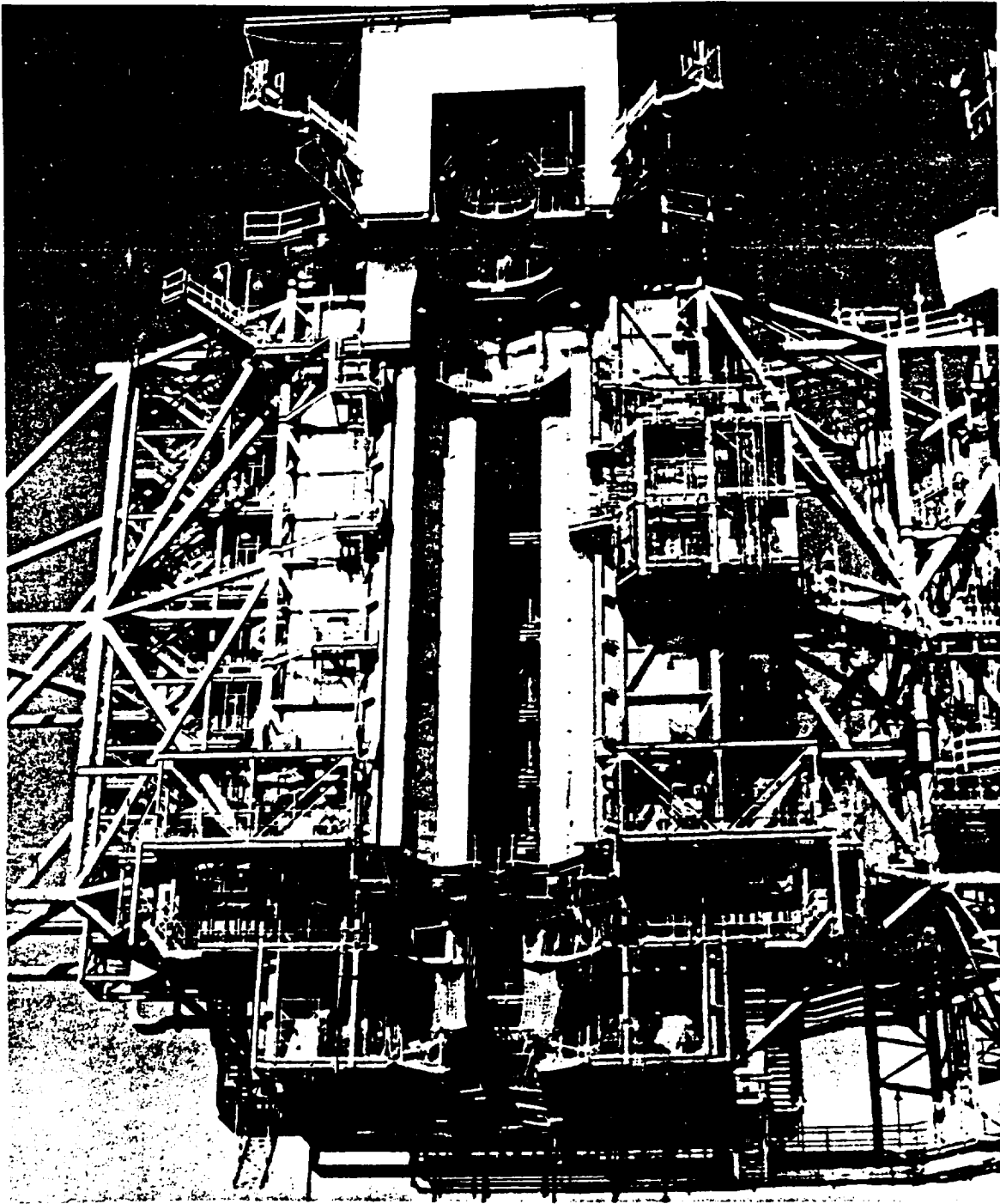


FIGURE 8. PCR MAIN BI-FOLD DOORS

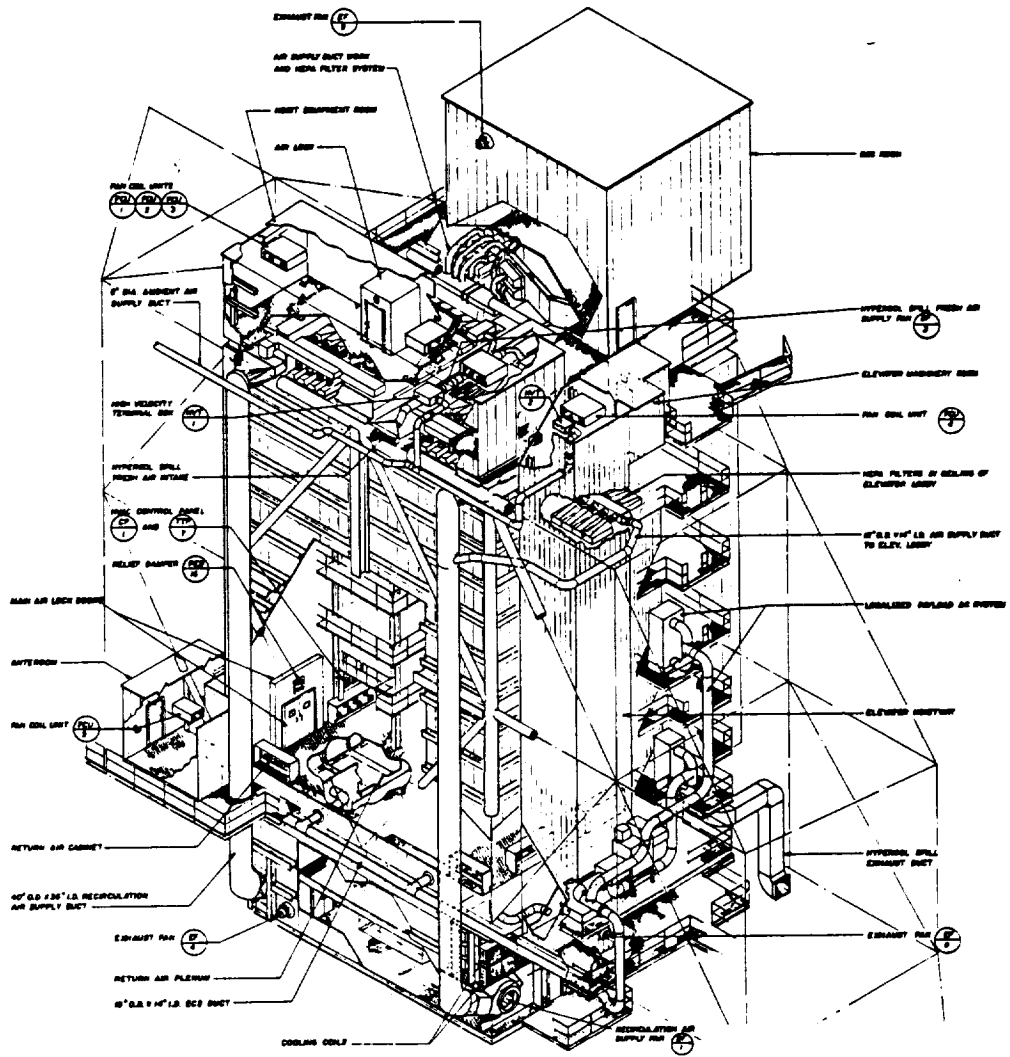


FIGURE 9. PCR CONTROLLED ENVIRONMENT SYSTEM

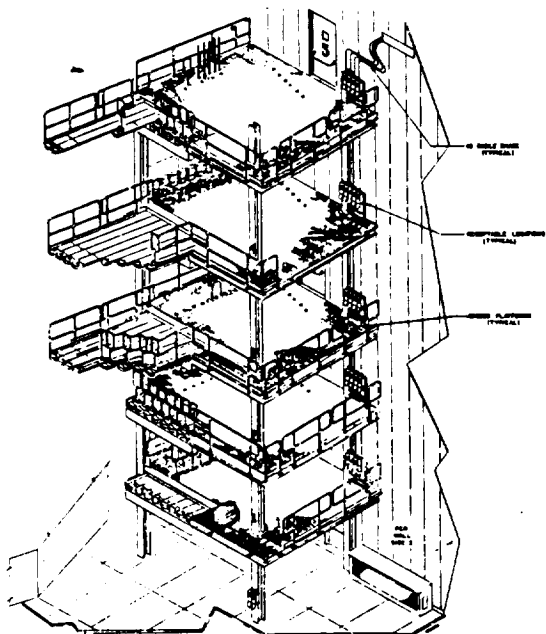


Figure 10A. Extendable Payload Access Platforms



Figure 10B. Orbiter LRU Access Platform

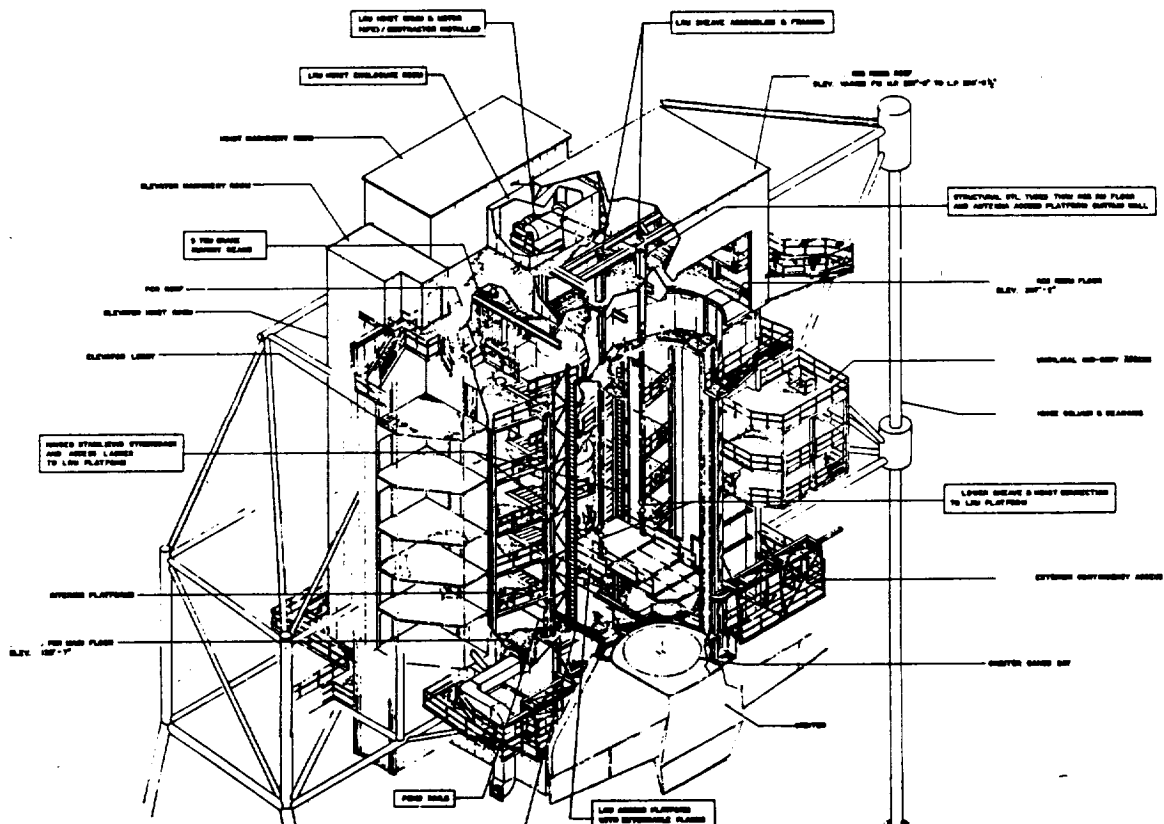


FIGURE 10. ORBITER LRU ACCESS AND PAYLOAD EXTENDABLE ACCESS PLATFORMS

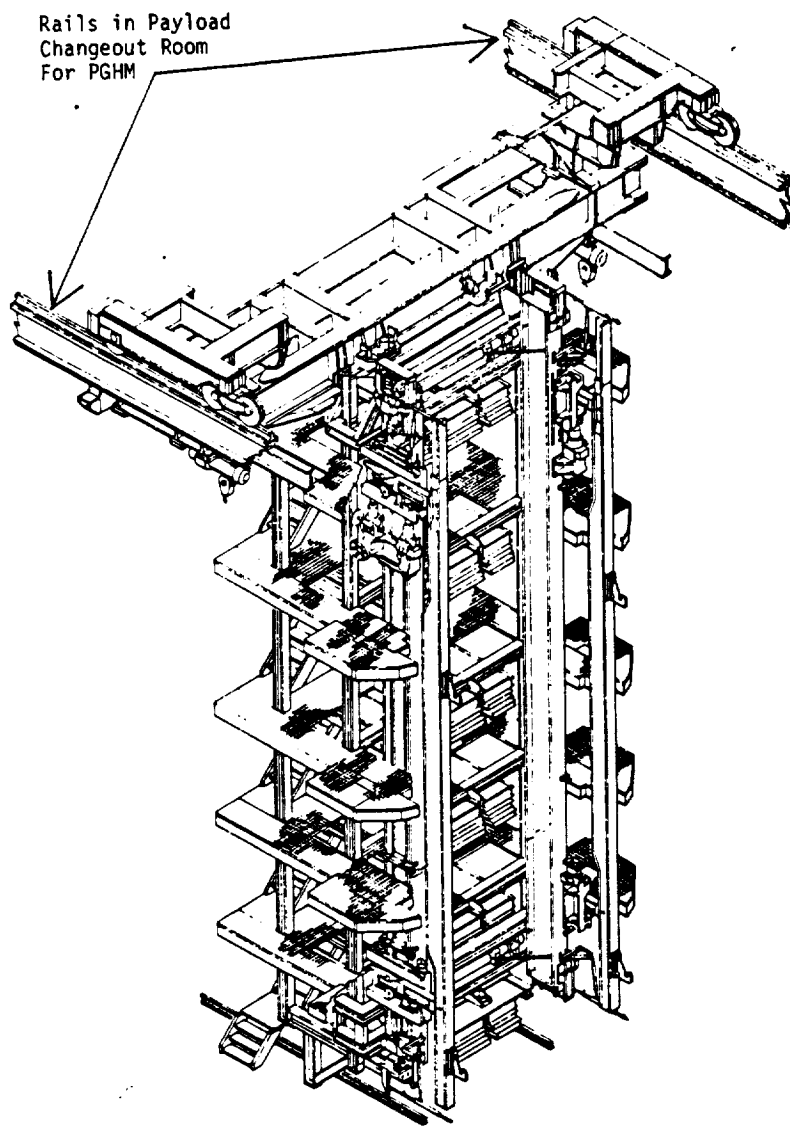


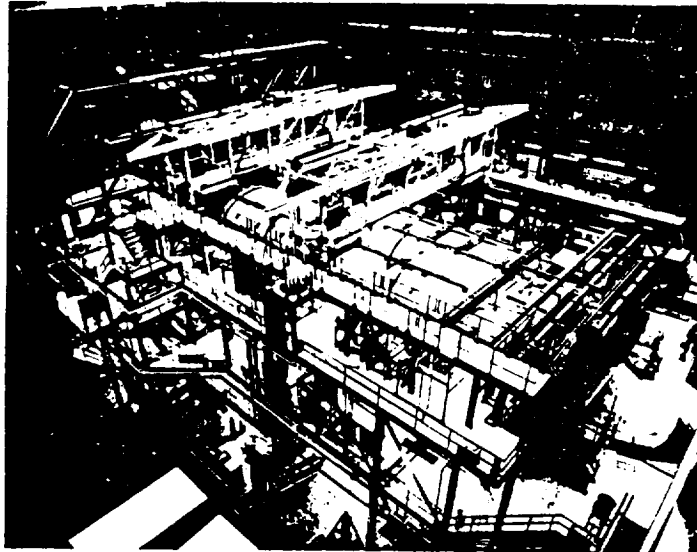
FIGURE 11. PAYLOAD GROUND HANDLING MECHANISM (PGHM)

OF PSC

ORBITER PROCESSING FACILITY: ACCESS PLATFORMS
KENNEDY SPACE CENTER, FLORIDA
"FROM CHALLENGE TO ACHIEVEMENT"by Michael Haratunian, P.E.
President
Seelye Stevenson Value & KnechtABSTRACT

The challenge presented to Seelye Stevenson Value & Knecht (SSV&K) by the National Aeronautics and Space Administration (NASA) was to provide a system of access platforms and equipment within the Orbiter Processing Facility to completely service the orbiter. NASA presented unusual design criteria to the firm: create a structure that allows service access to all areas of the orbiter without the need to step or lean on any portion of the craft; create a design that does not interfere with the movement of the orbiter during roll-in or roll-out of the facility; and, due to the concurrent development of the final version of the orbiter's geometry, design the structure with minimum clearances using preliminary data for Outer Mold Lines.

Towards this end, SSV&K developed a system of platforms that is responsive to the maintenance and testing requirements of the orbiter between space missions.



Orbiter Challenger in OPF.

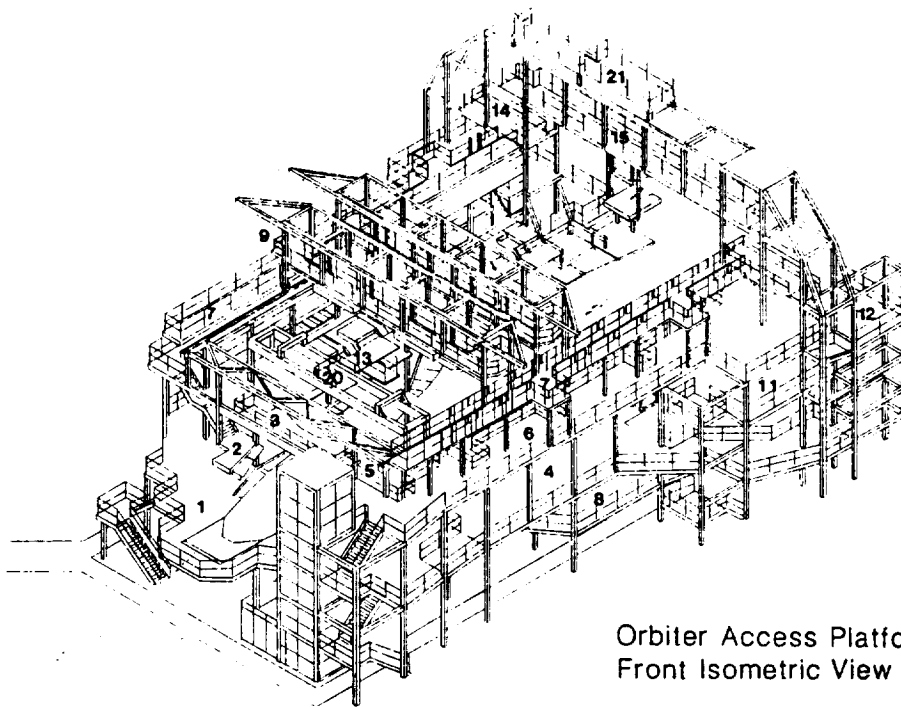
INTRODUCTION

Specified design criteria was met by the firm through research and development. Numerous studies were made using the clearance and load criteria specified by NASA. Final design was met by the interplay of concepts between NASA and SSV&K engineers during the detailed review of each section's needs. For example, the hydraulic actuators used for the platform's movements were chosen after discarding previous suggestions: use of an electric motor was rejected due to the danger of sparking within a hazardous environment; a non-sparking motor was eliminated due to excessive cost; and the use of compressed air was also contemplated, but was rejected due to lack of its availability at the site. Oil hydraulic actuators, fully sealed to prevent oil spillages, were finally chosen as the most advantageous method of providing the platform movement.

The design of the overhead bridge was also developed through close collaboration. The need for further access to the top of the Orbiter and payload bay was desired. Towards this end, the concept of an overhead structure was quickly recognized. By adding movement to this overhead structure, its versatility was greatly increased. A combination of longitudinal, transverse, vertical and rotating movements were subsequently developed.

The platform system which was ultimately developed consists of a series of fixed, moveable and cantilevered platforms. The moveable platforms include flip-up, flip-down, telescoping horizontal and vertical, scissor-type and completely moveable units. The overall platform structure is some 140 feet long, 91 feet wide and 58 feet high, and can support substantial dead loads, hoist loads, and live loads. Fixed stationary platforms were first developed, for required access elevations of the orbiter by working closely with NASA as the concurrent design of the orbiter was progressing. From these fixed areas, the moveable platforms were subsequently designed. These non-stationary platforms, closing within eight inches of the orbiter, are moved by manual or mechanical means in accordance with the size, location and type of motion required. To permit the orbiter uninterrupted access and egress into the OPF, the platforms flip-up, retract or swing free from the main structure. They are closed around the orbiter once it is in place and ready for servicing. Another feature of the design included the ability to cut back on the platform edges without affecting the structure's integrity. Therefore "hard steel", as we called it, was set back seven inches from the edge of platform. This seven inch section became known as "soft steel".

To facilitate design, a working scale model was constructed by SSV&K. This model proved to be a great aid to the firm and NASA in furthering the design to the construction stage.



Orbiter Access Platform
Front Isometric View

NASA Clearance Envelopes

The concurrent design of the orbiter along with OPF platforms presented an unusual design challenge for the firm. Achieving platform clearances specified by NASA required close collaboration between NASA and SSV&K engineers. During orbiter roll-in/out, jacking, and leveling, a minimum of 18 inch as clearance was permitted from the orbiter's Outer Mold Lines to each platform edge. Once the orbiter is in position and ready for servicing, a eight inches was permitted between the platform and the orbiter. During the moveable operation of a platform, four inches clearance from any moveable part of the platform to the orbiter was allowed. As mentioned earlier, the outer seven inches of each panel was constructed of "soft steel" to allow notching, penetrations or cutting away without affecting the structural integrity of the panel. The main structural support of each platform was set back seven inches from the panel edge. This became known as "hard steel". This ability to cut away portions of the platforms greatly increased the flexibility of the platform's design.

Load Criteria

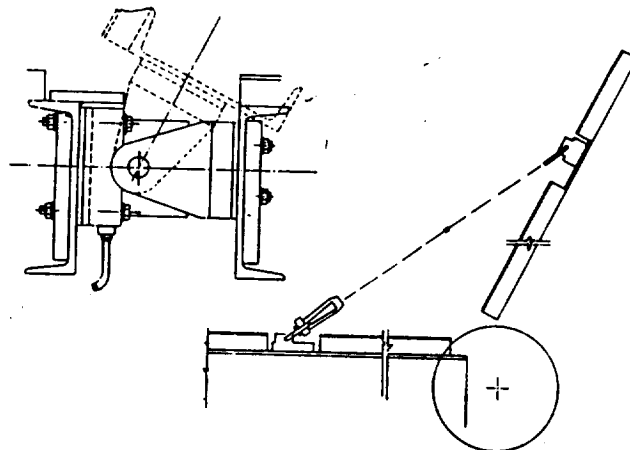
Another challenge presented to the firm was to design cantilevered and moveable platforms that also meet unusual live loads and deflection restrictions. SSV&K engineered a structural design that met deflections limited to $L/360$ of the span for nearly all platforms. Cantilevered elements, and the panels that swing-up and down were limited to $L/240$ of the span for live loads and equipment wheel loads.

Platform Movements

The movements of the platforms are an integral aspect of the design scheme. To provide complete accessibility as well as to maintain required clearances, platform extremities are made of hinged panels. The hinges are designed for both the swinging movement of the panels and as a support when the panels are in service.

The direction of a platform's movement was determined by the clearances below and above each platform. When a platform swings up, the hinge uses an integral bolt stop; when it swings down, the same hinge is rotated 180 degrees, and is supplemented with a toggle latch. This design permitted the use of a simple clevis-type hinge.

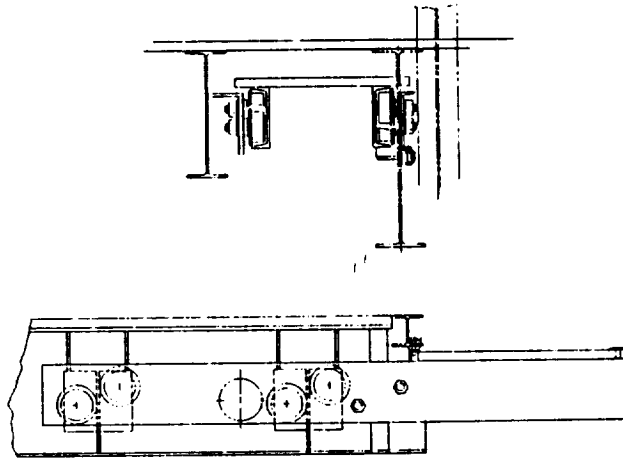
Several means of panel actuation are provided for swing-up platforms: a simple bar for lighter panels and manually operated winchs, and hydraulic rotary actuators for larger, heavier platforms. Hydraulic rotary actuators consist of a vaned heavy-duty torque motor with integral load-carrying bearings. In this case, the unit functions as both a hinge and actuator.



Swing Up/Down Platform
Hinged w/ Actuator

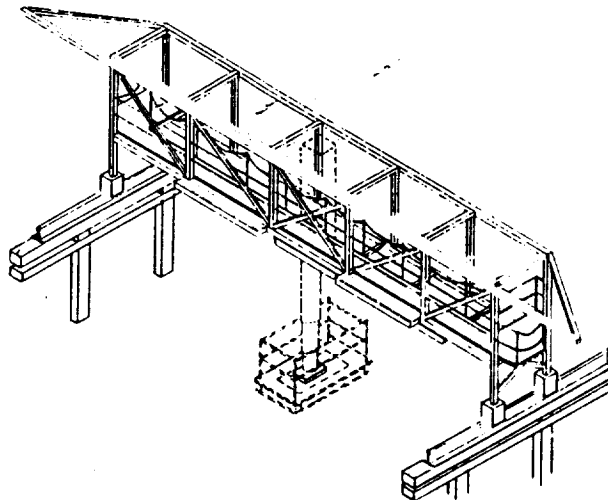
Where clearances were such that a hinged platform interfered with the orbiter's movement, platforms were made extensible by telescoping. The telescoping platforms are manually activated and have anti-friction bearing rollers that ride on hardened steel guides.

Manually operated hoists are also used for lighter swing-up and down platforms. These are of a simple-geared winch type with removable hand cranks.



Horizontal Telescoping Platform

Augmenting the main structure of platforms are two 50,000 pound moveable bridges that traverse along the length of the orbiter's 60 foot payload bay. Each bridge has two vertically telescoping platforms that move laterally across the width of the bridge as well as in a 360 degree rotation. These four vertically telescoping platforms (also called telescoping buckets) further enhance accessibility into and about the orbiter. A dual electrical motorized trolley system directs these 9 foot x 3 foot buckets transversely. They are positioned vertically using an electrically powered variable speed two-rope winch which actuates the telescoping bucket support. These buckets are supported by two electrically motor drawn bridges which use a chain drive system. The bridge rides on flanged wheels upon a rail equipped with anti-trip rollers for stability.



Rolling Bridges w/Buckets

APPLICATIONS OF MOVEABLE PLATFORMS

Using the series of movements, the platforms are flexible enough to successfully service the orbiter in accordance with each section's special needs.

Beginning with the front section of the craft, Platforms 1, 2, and 3 provide service personnel access to the nose, using flip-up and down movements. When these platforms are raised, they are secured away from the entering orbiter's nose section. Once the orbiter is in place, these platforms flip down and permit servicing of the instrumentation in this section, including antennae, the Orbiter Reaction Control Subsystem, and Startracker Well.

The Startracker Well requires a Class 10,000 clean room for servicing. To meet this need, a moveable anti-static nylon closure was devised to ride on fixed guide tracks and sliding assemblies. An air distribution system was also designed providing a positive air atmosphere.

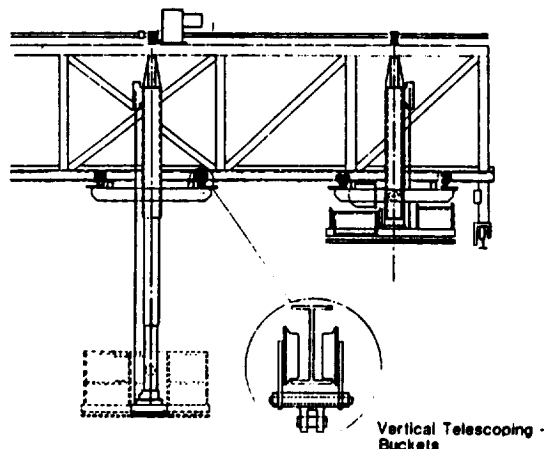
To permit the use of normal service equipment and consoles, these platforms are designed to hold a live load of 100 pounds per square foot, or 2,000 lbs. concentrated load over a 2'-6" square area.

Servicing the wing sections are Platforms 4 and 8. These also flip-up and down permitting safe roll-in, jacking, and leveling of the orbiter. The larger platforms in this section are powered by hydraulic actuators, while the smaller panels are manually raised and lowered, using a special hook designed for this purpose. These platforms permit service personnel to perform general maintenance on the wing, such as replacing the thermo-tiles. Platforms 4 and 8 can handle live loads of 100 pounds per square foot.

The payload bay area, 60 feet long with a 15 foot diameter, posed another special challenge in the design of the platform system: providing access to this section with the payload bay doors in a fully opened, closed or 145 degree, partially opened position.

This was accomplished using the combined movements of Platforms 11, 11a, 12, and 13. Platform 13 swings up and down along the length of the payload bay doors, and is therefore able to service the skin of the orbiter when the doors are fully closed. It also provides access into the payload bay cavity when the doors are fully extended by precisely fitting over the opened doors.

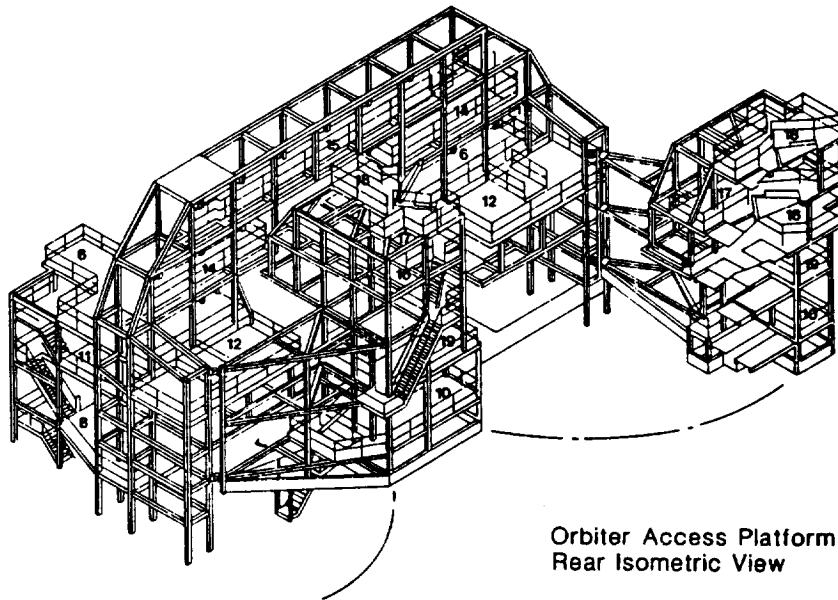
The overhead bridge and telescoping buckets further facilitate accessibility using four separate movements: the bridge with the telescoping buckets can move laterally along the length of the bay; the bucket platforms telescope vertically, up to 20 feet in either direction, thereby servicing the payload bay cavity itself or servicing the orbiter's skin when the cargo bay doors are closed; it can rotate 360 degrees and can also move along the width of the bridge, and therefore the orbiter. The 360 degree movement is controlled by a hand cranked gear reduced system operated from the bucket. A catwalk runs along the length of each bridge. This serves as a crossover platform as well as a service platform for the bridge and bucket drive system. Each bucket can support a 500 lb. load, while the bridge can accommodate 1000 lbs.



The design of the two bridges included provisions for support of the Zero- Gravity device used in opening and closing the payload doors.

Clearance of the C-Frame Support posed a serious problem. The C-Frame, which is attached to the Cargo Door Strong Back, swings down in an arc past the plane of the main platform truss line. Clearance envelopes were therefore developed and truss members positioned and shaped to give maximum clearance. There are six C-Frame locations on each side of the orbiter.

Platforms 10, 16, 17, 18 and 19 service the Rear Section, comprised of the Vertical Fin, Air Brake Actuator, Elevons, Orbiter Maneuvering System Pod and Main Engines. These platforms, composed of five levels, actually constitute a single structure, hinged to the fixed platforms.



Orbiter Access Platform
Rear Isometric View

Split into two hinged sections, the overall size of each is 17 feet x 20 feet x 50 feet high. Platforms 10, 16 and 19 swing up and down and service the engines and parts of the fin. They operate using hydraulic actuators and also telescope horizontally.

This section posed a major challenge: provide personnel access to external and internal service points at the rear of the Orbiter while also permitting the orbiter unobstructed movement during roll-in and roll-out.

After much research and study, the two 50 foot high rear swing platforms were each attached the main platform structure using a column as a pivot point, and then were swung from this point on a single rail embedded in the building floor. Each half of the platform structure has a 103 degree maximum swing, weighs a total of 98,000 lbs. and is operated by an electric motor drive.

The design of platforms which service the rudder and air brake actuators presented a further challenge to the firm. This required two sets of platforms of different configurations that can occupy the same area at different times. To meet this challenge, Platforms 17 and 18 were placed in this section with hinges at right angles to each other. Panel sections 3 and 6 of these platforms service the outer skin of the rudder, while sections 4 and 5 of the platforms service the rotary actuators inside, as well as the inner surface of the speed brake. Using this design, the two platforms can occupy the same area.

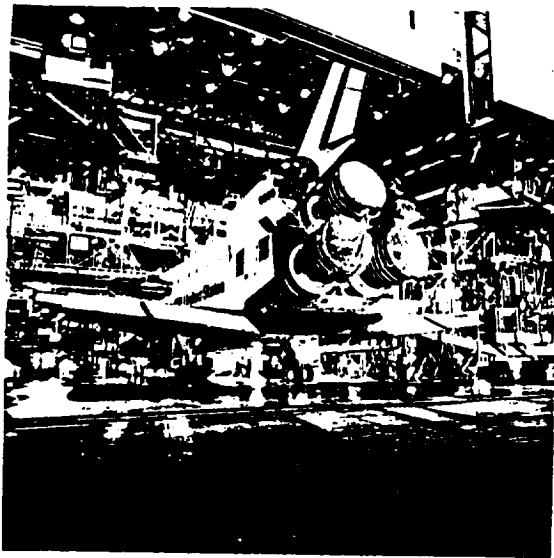
Removal of the Orbiter Manuevering System Pod required very close coordination between NASA and SSV&K, due to the concurrent design of the handling fixture and their respective platforms. Platforms 6, 11, 12 and 15 were designed to handle this section. The trolley and hoist used to remove the Pod is supported from platform 15. The Pod is then transferred to the overhead building crane.

Platforms 5, 6, 20 and 21 are stationary platforms. Platform 6 acts as a transit level to other platforms. Platform 21 is used for testing the antennae.

CONCLUSION

The concurrent design of the orbiter and the facility that would maintain it required close collaboration between SSV&K and NASA. The design of the system of platforms was the most challenging of the entire Orbiter Processing Facility concept. Near the end of the platform system's design, NASA developed, as a final check, a clearance envelope using a computerized matrix for the orbiter. A similar envelope was developed for the OPF platforms and their movements. Entry of the orbiter was then demonstrated using these two clearance envelopes. Only one platform within the entire system interfered with the orbiter clearances, which was easily rectified by cutting back part of the 7 inch soft steel section.

Our engineers recognized the need for a versatile and responsive system of movable and stationary platforms to meet all the needs of the service personnel in the maintenance and repair of the orbiter. The series of movements that were subsequently developed, and the mechanisms that permitted these movements, have resulted in a flexible system that permits free access around and within all areas of the orbiter.



Shuttle entering the Orbiter Processing Facility (OPF).

The principle SSV&K engineers of the OPF platform project were Fidele V. Plastini, P.E., project manager, Albert Thompson, P.E., structural, and James Campbell, P.E., mechanisms. Assisting in the preparation of this paper was Jill Bonamusa and Fidele V. Plastini. Graphics by Michael Bell, Peter Ruiz, and William Soto. The NASA KSC Project Manager was Ron Hinson.

Photos courtesy of NASA.

D32
N85-16969

EXTERNAL TANK GH₂ VENT ARM

Garland E. Reichle
NASA-KSC
KSC, Florida

and

Charles W. Glassburn
Planning Research Corp.
KSC, Florida

ABSTRACT

Because the venting of free hydrogen gas to the atmosphere presents an extremely hazardous situation, it was necessary to devise a means for safe, controlled venting of the Shuttle external tank (ET) gaseous hydrogen (GH₂) during and after liquid hydrogen (LH₂) tank loading. Several design concepts that were considered initially were discarded as unfeasible because of vehicle weight restrictions, high cost, and because the proposed structure was itself deemed a hazard due to the vehicle's nonvertical launch trajectory. A design concept employing a support structure/access arm attached to the Fixed Service Structure (FSS) was finally selected. The various design problems resolved included vent arm disconnect/drop interference, minimizing refurbishment due to launch damage, disconnect reliability, vehicle movement tracking, minimizing vent line pressure drop, and the presence of other vehicle services at the same centralized supply area. Six launches have proven the "system" to be reliable, efficient, and of nearly zero refurbishment cost.

INTRODUCTION

After a device or system has been developed, even we engineers who were involved in the development sometimes tend to look at the end product in its most obvious and most simplified form without thinking about how it got to be what it is. In almost all cases (be it a washing machine, car, house, or Shuttle system), that end product has evolved. The evolution is initiated by a need, which in turn causes development facets which we label design concept, analysis, hard design, fabrication, testing, and utilization. In between are literally hundreds of steps, decision points, and iterations that influence the end product. The most obvious major influences, though, are requirements, requirement changes, design accuracy as proven by test, and subtle operational changes that only become visible during the testing and operations application.

Such complexity as noted above is related in this paper on the Space Shuttle ET hydrogen vent arm system. The history of how that system evolved is an interesting blend of requirements and technology utilization.

The basic requirement that initiated the vent arm design effort was, and still is, to provide a controlled means of safely venting the GH₂ that is boiled off in the Shuttle LH₂ ET during and after LH₂ loading. This paper relates how that requirement was met. We will start where the initial need was first delineated and the challenge set. We will then progress through each step of the evolution to relate what was done and why, and will conclude with the present system.

THE CHALLENGE

As noted earlier, the basic requirement was to safely vent the GH₂ that is boiled off during and after ET LH₂ loading. This translated into more specific requirements as follows:

- o Provide a system to transfer the GH₂ boiloff to cross-country vent piping and thence to a burn pond.
- o Ensure that the system is connected and operable until Shuttle launch is certain.
- o Track all vehicle motions due to wind, solar, cryo, or other effects.

A secondary (but important) requirement was to provide an intertank purge system. This was never a design driver, but it is noted herein because the purge system was always considered to be coincidental with the GH₂ vent system. The systems physically had to go to the same vehicle area and could thus physically be (literally) tied to each other.

CONCEPT I

The initial concept was a straightforward and simple venting method. As shown in figure 1, the system would pipe the GH_2 directly from the top of the LH_2 tank down the side of the ET to a rise-off umbilical disconnect system in a tail service mast (TSM). From there, the GH_2 would be piped around the Mobile Launcher Platform (MLP) to the LH_2 disconnect tower and then to the burn pond.

Although this concept was simple, it was shelved rather quickly. At the same time the concept was being developed, Shuttle weight was becoming more and more a prime design driver. In the concept's final form, the weight of the piping, insulation, and tunneling was considered excessive unless no other viable alternative could be found.

CONCEPTS II AND III

The obvious approach to reducing vent system and purge system weight was to pipe directly from/to the intertank area. The major portion of the piping system's weight, then, would not be a direct part of the Shuttle. To do this would require a new umbilical plate, some sort of hanging or extended piping, and a disconnect method. Two concepts were thence developed which utilized tall structures to satisfy the accompanying vent and purge lines location, type of routing, and control needed. Concept II is shown in figure 2. It would utilize a new tower that would be built on the north end of the MLP. Concept III is shown in figure 3. It would utilize the FSS as its design base, namely, one corner of the 203-ft level. Both concepts first used the traditional horizontal swing-away umbilical system. However, in both cases, layouts and articulation analyses showed that the lengths of access arms needed, masses of the arms, and amount of rotation needed versus time to rotate for T-0 operations were all incongruent with design of a practical system. Thus, the drop-away umbilical-line approach was used, as shown in figures 2 and 3.

Both concepts had to meet the same physical restrictions of the Shuttle. These were: track the vehicle motions (regardless of cause), impose minimum forces on the Shuttle, and establish disconnect reliably, all without harming the vehicle. As the concepts developed, it became apparent that another requirement existed. The vehicle liftoff is not just up, but it also has an associated drift. Thus, whatever support structure was to be used and the vent and purge systems themselves could not be in the way of the vehicle. The restrictions on the physical location of Concept II's tower on the MLP were such that the tower would interfere with Shuttle liftoff. That in itself was enough to eliminate Concept II from further consideration. Added to this was the fact that the MLP would have to have major (expensive and technically undesirable) modifications to its north end to support the tower.

Concept III remained, then, as the most viable basic concept. As figure 3 shows, it consisted of a fixed arm, a retractable access (swing) arm for vent line hookup, and a vent line consisting of flexible and hard sections. (The intertank purge line would be piggyback.) The vent line was to be disconnected with a conventional mechanical advantage mechanism, i.e., a "hockey-stick" device, activated at the proper time by use of a lanyard. The vent line then would drop in a guided path. It would be expendable and thus be replaced after each launch.

At this point in time, many situations seemed to develop almost simultaneously. Studies of other ET systems kept resulting in more and more systems and requirements being added to the "vent arm assembly." Improvements in systems control, vehicle weight reduction, physical limitations or improvements, and/or safety aspects were the design drivers for these new systems requirements. It became apparent that a centralized access ground support equipment (GSE) grouping was needed. For example, GSE ET liquid oxygen (LOX) vent valve control was deemed necessary, so the pneumatic and electrical systems for that control were routed with the vent arm. Range safety needs (electrical), nose cone purge (pneumatics), ET instrumentation (electrical), and anti-icing/bipod heater power/control (electrical) were other needs routed with the vent arm. All of these, of course, affected the umbilical plate design itself and design iterations thereof. In addition, the access hatch to get into the intertank area was moved to the swing arm area to allow access on more than a contingency/emergency basis.

As the "group system" grew in total systems being accommodated, studies continued on the vent line itself. The line was sized several times. This was not an easy task because the diameter(s) had to be minimum to allow the total line to be manageable, hard sections were needed to support all of the pneumatic lines and electrical wires that were by then being routed with the vent line, and flexible sections were needed to account for vehicle tracking and similar movement aspects; yet the pressure drop through the line had to be minimal. (0.5 pound per square inch differential (psid) was the final design goal for the total vent line from the umbilical plate to the burn pond.)

One vent study showed that the line and its umbilical plate would, when released, scrape the side of the ET -- even if the vehicle did not "move into" the plate at disconnect. This situation forced a design change to provide for linear retraction of the vent arm at disconnect before the line would be

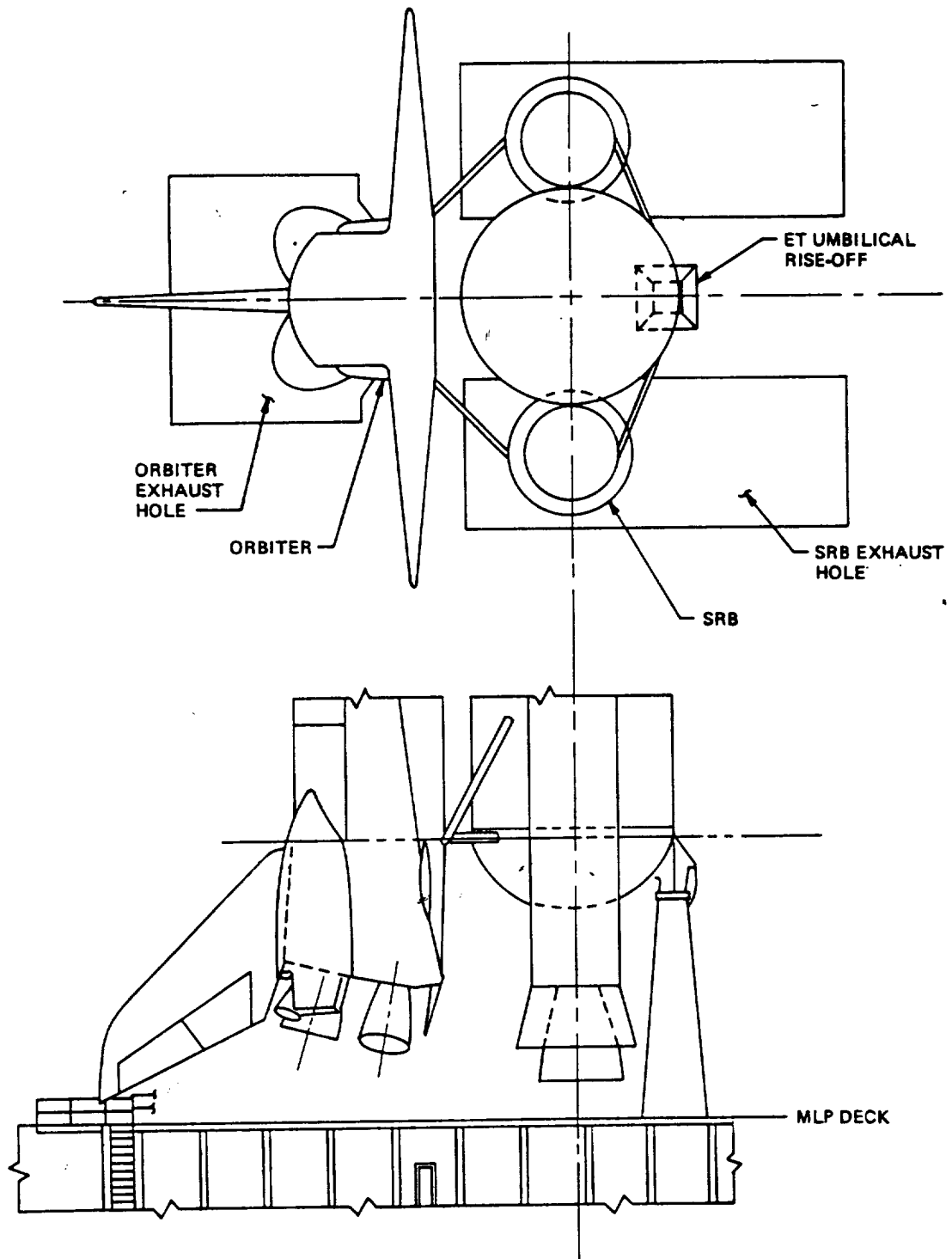


FIGURE 1. CONCEPT I (VENT THROUGH TSM)

ORIGINAL DRAWING
OF POOR QUALITY

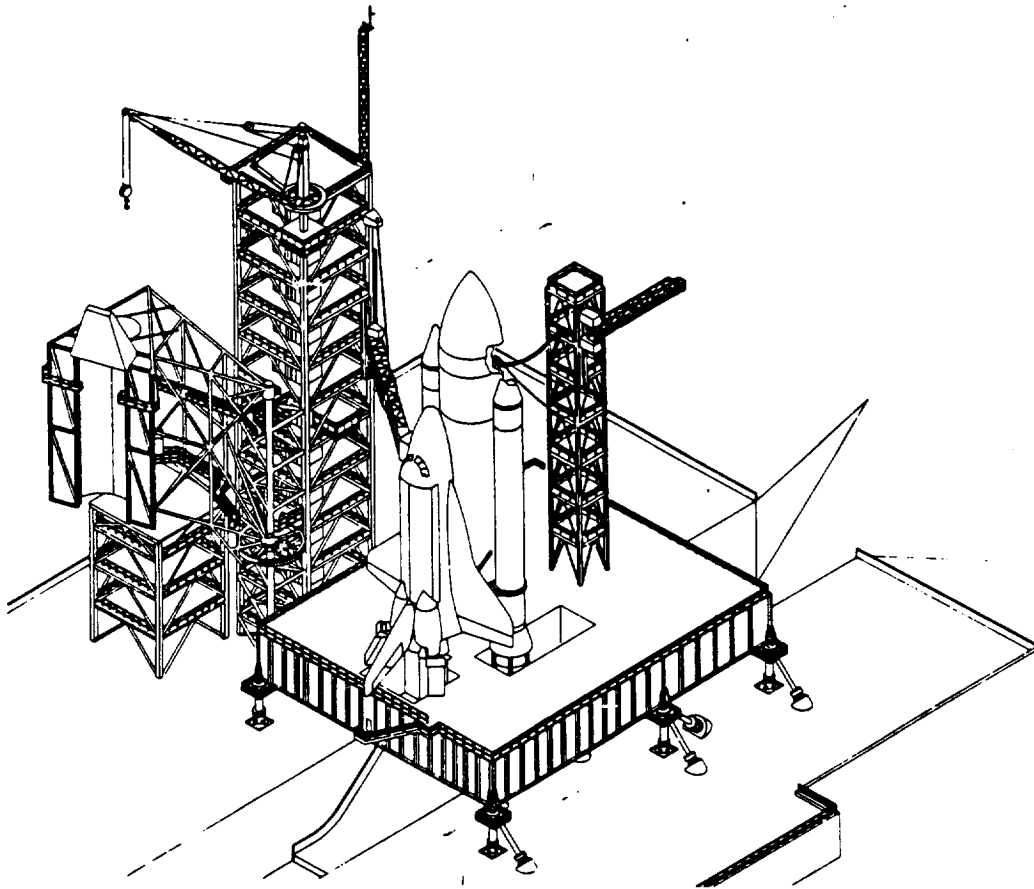


FIGURE 2. GH_2 VENT LINE CONCEPT II (TOWER ON MLP)

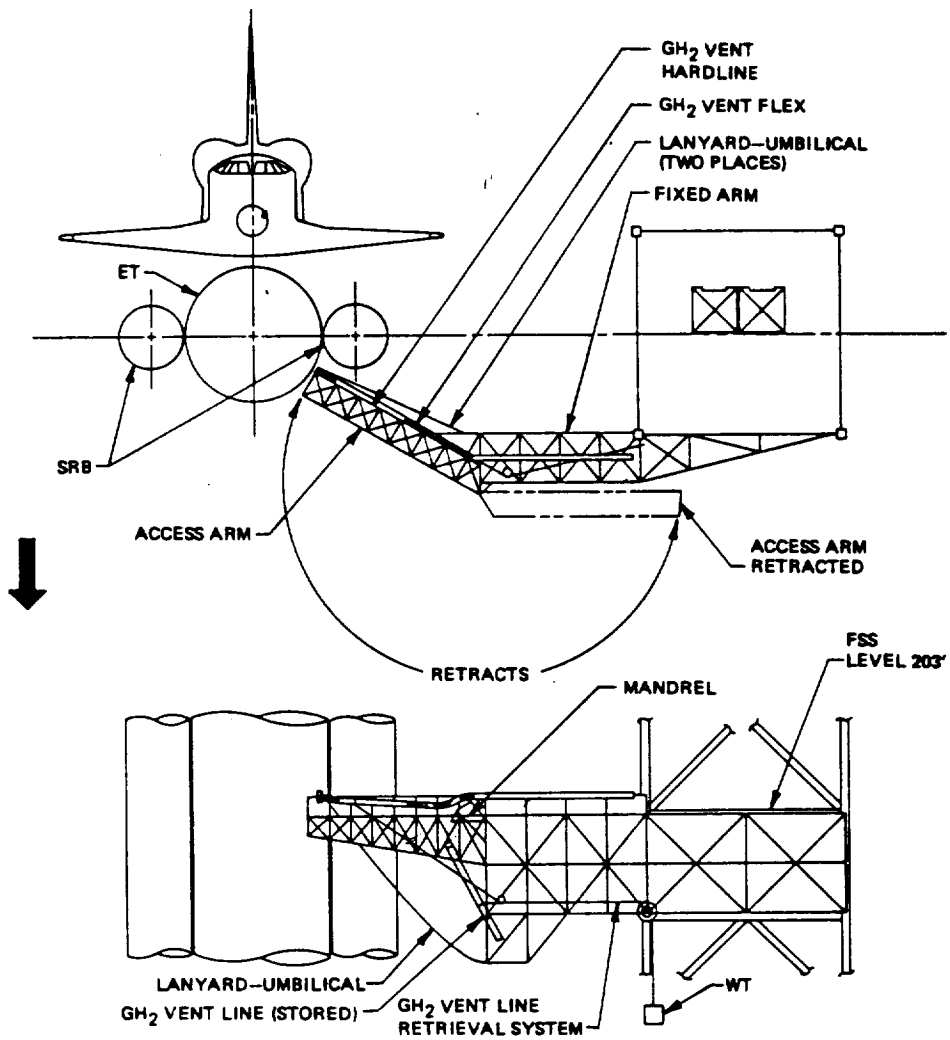


FIGURE 3. GH₂ VENT CONCEPT III (BASE FROM FSS)

allowed to "fall." That change was a dropweight mechanism balanced to pull back the vent line about 24 inches before line drop.

Due to tracking requirements and refined draft analysis, the lanyard-activated hockey stick umbilical disconnect device did not clear the vehicle trajectory in the worst case. It was considered that pyrotechnic bolts fired at T-0 would be a more positive and technically sounder way to release the ground-to-flight umbilical plates, giving the system more time to release and clear the vehicle. After much deliberation and many ministudies, it was decided to use the pyrotechnic bolts as the primary release and the lanyard as a backup. (The lanyard becomes taut only after the vehicle moves up 26 inches.)

Another major system study was cost. The expendable approach was shown to cost about \$50,000,000 for the Shuttle launch series of about 450 launches. That cost was excessive. So, a major effort was started to minimize launch damage. The result was to guide the vent arm back under a blast structure, put protective blankets over the flexible line sections, and install a deluge water system to saturate the vent arm during vehicle ascent. This was determined to reduce refurbishment cost to 25% of replacement cost. Indeed, these "fixes" have been good enough to reduce refurbishment cost to essentially zero.

TESTING

Testing was done primarily on a system basis. The total "group system" was tested at KSC's Launch Equipment Test Facility (LETF). The tests did not show any major design deficiencies. Basically, the system was fine tuned with the tests as well as being qualified mechanically. The only design aspect that was questioned aggressively, i.e., the disconnect method, was settled by the tests. The first concept verification testing (CVT) series of the lanyard umbilical disconnect was conducted before the pyrotechnic bolts were selected as the design approach. The second test series system qualification testing employed the bolts and proved the design concept.

PRESENT ASSEMBLY

In summary, the external tank GH₂ vent arm presently provides for more than just venting GH₂. It is an access system for the ET intertank area, and it provides for GH₂ venting, for all ET electrical and pneumatic support subsystems (including all gas purges), and for umbilical plate service in itself. The assembly is best described in two parts: ET vent umbilical system and intertank access arm.

ET HYDROGEN VENT UMBILICAL SYSTEM

This system provides for continuous venting of the Shuttle ET during and after LH₂ loading. It also provides the pneumatic line and electrical cables between the ground systems and the umbilical interface. The umbilical system disconnects at solid rocket booster (SRB) ignition command. The hydrogen vent line then pulls back, drops away, and is secured during vehicle liftoff. Figure 4 depicts the system.

Vent Line Assembly

This assembly consists of two vacuum jacketed flexhoses and one double wall hardline. The aft flexhose makes the connection between the hardline subassembly and the facility vent line interface. The forward flexhose makes the connection between the hardline subassembly and the intertank hydrogen vent umbilical interface.

Structural Platform Extension

The platform extension has four levels floored with steel grating. It provides space for equipment installation and personnel access for service, maintenance, and checkout of the vent line and access arm. A platform is attached to the side of the main platform providing a base for mounting the hinge actuation mechanism of the access arm, the haunch pivot fixture, the withdrawal mechanism, and the deceleration unit.

Haunch Pivot Fixture

This is a structural enclosure mounted on the top level of the fixed platform extension. The haunch pivot fixture contains the pivot links which support the facility end of the vent line and allow the vent line to adjust for vehicle movement and misalignment. The haunch also provides mountings

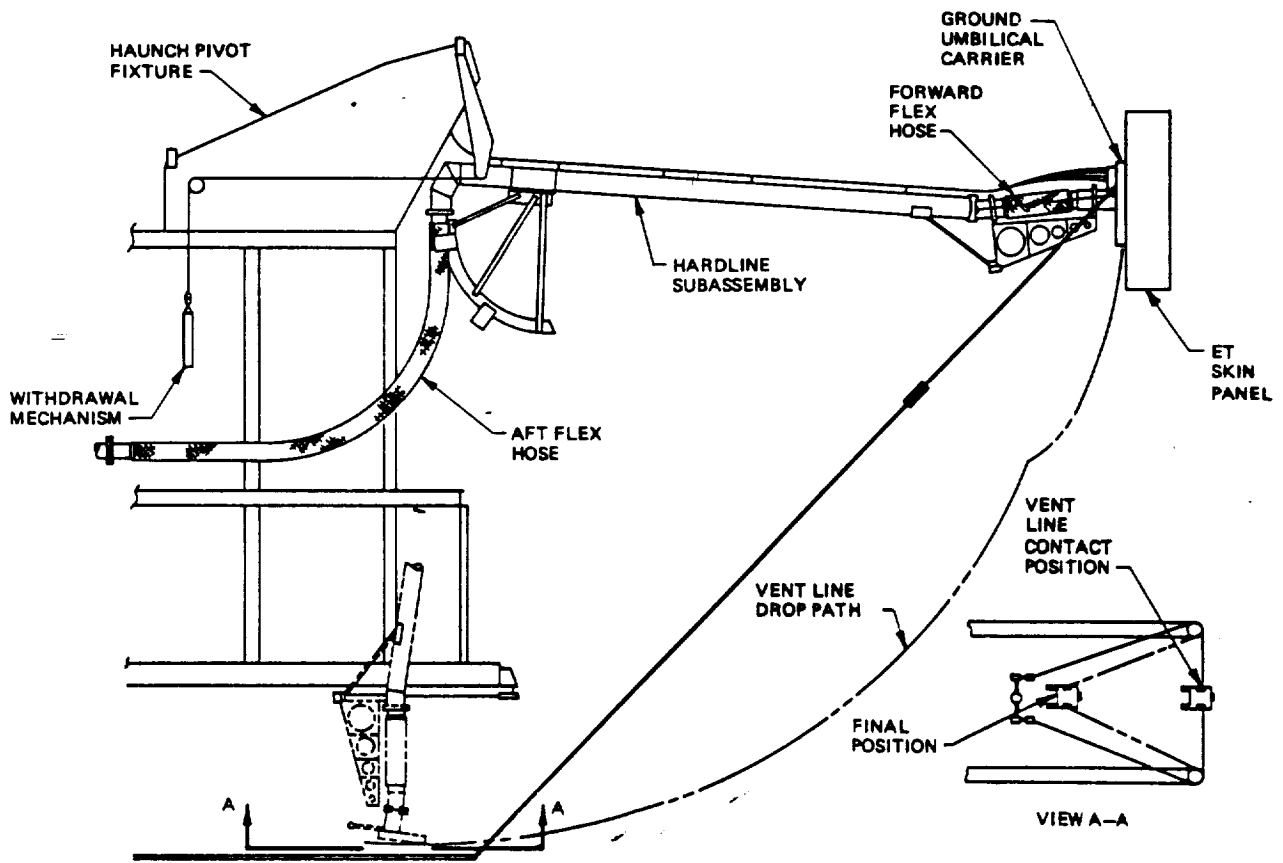


FIGURE 4. ET HYDROGEN VENT UMBILICAL SYSTEM

for the pivot link shock absorbers, latch back mechanism, guide sheaves for the withdrawal weight cables, and bulkhead for pneumatic and electrical interface with the vent line.

Withdrawal Mechanism

This mechanism is located at the back of the haunch fixture. The mechanism has side rails which guide a dropweight. Wire rope cables attached to the weight are routed over the guide sheaves in the rear of the haunch and are connected to the pivot links.

The potential energy of the suspended weight retracts the vent line via the pivot links after umbilical disconnect. The unit utilizes a manually operated winch to raise and reset the dropweight and shock absorbers mounted at the bottom of the side rail frame to decelerate the dropweight at the end of its travel.

Deceleration Unit

The deceleration unit is an arresting device utilizing a tension shock absorber. A cross beam with sheaves is attached to the rod end of the shock absorber. The wire rope arresting cable is routed through sheaves located horizontally and vertically. The routing geometry of the arresting cable allows the falling vent line to be decelerated and stopped approximately 92 inches after contact with the vent line support bracket. A mechanical latching device secures the vent line in the retracted position.

Ground Umbilical Carrier Assembly

The ground umbilical carrier assembly is a structural housing for the ET service line couplings which are mated to the ET umbilical panel. The carrier assembly is attached with a pyrotechnic separator which bolts the carrier assembly to the ET skin panel. The umbilical carrier is released from the ET panel when the pyrotechnic separator receives a triggering signal.

Static Lanyard Mechanism

The static lanyard mechanism is designed to increase the reliability of the ET vent line disconnect function by providing a secondary release system. The static lanyard is attached to each side of the ground umbilical carrier plate and to the structural platform extension. The lanyard is routed through a sheave and pivot arm mechanism, which allows the lanyard to track the vehicle during prelift-off excursions. The pivot arm is weighted to maintain lanyard tension and to minimize lanyard catenary. The mechanism is designed to allow 6 inches of cable feedout prior to the secondary disconnect.

INTERTANK ACCESS ARM

The intertank access arm provides a movable work platform for prelaunch servicing and checkout of the Space Shuttle ET intertank area. It provides the capability of lifting and positioning the vent line, installation with the ground umbilical carrier plate, personnel access for umbilical servicing, personnel access to the intertank tank compartment, AC power, lighting, and environmental control system service. Figure 5 depicts the arm.

Truss Assembly

The top surface of the truss is floored with grating, which serves as a walkway for personnel access. The line handling fixture is attached to the outer end of the truss and provides an air motor driven winch. The winch is used for lifting the vent line into position for installation with the umbilical and supports the vent line until the access arm is retracted.

Hinge Actuating Mechanism

The hinge actuating mechanism is a hydraulic cylinder actuated roller chain and sprocket drive unit. The two hydraulic cylinders are powered by hydraulic fluid supplied from the facility hydraulic system. A manual valve on the control panel controls rotation of the access arm.

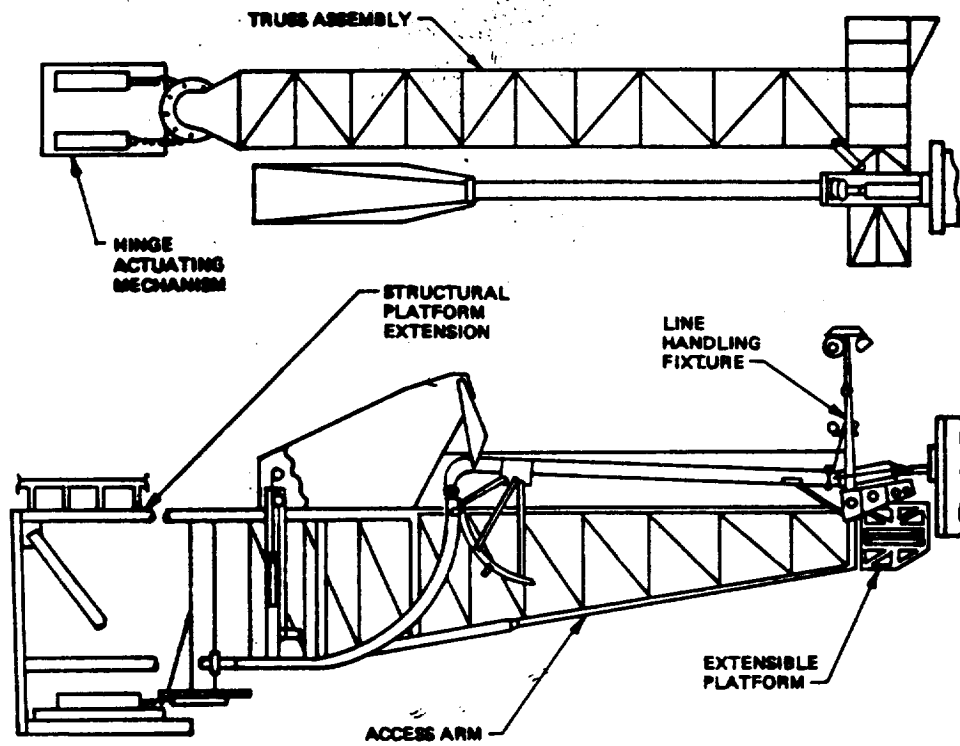


FIGURE 5. INTERTANK ACCESS ARM

The roller chain is a triple-strand chain which drives a sprocket. The sprocket is attached to the bottom of the hinge assembly, which is supported by a large self-aligning spherical roller bearing. This bearing acts as the lower pivot of the hinge and carries the thrust and radial loads of the access arm. The upper pivot of the hinge assembly has a smaller self-aligning spherical roller bearing, which carries the moment loads of the access arm.

Extensible Platform Assembly

This assembly consists of a fixed platform attached to the outboard end of the truss assembly to provide personnel access to the intertank area. A sliding platform can be extended from the side of the fixed platform, allowing personnel access for servicing the hydrogen vent umbilical, pneumatic service lines, and vent line. The sliding platform is extended or retracted by a handwheel-operated chain and sprocket drive.

SUMMATION

The challenge to provide a safe and reliable means to vent the hydrogen from the Shuttle ET was met through innovative design of a mechanism evolving from changing requirements and employment of basic concepts striving to be both cost effective and highly reliable. The Shuttle ET GH₂ vent arm "system" began as a simple vent line running down the side of the ET and ended as a rather complex centralized servicing system built onto and out from the FSS. Primary design drivers were vehicle weight, vehicle movement on the pad, vehicle launch trajectory, launch damage/refurbishment/replacement costs, physical limitations to ensure no damage to the vehicle at disconnect, and the number of vehicle services other than GH₂ venting through or at the same location. The "system" has operated almost flawlessly for six launches, with refurbishment costs nearly zero.

POOR QUALITY

D33
N85-16970

PAYLOAD TRANSPORTATION AT KSC

Michael E. Donahue
Planning Research Corp.
KSC, Florida

ABSTRACT

Cargo ground processing at John F. Kennedy Space Center (KSC) involves either a horizontal or vertical mode of assembly and processing of the Shuttle Transportation System (STS) payloads. Consequently, cargos are commonly referred to as horizontal or vertical payloads. The process flow for each mode requires different facilities and transportation requirements. Occasionally, a mixed mission cargo containing both horizontal and vertical payload elements will require a combination of horizontal and vertical transportation between facilities. This paper presents some of the engineering challenges and innovative solutions to satisfy the unique on-site payload transportation requirements at KSC. In particular, some of the more demanding design requirements of the Multiuse Mission Support Equipment are presented, and the resulting engineering designs and unique solutions are outlined.

INTRODUCTION

Horizontal cargos are assembled and tested in the Operations and Checkout Building (O&C) where all electrical, fluid, and mechanical interfaces between payload segments and Shuttle Orbiter are checked and tested. When integration and testing are complete, the payload is transported to the Orbiter at the Orbiter Processing Facility (OPF) and installed in the Orbiter payload bay. A vertical payload undergoes similar assembly and integration at the Vertical Processing Facility (VPF) and is then transported to the Shuttle launch pad where it is hoisted up to the Payload Changeout Room (PCR), a part of the Rotating Service Structure (RSS). It is then picked up by the payload ground handling mechanism (PGHM) for installation into the Shuttle Orbiter.

Mixed payloads require a combination of horizontal and vertical processing that culminates in the vertical transportation of the mixed cargo to the launch pad PCR. The rotation from horizontal to vertical is accomplished using two bridge cranes at the Vehicle Assembly Building (VAB). A flow chart of these requirements is shown in figure 1. The system created to accomplish the unique on-site transportation requirements for complete payload cargos and/or payload segments during line STS processing is called the Multiuse Mission Support Equipment (MMSE).

MMSE

The MMSE system was conceived to include a payload canister to structurally support and environmentally protect the payload during transportation operations, and a transporter to move the canister with the payload between KSC facilities for processing into the STS Orbiter. In addition, a complement of payload services to support the payload during transportation is required. It includes an electrical power unit, an environmental control unit, a fluid and gas services supply unit, and an instrumentation module to monitor the payload environment and critical payload measurements. The design and operational requirements for each element of the MMSE presented a unique engineering challenge.

PAYLOAD CANISTER

The payload canister must support all payloads that are possible for an STS mission; therefore it must accommodate a cargo volume of 15 feet in diameter and 60 feet long, with a maximum cargo weight of 65,000 pounds. The cargo can consist of one to five segments at one time, and the payload must be kept in a clean-room environment during transportation operations. The canister with payload has to be hoisted and rotated between the horizontal and vertical positions with only small deflections allowed in the canister structure so that loads are not induced into the payloads. This dictated a relatively stiff structure; however, gross weight is limited to 180,000 pounds because of the hoisting capacity at the launch pad for lifting the payload up to the PCR. Also, the canister must physically fit into all payload facilities (PCR, O&C, VPF, OPF) with its payload doors opened for removal of the payload.

The evolution of the canister design resulted in the configuration shown in figure 2, which is very similar in shape to the center body of the Shuttle Orbiter. The basic outside dimensions are 65 by 18 by 18 feet 7 inches high when horizontal (22 feet 7 inches high to the tip of the spike on the aft bulkhead). The inside geometry approximates that of the Shuttle Orbiter payload bay.

ORIGINAL DESIGN
OF POOR QUALITY

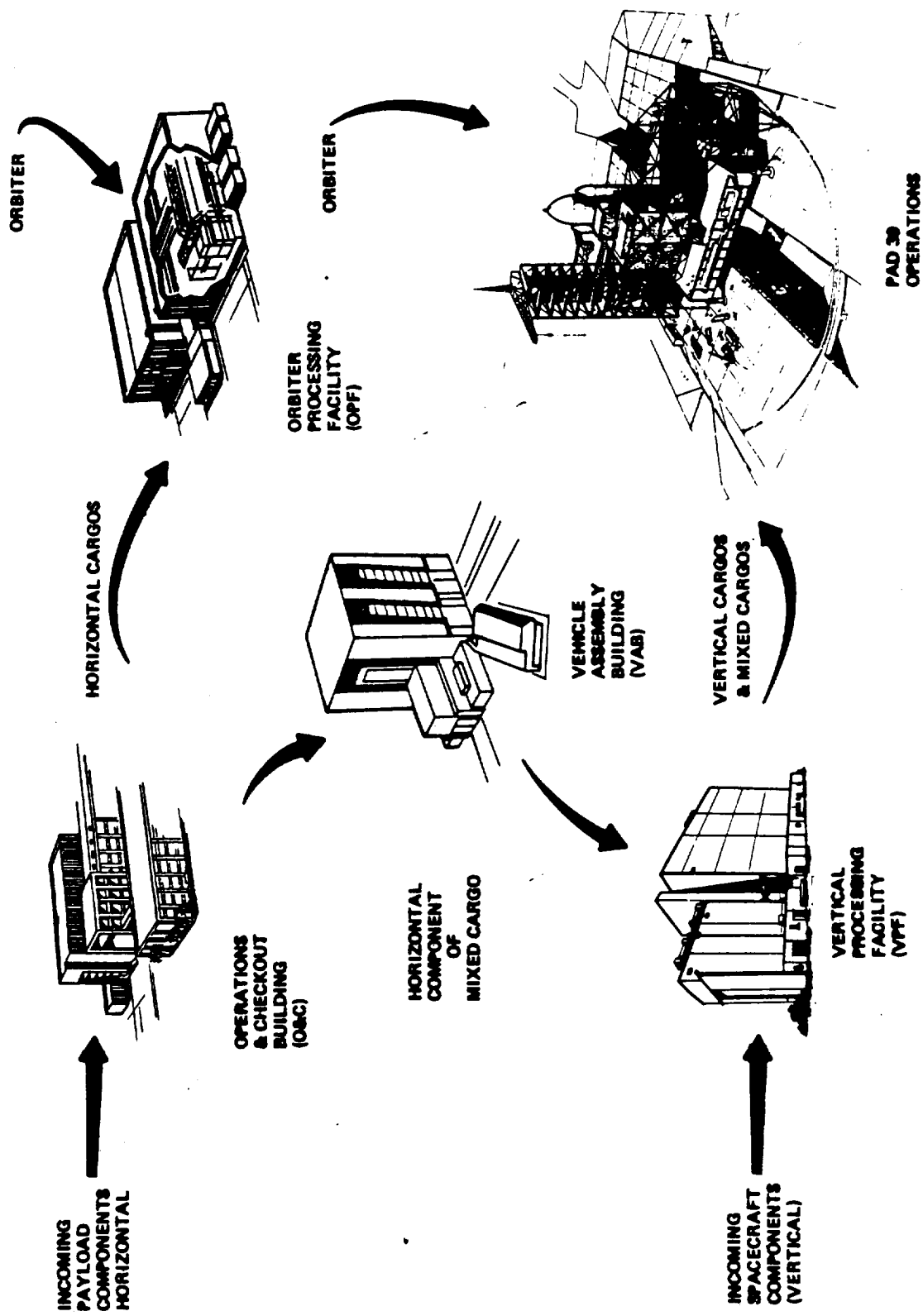


FIGURE 1. PAYLOAD TRANSPORTATION FLOW AT KSC

OR FOUR QUALITY

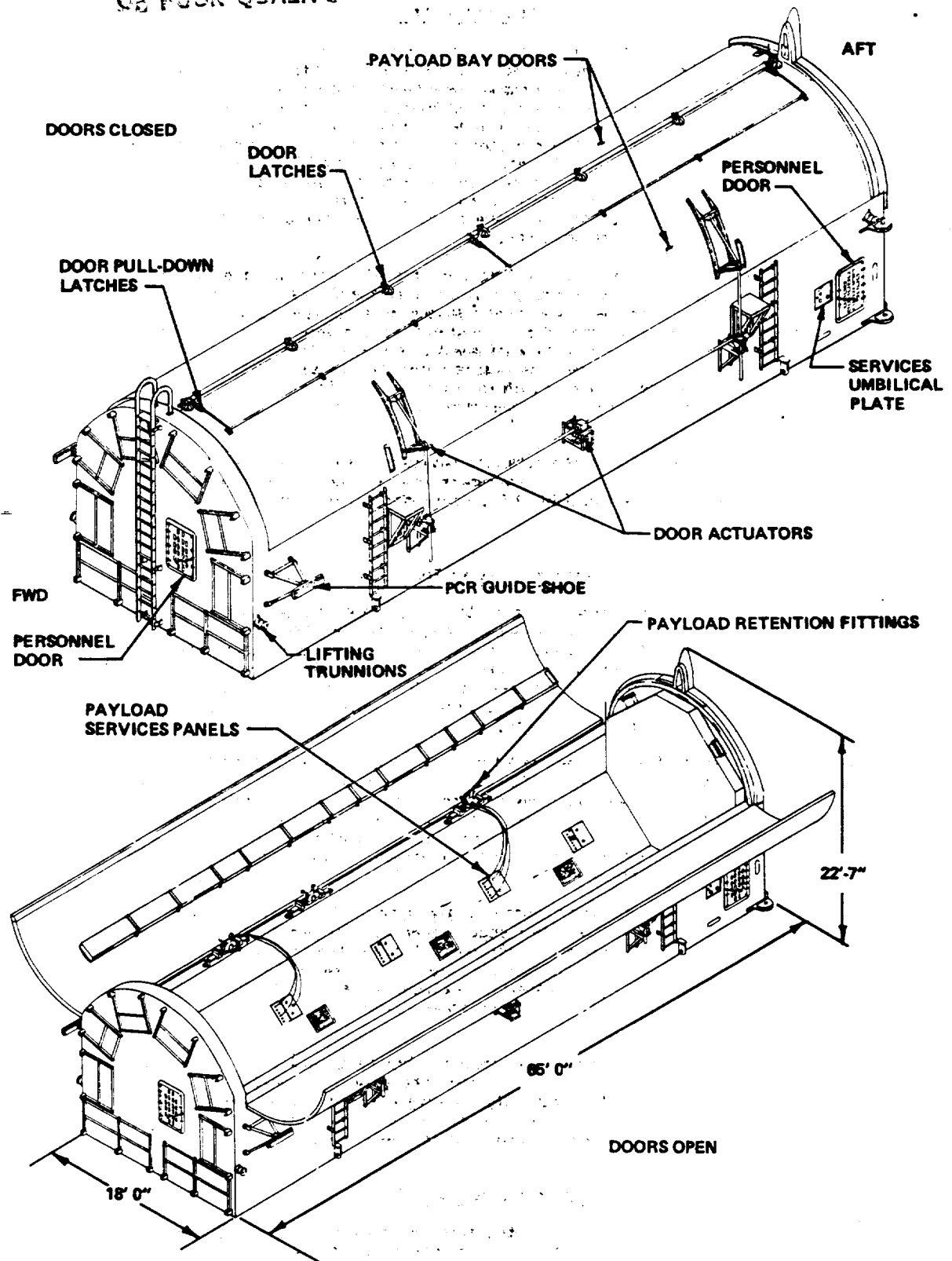


FIGURE 2. PAYLOAD CANISTER

Canister Structure

To satisfy the strength and particularly the rigidity requirements, the canister structural design consists of rigid steel "U"-shaped frames located approximately 10 feet apart with rigid steel bulkheads on each end of the payload bay. The frames are tied together with four steel rectangular box beams and a keel beam along the center of the canister bottom. Two of the box beams, called the longeron beams, along the side of the canister also provide support for the longeron trunnions of the payload, and they anchor the hinged end of the canister payload doors. The outside steel skin of the canister acts as a shear plate to stiffen the entire structure. To the inside of the skin are bonded blocks of rigid foam for insulation. The inside of the canister payload bay is lined with aluminum sheet to provide a floor for personnel access and to environmentally seal the payload bay. Two personnel hatches for access to the payload bay are provided, one through the forward bulkhead and one through the side of the structure at the aft end.

On the inside of the canister at each end, lifting trunnions are provided for both horizontal and vertical hoisting and for rotation between horizontal and vertical. All lifting is accomplished with two cranes except at the launch pad where a single 90-ton hoist is used to lift the vertical canister up to the PCR for payload transfer to the PGHM. To stabilize the canister during this lift, a pair of retractable guide shoes are provided on the forward end of the canister. These shoes "slip" into guide channels on both sides of the PCR to preclude swaying of the canister during hoisting. Since the weather seals around the payload door opening of the PCR must interface with the Shuttle Orbiter during STS operations, their geometry, as well as the geometry of the canister bulkheads, must duplicate the mold line of the Orbiter.

Installed in the aluminum floor of the canister payload bay are five payload interface panels that provide electrical power, fluid and gas, and instrumentation hookups for the payload. These panels are connected to umbilical panels on the outside of the aft end of the canister to which service is supplied from outside the canister.

Canister Payload Bay Doors

The canister payload bay doors posed a particularly challenging engineering problem in that they had to be thin in order to be opened in the space available at the PCR and in the OPF for removal of the payload and yet be strong and stiff enough to contribute to the structural integrity of the canister. When the payload doors are opened with the canister horizontal, the free edges must not sag into the payload envelope over their entire 60-foot length. With the doors closed, the doors needed to be an integral part of the load-carrying structure to provide rigidity to the canister, thus minimizing deflections during transportation of the payload.

The demanding requirements for the payload bay door design are satisfied by utilizing an aluminum monocoque structure very similar in construction to an airplane wing. The doors encompass the entire upper half of the canister; therefore, each door is configured into a quarter segment of a circle with an 8-foot radius and 5 inches thick. The design utilized "ribs" and "spars" bent from aluminum sheet and riveted between aluminum skins. The doors are attached to the lower structure by a continuous hinge between the door and the longeron beams of the lower structure. For a horizontal canister, the open doors provide a convenient personnel access along the longerons of the payload bay.

Special load-carrying latch mechanisms were designed to lock the two doors together along their interface at the top of the canister. The door latch mechanisms can be actuated from either end of the door by a torque tube that runs the length of the door. As a latch is locked utilizing an over-center mechanism, the torque is transferred to the next latch until all seven latches on the door are locked. Torque is applied to the torque tube by a ratchet turnbuckle-lever arm tool that is attached to either end of the torque tube. With the doors closed and locked, a pneumatically inflated seal is activated to environmentally seal the doors.

With the canister horizontal, the doors are opened using a screwjack mechanism that is mounted on the sides of the canister lower structure. The end of the screw is attached to a fold-down lever arm bracket mounted on the outside of the door. Two screwjacks and one air motor actuate each of the doors. With a vertical canister, the doors are operated manually with a technician pushing the doors by hand. During vertical operations, the door power mechanisms are folded out of the way and stored.

Payload Support Fittings

Payloads are supported in the canister in the same way they are supported in the Shuttle Orbiter. Primary longeron payload trunnions are supported in both the longitudinal (X_0) and vertical (Z_0) directions; secondary trunnions are supported only in the Z_0 direction. A split-block bearing housing

mounted on a slide rail is used such that the secondary fitting is allowed to slide along the X_0 direction, yet remain fixed in plus or minus Z_0 direction. For primary trunnion support, shear blocks are added to each side of the fitting to lock it to the rail for reaction of loads in the X_0 direction. Before insertion of a payload into the retention fittings, a spherical bearing is slipped onto the payload trunnion. During insertion of the payload, only the outer race of the GSE bearing contacts the housing of the retention fittings, thus protecting the polished surface of the payload trunnion.

The payload keel trunnion is supported in the canister between two longitudinal support rails that are mounted to the bottom of the canister payload bay. The keel trunnions require support only in the lateral direction (Y_0). To protect the surface finish on the keel trunnion and to act as a guide for the payload during insertion, a trunnion cover is placed on the keel trunnion prior to insertion of the payload into the canister.

PAYLOAD CANISTER TRANSPORTER

A vehicle to transport the payload canister required a motorized prime mover capable of transporting the canister in either a vertical or horizontal position at speeds up to 5 mi/h loaded (10 mi/h unloaded) and able to carry the necessary modules that provide services to the payload during transport in addition to the 90-ton maximum weight of the loaded canister.

To solve the transporter problem, technology was borrowed from the heavy construction industry -- particularly shipbuilding, where prime movers are used to transport large hull structures in the assembly of ships.

Description

The payload canister transporter, procured by performance specification, consists of a flat structural bed approximately 60 feet long and 22 feet wide, supported on twelve hydraulically lifted and steered bogies with four rubber tire wheels per bogie (see figure 3). Motive power is provided by hydraulic motors on the drive bogies. The transporter has two operator cabs, one on each end, and it can be controlled from either cab. The steering system, which is a servo-control system, allows the transporter to operate in a conventional Ackermann steering mode, a diagonal/transverse mode, or a carousel mode in which the transporter can turn about its own centerline axis. This steering capability allows operation in very close quarters and provides a transporter/canister positioning accuracy of ± 0.25 inches.

Transporter lifting power, steering power, and motive power is provided by hydraulics. The hydraulic pump system is driven mechanically by a diesel engine or, alternatively, by electric motors. This allows the transporter to be propelled by an internal combustion engine while over the road, by plug-in electrical power while inside clean-room payload facilities, and by an external electrical power generator in emergencies.

Transportation, Rotating, and Hoisting Operations

The bottom of the canister has four steel-plate pads on which the canister rests when horizontal and four similar pads on the aft bulkhead on which it rests when vertical. The transporter bed has mating steel pads which support the canister both horizontally and vertically. Holddowns are provided at the four support points to stabilize the canister when it is in the vertical transportation mode and to keep it from overturning. Vertical operations can proceed in winds up to 39 knots. The horizontal and vertical modes of transportation are shown in figure 4.

During transportation operations the MMSE payload services are provided to the payload through the umbilical panels on the canister. The umbilical lines, including supply and return air ducts for the environmental control system (ECS), are laid on the transporter deck. Sufficient length is provided for the drag-on lines so that they can remain attached and supplying services during hoisting and rotation operations at the VAB and during hoisting of the canister up to the PCR at the launch pad.

During hoisting operations at the launch pad when the vertical canister is lifted off the transporter by a single hook, the canister-payload center of gravity (cg) is placed under the hook by utilizing the bec-tilting feature of the transporter. To preclude the bottom (aft bulkhead) from "kicking-out" at the start of the lift, the transporter bed and the vertical canister are pitched over to allow the cg and the forward lifting trunnions on the canister to align with the lifting cable. The design of the canister is such that with any possible payload-canister cg the tilting is always in the same direction from vertical. The pad hoisting operation is shown in figure 5.

OF PERFORMANCE

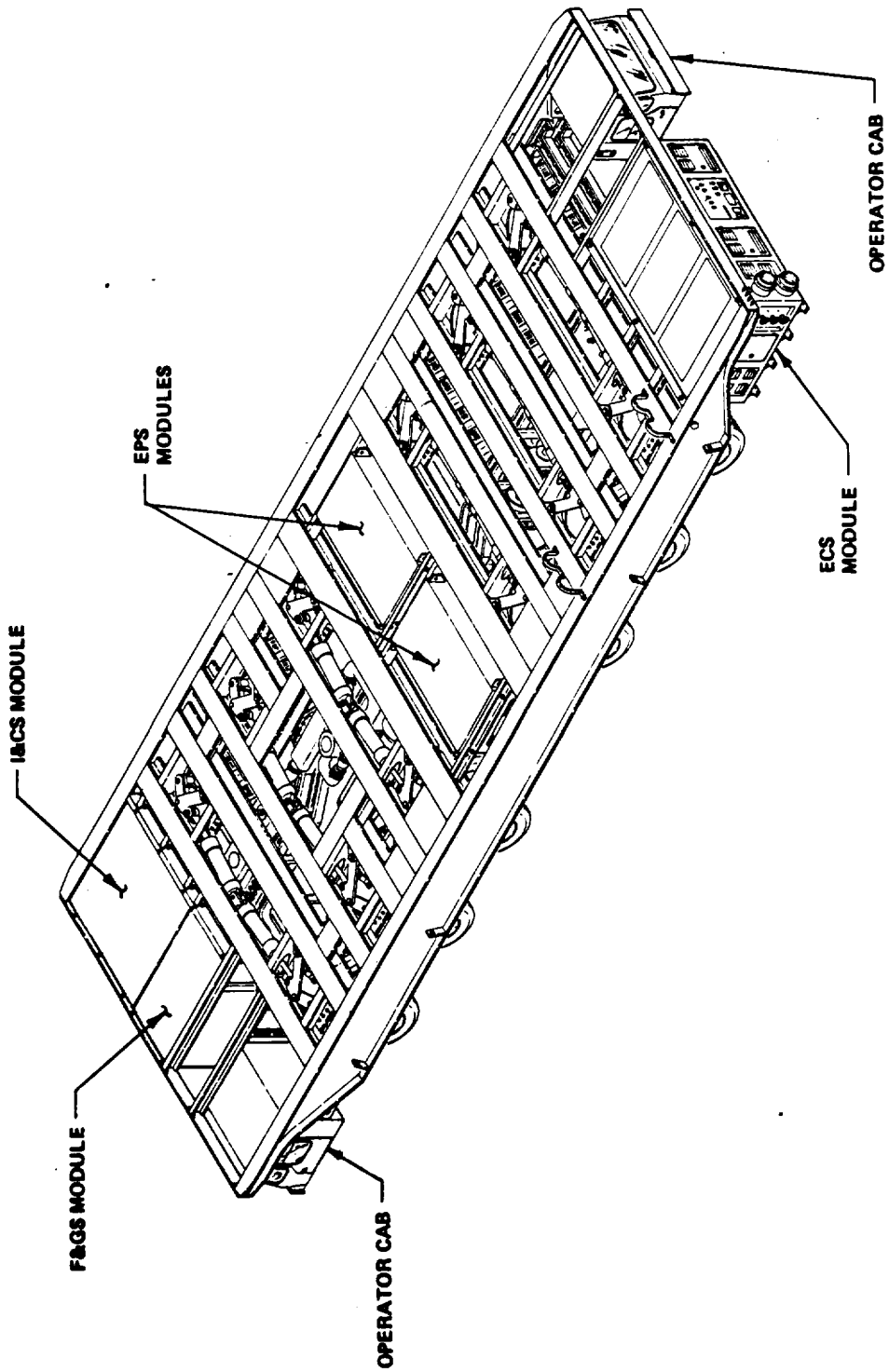


FIGURE 3. TRANSPORTER

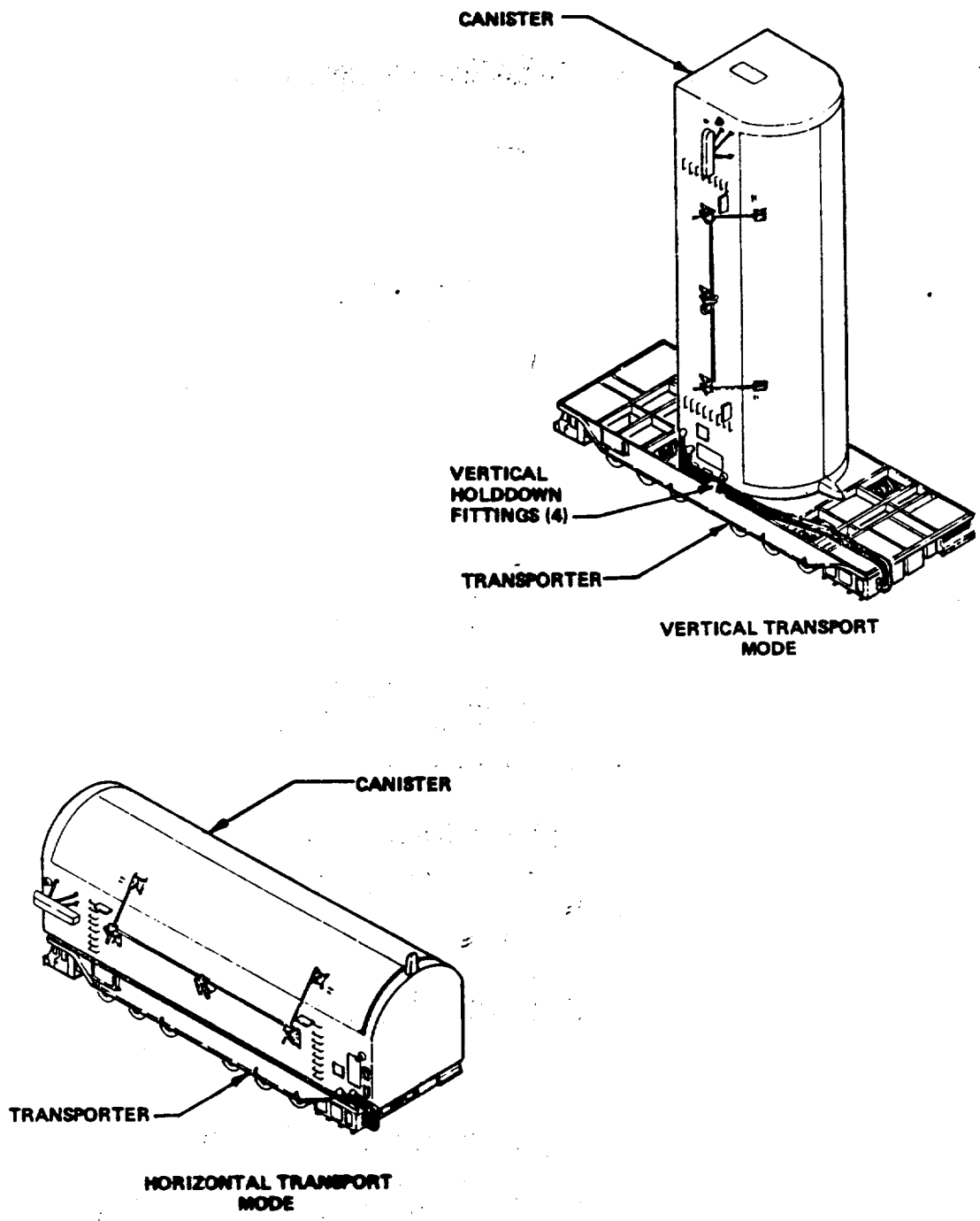


FIGURE 4. CANISTER-TRANSPORTER TRANSPORT MODES

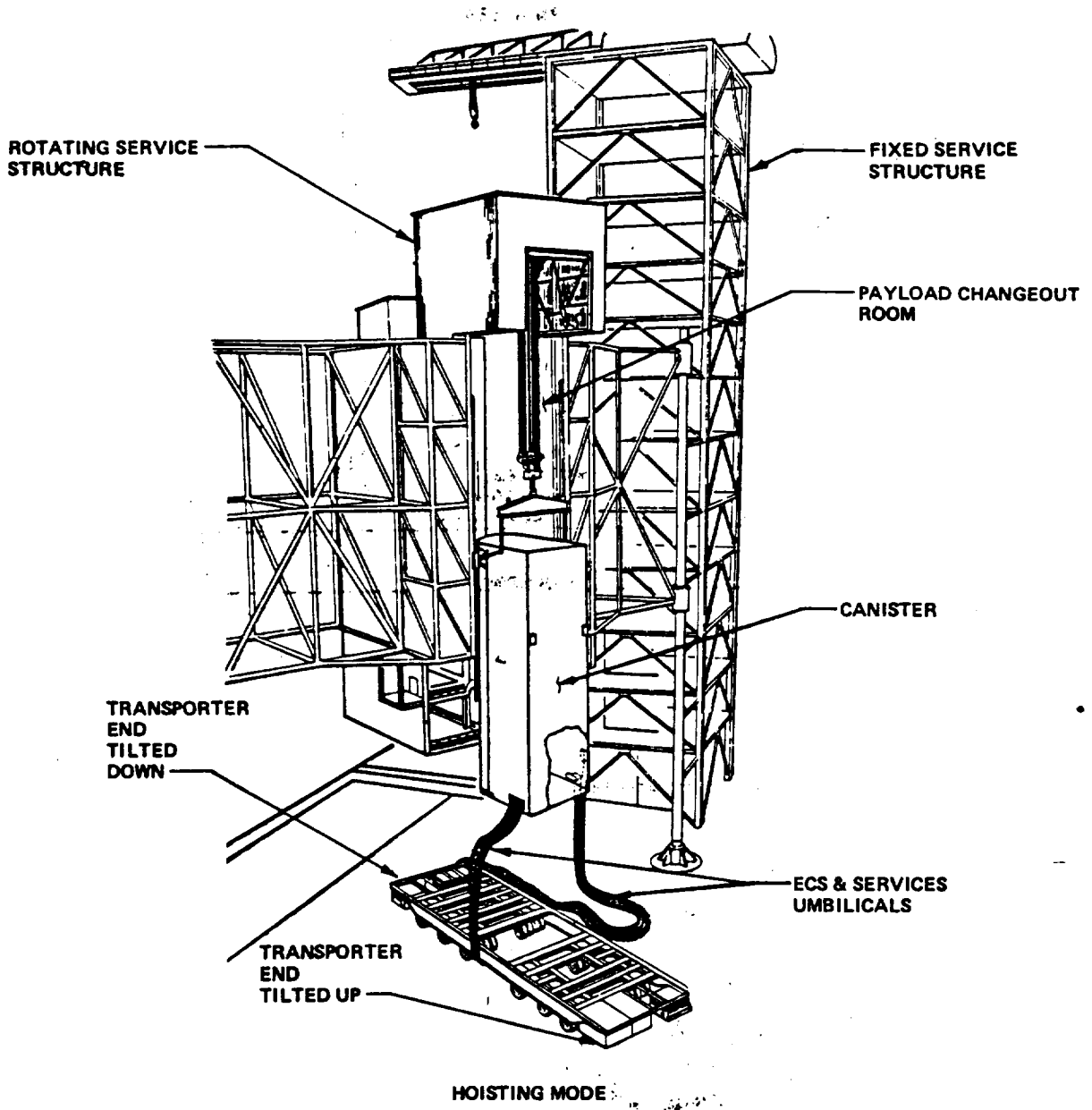


FIGURE 5. CANISTER HOISTING AT LAUNCH PAD

MMSE SERVICES SUBSYSTEMS

The electrical, environmental, fluid and gas, and instrumentation services required by the payload during transportation are supplied by separate subsystems. Because of the size and weight of these subsystems, it was necessary to keep them separate from the canister and to "pipe" the services to the canister through umbilical lines. The subsystem modules were uniquely packaged to fit under the bed of the transporter, allowing the most efficient use of space and maintaining a compact MMSE transportation system. The subsystem modules are identified in figure 3.

The ECS Module

The ECS module, mounted under the front end of the transporter bed, provides conditioned air to the payload through flexible supply and return ducts. Air is maintained at 65° to 75°F, 30% to 50% R.H., and Class-5000, with a flow rate of 75 to 150 pounds per minute.

The Fluid and Gas Subsystem (F&GS) Module

The F&GS module consists of K-bottles, a mounting rack, and a control panel. It can provide 30-pounds-per-square-inch-gage (psig) gaseous helium (GHe) and 30-psig gaseous nitrogen (GN₂) to the payload canister interface panel through umbilical hoses. This module is mounted under the aft center of the transporter bed.

The Instrumentation and Communication Subsystem (I&CS)

The I&CS consists of various instrumentation, electronics, recording devices, and displays packaged primarily in a module under the aft end of the transporter. The system provides a real-time display and recording capability for payload environmental measurements and monitors payload parameters during transportation. The module allows for an operator and observer to ride along inside the I&CS module during transportation.

The Electrical Power Subsystem (EPS)

The EPS consists of two diesel-engine-generator modules, distribution and control panels, and necessary cabling. The diesel generator modules are mounted one on each side of the transporter. They supply 120 V ac, 1.8 kVA single-phase power to the payload, ECS power, and I&CS power. In addition, the units can be used to drive the motor pumps of the transporter in case its mechanical drive engine should fail.

SUMMARY

Payload transportation at KSC is accomplished with a MMSE system. The payload canister, the canister transporter, and the services subsystem modules represent a unique system solution of some very demanding and challenging design requirements. The challenge was magnified because a complete Shuttle cargo is transported, not just individual payload components. The overall system goals were accomplished by combining these subsystems into a versatile tool for the STS program.

Many of the detail designs that went into the systems presented an engineering challenge. Those mentioned here, namely, the canister structure, payload doors, door-latch mechanisms and opening machinery, payload retention fittings, the transporter prime mover, and the subsystem modules, represent only a few of the many unique detail design problems that had to be solved. The MMSE system has achieved the system design requirements. This has been demonstrated successfully by tests using simulated payloads in and between all the payload facilities at KSC and by the successful transportation of entire cargos in support of seven STS launches to date.

STS PAYLOAD GROUND HANDLING MECHANISM
AT JOHN F. KENNEDY SPACE CENTER

Vincent Cassisi
NASA DD-MED-34
KSC, Florida

and

Bemis C. Tatem, Jr.
Planning Research Corporation
KSC, Florida

ABSTRACT

This paper describes the payload ground handling mechanism (PGHM), which lifts payloads out of the payload canister that brings them to the launch pad. The PGHM then loads the payloads into the Orbiter through the wide-open payload-bay doors.

The challenge was to provide this capability in time for Space Transportation System Flight No. 5 (STS-5). Meeting this STS requirement was considerably more challenging than using the stacking method for loading payloads on top of expendable vehicles. This paper describes the new mechanism and its main features.

INTRODUCTION

The STS requires effective payload handling on the ground and specifically at the launch pad in order to carry out its mission. This has been accomplished with the new PGHM, which went on line at Launch Complex 39 Pad A for STS-5.

Expendable vehicles required a relatively simple means of payload loading for vertically stacking the payload on top of the carrier vehicle. One challenge of the STS was to provide an effective means of loading multiple payloads into the payload bay of the Orbiter through the large, open doors while the Orbiter is in a vertical position at the launch pad, which precludes the previous simple stacking approach. The challenge was met by the new PGHM.

Satisfying the numerous operational requirements placed on this mechanism provided no small technical challenge. In addition to the gross X, Y, and Z translations required to position the payload, the lifting hooks themselves required cushioned X and Z vernier adjustment as well as uncushioned Y vernier adjustment capabilities. The cushioning of X and Z is necessary to protect the bearing blocks that support the payloads in the Orbiter payload bay during flight. These bearing blocks have a somewhat limited tolerance to bumping of the trunnions against them during payload insertion. Wind causing small motions of the space vehicle (because of its large sail area) is also a factor.

Generally speaking, friction is a nuisance in a mechanical system that requires accuracy of control and positioning; however, an understanding of coulomb friction and how it functions can be used to advantage. It is this use that is considered a state-of-the-art improvement. There was a significant payoff in obtaining this understanding, as it led to elimination of the need for a complex, electronic, strain-gage, load-measuring system and also led to development of self-compensating means of load assumption. The latter takes advantage of coulomb friction's characteristic of pushing back only as hard as it is pushed upon, up to the point of incipient sliding.

The fitting designs are a state-of-the-art improvement in that, within a limited space, they provide the functions of the necessary X, Y, and Z compliance, including remote control of X and Z vernier adjustment by means of hydraulic power. The necessary cushioning of X and Z is provided by hydraulic accumulators precharged with gaseous nitrogen (GN₂).

OVERVIEW AT LAUNCH COMPLEX 39 PAD A

The Orbiter has about 75 percent of its cargo installed in its payload bay at the launch pad. A series of problems had to be understood and overcome to develop the PGHM, which was designed and installed at the John F. Kennedy Space Center, to do this. To understand the details of the design, some background information is required.

The STS has two solid rocket boosters (SRB's) with an external fuel tank supported between them. The Orbiter is then suspended from the side of the external tank, so the SRB's support the entire vehicle. At the launch pad, this assembly rests on the mobile launcher platform where a rotating service structure (RSS) can be positioned so that the payload changeout room (PCR) inside it encloses, but does not hold, the Orbiter. The payloads are inside the PCR, from which they are installed into the Orbiter (figure 1).

The portion of the Orbiter that carries the cargo is referred to as the payload bay and is a void large enough to contain a cylinder 15 feet in diameter, 60 feet long, and weighing 65,000 pounds (figure 2). While the cylinder represents the maximum space available for payloads, the actual payloads are of various shapes, sizes, and weights. There can be as many as five main elements on each flight, each individual in design but all having a common method of attachment to the Orbiter payload bay along the longeron beam and at a keel point with standard trunnions. The payload longeron trunnions are 3.25 inches in diameter by approximately 8.75 inches long, and the keel trunnion is 3 inches in diameter by approximately 11.5 inches long. They are made of heat-treated steel or titanium with a chrome plating polished to 8 microinch root mean square.

A TYPICAL PAYLOAD

Figure 3 shows two views of a simplified payload: a 90-inch-radius cylinder that has some arbitrary length. The top view shows that the payload trunnion line is offset by 14 inches from the geometric center of the allowable 15-foot-diameter circle. In general, but not always, the center of gravity (cg) of the payload is near the geometric center. From the lower view, it is evident that there is a moment caused by the cg that has to be counteracted by the Orbiter attach points.

PAYLOAD RETENTION IN THE ORBITER

Due to flight flexure of the Orbiter, each attach point has a certain job to perform and is explained using the Orbiter coordinate reference system (figure 3). The X direction runs from nose to tail, the Y direction is from wing tip to wing tip, and the Z direction is from belly to payload-bay doors.

During flight, the Orbiter flexes and twists; and if the payload were firmly fixed to the Orbiter, it also would be caused to flex, twist, and pull. Therefore, to minimize unwanted stresses, the payload is restrained as follows: At the longeron area of the Orbiter there is a primary restraint that reacts the load in the X and Z directions but allows movement in the Y direction. A secondary restraint reacts the loads in the Z direction but allows free movement in the Y and X directions. The keel restraint reacts in the Y direction but allows free movement in the X and Z directions.

Figure 3 shows that force F_2 will counteract the weight in the X direction, and the couple F and $-F$ in the Z direction will counteract the moment of the weight W with its 14-inch offset. The keel only reacts side-to-side Y loads and thus mainly reacts flight loads.

The Orbiter has two types of longeron restraints. One, called the passive longeron fitting, is closed and bolted on the ground and stays that way for nondeployable payloads. The other is opened and closed remotely by the astronauts for deploying payloads in orbit and is known as the active longeron fitting. Both are attached to the longeron beam through use of a bridge assembly and both can be used as primary or secondary. In primary use, the fitting is firmly attached to the longeron beam; and in secondary application, it is allowed to slide.

The keel is attached to the bottom of the Orbiter payload bay by use of a bridge assembly and is powered open and closed by the astronauts. When open, it presents about a 9-inch-diameter opening. The closing motion draws both halves together linearly in the X direction until, at the closed position, there is only a 3-inch hole. When locked on the trunnion, motion is allowed by sliding the entire unit along the X direction, but the payload is held rigid in the Y-Y direction. The polished trunnion is allowed to slip longitudinally through the Orbiter fittings at all three attachments. Both the longeron fittings and the keel fitting contain a split bushing that could be damaged during payload installation if a misalignment of the trunnion to fitting causes a bushing force of approximately 3,000-lb shear.

VEHICLE AND PGHM STRUCTURE

The Orbiter is a cantilevered load hanging from the side of the fuel tank, which is a thin structural member that will flex under load. Deflections are produced when the load on the Orbiter is changed either by adding or removing a payload. The fuel tank is also suspended from the SRB's, so

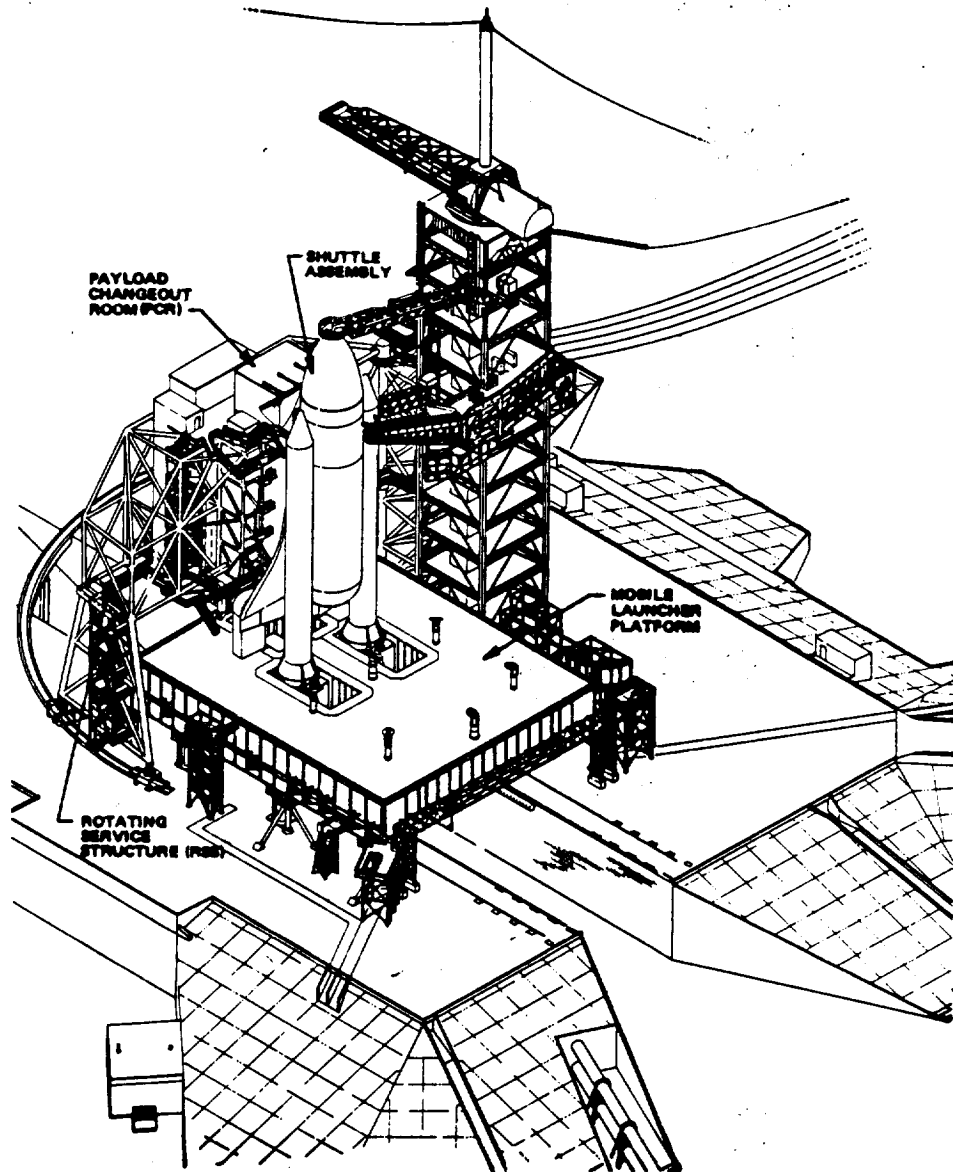
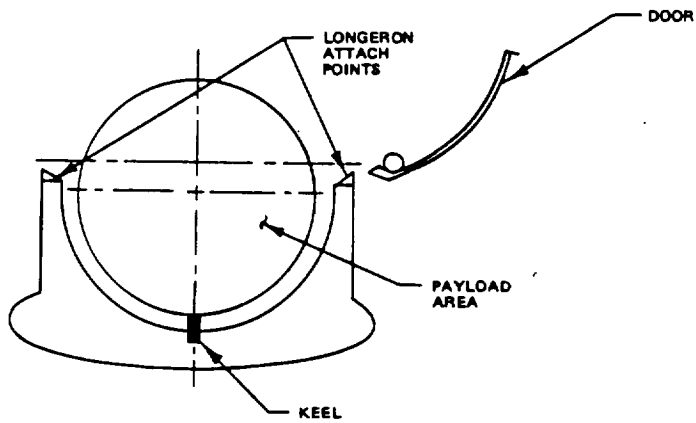


FIGURE 1. PAYLOAD CHANGEOUT ROOM WITH PGHM AND ACCESS STANDS



INSERT - SECTION THROUGH ORBITER PAYLOAD BAY

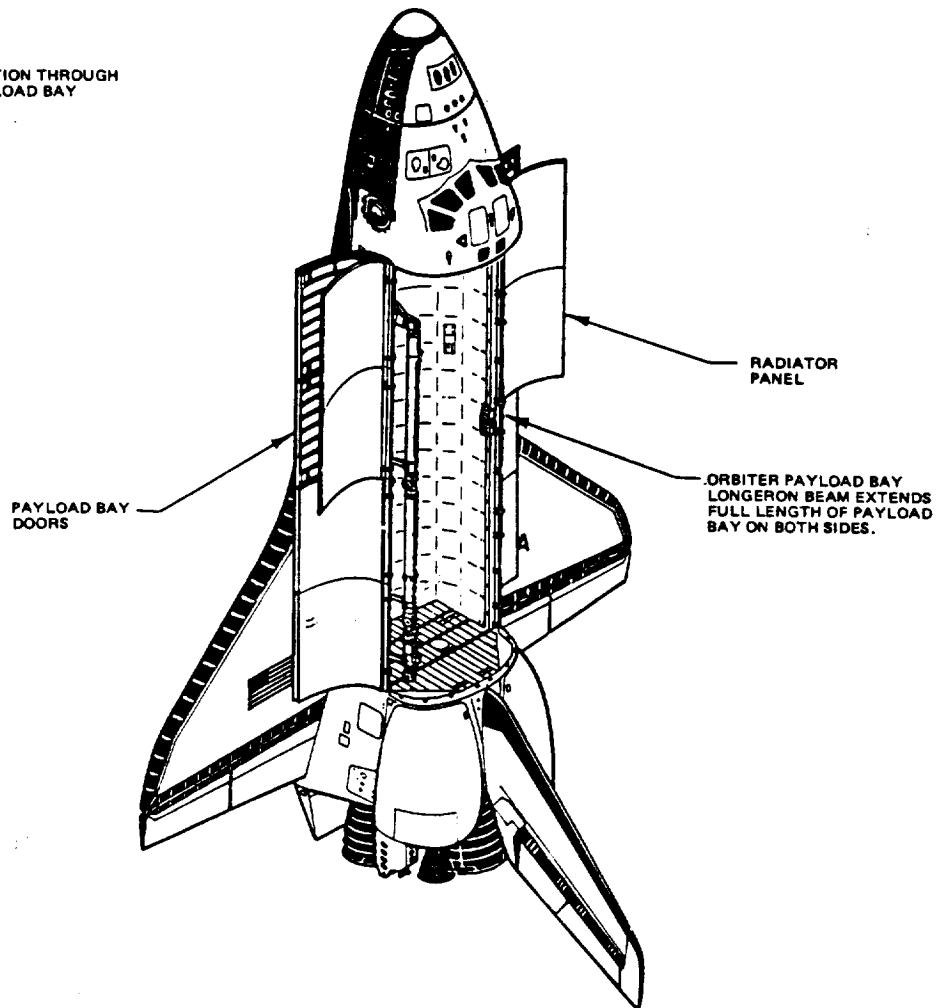


FIGURE 2. ORBITER CARGO BAY

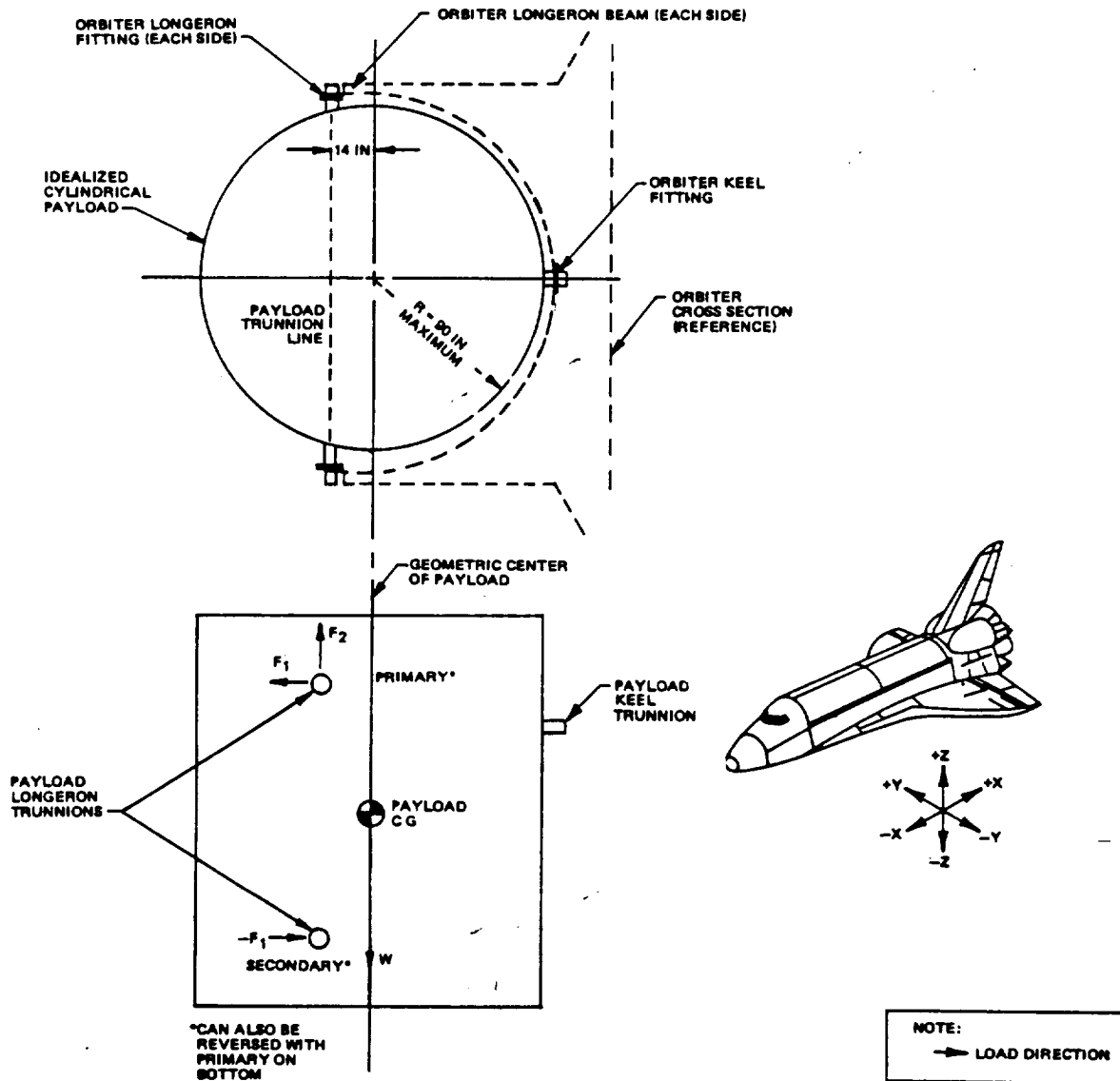


FIGURE 3. PAYLOAD TRUNNION FORCES

more flexibility is added to the system; the bending moment from the weight of the Orbiter and the payload will cause the SRB's to deflect. The assembled STS vehicle sitting at the pad also presents a sail area to the wind. These wind effects, which vary with direction and velocity, produce additional periodic movements that modify the static deflections. The result of all the loads is a deflection that has a point of apparent rotation located somewhere toward the base of the SRB segments. Looking at the STS vehicle from the side shows that the Orbiter is not only above but also off to the side of the vertical centerline of the SRB's. The effect of this is to create not only a deflection in the X direction, but a simultaneous deflection in the Z direction. The amount of deflection will vary along the length of the Orbiter, as can be seen by extending one radius line from the base of the SRB's to the top of the payload-bay area and another to the bottom. If both radii are rotated counterclockwise equally a few degrees, it is apparent that there are differences in the X and Z movements of the ends.

The structure that houses the PGHM is on a base separate from the STS vehicle. It also presents a sail area to the wind, resulting in a periodic deflection. The frequency of this movement is different from the frequency of the vehicle's movement. In addition, there are static deflections caused by variation in the amount and location of loads within.

Transferring a payload from the ground to the flight vehicle thus requires transferring the payload from one moving structure to another with the accuracy to align the trunnion to the flight fittings and to compensate for the additional change of deflections when the loads are actually transferred. At no time is the Orbiter tied to the ground, since this would cause unknown loads to be transmitted to the Orbiter and possibly damage the flight vehicle.

The new device is shown in figure 4. A bridge similar to that from a bridge crane is supported from ceiling rails that allow the unit to traverse the room from front to back to clear the doors that maintain clean conditions during absence of the Orbiter. Hanging from the bridge is a structural stem that is the supporting frame for the mechanisms mounted on its front (Orbiter) side. The stem also contains five levels for personnel and equipment, and slung below these levels are access platforms. These access platforms allow variable positioning for personnel to service the cargo elements.

GROSS PAYLOAD TRANSLATIONS

To best explain the operation of the mechanism, a typical usage will be described. This will cover the arrival of the cargo from its preparatory facility, the transfer of the cargo to the PGHM, and finally its insertion into the Orbiter.

The method chosen to carry the cargo around the John F. Kennedy Space Center is a simulated mid-body of the Orbiter called the payload canister. This structure duplicates the space within the Orbiter payload bay, along with the retention points and methods of holding the cargo. This canister is carried from point to point on its transporter; and for carrying payloads to the pad, it is used in the vertical position. Once it arrives at the pad, a 90-ton hoist on top of the PCR is used to lift the canister so that it is positioned in front of the PCR in exactly the same spot as the Orbiter will be later. Once it is secured to the PCR structure (which is the only difference between this operation and the Orbiter operation), the doors to the room and the doors to the canister are opened. This now allows the PGHM to move forward from the rear of the room so that it can remove the payloads from the canister. A fast movement is first used to approach the payload rapidly, but then motion automatically reverts to a slow mode for the final approach. Manual adjustments then make the final extension to engage the PGHM payload-retention fittings to the payload trunnions.

VERNIER PAYLOAD TRANSLATIONS

The payload fittings on the PGHM (figures 5 and 6) are pairs of small, relocatable mechanisms that allow the operator to create precise linear movements in three mutually perpendicular (X, Y, and Z) directions to engage the trunnion and then, after unlocking the canister retention fitting, to move the payload away from the canister. These fittings are positioned by use of water-based hydraulic systems. The primary fitting has independent adjustments in the X, Y, and Z directions, while the secondary fitting has a single powered movement in the Z direction and is allowed to pivot freely in the remaining directions. A compressed-GN₂ accumulator overload-protection system has been incorporated into the hydraulic system to protect the Orbiter from bearing contact damage. Any out-of-plane trunnion is automatically accounted for through this accumulator system. The use of this system will be discussed more later.

Once the payload weight has been assumed by the PGHM fittings, hydraulics are used to move the payload a few inches away from the canister fittings. Further retraction is made by use of manual adjusters contained in the front mechanisms, followed by engagement of the slow-speed movement and fast

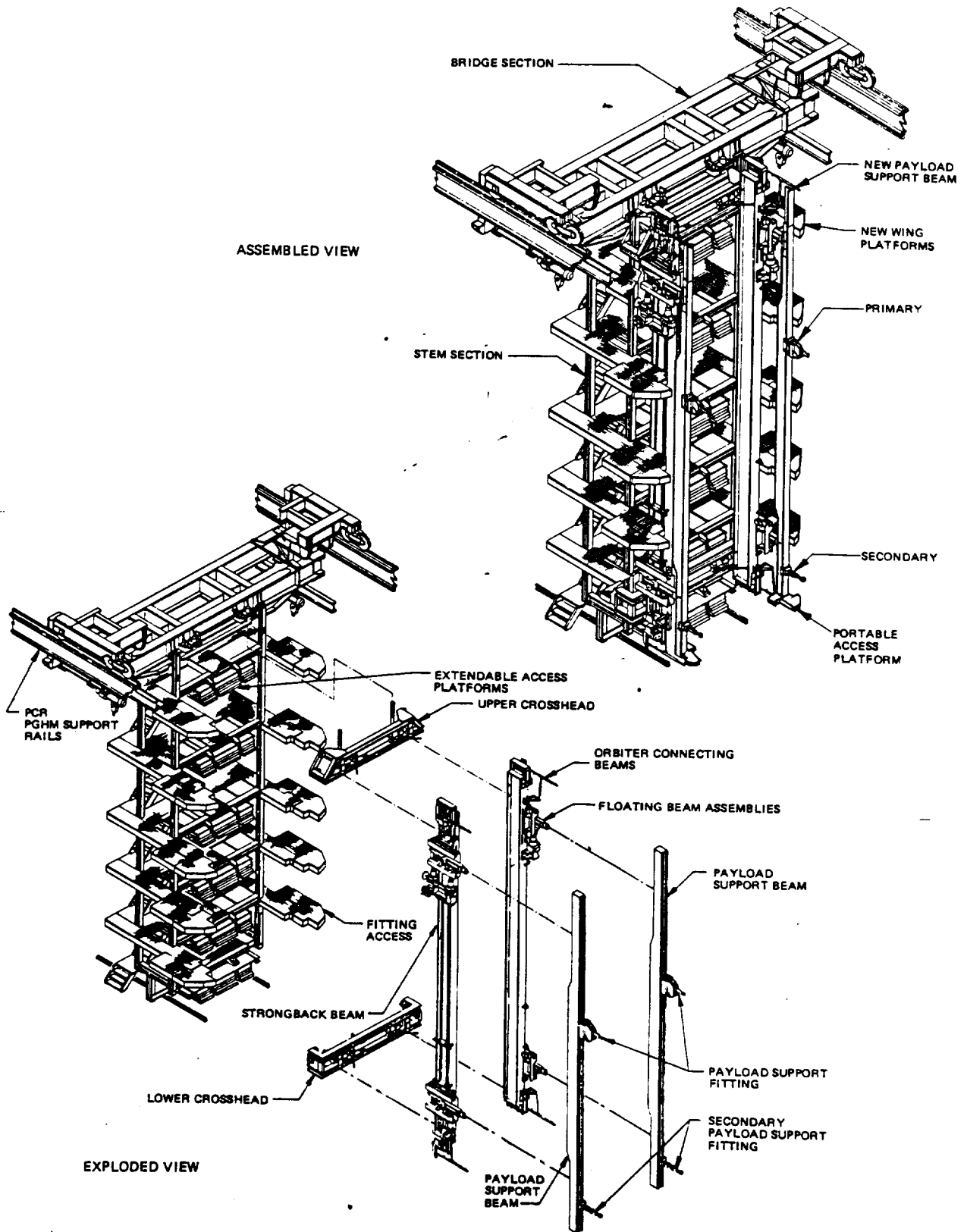


FIGURE 4. PAYLOAD GROUND HANDLING MECHANISM

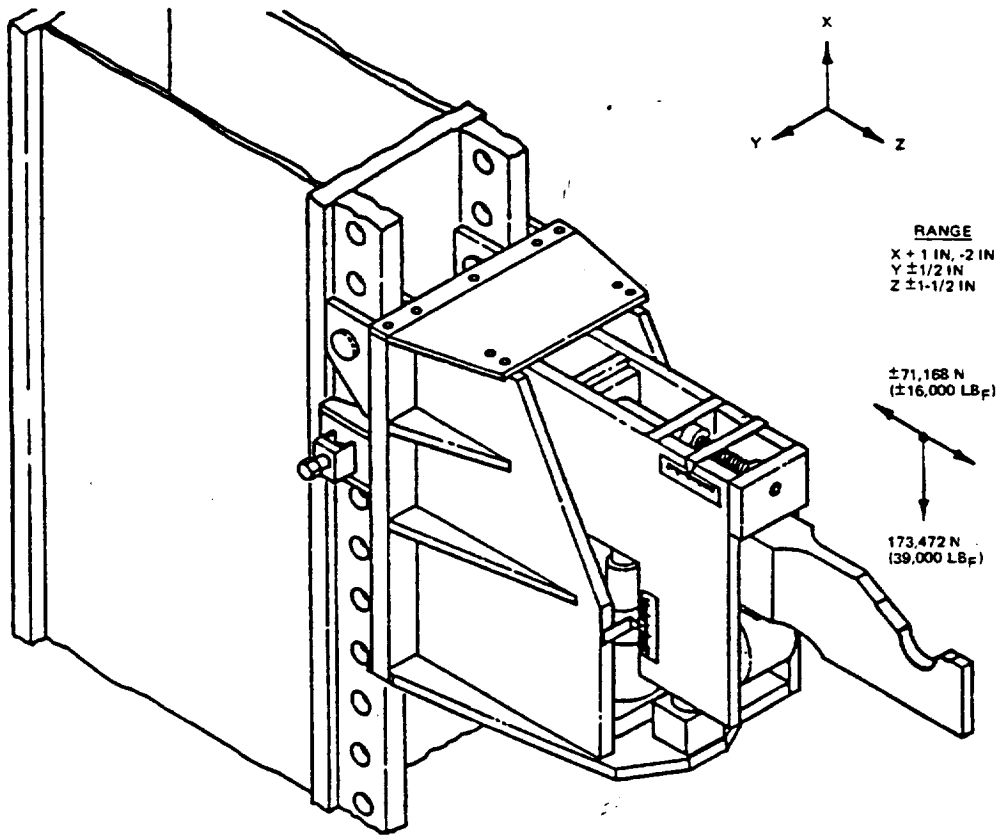


FIGURE 5. PRIMARY PAYLOAD SUPPORT FITTING MOUNTED TO SUPPORT BEAM

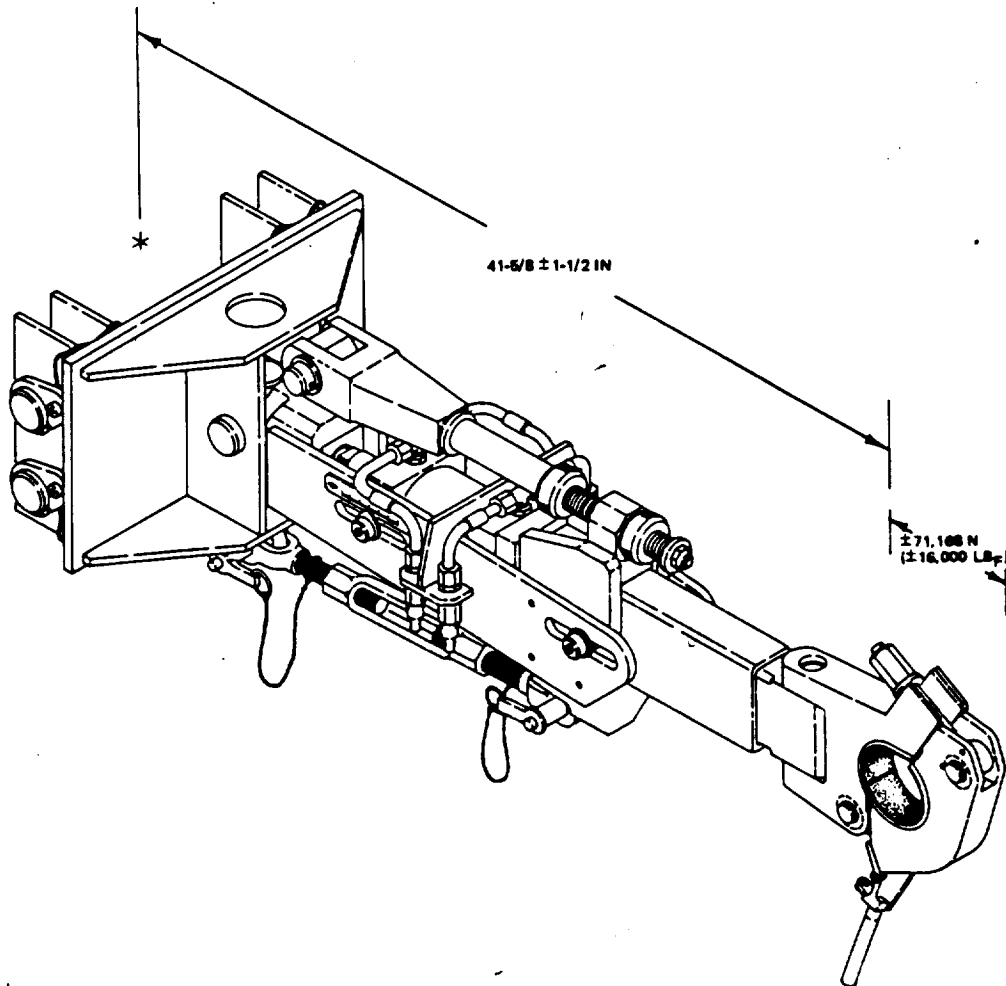


FIGURE 6. SECONDARY PAYLOAD SUPPORT FITTING MOUNTED TO SUPPORT BEAM

movement to the rear of the room. The doors to the canister are closed, the doors to the PCR are closed, and the canister is removed.

At the rear of the PCR, provisions have been made for accessing the various work points on the payloads (figure 1). When the Orbiter is ready to receive the payload, the RSS is pivoted around so that it encompasses the same portion of the Orbiter as it previously had on the canister. The difference now, however, is that the RSS does not hold on to the Orbiter as it did the canister, but, instead, stands free. The door to the PCR is again opened, and the doors to the Orbiter are opened. The PGHM moves forward, as it did before, and approaches the Orbiter. At this point, since the Orbiter and RSS are free of each other, different alignments must be made to account for tolerances inherent in the stacking and assembly of the STS vehicle. The Orbiter side of the PGHM contains adjusters that allow the entire cargo assembly to be moved as a unit to align with the plane of the Orbiter. The top of the mechanism contains large jackscrews for gross vertical adjustments; the crossheads contain side-to-side (Y) adjusters that move either together or opposite from each other to allow angular adjustment when combined with the vertical motion of the strongback beams. Individual adjustments can then be made on each side for X- and Z-direction motion. Once the payloads are aligned with the Orbiter, the hydraulic systems are used to place them within a fraction of an inch of seating in the Orbiter fittings. At this point, the Y adjuster on the PGHM fitting is used to center the payload keel in the Orbiter keel fitting prior to its closing.

CUSHIONING OF VERNIER TRANSLATIONS

The closing action of the Orbiter keel, if not precisely aligned to the keel trunnion, will side-load the payload. This side load will then cause a deflection within the hydraulic/pneumatic system of the PGHM fittings and allow compliance with the "wishes" of the Orbiter, thus preventing any possibility of Orbiter overload. The limitation of load is achieved by varying the pressure of the gas in the accumulators so that any additional load on the hydraulic cylinder will cause compression of the gas trapped within the system (figure 7). The force required to cause compression can be varied by the initial precharge pressure. Thus, any misalignment or movement between the Orbiter and the PCR will cause a deflection in the ground system through a force low enough to prevent damage to the Orbiter.

Once the keel is locked, the PGHM fittings move the payload trunnions into the Orbiter fittings, protecting them through the gas spring action, and the Orbiter fittings are locked. At this point, the PGHM is lowered away and prepared for retraction. Since the stem portion of the PGHM is hanging from the bridge on a pivot, a change of load on the front end could cause the stem to change the hang angle. This is prevented by use of clamps between the bottom of the stem and the PCR floor. Once the payloads are transferred onto the PGHM from the canister or given up to the Orbiter, the stem must be brought to its neutral angle for the new load condition. This is done simply by adjusting the screw-jacks between the stem and the floor. Once the load in the jack is zero, the clamps are opened and motion can begin.

TESTING

The completed PGHM was proofloaded at 125 percent of the maximum design load and then successfully used to install payloads in the Orbiter for STS-5.

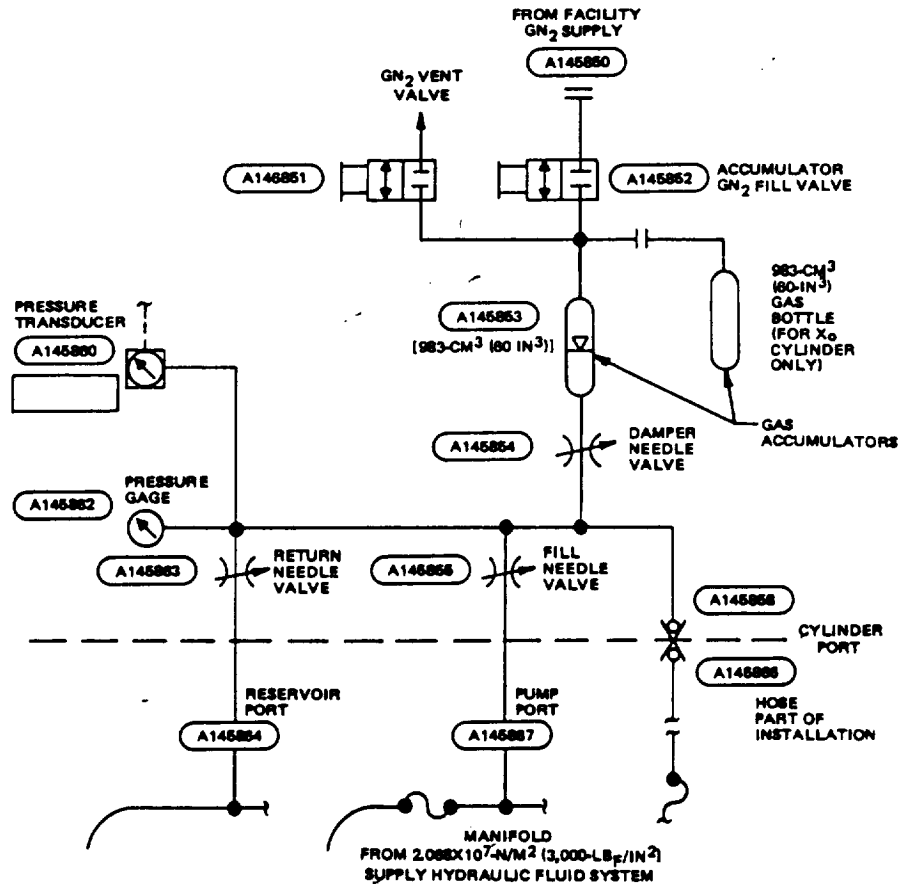


FIGURE 7. TYPICAL FITTING HYDRAULIC CONTROL SYSTEM (TYPICAL AT EACH RETRACT OR EXTENSION POSITION)

D35
N85-16972

THE ORBITER MATE/DEMATE DEVICE

Arthur J. Miller, P.E.
and
William H. Binkley, P.E.
Connell Associates, Inc.
Coral Gables, Florida

ABSTRACT

The purpose of this paper is to describe the numerous components and systems of the Orbiter Mate/Demate Device (MDD), with special emphasis on mechanisms and mechanical systems; to discuss in general their requirements, functions, and design; and, where applicable, to relate any unusual problems encountered during the initial concept studies, final design, and construction. The MDD and its electrical, machinery, and mechanical systems, including the Main Hoisting System, Power Operated Access Service Platform, Wind Restraint and Adjustment Mechanism, etc. were successfully designed and constructed. The MDD was used routinely during the initial Orbiter-747 Approach and Landing Test (ALT) and the more recent Orbital Flight Tests (OFT's) recovery and mate operations at the Dryden Flight Research Center (DFRC), Edwards Air Force Base, California.

INTRODUCTION

The Orbiter Mate/Demate Device is only one small part of NASA's overall Space Shuttle Program. However, at the time of its planning, development, design, and construction during the 1974 to 1976 period, it was of utmost importance. It was to be the only facility, at that time, capable of lifting and mating the Orbiter on the NASA 747 carrier aircraft and providing for all the numerous services and access requirements.

The firm of Connell Associates, Inc. was selected by NASA, Kennedy Space Center, Florida, to perform initial studies to develop, in a very limited amount of time (approximately 5 weeks), an acceptable MDD concept and, based on that acceptable concept, to provide the complete design. With the importance of the MDD in mind and aware of the very tight calendar time schedule, Connell Associates assigned its entire team of structural, machinery, electrical and mechanical engineers to the project to meet the challenge of developing an acceptable concept.

A schedule of mandatory coordination meetings, almost daily, between the engineering trades was initiated to expedite the concept design and to determine, as nearly as possible, the ideal geometry of the MDD structure and its principal components. An important design aid during this phase of the project was a scale model of the MDD which we made and continually revised as the concept was developed. The MDD model was constructed to the same scale as the model of the Orbiter, which was loaned to Connell Associates by NASA. The Orbiter model was mated on a plastic model of the Boeing 747 aircraft which we made from an "off-the-shelf" kit and then placed under the MDD model, thereby providing a three-dimensional view of the concept as it was being developed.

The concept design was successfully accomplished by preparing an Initial Studies Report and the model of the recommended concept and submitting them to NASA for review. After a few changes were incorporated into the design, the concept was approved and final design started. The on-going support, technical aid, and response provided by the NASA, KSC technical personnel of DD-MDD, DD-EDD, and DD-MED during all of the design phases were invaluable in helping to complete the project successfully and on schedule.

The MDD is a unique facility that could be classified somewhere between the categories of a conventional service structure and a fixed-frame multi-hook derrick. Its structure and components will be discussed in later paragraphs.

OUTLINE OF OPERATIONS, FUNCTIONS, AND SERVICE PROVIDED FOR ON THE MDD

The MDD is designed and constructed to routinely handle and accommodate the following operations, functions, and services:

1. Access to Orbiter jack points
2. Access to Orbiter fore and aft lift points
3. Hoisting the Orbiter high enough to allow a 747 aircraft to be positioned beneath it

4. Lowering the Orbiter and mating it with the 747 aircraft
5. Precise hoist load vertical positioning control system at each main hoist
6. Access for mating the Orbiter and 747 aircraft
7. Access for servicing each side of the Orbiter when it is in the following positions:
 - a. On jacks
 - b. Mated on 747
 - c. Secured for 40-knot wind while suspended from the MDD
8. Wind restraint and adjustment system to control positioning the Orbiter while it is suspended on the main hoists in winds up to 12 knots
9. Safety tie-down system to secure the Orbiter while suspended on the main hoists in winds up to 40 knots
10. Access/egress route to accommodate self-contained atmospheric protection ensemble (SCAPE)-suited personnel
11. All equipment/services are hazard proofed per KSC safety standards.
12. Accommodate services to the Orbiter such as APU hypergols and fuel cell gaseous oxygen and hydrogen. Requirements include cable trays, pipe traces, etc. for routing the services.
13. Installation of an airlock for access to the Orbiter crew hatch at on-jacks position and at the mated on 747 position.
14. Other components and systems provided or provided for on the MDD are the following:
 - a. Electrical systems such as electrical power service and distribution, lighting, receptacles, cable trays for GSE, fire alarm, obstruction lighting, and lightning protection
 - b. Mechanical (plumbing) systems such as compressed air system, wash-down stations, and personnel emergency shower system

GENERAL DESCRIPTION OF ORBITER/747 MATING OPERATIONS

The following events, in numerical sequence, are required to perform a typical Orbiter/747 mating operation at DFRC.

1. The Orbiter is towed into proper position at the mating device.
2. The Orbiter jack set is installed; connect hydraulic, cooling and electrical ground power lines; position Orbiter cabin access room.
3. Jack Orbiter to the "ground" service position (Orbiter ref: Zo = 400, 21'-1" above and parallel with ground surface).
4. Ingress ground crew and activate ECLSS, electrical power, and hydraulic systems.
5. Lower and position the power-operated access/service platforms to proper distance above the Orbiter (top of platform approx. 16'-1" above ground level) for servicing operations at the "ground" position.
6. Attach the fore and aft lifting slings to the Orbiter lift points.
7. Retract landing gear and doors.
8. Deactivate and secure system; egress ground crew.
9. Disconnect hydraulic lines and T-0 umbilical, and remove Orbiter cabin access room.
10. Prepare for hoisting Orbiter (detach jacks, etc.).
11. Retract (raise) the access/service platforms to proper position necessary.

12. Hoist the Orbiter to the "mate ready position" (to required elevation to provide clearance for 747).
13. Tow 747 into proper position beneath the Orbiter.
14. Utilizing the wind restraint and adjustment mechanism system, lower the Orbiter and mate to the 747.
15. Lower and position the access service platforms.
16. Remove the fore and aft lifting slings.
17. Complete servicing; perform final inspection and closeouts.
18. Retract (raise) the access service platforms to required height to clear Orbiter for tow away.
19. Perform pre-tow checklist.
20. Backtow 747 clear of mate/demate facility; tow to ramp area.

SPECIAL FEATURES

TRANSPORTABILITY OF THE MDD

A demanding feature of the MDD during the design and detailing was that all components of the facility, including the structural framing, platforms, machinery, electrical systems, mechanical (plumbing), etc., be designed and detailed for erection and disassembly into units for transport on either trucks or C5 cargo planes to relocation and routine reassembly at a different site. The structure, for example, consists of all-welded units which are sized to just fit in or on the carrier and to be reassembled using bolted connections. A similar solution is provided for the electrical system. A major portion of the electrical system's installation has been grouped together and mounted on a removable "ladder-like" substructure. The substructure and attached electrical installation is broken down into individual sections of nominal length and each section is independently bolted to the MDD main structure. The length of each section depends upon the spacing of the main members of the structural panel to which the section is attached. On one end of each section the wiring terminates in a large disconnect (splice box), and on the other end terminates with lengths of flexible conduit with circuit conductors extending from them. When in place on the MDD, one half of a union fitting on each flexible conduit of one section is joined with a matching half union fitting on the disconnect box of the adjacent section, and the circuit conductors are spliced to matching conductors inside the disconnect box. Each disconnect box is divided into two sections to isolate the control and power circuits as required by the code.

ACCESS/EGRESS ROUTE FOR SCAPE-SUITED PERSONNEL

An interesting requirement was to provide a safe method of access and egress from the ground level up to work positions at the outer end of the access service platform for personnel in heavy and cumbersome SCAPE suits. The SCAPE suit limits a person's movement and instead of stepping he must "shuffle along" at a slow pace, which could create a serious problem for the worker in an emergency situation when he needs to make a speedy exit. During the preliminary studies, several solutions were considered including using two mobile, self-powered, manually adjustable hydraulic platforms. However, after additional study, it was decided to provide a more conventional route of access and egress. Adjustable ramps are provided for access between the access service platforms and main level work platforms. For vertical transportation of the SCAPE-suited personnel, a personnel hoist is provided at the forward end of each of the two towers of the MDD. The personnel hoists are standard catalog units and have a cage size capable of accommodating several SCAPE-suited personnel at a time.

STRUCTURAL SYSTEM

The MDD structure is a fixed base (anchored) cantilevered-type space frame as indicated on plates 1, 2, 3, and 4. Its final size and geometry are the result of many trial concepts and provide the necessary horizontal and vertical clearance envelopes for accommodating the Orbiter and 747 aircraft and the numerous platforms and components required for the mating operations.

A strong effort was made during the design to keep the weight of the structure to a minimum due to the transportability requirement. Structural aluminum and also high-strength alloy steel were briefly

considered. However, these metals are not efficient when trying to limit deflection within that permitted by criteria; therefore, ASTM A36 steel was used for wide flange sections and ASTM A500, Grade B steel for the tubular steel members. The tubular steel sections, which have excellent torsion-resistant properties as well as efficient axial load members, were used throughout the structure for diagonal members. Wide flange sections were used for members subject to flexure and also for the main columns.

The structure is designed for universal-type loading criteria, including 125-mi/h hurricane winds, ar.J for Seismic Zone 4 (Z=1), the most severe earthquake loading. The space frame structure was designed by computer analysis using the MRI-STARZYNE III program.

MACHINERY

MAIN HOISTING SYSTEM

The main hoisting system is installed as an integral part of the MDD and is a special hoisting system consisting of three separate two-speed, 50-ton-rated hoist systems, each providing a separate pick-up point on the Orbiter. Each of the 50-ton-rated systems consists of a hoist machine, two deflector sheave blocks, a special three-sheave assembly, hook block with antifricition bearing swiveling safety latch hook, 50-ton hydra set unit, rope, and forged fittings. All of the above listed components for each system are identical for maximum interchangeability. The hoist machines are located at level 4'-0" in the base of the MDD towers. The deflector sheave blocks are located at approximate levels 80'-0" and 100'-0" and are at the top of the MDD towers and also at the top of the connecting framing between the towers. The three-sheave assemblies are located at level 100'-0" in the cantilever part of the MDD and are directly above the hook blocks. All three 50-ton-rated hoist systems are controlled from one plug-in portable operator-controlled station. There are two receptacles on the MDD that the operator control station can plug into, and these are located at level 5'-0" at columns 1A and 1D.

The operator control station controls all functions of the main hoisting system and has provisions for operating two or more of the 50-ton-rated hoists simultaneously. Also, each of the hoists can be operated separately and completely independently of one another. The operator control station controls the raising and lowering of the hook blocks in either of two fixed speeds and each speed has its own separate lever control. Each hoist has a control-on and control-off switch with a green light to indicate control-on condition. All hoisting controls have full inching capacity.

All hoist machinery for the main hoisting system is identical, and each consists of a 15/5 hp, 1800/600 rpm induction-drive motor; two fail-safe spring-set solenoid released shoe brakes immediately after the drive motor; double reduction Helical gear motor speed reducer; single grooving steel drum, wire rope, upper and lower geared limit switches; and a welded steel base. The total gear reduction is approximately 900:1, and all shafting is parallel. The drive motor is connected through a flexible coupling. The drive motor has discreet separate windings, one winding for low speed and one winding for high speed. Failure of either winding does not affect the use of the other speed.

Each of the three 50-ton-rated hoist systems is reeved 6 ps (6 parts single), and the wire rope is 1-1/8-inch diameter, improved plow steel, uncoated, bright, 6 x 19 INRC, preformed, prestressed, with 56.5 tons breaking strength.

Each hook of the three hoisting systems comprising the main hoisting system has a rated hook capacity of 50 tons and a rated maximum lift of 90 feet. Each hook has two fixed hoisting speeds: 1 fpm and 3 fpm, both raising and lowering.

Each of the three 50-ton-rated hooks is equipped with a 50-ton Hydra Set, which is positioned between the hook and the load. The Hydra-Set unit is a precision load positioner in the vertical axis and positions the load within 0.001-inch increments. The Hydra-Set unit works on the principle of a piston and cylinder, and during descent, oil is bled from the bottom of the piston; during ascent, oil is pumped to the bottom of the piston.

The MDD main hoisting system is designed to operate under the following duty cycle:

- a. Each hoist will raise and lower the specified rated hook load from ref. el. 0'-0" to 75'-10" for one full complete and continuous raising and lowering cycle at a sustained hook speed of 3 fpm.
- b. Two observer control stations, one port and one starboard, are provided at ground level with a "stop" button on a 100-foot cord plugged into a receptacle 5 feet above ground on the main structure. Operation of either "stop" button will trip the main hoist electric supply circuit

breakers, causing all three hoists to stop. The circuit breakers must be reset manually before any of the three hoists can be operated again.

POWER-OPERATED ACCESS/SERVICE PLATFORMS

The power-operated access/service platform system consists of two complete and identical, vertically adjustable, power-operated tilting platforms and their equipment, one on the port side and one on the starboard side of the MDD. This system provides the following:

- a. Access to the sides of the Orbiter above Orbiter wings and within longitudinal range of platform; access to the lift points and pins on the sides of the Orbiter; access for operation of the 50-ton Hydra Set precision vertical positioners; and all other access and service required within the operating range of the equipment.
- b. An adjustable pivoting ramp on the outboard side of the forward end of each of the two platforms. These ramps provide passageways for personnel and equipment to proceed on and off the platforms when the platforms are at their working positions.
- c. A manually operated ratchet hoist for each of the port and starboard side platforms to facilitate raising and lowering the small flip-down platforms positioned along the inboard edge of each of the two main platforms. The ratchet hoist positioned manually into and out of the row of pad eyes located along the center truss of each main platform.

Each of the two power-operated access/service platforms has its own separate operator control station located on the MDD tower on that platform side. Also, each platform has an observer control station provided with a "stop" button. Operation of the "stop" button will trip the access/service platform electric supply circuit breakers causing the platform to stop. The circuit breakers must be reset manually before the platform can be operated again.

The platforms have a vertical speed of 5 fpm both up and down, with full inching movement in both directions. Each of the two platforms is powered vertically by two self-locking worm gear hoisting systems, one hoisting the aft end of the platform. The two hoisting systems of any one platform can be run simultaneously or individually. When one hoist system of one platform is run individually, the platform will tilt, which is required to accommodate the various angular attitudes required of the Orbiter. When the Orbiter is in a tilt attitude, the power operated access/service platform has to be similarly tilted to provide the required access and service to the Orbiter. Each platform tilt is limited within a range of minus 5 degrees to plus 10 degrees, measured from horizontal in reference to the forward end of each platform. The platforms can be power hoisted in a tilted or horizontal attitude within the limits of the tilt.

Each platform is guided and supported by two sets of rectangular telescoping steel tubing. The aft set of telescoping tubes is connected to the top of the platform through a pivot pin joint, and the forward set of telescoping tubes is connected to the top of the platform through a link-pin joint. Through these two connections the platform can be tilted, within its tilt range, without binding the rigidly connected sets of telescoping steel tubing. All four sets of telescoping tubing assemblies are rigidly connected to the outside surfaces of the cantilever part of the MDD. A friction-type bearing for the sliding, telescoping tubing sections was selected instead of ball bearing. This was done to limit the freedom of the sliding action and with an average speed of 3 fpm (maximum of 5 fpm). This works well and produces a smooth running assembly. The antifriction bearing pads are preloaded with a precompressed silicone sponge rubber backing material. This produces an assembly with no shake and provides a cushioned and shock absorbing condition between the tubing sections.

The four self-locking worm gear hoisting machines are located on top of the 100-foot level of the cantilever part of the MDD. All are reeved 3 ps with 9/16 inch diameter wire rope, and the single part of rope proceeds from each hoist drum approximately horizontally to the side of the cantilever structure and in line with the vertically mounted, rectangular, telescoping steel tubing. At that point the rope is deflected through a double sheave deflector block vertically downward to a single sheave load block which is attached to the top of the inner section of the telescoping steel tubing. The rope then continues up to the double sheave and then down with dead end anchored to the single sheave load block.

Each platform is equipped with five, angled-arm-type limit switches mounted under the platform's personnel deck and arranged to prevent the extreme bottom outline of either platform from being less than 12 inches from the top of the Orbiter wing surface.

40-KNOT-WIND SAFETY TIE-DOWN SYSTEM

The Safety Tie-Down System is provided to secure the Orbiter while it is suspended on the main hoist hooks near level 60'-0" during strong wind conditions above 12 knots and to 40 knots maximum. The principal function of the wind ties is to limit horizontal or longitudinal movement of the Orbiter and prevent any damage to it due to contact with the MDD.

The tie-down system is symmetrical about the longitudinal centerline of the Orbiter and consists of anchorage mechanisms which secure the Orbiter's forward lift beam to the MDD and the aft lift beam to the access/service platforms. At the aft end, the anchorage mechanism consists of two assemblies extending horizontally at 45° from the access/service platform. Each of the assemblies consists of a combination tension-compression, barrel-enclosed spring assembly (8-1/2 ton rated), coupled to a reversible ratchet load binder. Each of these assemblies is rigid from end to end and provides push and pull capacity.

At the forward end, the anchorage mechanism consists of a single assembly similar to the assemblies at the aft end except it is an 8-ton tension type, connected directly to the adjacent MDD column at one end and to the Orbiter lift beam at the other end. It is designed and installed to pull parallel with the centerline of the Orbiter lift pin. Also, at the forward end and as part of the tie-down system is a mechanism which anchors the forward end of the access/service platform to the MDD main column. This mechanism includes two assemblies, one from each corner of the access/service platform to the connection plate at the column. Each assembly consists of a reversing ratchet and integral handle and has a 28-ton-rated capacity. This portion of the tie-down system pulls a wedge seat, provided on the forward end of the access/service platform, into and snug against a tapered wedge lug on the MDD and secures the platform to the structure.

PERSONNEL HOISTS

Two personnel hoists are provided, mainly for use by SCAPE-suited personnel. These personnel hoists are standard catalog units regularly manufactured for a variety of industrial uses. A personnel hoist is located next to the extreme forward side of the stairs of each of the two towers. The two personnel hoists are identical; each is a counterbalanced rack and pinion drive type. The hoisting pinion drive machinery is located in the cage, and the rack is attached to the mast. Each hoist has a single speed of 160 fpm raising and lowering and a live load capacity of 5,000 pounds.

A complete operator control panel is located inside the cage, and all control of the personnel hoist system is from within the cage, with the exception of a safety stop switch located on top of the cage (required by ANSI A10.4-1973). All cage gates and locks and all hoistway gates and locks are operable only from within the cage, with the exception of the lowest landing, and these have an exterior key lock in compliance with ANSI A10.4-1973.

A separate cage safety mechanism, a part of each cage hoisting machinery, tracks the primary hoisting rack attached to the mast. The cage safeties are of the rack and pinion type. A second pinion, running on and driven by the rack, is assembled together with the overspeed governor and the safety brake to form an integral unit. The governor, on the same shaft as the pinion, senses when the pinion exceeds normal rated speed and sets the safety brake. The safety brake, in turn, applies a retarding force on this shaft and, therefore, on the pinion gear, stopping the cage.

WIND RESTRAINT AND ADJUSTMENT MECHANISM

The wind restraint and adjustment mechanism is an integral part of the MDD and provides the following:

- a. Restraint to the movement of the Orbiter when suspended from the main hoisting system during a maximum 12-knot wind. The restraint provided is not 100%, but it reduces the amount of Orbiter movement to a workable and safe degree while it is being hoisted from the jacked position to the mated position. The restraint equipment provides a stiffness factor in the horizontal plane to the rope-suspended Orbiter and does not detract from the smooth and precise vertical positioning requirement. When the Orbiter is in the mating mode the restraint equipment prevents the Orbiter from excess movement that would bring it into contact with the access/service platforms and the MDD.
- b. Six-inch plus or minus adjustment of the Orbiter in the X-axis and the Y-axis horizontal plane when Orbiter is suspended from the main hoisting system. The adjustment is required for minute movement of the Orbiter during the process of mating and attaching the Orbiter to the pylons of the 747 and during the reverse process of demating the Orbiter from the pylons of the 747.

The wind restraint and adjustment mechanism is one complete system, and each of the two functions is achieved with the same equipment and simultaneously. At the same time that adjustment is being accomplished, restraint is inherent and automatic. The wind restraint and adjustment mechanism consists of four telescoping square steel tubing assemblies; fourteen universal joints; four ball joints; three 10-ton electric motor driven, machine screw, self-locking worm gear actuators, each with fail-safe motor brake and extreme travel, geared limit switches; three welded steel brackets for actuator mounts; two links; and one operator control station. The telescoping tube assemblies are mounted vertically, and the top end of each assembly is attached to the MDD at the approximate 100-foot level. A universal joint is provided between the top end and the 100-foot level connection. The lower end of each telescoping tube assembly is attached through ball joints to one of the two main hoisting system spreader bars. The spreader bars are part of the hoisting equipment between the Orbiter and the Hydra Set/hook assemblies. Two telescoping tube assemblies are vertically located in the Y-axis line of the Orbiter at X₀582 and the forward main hoisting hook, and two telescoping tube assemblies are vertically located in the Y-axis line of the Orbiter at X₀1307 and the aft main hoisting hooks.

The wind restraint and adjustment mechanism operates and produces adjustment of the Orbiter in a horizontal plane through the horizontally mounted, motor drive, screw actuators. The displacement of the actuators in the X and Y axes at the approximate 80-foot level is transmitted to the Orbiter through the telescoping steel tubing assemblies which are connected to the Orbiter lift system spreader bars. Because the tubing telescopes, the actuator movement at the 80-foot level can be transmitted to the Orbiter at any elevation within the range of the equipment. Wind restraint is simultaneously and automatically achieved with the same equipment used for Orbiter adjustment and restraints at any elevation within the range of the equipment. When the actuators are inoperative, the system equipment in a horizontal plane is rigid and provides the required wind restraint. Due to the telescoping capability of the tubing assemblies, precision vertical movement of the Orbiter is accomplished while horizontal wind restraint is functioning.

One operator control station controls all adjustment functions of this system. Each actuator has a separate and complete set of controls, and there is no provision for simultaneous control of any of the actuators. All movement controls have complete inching capacity and are "dead man" type of controls which return to "off" position when released.

MATING ACCESS SYSTEM

The mating access system provides access to the forward and aft attach points of the Orbiter to the pylons of the 747. The aft equipment portion of this system is government furnished equipment (GFE), consists of two manually adjustable hydraulic platforms, and is cataloged under KSC P/N 79K05143. One platform is required for the port pylon, and one is required for the starboard pylon.

The equipment that provides access to the single forward attach point pylon consists of two manually operated rolling platforms. One is located in the port side MDD tower, and the other is located in the starboard side MDD tower, both of which are at the approximate 35-foot level. The two forward rolling platforms are similar, one right hand and one left hand.

The forward access rolling platform is special, and each platform consists of a rolling platform, four vertical support roller assemblies, four horizontal side guide roller assemblies, one hand-operated winch and stand, 1/4"-diameter wire rope, three wire rope sheaves, two sheave brackets, one wire rope anchor bracket, forged fittings, ladder and landing to the rolling platform; two horizontal support beams that the platform rolls within.

Operation of each rolling platform is manual through the operation of a 1-ton hand winch. The winch has a gear ratio of 10.5:1; the rolling platform rolls on and is side guided by antifriction roller-bearing rollers.

Each of the rolling platforms is reeved 1 ps (one part single) with 1/4"-diameter, fiber-core pre-formed wire rope. This results in a safety factor of 1.74. The wire rope is one continuous piece and has three turns around the drum for good traction. A turnbuckle is provided in the reeving to maintain proper rope tension. Each rolling platform rolls out to the centerline of the MDD, and the two platforms provide 360-degree access to the forward pylon attach point to the Orbiter.

NOSE PLATFORMS WINCH SYSTEMS

A winch system is provided to raise and lower the nose platforms and the hinged access stairs at the 15'-7" level of the MDD. There are two winch systems, and they are similar -- one being left hand and one right hand. One is located in the port side MDD tower, and one is located in the starboard side MDD tower. Both systems are manually operated, and each winch system consists of two 1-ton hand-operated winches on one common stand, 1/4"-diameter wire rope, five snatch blocks, two swiveling safety

latch hooks, forged chain, fittings, and pad eyes. All components of both port and starboard winch systems are identical for interchangeability. The winches and stands are located on the 20'-10" level, and all pad eyes are located just under the 40'-0" level. When platforms are in the raised position, they are secured in a vertical position by safety chains.

ELECTRICAL SYSTEMS

The major electrical system installations provided on the MDD are electrical power service and distribution, lighting, receptacles, cable trays for GSE, fire alarm, obstruction lighting, and lightning protection. In addition to meeting their basic functional requirements, the design of the above installations includes special provisions for:

- a. Operation under hazardous conditions
- b. Demountability of electrical installations
- c. Minimum power operation

ELECTRICAL POWER SERVICE AND DISTRIBUTION

The electrical power service and distribution installation provided for the MDD is designed to receive a 480-volt, 3-phase, 3-wire electric service from the site on which it is erected; to distribute this 480-volt power to all 480-volt loads on the MDD and to several loads located on the site immediately adjacent to the MDD; to produce 208Y/120-volt, 3-phase, 4-wire power and distribute it to all 120-volt loads on the MDD; and to provide capacity for the future addition of a nominal amount of electrical load. The electric service from the site interfaces with the MDD at the line side connections of the main circuit breaker in a power panelboard on the outboard side of the MDD's port leg. This main breaker serves both as the service overload protection and disconnect. The breaker is equipped with a shunt trip coil controlled by a momentary contact switch located separately above the panelboard to permit rapid removal of all power from the MDD without having to open the panelboard enclosure. The electric service from the site must have a capacity of not less than 400 amperes at 480 volts. The total connected MDD load is 352 kVA with an estimated maximum concurrent demand of 282 kVA. Power is distributed to all 480-volt loads from two 480-volt distribution panelboards, one on each side of the MDD at ground level. The panelboards are located at ground level because the larger 480-volt loads are all at that level and also to allow ready access to the panelboards. Spare capacity has been provided in all panelboards in the form of spare circuit breakers and spaces for future circuit breakers.

LIGHTING

The lighting installation is designed to provide task and area illumination during MDD operational periods and minimum access illumination during nonoperational periods. Task and area lighting consists of floodlights mounted on poles that are separate from the MDD structure. This method was selected to permit locating the luminaires outside of the hazardous area of the MDD, thereby utilizing higher efficiency, nonexplosive-proof-type light sources. Supplementary floodlighting is provided on the two access/service platforms and nose platforms to provide a high level of illumination for localized work areas where the general task lighting may be inadequate. These floodlights are tungsten-halogen type, explosion proof because of their location on the MDD.

FIRE ALARM

The fire alarm system provided on the MDD comprises only one zone of a complete system for the entire Shuttle approach and landing test (ALT) facilities. The central control for this system is located in the nearby maintenance hangar and shops. One alarm-initiating circuit is extended from the system control panel to the MDD. This circuit is provided with manual stations and water flow switches. The flow switches are located upstream of the manual deluge valves and will operate upon opening of the respective valve. An alarm-sounding circuit is extended from the system control panel to the MDD. This circuit is provided with an alarm-sounding bell on the stairway for each of the MDD legs.

OBSTRUCTION LIGHTING

Obstruction lighting is provided on the MDD because its normal location will always be close to an operating airstrip. The obstruction lighting system is equipped with photoelectric control, mounted at the top of the MDD to automatically control the lights. A manual bypass switch is provided at ground level to override the photo control.

LIGHTNING PROTECTION

The lightning protection system is designed to provide protection for the entire structure and for personnel on the platforms and catwalks. The system design is based on the "cone of protection" concept using cones of 1 to 1 for a single point, and 2 to 1 between two adjacent points.

MECHANICAL (PLUMBING) SYSTEMS

COMPRESSED AIR SYSTEM

The air system is designed to supply shop air to pneumatically operated tools and purging air to electrical equipment located in a hazardous environment. The air system capacity will serve up to seven pneumatic tools in simultaneous operation and also provide a cubic-foot-per-minute airflow to 82 purging enclosures for a total air supply demand of approximately 115 cubic feet per minute. The air compressor is a self-contained factory package unit. The belt-driven air-compressor electric motor, starter, air receiver, and refrigerated air dryer are mounted on a common base and located at ground level, forward of the structure to avoid purging requirements of its electrical components due to the hypergol environment. The electrical components selected for the design are suitable for outdoor use.

The supply air piping system is divided at ground level for separate routing of shop air supply and purging air is reduced to 55 psig. The piping is routed through the tower to serve shop air outlets and purging enclosures on the left and right sides of the tower ("fixed levels") and, for shop air only, on left and right sides of the access/service platforms.

EMERGENCY SHOWER AND EYE/FACE WASH FIXTURES

A combination emergency shower and eye/face wash fixture is located on each side of the MDD "fixed" platforms at levels 20' and 40'. An eye/face wash fixture is located on each access/service platform. These units will serve as temporary relief for accidental spillage of hazardous or irritating fluids. The showers are designed for deluge type flow for full decontamination.

WASHDOWN STATIONS

The washdown stations will enable washing of inadvertent fuel spill on the Orbiter or adjacent areas. The stations are located on the access/service platforms and consist of a 40'-long, retractable water hose reel. The terminal fitting provided is a standard adjustable-type fog nozzle.

PERSONNEL SHOWER SYSTEM

A deluge-type shower system is designed for personnel protection against hypergol spills and ground level fire. The personnel shower system requires manual activation via two butterfly valves. Dual butterfly valves are used to preclude system flow by accidental opening of one valve. Manual activation will require two observers stationed on each side of the towers "fixed" level (either level 20 or level 40, depending on location of the access/service platform).

Each access/service platform has 30 spray nozzles. In addition, deluge-type sprinkler heads are located on the "fixed" levels to provide full egress protection between access/service platforms and "fixed" level stairways. Three additional spray nozzles are located on the access/service platform and are aimed toward the Orbiter's gaseous hydrogen and hydrazine servicing interfaces.

The entire system is supplied from an 8-inch underground main, reduced to 5 inches for routing to four separate manually controlled deluge stations located on the tower. Each control station (dual butterfly valves) has a waterflow detecting device electrically wired to an alarm system.

PIPING SPECIALTIES

The shop air, fire line, and potable water supply between the "fixed" level and access/service platform is supplied through flexible rubber hoses. The hoses must be disconnected when raising or lowering the access/service platform and reconnected to the applicable level (20 or 40) when the access/service platform is positioned at the desired level.

Swivel joints are located on the access/service platforms in order to maintain a vertical position at the hose connections while the access/service platforms are in variable tilting positions. This eliminates undue stress on piping and hoses.

Safety flow-cutoff valves are located in the air supply immediately upstream to the air hoses. These valves will automatically stop airflow in the event of hose rupture and eliminate hose whiplash.

CONCLUDING DISCUSSION

The Orbiter Mate/Demate Device at the Kennedy Space Center, Florida, is basically a twin facility to the MDD at DFRC, Edwards AFB, California, which is the subject of this paper. The two facilities have identical and interchangeable components and systems for mate and demate operations; however, some of the functions and services provided for at DFRC were not required for the design at KSC, such as the following:

- a. Access/egress route for SCAPE-suited personnel
- b. Personnel hoists
- c. Compressed air system
- d. Emergency shower and eye/face wash fixtures
- e. Washdown stations
- f. Personnel shower system

Both of these facilities have been used for each of NASA's Space Shuttle Orbiter's successful series of Orbital flight tests (OFT), with the recovery and mating operation at the MDD at DFRC and the demating operation at the MDD at KSC, where the Orbiter is prepared and readied for each of its space flights.

Related to the MDD's at DFRC and KSC is NASA's Orbiter Mate/Demate Stiffleg Derrick facility at the White Sands Missile Range, Northrup Strip, New Mexico (secondary landing site) (foundation and site design by Connell Associates under direction of NASA, KSC). It is designed and constructed to handle and accommodate the necessary operations, functions, and services for deservicing and mating the Orbiter for its return to KSC. This facility was recently used to recover the Orbiter after one of its OFT return flights and safe landing at WSMR.

In addition to the Orbiter mate/demate facilities at DFRC, KSC, and WSMR, to ensure safe landing, proper servicing, and quick turnaround for the next scheduled space flight, contingency landing sites (CLS's) have been selected by NASA around the world in case the Orbiter needs to make an emergency landing. The CLS's are located at the following airfields:

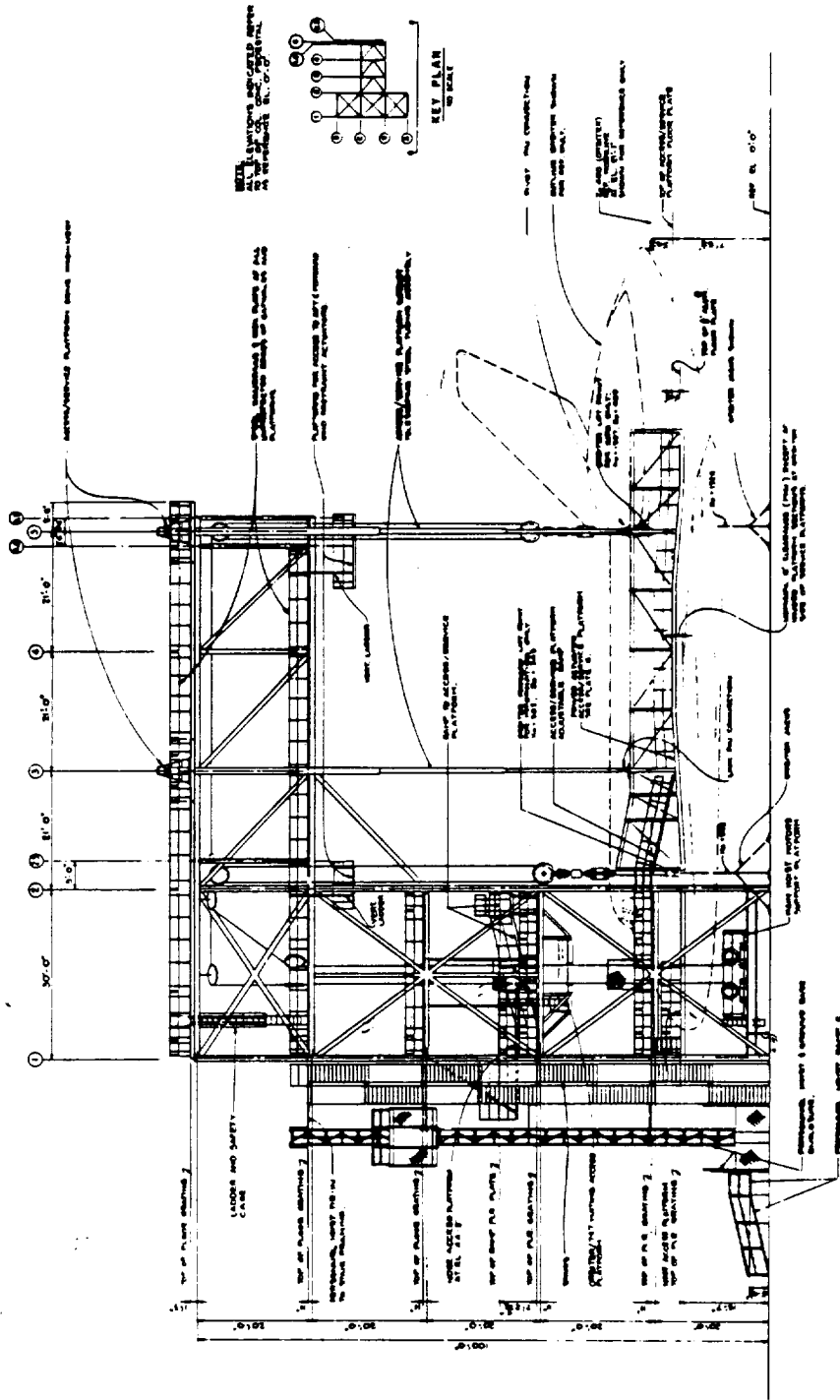
Naval Station, Rota, Spain
Kadena Air Base, Okinawa, Japan
Hickam AFB, Oahu, Hawaii
Dakar, Senegal

A Mate/Demate Stiffleg Derrick Universal Foundation has been designed for each of these sites to accommodate installation of the stiffleg-derrick system (GFE) and the forward and aft guy systems (GFE). All items needed to construct the facility, except for concrete and reinforcing steel, will be provided in a "fly-away foundation kit" which is GFE. Actual construction at any of the sites will not begin until an actual emergency landing of the Orbiter occurs at that particular site and the "go" signal is given by NASA.

REFERENCES FOR ADDITIONAL INFORMATION

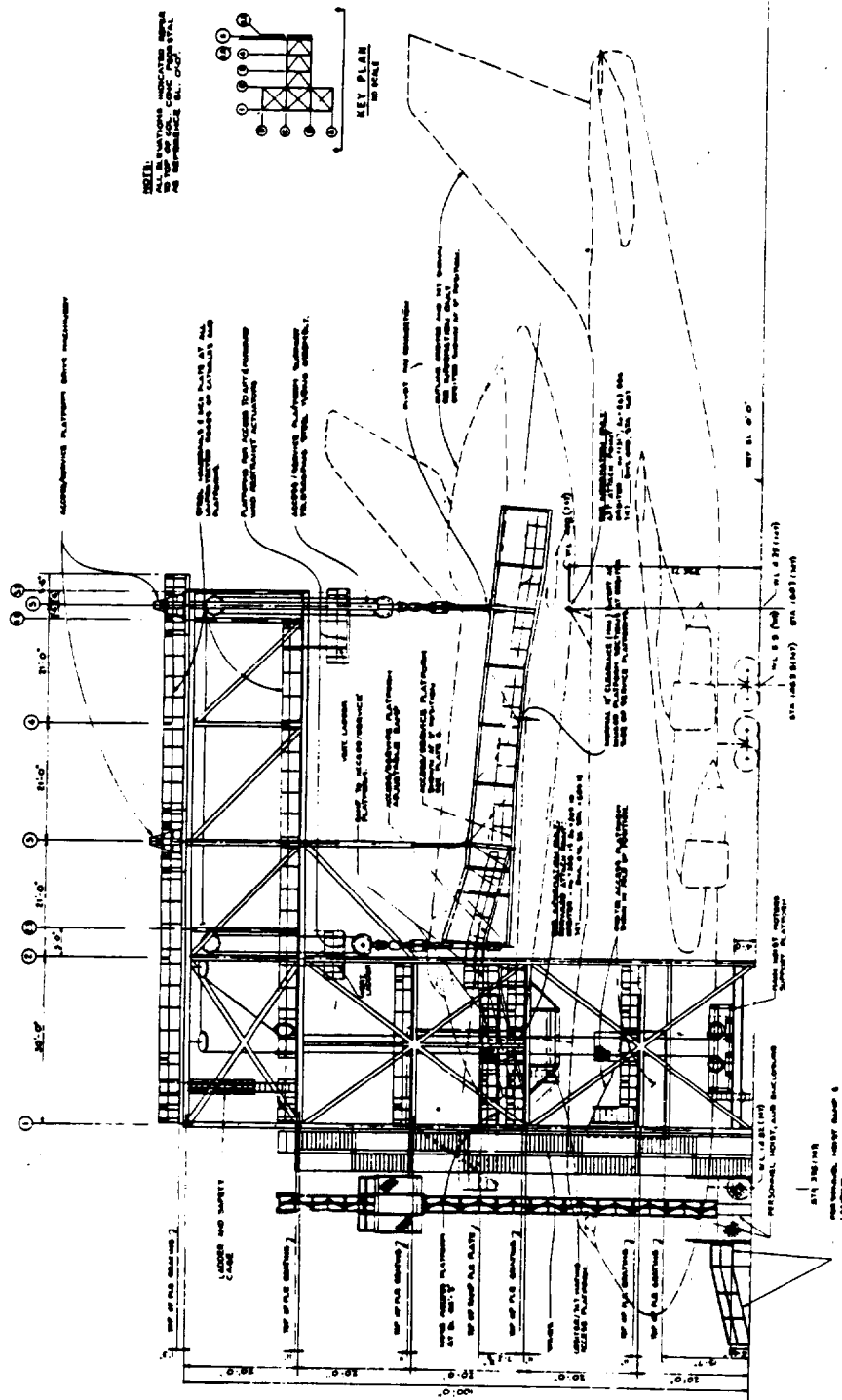
1. NASA Technical Report TR-1355, July 1975, Design Data Manual - Orbiter Mate/Demate Device, prepared by Connell Associates, Inc.
2. NASA Drawing No. 79K05459, Orbiter Mating Device, NASA DFRC, Edwards AFB, California (July 1975)
3. NASA Drawing No. 79K08112, Orbiter Mate/Demate Device, NASA, Kennedy Space Center, Florida (December 1976)
4. NASA Drawing No. 79K16871, Mate/Demate Stiffleg Derrick, White Sands Missile Range, N.M. (June 1979)
5. NASA Drawing No. 79K021033, Mate/Demate Stiffleg Derrick, Naval Station, Rota, Spain (March 1981)
6. NASA Drawing No. 79K21097, "Fly-Away" Foundation Kit CLS (A70-0873)

ORIGINAL DESIGNING
OF POOR QUALITY

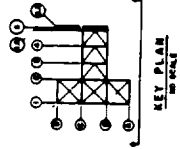


ORBITER MATING DEVICE
SIDE ELEVATION
ORBITER POSITIONED ON JACKS
PLATE NO. 1

ORBITER MATING DEVICE
OF POOR QUALITY



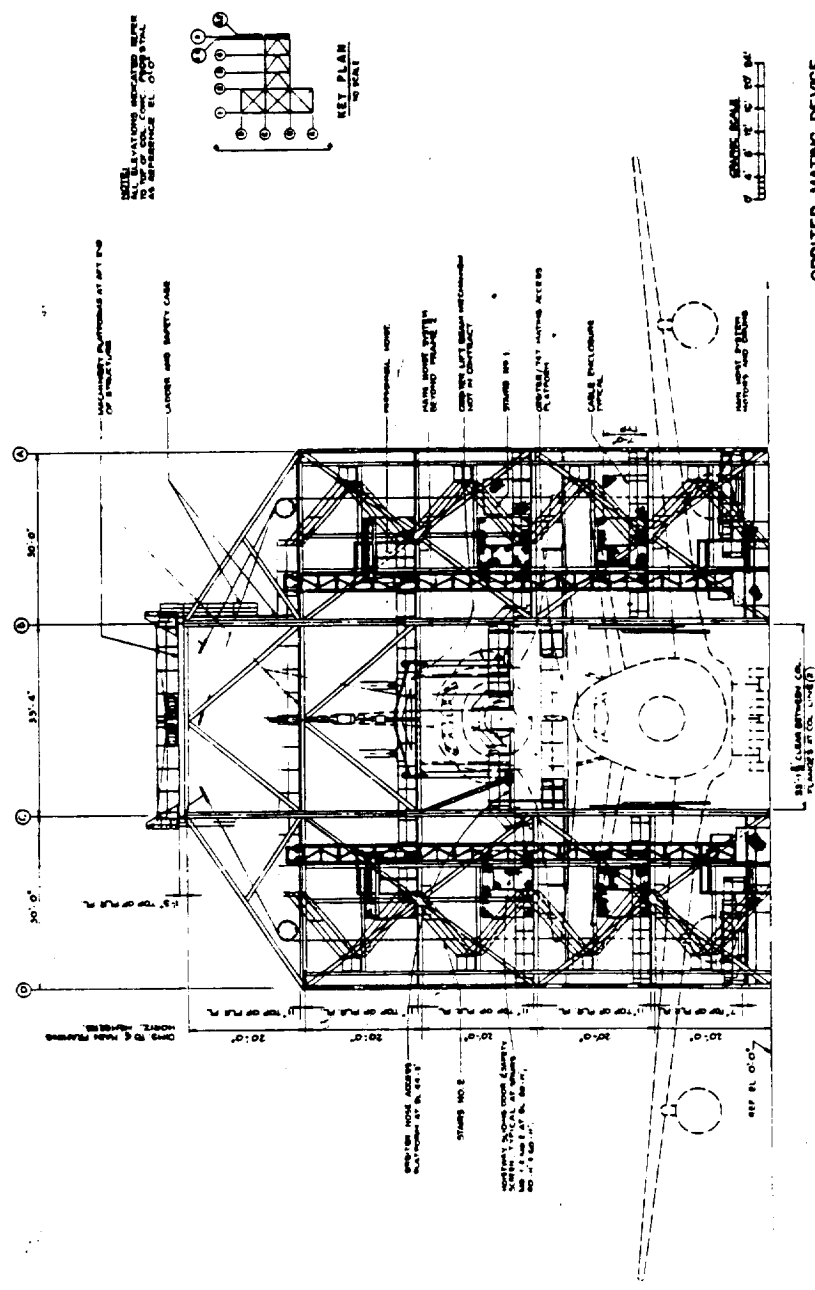
NOTE:
ALL DIMENSIONS INDICATED HEREIN
ARE TO BE CONSIDERED AS APPROXIMATE
AND NOT TO BE USED FOR FABRICATION



ORBITER MATING DEVICE
SIDE ELEVATION
ORBITER POSITIONED ON 747
PLATE NO 2

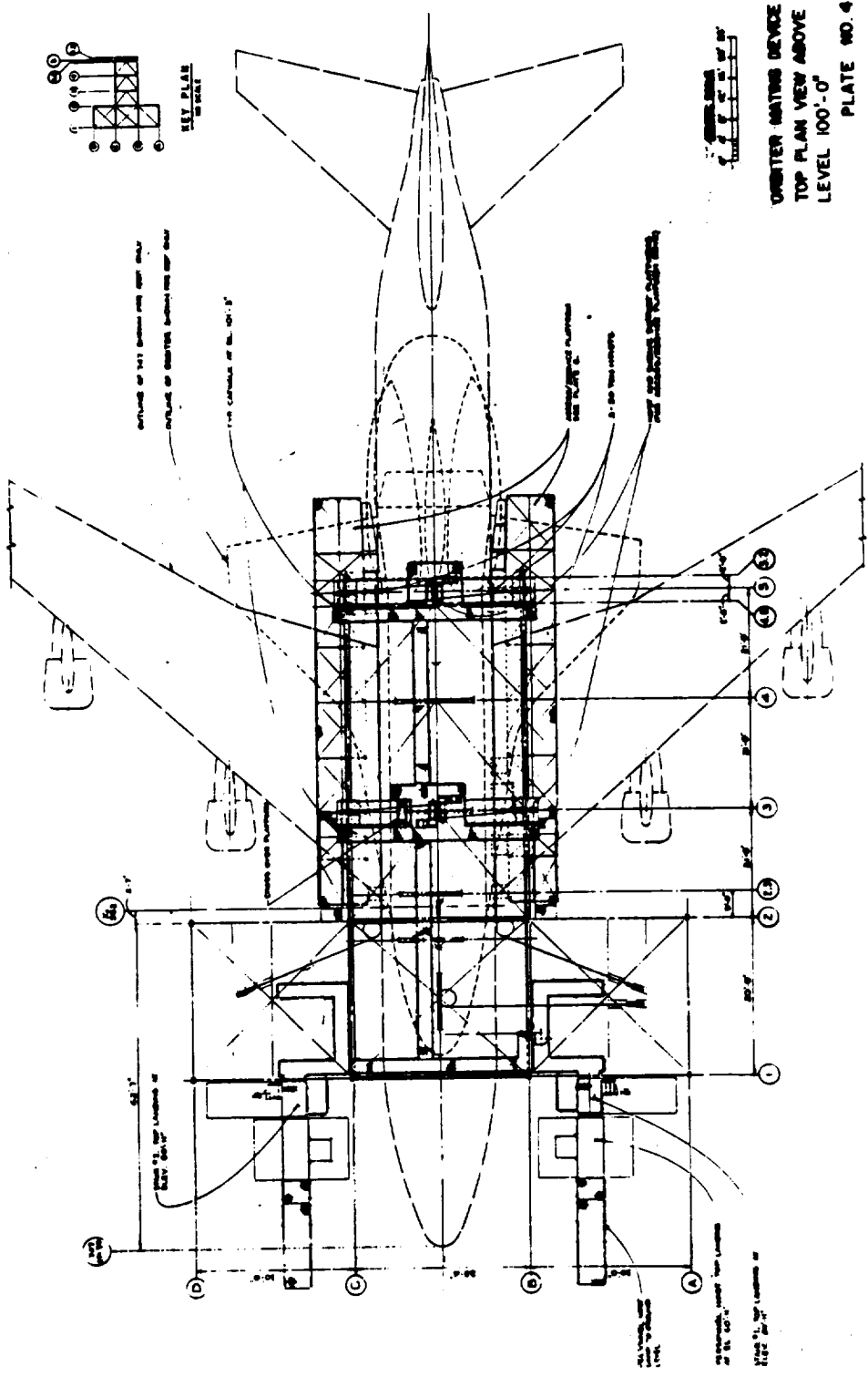


ORIGINAL FACED
OF POOR QUALITY



ORBITER MATING DEVICE
FRONT ELEVATION
ORBITER POSITIONED ON 747
PLATE NO. 3

CROSS SECTION OF
OF POOR QUALITY



D36

N85-16973

COMPUTER AIDED PROCESSING USING LASER MEASUREMENTS

Richard M. Davis, DF-PEO
and
John C. Koch, PRC Systems Services Co.
Kennedy Space Center, FL

ABSTRACT

We now have the challenge of processing the STS and its cargo through KSC facilities in the most timely and cost effective manner possible. To do this we have established a 3-D computer graphics data base into which we have entered the STS, payloads and KSC facilities. The facility drawing data are enhanced by laser theodolite measurements into an "as-built" configuration. We have combined elements of the data base to study orbiter/facility interfaces' payload/facility access problems and design/arrangement of various GSE to support processing requirements. With timely analysis/design utilizing the 3-D computer graphics system, costly delays can be avoided. Better methodology can be analyzed to determine procedures for cost avoidance. Some day we hope to have not only a KSC, but an inter-center data exchange network.

CHALLENGE

The challenge before us today is to process the Space Transportation System and its total complement of payloads (cargo) through the various facilities at the Kennedy Space Center in the most timely and cost effective manner possible.

One of our more pressing problems is the interaction of three primary elements: Space Shuttle, Cargo, and Facilities.

First, the Orbiter must be processed in the Orbiter Processing Facility (OPF) without interference from the many platforms necessary to gain access for post-flight inspection, maintenance, and pre-mate checkout prior to payload installation.

Next, Shuttle elements - the Orbiter, the External Tank (ET) and the Solid Rocket Boosters (SRB's) must be successfully integrated and stacked on a Mobile Launch Platform (MLP) inside the Vehicle Assembly Building (VAB) midst its assorted platforms and levels of access.

Numerous experiments and payload elements must be integrated into cargos for each mission. This integration and checkout is accomplished in the Horizontal Processing Facility (HPF), various hangars, and the Vertical Processing Facility (VPF). Each facility/MMSE (Multi-Mission Support Equipment) must be able to accept and not interfere with the myriad of payload elements.

Finally, the cargo must be entered into the Orbiter. This may be done either in the OPF or at the launch pad in the Payload Changeout Room (PCR). Here all three, the Shuttle, the cargo, and the facility, must interface precisely to accomplish a successful mission.

METHODOLOGY

Our methodology is common throughout for these challenges and their solutions; let us introduce our procedure.

We have established a computer graphics data base utilizing a three-dimensional color graphic system. The Shuttle configuration, the various cargos, and all the facilities utilized for buildup and processing are inserted into this data base utilizing dimensioned drawings and various input techniques. Single operator input time can vary from hours or a few days for a simple subject, to a month or more for a detailed facility.

Once the data base is built, it is relatively easy to produce the interrelationships between the three elements of Shuttle-Cargo-Facilities. Through the use of the computer graphics system, various components can be manipulated, shrunk, stretched, moved, modified, etc., at will. This is especially useful when arranging or modifying Ground Support Equipment (GSE), or moving an

experiment from one payload to another, or arranging different payloads according to the ever changing cargo manifests. Our zoom ability is very useful when a detail must be examined closely, plus, a measurement capability is available to determine clearances, interferences, line lengths, etc. Real-time working documentation can be obtained by a CRT copy machine. Final drawings are procured on a large 36" x 54" plotter on milar or vellum. This procedure, prior to the computer age, was accomplished by using basic drawing with overlays and cutouts.

A major uncertainty in facility definition is the difference between the design drawings and the final as-built configuration. To account for this variation, we at KSC have attempted to survey as much of each of the facilities as possible.

Our survey instrument is a laser theodolite, which is self-powered and field-transportable. It utilizes microprocessor calculation with digital display of the data. Data presented is horizontal distance, slant range, height, cross range, azimuth angle, and elevation angle. It does all this with an instrumentation accuracy of +5 mm in 5 km (0.0001%). The laser target is an optical prism, which is placed at the point to be measured. In its raw form, the transit data is not compatible with the format utilized by our computer; therefore, we have produced a special program that converts the theodolite data into our Orbiter X, Y, Z coordinate system.

Once we have the survey data entered into the computer graphics data base, we apply the selected points to the model constructed from the design drawings. Here is where you find the interesting discrepancies: doors are misaligned; walls are not plumb; platforms at odd levels; columns moved; and especially outlets for power, fluids, and gases seem to show up on the survey data as "as-built" locations. We have a very high level of confidence that our as-built computer models truly represent the actual facility.

The facilities we now have in our data base include the Vertical Processing Facility (VPF); Orbiter Processing Facility (OPF); Vehicle Assembly Building (VAB); Payload Changeout Room (PCR); and the Horizontal Processing Facility (HPF), including the N&S Level IV workstands, Spacelab workstands 2 and 3, Cargo Integration Test Equipment (CITE) workstand 4, Apollo Telescope Mount (ATM) cleanroom, and various Spacelab handling and access. We have recently completed the Launch Equipment Test Facility (LETF) where we check out the various umbilical and access arms utilized in Space Transportation System (STS) servicing at the launch pad. We can now analyze Orbiter/umbilical motion in three dimensions simultaneously. We do not necessarily have all of each facility surveyed at this time, but we are working on it.

The Orbiter contractor provided us with the Columbia's exterior mold lines, which we input into our data base. We also have Challenger's payload bay in the data base. While we have the Remote Manipulator System in the data base, we have input small details, such as the handrails and antenna, only when we were requested to work a specific problem. Results from various studies show that our Orbiter model is very accurate.

Starting with OSTA-1 which flew on STS-2, we began entering payload information into the data base to assure integrability with the various facilities. Some of our payload models were created from highly detailed drawings; others were created from drawings with very few dimensions that were digitized with our computer equipment.

Any payload in our data base can be positioned into any facility we identify as having a requirement for analysis. We can determine access problems in the various processing facilities. What may be easy access from a workstand in the horizontal position may present a difficult problem when inserted in the Orbiter in a vertical position with only limited levels from which to work. We have an overall high confidence level in our data facility/cargo base and feel comfortable with any challenge presented for solution.

ACHIEVEMENTS

We are utilizing our computer graphics capability to help simplify and expedite the STS and cargo processing at KSC. The survey enhanced data base has enabled us to analyze difficult three-dimensional problems quickly and with a very high level of confidence in the answers. We have studied a rather broad spectrum of problems from orbiter stacking and payload access to facility/GSE layout.

EXAMPLES

The following is a sampling of how our system is being utilized with examples taken from studies that have been performed at KSC.

Assure Orbiter/OPF Compatibility

Prior to the arrival of Columbia at KSC, there was concern if any of the access and service platforms in the OPF would interfere or damage the Orbiter when placed in position.

The Orbiter was moved into the OPF; the OPF workstands were positioned around the Orbiter--all done with the computer graphics system! At those points where interferences were identified on the computer simulation, platforms were physically modified to give adequate clearance. The simulation was verified when the Columbia was actually towed into the OPF; the platforms were moved into position--and no interference! Note Figures 1 and 2 which also indicate our zoom capability.

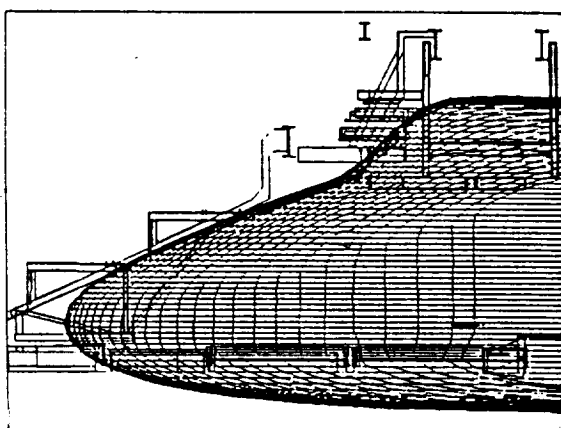


Figure 1.

ORBITER/OPF MOVEABLE ACCESS PLATFORMS

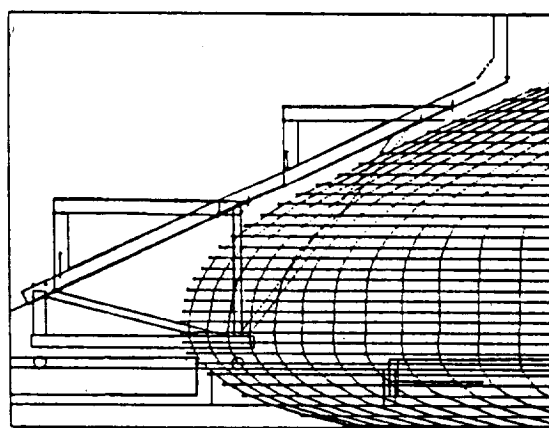


Figure 2.

Orbiter/ET/SRB Stacking Enhancement

On STS-6, the MLP was placed 1.5 inches off the predetermined set point. The stacked configuration of the Orbiter/ET/SRB on the off-center MLP was constructed in the data base. Then the VAB extendable platforms were moved into position around the off center stacked configuration. No excessively close tolerances were observed at any of the work levels; therefore, the MLP was allowed to remain off center, and the stacking effort continued without having to move the MLP. But more importantly, time was not wasted, personnel were not endangered and STS equipment was not damaged.

A similar condition occurred when we were asked if the Orbiter could be lowered through the platforms in the VAB with the forward bipod already attached to the ET (Figure 3). Previously, the bipod was attached after the Orbiter was lowered and soft mated to the rear struts -- a difficult and time-consuming operation. Again the model was constructed in the data base, and the operation proved that the Orbiter could be successfully lowered through the platforms, past the bipod, without interference.

Another exercise was run to see if the body flap in a 20° below the null location could be passed by the bipod. Again, the simulation indicated that we could lower the Orbiter with the body flap in the designated configuration. This exercise eradicated the need to power up the Orbiter after transfer from OPF to VAB to allow hydraulics to zero the control surfaces before stacking in the VAB.

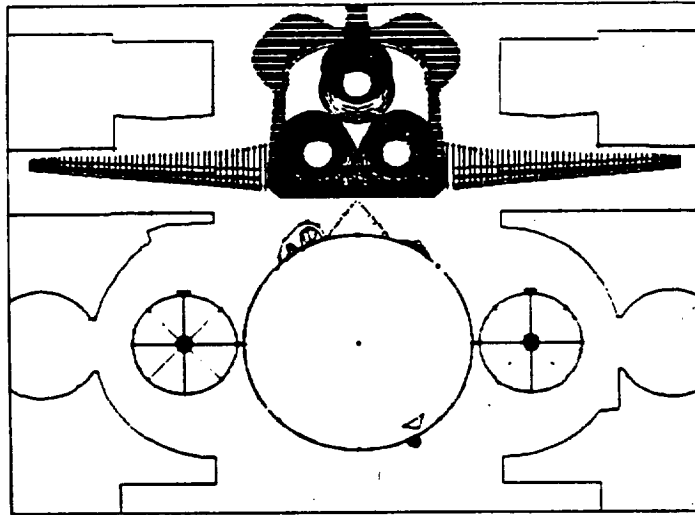


Figure 3. ORBITER/BIPOD CLEARANCE DURING MATING

Filament Wound SRB Study

The proposed filament wound SRB will have more flexibility than the present steel cases. This will result in greater Orbiter/ET umbilical connection motion. The Tail Service Mast (TSM), which contains the T-O umbilical and linkage was modeled to study the motion in three dimensions to determine maximum travel limits and element fatigue levels. Various T-O excursions were analyzed to determine what facility modifications would be necessary (Figure 4). In addition, the entire Launch Equipment Test Facility (LETF) was input into the data base to determine what modifications were required on the LETF to test these new excursions. This facility consists of five major test structures/systems.

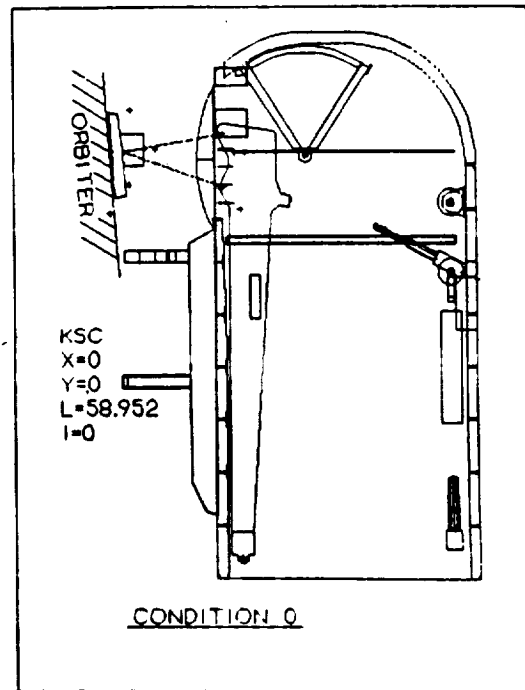


Figure 4. FILAMENT WOUND SRB EXCURSION STUDY
TSM MOD ANALYSIS

Parallel Processing of Cargo in the HPF

In order to study the impact of increased traffic in the out years, all cargo processing equipment and facilities are being entered into the data base. We have already taken a look at the problem of having SL-2, SL-3, and three elements of mixed cargo in the Level IV workstands at the same time. Various elements of access GSE were modeled to determine optimum use with minimum modification, or hindrance to other elements. It is very easy to cut and try with this system. We plan to model all the handling equipment and GSE necessary to identify all cargo placement in each workstand, at a given time slice, per month and year. This will provide maximum GSE utilization (Figures 5 and 6).

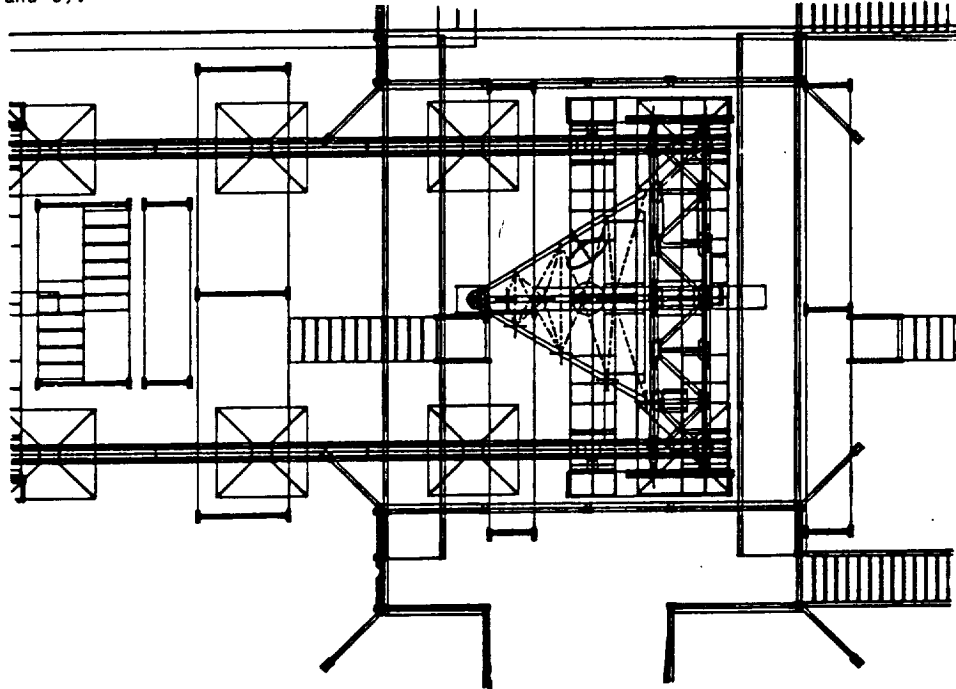


Figure 5. OAST-1 ACCESS STANDS -- O&C LEVEL IV
INTEGRATION AREA (PLAN VIEW)

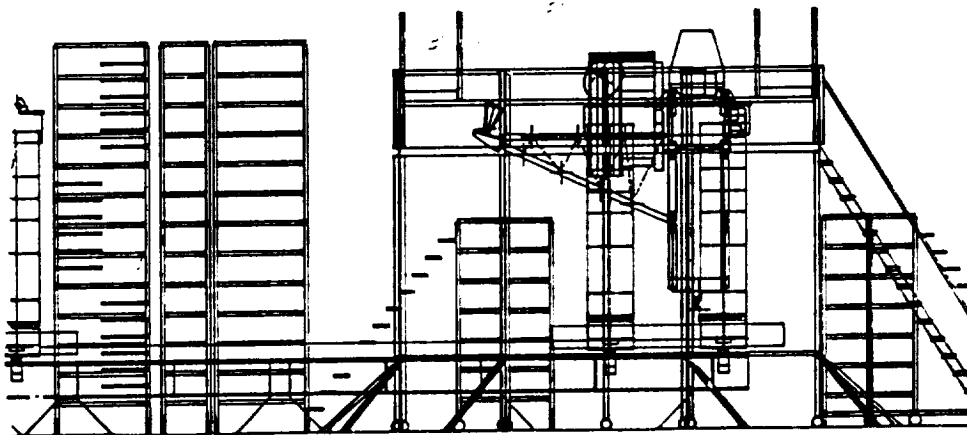


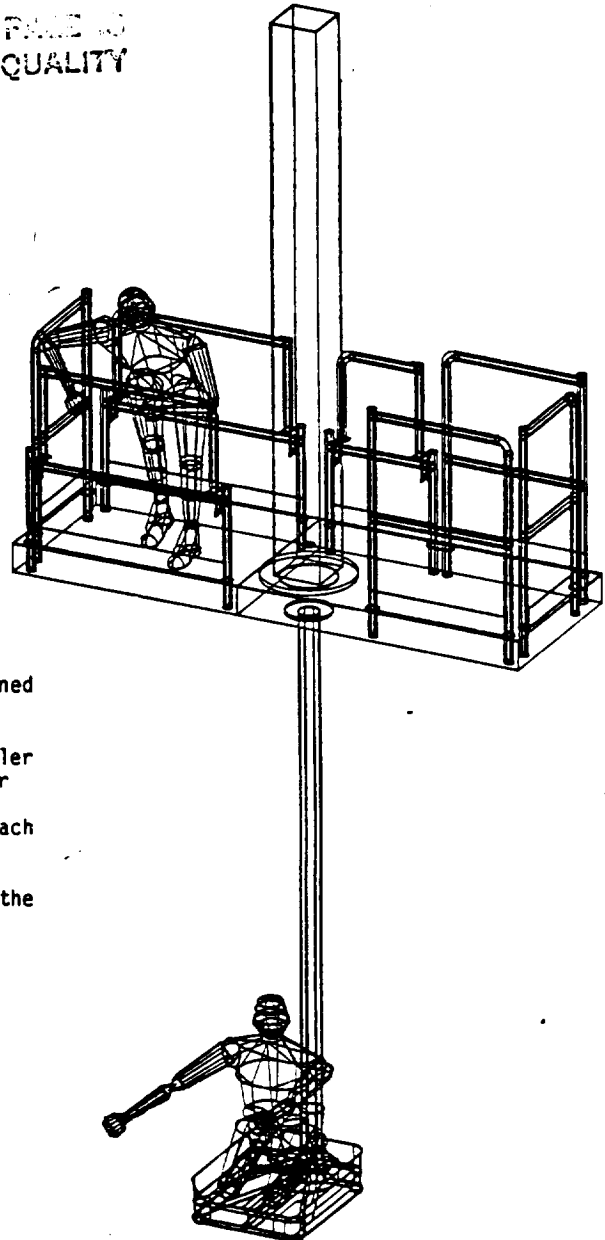
Figure 6. OAST-1 ACCESS STANDS -- O&C LEVEL IV
INTEGRATION AREA (ELEVATION VIEW)

Accessibility of Cargo in Facilities

Accessibility is always a critical element at KSC, and when the cargo is placed into the Orbiter, things get even more difficult.

One of the first challenges we met was determining placement of a Dewar on the platforms in the OPF and PCR. This placement is necessary for servicing two experiments utilizing cryogenics, and line length is critical.

ORIGINAL PAGE IS
OF POOR QUALITY



To service experiments on SL-1, it was determined that the present extendable bucket originally designed for access in the payload bay was too large for the limited space available. A smaller 16" x 20" platform was designed on the computer graphics system. An orthomorphic man was designed to test positioning, movement, and reach from the platform. Engineering and cargo operations conducted the CDR on the computer. This was a first for us, but we believe it is the beginning of many more to follow (Figure 7).

Figure 7. ACCESS PLATFORMS/ORTHOPORMOPHIC MEN

We have simulated several different cargo elements in the VPF to determine access from its work platforms. One of our more famous elements is the space telescope, which requires considerable access to several different panels and compartments on board (Figure 8).

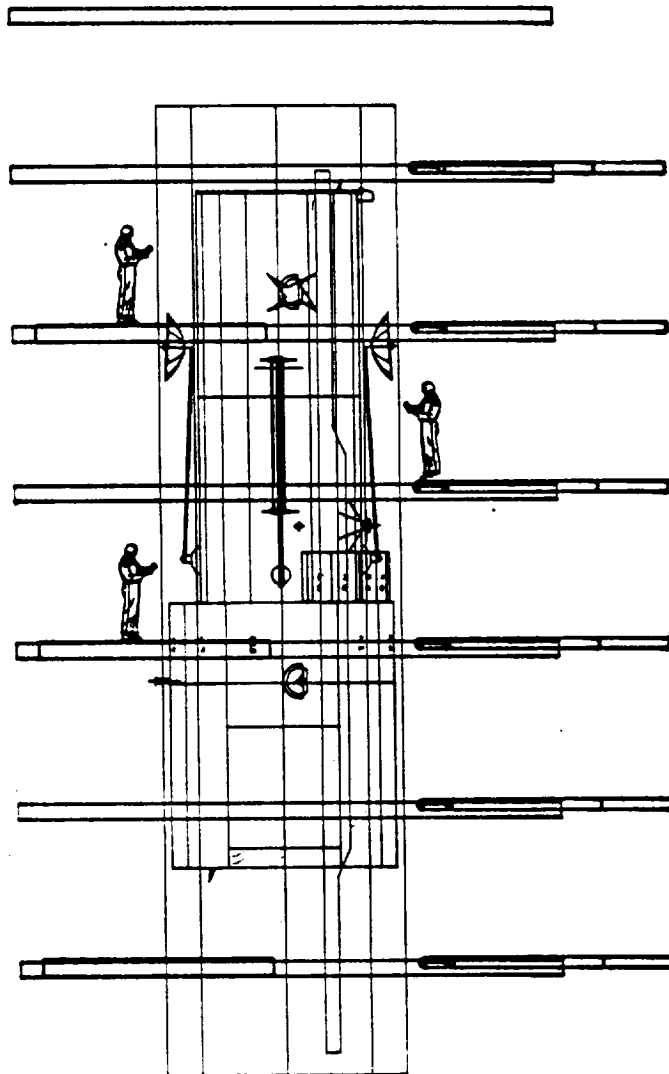


Figure 8. SPACE TELESCOPE IN VPF

The PCR at the Pad provides many challenges for our computer graphics system. Here in the PCR, is where all elements of the mission finalize. Often experiments have late access requirements, which are sometimes quite difficult to achieve in an environment that has rotated 90 degrees, and are now confined by the envelope of the payload bay. OSTA-1 battery access was our first exercise in the PCR. SL-2 cryogenic servicing is a persistent problem we are still modeling (Figure 9).

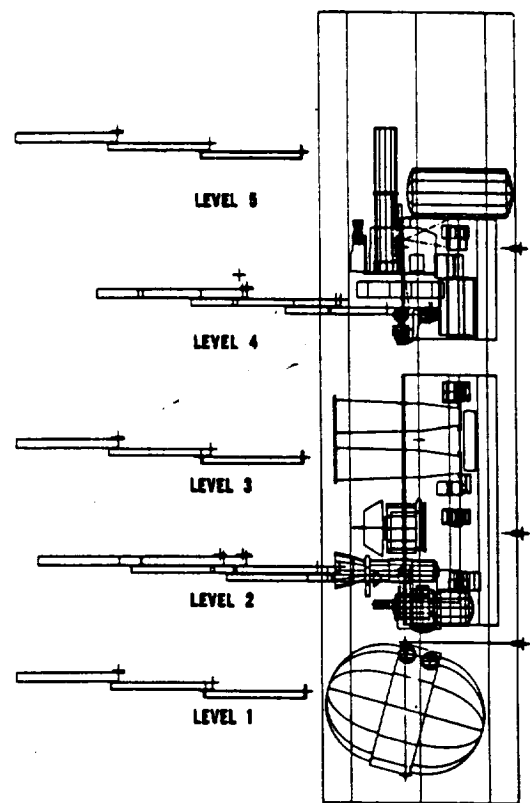


Figure 9. SL-2 IN PCR -- PGHM LEVELS 1-5

We have recently started constructing the data base to model the GSE necessary for a contingency landing site. Here, we must have maximum utilization from a minimum amount of equipment.

Sometimes, when a problem is identified to us, we can point to a solution that saves a great deal of time and money, such as the stacking exercises mentioned earlier, which can be equated in time and dollars saved. Sadly, we sometimes also prove that a clever idea just won't work.

We also must realize that there is a cost saving in preventing problems. These are very hard to quantify. A lot of the things done in the cargo processing world could be done on a drafting board or just by going out and measuring something (sometimes a brave or foolhardy thing to do at the VPF or PCR). As an example, we didn't have to service the OSTA-1 battery at the pad, but we knew that if we had to, we could not extend the center platform past the antenna. So, an alternate method had to be worked out in advance in the event servicing was necessary. How much do you save by putting the access stand up once, right, the first time?

We feel that one of the most valuable things we save is analysis time; time we don't have as the traffic increases.

PROPOSED RESPONSE TO MEET FUTURE CHALLENGES

At this time, KSC Engineering Development is making an in-depth study to determine our next generation computer system. We have asked our friends in the cargo and vehicle processing world to coordinate their efforts with us to provide an optimum system capable of meeting all our needs. Design engineering requires a large scientific computational capability while, in addition, Operations requires considerable graphics capability. Our intentions are that, in the future, we will design, coordinate, review, and sign off on the computer.

We intend to strive toward a controlled data base. With the new generation of engineers who are accustomed to working with computers we believe an entire engineering effort can be accomplished within the computer data base system.

Once a facility, cargo or flight vehicle, has been defined, it can be baselined and controlled within the system. Engineers can draw this information out of the controlled memory data base and perform operations or modifications at a remote terminal. However, the system would require appropriate sign-off/releases for the mods to be incorporated into the controlled data base. We believe this would also reduce/eliminate the huge volume of paper required and time consuming release boards. We have made the first steps towards these goals and when our new generation system comes on line, we hope to attain all of our goals.

Another important step we would like to propose is to have inter-center coordination for all of our common information requirements. At the present time, our computers and their great store of information in their data bases cannot communicate with each other. KSC has very detailed launch and cargo processing information and other centers such as MSFC, JSC and GSFC have payload information in their computers. Currently, KSC cannot transfer this information from one system to another.

We would like to propose a NASA-wide common data base where we all could exchange information. Perhaps we all do not require the same type of computer, but we should coordinate the effort so that the data bases are compatible, thereby releasing a great amount of transferable detailed information.

We believe that by utilizing such state-of-the-art technology to its fullest, we can minimize unknowns and process Shuttles and their cargo in a timely and cost effective manner. That is the ever present challenge.

IN-FLIGHT TESTING OF THE SPACE SHUTTLE ORBITER
THERMAL CONTROL SYSTEM

J. Thomas Taylor
NASA Lyndon B. Johnson Space Center
Houston, Texas 77058

ABSTRACT

The challenge of defining and successfully executing in-flight thermal control system testing of a complex manned spacecraft such as the Space Shuttle Orbiter and the considerations attendant to the definition of the tests are described in this report. Design concerns, design mission requirements, flight test objectives, crew vehicle and mission risk considerations, instrumentation, data requirements, and real-time mission monitoring are discussed. In addition, an overview of the test results is presented.

INTRODUCTION

The value and utility of a manned spacecraft such as the Space Shuttle Orbiter are enhanced greatly by its operational flexibility and capability to perform a multitude of varied and partly undetermined mission objectives. In this light, it was the initial design goal that the thermal design of the Orbiter be accomplished with minimum constraints with respect to vehicle attitude and time in attitude as well as power and weight.

The classical approach, whether for an unmanned or a manned spacecraft, is to define a thermal design mission which provides a design envelope and then to verify the design performance by ground testing to the extreme environments of the envelope, or by performing a simulated mission profile with minimal in-flight testing supported by analyses. This approach, however, was fostered in part by the fact that previous spacecraft were not reusable and a high degree of confidence in the design was necessary before committing to flight.

Program funding limitations and the fact that the Orbiter was a reusable spacecraft led to the consideration of in-flight testing for thermal design verification. At first glance, it would appear that this was a high-risk approach from a crew and vehicle safety standpoint as well as for mission success. Also of concern was the potential impact to the overall program schedule which might result if far-reaching design changes were necessary. However, systems redundancy, failure design requirements, and the capability to return to Earth in a short time minimized these risks. The overall test/verification approach and considerations which led to the total definition are described.

In-flight testing of the Space Shuttle Orbiter integrated thermal control design was successfully completed during the initial five orbital flights of the Space Transportation System (STS). The data base for verification of the thermal design to meet specified operational requirements was obtained with minimal ground tests through the definition and implementation of a comprehensive in-flight test program. Adequate data were obtained to either demonstrate capability or provide a data base for correlation of the vehicle- and subsystems-level thermal math models (TMM's) for analytical definition of the vehicle thermal performance capability.

TCS DESIGN OVERVIEW

The Orbiter thermal control system (TCS) is required to control and establish the thermal environments for all systems outside the crew module. However, certain systems that require internal thermal control as an intimate part of their operations are not included in the TCS. These are the fuel cells, the auxiliary power units (APU's) and cryogenic tank internal heaters, the active thermal control system Freon loop, the flash evaporator and steam ducts, and the hydraulic system water-boiler heaters.

The Orbiter TCS maintains subsystems and components within specified temperature limits for all mission phases (prelaunch, ascent, Earth orbit, entry, and postlanding). Integrated thermal control management is accomplished through use of fibrous and multilayer insulation (MLI) blankets, and available heat sources and heat sinks supplemented by passive thermal control (PTC) techniques such as coatings, heaters, thermal isolators, and, where practical, subsystems operating modes.

The basic insulation design consists of bulk fibrous insulation (TG-15000) sized to protect subsystems from overheating during entry and postlanding thermal soakback and supplemented by MLI for low weight, high thermal efficiency on orbit. The general vehicle-level application of bulk insula-

tion and MLI is shown in figures 1 and 2. A typical frame insulation installation is shown in figure 3, and typical fluid line applications are shown in figure 4.

Heater systems are used extensively as depicted in figure 5. These consist predominantly of two types: rope for fluid lines and patch heaters for area radiant heating and direct component heating such as aerodynamic control surface (aerosurface) actuators. A typical fluid line installation is shown in figure 6. Radiant heater designs are applied in the forward reaction control sys-

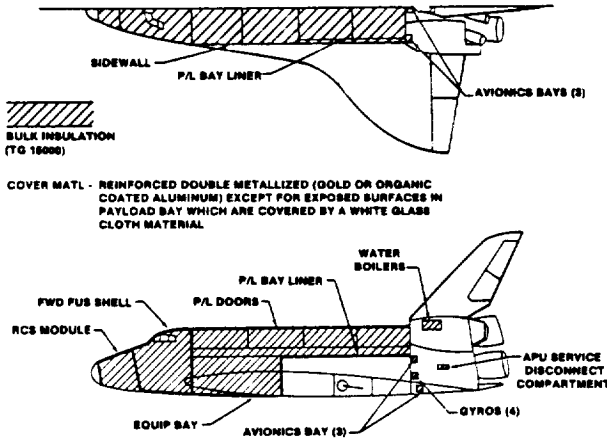


FIGURE 1.- THERMAL CONTROL SYSTEM BULK INSULATION.

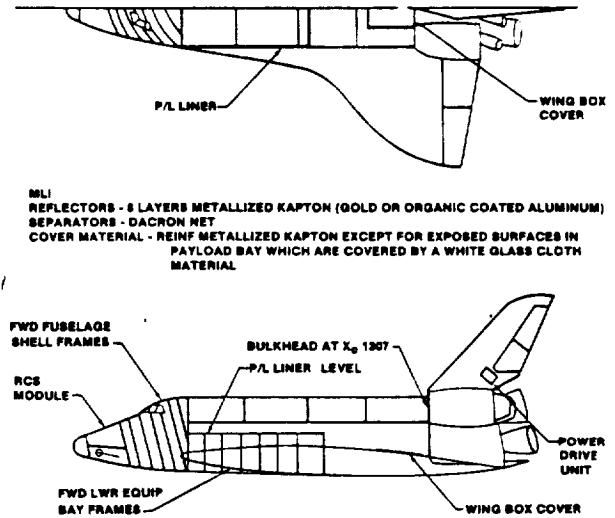


FIGURE 2.- THERMAL CONTROL SYSTEM MULTILAYER INSULATION.

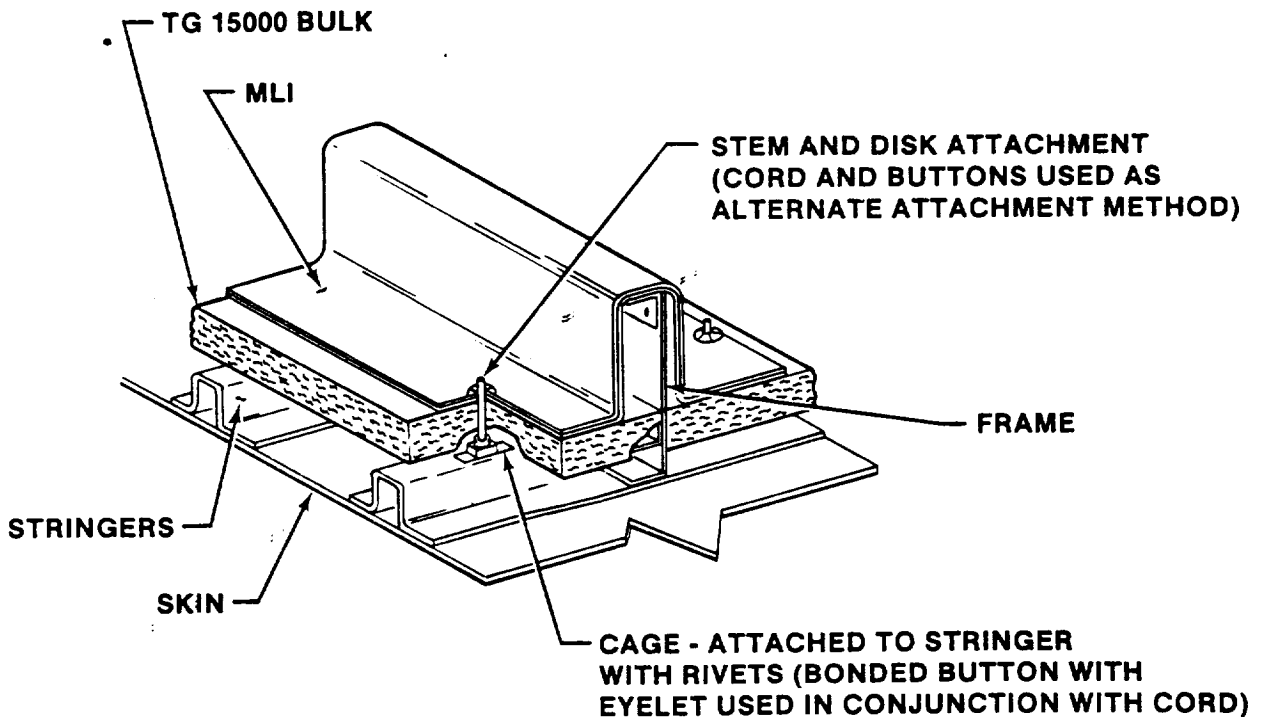
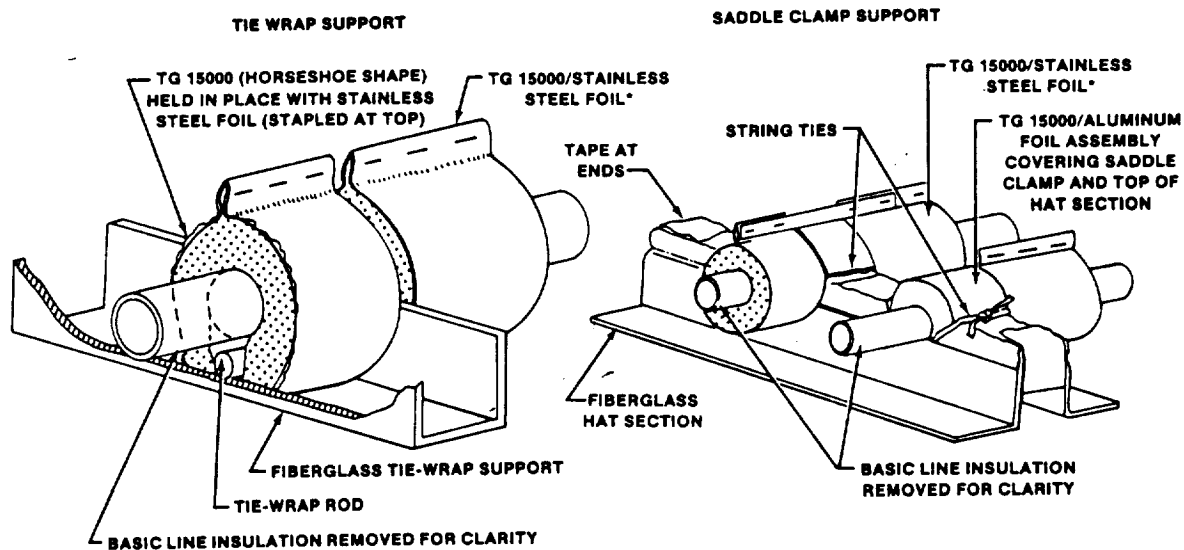


FIGURE 3.- TYPICAL FRAME SECTION MLI AND BULK INSULATION BLANKETS.

tem (RCS) compartment and the auxiliary propulsion system (APS) pods. The APS pod radiant heaters consisted of patch heaters applied to existing structural panels as depicted in figure 7. Most Orbiter heater systems are thermostatically controlled; exceptions are heaters required for special systems functions and operating modes, such as fuel cell purge line and vent heaters and main landing gear brakeline heaters, which are manually controlled.



*NEW VEHICLES SUBSTITUTE NONMETALLIZED POLYIMIDE FILM

FIGURE 4.- LINE INSULATION CONFIGURATION AT SUPPORTS.

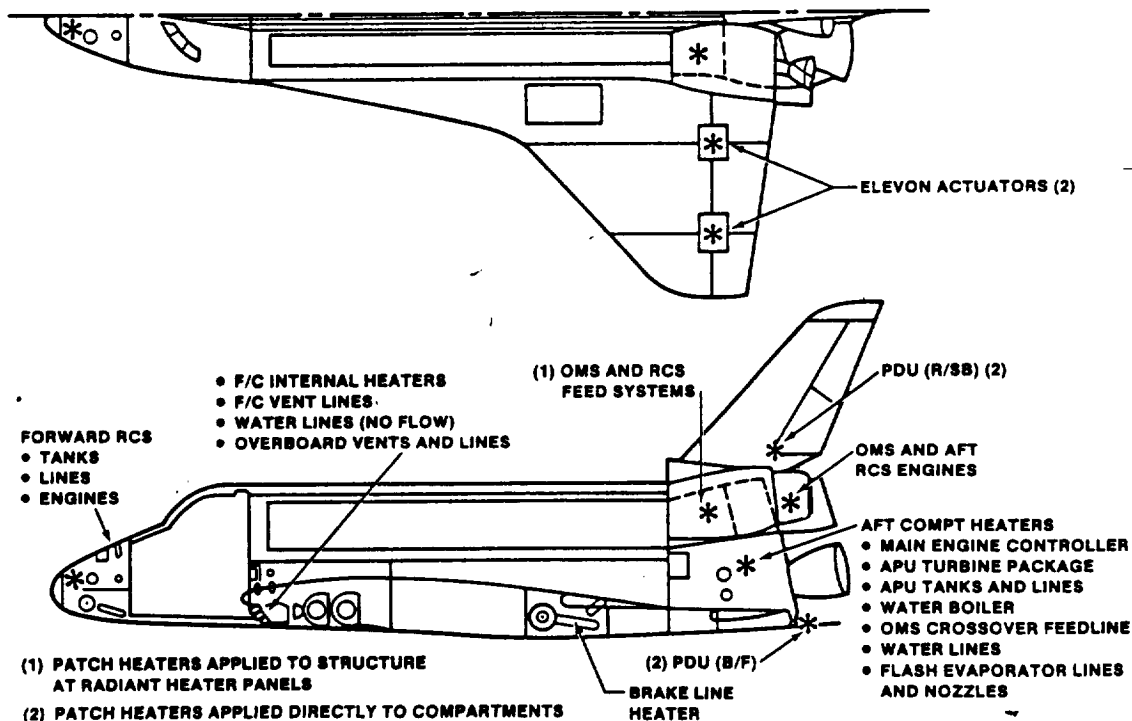


FIGURE 5.- ORBITER HEATER SYSTEMS.

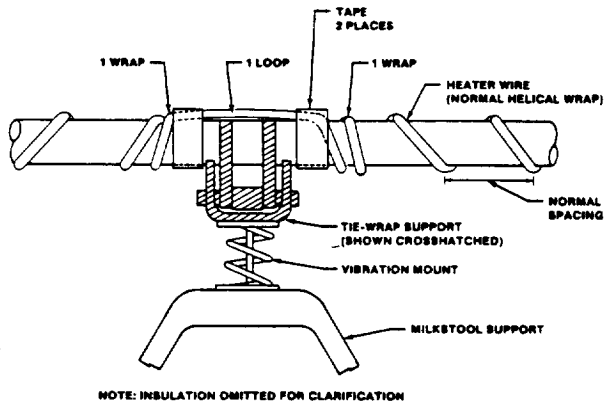


FIGURE 6.- TYPICAL HEATER INSTALLATION: LOCAL HEATING AT TIE-WRAP SUPPORT.

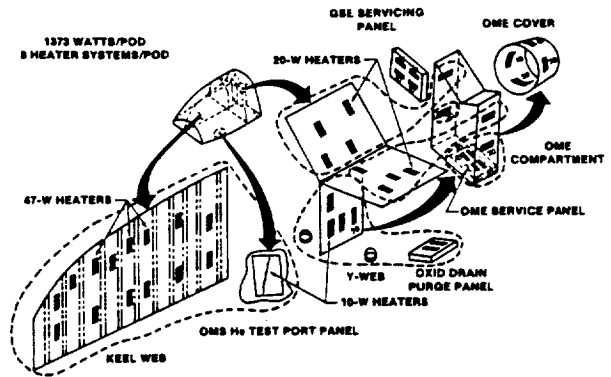


FIGURE 7.- APS POD HEATER AND THERMOSTAT ARRANGEMENT.

Except for drain lines and actuators, where heaters are applied for local thermal control, Orbiter hydraulic system temperatures are maintained on orbit by operation of circulation pumps which distribute the pump waste heat and heat picked up by way of a heat exchanger from the active TCS waste-heat-rejection loop to the various lines and components. The initial thermal requirement for the pumps was for prelaunch thermal conditioning of the main propulsion system (MPS) engine components and also for postlanding thermal conditioning to prevent local overheating of hydraulic system seals resulting from entry-heating soakback into the vehicle. On-orbit control of the circulation pump operation is achieved by a software thermostat mode driven by 40 temperature transducers located in the 3 hydraulic systems or by a computer-driven timer mode. In addition, specified movement of the aerosurfaces during main pump operations before entry interface is required to flush cold hydraulic fluid from stagnant lines and components to achieve full performance temperature levels during entry.

The vehicle-level air and gaseous nitrogen purge system (fig. 8) provides supplemental environment conditioning during prelaunch and postlanding phases. The primary thermal control function of the purge system before launch is to minimize heater usage and thereby to lower peak power requirements at lift-off and, in particular, to minimize stratification in the aft fuselage compartment during the MPS cryogenic chilldown conditioning and to raise the resulting compartment temperature levels. During the postlanding entry-heating-soakback period, the purge provides attenuation of the potential peak temperatures to which subsystems components would be subjected without the purge.

External vehicle surface coatings were dictated by thermal protection system (TPS) requirements for a black coating on the high-temperature reusable insulation and leading edges and a white coating on the low-temperature reusable insulation and felt (fig. 9). A white glass-fabric material was

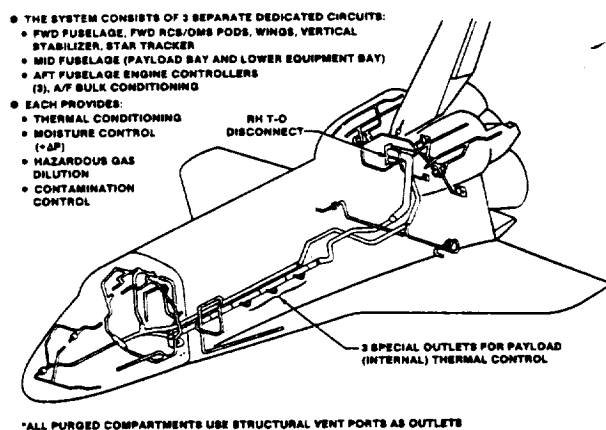


FIGURE 8.- PURGE SYSTEM, OV-102.

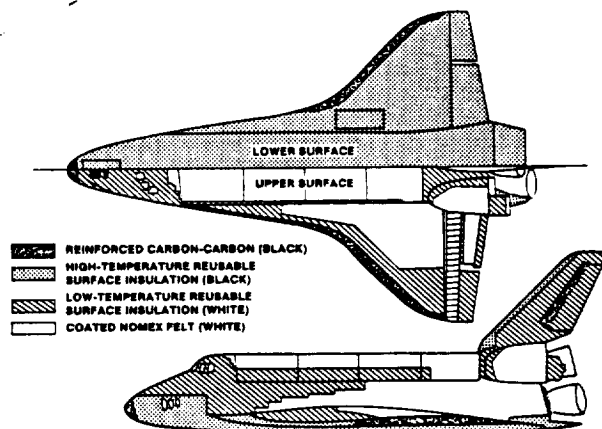


FIGURE 9.- OV-102 THERMAL PROTECTION SUBSYSTEM.

chosen for payload insulation blanket covers to reduce the effect of direct solar heating in the cavity and to provide acceptable temperatures for payloads. Internal insulation surfaces are metallized to provide a low emittance and thereby to reduce heat transfer to and from the structure.

THERMAL DESIGN MISSION

The initial thermal design mission definition for the Orbiter was quite simple; that is, provide adequate thermal design capability for the prelaunch, ascent, entry, and postlanding thermal environments and provide a 160-hour attitude-hold capability on orbit. The only constraints to the attitude-hold capability which evolved early in the Orbiter development were associated with preventing violation of the external TPS and structural bondline lower temperature and, in a hot case, providing preentry conditioning to cool the TPS bondlines below allowable maximum initial entry temperature levels.

The TPS bondline lower limit of -170°F could potentially be violated for any attitude which allowed continuous deep-space viewing. This possibility led to the requirement to limit such attitude holds to 6 hours followed by 3 hours of thermal conditioning before resuming the hold. This requirement applied only to attitudes that excluded solar or planetary exposure to a surface of the Orbiter during an orbit period. These attitudes were local-vertical orientations at high beta angles. A beta angle of 60° to 90° was chosen to define these orbital conditions. The beta angle is defined as the angle between the Earth-Sun line and the orbit plane.

During the course of the development program, additional attitude constraints were accepted by program management in lieu of design changes. These constraints are as follows.

1. Earth or solar viewing by the active thermal control system radiators is limited; the limitation varies dependent on water storage and power levels.
2. Tail to Sun attitudes are limited to 24 hours to prevent overheating of orbital maneuvering system (OMS) engine feedlines.
3. Nose, tail, and side Sun attitudes are limited to 33 hours to prevent violation of the main landing gear strut actuator and hydraulic dump valve lower limit of -35°F .

An additional requirement arose by which, for contingency early mission termination, thermal conditioning would be limited to 155 minutes and should not result in catastrophic conditions during entry or after landing. However, degradation in mission life would be accepted. The basic thermal design mission is outlined in figure 10; the basic thermal conditioning mode (PTC) and the beta angle (β) are illustrated.

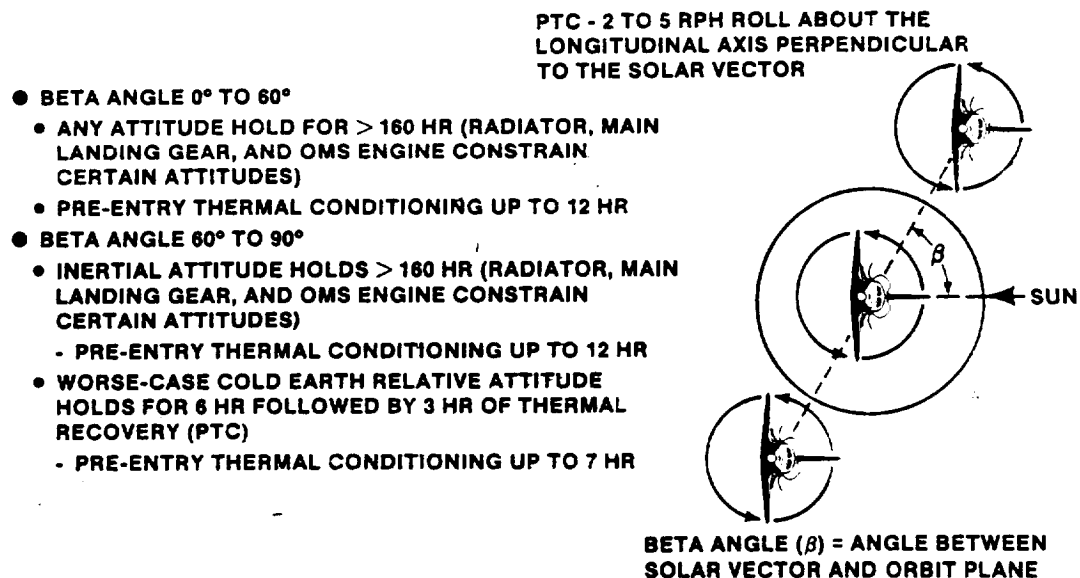


FIGURE 10.- THERMAL DESIGN MISSION PROFILE.

CONCERNS AFFECTING ON-ORBIT TEST DEFINITION

The initial program decision to consider in-flight thermal test and verification in lieu of ground thermal vacuum tests understandably caused much apprehension and concern. Verification by means of thermal ground tests and analysis supported by a minimum of in-flight testing was considered as the optimum technical approach. This conclusion was fostered in part by the design immaturity and unknown design problems at that time (late 1974 and early 1975).

Major concerns centered around (1) potential impacts to the thermal test time lines by other mission objectives, (2) the adequacy of flight instrumentation from the standpoint of quantity and location for both real-time anomaly identification and math model correlation, (3) the potential for early mission termination (mission success), (4) potential design changes which could impact the total orbital flight test (OFT) program, (5) commitment to flight by unverified analyses, and (6) the question of whether adequate thermal response for math model validation could be obtained. Ideally, the best approach for determining full capability and for providing sufficient data for math model verification and analytical extrapolations to actual flight design environments is to subject the vehicles and subsystems to the extreme hot and cold environments. This situation obviously is not desirable on initial flights from a crew or vehicle safety standpoint or for mission success. Basic advantages and disadvantages of ground thermal vacuum testing and in-flight testing were presented and summarized (tables 1(a) to 1(c)) along with the thermal vacuum test requirements (table 2).

Although Orbiter systems redundancy had a major impact in negating some of the basic risks and safety concerns, the potential of basic design flaws had to be faced in the design of redundant heater systems. A number of small fluid line heater tests were implemented to provide a level of confidence in the design approach. The in-flight tests, which are discussed later, were designed to minimize the impact of design flaws.

Other vehicle design features such as the caution and warning and the fault detection and annunciation (FDA) systems provide a method of defining systems failure redlines for early anomaly identification and resolution. These systems are used extensively for monitoring heater system performance. In addition, concerns over undercooling or overheating of RCS engines due to either heater system inadequacy or engine firing effects are minimized by an automatic deselect system.

VEHICLE MONITORING AND INSTRUMENTATION

Of major importance in any type of testing is the adequacy of the test instrumentation. As previously mentioned, this factor was a prime concern since a flight vehicle has inherent limitations as to the number of instruments that can be accommodated. In addition to the basic instrumentation needed to control operating modes of the various subsystems and to determine their general status, instrumentation was required to meet the objectives of the thermal flight tests. The overall verification and subsystem requirements which led to the definition of the flight test instrumentation are delineated in table 3.

Each subsystem area was reviewed for instrumentation to verify thermal math models for design-peculiar problems and for minimum real-time flight monitoring. The initial requirement was to add, to the existing 219 real-time operational flight instruments (OFI's) and 633 recorded development flight instruments (DFI's), 1460 new DFI's, of which 441 would be available in real time over the OFI system to support real-time monitoring and anomaly identification and resolution. This assessment was conservative but provided for the highest level of confidence in correlating math models for analytical design verification. However, such programmatic considerations as modifications, added costs, and schedule impacts inherent in accommodating this large amount of instrumentation on the vehicle suggested an alternate approach. Such an approach which would provide acceptable real-time monitoring capability but represented minimal instrumentation for math model verification purposes was presented and accepted. The former consideration affected to a great extent the definition of the flight test program, which is discussed later. It was agreed to add 410 DFI sensors to the Orbiter and to provide 410 data channels for real-time monitoring of selected existing and new DFI sensors. This addition brought the initial complement of real-time and recorded thermally related sensors to 629 and 633, respectively.

As a result of design changes and particular problems or concerns that arose during the design, development, and test phases of the vehicle, the number of real-time sensors approached 800. It was evident that such a large number of sensors could not be monitored adequately by means of manual plotting. Since no preflight data on vehicle thermal control performance were available to provide intelligence as to actual thermal response times or time to reach limits, it became evident that a real-time or near-real-time system of monitoring temperature response and trends was required. A summary of real-time monitoring requirements is presented in table 4. It was estimated that approximately 90 people (30 per 8-hour shift) with expertise in the thermal design area would be required

TABLE 1.- ADVANTAGES AND DISADVANTAGES OF INTEGRATED GROUND THERMAL VACUUM TEST AND ORBITAL FLIGHT TEST

(a) Integrated ground thermal vacuum test

Advantages	Disadvantages
<ul style="list-style-type: none"> • Flexibility in varying and controlling known environment • High level of confidence • Early design verification • Minimizes program impact • Supports operational data book (ODB) • Provides flexibility in obtaining additional data as warranted by prior test phase results (test conditions and additional instrumentation) • Allows testing to extreme conditions (capability determination and failure stimulation) 	<ul style="list-style-type: none"> • Test data will still require some interpretation and extrapolation to flight configuration and flight environments • Requires dedicated test articles or shared test articles with high potential for scheduling impact

(b) Orbital flight test

Advantages	Disadvantages
<ul style="list-style-type: none"> • Actual environment • Actual engine firings 	<ul style="list-style-type: none"> • Commitment to flight by analysis only • Crew time line impacted for thermal requirements • Determination of environment difficult • Large amount of instrumentation • Limited real-time data • Dedicated thermal flight test - Minimize impact from other mission objectives • Monitoring system for equipment duty cycles and power loads required • Insufficient intelligence for placement of instrumentation and heater controls • Insufficient intelligence to determine which instrumentation is required in real time • Dictates conservative flight test time line to avert potential problems (mission success, crew safety) • High probability of inadequate data (additional flight test required) • Questionable capability for real-time anomaly resolution and evaluation of flight plan changes • High program impact potential

(c) Summary

Test	Characteristic
Integrated thermal vacuum test	<ul style="list-style-type: none"> • Highly desirable for "no attitude constraints" thermal design • Mandatory for fixed-attitude/time-limit design if program does not provide dedicated thermal OFT and instrumentation or does not provide flexibility for more than one multiple-objective OFT with sufficient instrumentation • Minimum supplemental OFT instrumentation • Certification by test and analysis before flight
Orbital flight test	<ul style="list-style-type: none"> • Dedicated thermal OFT mandatory • Several flight tests required • High potential for large program impact • Greatly increased instrumentation and scar weight • Mission success questionable • Commitment to manned flight by analysis only

TABLE 2.- REQUIREMENTS FOR THERMAL VACUUM TESTS

- INTEGRATED THERMAL CONTROL SYSTEM VERIFICATION
 - Functional verification of integrated subsystems, interfaces, and active/passive thermal control systems while exposed to extreme mission environments
 - Subsystems qualification environment verification
 - Flight operations support by demonstrating off limits and contingency operation of subsystems
- OBTAIN DATA FOR CORRELATION OF THERMAL ANALYTICAL MATH MODEL
 - Certification analysis tool
 - Mission planning tool
 - Establish operational capability (operational data book)
 - Real-time mission support tool

per flight to plot data and identify potential problems and to support real-time decision activities for problem resolution.

An interactive computer terminal system, or trend monitoring system (TMS), was instituted by which six terminals were provided for retrieval and plotted display of data in near real time. The number of terminals was determined by appropriate grouping of subsystems and major vehicle areas allowing the use of minimum personnel while not overloading a particular individual. Data were provided to the host computer by computer-compatible tapes (CCT's) obtained from the Mission Control Center network interface processor (NIP). The normal lag between real-time data and TMS data-base updates was approximately 2 hours. Use of an on-line printer enabled review and scanning of real-time cathode-ray tube (CRT) data displays by the thermal analysts. Data comparison with preflight prediction and previous flight data, data extrapolation, flight plan changes, and real-time anomaly investigations were supported by the real-time CRT data displays and TMS data sources, which proved to be a very effective combination. The real-time data flow and analysis is depicted in figure 11.

IN-FLIGHT TEST PHILOSOPHY AND APPROACH

As in the case of ground thermal vacuum testing, it would have been ideal from a thermal standpoint to subject the vehicle to design conditions immediately during the flight test program. This exposure would have the advantage of providing the best possible data for design verification as well as of minimizing the number of test conditions and the flight test time. However, as discussed previously, crew safety and mission success considerations were primary. Basic to these considerations was the demonstration of launch, orbit insertion, deorbit, entry, and landing capabilities and procedures. In addition, such an approach would require that critical procedures for payload bay door closure, TPS preentry thermal conditioning, and hydraulic system entry warmup as well as the wheel brakeline heaters (which are only used just before and during entry) would have to work properly the first time. With these considerations and concerns in mind, the philosophy was adopted to subject the vehicle initially to a benign thermal environment to allow identification of any gross design flaws and to minimize the potential risk and mission impact. The vehicle would, within the OFT program constraints such as launch schedules, number of flights, mission length, and payload requirements, then be subjected to increasingly more severe thermal environments on follow-on flights.

In line with the stated philosophy, it was necessary that such test requirements as environments, vehicle attitudes, and special tests be defined consistent with program constraints and still provide for in-flight capability demonstration or provide adequate data for correlation of TMM's to be used for analytical design verification. This need resulted in requirements for both low- and high-beta-angle flights. The distinction between high and low beta angles is that high beta angles (60° to 90°), depending on orbit altitude, approach or provide 100 percent sunlight conditions or no Earth shadow time as opposed to low beta angles. The rationale for low-beta-angle missions was as follows.

1. To provide benign environment for early identification of gross design inadequacies
2. To provide level of confidence in design to commit to more severe environments

TABLE 3.- THERMAL TEST INSTRUMENTATION

REQUIREMENT FOR ADDITIONAL THERMAL INSTRUMENTATION

- Integrated thermal control system verification
 - Obtain data for thermal math model correlation and subsequent verification by analysis
- Operational program support
 - Mission planning tool
 - Data source for ODB
 - Real-time mission support and contingency identification and resolution

INSTRUMENTATION IDENTIFICATION GROUND RULES

- Utilize vehicle/subsystems design symmetry and similarity to minimize number of measurements
- Identify critical areas required for real-time on-orbit monitoring to prevent contingencies

STRUCTURE/SUBSYSTEM REQUIREMENTS

- Tanks
 - Identify gradients caused by heaters and local environment
 - Determine heat gain/loss through mounts
 - Determine interaction with surrounding structure/subsystems
 - Determine heater sizing and controller location adequacy
- Lines
 - Identify cold spots and verify heater/insulation sizing and controller location
 - Determine heat gain/loss through mounts
 - Determine interaction with surrounding structure/subsystems
- Heat-generating equipment (fuel cells, APU, pumps, etc.)
 - Determine interaction with surrounding structure/subsystems (heat balance and heat distribution)
 - Verify design environments
- Insulation
 - Verify adequacy of performance in installed configuration
 - Verify design environments
- Structure
 - Verify subsystems design environments (boundary conditions)
 - Bondline measurements for preentry thermal conditioning, verify structural gradients
 - Verify cabin heat leak
- Hydraulics
 - Verify circulation loop flow balance and duty cycle required for on-orbit thermal control
 - Verify adequate temperature control during main pump operations
 - Verify heater/insulation sizing and controller locations for stagnant lines and associated components
- RCS/DMS engines
 - Verify engine firing soakback effects
 - Verify engine heater sizes/duty cycles
 - Determine heat gain/loss through engines
- MPS
 - Determine local cooling effects from cryogenic lines and effect of engine firing on aft fuselage subsystems
 - Determine effects of heat gain/loss through engine on aft compartment and subsystems
- Payload bay (PLB)
 - Verify effects of open doors on lower midfuselage components
 - Verify PLB environments
- PLB doors
 - Substantiate analytical design gradients as they affect door operations
 - Verify temperatures of seals and mechanisms
- General - Verify OFI and heater controller locations

TABLE 4.- REQUIREMENTS FOR REAL-TIME THERMAL FLIGHT DATA

- GENERAL - Provide intelligence for precluding, identifying, and resolving anomalous conditions in those areas where analysis and ground test data are inadequate for preflight verification
- SPECIFIC REQUIREMENTS
 - Adequacy of hydraulic circulation pump for on-orbit operation and preentry aerosurface actuator/power drive unit warmup
 - Monitor operation of subsystem heaters (heater sizing, controllers and OFI instrumentation location)
 - Monitor areas which constrain vehicle attitudes
 - Effect of OMS/RCS engine firing/soakback on subsystem components and interfaces
 - Requirement for and adequacy of preentry thermal conditioning of TPS/structure and related door closure components (seals, motors, etc.)
- THERMAL MONITORING REQUIREMENTS
 - Lack of test data and knowledge of vehicle/subsystems response characteristics and TCS design adequacy requires timely access to real-time data and playback (as available) in a readily available and usable form for evaluation and decisionmaking to:
 - Determine vehicle status
 - Identify/forecast potential or impending anomalous conditions
 - Recommend or concur on remedial actions or flight plan changes
 - Approximately 800 temperatures must be monitored
 - Additional data required (available from existing sources) - Vehicle Earth/Sun look angles, orbital position, systems configuration and operating modes, power loads, engine firing times, overboard dump time lines, and consumables usage history
- VEHICLE STATUS REQUIREMENTS
 - High and low limit flags
 - Thermal summary tabs - Quick scan of all real-time thermal data
- PROBLEM IDENTIFICATION/FORECASTING REQUIREMENTS - Real-time temperature history plots
 - Capability to select parameters and plot scale (real-time update and playback interleaved)
 - Storage and retrieval
 - Overlay/comparison of predicted and flight data
 - Vehicle-Earth/vehicle-Sun look-angle plots
- REMEDIAL ACTION/FLIGHT PLAN CHANGE REQUIREMENTS - Same as problem identification/forecasting
- WHY ARE NEAR-REAL-TIME PLOTS WITH INTERLEAVED PLAYBACK AND STORAGE RETRIEVAL CAPABILITY REQUIRED?
 - Manned Test - Requires timely recognition of impending problems and definition of alternative solutions
 - Lack of test experience - Unknown level of confidence in preflight analyses requires thorough understanding of available flight data be maintained at all times
 - Flight data will be the major tool for recognizing potential problems and recommending avoidance actions and flight plan changes
 - Time to reach limits - Transient thermal response, which is dependent on environment, heater size, and design, can only be obtained from plotted data
 - Data extrapolation for more than a few hours (depending upon response rate) is questionable
 - Volume of data - Volume of data cannot be efficiently managed, plotted, handled, or understood without adequate computer hardware/software support

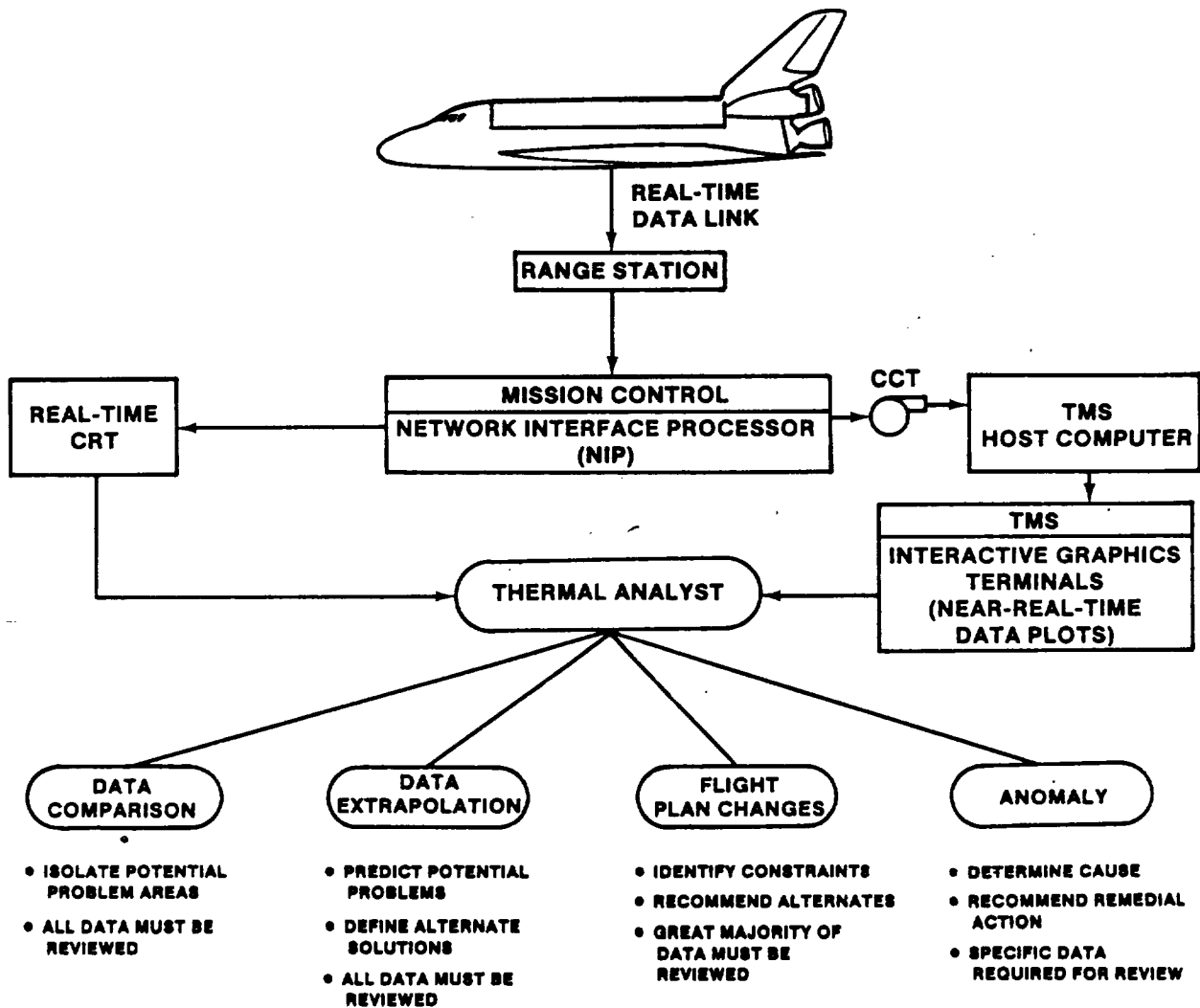


FIGURE 11.- REAL-TIME DATA FLOW AND ANALYSIS SCHEMATIC.

3. To gain level of confidence in analytical capability required for in-flight problem resolution and to support mission planning

4. Potentially inadequate data availability, both in sensor quantity and in sensor locations as well as that associated with long periods between ground station passes at high beta angles, requires previous flight test experience in support of anomaly resolution and mission planning

High-beta-angle flight requirements stemmed from the following.

1. Concern that temperature levels and the amplitude of transient responses at low beta angles would be inadequate for TMM correlation and analytical verification

2. Opportunity afforded at high beta angles to subject the vehicle or portions of the vehicle to extreme hot or cold conditions and provision of the best environments for TMM correlation or demonstration of design capability

FLIGHT TEST REQUIREMENTS AND TEST DEFINITION

The fundamental driver for test definition was to prove the thermal capability of the various

subsystems to meet the thermal design mission and to identify any existing constraints for the purpose of determining operational acceptability or redesign requirements and providing basic capability definition to support operational mission planning. To obtain the necessary test data, each system must be subjected to cold and hot environments during each mission phase to either demonstrate capability or correlate thermal math models. Since each vehicle compartment area with few exceptions can be treated as a box, the basic on-orbit test attitudes were defined to subject each side to hot and cold environments with variations dependent on peculiar subsystems and component test requirements.

In addition to determining environmental test requirements, it was also necessary to define specific systems functional tests to verify thermally sensitive operating modes. Initial test requirements and test definition were derived from the thermal design data-base analyses which identified vehicle and subsystems sensitivities. This process obviously was iterative since the overall thermal design was subject to the design maturity of other subsystems which affected the integrated thermal characteristics of the vehicle. A number of analysis cycles were required to update test requirements in addition to mission planning and actual preflight time-line analyses to arrive at the final test definition. The manner in which the various analyses are fed into the test definition and ultimately support the data correlation activities leading to the final TCS verification is shown in figure 12.

Prelaunch and ascent testing was basically a matter of obtaining data since systems operating modes are defined by launch operations and the external environment cannot be controlled. Likewise, systems test requirements, other than TCS, critical to entry defined the entry phase requirements. Each system was reviewed to determine data and test requirements for each mission phase. The general requirements are delineated in table 5.

Flight test requirements can be divided into two test groups.

1. Normal system operation and response to a given or specified environment
2. Operation of a system in a specified mode in a given or specified environment

Therefore, the first task in defining the flight test was to identify the required environments and vehicle on-orbit attitudes. Since the prelaunch, ascent, and entry phase environments and systems operating modes could not be varied to any great extent for TCS testing, the major portion of TCS tests was centered around the on-orbit phase. As discussed previously, it would have been ideal to subject the vehicle to extreme environments, which could be achieved by testing at high beta angles. This approach would also result in a minimum number of test conditions. However, in addition to the

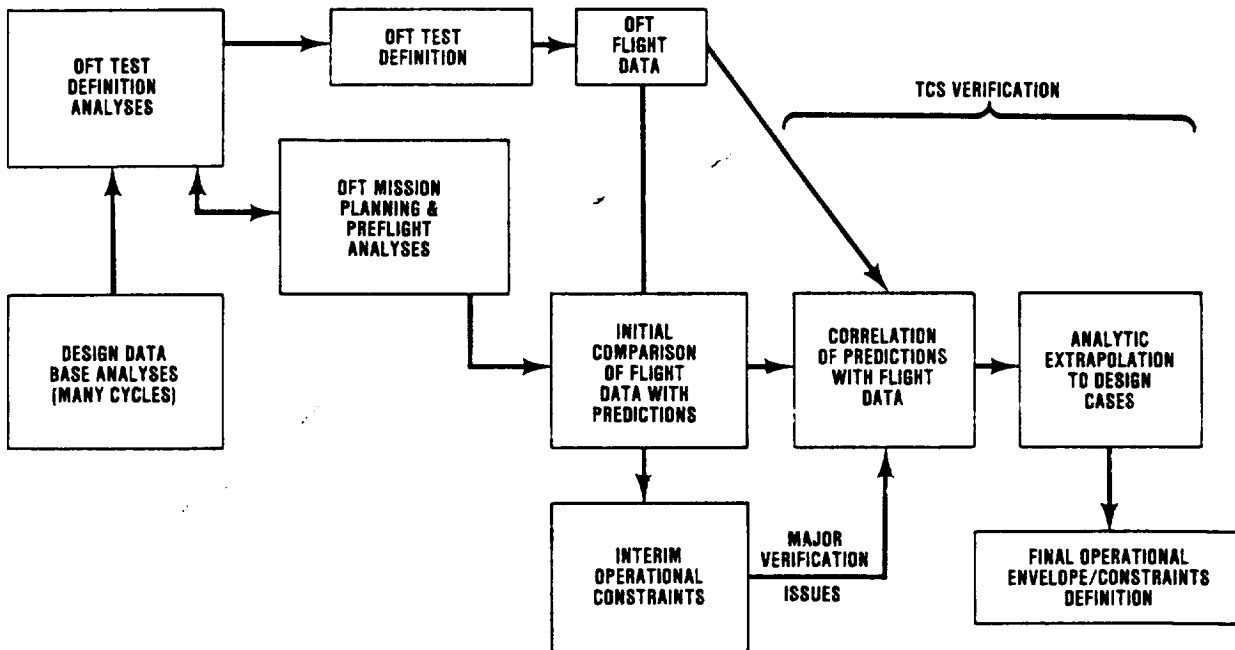


FIGURE 12.- TEST DEFINITION DETERMINATION.

TABLE 5.- SYSTEMS TEST REQUIREMENTS

1. GENERAL
 - a. Verify adequacy of heater system designs to maintain temperatures during all mission phases
 - b. Verify adequacy of insulation system in conjunction with the TPS to protect subsystems during aeroheating phases and postlanding entry-heating soakback
 - c. Verify that subsystem allowable environments are maintained during all mission phases
2. THERMAL PROTECTION SYSTEM
 - a. Define on-orbit cold attitude-hold capability and thermal conditioning requirement
 - b. Determine preentry thermal conditioning requirements to prevent violation of maximum allowable initial entry temperatures
3. STRUCTURES
 - a. Determine structural gradients to support entry and landing stress and loads analyses
 - b. Provide data to support determination of structural deflection effects on payload bay door (PLBD) closure and payload interfaces
4. HYDRAULICS
 - a. Verify adequacy of prelaunch hydraulic system thermal conditioning of main propulsion system
 - b. Verify adequate temperature control of hydraulic system during main pump operations for all mission phases
 - c. Determine adequacy of circulation pump on-orbit operation as a means of maintaining hydraulic system temperatures
 - d. Determine minimum preentry main pump operation and aerosurface actuator activity to achieve minimum full performance system and actuator temperatures
 - e. Determine postlanding circulation pump operational period to prevent local system overheating resulting from entry-heating soakback
5. RCS/QMS ENGINES
 - a. Verify that acceptable structure and subsystems temperatures are maintained following engine firings
 - b. Determine engine firing constraints (i.e., overheating or undercooling of engine components), if any.
 - c. Verify QMS engine feedline tail to Sun attitude-hold constraint
6. MAIN PROPULSION SYSTEM - Determine effect of main engine cryogenic chilldown during prelaunch and ascent and verify aft fuselage subsystem environments.
7. PAYLOAD BAY DOOR MECHANISMS
 - a. Verify that door latches, drive motors, mechanisms, and seals can be maintained within allowable temperature limits
 - b. Verify closure capability for various vehicle on-orbit attitudes
8. PAYLOAD BAY
 - a. Verify environment definition for payload integration for all mission phases
 - b. Verify adequate insulation performance at payload bay and lower equipment bay interface to maintain acceptable lower equipment bay subsystems environments
9. MAIN LANDING GEAR (MLG) - Verify or determine cold attitude-hold constraints envelope to prevent violation of strut actuator and hydraulic dump valve minimum allowable temperature
10. STAR TRACKER - Verify that hot and cold attitudes do not result in thermal distortions affecting star-tracker accuracy
11. PAYLOAD RETENTION FITTINGS
 - a. Obtain data for math model correlation to support payload integration analyses for definition of retention-fitting temperatures affecting payload and Orbiter interface loads
 - b. Determine preentry thermal conditioning requirements to prevent violation of specific payload retention-fitting minimum temperature allowables

concerns which guided the test philosophy, there were also flight schedules which dictated the capability to achieve high beta angles. Also, the number of test flights initially was uncertain.

Since the number of flights and the beta-angle conditions which could be achieved were uncertain, a matrix of attitudes and beta-angle conditions categorized as mandatory, highly desirable, and desirable was developed. This matrix formed the basis for defining flight tests which best fit the overall objectives for a given mission. Table 6 is a summary of test attitudes, purpose, beta angles, and hold time. The attitudes are defined in vehicle coordinates: -X nose, +X tail, +Z top, -Z bottom, +Y starboard side, and -Y port side. The attitude holds are defined as solar inertial (SI) or three-axis hold, Earth local vertical (LV), and orbital rate or single-axis inertial.

Passive thermal control, which consists of a continuous roll of 2 to 5 revolutions per hour about the X-axis with the X-axis perpendicular to the solar vector, and +ZLV (payload bay or top to Earth) for low beta angles were chosen as the most thermally benign attitudes to best satisfy the desire of minimizing the vehicle and subsystems thermal stress for the first mission. Also, PTC was chosen as a method of thermally conditioning the vehicle before entry to satisfy TPS initial entry requirements and before test attitude holds to minimize structural gradients and provide initial known temperature levels to minimize the error associated with initiating thermal math models for analyses and comparison with flight data. The +XSI, tail to Sun attitude provided a relatively cold environment for forward fuselage and midfuselage heaters, the hydraulics system, the star tracker, structural thermal deflection analyses (relating to payload bay door closure), and the main landing gear, as well as a hot condition for the OMS engine and aft RCS engine housing.

The -ZSI, bottom to Sun attitude provided a hot environment for TPS and structural heating, warm lower midfuselage systems environment, and structural gradients for thermal deflection analysis support. This attitude followed by PTC provided data for verification of the preentry thermal conditioning of the TPS bondlines to meet entry temperature constraints.

The +YSI, starboard side to Sun attitude subjects one OMS pod to a relatively hot environment and the other (port) pod to a cold environment to obtain heater performance data. Other objectives were to obtain side-to-side gradients to support thermal deflection analyses and to obtain additional main landing gear constraint data. The -XSI attitude with the nose pitched up 10° immediately following the +YSI attitude provided for a prolonged port OMS pod cold soak, which was desired, and provided data to verify the Sun-angle envelope associated with the main landing gear constraint.

The main objective of the pure -XSI (nose to Sun) attitude was to obtain data on aft fuselage systems and heaters in a cold environment, to verify another portion of the expected main landing gear cold attitude-hold constraint, hydraulic system response, and to provide a moderately warm environment for the forward RCS compartment. A secondary objective was to obtain additional OMS pod heater performance data.

Two attitudes, tail to Sun with top to space orbital rate roll followed by 3 hours of PTC for three cycles and pure tail to Sun with top to space orbital rate roll, were identified as candidates to provide the best data for cold TPS bondline, payload bay environment, and payload retention-fitting thermal response as well as to provide data on the cold main landing gear and hot orbital maneuvering engine (OME) line constraints. The +ZSI (payload bay to Sun) attitude was identified to support verification of payload maximum environments, payload retention-fitting warmup response, and star-tracker performance in a hot environment, and to provide additional data for structural thermal deflection analysis for top-to-bottom thermal gradients which affect payload bay door closure. This attitude also provides the best environment for K_u -band antenna performance in a hot environment, whereas the +XSI (nose pitched down 15°) attitude would provide for the best K_u -band antenna performance in a cold environment.

Two additional attitudes of lower priority, +YSI (side to Sun) with payload bay of +Z-axis rolled 40° toward the Sun and +XLV (nose to Earth) as described in table 6, were identified for flight tests if they could be flown with minimal impact. The attitudes categorized as mandatory represent the minimum set of data required for TCS verification. Beta-angle ranges were identified as shown in table 6 as acceptable, highly desirable, and no requirement. This tabulation provided a guide for determining the most appropriate mission for planning specific tests. As can be seen, the highly desirable category fell mainly in the high-beta-angle range since this range provides the opportunity for actual demonstration of capability with minimum reliance on thermal math model correlation to data at lower beta angles. Attitude-hold periods were best estimates, based on analyses, of time required to approach steady-state structural temperatures.

The second task was to identify subsystems functional tests for verifying thermally sensitive operating modes. The subsystems test objectives and test attitudes are summarized in table 7. These tests required specific crew activity to implement particular subsystems operations which would not normally occur.

TABLE 6.- THERMAL TEST MATRIX

Generic attitude (given in Orbiter structural body coordinate system)	Purpose	Attitude demo require- ment during OFT	Beta angle and approximate time requirements ^a		
			Low beta (0° to 45°)	Moderate beta (45° to ~73°)	High beta/ 100% Sun (>73°)
PTC	Benign env and initial conditioning before any mission thermal attitude sequence	M ^b	A ^c (10 hr)	A	HD ^d
+ZLY (top Earth, X on Y)	Benign env Earth viewing	M	A (72 hr)	NR ^e	NR
+XSI (tail Sun, SI)	Cold att for fwd RCS, star tracker, PLBD closure, and hyd. MLG constrained attitude	M	A (80 hr)	A	A
	Hot DME lines at high beta	M	No reqn't	No reqn't	H ^g (40 hr for DME lines)
-ZSI/PTC (bott Sun, SI/PTC) sequence mandatory	PLBD closure, warm bott structure/recovery to below design entry interface temps	M	A (40/10 hr)	A	HD ^f
+YSI (STBD side Sun, SI)	APS htr demo, nonsymmetric attitude for hyd and PLBD. MLG constrained att	M	A (40 hr)	A	HD
-XSI (nose Sun, SI)	Cold att for mid, aft, and APS htr systems and hyd. MLG constrained att	M	A (80 hr)	A	HD
-XSI (nose up 10°)	Same as above, only colder for APS pod htrs and an MLG constraint envelope limit	M	A (40 hr)	A	HD
6/3 demo (tail Sun, top space orb rate for 6 hr. Then, 3 hr PTC, then repeat cycle 2 more times with final PTC of 10 hr, i.e., 6/3/6/3/6/10)	Cold bondline constraint, deep-space viewing, PLBD closure, coldest PLB liner, cold P/L attachments	M	No reqn't	A (34 hr)	HD ^f
+ZSI (top Sun, SI)	Hot PLB and warm overall Orbiter; warm star tracker	M	A (40 hr)	A	HD ^f
	Hot K _u -band antenna ^g	(g)	No reqn't	No reqn't	HD (=20 hr)
+YSI top rolled towards Sun 40°	MLG constraint envelope limit	HD	HD (40 hr)	A	A
Tail Sun, top space orb rate	Cold bondline constraint, deep-space viewing at moderate beta, cold PLB liner, cold P/L attachments	HD	No reqn't	HD (20 hr)	No reqn't
+XLV (tail Earth LV)	Benign or possibly cold bondline constraint at moderate beta	D ^h	NR	D (20 hr, B ≤ 60°)	No reqn't
+XSI (nose down 15°)	Cold K _u -band antenna ^g	(g)	A (~5 hr)	A	A

^aThe assignment of categories (mandatory, highly desirable, acceptable, etc.) relative to beta angle is based solely on analysis and subject to change as later data become available. Time (duration) requirements depend on attitude sequences to some extent. (See note following footnotes.)

^bM = mandatory.

^cA = acceptable.

^dHD = highly desirable.

^eNR = not required if mandatory, highly desirable, acceptable, or desirable category achieved.

^fAdditional risk in overall certification may exist if these attitudes not demonstrated at high beta angle.

^gIf K_u-band antenna is not installed during OFT flights, generic demonstration attitudes similar to these are required after OFT (unless adequate ground thermal vacuum testing occurs).

^hD = desirable.

NOTE:

- ATTITUDE SEQUENCES: (1) It is highly desirable that the -XSI, nose pitched up 10° attitude follow the +YSI attitude to provide a long combined APS heater system demonstration.
(2) It is highly desirable that the -ZSI/PTC sequence and the +ZSI attitude follow a cold vehicle attitude (such as +XSI or -XSI) to demonstrate vehicle warmup from cold conditions.

TABLE 7.- SUBSYSTEMS FUNCTIONAL THERMAL TESTS

Subsystem	Test objective	Test attitude
Payload bay doors	<ul style="list-style-type: none"> • Demonstrate door closure capability • Determine effect of structure thermal deformation in various attitudes • Determine any constraints to payload bay door closure 	<ul style="list-style-type: none"> • PTC (benign), +ZLV (benign), +XSI, -XSI, +ZSI, -ZSI, and +X to Sun with +Z to deep space orbital rate
RCS engines	<ul style="list-style-type: none"> • Obtain RCS engine continuous and duty cycle firing thermal data to support analytical definition of any firing constraints which might exist (9 tests total) 	<ul style="list-style-type: none"> • Forward engines - +XSI, -ZSI, or +ZLV • Port aft engines - -XSI, -ZSI, +YSI, or +ZLV
OMS engine	<ul style="list-style-type: none"> • Obtain thermal response data to assess thermal soakback effects on engine components and Orbiter structure and subsystems 	<ul style="list-style-type: none"> • Port engine - -XSI, +YSI, or +ZLV
Hydraulics	<ul style="list-style-type: none"> • Operate each hydraulic system circulation pump to obtain independent thermal performance data (no thermal interaction test) • Operate all three hydraulic systems sequentially to obtain interactive thermal performance data (3 systems interaction test) • Demonstrate circulation pump operation in the software thermostat mode in a benign environment (single system thermal test) • Obtain data to verify aerosurface actuator cycling as a viable technique for obtaining operational hydraulic fluid temperatures to provide proper actuator response during entry aerodynamic operations (entry thermal conditioning) • Provide data to verify the automatic software timer mode operation of the hydraulic circulation pumps 	<ul style="list-style-type: none"> • +ZLV (benign) • +ZLV (benign) • +ZLV (benign) • +ZLV or postentry interface period following a benign attitude • +XSI (tail to Sun)
Star tracker	<ul style="list-style-type: none"> • Obtain data in nonoperating and operating modes under hot and cold environmental conditions to determine thermal effects on star-tracker accuracy 	<ul style="list-style-type: none"> • +ZSI (top Sun) +XSI (tail Sun)
Flash evaporator system feedwater lines	<ul style="list-style-type: none"> • Inhibit flash evaporator operation to obtain line heater performance during a period of fixed cold bias environmental conditions with no waterflow 	<ul style="list-style-type: none"> • -XSI (nose to Sun)
Potable water and wastewater dump lines and nozzles	<ul style="list-style-type: none"> • Obtain data during a defined water dump period in a cold bias environment to verify line and nozzle heater performance 	<ul style="list-style-type: none"> • -X or +XSI
K _u -band antenna	<ul style="list-style-type: none"> • Post-OFT, obtain data in the heater-only mode in both cold and hot environments followed by a defined period of operation in the minimum and maximum heat dissipation operating modes, respectively, to verify thermal performance 	<ul style="list-style-type: none"> • +XSI, nose pitched down 15° (cold) • +ZSI, top Sun (hot)

AS-FLOWN OFT THERMAL TEST PROGRAM

As the OFT program solidified, it became evident that the high-beta-angle tests could not be accomplished within the designated four flights. In conjunction with this limitation, program management recognized that a number of tests would have to cascade into the post-OFT or operational phase of the Space Shuttle Program. As a result, it became necessary to identify post-OFT test requirements and instrumentation at an early stage for the purpose of defining and implementing instrumentation hardware requirements and to facilitate mission planning.

In light of the concerns over the adequacy of low-beta-angle data for verification, it was decided to fly as many of the mandatory tests as practical during OFT at low beta angles, even though the high-beta-angle tests were more desirable, and to define a critical set for post-OFT testing at high beta angles. This approach would allow getting the plan in place to assure adequate verification but would also allow cancellation of the post-OFT tests if the data from the first four flights proved to be adequate.

The first Space Transportation System flight (STS-1) was flown in a +ZLV attitude with the tail or +X-axis on the velocity vector to provide the desired benign environment. Program payload commitments prevented accomplishment of TCS attitude tests during the STS-2 flight, which was flown in a +ZLV attitude with the nose or -X-axis on the velocity vector as required by the payload. However, scheduling changes for delaying removal of flight test instrumentation until after the fifth flight (designated as the first operational flight) enabled accomplishment of the four flight test programs in the first five flights.

In figures 13(a) to 13(c), STS-3 to STS-5 test attitudes are shown. The attitudes chosen for STS-3 were PTC for thermal conditioning before and after the first attitude hold of +X (tail to Sun with top to space) orbital rate roll followed by -XSI (nose to Sun) and +ZSI (top to Sun). It should be noted here that, contrary to the initial categorization shown in table 6, the continuous +X to Sun

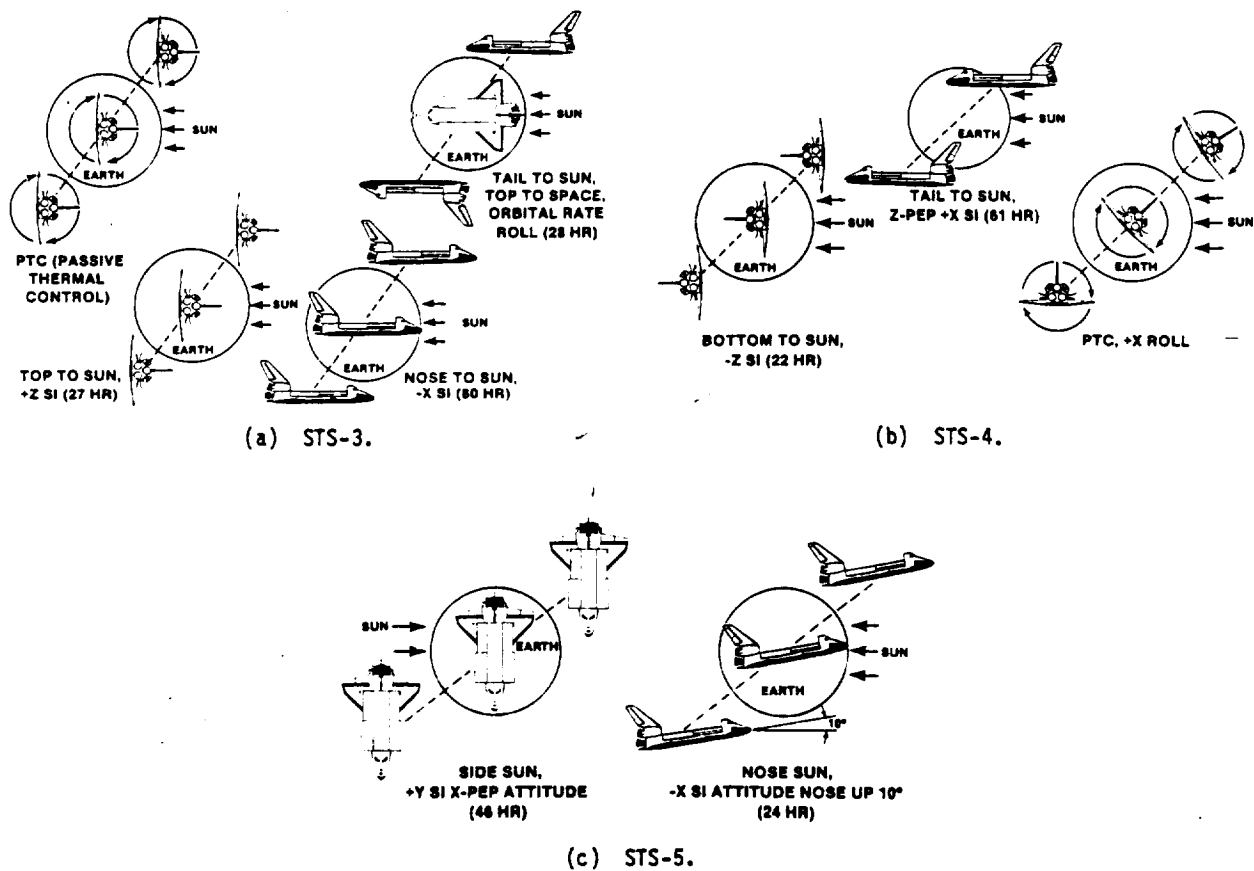


FIGURE 13.- THERMAL TEST ATTITUDES.

orbital rate roll test condition was chosen over the three cycles of 6 hours of +X orbital rate roll followed by 3 hours of PTC test condition. It was determined that a continuous hold would provide better response data for TPS bondlines and the payload bay, for the beta angles that would be encountered, than would the cyclic test condition. The +XSI (tail to Sun) and -ZSI (bottom to Sun) attitudes followed by PTC were flown on STS-4. The STS-5 test attitudes were +YSI (starboard side to Sun) followed by -XSI (nose to Sun) pitched up 10°. In figure 14, simplified attitude time lines flown on STS-1 to STS-5 are shown.

In general, the TCS test attitudes were flown as planned. An exception was STS-4, during which it was determined that an unacceptable quantity of moisture had been ingested by the TPS tiles and bakeout of the tiles was required. This determination resulted in reversing the attitude profile sequence from +XSI and -ZSI followed by PTC to +ZSI, PTC, and +XSI. Loss of data for thermal response of the black TPS tiles from a cold to a hot condition resulted.

Four test attitudes were designated as post-OFT test requirements: +ZSI, +XSI, -ZSI followed by PTC, and the cyclic 6 hours of +X to the Sun with -Z to Earth orbital rate roll followed by 3 hours of PTC. The post-OFT tests and objectives are summarized in table 8. Since the K_U-band antenna would initially be flown in benign environments in the post-OFT period and in light of ground thermal test results, it was determined that the two test attitudes, +ZSI and +XSI (nose down 15°), for the K_U-band could be treated as demonstration tests when convenient. All systems functional tests were completed with the exception of the OME engine firing tests, one of nine RCS engine firing thermal soakback tests, the potable water and wastewater dump tests, and two payload bay door closure tests. In addition, three hydraulic system tests were abbreviated and redefined as a result of STS-2 being shortened from 5 days to approximately 54 hours because of a fuel cell failure (table 9).

The OME firing and water dump tests were deleted since adequate data were obtained as a matter of course. In the case of the OME firing, the requirement was reevaluated because of propellant

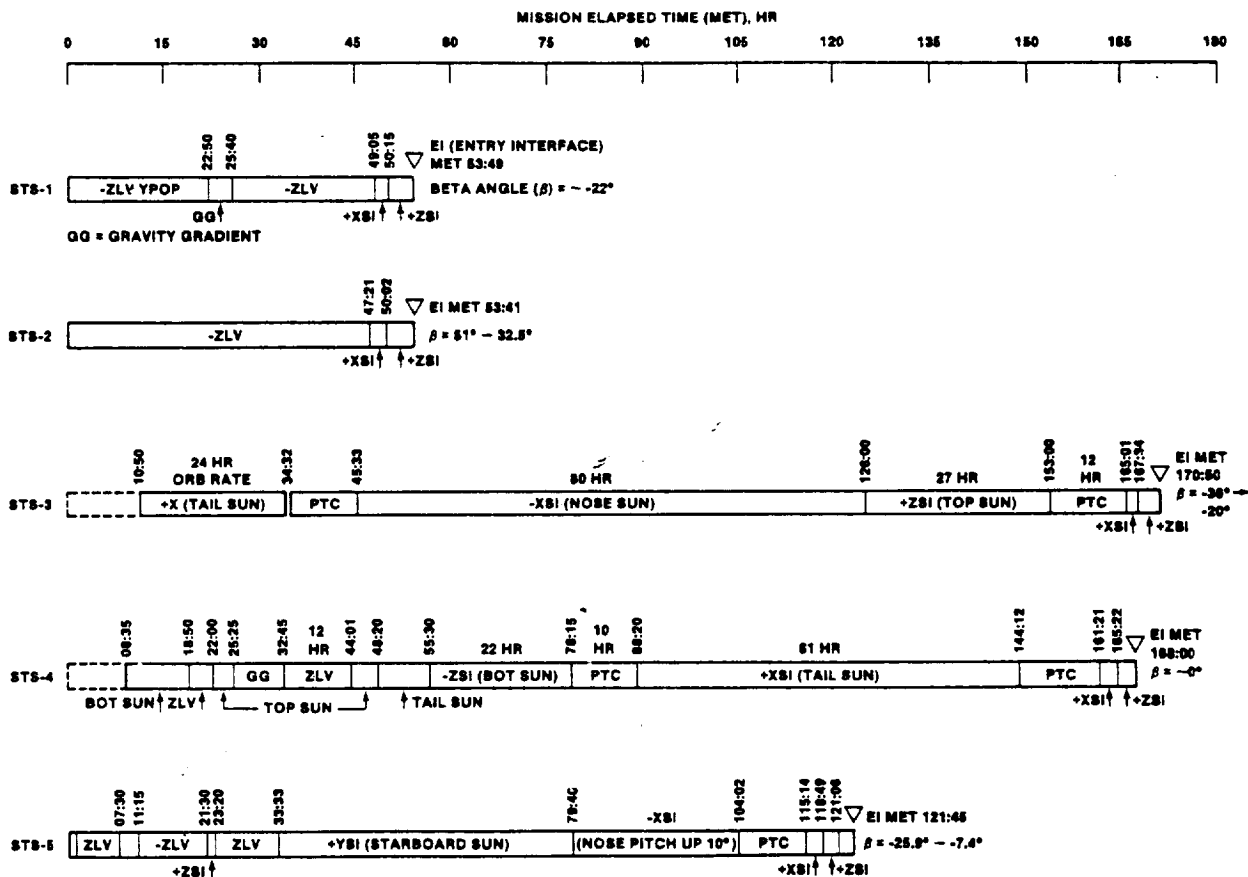


FIGURE 14.- STS FLIGHT TEST ATTITUDE TIME LINE.

TABLE 8.- POST-OFT TCS HIGH-BETA-ANGLE FLIGHT TESTS

Vehicle attitude	Primary test objectives
+ZSI (top to Sun)	<ul style="list-style-type: none"> Hot payload bay environment verification Determine effects of hot payload bay on lower midfuselage subsystems environments Payload bay door (PLBD) closure demonstration
+XSI (tail to Sun)	<ul style="list-style-type: none"> Identify and define OME propellant feedline hold constraint to prevent exceeding maximum allowable operational temperature Demonstrate MLG cold attitude-hold capability PLBD closure demonstration
6/3 attitude cycle	<ul style="list-style-type: none"> Define cold TPS bondline constraint Cold payload bay, cold environment verification and obtain payload retention-fitting thermal response data
-ZSI (bottom to Sun) followed by PTC	<ul style="list-style-type: none"> Demonstrate maximum TPS bondline temperatures and thermal conditioning recovery required to cool to maximum allowable initial entry temperature levels Determine effects on lower midfuselage subsystems environments

TABLE 9.- TCS FUNCTIONAL TEST ACCOMPLISHMENTS

Test planned	Flight				
	STS-1	STS-2	STS-3	STS-4	STS-5
Payload bay door closure	• +ZLV		<ul style="list-style-type: none"> +X orbital rate (required thermal conditioning to close and latch) -XSI +XSI (deleted real time) +ZSI 	<ul style="list-style-type: none"> -ZSI (required thermal conditioning to close and latch) +XSI (deleted real time) 	• +YSI (deleted)
RCS engine firings			<ul style="list-style-type: none"> -XSI (2 tests) 	<ul style="list-style-type: none"> +XSI (3 tests) -ZSI (1 test deleted) 	<ul style="list-style-type: none"> +YSI (2 tests) -XSI pitched up 10° (1 test)
Hydraulics		<ul style="list-style-type: none"> +ZLV (3 tests redefined real time for shortened mission) +ZLV 		• +XSI	
<ul style="list-style-type: none"> No thermal interaction, 3 system interaction, and single system thermostat test (3 tests) Entry thermal conditioning Circulation pump timer mode 					
Star tracker			• +ZSI	• +XSI	
Flash evaporator system feedwater lines			• -XSI		
Potable water and wastewater dump lines and nozzles				• Deleted (data obtained from flight 3)	
Vernier RCS engine heater test		• +ZLV (added following STS-1)			
APU fuel and water line thermal response with heaters "off"				• +ZLV	

availability. The RCS engine firing, a 100-second continuous burn of the aft-firing port engine, was deleted in real time as a result of other mission conflicts and was not rescheduled. A program management decision was made during the STS-4 mission to discontinue actual closing and latching of payload bay doors in the thermal test attitudes. However, thermal data and structure deflection measurements were obtained to support payload bay door verification.

Two functional tests were added during the OFT program. As a result of in-flight evidence that the forward vernier RCS engine heaters appeared to be incapable of maintaining temperatures above those indicative of leaking propellant valves during prolonged nonfiring periods, a special test was defined and performed on STS-2 to provide engine thermal response with the engines inhibited. Results of the test proved that either a hardware redesign or operational procedures would be required. The second test resulted from concern over "failed on" APU fuel line heaters overheating the fuel lines during entry and posing a safety hazard. The only immediate solution would be to inhibit the heaters; therefore, a test of the fuel line thermal response with heaters inhibited was implemented on STS-4 to determine whether the lines would freeze before landing. This problem is discussed in the following section.

FLIGHT TEST RESULTS OVERVIEW

The data presented herein are intended as an overview only for completeness of this report. Detailed evaluation, correlation of thermal math models, and TCS analyses to verify the Orbiter design are expected to be complete approximately 1.5 years following completion of the required TCS tests.

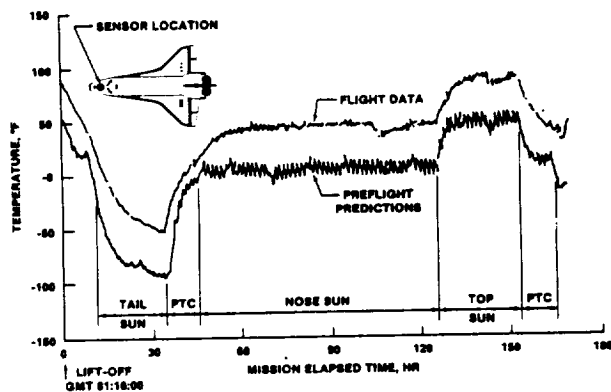
The primary prelaunch concerns were with the aft fuselage cooldown associated with the main propulsion system cryogenic propellant effects, which normally occur approximately 4 hours before launch when initial filling and conditioning of propellant lines within the aft fuselage begins. The aft fuselage prelaunch thermal model which was correlated to main propulsion system ground test data provided very good predictions for the actual vehicle. Bulk gas and structure temperature predictions were a maximum of 14° F warmer than actual prelaunch data (table 10).

On-orbit structure and TPS bondlines generally were warmer in flight than predicted. Figures 15(a) to 15(c) are comparisons of STS-3 flight temperatures with preflight predictions for two representative forward fuselage locations and one OMS pod TPS bondline location. Maximum deviations are on the order of 30° F. It can also be seen that the structure transient thermal response tends to be slower than predicted. In figure 16, the large gradients between the starboard (+Y) and port (-Y) midfuselage sides experienced during the +YSI attitude on STS-5 are shown.

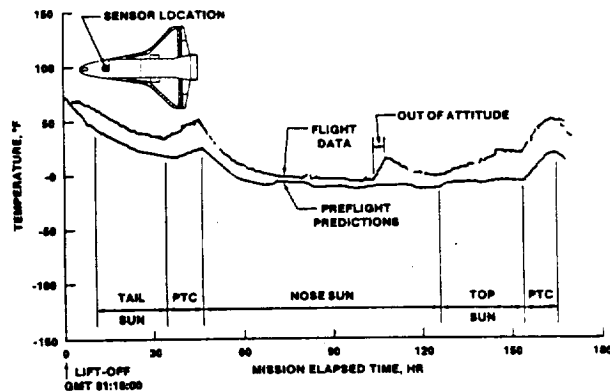
Most Orbiter heater systems performed better than predicted as would be expected in light of the warmer structure temperatures experienced. In instances in which heater duty cycles were greater than predicted, the increase was not of a magnitude that would cause alarm. Design performance acceptability will be determined in the verification program. Exceptions were the forward vernier RCS engine and forward RCS compartment radiant heater panels.

TABLE 10.- SUMMARY OF AFT FUSELAGE ANALYTICAL PREDICTIONS
VERSUS STS-1 DATA BEFORE LIFT-OFF

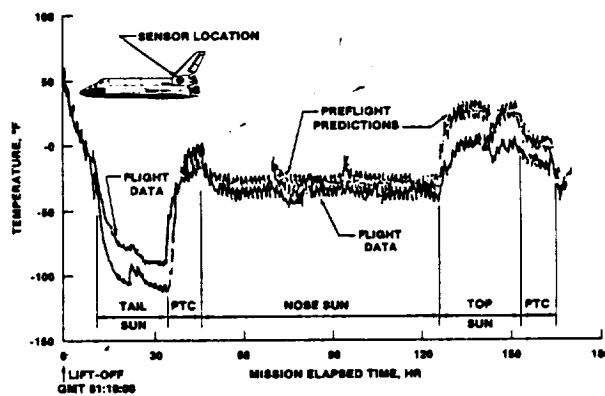
Aft fuselage location	Temperature, °F	
	STS-1 data	Preflight predictions
Forward bulk gas	66	70
Mid bulk gas	43	53
Aft bulk gas	35	40
Fuselage port sidewall	47	44
Fuselage starboard sidewall	40	43
Fuselage bottom centerline	40	43
Base heat shield	32	46



(a) FORWARD FUSELAGE TOP.



(b) FORWARD FUSELAGE BOTTOM.



(c) PORT SIDE OMS POD.

FIGURE 15.- STS-3 ON-ORBIT STRUCTURE TEMPERATURE PROFILE.

During a 4-hour period on STS-1, the vernier RCS engines were inhibited from firing. The engine heaters exhibited a 100-percent duty cycle, and temperatures continued to drop until the engines were enabled to fire. Data from STS-1 were inadequate for analysis; therefore, a test was implemented on STS-2 for a prolonged nonfiring period to obtain heater response data. In figure 17, the response of the port and starboard vernier engine oxidizer injector tubes, which are indicative of heater performance and are also used for leak detection, is shown. The differences in temperature response and heater "on" times result from the fact that, because of the moderate beta angle and +ZLV attitude being flown, sunlight was impinging on the port engine. The decrease in starboard engine temperature continued after the heater activated, and the temperature reached the engine valve leak detection limit of 130° F in approximately 5 hours 45 minutes after engine firing was inhibited. Inspection of engine installations revealed higher than expected conduction shorts and increased radiation losses.

Also on STS-1, the forward RCS compartment radiant panel heaters exhibited a 100-percent duty cycle until they were disabled for entry (fig. 18). The heaters had been predicted to function initially at a mission elapsed time (MET) of 16 hours as compared to an actual time of 35 hours 20 minutes at a duty cycle of 25 percent. Inspection of the thermostat installation disclosed that the propellant line bracket next to the thermostat was made of aluminum rather than fiber glass and was attached to an RCS purge and drain panel, which was more closely thermally coupled to the vehicle cold structure than had been calculated. The increased conduction and the high radiant view factor from the thermostat to the panel caused the high heater duty cycle. The initial concerns were that overheating of RCS system components could occur and that an unnecessary amount of power was being consumed. However, further analyses and flight data showed that overheating would not be a problem, and the increased power usage did not justify a redesign.

Failed-on APU fuel line heaters during entry would require a crewman to deactivate the failed heaters during a high crew activity period and therefore was undesirable. To negate this possibil-

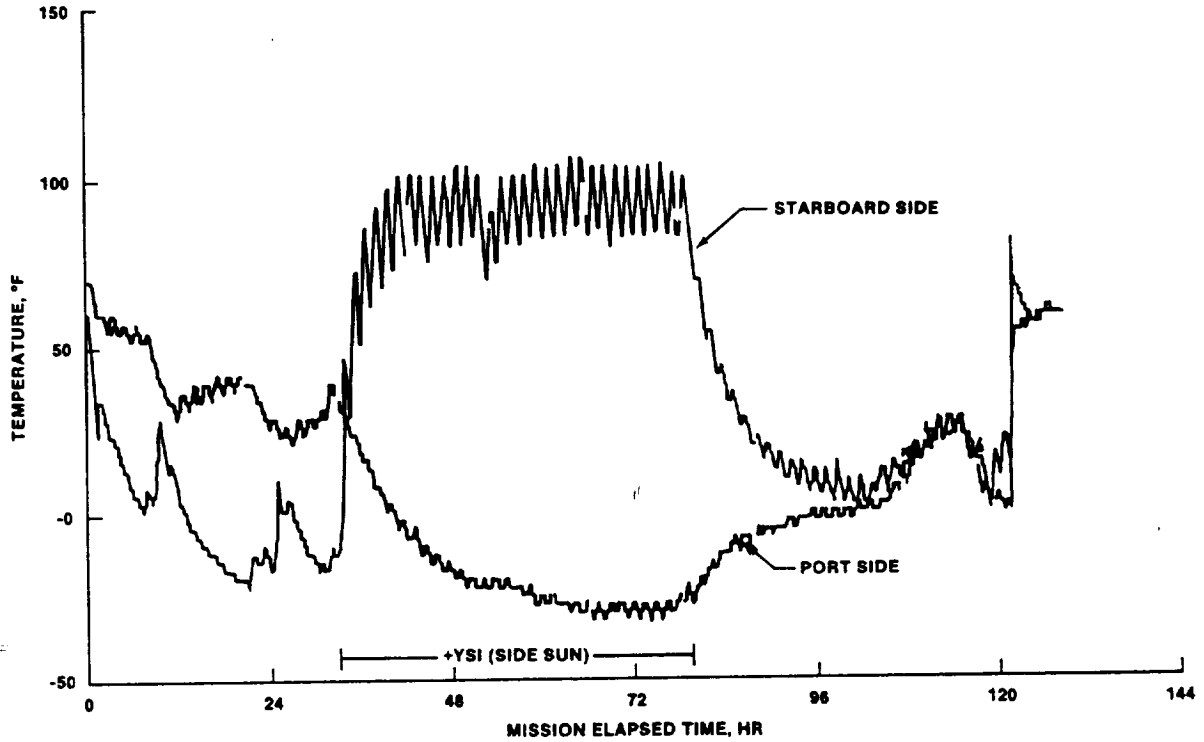


FIGURE 16.- STS-5 MIDFUSELAGE SIDE BONDLINE TEMPERATURE PROFILE.

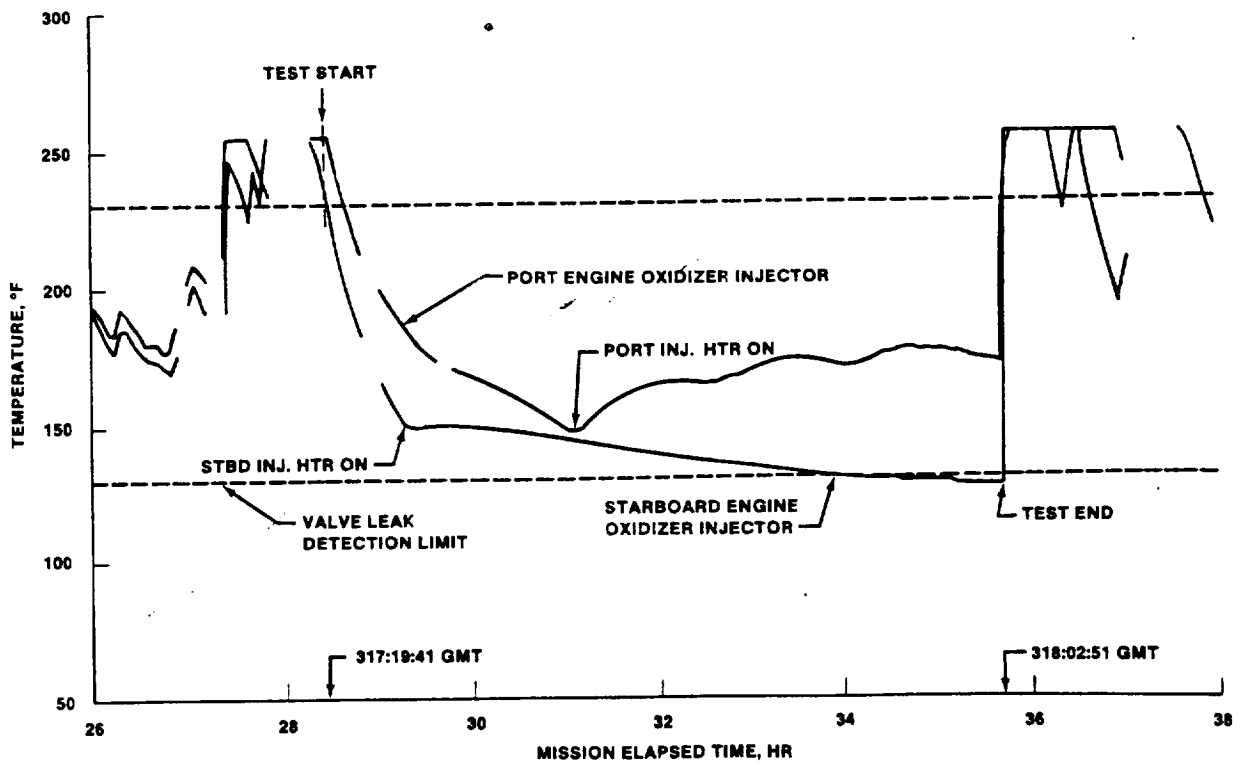


FIGURE 17.- STS-2 VERNIER RCS ENGINE HEATER TEST.

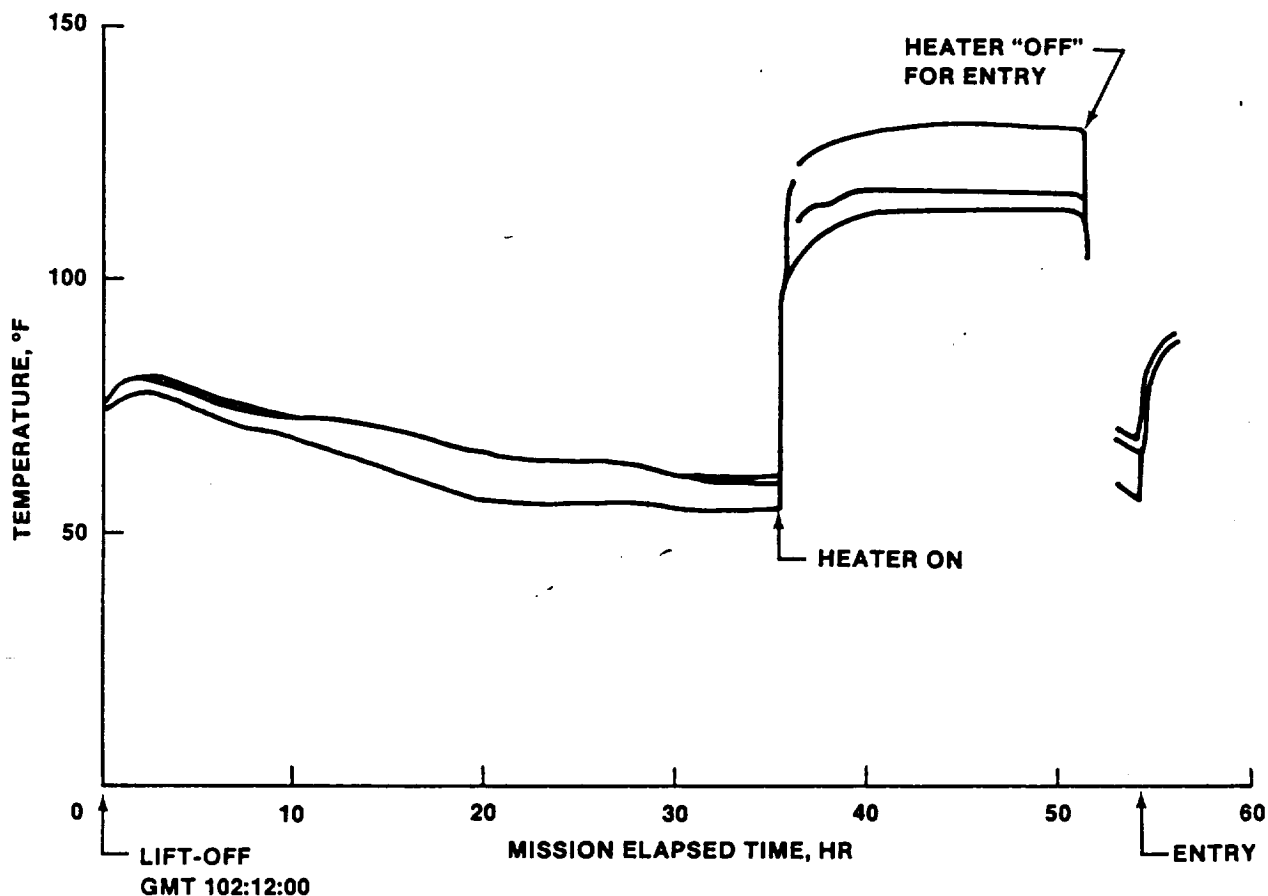


FIGURE 18.- STS-1 FORWARD RCS COMPARTMENT PORT HEATER PANEL TEMPERATURE PROFILE.

ity, it was desirable to determine whether the heaters could be deactivated before entry without freezing before ground power hookup after landing. A test was conducted on STS-4 by deactivating the heaters in an environment representative of that expected just before entry. In figure 19, the cooldown response of three locations on the APU 1 fuel service line is shown. It can be seen that the coldest location, curve 1, near the thermostat would reach the APU fuel freezing temperature of 35° F in less than the 3 hours desired by flight operations and would require crew intervention. Therefore, the heaters were not deactivated for entry.

The first data for determining the tail to Sun attitude-hold constraint for the OME feedlines were obtained on STS-3 during the 24 hours of +X to Sun orbital rate attitude. Temperature of the engine feedlines reached 110° F at the end of the hold and was still increasing. Extrapolation of the flight data indicated that the equilibrium temperature for the moderate beta angle that was flown would have been 120° F if the attitude had been held longer. This indication was verified during the 67-hour +XSI attitude hold on STS-4, in which the oxidizer line temperature reached approximately 120° F (fig. 20). Results of preliminary analyses indicate that the lines will exceed the 145° F limit for engine firing at beta angles exceeding 60°.

As expected, STS-4 provided the best data for supporting definition of the main landing gear strut actuators and hydraulic dump valve cold attitude-hold capability. The actuators and dump valves reached minimum temperatures of -24° F and -28° F (-35° F minimum allowable), respectively, at the end of the 67-hour +XSI attitude hold. The flight and predicted response for the strut actuator is shown in figure 21. Thermal model correlation and analyses will be required to define the constraint envelope.

The first flight data on the adequacy of running the hydraulic system circulation pumps on orbit as a means of maintaining fluid temperatures above the minimum limit of 0° F were returned on STS-2. A typical hydraulic line (system 2 body flap) response to a series of approximately 20 minutes "on,"

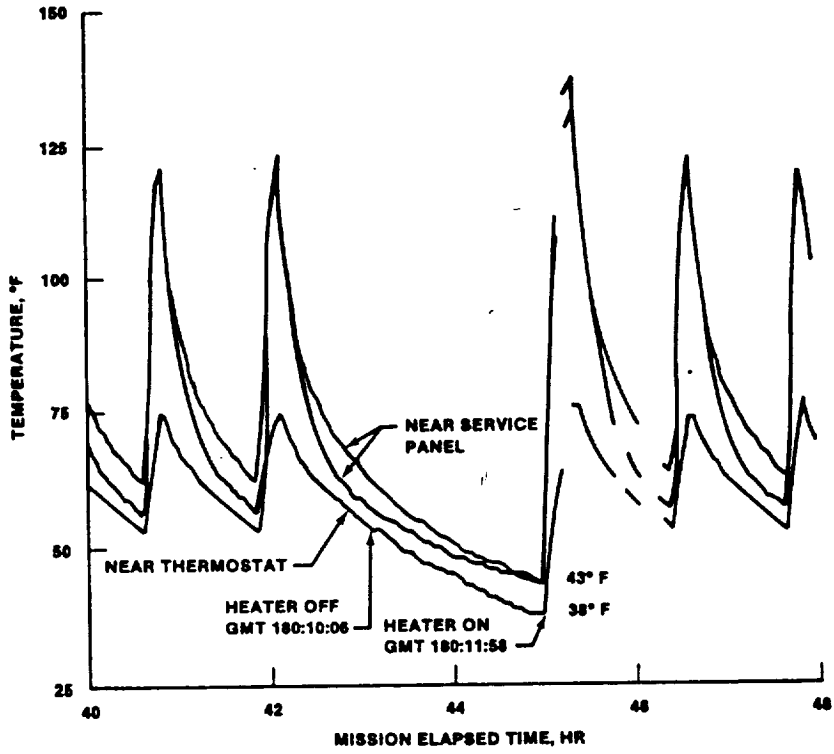


FIGURE 19.- STS-4 APU 1 SERVICE LINE TEMPERATURE PROFILE.

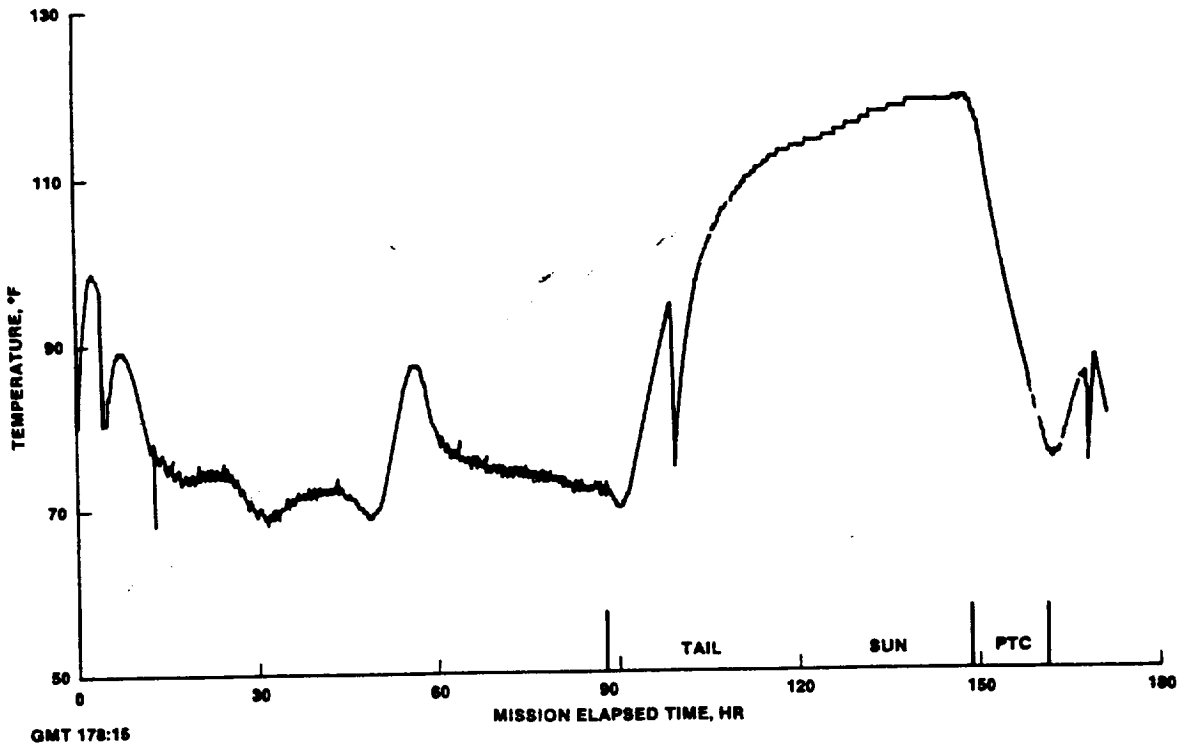


FIGURE 20.- STS-4 PORT ONE OXIDIZER LINE TEMPERATURE PROFILE.

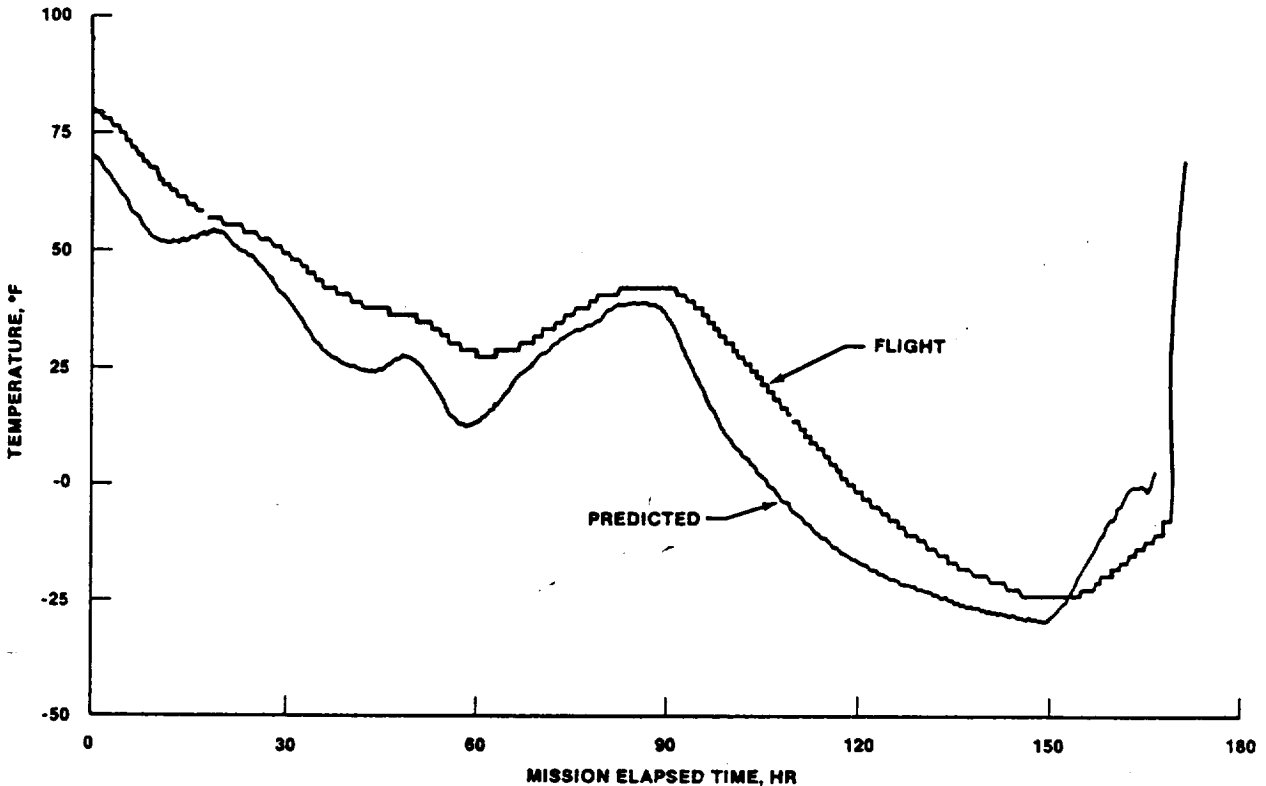


FIGURE 21.- STS-4 STARBOARD MAIN LANDING GEAR STRUT ACTUATOR TEMPERATURE PROFILE.

45 minutes "off" cycles (manual operation by the crew) is compared with predictions in figure 22. It can be seen that the temperature rise rate and levels are higher than predicted. Follow-on flight results have shown required pump duty cycles to be much less than predicted.

The thermal response of a forward primary RCS engine during and after a 30-second continuous test firing on STS-4 is shown in figure 23. Shown are the oxidizer and fuel injector tube and oxidizer valve temperatures. The cooling effects of propellant flow and postfiring propellant evaporative cooling can be seen beginning with the initiation of the firing at 142 hours 47 minutes MET followed by a temperature rise as a result of thermal soakback after the firing. The data provide a portion of the data base for thermal model correlation used to define any potential engine firing constraints.

Entry and postlanding thermal soakback effects on subsystems were minimal for the first five flights. Detailed analyses will be required for hotter entry environments than those flown. However, no problems are anticipated.

POST-OFT TESTING

During the course of the first five test flights, it became evident that the quality and the fidelity of the flight test data were much better than expected. More importantly, the TCS design appeared in most areas to exhibit greater margins and capability with respect to specified requirements when compared to preflight uncorrelated analytical predictions. A recommendation was made and accepted by the program management to accept the data from the first five flights as a basis for design verification. Also, except for some minor tests to investigate design differences between vehicles, the post-OFT TCS tests were deleted.

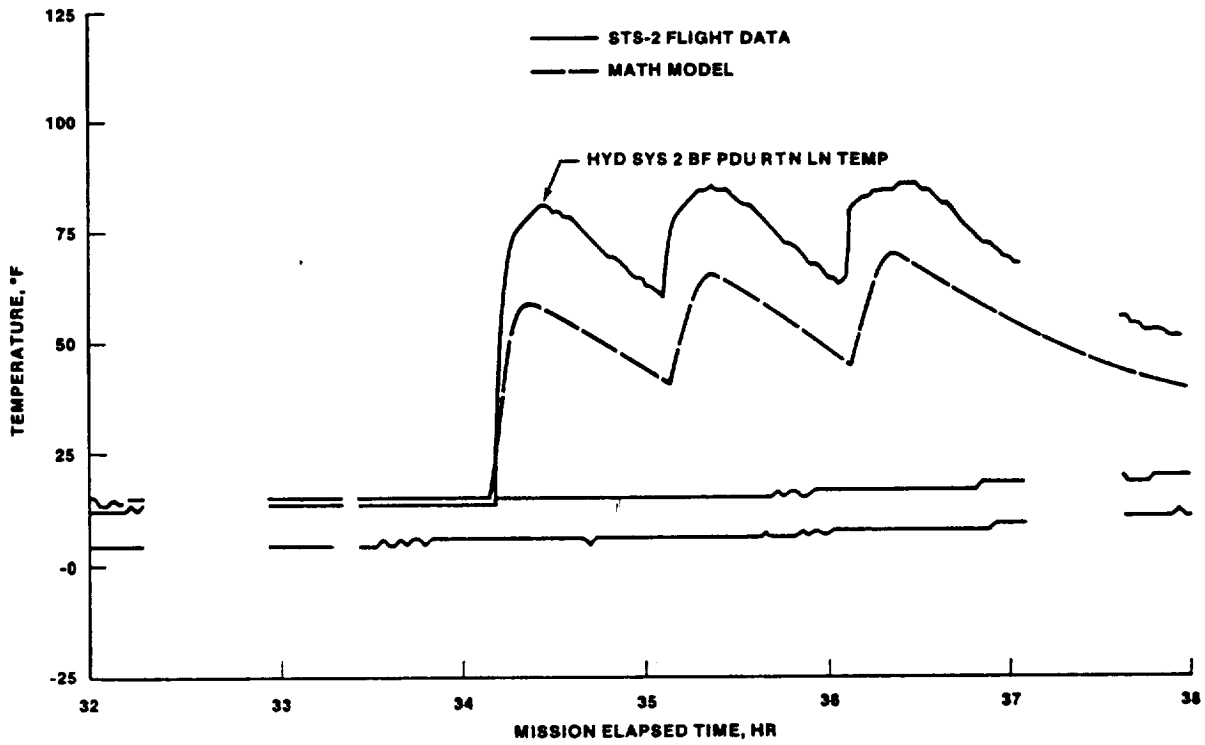


FIGURE 22.- STS-2 BODY FLAP OUTBOARD RETURN LINE TEMPERATURE PROFILE.

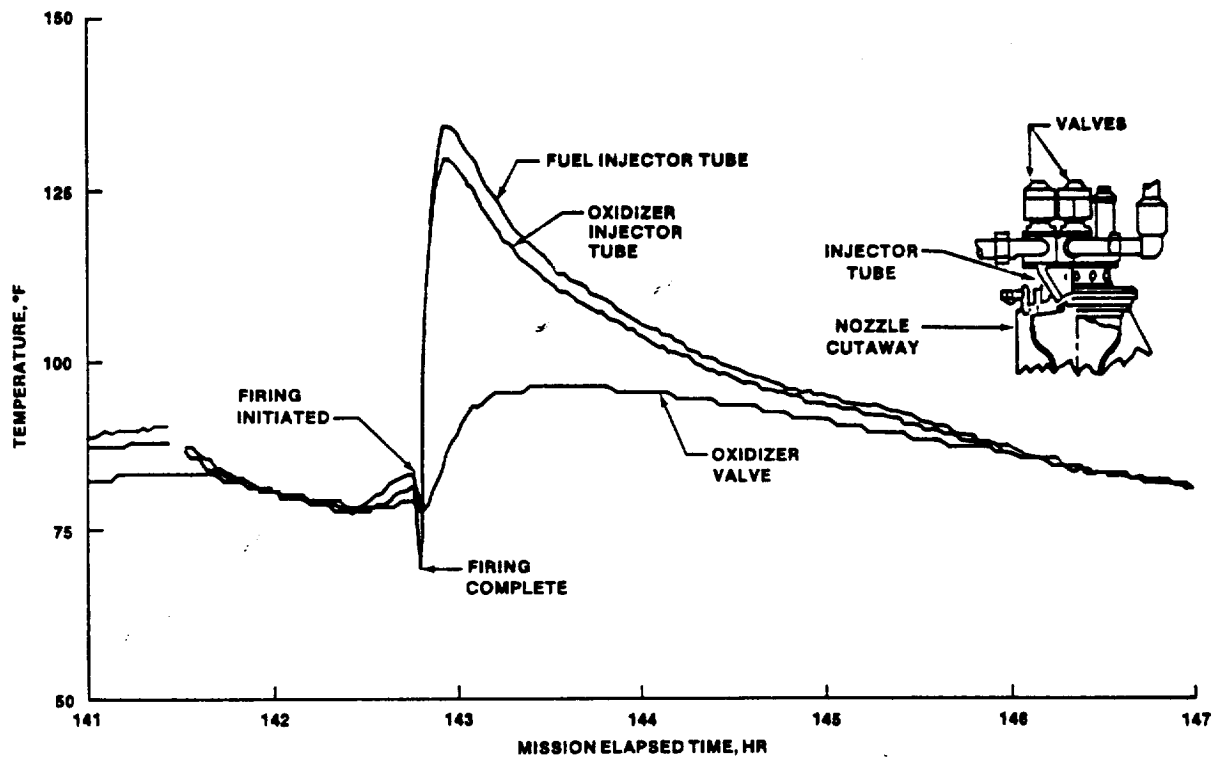


FIGURE 23.- STS-4 FORWARD PRIMARY RCS ENGINE TEMPERATURE RESPONSE TO 30-SECOND FIRING.

CONCLUSIONS

The definition of comprehensive thermal test requirements and integration of these requirements with basic mission objectives, operational and crew activities, payloads, and other systems test requirements led to the successful implementation and completion of the OFT thermal flight test program. The approach of initially testing in benign environments to minimize risk and gain confidence in the design before thermally stressing the vehicle proved to be sound. The approach also provided a basis of known performance for mission planning in critical areas such as payload bay door closure and preentry thermal conditioning.

The success of the test program was due largely to the dedication of mission planning, program requirements, and engineering personnel working as a team to integrate the various objectives and requirements into cohesive and practical crew activities and time lines for each test flight. Adequate data were obtained to support verification of the Orbiter TCS design. Results of preliminary analyses indicate that the TCS design will meet or exceed the vehicle specification requirements.

D33 N85-16975

SHUTTLE SYSTEM ASCENT AERODYNAMIC
AND PLUME HEATING

Lee D. Foster and Terry F. Greenwood
NASA George C. Marshall Space Flight Center
Huntsville, Alabama

Dorothy B. Lee
NASA Lyndon B. Johnson Space Center
Houston, Texas

ABSTRACT

The Shuttle program provided a challenge to the aerothermodynamicist due to the complexity of the flowfield around the vehicle during ascent, since the configuration causes multiple shock interactions between the elements. An extensive wind tunnel test program was required to obtain data for the prediction of the ascent design heating environment which involves both plume and aerodynamic heating phenomena. This paper discusses the approach for the heating methodology based on ground test firings and the use of the wind tunnel data to formulate the math models.

INTRODUCTION

The Space Shuttle is America's most versatile space vehicle. It is the first to be designed for reusability. This concept of reusability not only provided the economic payoffs which led to the existence of the Space Shuttle, but also provided the designers with unique challenges requiring innovative solutions. The economic and reuse considerations, in conjunction with the ambitious launch schedule (up to 60 launches per year originally projected), dictated the parallel burn concept and required that each element's design enable ease of manufacture and assembly.

The Space Shuttle (fig. 1) is composed of elements which include an Orbiter, three main engines (SSME), two solid rocket boosters (SRB) and an external tank (ET). The complexity of this arrangement required an extensive wind tunnel test program. This wind tunnel test program provided data to predict the design heating environment for the launch vehicle. The design evolution of the launch vehicle configuration and the wind tunnel test program is discussed in reference 1.

The configuration of the Space Shuttle provided unique challenges to the aerothermodynamicists. Never before has there been a launch vehicle with so many elements and one held together with so many struts. The flowfield around and through this configuration, compounded by the presence of interacting shocks, is exceedingly complex. Adding to the complexity of the flowfield is the presence of distinctive protuberances on each element quite different from the aerodynamically shaped fairings used on previous launch vehicles. As examples, the SRBs have several thousand boltheads protruding above the skin line and several structural rings of T-shaped cross section which present a thin "lip" to the approaching flow leading to high localized heating. The ET has cable trays and various fuel and pressurization lines which are elevated above the surface of the tank. Also the spray-on foam insulation (SOFI) which covers the ET results in a rough and wavy external surface.

The ascent design environment involves two types of heating phenomena: plume heating and aerodynamic heating. Plume heating consists of radiative and convective heating from the solid rocket motor (SRM) and main engine plumes. Plume radiative environments were generated analytically with the use of several different computer models. The plume convective heating environments were developed with the use of a combined analysis/wind tunnel approach. The aerodynamic heating predictions were developed from math models formulated on wind tunnel data obtained for a range of angles of attack and yaw, Reynolds numbers and Mach numbers.

TRAJECTORY

Choosing a thermal design trajectory for ascent was an important challenge faced by the aerothermodynamicists. Total system integration analysis cycles are required to develop trajectories. Thus, trajectories were not frequently updated through the Shuttle design phase. Each cycle provided trajectories for a myriad of conditions such as launch from the Kennedy Space Center (KSC) and Vandenberg Air Force Base (VAFB), all potential flight missions, nominal and abort cases, and cases with dispersed atmospheric conditions, wind intensities, and wind directions. Thermal assessment showed the mission 3A trajectory launched from VAFB to be the most severe. Characteristics of this thermal design trajectory are: 1) launch into a polar orbit with a 32,000 pound payload; 2) a 95 per-

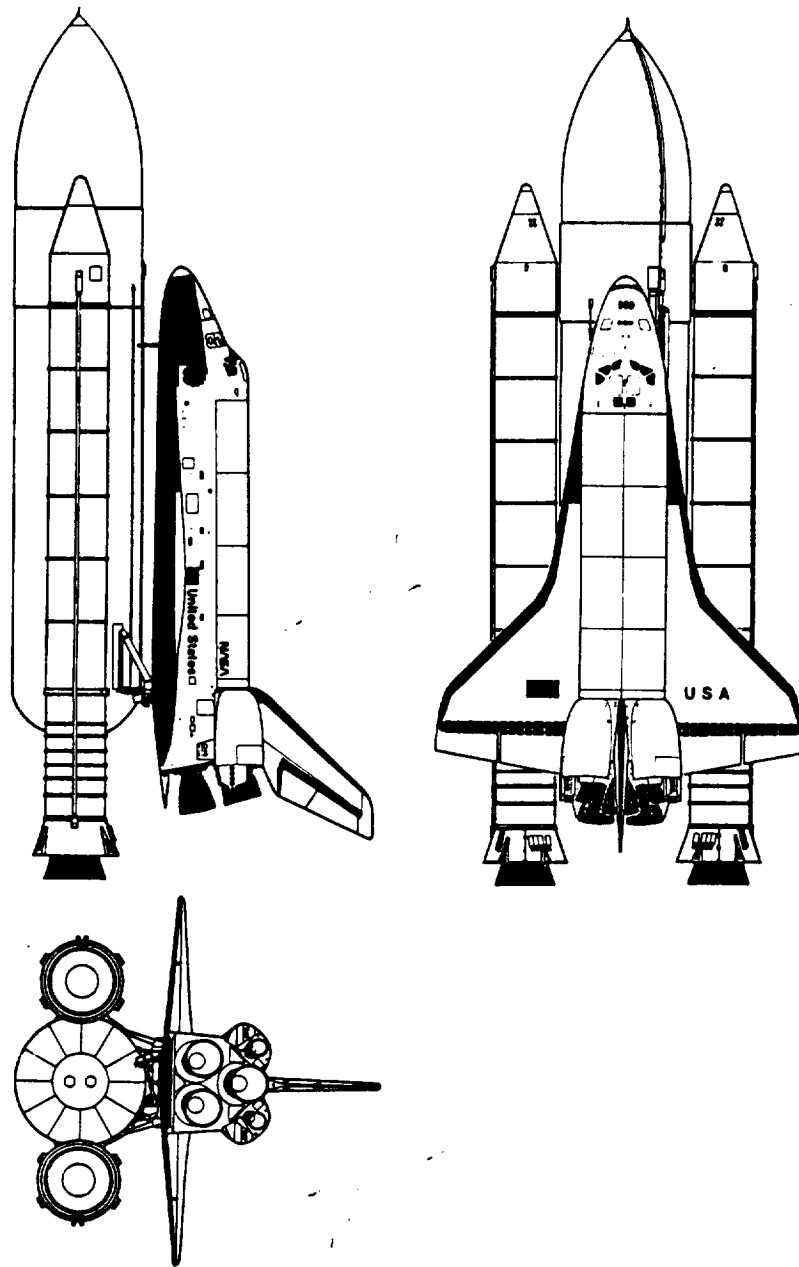


FIGURE 1.- SHUTTLE LAUNCH CONFIGURATION.

centile wind profile with a right quartering head wind direction; 3) the equivalence of 3σ dispersions on parameters that affect the trajectory (atmosphere, thrust, guidance and control parameters, etc.), and 4) one SSME out at 260 seconds into flight necessitating an abort-once-around (AOA) where the ET is separated at an altitude of 57 nautical miles and the Orbiter makes one revolution before landing at the launch site. Some properties of this thermal design trajectory are shown in figure 2. The heating indicator (Q_{HJ}) which is the heating to a one-foot sphere flying this trajectory, shows that the highest heating rates are associated with first stage flight. Figure 3 shows the envelope of possible vehicle attitudes during first stage flight. The excursions in sideslip angles around 115 seconds are caused by the potential differential thrust in the SRB's during tailoff.

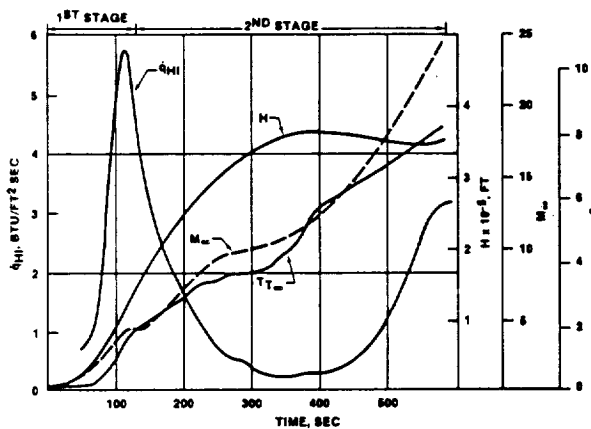


FIGURE 2.- ASCENT AERODYNAMIC HEATING DESIGN TRAJECTORY.

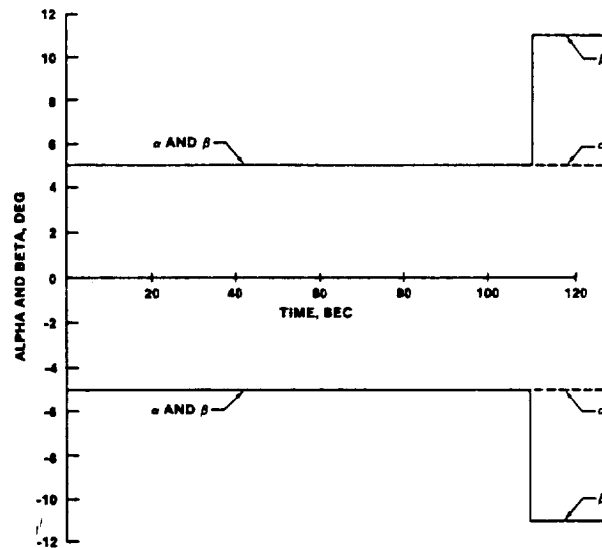


FIGURE 3.- ENVELOPE OF POSSIBLE ATTITUDES - FIRST STAGE FLIGHT.

During the second stage flight, many abort conditions are possible. Early in this portion of the flight, the Orbiter/ET can be turned around for a return to the launch site. This maneuver, called a return to launch site (RTLS) abort, is very risky and involves flying backwards into the SSME plumes. If an abort condition occurs later in the flight, an AOA or a Transatlantic (or Pacific) abort landing (TAL) would be elected depending on the number of SSME's which fail. Each of these aborts involves different flight conditions and were analyzed in the design cycle.

PLUME HEATING

An extensive effort to accurately predict the ascent base heating environment was undertaken early in the Shuttle program. A paper documenting the preflight Shuttle base heating methodology is given in reference 2. The ascent base heating environment is a combination of SSME and SRM plume radiation, freestream air convective cooling, and reversed plume flow convective heating. Each base region design point receives different levels of radiation and convective heating depending upon its location relative to the plumes, base gas absorption, structural blockage, general base configuration, and local surface temperature. The radiation environment varies with the plume shape and the incident radiation to any base location depends upon the emission/absorption and afterburning characteristics of each contributing plume and by the magnitude of attenuation of the base region gases. Convective cooling occurs during early first stage flight as cool freestream air is drawn through the base by the aspirating action of the plumes. At higher altitudes when the plumes become highly expanded and interact, hot gases from the SSME and SRM nozzle boundary layers are reversed into the base resulting in base convective heating to most base surfaces. The magnitude of this reversed flow convective heating during the last 30 to 40 sec. of first stage flight is significantly greater. It affects more surfaces than was anticipated before flight data were obtained. Photographs taken of the ET base during this time period show the reverse flow is so strong that the ET base appears to be burning. Actually, this observation is caused by aluminum oxide particles and ET aft dome ablation products glowing in the reversed flowfield.

Typical flight data measured at the center of the Orbiter heat shield illustrate the various environment components and their relative magnitudes throughout ascent in figure 4. Base heating is significant at this location from SSME ignition until main engine cutoff (MECO). Radiation during first stage flight is at a maximum near sea level, decreases as the altitudes increases, and is reduced by convective cooling during the first 70 seconds of flight. At 70 seconds, the plume boundaries intersect and begin to recirculate exhaust gases toward the base. There is then a rapid buildup in convective heating until SRM thrust tail-off begins which reduces the intensity of the reverse flow (and the heating). Approximately 7 seconds before SRB separation, a sharp spike in heating occurs associated with SRM shutdown. This "shutdown" heating spike is the result of motor liner material and other high radiators burning and flowing out the nozzle.

ORIGINAL PAGE IS
OF POOR QUALITY

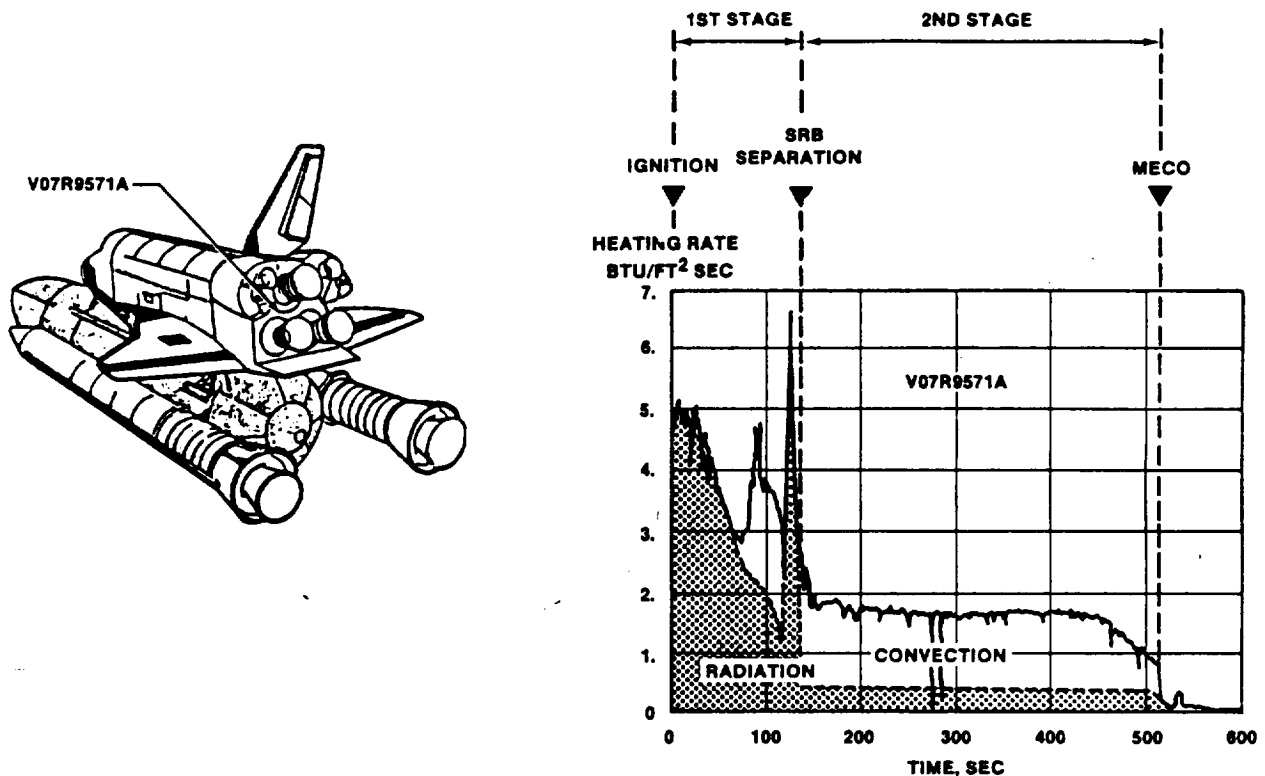


FIGURE 4.- TYPICAL ASCENT BASE HEATING ENVIRONMENT.

During second stage flight, the SSME plumes radiate at a nearly constant low level (note shaded area of figure 4). Convective heating is essentially constant as the flow into and out of the Orbiter base reaches a choked condition and becomes independent of altitude. This convective heating declines at the center of the Orbiter heat shield when the SSMEs throttle down at approximately 450 seconds. This decline is a result of flowfield changes in the base caused by variations in the main engine pitch position.

Radiative and convective heating components of the total base heating environment prediction methodology have different methods. They are computed independently and are summarized in the following paragraphs.

RADIATIVE PLUME HEATING

Solid Rocket Motor

The sea level math model for the SRM plume radiation was originally based on experimental data taken on sea level firings of the Titan IIIC solid motor³. Then it was scaled to the SRM motor size. This sea level model was subsequently updated based on data obtained during static firing tests of the SRM. Narrow view angle radiometer data were obtained along the plume centerline. This was done to characterize the plume emissive power. Wide angle radiometer data were obtained at positions that simulated locations on the Shuttle vehicle. From these data, a new sea level plume emissive power radiation model was developed⁴. Subsequent testing of the SRM (QM-3) provided narrow view angle radiometer measurements near the nozzle exit plane. These were slightly higher than measurements taken earlier and the data resulted in an update of the SRM plume emissive power radiation model⁵.

With the math model for sea level plume emissive power defined, radiative heating rates to various design points on the Shuttle were calculated with a radiation view factor computer program⁶. Initial predictions assumed no altitude variation. Later predictions (before flight data became available) considered altitude effects with a Monte Carlo radiation code⁷. The predictions coupled with

detailed, two-phase plume flowfield calculations resulted in the plume model discussed in reference 8.

Space Shuttle Main Engine

Radiative heating rates from the SSME plumes were initially calculated using the basic NASA band model gaseous radiation program⁹. An extensive effort was made to correctly model the Mach disk region and the viscous shear layer of the plume. To calculate SSME radiation to the large number of design points required for a design environment, a geometrical representation of the SSME plume radiation model was constructed. This allowed for view factor calculations to be made². At low altitudes, the plumes do not interact. Therefore, detailed radiation calculations were made for each plume. The environment was generated at a given design location by adding the contributions from each plume. The complex three-dimensional flowfield which occurs at high altitudes was approximated using two-dimensional techniques².

CONVECTIVE BASE HEATING

Convective base heating predictions were based almost entirely on short duration, hot firing model test data. Eight separate base heating test programs were conducted to support the convective environment analysis.^{10,11} The model used throughout these tests for first stage conditions was a 2.25% scale model of the fully integrated launch vehicle. These tests had short duration techniques that included hot firing hydrogen-oxygen simulation of the SSME, hot firing simulation of the booster SRM, and simulated external air flow over the model. The model used for second stage test conditions was a 4% scale model of the Orbiter base region, vertical fin, OMS pod, and body flap which included hot firing hydrogen-oxygen simulation of only the SSMEs. These tests were conducted in altitude chambers with no external flow, only a variable chamber back pressure.

During these tests, model heating rates and gas temperatures were measured over a range of simulated altitudes. All factors affecting convective base heating were parametrically varied to provide a detailed base heating data base. When the flight conditions were established, this data base was used to extract the model heat transfer coefficient corresponding to the specific flight condition. The techniques used to scale from model to full scale were based on the Colburn Turbulent Scaling Law. Analytical predictions for the mass average base gas recovery temperature were made by estimating the mass flowrate of exhaust products into the base region. Then integrating the total energy flowrate in the nozzle boundary layer from the nozzle wall to this mass flowrate. Details of these analytical techniques are provided in reference 2.

FLIGHT RESULTS

Flight instrumentation to monitor ascent base heating consisted of total calorimeters, radiometers, and gas temperature probes. With the exception of the gas temperature measurements, the data were generally good, consistent from component to component, and were of significant value in understanding the base heating environments. No valid gas temperature measurements were obtained. Complete presentations of all base heating data for STS-1 through 5 are presented in references 12 through 16. An overview of all the base heating flight data is given in reference 10.

Close examination of the flight data indicates that two changes were necessary in the basic SRM plume radiation prediction methodology. One change involved the sea level radiation model modified to account for the combustion zone between the SRMs from the outgassing ET base TPS material combusting as it flows downstream between the SRM plumes. The other change was a correction factor to account for altitude changes developed from the flight experience. The altitude correction factor eliminated the launch stand correction factor that was present in the earlier methodology. It also accounted for the SRM shutdown spike at the end of the SRM burn. These methodology changes are discussed in reference 11.

The Shuttle flight data generally validated the convective methodology. For most base surfaces, the good agreement between prediction and flight data indicated that the scaling methods were correct. However, at three distinct base locations, the prediction methodology was obviously incorrect. These locations were the upper interior region of the Orbiter base heatshield, the upper ET aft dome surface, and the outboard SRB skirt. At the upper heatshield location, the preflight methodology overpredicted convective heating during second stage. Conversely, the methodology underpredicted ET dome and outboard SRB skirt convective heating during the intense recirculation period at the end of first stage boost. Final operational flight environments will account for these discrepancies.

A comparison of actual flight data with the DCR environments and the current operational environments is shown in figure 5. This comparison is representative of the complete data base obtained on

Shuttle flights STS-1 through 5. There was generally good agreement overall between flight data and preflight prediction.¹⁷

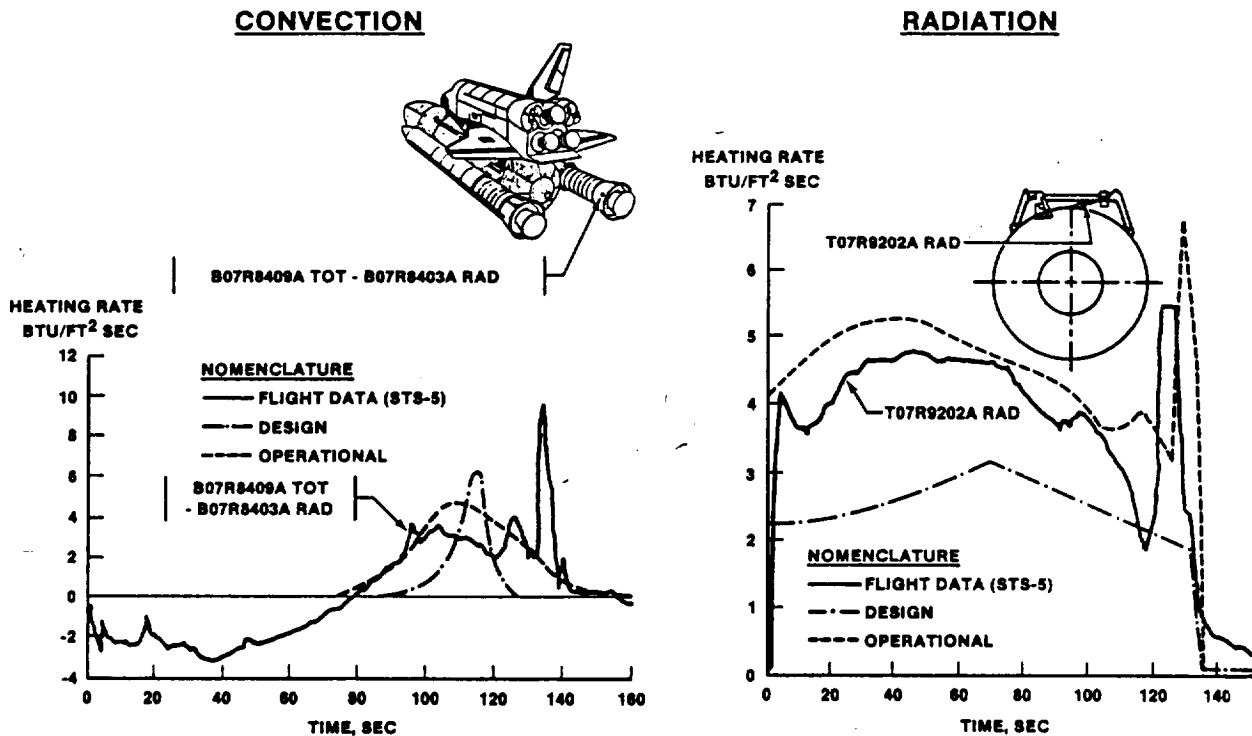


FIGURE 5.- COMPARISON OF PREDICTION WITH FLIGHT DATA.

AERODYNAMIC HEATING

The choice of aerodynamic heating methodology and the technique of generating the thermal design criteria proved to be the most important challenge faced during the Shuttle ascent design effort. While heating to the Orbiter was assessed for ascent flight, the majority of the Orbiter thermal protection system (TPS) was designed by the entry environment. The base region was designed by ascent plume heating. To develop a comprehensive ET and SRB TPS design, the thermal analysts required ascent heating prediction environments at many locations (body points) on the elements. The ET has approximately 1600 body points, the SRB approximately 600, and the Orbiter approximately 2000. Math models and computer programs had to be developed that were capable of accurate but rapid calculations. These calculations would accommodate the large number of body points and trajectory time steps. Simplified flowfield and heat transfer models were derived and checked with wind tunnel test data and results from large and cumbersome exact analytical solutions.

The wind tunnel test program¹ for the baseline Space Shuttle configuration began in 1973 and continued through late 1982. Thousands of hours of wind tunnel facility time were used to test the Orbiter, ET and SRBs as individual elements and as integrated vehicles for the first and second stage flight configurations. There are a limited number of aerothermal test facilities and those used were Arnold Engineering and Development Center (AEDC), NASA Ames, Langley, and Cornell Aeronautical Laboratory (CAL). Testing was performed on small scale models mainly with the use of thin-skin thermocouple-instrumented models. Additional testing was done with the phase change paint technique where stycast models are coated with paint which melts at known temperatures. One of the challenges involving the wind tunnel testing was associated with small scale models. Very little data were obtained for protuberances. A scaled Shuttle vehicle limits the size of a protuberance which precludes obtaining meaningful data. Therefore, data from the literature were used to develop heating predictions for most protuberances. A few tests were conducted with large scale protuberances mounted on flat plates. Another challenge was that the flowfield over the models differed from flight because of size limitations in the wind tunnels, facility flight simulation constraints and lack of plume simulation for the SRM and SSME.

The basic methodology for the calculations of the design heating rates involved analytically calculating undisturbed heating histories for each element and modifying these histories for interference effects of the integrated elements measured in the wind tunnel. Undisturbed heating is defined as the heat flux to the single element without protuberances. The analytical predictions were verified with wind-tunnel data obtained on each element without protuberances.

Early in the program a conservative design philosophy was adopted to assure safety of flight. This philosophy consisted of the worst possible vehicle orientation for the undisturbed heating calculations coupled with the worst vehicle attitude for the interference heating. This conservatism was identified as the envelope technique which used the maximum values of interference over undisturbed heat transfer coefficients (h_i/h_u).

FLIGHT RESULTS

The first six Space Shuttle flights were instrumented with heat flux sensors (calorimeters) on the ET and SRBs to measure heating rates to verify or modify the prediction methods. Instrumentation installation of the SRBs was relatively straightforward. However, installing sensors on the cryogenic ET proved to be a challenge. The sensors had to be placed in islands to insulate them from the cold structure and to preclude ice formation. Since this concept protruded above the surrounding TPS, shallow angle ramps were designed to surround the islands to minimize local flow disturbances. Surface thermocouples and pressure taps were installed in the Orbiter TPS tiles to measure surface temperatures and local static pressure. The surface temperatures were used to obtain heating rates for comparison with preflight predictions.

Examination of ET flight data became a new challenge with the necessity to "correct" the flight measurements. Calorimeters on the forward ogive of the ET were affected by wall temperature mismatch. This occurs when the air flows from the hot Spray on Foam Insulator (SOFI) surface to the cold calorimeter surface resulting in an erroneously high heat transfer measurement. Once these corrections and other data manipulations were made, such as subtracting out the radiation heating from those sensors which measure both convective and radiative aerodynamic heating, the flight data were then compared with the predictions.

The flight data evaluation has revealed that on the ET nose cap, the flight data were higher than the predictions. This is because the predictions were based on laminar flow wind tunnel data whereas during flight the flow was turbulent. This was a very localized effect and the predictions were updated to reflect this higher testing.

For most of the Space Shuttle areas the flight data are in reasonable agreement with the predictions when they are based on the actual flown trajectory. This gives confidence in the calculation of the undisturbed heating and in the applicability of the wind tunnel derived interference factors. The design values, however, are significantly higher than the flight data. This is because worst-on-worst trajectory parameters were used in the design environments. Removing the undue conservatism caused by the worst-on-worst envelope approach is the biggest remaining challenge. New approaches using exact vehicle attitudes have been developed resulting in optimized environments when the upcoming operational flight design heating values are published.

CONCLUSIONS

The Space Shuttle Program provided the opportunity to develop a complex two-phase plume flow-field calculation which will contribute immeasurably to future predictions of plume radiative heating. Flight results revealed the combustion affects of TPS outgassing on the sea level plume radiation model. Also they provided corrections for altitude effects near sea level and effects of the shutdown spike at the end of SRM burn.

The plume convective methodology was generally validated with flight data. However, the preflight methodology overpredicted the plume heating at the upper exterior region of the Orbiter base heat shield during second stage. And it underpredicted the ET dome and outboard SRB skirt during the recirculation period at the end of first stage.

The aerodynamic heating predictions are in reasonable agreement with the flight data everywhere except the ET nose cap. There the measurement exceeded the prediction because of an assumed laminar flow for an actual turbulent flow environment. The design values greatly exceeded the measured flight values since a conservative dispersed trajectory was used for predicting the design heating environment. An exact vehicle attitude method will reduce the preflight envelope technique. Reduced trajectory dispersions and updated aerodynamic heating math models should lower the design operational values sufficiently to reduce the ET and SRB TPS requirements.

ACKNOWLEDGEMENTS

The authors wish to thank all the aerothermodynamic personnel who participated in the design and evaluation of the ascent heating environment; particularly those at Remtech, Inc., Lockheed Missiles and Space Co., of Huntsville, AL, Rockwell Ascent Heating Group and MSFC Thermal Environment Branch. Special thanks goes to Messrs. John D. Warmbrod, Dave Seymour and the late Mr. Robert R. Watanabe.

REFERENCES

1. Whitnah, A. M. and Hillje, E. R.: Space Shuttle Wind Tunnel Testing Program. Paper 82-0562, AIAA 12th Aerodynamic Testing Conference, Williamsburg, VA, March 22-24, 1982.
2. Greenwood, T. F., Seymour, D. C., and Bender, R. L.: Base Heating Prediction Methodology Use for the Space Shuttle. JANNAF 10th Plume Technology Meeting, Volume II, San Diego, CA, Sept. 13-15, 1977.
3. Kramer, O. G.: Evaluation of Thermal Radiation from the Titan III Solid Rocket Motor Exhaust Plumes. Paper 70-842, AIAA 5th Thermophysics Conference, Los Angeles, CA, July 1970.
4. Carter, R. E.: Space Shuttle SRB Plumes-Thermal Radiation Model. LMSC-HREC TR D568530, Lockheed Missiles & Space Co., Huntsville, AL, Dec. 1978.
5. Greenwood, T. F.: Improved SRM Plume Radiation Design Heating. NASA MSFC memo ED33-80-45, Nov. 6, 1980.
6. Lovin, J. K. and Lubkowitz, A. W.: User's Manual (RADFAC) A Radiation View Factor Digital Computer Program. LMSC-HREC TN D148620, Lockheed Missiles & Space Co., Huntsville, AL, Nov. 1969.
7. Watson, G. H. and Lee, A. L.: Thermal Radiation Model for Solid Rocket Plumes. Journal of Spacecraft and Rockets, Vol. 14, No. 11, Nov. 1977, pp. 641-647.
8. Carter, R. E. and Lee, A. L.: Space Shuttle SRB Plume Radiation Heating Rate Prediction with Altitude Corrections. LMSC-HREC TM D497262, Lockheed Missiles & Space Co., Huntsville, AL, Sept. 1977.
9. Reardon, J. E. and Lee, Y.: Space Shuttle Main Engine Plume Radiation Model. RTR 014-7, REMTECH, Inc., Huntsville, AL, Dec. 1978.
10. Greenwood, T. F., Lee, Y. C., Bender, R. L. and Carter, R. E.: Shuttle Base Heating. AIAA Paper 83-1544, Presented at the 18th Thermophysics Conference, Montreal, Quebec, Canada, June 1-3, 1983.
11. Greenwood, T. F. et, al.: Development of Space Shuttle Base Heating Methodology and Comparison with Flight Data. JANNAF 13th Plume Technology Meeting, Houston, TX, April 27-29, 1982.
12. NASA MSFC: Space Shuttle STS-1 Final Flight Evaluation Report: Volume II, Base Heating Section VI. July 22, 1981.
13. Greenwood, T. F.: STS-2 Flight Evaluation Report: Base Heating. NASA MSFC Memo ED33-82-3, Jan. 15, 1982.
14. Greenwood, T. F.: STS-3 Flight Evaluation Report: Base Heating. NASA MSFC Memo ED33-82-25, April 25, 1982.
15. Greenwood, T. F.: STS-4 Flight Evaluation Report: Base Heating. NASA MSFC Memo ED33-82-46, Aug. 10, 1982.
16. Greenwood, T. F.: STS-5 Flight Evaluation Report: Base Heating. NASA MSFC Memo ED33-82-65, Dec. 2, 1982.
17. Greenwood, T. F., Lee, Y. C., Bender, R. L. and Carter, R. E.: Calculation of Shuttle Base Heating Environments and Comparison with Flight Data. Langley Conference on Shuttle Performance: Lessons Learned, Langley Research Center, Hampton, VA, March 8-10, 1983.

D39

N85-16976

THERMAL DESIGN OF THE SPACE SHUTTLE SOLID ROCKET BOOSTER

Robert R. Fisher, Jerold L. Vaniman, and William J. Patterson
NASA/Marshall Space Flight Center
Marshall Space Flight Center, Alabama 35812

ABSTRACT

The challenge of designing reusable space transportation systems has resulted in defining new and unique requirements. These requirements led to development of new Thermal Protection Systems (TPS) to meet the quick turnaround and low cost required for reuse of the SRB hardware. The TPS development had to take into account the ease of application, changing ascent/reentry environments, and the problem of cleaning the residual insulation upon recovery. This development led to a sprayable ablator TPS material which was developed at the Marshall Space Flight Center (MSFC). This paper discusses the challenges that were involved in designing and development of this unique thermal system.

INTRODUCTION

During the early stage of the Solid Rocket Booster (SRB) design, thermal design environment data were not well developed. The initial low heating rates predicted indicated that a "heat sink" design approach would be feasible and that no thermal protection material would be required. The structural design approach of the external skin line was primarily to simplify manufacture. Examples of the structural design approach are shown in Figure 1 by the attach ring and kick ring protuberances, the protruding bolts in the nose cap, frustum, and aft skirt, and the externally milled-out forward skirt.

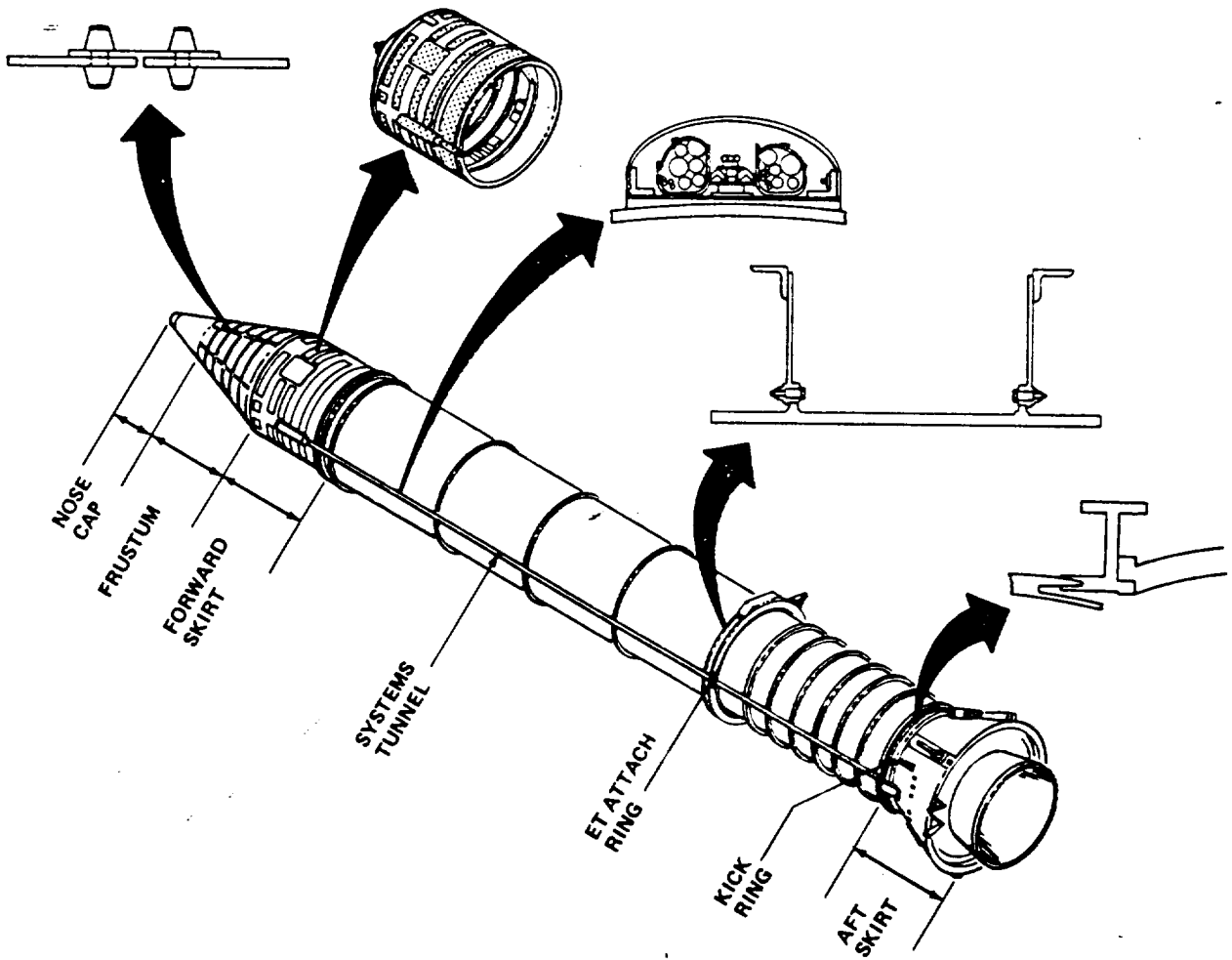


Figure 1. Sketch of SRB Showing Structural Elements.

As design trajectories changed and aerodynamic heating data from wind tunnel tests became available, the thermal design environment became much more severe, significantly increasing the predicted structural temperature levels. Maximum structural temperatures predicted for an uninsulated SRB are shown in Table 1. The allowable maximum temperatures for all SRB elements with the exception of the steel Solid Rocket Motor (SRM) case were exceeded, as shown by comparison to Table 2. Therefore, it was concluded that the "heat sink" approach was no longer feasible and that an external TPS would be required to maintain acceptable temperatures.

TABLE 1. MAXIMUM STRUCTURAL TEMPERATURES PREDICTED FOR AN UNINSULATED SRB

<u>SRB Element</u>	<u>Maximum Temperature Range</u>
Aluminum Structure	
o Nose Cap	310°F to 820°F
o Frustum	310°F to 460°F
o Forward Skirt	240°F to 500°F
o Systems Tunnel	410°F to 590°F
o Aft Skirt	295°F to 530°F
Steel Structure	
o ET/SRB Attach Ring	380°F to 700°F
o Kick Ring	425°F to 600°F
o SRM Case	140°F to 480°F

TABLE 2. SELECTED SRB THERMAL DESIGN LIMITS

<u>Component</u>	<u>Maximum Allowable Temperature</u>
o Reuseable Structure	
- Aluminum	300°F
- Steel	500°F
o Parachutes	200°F
o Electrical Wiring	200°F to 250°F
o Pyrotechnic Components	120°F to 250°F
o Sealant Material (Fastener and faying surfaces corrosion protection)	300°F
o Electronic Components	122°F to 185°F

TPS DEVELOPMENT CHALLENGE

The initial material under consideration was bonded cork, due to its availability and extensive prior use as an ablative insulation. However, it was recognized early in this program that the cork presented serious drawbacks from initial application time/cost and refurbishment for multi-flight use. The cork bonding process on major flight hardware structures is extremely labor intensive, resulting in significant cost penalties over a large number of vehicles. Also, the high density cork with its discreet layer of adhesive on the metallic substrate proved to be extremely difficult to remove during refurbishment studies.

Therefore, the initial challenge to the SRB project was the development/qualification of a primary TPS system for large acreage application (nose cap, frustum, and forward skirt). The drivers for this development were as follows:

- a. Thermal performance in 10 to 15 Btu/ft²-sec range.
- b. Low material density/high thermal efficiency.
- c. Low material cost.
- d. Applicable to spray processing utilizing robot technology.
- e. Compatible with the Environmental Protection Agency (EPA), Occupational Safety and Health Administration (OSHA), and Kennedy Space Center (KSC) facility restrictions.
- f. Spray/cure process relatively insensitive to environment variables.
- g. High material strength/damage tolerance.
- h. Ease of removal for refurbishment.

This rather formidable set of requirements was the focus of a large scale development activity by Materials and Processes Laboratory within MSFC. Following an intensive formulation screening and spray development phase, a system was chosen which utilized an aromatic, amine-cured, urethane-modified epoxy binder (or matrix resin) filled with glass and phenolic microballoons as well as glass reinforcing fibers. The system was demonstrated to be routinely sprayed in 1/4-in. thickness using chlorinated solvents as the spray carrier. The ablator composition, designated as Marshall Sprayable Ablator (MSA-1) is shown in Table 3.

The ablator is routinely sprayed in a spiral-wrap, continuous mode by robot manipulator and requires an elevated temperature cure of 150°F to 160°F for a 6-hr period. The cured MSA-1 material is characterized by properties as shown in Table 4.

TABLE 3. MSA-1 FORMULATION

Component	% By Weight
Phenolic Microballoons	37.7
Glass Microballoons	12.6
Chopped Glass Fibers (1/4 in.)	1.3
Milled Glass Fibers (1/16 in.)	3.1
Crest 7344 (Resin)	36.8
Crest 7119 (Catalyst)	5.1
Bentone 27 Clay	3.5
Ethanol (Bentone Activator)	-

Spray Solvents: 60/40 volume percent of methylene chloride to perchloroethylene

TABLE 4. MSA-1 CURED MATERIAL PROPERTIES

Flatwide tensile strength	80 to 100 psi at 75°F
Density	15 to 17 lbs/ft ³
Strain compatibility	1.6% at 75°F
Thermal conductivity	0.48 to 0.6 Btu-in/ft ² -hr-°F
Heat rate limit	10 to 15 Btu/ft ² -sec
Flammability	Self extinguishing on 1/8-in. Al substrate (NHB 8060.1)

THERMAL CHARACTERIZATION

Once the MSA-1 met the material requirements, thermal characterization was required for development of computer thermal models which could size the SRB TPS. The MSA-1 material performs as a charring ablator and, therefore, requires that the material ablation properties be determined, as well as the usual thermal properties of specific heat and thermal conductivity, etc. Thermal test facilities utilized for the MSA-1 thermal characterization were selected on their ability to simulate design thermal environment parameters such as heat rate, enthalpy levels, and aerodynamic shear forces. A Hot Gas Facility (HGF) was designed and built at MSFC for the purpose of screening candidate TPS and verifying design configurations. The von Karman Gas Dynamic Facility wind tunnel "C" at the Arnold Engineering and Development Center (AEDC), Tullahoma, Tennessee, was used extensively to obtain TPS thermal characterization data.

Flat panel specimens were prepared with the MSA-1 material sprayed on an aluminum substrate with the same surface finish as the SRB structure as shown on Figure 2. The panels were subjected to known heating rates for specific periods of time. The aluminum substrate temperature was monitored during the test and the MSA-1 material remaining after the test was measured. A typical post-test MSA-1 panel is shown in Figure 3. An ablation rate was determined by dividing the amount of material lost by the total test time. This type of data was obtained over the applicable heat range for the MSA-1, plotted and a nominal curve fit determined as shown on Figure 4. Thermal computer models were developed using the ablation rate curve. Effective MSA-1 material properties, such as ablation temperatures, heat capacitance, and thermal conduction values were adjusted in the computer models until the best correlation was obtained. With the thermal characteristics for the MSA-1 determined (Table 5), thermal models were developed to predict inflight structural temperatures with a specified thickness of MSA-1 material.

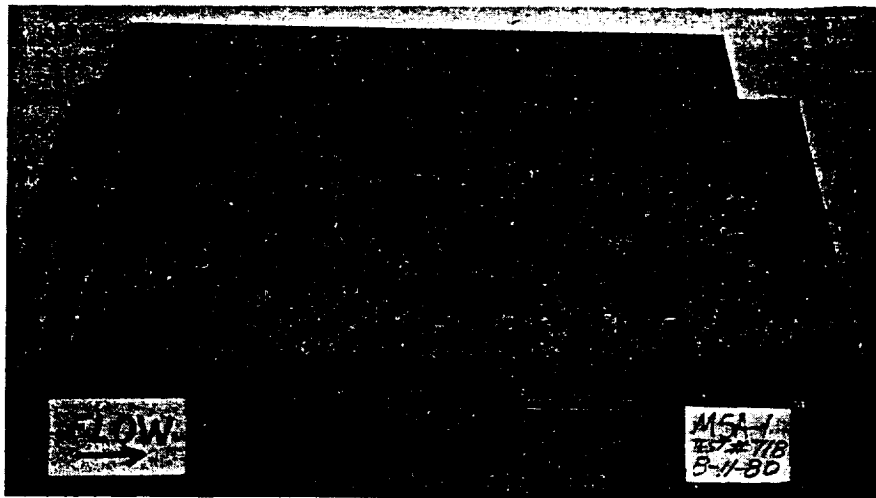


Figure 2. Pretest Photo of 1/4-in. Thick MSA-1 Panel to be Tested in Hot Gas Facility.

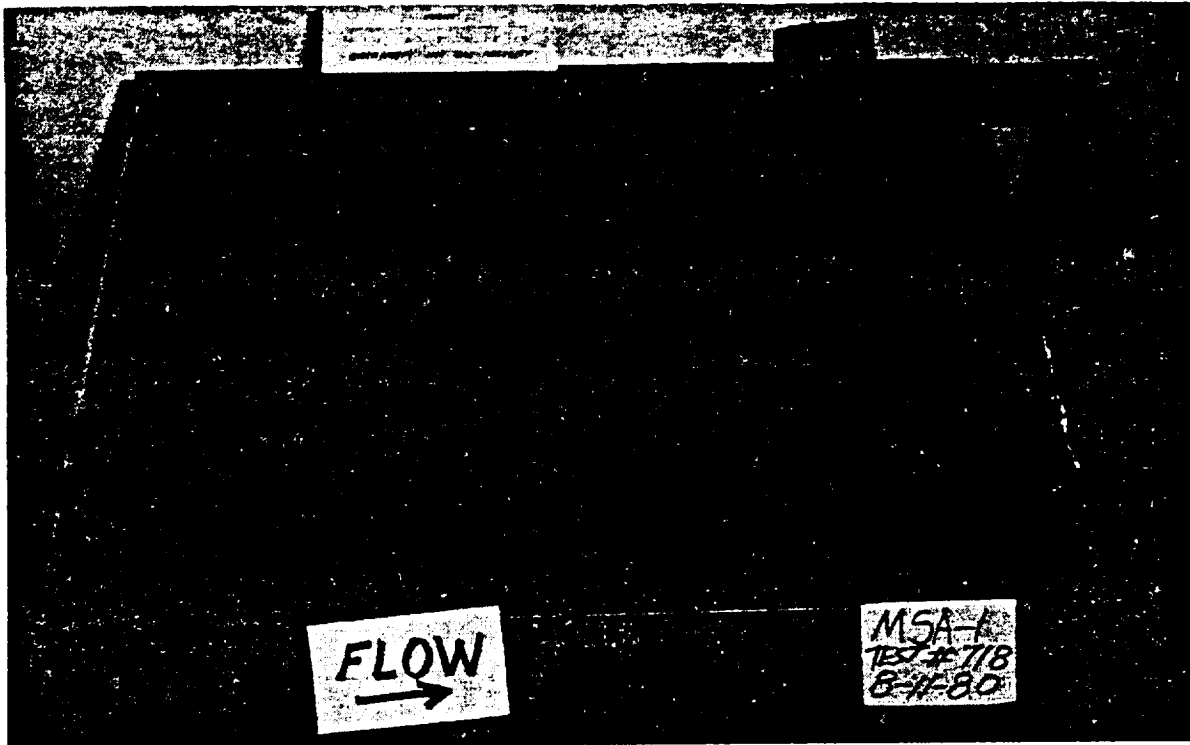


Figure 3. Post-Test Photo of 1/4-in. MSA-1 Panel Tested in Hot Gas Facility. Test Duration: 60 sec; Average Heating Rate: 13.5 Btu/ft²-sec (12 to 39 Btu/ft²-sec)

TABLE 5. MSA-1 THERMAL CHARACTERISTICS
USED IN COMPUTER MODEL

Parameter	Value
Density, lb/ft ³	16
Thermal Conductivity, Btu-in/ft ² -hr-°F	70°F to 600°F; 0.32 to 0.46
Specific Heat, Btu/lbm-°F	70°F to 600°F; 0.17 to 0.35
Recession Rate, mil/sec	0.0501 Q _{cw} ^{1.754}
Ablation Temperature, °F	620

Note: Q_{cw} = Cold Wall Heat Rate

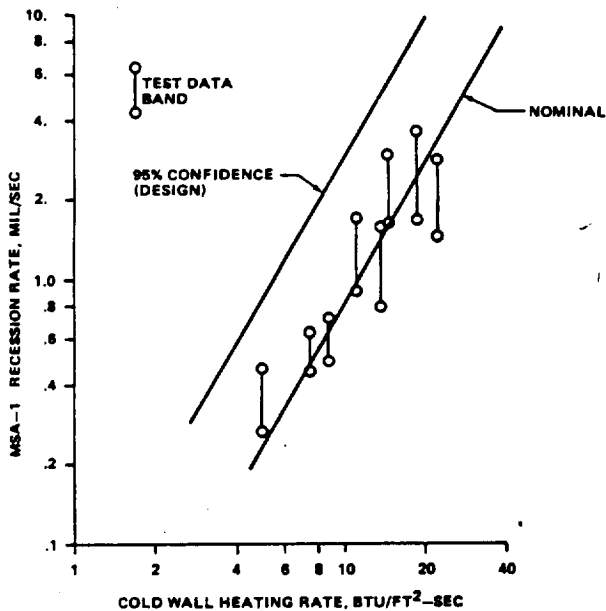


Figure 4. Recession Rate Versus Heating Rate for MSA-1 Panels Run at AEDC in Tunnel C.

TPS SIZING

After thermal computer models were developed, the next challenge was to size the TPS to the SRB. A 95 percentile deviation of the nominal ablation rate curve (Fig. 4) was used to size the MSA-1 thicknesses for the SRB structure. This conservative design approach ensures adequate thermal protection without undue weight penalty. A "design" heating environment, developed by perturbing trajectory parameters such as air density, vehicle angle of attack, wind direction, etc., was also utilized for sizing the TPS to cover "worst case" conditions. Aerodynamic heating rates vary at different locations on the SRB due to boundary layer growth, SRB configuration, influence of adjacent protuberances and influence of the adjacent External Tank (ET) and Orbiter. The aft areas of the SRBs are heated by radiation from its own SRM plume and from the Orbiter engine plumes. Thermal computer models were constructed for each SRB structural configuration requiring TPS and the appropriate heating environments for the ascent and descent portions of the flight imposed. Various MSA-1 thicknesses were then analysed at each location until one was found that would maintain the structure within the design temperature limits. Results of these analyses indicated MSA-1 material could furnish adequate thermal protection on the SRB nose cap, frustum, forward skirt, and a significant portion of the systems tunnel, as shown on Figure 5. However, the maximum sprayable thickness of MSA-1 was found to be limited to 1/4 in. to ensure consistent material characteristics. High heating rates on the aft attach ring, kick ring, aft portion of the systems tunnel and the aft skirt precluded utilization of MSA-1 on these structures due to thickness limitation, and/or low tolerance to airstream shear forces. Consequently, cork insulation was utilized on the aft skirt and local areas on the systems tunnel. However, phenolic glass fairings were selected to protect the aft attach ring and kick ring areas. This design was driven by the requirement for easy refurbishment, the ring structural configurations and the high (130 Btu/ft²-sec) Space Shuttle Main Engine (SSME) plume impingement heating during SRB separation. The SRB TPS is shown on Figure 6.

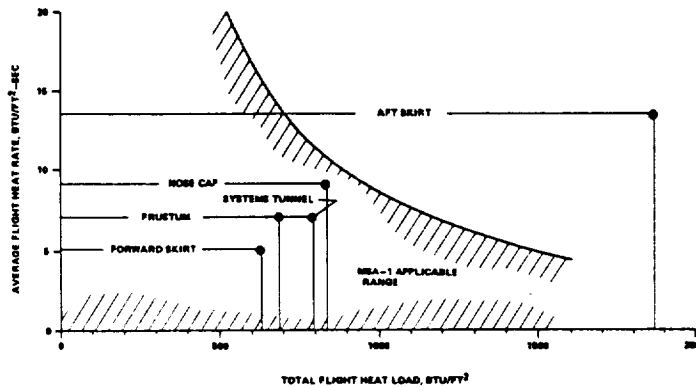


Figure 5. SRB Elements TPS Thermal Requirements Compared with the Thermal Capability of MSA-1.

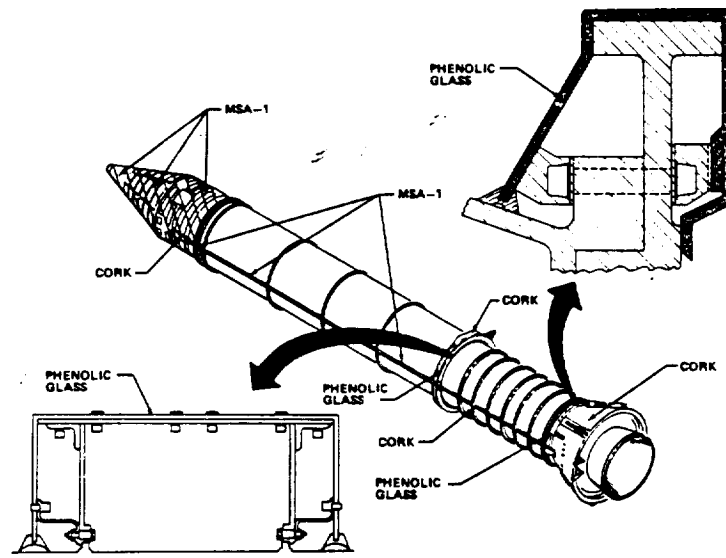


Figure 6. Sketch of SRB Showing TPS Utilized.

TPS VERIFICATION

OF HIGH QUALITY

After the MSA-1 had been analytically sized, verification tests were performed to verify the thermal and structural integrity of the baselined TPS to physically survive simulated flight pressure and thermal loads.

The philosophy used in planning the verification test conditions was:

- a. Utilize a heating rate representative of the average expected during ascent, staging, and descent.
- b. Select a test time adequate to produce the maximum predicted integrated flight heat load.
- c. Orientate the TPS test panel in the test facility such that the flight aerodynamic pressure loads can be simulated without compromising the average heating rate determined in (a) above.
- d. Provide a combined environments test to simulate heating simultaneously with structural and acoustic loads.

The success criteria established for the TPS verification tests were as follows:

- a. The predicted integrated flight heat load must be applied.
- b. The measured TPS recession rate must not exceed the 95 percentile design value.
- c. The substrate temperature must not exceed the maximum predicted flight temperature.
- d. The TPS must physically survive the combined imposed environments of thermal, shear, acoustic, and pressure loads.

After the TPS successfully completed the verification test phase, it was certified as flight-worthy, and requirements for the minimum thicknesses were specified to the designers. Actual TPS coverage on an SRB may be greater than analytically determined patterns because of the economics involved in TPS application.

The MSA-1 spray development optimization, accomplished at MSFC, allowed a technology transfer to KSC where the SRB prime contractor, United Space Boosters, Inc. (USBI), currently applies MSA-1 to all forward elements of SRB flight hardware (as well as to systems tunnel cover segments). Application of MSA-1 on the frustum is shown on Figure 7. This material has proven to be totally compatible with the

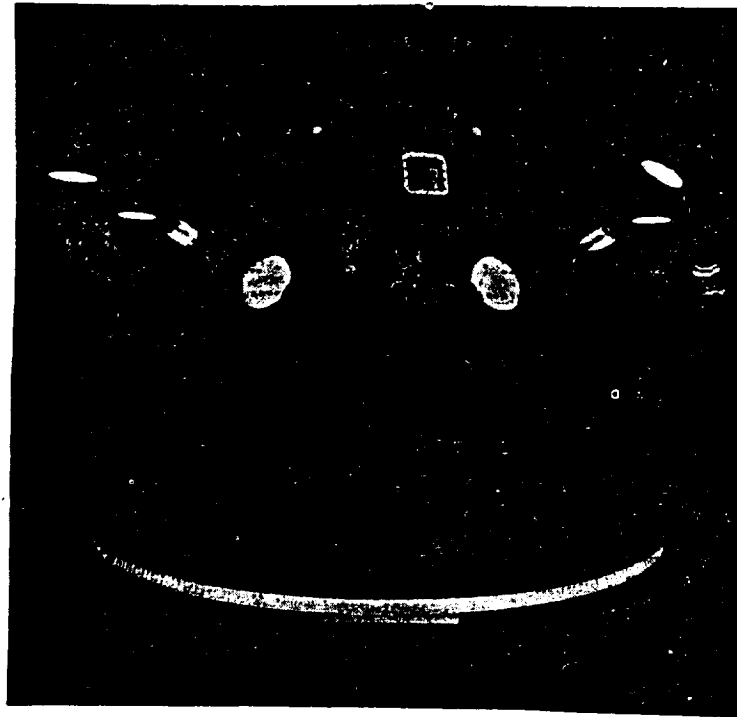


Figure 7. SRB Frustum with MSA-1 Applied.

ORIGINAL FACT IS OF POOR QUALITY

rigorous Florida EPA requirements and is applied in the vertical assembly building (VAB) low bay area with only modest temperature/humidity controls. The nonflammable spray solvents are compatible with the stringent VAB flammability requirements. The ease of removal of MSA-1 by high pressure water impingement (hydrolaser) has proven to be exceptionally valuable, since it allows rapid removal of material from a recovered structure and results in a residue-free surface without damaging the protective Bostik paint system on the aluminum. The cured MSA-1 is typically sprayed with a white hypalon-based topcoat (Fig. 8) to minimize moisture absorption.

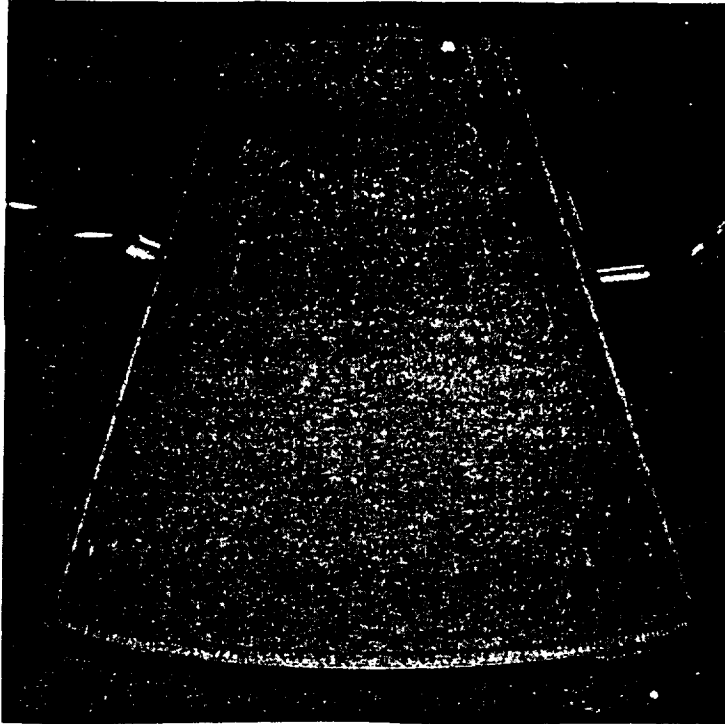


Figure 8. SRB Frustum with MSA-1 and Hypalon Paint Applied.

Replacement of the labor-intensive cork bonding operation by robotic spray application of MSA-1 results in a cost reduction of at least \$100,000 per shipset (based on two nose caps, two frustums, and two forward skirts). This estimate includes the significant savings realized in removal of MSA-1 versus cork on the forward skirts and frustums.

CONTINUING TPS CHALLENGES

Although MSA-1 has effectively met the challenges of cost and refurbishment for the nose cap, frustum, and forward skirt, the aft skirt still requires cork insulation. The thermal environments for this structure were predicted to be considerably above the performance range for MSA-1, considering its thickness limitation (1/4 in.). Considering the undesirable features of cork mentioned earlier, a second challenge was presented in the form of an improved ablation system which could accommodate greater application thicknesses to provide more thermal protection.

Thus, as soon as the MSA-1 optimization/qualification was completed, the development of a second generation sprayable ablator was undertaken to provide a system that could be sprayed in thicknesses up to 1/2 in. to replace cork on the clean-skin areas of the aft skirt. The MSA-2 development philosophy was based on minimizing the modification of MSA-1 formulation/processing to allow carryover of the maximum amount of MSA-1 experience and technology, as well as maintaining its favorable chemical and thermal properties. While the specific target for MSA-2 was to replace bonded cork on the aft skirt, it is currently planned to utilize MSA-2 as a single system for all SRB sprayed ablator requirements.

The original MSA-2 formulation development work involved screening several epoxy and modified epoxy resin binders, including conventional Epon 828 resin, rubber-modified 828, and phenolic-modified 828. As these formulations were screened by spraying 1/2 in. thick test panels, it became evident that curing stresses and shrinkage considerations would be the overriding factors in defining the formulation. A substantial effort was carried out to minimize cure stress, both from formulation ingredient selection

and application/cure parameters. As a result of this effort, the flexible epoxy resin EC-2216 (3M Company) was chosen as the binder, together with replacement of 15 percent by volume of phenolic microballoons (from the MSA-1 formulation) with ground cork. The cork particles provided additional stress relief in the matrix resin to minimize cracking/delamination. The final MSA-2 formulation is represented in Table 6. The sprayed formulation is typically applied to the substrate in two 1/4-in. layers, with up to 1 hr delay between applications. The current elevated temperature cure utilized for test panels is 150°F to 160°F for a 6-hr period.

TABLE 6. MSA-2 FORMULATION

Component	% By Weight
EC-2216 Resin/Catalyst	43.04
Ground Cork	3.12
Phenolic Microballoons	32.88
Glass Microballoons	12.89
Chopped Glass Fibers (1/4 in.)	1.29
Milled Glass Fibers (1/16 in.)	3.22
Bentone 27 Clay	3.55

(A small amount of ethyl alcohol is added to activate the Bentone for viscosity control.)

SPRAY SOLVENTS: 1/1 mixture of perchloroethylene and methylene chloride.

The cured ablator, MSA-2, is characterized by the properties as shown in Table 7. Recession rates for MSA-2 as a function of cold wall heating rate derived from TPS panels tested at AEDC are shown on Figure 9. The thermal evaluation performed to date on 1/2-in. thick MSA-2 panels has been quite successful, and this system potentially provides the means for replacing cork on the aft skirt as shown on Figure 10. The MSA-2 system appears, at this point in its development, to meet all the design challenges. The development/qualification schedule for MSA-2 calls for qualification testing and all-up spray verification to occur in late 1983 with implementation on SRB hardware by early 1984.

TABLE 7. MSA-2 CURED MATERIAL PROPERTIES

Flatwise tensile strength	60 to 80 psi at 75°F
Density	16 to 18 lbs/ft ³
Strain compatibility	1.4 to 1.6%
Thermal conductivity	0.4 to 0.5 Btu-in/ft ² -hr-°F
Heat rate limit	10 to 15 Btu/ft ² -sec
Flammability	Self extinguishing on 1/8-in. Al substrate (NHB 8060.1)

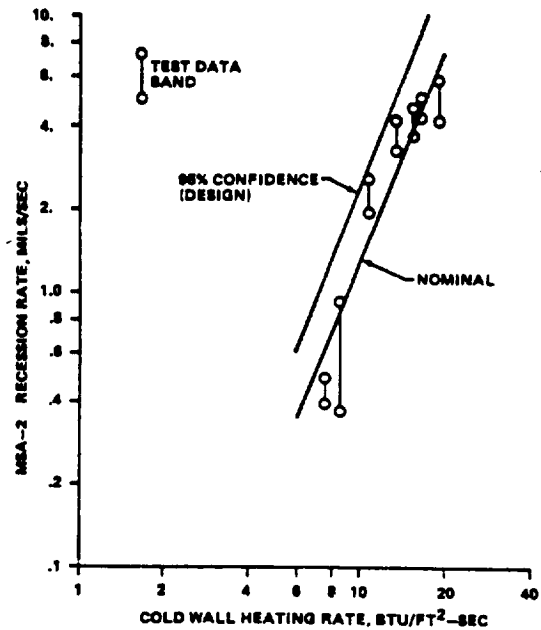


Figure 9. Recession rate versus heating rate for MSA-2 Panels Run at AEDC in Tunnel C.

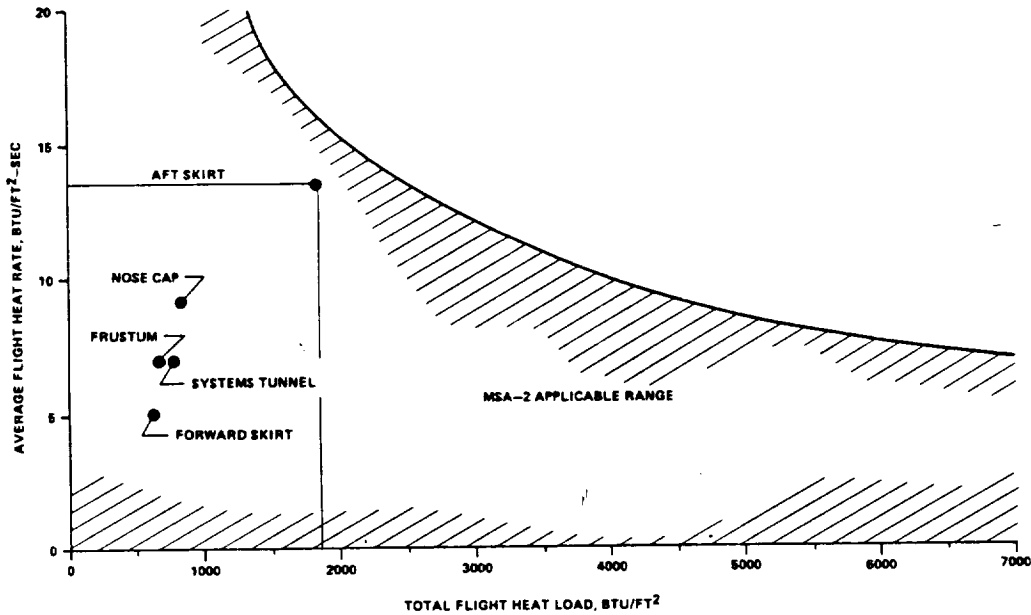


Figure 10. SRB Elements TPS Thermal Requirements Compared with the Thermal Capability of MSA-2.

The estimated cost reduction in replacing cork with MSA-2 on the aft skirt is at least \$50,000 per shipset (2 aft skirts). This estimate includes the significant cost savings in refurbishment for MSA-2 versus cork.

FLIGHT RESULTS AND FUTURE IMPROVEMENTS

The MSA-1 thermal protection material has been successfully flown on six Space Shuttle flights and has performed as expected. Temperature sensors were installed at selected locations on the SRB structure covered by MSA-1 and were recorded throughout flight. These temperature measurements correlated well with the predicted temperatures as shown on Figure 11. However, the flight trajectories flown to date have resulted in aerodynamic heating environments that are significantly less severe (>50%) than the design heating environment used to size the SRB TPS. Consequently, only limited MSA-1 ablation has occurred on the Space Shuttle flights to date. This has instigated a SRB TPS optimization study at MSFC with the goal to minimize SRB TPS requirements. It is believed that the current thermal design environments can be made more commensurate with planned flight thermal environments by revising the current methodology applied, and by incorporating new data obtained from flight and wind tunnel tests.

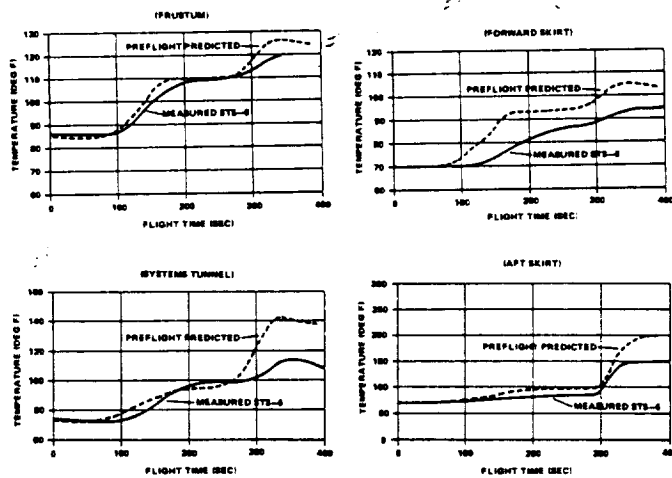


Figure 11. Typical SRB Structural Temperature Responses when Protected with MSA-1.

Changes in the ground rules for establishing SRB TPS are also being contemplated. The SRB TPS requirements were determined based on a design heating environment with the structural constraint being reusability. However, the design environment would seldom be encountered during an actual flight. Therefore, TPS reductions on the SRB should be possible if the TPS requirements for reusability were based on a "nominal" heating environment and the design thermal environment considered only for the ascent portion of flight to assure SRB structural integrity. If a design heating level was encountered, Space Shuttle safety would not be compromised, but the SRB reusability would have to be evaluated.

Studies are also in progress to simplify TPS closeout and installation on the SRB systems tunnel and the aft attach ring areas. The attach ring structural configuration modification being pursued is to change the angle stiffener at the edge of the ring to a flat ring stiffener. This change will significantly reduce aerodynamic heating effects as it will eliminate the small radius angle edge projecting into the airstream. Flight experience has also enabled a significant reduction in the design SSME plume impingement heating rates that occur during SRB separation. However, the sealant material on the ring fasteners will still have to be thermally protected or a new sealant material selected that will survive temperatures in the neighborhood of 500°F to 600°F. The systems tunnel configuration currently used requires a significant amount of time to close out the gap between the systems tunnel fairing and the tunnel floor plate. This precludes hot gas (high temperature boundary layer air) intrusion which would damage electrical wiring and could auto-ignite the range safety linear shaped charge housed within the fairing. This closeout is required after the SRB's are stacked on the Mobile Launch Platform (MLP), and has a direct impact on the launch turnaround time. An entirely new systems tunnel design is being evaluated that would significantly reduce the TPS closeout time on the MLP.

SUMMARY

The challenge of effectively providing thermal protection for the SRB has been accomplished. A TPS material, MSA-1, has been developed at MSFC and flown successfully on six Space Shuttle flights. However, cork insulation is currently being flown on the aft skirt because the thermal environments are considerably above the performance range for MSA-1, considering its thickness limitation of 1/4 in. Application/refurbishment costs of this cork is not cost effective. Consequently, development of a second generation sprayable ablator, MSA-2, is underway at MSFC to furnish an economical replacement for the cork. Results of thermal tests performed to date on 1/2-in. thick MSA-2 panels have met all expectations. The development/qualification schedule for MSA-2 calls for qualification testing and all-up spray verification to occur in late 1983 with implementation on SRB hardware by early 1984.

Flight experience, wind tunnel thermal data, and thermal protection material improvements are continuing to be utilized at MSFC to make the SRB TPS more efficient and economical. Structural configuration changes for the aft attach ring and systems tunnel are also being pursued to further simplify/eliminate SRB TPS requirements. Consequently, challenges still exist to establish a thermal protection system for the SRB that can truly be considered as operational.

REFERENCES

1. "Space Shuttle Aerodynamic Heating Data Book," Shuttle Vehicle Booster-Ascent - Volume III, SD73-SH-0180-3A, September 1978.
2. "Preliminary Shuttle Operational Flight Environments - SSME Plume Impingement to SRB's During Staging," ED33-83-2, January 12, 1983.
3. "SRB Reentry Thermal Environment Data Book," SE-019-053-2H, Rev. C, August 1981. Part 1 of 3, Part 3 of 3 and Appendix C.
4. "Space Shuttle Program Thermal Interfaces Design Data Book." SD74-SH-0144D, December 1977.
5. "Natural Environments for the Space Shuttle Solid Rocket Motor Booster," SE-019-043-2H, May 1975.
6. "SRB Thermal Design Data Book," SE-019-068-2H, April 1976.
7. "Tests to Evaluate an Expediting Technique for Postflight Refurbishment of SRB TPS," EP44(82-71), July 1982.
8. "Data Report for MSA-2 Development Tests," EP44(82-72), July 1982.
9. "SRB TPS Aeroheating Test Data Assessment," EP44(83-77), May 1983.

10. "SRB Materials Test and Evaluate in NASA-MSFC Hot Gas Facility, NASA-Ames 36 Foot HWT and AEDC Tunnel C," LMSC-HREC TMD 497497, November 1977.
11. "SRB TPS Verification Test Report," SE-019-186-2H, January 1981.
12. Vaniman, J., Fisher, R., Wojciechowski, and Dean, W.: "Ablative Thermal Protection System," presented at the International Conference on High Temperature Corrosion, March 2-6, 1981.
13. Solid Rocket Motor Thermal Protection System Materials Processing and Refurbishment Data Transfer Document, NASA IN-EH-77-01, 1977.
14. Patterson, W. J.: Strain Compatibility Assessment for SRB Sprayable Ablator MSA-1, NASA TM-78228, 1979.

THERMAL DESIGN OF THE SPACE SHUTTLE EXTERNAL TANK

Frederick D. Bachtel, Jerold L. Vaniman, and Dr. James M. Stuckey
NASA/Marshall Space Flight Center
Marshall Space Flight Center, AL 35812

Carroll Gray and Bernard Widofsky
Martin Marietta Corporation, Michoud Operations
New Orleans, LA

ABSTRACT

The Shuttle External Tank thermal design presented many challenges to NASA and the aerospace industry in meeting the stringent requirements established by the structures, main propulsion systems, and Orbiter elements. The selected thermal protection design had to meet these requirements, as well as take into account ease of application, suitability for mass production considering low weight, cost, and high reliability. This development led to a spray-on-foam (SOFI) which covers the entire tank. This paper discusses the need and design for a SOFI material having a dual role of cryogenic insulation and ablator, and the development of the SOFI over SLA concept for high heating areas. Further issues of minimum surface ice/frost, no debris, and the development of the TPS spray process considering the required quality and process control are discussed.

INTRODUCTION

The External Tank (ET) is the largest of the Space Shuttle Vehicle elements and serves as the fuel tank for the liquid oxygen (LO_2) and liquid hydrogen (LH_2) propellants used by the Orbiter's three main engines. Since both of the propellants are cryogenic (LO_2 at $-297^\circ F$ and LH_2 at $-423^\circ F$) the Thermal Protection System (TPS) for the ET must function as a cryogenic insulation to limit propellant boiloff and thus maintain the propellant quality. Furthermore, during ascent the ET experiences heating from aerodynamic and plume sources which requires the TPS to also function as an ablator providing protection against structural overheating. The challenge to the ET designers was: provide a low cost, lightweight, and reliable TPS, capable of providing the required protection while maintaining its integrity over the wide range of operating temperatures.

INITIAL ET TPS CONCEPT

Although the current ET design is much the same as the design which existed at the inception of the ET program in 1972, there has been a significant TPS design evolution driven by both changes in requirements and the design maturing. The ET with the initial TPS design as it existed in 1972 is shown in Figure 1. The ET consists of an ogive-shaped LO_2 tank with attached nose cap and a larger LH_2 tank supporting the orbiter and the SRBs. An intertank structure connects the two propellant tanks and reacts the SRB thrust load. Both the intertank and the nose cap form separate compartments which contain various electrical and propulsion components. Exterior to the tank are a multitude of protuberances on an otherwise smooth configuration - propellant lines, cable trays, and interface structural members.

The initial TPS design shown in Figure 1 consisted of BX-250 spray-on foam insulation (SOFI) on most of the LH_2 tank and an ablator, SLA-561s, on high heating areas of the LO_2 tank, the Intertank, and the LH_2 aft dome. Although these materials had been used on previous programs, both were being utilized in a novel way on the ET program.

BX-250 is a low density SOFI (2.0 pcf density) which was used on the Saturn S-II stage and also commercially as a cryogenic insulation. This material is a rigid closed cell polyurethane foam which has excellent insulation qualities at low temperatures. Therefore it is possible to limit the heat transfer through the insulation (and ultimately into the propellant) with a minimum of foam thickness. BX-250 was applied to the entire LH_2 tank (except the aft dome) to control boiloff of the super-cold LH_2 and to prevent the formation and runoff of liquid air. SOFI materials of this type are generally not thought of as being capable of withstanding the high temperatures expected from aerodynamic heating. For example, BX-250 begins to decompose at $255^\circ F$ whereas the insulation surface temperatures could be expected to reach $1500^\circ F$ or higher during ascent. Early testing of BX-250 however, showed that it responded favorably to moderate heating rates, and acted similar to an ablator, providing limited protection from ascent heating.

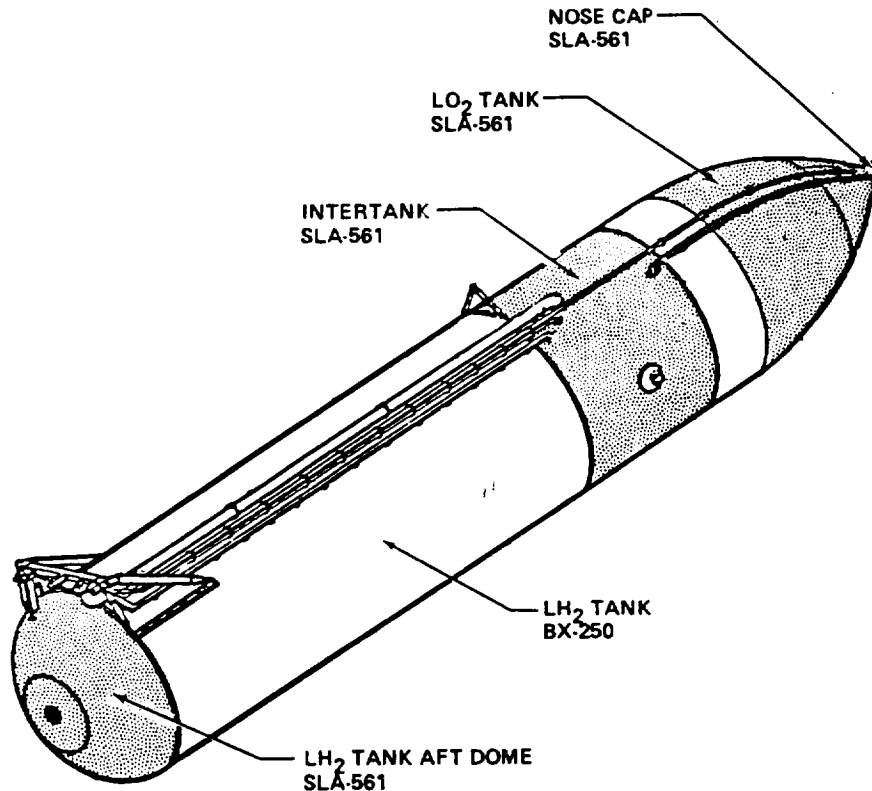


Figure 1. Initial ET TPS Configuration.

An "ablator" is a material which is designed specifically to withstand high temperatures through controlled sacrificial degradation (energy absorption) and is traditionally used in areas which require protection from high ascent or re-entry heating. Ablators can thus withstand significantly higher heating rates than foams, however, ablators are heavy and do not provide the same degree of cryogenic insulation properties. The ablator selected for the ET was sprayed SLA-561 (16 pcf density), a derivative of the light weight ablator developed on the Viking Project.

Prior to the ET program, whenever protection of cryogenic surfaces was involved, ablators were generally applied to separately attached heat shields or standoff panels. This was due in part to the implied problems of strain compatibilities between the substrate and the ablator material when subjected to cryogenic temperatures. The Martin Marietta Corp., recognizing the cost and weight advantage of applying an ablator directly to the cryogenic substrate, performed a feasibility program to develop this type system with SLA561. Based on the successful results of this study, the application of SLA561 directly to the LO₂ and LH₂ tanks was baselined initially and maintained to the current design.

Therefore the early design philosophy for the ET TPS was to utilize the capability of the SOFI wherever possible, supplementing with an ablator applied directly to the cryogenic tank wall. Although this was later impacted by an increase in the predicted ascent heating environments, this novel approach - using a foam insulation as both a cryogenic insulation and an ablator - continued throughout the program.

CHALLENGES IN THE TPS DEVELOPMENT

Since the ET is not reusable (discarded just prior to orbit) the total program cost of the ET is sensitive to recurring (per vehicle) costs, which of course is affected by TPS related labor and material costs. In addition, TPS contributes a small but significant part of the ET weight. The original thermal requirements imposed on the ET TPS design did not present significant challenges per se, since there were state-of-the-art TPS materials and techniques available; however, the weight and cost impacts would have been high. The challenge was to use the existing materials or their derivatives in new ways to develop a highly efficient, lightweight, and low cost system which would be consistent with a mass produced disposable vehicle such as the ET while maintaining the quality and reliability which is required of spacecraft design.

TPS MATERIALS

The first key to an efficient TPS was the use of a SOFI in a dual role of cryogenic insulator and ablator as discussed earlier. Shortly into the program, however, increases in predicted ascent heating quickly exceeded the capability of the original SOFI (BX-250) and the system became unable to accommodate the new environment without a major increase in the use of the SLA-561 ablator. A new urethane modified isocyanurate foam material (CPR-421) was selected to replace the BX-250 foam and concurrently reduce the quantity of SLA-561 required. This new material (selected from commercially available "high temperature" foams) possessed the required ablation characteristics and was compatible with the as-designed production concepts. This material was not flight qualified however and tighter control on processing parameters would be necessary to assure the desired material properties. It should be noted that this material was to be used in an environment unlike any previous commercial use and required considerably greater quality control than in previous applications. Material properties such as consistent density, bondline strength, tensile strength, and ablation characteristics were imperative for success on the ET whereas its low conductivity and durability were always important in commercial uses. Therefore, a complete development and verification program was initiated to characterize this "off the shelf" product. Early in this development program, the material was reformulated as CPR-488 to enhance its ablation characteristics and eliminate any toxic concerns.

A light-weight ablator capable of being applied directly to the cryogenic tank surface was the second key to an efficient TPS. Beginning with the baseline sprayed version, the ET SLA development extended to the installation options of mold-in-place, premold-and-bond, and hand packed in place, each tailored to suit design and production needs. However as the ablator thickness was later increased in response to growing ascent heat loads, problems began to appear with bondline integrity. This led to a substantial analytical and test effort to understand and characterize the stress relationships between the ablator and the substrate at cryogenic temperatures. Because of the inherent variability of material properties in composite mixtures and the low margin in the SLA561 bondline strength at flight conditions, the challenge was to control processing parameters and thus material properties to maintain a positive margin.

ICE/FROST AND DEBRIS REQUIREMENTS

The problem of ice forming on the ET cold surfaces during loading operations and then dislodging during ascent and damaging some other portion of the vehicle was recognized initially as a potential issue. However, no attempt was made in the design to preclude ice until later in the program when a "no ice/debris" requirement was imposed. At that time the LO₂ barrel was bare and was thus a large potential area for ice formation.

Icing on the general tank acreage was eliminated by adding an appropriate layer of SOFI, with the associated weight impact. The prevention of ice at the numerous protuberance areas however was a much more difficult design problem since these areas typically involved movable joints which are difficult to insulate. In addition, SOFI and ablator stress cracking, SOFI divots due to cryopumping, and other minor TPS discontinuities or anomalies which had previously been tolerated now could be a source of ice and/or TPS debris which had to be addressed. The challenge of preventing ice and TPS debris was compounded by the fact that most of the vehicle and ground systems had already been designed.

ET TPS DESIGN

Today's TPS design, although greatly evolved from the original concept, still adheres to the basic design philosophies of a SOFI and ablator system. Because of increased heating environments and the requirement to preclude ice formations on the tank, 1 in. or more of SOFI is now specified for all cryogenic surfaces. In those local areas where the capability of the SOFI is exceeded (generally near and around protuberances) an underlayer of ablator is retained. The latest ET TPS design showing the areas of SOFI and ablator coverage as well as other TPS elements is shown in Figure 2. The majority of the ET TPS is CPR488 SOFI, used on all exterior acreage except the aft dome. Ancillary to this, urethane foams (BX-250 or PDL-4034) are used for closeouts, ramps, and the domes within the intertank due to these foams' liberal application parameters. Another commercially available polyisocyanurate SOFI, modified for ET use (NCFI 22-65) was selected for the LH₂ aft dome where the high plume heating rates exceeded the capability of CPR488.

The ET TPS uses two ablator materials. SLA-561 is for primary use on the general acreage under the SOFI and most attachments, and MA25s is used on a few select protuberances which experience heating in excess of the capability of SLA-561.

The SOFI design thicknesses are basically defined by prelaunch requirements where maintaining good quality and stable propellants and minimizing ice are the primary considerations. A low heat transfer rate through the insulation is desired to maintain the insulation surface temperature above freezing (to preclude icing) and to limit propellant boiloff. Figure 3 shows propellant boiloff rate and a

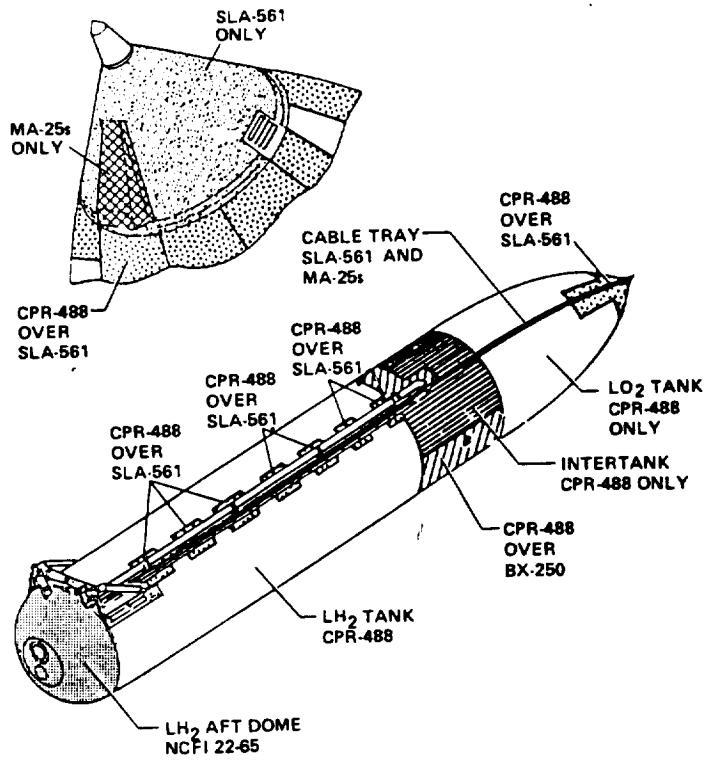


Figure 2. TPS Configuration.

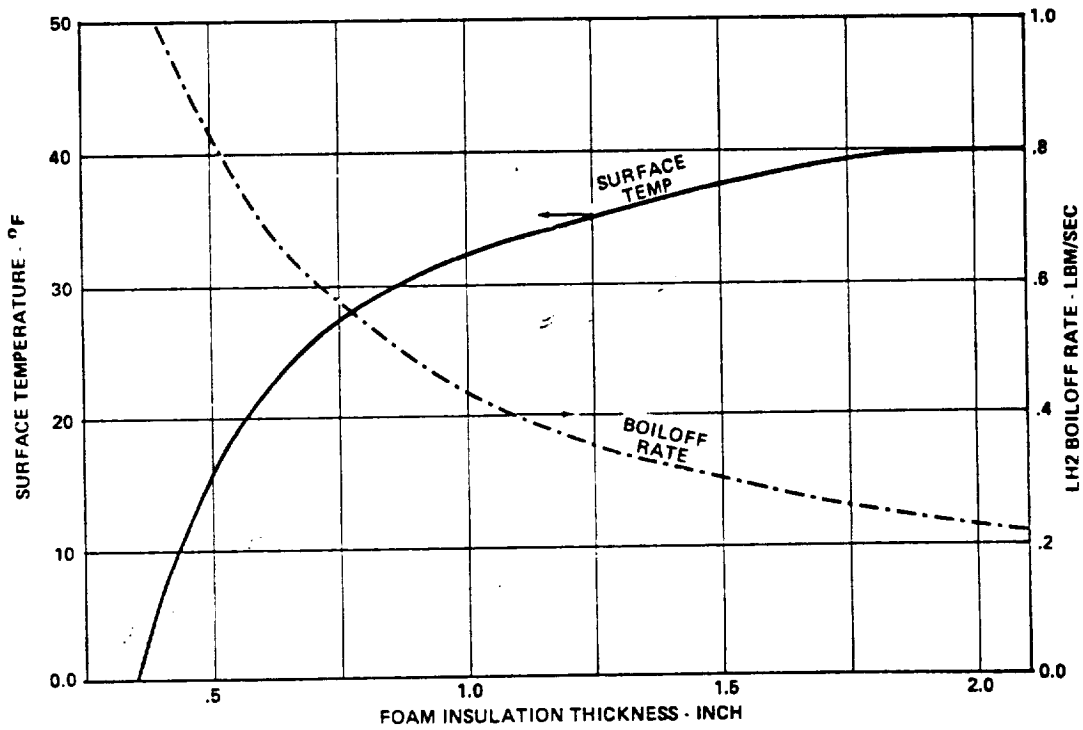


Figure 3. Typical Foam Insulation Performance.

typical surface temperature versus CPR-488 SOFI thickness for the LH₂ tank. The surface temperature is based on a set of combined ambient environments (i.e., wind, temperature, humidity, etc.) which represent the 95% cold conditions at KSC. As seen from this data, a 1-in. thickness of SOFI is very effective in limiting propellant boiloff and maintaining a surface temperature close to ambient (ambient is 55°F for this case). Increasing the thickness above 1 in. provides minimal improvement considering the corresponding weight increase. Therefore, a 1-in. thickness of SOFI was selected for the LH₂ and LO₂ tank acreages.

The ascent environments primarily define the ablator thicknesses and the thickness of the SOFI on the LH₂ tank aft dome. Maintaining the primary structure and subsystem components within the design temperature limits and minimizing unusable propellants due to stratification are the primary considerations. The thermal environments considered include: aerodynamic heating, radiant and convective heating from the engine exhaust plumes, SRB separation motor plume impingements, radiative and conductive transfer with the other elements of the Shuttle vehicle, and internal heating due to the autogenous tank pressurization gas. The TPS requirements were determined analytically based on these environments and material properties derived from test data.

Another function of the TPS occurs during ET entry when structural temperatures and tank pressures contribute to the ET fragmentation and the subsequent debris size and impact footprint. Except for some sections of the cable tray where MA25s ablator was added to protect RSS charges, the TPS defined by ascent requirements is adequate to meet entry requirements.

Other elements related to the thermal design of the ET include thermal isolators on LH₂ tank attachments, cryopumped propulsion lines, electrical heaters primarily for ice/frost protection, and several heated purge systems for compartment conditioning and also for ice/frost protection. The icing problem at the several brackets and attachments which penetrate the general acreage SOFI was eliminated by various combinations of insulation, isolators, heaters and purges.

TPS DEVELOPMENT AND VERIFICATION

The development and design verification effort for the ET TPS involved many activities ranging from material ablation testing to development of manufacturing techniques. All of these efforts can not be addressed adequately in a paper of this scope, therefore the following is an overview of the more important and unique aspects of this effort.

PROCESS DEVELOPMENT

As discussed earlier, the original SOFI, BX-250 was replaced by a new material CPR-421 which was subsequently reformulated as CPR-488. Results from the CPR-488 development program revealed that the critical materials properties required by the flight mechanical and thermal loads were predominantly influenced by applications processing parameters. Systematic material evaluations were undertaken to develop the acceptable ranges of critical processing conditions. It was determined that material temperatures at application had to be controlled to near 135°F and tank substrate temperatures to 140°F. The spray envelope of ambient temperature and relative humidity was also found to be more restricted than the conventional BX-250 foam as shown in Figure 4. In addition, spray overlap time and gun-to-tank separation distance was also found to be critical and needed proper controls.

With these very restrictive processing controls in place, critical material performance parameters, including structural strain compatibility, insulation efficiency, and ablation rates, were all consistent and repeatable.

The SLA-561 ablator material exists in three application modes; bonded premolded panels, a sprayable mix for large or complex surfaces, and a trowelable version for small closeouts and repairs. The primary focus of the development program was to develop a process for the sprayable ablator material which yielded repeatable physical properties of strength and density. Systematic material evaluations determined the need to seal the surfaces of the cork filler particles to minimize the absorption and subsequent retention of the spray solvent. The retention of this solvent was found to inhibit the cure of the silicone resin binder with resultant large variations in material properties. A cork coating process utilizing an epoxy resin was developed to control the solvent absorption and provide the required consistency in materials properties.

MANUFACTURING AND QUALITY CONTROL

The key to meeting high volume production, schedule, and budget constraints was to facilitate for critical TPS manufacturing operations using automated techniques in large environmentally-controlled TPS application cells. The two-component SOFI is sprayed using totally automated apparatus, where a

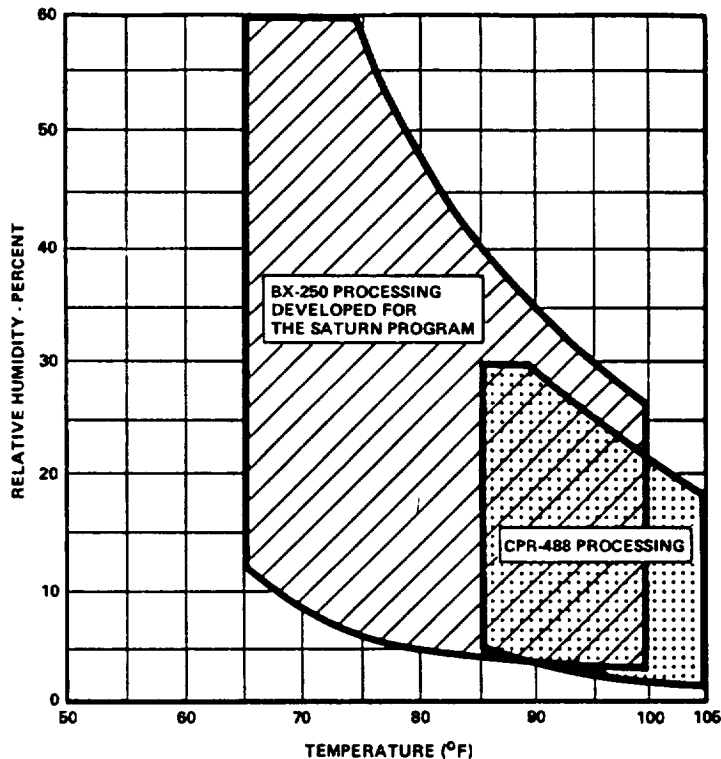


Figure 4. Temperature Versus Relative Humidity Requirements.

computer system is employed to control and monitor spray applications to the LH₂ tank and the LO₂/IT subassembly. All parameters during production runs are controlled and recorded throughout the spray operation. Each tank is coated as a single unit on a large rotating turntable. Spraying begins at the bottom and the gun carriage progresses upward at a predetermined rate to produce a uniform foam thickness of shingled layers. This technique with tight control on the processing parameters enables the system to produce a finished product on one pass with no machining of the "net sprayed" surface required afterward.

In acreage applications, SLA ablator is premolded to required thickness, cured, and then bonded to the tank using vacuum bagging techniques since this pliant material conforms to the large curvature. In complex configuration/large applications, such as the nose cap and the crossbeam, the SLA, thinned to a slurry with solvent, is hand sprayed, heat cured, and trimmed. Small complex components such as cable tray brackets have mole-in-place SLA applied.

Quality control for both SOFI and ablator application is effected by inspections, testings, and process control starting with material receiving and continuing through application to the tank. In the case of automated processes, all parameters are recorded and the process is automatically aborted if parameters are out of range. For material formulation and applications, witness coupons are simultaneously produced and later tested for certain key properties. Selected post-manufacturing tests including TPS plug pulls and an adhesive plough test are also performed at selected tank locations.

The most critical defect which must be controlled and is also difficult to detect, is a weak TPS bondline. This type of defect typically manifests itself only under loaded cryogenic conditions at which time the TPS may debond. Therefore, the first several tanks produced have had a cryogenic "TPS proof test" performed at KSC, which is basically a propellant loading test designed to load the TPS above flight loads. The successful results from these tests have verified the quality and process controls currently in place, and the "TPS proof test" are to be discontinued.

TPS STRUCTURAL CONSIDERATIONS

The ablator material, which is an elastomer at room temperature undergoes a change of state at approximately -180°F and becomes brittle due to the silicone resin binder passing through the brittle transition temperature. In this state the strain capability of the ablator is limited and excess loads,

particularly in thick layers undergoing flexure, may cause the material to crack and ultimately debond. During the ET design phase, the predicted heating environments increased significantly driving the program to ablator thickness in excess of 0.75 in. under which the induced loads were near the strain capability of the material with little margin remaining. To regain an acceptable TPS structural margin, a re-ordering of the launch procedures was implemented to take advantage of the change in the ablator's properties with temperature.

Normally the ET is loaded with little or no ullage pressure in the tanks. The tanks are then subsequently pressurized for launch and ascent to meet structural and propellant delivery requirements. The two primary loads applied to the ablator are due to the cryogenic chilldown of the tank (thermal strain) and to the internal tank pressure (substrate strain). It was shown analytically (and by test) that if the strain due to tank pressurization is applied prior to loading when the ablator is near room temperature, rather than after loading when the ablator is at cryogenic temperatures, that the resultant ablator structural margin is increased. This is because the final stress in the ablator is dependent on the temperature varying material properties that exist when the loads are applied. Therefore, the current propellant loading procedure for the ET LH₂ tank is to pressurize prior to loading. This provides an increase in TPS margin at the expense of a longer propellant loading timeline. Reductions in ablator coverage since the first vehicle have lessened the need for this procedure, and continuing efforts to reduce ablator application will hopefully eliminate the need altogether.

ET TPS ABLATION TESTING

Design and testing of ablative heat shields for spacecraft had traditionally been performed by testing materials in plasma arc facilities and correlating the erosion and pyrolysis reactions with kinetic chemical reactions in complex computer programs. This technique was necessary because most applications involved subjecting materials to the wide range of environments associated with re-entry or ballistic applications which did not always match the test (plasma arc) environment. Although this approach was used in the initial ET design phase it was subsequently replaced with a simpler semi-empirical design method.

The most significant difference between the ET program and other programs was that the primary ET TPS material was an extremely low density polyurethane foam rather than the normal higher density ablators. The foam recession appeared to be more of a char erosion process than actual ablation. In addition facilities and techniques were used which allowed TPS testing in environments which closely approximated those expected during flight.

The von Karman Gas Dynamic Facility's tunnel "C" at the Arnold Engineering and Development Center (AEDC) was selected to characterize the ET TPS as an alternative to plasma arc testing. This facility was chosen because it had the capability of matching flight recovery temperature and had a flow field which could produce turbulent flow heating and shear conditions over the range of flight environments. It was also capable of testing large samples (17 x 24 in. versus 6 x 6 in. for plasma arc) and had multiple test specimen capability.

Ablation test data obtained from this facility was correlated with test conditions and an empirical relationship established between material recession rate and heating rate. This relationship was then used with the predicted flight heating profile to perform the flight erosion analysis. This simplified technique (rather than the previously mentioned complex computer programs) was possible due to the close approximation of the test to flight environment offered by this facility.

When the design environments were increased, however, the AEDC facility could not produce turbulent heating at levels as high as required, particularly for ablator testing. The AMES 3.5 ft hypersonic wind tunnel with the Mach 7 nozzle was selected for TPS testing since it could achieve the higher environments and offered most of the same desirable aspects as the AEDC facility. Tests in the Ames facility provided the ablation data at the higher heating rates, and also duplicated and provided confidence in the AEDC simulation.

TPS testing in these facilities also included tests with simulated interference heating. This was accomplished by generating shock waves which were allowed to impinge on the TPS sample. Another approach used was to include a protuberance directly on the TPS sample. The heating rates obtained in these tests, however, were often too high to test SOFI materials due to the inherent tunnel conditions (Mach numbers of 7 and 10 as compared to 4 in flight). Lower heating rates could only be obtained with flat plate (shockless) testing although in many cases they represented an interference heating area on the ET. This presented a design concern, since the flat plate type testing was not representative of these special design cases, and because of this a substantial design margin was used for TPS sizing.

In early 1981, AEDC modified the Tunnel "C" facility with the addition of a Mach 4 nozzle. No facility previously existed at Mach 4 with corresponding total temperature and heating rate capabilities.

Test hardware was developed and calibrated to obtain the shock impingement environments in a flow field duplicating the flight environments at the lower heating rates needed for SOFI testing. Results of tests on the SOFI materials have provided the data and confidence to further utilize the ablative capabilities of CPR-488 with a subsequent substantial reduction of ablator coverage required on the ET.

Testing techniques are currently being developed to further reduce the ablator coverage on the ET. The technique involves a specimen design which will form an extension of the Mach 4 nozzle and take advantage of the relatively thick boundary layer in the nozzle (as compared to testing on a wedge shaped holder in the stream centerline). Specimens simulating the ice/frost ramps on the hydrogen tank at the cable tray/barry mount locations will be tested to demonstrate that the protection provided by the ramps is sufficient to virtually eliminate ablator coverage on the hydrogen tank at the attachment region of these brackets.

TPS VERIFICATION TESTING

The verification test program for the ET TPS included the wind tunnel tests discussed above together with several cryogenic, radiant heating, and combined environment tests. These tests were designed to verify the TPS integrity under the various predicted flight induced environments. There was no one test (other than flight) which simulated all of the pertinent flight parameters. Confidence in the TPS system was achieved by the successful results of these tests taken together.

Minitank tests were used to evaluate TPS cryo-strain compatibility, primer and TPS adhesion, and TPS cracking and susceptibility to cryopumping. The minitanks were 3-ft diameter aluminum tanks with TPS applied and were tested under repeated cryogenic fill, drain and pressurization cycles. These tests did not simulate any ascent pressure, heating or acoustics loads.

A larger 10-ft cryogenic tank was also tested similar to the minitanks to assess any large scale application issues. The 10-ft tanks, like the minitanks, were tested with LH₂ under repeated cryogenic cycles. The 10-ft tank also included a radiant heat test to assess TPS recession and propellant quality on a large scale tank. Note that the 10-ft tank was the largest scale application of flight type TPS prior to STS-1.

Radiant heating tests were conducted to verify the TPS recession characteristics under the aft dome environment where heating was due primarily to the exhaust plume radiation and recirculation, rather than aeroheating as simulated in the windtunnel tests. These tests were conducted in two facilities; one simulated radiant heat and acoustics, and the other radiant heat and ascent pressure decay.

The key element in the TPS qualification was the "combined environment" tests conducted on 4 x 4 ft TPS panels configured to represent the substrate and TPS in specific critical areas on the ET. These panels were subjected simultaneously to biaxial substrate loads, cryogenic backface temperature, ascent heat load (radiant), and either acoustics or ascent pressure. The panels were tested in a thermal/vacuum chamber, and/or in a thermal/acoustic facility depending on the specific test objective. Both facilities employed a large load cell structure which could be programmed to induce biaxial load profiles in either tension or compression. These were used to simulate various degrees of predicted flight substrate loads to demonstrate the TPS structural margin. The panels were cooled with liquid helium to simulate hydrogen tank substrate temperatures and the flight heat loads were simulated by an infrared lamp bank. These unique tests allowed the TPS to be subjected to nearly all the flight conditions (except aeroheating) and on a scale large enough to verify production methods.

FLIGHT RESULTS

The first six ETs were instrumented to provide flight verification of the thermal analysis and TPS design. The prime interest in evaluation of TPS performance are the heating rate and structural temperature data. Many of the instruments were intended to measure the conditions in the boundary layer on the ET TPS surface. The challenge was to mount this instrument such that it would not create a disturbance which would alter the parameters being measured, and such that the instruments would not be exposed to cryogenic temperature which would render them useless. Since the general TPS thickness on the ET is 1 in., there was very little room within the ET moldline to mount the transducers and still maintain isolation from the cryogenic tank wall. Furthermore the TPS surface may be receding due to heating during flight which would uncover the instruments. To overcome these problems, the transducers were mounted in hardened instrumentation islands as shown in Figure 5. The islands were "hardened" to the aeroheating environment by surrounding the island core with a non-receding ramp which would maintain a constant geometry during ascent. The transducers were mounted within the core which was isolated and insulated from the tank wall. This resulted in transducer temperatures that were acceptable and a stable surface surrounding the measurements.

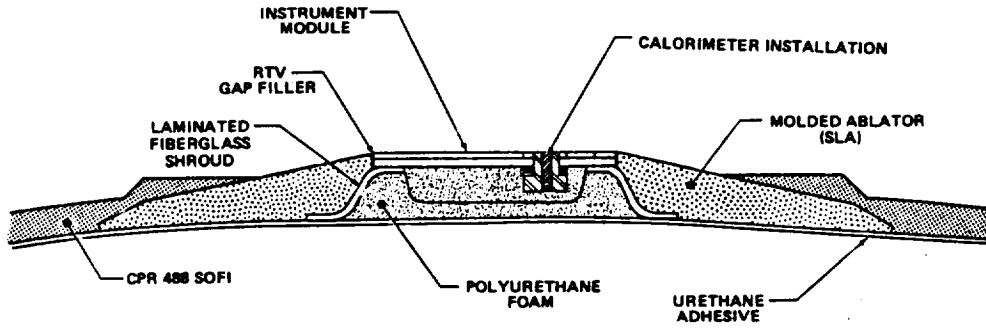


Figure 5. Hardened Instrumentation Island.

Flight instrumentation included aerodynamic heating measurements at 30 locations on the tank side-wall and at 8 locations in the base region. In addition, temperatures at 59 locations on the tank structure were also measured during flight. A comparison of the predicted temperature and measured temperatures from STS-5 for the LO_2 tank and LH_2 tanks are shown in Figures 6 and 7, respectively. The good correlation was part of the total TPS verification. In addition to the flight instrumentation data, cameras mounted in the orbiter were used to photograph the ET during ascent and after ET/orbiter separation. These photographs confirm the location of the higher heating regions and the adequacy of the ET TPS.

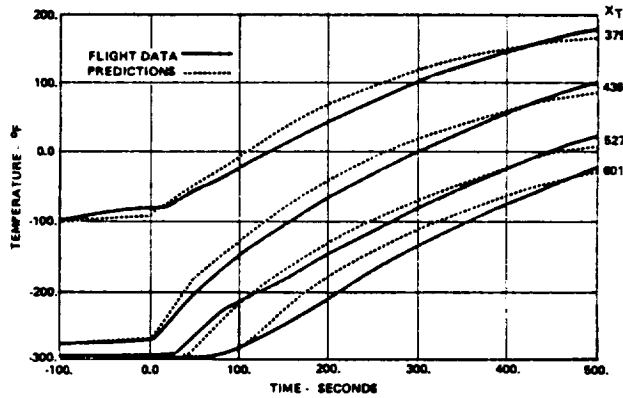


Figure 6. LO_2 Tank Structural Temperatures.

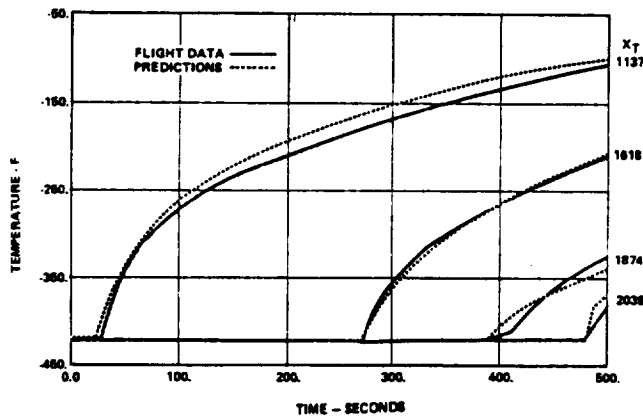


Figure 7. LH_2 Tank Structural Temperatures.

SUMMARY AND CONTINUING CHALLENGES

The major remaining challenges of the ET TPS design are to further reduce cost and weight and to enhance launch operations. In 1982, the first lightweight ET was delivered with a reduction of 6000 lb (including TPS) from the vehicle weight of the first series of tanks. Additional improvements are near term, such as the ablator reduction effort discussed earlier. Other efforts include the reduction of design heating rates and alternate designs which would not require ablators. This is basically a "fine tuning" of the design based on the experience and confidence gained from both production and flight results.

Components which still receive a covering of SLA will have automated ablator application using one of the newly developed methods of GIM, VIM or SAM (gas injected, vented injected, screen and applied molding), each of which eliminates final machining. Components requiring foam coverages or ramps made of foam will use the industrially familiar RIM (reaction injection molding). These are processes which will save material, reduce touch labor, and yield consistent sub-products.

Alternate and back ups to the primary TPS materials and their precursor ingredients are being identified and qualified in the event of supplied problems. Also, since the SLA-561 is essentially being underworked in ET environments, efforts are underway to tailor formulations into cheaper/lighter ablators (and/or cheaper/heavier foams) to replace the SLA-561 completely.

Efforts related to the enhancement of launch operations include the elimination or simplification of TPS closeout required at the launch site, simplification of the active thermal control systems (purges and heaters), and elimination of the residual Ice/Frost problem, particularly at the Vandenberg launch site.

Based on the present TPS design, weather conditions at VAFB result in a much higher probability of ice formation and thus launch delays than at KSC (23% versus 5%). Increasing the SOFI thickness would decrease the icing probability, however, the weight impact would not be acceptable at VAFB where Shuttle performance is already marginal. Many concepts were investigated to decrease the probability of forming ice. The concept finally selected, based on an analytical effort performed by CHAM of North America, Inc., consisted of two hot air jets directed vertically between the ET and Orbiter. The two jets entrain and mix with the ambient air and result in a warm high velocity flow over the tank surface which maintains the surface above freezing. The concept is currently undergoing scale model testing and the results look very promising.

The challenge of developing an efficient TPS system for the ET has been accomplished. Additional effort is continuing to upgrade the design based on flight and production experience. Today's ET TPS designers and engineers are addressing the technologies which will assure the future delivery of an already good product.

REFERENCES

- Warmbrod, J. D.; Elam, B. F.; Vaniman, J. L.: Thermal Design of the Space Shuttle External Tank. ASME 11th Intersociety Conference on Environmental Systems, July 13, 1981.
- External Tank LWT Thermal Data Book. MMC Dwg No. 80900200102, July, 1982, NASA Contract NAS8-30300.
- System Definition Handbook, Space Shuttle External Tank. MMC-ET-SE25-0, August 1980, NASA Contract NAS8-30300.
- Singhal, A. K.; Tam, L. T.: Numerical Modeling of Flow Around a 2% Scale Model of Space Shuttle. Final report on NASA contract NAS8-34940, November, 1982.

ORBITER ENTRY AEROTHERMODYNAMICS

Robert C. Ried
NASA Lyndon B. Johnson Space Center
Houston, Texas 77058

ABSTRACT

The challenge in the definition of the entry aerothermodynamic environment arising from the challenge of a reliable and reusable Orbiter is reviewed in light of the existing technology. A balanced use of prior, current, and advanced levels of technological sophistication was employed to achieve reasonable design requirements, design heating, and preflight confidence, respectively. Select problems pertinent to the Orbiter development are discussed briefly with reference to more comprehensive treatments. These problems include boundary-layer transition, leeward-side heating, shock/shock interaction scaling, tile gap heating, and nonequilibrium effects such as surface catalysis. Sample measurements obtained from test flights of the Orbiter are presented with comparison to preflight expectations. In summary, a reliance on both numerical and wind-tunnel simulations has afforded an efficient means for defining the entry environment and an adequate level of preflight confidence. The high-quality flight data provide an opportunity to refine the operational capability of the Orbiter and serve as a benchmark both for the development of aerothermodynamic technology and for use in meeting future entry heating challenges.

INTRODUCTION

The goals of the Space Transportation System (STS) have been to provide routine, cost-effective, and reliable means for carrying man and cargo to Earth orbit and return. Evaluations of achieving these goals led to the challenges of designing and developing a reusable Orbiter vehicle which could both perform atmospheric braking and achieve a land landing. These conflicting configuration requirements for the Orbiter were reconciled by altering the flight configuration with a high angle of attack for entry and then a low angle of attack for approach and landing. The high angle-of-attack entry configuration, the associated entry flight regime, and the relatively large size of the Orbiter provided some relief for the development of a weight-effective and reusable entry thermal protection system (TPS).

Guidelines for the Shuttle program (emanating from constraints on funding rate and minimum development costs) included limiting technology development, except as required, to meet the program goals. The development of reusable engines and a reusable TPS, however, required the development of conceptually new systems and an associated level of technology necessary to provide a level of confidence that these systems could perform adequately to meet the program goals. The challenge for the definition of the Orbiter entry heating was to develop reliable predictions on the basis of existing facilities and state-of-the-art capabilities, supplemented (as required) by advances in technology and understanding necessary to provide preflight confidence of success. This challenge was significant in light of the geometric complexity of the Orbiter configuration, the penalties of unnecessary weight in the system, the reuse requirement, and the basic severity of the entry environment. The Orbiter could not afford the weight associated with a conservative approach toward defining the entry TPS requirements. This approach would have mitigated the challenge and maintained the precedent set by previous entry vehicle designs.

A quantitative understanding of the entry heating phenomena for the windward surface of simple configurations was well established in the 1950's. Analysis and experiment had characterized convective heat transfer in a highly dissociated gas including the basic effects of finite-rate chemical and thermodynamic reactions. The flight mechanics leading to an optimum entry from the standpoint of entry heating for simple configurations was also well established in this era. This technology was used in the design and development of the orbital entry Mercury and Gemini vehicles and extended for the design and development of the more severe lunar return of the Apollo command module. These capsules all employed nonreusable ablators, but most important, they were designed with a level of conservatism which could not be tolerated on the Orbiter. This conservatism stemmed from the compounding of conservatism in the TPS requirements, the TPS performance, and the entry heating. An additional level of sophistication required by the Orbiter was the imposition of heating-rate and boundary-layer transition constraints on the entry flight trajectories to accommodate the reusable TPS capabilities and the insulation requirements, respectively.

TRIAD DILEMMA AND APPROACH

The Orbiter system and performance requirements dictated a more accurate, more precise, and more intricate definition of entry heating than for any previous system. On the other hand, the three-dimensional geometric complexity and the large scale of the Orbiter (compared to wind-tunnel models) posed a greater challenge to the definition of the entry flowfield and subsequent heating than had any previous system. To complete the triad, resources were extremely limited, particularly with regard to technology development. This triad dilemma was dealt with by a triad approach based heavily on experience with previous entry heating problems (ref. 1). The lowest level was a simplified heating model (developed at representative locations on the vehicle) for early system design and for entry trajectory design (ref. 2). The second level of the approach, the design methodology, employed the current state-of-the-art aerothermodynamic technology in ground testing, data correlation, and analysis of both ground test and flight (ref. 3). This effort provided "nominal" entry heating for all locations on the vehicle as TPS design requirements (ref. 4). This heating was considered "nominal" since no uncertainties or conservative factors were applied to the correlation of wind-tunnel data or analysis of the design environment for the design trajectory. To provide adequate preflight confidence in the use of "nominal" heating for design and to address technology deficiencies, the third level of the approach involved select advanced state-of-the-art efforts (ref. 5), parametric studies, and preflight uncertainty evaluations of the entry heating and TPS performance (ref. 6).

SIMPLIFIED HEATING MODEL

The simplified heating model used on the Orbiter was comparable to the design methodology used on the previous blunt manned entry capsules. At representative locations on the Orbiter, a first-order scaling of wind-tunnel data to flight conditions was performed for laminar and turbulent convective heating as well as for boundary-layer transition. Local heat transfer at a given angle of attack was correlated with the heat transfer to the stagnation point of a sphere (assuming equilibrium air). Boundary-layer transition and turbulent heating were correlated as a function of the Reynolds number behind a normal shock. Use of this Reynolds number is a first-order attempt to account for the equilibrium real air effects between flight and wind tunnel and is particularly applicable to blunt entry vehicles dominated by high-entropy flow. This approach was sufficiently straightforward to incorporate into the entry flight mechanics trajectory design (ref. 7). Thus, entry trajectories which were consistent with reusable TPS material capabilities were obtained as illustrated in figure 1. The reusable TPS requirement was a constraint on the geometric configuration and primarily on the entry trajectory corridor. Previous manned entry vehicle trajectories, such as Apollo, were only constrained by acceleration (dynamic pressure) and control.

This simplified model was also used to eliminate the largest contribution to unnecessary conservatism in previous manned entry vehicle TPS design: the difference between design and actual requirements. The value of this activity is illustrated in figure 2 by comparison of the Shuttle Orbiter and the Apollo command module experience. The small difference between the STS-1 environment and the design environment was within the preflight uncertainty of the environment and TPS performance (ref. 6). Also, comparison of the Apollo orbital test environments with the Shuttle Orbiter environment is a valid illustration of the heat-load penalty incurred as a result of the reusable TPS requirement. For a given insulation material, the required thickness is roughly proportional to the square root of the heat load.

DESIGN METHODOLOGY

As with previous manned entry vehicles, the foundation for the definition of the entry aerothermodynamic environment for the Shuttle Orbiter was based on wind-tunnel data taken on geometrically scaled models of the Orbiter. Extensive parametric testing was not performed; rather, testing was performed only where the best local flow parameters of significance to the high-heating flight regime could be approached. Despite the fact that wind-tunnel enthalpies are on the order of one-fiftieth of flight (a suitable dimensionless enthalpy parameter for this scaling does not exist), a wind-tunnel free-stream Mach number of about 8 provides the best simulation of the Orbiter entry heating flight regimes (ref. 1). Early aerothermodynamic model testing was performed with a phase-change paint test technique, but the bulk of the design test data were obtained with thermocouple-instrumented models at the Arnold Engineering Development Center, Tunnel 8.

The flight design entry heating data were obtained by analysis and correlation normalized by wind-tunnel data. Correlations of equilibrium boundary-layer solutions (and turbulent correlations) obtained for simple (two-dimensional) flowfields (refs. 3 and 8) were applied and normalized at wind-tunnel conditions. These normalized correlations were then applied to flight conditions along an entry trajectory (ref. 4). This process is illustrated schematically in figure 3. It should be noted that the Orbiter entry configuration is not a true blunt entry vehicle nor is it a slender flight vehicle. The flow dynamics vary along the vehicle from the high-entropy blunt-body nose flow to an asymptotic approach toward low-entropy slender-body flow (ref. 9).

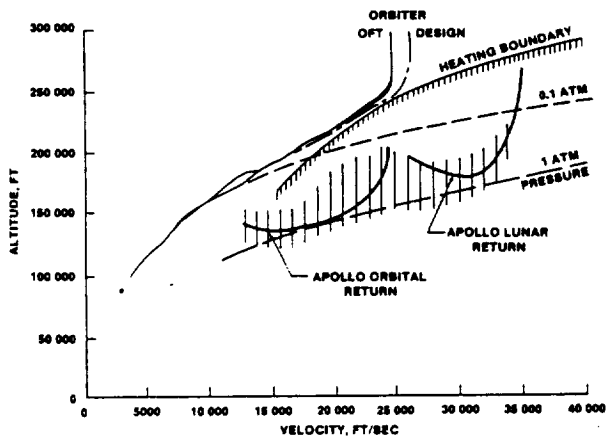


FIGURE 1.- ENTRY FLIGHT REGIMES: APOLLO COMMAND MODULE AND SHUTTLE ORBITER.

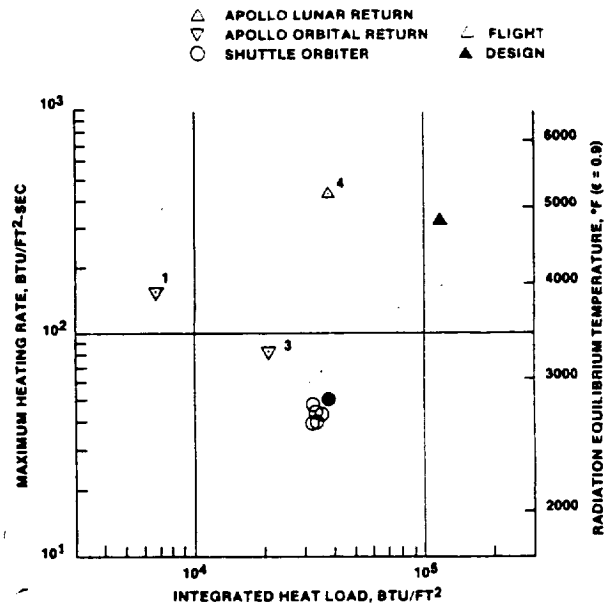


FIGURE 2.- TPS DESIGN AND FLIGHT TEST ENVIRONMENTS.

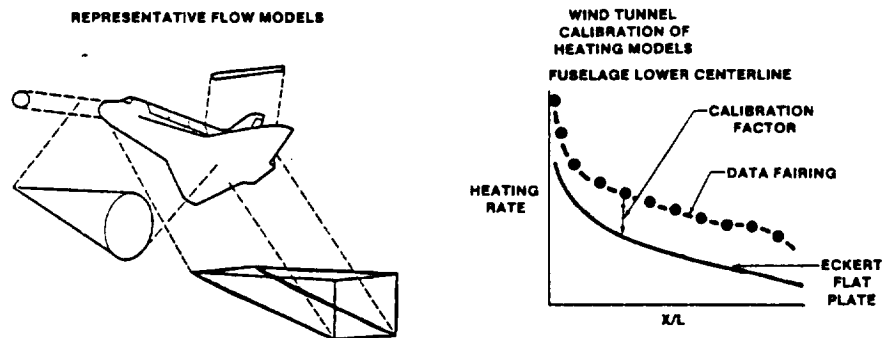


FIGURE 3.- DESIGN HEATING METHODOLOGY.

Smooth-body boundary-layer transition at any location on the vehicle was found to correlate at wind-tunnel conditions by momentum-thickness Reynolds number divided by local Mach number (ref. 4). This correlation was then applied to flight in terms of the same parameter. The results were not drastically different from those for the simplified model. It should be noted, however, that the Orbiter shape had to be "smoothed" to obtain a laminar entry heating vehicle. It had been observed experimentally that configurations without a continuously differentiable windward surface geometry gave rise to premature boundary-layer transition (refs. 1 and 10). This is an overall configuration effect as opposed to a local surface-roughness tripping effect.

TECHNOLOGY ADVANCEMENT

Although there can sometimes be a subtle distinction between state-of-the-art and advanced technology, aerothermodynamics is in the midst of a revolutionary change from a predominantly experimental simulation base to a heavy reliance on numerical simulation. In the case of the Orbiter, entry heating numerical simulations (fig. 4) provided benchmark information for incorporation into the design methodology (refs. 9 and 11 to 18). This information included the scaling of three-dimensional flows and heating from wind tunnel to flight as well as addressing the influences of finite-rate chemistry on the flow and heating. Although numerical flowfield computations have not yet encompassed the entire Orbiter, if the Shuttle program were initiated today, this capability would be the foundation of the design methodology.

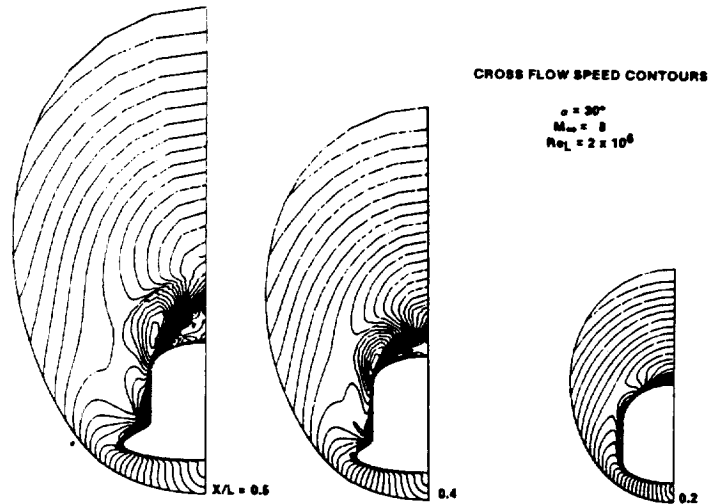


FIGURE 4.- ORBITER FLOWFIELD RESULTS.

Parametric analyses, tests, and data correlations were performed to obtain a better understanding of critical flow phenomena and the sensitivity of the environment and system. Off-nominal testing and analysis were discouraged as a main-line activity (to reduce development cost), but in-house and university studies (refs. 19 to 21) accomplished the required activity. The numerical flowfield simulations were extremely valuable for quantifying the sensitivities to given uncertainty parameters (ref. 6).

Early in the Shuttle program, arc-jet testing of candidate Orbiter TPS materials pointed to the significance of atom recombination surface catalysis to the Orbiter entry heating. Resource limitations prohibited completion of the necessary test data and analyses for the design. However, surface catalysis was characterized before flight (ref. 22). The process for obtaining flight predictions of this phenomenon is illustrated schematically in figure 5. In previous entry vehicle design, this phe-

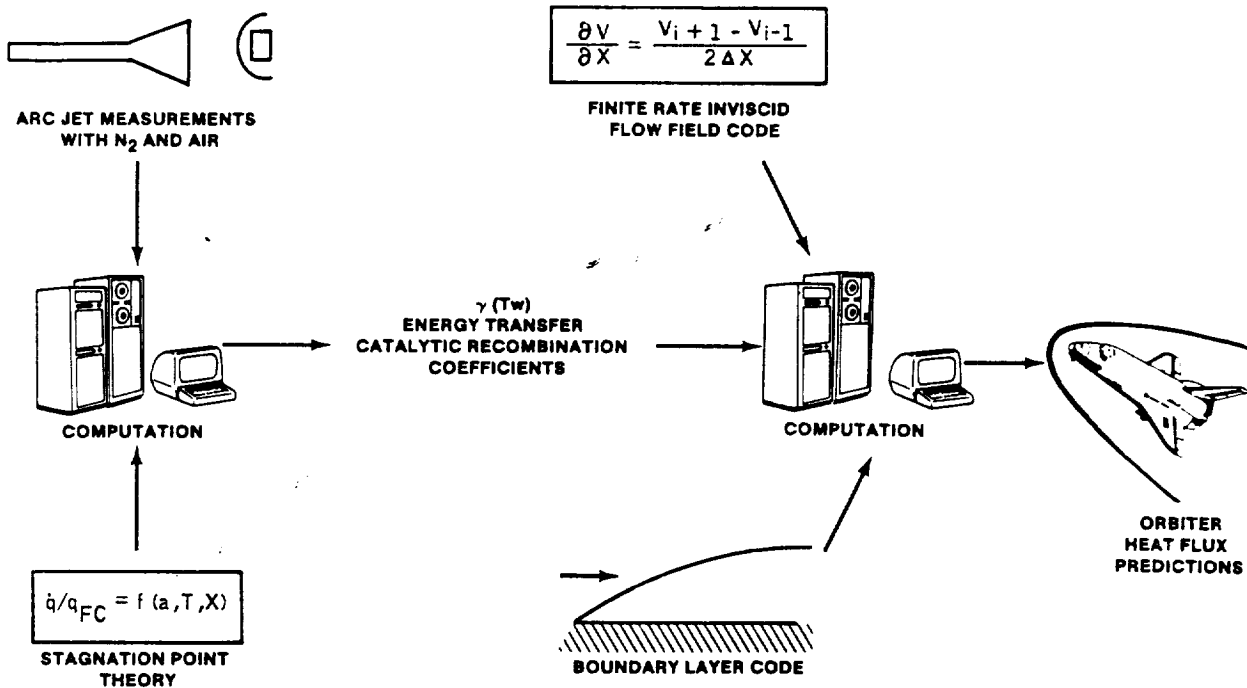


FIGURE 5.- SURFACE CATALYSIS FLIGHT PREDICTION PROCESS.

nomenon had always been masked by the complex processes associated with ablation.

A number of technology questions and issues have arisen as a result of the development of the Orbiter entry heating model. Several of these are addressed under the particular problem area.

SELECT PROBLEMS

BOUNDARY-LAYER TRANSITION

The phenomena of turbulent flow and boundary-layer transition have been under intense investigation for more than a century with somewhat limited success. This limitation is possibly measured by the anxiety which develops when engineers are required to predict boundary-layer transition outside the range of experimental data. The approach to predicting smooth-body transition has already been discussed. Early assessments of the influence of roughness on boundary-layer transition on the Orbiter did not indicate a problem; however, concern arose based on slender-body experience, the large difference between wind-tunnel and flight wall/gas temperature ratio, and the significance of early boundary-layer transition to the TPS. The ensuing activity pushed geometric similitude in wind-tunnel models of entry vehicles to new limits and incorporated pretest chilling of the model to cryogenic temperatures (refs. 23 to 25). Specialized testing, correlation, analysis, and debate finally led to an acceptable level of confidence that roughness associated with the Orbiter TPS tiles would not significantly alter boundary-layer transition from the smooth-body design methodology predictions. The approach used to establish the influence of distributed tile roughness is illustrated in figure 6.

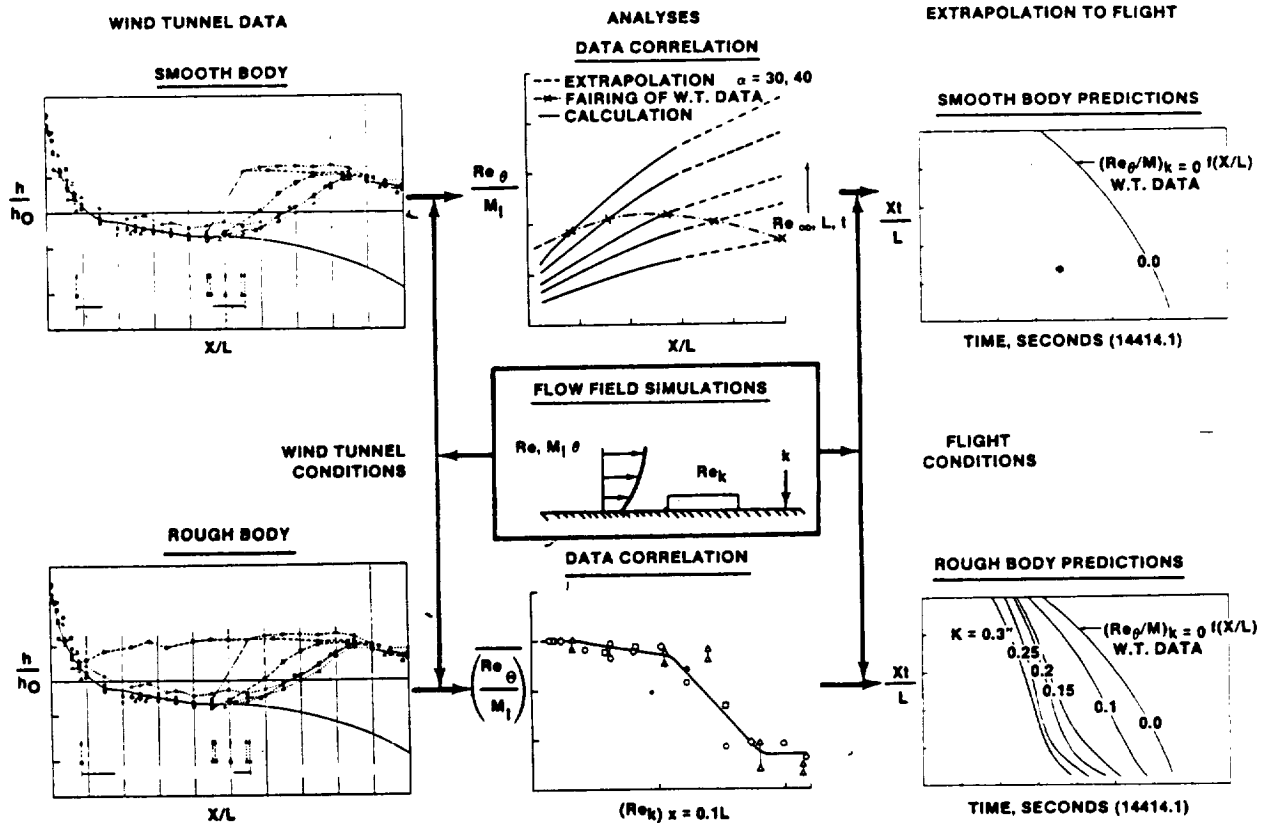


FIGURE 6.- LOGIC FOR PREDICTING BOUNDARY-LAYER TRANSITION ON THE ORBITER.

LEeward HEATING

Previous experience with entry vehicle leeward TPS design had generally resulted in a very conservative approach because of the large uncertainty in the hypersonic near-wake flowfield. This uncertainty was of particular importance to the Orbiter because of its large size and the fact that more than half the exterior surface is in a separated-flow regime during significant entry heating. The uncertainty with regard to the leeward environment still exists. However, the conservatism in the leeward TPS was minimized by a reliance on experience with previous manned entry vehicles. This experience is tantamount to assuming a blunt-body controlled flow in that the leeward wind-tunnel data were normalized by heat transfer to the stagnation point of a sphere and applied directly to flight. This problem remains empirical and awaits advances in numerical fluid mechanics simulation capability and efficiency.

SHOCK/SHOCK INTERACTION

Although the Shuttle Orbiter at angle of attack is a relatively clean configuration, there are areas of complex flows which cause concern as to local entry heating and in particular the scaling of wind-tunnel data to flight. One of these areas is the intersection of the fuselage shock and the wing shock. After rather sophisticated wind-tunnel testing, data correlation, and first-order analysis, it was judged that the angle of attack and the wing sweep of the Orbiter did not indicate an overly severe local heating problem for the wing leading edge (ref. 26). However, it was discovered in the pursuit of this problem that scaling of wind-tunnel data to flight when the flow has encountered two shocks (inboard of the shock/shock interaction) resulted in an amplification relative to single-shock scaling (ref. 27). The entropy change obtained by a dual-shock process can be less than that obtained for a single shock. This dual-shock scaling was incorporated in the preflight certification heating environment.

TILE GAP HEATING

Much to the chagrin of the aerothermodynamicist, the Orbiter entry TPS has thin gaps between the 6-inch-square surface insulation tiles. The resulting heat leak afforded by these gaps is a complex coupling of convective heating, radiation exchange, and predominantly conduction down the sidewall of the tile. On the basis primarily of arc-jet tests (which attempt to simulate this coupled environment/system interaction) and analysis, this heat leak can generally be accommodated by an increase in the average insulation thickness. The exception occurs when a pressure gradient causes a hot breeze into the gap (refs. 28 to 30). In this case, it became necessary to stuff the gaps to prevent flow intrusion along with the associated heating. It should be noted that since the nonadiabatic flow of air through a gap is driven by the pressure distribution and the pressure level, the importance of gap convective heating is greatest late in the trajectory after peak surface heating. This behavior was first realized when calculations were performed to ascertain the elevon/wing seal requirements (ref. 21). A postflight assessment is that the late turbulent flow regime is of greater significance to gap convective heating.

NONEQUILIBRIUM EFFECTS

Although significant entry heating occurs in the continuum gas dynamic regime, manned entry vehicles fly at sufficiently low pressure levels that chemical and thermodynamic nonequilibrium air phenomena are a concern (refs. 31 and 32). This concern was particularly significant for the Orbiter since it was constrained to lower pressures by the heating rates required for a reusable TPS (fig. 1). A considerable effort was required to confirm that the finite-rate air chemistry does not significantly alter the Orbiter windward flow dynamics (ref. 14). This same question has not yet been answered for the leeward region, where the potential influence of finite-rate chemistry on the gas dynamics is much greater. The finite-rate air chemistry and thermodynamics do, however, significantly alter the entry heating depending on the catalysis characteristics of the particular surface coating. This aspect is discussed in the Orbital Flight Test (OFT) Program results.

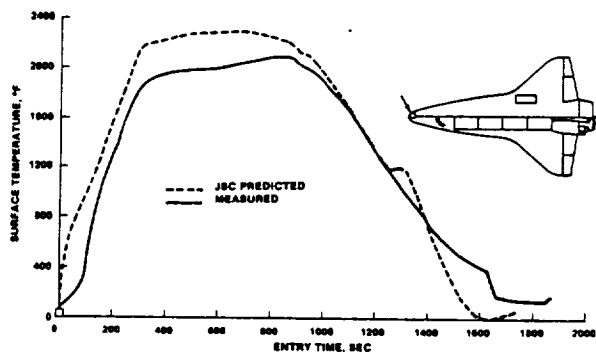
FLIGHT TEST RESULTS

The success of the Space Shuttle Program is very evident from the flight experience to date. An assessment of the job done in defining the entry heating and the flight capability of the Orbiter requires rather extensive analysis of the OFT data. The predominant source of entry heating data consisted of surface thermocouples mounted all over the Orbiter (ref. 33). These thermocouples were installed in the same fashion as in ground arc-jet and radiant tests of the TPS. The OFT Program has

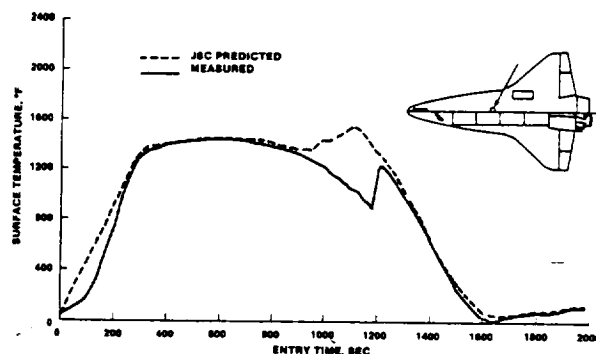
provided a large amount of high-quality data for ascertaining the entry heating on the Orbiter configuration. In turn, these data have given rise to a large number of publications comparing predictions and data with a definite trend toward convergence. However, the most important achievement in entry heating has been the contribution toward an adequately designed system (refs. 5 and 34) and well-designed entry trajectories (ref. 7).

Figure 7 is a comparison of selected flight measurements with preflight predictions (refs. 5 and 35). All predictions of boundary-layer transition were conservative, although some were close (refs. 6 and 23 to 25). A detailed presentation of the Orbiter flight boundary transition data is contained in reference 36. The data indicate a definite "tripping" and rapid transition, although whether the cause is distributed roughness (ref. 36), single governing roughness (ref. 37), or configuration (ref. 1) is under debate. Predictions of laminar convective heating are generally conservative (ref. 38), although the extent to which this is due to flowfield assumptions or to surface catalysis effects is under study (refs. 37 to 41). Fortunately, a series of Shuttle flight experiments with catalytically coated tiles (refs. 42 and 43) has provided vivid illustration of finite surface catalysis effects (fig. 8). Turbulent heating levels were very well predicted on the basis of normalization to wind-tunnel data. This agreement was somewhat expected because of the lower sensitivity of turbulent heating to local flow parameters when compared to the laminar case. It should be noted that there is an apparent trend for the entry heating in the highest temperature surface areas to increase (refs. 40 and 44) with flight experience. This trend would indicate changes in surface properties such as emittance or catalycity. Except for this observation, the flight data are quite repeatable.

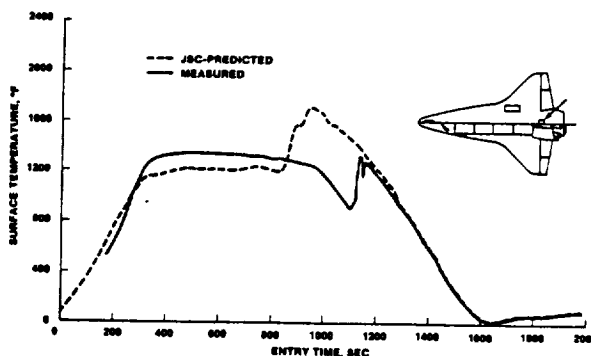
In the light of the complexity of the Orbiter flowfield, the various phenomena involved, and the limitations of wind tunnels in simulating the flight environment, it is fortuitous that the simplified model works quite well. On the leeward side of the vehicle, where the simplified model equals the current level of sophistication, agreement is also reasonable. Figures 9 and 10 illustrate the normalized film heat-transfer coefficient (inferred (ref. 45) from surface temperature measurements) as a function of Reynolds number and angle of attack, respectively. As can be seen, the flight data are quite repeatable and the potential for heat transfer is quite sensitive to angle of attack.



(a) FORWARD WINDWARD CENTERLINE.



(b) MIDBODY WINDWARD CENTERLINE.



(c) AFT WINDWARD CENTERLINE.

FIGURE 7.- COMPARISON OF STS-3 FLIGHT DATA WITH PREFLIGHT TEST PREDICTIONS.

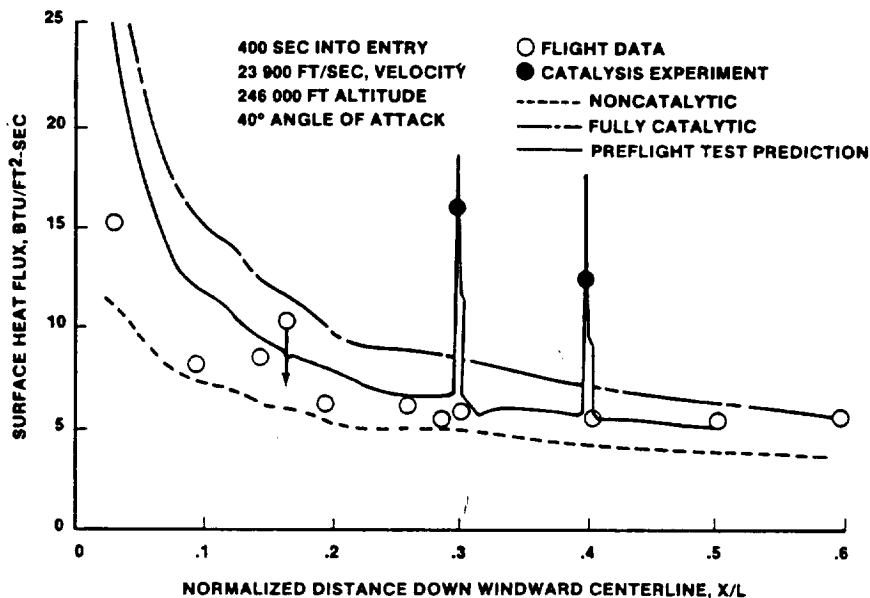


FIGURE 8.- ORBITER INFERRED AND PREDICTED HEAT FLUX, STS-3.

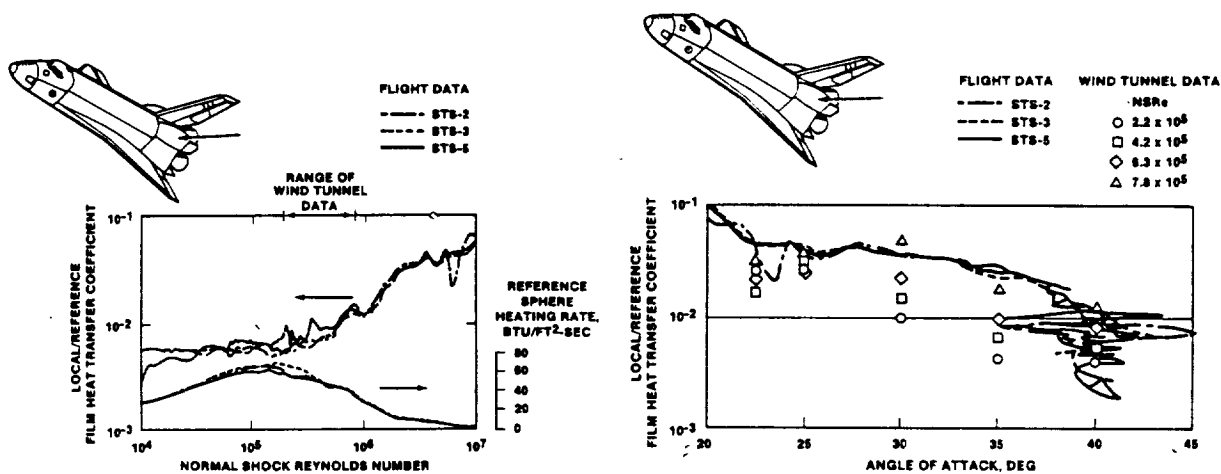


FIGURE 9.- LEEWARD SURFACE FLIGHT DATA VERSUS REYNOLDS NUMBER.

FIGURE 10.- LEEWARD SURFACE FLIGHT DATA VERSUS ANGLE OF ATTACK.

CONCLUSIONS

The definition of entry heating to the Space Shuttle Orbiter was an exciting challenge to the aerothermodynamics community from the standpoint of technology, engineering, and management. It was met by a balanced effort of varying levels of sophistication weighted heavily with experience and adherence to basic engineering principles such as similitude. The use of nominal heating predictions for design was not a low-risk approach but one that helped to provide vehicle performance and an adequate TPS. The treatment of boundary-layer transition is without precedent, except perhaps for the design of a wing for the P-51 airplane.

The reliance on both numerical and wind-tunnel simulations has afforded an efficient means of defining the entry environment and an adequate level of preflight confidence. The high-quality flight data provide opportunity to refine the operational capability of the Orbiter and serve as a benchmark both for the development of aerothermodynamic technology and for use in meeting future entry heating challenges.

ACKNOWLEDGMENTS

The many talented and dedicated technicians, managers, engineers, and scientists who helped make the Shuttle program a success through their contributions to the definition of the Orbiter entry heating are acknowledged. In particular, the Aerothermodynamics Subsystem Manager, Mrs. Dorothy Lee; the Manager of Aerothermal Analysis, Rockwell, Mr. Mark Harthun; and lead champions of the truth, Drs. Winston Goodrich, Carl Scott, and Chien Li are recognized.

REFERENCES

1. Ried, R. C., Jr.; Goodrich, W. D.; Strouhal, G.; and Curry, D. M.: The Importance of Boundary Layer Transition to the Space Shuttle Design. Proceedings of the Boundary Layer Transition Workshop, Nov. 3-5, 1971. Aerospace Report No. TOR-0172 (S2816-16) -5, Dec. 20, 1971.
2. Curry, D. M.; Tolin, J. W., Jr.; and Goodrich, W. D.: Effects of Selected Trajectory Parameters on Weight Trends in the Shuttle Thermal Protection System. NASA TM X-58113, Jan. 1974.
3. Entry Aeroheating Design Methods Handbook. Rockwell International Space Division (Downey, Calif.). (To be published, 1983.)
4. Haney, J. W.; and Petrilla, C. T.: Space Shuttle Orbiter Entry Aerodynamic Heating Data Book. Rockwell International Space Division (Downey, Calif.) SD73-SH-0184C, Oct. 1978.
5. Ried, R. C., Jr.; et al.: Space Shuttle Orbiter Entry Heating and TPS Response: STS-1 Predictions and Flight Data. Computational Aspects of Heat Transfer in Structures, NASA CP-2216, 1982.
6. Goodrich, W. D.; Derry, S. M.; and Maraia, R. J.: Effects of Aerodynamic Heating and TPS Thermal Performance Uncertainties on the Shuttle Orbiter. Entry Heating and Thermal Protection, Vol. 69 of Progress in Astronautics and Aeronautics, Walter B. Olstad, ed., 1980, pp. 247-268.
7. Joosten, B. K.; and Silvestri, R. T.: Descent Guidance and Mission Design for Space Shuttle. Paper presented at Space Shuttle Program Technical Conference (Houston, Tex.), June 28-30, 1983.
8. Hender, D. R.: A Miniature Version of the JA70 Aerodynamic Heating Computer Program, H800 (MINIVER). MDC G0462, McDonnell-Douglas Astronautics Co. (Huntington Beach, Calif.), June 1970 (Revised Jan. 1972).
9. Goodrich, W. D.; Li, C. P.; Houston, C. K.; Meyers, R. M.; and Olmedo, L.: Scaling of Orbiter Aerothermodynamic Data Through Numerical Flow Field Simulations. NASA SP-347, Part 2, Mar. 1975, pp. 1395-1410.
10. Young, C. H.; Reda, D. C.; and Roberge, A. M.: Hypersonic Transitional and Turbulent Flow Studies on a Lifting Entry Vehicle. AIAA Paper 71-100, Jan. 1971.
11. Goodrich, W. D.; Li, C. P.; Houston, C. K.; Chiu, P. B.; and Olmedo, L.: Numerical Computations of Orbiter Flow Fields and Laminar Heating Rate. J. Spacecraft & Rockets, vol. 14, no. 5, May 1977, pp. 257-264.
12. Rakich, J. V.; and Lanfranco, M. J.: Numerical Computation of Space Shuttle Laminar Heating and Surface Streamlines. J. Spacecraft & Rockets, vol. 14, no. 5, May 1977, pp. 265-272.
13. Li, C. P.: Numerical Simulation of Reentry Flow Around the Shuttle Orbiter Including Real Gas Effects. Paper presented at Symposium on Computers in Flow Predictions and Fluid Dynamics Experiments, ASME Winter Annual Meeting (Washington, D.C.), Nov. 1981.
14. Rakich, J. V.; Bailey, H. E.; and Park, C.: Computation of Nonequilibrium Three-Dimensional Inviscid Flow Over Blunt-Nosed Bodies Flying at Supersonic Speeds. AIAA Paper 75-835, June 1975.
15. Scott, C. D.: Space Shuttle Laminar Heating with Finite-Rate Catalytic Recombination. AIAA Paper 81-1144, June 1981.
16. Li, C. P.: A Numerical Study of Laminar Flow Separation on Blunt Flared Cones at Angle-of-Attack. AIAA Paper 74-585, June 1974.

17. Kutler, P.; Reinhardt, W. A.; and Warning, R. F.: Multishocked Three-Dimensional Supersonic Flow Fields with Real Gas Effects. AIAA J., vol. 11, May 1973, pp. 657-664.
18. Rakich, J. V.; and Mateer, G. G.: Calculation of Metric Coefficients for Streamline Coordinates. AIAA J., vol. 10, no. 11, Nov. 1972, pp. 1538-1540.
19. Bertin, J. J.; and Goodrich, W. D.: Effects of Surface Temperature and Reynolds Number on Leeward Shuttle Heating. J. Spacecraft & Rockets, vol. 13, no. 8, Aug. 1976, pp. 473-480.
20. Bertin, J. J.; and Goodrich, W. D.: Aerodynamic Heating for Gaps in Laminar and Transitional Boundary Layers. Aerothermodynamics and Planetary Entry, Vol. 77 of Progress in Astronautics and Aeronautics, A. L. Crosbie, ed., 1981, pp. 3-35.
21. Scott, C. D.; Murray, L. P.; and Milhoan, J. D.: Shuttle Elevon Cove Aerodynamic Heating by Injected Flow. Progress in Astronautics and Aeronautics, Vol. 59, L. S. Fletcher, ed., 1978, pp. 27-48.
22. Scott, C. D.: Catalytic Recombination of Nitrogen and Oxygen on High Temperature Reusable Surface Insulation. AIAA Paper 80-1477, June 1981.
23. Goodrich, W. D.; and Stalmach, C., Jr.: Effects of Scaled Heatshield Tile Misalignment on Orbiter Boundary Layer Transition. J. Spacecraft & Rockets, vol. 14, Oct. 1977, pp. 638-640.
24. Bertin, J. J.; Idar, E. S., III; and Goodrich, W. D.: Effect of Surface Cooling and Roughness on Transition for the Shuttle Orbiter. J. Spacecraft & Rockets, vol. 15, Mar.-Apr. 1978, pp. 113-119.
25. Bertin, J. J.; Hayden, T. E.; and Goodrich, W. D.: Comparison of Correlations of Shuttle Boundary Layer Transition Due to Distributed Roughness. AIAA Paper 81-0417, Jan. 1981.
26. Bertin, J. J.; Williams, F. E.; Baker, R. C.; Goodrich, W. D.; and Kessler, W. C.: Aerothermodynamic Measurement for Space Shuttle Configuration in Hypersonic Wind Tunnel. NASA TM X-2507, Feb. 1972.
27. Bertin, J. J.; Mosso, S. J.; Barnette, D. W.; and Goodrich, W. D.: Engineering Flow Fields and Heating Rates for Highly Swept Leading Edges. J. Spacecraft & Rockets, vol. 13, no. 9, Sept. 1976, pp. 540-546.
28. Scott, C. D.; and Marafa, R. J.: Gap Heating with Pressure Gradients. Entry Heating and Thermal Protection, Vol. 69 of Progress in Astronautics and Aeronautics, W. B. Olstad, ed., 1980, pp. 269-286.
29. Throckmorton, D. A.: Pressure Gradient Effects on Heat Transfer to Reusable Surface Insulation Tile-Array Gaps. NASA TN D-7939, Aug. 1975.
30. Avery, D. E.: Aerodynamic Heating in Gaps of Thermal Protection System Tile Arrays in Laminar and Turbulence Boundary Layers. NASA TP-1187, 1978.
31. Ried, R. C., Jr.: Aerodynamic Heating. Ch. 6, Manned Spacecraft: Engineering Design and Operation, P. E. Purser, M. A. Faget, and N. F. Smith, eds., Fairchild Publications, Inc. (New York), 1964.
32. Ried, R. C., Jr.; Rochelle, W. C.; and Milhoan, J. D.: Radiative Heating to the Apollo Command Module: Engineering Prediction and Flight Measurement. NASA TM X-56834, Apr. 1972.
33. Smith, J. A.: STS-3 Structural and Aerodynamic Pressure, Aerothermodynamic and Thermal Protection System Measurement Locations. JSC-17889, Lyndon B. Johnson Space Center, Jan. 15, 1982.
34. Lee, D. B.; and Harthun, M. H.: Aerothermodynamic Entry Environment of the Space Shuttle Orbiter. AIAA Paper 82-0821, June 1982.
35. Scott, C. D.; and Derry, S. M.: Catalytic Recombination and the Space Shuttle Heating. AIAA Paper 82-0841, June 1982.

36. Goodrich, W. D.; Derry, S. M.; and Bertin, J. J.: Shuttle Orbiter Boundary Layer Transition at Flight and Wind Tunnel Conditions. Paper presented at Langley Conference on Shuttle Performance: Lessons Learned, Langley Research Center (Hampton, Va.), Mar. 8-10, 1983. NASA CP-2283, to be published.
37. Harthun, M. H.; Blumer, C. B.; and Miller, B. A.: Orbiter Windward Surface Entry Heating - Post-Orbital Flight Test Program Update. Paper presented at Langley Conference on Shuttle Performance: Lessons Learned, Langley Research Center (Hampton, Va.), Mar. 8-10, 1983. NASA CP-2283, to be published.
38. Haney, J. W.: Orbiter Entry Heating Lessons-Learned from Development Flight Test Program. Paper presented at Langley Conference on Shuttle Performance: Lessons Learned, Langley Research Center (Hampton, Va.), Mar. 8-10, 1983. NASA CP-2283, to be published.
39. Scott, C. D.: A Review of Nonequilibrium Effects and Surface Catalysis on Shuttle Heating. Paper presented at Langley Conference on Shuttle Performance: Lessons Learned, Langley Research Center (Hampton, Va.), Mar. 8-10, 1983. NASA CP-2283, to be published.
40. Scott, C. D.: Effects of Nonequilibrium and Surface Catalysis on Shuttle Heat Transfer: A Review. AIAA Paper 83-1485, June 1983.
41. Shinn, J. L.; Moss, J. W.; and Simmonds, A. L.: Viscous-Shock-Layer Heating Analysis for the Shuttle Windward Plane with Surface Finite Catalytic Recombination Rates. AIAA Paper 82-0842, June 1982.
42. Stewart, D. A.; Rakich, J. V.; and Lanfranco, M. J.: Catalytic Surface Effects Experiment on the Space Shuttle. Thermophysics of Atmospheric Entry, Vol. 82 of Progress in Astronautics and Aeronautics, T. E. Houston, ed., 1982, pp. 248-272.
43. Rakich, J. V.; Stewart, D. A.; and Lanfranco, M. J.: Results of a Flight Experiment on the Catalytic Efficiency of the Space Shuttle Heat Shield. AIAA Paper 81-0944, June 1982.
44. Williams, S. D.; and Curry, D. M.: An Assessment of the Space Shuttle Orbiter Thermal Environment Using Flight Data. AIAA Paper 83-1488, June 1983.
45. Williams, S. D.: Columbia: The First Five (5) Flights. Entry Heating Data Series: Vol. 2, The OMS POD, NASA CR-171657, May 1983; Vol. 3, The Lower Windward Surface Centerline, NASA CR-171665, May 1983; Vol. 4, The Lower Windward Wing 50% and 80% Semi-Spans, NASA CR-171666, May 1983.

D42
N85-16979

ORBITER THERMAL PROTECTION SYSTEM

Robert L. Dotts, Donald M. Curry, and Donald J. Tillian
NASA Lyndon B. Johnson Space Center
Houston, Texas 77058

ABSTRACT

The major material and design challenges associated with the Orbiter thermal protection system (TPS), the various TPS materials that are used, the different design approaches associated with each of the materials, and the performance experienced during the flight test program are described. The first five flights of the Orbiter Columbia and the initial flight of the Orbiter Challenger have provided the necessary data to verify the TPS thermal performance, structural integrity, and reusability. The flight performance characteristics of each TPS material are discussed. This discussion is based on postflight inspections and postflight interpretation of the flight instrumentation data. The flights to date indicate that the thermal and structural design requirements for the Orbiter TPS have been met and that the overall performance has been outstanding.

INTRODUCTION

One major technical accomplishment of the Space Shuttle program involved the development of a reusable thermal protection system (TPS). To meet the challenge of providing a reusable TPS for the Orbiter, new concepts of thermal protection materials and design approaches were necessary. Before the Shuttle Program, all manned space vehicles had used ablator materials having a one-mission capability. In contrast, the TPS for the Shuttle Orbiter had to be reusable for 100 missions to minimize operational costs. It also had to be extremely weight-efficient to meet vehicle performance requirements.

Four principal thermal protection concepts appeared to have potential application for the Shuttle Orbiter program. These concepts included (1) replaceable ablator panels, (2) nonablating, nonmetallic insulative-reradiative materials, (3) metallic reradiative heat shields, and (4) carbon-carbon reradiative hot structures. Extensive technology development activities were undertaken at the various National Aeronautics and Space Administration (NASA) centers and by the major aerospace firms from 1969 to 1972. Although the ablator technology was well developed at the time, it was not economically feasible to develop a low density replaceable system. The metallic reradiative heat shields had significant disadvantages as far as temperature limitation, expensive manufacturing, and difficult inspection techniques. The nonreceding, nonmetallic ceramic heat shield possessed two unique advantages from the onset; that is, design simplicity and reuse capability. In contrast, the metallic heat shields were quite complex due to the design features needed to minimize thermal distortion, panel-to-panel joints, as well as the insulation with its packaging that would be required to protect the vehicle primary structure. The carbon-carbon material was the only known material that showed potential for providing reuse capability for the high temperature areas of the Orbiter (>2300° F) such as the wing leading edge and nose cap regions.

It was recognized that major technological developments would have to be undertaken to bring the nonmetallic ceramic materials from the laboratory state to actual vehicle application. However, the significant weight savings and design simplicity inherent with the ceramic materials led to their selection as the primary Orbiter TPS. The carbon-carbon was the clear choice for leading-edge applications where a durable reusable material was required. Its temperature capability also added to its preference. However, significant developments in coatings preventing oxidation would have to be made to make carbon-carbon a multi-mission material.

This paper will cover the development activities that were undertaken for the TPS materials selected for the Orbiter, the major pacing material and design issues that evolved, and finally the performance based on the recent flight test program.

DESIGN REQUIREMENTS - GENERAL

The thermal protection for the Orbiter is designed to operate successfully over a spectrum of environments typical of both aircraft and spacecraft as shown in figure 1. During the ascent and entry phases of the mission, the Orbiter structure must be maintained at temperatures less than 350° F. In addition to withstanding the thermal environments, the TPS must also perform satisfactorily in other induced environments, such as launch acoustics, structural deflections induced by aerodynamic loads, and onorbit cold soak as well as the natural environments such as salt fog, wind, and rain.

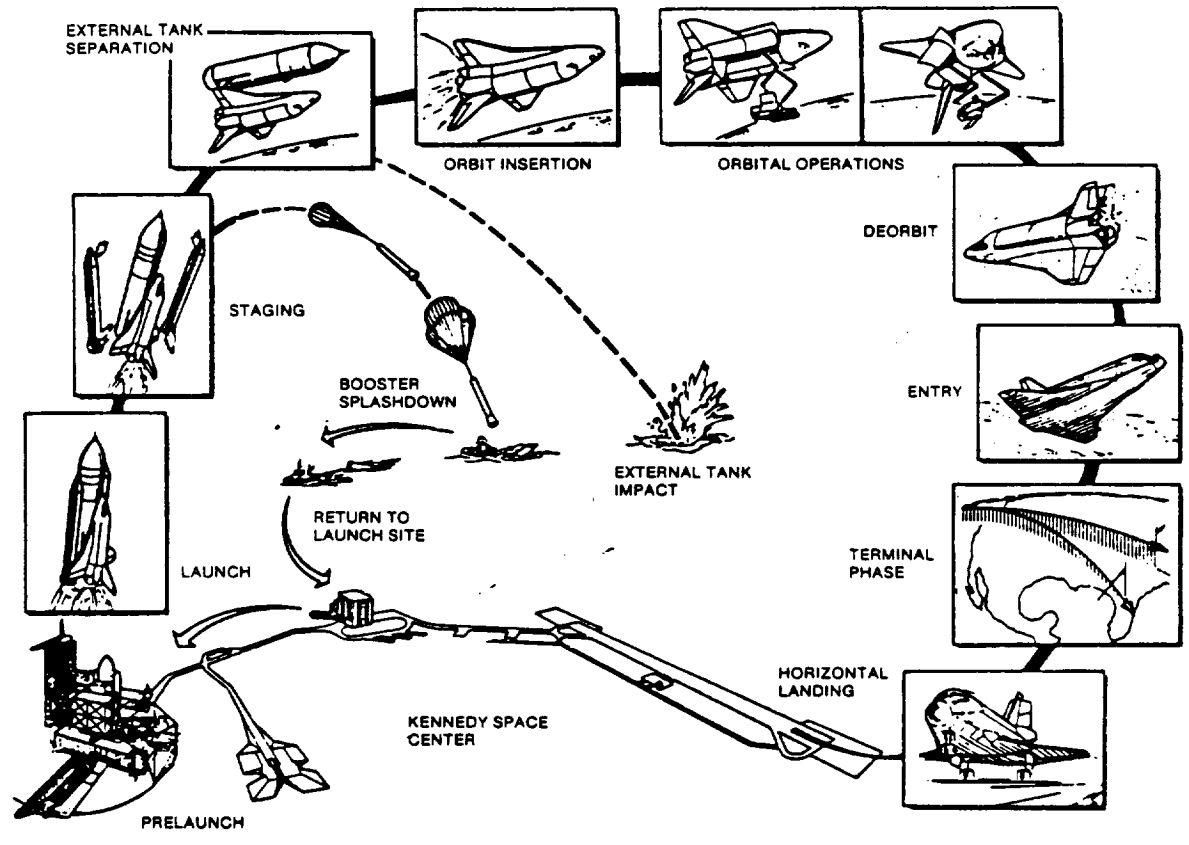


FIGURE 1.- ORBITER MISSION SEQUENCES.

The exterior surfaces of the TPS must also provide an acceptable aerodynamic surface to avoid early tripping of the high-temperature boundary layer (from laminar to turbulent flow). This would significantly increase the thermal heat load to the structure. This requirement resulted in maintenance of rigid fabrication tolerances during the manufacture of the TPS.

The key driver to the design of the TPS has been the requirement for the TPS to function for 100 missions with minimal weight, maintenance, and refurbishment.

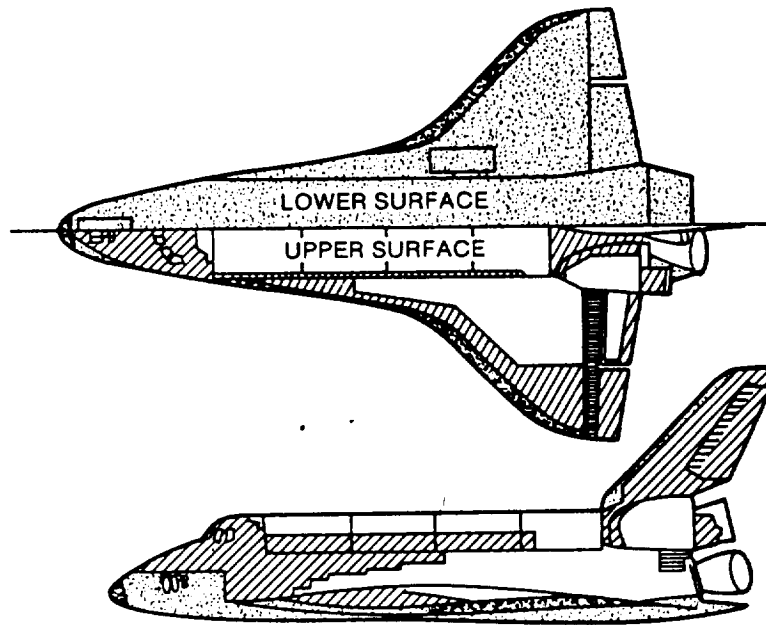
THERMAL PROTECTION MATERIALS

The location of the various thermal protection materials that are applied to the Orbiter structure is shown in figure 2. The allocation was based primarily on the inherent temperature capability of the materials. The following sections cover the individual material characteristics.

RSI TPS

Three material systems applied to the Orbiter are broadly characterized as reusable surface insulation (RSI). Low-density silica ceramic insulation comprises two of these material systems. The third material consists of a coated nylon felt system.

The ceramic tiles are classified in two categories: the high-temperature reusable surface insulation (HRSI) and the low-temperature reusable surface insulation (LRSI). The primary difference in these material systems is in the surface coating. The HRSI tiles (predominantly on the lower Orbiter surfaces) are coated with a black borosilicate glass. Whereas, the LRSI tiles contain a white coating. Both the HRSI and the LRSI TPS tiles are manufactured by the Lockheed Missiles and Space Company (LMSC). The actual tile installation on the Orbiter structure is performed by Rockwell International.








-  REINFORCED CARBON-CARBON
-  HIGH-TEMPERATURE REUSABLE SURFACE INSULATION
-  LOW-TEMPERATURE REUSABLE SURFACE INSULATION
-  COATED NOMEX FELT
-  METAL OR GLASS

FIGURE 2.- THERMAL PROTECTION SUBSYSTEM.

The basic insulation material for the tile is manufactured in two densities: 9 lb/ft³, which is identified as LI-900 and 22 lb/ft³ which is identified as LI-2200. These materials cover approximately 70% of the surface area of the Orbiter structure. Most of this area is covered with LI-900 tiles, with the higher density material used in areas of door edges and penetrations where use of a stronger more durable material is required.

The basic raw material for the all-silica TPS tile consists of short-staple, 99.6% pure amorphous silica fiber manufactured by Johns Manville. At LMSC, the fibers are felted from a slurry, pressed, and sintered in the form of rigidized blocks of insulation material. Tiles which have been sized for specific thermal environments are then cut from these blocks of insulation material. The majority of these tiles are cut with a square planform. However, other tile shapes are required because of vehicle geometry. The tiles are then coated with a thin borosilicate glass coating. The HRSI tiles have a coating containing a black pigment (silicon tetraboride) for the proper high-temperature emittance value ($\epsilon > 0.8$) which is needed in the high-temperature applications on the Orbiter. This coating also provides a barrier to moisture absorption. The LRSI tiles have a white coating with the proper optical properties (solar absorptance to total hemispherical emittance ratio ($\alpha/\epsilon < 0.4$)) that is needed to maintain the proper onorbit temperatures for vehicle thermal control purposes. After the coating process, the tiles are treated with a water repellent material under controlled heating/vacuum conditions that imparts a hydrophobic film. This prevents water absorption by the low-density insulation. The tile insulation then remains water repellent until exposure to temperatures greater than 1050° F. The tiles are then shipped to Rockwell in the form of large arrays (√20 tiles/array) which are applied to the Orbiter structure.

The flexible reusable surface insulation (FRSI), which is the simplest TPS used on the Orbiter, consists of a needled Nomex felt. It is coated with a thin silicone elastomeric film. This material is provided in the form of 3- by 4-foot sheets ranging in thickness from 0.16 to 0.32 in. by the Globe Albany Company. This material is installed on the Orbiter structure by Rockwell International.

RCC MATERIAL

A unique structural material called reinforced carbon-carbon (RCC), manufactured by the Vought Corporation, protects the Orbiter's nose cap and wing leading edge in the regions of highest temperature on the Orbiter.

The fabrication of the RCC begins with a rayon cloth, which is graphitized and impregnated with a phenolic resin. This impregnated cloth is layed up as a laminate and cured in an autoclave. After cure, the laminate is pyrolyzed (baking the resin volatiles out) at high temperature to convert the resin to carbon. The part is then impregnated with furfural alcohol in a vacuum chamber, cured, and pyrolyzed again to convert the alcohol to carbon. This process is repeated three times until the required carbon-carbon density of 90 to 100 lb/ft³ is achieved.

The resulting RCC part is a hard carbon structure possessing reasonable strength and low coefficient of thermal expansion. This provides excellent resistance to thermal stresses and shock. The carbon-carbon is protected from oxidation by converting the outer surface to silicon carbide (SiC) in a diffusion coating process. The oxidation-resistant coating is applied to the part by packing it in a retort with a dry-pack material made up of a mixture of alumina, silicon, and silicon carbide. The retort is placed in a furnace and the coating process takes place in argon with a stepped time-temperature cycle of up to 3200° F. A diffusion reaction occurs between the dry pack and carbon-carbon. This causes the outer layers of the carbon-carbon to convert to silicon carbide (whitish-gray color) with effectively no thickness increase of the uncoated part.

Further oxidation resistance is provided by impregnation with tetrethyl-orthosilicate (TEOS). When cured, TEOS leaves a silicon dioxide (SiO₂) residue throughout the coating and substrate to further reduce the area of exposed carbon. The final step in the fabrication process is the application of a surface sealant (sodium silicate/SiC mixture) to fill any remaining surface porosity or microcracks.

THERMAL PROTECTION DESIGN

RSI DESIGN

The HRSI and LRSI tiles are bonded to the Orbiter structure. A silicone adhesive and an intervening layer of nylon felt material as shown in figure 3 are used. The low-density silica tile is an excellent thermal insulator. However, as it is a ceramic material, it possesses low strength and is brittle. For that reason, a nylon felt material, known as a strain isolation pad (SIP), is used to isolate the structural strains and deflections of the Orbiter airframe from inducing critical stresses in the tile. Tiles are densified by a ceramic slurry process at the inner moldline assuring adequate strength at the tile/SIP interface. Densification was implemented to assure adequate tile structural margins for the predicted load cases. Since so many parts are involved (approximately 31,000 tiles), pull tests were performed to verify that each tile system (tile/SIP/bond) installed on the Orbiter possessed adequate strength margin. Tile-to-tile contact resulting from acoustic-induced tile movement or from contraction of the airframe in the cold extremes of space is prevented by providing gaps between the tiles. The filler bar material in the bottom of the tile-to-tile gaps is used for thermal insulation from tile-to-tile gap heating.

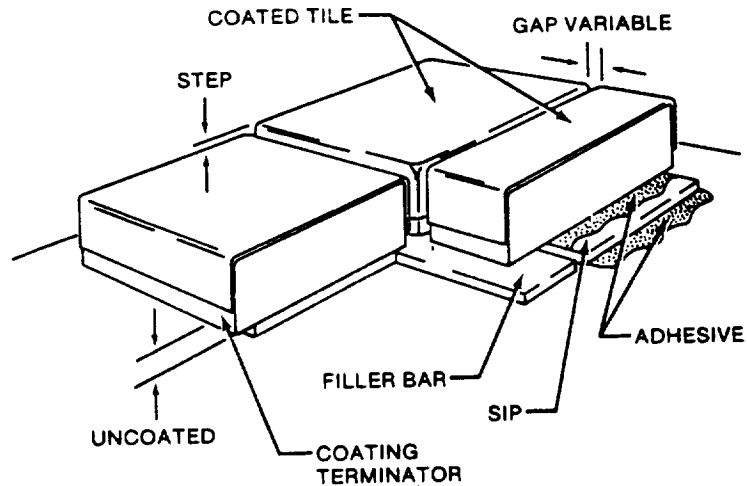
In the higher pressure gradient regions of the Orbiter, open tile-to-tile gaps could result in sufficient ingestion of high-temperature gas flow during entry. This could cause local overtemperature of the various TPS components and the structure. To preclude this from happening, two basic types of gap fillers, "pillow" or "layer", are bonded to the top of filler bar as shown in figure 4. Thermal barriers made from the same cloth and filled with soft insulation and metallic springs are used to fill the larger tile-to-tile gaps around movable hatches and doors.

The FRSI TPS installation is the least complex of the TPS materials used on the Orbiter. In this case, 3- by 4-foot blankets of Nomex felt which has been heat-treated and coated with silicone elastomer are bonded with a silicone rubber adhesive to the structure. Figure 5 shows a cross section of this insulation system.

The RSI material characteristics and detailed description of the design applications have been presented in reference 1-3.

LESS DESIGN

The leading-edge structural system (LESS) of the Orbiter consists of the RCC nose cap (figure 6) and wind leading-edge panels (figure 7), the metallic attachments to the Orbiter structure, the inter-



MATERIALS

- TILE - 22 LB/FT³ PURE SILICA FIBER-FIRED AT 2300° F
- 9 LB/FT³
- COATING - BOROSILICATE (GLASS) FOR WATER-PROOF AND OPTICAL PROPERTIES
- SIP - NOMEX FELT
- FILLER BAR - COATED NOMEX FELT
- ADHESIVE - ROOM-TEMPERATURE VULCANIZING (RTV) SILICONE

FIGURE 3.- TILE SYSTEM CONFIGURATION.

nal insulation system, thermal barriers, and the interface tiles between the RCC and acreage reusable surface insulation.

The wing leading edge and the nose cap are structural fairings which transmit aerodynamic loads to the forward bulkhead or to the wing spar through discrete mechanical attachments. Inconel 718 and A-286 stainless steel fittings are bolted to flanges formed on the RCC components. They are attached to the aluminum wing spar and fuselage forward bulkhead. The fitting arrangement provides thermal isolation, allows thermal expansion, and accommodates structural displacement. The wing leading edge consists of 22 panels joined by 22 T-seals. This segmentation is necessary not only to facilitate the high-temperature fabrication process but also to accommodate the thermal expansion during entry of the leading edge while preventing large gaps or interference between the parts. In addition, the T-seals prevent the direct flow of hot boundary-layer gases into the wing leading-edge cavity during entry. The nose cap seal design and structural attachments are similar to the wing leading edge.

The RCC parts form a hollow shell, which promotes internal cross radiation from the hot stagnation region to the cooler leeward surface area. This reduces the stagnation temperatures and thermal gradients around the shell. The operational temperature range of the RCC is from -200° to 3000° F. Since RCC is not an insulator, the adjacent aluminum and the metallic attachments are protected from internal radiant heating by internal insulation. Dynaflex insulation, contained in formed and welded Inconel foil, protects the metallic attachment fittings from the heat emitted from the inner surfaces of the RCC wing panels. The nose cap internal insulation system consists of blankets fabricated from AB-312 ceramic cloth, saffil and Dynaflex insulation. HRSI tiles protect the nose cap bulkhead access door from the heat emitted from the hot inside surface of the RCC.

The RCC material characteristics and detailed description of the design application have been presented in references 4-7.

ELEVON/ELEVON ABLATOR

Before the first flight of Columbia and late in the Orbiter fabrication cycle, thermal analysis/wind tunnel testing indicated that the areas between the inboard and outboard elevons would

ORIGINAL
OF POOR QUALITY

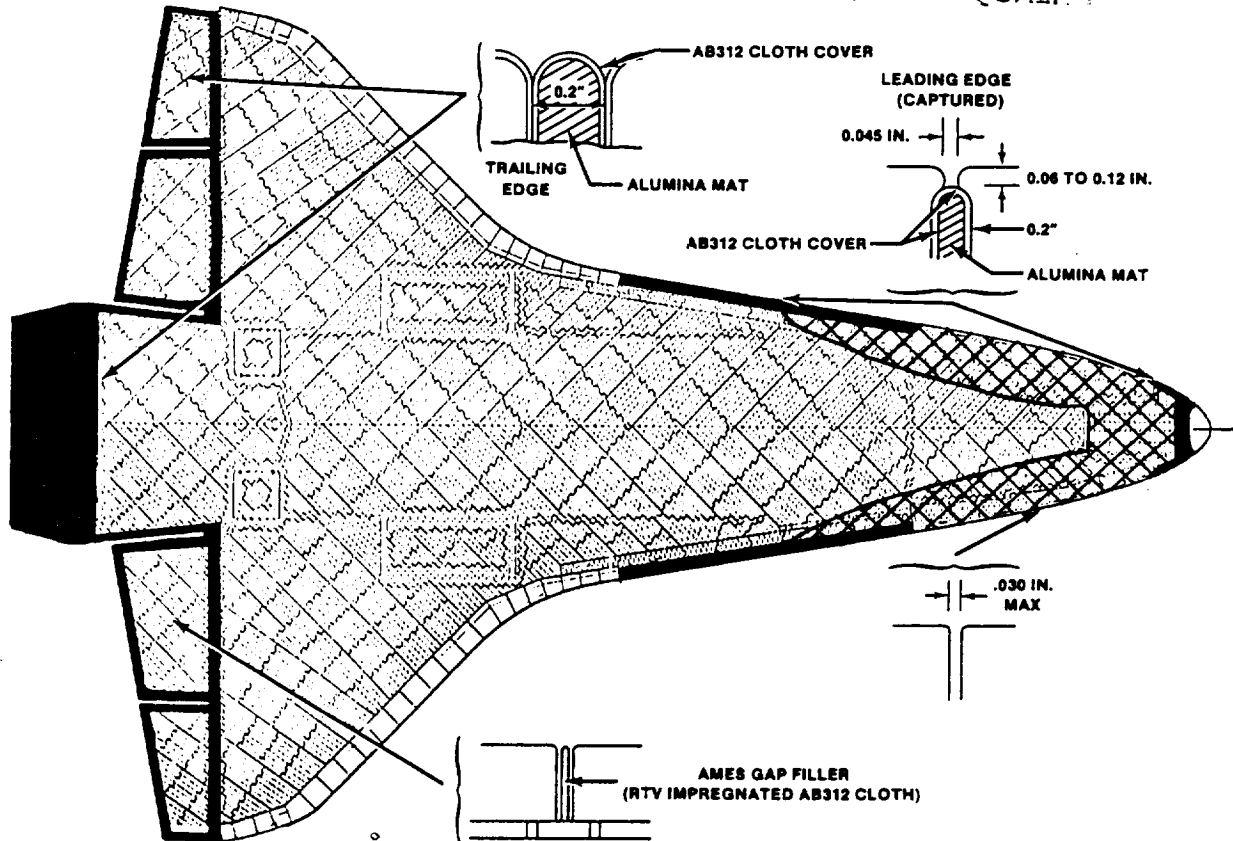


FIGURE 4.- HIGH DELTA-P GAP FILLER ZONES.

encounter temperatures that were too high for tiles to survive even a single mission ($\sqrt{32000}$ F). Therefore, an ablative material was installed between the split segments of the elevons (outboard end of each inboard elevon and inboard end of each outboard elevon) as shown in figure 8. The ablative material (AVCOAT 5026-39HC/G) was the same as the Apollo heat shield material. It consisted of an epoxy-novolac resin filled with microballoons and a mixture of silica and E-glass fibers. The resin mixture was injected into a fiberglass, open-faced honeycomb core which was bonded to an aluminum plate. Since the ablator chars and undergoes surface erosion, it was replaced after each flight. As a result, the ablator system was mechanically attached to the wing structure for easy installation and removal. The first five flights indicated lower temperatures than initially predicted. All Orbiters are now being returned to the original reusable silica tile design in the elevon split area.

THERMAL PROTECTION SYSTEM TECHNOLOGY

RSI MATERIAL SELECTION

Early in the 1970's, contractors began developing a lightweight, rigid ceramic TPSs for the Shuttle program. The technology programs from 1970 to 1972 consisted of three distinct development phases. The first phase covered materials screening and initial laboratory formulation of materials. Lockheed developed the all-silica system. A mullite system was developed by McDonnell-Douglas. During this phase, initial mechanical and thermal properties were obtained from materials produced in the laboratory. A second phase of development activities was undertaken with the initial contractors as well as with General Electric who was also using mullite materials at the time. During this phase, the design methodology for these brittle materials was developed and a reasonable understanding of the behavior under various load conditions evolved. A major advance occurred with the improvements of the thermal stability characteristics of the silica fiber. A third technology phase was implemented with these contractors. The primary emphasis during this phase was the development of attachment methods for these low density ceramic materials. These materials possessed a low strain

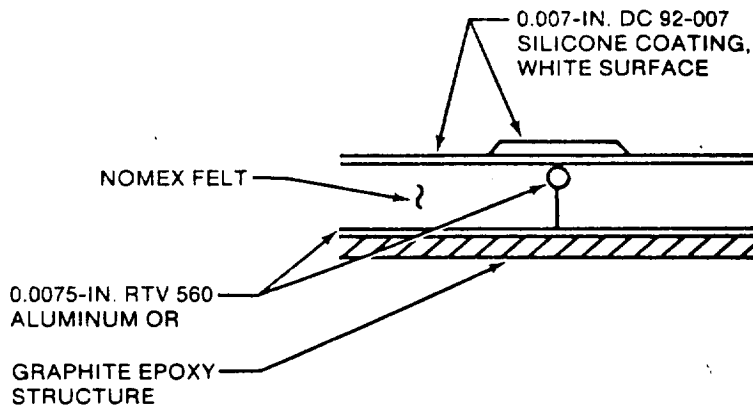


FIGURE 5.- FRSI TPS INSTALLATION.

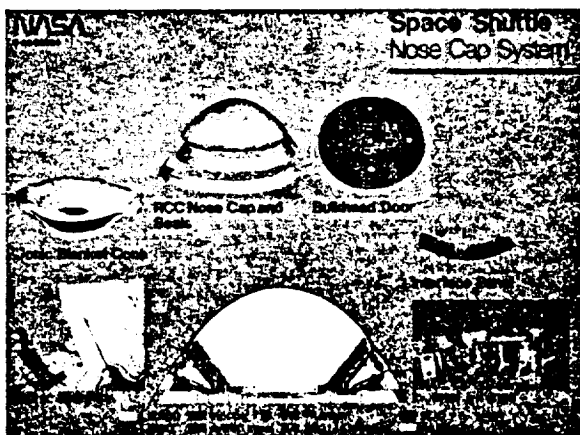


FIGURE 6.- SPACE SHUTTLE NOSE CAP SYSTEM.

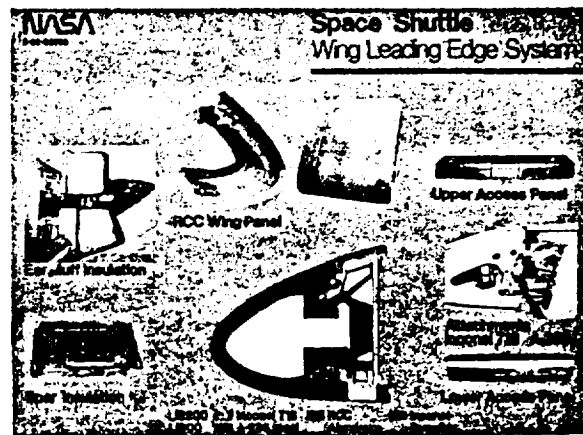


FIGURE 7.- SPACE SHUTTLE WING LEADING EDGE SYSTEM.

to failure capability. The very low density silica material LI-900 proved to be a feasible material. Enough experience had been gained through these technology programs to undertake the selection process for the Orbiter TPS. It was found that the silica strength properties were not adversely affected by high temperature exposure. In contrast, the mullite material had significant strength loss with temperature. Additionally, the mullite contractors failed to strengthen the mullite material to levels compatible with the induced thermal stresses of entry heating. Failures were predicted and experienced during test. Mullite materials initially were expected to have higher temperature capability than silica. However, the low density silica possessed better thermal performance characteristics due to the small fiber diameter material used in its formulation. All of these factors clearly indicated that the rigidized silica ceramic material was the superior product. It was selected in January 1973 as the baseline TPS material. The evolution of the RSI TPS has been presented at a number of conferences (references 8-10).

PRODUCTION

In June 1973, Lockheed was selected to provide the silica RSI TPS for the Orbiter. The reusable ceramic tile engineering, design, and installation to the Orbiter remained a Rockwell responsibility. This allowed for integration of the tile system with the structure design and numerous TPS penetrations that were required. This was in contrast to the leading-edge structural system which was awarded to the Vought Corporation. Vought was responsible for the design, manufacturing, and engineering for the RCC parts. Whereas Rockwell was responsible only for the attachment interface to the structure and the internal insulation. This separation of the design was acceptable because of the configuration of the Leading Edge Structural Subsystem (LESS).

The transition from laboratory and pilot plant production of the silica RSI to a full production status was not accomplished without the usual attendant scale up problems. One key aspect in the ini-

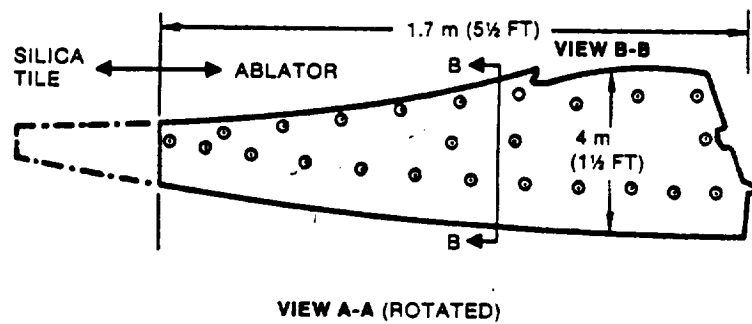
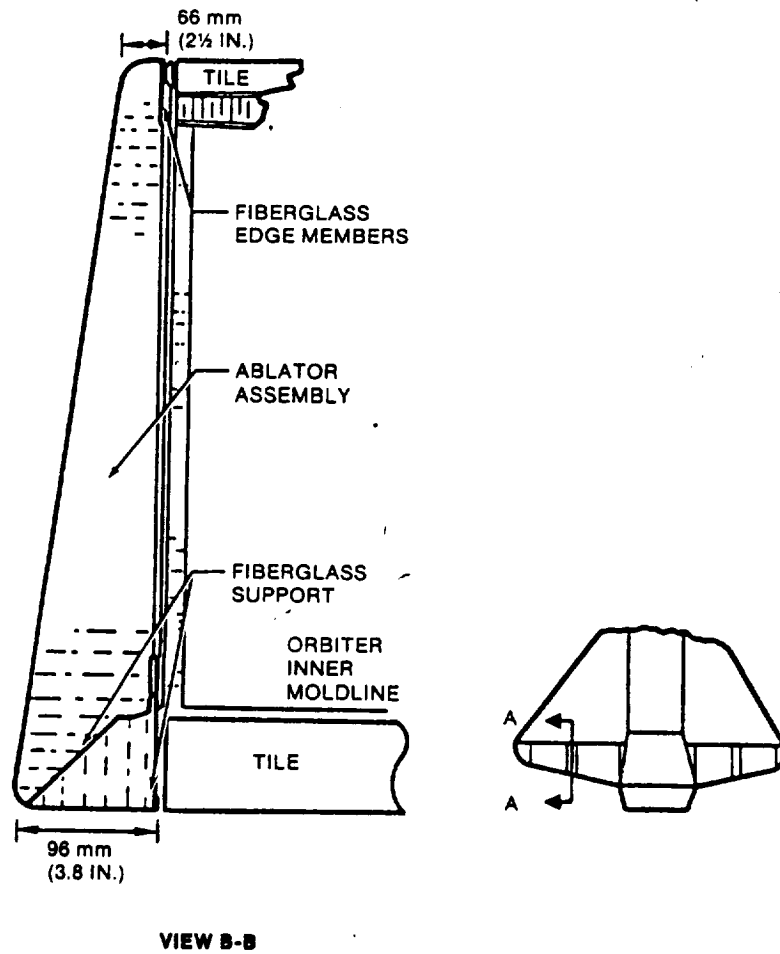


FIGURE 8.- ELEVON/ELEVON ABLATOR INSTALLATION.

tial process developing phase was control of the purity and consistency of the silica fibers. The amorphous silica fiber, a key ingredient in the production of the silica tile, impedes the formation of crystalline forms of the silica. These crystalline forms have a thermal expansion coefficient 30 times greater than the amorphous form. Transformation from the amorphous structure to crystalline form is associated with totally unacceptable shrinkage and distortion of the sintered silica composite. To achieve the required dimensionally stability ultra pure silica fiber greater than 99.6% pure was necessary.

Early in the production phases, fiber with sufficient purity to meet the high production capability for the Orbiter became a major concern. The fiber delivered by Johns-Manville did not meet all the purity requirement and extensive post-treatment was needed. At one point, an alternate high purity fiber source was considered. However, the fiber diameters were larger than the JM fibers which would have adversely affected the thermal performance. Rigid process controls were established from the starting point, that is, from the sand used in making the fiber, through to the fiberizing and cleaning process. These controls minimized contaminants and lead to the delivery of sufficiently pure fibers for the Orbiter tile application.

The next key material development issue encountered during the production phase involved the glass coating. During manufacturing and during thermal tests, the multi-layer glass coating applied to the tile had a tendency to crack or foam. This caused problems related to tile moisture absorption and dimensional stability. A single layer coating, Reaction Cured Glass (RGG), was developed at the Ames Research Center. It did not foam during processing and had a better match with the thermal expansion coefficient of the silica insulation material. This process was eventually implemented in the LMSC production facility after a lengthy verification test program. These tests demonstrated its superior performance as compared to the previous multi-layer coating system.

Rigid process controls were needed to take the tile from the laboratory to production scale-up. A modern manufacturing facility was created at LMSC's main plant in Sunnyvale, California. That plant contained the latest blending and slurry casting and coating equipment, precision controlled kilns and furnaces with low contaminant requirements, and sophisticated numerically controlled machinery to fabricate the TPS tile. Fabricating the tile from a basic block of insulation material was indeed a formidable engineering manufacturing task. The Rockwell master dimension engineering data base and vehicle configuration coordinates were converted into computer tapes that drove the numerically controlled mills that machined the tiles to precise dimensions. After the coating and waterproofing process, Lockheed's job was finished. The tiles in large array form were shipped to Rockwell. Rockwell subsequently bonded them to the Orbiter structure.

RSI DESIGN CHALLENGE

First the RSI material is produced in the form of tiles with dimensionally stable planforms. The next major technical problem became one of assuring adequate attachment to the Orbiter vehicle structure. As mentioned previously, the RSI ceramic TPS is a relatively brittle, low strength material. Therefore, a strain isolation system is needed providing mechanical isolation of the tile from structure deformations. To accomplish this function, the tile was bonded to a low-modulus nylon felt pad with a silicone adhesive. Then the composite was bonded to the structure with the same adhesive. For the load conditions predicted during the initial design study there was every reason to believe that the design approach would function properly. However, as the mission requirements became better defined, the updated environments indicated higher load conditions. These loads would have exceeded the strength capability of the low density tile/SIP system. In addition, structural integrity tests of the tile/SIP system indicated the presence of discrete stress concentrations. They were caused by the needling characteristics of the SIP, which significantly reduced the strength of the system. Many different approaches were explored to solve this problem. The most effective procedure involved a densification process. The inner mold line of the tile was densified by filling the voids in the tile fiber material with a ceramic slurry. It was found that this densification process distributed the loads induced by the individual fiber bundles in the SIP. It also provided adequate strength such that the failure of the tile/SIP system always occurred in the tile and not at the SIP to tile joint. With this deficiency corrected, a truly functional design of the Orbiter TPS had been achieved. The various sources of tile stresses, the stress analysis methodology, description of the various structural integrity tests, and verification activities were described in reference 11.

REINFORCED CARBON-CARBON

Materials Selection

Carbon-carbon material development during the Shuttle technology phase programs in the early 1970's was conducted at the McDonnell-Douglas and Vought Corporations (reference 12 and 13). These early material investigations were divided into two classes, substrates and coatings. The ultimate test of the materials was their compatibility as a system. Many combinations of carbon filaments, binder materials, inhibiting and coating materials were developed and tested. Both yarns and cloths of carbon and graphite, with phenolic and epoxy as initial binders were evaluated for basic strength properties. Further strengthening was accomplished by the chemical vapor deposition (CVD) reimpregnation process and by reimpregnation with pitch and furfural alcohol. Various metal and boride oxidation inhibitors were considered as diffused-in coatings and as additives to the initial binders. The

add-mix oxidation inhibitors reduced the interlaminar strength properties. Extensive oxidation and structural testing indicated that the cloth with carbon binder and a silicon carbide diffusion coating provided the highest temperature and strength reuse capability.

The selected material used on the Orbiter is an all-carbon composite produced by the Vought Corporation. Graphite fabric, preimpregnated with phenolic resin, is laid-up in complex shaped molds and cured. Once cured, the resin polymer is converted to carbon by pyrolysis. The part is then impregnated with furfuryl alcohol and pyrolyzed three more times to increase its density and strength. The carbon-carbon is protected from oxidation by converting the outer carbon plies to silicon carbide in a diffusion coating process. Further oxidation protection is provided by (1) impregnation of the laminate with tetraethyl orthosilicate (TEOS) which, when cured, leaves a silicon dioxide residue throughout the coating and substrate and (2) a final surface sealant treatment consisting of sodium silicate and graphite fibers.

LESS DESIGN CHALLENGES

The primary purpose for the LESS is to provide thermo-structural capabilities for the regions of the Orbiter that exceed 23000° F. Operational requirements include the retention of aerodynamic shape of the outer moldlines and interface control between the RCC and the RSI tiles. Additionally, control of the aluminum structure temperature to less than 350° F., servicability for easy access and removal of the RCC components, and the capability to sustain 100 missions with minimal refurbishment are required.

The life expectancy of the RCC system is reached in one of two ways. The first is by erosion of the SiC coating which exposes the unprotected carbon substrate to direct oxidation. The second is by subsurface oxidation where the substrate is oxidized with the coating intact in such a way that either the strength of the substrate is diminished or the adherence of the coating is lost.

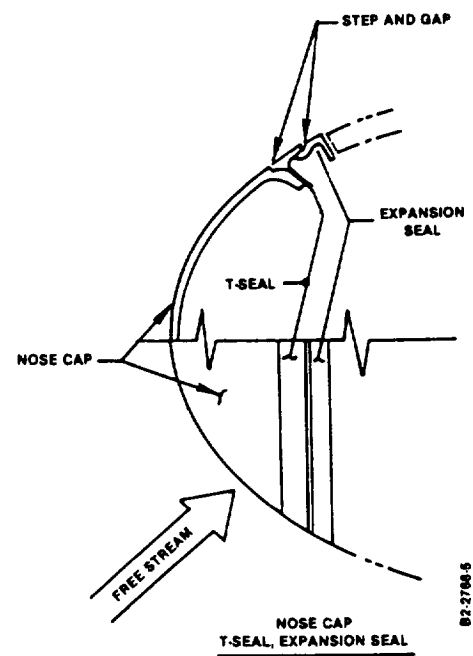
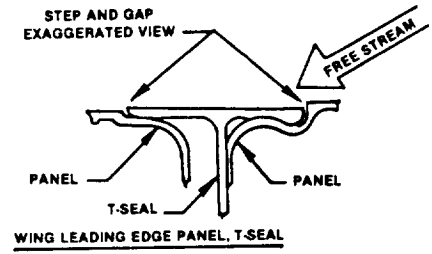
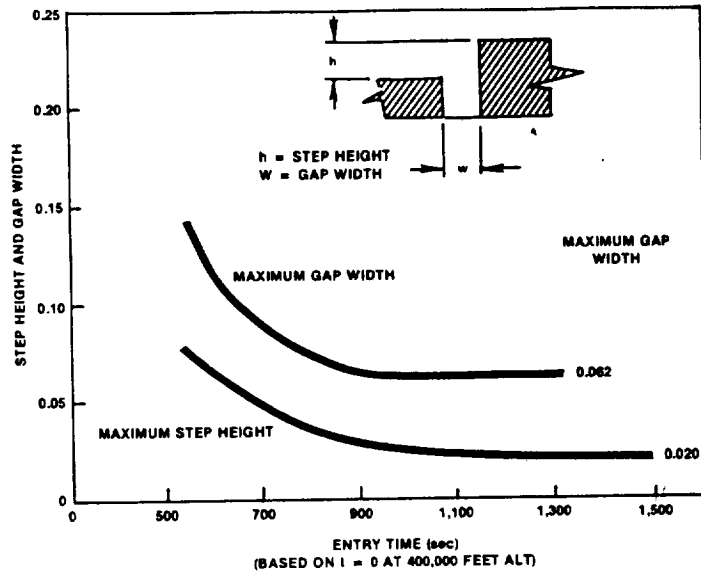
During the NASA technology phases (1970), coating erosion performance was primarily emphasized. At temperatures above the oxidation threshold of silicon carbide (2700° F), the coating will ablate. Thus it will tolerate only a limited number of entries (ref. 14). Therefore, a post-coating heat treat process was applied to the coated RCC part at 3200° F for 45 minutes in argon. This process step was a standard procedure to enhance the coating resistance to oxidation. However, plasma arc tests performed in 1972-73 at NASA/JSC and NASA/Ames indicated that non-heat treated RCC specimens experiences less mass loss than the heat treated RCC. Further investigation revealed oxidation of the substrate at the coating substrate interface. This was a result of inherent microcracks in the silicon carbide coating. Extensive air oxidation tests over a wide range of temperature and pressures, microanalyses, and mechanical property tests were conducted. These tests characterized the subsurface oxidation and its impact on RCC mission life (ref. 15 and 16).

The resultant strength degradation caused by the substrate mass loss restricts the mission life capability through the inability of the RCC to sustain the predicted loads. Therefore, the TEOS impregnation process was developed which infiltrated the silicon carbide coating and carbon substrate. This resulted in increased oxidation protection. Before delivery of the Columbia, element tests revealed the possibility of getting porous substrate in some areas of the production parts. High porosity in the substrate reduces the effectiveness of the basic SiC coating and the TEOS impregnation. Consequently, the oxidation rate in the porous region is increased. In some cases, the mission life of the affected part is reduced. A post-coating treatment of sodium silicate and graphite fiber sealing the surface porosity has minimized this undesirable surface condition.

Critical manufacturing challenges were to hold ± 10 mil tolerance on large molded parts. Additional challenges were high temperature tooling and developing Non Destructive Evaluation (NDE) techniques to monitor process and insure consistent hardware.

The most difficult technical problem was maintaining dimensional tolerances for the gap and step requirements (fig. 9) in the LESS design. An extensive manufacturing tolerance and process program characterized the dimensional changes of an RCC part. Dimensional fit and control was then achieved by designing the growth and expansion of the RCC into all stages of tooling. Since all trim and drilling of the RCC parts is performed before the coating process, the ability to predict any growth or shrinkage after coating is most important. A final assembly fixture (fig. 10) was used for fit-up of the RCC wing panels and seals just before coating as well as for final assembly of the coated panels with the attach fittings. A similarly employed assembly fixture is used for the nose cap and seals.

Continual inspection, acceptance testing, and weight measurements are performed during the RCC fabrication process. NDE inspection (visual, x-ray, ultrasonic and eddy current) of the parts along with strength and mass loss testing of control panels processed with each part assures acceptable substrate in all hardware.



B2-2764-5

FIGURE 9.- SPECIFICATION REQUIREMENTS (STEPS AND GAPS).

Elevated temperature is the primary factor in the design of the attach fittings, the internal insulation system for the protection of these attachments, and the adjacent aluminum structure. Thermophysical properties of the RCC material (i.e., good conductor) and the hollow shell design promote internal cross-radiation from the hot stagnation region to the inherently cooler regions. Since structural fasteners were required to be held below 1200° F., they needed to be located inside the outer moldline (OML). However, as the attachment flange was lengthened, it also intercepted more cross-radiation from the panel surface. Since the attach hardware also intercepted the OML radiation, it was necessary to provide insulation to limit the temperatures. Heat resistant metals such as Inconel 718 and A-286 steel interface between the RCC and aluminum support structure. These metal components are protected with various insulation packages composed of Dynaflex, AB-312 ceramic cloth, saffil or RSI tiles. Dynaflex contained in formed and welded Inconel 601 foil, is the primary insulation system used in the wing leading edge. Blankets of Dynaflex and saffil wrapped with AB-312 cloth are used in the nose cap cavity along with RSI tiles on the forward face of the access door. Paradoxically, the internal insulation which prevents exceeding the maximum temperature for the metallic attachments also retards the cooling rate of the RCC lugs. This contributes to the undesirable oxidation rate.

ORBITER FLIGHT PERFORMANCE

RSI FLIGHT PERFORMANCE

The RSI tile performs its required thermal protection function during entry by two primary means of heat dissipation. A large percentage (~98%) of the heat energy is reradiated to the atmosphere by the high-emittance glass coating on the tile surface. The remaining heat energy is effectively retarded by the low diffusivity of the basic insulation material. The basic thermal performance of the RSI tiles can be evaluated by three important parameters: the induced surface temperature profile, the transient response of the RSI interior, and the structural temperature response.

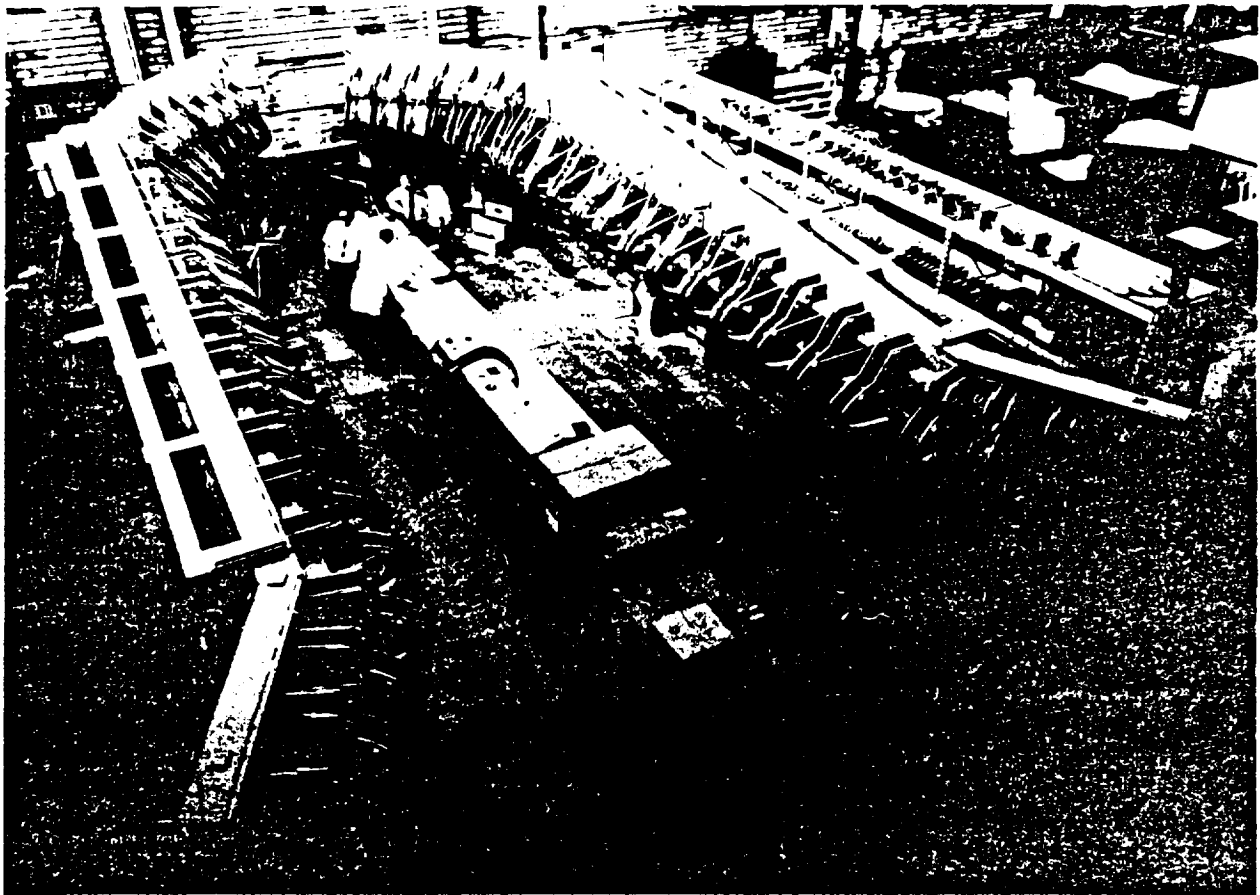


FIGURE 10.- WING LEADING EDGE FINAL ASSEMBLY FIXTURE.

Figures 11 to 13 show comparisons of flight data from STS-5 with predicted performance. In this case, the measured RSI surface temperature was the driving function for the thermal math model. In general, good agreement is shown between the flight data and predictions. Figures 14 and 15 show the distribution of peak surface temperatures and structural temperatures experienced during representative Orbiter test flights. The temperatures on some localized areas such as the OMS pods were higher than expected. Therefore, modification of the TPS was required for the later vehicles that will be flown at the more severe entries typical of the Western Test Range. For the most part, the measured surface temperatures during entry have been lower than expected for the flight tests flown from the Eastern Test Range. The lower surface temperatures indicate lower surface heating rates and a lower heat load into the structure. The lower heating rates are attributed to the noncatalytic effects of the TPS tile coatings. Other contributing factors include later than expected transition from laminar to turbulent flow and internal convective cooling effects on the structure during the later part of entry which had not been accounted for in the thermal math models. These effects are summarized in figure 16.

Tile structural integrity for the most part has been excellent during the flight test program. Since there are so many parts (~31,000 tiles), the tile attachment to the structure has always been one of the major concerns. None of the HRSI tiles on the lower surface have been lost during the flight test program. Some undensified white tiles were lost on the OMS pods during STS-1. This was because of improper machining operations of the diced LRSI tiles in this area. Also, loss of undensified tiles during the STS-3 mission on the upper forward fuselage area and the upper body flap area was attributed to excessive application of the tile rewaterproofing agent. Keeping moisture out of the tile has been one of the major technical problems encountered during the flight test program. The anomalies due to moisture absorption that have occurred during the flight test program, the corrective actions, and ongoing improvement activities are discussed in reference 17.

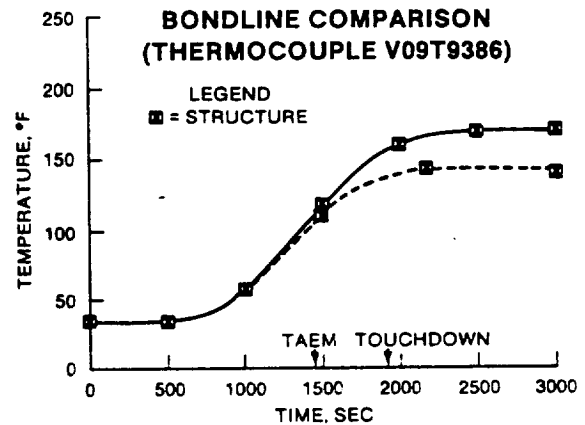
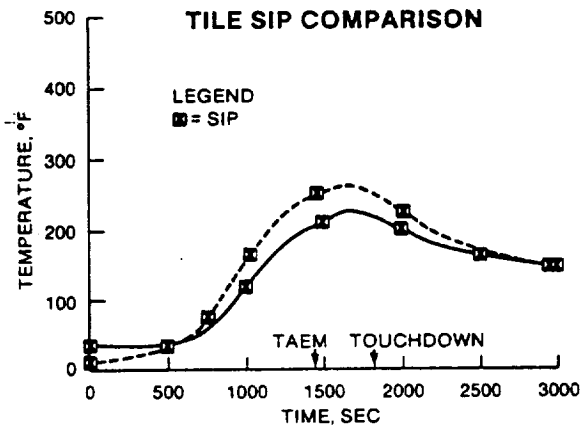
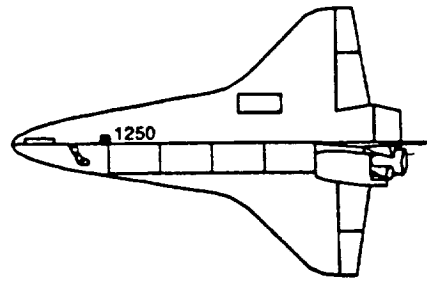
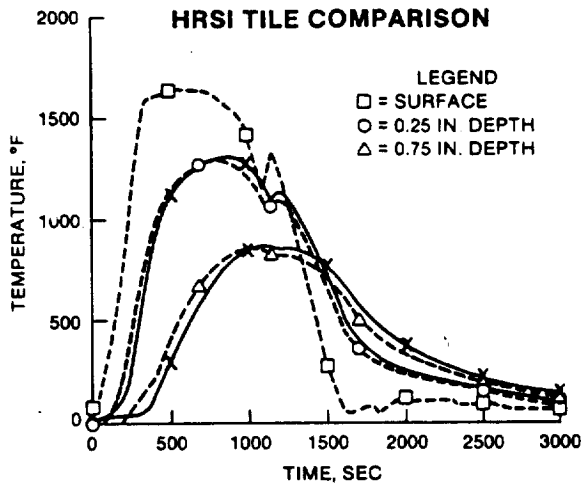


FIGURE 11.- STS-5 FLIGHT DATA (DASHED LINES) VERSUS ANALYSES (SOLID LINES): BODY POINT 1250.

Overall, the TPS tiles have performed exceptionally well despite exposure to adverse weather conditions and debris damage during ascent. Because this material has low impact resistance, minor surface damage in the form of dents, gouges, and coating chips has occurred during all of the flights. This damage is attributed to ascent debris from the external tank and the solid rocket boosters (SRB). A worse case example after entry is shown in figure 17. Some of the conditions have been corrected. A smaller amount of damage occurred during the STS-4, STS-5 and STS-6 flights. The damage that has occurred has not resulted in any significant degradation of the overall Orbiter tile thermal performance. The majority of the damaged areas were readily repairable by use of ceramic filler agents. There has also been some surface contamination of the TPS outer surface. This contamination comes primarily from the decomposition of silicone materials that are used in the gap fillers. Additional contamination is from the aluminum oxide in the SRB plumes and decomposed external tank insulation. The deposits for the most part are surface effects and have not resulted in any loss of thermal performance or life.

Excessive tile-to-tile gap heating has occurred in a number of locations and has been a continual problem during the flight test program. Extensive analyses of the flight data and ground test results have been undertaken to understand this complex flow phenomenon. The excessive gap heating, attributed primarily to excessive tile-to-tile steps and gaps, has resulted in tile sidewall shrinkage, filler bar charring, and localized severe structural temperature gradients in one instance. Gap fillers that have been installed in those areas where excessive gap heating occurred have been completely effective.

In conclusion, even though a number of anomalies have occurred during the first five flights of the Orbiter Columbia and the first flight of the Challenger, the overall thermal-structural performance of the ceramic silica tiles has been far better than expected. The flight performance characteristics of the RSI TPS during the STS-1 through STS-5 missions has been presented in reference 2, 3, and 18.

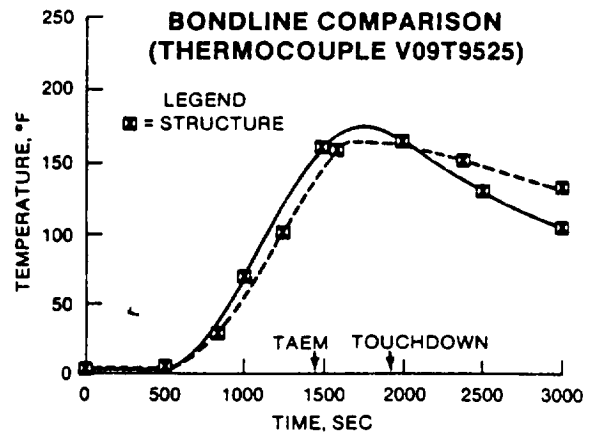
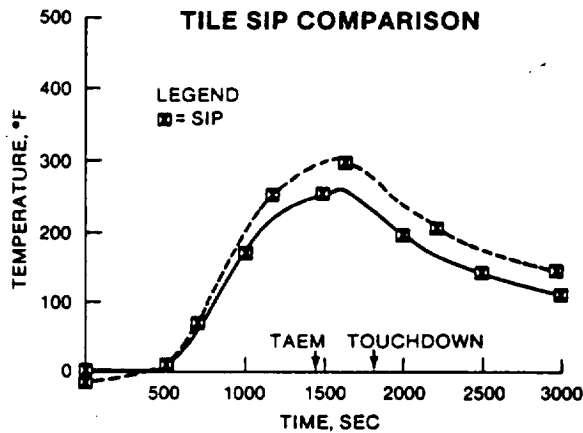
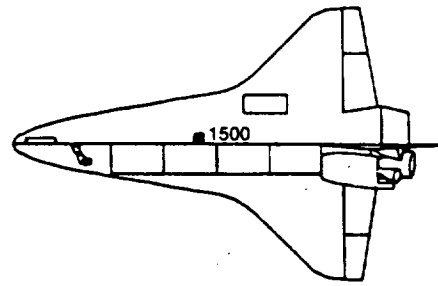
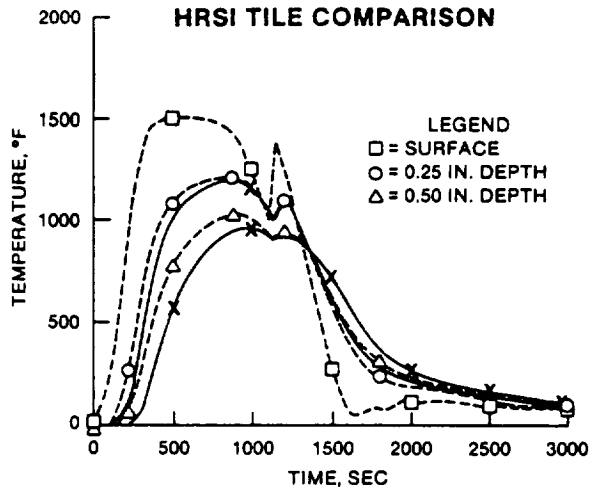


FIGURE 12.- STS-5 FLIGHT DATA (DASHED LINES) VERSUS ANALYSES (SOLID LINES): BODY POINT 1500.

LESS FLIGHT PERFORMANCE

Successful completion of the first five development flights of the Orbiter Columbia have provided sufficient engineering data, coupled with postflight inspections after each flight, to assess the thermostructural design and capability of the LESS. Peak nose cap radiometer temperature measurement (STS-5) of the inner moldline (IML) of the RCC shell are presented in figure 18. A comparison of the predicted and measured stagnation point-IML transient temperature histories (fig. 19) shows the STS-5 flight data 180° F. higher than the prediction but approximately equal to the predicted design temperature using the 14414.1C design trajectory.

Nose cap internal insulation, attachment, and bulkhead measured temperatures for the STS-2, 3 and 5 flights are shown in figure 20. These temperatures agree with predictions made using the thermal math models developed to support flight certification. Postflight visual inspections of the RCC external surface and the nose cap conic internal insulation blankets have indicated no anomalies or degradation. However, damage to the nose cap's lower windward surface interface tiles has occurred as a result of excessive tile-to-tile and RCC-to-tile gap heating. Corrective action in terms of redesigned gap fillers and flow stoppers has been incorporated into this interface area. This eliminates the overheating condition. Radiometer measurement of wing leading edge IML temperature as a function of semi-span is shown in figure 21. The maximum heating zone (45% to 55% semi-span) results from the interaction of the nose cap bow shock and wing shocks producing higher boundary-layer pressures and heat rates. Comparing predicted and measured RCC shell IML temperatures indicates heat flux levels substantially lower than predicted for panels 4 and 22. There was excellent agreement for panel 16 and heat flux levels higher than predicted for panel 9. Wing panel 9 is located in the "double shock" heating zone. The results shown in figure 22 indicate the measured RCC IML tempera-

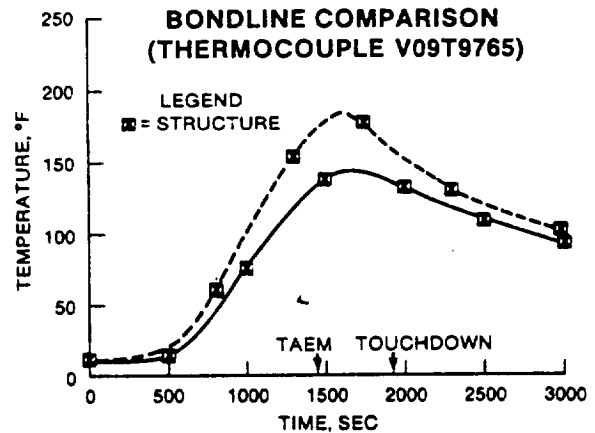
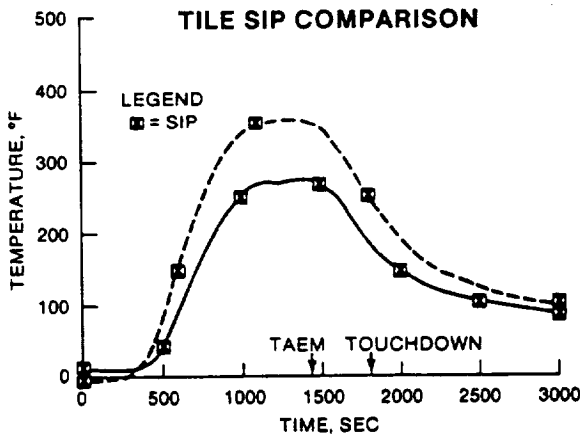
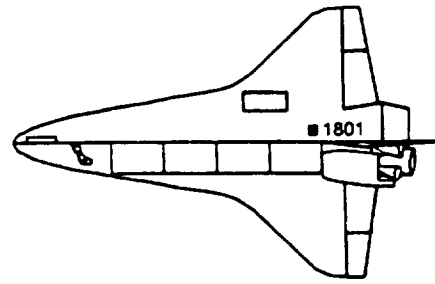
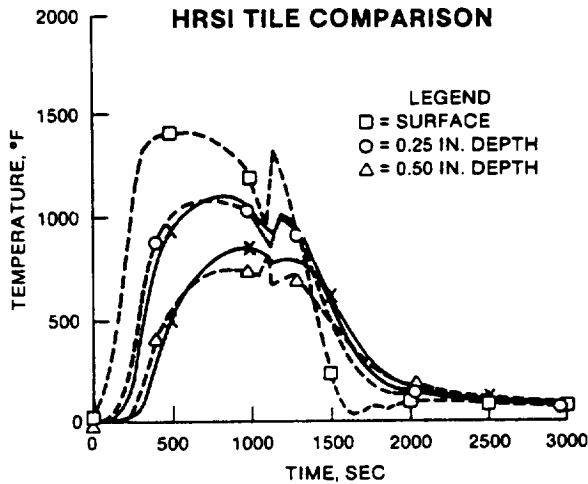


FIGURE 13.- STS-5 FLIGHT DATA (DASHED LINES) VERSUS ANALYSES (SOLID LINES): BODY POINT 1801.

ture (2601° F.). A comparison of measured temperatures of the RCC attachment hardware, internal insulation, and wing spar structure for the STS-2, 3 and 5 flights are shown in figure 23. These temperatures agree with the preflight/postflight predictions made using the math models verified from certification tests.

The wing leading edge panels have all been examined externally for evidence of any anomalies, i.e., coating chips, cracks, etc., after each STS flight. In addition, selected wing panels have been removed for detailed internal inspection of the interior surfaces of the RCC, attachment hardware and Inconel/Dynaflex insulation. The associated upper and lower access panels have also been inspected after flight for evidence of deterioration.

During the STS-2 postflight inspection, areas of discoloration were evident on the wing leading-edge upper access interface panel at RCC left-hand panels 9 through 13 and right-hand panels 10 through 13. This discoloration (white deposit/streaking on black tiles) was the result of gas flow through the subject panels entering the RCC/RSI lower access panel interface. An examination of the lower access panels show gap filler/thermal barrier heating, embrittlement, and discoloration. Inspection of the wing leading-edge front spar showed evidence of gas flow streaking and heating of the tile filler bar (discoloration, scorching, burning) at the RCC panel/T-seal joints. Before the STS-3 flight, larger diameter corner gap fillers were added to the four corners of the lower access panels. Postflight inspections of STS-3 - 5 indicate virtual elimination of hot gas flow-through in those RCC panels which had experienced extensive flow-through heating on STS-1 and 2. The flight performance characteristics of the LESS during the STS-1 through STS-5 missions has been presented in references 6, 7 and 19.

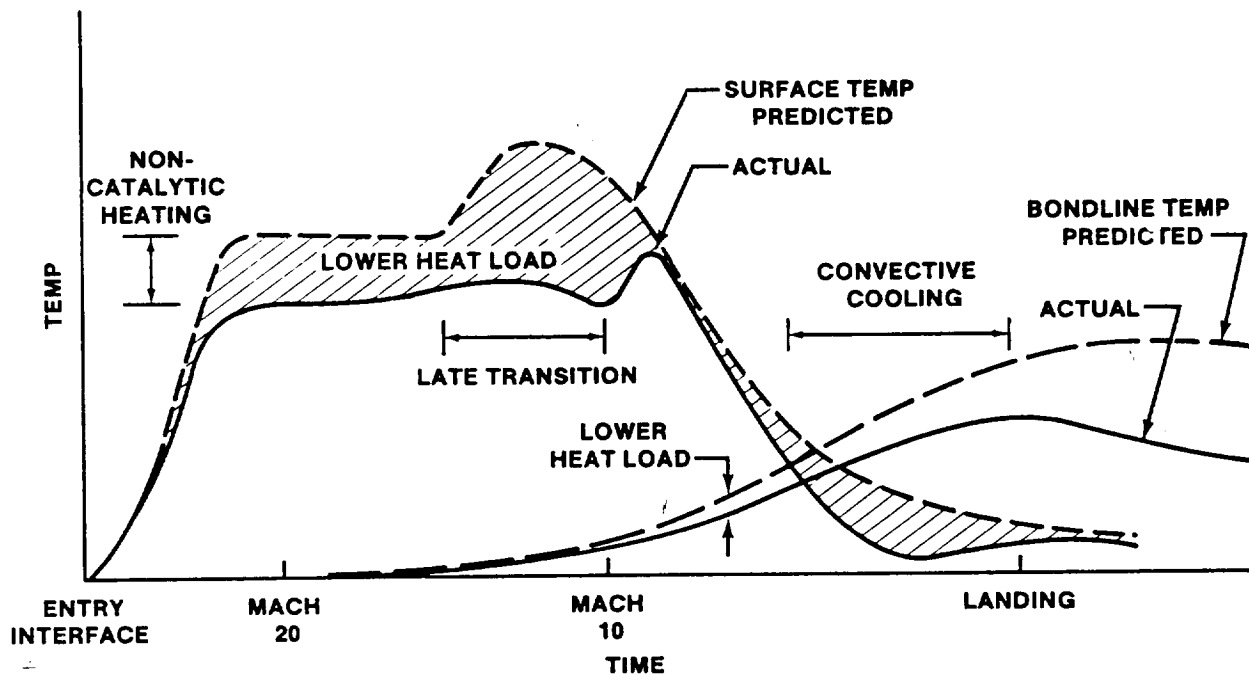


FIGURE 16.- GENERALIZED LOWER SURFACE THERMAL PERFORMANCE RESULTS: STS-1 TO STS-5.

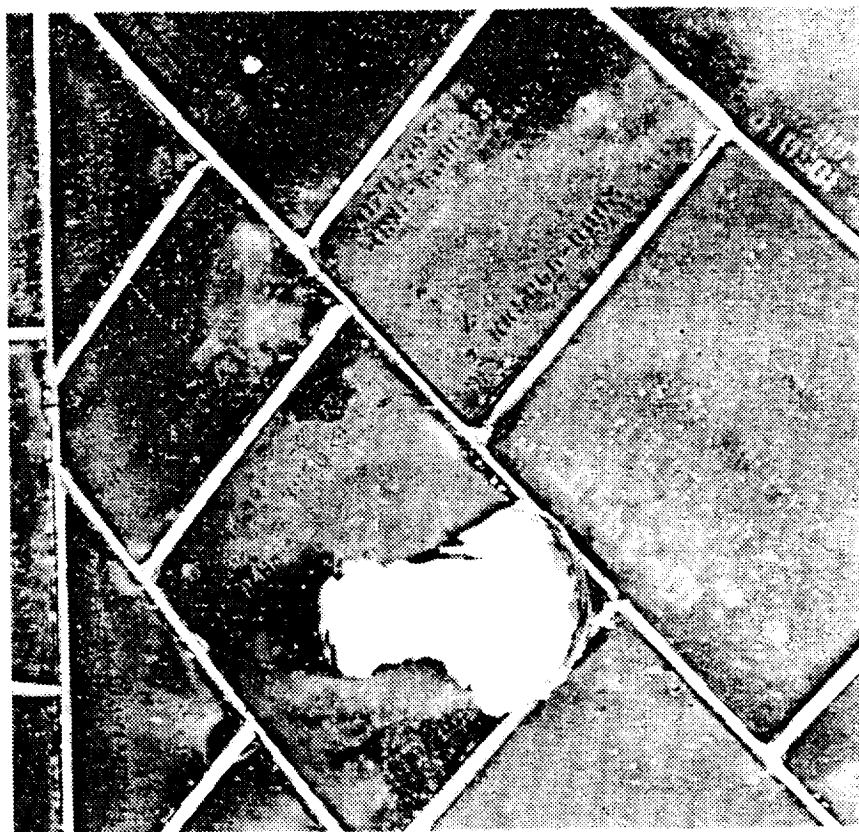


FIGURE 17.- STS-1 DAMAGE AND ENTRY HEATING EFFECTS, BODY FLAP.

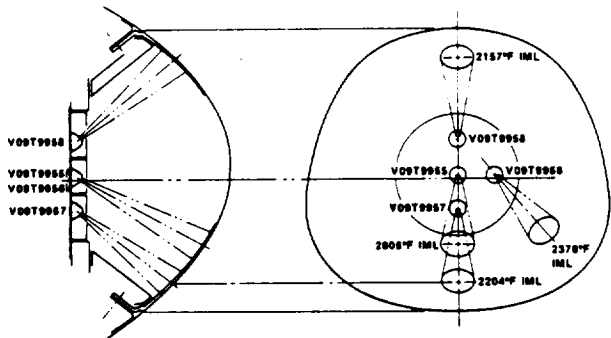


FIGURE 18.- STS-5 NOSE CAP FLIGHT DATA: PEAK RCC IML TEMPERATURES.

ST-5
OF STS-5

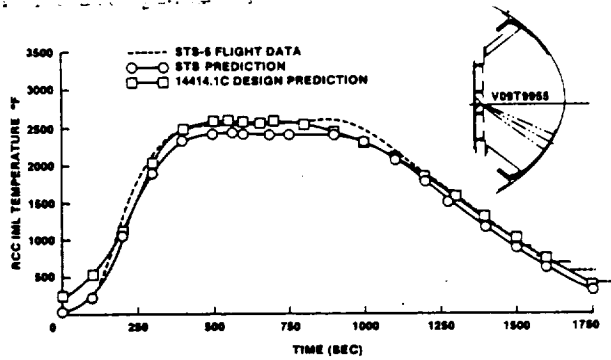


FIGURE 19.- NOSE CAP RCC IML TEMPERATURE.

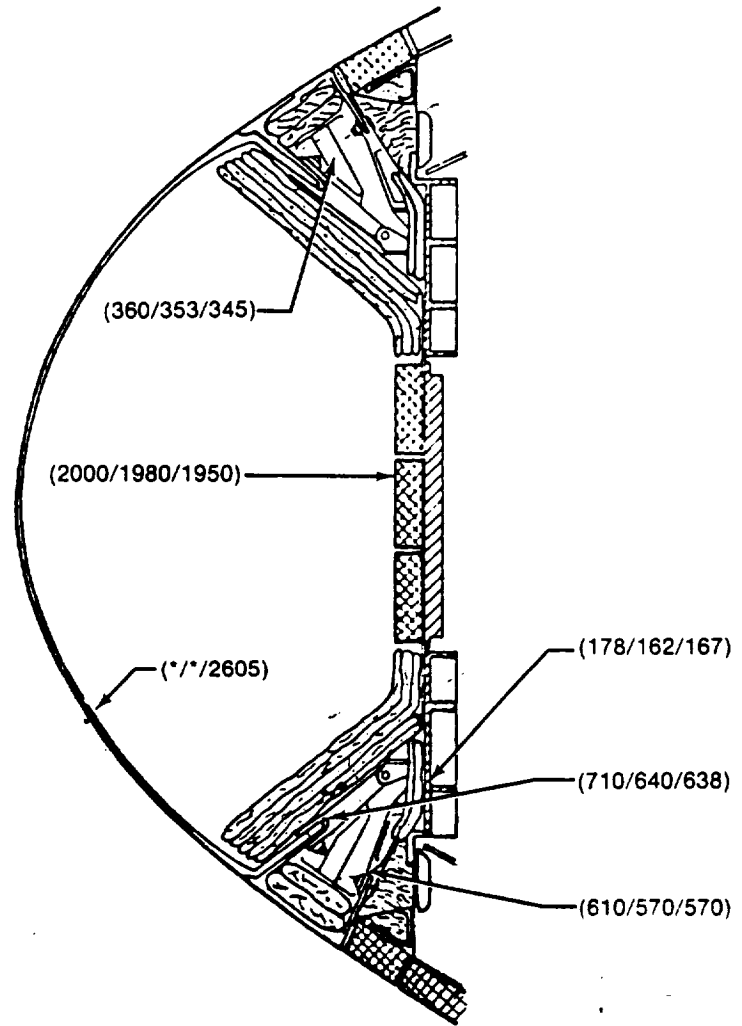


FIGURE 20.- STS-2, STS-3, AND STS-5 PEAK TEMPERATURE (°F): LESS NOSE CAP.

ORIGINAL FACE
OF POOR QUALITY

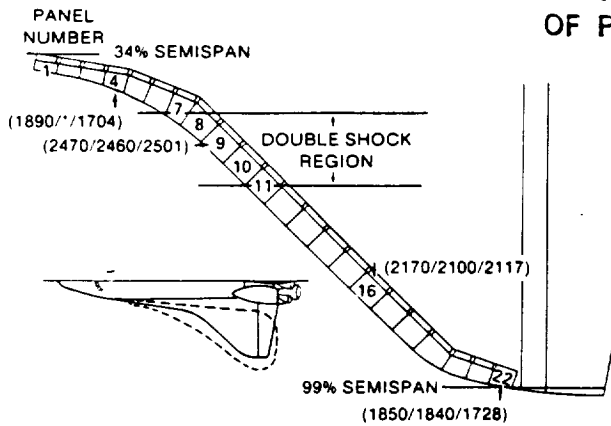


FIGURE 21.- STS-2, STS-3, AND STS-5 PEAK TEMPERATURE (°F): LESS WING LEADING EDGE.

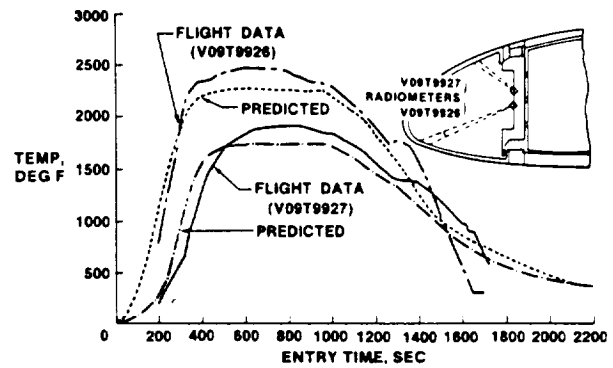


FIGURE 22.- STS-2 FLIGHT RESULTS: LESS-RCC PANEL 9 IML TEMPERATURES.

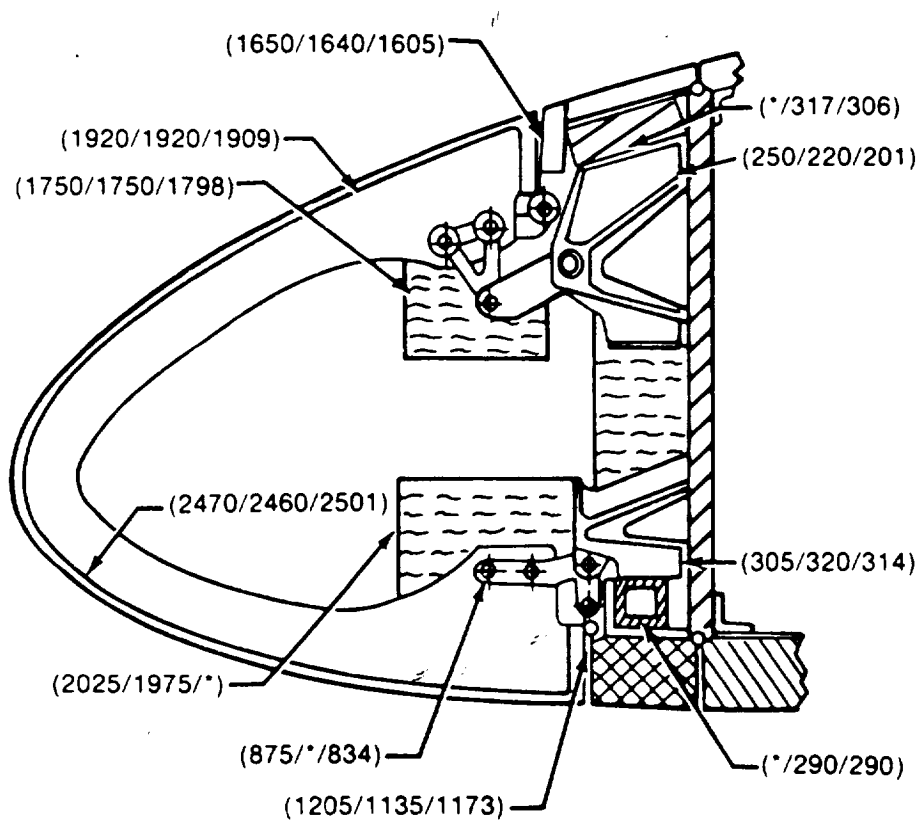


FIGURE 23.- STS-2, STS-3, AND STS-5 PEAK TEMPERATURE (°F): LESS PANEL 9.

CONCLUDING REMARKS

Five successful flights have been accomplished on the Orbiter Columbia TPS and one on the Orbiter Challenger. Satisfactory thermal/structural performance during these flights indicates that the proper thermal protection materials and design approaches were selected for the Orbiter. There are some minor localized areas of the Orbiter where heating or damage exceeded expectations. However, these areas are amenable to minor design modifications. Satisfactory performance is expected during the operational phases of the Shuttle. Degradation of the Orbiter thermal protection system (RSI and LESS) has been minimal, and satisfactory vehicle turnaround operations have been accomplished.

REFERENCES

1. Korb, L. J. and Clancy, H. M., Space Shuttle Orbiter Thermal Protection System: A Material and Structural Overview, 26th National Symposium Society for the Advancement of Material Process Engineering, Los Angeles, CA, April 28-30, 1981.
2. Dotts, R. L., Battley, H. H., Hughes, T. J., and Neuenschwander, W. D., Space Shuttle Orbiter Reusable Surface Insulation Subsystem Thermal Performance, AIAA 20th Aerospace Science Meeting, Orlando, FL, January 11, 1982.
3. Dotts, R. L., Tillian, D. J., and Smith, J. A., Space Shuttle Orbiter-Reusable Surface Insulation Flight Performance AIAA/ASME/ASCE/AHS 23rd Structures, Structural Dynamics and Material Conference, New Orleans, LA, May 10-12, 1982.
4. Smith, T. W., Leading Edge Structural Subsystem Mechanical Design Allowables for Material with Improved Coating System, Report No. 221RPO0614, Vought Corporation, July 1977.
5. Curry, D. M., Scott, H. C., and Webster, C. N., Material Characteristics of Space Shuttle Reinforced Carbon-Carbon, Proceedings of 24th National SAMPE Symposium, Volume 24, Book 2, 1979.
6. Curry, D. M., Cunningham, J. A., and Frahm, J. R., Space Shuttle Orbiter - Leading Edge Structural Subsystem Thermal Performance, AIAA Paper No. 82-0004, AIAA 20th Aerospace Sciences Meeting, January 11-14, 1982.
7. Curry, D. M., Latchem, J. W., and Whisenhunt, G. B., Space Shuttle Orbiter Leading Edge Structural Subsystem Development, AIAA Paper No. 83-0483, AIAA 21st Aerospace Sciences Meeting, January 10-13, 1983.
8. Greenshields, D. H., Strouhal, G., Tillian, D. J., and Pavlosky, J., Development Status of Reusable Nonmetallic Thermal Protection NASA Space Shuttle Technology Conference, Langley Research Center, Hampton, Virginia, March 2-4, 1971, NASA TMX-2273, April 1971.
9. Greenshields, D. H., Meyer, A., Tillian, D. J., Status of RSI TPS Technology Programs, NASA Space Shuttle Technology Conference, San Antonio, Texas, April 14, 1972, NASA TMX-2570, July 1972.
10. Strouhal, G., Tillian, D. J., Reusable Surface Insulation thermal Protection System Test Evaluation Status, NASA Symposium on Reusable Surface Insulation for Thermal Protection of the Space Shuttle, Ames Research Center, Nos. 1-3, 1972, NASA TMX-2720.
11. Moser, T. L. and Schneider, W. C., Strength Integrity of the Space Orbiter Tiles, AIAA/STEP/STFE/SAE/ITEA/IEE 1st Flight testing Conference, Las Vegas, NV, November 11-13, 1981.
12. Development of a Thermal Protection System for the Wing of a Space Shuttle Vehicle, Phase I Final Report, LTV/VSD Report No. TR143-5R-00044, February 22, 1971 (NASA Contract NAS9-11224).
13. Development of a Thermal Protection System for the Wing of a Space Shuttle Vehicle, Final Report MDC E0319, February 24, 1971 (NASA Contract NAS9-11223).
14. Medford, J. E., Multi-Cycle Plasma Arc Evaluation of Oxidation Inhibited Carbon-Carbon Material for Shuttle Leading Edges, ASME Paper No. 72-ENAV-26, August 14-16, 1972.
15. McGinnis, F. K., Shuttle LESS Subsurfaces Attach Investigation Final Report, Report No. 221RPO0241, Vought Corporation, December 1974.
16. Curry, D. M., Johansen, K. J., and Stephens, E. W., Reinforced Carbon-Carbon Oxidation Behaviour in Convective and Radiative Environments, NASA Technical Paper 1284, August 1978.
17. Schomberg, C., Dotts, R. L., and Tillian, D. J., Moisture Absorption Characteristics of the Orbiter Thermal Protection System and Methods Used to Prevent Water Ingestion, Paper to be Presented at Intersociety Conference on Environmental Systems (ICES), San Francisco, CA, July 11-15, 1983.
18. Dotts, R. L., Smith, J. A., and Tillian, D. J., Space Shuttle Orbiter Reusable Surface Insulation Flight Results. Langley Conference on Shuttle Performance Lessons Learned, Langley Research Center, March 8-10, 1983.
19. Curry, D. M., Johnson, D. W., and Kelly, R. E., Space Shuttle Orbiter Leading Edge Flight Performance Compared to design Goals, Langley Conference on Shuttle Performance - Lessons Learned, NASA Langley Research Center, March 8-10, 1983.

D43
N85-16980

SHUTTLE ON-ORBIT CONTAMINATION AND ENVIRONMENTAL EFFECTS

L. J. Leger, S. Jacobs, and H. K. F. Ehlers
NASA Lyndon B. Johnson Space Center
Houston, Texas 77058

E. Miller
NASA George C. Marshall Space Flight Center
Marshall Space Flight Center, Alabama 35812

ABSTRACT

One of the many challenges presented by the development of the Space Shuttle system was ensuring compatibility of the system with payloads and payload measurements. Early in the development of the system, the contamination environment associated with Shuttle flight was addressed through working group activities involving broad representation. Through these activities, an extensive set of quantitative requirements and goals was developed and implemented by the Space Shuttle Program management. Assessment of performance of the Shuttle system as measured by these requirements and goals has been partly obtained through the use of the induced environment contamination monitor on Shuttle flights 2, 3, and 4. Contamination levels are low and generally within the requirements and goals established. Additional data expected to be available from near-term payloads and already planned contamination measurements will complete the environment definition and allow for the development of contamination avoidance procedures as necessary for any payload.

INTRODUCTION

The Space Shuttle was originally conceived and developed to be the primary space transportation system for the United States through the 1990's. Development of the components of the system presented a unique challenge in many aspects such as development of reusable thermal protection systems and primary propulsion engines as well as other devices such as the remote manipulator system. Equally unique was the challenge of providing maximum operational flexibility and at the same time satisfying the needs of the wide range of payloads which were to use this orbital delivery system. Previous experience was very limited or not available since prior space programs had specific objectives to achieve and other delivery systems did not have to be reusable or manned or be compatible with measurements from attached payloads. To ensure a successful operational system, therefore, it was necessary to effectively integrate the wide range of requirements presented by Space Shuttle development.

To address requirement development and integration, the Space Shuttle Program management established working groups to address each of several critical areas. These working groups had broad membership, generally including each cognizant NASA center as well as representatives from the user community, and were responsible for addressing needs, developing requirements, and guiding program implementation of these requirements. One of the critical areas defined was control of the environment to which the payload would be exposed during Shuttle flight. Aspects of the environment which were to be addressed consisted of mechanical loads, both static and dynamic; thermal, electromagnetic, and contamination (used here to refer to particles and gases in the environment which produce undesirable effects primarily on payload optics). A historical description of the activities associated with the contamination requirement development is provided with emphasis on particular challenges and problems encountered. Also, measurements made to define this aspect of the environment are summarized and system performance is assessed by comparing the results of these measurements with program requirements.

SHUTTLE CONTAMINATION ORGANIZATION APPROACH

The Shuttle contamination working group (initially called the Particles and Gases Working Group (PGWG)) was established in 1973 at the NASA Lyndon B. Johnson Space Center (JSC) and initially consisted of representatives from JSC, the NASA Goddard Space Flight Center (GSFC), the NASA George C. Marshall Space Flight Center (MSFC), the NASA John F. Kennedy Space Center (KSC), the NASA Ames Research Center (ARC), NASA Headquarters, Rockwell International, Aerospace Corporation, and the European Space Research and Technology Center/European Space Research Organization (ESTEC/ESRO). This group, currently called the Particles and Gases Contamination Panel (PGCP), is primarily responsible for contamination requirements implementation. Concurrently, a group was formed at MSFC in 1974 (the Contamination Requirements Definition Group (CRDG)), with membership similar to that of the PGCP with the addition of U.S. Naval Research Laboratory and NASA Langley Research Center (LaRC) representatives. The CRDG was primarily responsible for developing a complete set of contamination requirements, the evolution and definition of which are discussed in the following section.

REQUIREMENTS DEVELOPMENT AND DEFINITION

No clear precedents existed at the inception of the Space Transportation System (STS) Program for the development and incorporation into documentation of a complete set of contamination requirements for a reusable space transportation system. Somewhat of a previous experience base had been developed for the Skylab Program in invoking contamination control measures for the Apollo telescope mount (ATM). At about the same time (circa 1972), a group of scientists with a common interest in using the Space Shuttle system convened at Wood's Hole, Massachusetts. Out of the discussions, which were centered around the Orbiter-induced environment and potential effect on payloads, came a set of proposed requirements for the environment surrounding the vehicle in orbit. Using this set of generalized requirements and the Skylab experience, the Particles and Gases Contamination Panel developed workable and realistic requirements which could be feasibly implemented into the STS Program documentation. Whereas molecular contamination on orbit was mainly addressed by the Wood's Hole group, ground facilities contamination control and the Orbiter's exposure to these ground facilities as well as to the launch, on-orbit, and entry environments from a molecular and particulate standpoint had to be addressed.

Part of the problem in addressing ground particulate contamination control was the nomenclature in use at the time for previous programs. Contamination control on the ground was based on the concept of "clean room cleanliness," such as class 10 000, class 100 000, and so on, specifying particles suspended in the air. This concept was not appropriate for use on the Shuttle program in that payload integration to the Orbiter required that any payload area be exposed to a large airplane, or at least part of it, for a considerable length of time. Therefore, a somewhat new approach to defining the cleanliness levels associated with Shuttle flight had to be developed. The "clean room" concept was replaced with a definition of the extent of control on all aspects of the environment such as temperature, humidity, condensable gases, and particulate control both on surfaces and in free air. Approaches developed had to be flexible enough to serve a wide variety of needs yet be constrained to be compatible with the relatively short Shuttle ground turnaround and with operational cost. As a result, the standard cleanliness approach developed was based on a "visibly clean" surface criterion. This category of requirements has been subsequently divided into three levels of surface contamination control and along with other parameters, such as free air cleanliness, and temperature and humidity, form the basis for ground contamination control. The complete set of requirements developed for contamination control was incorporated into the Shuttle documentation, specifically Volume X of JSC-07700 (ref. 1).

In contrast to contamination control during ground-based operation for which requirements are qualitative and general, requirements for on-orbit contamination control can almost be completely defined quantitatively. To address all aspects of the environment, these requirements are of necessity complex and extensive. This complexity presented problems in implementing these requirements in that program management was concerned about the difficulties created and the program capability to verify performance to these requirements. Because of this concern, most of the on-orbit environmental requirements were accepted by the Shuttle program as "goals." The key parameters of the environment such as gas cloud density definition and particle release requirements were included in the baseline Shuttle documentation. A more detailed set of environmental definitions developed by the CRDG (ref. 2) essentially constitutes the set of Shuttle goals for control of the gases and particles associated with the environment and their effect on background light scattering and emissions.

A summary of the requirements and goals applicable to the on-orbit, or more generally flight phase, environment is included in table 1. Key parameters addressed are molecular column density, which defines the gas cloud density associated with the Orbiter vehicle, and return flux, which addresses the component of this cloud which is scattered back to surfaces in the payload bay because of interaction with the ambient environment. Other requirements address deposition of matter on surfaces either directly or by scattering by the atmosphere and light background in the various spectral regions also essentially due to the gases or particulates in the environment. These requirements and goals were implemented in the Shuttle program in March 1974. No changes or revisions of these requirements have been necessary over the intervening years.

REQUIREMENT IMPLEMENTATION

As inferred previously, the STS Program management was hesitant in accepting the outlined requirements unless there was some reasonable assurance that these "goals" were viable; that is, assurance that they could be met by the STS. Two methods of "verification" were considered and implemented: analysis and measurements. The subject of performance assessment using onboard measurements is discussed in the next section. Although Skylab used math modeling somewhat in performing contamination analysis, the STS Program marked the first time that the development of a contamination math model coincided with the development of a space vehicle. This coincidence allowed, for the first time, the use of contamination modeling as a design tool in the performance of trade studies.

TABLE 1.- SUMMARY OF CONTAMINATION SPECIFICATION
AND MEASUREMENT REQUIREMENTS ON ORBIT

Contamination specifications	Specific references	Measurement required
Molecular column density less than:		
- 10^{12} H ₂ O particles/cm ²	1	Molecular column density
- 10^{11} H ₂ O + CO ₂ particles/cm ²	2	
- 10^{13} N ₂ + O ₂ particles/cm ²	2	
- 10^{10} other molecules/cm ²	2	
Scattered/emission light background less than:		
- $m_v = 20$ th magnitude star/arc-s ² (10^{-12} B ₀ in ultraviolet)	1	Background spectral intensity
- $10^{-14.2}$ B ₀ in visible	2,3,5	
- $10^{-14.0}$ B ₀ in ultraviolet	2,3,5	
- 10^{-11} W/m ² /sr/nm $\lambda < 30$ μ m	2,3,5	
- 10^{-10} W/m ² /sr/nm $\lambda < 30$ μ m	2,3,5	
Fewer than one 5- μ m particle per orbit in 1.5×10^{-5} -sr field of view	1,2	Particle size and velocity distribution
Molecular return flux such that:		
- H ₂ O $< 10^{12}$ molecules/cm ² /s	1	- Molecular return flux
- Deposition $< 10^{-7}$ g/cm ² /30 days 0.1 sr on 300-K surface	2	- Molecular deposition on an ambient surface
- Deposition $< 10^{-5}$ g/cm ² /30 days 2π sr on 300-K surface	2	- Molecular deposition on an ambient surface
- Deposition $< 10^{-5}$ g/cm ² /30 days 0.1 sr on 20-K surface	2	- Molecular deposition on a cryogenic surface
- Degradation of optics $< 1\%$	1	- Degradation of optical surfaces

The (molecular) contamination math model, as developed by JSC with Martin-Marietta Aerospace as subcontractor, is a computer program which accepts certain time-dependent input parameters such as materials gas emission, reflection, and adsorption characteristics, engine and vent characteristics, ambient and emitted gas interaction, and their associated mass transport mechanism and vehicle geometry. The model provides a time-dependent output of such parameters as gas density, column density, return flux, and deposition which define the induced environment of the Space Shuttle Orbiter and payload on orbit. The model is currently being used for special studies associated with flight data correlation and STS performance assessment as well as payload integration activities.

During the 1973-74 time frame, the model was used to assess the effects of design changes such as reaction control engine location on the upper payload bay viewing region. Additionally, locations of the supplemental flash evaporator system (FES) nozzles, which are used to dump as much as 7.2 kilograms of water per hour in orbit, were selected on the basis of model output.

The larger benefit derived from having a functional model during the Space Shuttle development was the ability to understand the design relative to its performance from a contamination standpoint. This understanding not only provided confidence to program management that acceptable designs were being developed but also provided effective description of the evolving system and its associated environment to potential users. It is strongly recommended that such a model be formulated in future programs at the earliest stage of development.

PERFORMANCE ASSESSMENT

In addition to the extensive modeling efforts to describe and better understand the Shuttle contamination environment, a program was established to make measurements of the environment on the early flights to assess performance and provide data for correlation with and refinement of the model. The large number of environmental parameters to be measured resulted in the need for 10 instruments. This group of instruments was integrated into one package referred to as the induced environment contamination monitor (IECM), which was funded jointly by the Space Shuttle Program and the NASA Office of Aeronautics and Space Technology. The Marshall Space Flight Center provided the technical development and management for the IECM.

At the onset of this measurement program, it was understood that the IECM would provide definitions of most aspects of the environment. Certain parameters, especially those related to far infrared and far ultraviolet measurements, are best obtained from near-term payloads. Originally, the IECM was planned for six flights of the first Shuttle Orbiter. For several reasons, this schedule was abbreviated to three flights, which are reported here and seem adequate for the intended objectives.

INDUCED ENVIRONMENT CONTAMINATION MONITOR

Background

The objectives of the IECM project were to provide a self-contained instrument complement compatible with the development flight instrumentation (DFI) pallet and to provide capabilities to do the following.

1. Measure major aspects of the particle and gaseous contamination during ground handling, launch preparation, ascent, orbital operation, descent, landing, and payload removal to verify the requirements and goals developed by the PGCP and the STS Payload CRDG.
2. Provide diagnostic data to identify any sources that contribute to out-of-specification conditions so that corrective action may be taken.
3. Measure the contamination effects from delivery, deployment, retrieval, and landing of a free-flying payload.
4. Perform routine monitoring to detect any anomalous operation conditions such as leaks in the hydraulic, coolant, or fuel system; sloughing-off of particulates from the thermal protective surface, insulation, or experiments; and outgassing from new components or various experiments.

Brief IECM Description

The IECM (fig. 1) is a 355-kilogram, desk size (121.3 centimeters long by 82.2 centimeters wide by 79.1 centimeters high) package and consists of 10 instruments designed to obtain environment and induced contamination measurements during preflight ground operations and ascent, on-orbit, descent, and postlanding operations. The 10 instruments and their functions are (1) a humidity monitor; (2) a dewpoint hygrometer, which measures water vapor content and air temperature on the ground and during ascent and descent; (3) an air sampler, which provides sampling for hydrocarbons, hydrogen chloride (HCl), and nitrogen oxide (NO) products in the cargo bay; (4) a cascade impactor, which measures size and quantity of airborne particulates in the cargo bay; (5) an optical effects module (OEM); (6) a passive sample array (PSA), which provides a measure of molecular contamination effects on optical properties as well as size distribution and effects of particulate accumulation; (7) a temperature-controlled quartz crystal microbalance (TQCM); (8) a cryogenic quartz crystal microbalance (CQCM), which measures nonvolatile residue at various temperatures; (9) a camera/photometer, which measures size, range, and velocity of on-orbit particulates as well as background brightness; and (10) a mass spectrometer, which measures quantity and mass of molecular flux. Table 2 gives the IECM instrument characteristics and description summary.

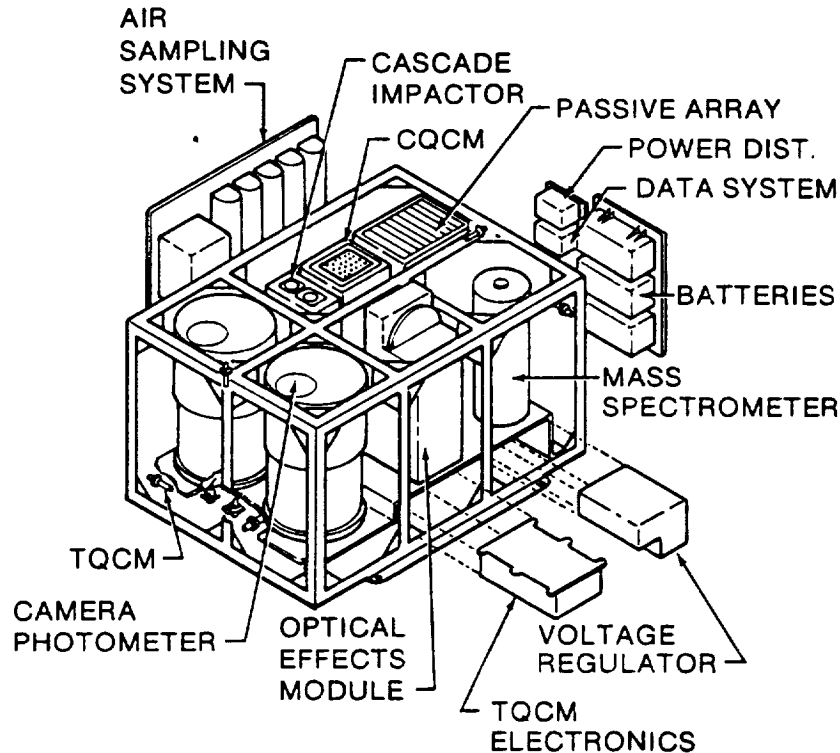


FIGURE 1.- INDUCED ENVIRONMENT CONTAMINATION MONITOR.

The IECM engineering subsystems consist of a programmable, microprocessor-based data acquisition and control system (DACS), a power distribution and control unit (PDCU), and a thermal control system. Reference 3 gives a more complete description of the IECM instruments and subsystems.

The IECM and the release/attach mechanism (REM) were mounted on the DFI at station $x_0 = 1179$, $y_0 = 0$, $z_0 = 474$ (top center of IECM). The REM was developed at MSFC to provide release/attach capabilities for small payloads such as IECM and the University of Iowa's plasma diagnostic package (PDP).

Flight History

The IECM was installed in the Columbia for the STS-1 flight. It was later decided that the IECM would be deleted from the flight to improve weight margins. Considerable effort was made at this late date to install a passive optical sample assembly (POSA) to obtain some, albeit limited, contamination data from the first flight. Following the success of this effort, permission was obtained to install another POSA at the landing site for the ferry flight.

The IECM subsequently was flown on STS-2, STS-3, and STS-4. Between each flight, the entire package was returned to MSFC for refurbishment that included (1) postflight functional tests, (2) individual instrument refurbishment on changeout, (3) reprogramming the DACS for next flight operational requirements, (4) cleaning and thermal vacuum bakeout, (5) installation of new batteries, and (6) preflight functional tests. Turnaround time for these activities at MSFC was as short as 10 days (between STS-3 and STS-4). The REM was also returned to the MSFC for checkout and refurbishment between each flight.

Measurements

The IECM measurements began on each mission following installation and checkout of the package in the Orbiter payload bay during the Orbiter Processing Facility (OPF) operations. Measurements of temperature, humidity, aerosols, hydrocarbons, and nonvolatile residues were made over a 12-hour period

TABLE 2.- IECM INSTRUMENT CHARACTERISTICS AND DESCRIPTION SUMMARY

Instrument (a)	Measurement	Operation (b)	Resolution
Humidity monitor	Relative humidity, temperature	GPL,A,D,PL	$\pm 0.5\%$
Dewpoint hydrometer	Dewpoint	GPL,A,D,PL	$\pm 0.5\%$
Air sampler	Gaseous contaminants	GPL,A,D,PL	~ 1 ppm
Cascade impactor	Particulate contamination of nonvolatile residue	GPL,A,O,D,PL	$\pm 1.5 \times 10^{-9}$ g
PSA	Optical degradation due to accumulated contamination	GPL,A,O,D,PL	(c)
OEM	Degradation of optics at 253.65 nm	GPL,O,D,PL	$\pm 0.8\%$
TQCM	Condensed molecular contamination at 213 to 303 K (-60° to +30° C)	GPL,A,O,D,PL	$\pm 1.56 \times 10^{-9}$ g
CQCM	Condensed molecular contamination at 133 K (-140° C) to ambient	GPL,A,O,D,PL	$\pm 1.65 \times 10^{-9}$ g
Camera/photometer	Particulate velocity, direction; photometry	0	25- μ m particle at 1 m/s
Mass spectrometer	Molecular return flux	0	± 1 count

aPSA = passive sample array, OEM = optical effects module, TQCM = temperature-controlled quartz crystal microbalance, and CQCM = cryogenic quartz crystal microbalance.
 bGPL = ground prelaunch, A = ascent, O = on orbit, D = descent, and PL = postlanding.
 cSamples for lab analysis.

when Orbiter power was available and the payload bay doors were open. Dustfall and residues from the total stay time in the OPF were measured from PSA-exposed samples. On STS-4, the payload bay doors were opened on the pad and the preflight measurements were obtained for the periods between the OPF and the Payload Changeout Room (PCR) and during the time the payload bay doors were open to the PCR. These measurements were also performed during ascent and descent and after landing. In addition, air was sampled for exhaust gas products ingested into the payload bay.

The on-orbit measurements consisted of continuous monitoring of optical transmittance at a wavelength of 253.7 micrometers, return flux of molecular species emanating from the Orbiter, molecular mass deposition at various substrate temperatures, and particulates and induced brightness from scattered light. During the STS-4 mission, the IECM was maneuvered about the Orbiter to more directly measure outgassing, leaks, vernier reaction control system (VRCS) exhausts, and FES effects.

OTHER MEASUREMENTS

In addition to the aforementioned POSA and ferry flight POSA (flown on STS-1 to STS-4), Orbiter and payload facilities environment data were monitored by KSC personnel. Postflight nonvolatile residue measurements were made on the Orbiter radiator surfaces. Visual and laboratory measurements were made on various Orbiter and payload materials, surfaces, and paints (including the IECM paint) for contamination and environmental effects. Flight crewmembers were queried about contamination observations and impressions (window fogging, particles, engine firing, and water dump events). Onboard video and film photographs were reviewed for further information.

RESULTS AND COMPARISON TO GOALS

During the preflight 12-hour sampling periods, the IECM data showed that the facilities were within specifications for air temperature and relative humidity: $22^{\circ} \pm 2^{\circ}$ C and 30 to 50 percent, respectively. Nonvolatile residue was not detected to $<10^{-7}$ -g/cm² levels on surfaces exposed during the entire ground flow. (Goal is $<10^{-6}$ g/cm².) Table 3 gives the particle fallout measurements from the PSA during ground flow for STS-2 to STS-4. These results generally exceed Level 300A but show improvement on STS-4.

Particle accumulation was subsequently measured by the cascade impactor during ascent and descent, where redistribution is provided by airflows. These results are given in table 4 for different particle sizes contained in a volume of air. Comparing these results to 100K clean-room-air aerosol content goal, the results from STS-2 and STS-4 indicate that this goal was exceeded for particles as large as 5 micrometers diameter. These results are, however, highly dependent on assumed values for density and average diameter. The air sampler results indicate that engine exhaust products are not ingested into the payload bay during ascent or descent. Some volatile hydrocarbons were trapped and analyzed. Tables 5 and 6 summarize the air sampler results. Slight molecular mass depositions (~ 100 ng/cm²) detected on the TQCM's during the first minute after launch subsequently dissipated within 15 minutes.

Descent and postlanding temperatures of air pumped into the IECM air sampler manifold were between about 10^o and 20^o C and the relative humidity ranged between 15 and 25 percent on the three flights (figs. 2(a) and 2(b)). Ascent temperature change and relative humidity were not measurable in the dry nitrogen purge gas.

The on-orbit goals for molecular flux scattered back into the payload bay (-z-axis return flux) is $<10^{12}$ water (H₂O) molecules/cm²/s and mass deposition of $<10^{-5}$ g/cm²/30 days. Table 7 gives the mass spectrometer H₂O return flux and resultant calculated column densities for the three flights. This goal, a particular concern for infrared observations, was attained on the STS-3 mission, which was free from water absorption by the thermal protection system (TPS) as occurred on STS-2 and from hail damage as occurred on STS-4. The goal was exceeded, as anticipated, during door closing and primary reaction control system (PRCS) engine tests.

TABLE 3.- PREFLIGHT PARTICLE FALLOUT, PASSIVE SAMPLE ARRAY

Contamination specification	Averaged preflight exposure results
Particle density - optical surfaces \leq Level 300	STS-2 19 days exposure: OPF $\rho = 1.4 \times 10^4$ particles/cm ² Level 750 to 1500
Orbiter Processing Facility (OPF) at KSC subjected to cleanup following rollout of STS-2	STS-3 19 days exposure: OPF $\rho = 6.5 \times 10^3$ particles/cm ² Level 500 to 1500
During OPF operations, samples and instruments of the IECM designated for flight were protected by covers until final access prior to rollout	STS-4 5 days exposure: OPF $\rho = 1.3 \times 10^3$ /cm ² Level 500 to 750
	In-transit OPF-PCR (26 days) $\rho = 6.7 \times 10^2$ /cm ² Level 200 to 500
	16 days exposure in PCR $\rho = 5 \times 10^2$ /cm ² Level 300 to 750
	Samples exposed from first access OPF to last access PCR $\rho = 2.7 \times 10^3$ /cm ² Level 500 to 750

TABLE 4.- STS-2 to STS-4 SUMMARY RESULTS - CASCADE IMPACTOR

Measurement	Requirements	Mission	Results, $\mu\text{g}/\text{m}^3$	
			Ascent	Descent
>5- μm size particles	<375 $\mu\text{g}/\text{m}^3$ (assuming $d = 25 \mu\text{m}$, $\rho = 2 \text{ g}/\text{cm}^3$)	STS-2	✓30	✓10
		STS-3	✓10	✓10
		STS-4	Non-functional	✓20
1- to 5- μm size particles	<100 $\mu\text{g}/\text{m}^3$ (assuming $d = 5 \mu\text{m}$, $\rho = 2 \text{ g}/\text{cm}^3$)	STS-2	✓500	✓250
		STS-3	<10	<10
		STS-4	✓400	✓10
0.3- to 1- μm size particles	<10 $\mu\text{g}/\text{m}^3$ (assuming $d = 1 \mu\text{m}$, $\rho = 2 \text{ g}/\text{cm}^3$)	STS-2	✓250	✓125
		STS-3	<10	<10
		STS-4	≈150	Non-functional

TABLE 5.- INDUCED ENVIRONMENT CONTAMINATION MONITOR - AIR SAMPLER RESULTS: CONTAMINANT TOTALS FOR REPRESENTATIVE ASCENT AND DESCENT PHASES

Location	Species	Levels expected, spec.	Detection method (a)	Observed
Ascent	Volatile hydrocarbons ^b	Unknown, no spec.	A	✓50 ppm by weight, ✓10 ppm by volume ^b
Ascent	Reactive HCl	Unknown, no spec.	B	None detected to 1 ppm sensitivity
Descent	Reactives NO, NO ₂ , NH ₃	Unknown, no spec.	C	None detected to 1 ppm sensitivity
Descent	Volatile hydrocarbons ^b	Unknown, no spec.	A	✓20 ppm by weight, ✓4 ppm by volume ^b

^aA - concentration on adsorbent; postflight gas chromatograph/mass spectrometer (GC/MS) analysis.

^bB - reaction with silver oxide/hydroxide surfaces; postflight analyses by electron spectroscopy for chemical analysis (ESCA).

C - reaction with ruthenium trichloride surfaces; postflight analyses by ESCA.

^bCovers C₉ to C₂₄ range and uses ✓C₁₂ as average molecular weight to obtain ppm by volume.

TABLE 6.- AIR SAMPLER RESULTS: CONTAMINANT TOTALS FOR REPRESENTATIVE STS GROUND, ASCENT, AND DESCENT PHASES

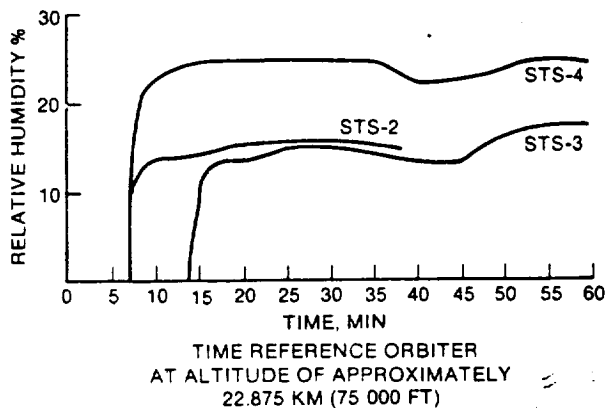
Mission phase	Species	Detection method (a)	Observed
Preflight (OPF)	Volatile hydrocarbons ^b	A	3 ppr. by weight 1 ppm by volume
Ascent	Volatile hydrocarbons ^b	A	50 ppm by weight 10 ppm by volume
Ascent	Reactive HCl	B	None detected to 1 ppm sensitivity
Descent	Reactives NO, NO ₂ , NH ₃	C	None detected to 1 ppm sensitivity
Descent	Volatile hydrocarbons ^b	A	20 ppm by weight 4 ppm by volume

^aA - concentration on adsorbent; postflight GC/MS analysis.

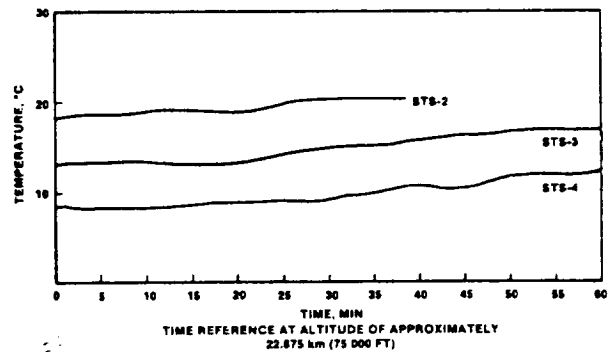
B - reaction with silver oxide/hydroxide surfaces.

C - reaction with ruthenium trichloride surfaces.

^bCovers C₉ to C₂₄ range and uses $\sqrt{C_{12}}$ as average molecular weight to obtain ppm by volume.



(a) RELATIVE HUMIDITY DURING DESCENT.



(b) TEMPERATURE DURING REENTRY.

FIGURE 2.- IECM MEASUREMENTS ON STS-2 TO STS-4.

Table 8 gives a summary of -z-axis mass deposition at a sensor temperature of 30° C, also extrapolated to 30 days for STS-3 and STS-4. (STS-2 -z-axis TQCM sensor was inoperative.) Only for a short period of time on STS-3 did the deposition rate exceed 1×10^{-5} g/cm²/30 days. Further, table 9 gives a similar summary for an average of all five TQCM sensors (+x, +y, -z directions). These data indicate that mass depositions on surfaces with direct views to the Orbiter should not be significant. The CQCM (-z-axis) sensors, with temperatures ranging between -101° and 35° C, indicated even less total mass accumulation during the missions, ranging from 3.5×10^{-6} g/cm²/30 days on STS-2 to negative values on STS-4. The OEM optical samples showed 1 to 2 percent increased transmittance trends, and the mass spectrometer indicated insignificant return flux for masses greater than 50 amu.

The TQCM, the CQCM, and the mass spectrometer were used to monitor the STS-3 PRCS engine test (L2U test). The accumulation on the QCM's dissipated with 1/e time constant of about 15 minutes at 30° C sensor temperature. The mass spectrometer measured pressures to its limit of about 5×10^{-5}

TABLE 7.- H₂O RETURN FLUX AND CALCULATED COLUMN DENSITIES

Mission	Return flux, particles/cm ² -sr-s		Column density, particles/cm ²	
	Maximum ^a	Final	Maximum	Final
STS-2 ^b	1.5 × 10 ¹⁴	1.8 × 10 ¹³	2.0 × 10 ¹³	2.7 × 10 ¹²
STS-3	9.8 × 10 ¹¹	2.6 × 10 ¹¹	1.5 × 10 ¹¹	4.0 × 10 ¹⁰
STS-4	2.1 × 10 ¹⁴	6.6 × 10 ¹²	3.2 × 10 ¹³	1.0 × 10 ¹²

^aExcept for PRCS firings and payload bay door closings.

^bThe STS-2 values are considered upper limits.

TABLE 8.- DATA FROM -Z-AXIS TOCM MASS DEPOSITION SENSORS AT 300° C EXTRAPOLATED TO 30-DAY MISSION

MET, hr	Mission	Measured value, ng cm ⁻² hr ⁻¹	Value extrapolated to 30-day mission, gm cm ⁻² /30 days
003.8	STS-3	<0	<0
016.6	STS-4	5.7	4.1 × 10 ⁻⁶
021.9	STS-3	14.6	1.0 × 10 ⁻⁵
034.9	STS-4	3.2	2.3 × 10 ⁻⁶
040.0	STS-3	1.0	7.2 × 10 ⁻⁷
058.0	STS-3	0	0
076.0	STS-3	<0	<0
084.7	STS-4	.4	2.9 × 10 ⁻⁷
102.9	STS-4	4.2	3.0 × 10 ⁻⁶
112.5	STS-3	14.8	1.1 × 10 ⁻⁵
121.4	STS-4	4.2	3.0 × 10 ⁻⁶
125.7	STS-3	<0	<0
139.5	STS-4	7.6	5.5 × 10 ⁻⁶
157.9	STS-4	<0	<0

TABLE 9.- DATA FROM ALL TOCM SENSORS AT 300° C EXTRAPOLATED TO 30-DAY MISSION

MET, hr	Mission	Measured value, ng cm ⁻² hr ⁻¹	Value extrapolated to 30-day mission, g cm ⁻² /30 days
2.1	STS-2	<0	<0
3.8	STS-3	<0	<0
13.8	STS-2	20	1.4 × 10 ⁻⁵
16.6	STS-4	<0	<0
21.9	STS-3	5	3.6 × 10 ⁻⁶
25.4	STS-2	7.7	5.5 × 10 ⁻⁶
34.9	STS-4	1.8	1.3 × 10 ⁻⁶
38.2	STS-3	4.6	3.3 × 10 ⁻⁶
40.0	STS-3	23	1.7 × 10 ⁻⁵
50.0	STS-2	22.6	1.6 × 10 ⁻⁵
58.3	STS-3	9.7	7.0 × 10 ⁻⁶
76.3	STS-3	7.9	5.7 × 10 ⁻⁶
84.7	STS-4	<0	<0
94.4	STS-4	35.3	2.5 × 10 ⁻⁵
102.9	STS-4	2.5	1.8 × 10 ⁻⁶
112.5	STS-3	11.1	8.0 × 10 ⁻⁶
121.4	STS-4	3.8	2.7 × 10 ⁻⁶
125.7	STS-3	<0	<0
139.5	STS-4	2.7	1.9 × 10 ⁻⁶
157.9	STS-4	<0	<0

torr during door closings. Partial pressures of carbon dioxide, also a concern for infrared observations, were insignificant.

The STS-4 contamination mapping with the IECM using the remote manipulator system (RMS) results indicate qualitative agreement of direct molecular flux and return flux outgassing levels of high molecular weight (>50 amu) too small to be quantified, and cabin leakage was not detectable. A Freon 12 leak in the FES/cooling system loop was clearly detected.

More detailed IECM results are given in references 4 and 5. The camera/photometer stereopair provided 0.24-steradian (32°) field-of-view film records of contaminant particles as small as 25 micrometers illuminated by the Sun against a dark sky or Earth background, and background brightness levels during these periods as well as levels during orbital nighttimes. A summary of particles detected during the first 48 hours of the missions is given in figure 3, excluding water dumps. Only the first 48 hours are shown because of the short mission time of STS-2 and camera failure at 50 hours mission elapsed time (MET) on STS-3. On STS-4, continued low levels of particles are shown beyond 48 hours. The particle population goal is less than one 5-micrometer particle/orbit in a 1.5×10^{-5} -steradian field of view. After about 15 hours MET, the number of >25-micrometer particles observed is about 0.03/orbit in a 1.5×10^{-5} -steradian field of view, sufficiently small to make it unlikely that the goal would be exceeded significantly by smaller particles. During water dumps, the particulate count is very high, again as expected and excluded by the goal definition (>100/frame), and the scattered light from the particles limits the photometer-controlled exposure to 1 second. When the water dumps are terminated, the particle count decays rapidly with a time constant $1/e$ of 5 minutes as shown in figure 4. Particle count increases have not been seen with operation of the FES.

Sky background brightness after about 15 hours MET and during the absence of water dumps consistently shows no difference during orbital nighttimes and daytimes, indicative of no contribution from molecular or particulate scattering, which is a requirement goal. Stars as faint as $m_v = 10$ are consistently seen during these day and night observations; the exposures were terminated by integrated starlight in both cases. No evidence has been found of light that can be attributed to the glow phenomenon.

ENVIRONMENT INTERACTIONS

The OEM and PSA samples show no discernible optical or physical effects on such optical materials and coatings as lithium fluoride, calcium difluoride, magnesium difluoride (MgF_2), barium difluoride,

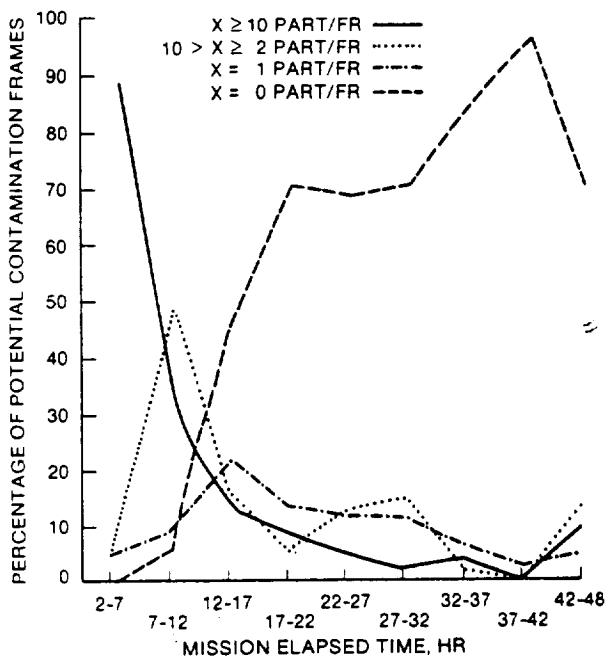


FIGURE 3.- PARTICLE DENSITY ON FRAMES.

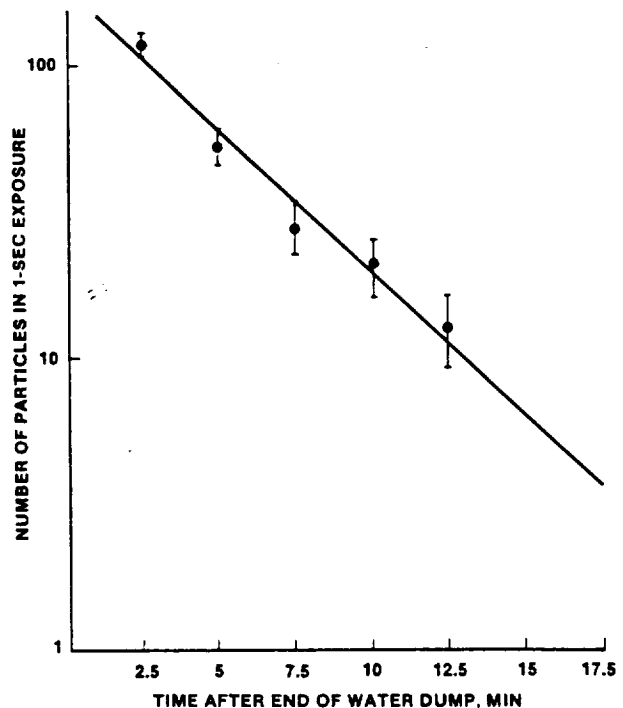


FIGURE 4.- PARTICLE COUNT DECAY AFTER WATER DUMP TERMINATION.

sapphire, crystalline quartz, fused silica, gold, platinum, MgF₂ over aluminum, and pyrex. Some coatings, however, apparently formed oxide resulting from the exposure to oxygen atoms. Thin films of osmium (15 nanometers) on fused silica flown on STS-3 and STS-4 were removed, presumably, by the formation of osmium tetroxide, which has a vapor pressure of 760 torr at 25° C. A vacuum-deposited 300-nanometer carbon film and a 255-nanometer silver film, both on quartz, were added to STS-4. The carbon film was removed and the silver film was converted to a transparent blue-green film, determined to be Ag₂O (ref. 6).

Silver-plated nuts on the PSA and the fixed part of the REM for the PDP showed apparent heavy oxidation, even though located such that a direct view to space was never possible. Osmium films deposited over a flash coating of nickel were flown on STS-5. The samples were positioned to have both direct and indirect view to space. The results indicate that most, if not all, of the osmium was removed (ref. 7).

Leger (refs. 8 and 9) has reported weight loss of various organic materials exposed to atomic oxygen. Mass measurements on Kapton surfaces showed losses of as much as 4 to 5 micrometers thickness on STS-3. Other film samples and Orbiter organic paints showed effects such as mass loss and loss of binder, leaving pigment-rich surfaces. The SI3G silicone-based paint on the IECM, however, did not degrade physically or optically during the mission.

OPEN ISSUES

Several of the requirements and goals listed in table 1 could not be completely verified using IECM data. One example not completely verified is the particle environment during the on-orbit phase of flight since the IECM camera particle size detection limit is 25 micrometers and the goal addresses particle size down to 5 micrometers. Verification of this requirement will require data generated by a cryogenically cooled infrared telescope. Such a device is planned for flight on the Spacelab II mission, and plans have already been made to examine data generated by this system for contamination effects. Data from other near-term payloads will also be examined and used to provide a complete definition of the environment and acceptable operational techniques for hopefully all types of payloads.

One aspect of the Shuttle system which was not covered by the use of the IECM was contamination of the upper stages. Measurements now being planned should provide the necessary data.

The complete approach for control of contamination during ground turnaround is still being developed. Part of the reason for this delayed development was the lack of an experience base associated with operation of the Shuttle in ground facilities. The necessity for the development of this data base was recognized during the development of the requirements; however, progress has been somewhat slow in this area. This problem was highlighted by the contamination concerns which developed during preparations for launch of the Tracking and Data Relay Satellite A (TDRS A) on STS-6. With the emphasis generated by this event and some additional test data, detailed contamination control procedures which will be acceptable to all can be developed.

CONCLUSIONS

The Space Shuttle contamination control program has been completed with the measurements of the environment made during the orbital flight test program using the IECM. Performance of the Shuttle system has been assessed by comparing the measured environment with the contamination requirements and goals developed by the two contamination working groups. This comparison shows that, in general, where measurements were performed, contamination requirements and goals have been met. Molecular contamination, in terms both of gaseous and condensable species, is below the requirement levels and should be adequate for all payloads with minimal need for covers or other forms of protection. Particle release rates during quiescent periods appear to be within the requirements established based on cryogenic infrared telescope needs. Further measurements are required to fully verify this requirement for particles smaller than 25 micrometers. Except for surface glow effects first observed and photographed on STS-3, light background levels in the visible spectral region are within required levels. Verification of this requirement for the infrared and ultraviolet spectral regions will have to await further elements by near-term payloads. Light emitted by the primary and vernier reaction control system jets during firings may require changes from standard operational techniques for certain contamination-sensitive payloads.

Ground contamination control needs additional definition of procedures to be used for payload integration and ground facility operation. Part of the higher than expected particle content in the payload bay during ascent may be due to a lack of implementation of adequate control during ground turnaround for the early Shuttle missions. This situation should improve with continued emphasis and the development of a significant experience base.

The approach used for the development of the contamination control program was very effective in developing a system with excellent performance and in defining the vehicle-associated environment. Broad participation in panel activities led to a better understanding of payload concerns by system design engineers and also to a better understanding of Shuttle development problems on the part of payload developers and the scientific community in general. Indeed, contamination control was treated in Shuttle development as a full-fledged discipline for perhaps the first time, in that the program provided support from requirements development to the final environmental measurements.

REFERENCES

1. Space Shuttle Flight and Ground System Specification. JSC-07700, Vol. X, Apr. 27, 1978.
2. Payload Contamination Control Requirements for Space Transportation System (STS) Induced Environment. STS Payload Contamination Requirements Definition Group Report, NASA Marshall Space Flight Center, Huntsville, Alabama, July 22, 1975.
3. Miller, E. R.; and Decker, R.: An Induced Environment Contamination Monitor for the Space Shuttle. NASA TM-78193, Aug. 1978.
4. Ehlers, H. K. F.; Jacobs, S.; Leger, L. J.; and Miller, E.: Space Shuttle Contamination Measurements From Flights STS-1 Through STS-4. AIAA Paper 83-0331, Jan. 1983.
5. Miller, Edgar R., ed.: STS-2, -3, and -4 Induced Environment Contamination Monitor (IECM) Summary Report. NASA TM-82524, Feb. 1983.
6. Peters, P. N.; Linton, R. J.; and Miller, E. R.: Results of Apparent Atomic Oxygen Reactions on Ag, C, and Os Exposed During the Shuttle STS-4 Orbits. Submitted to Geophysical Research Letters.
7. Gull, Theodore: Private Communication. NASA Goddard Space Flight Center, Mar. 1983.
8. Leger, L. J.: Oxygen Atom Reaction With Shuttle Materials at Orbital Altitudes. NASA TM-58246, May 1982.
9. Leger, L. J.: Oxygen Atom Reaction With Shuttle Materials at Orbital Altitudes - Data and Experiment Status. AIAA Paper 83-0073, Jan. 1983.

INDEX

- Abner, Charles A., 81
 Anderson, Judith A., 97
 Arrington, James P., 209
 Austin, L. D., 177
- Bacchus, D. L., 189
 Bachtel, Frederick D., 1041
 Bailey, William W., 532
 Batson, Bartus H., 767
 Binkley, William H., 972
 Blackmon, F. Herb, 76
 Blevins, Donald R., 656
 Boggs, Clifton R., 910
 Boykin, Jack C., 1
 Boyle, W. W., 151
 Braun, Walter R., 798, 804
 Bromley, Linda K., 831
 Burghduff, Richard D., 47
- Campbell, Carlisle C., Jr., 850
 Carpenter, J. E., 498
 Carsley, Renton B., 872
 Cassisi, Vincent, 961
 Chase, Charles A., 628
 Chevers, Edward S., 30
 Coldwater, Harold R., 357
 Cole, Timothy W., 585
 Cooke, Douglas R., 264
 Craig, M. K., 151
 Crump, John M., 920
 Curry, Donald M., 1062
- Davis, Richard M., 986
 Decrisantis, Angelo, 414
 Dessouky, Khaled, 815
 Dill, Charlie C., 151
 Doetsch, K. H., 892
 Donahue, Michael E., 952
 Dotts, Robert L., 1062
 Dutton, Jon A., 357
- Edson, William F., Jr., 525
 Eggers, D. S., 720
 Ehlers, H. K. F., 1082
- Felder, G. L., 857
 Ferguson, Robert M., 565
 Fisher, Robert R., 1030
- Foll, Richard R., 357
 Foster, Lee D., 1022
 Fouts, W. B., 64
- Gaines, L. M., 177
 Gamble, Joe D., 209, 264
 Gatto, Ralph E., 335
 Gibb, John W., 414, 465
 Gibson, Cecil R., 639
 Gilbert, David W., 137
 Glassburn, Charles W., 942
 Glynn, Philip C., 345
 Godfrey, Robert D., 787
 Gray, Carroll, 1041
 Greenwood, Terry F., 1022
 Griffin, J. W., 757
- Hamilton, J. T., 151, 177
 Hampton, P. W., 54
 Haratunian, Michael, 935
 Hardee, J. H., 883
 Heinrich, Steven R., 465
 Helms, William R., 573
 Henderson, John, 656
 Henderson, O. L., 19
 Hendrickson, Kenneth O., 97
 Herr, Denver W., 821
 Hillje, Ernest R., 209, 313
 Hohmann, Carl, 656
 Homan, David, 295
 Hondros, J. G., 177
 Hooks, Ivy, 295
 Howell, Gayle J., 357
 Howell, H. R., 480
 Hughes, Robert W., 690
 Humphrey, Terry D., 35
 Humphries, Clarence, 639
 Huth, G. K., 757
- Jacobs, Steve, 1082
 Jamieson, John R., Jr., 585
 Joosten, B. Kent, 113
- Karakulko, W., 656
 Kelley, J. S., 757
 Kilminster, Joe C., 618
 Koch, John C., 986

Koszinski, E. P., 465
Kross, D. A., 189

Lak, Tibor I., 585
Lance, Renee, 673
Lee, Dorothy B., 1022
Leger, L. J., 1082
Lenett, S. D., 720
Lewis, James L., Jr., 47
Lewton, W. A., 720
Lindsey, William C., 810

Mackey, Alden C., 335
McBarron, James W., II, 435
McCarty, John P., 600
McIntosh, M. E., 465
McKenzie, Teresa M., 798, 804
McMann, Harold J., 435
Mangialardi, J. K., 465
Mesmer, J., 64
Miller, Arthur J., 972
Miller, E., 1082
Miller, Glenn J., 403
Miller, John Q., 618
Mitchell, Walter T., 38
Modest, M. F., 480
Modlin, C. Thomas, Jr., 325
Moog, R. D., 189
Moser, Thomas L., 345
Munafa, Paul M., 386
Muratore, John F., 87
Murray, R. W., 465
Murray, S. V., 125

Naber, Ruth A., 905
Nason, John R., 450
Novosad, S. W., 720

Olsen, Deloy C., 209
Ord, George R., 414
Oren, J. A., 480

Patterson, William J., 1030
Pawlowski, J. F., 720, 767
Plowden, John B., 558
Porter, J. A., 720
Powers, Bruce G., 143
Price, Charles R., 35
Prince, R. Norman, 414

Rasmussen, Anker M., 505
Reichle, Garland E., 942

Ried, Robert C., 1051
Riles, Warren L., 510
Ripley, John G., 861
Roberts, B. B., 151, 209
Romere, Paul O., 209, 295
Rudolph, James W., 539
Runkle, Roy E., 365
Ryan, Robert S., 386

Salter, Larry D., 386
Scallion, William I., 209
Schelkopf, J. D., 465
Schuesser, Emil R., 102
Schlosser, Donald C., 264
Schmidt, Oron L., 767
Schneider, Henry E., 1
Schneider, William C., 403
Schubert, Franz, 465
Schwartz, John J., 777, 821
Schwartz, Richard, 490
Searle, Richard F., 38
Seibert, W. W., 720
Seyl, J. W., 720
Simon, William E., 702
Smith, Gerald W., 628
Smith, H. E., 64
Spearing, Robert, 777
Spencer, Bernard, Jr., 209
Steele, Mike, 465
Steiner, A. W., 757
Stoker, C. Jack, 831
Stone, Howard W., Jr., 264
Stuckey, James M., 1041
Surber, T. E., 177
Swider, Joe, 414

Taeuber, Ralph J., 656
Tatem, Bemis C., Jr., 961
Taylor, J. Thomas, 995
Teasdale, William E., 767
Thibodaux, Joseph G., Jr., 581
Thibodeau, Joseph R., 1
Thomas, Emory, 465
Tillian, Donald J., 1062
Tory, Edward G., 550
Townsend, Don H., 81

Underwood, Jimmy M., 209, 264
Ussher, T. H., 892

Vang, H. A., 720, 757
Vaniman, Jerold L., 1030, 1041
Vick, H. G., 54

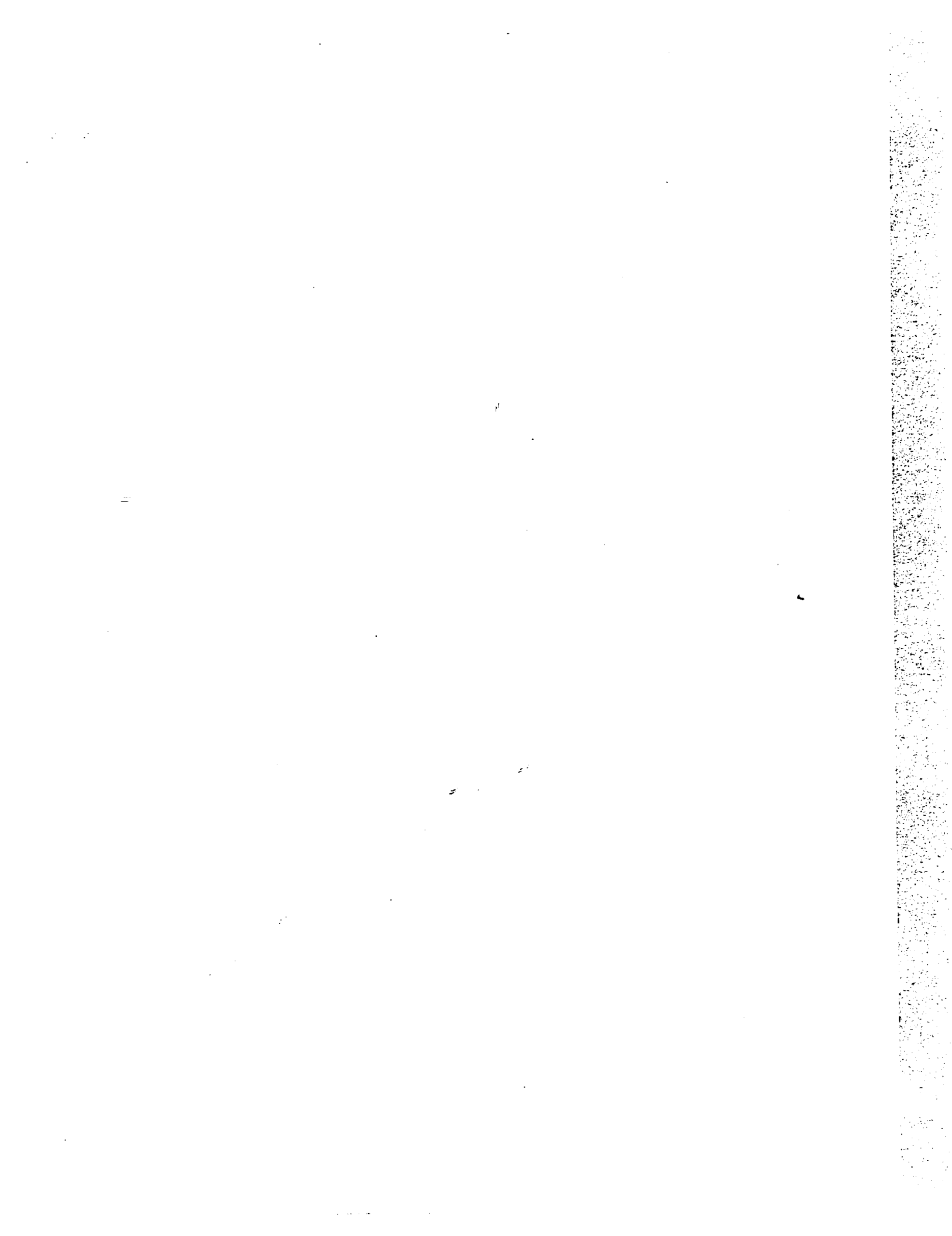
Wallace, R. O., 177
Walleshauser, James J., 414
Walvis, Dirk J. M., 821
Ware, George M., 209
Weary, Dwayne P., 673
Weinberg, Aaron, 777, 821
Whitcomb, Kathy K., 87
Whitnah, Arthur M., 209
Widofsky, Bernard, 1041
Wierum, Frederic A., 450

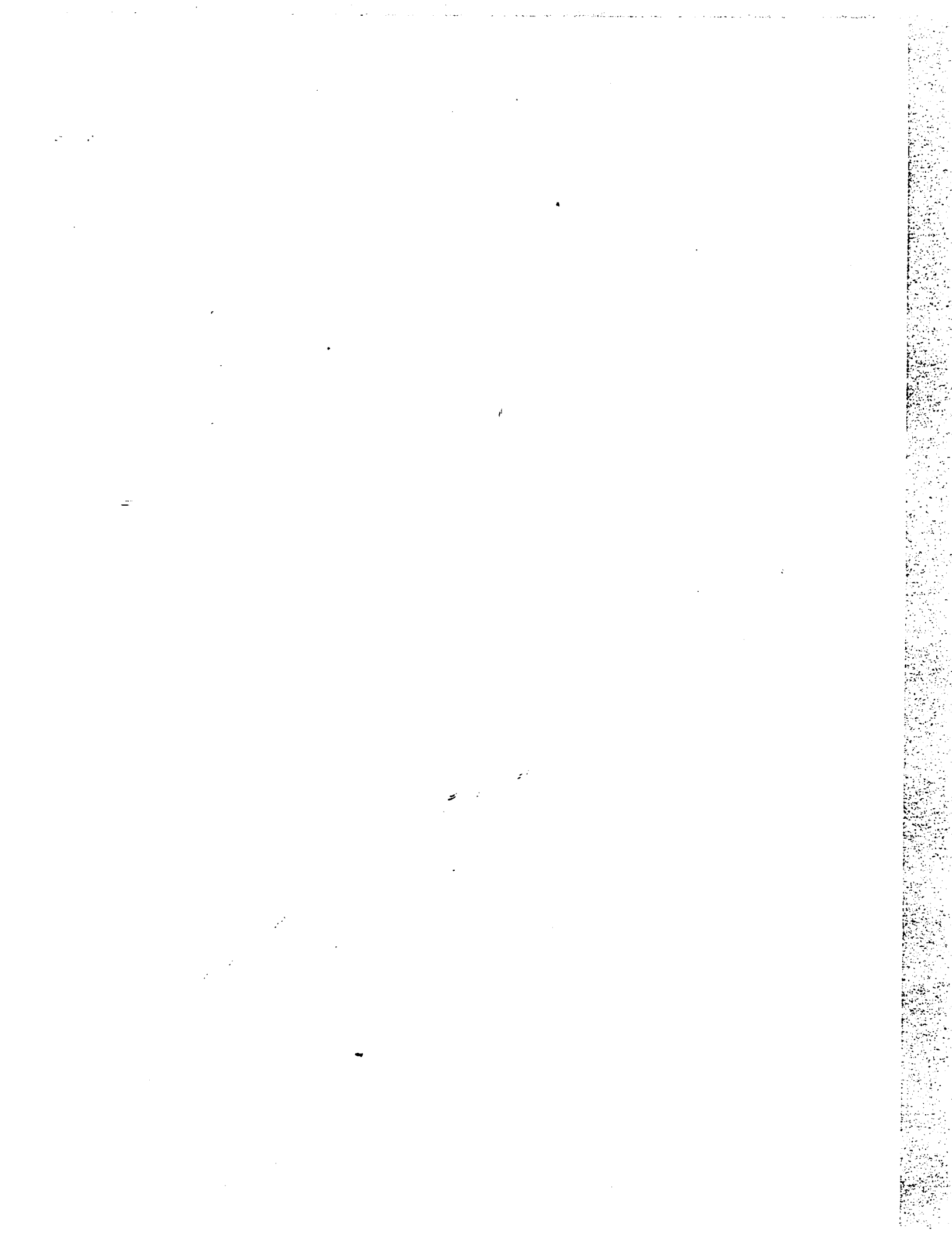
Williams, J. L., 480
Wojnarowski, John, 414
Wood, Byron K., 600
Woodis, William R., 365
Woolford, Barbara, 426
Worlund, Armis L., 585
Wynveen, R. A., 465

Yanosy, James L., 450
Young, George M., III, 386
Young, J. C., 151, 209

Zrubek, W. E., 757
Zupp, George A., Jr., 325







1. Report No. NASA CP-2342, Part 2	2. Government Accession No.	3. Recipient's Catalog No.	
4. Title and Subtitle Space Shuttle Technical Conference		5. Report Date January 1985	
		6. Performing Organization Code	
7. Author(s) Norman Chaffee, Compiler		8. Performing Organization Report No. S-539	
		10. Work Unit No. 953-36-00-00-72	
9. Performing Organization Name and Address NASA Lyndon B. Johnson Space Center Houston, Texas 77058		11. Contract or Grant No.	
		13. Type of Report and Period Covered Conference Publication	
12. Sponsoring Agency Name and Address National Aeronautics and Space Administration Washington, D. C. 20546		14. Sponsoring Agency Code	
15. Supplementary Notes *Because of the large volume of material prepared for the conference, this publication is divided into two parts. Part 1 - 597 pages, Part 2 - 530 pages.			
16. Abstract This publication is a compilation of the papers prepared for the Space Shuttle Technical Conference held at the NASA Lyndon B. Johnson Space Center, Houston, Texas, June 28-30, 1983. The purpose of this conference was to provide an archival publication for the retrospective presentation and documentation of the key scientific and engineering achievements of the Space Shuttle Program following the attainment of full operational status by the National Space Transportation System. To provide technical disciplinary focus, the conference was organized around 10 technical topic areas: (1) Integrated Avionics, (2) Guidance, Navigation, and Control, (3) Aerodynamics, (4) Structures, (5) Life Support, Environmental Control, and Crew Station, (6) Ground Operations, (7) Propulsion and Power, (8) Communications and Tracking, (9) Mechanisms and Mechanical Systems, and (10) Thermal and Contamination Environments and Protection Systems. The papers in each technical topic which were presented over the 3-day conference period provide a historical overview of the key technical problems and challenges which were met and overcome during the development phase of the Space Shuttle Program. Taken as a whole, these papers provide a valuable archival reference to the magnitude and scope of this major national achievement.			
17. Key Words (Suggested by Author(s)) Space Shuttle; Orbiter; Avionics; Guidance; Navigation; Control; Aerodynamics; Structures; Life Support; Environmental Control; Ground Operations; Propulsion; Power; Communications; Tracking; Mechanisms; Mechanical Systems; Thermal Protection; Contamination		18. Distribution Statement Unclassified - Unlimited Subject Category 12	
19. Security Classif. (of this report) Unclassified	20. Security Classif. (of this page) Unclassified	21. No. of Pages 530	22. Price A23

*For sale by the National Technical Information Service, Springfield, Virginia 22161